ICCMSE

Preface: Proceedings of the International Conference of Computational Methods in Sciences and Engineering 2019 (ICCMSE-2019)

The International Conference of Computational Methods in Sciences and Engineering 2019 (ICCMSE-2019) was taken place at Sheraton Rhodes Resort, Rhodes, Greece, between 1st and 5th May 2019.

The aim of the conference is to bring together computational scientists and engineers from several disciplines in order to share methods, methodologies and ideas and to attract original research papers of very high quality.

More than 300 papers have been submitted in order to be considered for presentation at ICCMSE-2019. The selection of the papers included in this Volume was based on an international peer review procedure by at least two independent reviewers.

We would like to thank:

- The eminent Scientific Committee of ICCMSE-2019 for their help and support (see the Conference Details in subsequent pages). We want to express special thanks to Professor Charalambos Tsitouras, Professor Zacharoula Kalogiratou and Professor Theodore Monovasilis for their help in the Editorial work for the selection of the papers via international peer review procedure.

- The Symposia and Sessions organizers for their considerable effort, as well as for their valuable job in relation to the further development of the conference.

- The distinguished invited speaker Professor Dr. Paul Mezey for his acceptance to give keynote lecture on his respective fields of expertise.

- The Organizing Committee (Mrs Eleni Ralli-Simou (Secretary of ICCMSE), Mr. Sotitis Economou, Mr. Konstantinos Giannakopoulos, Mrs. Danae Grypari, Mrs. Marianna Grypari, Mr. Nikolaos Simos, Mr. George Vordonis) for their valuable assistance.

- Special thanks to Mr. G. Vordonis for his help in typesetting of this Volume.

- Special thanks to the Secretary of ICCMSE-2019, Mrs Elena Ralli (who is also the Administrative Secretary of the European Society of Computational Methods in Sciences and Engineering (ESCMSE)) for her excellent job.

- Special thanks to the American Institute of Physics for the inclusion of these Proceedings into the famous series of the AIP Conference Proceedings

- Special thanks and acknowledgments to the REGALSCOPE LTD for their organization

Professor Dr. T.E. Simos, Editor
President of the European Society of Computational Methods in Sciences and Engineering (ESCMSE), Active Member of the European Academy of Sciences and Arts; Active Member of the European Academy of Sciences; Neijiang Normal University, P.R. China and University of Peloponnese, Greece

Professor Dr. Zacharoula Kalogiratou, Co-Editor, Vice-Chairman, Technological Educational Institute of Western Macedonia, Greece

Associate Prof. Dr. Theodore Monovasilis, Co-Editor, Vice-Chairman, Technological Educational Institute of Western Macedonia, Greece

October 2019

CONFERENCE DETAILS

International Conference of Computational Methods in Sciences and Engineering 2019 (ICCMSE-2019), Sheraton Rhodes Resort, Rhodes, Greece, 1-5 May 2019.

Chairman and Organiser

Professor T.E. Simos, Data Recovery Key Laboratory of Sichuan Province, College of Mathematics and Information Science, Neijiang Normal University, Neijiang 641100, PR China and Laboratory of Computational Sciences, Department of Informatics and Telecommunications, Faculty of Economy, Management and Informatics, University of Peloponnese, GR-221 00 Tripolis, Greece, Member of the Presidium of the European Academy of Sciences, President of the European Society of Computational Methods in Sciences and Engineering (ESCMSE), Active Member of the European Academy of Sciences and Arts (EASA), Active Member of the European Academy of Sciences (EAS), Corresponding Member of European Academy of Arts, Sciences and Humanities (EAASH).

Co-Chairwoman and Co-Chairman

Professor Dr. Zacharoula Kalogiratou, Technological Educational Institute of Western Macedonia.
Associate Prof. Dr. Theodore Monovasilis, Technological Educational Institute of Western Macedonia.

Scientific Committee

- **Prof Zacharoula Kalogiratou,** Greece
- **Prof. Vladislav N. Kovalnogov,** Russian Federation
- **Prof. Paul G. Mezey,** Canada, Hungary and Romania
- **Associate Prof. Theodore Monovasilis,** Greece
- **Dr. Taku Onishi,** Japan, Norway
- **Prof. T.E. Simos,** Greece
- **Prof. Dr. Ajit J. Thakkar,** Canada
- **Prof. Ch. Tsitouras,** Greece
- **Prof. Zhigang Jiang,** USA

Invited Speakers

- **Paul Mezey,** Canada Research Chair in Scientific Modelling and Simulation Department of Chemistry Memorial University of Newfoundland St. John's, CANADA

European Society of Computational Methods in Sciences and Engineering (ESCMSE)

AIMS AND SCOPE

The ***European Society of Computational Methods in Sciences and Engineering (ESCMSE)*** is a non-profit organization. The URL address is: http://escmse.eu/

The aims and scopes of ***ESCMSE*** is the construction, development and analysis of computational, numerical and mathematical methods and their application in the sciences and engineering.

In order to achieve this, the ***ESCMSE*** pursues the following activities:

• Research cooperation between scientists in the above subject.
• Foundation, development and organization of national and international conferences, workshops, seminars, schools, symposiums.
• Special issues of scientific journals.
• Dissemination of the research results.
• Participation and possible representation of Greece and the European Union at the events and activities of international scientific organizations on the same or similar subject.
• Collection of reference material relative to the aims and scope of ***ESCMSE***.

Based on the above activities, *ESCMSE* has already developed two international scientific journals called:

Journal of Numerical Analysis, Industrial and Applied Mathematics (JNAIAM). This is a journal under the copyright of ESCMSE. This is the journal for original research papers, review papers and letters. We note that this journal is electronically free for the academic community. URL address: **http://www.jnaiam.org**

Computing Letters (CoLe). This is a journal under the copyright of ESCMSE. This is the journal for original research papers, review papers and letters. We note that this journal is electronically free for the academic community.

CATEGORIES OF MEMBERSHIP

European Society of Computational Methods in Sciences and Engineering (ESCMSE)

Initially the categories of membership will be:

• **Full Member (MESCMSE):** PhD graduates (or equivalent) in computational or numerical or mathematical methods with applications in sciences and engineering, or others who have contributed to the advancement of computational or numerical or mathematical methods with applications in sciences and engineering through research or education. Full Members may use the title MESCMSE.

• **Associate Member (AMESCMSE):** Educators, or others, such as distinguished amateur scientists, who have demonstrated dedication to the advancement of computational or numerical or mathematical methods with applications in sciences and engineering may be elected as Associate Members. Associate Members may use the title AMESCMSE.

• **Student Member (SMESCMSE):** Undergraduate or graduate students working towards a degree in computational or numerical or mathematical methods with applications in sciences and engineering or a related subject may be elected as Student Members as long as they remain students. The Student Members may use the title SMESCMSE

• **Corporate Member:** Any registered company, institution, association or other organization may apply to become a Corporate Member of the Society.

REMARKS

1. After three years of full membership of the European Society of Computational Methods in Sciences and Engineering, members can request promotion to Fellow of the European Society of Computational Methods in Sciences and Engineering. The election is based on international peer-review. After the election of the initial Fellows of the European Society of Computational Methods in Sciences and Engineering, another requirement for the election to the Category of Fellow will be the nomination of the applicant by at least two (2) Fellows of the European Society of Computational Methods in Sciences and Engineering.

2. All grades of members other than Students are entitled to vote in Society ballots.

3. All grades of membership other than Student Members receive the official journal of the ESCMSE.

A Functorial Approach to Analogous Molecular Systems

Paul G. Mezey

Editor-in-Chief, Journal of Mathematical Chemistry, Springer,
Distinguished Visiting Professor,
International Research Unit of Advanced Future Studies, Yukawa Institute for Theoretical Physics,
Kyoto University, Kyoto 606-8502, Japan
Professor of Chemistry,
Canada Research Chair, Tier 1, 2003-2017, Scientific Modelling and Simulation
Department of Chemistry and Department of Physics,
Memorial University of Newfoundland, St. John's, NL, CANADA ,
Professor of Chemistry ("Magantanar"),
Institute of Chemistry, Eötvös University of Budapest
Budapest, Hungary
Guest Professor,
Faculty of Chemistry and Chemical Engineering, Babes-Bolyai University,
11 Arany Janos st., RO-400028, Cluj-Napoca, Romania

Email : paul.mezey@gmail.com

Abstract. Functorial models of category theory are powerful tools used in many branches of mathematics, even in various computer languages such as Python, however, on an applied mathematics level, functors can also provide novel approaches and new types of systematizations of interrelations among scientific concepts and representations. In a somewhat simplified way, a functor can be thought of as a mathematical tool doing two things all at once: transforming both sets and mappings between those sets. For example, a functor can establish a connection between one entity, involving two sets and a family of transformations between them, and another entity, also involving some two sets and the family of transformations between those. In other words, such a functor transforms one pair of sets and the relations between them to another pair of sets and the relations between them.

A Functor Model for Molecular Analogies

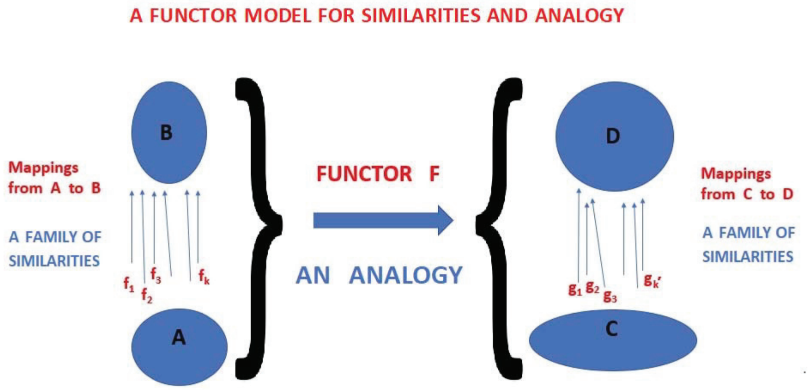

In fact, a functor has a dual role: providing a transformation not only between sets of objects, but also transforming the mappings between those sets. In some cases, the mappings connecting the elements of the pair of objects in one entity can be interpreted as pairwise expressions of certain kind of ***similarities*** between the elements of sets assigned to each other in the first entity, and in the same way, the mappings between the elements of the two sets in the second entity may be regarded as expressions of ***similarities*** between those elements.

The functor itself, connecting, on the one hand, the entire first entity involving the pair of sets with all their elements as well as all their associated mappings, with the entire second entity involving the pair of those sets with all their elements and also all their associated mappings, this functor can then be interpreted as some "higher level similarity", involving both elements of sets and relations between them. This higher-level similarity, the "similarity of similarities" of elements of sets, involving the similarity of relations between those sets, is certainly more complex than some ordinary similarity, and we may consider this multitude of similarities as an "analogy". In this contribution an efficient mathematical tool, a functorial approach is used for the description and treatment of families of molecular similarities, leading to a well-defined interpretation of analogies between molecular families, and in an even broader context, analogies within the field of chemistry.

Although traditionally molecular similarity has been used very successfully on very many occasions for connecting theoretical descriptions, such as molecular wavefunctions or even molecular graphs to experimentally determined molecular properties, as it has been described in some of the early expositions of the subject [1-3], many of the similarity analyses have been focusing on one, or only few properties at a given time. Much of the related approaches have involved the concept of shape, for example, the local and global shapes of molecular electron density clouds and their similarities [4-16], but also the shapes of potential functions, even the higher-dimensional shapes of potential energy hypersurfaces, relevant to the study of chemical reactions and conformational changes [17,18].

However, when extending the similarity concepts to analogies, then a more complex, yet a more exhaustive comparison becomes possible, and the mathematical tools of functors appear to be ideal for this purpose. In fact, the functor approach to analogies is providing a mathematically well-defined way to establish analogies between molecular systems involving very large number of molecules, with very large number of relevant properties. If such analogies, represented as functors, are taken as interrelations between entire systems of similarities, this approach still retains, on a simpler level, the use of individual similarities, described as mappings interrelating individual molecules. Consequently, analogies between molecular systems and their detailed interrelations are treated as "higher level similarities" represented by functors, themselves taken as transformations between molecular families together with their interrelations by various, often highly involved similarity mappings.

Whereas it is customary to discuss molecular shape and molecular similarity with a focus on nuclear coordinates, in the context of analogies and functors, it is more revealing to use families of similarities for characterization by focusing on the shape and shape changes of the electron density clouds. Such an approach can provide useful alternatives for the traditional molecular characterizations in applied fields, such as the QShAR, Quantitative Shape-Activity Relations approach in pesticide and herbicide research, as well as in pharmaceutical drug design. A rather multi-faceted collection of similarity concepts, hence, a good example for rather complex and extensive analogies is at the basis of a specific approach exploiting interrelations between molecules if the nuclear charges are regarded as abstract variables, leading to the reference cluster approach for symmetry utilization [16], and in a more extreme case, to the Universal Molecule model [17,18].

References

1. R. Carbo, L. Leyda, L. and M. Amau, "An electron density measure of the similarity between two compounds." Int. J. Quantum Chem. 17, 1185-1189 (1980).
2. M.A. Johnson and G.M. Maggiora, Eds., *Concepts and Applications of Molecular Similarity,* Wiley, New York, 1990.
3. P. M. Dean (Ed.), *Molecular Similarity in Drug Design*, Blackie Academic & Professional, 1995.
4. P.G. Mezey, "Classification Schemes of Nuclear Geometries and The Concept of Chemical Structure. Metric Spaces of Chemical Structure Sets Over Potential Energy Hypersurfaces", *J. Chem. Phys.,* **78**, 6182-6186 (1983).
5. P.G. Mezey, "Reaction Topology of Excited State Potential Energy Hypersurfaces", *Can. J. Chem.,* **61**, 956-961 (1983).
6. P.G. Mezey, "A Global Approach to Molecular Symmetry: Theorems on Symmetry Relations between Ground and Excited State Configurations", *J. Amer. Chem. Soc.,* **ll2**, 3791-3802 (l990).
7. P.G. Mezey, *Shape In Chemistry: An Introduction To Molecular Shape And Topology,* New York: VCH Publishers, 1993.
8. P.G. Mezey, "Semi-Similarity of Molecular Bodies: Scaling-Nesting Similarity Measures", *Int. J. Quantum Chem.,* **51**, 255-264 (1994).

9. P.G. Mezey," Two Symmetry Constraints on the Identity and Deformations of Chemical Species", *J. Phys. Chem.,* **99**, 4947-4954 (1995).
10. P.G. Mezey, "The T-Hull Approach to Shape Analysis", *Theor. Chim. Acta,* **91**, 67-71 (1995).
11. P.G. Mezey, "Three Properties of Relative Shape Envelopes of Molecular Electron Density Contours", *Theor. Chim. Acta,* **92,** 333-338 (1995).
12. D.J. Klein and P.G. Mezey, " T-Hull Relations for Shape Envelopes of Molecular Contours", *Theor. Chim. Acta,* **94**, 177-182 (1996).
13. P.G. Mezey, "Theorems on Molecular Shape-Similarity Descriptors: External T-Plasters and Interior T-Aggregates",*J. Chem. Inf. Comp. Sci.,* **36**, 1076-1081 (1996).
14. P.G. Mezey, "A Proof of the Metric Properties of the Symmetric Scaling-Nesting Dissimilarity Measure and Related Symmetry Deficiency Measures", *Int. J. Quantum Chem.,* **63**, 105-109 (1997).
15. P.G. Mezey, "Natural Molecular Fragments, Functional Groups, and Holographic Constraints on Electron Densities", Phys. Chem. Chem. Phys., 14, 8516-8522 (2012).
16. P. G. Mezey: "Relations Between Real Molecules Through Abstract Molecules: The Reference Cluster Approach" (Invited paper to the Peter Surjan Festschrift). 134:134 DOI 10.1007/s00214-015-1728-1 Theor. Chem. Acc. **2015**, 25-30 (2015).
17. P. G. Mezey, Topological tools for the study of Families of Reaction Mechanisms: the Fundamental Groups of Potential Surfaces in the Universal Molecule Context. Chapter 9, In: Challenges and Advances in Computational Chemistry and Physics, Vol 22, "Applications of Topological Methods in Molecular Chemistry", Springer. Editors: Esmail Alikhani, Remi Chauvin, Christine Lepetit, and Bernard Silvi, DOI: 10.1007/978-3-319-29022-5_9 Challenges,Comp.Chem.,Phys., **22**, 243-255 (2016).
18. P.G. Mezey, "Shape-Similarity Measures of Transition Structure Electron Densities as Tools to Assess Similarities of Reactions and Conformational Changes of Molecules", Chapter 2, in "Quantum Chemistry at the Dawn of the 21st Century", Ed. T. Chakraborty and R. Carbó-Dorca, AAP Apple Academic Press (CRC Press, Taylor and Francis Group), Wareton, NJ, USA, 2018, pp 35-58.

Keywords: Similarity and Analogy, Functor and Category Theory, Shape Analysis, Molecular Shape, Molecular Families QSAR, Pharmaceutical Drug Design. PACS: **31.10+z, 31.15-p**

Preface of “The 5th Computational Chemistry (CC) Symposium”

Taku Onishi[1-2]

[1]*Graduate School of Engineering, Mie University, Japan*
[2]*Hylleraas Centre for Quantum Molecular Sciences, Department of Chemistry, University of Oslo, Norway*

Corresponding author: taku@chem.mie-u.ac.jp, taku.onishi@kjemi.uio.no
URL: https://sites.google.com/site/cc2019iccmse/

Group Photo with CC Symposium Participants
(Sheraton Rhodes Resort: 2 May 2019)

The 5th Computational Chemistry (CC) symposium was held as the main symposium of ICCMSE 2019, with the cooperation of Prof. Theodore Simos (Chair of ICCMSE 2019) and Dr. Tokuei Sako. Our symposium purpose is to offer an opportunity to build a scientific friendship through interdisciplinary discussion, between outstanding chemists and physicists from all around the world.

In CC symposium, topics are largely divided into three: Materials; Biology; Chemical Reaction. Not only chemists but also physicists gave presentations from the different viewpoints. To discuss basic science in collaboration with theoretical physicists, quantum physics such as cosmology, particle and quantum methodology was actively discussed.

I would like to thank all participants. Due to their scientific contributions to CC symposium, new types of collaborations were born. From ICCMSE 2020, to accelerate interdisciplinary discussion with physicists, computational and theoretical physics will be more focused on.

Chair of CC symposium

Taku Onishi, PhD

Taku Onishi was born in Kobe, Japan. He graduated from Department of Chemistry, Osaka University, and received PhD from Osaka University in March 2003. He has been working as an assistant professor at Mie University since 2003. He has served on international scientific committee and editorial board: Science committee of ICCMSE, Editorial board of Journal of Computational Methods in Sciences and Engineering (JCMSE), Cogent Chemistry and Cogent Engineering etc. He has been a guest researcher of Department of Chemistry, University of Oslo.

Research field: Quantum Chemistry, Computational Chemistry, Materials Science

Book: Quantum Computational Chemistry - Modelling and Calculation for Functional Materials (Springer Nature, 2018)

Proton Conducting Mechanism in Perovskite Metal Oxides From Viewpoints of Local Structural Relaxation and Local Chemical Bonding Change

Taku Onishi[1-2]

[1]*Graduate School of Engineering, Mie University, Japan*
[2]*Hylleraas Centre for Quantum Molecular Sciences, Department of Chemistry, University of Oslo, Norway*

Corresponding author: taku@chem.mie-u.ac.jp, taku.onishi@kjemi.uio.no

Abstract. From our previous molecular orbital calculations using hybrid density functional theory for proton-conducting perovskite metal oxides, it was found that proton pumping effect is combined during proton-conduction, and covalent bonding change occurs in a diagonal line. It is known that pure perovskite metal oxides are regarded as boundary system. It is because they consist of the same unit structures. However, during proton-conduction, both local structural relaxation and local chemical bonding change must be taken into consideration. In this paper, the proton-conducting mechanism is explained from the different viewpoints of local structural relaxation and local chemical bonding change.

INTRODUCTION

Hydrogen has been much expected for next generation energy carrier. In industry all over the world, fuel cell (FC) has been actively developed, because practical electricity production is possible through direct utilization of hydrogen (sometimes through reforming from natural gas). Among several FCs, solid oxide fuel cell (SOFC) has been much expected as most practical one, due to structural stability and safety. In SOFC, proton-conducting [1-2] or oxide ion-conducting perovskite metal oxides [3-5] are used as solid electrolyte. It was demonstrated that proton-conducting mechanism in perovskite type metal oxides can be explained by proton pumping effect and chemical bonding change [6-8] (see Figure 1). In this paper, we explain proton-conducting mechanism from different viewpoints of <u>local structural relaxation and local chemical bonding change</u>.

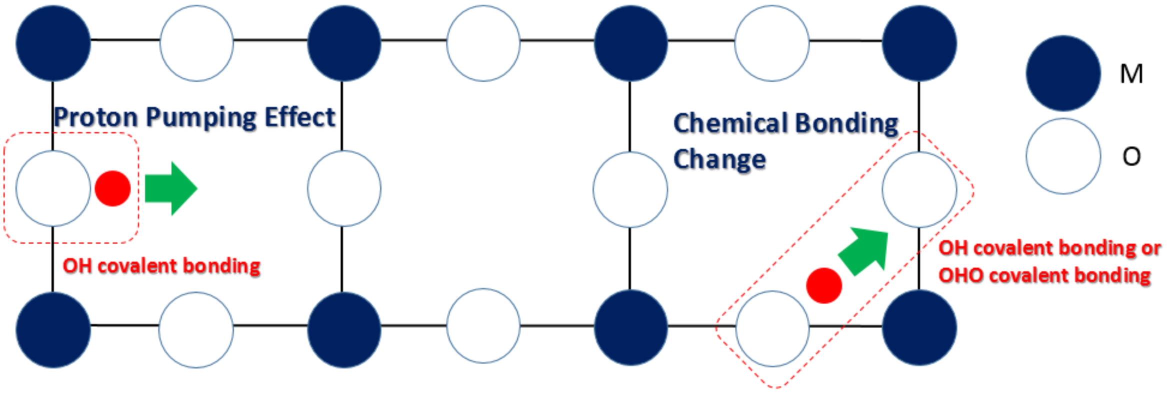

FIGURE 1. Schematic figure of proton-conduction in AMO_3 perovskite oxide (A= Counter Cation; M=Metal)

EQUALITY OF UNIT MODEL

In ideal solid, the same unit structures are continuously allocated. In cluster model calculation, minimum cluster model corresponding to minimum unit structure is constructed. It is because the cluster is regarded as a part of solid. In larger cluster model, which consists of many unit structures, the equality of electronic state per each unit structure is not kept. It is noted that three conditions are required: (1)No neutral condition (Neutral total charge is not always required); (2) No geometry optimization; (3) Experimental lattice distance. The details are explained in Ref. [9].

In band calculation, electrons only for one unit cell are considered as same as cluster model calculation. Though boundary property is mathematically included in the wave-function by using Bloch theorem, orbital overlap and electron spread between different unit cells cannot be property taken into account. It is hence found that dangling bond also exists in band model.

For example, let us consider antiferromagnetic M_2O layer, where superexchange interaction exists between metals via oxygen atom [10]. As shown in Figure 2, if unit cell is terminated at oxygen atom, no orbital overlap throughout M-O-M is represented in wave-function. Considering the effect, the scientific reasonable unit model must be constructed in both cluster model and band calculations.

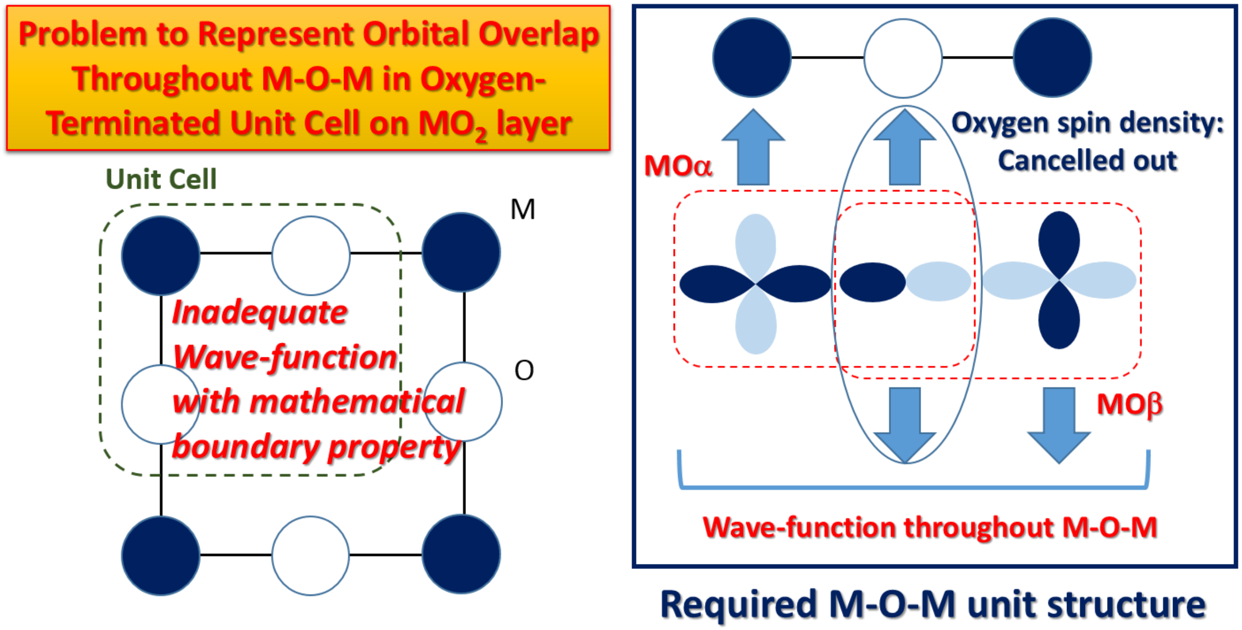

FIGURE 2. Schematic figure of problem in oxygen-terminated unit cell to represent superexchange interaction. MO denotes molecular orbital.

TWO LOCAL EFFECTS

Local Structural Relaxation: Proton Pumping Effect

When investigating solid state ion-conduction, a large structural relaxation can be negligible. It is because stable ion-conduction will not be observed, when it is largely distorted. However, since there is a possibility of a large surface structural relaxation, it must be discussed as surface proton-conduction.

AMO_3 type perovskite metal oxides, where A and M denote counter cation and metal, respectively, consist of M_4O_4 square, which is a minimum unit. In pure perovskite metal oxides, all units ideally have the same electronic structure. It implies that M_4O_4 square is a boundary unit. On the other hand, in proton-doped perovskite metal oxides, proton is irregularly doped (see Figure 3). M_4O_4 square including proton is hence non-boundary unit. For example, one neighbouring unit includes proton, whereas the other does not.

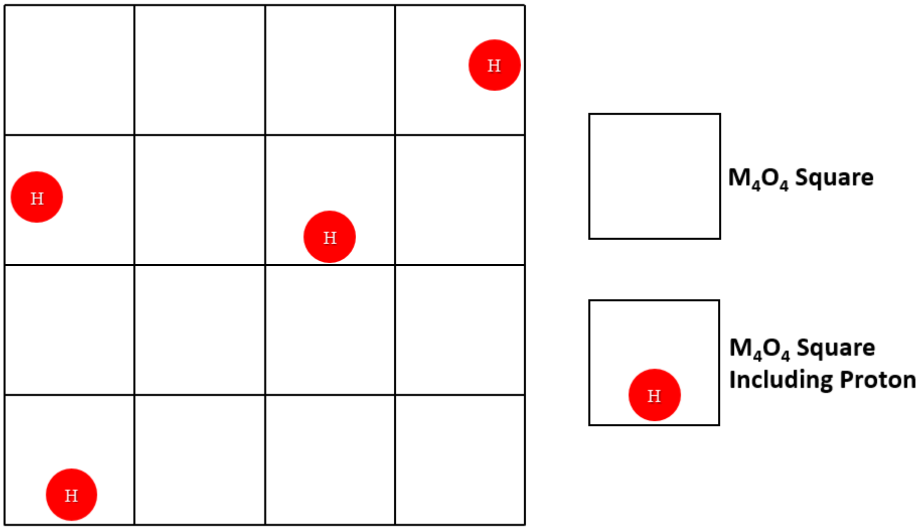

FIGURE 3. Schematic figure of MO_2 layer of proton-conducting AMO_3 type perovskite oxide (A= Counter Cation; M=Metal)

It is known that as shown in Figure 1, O-H is pumped into the square centre, whereas metal and other oxygen atoms consisting of M_4O_4 square are all kept fixed (proton pumping effect). It is noted that covalent bonding between oxygen and hydrogen atoms is kept during O-H migration.

OH migration can be regarded as local and temporal structural relaxation (see Figure 4). It is because oxygen atom is displaced from the lattice position, and the phenomenon is observed only at specific unit, where proton exists.

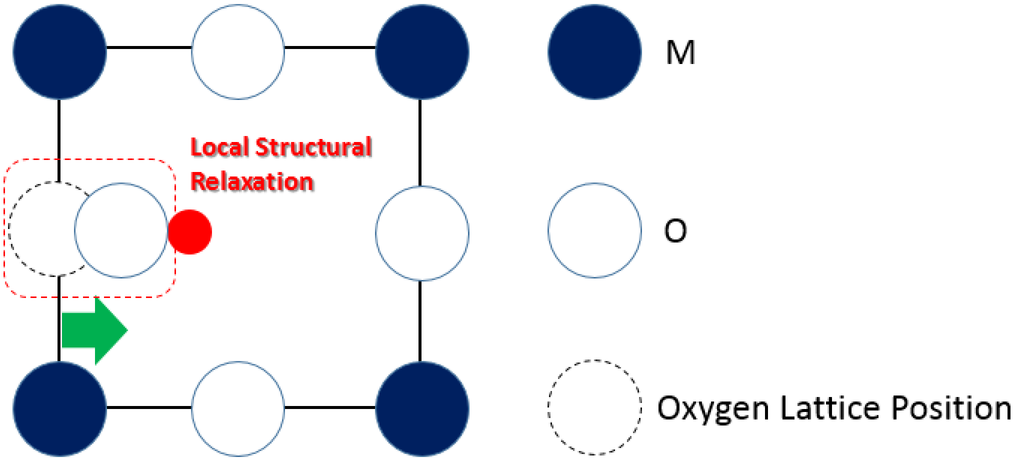

FIGURE 4. Schematic figure of local and temporal O-H migration within M_4O_4 square

Local Chemical Bonding Change

Local chemical bonding is observed in proton-conducting AMO_3 perovskite (see Figure 5). During proton-conduction in a diagonal line (connecting two oxygen atoms), hydrogen forms covalent bonding with one oxygen atom (O-H covalent bonding), when hydrogen is allocated near the oxygen atom. On the other hand, at the middle of a diagonal line, hydrogen atom forms covalent bonding with both oxygen atoms (O-H-O covalent bonding). It is noted that the chemical bonding change locally and temporarily occurs during proton-conduction.

FIGURE 5. Schematic figure of (1) O-H and (2) O-H-O covalent bonding formations during proton-conduction in a diagonal line

SUMMARY

During proton-conduction in perovskite metal oxides, two local effects cannot be negligible. One is local oxygen relaxation. In proton pumping, oxygen atom is displaced from lattice position, forming O-H covalent bonding. It can be hence regarded that local structural relaxation occurs. The other is local chemical bonding change. During proton-conduction in a diagonal line, O-H or O-H-O covalent bonding is formed. It is noted that both local effects temporarily appear during proton-conduction. Thus, when investigating proton-conduction, two local effects must be properly taken into consideration. Molecular orbital calculation for cluster model is very useful for the investigation.

ACKNOWLEDGEMENTS

This work was partially supported by the Research Council of Norway through its Centres of Excellence scheme, project number 262695.

REFERENCES

1. J. M. Polfus, T. Norby, R. Haugsrud, *Dalton Trans* **40**, 132 (2011)
2. T. Norby, *Perovskite Oxide for Solid Oxide Fuel Cell* (Springer Nature), Chapter 11 (2011)
3. T. Ishihara, *Perovskite Oxide for Solid Oxide Fuel Cell* (Springer Nature), Chapter 4 (2009)
4. T. Onishi, *Int. J. Quant. Chem.* **110**, 2912–2917 (2010)
5. T. Onishi, *Adv. Quant. Chem.* **64**, 31-81 (2012)
6. T. Onishi, *Adv. Quant. Chem.* **70**, 31-67 (2015)
7. T. Onishi, T. Helgaker, *Advances in Quantum Methods and Applications in Chemistry, Physics, and Biology* (Springer Nature) Chapter 14 (2013)
8. T. Onishi, *Quantum Computational Chemistry -Modelling and Calculation for Functional Materials* (Springer Nature) Chapter 14 (2018)
9. T. Onishi, *Quantum Computational Chemistry -Modelling and Calculation for Functional Materials* (Springer Nature) Chapter 9 (2018)
10. T. Onishi, *Quantum Computational Chemistry -Modelling and Calculation for Functional Materials* (Springer Nature) Chapter 10 (2018)

The Adiabatic Potential of the He-H Interaction

Elena V. Orlenko[1, a)], Andrey Barilov[2, b)], and Fedor Orlenko[3]

[1]*Theoretical Physics Department, Peter the Great St. Petersburg Polytechnic University, Polytechnicheskaya St. 29, 195251, St. Petersburg, Russia.*
[2]*Department of Physical Electronics, Peter the Great St. Petersburg Polytechnic University, Polytechnicheskaya St. 29, 195251, St. Petersburg, Russia.*
[3]*Department of Physics, Saint Petersburg State Chemical Pharmaceutical Academy (SPCPA), Professor Popov St., 14, Lit. A, 197376 St. Petersburg, Russia.*

[a)]Corresponding author: eorlenko@mail.ru
[b)]andreybarilov@gmail.com

Abstract. We compute an adiabatic potential of the Hydrogen-Helium interaction by using a new approach based on the regular method of the Exchange perturbation theory (EPT). We present the results in the analytical form. A proofed completeness property for a non-orthogonal set of anti-symmetrized wave functions allows to present solution as an expansion on this set. The corrections to the antisymmetrized wave functions of zeroth approximation are properly antisymmetric.

INTRODUCTION

Besides, of hydrogen molecule, helium hydride is the second of the most elementary molecules. In their pioneer work, Micelle and Harris [1] have predicted the existence of the bound exited states of helium hydride by using a molecular orbital calculation. The ground state of this system is repulsive; it is shown by numerous experiments and theoretical calculations [2]. Now, it is not only helium hydride, but also the systems, like, NeH and ArH, have only repulsive ground state; nevertheless they possess a series of bound excited Rydberg states [2 - 4]. The first observation supporting the existence of bound, excited states of HeH was performed in the experiment of Möller et. all [5]. In the work [6] authors reported on the spectroscopic proof of the existence of rather long-lived excited states of HeH. In the experiment W. Ketterle, et all have observed the discrete emission spectra [7]. It was the ultimate proof of the bound state existence foe the helium hydride. Theoretical investigations of noble gases hydrides performed by numerical calculations have used an Atomic Orbital technique (LCAO), or Hartree-Fock methods [8], [9]). The reference spaces consisted of the symmetry-adapted functions configurations or contracted Gaussian-type functions [2] to avoid their overlapping basis overfilling problem. Due to the absence of a regular method of the probe-wave functions have been constructed half-intuitive. A perturbation theory (PT) method gives certain advantages in comparison with variation methods. So, the representation of the interaction energy in PT as a sum of different terms, each having a specific physical meaning, allows to associate this energy with the physical characteristics of the interacting system of atoms ([10, 11]. There are two types of multi-electronic systems according to the construction of the antisymmetric wave functions and their inputs to exchange contributions, first, *single-centred* systems and *manifold centered*, or molecular systems. In the first case, the "zeroth" Hamiltonian $\hat{H}_0$ describing the non-interactive system and a perturbation operator $\hat{V}$ accounting for all electron-electron interactions the same as a total Hamiltonian $\hat{H} = \hat{H}_0 + \hat{V}$ are invariant to the antisymmetrization operation $\hat{A}$, that takes into account all electron permutations: $\left[\hat{H}_0, \hat{A}\right] = 0$, $\left[\hat{V}, \hat{A}\right] = 0$, $\left[\hat{H}, \hat{A}\right] = 0$. It is commonly accepted in the "single-centered" case to use the antisymmetrized wave functions in a Slater determinant form. For the second case, both the "zeroth" Hamiltonian

$\hat{H}_0$ describing a manifold centred multielectron system without interatomic interaction and perturbation operator $\hat{V}$, that describes an interatomic interaction are non-invariant to the antisymmetrisation accounting for the electron permutations among the atomic centres: $\left[\hat{H}_0, \hat{A}\right] \neq 0$, $\left[\hat{V}, \hat{A}\right] \neq 0$. At that time, the total Hamiltonian of the system preserves its invariance $\left[\hat{H}, \hat{A}\right] = 0$ [11-13]. Contrary to the single-center case, a zeroth approximation wave function antisymmetrized with respect to intercentre electron permutations is not an eigenfunction of the non-invariant Hamiltonian [10, 11]. Respectfully to the mentioned problems, an exchange perturbation theory (EPT) formalism has been formulated [11-13] in such a way that, first, the zeroth approximation antisymmetrized wave function should be an eigenfunction of the Hamiltonian which describes the non-interactive subsystems forming the total system. Second, corrections of any order to the wave function accounting for the perturbation should have properly antisymmetric form. It takes into account an another difficulty related to the non-orthogonality of a zeroth approximation antisymmetrized wave functions set commonly called as "an overfilling catastrophe". It was shown that under certain conditions a non-orthogonal basis of antisymmetrized wave functions constitutes a complete set. An overview and a classification of the existed EPT formalisms can be found in Ref.[10]. There are two groups: (I) formalisms with non-symmetric unperturbed Hamiltonian and non-symmetric perturbation; (II) formalisms with symmetric zero-approximation Hamiltonian and symmetric perturbation. The first type of formalisms, also called symmetry-adapted EPT formalisms, have an advantage of being a simple representation of zero-approximation Hamiltonian and a perturbation operator. The drawback of these formalisms is that they require a *post factum* antisymmetrization that need in the additional variation procedure for obtaining the corrections within the perturbation theory, as seen in [10, 14]. (II) The second type of formalisms allows the standard perturbation theory methods by constructing a symmetric zero-approximation Hamiltonian and perturbation. As a result, a symmetric unperturbed Hamiltonian with antisymmetric eigenfunctions have a non-Hermitian form [10, 15]. The practical applicability of this Hamiltonian is restricted to two-electron systems. In the present work, we use the EPT formalism developed in a general form [11-13, 16]. The presentation of the energy and the wave function corrections contain a special symmetric form of the perturbation operator. The represented EPT formalism has a standard form of an Invariant exchange perturbation theory (IEPT) and takes into account intercentre permutations of electrons among overlapping states and then reduced to the symmetry-adapted form. We apply EPT formalism for describing and computing a Helium – Hydrogen adiabatic potential of an interaction.

THE ADIABATIC POTENTIAL OF THE *HE-H* INTERACTION

As an initial wave function of the neutral (total charge Q=0) system noninteractive *He-H* we take the form of the simple product of two atomic wave functions, dependent on their spatial and spin parts, for the ground state (doublet spin state) is:

$$\Phi_0(\mathbf{r}_1,\mathbf{r}_2,\mathbf{r}_3;\xi_1,\xi_2;\xi_3) = \Phi_{He}(\mathbf{R}-\mathbf{r}_1,\mathbf{R}-\mathbf{r}_2;\xi_1,\xi_2)\cdot\psi_H(\mathbf{r}_3)\cdot\chi_H(\xi_3);$$

$$\Phi_{He}(\mathbf{R}-\mathbf{r}_1,\mathbf{R}-\mathbf{r}_2;\xi_1,\xi_2) =^1 S_{0He}(1,2) = \left(\varphi_{1s}(\mathbf{R}-\mathbf{r}_1)\varphi_{1s}(\mathbf{R}-\mathbf{r}_2)\right)\cdot\frac{1}{\sqrt{2}}\left(\alpha1\beta2-\beta1\alpha2\right). \tag{1}$$

Here $\mathbf{R}$ is a vector originating at the Hydrogens nucleus and pointing to the Helium nucleus; $\mathbf{r}_i$ - is the radius vector of the electron, numbered *i*, originating at the Hydrogen nucleus; ξ_i – is the spin variable of the electron *i*. The atomic function $\Phi_{He}(\mathbf{R}-\mathbf{r}_1,\mathbf{R}-\mathbf{r}_2;\xi_1,\xi_2)$ of Helium atom is a ground state antisymmetrized function accounted the internal electron permutations, where α and β are the one-electron spin functions, corresponding to the "up" and "down" spin states, respectively. The ordinary non-symmetric form of the unperturbed system Hamiltonian and a perturbation operator are

$$H^0(1,2,3) = -\frac{\hbar^2}{2m}(\nabla_1^2+\nabla_2^2+\nabla_3^2) - \frac{2e^2}{r_{He1}} - \frac{2e^2}{r_{He2}} + \frac{2e^2}{r_{12}} - \frac{e^2}{r_{H3}}, V_{p=0} \equiv V(12,3) = -\frac{2e^2}{r_{He3}} - \frac{e^2}{r_{H1}} - \frac{e^2}{r_{H2}} + \frac{2e^2}{R} + \frac{e^2}{r_{23}} + \frac{e^2}{r_{13}}, \tag{2}$$

where we denote $r_{He1} = |\mathbf{R} - \mathbf{r}_1|$ the distance between electron, numbered 1, and its own Helium nucleus; $r_{12} = |\mathbf{r}_1 - \mathbf{r}_2|$ -- a distance between electrons, numbered 1 and 2, respectively, that belong to the same centre, the Helium nucleus, with $r_{H3} = |\mathbf{r}_3|$ being a distance between electron, numbered 3 and its own centre, originating at the Hydrogen nucleus.

The function (1) is an eigenfunction for the Hamiltonian (2). For the antisymmetrisation of the three-electron system, *He-H*, where both electrons occupy the $1s^2$ orbital in a singlet state, only [21]-type Young diagram is possible. Here the superscript [21] will describe the ordering of empty boxes in the Young diagram: two boxes in the upper row and one box in the bottom row, and the subscript describes the different art of the boxes filling Ref.[17]. Antisymmetrization of the atomic wavefunfction given by Eq. (1) over interatomic electrons permutations performed using the four independent Young's operators corresponding to the Young diagram: $\omega_{11}^{[21]};\omega_{12}^{[21]};\omega_{21}^{[21]};\omega_{22}^{[21]}$, where, $\omega_{11}^{[21]}=\frac{1}{\sqrt{12}}(2+2P_{12}-P_{23}-P_{13}-P_{123}-P_{132})$, $\omega_{12}^{[21]}=(P_{23}-P_{13}-P_{123}+P_{132})$, P_{12} denotes the permutation of electrons 1 and 2; P_{123} denotes the cyclic permutation of electrons 1, 2 and 3. We obtain the antisymmetric wave function by applying the normalized Young operator [17] to the wave function of the Hydrogen–Helium system as follows:

$$\Psi=\frac{1}{f_0}\left(\Psi_1(\mathbf{r}_1,\mathbf{r}_2,\mathbf{r}_3)\mathrm{X}_{HeH1}(1,2,3)+\Psi_2(\mathbf{r}_1,\mathbf{r}_2,\mathbf{r}_3)\mathrm{X}_{HeH2}(1,2,3)\right). \tag{3}$$

Here is the normalized factor f_0, determined by $f_0=\frac{\sqrt{3}}{2}\langle\Psi_1(\mathbf{r}_1,\mathbf{r}_2,\mathbf{r}_3)|\Psi_{\mathrm{He}}(\mathbf{r}_1,\mathbf{r}_2,)\psi_{\mathrm{H}}(\mathbf{r}_3)\rangle$. The spatial parts are

$$\Psi_1(\mathbf{r}_1,\mathbf{r}_2;\mathbf{r}_3)=\omega_{11}^{[21]}\Phi_{He}(\mathbf{R}-\mathbf{r}_1,\mathbf{R}-\mathbf{r}_2)\Phi_H(\mathbf{r}_3);\Psi_2(\mathbf{r}_1,\mathbf{r}_2;\mathbf{r}_3)=\omega_{12}^{[21]}\Phi_{He}(\mathbf{R}-\mathbf{r}_1,\mathbf{R}-\mathbf{r}_2)\Phi_H(\mathbf{r}_3)=0, \tag{4}$$

whereas the corresponding spin parts are: $\mathrm{X}_{He_H1}=\omega_{22}^{[21]}|\alpha1\beta2\alpha3\rangle=\frac{\sqrt{3}}{2}\{|\alpha1\beta2\alpha3\rangle-|\beta1\alpha2\alpha3\rangle\}$,

$$\mathrm{X}_{He_H2}=\omega_{21}^{[21]}|\alpha1\beta2\alpha3\rangle=\frac{1}{2}\{-2|\alpha1\alpha2\beta3\rangle+|\alpha1\beta2\alpha3\rangle+|\beta1\alpha2\alpha3\rangle\}. \tag{5}$$

According to EPT [11-13], the energy of *He-H* interaction in the first approximation has a form

$$E(R)=E_i^1=\langle\Psi|V_{p=0}|\Phi^{p=0}\rangle=\frac{1}{f_0(R)}(4K(R)-3A_{23}(R)-A_{31}(R)), \tag{6}$$

Here, bra-vector $\langle\Psi|$ has the antisymmetric form (5) and ket-vector $|\Phi^{p=0}\rangle$ determined by (1), $f_0(R)=\frac{2(1-S^2(R))}{3}$

$A_{23}(R)=(\varphi_{He}(1)\varphi_{He}(3)\psi_H(2)|V(12,3)|\varphi_{He}(1)\varphi_{He}(2)\psi_H(3))$, $A_{13}=(\varphi_{He}(2)\varphi_{He}(3)\psi_H(1)|V(12,3)|\varphi_{He}(1)\varphi_{He}(2)\psi_H(3))$, $S=\int\psi_H(\mathbf{r})\varphi_{He}(\mathbf{R}-\mathbf{r})d^3\mathbf{r}$. A "direct" contribution K is the integral $K=(\varphi_{He}(1)\varphi_{He}(2)\psi_H(3)|V(12,3)|\varphi_{He}(1)\varphi_{He}(2)\psi_H(3))$. The initial electron states of Helium-atom has a from [18]: $\psi(\mathbf{R}-\mathbf{r}_i)=(\alpha^3/\pi)^{1/2}\exp(-\alpha|\mathbf{R}-\mathbf{r}|),\alpha=27/16$. A ground state of the electron in a Hydrogen atom is described by the single-electron wave function:

$$\psi_H(r_H)=\psi_{nlm}(r,\theta,\varphi)=\frac{1}{\sqrt{(2n\cdot(n-l-1)!\cdot(n+l)!)}}\cdot(2/na_0)^{\frac{2}{3}}\cdot e^{-\frac{r}{na_0}}\cdot\left(\frac{2r}{na_0}\right)^l L_{n-l-1}^{2l+1}(2r/na_0)\cdot Y_{l,m}(\theta,\varphi),$$

where a_0 - is a Bohr radius, $L_{n-l-1}^{2l+1}\left(2r/na_0\right)$ - generalized Laguerre polynomial of degree $n-\ell-1$, $Y_{l,m}(\theta,\varphi)$ is a spherical harmonic function of degree ℓ and order m. To evaluate all above-mentioned integrals we use the elliptical coordinates for each i-th electron.

Results and Conclusion

A Computation of the potential E(R), given by the Eq. (6) with expressions for the exchange contributions and for the direct Coulomb contribution gives the results presented by curves on the Figs.2 (a, b, c, d). E(R) show only potential of the interatomic interaction in the Hartree units E_h, whereas an interatomic distance has been taken in Bohr radius a_0. Analysing the interaction potential may to choose the most preferable excited states of Hydrogen atom for the Helium hydride creation. They are: s-state (n=2, l=0, m=0) with bond energy E_{bond}=0.01 Hartree; p-state (n=2, l=1, m=0) with bond energy E_{bond}=0.007 Hartree and d-state (n=3, l=2, m=0) with bond energy E_{bond}=0.009 Hartree. It is well known, that the ground state of Hydrogen atom is repulsive and does not form the helium hydride state. Our results shown on the Fig. 2a demonstrate such a repulsive potential.

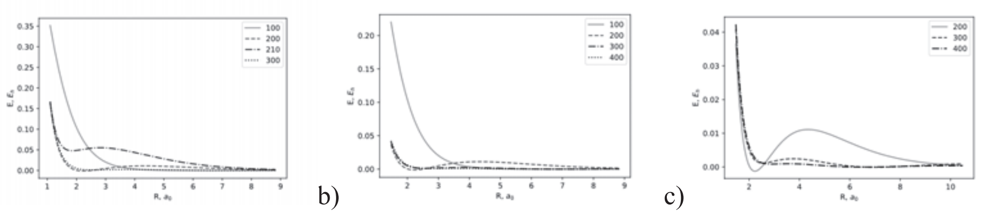

a) b) c)

FIGURE 1. The potential of the interatomic interaction in the Hartree units E_h, whereas an interatomic distance is taken in Bohr radius a_0 for the ground state of He-atom and a) a ground state (n=1, l=0, m=0), or (100) and excited s-states of Hydrogen atom (200), (300), (400) and p-state (210). b) a ground state (*n*=1, *l*=0, *m*=0), or (100) and excited s-states of Hydrogen atom (200), (300), (400); c) excited s-states of Hydrogen atom (200), (300), (400).

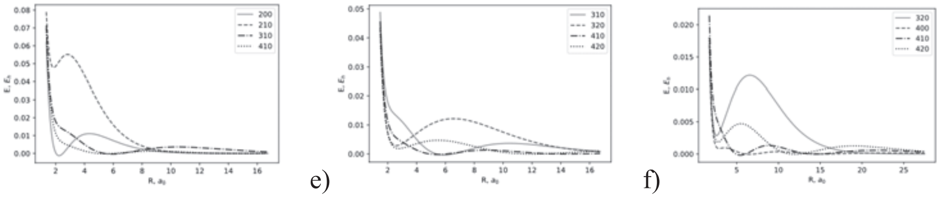

d) e) f)

FIGURE 2. The potential of the interatomic interaction in E_h, interatomic distances are in a_0 for the ground state of He-atom and d) excited p-states of Hydrogen atom (210), (310), (410) in compare s-state (200); e) excited H-states (*n*=3, *l*=1, *m*=0) (p-state), d-state-(320), p-state (410), d-state-(420); f) excited H states (*n*=3, *l*=2, *m*=0) (d-state), s-state-(400), p-state (410), d-state-(420);

The interaction energy $E(R)$ should include the atomic eigenstates energy: $E(R) = E_{He}^0 + E_{He}^0 + U_{\text{int}}(R) = -\left(Z - \frac{5}{16}\right)^2 \frac{e^2}{a_0} - \frac{e^2}{2a_0 n^2} + U_{\text{int}}(R)$. Here Z – is a real Helium nuclear charge, Z=2. So that, the each term have the following energy shift: $X^2\Sigma^+(n=1, l=1), \Delta E = -3,35E_h$; $A^2\Sigma^+(n=2, l=0), \Delta E = -2.97E_h$ $B^2\Pi(n=2, l=1), \Delta E = -2.97E_h$; $C^2\Sigma^+(n=3, l=0), \Delta E = -2.903E_h$; $C^2\Pi(n=3, l=1), \Delta E = -2.903E_h$; $C^2\Delta(n=3, l=2)$, $\Delta E = -2.903E_h$. These results are in a good agreement with the experimental dates [7, 8] [2], [7], [19].

Acknowledgments

The authors greatly appreciated the Peter the Great St. Petersburg Polytechnic University, and its Program 5-100-2020, for the financial support for the participation in the ICCMSE Conference 2019.

REFERENCES

1. H. H. Michels and F. E. Harris, J. Chem. Phys. **39**, 1464 (1963).
2. G. Theodorakopoulos, S. C. Farantos, R. J. Buenker, and S. D. Peyerimhoff, J. Phys. B **17**, 1453 (1984).
3. V. Bondybey , P.K. Pearson and H.F. Schaefer, J. Chem. Phys. **57**, 1123, (1972)
4. J. W. C. Johns, J. Mol. Spectrosc. **36**, 488 (1970).
5. T. Möller, M. Beland, J. Stapelfeldt, and G. Zimmerer, in Book of Abstracts, Second European Conference on Atomic and Molecular Physics, Amsterdam, 1985, edited by A. E.de Vries and M. J. van der Wiel, (Amsterdam, 1985)
6. Th. Möller, M. Beland, and G. Zimmerer, Phys. Rev. Lett., **55**, 20 , 2145-2148, (1985).
7. W. Ketterle, H. Figger, and H. Walther, Phys.Rev.Lett., **55**, 27, 2941-2944, (1985).
8. G. Theodorakopoulos, I. D. Petsalakis , C. A. Nicolaidest and R. J. Buenker, J. Phys. B: At. Mol. Phys. **20** 2339-2345, (1987).
9. J. R. Peterson and Y. K. Bae, Phys. Rev. A **34**, 3517 (1986).
10. I.G. Kaplan, *Intermolecular interactions: physical picture, computational methods, and model potentials* (Wiley, New York. 2006), pp. 380.
11. Elena V. Orlenko, Chapter 1. Exchange Perturbation Theory in *Perturbation Theory: Advances in Research and Applications*. Edited by Zossima Pirgov, (Nova Science Publishers, New York 2018) p.p. 1-60.
12. E. V.Orlenko, T. Yu. Latychevskaia, JETP, **86**, 1167-1176, (1998). .
13. E.V.Orlenko, T. Latychevskaya, A.V. Evstafev, F.E. Orlenko, Theor. Chem. Acc., **134,** (5), 28, (2015).
14. Mayer, I. Chem. Phys. Lett.,**332**, 381-392, (2000).
15. Sternheimer, R. M. Phys. Rev.,**96**, 951, (1954).
16. Orlenko, E.V.; Rumyantsev, A.A. JETP, **97**, 439-448, (1990).
17. I.G. Kaplan, *Symmetry of many-electron systems* (Academic: New York. 1975), pp 372.
18. P.Gombas, T. Szondy, *Solutions of the simple self-consistent field for atoms*. (Acad. Kiodo: Budapest, 1970), pp.82.
19. J. Römelt, S. D. Peyerimhoff, and R. J. Bünker, Chem. Phys. **41**, 133 (1979); T. E. Sharp, At. Data **2**, 119 (1971).

Some Observations on the Performance of the Most Recent Exchange-Correlation Functionals for the Large and Chemically Diverse GMTKN55 Benchmark

Golokesh Santra[1] and Jan M.L. Martin[1, a)]

[1] *Department of Organic Chemistry, Weizmann Institute of Science, 76100 Reḥovot, Israel*

[a)]Corresponding author: gershom@weizmann.ac.il

Abstract. Benchmarks that span a broad swath of chemical space, such as GMTKN55, are very useful for assessing progress in the quest for more universal DFT functionals. We find that the WTMAD2 metrics for a great number of functionals show a clear "Jacob's Ladder hierarchy"; that the "combinatorial" development strategy of Head-Gordon and coworkers generates "best on rung" performers; that the quality of the nonlocal dispersion correction becomes more important as functionals become more accurate for nondispersion properties; that fitting against small, unrepresentative benchmark sets leads to underperforming functionals; and that ωB97M(2) is currently the best DFT functional of any kind, but that revDSD-D4 functionals are able to reach similar performance using fewer parameters, and that revDOD-D4 in addition permits reduced-scaling algorithms. If one seeks a range-separated hybrid (RSH) GGA that also performs well for optical excitation energies, CAM-QTP-01 may be a viable option. The D4 dispersion model, with its partial charge dependence, appears to be clearly superior to D3BJ and even possibly NL. Should one require a double hybrid without dispersion model, noDispSD-SCAN is a viable option. Performance for the MOBH35 transition metal benchmark is different: the best double hybrids are competitive but not superior to ωB97M-V, which offers the best performance compromise for mixed main group-transition metal problems.

INTRODUCTION

Recently, Goerigk and coworkers released the GMTKN55 benchmark[1] for density functional methods, which is both large (1,500 reaction energies) and chemically diverse (55 different types of properties, which can be grouped into five major categories: small molecule thermochemistry, large molecule reactions, barrier heights, intermolecular noncovalent interactions, and intramolecular/conformational ones). These authors covered a great many exchange-correlation functionals, but a number of more recent ones such as ωB97M(2)[2] went unexplored for technical reasons. In addition, a set of revised[3] DSD double hybrids has meanwhile been fitted to GMTKN55, improving substantially on the original ones.[4] The purpose of the present short paper is to summarize these data and stress the strengths and weaknesses of these methods.

In Perdew's "Jacob's Ladder" metaphor,[5] we climb a ladder from Hartree's "vale of tears" to the heaven of chemical accuracy by introducing an XC (exchange-correlation) functional and adding explicit dependence on additional pieces of information on each rung: on rung 1 (LDA) just the local density ρ; on rung 2 (GGA) the reduced density gradient $\rho^{-4/3}\nabla\rho$; on rung 3 (mGGA) the Laplacian or (contains equivalent information) the kinetic energy density τ; on rung 4 the occupied orbitals (of which hybrids are the most common special case);[6] and finally on rung 5 the unoccupied orbitals (e.g., double hybrids[7] based on GLPT2, 2nd-order Görling-Levy[8] perturbation theory).

In the development of DFT functionals, physicists have traditionally strived for nonempirical functionals with parameters derived from known constraints, while chemists have embraced empiricism. The proliferation of empirical parameters in functionals like M06[9] and MN15[10] has inspired the "combinatorial optimization" approach of Mardirossian and Head-Gordon,[11] in which the parameter space is carefully pruned for statistical significance: this has resulted in the ωB97X-V,[11] B97M-V,[12] ωB97M-V,[13] and ωB97M(2) functionals.[2] From a different perspective,

the DSD functionals (dispersion-corrected, spin-component scaled, double hybrid) developed in our group[3,4,14] reduce empirical parameters to a mere handful at the expense of introducing the GLPT2 step.

COMPUTATIONAL METHODS

All quantum chemical calculations were performed using Q-CHEM[15] versions 5.1.1 and 5.2 running on the Faculty of Chemistry HPC facility. SG-3 or better integration grids were used throughout; basis sets were def2-QZVPP except for some anionic subsets where diffuse functions could matter much, where we employed def2-QZVPPD instead. For further details see Ref. [3]

The primary metric and "objective function" employed is the WTMAD2 (weighted mean absolute deviation, type 2) as defined by Goerigk et al, defined as follows:

$$\mathrm{WTMAD2} = \frac{1}{\sum_i^{55} N_i} \cdot \sum_i^{55} N_i \cdot \frac{56.84\ \mathrm{kcal/mol}}{\overline{|\Delta E|}_i} \cdot \mathrm{MAD}_i$$

in which division by $|\Delta E|_i$, the mean absolute value of all the reference energies for subset *i*, seeks to compensate for the different energy scales. N_i the number of data points in the subset, and MAD_i represents the mean absolute difference between calculated and reference reaction energies for subset *i*. We note that MAD is a more "robust statistic"[16] than the root mean square deviation, in the statistical sense that MAD is less sensitive to "outliers" than the RMSD (root mean square difference), conversely, RMSD is more useful for spotting outliers.

Aside from ωB97M(2) and the original[4] and revised[3] double-hybrid functionals, in order to "compare apples to apples", we also evaluated WTMAD2 in the exact same manner for some additional functionals on rungs 2–4. They were the GGAs PBE,[17] revPBE,[18] and B97-D3BJ;[19] the meta-GGAs TPSS,[20] revTPSS,[21] SCAN,[22] and B97M-V,[12] the global hybrid GGAs B3LYP,[23,24] PBE0,[25] and its analog revPBE0;[25] the global hybrid meta-GGAs PW6B95,[26] M06,[27] revM06,[28] M06-2X,[27] SCAN0,[29] and MN15,[10] the range-separated hybrids M11,[30] revM11,[31] CAM-QTP00 and CAM-QTP01,[32] as well as ωB97X-V,[11] and the range-separated hybrid meta-GGA ωB97M-V.[13] For additional references, see Refs.[1,3,33]

Parameters for the D3BJ[34] and D4[35] dispersion corrections were taken from Ref.[1] where necessary; where unavailable, they were obtained in this work by minimizing the GMTKN55 WTMAD2 in function of the dispersion terms using an adaptation of Powell's BOBYQA derivative-free bounded optimizer. [36]

RESULTS AND DISCUSSION

Values of the WTMAD2 metric, as well as of its subtotals for the five principal subcategories, are given in Table 1 relative to the popular M06-2X functional, which is popular among mechanistic researchers owing to its good performance for both thermochemistry and barrier heights.

As concerns Jacob's Ladder, we can state that it is well preserved along the sequence LDA → PBE → SCAN → SCAN0 → SCAN0-2, and more clearly still along the pathway LDA → B97-D3 → B97M-V → wB97M-V → wB97M(2): each of these latter functionals is "best in class" on its rung except for B97-D3 which is slightly surpassed by revPBE-D3BJ.

Concerning the PBE variants, we note that PBEsol,[37] the solids version of PBE, leads to an unacceptable deterioration for molecules; Weitao Yang's modified revPBE,[18] in contrast, yields clearly improved performance. RPBE is comparable to PBE here, with some variation in the subsets.

The CAM-QTP01 RSH originated as a reparametrization of CAM-B3LYP[38] by the Bartlett group[32] in order to minimize deviations from the ionization potential theorem and thus improve performance for electronic spectroscopy (in what could be called a "globalized" take on the tuned range separated hybrids of Baer and Kronik,[39,40]). After fitting a D3BJ dispersion correction for it to the whole GMTKN55 set, we found that CAM-QTP01-D3BJ performs comparably to popular hybrids like PBE0-D3BJ and B3LYP-D3BJ for equilibrium thermochemistry — but, intriguingly, CAM-B3LYP-D3BJ beats them both, owing primarily to the noncovalent subsets.

As for empirical vs. nonempirical functionals: on rung 2 revPBE-D3BJ bests B97-D3BJ (principally for large-molecule reactions), but on rung 3, B97M-V[12] has a clear advantage over SCAN-D3BJ and indeed outperforms the two most popular *hybrids*, B3LYP-D3BJ and PBE0-D3BJ. On rung 4, the advance of ωB97M-V over revPBE0-D3BJ (the best nonempirical performer) is even more lopsided, as is the advantage on rung 5 of DSD-SCAN-D3BJ over the nonempirical SCAN0-2. [29] The superiority of empirical over "nonempirical" double hybrids[41] like SCAN0-2 was demonstrated in great detail by Goerigk and coworkers.[42]

TABLE 1. Performance of functionals for the GMTKN55 benchmark and its five major subsets, relative to the popular M06-2X functional, plus MAD (kcal/mol) for the MOBH35 transition metal barrier benchmark of Iron and Janes.[33] Blue shading represents better performance, and red shading worse performance, than M06-2X.

Functionals	Rung	Empiricity	WTMAD2	Thermo-chem.	Barrier heights	Large mol. reactions	Conformer Equilibria	Inter-molecular	MOBH35 Ref.[33]
LDA(SPW92)	1	0	4.74	5.19	8.40	2.75	4.15	5.35	7.10
PBEsol-D3BJ	2	0[37]	2.98	3.39	6.45	2.09	2.55	2.52	
PBE-D3BJ	2	0[17]	2.18	2.44	4.99	1.86	1.54	1.79	5.00
rPBE-D3BJ	2	0[43]	2.18	2.40	4.76	1.50	1.28	2.53	
TPSS-D3BJ	3	0[20]	1.91	2.15	4.43	1.88	1.31	1.34	4.70
B97-D3BJ	2	M[19]	1.80	2.12	3.60	2.11	1.26	1.08	5.60
revTPSS-D3BJ	3	0[21]	1.76	2.26	4.22	1.64	1.08	1.18	4.70
revPBE-D3BJ	2	0[18]	1.74	2.07	4.24	1.58	1.26	1.11	5.30
SCAN-D3BJ	3	0[44]	1.66	1.95	4.05	1.21	1.06	1.51	4.00
M06-D3zero	4MX	L[27]	1.62	1.34	1.33	1.35	2.43	1.34	3.90
SCAN0	4MX	0[29]	1.61	1.91	2.14	1.22	1.39	1.74	2.00
CAM-QTP-02-D3BJ[a]	4GR	S[45]	1.52	1.53	1.90	1.18	1.56	1.65	2.90§
CAM-QTP-01-D3BJ[b]	4GR	S[32]	1.42	1.46	1.94	1.12	1.48	1.40	2.40§
CAM-QTP-00-D3BJ[c]	4GR	S[32]	1.35	1.92	2.23	1.18	1.04	1.05	4.10§
PBE0-D3BJ	4GX	0[25]	1.37	1.60	2.50	1.27	1.03	1.17	2.70
B3LYP-D3BJ	4GX	S[23,24]	1.36	1.53	2.37	1.54	0.94	1.08	3.90
M11	4MR	L[30]	1.34	1.12	1.18	1.02	2.07	1.09	2.60
B97M-V	3	M[12]	1.33	1.39	2.08	1.45	1.44	0.74	3.00
SCAN0-D3BJ[d]	4MX	S[29]	1.30	1.94	2.26	1.09	0.86	1.09	2.20§
MN15-D3BJ	4MX	L[10]	1.21	1.16	1.08	0.94	1.74	0.97	2.50
revM11	4MR	L	1.20	1.31	1.58	1.19	1.32	0.83	2.10
PW6B95-D3BJ	4MX	S[26]	1.15	1.22	1.64	1.38	1.07	0.75	2.50
LC-wPBEh-D3BJ[e]	4GR	S[46]	1.15	1.54	1.97	1.15	0.93	0.74	2.50§
revPBE0-D3BJ	4GX	0[25]	1.13	1.59	2.00	0.98	0.93	0.80	2.90§
BHandHLYP	4GX	0[47]	1.16	1.84	1.70	1.17	0.79	0.80	3.50§
CAM-B3LYP-D3BJ	4GR	S[38]	1.11	1.32	1.83	1.17	1.01	0.71	2.40§
revM06	4MX	L	1.11	1.18	1.09	1.07	1.37	0.82	2.10
M06-2X	4MX	L[27]	1 by def.	1 (unity) by definition					2.90
Actual values for M06-2X (kcal/mol)			**4.79**	**0.86**	**0.48**	**1.08**	**1.22**	**1.14**	
SCAN0-2	5	0[29]	0.98	1.14	1.36	1.00	0.77	0.90	3.20
ωB97X-D3BJ	4GR	M[48]	0.98	1.14	1.36	1.00	0.77	0.90	2.30
ωB97X-V	4GR	M[11]	0.83	1.19	1.16	0.99	0.60	0.51	2.00
ωB97M-D3BJ	4MR	M[49]	0.79	0.86	0.85	0.76	0.73	0.79	1.90
ωB97M-V	4MR	M[13]	0.69	0.85	0.94	0.59	0.73	0.50	1.70
B2GP-PLYP-D3BJ	5	S[50]	0.67	0.73	0.86	0.61	0.52	0.74	2.60
DSD-PBE-D3BJ	5	S[4]	0.66	0.77	0.85	0.50	0.60	0.72	2.80
DSD-PBEP86-D3BJ	5	S[4,14]	0.65	0.64	0.93	0.45	0.53	0.85	2.70
noDispSD-SCAN69	5	S[3]	0.62	0.68	1.09	0.62	0.39	0.64	3.10
ωB97X-2(TQ)	5R	M	0.62	0.69	0.76	0.55	0.41	0.81	2.80
revωB97X-2	5R	M	0.59	0.68	0.77	0.54	0.41	0.67	2.70
DSD-BLYP-D4	5	S[4,35]	0.59	0.68	0.79	0.55	0.55	0.52	2.80
revDSD-PBEB95-D4	5	S[3]	0.56	0.74	0.64	0.41	0.64	0.46	2.00
DSD-PBEP86-D4	5	S[4,35]	0.55	0.63	0.76	0.59	0.45	0.49	2.40
DSD-PBEP86-NL	6	S[4,48]	0.55	0.68	0.82	0.53	0.44	0.49	2.60
DSD-PBE-D4	5	S[4,35]	0.55	0.71	0.80	0.52	0.43	0.48	2.40§
DSD-SCAN-D4	5	S[3]	0.55	0.70	0.82	0.58	0.37	0.49	2.00
revDSD-BLYP-D4	5	S[3]	0.54	0.66	0.71	0.53	0.39	0.55	2.10
revDSD-PBEP86-D3BJ	5	S[3]	0.51	0.62	0.64	0.51	0.37	0.50	2.10
revDSD-PBE-D4	5	S[3]	0.51	0.75	0.73	0.49	0.35	0.43	2.10
revDSD-PBEP86-NL	5	S[3]	0.51	0.64	0.62	0.51	0.38	0.50	[1.90]
revDOD-PBEP86-D4	5	S[3]	0.49	0.69	0.62	0.55	0.33	0.41	1.80
revDSD-PBEP86-D4	5	S[3]	0.49	0.65	0.65	0.53	0.33	0.42	1.90
ωB97M(2)	5	M[2]	0.46	0.52	0.54	0.39	0.47	0.43	2.40

Empiricity: 0=nonempirical, S=small (≤6 empirical parameters), M=medium (about a dozen parameters), L=large (several dozen parameters)

Rung 4 subsets: G=GGA, M=mGGA, X=global hybrid, R=range-separated hybrid

(a) a_1=0.270; a_2=7.338; s_6=1; s_8=1.037 (this work); (b) a_1=0.270; a_2=7.040; s_6=1; s_8=1.230 (this work); (c) a_1=0.377; a_2=6.186; s_6=1; s_8=2.415 (this work); (d) a_1=0; a_2=7.9042; s_6=1; s_8=0;[3] (e) a_1=0.426; a_2=4.982; s_6=1; s_8=1.752 (this work)

§ M. A. Iron, personal communication (supplemental to Ref.[33])

At first sight, the DSD double hybrids offer only ωB97M-V like performance. However, some of that is due to deficiencies of the D3BJ dispersion model: when substituting the newer D4 model or the VV10 nonlocal dispersion functional (NL) as a “drop-in replacement”, statistics improve considerably. Indeed, when the functional is

reoptimized together with D4 over the whole GMTKN55 dataset, we are able to lower WTMAD2 for this revDSD-PBEP86-D4 functional to a value statistically equivalent to the "best in class" ωB97M(2). What's more, revDSD-PBEP86-D4 contains just four true fitting parameters, plus three additional parameters that can be fixed at reasonable values over a broad range — about one-third or one-half the parameters in ωB97M(2), depending on whether includes the three "semi-arbitrary" ones in the count.

Let us briefly turn to the major subsets. Barrier heights are the most demanding, with most functionals above M06-2X in the table running 2-5 times worse: the three main exceptions, M11, M06-D3, and MN15-D3BJ all show severely degraded performance for conformers (which are driven primarily by intramolecular interactions). If one wishes to exceed the already good performance of M06-2X for barriers *and* for thermochemistry, one needs to resort to either ωB97M-{V,D3BJ} or to a double hybrid, the latter with improved performance for other properties in the bargain.

(Speaking of subsets, we note that ωB97M-D3BJ is noticeably inferior to wB97M-V for noncovalent interactions as well, as is ωB97X-D3BJ relative to ωB97X-V. On the other hand, barrier heights and general thermochemistry are not impacted thus, and hence ωB97X-D3BJ and ωB97M-D3BJ become attractive for mechanistic exploration, as analytical 1st and 2nd derivatives are readily available.)

If one wishes to eliminate the dispersion correction entirely, the best option appears to be the noDispSD-SCAN double hybrid.[3] While somewhat inferior in performance to the revDSD-PBEP86 variants, it still represents a significant improvement over ωB97M-V, and moreover entails just three parameters (namely, $c_{C,DFT}$, c_{2ab}, and c_{2ss}).

How do these observations for the main group square with performance for transition metal systems? The final column of Table 1 shows MSDs for the MOBH35 (metal-organic barrier heights) of Iron and Janes.[33] One can see there that what holds true for main group does not necessarily hold true for transition metals: for instance, PBE0-D3BJ is clearly superior to B3LYP-D3BJ for transition metal reactions, even though the two functionals are comparable in quality for the main group. SCAN0 and SCAN0-D3BJ, despite unremarkable performance for main-group problems, are among the best performers for MOBH35. The three QTP range-separated hybrids CAM-QTP0*x*-D3BJ (*x*=0,1,2) perform comparably for main-group elements, but QTP01 is markedly superior for transition metals, and indeed the original CAM-B3LYP matches QTP01 for transition metals while outperforming it for GMTKN55. What CAM-QTP01 and CAM-B3LYP have in common with each other and with wB97X-V and wB97M-V are a relatively modest percentages of short-range HF exchange (23, 19, 17, and.15%, respectively), where CAM-QTP00 has 54% and CAM-QTP02 28%. We note that the Becke half-and-half hybrid (which has 50% over the whole distance range) likewise does not perform well for MOBH35 —and neither does B3LYP, which has 20% across the distance range (and hence does not benefit from reduced self-interaction error like the RSHes do). Double hybrids do not necessarily offer advantages for transition metal systems: In fact, the main group "top scorer" ωB97M(2) turns out to be inferior to ωB97M-V for MOBH35. (We note in passing that BH&HLYP actually has a lower WTMAD2 than B3LYP, owing to improved performance for barriers at the expense of small-molecule thermochemistry: handling both well in a global hybrid requires both elevated HF exchange and a meta-GGA, as was demonstrated first with the BMK functional,[51] and later applied to good effect in M06, M06-2X, and other Minnesota functionals. We also note in passing that revM06 represents a substantial improvement over the original M06 for both GMTKN55 and MOBH35.)

While our original DSD double hybrids, fitted to a smallish training set, leave something to be desired for MOBH35, the revised fits[3] to GMTKN55 like revDSD-PBEP86-D4 are comparable to the best performers, despite no transition metal systems at all being present in GMTKN55. This implies that refitting to the much larger and more diverse main-group dataset helped up capture broader molecular physics, rather than add to the plethora of functionals good for specific properties of specific system.

Results for the revDOD-PBEP86-D4 functional, which eliminates the same-spin GLPT2 term, are essentially indistinguishable for main-group systems and even slightly better for MOBH35. This is quite useful, since spin-opposite MP2 viz GLPT2 can be performed using reduced-scaling $O(N^4)$[52–54] or even $O(N^3)$ algorithms.[55]

A summary of our main conclusions has been given in the abstract. If we had to single out just two take-home messages, however, it would be that: (a) ωB97M-V is hard to beat as a "workhorse functional"; (b) for any further improvement beyond that, mildly empirical double hybrids such as revDSD-PBEP86-D4 look most promising.

ACKNOWLEDGMENTS

This research was supported by the Israel Science Foundation (grant 1358/15), the Minerva Foundation, and the Helen and Martin Kimmel Center for Molecular Design (Weizmann Institute of Science). We thank Nitai Sylvetsky for critical reading of the manuscript and Dr. Mark Iron for helpful discussions and some additional data not present in the preprint version of Ref.[33]

REFERENCES

1 L. Goerigk, A. Hansen, C. Bauer, S. Ehrlich, A. Najibi, and S. Grimme, Phys. Chem. Chem. Phys. **19**, 32184 (2017).
2 N. Mardirossian and M. Head-Gordon, J. Chem. Phys. **148**, 241736 (2018).
3 G. Santra, N. Sylvetsky, and J.M.L. Martin, J. Phys. Chem. A **123**, ASAP (2019). http://doi.org/10.1021/acs.jpca.9b03157
4 S. Kozuch and J.M.L. Martin, J. Comput. Chem. **34**, 2327 (2013).
5 J.P. Perdew and K. Schmidt, AIP Conf. Proc. **577**, 1 (2001).
6 S. Kümmel and L. Kronik, Rev. Mod. Phys. **80**, 3 (2008).
7 S. Grimme, J. Chem. Phys. **124**, 034108 (2006).
8 A. Görling and M. Levy, Phys. Rev. A **50**, 196 (1994).
9 Y. Zhao and D.G. Truhlar, Acc. Chem. Res. **41**, 157 (2008).
10 H.S. Yu, X. He, S.L. Li, and D.G. Truhlar, Chem. Sci. **7**, 5032 (2016).
11 N. Mardirossian and M. Head-Gordon, Phys. Chem. Chem. Phys. **16**, 9904 (2014).
12 N. Mardirossian and M. Head-Gordon, J. Chem. Phys. **142**, 074111 (2015).
13 N. Mardirossian and M. Head-Gordon, J. Chem. Phys. **144**, 214110 (2016).
14 S. Kozuch and J.M.L. Martin, Phys. Chem. Chem. Phys. **13**, 20104 (2011).
15 Y. Shao, Z. Gan, E. Epifanovsky, A.T.B. Gilbert, P.M.W. Gill, M. Head-Gordon, *et al.* Mol. Phys. **113**, 184 (2015).
16 P.J. Huber and E.M. Ronchetti, *Robust Statistics* (John Wiley & Sons, Inc., Hoboken, NJ, USA, 2009).
17 J.P. Perdew, K. Burke, and M. Ernzerhof, Phys. Rev. Lett. **77**, 3865 (1996).
18 Y. Zhang and W. Yang, Phys. Rev. Lett. **80**, 890 (1998).
19 S. Grimme, J. Antony, S. Ehrlich, and H. Krieg, J. Chem. Phys. **132**, 154104 (2010).
20 J. Tao, J. Perdew, V. Staroverov, and G. Scuseria, Phys. Rev. Lett. **91**, 146401 (2003).
21 J. Perdew, A. Ruzsinszky, G. Csonka, L. Constantin, and J. Sun, Phys. Rev. Lett. **103**, (2009).
22 J. Sun, A. Ruzsinszky, and J.P. Perdew, Phys. Rev. Lett. **115**, 036402 (2015).
23 A.D. Becke, J. Chem. Phys. **98**, 5648 (1993).
24 P.J. Stephens, F.J. Devlin, C.F. Chabalowski, and M.J. Frisch, J. Phys. Chem. **98**, 11623 (1994).
25 C. Adamo and V. Barone, J. Chem. Phys. **110**, 6158 (1999).
26 Y. Zhao and D.G. Truhlar, J. Phys. Chem. A **109**, 5656 (2005).
27 Y. Zhao and D.G. Truhlar, Theor. Chem. Acc. **120**, 215 (2008).
28 Y. Wang, P. Verma, X. Jin, D.G. Truhlar, and X. He, Proc. Natl. Acad. Sci. **115**, 10257 (2018).
29 K. Hui and J.-D. Chai, J. Chem. Phys. **144**, 044114 (2016).
30 R. Peverati and D.G. Truhlar, J. Phys. Chem. Lett. **2**, 2810 (2011).
31 P. Verma, Y. Wang, S. Ghosh, X. He, and D.G. Truhlar, J. Phys. Chem. A **123**, 2966 (2019).
32 Y. Jin and R.J. Bartlett, J. Chem. Phys. **145**, 034107 (2016).
33 M.A. Iron and T. Janes, J. Phys. Chem. A **123**, 3761 (2019).
34 S. Grimme, S. Ehrlich, and L. Goerigk, J. Comput. Chem. **32**, 1456 (2011).
35 E. Caldeweyher, S. Ehlert, A. Hansen, H. Neugebauer, S. Spicher, C. Bannwarth, and S. Grimme, J. Chem. Phys. **150**, 154122 (2019).
36 M.J.D. Powell, *The BOBYQA Algorithm for Bound Constrained Optimization without Derivatives (DAMPT Report 2009/NA06)* (Department of Applied Mathematics and Theoretical Physics, University of Cambridge, UK, 2009).
37 J.P. Perdew, A. Ruzsinszky, G.I. Csonka, O.A. Vydrov, G.E. Scuseria, L.A. Constantin, X. Zhou, and K. Burke, Phys. Rev. Lett. **100**, 136406 (2008).
38 T. Yanai, D.P. Tew, and N.C. Handy, Chem. Phys. Lett. **393**, 51 (2004).
39 R. Baer, E. Livshits, and U. Salzner, Annu. Rev. Phys. Chem. **61**, 85 (2010).
40 L. Kronik, T. Stein, S. Refaely-Abramson, and R. Baer, J. Chem. Theory Comput. **8**, 1515 (2012).
41 E. Brémond, I. Ciofini, J.C. Sancho-García, and C. Adamo, Acc. Chem. Res. **49**, 1503 (2016).
42 N. Mehta, M. Casanova-Páez, and L. Goerigk, Phys. Chem. Chem. Phys. **20**, 23175 (2018).
43 B. Hammer, L.B. Hansen, and J.K. Nørskov, Phys. Rev. B **59**, 7413 (1999).
44 J.G. Brandenburg, J.E. Bates, J. Sun, and J.P. Perdew, Phys. Rev. B - Condens. Matter Mater. Phys. **94**, 17 (2016).
45 R.L.A. Haiduke and R.J. Bartlett, J. Chem. Phys. **148**, 184106 (2018).
46 M.A. Rohrdanz, K.M. Martins, and J.M. Herbert, J. Chem. Phys. **130**, 054112 (2009).
47 A.D. Becke, J. Chem. Phys. **98**, 1372 (1993).
48 A. Najibi and L. Goerigk, J. Chem. Theory Comput. **14**, 5725 (2018).
49 N. Mardirossian and M. Head-Gordon, J. Chem. Phys. **145**, 186101 (2016).
50 A. Karton, A. Tarnopolsky, J.-F. Lamère, G.C. Schatz, and J.M.L. Martin, J. Phys. Chem. A **112**, 12868 (2008).
51 A.D. Boese and J.M.L. Martin, J. Chem. Phys. **121**, 3405 (2004).
52 J. Almlöf, Chem. Phys. Lett. **181**, 319 (1991).
53 M. Häser, Theor. Chim. Acta **87**, 147 (1993).
54 M. Häser and J. Almlöf, J. Chem. Phys. **96**, 489 (1992).
55 C. Song and T.J. Martínez, J. Chem. Phys. **144**, 174111 (2016).

Coupled Cluster Benchmark of New Density Functionals and of Domain Pair Natural Orbital Methods: Mechanisms of Hydroarylation and Oxidative Coupling Catalyzed by Ru(II) Chloride Carbonyls

Irena Efremenko[1] and Jan M.L. Martin[1, a)]

[1] *Department of Organic Chemistry, Weizmann Institute of Science, 76100 Reḥovot, Israel*

[a)]Corresponding author: gershom@weizmann.ac.il

Abstract. In the present work we tested the performance of several new functionals for studying the mechanisms of concurrent reaction of hydroarylation and oxidative coupling catalyzed by Ru(II) chloride carbonyls. We find that DLPNO-CCSD(T) is an acceptable substitute for full canonical CCSD(T) calculations; that the recent ωB97X-V and ωB97M-V functionals exhibit superior performance to commonly used DFT functionals; and that the revised DSD-PBEP86 double hybrid represents an improvement over the original, even though transition metals were not involved in its parametrization.

INTRODUCTION

Synthetic methods allowing one-step C-C bond formation through homogenous-catalyst-mediated transformation of C-H bonds have become increasingly important in both industry and academia.[1,2] Potential routes for selective C-H bond activation and subsequent C-C bond formation in alkenes and aromatic compounds include hydroarylation by addition of aromatic C–H bonds across an unsaturated C=C bond, or an oxidative coupling that preserves the double bond. The latter reaction, while a highly desirable industrial goal, is challenging from the synthetic point of view. Pioneering examples of Ru-catalyzed coupling of aromatic carbon-hydrogen bonds with olefins were reported two decades ago.[3,4] Since then (for a review, see Ref. 2), an increasing number of examples catalyzed by Rh, Ru and Pd have been published, but the mechanistic aspects of the reactions have only been addressed by experimental methods.

Motivated by the experimental results of Milstein and coworkers,[4] over a decade ago we started to explore the mechanisms of the concurrent reactions of oxidative coupling and hydroarylation of methyl acrylate (MA) catalyzed by Ru carbonyl complexes (Scheme 1) using hybrid and double hybrid DFT families. These calculations showed that either proton elimination by chloride ion, or hydrogen transfer to coordinated olefin, can serve as the initial step of aromatic C-H bond activation, while oxidative addition mechanism could be excluded. Proton elimination proceeds via transition state **TS1** and initiates oxidative coupling with olefin (**TS2**) according to Scheme 2a. Next, interaction of Ru hydride intermediate **Int3** with MA and HCl regenerates the initial $RuCl_2$ carbonyl (**TS4a**). Alternatively, the catalytic cycle could be closed by interaction of **Int3** with MA and benzene, yielding **Int1** (**TS4b**). Hydrogen transfer to MA (**TS1a** and **TS1b**) causes coexistence of phenyl and one of the two isomeric alkyl ligands in

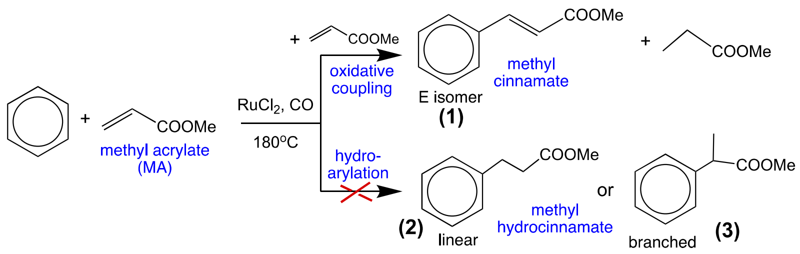

Scheme 1. *Possible interactions between MA and benzene in presence of Ru(II) chloride carbonyl complexes in benzene solution: oxidative coupling (observed) and hydroarylation (not observed).*

the Ru coordination sphere (**Int4** and **Int5**). This mainly leads to the hydroarylation products via **TS3** and **TS3a** (Scheme 2,b), but coordination of the second olefin molecule followed by oxidative coupling is also possible.

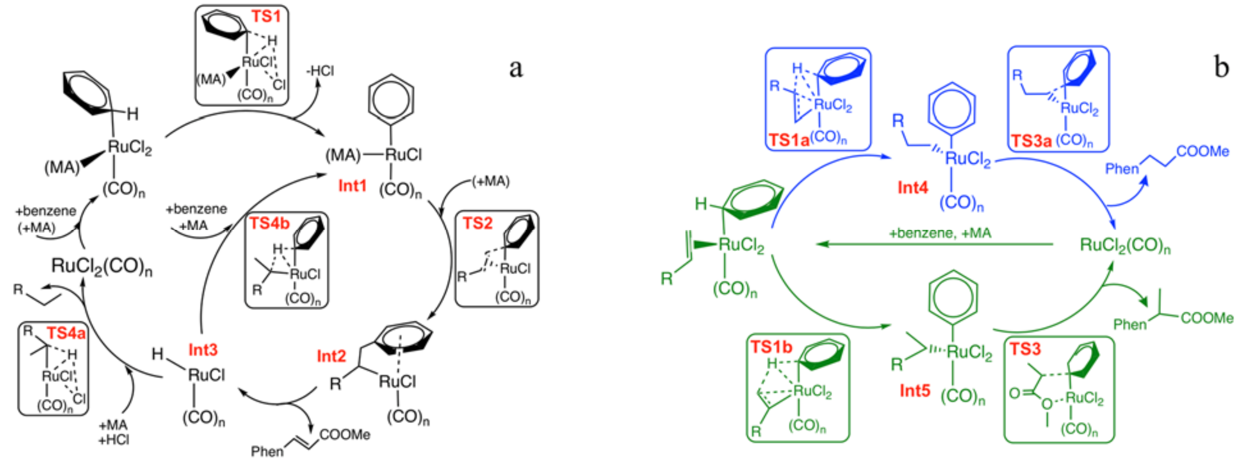

Scheme 2. *Mechanisms of MA interactions with benzene in presence of Ru(II) chloride carbonyl complexes: oxidative coupling (a) and hydroarylation (b).*

We found that the activation barriers, the relative energies of the key intermediates, and the overall direction of the catalytic reaction strongly depend on the composition of the Ru coordination sphere. Ru complexes that could form in the reaction mixture, and serve as initial species of catalytic cycles ,are shown in Scheme 3. In all the complexes, chloride anions are strongly bound to the metal atom; the only exception is $RuCl_2(CO)_4$(benzene) (rightmost complex in the 2nd row of Scheme 3) showing CO insertion into one of the Ru-Cl bonds. Moreover, the energetic results, particularly calculated activation barriers, differ between computational approaches and were hard to reconcile with experimental observations.

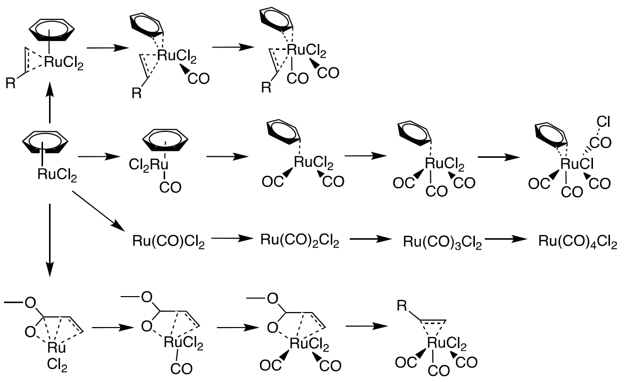

Scheme 3. *Calculated $RuCl_2$ complexes with benzene, CO and MA. Arrows indicate that complex [$RuCl_2$(benzene)] is used as a reference.*

Therefore, for this specific case, we will attempt to obtain rigorous first-principles results by means of coupled cluster theory near the complete basis set limit, and use these results to assess the performance of more affordable computational methods. We believe our results have broader relevance for modeling mechanisms of catalytic reactions mediated by transition metal complexes.

The CCSD(T) method[5] is considered the "gold standard" of quantum chemistry. However, the computational cost of canonical CCSD(T) calculations scales as $O(N^7)$ and becomes prohibitively high for mechanistic studies of practical transition metal catalysis problems. Recently developed domain pair natural orbital methods, such as DLPNO-CCSD(T) of Neese and coworkers[6] and PNO-LCCSD(T) of Werner and coworkers,[7] scale almost linearly with system size (at least for closed-shell cases) and, in the main group, provide similar accuracy to the corresponding canonical calculation. Recently, benchmark studies of the performance of density functionals for transition metal problems, using DLPNO-CCSD(T) for calibration, have started appearing for reaction energies[8] and barrier heights.[9] Since the Ru complexes shown in Schemes 2 and 3 are still barely tractable by canonical methods, this enables us to assess the "domain error" for real-size transition metal complexes. In this paper, we assess both DFT and PNO methods against canonical CCSD(T) for the hydroarylation and oxidative coupling of benzene and methyl acrylate (MA) catalyzed by $RuCl_2$-carbonyl complexes, as a representative example for the complex mechanisms of homogeneous catalytic reactions.

Having in mind specific computational problems usually addressed in such mechanistic studies, the calculations were divided into four groups: (i) overall reaction energies (Scheme 1) that do not involve transition metals; (ii) relative energies of stable $RuCl_2$ complexes with CO, benzene and MA (Scheme 3) that should reproduce breaking

and formation of the metal-ligand bonds and deep alterations of the coordination sphere and electronic structure of the metal atom; (ii) energies of key intermediates along reaction pathways catalyzed by different Ru complexes (Scheme 2) and (iv) barrier heights along these reaction pathways. It would be natural to calculate relative energies of the carbonyl complexes relative to $RuCl_2$, however, our calculations revealed that it has a triplet ground state, and that the singlet is essentially purely biradical (which is also reflected in the pathological D_1 diagnostic[10] value of 0.435). Discussion of the open-shell calculations are beyond the scope of this preliminary report; therefore, we used $RuCl_2$(benzene) as a reference, as $RuCl_2$ will anyway have no independent existence under the experimental conditions (benzene solvent). At all levels, 1:1 exchange of benzene with CO or MA is energetically unfavorable; all other complexes are exothermic with respect to the reference. The relative energies of key intermediates and transition states along each reaction path were calculated relative to the initial form of the catalyst, $(C_6H_6)(CO)_nRuCl_2$ (n=0-4).

COMPUTATIONAL METHODS

The Weigend-Ahlrichs basis set family[11] def2-TZVP, def2-TZVPP, and def2-QZVPP was used throughout.

Reference geometries were optimized at the PBE0-D3BJ/def2-TZVP level[12,13] using Gaussian 09;[14] identities of transition states were verified by frequency and intrinsic reaction coordinate calculations.

At the final geometries, canonical CCSD(T)/def2-TZVPP single-point energy calculations were performed using MOLPRO 2018,[15] both using default frozen cores and including Ru(4s,4p) subvalence orbitals (which *are* correlated by default in ORCA. We found in this work that the mean absolute effects of Ru(4s,4p) subvalence correlation on carbonyl ligand energies and transition states are both a nontrivial 1.0 kcal/mol.) DLPNO-CCSD(T)[16] and the version with improved iterative triples, DLPNO-CCSD(T1),[17] were calculated with the def-TZVPP basis set using ORCA,[18] likewise DLPNO-CCSD(T)/def2-QZVPP calculations were done for basis set extrapolation using the simple L^{-3} formula.[19] TightPNO cutoffs[20] were used to reduce domain discretization error; we found in the present work that DefaultPNO causes errors up to 3.5 kcal/mol in energy differences, and hence do not recommend its use.

In addition, single-point DFT calculations with a number of DFT functionals were carried out using ORCA. Aside from PBE0 already mentioned, these include: (a) the Berkeley "combinatorially optimized"[21] B97M-V, ωB97X-V and ωB97M-V; (b) the M06 family:[22] M06-L, M06 and M06-2X; (c) TPSS[23] and two different hybrids thereof, namely, TPSSh and TPSS0 (10% and 25% HF exchange, respectively); (d) both the original double-hybrid DSD-PBEP86-D3BJ[24] and its reparametrized version revDSD-PBEP86-D4;[25] in the latter, D3BJ also replaced with the very recently published next-generation D4 model.[26] As basis set convergence of double hybrids tends to be dominated by the MP2-like term, we carried out def2-TZVPP and def2-QZVPP calculations and applied L^{-3} basis set extrapolation;[27] for the remaining DFT functionals we applied def2-TZVPP except for ωB97, which were accurate enough that we also tried def2-QZVPP. (Changes are on the order of 1 kcal/mol.) GRID6 was used in all DFT calculations.

In all Orca calculations, the RIJCOSX approximation[28] was employed, as well as the RI-MP2 approximation[29] for the double hybrids, in conjunction with the respective appropriate auxiliary basis sets[30,31] for the def2 family.

RESULTS AND DISCUSSION

MAD (mean absolute deviation) and RMSD (root mean square deviation) error statistics with respect to our best CCSD(T) basis set limit estimates are shown in Figure 1 for the four types of energy differences. As expected, the smallest deviations were found for the overall reaction energies, which involve only main group elements. The hybrid functionals of the M06 family (MAD=0.68 and 0.57 kcal/mol for M06 and M06-2X, respectively) and double hybrid revDSD-PBEP86 functionals (MAD=0.64) show the best performance in this group. However, overall for the four criteria, the best results were obtained using ωB97M-V and ωB97X-V range-separated hybrids as well as by the revDSD-PBEP86 double hybrid, with accuracy between DLPNO-CCSD and DLPNO-CCSD(T). On the 3rd rung (meta-GGA) of the Jacob's Ladder, B97M-V performed best for reaction energies and carbonyl complex stabilities; however, M06-L showed similar performance, and TPSS outperformed them for barrier heights (MAD 3.69 vs. 4.54 for M06-L and 5.47 for B97M-V). The revDSD-PBEP86 functional outperforms the original DSD-PBEP86 for all four groups of calculations, whereas DSD-SCAN-D4 improved on DSD-PBEP86-D3BJ only for the carbonyl complexes. The DLNPO-CCSD(T) approach shows very close agreement (MAD=0.35 kcal/mol) with canonical CCSD(T) for the reaction energies, while for other groups there is a bit more daylight between them (MAD=1.04 for carbonyls, 1.56 for intermediates, and 1.58 kcal/mol for TSes). Using the DLNPO-CCSD(T1) approach with improved perturbative triples decreases these statistics to 0.60, 0.80, and 1.02 kcal/mol, respectively. The RMSD/MAD ratios are close to the theoretical value[32] (for a normal distribution) of $\sqrt{(\pi/2)}\approx 1.2533$, for carbonyls and intermediates but

much larger for TSes, indicating an outlier (RMSD=0.80, 0.86, 2.05 kcal/mol): we note that TS2-CO2 is essentially biradical (and has D_1>0.4). If we exclude it, MAD and RMSD drop to quite pleasing values of 0.63 and 0.73 kcal/mol, respectively.

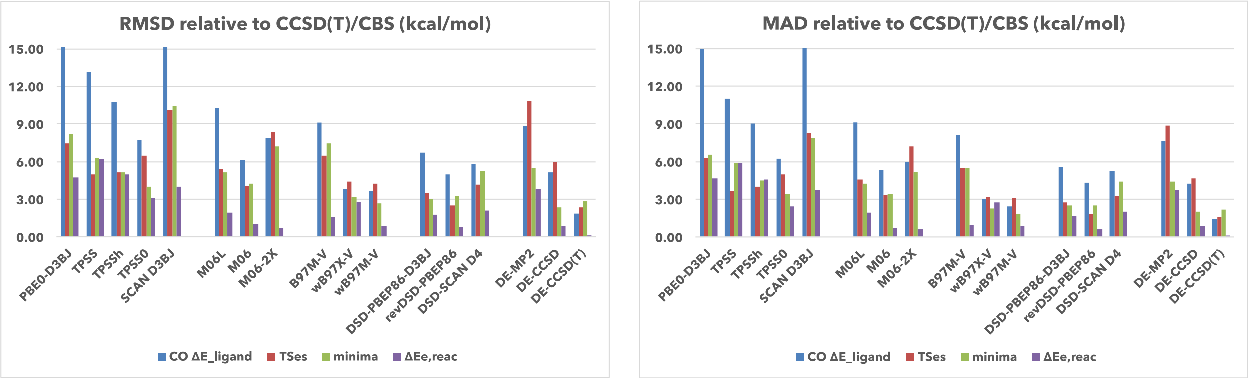

FIGURE 1. RMSD and MAD relative to CCSD(T)/CBS for the four types of energetics considered.

At all levels except for DLPNO-MP2, the highest RMSD and MAD values were found for the first reaction, i.e. dissociation of benzene and association of CO and MA ligands. Most density functionals tend to overbind the ligands; detailed analysis shows that for one group of functionals (PBE0-D3BJ, SCAN-D3BJ, TPSS, M06L and DSD-PBEP86 family, Fig. 2a) the error becomes greater with increasing number of CO ligands; the other group (M06, M06-2X, TPSS0, TPSSh, and B97, Fig. 2b) exhibits a less pronounced opposite trend, especially in the presence of coordinated benzene.

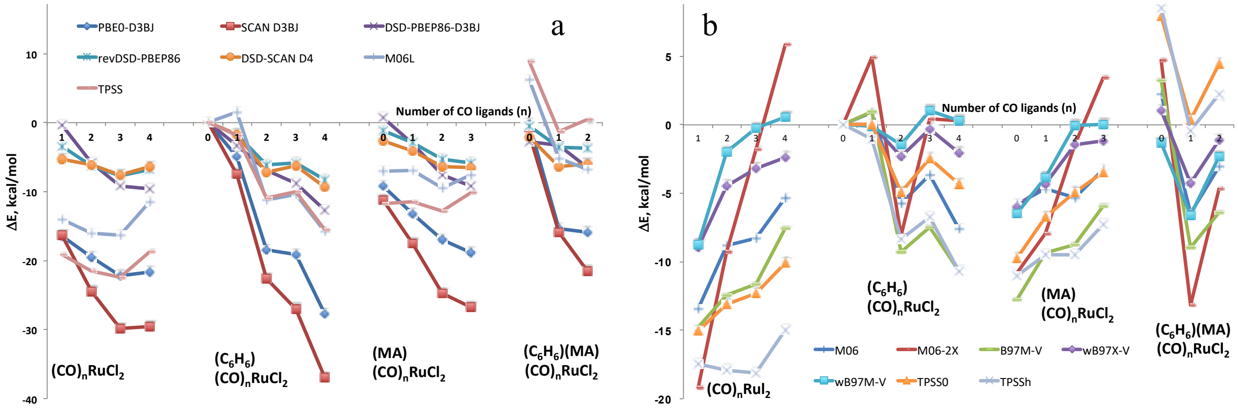

FIGURE 2. Energy deviation relative to CCSD(T)/CBS in different $RuCl_2$ $(CO)_n$ complexes as a function of n.

Our findings are consistent (see also our companion paper in the present volume) with the findings of Najibi and Goerigk[33] and ourselves[25] for the very large GMTKN55 main-group benchmark[34] and of Iron and Janes[9] for the MOBH35 transition metal reaction benchmark: Notably, that the range-separated hybrids ωB97X-V and ωB97M-V acquit themselves particularly well, that revDSD represents an improvement over the original DSD not just for the main group but also transition metals, and that unlike for the main group where empirical double hybrids are clearly superior, they offer no clear advantage over ωB97M-V for transition metal reactions. Unlike Iron and Janes, however, who found the new DSD-SCAN double hybrid[25] to be among the best performers for MOBH35, we find it to be inferior to revDSD-PBEP86 and the ωB97*n*-V family for the present problem (Figure 1).

ACKNOWLEDGMENTS

This research was supported by the Israel Science Foundation (grant 1358/15), the Minerva Foundation, and the Helen and Martin Kimmel Center for Molecular Design (Weizmann Institute of Science).

REFERENCES

1 S. Murai, F. Kakiuchi, S. Sekine, Y. Tanaka, A. Kamatani, M. Sonoda, and N. Chatani, *Nature* **366**, 529 (1993); J. Kischel, I. Jovel, K. Mertins, A. Zapf, and M. Beller, *Org. Lett.*, **8**, 19 (2006); H. A. Zhong, J. A. Labinger, and J. E. Bercaw, *J. Am. Chem. Soc.* **2002**, *124*, 1378; C. Jia, D. Piao, J. Oyamada, W. Lu, T. Kitamura, and Y. Fujiwara, *Science* **287**, 1992 (2000).

2 (a) *From C-H to C-C Bonds: Cross-Dehydrogenative-Coupling*, Chao-Jun Li, ed. Royal Society of Chemistry, 2014. (b) *Catalytic Arylation Methods: From the Academic Lab to Industrial Processes***,** A. J. Burke, C. S. Marques, Ed.. Wiley, 2015.

3 F. Kakiuchi, T. Sato, M. Yamauchi, N. Chatani and S. Murai, *Chem. Lett.* **28**, 19 (1999).

4 H. Weissman, X. Song, and D. Milstein, *J. Am. Chem. Soc.* **123**, 337 (2001). D. Milstein, D. *Pure Appl. Chem.* **75**, 445 (2003).

5 I. Shavitt and R.J. Bartlett, *Many – Body Methods in Chemistry and Physics* (Cambridge University Press, Cambridge, 2009).

6 C. Riplinger, B. Sandhoefer, A. Hansen, and F. Neese, *J. Chem. Phys.* **139**, 134101 (2013).

7 Q. Ma and H. Werner, *WIRes Comput. Mol. Sci*. **8**, e1371 (2018) and references therein.

8 S. Dohm, A. Hansen, M. Steinmetz, S. Grimme, and M.P. Checinski, *J. Chem. Theory Comput.* **14**, 2596 (2018).

9 M. A. Iron, and T. Janes. *J. Phys. Chem. A* **123**, 3761-3781 (2019).

10 C. L. Janssen and I. M. B. Nielsen, *Chem. Phys. Lett.* **290,** 423–430 (1998).

11 F. Weigend and R. Ahlrichs, *Phys. Chem. Chem. Phys.* **7**, 3297 (2005)

12 C. Adamo and V.Barone, *J. Chem. Phys.* **110**, 6158 (1999) and references therein.

13 S. Grimme, S. Ehrlich, and L. Goerigk, L. *J. Comput. Chem.* **32**, 1456 (2011) and references therein

14 M. J.Frisch, *et al.*, Gaussian09, Revision C.01wis4; Gaussian, Inc.: Wallingford, CT, **2009**. Website: http://www.gaussian.com

15 H.-J. Werner *et al.*, MOLPRO 2018.2, a package of ab initio programs. Cardiff, UK, 2018. Website: http://www.molpro.net.

16 M Saitow, U Becker, C Riplinger, E Valeev, F Neese, *J. Chem. Phys.* **146** 164105 (2017).

17 Y. Guo, C. Riplinger, U. Becker, D.G. Liakos, Y. Minenkov, L. Cavallo, and F. Neese, *J. Chem. Phys.* **148**, (2018).

18 F. Neese, F. *WIREs Comput. Mol. Sci.* **8**, e1327 (2018) and references therein.

19 A. Halkier, T. Helgaker, P. Jørgensen, W. Klopper, H. Koch, J. Olsen, and A.K. Wilson, *Chem. Phys. Lett.* **286**, 243 (1998).

20 D.G. Liakos, M. Sparta, M.K. Kesharwani, J.M.L. Martin, and F. Neese, *J. Chem. Theory Comput.* **11**, 1525 (2015).

21 N. Mardirossian and M. Head-Gordon, *PCCP* **16**, 9904 (2014); *J. Chem. Phys.* **142***,* 074111(2015); *ibid.* **144***,* 214110 (2016).

22 Y. Zhao and D. G. Truhlar, *J. Chem. Phys.* **2006**, *125*, 194101; idem, *Theor. Chem. Acc.* **2008**, *120*, 215-241.

23 J. Tao, J. Perdew, V. Staroverov, and G. Scuseria, *Phys. Rev. Lett.* **91**, 146401 (2003).

24 S. Kozuch and J.M.L. Martin, *PCCP* **13**, 20104 (2011); *J. Comput. Chem*. **34**, 2327 (2013).

25 G. Santra, N. Sylvetsky, and J. M. L. Martin, *J. Phys. Chem. A*, **123**, ASAP (2019) (Leo Radom festschrift). DOI: 10.1021/acs.jpca.9b03157

26 E. Caldeweyher, S.Ehlert, A.Hansen, H.Neugebauer, S.Spicher, C.Bannwarth, S. Grimme, *J. Chem. Phys.* **150**, 154122 (2019).

27 A. Halkier, T. Helgaker, P. Jørgensen, W. Klopper, H. Koch, J. Olsen, and A.K. Wilson, *Chem. Phys. Lett.* **286**, 243 (1998).

28 S. Kossmann and F. Neese, *J. Chem. Theory Comput.* **6**, 2325–2338 (2010) and references therein

29 For a review, see: D. E. Bernholdt, *Parallel Computing* **26**, 945 (2000)

30 F. Weigend, *PCCP* **8**, 1057 (2006); F. Weigend, *J. Comput. Chem.* **29**, 167 (2008).

31 C. Hättig, *PCCP* **7**, 59 (2005); A. Hellweg, C. Hättig, S. Höfener, and W. Klopper, *Theor. Chem. Acc.* **117**, 587 (2007).

32 R. C. Geary, *Biometrika* **27**, 310-332 (1935)

33 A. Najibi and L. Goerigk, *J. Chem. Theory Comput.* **14**, 5725 (2018).

34 L. Goerigk, A. Hansen, C. Bauer, S. Ehrlich, A. Najibi, and S. Grimme, *PCCP* **19**, 32184 (2017).

Ultrafast Spectral Dynamics of Fluorescence in EDACs: Numerical Algorithms and Test Simulations

S.V. Feskov

Volgograd State University, Universitetskiy prospect, 100, 400062, Volgograd, Russia

serguei.feskov@volsu.ru

Abstract. Photochemical processes in electron-donor-acceptor complexes (EDACs) involving ultrafast hot charge recombination to the ground electronic state are considered within the extended stochastic model of electron transfer. An expression for the transient fluorescence spectra of the non-equilibrium photochemical system is derived in the resonant approximation. Numerical schemes for simulation of the spectral profiles dynamics are proposed and adapted for use with the Brownian simulation algorithm. Several optimization procedures are suggested, allowing to improve computational efficiency of the proposed schemes. Results of some illustrative simulations are presented.

INTRODUCTION

Electron donor-acceptor complexes are known to be one of the most convenient tools for studying relaxation processes in the reactant molecules, as well as in the surrounding solvent [1, 2, 3, 4, 5]. Excitation of a charge transfer (CT) band in EDAC by a short laser pulse launches a series of ultrafast processes involving formation of a contact ion pair with subsequent intramolecular and solvent relaxation, hot charge recombination to the ground state of the complex and separation of ions to the bulk. These processes generally proceed according to the following scheme

$$[DA] \underset{k_{CR}}{\overset{h\nu}{\Longleftrightarrow}} [D^{+}A^{-}] \overset{\varphi}{\longrightarrow} D^{+} + A^{-}$$

Here D and A are the electron donor and acceptor, $h\nu$ indicates photoexcitation of the CT band, k_{CR} is the rate of intermolecular charge recombination (CR) and φ is the quantum yield of free ions.

Subpicosecond dynamics of fluorescence spectra in EDACs contains important information on ultrafast processes in the DA pair, but this dynamics is often difficult to interpret, because such interpretation implies self-consistent analysis of large amounts of spectroscopic data. Large spectral width of the excitation pulse, used in the time-resolved experiments, complicates the analysis too. The recorded signal in this case traces a variety of processes involving many electronic-vibrational states and occurring simultaneously. One of the possible ways of analysis in this case could be fitting the results of numerical simulation to the experimental data [6, 7, 8].

Intermolecular CT in polar solvents is generally accompanied by excitation of a large amount of vibrational modes, both in the DA-pair and nearby medium. A part of these modes relates to the reorganization of solvent dipoles, while the other is associated with the intramolecular reorganization of the reactants and products. Solvent modes in these reactions are usually low-frequency ($\hbar\Omega \ll k_B T$) and thus classical [9]. The characteristic values of the solvent reorganization energy lie in the range $\lambda = 0.2 \div 0.5$ eV. On the other hand, intramolecular vibrations are often high-frequency ($\hbar\Omega \gg k_B T$), so the corresponding modes are treated as quantum (discreet) coordinates [10]. Typically, ultrafast CT in EDACs is accompanied by excitation of several high-frequency modes with a total reorganization energy $\lambda_v = 0.2 \div 0.6$ eV. The total amount of active vibrational substates can reach 10^4 – 10^6.

We consider here efficient numerical schemes for simulation of the transient fluorescence spectra in EDACs within the extended (multimode) stochastic model of electron transfer. The model takes into account the effective intramolecular high-frequency vibrational mode and a set of low-frequency coordinates, which are associated here with different solvent relaxation modes. Following the Zusman's approach [11], the system evolution along these

(collective) solvent coordinates is treated as a stochastic motion, and the diffusion approximation is used for its description. As a numerical method we adopt here the RABS technique [6, 12], which has demonstrated its efficiency in solving the stochastic model equations. The main factors affecting the spectral dynamics of highly exergonic EDACs are known to be intramolecular vibrational relaxation in reactants and dielectric relaxation of the solvent in vicinity of the ion pair. In this study we obtain exact analytic expressions for fluorescence profiles in the two limiting cases when one of the relaxation channels dominates another. The influence of solvent and intramolecular reorganization energies on the EDAC fluorescence profiles is analyzed.

TRANSIENT SPECTRA: MODEL AND COMPUTATIONAL SCHEME

To describe photochemical reaction in EDAC, we use the standard two-electronic-state model of electron transfer and denote the ground (neutral) and the excited (ionic) states of the complex as $|1\rangle$ and $|2\rangle$. A bath of solvent molecules is described by a set of polarization coordinates $\mathbf{Q} = (Q_1, Q_2, ..., Q_K)$ [11], while intramolecular high-frequency vibrations are represented by the effective quantum mode with the frequency Ω. The free energy surfaces of the electronic-vibrational states of the system in these coordinates are

$$G_1^{(m)}(\mathbf{Q}) = \sum_k \frac{Q_k^2}{4\lambda_k} + m\hbar\Omega + G_1, \quad G_2^{(n)}(\mathbf{Q}) = \sum_k \frac{(Q_k - 2\lambda_k)^2}{4\lambda_k} + n\hbar\Omega + G_2, \tag{1}$$

where λ_k is the kth component of the solvent reorganization energy $\lambda = \sum \lambda_k$, n and m are vibrational quantum numbers, $\Delta G_{\mathrm{CR}} = G_1 - G_2$ is the free energy of charge recombination.

Employing the Golden Rule expression for the rate of the $|2, n\rangle \to |1, m\rangle$ fluorescent transition one obtains

$$K^{m,n}(\omega) = \frac{2\pi |V_{m,n}|^2}{\hbar}\, \delta\left(\Delta G_{21}^{m,n} - \hbar\omega\right), \qquad \Delta G_{21}^{m,n} = G_2^{(n)} - G_1^{(m)},$$

where $V_{m,n}$ is the coupling energy between the two states, $|V_{m,n}|^2 \propto F_{m,n}$. In the absence of spectral broadening, fluorescent transition from the nth vibronic sublevel of the excited state is then characterized by the spectral density

$$S_{\mathrm{fl}}^{(n)}(\omega) = A P_n \sum_m F_{m,n}\, \delta\left(\Delta G_{21}^{m,n} - \hbar\omega\right),$$

where $A = \mathrm{const}$, P_n is the population of the nth vibrational sublevel of the excited state. The entire spectral profile $S_{\mathrm{fl}}(\omega)$ is

$$S_{\mathrm{fl}}(\omega) = \sum_n S_{\mathrm{fl}}^{(n)}(\omega) = A \sum_n P_n \sum_m F_{m,n}\, \delta\left(\Delta G_{21}^{m,n} - \hbar\omega\right).$$

Since photochemical processes in EDACs are described by evolution of the time-dependent probability distribution functions $\rho_n(\mathbf{Q}, t)$ one gets the following result

$$S_{\mathrm{fl}}(\omega, t) = A \sum_n \int \rho_n(\mathbf{Q}, t) \sum_m F_{m,n}\, \delta\left(\Delta G_{21}^{m,n}(\mathbf{Q}) - \hbar\omega\right) d\mathbf{Q}. \tag{2}$$

To calculate the integral in this equation we introduce the collective energy coordinate $Z = \sum_k Q_k$. From Eq. (1) one finds

$$\Delta G_{21}^{m,n}(\mathbf{Q}) = Z_{m,n}^{\dagger} - Z, \quad \text{where } Z_{m,n}^{\dagger} = \lambda + G_2 - G_1 + (m - n)\hbar\Omega,$$

$$S_{\mathrm{fl}}(\omega, t) = A \sum_{n,m} F_{m,n}\, \rho_n\left(Z - Z_{m,n}^{\dagger} + \hbar\omega, t\right). \tag{3}$$

We further adapt this general result for the use with the recrossing-algorithm of the Brownian simulation (RABS) method [12]. We introduce an ensemble of quasi-particles $\left\{\mathbf{Q}^{(i)}\right\}_{i=1}^{M}$ representing evolution of density distribution functions $\rho_n(\mathbf{Q}, t)$ in the configuration space as

$$\rho_n(\mathbf{Q}, t) = \sum_{i=1}^{M} \delta_{n,n_i} \prod_k \delta\left(Q_k - Q_k^{(i)}(t)\right), \tag{4}$$

The $Q_k^{(i)}(t)$ quantity here is the reactive trajectory of the quasi-particle, calculated using RAMB. From Eq. (4) and Eq. (3) one gets the fluorescence spectrum

$$S_{\mathrm{fl}}(\omega,t) = A \sum_{i=1}^{M} \sum_{m} F_{m,n_i}\, \delta\left(Z^{(i)}(t) - Z^{\dagger}_{m,n_i} + \hbar\omega\right). \tag{5}$$

Computational scheme Eq. (5) allows estimating the complexity of the proposed algorithm as $\overline{O}(N \cdot M)$, where N is the number of active vibrational sublevels of the excited state, and M is the number of Brownian quasi-particles. For typical values $N = 10^4$ and $M = 10^6$, this gives an estimation $C = 10^{10}$ for the total number of operations in calculations of each $S_{\mathrm{fl}}(\omega,t)$ profile.

The result Eq. (5) can be easily expanded to the case of homogeneous or inhomogeneous spectral broadening. For example, for the Gaussian broadening due to the finite duration of the probe pulse τ_p one can easily obtain the following computational scheme

$$\widetilde{S}_{\mathrm{fl}}(\omega,t) = A \sum_{i=1}^{M} \sum_{m} F_{m,n_i}\, \exp\left(-\frac{\tau_p^2}{2\hbar^2}\left[Z^{(i)}(t) - Z^{\dagger}_{m,n_i} + \hbar\omega\right]^2\right). \tag{6}$$

We consider now some possibilities of increasing the efficiency of $S(\omega,t)$ calculations taking into account the structure of the expressions (5) and (6). First of all we note, that evolution of the $S_{\mathrm{fl}}(\omega,t)$ and $\widetilde{S}_{\mathrm{fl}}(\omega,t)$ profiles is entirely due to the motion of quasi-particles, i.e. their Brownian trajectories $Z^{(i)}(t)$. Since the structure of the free energy levels in EDAC remains unchanged, only the argument in expressions (5) and (6) depends on time, but not the function itself. This allows us to rewrite Eq. (5) in the form

$$S_{\mathrm{fl}}(\omega,t) = A \sum_{i=1}^{M} I_{n_i}\left(Z^{(i)}(t) + \hbar\omega\right), \qquad \text{where} \quad I_n(Z) = \sum_{m} F_{m,n}\, \exp\left(-\frac{\tau_p^2}{2\hbar^2}[Z - Z^{\dagger}_{m,n}]^2\right). \tag{7}$$

It is important here that the dependencies $I_n(Z)$ can be precalculated only once and stored in RAM as indexed arrays with the possibility of quick fetching for any Z. Calculation of the $S_{\mathrm{fl}}(\omega,t)$ profile in this case is reduced to the calculation of the sum over the ensemble of quasi-particles, Eq. (7). The complexity of the algorithm is now estimated as $\overline{O}(M)$, which requires only 10^6 operations per spectrum in a typical calculation.

TESTING OF THE ALGORITHM. ILLUSTRATIVE SIMULATIONS

In this study the numerical scheme (5) has been implemented within the `QM2L` software package [6] and validated using several test simulations. An agreement with known analytic solutions of model equations in the limiting cases was obtained. The results of one of the simulations are presented in Fig. 1, where the calculated spectral profiles of the EDAC excited state fluorescence are pictured in the (0.5 eV – 3.0 eV) region and in time interval up to 1 ps. The following values of the model parameters are used in simulations: solvent reorganization energy $\lambda = 0.5$ eV, reorganization energy of the intramolecular high-frequency vibrational mode $\lambda_v = 0.45$ eV, vibrational quantum $\Omega = 0.15$ eV, free energy of CR $\Delta G_{\mathrm{CR}} = -1.35$ eV, bath temperature $k_{\mathrm{B}}T = 0.025$ eV, vibrational relaxation time $\tau_v = 0.3$ ps. These parameters correspond to a typical charge transfer complex in a polar solvent, for example, the complex composed of hexamethylbenzene (HMB) as an electron donor and tetracyanoethylene (TCNE) as an acceptor [13]. The number of Brownian particles is $M = 10^6$, which provides satisfactory accuracy of the numerical results. The longitudinal dielectric relaxation time of the solvent τ_{L} in these simulations was set to infinity, which enable us to compare the numerical results with an analytic expression for the $S_{\mathrm{fl}}(\omega,t)$ in the limiting case $\tau_{\mathrm{L}} \gg \tau_{\mathrm{v}}$

$$S_{\mathrm{fl}}^{(\mathrm{vib})}(\omega,t) = A\left[\sum_{m} F_{0,m}\left(1 - e^{-t/\tau_v}\sum_{n=1}^{n_0}\frac{(t/\tau_v)^{n_0-n}}{(n_0-n)!}\right)\frac{1}{\sqrt{2\pi\sigma_q^2}}\exp\left\{-\frac{(Q^{\sharp}_{0,m} - 2\lambda + \hbar\omega)^2}{2\sigma_q^2}\right\} + \right.$$
$$\left. + \sum_{n=1}^{n_0}\sum_{m} F_{n,m} e^{-t/\tau_v}\frac{(t/\tau_v)^{n_0-n}}{(n_0-n)!}\frac{1}{\sqrt{2\pi\sigma_q^2}}\exp\left\{-\frac{(Q^{\sharp}_{n,m} - 2\lambda + \hbar\omega)^2}{2\sigma_q^2}\right\}\right], \tag{8}$$
$$\sigma_q^2 = 2\lambda k_{\mathrm{B}}T, \qquad Q^{\sharp}_{n,m} = \lambda + \Delta G_{\mathrm{CR}} + (m-n)\hbar\Omega.$$

This expression is obtained using the method described in [14]. Comparison between analytic and simulation results shows their correspondence within the accuracy of the numerical method.

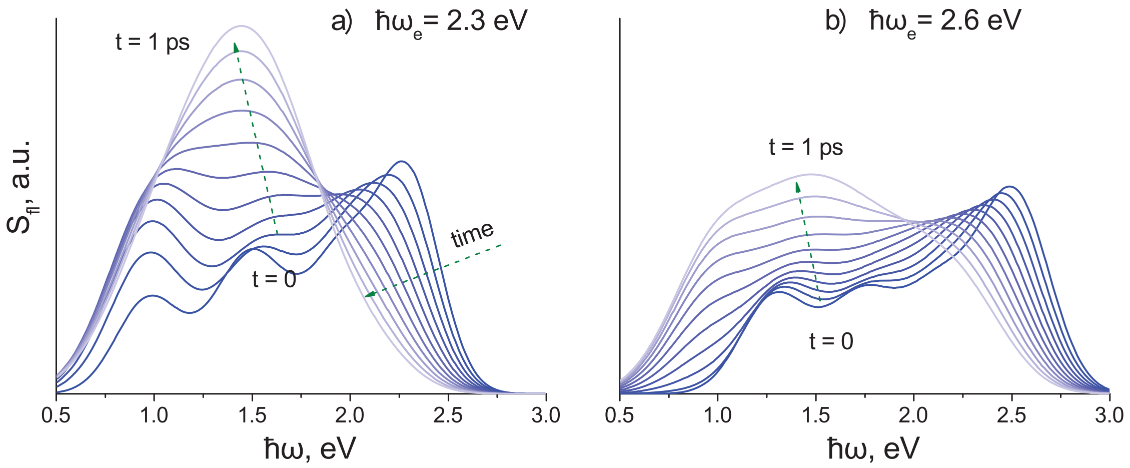

FIGURE 1. Ultrafast spectral dynamics of the EDAC fluorescence in the slow solvent limit ($\tau_L \gg \tau_v$), i.e. due to intramolecular vibrational relaxation in the excited electronic state $[D^+A^-]$. Simulations are performed using the `QM2L` package with $N = 10^6$ Brownian particles. Panels (a) and (b) correspond to different frequencies of the excitation pulse (indicated in the figure). The values of other parameters are given in text.

Test simulations in Fig. 1 do not take into account relaxation of solvent polarization in the vicinity of reactants, but, however, demonstrate the role of intramolecular high-frequency vibrations associated with CT transitions in EDACs. Specifically, in highly exergonic complexes ($-\Delta G_{CR} > \lambda + \lambda_v$), vibrational relaxation of the excited electronic state appears in spectral dynamics of fluorescence as clearly visible red shift (see Fig. 1, panels (a) and (b)). The role of electron-vibrational interactions in these photoprocesses is also revealed by the test simulations. Electron-vibrational interactions manifest themselves as an effective broadening of fluorescence profiles at short timescales. These results are in qualitative agreement with known features of transient fluorescence spectra of the excited electron-donor-acceptor complexes in polar solvents.

ACKNOWLEDGMENTS

The work was supported by the Russian Science Foundation (project 16-13-10122).

REFERENCES

[1] O. Nicolet and E. Vauthey, J. Phys. Chem. A **106**, 5553–5562 (2002).
[2] O. Nicolet, N. Banerji, S. Pagès, and E. Vauthey, J. Phys. Chem. A **109**, 8236–8245 (2005).
[3] A. Samanta, J. Phys. Chem. B **110**, p. 1370413716 (2006).
[4] C.-C. Chiu, C.-C. Hung, C.-L. Chen, and P.-Y. Cheng, J. Phys. Chem. B **117**, 9734–9756 (2013).
[5] C.-C. Chiu, C.-C. Hung, and P.-Y. Cheng, J. Phys. Chem. B **120**, 12390–12403 (2016).
[6] S. V. Feskov, V. N. Ionkin, and A. I. Ivanov, J. Phys. Chem. A **110**, 11919–11925 (2006).
[7] S. V. Feskov and A. I. Burshtein, J. Phys. Chem. A **113**, 13528–13540 (2009).
[8] S. V. Feskov, A. O. Kichigina, and A. I. Ivanov, J. Phys. Chem. A **115**, 1462–1471 (2011).
[9] R. A. Marcus and N. Sutin, Biochim. Biophys. Acta. **811**, 265–322 (1985).
[10] J. Jortner and M. Bixon, J. Chem. Phys. **88**, 167–170 (1988).
[11] L. D. Zusman, Chem. Phys. **119**, 51 – 61 (1988).
[12] S. V. Feskov and A. I. Ivanov, J. Chem. Phys. **148**, p. 104107 (2018).
[13] F. Markel, N. S. Ferris, I. R. Gould, and A. B. Myers, J. Am. Chem. Soc. **114**, 6208–6219 (1992).
[14] S. V. Feskov, Opt. Spectrosc. **123**, 699–704 (2017).

Brownian Simulation Algorithm for the Coherent Optical Excitation of Electron-donor-acceptor Complexes

D.E. Kononov and S.V. Feskov[a)]

Volgograd State University, Universitetskiy prospect, 100, 400062, Volgograd, Russia

[a)]serguei.feskov@volsu.ru

Abstract. A stochastic model of electron-donor-acceptor complex (EDAC) interacting coherently with a short laser pulse within the charge transfer band is considered in the low-field approximation. An analytical expression for the probability of detection the complex in the excited electronic state is obtained within the perturbation theory in the optical coupling parameter. New computational scheme for numerical simulations of coherent optical excitation in EDACs is proposed. This scheme extends the recrossing-algorithm of the Brownian simulation (RABS) method developed earlier for simulations of nonequilibrium electron transfer within the multimode Zusman/Jortner-Bixon model. The proposed algorithm implies calculations of stochastic trajectories of quasiparticles in multidimensional space of solvent coordinates, as well as transitions between different electronic and vibrational states of EDAC. Applicability conditions and efficiency of the algorithm are discussed.

INTRODUCTION

Ultrafast photochemical processes, involving intermolecular electron transfer (ET) in polar solvents, often proceed at short (sub-picosecond) timescales comparable with duration of the pump pulse. Hot charge recombination (CR) in EDACs is one of the well-known reactions of this kind, extensively studied both experimentally [1, 2, 3, 4] and theoretically [5, 6, 7, 8]. Several approaches to numerical simulation of these reactions rely on the "instantaneous pump" approximation, assuming the vibrational modes of the reactants and solvent to be "frozen" in the course of the optical excitation (see, for example, [5, 7]). This approximation however is not always justified, especially if hot CR proceeds with participation of vibrationally excited states of the ionic pair. The rate of this reaction often exceeds the rate of solvent relaxation [2], while a duration of the excitation pulse is larger than the time of CR. This study aims to the development of efficient numerical schemes for ultrafast nonequilibrium photoreactions in EDACs within the RABS method [5, 9]. We propose new algorithm for simulations of coherent optical excitation in these complexes, that extends the applicability of the previous (incoherent) one. The previously suggested computational scheme [10] was based on the well-known kinetic (rate) approximation and described the optically induced electronic transitions as a first-order process. The present scheme employs a more rigorous Hamiltonian description of optical pumping in EDACs and allows one to take into account coherent evolution of the molecular system under the action of the laser pulse. An analytic expression for the probability of a quantum transition to the excited electronic state is obtained within a two-level/weak-coupling model. The algorithm can be extended further and applied to models, involving several classical solvent coordinates and high-frequency quantum vibrational modes. The advantage of the suggested approach is its higher performance with respect to the standard methods based on the numerical solution of the Schrodinger equation.

MODEL AND NUMERICAL METHOD

Charge transfer in EDACs is traditionally described as a quantum transition between the two electronic states corresponding to the neutral ($[DA]$) and charged ($[D^+A^-]$) components of the complex. In weakly coupled systems, CT transitions are of the resonant nature, i.e. proceed only in those nuclear configurations that provide equal energies of the complex + solvent system both in the reactant and product states [11]. Compact description of the CT transitions,

assisted by vibrational excitation of the CT product, is given by the Zusman/Jortner-Bixon model of ET [12, 13]. This model is used here as a basis for description of ultrafast ET in EDACs. Evolution of the particle density profiles in the ground and excited states of the complex is described by the system of coupled equations

$$\frac{\partial \rho_1^{(n)}}{\partial t} = \hat{L}_1 \rho_1^{(n)} - \sum_m 2\pi V_{n,m}^2 \hbar^{-1} \delta(q - q_{n,m}^\dagger) \left(\rho_1^{(n)} - \rho_2^{(m)}\right), \tag{1}$$

$$\frac{\partial \rho_2^{(m)}}{\partial t} = \hat{L}_2 \rho_2^{(m)} - \sum_n 2\pi V_{m,n}^2 \hbar^{-1} \delta(q - q_{n,m}^\dagger) \left(\rho_2^{(m)} - \rho_1^{(n)}\right). \tag{2}$$

In these equations, $\rho_1^{(n)} = \rho_1^{(n)}(q,t)$ and $\rho_2^{(m)} = \rho_2^{(m)}(q,t)$ are the time-dependent distributions of particles in the $|1,n\rangle$ and $|2,m\rangle$ states, respectively, n and m are vibrational quantum numbers, $V_{n,m} = V_{m,n}$ is the coupling energy between the $|1,n\rangle$ and $|2,m\rangle$ states, $q_{n,m}^\dagger$ is the crossing point of the $U_1^{(n)}(q)$ and $U_2^{(m)}(q)$ diabatic free energy surfaces (FESs). The Smoluchowski operators $\hat{L}_k$ in Eqs. (1)-(2) describe relaxation of solvent polarization in vicinity of the complex to the thermodynamic equilibrium

$$\hat{L}_k = D_q \frac{\partial}{\partial q} \exp\left(-\frac{U_k(q)}{k_B T}\right) \frac{\partial}{\partial q} \exp\left(\frac{U_k(q)}{k_B T}\right), \qquad (k = 1, 2). \tag{3}$$

Here $D_q \equiv 2\lambda k_B T/\tau_L$ is the diffusion coefficient, τ_L is the longitudinal dielectric relaxation time of the solvent, λ is the solvent reorganization energy, and T is the bath temperature. It should be noted here, that in non-Debye solvents the Marcus polarization coordinate q can be split into several relaxation components $\mathbf{q} = (q_1, q_2, \ldots, q_r)$, making the configuration space multidimensional. Generalization of the model to the multidimensional case has been done earlier in several important works [12, 14]. For the sake of simplicity, we consider here a simple model with only one classical and one quantum coordinate.

The main difficulty of numerical solution of Eqs. (1)-(2) is due to the dimensionality of the configuration space. Indeed, the number of coupled equations can reach 10^4 - 10^5 if several quantum intramolecular modes are active in CT and taken into consideration. Another problem arises from the presence of multiple delta-localized coupling terms, describing resonant CT transitions in EDACs (the second term in the rhs of Eqs. (1)-(2)). These difficulties make standard numerical techniques (such as grid-based algorithms or Monte-Carlo methods [15]) ineffective and require the development of more specific approaches.

A family of methods based on the recrossing-algorithm of the Brownian simulation (RABS) scheme has been suggested earlier [16] and implemented within the `QM2L` and `BSM Kinetics` packages [9, 17]. The complexity of the RABS scheme is linear with respect to the number of solvent and intramolecular modes, which makes the scheme efficient in multidimensional models. The basic RABS algorithm implies generation of unreactive stochastic trajectories of quasi-particles on the free energy surfaces of electron-vibrational states of the complex, $U_k^{(n)}$. The CT transitions in this technique are implemented as "hops" of quasi-particles between FESs with different localization of the electron, $U_1^{(n)}$ and $U_2^{(m)}$. In the Zusman approximation, such hops are allowed only in the region of the FESs intersection, $U_1^{(n)} = U_2^{(m)}$, that is at the $q_{n,m}^\dagger$ points. We refer to the passage of the Brownian trajectory through the $q_{n,m}^\dagger$ point as the "recrossing" event. The criterion for a surface hop in this scheme is determined by the particle's velocity at the instant of the recrossing [17].

COHERENT OPTICAL TRANSITIONS

To introduce coherent optical electronic transitions to the RABS scheme we consider here as a starting point a simple two-level quantum system, thus neglecting vibrational sublevels of the excited state. Evolution of this system under the action of a short laser pulse is governed by the spin-Hamiltonian

$$\hat{H}(t) = -\frac{\hbar\omega_0}{2} \hat{\sigma}_z + \frac{\hbar\Omega}{2} \hat{\sigma}_x F(t) \cos\omega t - \frac{\hbar\Omega}{2} \hat{\sigma}_y F(t) \sin\omega t, \tag{4}$$

where ω is the carrier frequency of the laser pulse, σ_i $(i = x, y, z)$ are the Pauli matrices, ω_0 is the Bohr frequency of optical transition, and Ω is the Rabi frequency (ω, ω_0 and Ω are model parameters). The first term in the right-hand side of Eq. (4) describes two split energy levels corresponding to the neutral $[DA]$ and ionic $[D^+A^-]$ states of EDAC,

while the second and third terms represent the time-dependent optical interaction between these states. Assuming the laser pulse to be Gaussian, we put $F(t) = \exp\left(-(t-t_0)^2/2\tau_e^2\right)$, with τ_e being its duration. In the low-field limit the Schrodinger equation for the spin-Hamiltonian Eq. (4) can be solved analytically, and the dynamics of the excited state population is given by the equation

$$P_2(t) = \frac{\pi\Omega^2\tau_e^2}{8}\left|\exp\left(-\frac{\Delta\omega^2\tau_e^2}{2} - i\Delta\omega t_0\right)\left(1 + \mathrm{erf}\left(\frac{t-t_0}{\sqrt{2}\tau_e} + \frac{i\Delta\omega\tau_e}{\sqrt{2}}\right)\right)\right|^2, \qquad \Delta\omega \equiv \omega_0 - \omega. \tag{5}$$

Now we transform this result into a form that is more convenient for calculations, using the well-known Faddeeva function $w(z)$ of the complex argument, $w(z) \equiv \exp(-z^2)(1 - \mathrm{erf}(-iz))$. Denoting $z \equiv (t-t_0)/\sqrt{2}\tau_e + i\Delta\omega\tau_e/\sqrt{2}$ one gets from Eq. (5)

$$P_2(t) = \frac{\pi\Omega^2\tau_e^2}{8}\left|\exp\left(-\frac{\Delta\omega^2\tau_e^2}{2} - i\Delta\omega t_0\right)\left(1 + \mathrm{erf}\left(2 - e^{-z^2}w(iz)\right)\right)\right|^2. \tag{6}$$

In this study we utilize Eq. (6) using the following computational scheme. An optically driven hop of a particle from the ground to the excited state can be simulated using the calculated probability ΔT_{up} for a particle to undergo quantum transition to the upper FES during the time interval $[t_k, t_k + \Delta t_k]$ provided that at t_k it is on the lower FES. This probability is

$$\Delta T_{\mathrm{up}}(t_k, \Delta t_k) = \frac{E_2(t_k + \Delta t_k) - E_2(t_k)}{1 - E_2(t_k)}, \tag{7}$$

where $E_2(t) \equiv 2P_2(t)/\pi\Omega^2\tau_e^2$ is the normalized excited state kinetics. Such a normalization is introduced here to improve the efficiency of simulations, thus providing *all* the particles in the ground state to undergo optical transition to the excited state at $t \to \infty$.

It should be noted here that Eq. (7) can be actually employed only if the numerator in this expression is non-negative, $E_2(t_k + \Delta t_k) - E_2(t_k) \geq 0$, that is if transition is locally irreversible. This condition is not generally met in quantum systems, the phenomenon is often referred to as quantum beats. To simulate an outflow of the excited state population back to the ground state due to coherent evolution of the quantum system, we apply the same strategy as above and introduce the probability of the "down" transition as

$$\Delta T_{\mathrm{dn}}(t_k, \Delta t_k) = \frac{E_2(t_k + \Delta t_k) - E_2(t_k)}{E_2(t_k)}, \tag{8}$$

Employing expressions (7) and (8) as surface hop criteria within the RABS scheme, one gets the following computational algorithm

1. during the action of the excitation pulse, calculate the quantity $\delta E_2 = E_2(t_k + \Delta t_k) - E_2(t_k)$ at each time step Δt_k;
2. if $\delta E_2 > 0$ then
   (a) calculate the probability of up-transition from Eq. (7),
   (b) for each particle on the lower FES, apply a surface hop criterion by comparing ΔT_{up} with a random number sampled from the (0.1) interval;
3. if $\delta E_2 < 0$ then
   (a) calculate the probability of down-transition from Eq. (8),
   (b) for each particle on the upper FES, apply a surface hop criterion by comparing ΔT_{dn} with a random number sampled from the (0.1) interval.

It should be noted here that the Faddeeva function of a complex argument $w(iz)$ can be easily evaluated using `Algorithm 916` by Zaghloul and Ali [18].

We consider now the results of several test simulations illustrating an accuracy of the method. Numerical experiments were carried out using the `QM2L` code with $N = 10^6$ Brownian particles. Fig. 1A shows simulated kinetics of the excited state population in the absence of CR at different values of $\Delta\omega$ (indicated in the figure caption). $E_2(t)$ curves here reproduce exactly the solution of the Schrodinger equation in the weak-field limit, Eq. (5), for all values of $\Delta\omega$ (not shown in Fig. 1A). In the case of the resonant excitation, $\Delta\omega = 0$, the upper curve in Fig. 1A demonstrates a transition of the excited state population to unity at $t \to \infty$, thereby ensuring participation of the entire ensemble of quasi-particles in simulations of the optical excitation. Another important result in Fig. 1A is a partial depopulation of the excited state at $\hbar\Delta\omega \geq 6$ meV, which is clearly seen at large t, when the pulse weakens.

Another simulation, presented in Fig. 1B, demonstrates the dependence of the excitation yield (that is, the normalized population of the excited state at $t \to \infty$) as a function of $\Delta\omega$. The yield expectedly drops rather fast when the pulse frequency shifts out of resonance, $|\Delta\omega| > 0$. This result is easy to understand if we take into account spectral density of the pulse. Indeed, the spectrum of the $F(t)$ pulse is also Gaussian, and in Fig. 1B it completely reproduces the profile of the excitation yield at a given τ_e.

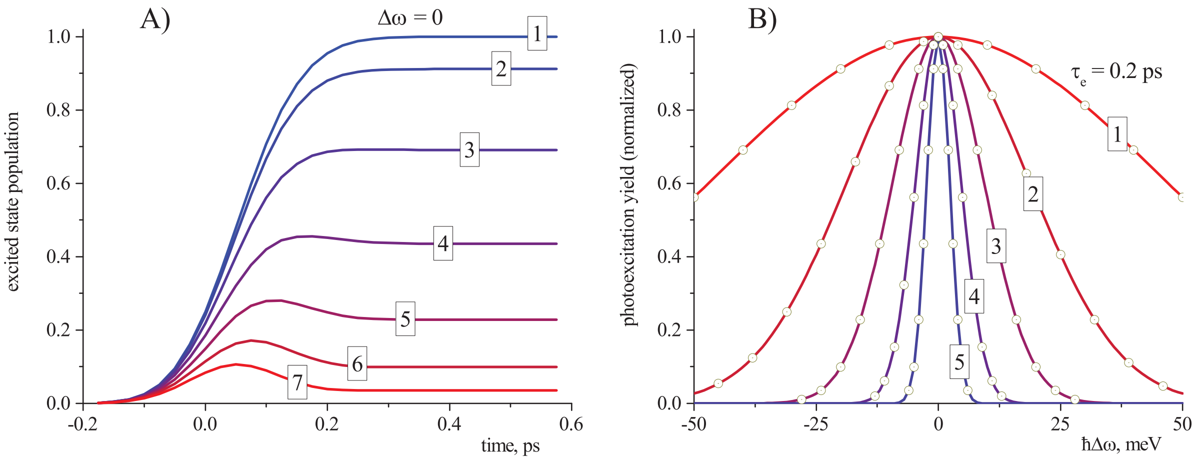

FIGURE 1. Panel A: coherent dynamics of the excited state population in EDAC driven by a short laser pulse. Simulations are performed with the `QM2L` code using the suggested computational scheme. Simulation parameters: $\tau_e = 0.1$ ps, $\hbar\Delta\omega$ = 0.0(1), 2.0(2), 4.0(3), 6.0(4), 8.0(5), 10.0(6), 12.0(7) meV. Panel B: normalized quantum yield of photoexcitation as a function of $\Delta\omega$. Lines – simulation results, dots – spectral density of the excitation pulse.

ACKNOWLEDGMENTS

This work was supported by RFBR and the Government of the Volgograd region (project 19-47-340020), and by the Ministry of Science and Higher Education of the Russian Federation (project 2.852.2017/4.6).

REFERENCES

[1] N. Mataga, H. Chosrowjan, and S. Taniguchi, J. Photochem. Photobiol. C **6**, 37–79 (2005).
[2] O. Nicolet, N. Banerji, S. Pagès, and E. Vauthey, J. Phys. Chem. A **109**, 8236–8245 (2005).
[3] J. Tsutsumi, H. Matsui, T. Yamada, R. Kumai, and T. Hasegawa, J. Phys. Chem. C **116**, 23957–23964 (2012).
[4] C.-C. Chiu, C.-C. Hung, C.-L. Chen, and P.-Y. Cheng, J. Phys. Chem. B **117**, 9734–9756 (2013).
[5] S. V. Feskov, V. N. Ionkin, and A. I. Ivanov, J. Phys. Chem. A **110**, 11919–11925 (2006).
[6] V. V. Yudanov, V. A. Mikhailova, and A. I. Ivanov, J. Phys. Chem. A **114**, 12998–13004 (2010).
[7] S. V. Feskov, A. O. Kichigina, and A. I. Ivanov, J. Phys. Chem. A **115**, 1462–1471 (2011).
[8] G. Piacente, A. Amadei, M. D'Abramo, I. Daidone, and M. Aschi, Phys. Chem. Chem. Phys. **16**, 20624–20638 (2014).
[9] A. E. Nazarov, R. G. Fedunov, and A. I. Ivanov, Comp. Phys. Comm. **210**, 172–180 (2017).
[10] S. V. Feskov and S. N. Osipova, Sci. J. VolSU. Math. Phys. **24**, 62–72 (2014).
[11] R. A. Marcus and N. Sutin, Biochim. Biophys. Acta. **811**, 265–322 (1985).
[12] L. D. Zusman, Chem. Phys. **119**, 51 – 61 (1988).
[13] J. Jortner and M. Bixon, J. Chem. Phys. **88**, 167–170 (1988).
[14] H. Sumi and R. A. Marcus, J. Chem. Phys. **84**, 4894–4914 (1986).
[15] M. P. Allen and D. J. Tildesley, *Computer Simulation of Liquids* (Clarendon Press, New York, 1989).
[16] R. G. Fedunov, S. V. Feskov, A. I. Ivanov, O. Nicolet, S. Pagès, and E. Vauthey, J. Chem. Phys. **121**, 3643–3656 (2004).
[17] S. V. Feskov and A. I. Ivanov, J. Chem. Phys. **148**, p. 104107 (2018).
[18] M. R. Zaghloul and A. N. Ali, ACM Trans. Math. Softw. **38**, 15:1–15:22 (2012).

Application of Spaces in Conjugate Coordinates for Decoupling and Calculating Systems of Phase Equilibrium Equations and Searching for the Minimum of the Total Energy in the Framework DFT for Physical Materials Science

Alexander L. Udovsky[1, a)]

[1]*Baikov Institute of Metallurgy and Materials Science of RAS, Moscow, Russia*

[a)]Corresponding author: audovskiy@imet.ac.ru

Abstract. The space in coordinates, the scalar convolution of which contributes to the Gibbs energy or energy, is called the space in conjugate coordinates (CCs), for example, the P -V space (pressure-volume coordinates. The report examines the use of spaces in conjugate coordinates both for implementing the method for calculating the system of phase equilibrium equations in the field of chemical thermodynamics, and for finding the minimum of the total energy in terms of the electron density functional depending on the volume variation for intermetallic phases with a tetragonal crystal lattice: C14 Laves - and Sigma - phases in P - V space.

INTRODUCTION

In [1], van der Waals, analyzing the equation of state proposed by him, gives the rule of equality of Maxwell squares as a calculation method in the P - V (pressure - volume) coordinates of the equilibrium values of the volumes of the condensed and gas phases under the condition of constant temperature for single-component systems (1CS). The book [2] demonstrated that the application of the Maxwell rule for isotherms that are below the critical point and have a non-monotonic form is equivalent to the condition of equal chemical potentials of the liquid and gas phases for 1CS. The Maxwell's idea stimulated the author of this report for its generalization and application to the creation of a general method for calculating the system of equilibrium equations for binary systems. Minimization of the Gibbs molar thermodynamic potential (GTP) in composition for two-phase closed 2CS under conditions of constant temperature and pressure leads to a set of Phase-Equilibrium Equations (SPEE) with unknown compositions of equilibrium phases. The presence of configuration entropy in GTP leads SPEE to a system of two transcendental equations. It is known that in the general case there is no calculation algorithm that leads to a convergent iterative procedure for solving a system of transcendental equations with a given accuracy [3]. An attempt to take into account the short-range order in 2CS leads to the need to use the GTP functional depending on the internal (configuration) degrees of freedom, the composition of the closed 2CS and the temperature. A similar problem arises in the application of statistical models in simulating the filling with atoms of both components of different sub-lattices of chemical compounds, taking into account the existence of their homogeneity region. Thus, the construction of an autonomous algorithm for calculating a SPEE, independent of the models used, has lasting value.

METHODOLOGY

Within the framework of Gibbs thermodynamics, the Maxwell rule applied for 1CS G = G (T, P) in the space of P - V coordinates corresponds to the manipulation in the space of conjugate coordinates generalized force - and the generalized “displacement” it ($V=\partial G/\partial P$) at T = const. For 2CS, the molar TPG of any of the phases is $G^i=G^i(T,P,x),\ i=\alpha,\beta$ phases, the conjugate variables under the condition $T = const$ is a partial derivatives of

$(\mu_2^i - \mu_1^i) = \partial G^i / \partial x$. Fragments of the phase diagram of a closed 2CS are built in Figure 1, the upper parts in the *T- x* coordinates (*P = const*) (the stratification is shown on the left; the equilibrium of non-isomorphic solutions is on the right). Under the condition *T = const* = T_0, the compositions of the equilibrium phases correspond to the abscissas of the tangency points of the common tangent constructed in the *G-x* space or in the *GTP* space (middle parts of Figure 1).

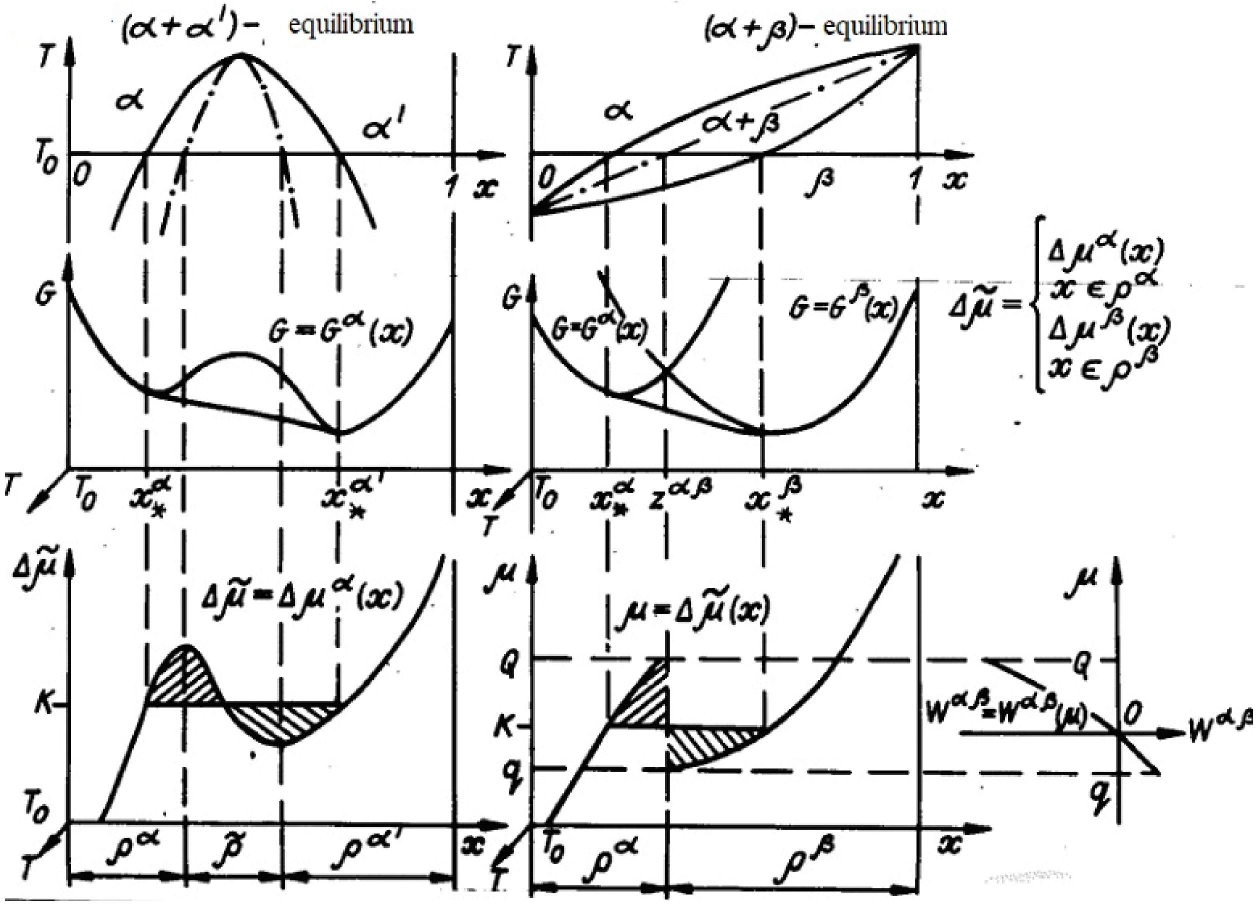

FIGURE 1. A geometrical illustration of the Maxwell's rule of equality of squares (shaded areas): on the left –for miscibility gap of isomorphic solutions; right - for competing structures

The compositions of the alloys for the inflection points x1 and x2 (spinodal points) are the roots of the equation

$$\partial^2 G^i / \partial x^2 = 0, \quad \forall x \in (0; x_c) \text{ or } \forall x \in (x_c; 1), \tag{1}$$

where x_c is the composition of the critical point. At these points, the values $\Delta\mu(x_1) = \mu_2(x_1) - \mu_1(x_1) = \partial G / \partial x\big|_{x_1}$ and $\Delta\mu(x_2) = \mu_2(x_2) - \mu_1(x_2) = \partial G / \partial x\big|_{x2}$ are the local maximum and minimum in the space of conjugate variables $\Delta\mu(x) - x$ (lower part of Figure 1) equal to Q and q, respectively, are also the boundaries of the range of permissible values (RPV) for function (2) (see the right fragment in the lower part of Figure 1):

$$W^{aa'}(x^a,\ x^{a'})^o = G^a(x^a)\ -\ x^a\ ¶(G^a / ¶x)_{x^a} - \{\ G^{a'}\left(x^{a'}\right)\ -\ x^{a'}(¶G^{a'} / ¶x)_{x^{a'}}\} = 0 \tag{2}$$

The geometric meaning of the function (2) consists in the description of the difference between the scratched areas, and from the point of view of analytics it is the 2nd equation of the SPEE, the function (2) is shown in the lower part of Figure 1 - on the left. The calculation cycle:

1) Fixed temperature value $T = T_1$.
2) Begins with the calculation of the 1st value $k_1 = (Q + q) / 2$;
3) The intersection of the straight line k_1 with the curve $\Delta\mu(x) = k_1,\ \forall x \in (0; x_{sp1})$ the root of which is the approximate value of the composition x_1^{α}, and the equation $\Delta\mu(x) = k_1,\ \forall x \in (x_{sp2}; 1)$, the root of which is the approximate value of the composition $x_1^{\alpha-prim}$.
4) Substituting the values of k_1, x_1^{α} and $x_1^{\alpha-prim}$ into function (2) allows you to determine the sign and value of the function $W^{\alpha\alpha-prim}{}'(k_1, x_1^{\alpha}, x_1^{\alpha-prim})$.
5) Given that $W^{\alpha\alpha-prim}(Q) < 0$ and $W^{\alpha\alpha-prim}(q) > 0 >$ 0, using the dichotomy method allows us to obtain new boundaries {Q1; q1} the area of valid values for the function (2).
6) In the new range of acceptable values, the new value $k_2 = (Q1 + q1) / 2$ is calculated and all operations (2-5) are repeated.
7) The condition of continuity of chemical potentials at the boundaries between the first derivatives of G in composition on the boundaries of single-phase and two-phase fields ($\alpha/(\alpha+\alpha$-*prim* and *a-prim*/($\alpha+\alpha$-*prim*)) are checked.
8) If the exit criterion is not met, all operations (2-7) are repeated.

If the criterion for continuity of chemical potentials at one / two-phase boundaries is satisfied, then the cycle to *k* ends and proceeds to the next value of temperature (item 1).

THE RESULTS

In more detail, a generalization of the Maxwell rule (GMR) for the equilibrium of both isomorphic and non-isomorphic solutions is presented in [4]. The convergence of the algorithm for GMR is quadratic, (as in Newton's method) was proved in [5]. The use of GMR allowed us to carry out calculations with an accuracy of 10^{-5} at.% for the example of the Al – Si system, Figure 2.

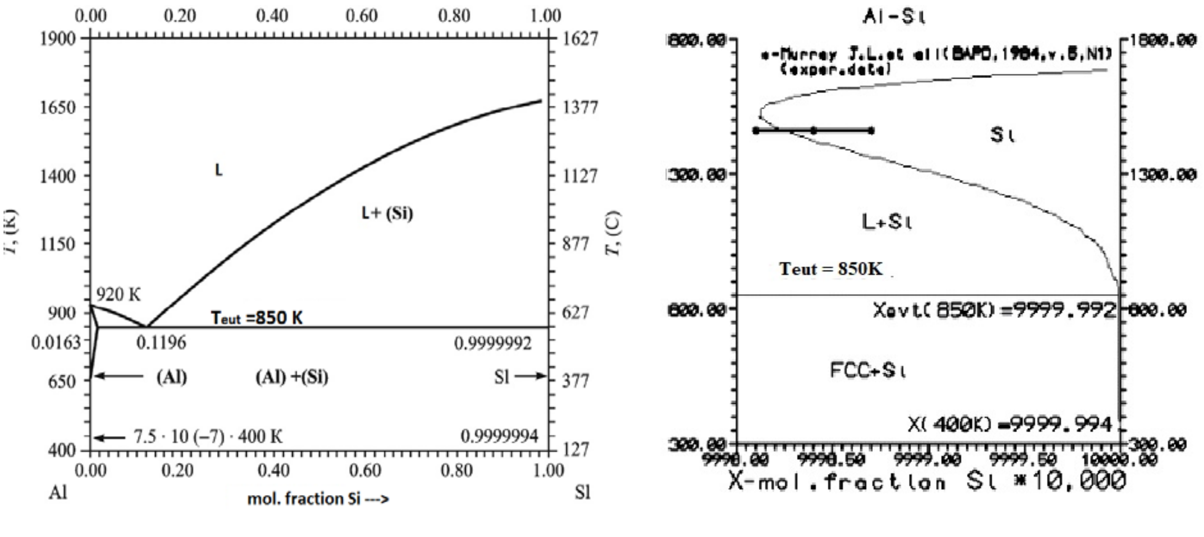

FIGURE 2. The CALPHAD-optimized Al-Si system phase diagram (left) and its fragment (enlarged 5000 times) for silicon-rich alloys (right). L+(Si) and (Al)+(Si) are abbreviations correspond to two - phase fields, including as Liquid - phase and Si-rich solid solution for as Al-rich and Si-rich solid solutions.

In [6], a SPEE was obtained in a covariant form for 3CS or more component systems. Its representation in the polar coordinate system (ρ, φ) for 3CS also made it possible to generalize the Maxwell's rule on equality of areas in the

coordinates $\partial G / \partial \rho - \rho$ at φ = *const,* where ρ , φ - modulus of the vector and the angle of inclination of the desired vector of two-phase tie-line for 3CS [6-7]. The developed algorithm and computer program were applied to calculate the equilibrium between the fcc - and liquid phases for Ni-rich alloys in the Ni-Al-W 3CS in the range of 1685 - 1806 K, the family of liquids and solidus isotherms were calculated, as well as the evolution of fractions of liquid and solid phases as function on temperature for fixed composition alloys [8].

APPLICATION OF CONJUGATE SPACE FOR DFT CALCULATIONS OF INTERMETALLIC PHASES

For tetragonal phases, the volume of the crystal lattice is equal to $V(a,c) = (\sqrt{3}/2)a^2\mathrm{c}$, then, by definition, the total pressure is equal to

$$P = -\frac{\partial E_{tot}}{\partial V} = -(1/V) * \left\{ 2\left(\frac{\partial \ln a}{\partial E_{tot}}\right)_c + \left(\frac{\partial \ln c}{\partial E_{tot}}\right)_a \right\}^{-1} \quad (3)$$

Calculations of the total energy (E_{tot}) for the ground state were carried out first depending on one variable, for example, E_{tot} *(a)*, under the condition *c = const*, and then depending on E_{tot} *(c)* under the condition *a = const*. In the works [9-10], it was shown that acceptable accuracy of E_{tot} is achieved when calculating E_{tot} on 9 nodes in any direction. Finding a minimum in the E_{tot} *-V* space is equivalent to finding a solution to a system of equations in the 3-dimensional space *P – a – c.* After localization of the minimum domain E_{tot}*,* linearization is performed on neighboring nodes and the roots of the equations *P{V (a; c = const)} = 0* and *P{V (c; a = const)} = 0* are calculated using a cyclic procedure. Next, a numerical differentiation is made according to the 5-point formula for the central differences in both E_{tot} *– a – c* and *P – a – c* spaces to calculate the bulk modulus of elasticity.

ACKNOWLEDGMENTS

The reported study was funded by RFBR according to the research project № 19-03-00530.

REFERENCES

1. J. D.v.d. Waals, Ph. Konnstamm. Lehrbuch der Thermostatik. Erster Tell. Allgemeine Thetmostatic. Verlag von Johann Ambrosias Barth, Leipzig, 1927.
2. L. D. Landau, E. M. Lifshitz. Statistical Physics (Science, Moscow, 1976), p.287 (in Russian).
3. J. M. Ortega, W. C. Rheinboldt. Iterative solution of nonlinear equations in several variables. (Acad. Press. New York and London, 1970).
4. A. L. Udovsky, Izvestya Akademii Nauk SSSR, Russian Metally N 2, 136–157 (1990).
5. A. L. Udovsky, V. N. Karpushkin, E. A. Kozodaeva, CALPHAD v. 19, N 3, 245-277 (1995).
6. A. L. Udovskii. Doklady Physics, vol.46, No. 4, 247-250 (2001).
7. A. Udovsky, Proceedings Joint European Thermodynamics Conference IX JETC IX – 12-15 June 2007, edited by Bernard Guy and Daniel Tondeur. (Ecole Nationale Superieure des Mines, Saint_Etienne), pp.189-193.
8. A. Udovsky, M. Kupavtsev. Ibid, pp. 194-198.
9. A. Udovsky, D. Vasilyev. 17th ISRAELI-RUSSIAN BI-NATIONAL WORKSHOP 2018 "The optimization of the composition, structure and properties of metals, oxides, composites, nano and amorphous materials", August 13 – August 17, 2018, pp. 229-238. http://www.ariel.ac.il/sites/conf/mmt/ws2018cd/Service%20files/papers/229-238.pdf
10. A. Udovsky. HTMC XVI – 16th UIPAC High Temperature Material Chemistry Conference (HTMC XVI) July 2-6, 2018, Yekaterinburg, Russia, Book of abstracts, p.46.

Recent Progress of Protein Canonical Molecular Orbital Calculation by the Third Generation Density Functional Method

Toshiyuki Hirano[1, a)] and Fumitoshi Sato[1, b)]

[1] *Institute of Industrial Science, the University of Tokyo, Japan*

[a)] Corresponding author: t-hirao@iis.u-tokyo.ac.jp
[b)] satofumi@iis.u-tokyo.ac.jp

Abstract. Although canonical molecular orbital (CMO) calculations for proteins are very useful for protein engineering, they are computationally expensive and difficult to achieve because proteins are large molecules. We had developed the third-generation density functional (3G DF) method, which performed electronic state calculation with high efficiency in parallel computer by performing only matrix operation during the SCF calculation. In this study, by applying the powerful computing platform of graphic processing unit (GPU) to our 3G DF calculation method, we constructed a computing environment that achieved the large-scale CMO computation with high efficiency.

INTRODUCTION

The canonical molecular orbitals (CMOs) provide insights into characteristics of molecule. Nowadays, it is indispensable to use theoretical calculation and experiment complementarily in small molecule research. Although it is difficult to perform the CMO calculation of protein, the results give us important information to not only theoretical but also experimental researchers [1-3].

We have developed CMO calculation program for proteins, ProteinDF [4], which is written by the object-oriented language, C++. The simulation approach is based on the density functional (DF), and implemented by using the third generation (3G) DF calculation method [5], which means that it follows FILE and direct methods. The Kohn-Sham (KS) (or Fock) matrix has been iteratively evaluated by molecular integrals in the direct method which is commonly used, but in the 3G DF method it is given by only simple matrix operations in the SCF routine. The matrix operations are easier to achieve even load balance than the complicated molecular integrals in the current distributed-memory type parallel computer. In addition, it is expected that the whole CMOs calculation will be time-shortened by using machine-optimized linear algebra libraries such as BLAS/LAPACK.

In this study, implementation of the linear algebra routines with the use of the ViennaCL [6], which supports the OpenCL, has been achieved for the ProteinDF. By using the OpenCL, it was possible to use not only NVIDIA's GPUs but also AMD's. The 3G DF method provided an easy way to implement the GPU computing on the large-scale CMO calculation. The fast matrix operations with the GPU gave a beneficial effect on the 3G DF scheme. In this article, we will introduce the implementation of 3G DF method on the ProteinDF, and report the benchmark results on GPUs.

METHOD

Simple summary of the 3G DF scheme

In this section, we will briefly introduce the 3G DF scheme. The Kohn-Sham (KS) orbitals are determined by solving the following eigenvalue equation, which is similar manner as the Hartree-Fock (HF) method.

$$\boldsymbol{FC} = \boldsymbol{SC\epsilon} \tag{1}$$

Here, $\boldsymbol{F}$, $\boldsymbol{C}$, $\boldsymbol{S}$ and $\boldsymbol{\epsilon}$ are the KS (or Fock) matrix, the coefficients matrix, the overlap matrix and the diagonal matrix of orbital energies, respectively. The KS (Fock) matrix depends on the coefficient matrix, $\boldsymbol{C}$, via the density matrix, $\boldsymbol{P}$. So, the self-consistent field (SCF) calculation method is applied to solve that eigenvalue equation. In the SCF calculation, building the Coulomb ($\boldsymbol{J}$) and Fock exchange ($\boldsymbol{K}$) terms, which are components of the KS (Fock) matrix, are bottleneck steps because these terms are obtained by time-consuming molecular integral, four-center-two-electron repulsion integral (ERI). The ERI, $\langle pq|rs\rangle$, is determined as follows.

$$\langle pq|rs\rangle = \iint g_p^*(\boldsymbol{r}_1)g_q^*(\boldsymbol{r}_2)\frac{1}{|\boldsymbol{r}_1-\boldsymbol{r}_2|}g_r\ (\boldsymbol{r}_1)g_s\ (\boldsymbol{r}_2)d\boldsymbol{r}_1 d\boldsymbol{r}_2 \tag{2}$$

, where $g(\boldsymbol{r})$ represents basis set function on the electron coordinate, $\boldsymbol{r}$. Now, we introduce the Cholesky vectors ($\boldsymbol{L}$) of the super-matrix, $\boldsymbol{V}$, whose element is evaluated by the ERI.

$$V_{pq,rs}^{ERI} = \langle pq\,|\,rs\rangle \approx \sum_{I=1}^{M} L_{I,pq}^{ERI} L_{I,rs}^{ERI} \tag{3}$$

After the Cholesky vectors $\boldsymbol{L}$ were gained, the $\boldsymbol{J}$ and $\boldsymbol{K}$ terms were solved as follows:

$$J_{pq} = \sum_{rs} P_{rs}\langle pq|rs\rangle \approx \sum_{rs}\sum_{I}\ L_{I,pq}^{ERI} L_{I,rs}^{ERI} P_{rs} \tag{4}$$

$$K_{pq} = -\frac{1}{2}\sum_{rs} P_{rs}\langle pr|qs\rangle \approx \sum_{r}\ \sum_{I}\ L_{I,pq}^{ERI} L_{I,rs}^{ERI} P_{rs} \tag{5}$$

$$X_{I,pi} = \sum_{r}\ L_{I,pr}^{ERI} Q_{ri} \tag{6}$$

$$P_{rs} = \sum_{i}\ Q_{ri}Q_{si} \tag{7}$$

In case of density functional calculation, the exchange-correlation term could be obtained by similar matrix operations using the grid-free method. Here, we would like to emphasize that the $\boldsymbol{J}$ and $\boldsymbol{K}$ terms are evaluated by the matrix-matrix multiplications only. Therefore, the KS (Fock) matrix is obtained by simple linear algebraic procedure. Even load balancing is strongly desired in the many-core computing system, but the matrix operations are simpler than the molecular integrals and easy to achieve it. The 3G DF calculation scheme is suitable for the modern HPC machines prepared the optimized linear algebra software library.

GPU acceleration of the matrix-matrix multiplication

Nowadays, the computing performance of graphics processing units (GPU) is superior to that of the CPU for specific purpose such as matrix operations. General-purpose computing on graphics processing units (GPGPU) is an essential way for the high-performance computing (HPC).

The ProteinDF has already implemented and used the well-known BLAS/LAPACK library as linear algebra operation library. In order to use the GPU computing on the linear algebra operations, we use the ViennaCL library for the ProteinDF in this study. The ViennaCL supports CUDA, OpenCL and OpenMP. In this study, we would like to use not only NVIDIA's GPU but also AMD's, so the ViennaCL library was used on the OpenCL environment. Besides, Eigen library was also utilized as the linear algebra computing for the ProteinDF. The ViennaCL has interfaces to matrix built by the Eigen, and CPU-GPU data transfer is easy to use. Both of the ViennaCL and Eigen are C++ template library with affinity to C++ application such as the ProteinDF.

In order to use the BLAS/LAPACK, Eigen and ViennaCL library, the corresponding matrix classes were written in the ProteinDF. Since the matrix operations and algorithms relating to build the KS (Fock) matrix and the eigenvalue problem were common regardless of the linear algebra packages, we decided to unify the interface of the matrix classes by using the bridge design pattern.

RESULTS AND DISCUSSION

As mentioned above, in the 3G DF calculation scheme, there are many matrix-matrix multiplications (DGEMM) during the SCF calculation. So, the benchmark test of the matrix multiplication for comparing various linear algebra packages was performed. In addition to this, because there is solving for the eigenvalue problem in the SCF calculation, the elapsed time of the calculation was also investigated. These benchmark tests were carried out on the Intel Core-i5 4590S and 32 GB mem. The NVIDIA GeForce GTX 1070, Tesla P100, AMD Radeon RX480, and Vega 56 were used as the GPU.

Figure 1-(a) shows the logarithmic chart of the performance of the matrix-matrix multiplication in comparing linear algebra packages and GPUs. The horizontal axis indicates the size of matrix. And, the vertical axis is for the computing performance as floating-point operations per second (FLOPS). The higher the FLOPS value is, the better the computing performance is. In the linear algebra packages using a CPU such as BLAS and Eigen, the FLOPS value

was almost constant with the size of the matrix. Since, the theoretical peak of the CPU (Intel Core i5-4590S; code name: Haswell) was about 192 GFLOPS, it could be said that half or more performance had been achieved. On the other hand, when the GPU was used in the multiplication of smaller size matrices, the computing performance was decreased. The low performance on the small matrix operation may be attributed to the latency involved in data transfer between CPU and GPU. These results showed that the GPU computing was superior to CPU for matrix-matrix multiplication of about 10,000 or more, although depending on the type of GPU. The matrix size corresponds to the number of atomic orbitals (AOs) in the CMO calculation. Using double-zeta basis sets, the number of AOs in the CMO calculation of protein assembled with about 100 amino-acid residues estimates 10,000 or more. So, our results suggested that the GPU computing dominated in the CMO calculations of these molecular sizes.

The comparing elapsed time of solving eigenvalue problem using logarithmic chart is presented in Fig. 1 (b). It was generally observed that GPUs tend to perform processing in a shorter time than CPUs. All libraries had almost the same size dependency, and it might be inferred that the algorithms were almost identical. The reason why the GPUs computing was faster than the CPUs was considered that the GPUs having a high memory transfer speed was more advantageous, once the matrix was expanded on the GPU. On the other hand, as a drawback of GPUs, the amount of memory installed in GPUs was extremely small compared to that of CPUs. So, for GPUs with 8 GB of physical memory, the size of the eigenvalue problem that could be calculated was limited to about 8,000. When solving a protein of 100 residues or more with GPUs, a lot of ingenuity is required.

Using the developed program in this study, we performed benchmark test on actual proteins. The elapsed times of 1 SCF cycle in HF calculation using CPU and GPU were shown in Fig. 2. The used model proteins were RGD peptide (PDB ID: 1FUL, 11 amino-acid residues, 138 atoms, 1375 AOs) and glucagon analog (PDB ID: 1GH0, 29 amino-acid residues, 474 atoms, 451 AOs). The performance tests were carried out on Intel Xeon E5-2620 (16 cores), 128 GB mem and NVIDIA Tesla P100 GPU. In the ProteinDF, unnecessary matrices were saved to disk for effective use of limited physical memory, and these results included the file I/O times. As expected, most of the time were spent calculating the Fock exchange term ($\boldsymbol{K}$). As shown in the Eq. 5, matrix-matrix multiplications were repeatedly performed for calculation of the Fock exchange term. By using the GPU, the matrix-matrix multiplication could be performed quickly and calculated in a short time. However, the computation time of the Coulomb term ($\boldsymbol{J}$) was slower on the GPU than the CPU. In the 3G DF calculation scheme, since the Coulomb term was obtained by the sum of dot product of vectors, it was considered that the data transfer time between the CPU and the GPU was rate-limiting step. The theoretical peak (FP64) of the NVIDIA Tesla GPU P100 was about 4.8 TFLOPS. According to the previous results, even matrix-matrix multiplication had achieved less than a quarter of theoretical performance. Further improvements are needed, such as data transfer between CPU and GPU in the background.

SUMMARY

In the recent HPC environment, utilization of GPUs is an indispensable technology. The powerful computing power of GPUs is very attractive for large-scale CMO calculation. In general, however, GPU computing is highly specialized, difficult to program, and has problems with portability. The 3G DF calculation method was able to achieve SCF calculation only by matrix operations. A large-scale CMO computing environment using GPU was constructed by applying the ViennaCL based on the OpenCL as linear algebra library to the ProteinDF. And, the 3G DF method has been verified to be useful for GPU computing.

ACKNOWLEDGMENTS

This work was partly-subsidized by JSPS/MEXT KAKENHI Grant Numbers JP17K00395. The computation in this work has been done using the facilities of the Institute of Statistical Mathematics.

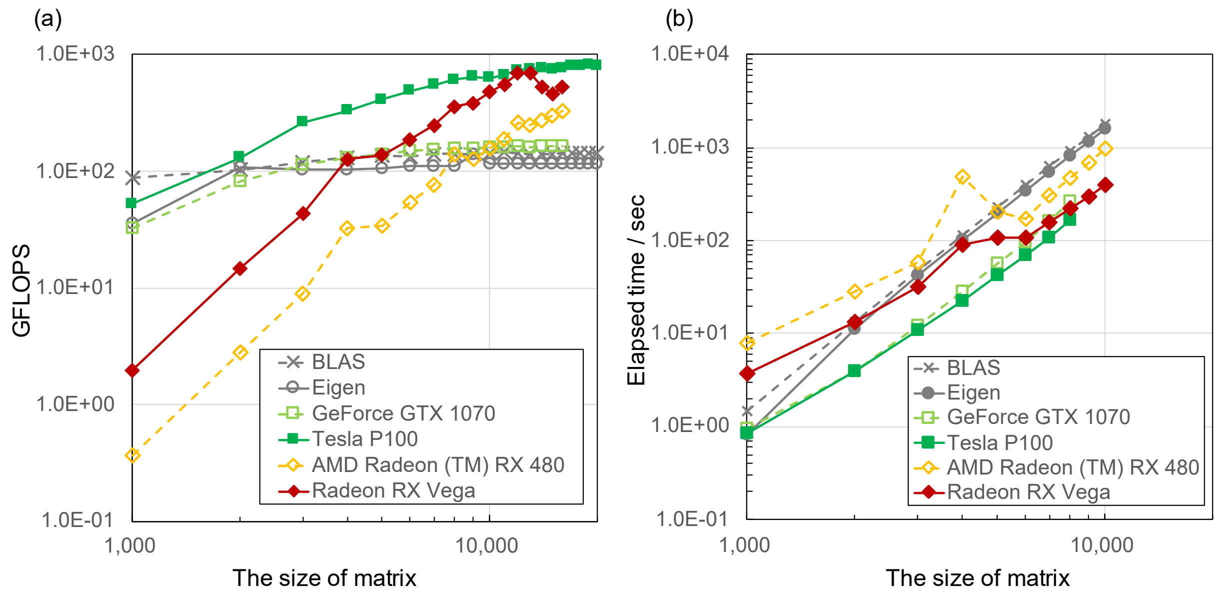

FIGURE 1. The logarithmic charts of the performance of matrix operations by using various linear algebra packages: (a) matrix-matrix multiplication (b) eigenvalue problem; The horizontal axis indicates the number of square matrix size, and the vertical one is for the FLOPS (a) and the elapsed time of calculation (b).

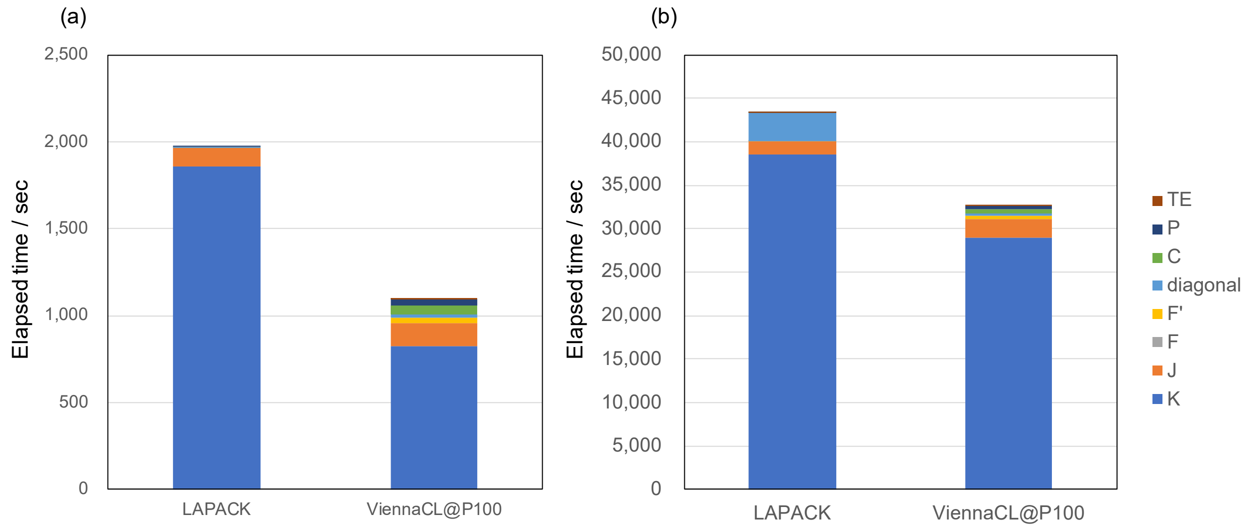

FIGURE 2. The elapsed time of 1-cycle SCF calculation on the ProteinDF: (a) PDB ID: 1FUL (b) PDB ID: 1BH0.

REFERENCES

1. K. Chiba, T.Hirano and F.Sato, Int. J. Quant. Chem., **113**, 2345 (2013).
2. Y.Yagi and Y.Naoshima, Trans. Jpn. Soc. Sim. Tech., **4**, 127 (2012).
3. Y.Tokita, S. Yamada, and W.Luo, Angew. Chem., **50**, 11663 (2011).
4. https://proteindf.github.io/
5. T. Hirano and F. Sato, Phys. Chem. Chem. Phys., **16**, 14496 (2014).

K. Rupp, Ph. Tillet, F. Rudolf, J. Weinbub, A. Morhammer, T. Grasser, A. Jüngel and S. Selberherr, SIAM J. Sci. Comput., **38**, S412 (2016).

Pyridine-Cyanoanthracene Bonded Exciplex

Iria Bolaño[1], Fereshteh Naderi[2] and Valera Veryazov[1,a)]

[1]*Department of Theoretical Chemistry, Chemical Center, Lund University, Lund, Sweden*
[2]*Department of Chemistry, Shahr-e-Qods Branch, Islamic Azad University, Tehran, Iran*

[a)]Corresponding author*:* valera.veryazov@teokem.lu.se

Abstract. Exiplexes are a special kind of molecular complexes, which exist only due to a weak bond in an excited state. The theoretical description of these complexes requires the usage of multiconfigurational theory (CASSCF or RASSCF) followed by second order of perturbation theory. Formation of exiplex complex from pyridine and cyano-anthracene has been studied.

INTRODUCTION

An interaction between two molecules can be repulsive or attractive with the formation of a covalent bond, a charge transfer or weak a van der Waals interaction. Usually, this interaction occurs in the ground state. However, there is a rather rare type of interactions between two molecules, where the ground state is repulsive, but the excited state is slightly binding, creating so-called exciplexes [1-2].

The highly conjugated derivatives of anthracene and naphtalene leads to a wide variety of photochemical processes after light absorption. These derivatives can interact with another organic molecules by the formation of a weak bond emerging the bonded exciplexes [3-5]. The phenomena has been experimentally reported by Wang et al [6]. They described the capability of pyridine molecule to allow charge transfer reaction with cyanoaromatic molecules such as 9-cyanoanthracene (9CA), leading to quenching processes. Theoretically exciplexes are difficult to study due to the need to describe the excited states with a high precision, thus there are very few calculations of exciplex complexes. In the current paper we used the computational set up similar to [7], where the electronic structure of the complex between cyan-naphtalene and pyridine has been reported.

COMPUTATIONAL DETAILS

An important decision about the set up of the project is the choice of geometry of the molecules during their interaction. The minimum energy path (MEP) of the interacting pyridine-cyanoanthracene complex were calculated by optimizing the geometries at sequential constrained monomers distances. Full optimizations (with constrained distance between molecules) were performed at DFT with the B3LYP functional and Pople's basis set (6-31G*) using Gaussian03 program [8]. The results of geometry optimization shows relaxation of anthracene molecule hydrogen atom, connected to carbon, which is attracted by pyridine, moves out of the plane.

In order to describe exciplexes, we need a computational method that is capable to describe both the ground state and excited states. Time dependent DFT (TDDFT) is known as a simplest method to describe the excited states. However, the method assumes similarities between ground and excited states and it only vertical excitations are considered. Applied to pyridine-9CA complex, TDDFT calculations with B3LYP functional and def2-TZVP basis set by using Orca 4.1.1 program [9] show minimum in the ground, which is fully repeated in the excited states. No formation of exciplex can be confirmed from TDDFT calculations. Hence, following the recommendations from [7], the energy profiles were computed by performing punctual calculations with the complete active space self-consistent field (CASSCF) and recalculated using perturbation theory of second order with CASPT2 methods to recover the effect of dynamic correlation, both methods implemented in Molcas-8 package [10]. Equal contribution

for each state were set up in the state averages in CASPT2 calculations. The same active space of 14 electrons in 14 π orbitals /0/14/0/ were taken for all complexes with the basis set ANO-L-VDZP.

Same strategy were kept up but using the restricted active space (RASSCF and RASPT2) methodology performing a full CI between the HOMO-1 and LUMO+1 π orbitals and an up to double excitation strategy between eight occupied π orbitals and eight virtual π orbitals, this is an /8/4/8/sd active space.

RESULTS AND DISCUSSION

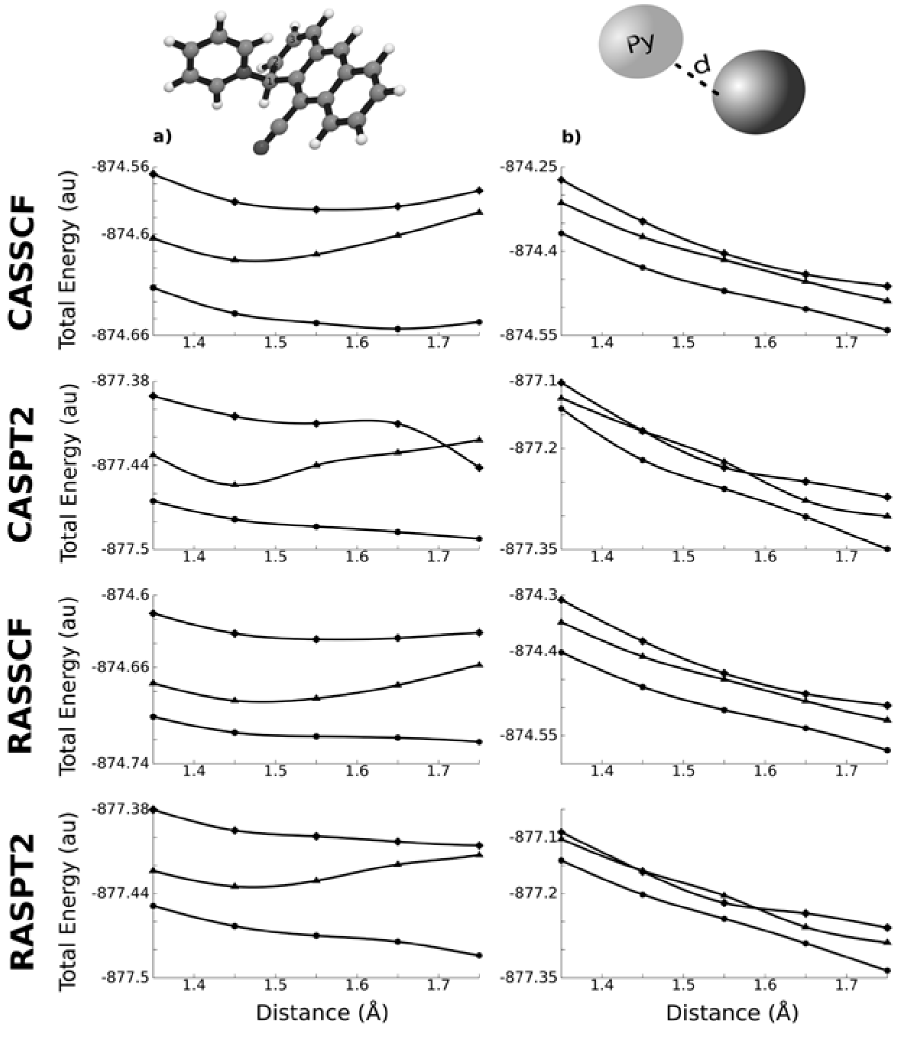

FIGURE 1. Minimum energy paths at CASSCF, CASPT2, RASSCF and RASPT2 level of theory for the interacting pyridine and 9CA complex at varied distances between the pyridine nitrogen and C1 in the anthracene skeleton a) full optimizing the geometries b) the geometries are frozen and not modifying during the reaction. Circles indicate the ground state, triangles the first excited state and diamonds the second excited state.

The systems in charge transfer quenching events are characterized for being highly conjugated aromatic compounds with a large amount of orbitals and electrons involved in the chemical bonds. Such systems are almost impossible to handle by ab initio, parameter-free level of theory. The another complication comes from the large amount of internal coordinates involved into reaction between molecules. As an attempt to simplify the calculations, it was considered a model, where individual molecules are frozen and the only parameter of the chemical reaction is the distance between the molecules.

CASSCF and CASPT2 comparison of the MEP

The main outcome extracted from the MEP profiles at CASSCF and CASPT2 level is the smooth minimum in the first excited state at around 1.45 Å. The ground state remains repulsive along the internal coordinate calculations although at large distances the CASSCF calculations could not describe properly the behavior of the exciplexes ground state (Figure 1 a)). The same discrepancy at CASSCF level arises with the trend of the excited states as the monomers distance increases, with no stabilization of the energy according to bonded exciplexes model [7]. An unexpected sharp minimum in the second state of CASSCF energy profile also supports the point that the dynamic correlation must be decisive in the description of bonded exciplexes.

Similar features of the energy profile found in CAS outcomes can be also noticed at the RAS level although the minimum is slightly displaced. At short distances, RASSCF and RASPT2 calculations agree really good but as the distance increases, RASPT2 excited states converge to slightly lower energies. The second excited state presents less repulsive trend in the RASSCF landscape. The RAS and CAS energy profiles scarcely differ so the use of the cheaper RASPT2 method is a wise choice in the study of bonded exciplexes.

Frozen monomers

To understand the importance of observed in our calculations the geometry relaxation of anthracene, we considered a model where individual molecules had a frozen geometry. The results are presented at Figure 1b. The results shown a constant repulsive trend in ground and excited states as the monomers distance increases. Then the distance is not the main responsible of the complex stabilization. The nature of the transitions is not any more the same as in the one of the MEP, specially the electronic transition on the anthracene skeleton. Otherwise at the long distances the energetic trend for the ground and excited states proceeds in the same direction as MEP profile. This fact is expected at some point as the interaction between monomers starts to weaken and no change transfer is observed.

It is clear that the proposed model outcomes do not fit with the relaxed system results but it clarify the importance of the rearrangement of the geometry. The anthracene molecule needs to be distorted and kept the aromaticity of the neighbor carbon rings to allow the formation of the bonded exciplexes.

Minimum energy results

The low distance at which both monomers stabilized in the First excited state suggests the presence of a mild bond between pyridine and cyano-anthracene. Due to this new bond between monomers, the planarity of the anthracene is distorted. As consequence, the C1 lose its sp^2 hybridization to a sp^3 one as the bond is being formed increasing the distances of C1 with C2 and C6. The remaining distances between atoms scarcely varies during the reaction, specially the ones on the fuse six-membered rings.

TABLE 1. Number occupations for the ground state, first excited state and second excited state at the CAS and RAS level at monomers distance of 1.45 Å. The shape of HOMO, LUMO and LUMO+1 orbitals is shown at Figure 2.

	S_0^{CAS}	S_1^{CAS}	S_2^{CAS}	S_0^{RAS}	S_1^{RAS}	S_2^{RAS}
HOMO	1.88	1.44	1.01	1.84	1.76	1.03
LUMO	0.12	0.56	0.07	0.15	0.23	0.05
$LUMO^{+1}$	0.07	0.02	0.99	0.09	0.09	0.98

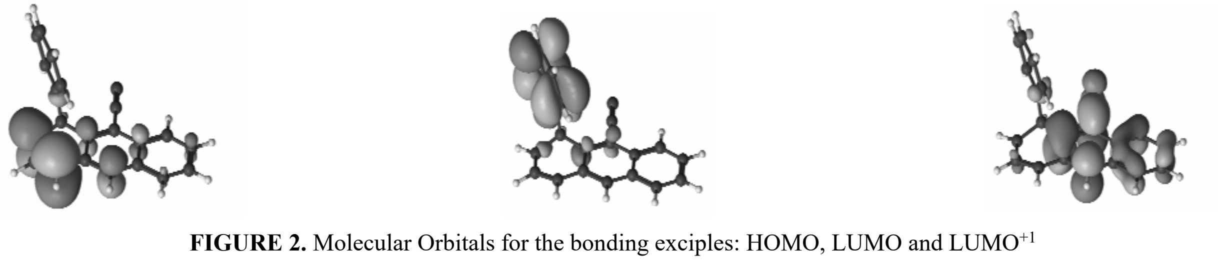

FIGURE 2. Molecular Orbitals for the bonding exciples: HOMO, LUMO and $LUMO^{+1}$

The orbitals involved in the main electronic transitions along the distance, the first excited state at 1.45 Å are mainly due to the charge transfer within the anthracene molecule, from the modified carbon ring to the remaining conjugated system and cyan group. The amount of transferred electrons is 0.56 at CAS and 0.23 at RAS level (Table 1). The second most important transition corresponds to the ground state. Otherwise the second excited state main contribution is a charge transfer between anthracene moiety to pyridine meanwhile the second most important configuration is due to the anthracene charge rearrangement (0.99 and 0.98 occupation numbers at CAS and RAS respectively). At longer distances though, the nature of the transition swap. So the first excited state is now principally due to a charge transfer between monomers.

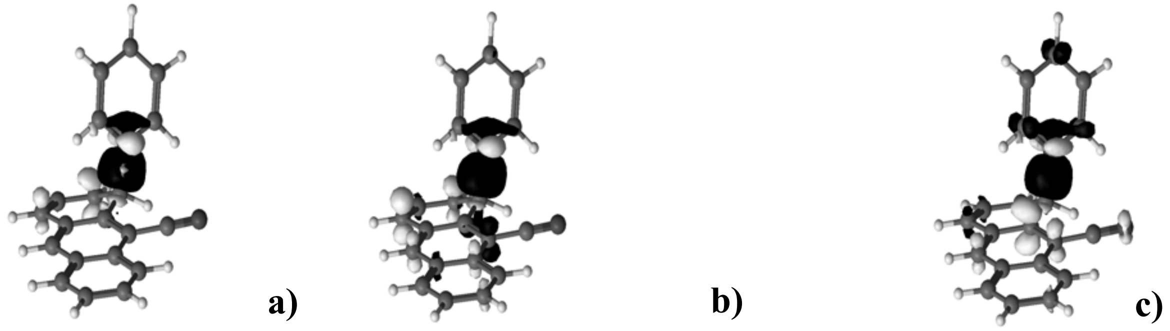

FIGURE 3. Electron density variance in Pyridine-9CA at the minimum in a) ground state b) first excited state c) second excited state. Black color indicates the gain of electron density and white color the lost of electron density.

The minimum presents a particular high dependence on an internal charge transfer that therefore must be relevant to host the new charge incoming from the pyridine. Plotting the electron density movements at 1.45 Å monomers distance, the charge is being accumulated around the bond formation area, specially in the first excited state (Figure 3). The same tendency of the electron density to be located around the ongoing bond can be noticed in the ground state as well, since there is still a high contribution of the HOMO-LUMO configuration. This can explain the breakage of the anthracene symmetry when the geometry is optimized in the ground state.

CONCLUSIONS

Pyridine and cyano-anthracene forms an exciplex complex, repulsive in the ground state, but binding in the first and second exited states. The deformation of the valence angle on the carbon atom from anthracene, which is nearest to pyridine, has been shown to be important for the formation of the bond.

ACKNOWLEDGEMENT

The work was supported by the Chamber of Commerce of Spain. Thanks to the Swedish National Infrastructure for Computing (SNIC) through LUNARC, the Center for Scientific and Technical Computing at Lund University.

REFERENCES

[1] R. A. Krueger and G. Blanquart, J. Phys. Chem. A 123, 1796−1806 (2019).
[2] A. A. Safonov, A. A. Bagaturyants and V. A. Sazhnikov, J. Phys. Chem. A 119, 8182−8187 (2015).
[3] V. A. Spata and S. Matsika, J. Phys. Chem. A 117, 8718–8728 (2013).
[4] V. A. Spata, W. Lee and S. Matsika, J. Phys. Chem. Lett. 7, 976-984 (2016).
[5] Y. Wang, O. Haze, J. P. Dinnocenzo, S. Farid, R. S. Farid and I. R. Gould, J. Phys. Chem. A 112, 13088–13094 (2008).
[6] Y. Wang, O. Haze, J. P. Dinnocenzo, S. Farid, R. Farid and I.Gould, J. Org. Chem. 72, 6970–6981 (2007)
[7] V. Veryazov, P Å Malmqvist, B.O. Roos, Int. J. Quant. Chem, 111, 3329-3338 (2011).
[8] M. J. Frisch, et al. Gaussian 03; Revision B.02, Gaussian, Inc.: Pittsburgh, PA, (2003).
[9] F. Neese, WIREs Comput. Mol. Sci. 2, 73–78 (2012).
[10] F. Aquilante, et al. J. Comput. Chem. 37, 506-541 (2016).

Computational Investigations of Bioinorganic Complexes: The Case of Calcium, Gold and Platinum Ions

Roberto Paciotti, Iogann Tolbatov, Alessandro Marrone, Loriano Storchi, Nazzareno Re, Cecilia Coletti [a)]

Dipartimento di Farmacia, Università G. d'Annunzio Chieti-Pescara, Via dei Vestini 31, I-66100 Chieti, Italy

[a)]Corresponding author: ccoletti@unich.it

Abstract. Metals play an important role in many biological systems, not to mention that their use in the formulation of drugs with novel modes of action has boosted the investigations aimed at elucidating their reaction mechanisms. At variance with carbon-based (or purely organic) molecules which nowadays may be described rather satisfactorily with molecular mechanics, molecules involving metals cannot do without a proper quantum mechanical treatment of the metal atoms. For this reason, in the last years we have been investigating a wealth of methods ranging from pure quantum mechanical ones to multilayered approaches which allow the calculation of detailed information related to the structure, the dynamics and the reaction mechanisms of metal-based biomolecules or drugs.

Introduction

Metals are characterized by an extremely rich and versatile chemistry that motivates the seminal importance of these elements in a wide range of fields like material sciences, electronics, catalysis, biology, medicine [1]. Life itself is not possible in the absence of essential metal elements. The physiological concentration of these elements in the biological media has allowed a classification of essential metals into two groups. In a first group is made of hard cations such as Na^+, K^+, Mg^{2+} and Ca^{2+} that are typically found at high concentrations (10–150 mM) in the biological fluids [2] because of their role in either regulation of ionic or electrical gradients (Na^+, K^+: heart beating, neuronal transmission), generation of cellular signaling based on ionic fluxes (Ca^{2+}, neuronal transmission, muscle contraction), or being structural constituents (Ca^{2+}: bone tissue, proteins; Mg^{2+}: DNA, proteins). A second group is formed by transition metals like Fe, Cu, Zn, and Mn in wider spread of oxidation states and hard-soft character that are present at much lower concentration and more typically exerting their physiological role through the binding at specialized proteins [2]. Beside constitutive elements, other transition metals have been recognized to form complexes with a specialized biological activity like Pt [3], Ru, and Au, [4] or to be intrinsically toxic like Hg and Cd [5].

Most of the "success" of metals in the biological world reflects the extraordinary versatility of the coordinative bond of inducing i) orientational and positional patterns for the binding ligands, ii) reciprocal modulation of the electronic structure of both metal center and bound ligands, iii) activation of naïve reactivity on ligands otherwise particularly challenging in aqueous media [6]. A complete elucidation of the structure and reactivity of bioinorganic systems may thus be very important to achieve an in-depth understanding of the structure-biological activity relationships and to provide for the basis for the rational design of new biologically active metal complexes [7]. Hence, to consolidate our understanding of the interaction of metals with and/or within biomolecules, the investigation of electronic structure and coordination of these elements is essential and paves the way to quantum chemistry approaches specifically addressed to the description of bioinorganic systems. Reduced models of the first coordination sphere are adequate and suitable to a full QM description, thus allowing to gain an accurate description of both the electronic and steric effects related to the metal coordination. In other cases, structural rearrangements

occurring in the biological target could affect the metal coordination, so that an adequate elucidation of the metal-target interaction can only be achieved by the QM investigation of large portions of the system and at the cost of dramatically increasing the computational burden. For this reason, multiscale, hybrid or multilayered methods (molecular dynamics, computational docking, QM/MM studies, etc.) are often essential to adequately capture all the aspects of metal-target interaction.

In this report, we discuss the application of multilayered computational schemes for the investigation of the metal elements interaction with biomolecules.

Calcium ions mediating the prion protein aggregation.

The possible role played by Calcium ions in the prion protein (PrP) assembly has been recently assessed [8,9]. The pathogenic conversion of natively folded prion protein (PrP^C) into misfolded or "scrapie" isoform (PrP^{Sc}) has been identified as the major event in the formation of prions: the infectious entities of transmissible spongiform encephalopathy (TSE) [10,11]. Among the most accredited molecular mechanisms, the nucleated conformational conversion (NCC) of Lindquist is consistent with most of the evidences about prion formation [12]. According to this model, the aggregation propensity of PrP^C turns out to be essential and a pathogenic stimulus of the $PrP^C \rightarrow PrP^{Sc}$ conversion can be newly interpreted as any structural event prompting PrP^C into an aggregation-prone status. Recently, we applied a computational approach to elucidate the aggregation propensity of PrP^C protein systems in response to an increased concentration of Ca^{2+} ion.[9] The combination of molecular dynamics and molecular interaction fields analyses allowed to accurately map the PrP surface and locate the calcium binding sites. By assessing the effect of increasingly [Ca^{2+}], our computational scheme allowed to spotlight a peculiar dinuclear Ca^{2+} binding motif (DBM) in proximity of the S2-H2 loop for [Ca^{2+}] > 5 mM [9]. By assuming an assembly scheme analogous to the one detected for the E200K mutant, we showed that the metal-bound PrP^C units may undergo a self-interaction process through the formation of DBM. In particular, we detected two protein portions, i.e. region 1 (hosting the DBM) and region3, together locating the majority of Ca^{2+} coordination sites and in close proximity to the complementary interfaces detected on E200K mutants [9,13]. In our hypothesis, the approach of two Ca^{2+} coordination sites may lead to a ligand rearrangement, and, eventually, to the formation of an interunit Ca^{2+} complex. Quantum chemical calculations were performed to investigate the thermodynamics of the possible Ca^{2+}-mediated condensation of reduced models of region 1 and 3 ([8, Figure 8]. The reaction of DBM with propanoate coordinating one $[Ca(H_2O)_5]^{2+}$ moiety resulted to be endergonic by 1.5 kcal/mol, thus corresponding to a slightly left-shifted equilibrium. This process would resemble the approach of DBM with a Ca^{2+}-bound carboxylate, i.e. any other Ca^{2+} coordinating group on PrP^C, inducing ligand exchange and release of a $[Ca(H_2O)_5]^{2+}$ moiety in the bulk. On the other hand, the coordination of a free propanoate group at DBM, i.e. a model of not coordinated Glu or Asp side chains coordinating at the dinuclear motif, was found to be largely favored with a free energy gain of –26 kcal/mol. Also, the process resembling the interunit approach between an uncoordinated Asp or Glu residue with an occupied Ca^{2+}-binding sites is exergonic by –21.5 kcal/mol, and, thus, represents a further example of Ca^{2+}-mediated interaction occurring in the PrP self-assembly.

Gold(I) NHC complexes targeting "soft" aminoacids.

Neutral N-heterocyclic carbene gold(I) compounds, such as [Au(I)(NHC)Cl], are extensively utilized in medicinal chemistry as promising antitumor agents [14]. Unlike to platinum-based drugs the primary target of which is DNA, these gold-based cytotoxic agents modify selected proteins disrupting their normal functioning. Several recent studies have investigated the interaction of gold carbene compounds with a plethora of proteins [15,16], yet the detailed mechanisms of reaction with protein side chains still lack. In order to shed light on the reactivity of [Au(I)(NHC)Cl] with protein side chains, we have performed DFT calculations on the thermodynamics and kinetics of their reaction with water and various nucleophiles as model of the probable protein binding sites. Our results permit to determine an order of reactivity for its binding to protein residues: "Sec > Lys > activated-Gln/Asn > activated- Cys > Cys > Met > Arg > N-terminal > Hys > Gln/Asn ≈ Glu/Asp > H_2O" [17]. The lowest barriers are computed for Cys and Sec (13-18 kcal/mol), indeed, they agree with the experimental evidence demonstrating the prevalent binding of the $(Me_2Imy)Au^+$ moiety to the selenocysteine and cysteine residues of thioredoxine reductase. Comparatively low barriers calculated for the N-based nucleophile sites, lysine, arginine and N-terminal amine (16-

20 kcal/mol) suggest little discrimination in terms of reactivity within either S/Se or N-based nucleophile sites, indicating that that these N-based sites could also bind an $Au(NHC)^+$ fragment whenever cysteine or selenocysteine residues are absent or less accessible/buried.

Gold(III) complexes blocking the glycerol-transport mediated by AQP3

The activity of Au(III) bipyridyl complexes as selective inhibitors of the human aquagliceroporin-3 (AQP3) has been recently ascertained to be based on the coordination at a specific AQP3 cysteine residue [18]. The control of the transport of small molecules across cell membrane makes these channel proteins suitable anticancer targets [19], although a full elucidation of the chemical processes overseeing the structural changes required to block the AQP3 channel is still lacking. Thus, we designed a multilayered computational scheme combining density functional theory, classical molecular dynamics and quantum mechanical/molecular mechanics approaches to investigate the interaction of the $[Au(bipy)Cl_2]^+$ (Aubipy) with AQP3 [20]. Our calculations clearly indicated that Aubipy binds at AQP3 periplasmic pore in the chloro-hydroxo form initially through π-stacking interactions involving the metal center. The non-coordinative binding is crucial in making energetically affordable the approach of Au(III) center to the final (coordinative) cysteine site. The same computational workflow was then applied to investigate the binding proprieties of a series of phenantroline complexes of Au(III) [21]. QM calculations evidenced how these complexes are stable and the periplasmic pore of AQP3 in their dichloro form in physiological conditions. This study corroborated the importance of non-coordinative binding at AQP3 and showed at which extent decoration of the phen ligand could influence the biological activity of these complexes [21].

Platinum-based anticancer complexes

Cisplatin, *cis*-diamminedichloroplatinum(II), and its derivatives are the first and more successful metal-based complexes to be used in antitumor therapy [22]. Nowadays cisplatin still represents the reference molecule for a large number of platinum(II) and platinum(IV) compounds, being designed and tested for tumor growth inhibition. Binding of cisplatin to DNA is ultimately responsible for cell death and occurs via stepwise replacement of chlorido ligands by a solvent assisted mechanism. Besides DNA, cisplatin is known to bind proteins and small biomolecules through sulfur or nitrogen atoms [23]. Given the high interest for cisplatin reactions with biomolecules, a considerable number of mechanistic studies have been devoted to clarify ligand substitution processes of platinum(II) complexes. To fully elucidate these mechanisms and in general interactions of cisplatin with biomolecular targets such natural aminoacids at a molecular level, in the last years we focused on the combined experimental-theoretical characterization of cisplatin-related complexes formed in aqueous solution, isolating them in a highly diluted environment [24-27]. Such conditions (obtained by electrospray ionization, used to deliver ions formed in solution into the gas phase, where they are structurally interrogated by vibrational "action" spectroscopy) allow indeed a detailed characterization of the species involved in the reaction mechanism when supported by very high level (up to post Hartree-Fock methods coupled with large basis sets and the use of anharmonic corrections for the determination of vibrational frequencies) quantum mechanical calculations, which permit the identification of the relevant species (isomers and even conformers) [28] formed in the interaction of cisplatin with simple biomolecules [26-29]. As a result, we were able to identify and characterize for the first time an elusive intermediate in the hypothesized mechanism of action of cisplatin with simple biomolecules, i.e. the encounter complex in the Eigen-Wilkins mechanism [30-32].

In turn, the clarification of this mechanism motivated us to deepen some aspects of the reactivity of cisplatin derivatives, already in use or in their first steps of in vivo/in vitro research as cytotoxic agents [33]. All these studies were performed with state of the art DFT functionals and post Hartree-Fock methods, which allow to calculate kinetic barriers and thermodynamic stabilities within a chemical accuracy (1 kcal/mol ca.) [34]. We started by investigating the possibility of the interaction of carboplatin, cis-diammine(cyclo-butane-1,1-dicarboxylato)-platinum(II), a second-generation platinum-based anticancer agent, with chloride [35] or carbonate ions [36], relevant in biological media. More recently we investigated in details the reduction mechanism of Pt(IV) complexes [37], which are thought to act as prodrugs, leading to cisplatin in the strongly reducing environment of tumor cells, limiting, in such a way, undesired reactions with biological molecules, responsible for many of the severe side effects of cisplatin and phenomena of acquired resistance to the therapy.

REFERENCES

1. H. B. Gray PNAS, **100**, 3563-3568 (2003).
2. R. R. Crichton Biological Inorganic Chemistry–An Introduction First edition 2008, Elsevier.
3. J. Reedijk PNAS **100**, 3611-3616 (2003).
4. (a) B. K. Keppler, M. Henn,U. M. Juhl, M. R. Berger, R. Niebl, F. E. Wagner, Progr. Clin. Biochem. Med. **10**, 41-69 (1989). (c) S. Spreckelmeyer, C. Orvig, A. Casini Molecules **19**, 15584-15610 (2014).
5. M. Valko, H. Morris, M. T.D. Cronin. Curr. Med. Chem. 12, Issue 10 (2005).
6. P. J. Deuss, R. Denheeten, W. Laan, P.C. J. Kamer, Chem. Eur. J. **17**, 4680-4698 (2011).
7. S. Komeda, A. Casini Curr. Top. Med. Chem. **12**, 219-235 (2012).
8. L. Storchi, R. Paciotti, N. Re, A. Marrone, Proteins, **83**, 1751-1765 (2015).
9. A. Marrone, N. Re, L. Storchi PLoS ONE **11**, e0168039 (2016).
10. S. B. Prusiner New Engl. J. Med. **344**, 1516–1526 (2001).
11. S. B. Prusiner Proc. Natl. Acad. Sci. USA **95**, 13363–13383 (1998).
12. T.R. Serio, A.G. Cashikar, A.S. Kowal, G.J. Sawicki, J.J. Moslehi, L. Serpell et al. Science **289**, 1317–1321 (2000).
13. R. Paciotti, L. Storchi, A. Marrone Proteins **87**, 51-61 (2019).
14. I. Ott, Coord. Chem. Rev. **253**, 1670-1681 (2009).
15. A. Bindoli, M.P. Rigobello, G. Scutari, C. Gabbiani, A. Casini, L. Messori, Coord. Chem. Rev. **253**, 1692-1707 (2009).
16. B. Bertrand, A. Casini, Dalton Trans. **43**, 4209-4219 (2014).
17. I. Tolbatov, C. Coletti, A. Marrone, N. Re, Int. J. Mol. Sci. **20**, 820:1-15 (2019)
18. G. Soveral, S. Nielsen, A. Casini, *Aquaporins in health and disease: new molecular targets for drug discovery*, Eds. CRC Press, Taylor & Francis Group, **2016**.
19. M. C. Papadopoulos, S. Saadoun, Biochim. et Biophys. Acta **1848**, 2576–2583 (2015)
20. V. Graziani, A. Marrone, N. Re, C. Coletti, J.A. Platts, A. Casini, Chem. Eur. J. **23**, 13802-13813 (2017).
21. M. N. Wenzel, A. F. Mósca, V. Graziani, B. Aikman, S. R. Thomas, A. De Almeida, J. A. Platts, N. Re, C. Coletti, A. Marrone, G. Soveral, A. Casini, Inorg. Chem. **58**, 2140-2148 (2019)
22. S.E. Sherman, S.J. Lippard, Chem. Rev. **87**, 1153-1181 (1987).
23. T. Boulikas, M. Vougiouka, Oncol. Rep. **10**, 1663 (2003).
24. D. Corinti, C. Coletti, N. Re, B. Chiavarino, M.E. Crestoni, S. Fornarini, Chem. Eur. J. **22**, 3794-3803 (2016)
25. R. Paciotti, C. Coletti, N. Re, D. Scuderi, B. Chiavarino, S. Fornarini, M.E. Crestoni, Phys. Chem. Chem. Phys. **17** (2015), 25891-25904
26. R. Paciotti, D. Corinti, A. De Petris, A. Ciavardini, S. Piccirillo, C. Coletti, N. Re, P. Maitre, B. Bellina, P. Barran, B. Chiavarino, M.E. Crestoni, S. Fornarini, Phys. Chem. Chem. Phys. **19** (2017), 26697-26707
27. D. Corinti, R. Paciotti, N. Re, C. Coletti, B. Chiavarino, M.E. Crestoni, S. Fornarini, Pure and Applied Chemistry, doi: https://doi.org/10.1515/pac-2019-0110
28. D. Corinti, A. De Petris, C. Coletti, N. Re, B. Chiavarino, M.E. Crestoni, S. Fornarini, Chem.Phys.Chem. **18**, 318-325 (2017)
29. A. De Petris, A. Ciavardini, C. Coletti, N. Re, B. Chiavarino, M.E. Crestoni, S. Fornarini, J. Phys. Chem. Lett., **4**, 3631-3635 (2013)
30. C. Coletti, N. Re, D. Scuderi, Ph. Maitre, B. Chiavarino, S. Fornarini, F. Lanucara, R.K.Sinha, M.E. Crestoni, Phys.Chem.Chem.Phys. **12**, 13455-13467 (2010)
31. D. Corinti, C. Coletti, N. Re, S. Piccirillo, M. Giampà, M.E. Crestoni, S. Fornarini, RSC Adv **26**, 15877-15884 (2017)
32. D. Corinti, C. Coletti, N. Re, R. Paciotti, Ph. Maitre, B. Chiavarino, M.E. Crestoni, S. Fornarini, Int. J. Mass Spectr., 435 (2019), 7-17
33. V. Graziani, C. Coletti, A. Marrone, N. Re, J. Phys. Chem. A **120**, 5175-5186 (2016)
34. J. K.-C. Lau, D. V. Deubel, J. Chem. Theory Comput. **2**, 103–106 (2006)
35. A. Ciancetta, C. Coletti, A. Marrone, N. Re, Dalton Trans. **41**, 12960-12969 (2012)
36. A. Ciancetta, C. Coletti, A. Marrone, N. Re, Theor. Chem. Acc. **129**, 757-769 (2011)
37. I. Tolbatov, C. Coletti, A. Marrone, and N. Re, Inorg. Chem. **57**, 3411-3419 (2018)

Molecular Dynamics Simulation of Myopathy-related Mutant FHL1 in Water and Analysis of Structure Stabilization

H. Takeuchi[1], H. Okajima[1], H. Itoga[1], K. Nobuoka[1], H. Yamada[1, 2], T. Miyakawa[1], R. Morikawa[1], Y. K. Hayashi[3], and M. Takasu[1, a)]

[1]*Tokyo University of Pharmacy and Life Sciences, Japan*
[2]*Institute of Statistical Mathematics, Japan*
[3]*Tokyo Medical University, Japan*

[a)]Corresponding author: takasu@toyaku.ac.jp

Abstract. Mutations in the *FHL1* gene can cause X-linked hereditary myopathy, which causes one of the rarest intractable diseases. The age of the disease onset is quite variable from early infancy to adulthood, and the patients show progressive muscle weakness and atrophy. The FHL1 protein is constituted by four and a half LIM domains. Each LIM domain contains two zinc fingers, which contribute to the structural stability of the LIM domain. A change in the cysteine or histidine residues in the 2nd LIM domain (LIM2) is closely associated with the disease severity. Therefore, LIM2 is suggested to have an essential role in maintaining the structure of FHL1. In this study, molecular dynamics simulation was performed on molecular models consisting of LIM1 and LIM2 of wild and mutant FHL1. We calculated the extent of distortion of zinc finger structure and measured the distance between zinc atom and Cα atom of zinc-coordinated residues. Our analysis showed that the correlation between these two quantities is larger in the mutants associated with severe myopathy.

INTRODUCTION

Hereditary myopathy is one of the rarest diseases and its symptoms include progressive muscle weakness and muscle atrophy[1]. The mutations in the *FHL1* gene are reported to be one of the causative genes for hereditary myopathy[2]. More than 40 types of variants in the *FHL1* gene have been reported[2]. There are a few hypotheses, which suggest that some functions of FHL1 protein are inactivated or regulated by mutations of the *FHL1* gene[2]. In addition, it is widely known that clinical symptoms are related to the type of variants. C101F, H123Y, C132F, C150Y are known to be variants that can cause severe myopathy[2, 3]. FHL1 protein contains four and a half LIM domains. A schematic diagram of FHL1 is shown in Fig. 1.

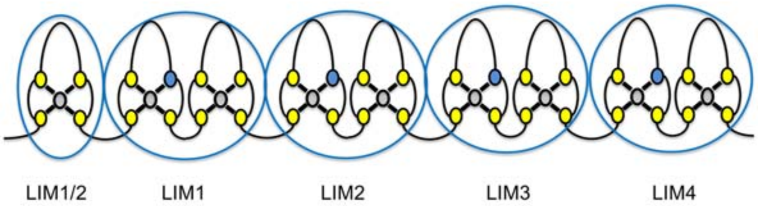

FIGURE 1. FHL1 structure. Yellow is cysteine, blue is histidine, and gray is zinc (Zn).

Each LIM domain is composed of two zinc fingers. They contribute to the structural maintenance of each LIM domain, and zinc finger of LIM2 domain is thought to be important for maintaining the three-dimensional structure of FHL1[2] because most cases of reported muscle diseases carry mutations of cysteine or histidine residue in LIM2.

Previously, Chen et al.[4] performed simulations using the structures of 98th to 158th residues and two zinc atoms of LIM2 domain, obtained by removing the loop region at the terminal. They reported that mutations in the LIM2 domain could cause aggregation of atoms in the protein, but mutations in the LIM2 domain had not caused significant distortions in the protein structure. Generally, mutant proteins are considered to have an increased tendency to aggregate[4].

In this study, we performed molecular dynamics simulations of FHL1 protein structure, consisting of the LIM1 and LIM2 domains in aqueous solution. Moreover, when we analyzed the distance $D_{\text{Zn-c}\alpha}$ between the zinc atom and Cα atom of each zinc-coordination residue, a difference was found for $D_{\text{Zn-c}\alpha}$ when mutation was introduced in this residue[5]. We analyzed the correlation between this change in $D_{\text{Zn-c}\alpha}$ and the change in zinc finger structure.

Simulation Methods

From an all-atom model of FHL1 protein, LIM1 and LIM2 domains (LIM1 + LIM2) were extracted, and the ff99SB-ILDN force field[6] was applied. Further, for zinc finger atoms, CCCC of ZAFF (Zinc Amber Force Field)[7] and force field of CCCH (C: cysteine, H: histidine)[7] were used.

LIM1 + LIM2 were arranged in a cuboid system with a periodic boundary condition. The TIP3P water model was added to these systems. We obtained the LIM1 (PDBID: 2CUP) and the LIM2 (PDB ID: 1X63) structures, determined by solution NMR, in order to create an initial structure of LIM1 + LIM2. The LIM1 + LIM2 structure is prepared using Modeller[8-11], which is a software for modeling protein structures. The Swiss-PdbViewer[12] was used to generate the mutant structure. Solvent and ions were added to the system containing LIM1 + LIM2 using AmberTools[13]. Following which, energy minimization was performed using GROMACS ver. 5[14, 15]. We performed MD simulation in advance for relaxation with NVT (constant volume and 300 K) and NPT (1 bar and 300 K) conditions and then performed under conditions for 500 ns.

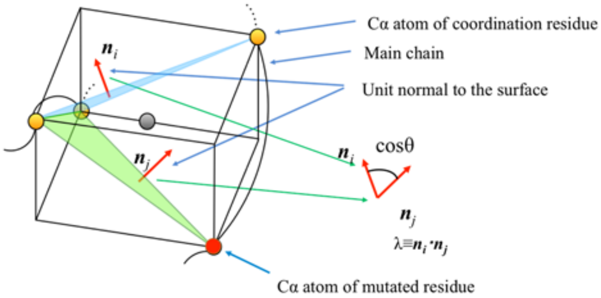

FIGURE 2. The schematic representation of determination of λ.

Two major analyses were carried out in this study. The first one was the distance from the zinc atom to the Cα atom of the residues that coordinate with Zn, denoted by $D_{\text{Zn-c}\alpha}$. The second analysis was the inner product λ of the normal of the dihedral two-faced surface consisting of Cα atoms of the four residues coordinating with the zinc atom (Fig. 2). In order to analyze whether the changes in $D_{\text{Zn-c}\alpha}$ could be related to the changes in the structure of the zinc finger, the correlation coefficient between $D_{\text{Zn-c}\alpha}$ and λ was determined.

The correlation ρ between $D_{\text{Zn-c}\alpha}$ and λ which shows structural stability between changing of $D_{\text{Zn-c}\alpha}$ and zinc finger is expressed by equation (1),

$$\rho(t_1,t_2)=\frac{\left\langle\left(\lambda(t)-\langle\lambda(t)\rangle_s\right)\left(D_{\text{Zn-c}\alpha}(t)-\left\langle D_{\text{Zn-c}\alpha}(t)_s\right\rangle\right)\right\rangle_s}{\sqrt{\left\langle\left(\lambda(t)-\langle\lambda(t)\rangle_s\right)^2\right\rangle_s\left\langle\left(D_{\text{Zn-c}\alpha}(t)-\langle D_{\text{Zn-c}\alpha}(t)\rangle_s\right)^2\right\rangle_s}}. \quad (1)$$

Here, $\langle\ \rangle_s$ represents an average of samples at times t_1 to t_2. When the value of |ρ| is close to 1, the Cα atom is displaced in the direction of the plane, which includes the Cα, and thus the correlation between the changes in $D_{\text{Zn-c}\alpha}$ and the changes in λ is large. So, they move nearly perpendicular to the surface as $D_{\text{Zn-c}\alpha}$ changes. Suppose that the same change in $D_{\text{Zn-c}\alpha}$ is recognized. Since the stability of the tetracoordinated structure depends on the dihedral angle constituting the tetrahedron, the structure is stable when $D_{\text{Zn-c}\alpha}$ is changed while maintaining the dihedral angle. This is the case of small |ρ|. On the other hand, when the dihedral angle changes with the $D_{\text{Zn-c}\alpha}$, the tetrahedral structure is distorted and unstable. This is the case of large |ρ|.

Criteria for determining the degree of correlation vary depending on the application, but the following criteria are widely used.

|ρ| = 0 to 0.2: almost no correlation, |ρ| = 0.2 to 0.4: weak correlation, |ρ| = 0.4 to 0.7: moderate correlation,
|ρ| = 0.7 ~ 1: strong correlation

In this study, the structures of five types of FHL1 were simulated including wild type, C101F, C104R, H123Y and C126Y. Among them, C101F and H123Y were reported to be associated with severe myopathy[2, 3].

RESULTS

The results for $D_{Zn\text{-}c\alpha}$ are shown in TABLE 1. For C101F, both the mean value and the fluctuation were considerably different, and the structure may be largely changed compared with the wild type.

TABLE 1. Average and standard deviation of $D_{Zn\text{-}c\alpha}$ for wild type 1) and mutant 2)

Residue number	Average and standard deviation (nm)	Average difference (nm)	Ratio to wild type standard deviation (fluctuation)
101	1) 0.4663±0.0072	-0.2319	18.3194
	2) 0.6982±0.1319		
104	1) 0.4017±0.0109	-0.1103	8.3211
	2) 0.5120±0.0907		
123	1) 0.4566±0.0106	0.0205	2.5
	2) 0.4361±0.0265		
126	1) 0.4699±0.0071	-0.1384	7.9437
	2) 0.6083±0.0564		

It is found that the fluctuations of each mutant are larger than that of the wild type. However, the correlation between the severity and structural change was not found. The result of λ is shown in Table 2. C101F shows larger average value and fluctuation than the wild type, and the structure may be largely changed compared with the wild type.

TABLE 2. Average and standard deviation of λ

Model	Average and standard deviation of λ (Average degrees)	Difference of λ (degrees)	Ratio to wild type standard deviation (fluctuation)
Wild	-0.8822±0.0184 (152.9)	0	1
C101F	-0.5582±0.2799 (123.9)	0.3360(29.0)	15.21
C104R	-0.9055±0.0429 (154.9)	-0.0233(-2.0)	2.33
H123Y	-0.8622±0.0333 (149.6)	0.02(3.3)	1.81
C126Y	-0.8884±0.0309 (152.7)	-0.0062(0.2)	1.68

Finally, we show the results of the correlation between $D_{Zn\text{-}c\alpha}$ and λ in Fig. 3. The relationship between $D_{Zn\text{-}c\alpha}$ and λ was shown graphically where the vertical axis is $D^{(n)}$ (($D_{Zn\text{-}c\alpha}$-<$D_{Zn\text{-}c\alpha}$>) / standard deviation), and the horizontal axis is $\lambda^{(n)}$, in accordance with the equation for finding the correlation coefficient ρ. ((λ-<λ>) / standard deviation)

In addition, there were cases where the correlation coefficient was divided into multiple time intervals for mutant types in accordance with the changes in $D_{Zn\text{-}c\alpha}$. TABLE 3 shows that there was no major structural change, and the value of ρ was low in wild type.

TABLE 3. Correlation coefficient ρ (t_1, t_2) for t_1=0 ns, t_2=500 ns of wild type

Residue number	Correlation coefficient
101	0.0482
104	-0.1323
123	-0.0834
126	-0.0137

TABLE 4. Correlation coefficient ρ (t_1, t_2) of mutants

Mutants	Correlation coefficient ρ
C101F (0-200 ns)	-0.693
200-230 ns	-0.192
230-250 ns	-0.468
250-270 ns	-0.541
270-280 ns	-0.816
280-500 ns	-0.233
C104R (0-100 ns)	-0.442
100-420 ns	-0.093
420-550 ns	-0.738
550-600 ns	-0.214
H123Y (0-500 ns)	-0.484
C126Y (0-500 ns)	-0.049

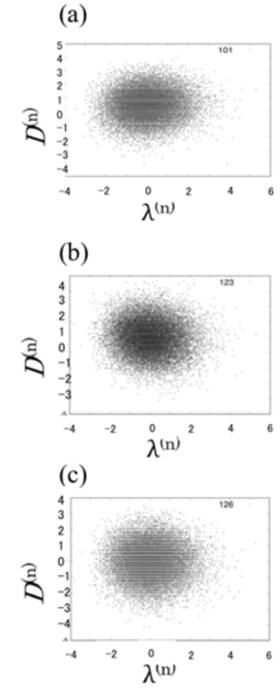

FIGURE 3. Correlation between $D_{Zn\text{-}c\alpha}$ and λ of wild type. (a) is C101F, (b) is H123Y, (c) is C126Y.

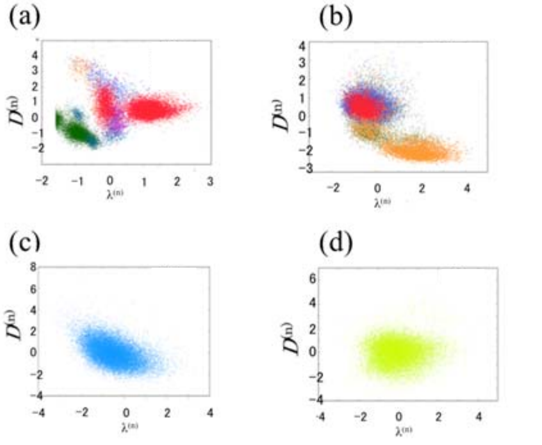

FIGURE 4. Correlation between $D_{\mathrm{Zn\text{-}c}\alpha}$ and λ of mutant. (a) is C101F, (b) is C104R, (c) is H123Y, (d) is C126Y.
In (a), green is 0-200 ns, yellow green is 200-230 ns, blue is 230-250 ns, purple is 250-270 ns, orange is 270-280 ns, and red is 280-500 ns.
In (b), green is 0-100 ns, blue is 100-420 ns, orange is 420-550, red is 550-600 ns.

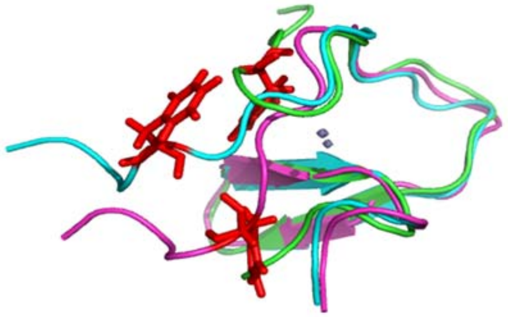

FIGURE 5. Structural changing of C101F. Green is initial structure of C101F. Light blue is during the structural change. Purple is C101F after structural changes. Red is 101st residue.

In TABLE 4 and Fig. 4, high correlation values are found for C101F and H123Y among the variant types. With C101F, we confirmed the structural change. The structure of C126Y was roughly the same as wild type. As shown in Fig. 5, changes in the periphery of the mutated residue shown in red were separated from the vicinity of the zinc atom.

DISCUSSION

In this study, we performed molecular dynamics simulations of FHL1 protein variants, and analyzed the structural stability of the wild type and compared it with that of the multiple variants. The results showed that the change in $D_{\mathrm{Zn\text{-}c}\alpha}$ is one of the factors that could distort zinc finger structure in the variants that are known to produce clinically severe forms of myopathy. Our results indicate that zinc finger structure is unstable in the mutants related to the severe forms of the disease because the fluctuation of $D_{\mathrm{Zn\text{-}c}\alpha}$ affects the maintenance of appropriate bond angle of coordinate bonds in the zinc finger.

As a future work, we will also perform the docking simulation of molecules that interact with LIM protein.

REFERENCES

1. T. Komagamine, M. Kawai, N. et al. J. Neurol. Sci. **318**, 163–167 (2012).
2. T. Shathasivam, T. Kislinger, and A. O. Gramolini. J. Cell. Mol. Med. **14**, 2702–2720 (2010).
3. S. Shalaby, K. Y. Hayashi, I. Nonaka, S. Noguchi, I. Nishino. Neurology. **72**, 375–376 (2009).
4. H. D. Chen, H. W. Raskind, et al. J. Neurol. Sci. **296**, 22–29 (2010).
5. H. Takeuchi, H. Okajima, et al, Proc. 8th Int. Conf. on Biosci. Biochem. and Bioinfo. 1–5 (2018).
6. K. Lindorff-Larsen, S. Piana, et al, Proteins. **78,** 1950–1958 (2010).
7. B. M. Peters, Y. Yang, et al, J. Chem. Theory Comput. **6,** 2935–2947 (2010).
8. B. Webb, and A. Sail. Curr. Protoc. Bioinformatics. 5.6.1–5.6.32. (2014).
9. A. M. Marti-Renom, A. Stuart, et al, Annu. Rev. Biophys. Biomol. Struct. **29,** 291–325 (2000).
10. A. Sali, and T. L. Blundell, J. Mol. Biol. **234,** 779–815 (1993).
11. A. Fiser, K. R. Do, and A. Sali, Protein Science. **9,** 1753–1773 (2000).
12. N. Guex, and M. C. Peitsch, Electrophoresis. **18,** 2714–2723 (1997).
13. A. D. Case, S. D. Cerutti, et al. AMBER 2017, University of California, San Francisco (2017).
14. S. Pronk, S. Páll, R. Schulz, et al, Bioinformatics. **29,** 845–854 (2013).
15. S. Páll, J. M. Abraham, C. Kutzner, B. Hess, and E. Lindahl, Proc of EASC 2015 LNCS. **8759,** 3–27 (2015).

Modified AMBER Force-Field (FUJI) Parameters for Sulfated and Phosphorylated Tyrosine Residues: Development and Application to CCR5-Derived Peptide Systems

Takefumi Yamashita, [1, a)] Ryo Okajima, [1, 2] Kazuhiro Miyanabe, [3]
and Kouhei Tsumoto [3, 4, 5]

[1]*Laboratory for Systems Biology and Medicine, Research Center for Advanced Science and Technology, the University of Tokyo, 4-6-1 Komaba, Meguro-ku, Tokyo 153-8904, Japan.*
[2] *Department of Basic Science, Graduate School of Arts and Sciences, the University of Tokyo 3-8-1 Komaba, Meguro-ku, Tokyo 153-8902, Japan.*
[3] *Department of Chemistry and Biotechnology, School of Engineering, the University of Tokyo, 7-3-1 Hongo, Bunkyo-ku, Tokyo 113-8656, Japan.*
[4] *Department of Bioengineering, School of Engineering, the University of Tokyo, 7-3-1 Hongo, Bunkyo-ku, Tokyo 113-8656, Japan.*
[5] *Laboratory of Medical Proteomics, Institute of Medical Science, the University of Tokyo, 4-6-1 Shirokanedai, Minato-ku, Tokyo 108-8639, Japan.*

[a)]Corresponding author: yamashita@lsbm.org

Abstract. Tyrosine phosphorylation and tyrosine sulfation are important post-translational modifications in biological systems. In this study, we developed FUJI force-field parameters for sulfo-tyrosine and phospho-tyrosine residues to investigate the effect of tyrosine modification. Then, we applied the new parameters to molecular dynamics simulations of CCR5-derived peptide (pep1) systems. We found that the effect of phosphorylation on the structure was much greater than that of sulfation. In addition, we characterized the effects of sulfation and phosphorylation on the interaction between pep1 and its antibody 4B08 by using the FUJI force-field parameters developed here.

INTRODUCTION

Post-translational modifications play various important roles in biological systems. One of the most common and important modifications is the tyrosine phosphorylation [1]. A tyrosine kinase catalyzing phosphorylation, BCR–ABL, causes chronic myeloid leukemia, and its inhibitor can be used as a therapeutic agent [2]. The tyrosine sulfation is also biologically important; sulfation of CC-chemokine receptor 5 (CCR5) initiates the entry of HIV-1 into the target immunological cell. Recently, Miyanabe et al. [3] studied the effect of tyrosine sulfation on the interaction between a CCR5-derived peptide (denoted by pep1), which includes sulfation-targeting tyrosine residues (Y4 and Y5), and its antibody, 4B08, by using various different experiments and molecular dynamics (MD) simulations. Interestingly, Cormier et al. [4] found that the effect of CCR5 sulfation was completely different from that of CCR5 phosphorylation, even though the sulfate group is chemically similar to the phosphate group.

To characterize the effect of sulfation and phosphorylation by using MD simulation, an accurate force field describing not only unmodified amino acid residues but also sulfo-tyrosine (sTyr, sY) and phospho-tyrosine (pTyr, pY) is necessary. Previously, we found that FUJI, a modified version of the AMBER force field [5], was one of the most reliable force fields for unmodified proteins [6-9]; thus, we applied FUJI to many unmodified protein systems

[10-14]. However, FUJI did not have parameters for sTyr and pTyr. In this study, we developed FUJI force-field parameters for sTyr and pTyr and then applied them to the pep1 and pep1–4B08 complex systems.

DEVELOPMENT OF FORCE-FIELD PARAMETERS

The FUJI force-field parameters for sTyr and pTyr were developed. To obtain sTyr and pTyr models consistent with unmodified amino acid residue models, partial charges derived through the standard AMBER-style procedure [15, 16] are necessary. Whereas the partial charges of pTyr were taken from Ref. [15], those of sTyr were newly derived (Table 1). Here the sTyr residue capped with ACE and NME was used to calculate the partial charges. Two conformations (α-helix and β-strand) were energetically optimized, and the electrostatic potentials were calculated with the HF/6-31G(d) level quantum chemistry method. All of the calculations were performed with the Gaussian 09 program. Then, a two-step RESP fit was conducted through the RED program [17]. All other parameters for sTyr and pTyr were derived through the FF–FOM method [18], taking the main chain parameters from Ref. [5].

TABLE 1. Partial charges of sTyr, pTyr, and Tyr

sTyr		**pTyr**		**Tyr**	
Atom	Charge	Atom	Charge	Atom	Charge
CA	0.0828	CA	0.141279	CA	−0.0014
HA	0.0981	HA	0.027982	HA	0.0876
CB	0.0257	CB	−0.251171	CB	−0.0152
HB1, HB2	0.0137	HB1, HB2	0.081930	HB1, HB2	0.0295
CG	−0.0078	CG	0.073446	CG	−0.0011
CD1, CD2	−0.2224	CD1, CD2	−0.198084	CD1, CD2	-0.1906
HD1, HD2	0.1453	HD1, HD2	0.112503	HD1, HD2	0.1699
CE1, CE2	−0.1509	CE1, CE2	−0.254266	CE1, CE2	−0.2341
HE1, HE2	0.1494	HE1, HE2	0.161606	HE1, HE2	0.1656
CZ	0.3166	CZ	0.477009	CZ	0.3226
OH	−0.4533	OH	−0.557944	OH	−0.5579
S	1.1855	P	1.380672	HH	0.3992
O1S, O2S, O3S	−0.6166	O1P, O2P, O3P	−0.943550		

EFFECTS OF MODIFICATION ON CCR5-DERIVED PEPTIDE SYSTEMS

First, we applied the new FUJI force field to a short CCR5-derived peptide, pep1, the sequence of which is DINYYTSEP. To compare the effect of sulfation with the effect of phosphorylation, we investigated three modification states: unmodified, sulfated, and phosphorylated. In sulfo-pep1 and phospho-pep1, both Y4 and Y5 were modified (Fig. 1a). For each modification state, five MD simulations were conducted for 600 ns under isothermal–isobaric conditions (298 K and 1 atm), where the Nose–Hoover thermostat (τ_T = 2 ps) and Berendsen barostat (τ_p = 10 ps) were used. The last 480 ns of data were used for the subsequent statistical analyses. Standard errors were calculated over the five sets of data. The pep1 system consists of one peptide, 1853 water molecules, 7 Na^+ ions, and 5 Cl^- ions; the sulfo-pep1 system consists of a peptide, 2173 water molecules, 10 Na^+ ions, and 6 Cl^- ions; and the phospho-pep1 system consists of a peptide, 2171 water molecules, 12 Na^+ ions, and 6 Cl^- ions. The FUJI and TIP3P models were adopted to describe protein and water, respectively. Initial structures were obtained by computationally modifying a crystal structure (PDB entry: 5YD3). The long-range electrostatic interaction was calculated with the particle-mesh Ewald method. The linear constraint solver method was used to constrain the bond lengths, and the MD time step was set to 3 fs. All MD simulations were performed with GROMACS ver. 4.6.7 [19].

To characterize the structure simply, we calculated the distribution of the distance between the center of mass of the benzene ring of Y4 and that of Y5 (Fig. 1b). This is denoted as the ring–ring distance. Sulfation shifts the distribution to the long-distance side. In particular, the distribution for pep1 has a shoulder at 0.45 nm, but the sulfation diminishes it significantly, probably due to the electrostatic repulsion between the two sulfate groups. Whereas the distribution for sulfo-pep1 is similar to that for unmodified pep1, phosphorylation changes the shape of the distribution drastically. The circular variance analysis [14] also shows that phosphorylation rigidifies the main chain motion more significantly than sulfation (data not shown). These results indicate that the difference between the dianionic and monoanionic effects is more significant than one might expect, which is consistent with previous

results [20]. In addition, we tested whether the naïve Bayes classifier can distinguish the three modification states only based on the ring–ring distance distribution (Fig. 1b). The procedure was the same as in Ref. [21], except that the input data are the ring–ring distances of modified pep1 systems. Three of six short trajectories were correctly classified for the sulfated system (Fig. 1c); all short trajectories were correctly classified for the phosphorylated system (Fig. 1d). This is because phosphorylation has a greater effect on the ring–ring distance distribution than sulfation.

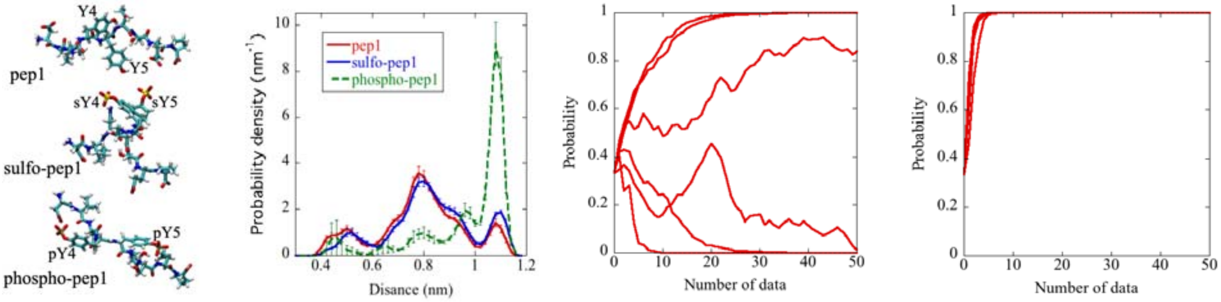

(a) (b) (c) (d)

FIGURE 1. (a) Snapshots of modified and unmodified peptides. (b) Distributions of ring–ring distance. Posterior probability that the classifier correctly classifies the given distance data of (c) sulfo-pep1 and (d) phospho-pep1.

Next, we applied the developed force field to MD simulations of the pep1–antibody complex systems, where anti-pep1 antibody, 4B08, has a single-chain variable fragment (scFv) form. The MD simulation conditions for the pep1–4B08 complex system were the same as for the pep1 system discussed above. The unmodified system consists of one peptide, one scFv, 11,354 water molecules, 34 Na^+ ions, and 34 Cl^- ions; the sulfated system consists of a peptide, one scFv, 11,734 water molecules, 37 Na^+ ions, and 35 Cl^- ions; and the phospholyrated system consists of a peptide, one scFv, 11,733 water molecules, 39 Na^+ ions, and 35 Cl^- ions.

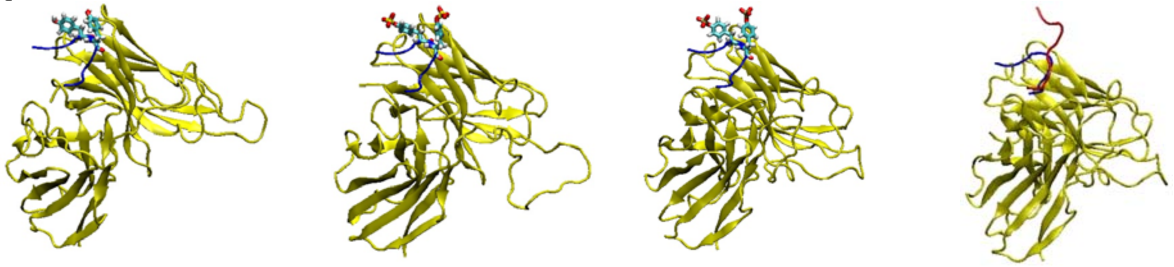

(a) (b) (c) (d)

FIGURE 2. Snapshots of MD simulations for (a) unmodified complex, (b) sulfated complex, and (c) phosphorylated complex. Yellow ribbons represent 4B08. (d) Blue and red tubes are snapshots of pep1 taken from t = 50 and 300 ns, respectively. The N-terminal part is bound to 4B08 in the former conformation, whereas it dissociates from 4B08 in the latter conformation.

As shown by X-ray crystallography, the side-chains of Y4 and Y5 do not interact with 4B08 directly (Fig. 2a–c). Interestingly, we observed that the N-terminal part of pep1 dissociated from the antibody in all of the modification states (Fig. 2d). The result for the unmodified system is consistent with the Ala-scanning experiments [22], which showed that substitutions of N-terminal residues did not markedly influence the binding affinity.

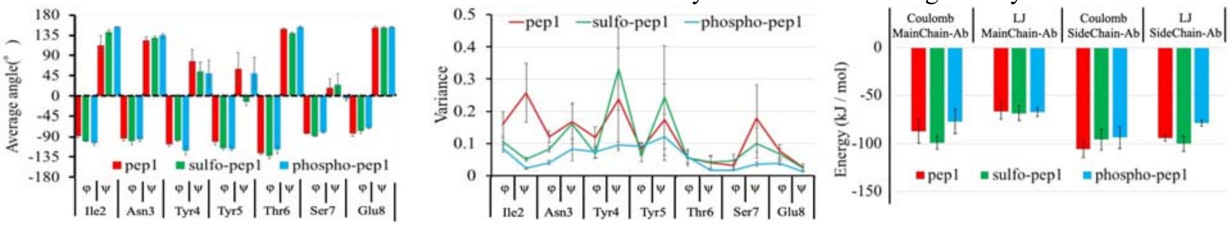

(a) (b) (c)

FIGURE 3. (a) Circular averages of φ/ψ angles. (b) Circular variances of φ/ψ angles. (c) Interaction energies between pep1 and 4B08. MainChain-Ab and SideChain-Ab mean the interaction between the main chain of pep1 and 4B08 and the interaction between the side chain of pep1 and 4B08, respectively.

Although comparison of the snapshots did not indicate any clear influence of modifications on the binding structure, the directional analysis detected several small but significant influences. For example, the circular average of the φ angle of Y4 is increased by sulfation but decreased by phosphorylation (Fig. 3a). The circular variances, which are related to the conformational entropy, show that phosphorylation suppresses the main chain motion of pep1 more than sulfation. However, we could not find any statistically significant effects of sulfation on the interaction energies, except that the Lennard–Jones (LJ) interaction between pep1 and 4B08 was slightly weakened by phosphorylation (Fig. 3c).

CONCLUSION

In this study, FUJI parameters for sTyr and pTyr were developed to be able to investigate the tyrosine sulfation and phosphorylation. In addition, the FUJI parameters of sTyr and pTyr were applied to the pep1 and pep1–4B08 complex systems. By using MD simulations, we found that the effect of phosphorylation on the pep1 conformation was clearly different from that of sulfation, despite the chemical similarity. This may explain the experimental results of Ref. [4]. The new parameters developed here will be useful for investigating post-translational effects in biological systems at the molecular level.

ACKNOWLEDGMENTS

This research used computational resources of the TSUBAME through the HPCI System Research Project (hp170130, hp180044, hp190117), and of the Research Center for Computational Science, Okazaki, Japan. T.Y. acknowledges support from the SIP program (SM^4I), Scientific Research (JSPS KAKENHI (S)15H05752, (C)15KT0103, (B)16KT0050, (C)18K05025), and Innovative Drug Discovery Infrastructure through Functional Control of Bio-molecular Systems (hp170255, hp180191, hp190171).

REFERENCES

1. G. Manning, D. B. Whyte, R. Martinez, T. Hunter and S. Sudarsanam, Science **298**, 1912-1934 (2002).
2. B. J. Druker, M. Talpaz, D. J. Resta, B. Peng, E. Buchdunger, J. M. Ford, N. B. Lydon, H. Kantarjian, R. Capdeville and S. Ohno-Jones, New Engl. J. Med. **344**, 1031-1037 (2001).
3. K. Miyanabe, T. Yamashita, Y. Abe, H. Akiba, Y. Takamatsu, M. Nakakido, T. Hamakubo, T. Ueda, J. M. Caaveiro and K. Tsumoto, Biochemistry **57**, 4177-4185 (2018).
4. E. G. Cormier, M. Persuh, D. A. Thompson, S. W. Lin, T. P. Sakmar, W. C. Olson and T. Dragic, Proc. Natl. Acad. Sci. U.S.A. **97**, 5762-5767 (2000).
5. H. Fujitani, A. Matsuura, S. Sakai, H. Sato and Y. Tanida, J. Chem. Theory Comput. **5**, 1155-1165 (2009).
6. T. Yamashita, Biomedical Sciences **2**, 34-47 (2016).
7. T. Yamashita, JPS Conf. Proc. **5**, 010003 (2015).
8. T. Yamashita, A. Ueda, T. Mitsui, A. Tomonaga, S. Matsumoto, T. Kodama and H. Fujitani, Chem. Pharm. Bull. **63**, 147-155 (2015).
9. H. Fujitani, K. Shinoda, T. Yamashita and T. Kodama, J. Phys.: Conf. Ser. **454**, 012018 (2013).
10. T. Yamashita, E. Mizohata, S. Nagatoishi, T. Watanabe, M. Nakakido, H. Iwanari, Y. Mochizuki, T. Nakayama, Y. Kado and Y. Yokota, Structure **27**, 519-527 (2019).
11. T. Yamashita, Int. Immunol. **30**, 133-140 (2018).
12. K. Sasaki, R. Okajima and T. Yamashita, AIP Conf. Proc. **2040**, 020015 (2018).
13. T. Yamashita and Y. Takamatsu, AIP Conf. Proc. **1906**, 030022 (2017).
14. T. Yamashita, AIP Conf. Proc. **1790**, 020026 (2016).
15. N. Homeyer, A. H. Horn, H. Lanig and H. Sticht, J. Mol. Model. **12**, 281-289 (2006).
16. P. Cieplak, W. D. Cornell, C. Bayly and P. A. Kollman, J. Comput. Chem. **16**, 1357-1377 (1995).
17. F.-Y. Dupradeau, A. Pigache, T. Zaffran, C. Savineau, R. Lelong, N. Grivel, D. Lelong, W. Rosanski and P. Cieplak, PCCP **12**, 7821-7839 (2010).
18. H. Fujitani, Y. Tanida and A. Matsuura, Phys. Rev. E **79**, 021914 (2009).
19. S. Pronk, S. Pall, R. Schulz, P. Larsson, P. Bjelkmar, R. Apostolov, M. R. Shirts, J. C. Smith, P. M. Kasson, D. van der Spoel, B. Hess and E. Lindahl, Bioinformatics **29**, 845-854 (2013).
20. C. Rapp, H. Klerman, E. Levine and C. L. McClendon, PloS one **8**, e57804 (2013).
21. T. Yamashita, R. Okajima and N. Shoji, AIP Conf. Proc. **2040**, 020014 (2018).
22. K. Miyanabe, H. Akiba, D. Kuroda, M. Nakakido, O. Kusano-Arai, H. Iwanari, T. Hamakubo, J. M. Caaveiro and K. Tsumoto, The Journal of Biochemistry **164**, 65-76 (2018).

Hyperspherical Coordinates and Energy Partitions for Reactive Processes and Clusters

Andrea Lombardi[1,3,a)], Federico Palazzetti[1] and Misha B. Sevryuk[2]

[1]*Dipartimento di Chimica, Biologia e Biotecnologie, Università di Perugia, Via Elce di Sotto 8, 06123, Perugia, Italy.*
[2]*Institute of Energy Problems of Chemical Physics, Russian Academy of Sciences, Leninskii pr. 38/2, Moscow, 119334 Russia*
[3]*Consortium for Computational Molecular and Materials Sciences (CMS)[2], Via Elce di Sotto, 8, 06123 Perugia, Italy*

[a)]Corresponding author: andrea.lombardi@unipg.it

Abstract.
The hyperspherical coordinate systems have been developed for the study of few-body scattering problems of nuclear and molecular physics, for example in the practical implementation of demanding quantum calculations typical of chemical reactions. The hyperangular momenta and their eigenfunctions, the hyperspherical harmonics, are the mathematical apparatus characterizing the hyperspherical representation of molecular dynamics. To circumvent the restriction to the application of the hyperspherical methods, due to exceedingly high computational costs, a classical mechanics hyperspherical formulation has been developed suitable for applications to clusters and large molecular system dynamics. The asymptotic theory of generalized harmonics connected with that of spin networks establishes semiclassical connections for treating discretization procedures, specifically, the hyperquantization algorithm treated by us elsewhere. **Keywords:** Hyperspherical coordinates, Hyperspherical harmonics, Energy partitions

Introduction

Methods based on hyperspherical functions [1–3] in atomic and molecular scattering calculations are widely employed. Considerable work has been done to develop hyperspherical harmonics basis sets mainly for three, four-body systems (see e.g [4–9]), due to their appealing property of being invariant with respect to the possible reaction channels. Hyperspherical methods are in this respect to be preferred to other approaches (see e.g. semiclassical [10–17]).

Besides their use as quantum scattering basis sets, hyperspherical functions are suitable to be applied to the representation of intermolecular and intramolecular interactions in collision studies [18, 19, 19–28, 28–46].

The limited applicability of hyperspherical coordinates, to just three of four-center systems can be in part bypassed developing a hyperspherical formulation of classical dynamics, by which medium size and large molecules and atomic and molecular clusters can be simulated, taking advantage of the lower computational cost of classical trajectories (see e.g. [47]). The classical Hamilton function and the degrees of freedom get separated into energy terms, corresponding to well defined kinetic energy contributions and homogeneous sets of variables Energy contributions, account for shape deformation, ordinary rotations and kinematic rotations [6, 48–50].

It is noticeable that in the separation scheme of hyperspherical coordinates two different sets of rotational degrees of freedom (ordinary rotations and rotations in the kinematic space) are present, so that the remaining three degrees of freedom turn out to be invariant with respect to both kinds of rotation action and solely depend on the global shape of the aggregates of particles. This “invariance‘” approach to structure and dynamics has been validated in a series of applications [48, 51–53]. Invariant hyperspherical deformation indices, a combination of invariant degrees of freedom, have been proposed for the study and classification of local and global minimum energy structures of atomic and molecular clusters.

Hyperspherical coordinates for atomic and molecular aggregates

Let us suppose we have a collection of $N \geq 2$ particles with masses $m_1, \cdots, m_N$ and positions identified by a set of radii vectors in the center of mass reference frame, $\mathbf{r_1}, \cdots, \mathbf{r_N}$. Mass *scaled* radii vectors $\mathbf{q}_\alpha = (m_\alpha/M)^{1/2}\mathbf{r}_\alpha$ ($1 \leq \alpha \leq N$), can be obtained, where $M = \sum_\alpha^N m_\alpha$ is the total mass of the system.
A $3 \times N$ position matrix denoted by Z containing column-wise the components of the mass scaled vectors, can be generated, as follows:

$$Z = \begin{pmatrix} q_{1,1} & q_{1,2} & \cdots & q_{1,N} \\ q_{2,1} & q_{2,2} & \cdots & q_{2,N} \\ q_{3,1} & q_{3,2} & \cdots & q_{3,N} \end{pmatrix}. \tag{1}$$

The coordinate frame can be rotated, acting (left-multiplication) on the position matrix by an orthogonal matrix R^t, transpose of a matrix $R \in O(3)$. A rotation of the coordinate frame can also be performed in the so called *kinematic space* [5, 49], by action of an orthogonal matrix (right-multiplication) $K \in O(N)$ on the position matrix Z, $Z' = ZK$.

It is possible to identify a subset of K matrices having the following form (see last column):

$$K = \begin{pmatrix} k_{1,1} & k_{1,2} & \cdots & (m_1/M)^{1/2} \\ k_{2,1} & k_{2,2} & \cdots & (m_2/M)^{1/2} \\ \cdots & \cdots & \cdots & \cdots \\ k_{N,1} & k_{N,2} & \cdots & (m_N/M)^{1/2} \end{pmatrix} \tag{2}$$

and its application generates a subset of all the possible Cartesian frames. Note that the last column of the above matrices is zero, due to the relation $\sum_\alpha^N m_\alpha^{1/2}\mathbf{q}_\alpha = 0$, valid for the mass scaled vectors. In such special cases, one only has to deal with a $3 \times (N-1)$ reduced Z matrix. The physical meaning of such condition is that one gets rid of the motion of the center of mass. This smaller matrix Z is called *reduced position matrix*.
The Jacobi vectors are defined as a linear combinations of the N Cartesian particle position vectors, with coefficients being a function of the particle masses [54, 55]. Kinematic rotations connect different Jacobi vector sets corresponding to the different coupling schemes and reactive channels of the system.
The *singular value decomposition* theorem [56] applied to the $3 \times n$ position matrix Z (where $n = N$ or $n = N - 1$) leads to the following product of three matrices:

$$Z = R\Xi K^t \tag{3}$$

where $R \in O(3)$ and $K \in O(n)$ are 3×3 and $3 \times n$ orthogonal matrices, respectively. The elements of the $3 \times n$ matrix Ξ are zeroes, with the possible exception of the diagonal entries, $\Xi_{11} = \xi_1, \Xi_{22} = \xi_2, \Xi_{33} = \xi_3$, which are subjected to the inequality $\xi_1 \geq \xi_2 \geq \xi_3 \geq 0$.
The values ξ_i, ($i = 1, 2, 3$) are called the *singular values* of the matrix Z and are uniquely determined, although the factors R and K in Eq. 3 are not. If $N \leq 3$ and Z is the full $3 \times N$ position matrix, then the smallest singular value ξ_3 is necessarily zero. An important relation can be easily obtained [48, 49]:

$$\xi_1^2 + \xi_2^2 + \xi_3^2 = \rho^2. \tag{4}$$

The ξ's are invariant under both ordinary rotations in the physical space and kinematic rotations [5, 6, 49, 57], a remarkable property, with possible applications to molecular dynamics [48, 58–61] and properties of the minimum energy structures of N-particle aggregates.
The symmetric case $n = 3$, corresponds to four particles or four center systems, is special, since the two matrices R and K cannot be chosen to be *special orthogonal* ($R \in SO(3)$ and $K \in SO(n)$), but are required to be just orthogonal matrices ($O(3)$). In this case, if the determinant of Z is lower than zero, its sign depends on the sign of the product of the ξ's, and so one has $\xi_3 \leq 0$. This fact is directly connected to the mirror image and chirality sign of the system [51, 62, 63].

Summary

We briefly summarized the relevant aspects of the hyperspherical coordinate approach to structure and dynamics of molecules and clusters and some interesting features, coming from invariance properties of coordinates and kinetic energy terms.

ACKNOWLEDGMENTS

A.L. and F. P. acknowledges financial support and from MIUR PRIN 2015 (Codice Progetto: 2015F59J3R_002) and from the Dipartimento di Chimica, Biologia e Biotecnologie dell'Università di Perugia (FRB, Fondo per la Ricerca di Base 2017). The authors acknowledge support through SIR 2014 Scientific Independence for Young Researchers (RBSI14U3VF) and the AMIS project through the program Dipartimenti di Eccellenza.

REFERENCES

[1] B. Zhao and H. Guo, WIREs Comput Mol Sci **7:e1301** (2017).
[2] D. Skouteris, J. Castillo, and D. E. Manolopoulos, Comput. Phys. Comm. **133**, 128–135 (2000).
[3] B. Lepetit and J. M. Launay, J. Chem. Phys. **95**, 5159–5168 (1991).
[4] V. Aquilanti, A. Beddoni, S. Cavalli, A. Lombardi, and R. Littlejohn, Molecular Physics **98**, 1763–1770 (2000).
[5] V. Aquilanti, A. Beddoni, A. Lombardi, and R. Littlejohn, International journal of quantum chemistry **89**, 277–291 (2002).
[6] V. Aquilanti, A. Lombardi, and R. Littlejohn, Theoretical Chemistry Accounts **111**, 400–406 (2004).
[7] A. Kuppermann, Isr. J. Chem. **43**, p. 229 (2003).
[8] D. De Fazio, S. Cavalli, and V. Aquilanti, .
[9] V. Aquilanti and S. Cavalli, **93**, 801–809 (1997).
[10] A. Laganà, S. Crocchianti, N. Faginas Lago, L. Pacifici, and G. Ferraro, Collect. Czech. Chem. Commun. **68**, 307–330 (2003).
[11] N. Faginas-Lago, A. Laganà, E. Garcia, and X. Gimenez, Computational Science and Its Applications–ICCSA 2005 29–39 (2005).
[12] N. Faginas-Lago and A. Laganá, AIP Conference Proceedings **762**, p. 920 (2005).
[13] N. Faginas-Lago and Laganà, J. Chem. Phys. **125**, p. 114311 (2006).
[14] N. Faginas-Lago, A. Costantini, and F. Huarte-Larrañaga, International Journal of Quantum Chemistry **110**, 422–431 (2010).
[15] N. Faginas, F. Huarte-Larranaga, and A. Laganà, Chem. Phys. Lett. **464**, 249–255 (2008).
[16] S. Rampino, N. Faginas-Lago, A. Laganà, and F. Huarte-Larrañaga, J. Comput. Chem. **33**, 708–714 (2012).
[17] A. Laganà, N. Faginas-Lago, S. Rampino, F. Huarte-Larrañaga, and E. García, Physica Scripta **78**, p. 058116 (2008).
[18] A. Lombardi, N. Faginas Lago, A. Laganà, and S. Falcinelli, in *Computational Science and Its Applications - ICCSA 2012*, Lecture Notes in Computer Science, Vol. 7333 (Springer, Berlin, Heidelberg, 2012), pp. 387–400.
[19] A. Lombardi, A. Lagan, F. Pirani, F. Palazzetti, and N. Faginas-Lago, in *Computational Science and Its Applications - ICCSA 2013*, Lecture Notes in Computer Science, Vol. 7972, edited by B. Murgante, S. Misra, M. Carlini, C. Torre, H.-Q. Nguyen, D. Taniar, B. Apduhan, and O. Gervasi (Springer Berlin Heidelberg, 2013), pp. 17–31.
[20] N. Faginas Lago, M. Albertí, A. Laganà, and A. Lombardi, in *Computational Science and Its Applications - ICCSA 2013*, Lecture Notes in Computer Science, Vol. 7971 (Springer, Berlin, Heidelberg, 2013), pp. 1–15.
[21] N. Faginas-Lago, M. Albert, A. Costantini, A. Laganá, A. Lombardi, and L. Pacifici, Journal of Molecular Modeling **20**, p. 2226 (2014).
[22] N. Faginas-Lago, D. Yeni, F. Huarte, M. Alcamì, and F. Martin, J. PHys. Chem. A **120**, 6451–6458 (2016).
[23] N. Faginas-Lago, A. Lombardi, M. Albertí, , and G. Grossi, Journal of Molecular Liquids **204**, p. 192 197 (2015).
[24] M. Albertí and N. Faginas Lago, Eur. Phys. J. D **67**, p. 73 (2013).
[25] M. Albertí and N. Faginas Lago, J. Phys. Chem. A **116**, 3094–3102 (2012).

[26] M. Albertí, N. Faginas Lago, and F. Pirani, J. Phys. Chem. A **115**, 10871–10879 (2011).
[27] N. Faginas-Lago, M. Albertí, A. Laganà, A. Lombardi, L. Pacifici, and A. Costantini, in *Computational Science and Its Applications-ICCSA 2014*, Lecture Notes in Computer Science, Vol. 8579, edited by B. Murgante and S. e. a. Misra (Springer International Publishing, 2014), pp. 585–600.
[28] N. Faginas-Lago, F. Huarte Larrañaga, and M. Albertí, Eur. Phys. J. D **55**, p. 75 (2009).
[29] M. Bartolomei, F. Pirani, A. Laganà, and A. Lombardi, J. Comp. Chem. **33**, p. 1806 (2012).
[30] A. Lombardi, N. Faginas-Lago, A. Laganà, F. Pirani, and S. Falcinelli, in *Computational Science and Its Applications – ICCSA 2012*, Lecture Notes in Computer Science, Vol. 7333, edited by B. Murgante, O. Gervasi, S. Misra, N. Nedjah, A. Rocha, D. Taniar, and B. Apduhan (Springer Berlin Heidelberg, 2012), pp. 387–400.
[31] M. Albertí, N. Faginas-Lago, A. Laganà, and F. Pirani, Phys. Chem. Chem. Phys. **13**, 8422–8432 (2011).
[32] M. Albertí, N. Faginas-Lago, and F. Pirani, J. Phys. Chem. A **115**, 10871–10879 (2011).
[33] M. Albertí and N. Faginas-Lago, Eur. Phys. J. D **67**, p. 73 (2013).
[34] M. Albertí, N. Faginas-Lago, and F. Pirani, Chem. Phys. **399**, p. 232 (2012).
[35] S. Falcinelli, M. Rosi, P. Candori, F. Vecchiocattivi, A. Bartocci, A. Lombardi, N. Faginas-Lago, and F. Pirani, in *Computational Science and Its Applications - ICCSA 2013*, Lecture Notes in Computer Science, Vol. 7971, edited by B. Murgante, S. Misra, M. Carlini, C. Torre, H.-Q. Nguyen, D. Taniar, B. Apduhan, and O. Gervasi (Springer Berlin Heidelberg, 2013), pp. 69–83.
[36] A. Lombardi, N. Faginas-Lago, L. Pacifici, and A. Costantini, J. Phys. Chem. A **117**, 11430–11440 (2013), http://pubs.acs.org/doi/pdf/10.1021/jp408522m .
[37] A. Lombardi, F. Pirani, A. Laganà, and M. Bartolomei, J. Comp. Chem. **37**, 1463–1475 (2016).
[38] L. Pacifici, M. Verdicchio, N. Faginas-Lago, A. Lombardi, and A. Costantini, Journal of Computational Chemistry **34**, 2668–2676 (2013).
[39] A. Lombardi, N. Faginas-Lago, L. Pacifici, and G. Grossi, J. Chem. Phys. **143**, p. 034307 (2015).
[40] A. Lombardi, N. Faginas-Lago, L. Pacifici, and A. Costantini, J. Phys. Chem. A **117**, 11430–11440 (2013).
[41] R. Celiberto, I. Armenise, M. Cacciatore, M. Capitelli, F. Esposito, P. Gamallo, R. Janev, A. Lagana, V. Laporta, A. Laricchiuta, *et al.*, Plasma Sources Science and Technology **25**, p. 033004 (2016).
[42] N. Faginas-Lago, A. Lombardi, and M. Albertí, Journal of Molecular Liquids **224**, 792–800 (2016).
[43] F. Palazzetti, E. Munusamy, A. Lombardi, G. Grossi, and V. Aquilanti, International Journal of Quantum Chemistry **111**, 318–332 (2011).
[44] A. Lombardi and F. Palazzetti, Journal of Molecular Structure: THEOCHEM **852**, 22–29 (2008).
[45] P. R. Barreto, A. F. Albernaz, F. Palazzetti, A. Lombardi, G. Grossi, and V. Aquilanti, Physica Scripta **84**, p. 028111 (2011).
[46] P. R. Barreto, A. F. Albernaz, A. Capobianco, F. Palazzetti, A. Lombardi, G. Grossi, and V. Aquilanti, Computational and Theoretical Chemistry **990**, 53–61 (2012).
[47] M. Nakamura, P.-Y. Tsai, T. Kasai, K.-C. Lin, F. Palazzetti, A. Lombardi, and V. Aquilanti, Faraday discussions **177**, 77–98 (2015).
[48] V. Aquilanti, A. Lombardi, and E. Yurtsever, Physical Chemistry Chemical Physics **4**, 5040–5051 (2002).
[49] M. B. Sevryuk, A. Lombardi, and V. Aquilanti, Physical Review A **72**, p. 033201 (2005).
[50] J. Castro Palacio, L. Velazquez Abad, A. Lombardi, V. Aquilanti, and J. Rubayo Soneira, The Journal of chemical physics **126**, p. 174701 (2007).
[51] A. Lombardi and F. Palazzetti, Journal of Physics: Condensed Matter **30**, p. 063003 (2018).
[52] A. Lombardi, F. Palazzetti, L. Peroncelli, G. Grossi, V. Aquilanti, and M. Sevryuk, Theoretical Chemistry Accounts **117**, 709–721 (2007).
[53] V. Aquilanti, G. Grossi, A. Lombardi, G. S. Maciel, and F. Palazzetti, Rend. Fis. Acc. Lincei **22**, 125–135 (2011).
[54] F. Gatti and C. Lung, J. Chem. Phys. **108**, 8804–8820 (1998).
[55] V. Aquilanti, A. Lombardi, and E. Yurtsever, Phys. Chem. Chem. Phys. **4**, p. 2002 (5040–5051).
[56] R. A. Horn and C. R. Johnson, *Matrix Analysis, 2nd ed.* (University Press, Cambridge, 1990).
[57] V. Aquilanti, A. Lombardi, and M. B. Sevryuk, J. Chem. Phys. **121**, p. 5579 (2004).
[58] V. Aquilanti, E. Carmona Novillo, E. Garcia, A. Lombardi, M. B. Sevryuk, and E. Yurtsever, Comput. Mat. Sci. **35**, 187–191 (2006).
[59] V. Aquilanti, A. Lombardi, M. B. Sevryuk, and E. Yurtsever, Phys. Rev. Lett **93**, p. 113402 (2004).
[60] F. Calvo, X. Gadea, A. Lombardi, and V. Aquilanti, J. Chem. Phys. **125**, p. 114307 (2006).
[61] A. Lombardi, V. Aquilanti, E. Yurtsever, and M. B. Sevryuk, Chem. Phys. Lett. **30**, 424–428 (2006).
[62] A. Lombardi, G. S. Maciel, F. Palazzetti, G. Grossi, and V. Aquilanti, Journal of the Vacuum Society of Japan **53**, 645–653 (2010).
[63] F. Palazzetti, P.-Y. Tsai, A. Lombardi, M. Nakamura, D.-C. Che, T. Kasai, K.-C. Lin, and V. Aquilanti, Rendiconti Lincei **24**, 299–308 (2013).

Screen Representation of Structural Properties of Alanine in Polypeptide Chains

Concetta Caglioti [1, a)], Robenilson dos Santos Ferreira [2, 3], Federico Palazzetti [1], Andrea Lombardi [1], Vincenzo Aquilanti [1, 4]

[1] *Dipartimento di Chimica, Biologia e Biotecnologie – Università di Perugia, via Elce di Sotto 8, 06123, Perugia, Italy.*

[2] *Instituto de Fìsica, Universidade Federal da Bahia, Campus Universitario de Ondina, Salvador, BA CEP 40210-340, Brazil.*

[3] *Instituto Federal de Alagoas-Campus Piranhas, Piranhas, AL CEP 57460-000, Brazil.*

[4] *Istituto di Struttura della Materia-Consiglio Nazionale delle Ricerche, 00016 Rome, Italy*

[a)] Corresponding author: concettacaglioti@hotmail.com

Abstract. Alternative to conventional structural diagrams that plot dihedral angles of aminoacids in in the protein chains, the proposed screen representation is based on significant distances in the aminoacid unit. Here, we report the case of alanine, the simplest chiral aminoacid, both isolated and participating in about fifty peptidic chains, of length included between 43 and 2238 aminoacid units. We present comparison with the most stable conformer in the isolated form (NH_2-CH-CH_3-COOH), in order to find possible effects in bond lengths due to aminoacid substituents. We have also found that serine is the aminoacid most frequently connected to alanine. Screen points of alanine, when bounded to serine, are displayed and highlighted in order to evidence how this aminoacid, exemplary for the substituent groups, affects the alanine structure.

INTRODUCTION

Proteins are among the most studied class of molecules, because of their involvement in many areas of sciences. Interest in them extended beyond the traditional research areas (such as industrial, pharmaceutical and medical chemistry) and raised interest among the astrochemical [1] (see also Ref. [2,3]) and astrobiological communities, especially for the issue related to the origin of the homochirality in nature, *i. e.* the phenomenon for which all the aminoacids in proteins are levorotatory and the sugars in biomolecules are dextrorotatory (for the possible origin of chiral discrimination see for example Refs. [4] and references therein, for experiments on the stereodynamical selectivity of chirality see Ref.[5], for the role of molecular alignment see Refs. [6–12], for chiral discrimination processes in photodissociation see Refs. [13–16] and in collisions see Refs. [17,18]). The enormous amount of data, that are often heterogeneous with considerable spread of accuracy, led to the use of methods that permit to compact and classify the information on this wide class of compounds. The Ramachandran plot [19] is the most famous among these methods and relies on dihedral angles. The screen is a representation alternative to the Ramachandran, based on the plot of significant distances of the system, represented by the six edges of a virtual tetrahedron built in the system itself. It has been initially applied to represent the range of existence and the Regge symmetries of 6*j*-symbols [20–22], the building blocks of spin networks[23–26] and to establish connections between the 6*j* symbols and the four-bar mechanical engineering mechanism, an archetypal mechanism of kinematics [27]. At the molecular level, it has been applied to peroxides [28–31] and persulfides[32,33], to visualize relevant kinetic and electric properties [34], and geometrical features related to dynamics [35] For this latter case, the screen has been built by plotting an intramolecular distance (and that corresponding to its opposite edge) sensitive to the torsional motion around the O – O (or S – S) bond [36], that leads to the transition between two mirror forms (see also Ref.[37]). For the present case, the system of interest is the alanine; a tetrahedron

is built in the aminoacid unit (Fig. 1a) and the six edges are the interatomic distances between the four vertices, *i. e.* the atoms directly connected to the central carbon: H_A, that indicates the hydrogen atom; C_B, the carbon of the methyl group; N, the nitrogen; C, the carbon of the carboxylic functional. The edges of the tetrahedron are formed by the interatomic distances: N-H_A, N-C_B, N-C, H_A-C_B, H_A-C, C-C_B. Since the screen presents plots of opposite edges of the tetrahedron, there are three possible choices: the distances H_A – C_B and N – C, N – H_A and C – C_B, N – C_B and H_A – C.

We report case studies on alanine in about fifty peptidic fragments, whose data have been extracted from Protein Data Bank (www.rcsb.org). Our objective is to verify changes in structural properties of this aminoacid, when it is bounded to other aminoacid units in peptide chains. Specific attention is devoted to possible effects due to the connection of alanine and serine, the most frequently aminoacid bounded to alanine in our sample of peptides.

SCREEN REPRESENTATION OF PEPTIDES

About 500 alanine structures have been taken from about fifty proteins, whose length is included between 43 and 2238 aminoacid units, from Protein Data Bank. Here, we report the four-character code that identifies the proteins: 5aht, 5jpx, 1hgv, 1hgz, 1hh0, 1nh4, 2n8t, 1new, 5lg7, 2ltf, 2cqj, 6axd, 2lze, 1x4q, 1e1g, 1e1j, 1e1p, 1e1s, 1e1u, 1e1w, 1hjm, 1hjn ,2l9q, 1xyk, 1xyj, 1xyw, 2ku4, 6gt7, 1lwb, 1k8h, 5v7z, 6do6, 2fe0, 6do7, 5w4s, 2lu5, 2i83, 1qlx, 1qlz, 6f2x, 5lg0, 2h35, 2m6z, 5kk3, 4gdi.

In Fig. 1b-d, we show plots of each pair of the opposite distances, focusing on the difference between the most stable conformer of isolated alanine and the alanine in the peptidic chain, where we suppose that aminoacids connected to alanine through bonds with N or C determine alterations in the interatomic distances. The interatomic distances of the most stable conformer of alanine (Berlin *ab initio* aminoacid DB, http://aminoaciddb.rz-berlin.mpg.de/) are H_A – C_B 2.16 Å, N – C 2.47 Å, N – H_A 2.15 Å, C – C_B 2.51 Å, H_A – C 2.13 Å and N – C_B 2.48 Å. The 10.8 % of the bonds that alanine forms with other aminoacids is established with serine, then 8.5 % with leucine, 7.9 % glycine, 6.8 % glutamic acid and isoleucine, 6.1 % valine, 5.4 % lysine, 4.7 % glutamine, 4.6 % tyrosine, 4.3 % proline and histidine, 4.2 % aspartic acid, 4.0 % phenylalanine, 3.2 % methionine, 3.0 % threonine, 2.5 % tryptophane, 2.3 % arginine, 1.4 % cysteine, finally, in the 6.5 % alanine binds another alanine. Being the alanine-serine the most common peptidic bond among the proteins represented in our screen, the distance points of alanine when connected to serine are highlighted in order to show possible effects to the alanine structure.

In Fig. 1b, the screen representation of the distances H_A – C_B and N – C is reported. Presence of aminoacid substituents may determine changes to the H_A – C_B length (y) from 2.16 Å to ca. 2.0 Å and to the N – C length (x) from 2.45 Å to 2.3 – 2.6 Å. The points are grouped into two main areas: the first one is included between H_A – C_B distance lower than 2.1 Å and in the range 2.35 - 2.5 Å for the N – C distance. The second one covers the range of H_A – C_B distance higher than 2.1 Å and 2.25 - 2.6 Å for the N – C distance. In Fig. 1c, we show the screen of the distances N – H_A and C – C_B. In the peptidic chain, the N - H_A length spans a range from *ca.* 1.95 to *ca.* 2.12 and the C – C_B length (x) from *ca.* 2.35 Å to *ca.* 2.62 Å. In Fig. 1d, we report the screen for the distances N – C_B and H_A – C. With respect to the isolated alanine, N – C_B distance (y) varies from 2.48 to Å *ca.* 2.35 – 2.55 Å, while H_A – C (x) varies from 2.13 Å to 2.05 – 2.20 Å. Similarly, to the case of Fig. 1b, the points are grouped in two main areas according to the value of the H_A – C distance: one covers the range 2.05 – 2.1 Å and the other one the interval 2.1 – 2.2 Å.

When connected to serine, interatomic distances in alanine presents a similar distribution to the overall distribution. However, it must be noted that the N – C length remains lower than 2.55 Å (Fig. 1b) and the distance N – C_B remains substantially lower than that of the isolated alanine (Fig. 1d). Comparison with distances of alanine connected to other aminoacids should permit to distinguish the effect of the various aminoacids to the alanine structure.

FINAL REMARKS

The screen defined as a square plot of selected intermolecular distances has been employed to display structural properties of alanine in a sample of about fifty peptides. The geometries have been extracted from Protein Data Bank. Role of substituent groups in enlarging or shortening distances between intermolecular groups is found and indicated as suggestive of bond weakening or strengthening. Specifically, effects of serine, the aminoacid mostly connected to alanine have been investigated. Future works, aiming at investigating the effect of other aminoacid connected to alanine, should permit to univocally distinguish alteration to the alanine structure due to the presence of other aminoacids.

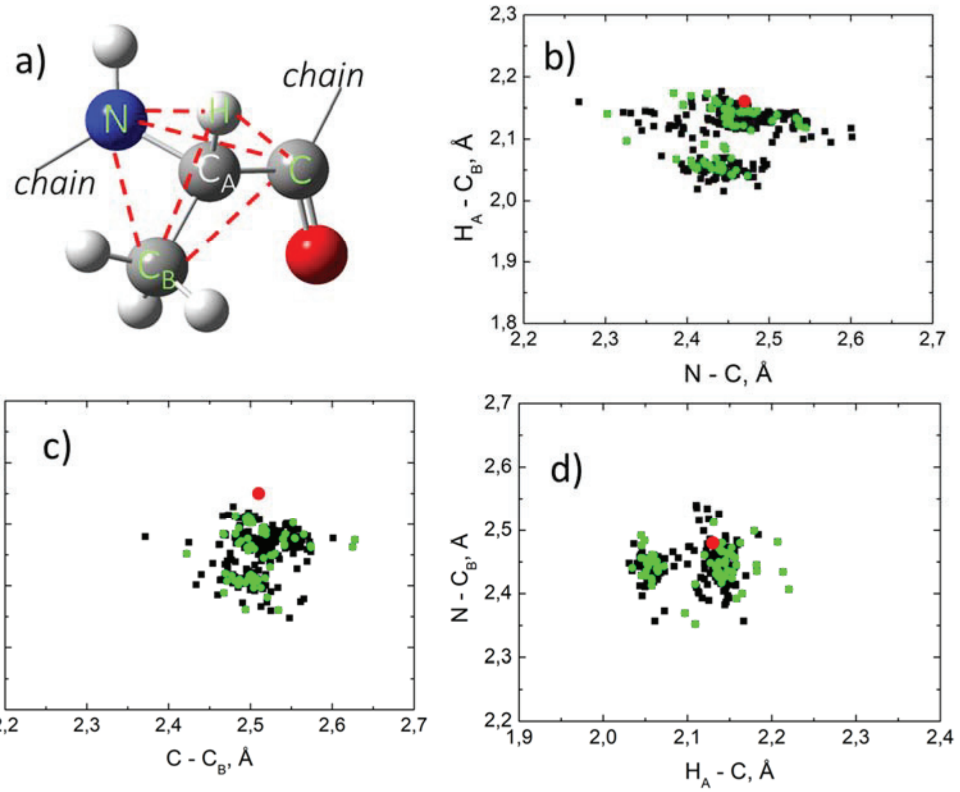

FIGURE 1. (a) . The virtual tetrahedron built in the alanine unit, the six edges are represented by red dashed lines, while the bonds are in light grey; the four vertices are: nitrogen (N, in blue), the carbon atom of the methyl group (CB, in grey), the hydrogen bounded to the central carbon (HA, in white), the carboxylic carbon atom (C, in grey). Note that the central carbon (CA, in grey) is not a vertex. b-d) Screen diagrams of alanine, plotting the following distances, in Å: b) $H_A – C_B$ *vs.* N – C, c) N – H_A *vs.* C – C_B, d) N – C_B *vs.* H_A – C. The red dot reports the distances related to the most stable conformer of isolated alanine; in black, the distances of alanine are shown; in green, we highlight the distances of alanine when connected to serine, the aminoacid most frequently bounded to alanine.

ACKNOWLEDGMENTS

The authors acknowledge the Italian Ministry for Education, University and Research, MIUR, for financial supporting through SIR 2014 Scientific Independence for young Researchers (RBSI14U3VF).

REFERENCES

1 F. Palazzetti, G.S. Maciel, A. Lombardi, G. Grossi, and V. Aquilanti, J. Chinese Chem. Soc. **59**, 1045 (2012).
2 F.A. Gianturco, M. Satta, M. Mendolicchio, F. Palazzetti, A. Piserchia, V. Barone, and R. Wester, Astrophys. J. **830**, 2 (2016).
3 A. Lombardi, A. Laganà, F. Pirani, F. Palazzetti, and N.F. Lago, Lect. Notes Comput. Sci. **7972**, 17 (2013).
4 V. Aquilanti, G. Grossi, A. Lombardi, G.S. MacIel, and F. Palazzetti, Phys. Scr. **78**, 058119 (2008).
5 T. Kasai, D.-C. Che, M. Okada, P.-Y. Tsai, K.-C. Lin, F. Palazzetti, and V. Aquilanti, Phys. Chem. Chem. Phys. **16**, 9776 (2014).
6 D.-C. Che, F. Palazzetti, Y. Okuno, V. Aquilanti, and T. Kasai, J. Phys. Chem. A **114**, 3280 (2010).
7 A. Lombardi, G.S. Maciel, F. Palazzetti, G. Grossi, and V. Aquilanti, J. Vac. Soc. Japan **53**, 645 (2010).
8 V. Aquilanti, G. Grossi, A. Lombardi, G.S. Maciel, and F. Palazzetti, Rend. Lincei **22**, 125 (2011).
9 D.-C. Che, K. Kanda, F. Palazzetti, V. Aquilanti, and T. Kasai, Chem. Phys. **399**, 180 (2012).
10 T.-M. Su, F. Palazzetti, A. Lombardi, G. Grossi, and V. Aquilanti, Rend. Lincei **24**, 291 (2013).
11 F. Palazzetti, G.S. Maciel, K. Kanda, M. Nakamura, D.-C. Che, T. Kasai, and V. Aquilanti, Phys. Chem. Chem. Phys. **16**, 9866 (2014).
12 F. Palazzetti, A. Lombardi, M. Nakamura, S.-J. Yang, T. Kasai, K.-C. Lin, P.-Y. Tsai, and D.-C. Che, "Stereodirectional photodynamics: Experimental and theoretical perspectives" in International Conference of Computa-

tional Methods in Sciences and Engeneering-2016, edited by T. E. Simos et al., AIP Conference Proceedings 1790, American Institute of Physics, Athens, Greece, 2016, pp. 020020.
13 F. Palazzetti, P.-Y. Tsai, A. Lombardi, M. Nakamura, D.-C. Che, T. Kasai, K.-C. Lin, and V. Aquilanti, Rend. Lincei **24**, 299 (2013).
14 F. Palazzetti, A. Lombardi, S.-J. Yang, M. Nakamura, T. Kasai, K.-C. Lin, D.-C. Che, and P.-Y. Tsai, "Rotational state-selection and alignment of chiral molecules by electrostatic hexapoles" in International Conference
of Computational Methods in Sciences and Engeneering-2016, edited by T. E. Simos et al., AIP Conference Proceedings 1790, American Institute of Physics, Athens, Greece, 2016, pp. 020019.
15 M. Nakamura, S.-J. Yang, P.-Y. Tsai, T. Kasai, K.-C. Lin, D.-C. Che, A. Lombardi, F. Palazzetti, and V. Aquilanti, J. Phys. Chem. A **120**, 5389 (2016).
16 M. Nakamura, F. Palazzetti, P.-Y. Tsai, S.-J. Yang, K.-C. Lin, T. Kasai, D.-C. Che, A. Lombardi, and V. Aquilanti, Phys. Chem. Chem. Phys. (2019).
17 A. Lombardi, F. Palazzetti, V. Aquilanti, and G. Grossi, "Chirality in molecular collisions" in International Conference of Computational Methods in Sciences and Engeneering-2017, edited by T. E. Simos et al., AIP Conference
Proceedings 1906, American Institute of Physics, Thessaloniki, Greece, 2017, pp. 030012.
18 A. Lombardi and F. Palazzetti, J. Phys. Condens. Matter **30**, 063003 (2018).
19 F. Carrascoza, S. Zaric, and R. Silaghi-Dumitrescu, J. Mol. Graph. Model. **50**, 125 (2014).
20 M. Ragni, A.C.P. Bitencourt, V. Aquilanti, R.W. Anderson, R.G. Littlejohn, Int. J. Quant. Chem. **110**, 731 (2010).
21 R.W. Anderson, V.Aquilanti, A.C.P. Bitencourt, D.Marinelli, M. Ragni, Lect. Notes Comput. Sci. **7972**,46(2013).
22 A.C.P. Bitencourt, M. Ragni, R.G. Littlejohn, R.W. Anderson, and V. Aquilanti, Lect. Notes Comput. Sci. **8579**, 468 (2014).
23 V. Aquilanti, A.C.P. Bitencourt, C. da S. Ferreira, A. Marzuoli, and M. Ragni, Theor. Chem. Acc. **123**, 237 2009).
24 V. Aquilanti, H.M. Haggard, A. Hedeman, N. Jeevanjee, R.G. Littlejohn, and L. Yu, J. Phys. A Math. Theor. **45**, 065209 (2012).
25 A.C.P. Bitencourt, A.Marzuoli, M.Ragni, R.Anderson, V.Aquilanti, Lect. Notes Comput. Sci. **7333**, 723 (2012).
26 R.W. Anderson and V. Aquilanti, J. Chem. Phys. **124**, 214104 (2006).
27 V. Aquilanti, A.C.P. Bitencourt, C. Caglioti, R.F. dos Santos, A. Lombardi, F. Palazzetti, and M. Ragni, Rend. Lincei **30**, 67 (2019).
28 P.R.P. Barreto, A.F.A. Vilela, A. Lombardi, G.S. Maciel, F. Palazzetti, and V. Aquilanti, J. Phys. Chem. A **111**, 12754 (2007).
29 P.R.P. Barreto, F. Palazzetti, G. Grossi, A. Lombardi, G.S. Maciel, and A.F.A. Vilela, Int. J. Quant. Chem. **110**, 777 (2010).
30 P.R.P. Barreto, A.F.Albernaz,F. Palazzetti,A. Lombardi, G.Grossi, and V.Aquilanti, Phys. Scr. **84**, 028111 (2011).
31 P.R.P. Barreto, A.F. Albernaz, and F. Palazzetti, Int. J. Quantum Chem. **112**, 834 (2012).
32 G.S. Maciel, P.R.P. Barreto, F. Palazzetti, A. Lombardi, and V. Aquilanti, J. Chem. Phys. **129**, 164302 (2008).
33 V. Aquilanti, C. Caglioti, P. Casavecchia, G. Grossi, A. Lombardi, F. Palazzetti, and F. Pirani, "The astrochemical observatory: Computational and theoretical focus on molecular chirality changing torsions around O – O and S – S bonds" in International Conference of Computational Methods in Sciences and Engeneering-2017, edited by T. E. Simos et al., AIP Conference Proceedings 1906, American Institute of Physics, Thessaloniki, Greece, 2017, pp. 030010.
34 C. Caglioti, R.F.Dos Santos, V. Aquilanti, A. Lombardi, and F. Palazzetti, "Screen mapping of structural and electric properties, chirality changing rates and racemization times of chiral peroxides and persulfides" in International Conference of Computational Methods in Sciences and Engeneering-2018, edited by T. E. Simos et al., AIP Conference Proceedings 2040, American Institute of Physics, Thessaloniki, Greece, 2018, pp. 020021.
35 V. Aquilanti, C. Caglioti, A. Lombardi, G. S. Maciel and F. Palazzetti, Lect. Notes Comput. Sci. **10408**, 354 (2017).
36 A. Lombardi, F. Palazzetti, G.S. Maciel, V. Aquilanti, and M.B. Sevryuk, Int. J. Quant. Chem. **111**, 1651 (2011).
37 F. Palazzetti, E. Munusamy, A. Lombardi, G. Grossi, and V. Aquilanti, Int. J. Quantum Chem. **111**, 318 (2011).

Rate Constants and *First-Principles* Trajectories for Attack at Tetrahedral Carbon: Role of Molecular Orientation on Chiral Selectivity

Marcos Vinícius C. S. Rezende[1], Priscila Gomes dos Santos[1], Nayara D. Coutinho[2], Federico Palazzetti[2,a], Andrea Lombardi[2] and Valter Henrique Carvalho-Silva[1]

[1]Grupo de Química Teórica e Estrutural de Anápolis, Campus de Ciências Exatas e Tecnológicas. Universidade Estadual de Goiás, Anápolis, Brazil

[2]Dipartimento di Chimica, Biologia e Biotecnologie, Università di Perugia, Perugia, Italy

[a)]federico.palazzetti@unipg.it

Abstract. The characterization of stereodynamics and the dependence of kinetics on molecular orientation presently can be experimentally an essential tool for controlling reactive and nonreactive encounters. The Aquilanti mechanism considers chiral selectivity due to collisions of oriented reactants: here, we demonstrate it by the first-time calculations of stationary points and collision simulations based on *first-principle* molecular dynamics to study prototypical bimolecular nucleophilic substitution Mechanisms (S_N2) and bimolecular Elimination (E2). The latter reactive channel exhibits enantiomeric discrimination.

INTRODUCTION

Chiral selectivity encompasses large areas of science, the characterization of processes determined by the enantiomeric specificity in nature. The phenomenon of homochirality of biomolecules, such as amino acids and sugars, stands out as significant factor for the study of this phenomenon [1-2]. The industrial, pharmaceutical and even astrochemical fields had a boosting impact [3-4] on studies of the stereodynamical origin of chiral discrimination, which is a groundbreaking concept in relation to conventional approaches [2].

The understanding of the mechanisms of a collisional process depends on all the kinetic aspects of a chemical reaction [5, 6]. The determination of molecular anisotropy behavior was possible due to advances in molecular beam techniques for analyses of enantioselective collisional processes [7, 8]. Significant advances have also been achieved in relation to the improvement of molecular alignment and orientation techniques [9, 10]. The natural alignment technique was developed in the Nineties, and is based on the expansion of a supersonic molecular beam sown in lighter atoms, where collisions point to a rotational relaxation of the molecule followed by alignment in relation to the direction beam propagation. The electrostatic hexapolar orientation aims to guide the molecules towards and direction, through a non-homogeneous electrostatic field generated by a hexapole followed by a homogeneous field [11-13].

The observation of chiral effects in molecular collisions occurring in spatial aspects are only possible due to the molecular orientation. The Aquilanti mechanism individuates the molecular orientation as capable of differentiating between a pair of enantiomers [14-17]. There are supporting theoretical evidences for the Aquilanti mechanism, which has been shown to be effective in studies of elastic collision simulations[18] of the H_2O_2 [19, 20] and H_2S_2 [21] chiral molecules with rare gas atoms. Here, it is demonstrated for the first time the performance of molecular orientation in reactive collisional processes, in a bimolecular nucleophilic substitution (S_N2) reaction.

In organic chemistry, the mechanisms of nucleophilic substitution S_N2 and second-order elimination reactions E2 stand out by the ability to demonstrate the stereospecific role of chiral substrates [22]. This work aims to improve the understanding of the chiral collisional mechanisms and to serve as a basis for studies focused on astrochemistry and biochemistry. Advanced theoretical studies of the interaction of nucleophilic species with chiral substrates were performed in the analysis of the stationary points in the HS^-+ CHFXY (X = CH_3 or CN and Y = Cl or I) reaction, along with the *ab initio* molecular dynamics trajectories for the HS^-+ CHFCNI reaction.

COMPUTATIONAL PROCEDURE

The geometry optimizations and energies of all participants in the reaction have been calculated at a ωB97XD/aug-cc-pVDZ level of theory. Higher level coupled cluster theory with triple excitations treated perturbatively CCSD(T) has been used to further refine the energies. The stationary points were characterized by analytic harmonic frequency calculations: the absence or existence of an imaginary frequency indicates that the optimized structures are local minima or transition-states, respectively. The zero-point vibrational energy (ZPVE) contributions were considered in the calculation of the energy barriers. Thermodynamic and kinetic energy parameters have been calculated as the difference between the energy of the products and reactants and the difference between the energy of the transition-state and that of the reactant structures, respectively. All calculations have been performed using the Gaussian09 package[23].

The reaction rate constant ($\boldsymbol{k}$) has been calculated by *deformed*-Transition state theory(d-TST) [24-28] using the Transitivity code (www.vhcsgroup.com/transitivity) [29-31]. Given A + B ⟶TS† ⟶ C, a generic bimolecular reaction, the calculation of the partition functions Q_1, Q_2 and $Q^{\dagger}$ has to be evaluated for the reagents (A e B) and for the transition-state (TS), respectively. Thus, the rate constant is given by:

$$k(T) = \frac{k_B T}{h} \frac{Q^{\dagger}}{Q_1 Q_2} \left(1 - d \frac{\varepsilon^{\ddagger}}{k_B T}\right)^{1/d}, \; d = -\frac{1}{3}\left(\frac{h\nu^{\ddagger}}{2\varepsilon^{\ddagger}}\right)^2, \tag{1}$$

where k_B is the Boltzmann's constant, h is the Planck's constant and $\varepsilon^{\ddagger}$ is the effective height of the energy barrier, given by $\varepsilon^{\ddagger} = V + \varepsilon_{ZPE}$, where ε_{ZPE} is the harmonic zero-point energy correction and V is the height of the potential energy barrier.

First-principles Born-Oppenheimer molecular dynamics (BOMD) simulations have been carried out using the CPMD 3.17.1 package [32]. Simulations have been performed for the two enantiomeric forms R and S, starting from the same initial configurations. The electronic structure has been treated within the generalized gradient approximation to density functional theory, using the Perdew–Burke–Ernzerhof (PBE) exchange–correlation functional. [33,34] Vanderbilt ultrasoft pseudopotentials have been employed to represent core-valence electron interactions [35]. The simulations have been conducted in a NVT ensemble at temperature of 200 K controlled using a Nosé-Hoover thermostat [36].

RESULTS AND DISCUSSION

In this work, focus has been on the mechanisms of anti-E2 reactions [(1) and (2) reactions] and SN2, [(3) to (6) reactions] are evaluated, since they are more favored [37]. In Figure 1(a), we demonstrated the transition-states molecular structures and observed that the anti-E2 and back-side S_N2 channels exhibit a simultaneous transition-state and great geometric similarity of the enantiomers.

Thermodynamic and kinetic parameters were calculated at CCSD (T)/aug-cc-pVDZ//ωB97XD/aug-cc-pVDZ level of calculation. The energy difference between the enantiomeric forms are checked to be negligible both in S_N2 and E2 channels. The S_N2 channels are exothermic processes and present greater spontaneity in the reactions (3) and (5), when Cl is the leaving group. The reactions E2: is thermoneutral when the Cl is the leaving group (1) and when the iodine is the leaving group (2), it is endothermic; both configurations (R, S) of the reaction (2) are thermodynamically unfavorable. The kinetic parameters identified the largest barrier heights in the elimination channels, being the highest when I is the leaving group.

The kinetic rate constants for HS-+ $CHFCH_3Y$ (Y = Cl and I) reactions was calculated using the *deformed* transition state theory (d-TST) in a wide temperature range (200-400 K) at CCSD (T)/Aug-CC-pVDZ//ωB97XD/Aug-CC-pVDZ level calculation. The branching ratios for the E2 and S_N2 channels are defined as $\frac{k_{channel}}{k_{E2}+k_{S_N2}}$. At low temperatures the S_N2 channel is preferred while at high temperatures there is larger contribution of the E2 channel.

Not unexpectedly, it was not possible to differentiate the chiral selectivity of the reactions studied through the calculations of stationary electronic structure, as reported in previous studies. Due to the high reactivity at low temperature of the back-side S_N2 channel with X = CN and Y = I which corresponds to the negative activation energy, an analysis be performed by *first-principles* molecular dynamics. Figure 1(b) shows the temporal evolution of

progression variable s. Both the enantiomers lead to S_N2 products, but R enantiomer decreases its reactivity, and it takes a longer time for the reaction revealing the role of the Aquilanti mechanism. The stereodynamic effect shown in the simulations discriminates in the kinetics of these forms: studies are being conducted with regard to a number statistically relevant of trajectories to substantiate the orientational alignment and will be presented in a future work.

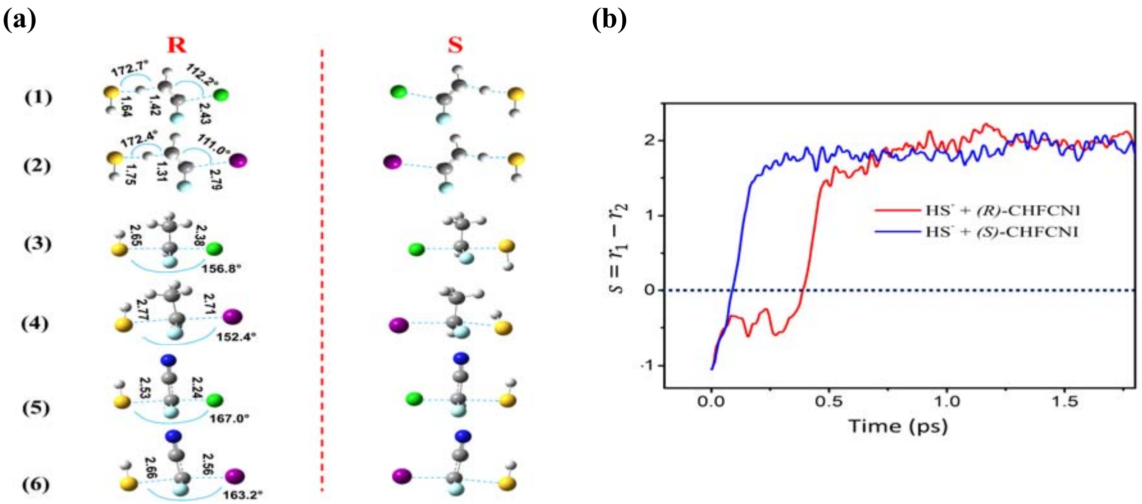

FIGURE 1. (a) Geometries and structural parameters optimized for the anti-E2 and side-back S_N2 transition-states of the HS^- + CHFXY (X = CH_3 and CN; Y = Cl and I) reaction in R and S configurations at ωB97XD/aug-cc- pVDZ level of calculation. Bond lengths are in angstroms and bond angles are in degrees. (b) Reactive trajectory for elementary S_N2 channel for HS^- + CHFCNI reaction in R and S configurations. The temporal evolution of the lengths of bond that is broken ($r_1 = C - I$) and the bond that is formed ($r_2 = C - S$) are reported. R enantiomer was observed to require longer time to react.

CONCLUSION

In this work, both thermodynamic and kinetic parameters were tackled to characterize the reaction mechanisms. The calculations of stationary electronic structure methods were not directly able to differentiate enantiomers, although allowing the choice of the reactional route, the back-side S_N2 with X = CN and Y = I. This process was verified as an interesting candidate for revealing the stereodirectional effect of chiral discrimination. The Aquilanti mechanism was observed for the CHFXY reaction (X = CN; Y = I) and HS^-: the control of the S_N2 channel trajectories allows the visualization of the R and S enantiomers, determining a lower reactivity to the R enantiomer.

ACKNOWLEDGMENTS

The authors are grateful for the support given by CAPES and CNPq. This research is also supported by the High Performance Computing Center at the Universidade Estadual de Goiás (UEG). Valter H. Carvalho-Silva thanks CNPq for the research funding programs [Universal 01/2016 - Faixa A - 406063/2016-8] and Organizzazione internazionale italo-latino Americana (IILA) for Biotechnology Sector-2019 scholarship. Federico Palazzetti, Nayara D. Coutinho and Andrea Lombardi acknowledge the Italian Ministry for Education, University and Research, MIUR, for financial support: SIR 2014 ‘‘Scientific Independence for young Researchers’’ (RBSI14U3VF).

REFERENCES

1. V. Aquilanti, G. Grossi, A. Lombardi, G. S. Maciel, and F. Palazzetti, Phys. Scr. **78**, 058119 (2008).
2. T. Kasai, D.-C. Che, M. Okada, P.-Y. Tsai, K.-C. Lin, F. Palazzetti, and V. Aquilanti, Phys. Chem. Chem. Phys. **16**, 9776 (2014).
3. V. Aquilanti and G. S. Maciel, Orig. Life Evol. Bios. **36**, 435-441 (2006).

4. T. -M. Su, F. Palazzetti, A. Lombardi, G. Grossi, V. Aquilanti, Rend. Fis. Acc. Lincei **24**, 291-297 (2013).
5. F. Palazzetti, G. S. Maciel, A. Lombardi, G. Grossi, and V. Aquilanti, J. Chinese Chem. Soc. **59** , 1 (2012).
6. V. Aquilanti, C. Caglioti, P. Casavecchia, G. Grossi, A. Lombardi, F. Palazzetti, and F. Pirani, "The astrochemical observatory: Computational and theoretical focus on molecular chirality changing torsions around O – O and S – S bonds" in International Conference of Computational Methods in Sciences and Engeneering-2017, edited by T. E. Simos et al., AIP Conference Proceedings 1906, American Institute of Physics, Thessaloniki, Greece, 2017, pp. 030010.
7. A. Lombardi and F. Palazzetti, J. Phys. Condens. Matter **30**, 063003 (2018).
8. L. G. Santin, E. M. Toledo, V. H. Carvalho-Silva, A. J. Camargo, R. Gargano, and S. S. Oliveira, J. Phys. Chem. C **120**, 19923 (2016).
9. A. Lombardi, G. S. Maciel, F. Palazzetti, G. Grossi, and V. Aquilanti, J. Vac. Soc. Japan **53**, 645 (2010).
10. V. Aquilanti, A. Lombardi, G. Grossi, G. S. Maciel, and F. Palazzetti, Rend. Acc. Fis. Lincei **22**, 125 (2011).
11. V. Aquilanti, M. Bartolomei, F. Pirani, D. Cappelletti, F. Vecchiocattivi, Y. Shimizu, and T. Kasai, Phys. Chem. Chem. Phys. **7**, 291 (2005).
12. D. -C. Che, F. Palazzetti, Y. Okuno, V. Aquilanti, and T. Kasai, J. Chem. Phys. A **114**, 3280-3286 (2010)
13. D. C. Che, K. Kanda, F. Palazzetti, V. Aquilanti, and T. Kasai, Chem. Phys. **399**, 180 (2012).
14. F. Palazzetti, G. S. Maciel, K. Kanda, M. Nakamura, D. -C. Che, T. Kasai, and V. Aquilanti, Phys. Chem. Chem. Phys. **16**, 9866-9875 (2014).
15. M. Nakamura, S. J. Yang, P. Y. Tsai, T. Kasai, K. C. Lin, D. C. Che, A. Lombardi, F. Palazzetti, and V. Aquilanti, J. Phys. Chem. A **120**, 5389 (2016).
16. M. Nakamura, F. Palazzetti, P. Tsai, and S. Yang, Phys. Chem. Chem. Phys. (2018). DOI: 10.1039/C8CP04270E
17. F. Palazzetti, P. -Y. Tsai, A. Lombardi, M. Nakamura, D. -C. Che, T. Kasai, K. -C. Lin, and V. Aquilanti, Rend. Acc. Fis. Lincei **24**, 299-308 (2013).
18. A. Lombardi, F. Palazzetti, G. S. Maciel, V. Aquilanti, and M. B. Sevryuk, Int. J. Quantum Chem. **111**, 1651 (2011).
19. P. R. P. Barreto, A. F. A. Vilela, A. Lombardi, G. S. Maciel, F. Palazzetti, and V. Aquilanti, J. Phys. Chem. A **111**, 12754 (2007).
20. Y. Alves, D. O. Só, P. Henrique, and D. O. Neto, Front. Chem. **6** , 1 (2019).
21. G. S. Maciel, P. R. P. Barreto, F. Palazzetti, and A. Lombardi, J. Chem. Phys. **164302**, 164302 (2008).
22. M. Smith, *March's Advanced Organic Chemistry : Reactions, Mechanisms, and Structure.* (Wiley, 2013).
23. M. J. Frisch *et al.* Gaussian 09 (2009).
24. V. H. Carvalho-Silva, V. Aquilanti, H. C. B. de Oliveira, and K. C. Mundim, J. Comput. Chem. **38**, 178 (2017).
25. N. D. Coutinho, F. O. Sanches-Neto, V. H. Carvalho-Silva, H. C. B. de Oliveira, L. A. Ribeiro, and V. Aquilanti, J. Comput. Chem. **39**, 2508 (2018).
26. F. O. Sanches-Neto, N. D. Coutinho, and V. H. Carvalho-Silva, Phys. Chem.Chem. Phys. **19**, 24467 (2017).
27. D. Claudino, R. Gargano, V. H. Carvalho-Silva, G. M. E Silva, and W. F. Da Cunha, J. Phys. Chem. A **120**, 5464 (2016).
28. V. Aquilanti, E. P. Borges, N. D. Coutinho, K. C. Mundim, and V. H. Carvalho-Silva, Rend. Fis. Acc. Lincei **29**, 787-802 (2018).
29. H. G. Machado, F. O. Sanches-Neto, N. D. Coutinho, K. C. Mundim, F. Palazzetti, and V. H. Carvalho-Silva, Submitted.
30. V. H. Carvalho-Silva, N. D. Coutinho, and V. Aquilanti, Front. Chem. **7**, 380 (2019).
31. V. Aquilanti, N. D. Coutinho, and V. H. Carvalho-Silva, Phil. Trans. R. Soc. A **375**, 20160201 (2017).
32. CPMD version 4.1, (2012).
33. J. P. Perdew, K. Burke, and M. Ernzerhof, Phys. Rev. Lett. **77**, 3865 (1996).
34. J. P. Perdew, K. Burke, and M. Ernzerhof, Phys. Rev. Lett. **78**, 1396 (1997).
35. D. Vanderbilt, Phys. Rev. B **41**, 7892 (1990).
36. G. J. Martyna, M. L. Klein, and M. Tuckerman, J. Chem. Phys. **97**, 2635 (1992).
37. L. Yang, J. Zhang, J. Xie, X. Ma, L. Zhang, C. Zhao, and W. L. Hase, J. Phys. Chem. A **121**, 1078 (2017).

Structures of Stable Oxide Cluster Ions of First-Row Late Transition Metals: An Ion Mobility-Mass Spectrometric Study

Fuminori Misaizu[1, a)], M. Abdul Latif[1, 2], Jenna W. J. Wu[1], Ryoichi Moriyama[1], Motoyoshi Nakano[1], Kiichirou Koyasu[1], and Keijiro Ohshimo[1]

[1] *Department of Chemistry, Graduate School of Science, Tohoku University, Sendai 980-8578, Japan*
[2] *Department of Chemistry, Faculty of Science, Begum Rokeya University, Rangpur-5400, Bangladesh*

[a)] Corresponding author: misaizu@m.tohoku.ac.jp

Abstract. Ion mobility mass spectrometry has been applied to unveil stable compositions and geometrical structures of oxide cluster ions of first-row late transition metals such as Fe, Co, Ni, Cu, and Zn. Geometrical structures were assigned by comparison of collision cross sections obtained by this experiment with those calculated for the structures predicted by quantum chemical calculations. Mass spectra of stable compositions of the metal oxide cluster ions resulting from collision-induced-dissociation in the ion drift cell have also been obtained. Oxides of the late transition metals except for Cu were found to have common stable compositions with the same numbers of metal and oxygen atoms, $(FeO)_n^+$, $(CoO)_n^+$, $(NiO)_n^+$, and $(ZnO)_n^+$, in addition to oxygen-rich $Fe_nO_{n+1}^+$ ions or oxygen-deficient $Co_nO_{n-1}^+$, $Ni_nO_{n-1}^+$, and $Zn_nO_{n-1}^+$ ions for n up to ≈10. As for the copper oxide clusters, $Cu_nO_m^+$ ions with n:m ≈ 2:1 were predominant in the mass spectrum. For the stable ions, structural transitions were commonly observed from two-dimensional (2D) cyclic or sheet structures to three-dimensional (3D) compact structures at around the size n smaller than 8. Both types of isomers coexist at n = 6-8 for $(FeO)_n^+$ and $(ZnO)_n^+$, and at n = 5 for $(NiO)_n^+$, whereas 3D structures were clearly observed from n = 6 for $(CoO)_n^+$. These structural transitions were characteristic for the oxide cluster ions of the late transition metals, in marked contrast to those of early transition metals.

INTRODUCTION

Metal oxide nanoparticles are regarded not only as local structure models of solids or surfaces but also as candidates of novel functional materials. In particular, nanoparticles of transition metal oxides are now widely utilized as catalysts, materials of electronic devices, magnetic storage media, and so on. The possibility of application of smaller sized particles, that is, nanoclusters or clusters, is also pursued extensively in the past few decades. It is important to investigate the size-dependent change of properties of the clusters, since most of the properties have strong size dependence. In addition, there are some structural isomers even if the cluster size was selected. Therefore, it is necessary to investigate the size- and isomer-selected clusters to unveil the pure properties of the clusters.

Spectroscopic techniques such as infrared spectroscopy and photoelectron spectroscopy have been applied for the determination of cluster structures. However, it is a long way to obtain the spectra of wide range of size-selected clusters. On the other hand, ion mobility spectrometry, which is an analytical and separation method using interaction of the target ions with buffer gas, is also a powerful method to assign geometrical structures of cluster ions in the wide size range from the determination of collision cross sections (CCSs). For the purpose of identifying cluster ion structures, ion mobility mass spectrometry (IM-MS), which is a combination of ion mobility spectrometry and mass spectrometry, was applied to various cluster ions such as metal clusters [1], group 14 clusters [2], ionic nanocrystals [3], molecular clusters [4], and also metal oxide clusters [5].

We have applied IM-MS to investigate stable compositions and geometrical structures of oxide cluster ions of first-row late transition metals, Fe [6], Co [7], Ni [8], Cu [9] and Zn [10]. In the present paper, we showed the results of the structure assignments for oxygen-equivalent cluster ions, $(FeO)_n^+$, $(CoO)_n^+$, $(NiO)_n^+$, and $(ZnO)_n^+$. This is the first comparative study of the structures of these metal oxide cluster ions, whereas such comparison was reported theoretically for neutral clusters [11].

EXPERIMENTAL AND THEORETICAL METHODS

Experiment was performed in a vacuum apparatus containing a cluster ion source, an ion-drift cell for ion mobility spectrometry, and a reflectron-type time-of-flight mass spectrometer (TOF-MS). The setup was already reported in detail elsewhere [5-10]. Metal oxide cluster cations were produced by laser vaporization of a metal rod and subsequent reaction with O_2 gas seeded in He which was expanded from a pulsed valve. The generated cluster ions were injected into the ion-drift cell with a given kinetic energy E_{inj} between 50-250 eV by a pulsed electric field. The ion-drift cell was filled with He buffer gas at 0.80 or 0.90 Torr and was cooled to 190 K. The ions were accelerated by the electrostatic field (E = 10 V/cm) in the drift cell. As a result of the balance between the collisions and electrostatic acceleration, the ions reached a constant drift velocity v_{d} which is proportional to E, that is, $v_{\mathrm{d}} = KE$. Here the coefficient K is called ion mobility. After exiting the cell, the ions were re-accelerated in an acceleration region of the reflectron TOF-MS at a given time Δt later from the ion-injection pulse. This delay time, Δt, was hereafter denoted as "arrival time". Finally, the ions were mass-analyzed by the TOF-MS. In the IM-MS measurement, we obtained a series of TOF mass spectra sequentially by scanning Δt. As a result, cluster ions with different cross sections were separately detected at different arrival times in a two-dimensional (2D) plot of TOF vs. arrival time.

The collision cross section Ω between the ion and a He atom was determined from the measurement of the ion mobility K using the following Eq. (1) based on the theory of ion transport [12].

$$K = \frac{3e}{16N}\left(\frac{2\pi}{k_{\mathrm{B}}\mu T_{\mathrm{eff}}}\right)^{1/2}\frac{1}{\Omega}, \tag{1}$$

where e is the elementary charge, N is the number density of the buffer gas, k_{B} is the Boltzmann constant, μ is the reduced mass of the ion and the buffer gas atom. The term T_{eff}, the effective temperature of the ions, is given by $T_{\mathrm{BG}} + m_{\mathrm{B}}v_{\mathrm{d}}^2/3k_{\mathrm{B}}$, where T_{BG} is the buffer gas temperature and m_{B} is the mass of buffer gas. The ion flight time in the drift cell t_{d} was first determined by subtracting the time flying the outside regions of the cell, which was calculated with solving the equations of motion of the ions, from the peak of the arrival time distribution of the ion. Then the drift velocity v_{d} and thus the ion mobility K were determined from t_{d}. Finally, Ω was determined from the Eq. (1). A TOF mass spectrum was also obtained from the 2D plot of TOF vs. arrival time noted above. In the present apparatus, after injection into the cell by a pulsed electric field, cluster ions diffuse spatially in their running direction depending on their cross sections before reaching the acceleration region of the TOF mass spectrometer. Therefore, the TOF mass spectrum was obtained by summing up all the TOF spectra measured at every arrival time because of the spread of arrival time distribution of the cluster ions.

Quantum chemical calculations for the geometry optimizations of metal oxide cluster ions were performed prior to calculations of collision integrals which can be compared with the CCSs of the ions. The geometry optimizations were carried out with 6-311+G(d) (Zn oxides) or 6-31+G(d) (Fe, Co, and Ni oxides) basis sets and B3LYP functional in Gaussian 09. Several spin states were examined in these calculations. The CCS of the ion with a He atom was calculated by the projection approximation method which is included in the MOBCAL program [13].

RESULTS AND DISCUSSION

Stable Compositions of Metal Oxide Cluster Ions

The observed cluster-ion compositions were strongly dependent on the ion injection energy E_{inj} to the ion-drift cell. In general, a few series of cluster ions were observed in the TOF mass spectra at high ion injection energy (E_{inj} = 250 eV) as shown in **FIGURE 1**. This is a result of collision induced dissociation just after injection into the ion-drift cell as discussed in previous papers [14], and therefore, the ions survived at high injection energies are stable compositions with respect to dissociation.

As a result, oxygen-equivalent cluster ions such as $(FeO)_n^+$, $(CoO)_n^+$, and $(NiO)_n^+$ were observed in these mass spectra. This result reflects that the late transition metals in general have an oxidation number of +2, although one electron is lacking in these singly charged cluster ions. In addition, one oxygen-rich series, $Fe_nO_{n+1}^+$, was also

observed for iron oxide cluster ions, due to the contribution of iron oxidation number of +3. By contrast, one oxygen-poor series, $Co_nO_{n-1}^+$ and $Ni_nO_{n-1}^+$, were also predominantly observed for Co and Ni oxide cluster ions, probably because of the total positive charge of the ions. As for the anions of these metal oxide clusters, more oxygen-rich clusters were observed as stable compositions. Also for the zinc oxide cluster ions, the $(ZnO)_n^+$ ions were exclusively observed in the mass spectrum under the similar conditions of **FIGURE 1** [10], which reflects the fact that the zinc has only an oxidation number of +2 in bulk compounds. Copper oxide cluster ions have, on the other hand, main compositions of $Cu_nO_{n/2}^+$ and neighboring series, which are probably due to the oxidation number of +1 of the copper atom [9].

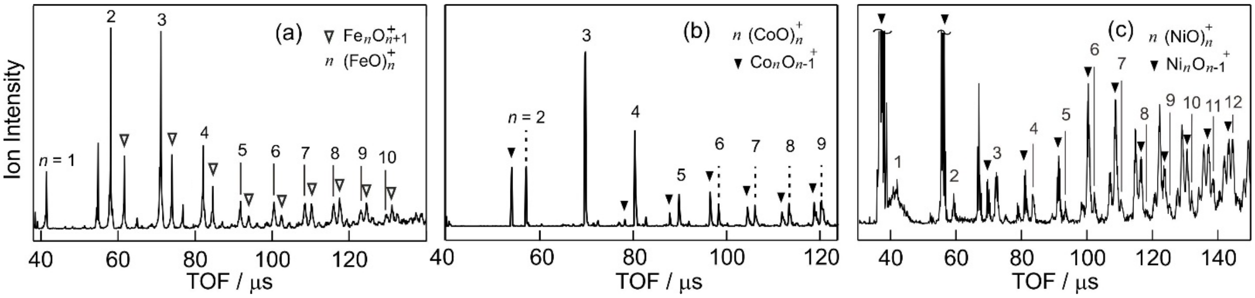

FIGURE 1. TOF mass spectra of cluster ions of (a) iron oxide, (b) cobalt oxide, and (c) nickel oxide with an ion-injection energy of 250 eV to the ion-drift cell. The pressures of the drift cell were 0.80 Torr for (a) and (b), and 0.90 Torr for (c). The cell temperature was kept at 190 K.

Collision Cross Sections (CCSs) and Structures of Metal Oxide Cluster Ions

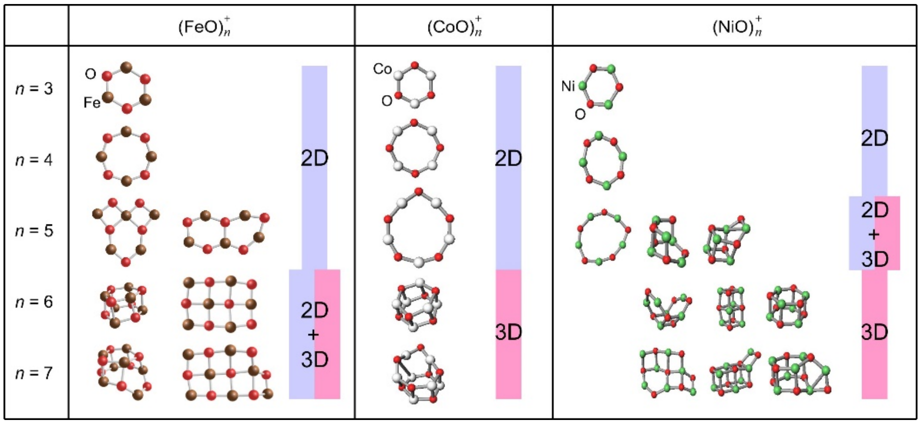

FIGURE 2. Typical structures of $(FeO)_n^+$, $(CoO)_n^+$, and $(NiO)_n^+$cluster ions for n = 3-7. These structures were assigned from the comparison between the CCSs determined by IM-MS measurements and those of the optimized structures by DFT calculations. 2D to 3D structural change was commonly found at n = 5 or 6 with increasing cluster size.

Here we summarized qualitatively the changes of the assigned structures of oxygen-equivalent metal oxide cluster ions, $(FeO)_n^+$, $(CoO)_n^+$, $(NiO)_n^+$, and $(ZnO)_n^+$, which are the stable compositions as noted above, with increasing cluster size up to n = 8. Typical structures for the former three cluster ions for n = 3-7 are shown in **FIGURE 2**, which were assigned from the comparison between the CCSs determined by IM-MS measurements and those of the optimized structures by DFT calculations. These structures were obtained for the cluster ions with different spin states, although the relative energy was dependent on the spin states. As for $(FeO)_n^+$, the ions were assigned to have 2D ring structures for n = 3-5, whereas three-dimensional (3D) tower structures exist in addition to 2D sheet isomers for n = 6 and 7. Similar isomer coexistence was also found for $(FeO)_8^+$. On the other hand, 2D to 3D structure change was clearly observed between n = 5 and 6 for $(CoO)_n^+$. Similar structural change was also

observed for $(NiO)_n^+$, excepting the 2D and 3D isomer coexistence at $n = 5$. Also for $(ZnO)_n^+$, similar change was discerned, and both 2D and 3D structures were found at $n = 6$-8. Therefore, structure transitions from 2D to 3D were commonly found at $n = 5$ or 6 with increasing cluster size for these oxygen-equivalent cluster ions of the late transition metal oxides. Another common feature in the structures of these metal oxide cluster ions is that the oxygen atoms are bridged between two metal atoms. This feature is a result of ionic bond nature between doubly charged metal atomic ions and O^{2-}. In fact, these structural features showed marked contrast with the oxide cluster ions of early transition metals, such as $(TiO_2)_n^+$ [5], $(V_2O_5)_{n/2}^+$ [15], and $(CrO_2)_n^+$ [16], and also with $Cu_nO_{n/2}^+$ ions [9]. The latter ions have more oxygen atoms than the metal atoms, and the oxygen atoms in most of the cluster ions are again bridged between metal atoms. Therefore, 3D complicated structures were already formed even at the smallest cluster size in the ions of these early transition metal oxides.

ACKNOWLEDGMENTS

This work was supported by Grants-in-Aid for Scientific Research (KAKENHI, nos. JP16K05641 and JP18K14173) from the Japan Society for the Promotion of Science (JSPS), the Research Seeds Quest Program (JST), and the Murata Science Foundation. The calculations were performed in part by using the facilities of the Research Center for Computational Science, Okazaki, Japan.

REFERENCES

1. S. Gilb, P. Weis, F. Furche, R. Ahlrichs, and M. M. Kappes, J. Chem. Phys. **116**, 4094–4101 (2002).
2. G. von Helden, P. R. Kemper, N. G. Gotts, and M. T. Bowers, Science **259**, 1300–1302 (1993).
3. R. R. Hudgins, P. Dugourd, J. M. Tenenbaum, and M. F. Jarrold, Phys. Rev. Lett. **78**, 4213–4216 (1997).
4. M. J. Rusyniak, Y. M. Ibrahim, D. L. Wright, S. N. Khanna, and M. S. El-Shall, J. Am. Chem. Soc. **125**, 12001–12013 (2003).
5. K. Ohshimo, N. Norimasa, R. Moriyama, and F. Misaizu, J. Chem. Phys. **144**, 194305 (2016). (8 pages)
6. K. Ohshimo, T. Komukai, R. Moriyama, and F. Misaizu, J. Phys. Chem. A **118**, 3899–3905 (2014).
7. K. Ota, K. Koyasu, K. Ohshimo, and F. Misaizu, Chem. Phys. Lett. **588**, 63–67 (2013).
8. K. Ohshimo, S. Azuma, T. Komukai, R. Moriyama, and F. Misaizu, J. Phys. Chem. C **119**, 11014–11021 (2015).
9. M. A. Latif, J. W. J. Wu, R. Moriyama, M. Nakano, K. Ohshimo, and F. Misaizu, ACS Omega **3**, 18705–18713 (2018).
10. K. Koyasu, K. Komatsu, and F. Misaizu, J. Chem. Phys. **139**, 164308 (2013). (6 pages)
11. G. L. Gutsev, K. G. Belay, K. V. Bozhenko, L. G. Gutsev, and B. R. Ramachandran, Phys. Chem. Chem. Phys. **18**, 27858-27867 (2016).
12. E. A. Mason and E. W. McDaniel, *Transport Properties of Ions in Gases* (Wiley and Sons, New York, 1988).
13. M. F. Mesleh, J. M. Hunter, A. A. Shvartsburg, G. C. Schatz, and M. F. Jarrold, J. Phys. Chem. **100**, 16082–16086 (1996).
14. K. Ohshimo, T. Takahashi, R. Moriyama, and F. Misaizu, J. Phys. Chem. A **118**, 9970–9975 (2014).
15. J. W. J. Wu, R. Moriyama, H. Tahara, K. Ohshimo, and F. Misaizu, J. Phys. Chem. A **120**, 3788–3796 (2016).
16. R. Moriyama, R. Sato, M. Nakano, K. Ohshimo, and F. Misaizu, J. Phys. Chem. A **121**, 5605–5613 (2017).

Precise Synthesis of Platinum and Alloy Clusters and Elucidation of Their Structures

Sakiat Hossain, Yukari Imai, and Yuichi Negishi[a)]

Department of Applied Chemistry, Faculty of Science, Tokyo University of Science, 1-3 Kagurazaka, Shinjuku-ku, Tokyo 162-8601, Japan

[a)] Corresponding author: negishi@rs.kagu.tus.ac.jp

Abstract. We report herein the new Pt and bi-/tri-metallic alloy clusters. For the Pt clusters, we have precisely synthesized the cationic Pt_{17} cluster, $[Pt_{17}(CO)_{12}(PPh_3)_8]^{n+}$ (n = 1, 2), protected by CO and triphenylphosphine (PPh_3) by a simple method. The study on the synthesized cluster revealed that $[Pt_{17}(CO)_{12}(PPh_3)_8]^{n+}$ (n = 1, 2) has a geometric structure similar to that of previously reported $Pt_{17}(CO)_{12}(PEt_3)_8$ (PEt_3 = triethylphosphine) and that $[Pt_{17}(CO)_{12}(PPh_3)_8]^{n+}$ (n = 1, 2) possessed a discretized electronic structure. For the bimetallic cluster, we have established a method to selectively synthesize hetero-biicosahedral $[Au_{24}Pd(PPh_3)_{10}(SC_2H_4Ph)_5Cl_2]^+$ (SC_2H_4Ph = phenylethanethiolate), in which a Pd atom replaces the central atom in one icosahedral Au_{13} core. The study on the synthesized cluster revealed that $[Au_{24}Pd(PPh_3)_{10}(SC_2H_4Ph)_5Cl_2]^+$ has dipole moment and is comparatively stable during cluster reduction. For the trimetallic cluster, we succeeded in the compositionally selective synthesis of $[Au_{\sim20}Ag_{\sim4}Pd(SC_2H_4Ph)_{18}]^0$ and $[Au_{\sim20}Ag_{\sim4}Pt(SC_2H_4Ph)_{18}]^0$. Single crystal X-ray structural analysis revealed the precise position of each metal element in these metal clusters. In this study, it was demonstrated that reacting with thiol at an elevated temperature is important to direct the metal elements to the most stable positions.

INTRODUCTION

In recent years, it has become possible to synthesize gold (Au) clusters[1] and silver (Ag) clusters[2] with atomic precision using thiolate (SR) or phosphine (PR_3) as a ligand. The electronic/geometric structures and size-specific physical/chemical properties of these metal clusters have also been investigated extensively. Applied research on these clusters has been conducted in a wide variety of fields such as sensing, imaging, cancer radiation therapy, catalysis, photocatalysis, solar cells, photosensitization, and single-electron devices.

Similar to these metal clusters, platinum (Pt) clusters have also attracted much interest. An attractive feature of Pt clusters is their high catalytic activity in a variety of reactions.[3] In particular, Pt clusters have recently attracted considerable attention from the viewpoint of the miniaturization of redox catalysts used in fuel cells. In the precise synthesis of these Pt clusters, carbon monoxide (CO) or PR_3 is used as the main ligand. However, little information has been obtained on the electronic structure and physical/chemical properties of $Pt_n(CO)_m(PR_3)_l$ clusters to date.

Alloy clusters have also attracted considerable attention from the viewpoint of generating nanomaterials with new physical/chemical properties and functionalities. Synthesis methods with atomic accuracy have already been established for several alloy clusters.[4] However, there are still many alloy clusters that cannot be synthesized with atomic precision.

Our group has been attempting to establish the method to precisely synthesize new Pt and alloy clusters and elucidate their geometrical and electronic structures. In this paper, we report three kinds of clusters, $[Pt_{17}(CO)_{12}(PPh_3)_8]^{n+}$ (n = 1, 2; PPh_3 = triphenylphosphine),[5] $[Au_{24}Pd(PPh_3)_{10}(SC_2H_4Ph)_5Cl_2]^+$ (Pd = palladium; SC_2H_4Ph = phenylethanethiolate),[6] and $[Au_{\sim20}Ag_{\sim4}M(SC_2H_4Ph)_{18}]^0$ (M = Pd or Pt),[7] which were recently synthesized in our group.

RESULTS AND DISCUSSION

Pt Cluster; $[Pt_{17}(CO)_{12}(PPh_3)_8]^{n+}$ (n = 1, 2)

In this research, the final objective was to obtain experimental information about the largely unknown electronic structure of $Pt_n(CO)_m(PR_3)_l$ clusters. To this end, we precisely synthesized a Pt_{17} cluster ($[Pt_{17}(CO)_{12}(PPh_3)_8]^{n+}$; n = 1, 2) protected by CO and PPh_3 by a simple method and studied its geometric and electronic structure.[5]

In previous work, neutral $Pt_{17}(CO)_{12}(PEt_3)_8$ (PEt_3 = triethylphosphine) was synthesized in the following three steps: 1) a Pt salt (Na_2PtCl_4) was reacted with CO to produce a $[Pt(CO)_2]_n$ oligomer, 2) the $[Pt(CO)_2]_n$ oligomer was reacted with PEt_3 to give $Pt_5(CO)_6(PEt_3)_4$, and 3) $Pt_{17}(CO)_{12}(PEt_3)_8$ was synthesized by thermal decomposition of $Pt_5(CO)_6(PEt_3)_4$.[8] In our study, we synthesized cationic $[Pt_{17}(CO)_{12}(PPh_3)_8]^{n+}$ (n = 1, 2) in quite a different way. Specifically, an ethylene glycol solution containing H_2PtCl_6 and NaOH was heated at 120 °C, which induced the reduction of Pt ions and the generation of CO by oxidation of ethylene glycol. Then, PPh_3 was added to the solution to prepare $Pt_n(CO)_m(PR_3)_l$ clusters containing both CO and PPh_3.

The mass spectrometry of the products revealed that the cationic $[Pt_{17}(CO)_{12}(PPh_3)_8]^{n+}$ (n = 1, 2) were synthesized by this simple method (Figure 1a). Single-crystal X-ray structure analysis of $[Pt_{17}(CO)_{12}(PPh_3)_8][(SbF_6)_n]$ (n = 1, 2; SbF_6 = hexafluoroantimonate) (Figure 1b) revealed that $[Pt_{17}(CO)_{12}(PPh_3)_8][(SbF_6)_n]$ (n = 1, 2) have a geometric structure similar to that of neutral $Pt_{17}(CO)_{12}(PEt_3)_8$. The optical absorption spectroscopy (Figure 1c) and electrochemical measurements (Figure 1d) demonstrated that $[Pt_{17}(CO)_{12}(PPh_3)_8][(SbF_6)_n]$ (n = 1, 2) has a discrete electronic structure similar to that of fine Au clusters.[9] The method used to synthesize $[Pt_{17}(CO)_{12}(PPh_3)_8]^{n+}$ (n = 1, 2) is extremely simple compared with those reported for other Pt clusters such as $Pt_{17}(CO)_{12}(PEt_3)_8$. Therefore, in the future, it is expected that more fundamental and applied research will be conducted on Pt clusters based on the results of this research.

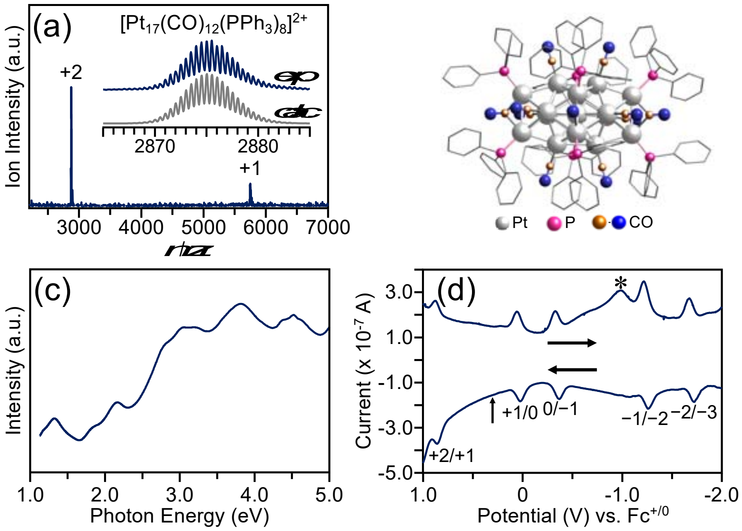

FIGURE 1. The results obtained for $[Pt_{17}(CO)_{12}(PPh_3)_8]^{n+}$ (n = 1, 2); (a) positive-ion electrospray ionization (ESI) mass spectrum, (b) geometrical structure of $[Pt_{17}(CO)_{12}(PPh_3)_8][SbF_6]$, (c) optical absorption spectrum, and (d) differential pulse voltammetry (DPV) curve. In (d), the vertical arrow indicates the open-circuit potential. The peak indicated by an asterisk (*) is presumed to be caused by impurities. Reproduced from reference 5. Copyright 2017 American Chemical Society.

Bimetallic Alloy Cluster; $[Au_{24}Pd(PPh_3)_{10}(SC_2H_4Ph)_5Cl_2]^+$

A recent study implied that a hetero-biicosahedral 25-atom cluster composed of two kinds of icosahedral 13-atom cores could serve as a molecular rectifier and dipole material.[10] However, no hetero-biicosahedral 25-atom clusters containing three types of ligands, PR_3, halogens, and SR, have been reported. In this study, we attempted to synthesize and elucidate the electronic structure of a hetero-biicosahedral 25-atom cluster in which the central atom of one icosahedral Au_{13} core is replaced by a hetero atom.

It has been reported that Pd substitutes with the central atom of Au_{13} (Pd@Au_{12}).[11] In addition, because the electronegativity of Pd (2.20) is lower than that of Au (2.54), charge transfer from Pd to Au is likely to occur in Pd@Au_{12}. Therefore, charge transfer and generation of a dipole moment are both expected to occur between the two icosahedral cores Pd@Au_{12} and Au@Au_{12} based on the difference in charge density of the central atoms. For these reasons, we selected Pd as the substituting element in this study.[6]

We established a method to selectively synthesize hetero-biicosahedral $[Au_{24}Pd(PPh_3)_{10}(SC_2H_4Ph)_5Cl_2]^+$, in which a Pd atom replaces the central atom in one icosahedral Au_{13} core (Figure 2a and 2b). Optical absorption spectroscopy suggested that the electronic structure of each individual icosahedral 13-atom core in $[Au_{24}Pd(PPh_3)_{10}(SC_2H_4Ph)_5Cl_2]^+$ was reasonably well maintained, similar to the case of $[Au_{25}(PPh_3)_{10}(SC_2H_4Ph)_5Cl_2]^{2+}$ (Figure 2c). Density functional theory calculation revealed that the peak splitting in the region below 2.0 eV of the optical absorption spectrum of $[Au_{24}Pd(PPh_3)_{10}(SC_2H_4Ph)_5Cl_2]^+$ (Figure 2c) is due to the splitting of highest occupied molecular orbitals and also suggested that this cluster has dipole moment. Electrochemical measurements showed that $[Au_{24}Pd(PPh_3)_{10}(SC_2H_4Ph)_5Cl_2]^+$ was relatively stable to reduction (Figure 2d). These results are expected to contribute to the development of molecular rectifiers and dipole materials based on hetero-biicosahedral 25-atom clusters.

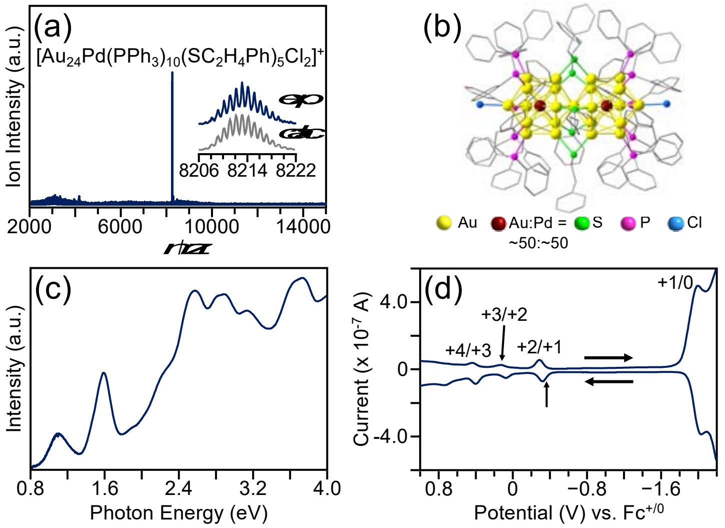

FIGURE 2. The results obtained for $[Au_{24}Pd(PPh_3)_{10}(SC_2H_4Ph)_5Cl_2]^+$; (a) positive-ion ESI mass spectrum, (b) geometrical structure of $[Au_{24}Pd(PPh_3)_{10}(SC_2H_4Ph)_5Cl_2]$Cl, (c) optical absorption spectrum, and (d) DPV curve. Reproduced from reference 6. Copyright 2018 Royal Society of Chemistry.

Trimetallic Alloy Cluster; $[Au_{\sim20}Ag_{\sim4}M(SC_2H_4Ph)_{18}]^0$ (M = Pd or Pt)

As shown above, bimetallic alloy clusters with a strictly controlled chemical composition and metal positions can be synthesized for the several bimetallic alloy clusters. Those clusters exhibit physical/chemical properties and functions that differ from those of related monometallic clusters. If the kind of metal elements were increased, the alloy clusters could exhibit further varied physical and chemical properties and functions. However, as the kind of metal elements in the clusters increases, control of the chemical composition of the alloy cluster becomes difficult. In fact, a distribution in the chemical composition exists in the reported trimetallic alloy clusters.[12] To understand the basic properties of trimetallic alloy clusters and to control their functions precisely, it is necessary to synthesize trimetallic alloy clusters with a controlled chemical composition.

In this study, we succeeded in the compositionally selective synthesis of two trimetallic $[Au_{\sim20}Ag_{\sim4}M(SC_2H_4Ph)_{18}]^0$ (M = Pd or Pt) alloy clusters with a well-controlled chemical composition and metal positions (Figure 3a and 3b).[7] By targeting controlled $[Au_{\sim20}Ag_{\sim4}M(SC_2H_4Ph)_{18}]^0$ (M = Pd or Pt), it is expected that a fundamental understanding of the physical and chemical properties of trimetallic alloy clusters and their origin could be obtained. In addition, this study demonstrates that geometric factor can be leveraged to control the Ag position on the surface of the Au–Ag alloy clusters. It is expected that the chemical composition and the metal position of many alloy clusters that contain Au and Ag could be controlled by a similar approach, and that many functionally controlled alloy clusters could be created in the future.

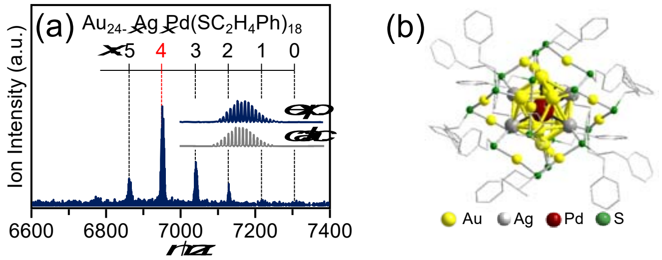

FIGURE 3. The results obtained for $[Au_{\sim20}Ag_{\sim4}Pd(SC_2H_4Ph)_{18}]^0$; (a) matrix-assisted laser desorption/ionization mass spectrum and (b) geometrical structure Reproduced from reference 7. Copyright 2017 American Chemical Society.

CONCLUSIONS

A precise synthesis method for Pt and bi- and tri-metallic alloy clusters has been successfully established. We have elucidated their geometrical structures, and have investigated their electronic structures. We expect that our findings might serve as clear design guidelines for creating new functional nanomaterials. In the future, we expect that techniques to regularly assemble alloy clusters will be developed to enable these applications.

ACKNOWLEDGMENTS

We thank Prof. De-en Jiang and Dr. Guoxiang Hu (University of California, Riverside) for theoretical calculation and Dr. Lakshmi V. Nair (National Institute of Technology Calicut) and Dr. Wataru Kurashige (Tokyo University of Science) for their technical assistance. This work was supported by the Japan Society for the Promotion of Science (JSPS) KAKENHI (grant numbers JP16H04099 and 16K21402), Scientific Research on Innovative Areas "Coordination Asymmetry" (grant number 17H05385). Funding from the Takahashi Industrial and Economic Research Foundation and Asahi Glass Foundation is also gratefully acknowledged.

REFERENCES

1. Kurashige, W.; Niihori, Y.; Sharma, S.; Negishi, Y. *Coord. Chem. Rev.* **2016**, *320–321*, 238–250.
2. Yang, H.; Wang, Y.; Huang, H.; Gell, L.; Lehtovaara, L.; Malola, S.; Häkkinen, H.; Zheng, N. *Nat. Commun.* **2013**, *4*, 2422.
3. Yamamoto, K.; Imaoka, T.; Chun, W.-J.; Enoki, O.; Katoh, H.; Takenaga, M.; Sonoi, A. *Nat. Chem.* **2009**, *1*, 397−402.
4. Hossain, S.; Niihori, Y.; Nair, L. V.; Kumar, B.; Kurashige, W.; Negishi, Y. *Acc. Chem. Res.* **2018**, *51*, 3114−3124.
5. Nair, L. V.; Hossain, S.; Wakayama, S.; Takagi, S.; Yoshioka, M.; Maekawa, J.; Harasawa, A.; Kumar, B.; Niihori, Y.; Kurashige, W.; Negishi, Y. *J. Phys. Chem. C* **2017**, *121*, 11002–11009.
6. Nair, L. V.; Hossain, S.; Takagi, S.; Imai, Y.; Hu, G.; Wakayama, S.; Kumar, B.; Kurashige, W.; Jiang, D.-e.; Negishi, Y. *Nanoscale* **2018**, *10*, 18969–18979.
7. Hossain, S.; Ono, T.; Yoshioka, M.; Hu, G.; Hosoi, M.; Chen, Z.; Nair, L. V.; Niihori, Y.; Kurashige, W.; Jiang, D.-e.; Negishi, Y. *J. Phys. Chem. Lett.* **2018**, *9*, 2590–2594.
8. Kurasov, S. S.; Eremenko, N. K.; Slovokhotov, Y. L.; Struchkov, Y. T. *J. Organomet. Chem.* **1989**, *361*, 405–408.
9. Negishi, Y.; Nobusada, K.; Tsukuda, T. *J. Am. Chem. Soc.* **2005**, *127*, 5261−5270.
10. Iwasa, T.; Nobusada, K.; Nakajima, A. *J. Phys. Chem. C* **2013**, *117*, 24586−24591.
11. Negishi, Y.; Kurashige, W.; Niihori, Y.; Nobusada, K. *Phys. Chem. Chem. Phys.* **2013**, *15*, 18736–18751.
12. Sharma, S.; Kurashige, W.; Nobusada, K.; Negishi, Y. *Nanoscale* **2015**, *7*, 10606−10612.

Preface of Symposium “Photonic Metamaterials”

Tatjana Gric

Department of Electronic Systems, Vilnius Gediminas Technical University, Vilnius, Lithuania, Aston Institute of Photonic Technologies, Aston University, Birmingham B4 7ET, UK, Semiconductor Physics Institute, Center for Physical Sciences and Technology, Vilnius, Lithuania

Tatjana.Gric@Dal.Ca

Session **Photonic Metamaterials**. Metamaterials have, in the last few decades, inspired scientists and engineers to think about waves beyond traditional constraints imposed by materials in which they propagate, conceiving new functionalities, such as subwavelength imaging, invisibility cloaking and broadband ultraslow light. While mainly for ease of fabrication, many of the metamaterials concepts have initially been demonstrated at longer wavelengths and for microwaves, metamaterials have subsequently moved to photonic frequencies and the nanoscale. At the same time, metamaterials are recently embedding new quantum materials such as graphene, dielectric nanostructures and, as metasurfaces, surface geometries and surface waves while also embracing new functionalities such as nonlinearity, quantum gain and strong light-matter coupling.

This Session, "Photonic Metamaterials" is devoted to exhibiting the current state of the art of the dynamic and vibrant field of photonic metamaterials reaching across various disciplines, suggesting exciting applications in chemistry, material science, biology, medicine, and engineering. It will illuminate recent advances in the wider photonic metamaterials field, such as (to mention a few) active metamaterials and metasurfaces, self-organized nanoplasmonic metamaterials, graphene metamaterials, metamaterials with negative or vanishing refractive index and topological metamaterials facilitating ultraslow broadband waves on the nanoscale and novel applications, such as stopped-light lasing.

Swift Heavy Ion Irradiated Planar Waveguides in a Rare Earth Doped Tungsten Tellurite Glass and a Tungstate Crystal

I. Bányász[1, a)], G.U.L. Nagy[2], I. Rajta[2], V. Havránek[3], V. Vosecek[3], M. Fried[4], P. Petrik[4], E. Agócs[4,] B. Kalas[4,] M. Veres[1] and R. Holomb[1]

[1] *Wigner Research Centre for Physics, Hungarian Academy of Sciences, P.O.B. 49, H-1525, Budapest, Hungary*
[2] *MTA Atomki, Institute for Nuclear Research, Hungarian Academy of Sciences, H-4001 Debrecen, P.O. Box 51 Hungary*
[3] *Nuclear Physics Institute AV CR, Řež near Prague, 250 68, Czech Republic*
[4.] *Research Institute for Technical Physics and Materials Science, Centre for Energy Research, Hungarian Academy of Sciences, Budapest, P.O.B. 49, H-1525 Hungary*
[a)] Corresponding author: banyasz.istvan@wigner.mta.hu

Abstract. Planar optical waveguides were designed and fabricated in an Er-doped Tungsten- Tellurite oxide glass and in a $KDy\,(WO_4)_2$ crystal by swift heavy ion irradiation. 12.5 MeV Au^{5+} ions were used in the first case and 10.5 MeV N^{4+} ions in the second one. Irradiated fluences were very low: $7\cdot10^{14}$ ions/cm^2 in the first experiment, and $4\cdot10^{15}$ ions/cm^2 ions/cm^2 in the second one. Micro Raman studies of both waveguides showed structural changes in the irradiated samples. Ellipsometric measurements showed the existence of ion beam irradiated thin film structures in both samples. M-line spectroscopic measurements were carried out to check functionality of the ion beam irradiated planar optical waveguides. One guided mode was detected in both samples at the wavelength of 632.8 nm both in TE and TM modes. However, amplitude and width of the detected m-lines indicate high propagation losses. According to our previous experiences, stepwise thermal annealing can largely reduce propagation losses, and even allow for guiding at the 1550 nm telecom band.

INTRODUCTION

Ion beam techniques are among the best methods for optical waveguide fabrication in crystalline and amorphous materials. The first report on waveguide fabrication in fused silica using proton beam was published by Schineller *et al.* in 1968 [1]. An important monograph of this field was written by Townsend *et al.* [2]. A detailed review of ion-implanted waveguides in optical materials has recently been published by Chen *et al.* [3].

Formation of adequate refractive index changes for waveguide fabrication requires relatively high fluences, in the 10^{15} - 10^{17} ions/cm^2 range, especially when mass and energy of the implanted ion are low. When ion mass and energy are higher, the electronic interaction becomes predominant over the nuclear one. First studies on the effects of swift heavy ion irradiation on the optical properties of materials date back to the 1990's [4]. Fabrication of waveguides with swift heavy and medium-light ions was demonstrated especially in $LiNbO_3$ crystals. The refractive index change needed to fabricate an optical waveguide has been produced either by the electronic interaction between the ions and the target atoms or by the creation of an optical barrier at the stopping range of the ions [5-7].

DESIGN AND FABRICATION OF THE WAVEGUIDES

The irradiations were carried out at Tandetron Laboratory of the Nuclear Physics Institute AV CR, Řež, Czech Republic. Ion species, energies and fluences for the fabrication of the planar optical waveguides were chosen so that the irradiated samples could work well at the design wavelengths.

The two materials were chosen because of their high importance in modern integrated optics. Rare earth doped glasses are widely used as lasers and amplifiers. However, due to their high susceptibility to chemical processing, alternative fabrication methods, such as direct laser writing and ion beam implantation were developed [8, 9]. Gold was chosen as the implanted ion to provide plasmonic enhancement of the luminescence of the Er-doped Tungsten Tellurite glass, and at the same time create a planar waveguide. Electronic and nuclear energy losses as well as Au ion ranges were calculated using the SRIM code [10], and are presented in Figure 1.a) and b).

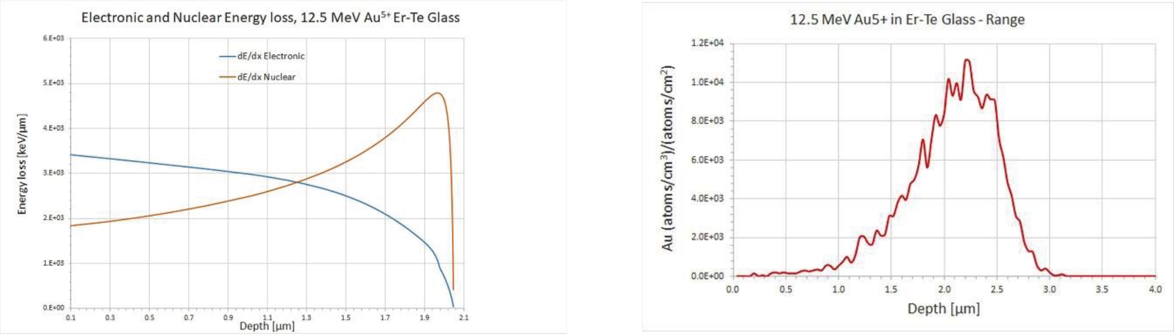

FIGURE 1. a) Electronic and nuclear energy loss *vs.* depth of 12.5 MeV Au^{5+} ions in Er-doped Te – W glass. b). Distribution of the implanted Au atoms in Er-doped Te – W glass.

It can be seen in Figure 1. that electronic and nuclear energy losses are of the same order of magnitude. The implanted gold atoms form a thick layer of 1.5 μm (at the level 1/e in Figure 1. b), centered at 2.1 μm.

KDy $(WO_4)_2$, as well as other tungstate crystals, is also a widely used material for the fabrication of integrated optical amplifiers and lasers [11-13]. Electronic and nuclear energy losses as well as N ion ranges were calculated using the SRIM code are shown in Figure 2.a) and b).

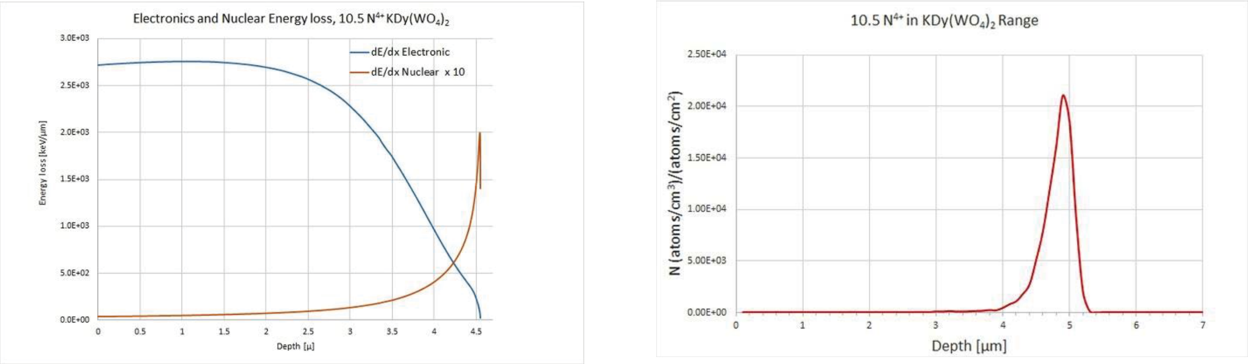

FIGURE 2. a) Electronic and nuclear energy loss *vs.* depth of 10.5 MeV N^{4+} ions in the KDy $(WO_4)_2$ crystal. b). Distribution of the implanted N atoms in the KDy $(WO_4)_2$ crystal.

Irradiated fluences were very low: $7{\cdot}10^{14}$ ions/^{cm2} in the first experiment, and $4{\cdot}10^{15}$ ions/cm^2 in the second one.

MICRO RAMAN MEASUREMENTS

The irradiated samples were studied by micro Raman spectroscopy to reveal structural changes due to the ion irradiation. The results are presented in Figure 3.a) and b).

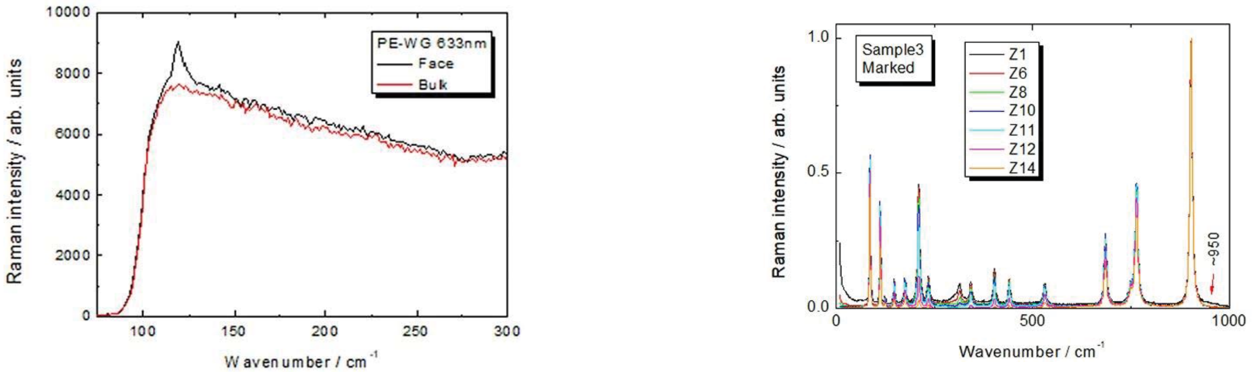

FIGURE 3. a) Micro Raman spectra of the bulk and 12.5 MeV Au^{5+} irradiated Er-doped Te-W-glass. b) Micro Raman spectra of the 10.5 MeV N^{4+} irradiated KDy $(WO_4)_2$ crystal.

Irradiation by the gold ions caused the appearance of a new band in the Raman spectrum of the Er-doped Te-W-glass, centered at 119.2 cm^{-1}. Similarly, a new band was created at 950 cm^{-1} in the Raman spectrum of the 10.5 MeV N^{4+} irradiated KDy $(WO_4)_2$ crystal.

SPECTROSCOPIC ELLIPSOMETRIC MEASUREMENTS

Both waveguides were measured by a WOOLLAM M-2000DI spectroscopic ellipsometer (SE) (λ = 193-1690 nm). A three-layer optical model was applied in the evaluation of the spectroscopic ellipsometry (SE) data. Results are shown in Figure 4.

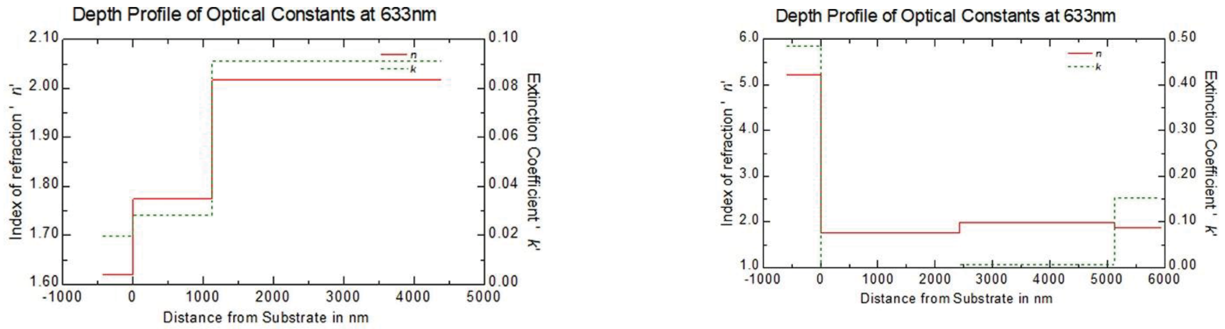

FIGURE 4. Depth profiles of the optical constants at 633 nm calculated from SE measurements a) of the 12.5 MeV Au^{5+} irradiated Er-doped Te-W-glass. b) of the 10.5 MeV N^{4+} irradiated KDy $(WO_4)_2$ crystal.

M-LINE SPECTROSCOPY

Functionality of the planar waveguides was tested by m-line spectroscopy. A Metricon 2010M Prism Coupler was used at 632.8 nm and 1534.9 nm, both in TE and TM modes. Guiding in the as-implanted waveguides could be proved only at the wavelength of 632.8 nm. TM m-line spectra taken at 632.8 nm are presented in Figure 5.

Effective refractive indices of the detected modes can be seen in Table 1.

TABLE 1. Effective refractive indices of the detected modes at 632.8 nm.

Waveguide name	n_{eff} TE	n_{eff} TM
Er-doped Te-W glass	2.1596	1.9564
KDy$(WO_4)_2$ crystal	-	2.0665

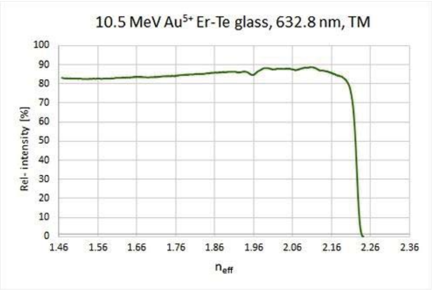

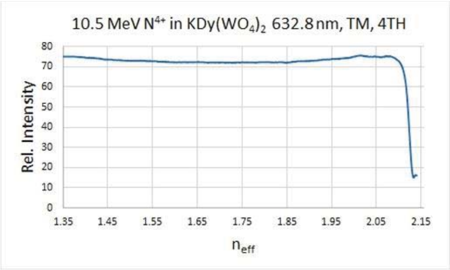

FIGURE 5. M-line spectra at 633 nm in TM mode a) of the 12.5 MeV Au^{5+} irradiated Er-doped Te-W-glass. b) of the 10.5 MeV N^{4+} irradiated KDy $(WO_4)_2$ crystal.

CONCLUSION

Fabrication of planar optical waveguides via swift heavy ion irradiation at low fluences in an Er-doped Tungsten – Tellurite glass and KDy $(WO_4)_2$ crystal was devised and performed. Structural studies proved the creation of the thin layers. M-line spectroscopic measurements of the samples showed that both waveguides could support one guided mode at 632.8 nm. However, the low amplitudes of the detected modes indicate relatively high propagation losses. Both the relevant scientific literature and our own experiences suggest that stepwise annealing of both samples could significantly reduce propagation losses of the waveguides. Even guiding at the telecom band of 1.5 μm can be expected.

REFERENCES

1. E. R. Schineller, R. P. Flam, and D. W. Wilmot, J. Opt. Soc. Am. **58**, 1171, (1968)
2. P. D. Townsend, P. J. Chandler and L . Zhang *Optical Effects of Ion Implantation*, Chapters 5– 7, (Cambridge University Press Cambridge, U.K., (1994)
3. F. Chen, X. L.Wang and K.M. Wang, Opt. Mat., **29**, 1523-1542, (2007).
4. P. Sreeramana Aithal, H.S. Nagaraja, P. Mohan Rao, D.K. Avasthi, Asati Sarma, Journal of Applied Physics, **81** 7526 (1997)
5. G. Szenes, Phys. Rev. B **52** 6154-6157 (1995).
6. G.G. Bentini, M. Bianconi, L. Correa, M. Chiarini, P. Mazzoldi, C. Sada, N. Argiolas, M. Bazzan, R. Guzzi, Journal of Applied Physics, **96** 242-247 (2004)
7. J. Olivares, G. García, A. García-Navarro, F. Agulló-López, O. Caballero, A. García-Cabañes, Appl. Phys. Lett., **86** 183501 (2005)
8. S. Berneschi, G. Nunzi Conti, I. Bányász, A. Watterich, N.Q. Khanh, M. Fried, F. Pászti, M. Brenci, S. Pelli, G.C. Righini, Appl. Phys. Lett **90** 121136 (2007
9. I. Bányász, S. Berneschi, M. Bettinelli, M. Brenci, M. Fried, N.Q. Khanh, T. Lohner, G. Nunzi Conti, S. Pelli, P. Petrik, G.C. Righini, A. Speghini, A. Watterich, Z. Zolnai, IEEE Photonics J. **4** 721-727, (2012).
10. J.F. Ziegler, J.P. Biersack, Nuclear Instruments and Methods in Physics Research Section B, **268** 1818-1823 (2010)
11. S.V. Kurbasov, L.L. Losev, Optics Communications **168** 227–232 (1999)
12. J.Liu, J. M. Cano Torres, F. Esteban-Betego, *et al.* , Optics & Laser Technology **39** 558–561 (2007)
13. C. A. Merchant, P. Scrutton, S. García-Blanco, C. Hnatovsky, R. S. Taylor, A. García-Navarro, G. García, F. Agulló-López, J. Olivares, A. S. Helmy and J. S. Aitchison, IEEE J. Quantum Electronics **45** 373-379 (2009)

Wave Polarisation in a Dynamic Elastic Lattice

G. Carta[1,a)], I. S. Jones[1,b)], N. V. Movchan[2,c)] and A. B. Movchan[2,d)]

[1]*Liverpool John Moores University, Mechanical Engineering and Materials Research Centre, L3 3AF Liverpool, United Kingdom*
[2]*University of Liverpool, Department of Mathematical Sciences, L69 7ZL Liverpool, United Kingdom*

[a)]Corresponding author: g.carta@ljmu.ac.uk
[b)]i.s.jones@ljmu.ac.uk
[c)]nvm@liverpool.ac.uk
[d)]abm@liverpool.ac.uk

Abstract. In an elastic lattice, the continuum notions of pressure and shear waves cannot be employed to describe waves propagating in the discrete medium, especially when the wavelength is comparable with the size of the elementary cell of the periodic system. Here, the concepts of lattice flux and lattice circulation of the displacement field are used to characterise waves propagating in the micro-structured medium. In particular, it is shown that the displacement field can be decomposed into flux-free and circulation-free components, that in the long wavelength limit correspond to shear and pressure waves. The proposed procedure can be applied for any value of the wave vector. A surprising result is that there are lines in the reciprocal space where waves in the lattice have similar features as those observed in the long wavelength limit.

INTRODUCTION

Models of discrete media have been proposed in the literature to describe phenomena that cannot be explained using continuum approximations. In particular, dynamic propagation of cracks can be predicted from analytical models of elastic lattices [1, 2]. In addition, discrete media exhibit dispersive properties and dynamic anisotropy [3, 4], that are not observed in continua. Dynamic anisotropy and preferential directionality is a property of so-called "hyperbolic metamaterials", which have been developed not only in elasticity but also in electromagnetism, nanophotonics and plasmonics [5, 6, 7, 8]. In recent years, special attention has been given to chiral lattices connected to gyroscopic spinners [9, 10], where extremely localised waveforms and unidirectional propagation can be obtained [11, 12].

Wave polarisation in discrete elastic systems is a fundamental problem to discuss in order to fully understand how waves propagate in such systems. In an infinite continuum, waves are generally distinguished into pressure and shear waves. These notions cannot be used in a discrete medium, in particular when the wavelength is comparable with the size of the elementary cell. Here, the concepts of lattice flux and lattice circulation, firstly introduced in [13], are used to characterise waves propagating in an elastic triangular lattice, for any value of the wave vector.

DISPERSION PROPERTIES OF A TRIANGULAR ELASTIC LATTICE

Propagation of elastic waves in the triangular lattice shown in Figure 1(a) is studied. The system consists of particles with mass m, arranged in a triangular periodic pattern and connected by elastic springs of stiffness c, length l and negligible inertia. The lattice particles are constrained to move in the x_1x_2-plane and their displacements are assumed to be small. Consequently, the equations of motion of the lattice particles are linear.

Using the analytical approach developed in [3], the time-harmonic equations of motion for any particle of the infinite periodic system in Figure 1(a) are determined and they are given by

$$\left\{c\left[3-2\cos(\zeta l+\xi l)-\frac{\cos(\zeta l)+\cos(\xi l)}{2}\right]-m\omega^2\right\}U_1+\left\{c\sqrt{3}\frac{\cos(\xi l)-\cos(\zeta l)}{2}\right\}U_2=0, \tag{1}$$

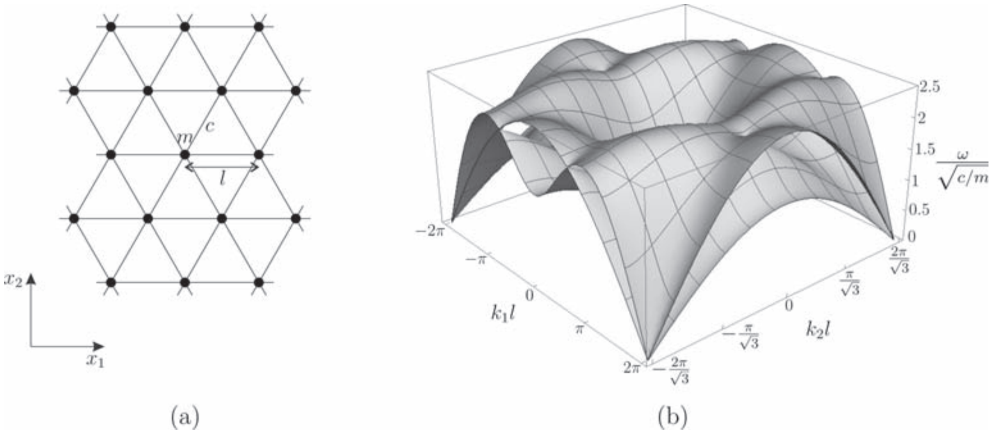

FIGURE 1. (a) Schematic representation of a triangular elastic lattice; (b) dispersion surfaces of the lattice.

$$\left\{c\sqrt{3}\frac{\cos(\xi l)-\cos(\zeta l)}{2}\right\}U_1+\left\{3c\left[1-\frac{\cos(\zeta l)+\cos(\xi l)}{2}\right]-m\omega^2\right\}U_2=0. \tag{2}$$

Here, $\boldsymbol{U} = (U_1, U_2)^{\mathrm{T}}$ is the vector of displacement amplitudes, ω is the radian frequency, $\zeta = k_1/2 + \sqrt{3}k_2/2$, $\xi = k_1/2 - \sqrt{3}k_2/2$ and $\boldsymbol{k} = (k_1, k_2)^{\mathrm{T}}$ is the wave vector.

Non-trivial solutions of Equation (1) and (2) are obtained by setting

$$\det\left(\boldsymbol{C}-\omega^2\boldsymbol{M}\right)\boldsymbol{U}=0, \tag{3}$$

where $\boldsymbol{C}$ is the stiffness matrix, whose entries are the coefficients of $\boldsymbol{U}$ in Equation (1) and (2), $\boldsymbol{M} = m\boldsymbol{I}$ is the mass matrix and $\boldsymbol{I}$ is the 2×2 identity matrix. The solutions of Equation (3), which is denoted as the *dispersion relation* of the system, are expressed by

$$\omega^{(1)}(\boldsymbol{k})=\sqrt{\frac{\mathrm{tr}(\boldsymbol{C})-\sqrt{\mathrm{tr}^2(\boldsymbol{C})-4\det(\boldsymbol{C})}}{2m}}, \tag{4}$$

$$\omega^{(2)}(\boldsymbol{k})=\sqrt{\frac{\mathrm{tr}(\boldsymbol{C})+\sqrt{\mathrm{tr}^2(\boldsymbol{C})-4\det(\boldsymbol{C})}}{2m}}. \tag{5}$$

The dispersion surfaces, given by Equation (4) and (5), are plotted in Figure 1(b). The two surfaces have six common points, referred to as *Dirac points* and labelled as D in Figure 3, where the group velocities are singular.

CHARACTERISATION OF WAVES IN A TRIANGULAR ELASTIC LATTICE

In [13], propagation of waves in a triangular elastic lattice is described by using the novel notions of lattice flux and lattice circulation, which are defined as

$$\Phi_{\boldsymbol{u}}=\mathrm{i}\frac{\sqrt{3}l}{2}\boldsymbol{u}\cdot\boldsymbol{f} \tag{6}$$

and

$$\Gamma_{\boldsymbol{u}}=-\mathrm{i}\frac{\sqrt{3}l}{2}\left(\boldsymbol{u}\times\boldsymbol{f}\right)\cdot\boldsymbol{e}_3, \tag{7}$$

respectively. In the formulae above, $\boldsymbol{e}_3$ is the unit vector of the x_3-axis and $\boldsymbol{u}(t) = \boldsymbol{U}\cos(\omega t)$ is the displacement as a function of time t of a lattice particle, whose eigenvector is given by $\boldsymbol{U}$. It is noted that the eigenvector $\boldsymbol{U}$ can be calculated for the lower or upper dispersion surface, hence the flux and circulation also depend on the choice of

the dispersion surface. The displacements $\boldsymbol{u}^{(j)}$ $(j = 1, 2)$ of each lattice particle corresponding to the two dispersion surfaces ($j = 1$ or $j = 2$) are straight lines, perpendicular to each other [13]. The vector $\boldsymbol{f}$ has the form

$$\boldsymbol{f} = \Big(2\sin(\zeta l + \xi l) + \sin(\zeta l) + \sin(\xi l)\,,\ \sqrt{3}\,\left[\sin(\zeta l) - \sin(\xi l)\right]\Big)^{\mathrm{T}}\,. \tag{8}$$

In the long wavelength limit as $\boldsymbol{k} \to \boldsymbol{0}$, the vector $\boldsymbol{f}$ and the wave vector $\boldsymbol{k}$ are parallel. From Equation (6) and (7), it is apparent that in the long wavelength limit zero flux corresponds to shear waves (for which $\boldsymbol{u}\cdot\boldsymbol{k} = 0$), while zero circulation corresponds to pressure waves (for which $\boldsymbol{u}\times\boldsymbol{k} = \boldsymbol{0}$). For large values of $|\boldsymbol{k}|$, the notions of shear and pressure waves have no significance, hence the definitions of lattice flux and lattice circulation should be used to characterise waves propagating in the discrete medium.

Lattice flux and lattice circulation are time-harmonic quantities, having the same radian frequency ω as the displacement $\boldsymbol{u}$ (see Equation (6) and (7)). Their respective amplitudes, $|\Phi_{\boldsymbol{u}}|$ and $|\Gamma_{\boldsymbol{u}}|$, are given by

$$|\Phi_{\boldsymbol{u}}| = \frac{\sqrt{3}l}{2}|\boldsymbol{u}||\boldsymbol{f}|\cos(\beta), \tag{9}$$

$$|\Gamma_{\boldsymbol{u}}| = \frac{\sqrt{3}l}{2}|\boldsymbol{u}||\boldsymbol{f}|\sin(\beta), \tag{10}$$

where $|\boldsymbol{u}|$ is the modulus of the displacement vector, $|\boldsymbol{f}|$ is the modulus of the vector $\boldsymbol{f}$ in Equation (8) and β is the acute angle between $\boldsymbol{u}$ and $\boldsymbol{f}$. The amplitudes of flux and circulation in the k_1k_2-plane for the lower ($j = 1$) and upper ($j = 2$) dispersion surfaces are shown in Figure 2(a) and 2(b). It is noted that the amplitude of flux calculated for one surface is equal to the amplitude of circulation determined for the other surface, due to the orthogonality of the eigenvectors [13]. The angles β as functions of the wave vector $\boldsymbol{k}$ corresponding to the two dispersion surfaces are plotted in Figure 2(c) and 2(d).

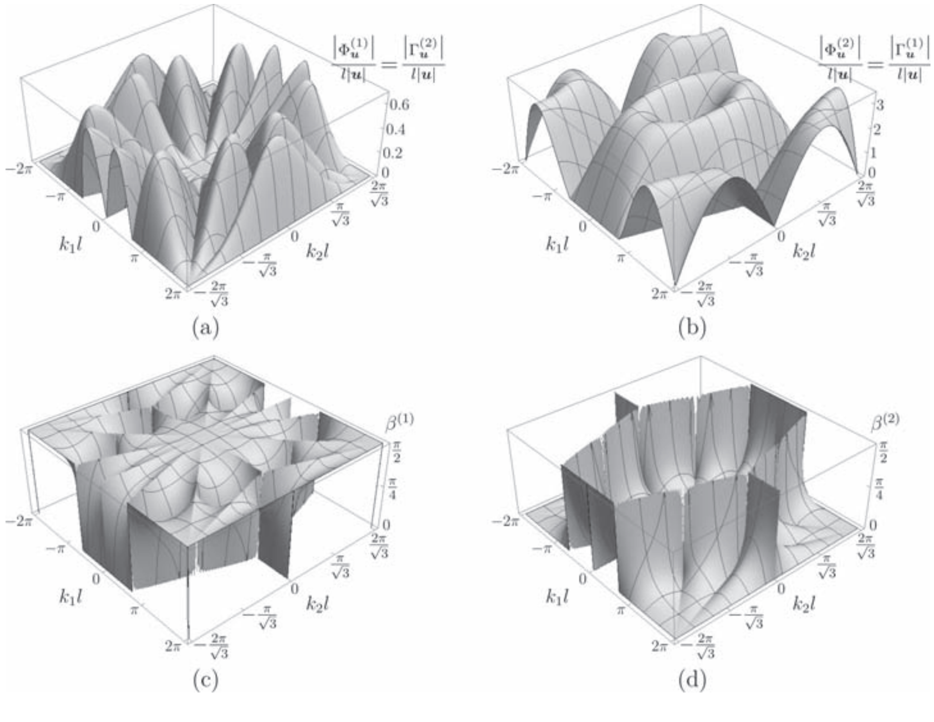

FIGURE 2. (a,b) Amplitudes of lattice flux and lattice circulation in the k_1k_2-plane for the lower ($j = 1$) and upper ($j = 2$) dispersion surfaces; (c,d) angles $\beta^{(j)}$ $(j = 1, 2)$ in the k_1k_2-plane.

Figure 2(c) and 2(d) show that in the lower dispersion surface the displacement vector $\boldsymbol{u}$ and the vector $\boldsymbol{f}$ are orthogonal ($\beta^{(1)} = \pi/2$) on the lines $k_2/k_1 = n\pi/6$ $(n = 0, 1, .., 11)$, while they are parallel ($\beta^{(1)} = 0$) on the hexagon connecting the Dirac points, i.e. points D in Figure 3. This is confirmed by the diagrams in Figure 2(a) and 2(b), which

show that the amplitude of lattice flux $\left|\Phi_{\boldsymbol{u}}^{(1)}\right|$ is zero on the lines $k_2/k_1 = n\pi/6$ ($n = 0, 1, .., 11$) and the amplitude of lattice circulation $\left|\Gamma_{\boldsymbol{u}}^{(1)}\right|$ is zero on the hexagon connecting the Dirac points. The opposite scenario is observed in the upper dispersion surface. For all the other values of the wave vector, waves are characterised by a mixture of flux-free and circulation-free waves.

Figure 3 summarises the results of Figure 2(a)-2(d). Lines of zero flux (dashed lines) and lines of zero circulation (dotted lines) are clearly identified. At the points where the dashed and dotted lines intersect, both flux and circulation are null. In the grey regions, waves possess non-zero values of flux and circulation.

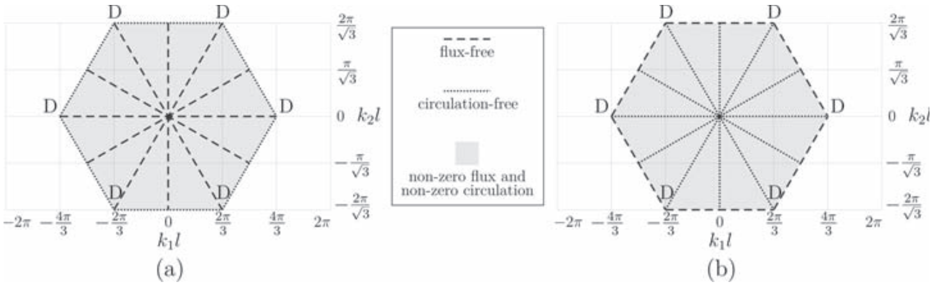

FIGURE 3. Types of waves in the elastic triangular lattice for (a) the lower and (b) the upper dispersion surface. Points D indicate the positions of the Dirac points in the reciprocal plane.

CONCLUSIONS

The displacement field in an elastic lattice can be decomposed into a flux-free and a circulation-free component. In the k_1k_2-plane, there are special lines where the dynamic response of the system for small wavelengths is similar to that observed in the long wavelength regime. Lattice flux and lattice circulation provide a novel means to characterise waves in a discrete medium, even when the wavelength is comparable with the size of the elementary cell. In the long wavelength limit, where the lattice approximates a continuum, flux-free and circulation-free waves correspond to shear and pressure waves, respectively.

ACKNOWLEDGMENTS

The authors would like to thank the EPSRC (UK) for its support through Programme Grant no. EP/L024926/1.

REFERENCES

[1] L. I. Slepyan, *Models and Phenomena in Fracture Mechanics* (Springer, Berlin, 2002).
[2] M. J. Nieves, G. S. Mishuris, and L. I. Slepyan, Int. J. Solids Struct. **97–98**, 699–713 (2016).
[3] P. G. Martinsson and A. B. Movchan, Q. J. Mech. Appl. Math. **56**, 45–64 (2003).
[4] M. Ayzenberg-Stepanenko and L. I. Slepyan, J. Sound Vib. **313**, 812–821 (2008).
[5] A. Poddubny, I. Iorsh, P. Belov, and Y. Kivshar, Nature Photon. **7**, 948–957 (2013).
[6] V. P. Drachev, V. A. Podolskiy, and A. V. Kildishev, Optics Express **21**, 15048–15064 (2013).
[7] T. Gric and O. Hess, Appl. Sci. **8(8)** (2018).
[8] A. Trofimov and T. Gric, J. Electr. Waves Appl. **32(14)**, 1857–1867 (2018).
[9] M. Brun, I. S. Jones, and A. B. Movchan, Proc. R. Soc. London A **468**, 3027–3046 (2012).
[10] G. Carta, M. Brun, A. B. Movchan, N. V. Movchan, and I. S. Jones, Int. J. Solids Struct. **51**, 2213–2225 (2014).
[11] G. Carta, I. S. Jones, N. V. Movchan, A. B. Movchan, and M. J. Nieves, Sci. Rep. **7** (2017).
[12] M. Garau, G. Carta, M. J. Nieves, I. S. Jones, N. V. Movchan, and A. B. Movchan, Proc. R. Soc. London A **474** (2018).
[13] G. Carta, I. S. Jones, N. V. Movchan, and A. B. Movchan, Phys. Mesomech. **22(2)**, 152–163 (2019).

Numerical and Analytical Models for Calculating Optical Forces Near Auxiliary Plasmonic Substrates

Alexander S. Shalin[1, a)], Aliaksandra Ivinskaya[1], Natalia Kostina[1], Mihail I. Petrov[1], Andrey A. Bogdanov[1], Sergei Sukhov[2] and Pavel Ginzburg[3].

[1] *"Nano-Optomechanics" Laboratory, Department of Nanophotonics and Metamaterials, ITMO University, Birzhevaja line, 14, 199034, St. Petersburg, Russia*

[2]*CREOL, The College of Optics and Photonics, University of Central Florida, Orlando, Florida, USA.*
[3]*School of Electrical Engineering, Tel Aviv University, Ramat Aviv, Tel Aviv 69978, Israel.*

[a)]Corresponding author: alexandesh@gmail.com

Abstract. The optical force acting on a nanoparticle near a planar substrate is governed by incident light and excitation of surface and volume modes of the substrate. The realization of negative optical forces ("tractor beams") via propagating plasmon-polaritones and volume modes will be shown and considered in detail on the basis of the described analytical and numerical models for certain types of anisotropic substrates. In addition, optical tweezers performance is investigated when the Gaussian beam is focused on the metal substrate with nanoparticle. When the beam is focused above the substrate optical force increases about an order of magnitude due to evanescent field of surface plasmon. Novel effect of repulsion from Gaussian beam ("anti-trapping") is obtained when the beam waist is moved below the substrate which is confirmed by both the analytical approach and finite element simulation.

INTRODUCTION

Mechanical momentum carried by electromagnetic radiation can be effectively transferred to a structure via scattering and absorption. A self-consistent electromagnetic field interacts with induced polarization charges and, as a result, an averaged macroscopic Newtonian force acts on the structure. Optomechanics is a powerful tool at nanoscale relying on unique properties of light to manipulate matter non-invasively. Biological samples and nanoparticles can be arranged according predefined pattern what is very important for nanophotonics, chemistry, biology and other scientific directions [1, 2].

When illuminated by an electromagnetic field, microscopic particles can form stable structures due to optical binding, an effect rooted in the mutual interaction and the corresponding optical forces that exist as long as the external excitation remains active. Optical binding was first studied in [3] and, since then, several aspects of it have been considered [4, 5].

Optical trapping experiments with focused laser beams (optical tweezers [6]), started the era of optical manipulation. Ever since then, this concept has been successfully applied to various fields of science and engineering, such as laser cooling, particle sorting, optomechanical light modulators, among many other research areas. One of the primary goals of optical manipulation research is to reduce the overall power of a trapping beam and to achieve stiff and highly localized potential light profiles [7]. Complex shaping of beams could improve the quality of trapping, however they present additional technical complications in comparison with traditional light sources.

The ways to control spatial position of particles range from free-space optics to utilization of auxiliary nanostructures for field and force shaping. While nanostructures localize particles at particular positions, i.e. at hot

spots of high field intensity, very simple planar substrate can serve as a platform for divers operations with nanoobjects. Here we are interested in the direction and strength of optical force when substrate is made of arbitrary anisotropic (i.e. hyperbolic) metamaterial [8-10] or metal [11] and supports surface plasmon-polaritones (SPP) and volume modes.

The ability to manipulate small objects with focused laser beams opened a venue for investigating dynamical phenomena relevant to both fundamental and applied science. Nanophotonic and plasmonic structures enable achieving superior performance in optical trapping due to highly confined near-fields. In this case, the interplay between the excitation field, re-scattered fields and the eigenmodes of a structure can lead to remarkable effects.

The optical force acting on a nanoparticle in the presence of a complicated structure giving rise to a number of surface or volume modes requires very strong analytical and/numerical models for efficient and comprehensive description. Hereinafter we consider some appropriate methods and compare them with each other. The analytical results will be supported by numerical calculations in COMSOL Multiphysics of different versions (4.3, 5.1) and the principal difference will be shown.

METAMATERIAL SUBSTRATES FOR OPTICAL PULLING FORCES

Theoretical Formalism

Recent progress in metamaterials span over fascinating applications relying on the control over the flow of light with transformation optics [12], spin Hall effect [13], subdiffraction resolution [14], surface waves at metasurfaces [15], [16], ect., what strongly motivates their application in the field of optomechanics.

The force on a dipole particle with polarizability α near semi-infinite substrate (Figure 1) can be written as [17]

$$F_x = \frac{1}{2}\mathrm{Re}(\alpha \mathbf{E}^{tot}\partial_x \mathbf{E}^{0*}) + |\alpha|^2\, \omega^2 \mu_1 \mu_0\, \mathrm{Im}(\mathrm{E}_x^{tot} \mathrm{E}_z^{tot*})\, \mathrm{Im}(\partial_x\, \mathrm{G}_{xz}), \tag{1}$$

where $\mathbf{E}^{\mathrm{tot}}$ is a local field at the particle location, $\mathbf{E}^0$ is incident field, **G** is Green's function. Green's function defines structure response to incident field and enters both expression for total field $\mathbf{E}^{\mathrm{tot}}$ and the force **F**.

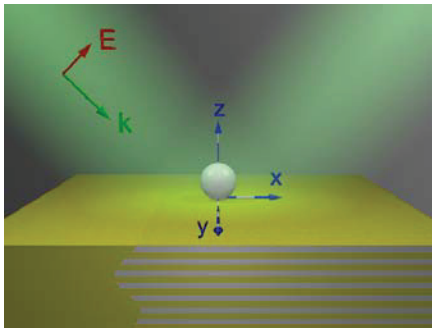

FIGURE 1. Optomechanically manipulated subwavelength dielectric particle (ε = 3, R = 15 nm, z = 15 nm) next to anisotropic (hyperbolic) metasurface. Plane wave of p-polarization is incident at 35°.

Discussion

The force map is built as a function of real parts of dielectric permittivities along the two main axes $\varepsilon_x = \varepsilon'_x + i\varepsilon''_x$ and $\varepsilon_z = \varepsilon'_z + i\varepsilon''_z$ of the crystal. Regions of positive and negative values are displayed with grey and color legends respectively (Figure 2).

Auxiliary metasurfaces introduce additional degree of freedom into optomechanical manipulation schemes. Here, optical forces, mediated by hyperbolic metamaterials, interfacing dielectric homogeneous spaces (e.g. air or water, in the case of fluidic applications) were investigated. Strong optical pulling forces were obtained over the broad spectral range and this new effect is attributed to the hyperbolic type of dispersion of electromagnetic modes. Analytical formalism of the phenomenon was developed and it relies on the self-consistent expressions for the total field at the particle location, given with the help of electromagnetic Green's function. Spectral decomposition of the

Green function enabled identifying contributions of different interaction channels into the total optical force. In particular, surface plasmon polaritons, having strongly resonant behavior, were separated from the hyperbolic bulk modes for the case of homogeneous hyperbolic material.

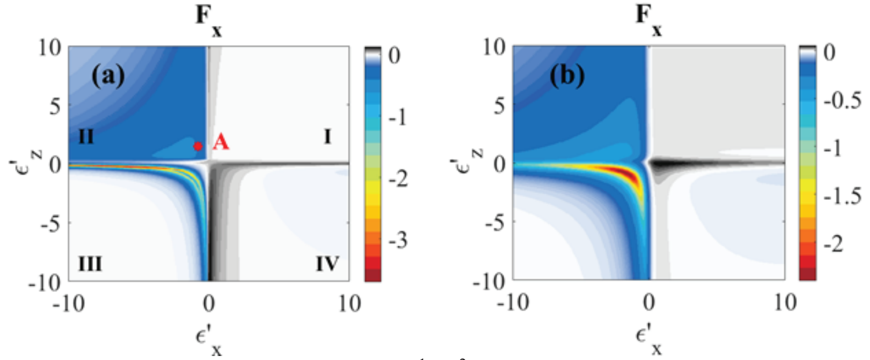

FIGURE 2. Colour maps of optical forces (in fN $mW^{-1}\mu m^2$) acting on a particle (ε=3, R=15 nm, z=15 nm) above an anisotropic material, as the function of substrate tensor.

Hyperbolic modes, having high density of electromagnetic states over a broad spectral range, are the preferable channel for scattering. It was shown that the hyperbolicity of the substrate plays the key role in delivering the overall effect in the broad spectral range. Nevertheless, for multilayered realization top metal layer interfacing the air, introduces an important contribution to the value of the pulling force. The broadband property and tunability have an additional key advantage over a single metal layer – optical attraction can be achieved at the infrared spectral range, which is highly important to many optomechanical applications. Metasurfaces, designed to control near-field interactions, open a venue for flexible optomechanical manipulation schemes. While the effect of optical attraction was demonstrated here, other important fundamental effects and applications, such as optical binding, sorting, trapping, to name just few, can be enabled by carefully designed optomechanical metasurfaces.

PLASMONIC TRAPPING AND ANTITRAPPING OF NANOPARTICLES

Gaussian Beam Focused at Metal Substrate

Optical trapping characteristics in the proximity to the beam waist of Gaussian beam and the impact of the focus position with respect to the surface were studied. Gaussian beam is focused above or below the substrate and the force acting on a dielectric bead (ε=3) of radius R=15 nm is calculated. Three different scenarios were considered: glass (ε_2=2.25) and silver substrates, and in the latter case the plasmonic contribution to optical forces can be switched 'on' and 'off' by either including evanescent harmonics or not. For f=100 μm the bead lying on the substrate (centered at z=15 nm) experiences attraction to the beam center (trapping) at all the cases (Figure 3B). This is a typical behavior for a deeply subwavelength low-index bead which has no resonances and is usually attracted towards the axis of free-space Gaussian beam. Comparison between the force values favors the silver substrate, which provides about an order of magnitude enhancement compared to the glass. Thus, the auxiliary metal substrate allows increasing the trap stiffness.

At the other hand, focusing the beam below the substrate (f=-100 μm) leads to completely different behavior (Figure 3C). While in both glass and 'silver with plasmon excluded' cases optical trapping is observed, real silver substrate leads to optical repulsion from the beam axis – anti-trapping, pushing the particle away from the region of high optical intensity. Anti-trapping stiffness (derivative of the force with respect to the coordinate) is several times larger than in the case of the glass substrate.

Surface plasmon excitation at the metal substrate plays a key role in tailoring optical forces acting on a nearby particle. Depending on whether the illuminating Gaussian beam is focused above or below the metal-dielectric interface, an order of magnitude enhancement or reduction of trap stiffness is achieved in comparison to standard glass substrates. Furthermore, a novel plasmon-assisted anti-trapping effect (particle repulsion from the beam axis) is predicted and studied. Highly accurate particles sorting scheme based on the anti-trapping effect is analyzed. The ability to distinguish and configure various electromagnetic channels through the developed analytical theory

provides the guidelines for designing auxiliary nanostructures and achieving an ultimate control over the mechanical motion at the micro- and nano-scales.

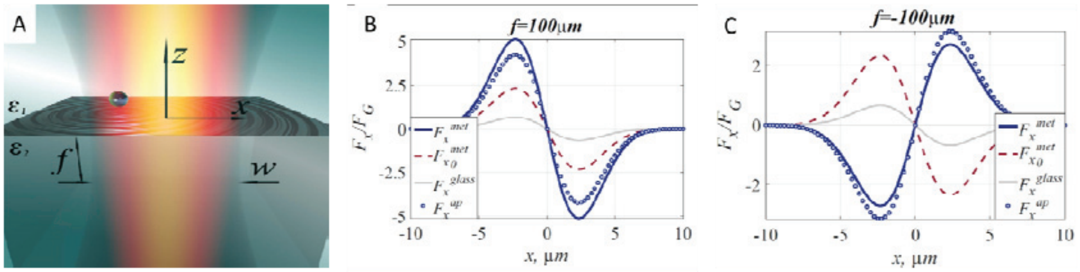

FIGURE 3. A) Schematics of the system. Gaussian beam with waist w is normally incident on a flat silver substrate; the focal position f along the z axis can be either above or below the interface. Optical forces acting on a spherical dielectric particle are formed by beam-particle, beam-substrate, and particle-substrate interactions. Optical force acting on a particle (ε=3, radius R=15 nm) in the Gaussian beam focused above (f=100 µm, B) and below (f=-100 µm, C) the substrate interface. Blue solid lines correspond to silver substrate; red dashed lines to the model without plasmon contribution; grey solid lines to the glass substrate. The beam waist diameter is w=10λ, the particle is touching the substrate.

ACKNOWLEDGMENTS

The authors acknowledge the financial support provided by Russian Fund for Basic Research (Projects No. 18-02-00414, 18-52-00005); Ministry of Education and Science of the Russian Federation (GOSZADANIE, Grant No. 3.4982.2017/6.7) and Government of Russian Federation, Grant 08-08. The force calculations were partially supported by Russian Science Foundation (Grant No. 18-72-10127).

REFERENCES

1. A. S. Shalin and S. V. Sukhov, Plasmonics **8**, 625-629, (2013).
2. A. S. Shalin, P. Ginzburg, P. A. Belov, Y. S. Kivshar, and A. V. Zayats, Laser Photonics Rev. **8**, 131–136, (2014).
3. M. M. Burns, J. M. Fournier and J. A. Golovchenko, Phys. Rev. Lett. **63,** 1233–6, (1989).
4. S. Sukhov, A. Shalin, D. Haefner, and A. Dogariu., Optics Express, **23**, 247-252 (2015).
5. N. Kostina, A. Ivinskaya, S. Sukhov, A. Bogdanov, I. Toftul, M. Nieto-Vesperinas, P. Ginzburg, M. Petrov and A. Shalin, Phys. Rev. B **99** 125416, (2017).
6. A. Ashkin, Phys. Rev. Lett. **24** 156–9, (1970).
7. A. Ivinskaya, M. I. Petrov, A. A. Bogdanov, I. Shishkin, P. Ginzburg and A. S. Shalin, Light: Science and Applications, **6**, e16258, (2017).
8. A. S. Shalin, S. V. Sukhov, A. A. Bogdanov, P. A. Belov, and P. Ginzburg, Physical Review A **91**, 063830, (2015).
9. A. A. Bogdanov, A. S. Shalin and P. Ginzburg, Scientific Reports **5**, 15846, (2015).
10. A. Ivinskaya, N. Kostina, A. Proskurin, M. I. Petrov, A. A. Bogdanov, S. Sukhov, A. V. Krasavin, A. Karabchevsky, A. S. Shalin, and P. Ginzburg, ACS Photonics **5**, 4371–4377, (2018).
11. M. I. Petrov, S. V. Sukhov, A. A. Bogdanov, A. S. Shalin, and A. Dogariu, Laser Photonics Rev. **10**, 116–122 (2016).
12. Alexander S. Shalin, Pavel Ginzburg, Alexey A. Orlov, Ivan Iorsh, Pavel A. Belov, Yuri S. Kivshar, and Anatoly V. Zayats, Phys. Rev. B, **91**, pp. 125426, (2015).
13. P. V. Kapitanova, P. Ginzburg, F. J. Rodríguez-Fortuño, D. S. Filonov, P. M. Voroshilov, P. A. Belov, A. N. Poddubny, Y. S. Kivshar, G. A. Wurtz, and A. V. Zayats, Nat. Commun., **5**, 3226, (2014).
14. X. Zhang and Z. Liu, Nat. Mater., **7**, 435–441, (2008).
15. O. Y. Yermakov, A. I. Ovcharenko, M. Song, A. A. Bogdanov, I. V. Iorsh, and Y. S. Kivshar, Phys. Rev. B, **91**, 1–7, (2015).
16. A. A. High, R. C. Devlin, A. Dibos, M. Polking, D. S. Wild, J. Perczel, N. P. de Leon, M. D. Lukin, and H. Park, Nature, **522**, 192–196, (2015).
17. L. Novotny and B. Hecht, *Principles of Nano-Optics* (2nd ed. Cambridge University Press, 2012), p. 559.

Preface of “The Third Symposium on Computational Methods in Economics and Nature Use”

Alexander N. Medvedev[a)] and Marina A. Medvedeva[b)]

Department of Systems Analysis and Decision Making, Ural Federal University, Mira 19, Yekaterinburg, Russia, 620002

[a)]Corresponding author: alnikmed52@gmail.com
[b)]marmed55@yandex.ru

"The Third Symposium on Computational Methods in Economics and Nature Use" is dedicated to the discussion of development and practical application of computational methods and information technologies in such important spheres of human activity as economics and nature use.

The presentations of representatives of academic and university science, as well as doctoral and master students were presented at the Symposium in oral and poster format.

The Symposium program included 20 presentations, which addressed newly created models and methods, as well as particular examples of their use for the evaluation, analysis and forecasting of different indicators in the field of economics, nature use, management, and related spheres.

Alexander N. Medvedev

Assoc. Prof. Dr. Alexander N. Medvedev works as a Scientific Secretary and a Leading Researcher of the Institute of Industrial Ecology of the Ural Branch of the Russian Academy of Sciences and as an Associate Professor (part time) of Department of Systems Analysis and Decision Making of Ural Federal University, Yekaterinburg, Russia.

He got his PhD in Technical Sciences at the Institute of Geophysics UB RAS, in 1990, under the supervision of Professor Valeriy V. Kormiltsev. His main scientific interests are in the field of application of computer modeling and experimental studies for solving the tasks in the sphere of nature use and environmental protection.

He participated in several International Conferences on Applied Mathematics and Geosciences (ICNAAM 2015-2018, Rhodes, Thessaloniki, Greece; ICCMSE 2017-2019, Rhodes, Thessaloniki, Greece; ICAMCS 2017, Rome, Italy; CAO 2015, Garmisch-Partenkirchen, Germany; AMEE 2015-2016, 2018, 2019 Sozopol, Bulgaria; SGEM 2014-2016, 2019, Albena, Bulgaria, etc.).

He organized 6 Mini Symposiums in the frames of ICCMSE and ICNAAM 2017-2019.

He is an author of more than 140 scientific articles and about 10 textbooks.

Alexander Medvedev is an Active Member of the European Academy of Natural Sciences (Hanover, Germany), Federal Expert on Nature Use (Moscow, Russia), and evaluator of international scientific-technical projects of the European Union (European and International Cooperation Projects Management Agency, Bonn, Germany).

Marina A. Medvedeva

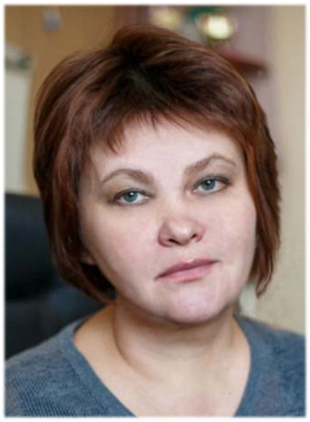

Assoc. Prof. Dr. Marina A. Medvedeva works as a Head of Department of Systems Analysis and Decision Making and Associate Professor of Ural Federal University, Yekaterinburg, Russia.

She got his PhD in Physics and Mathematics at the Institute of Industrial Ecology UB RAS in 2005, under the supervision of Professor Oleg I. Nikonov. Her main scientific interests are in the field of application of computer modeling and information technologies in economics, business, and education.

She was a participant of several International Conferences on Applied Mathematics and Informatics (ICNAAM 2009-2018, Greece; ICCMSE 2017-2019, Rhodes, Thessaloniki, Greece; CAO 2012, Rimini, Italy, CAO 2018, Yekaterinburg, Russia; MSCI 2015, Sliema, Malta; AMEE 2015-2016, Sozopol, Bulgaria; SGEM 2014-2016, Albena, Bulgaria, etc.).

She organized 6 Mini Symposiums in the frames of ICCMSE and ICNAAM 2017-2019.

She is an author of more than 100 scientific articles and about 11 textbooks.

Marina A. Medvedeva is a leader of the international master educational program on Business Informatics in Ural Federal University, Yekaterinburg, Russia.

Multicriterial Optimization of Transportation Based on Customers Probabilistic Preferences

Dmitry Zavalishchin[1,2,3,a)] and Galina Timofeeva[2,3,b)]

[1]*Department of Optimal Control, N.N.Krasovskii Institute of Mathematics and Mechanics, Ural Branch of the Russian Academy of Sciences, S. Kovalevskaya str., 16, Ekaterinburg, 620990, Russia*
[2]*Ural State University of Railway Transport, Kolmogorov str., 66, Ekaterinburg, 620034, Russia*
[3]*Ural Federal University named after First President of Russia B. N. Yeltsin, Mira str., 19, Ekaterinburg, 620002, Russia*

[a)]Corresponding author: zav@imm.uran.ru
[b)]gtimofeeva@usurt.ru

Abstract. In the situation of rapidly developing e-commerce, there is a need to expand the possibilities of cargo delivery. Of course, there is the problem of optimizing transport routes. The problem of probabilistic mathematical modeling of the carriers preferences of and their clients is considered. Patterns of preferences are formulated based on the solution of a multicriteria problem. Choosing a route by a random carrier is considered as an optimization problem with a random preference function. We investigate the case of a random delivery time. The results of this study can also be useful for mathematical modeling of transport networks.

Keywords: Transportation Network, Random Preference Function, Quantile Criterion, Multicriterial Problem, Transportation Planning, Uncertainty.
PACS: 02.50.Le, 02.60.Pn, 02.50.Ga.

INTRODUCTION

In the framework of previous researches [1, 2] a probabilistic model of preferences of passengers (and other consumers of transport services) based on a two-criterion approach with criteria for price and time of transportation was proposed. In this paper the preference of a randomly selected consumer is modeled as a solution to a problem with an objective function in the form of a linear convolution of criteria with random weights that reflect consumer preferences. The model makes it possible to predict changes in the distribution of freight traffic after the introduction of new routes. In addition, in the considered mathematical model of the route choice for cargo delivery the transportation time is a random variable. An approach to the route selection model based on the reduction from a probabilistic problem formulation to a deterministic problem with several criteria is proposed.

In modern times the transportation market is actively developing and there are many transport companies that work with small wholesale shipments of goods. They choose the route of delivery and carriers based on the cost constraints and requirements for delivery times. These requirements and restrictions may be offered by the Internet site itself. For example, on walmart.com, target.com, aliexpress.com and similar sites, the buyer immediately has a choice of delivery time in three options. Naturally, the way and therefore the cost depends on the delivery time. The carrier or decision maker as orders are received each time has the problem of choosing the route and mode of transport in the time and cost constraints. Thus we can talk about the preferences of carriers which are determined by several parameters.

The problem of optimizing multimodal transportation including under conditions of uncertainty is investigated in [3, 4]. There are many approaches to the study of such problems. As a rule these approaches consist in the combination and development of classical methods of operations research. For example dynamic programming for optimization problem of multi-modal transportation is used in [5, 6].

MATHEMATICAL FORMALIZATION OF THE CARRIERS PREFERENCE PROBLEM

It is assumed that the consumer has several possible alternatives. Let us introduce the following notations.

Let the consumer have a choice between possible n possible alternatives $x_1, \ldots, x_n$. Denote the set $X_0 = \{x_1, \ldots, x_n\}$. If a new route is added, then the set of alternatives expands. Denote the new set of alternatives after added a the route as X_1, $X_1 = X_0 \cup x_{n+1}$, where x_{n+1} is a new route. At this stage of the study, the question of partial intersection of routes, as well as restrictions associated with network load, are not considered.

We will describe the preferences of a randomly selected client by a random vector $\{\xi_0, \xi_1\}$, where ξ_i are dependent on each other discrete random variables that take values $\xi_i \in X_i$, $i = 1, 2$. The random variable ξ_0 indicates the distribution of preferences before the introduction of a new route for the transport network, and ξ_1 – after the introduction of a new one. The statistics show that the distribution of the random vector $\{\xi_0, \xi_1\}$ depends on the value of the $T(x_i)$ criteria – travel time and the cost of moving $C(x_i)$ on possible routes.

BICRITERIAL APPROACH

Denote the cost of each route by c_i, $i = 1, \ldots, n$, the time it takes to move from A to B each route by t_i, $i = 1, \ldots, n$. Other transportation conditions (such as convenience of the schedule, etc.) are not taken into account, and we obtain an optimization problem with two criteria for describing preferences of one carrier formulated in [2]

$$\begin{aligned} y_1 + \ldots + y_n &= 1, \quad y_i \in \{0; 1\} \\ T(Y) &= t_1 y_1 + \ldots + t_n y_n \to \min \\ C(Y) &= c_1 y_1 + \ldots + c_n y_n \to \min \end{aligned} \tag{1}$$

Definition 1. The solution $X^{(1)}$ is preferable to the solution (solution dominates) $X^{(2)}$ if one of the two conditions is fulfilled

$$T(Y^{(1)}) \le T(Y^{(2)}) \wedge C(Y^{(1)}) < C(Y^{(2)})$$

or

$$T(Y^{(1)}) < T(Y^{(2)}) \wedge C(Y^{(1)}) \le C(Y^{(2)}).$$

In contrast to the model with a single decision maker, we will consider a probabilistic model, when there are many consumers or decision makers. Their preferences can be studied on the basis of statistical data. For the mathematical description of probabilistic nature of consumer preferences we consider the following model.

As a criterion, we will use the generalized price of transportation, which is the sum of two criteria

$$f_\theta(X) = C(X) + \theta T(X),$$

where $\theta T(X) \ge 0$ is the "price" of the time spent by the consumer.

Thus, we get the problem of minimizing a criterion depends on the parameter $\theta \in [0, \infty)$

$$\begin{aligned} x_1 + \ldots + x_n = 1, \qquad & x_i \in \{0; 1\} \\ f_\theta(X) = C(X) + \theta T(X) \qquad & \to \min \end{aligned} \tag{2}$$

It can be assumed that a randomly selected consumer chooses a solution from the set A_0 based on the choice of the optimal solution of the problem (2) with a random objective function.

THE CASE OF RANDOM TIME AND UNCERTAINTY IN THE COST OF A TRIP

Within the model, consumers choose only Pareto–optimal solutions to problem (1), but in reality this is not quite so. Some (relatively small) part of the consumers prefers the dominant solutions. This can be explained by several reasons. The choice between effective solutions is made on the basis of a preference function, which is probabilistic in nature and depends on the preferences of a randomly selected consumer of transport services.

It is obvious that such problem is a certain simplification of the real situation, since the price is often determined ambiguously (there is a system of tariffs, discounts, etc.). Statistics show that the time of transportation is a random variable, the most important indicators of which are the statistical parameters of the distribution (such as the average time of transportation and its variance). Let us consider in more detail the preferences of the consumer of transport services, taking into account the fact that the transport time is random.

In the study of optimization problems with a probabilistic objective function the quantile criterion for choosing a solution is often used over the past decades. The properties of the quantile criterion optimization problems are investigated in [7]. So the duration of transportation guaranteed with a given probability α (for example, $\alpha = 0.95$) is minimized. The initial criterion of $T(Y) \to \min$ is converted to the quantile criterion for a fixed $\alpha \in (0.5; 1)$

$$q_\alpha(Y) \to \min \tag{3}$$

if the random nature of the delivery time and the risk of late delivery are taken into account.

When considering proposals one delivery time can be indicated (as a rule, this time is guaranteed by the service provider with some rather high probability). In the analysis of traffic for the estimated time the time specified in the schedule is often taken, but in reality the travel time is random.

Let the transportation time on the i-th route be modeled as a random variable η_i. Denote by $q_\alpha^{(i)}$ level quantile α random duration of transportation on the i-th route

$$q_\alpha^{(i)} = \{q : Pr\{\eta_i < q\} > \alpha\}.$$

We formulate a criterion for preference of the i -th route on the j-th criterion by the criterion of "shortest transit time", taking into account the random duration of transportation.

Definition 2. We say that a random travel time η_i is not greater than η_j if

$$q_\alpha^{(i)} \le q_\alpha^{(j)} \quad \forall \alpha \in [0.5, 1)\,.$$

If the inequality is strict on some interval, then the random time of transportation η_i is less than η_j. The ratio η_i less than η_j will be denoted by $\eta_i \prec \eta_j$.

If the time of transportation is modeled using the normal distribution (which is often used in practical research), then one can use the known relation to compare normally distributed random variables

$$\eta_i \prec \eta_j \quad \Leftrightarrow \quad E(\eta_i) < E(\eta_j) \wedge Var(\eta_i) < Var(\eta_j), \tag{4}$$

where $E(\eta)$ is the mathematical expectation of the random variable η and $Var(\eta) = \sigma^2(\eta)$ is its variance. It follows from the equality

$$q_\alpha(\eta) = E(\eta) + k_\alpha \sigma(\eta)$$

for the normal distribution of a random variable η and $\alpha \in (0.5; 1)$, here $k_\alpha > 0$ is a quantile of level α.

It should be noted that relation (4) is also true for some other distributions, for example, for the lognormal distribution. In financial analysis, the indicator $\sigma(\eta)$ characterizes the risk of financial investments, in the case when η characterizes the duration of delivery, its standard deviation $\sigma(\eta)$ is a measure of the risk of late delivery. The quantile criterion (3) can be replaced by two criteria

$$\begin{array}{ll} E(Y) & \to \min \\ \sigma(Y) & \to \min\,. \end{array} \tag{5}$$

Thus, we obtain the convolution of criteria with a parameter, k_α, which, generally speaking, is also not uniquely defined and depends on the consumer's assessment of the importance of accurately fulfilling the delivery schedule, which can be called "risk appetite".

When taking into account the random delivery time, a problem with two criteria turns to a problem with three criteria, which are the shipping cost, the average shipping time and the risk of deviations from the average. Denote

$$\bar{t}_i = E(\eta_i), \quad \sigma_i = \sigma(\eta_i), \quad i = 1, \ldots, n.$$

We get a multi–criteria problem of the alternatives choice

$$\begin{array}{c} y_1 + \ldots + y_n = 1, \quad y_i \in \{0; 1\} \\ \bar{T}(Y) = \bar{t}_1 y_1 + \ldots + \bar{t}_n y_n \to \min \\ V(Y) = \sigma_1 y_1 + \ldots + \sigma_n y_n \to \min \\ C(Y) = c_1 y_1 + \ldots + c_n y_n \to \min \end{array} \tag{6}$$

In the transition from a multicriteria problem to the optimization problem for the convolution of criteria, the following problem is obtained

$$
\begin{gathered}
y_1 + \ldots + y_n = 1, \;\; y_i \in \{0; 1\} \\
\theta_1 \bar{T}(Y) + \theta_2 V(Y) + C(Y) \to \min,
\end{gathered} \tag{7}
$$

where the parameters θ_1 and θ_2 determine the estimate of the significance of the average time and standard deviations for an individual consumer and can be considered as random.

CONCLUSION

We consider the problem of modeling the preferences of carriers and consumers of transport services for the optimal choice of route, taking into account the variation in transportation time. The quantile criterion for choosing the optimal route is investigated. In the designed multicriteria problem the convolution of criteria based on their importance for random chosen consumer is used. The proposed approach can be extended to a wide class of problems of choosing the optimal route.

Acknowledgements

The investigation was supported by the Russian Foundation for Basic Research, project no. 17-08-01123-a.

REFERENCES

[1] G. A. Timofeeva, A. V. Martynenko, "Analysis of Transport Network Development via Probabilistic Modelling", in *Stability and Oscillations of Nonlinear Control Systems (STAB): 14th Intern. Conf. (Pyatnitskiy's Conference)*, 2018, Moscow: Proceedings. 2 p. IEEE Xplore Digital Library.

[2] G. A. Timofeeva, A. V. Martynenko, D. S. Zavalishchin, "Probabilistic modeling of passengers and carriers preferences via bicriterial approach", in *17th IFAC Workshop on Control Applications of Optimization (CAO 2018)*, 2018, IFAC-PapersOnLine, **51**(32), pp. 496–498.

[3] Crespo–Pereira et al., "Hybrid Algorithm for the Optimization of Multimodal Freight Transport Services: Maritime Application", in *Proceedings of the Winter Simulation Conference*, 2013, pp. 3406–3417.

[4] José E. Flórez et al., "Planning Multi–Modal Transportation Problems", in *Proceedings of the XXIst International Conference on Automated Planning and Scheduling Computing Surveys, ICAPS-11*, 2011, pp. 66–73.

[5] D. S. Zavalishchin, G. A. Timofeeva, "Approach to Transportation Planning under Uncertainty", in AIP Conference Proceedings 1906, American Institute of Physics, NY, 2017.

[6] D. S. Zavalishchin, A. D. Popkov, "Dynamic programming method for optimization problem of multi-modal transportation", in *CEUR Workshop Proceedings*, Vol.1825, 2016.

[7] A. I. Kibzun, Y. S. Kan, *Stochastic Programming Problems with Probability and Quantile Functions*, Wiley, 1996, 316p.

Assessment of Risks and Threats to the Development of Socio-Economic System

Alexandr A. Tarasyev [1, a)], Gavriil A. Agarkov[1, b)],
Viktor A. Koksharov[1, c)], Camilo A. Ospina Acosta[2, d)]

[1]*Ural Federal University, 620002, Mira Street, 19, Yekaterinburg, Russia*
[2]*Aclate, 401 Congress Avenue, Suite 2650, Austin, TX 78701, USA*

[a)] Corresponding author: alextarassiev@mail.ru
[b)] g.a.agarkov@urfu.ru
[c)] v.a.koksharov@urfu.ru
[d)] camilo.ospinaa@gmail.com

Abstract. In recent years, the subjects of the Russian Federation are becoming increasingly independent in the areas of management, management and disposal of financial resources in the region. The trend of decentralization of management leads to an increase in the responsibility of regional authorities for the current socio-economic situation in their subordinate entities, as well as for its further development. Ensuring economic security is one of the priorities for the development and regulation of regional socio-economic systems. The need to maintain sustainable economic development is due to two components that form a generalized structure of the concept of sustainable development: ensuring the prerequisites for economic growth, improving the level and quality of life of the population of the region. Economic security is considered as a set of economic, geopolitical, environmental, legal and other conditions that provide prerequisites for its survival in the event of a crisis and for development in the future, protection of vital interests of the state in relation to its resource potential, balance and dynamics of development and growth. The paper presents a model for the overall assessment of the impact of adverse socio-economic factors on the formation of sustainable development of the economic system. Due to the use of the Cobb-Douglas production function, the influence of threats was taken into account by means of a model description of indicators describing the dynamics of financial and labor resources. As a result, a mathematical definition of risk for the development of socio-economic system, expressed as a risk for the formation of GRP. It is possible to obtain a rapid assessment of the impact of economic threats on the development of the economic system and to calculate the economic damage possible in the implementation of these threats.
Keywords: labor market, modeling, economic system, risk, GRP, Cobb-Douglas production function.

INTRODUCTION

The transition of the economy of Russia and its regions to an innovative way of development is currently one of the priority strategic tasks. It is necessary to carry out a comprehensive assessment of the potential risks and threats for each scenario of the economic system, taking into account the likelihood of negative economic phenomena. It is also necessary to create a positive investment climate by increasing the investment attractiveness of the regional economy [1] to stimulate the economic system development (figure 1). The basis of the process of forming the internal stability of the region are its components, which include the following: financial, industrial, labor. The inclusion in the structure of internal stability of the main areas of functioning of the region as a system ensures high reliability of its quantitative assessment.

The financial component of the study of the internal stability of the region is a reserve of funds and the possibility of its mobilization in the event of threats. A sufficient financial base ensures the independence of the region as a subject of economic relations, as well as determines the speed of adaptation of the region's systems to the new conditions of functioning. The financial component is considered in relation to three levels of functioning of the

regional economy: the state of the business sector, the stability of the budget system, the financial viability of the region as a whole.

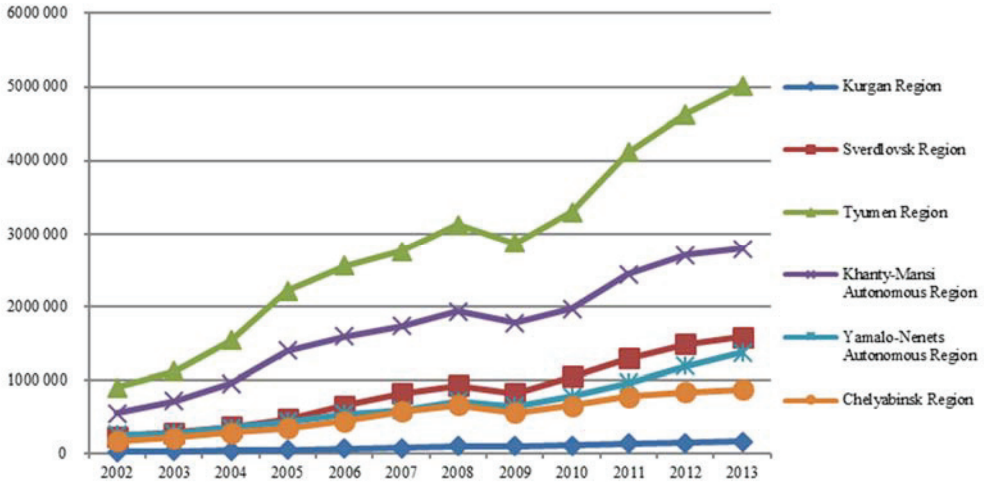

FIGURE 1. Dynamics of the gross regional product in the UrFO in current prices, million rubles

Taking into account the production component as part of the internal stability of the region provides an opportunity to assess the competitiveness of the production structure of the region, as well as its ability to quickly and with minimal losses to respond to emerging threats. As a production component, such characteristics of the real sector are taken into account, which provide the region with the opportunity to form an effective sectoral economy, as well as the territorial organization of production forces.

The labor component is considered from the position of assessing the availability of the resource base for the development of all areas of the region as a system. In an unstable economic situation, the security of the labor market, as well as the lack of demographic tension creates prerequisites for the formation of a high level of internal immunity of the region. The inclusion in the methodological apparatus of the considered parameters will allow to quantify the formed internal immunity of subjects.

The issues of regulation of investment flows and improving their efficiency by optimizing management are widespread in the works of foreign researchers. The main issue is the optimization of the use of investment flows, considered in the works of the authors (R. Ayres, V. Voudouris 2014) [3], (T. Palokangas 2014) [7], ways to improve their efficiency (L. Lambertini, A. Tamrieri 2015) [4], (L. Lambertini, A. Palestini 2014) [5], (S. M. Aseev 2014) [2], (B. K. Ane, A. tarasiev, CH. Watanabe 2007) [1]. Optimal management of investment flows (S. M. Aseev 2014) [2], (B. K. Ane, A. M. Tarasyev, A.m., Watanabe 2007) [1]. A number of works are devoted to the construction and analysis of risk management tasks in conditions of uncertainty of financial and, in particular, investment flows (Tarasyev A.A., Krivenko I.A., Pecherkina M.S., Kashina, T.O. 2016) [6]. Most of the authors are inclined to the principle of construction of differential models of financial flows management with the possibility of working out several scenarios of model dynamics management.

STATISTICS

Monitoring of socio-economic indicators is of particular importance in the context of the unstable economic situation in the Russian Federation in recent years. At the same time, it is necessary to obtain the calculated forecast trajectories reflecting the future dynamics of macroeconomic indicators used in the assessment of the socio-economic systems of the regions. Thus, the question arises of a mathematical model that takes into account the dynamics of the main indicators and observes the basic relations and the degree of interaction between them.

The Ural Federal district is a large region of Russia, both in terms of the occupied territory and the level of socio-economic development. Distribution of the population of the Urals Federal district by regions is uneven. The average annual population of the subjects in the period 2000-2013 is presented in table 1. Sverdlovsk (35.38 %) and Tyumen (28.78 %) regions can be identified as the regions with the largest share of the permanent population in 2013, and Kurgan region (7.26%) as the lowest. At the same time, the trend in the population dynamics of the UrFO

subjects can be characterized as ambiguous. In General, the population of the district in the period from 2000 to 2008 is declining, this trend is typical for most regions of the Ural Federal District, with the exception of the Northern subjects (Tyumen region, Khanty-Mansiysk, Yamal-Nenets Autonomous districts), showing a steady increase in population in the period under review.

The subjects of UrFO heterogeneous and the distribution of productive capacities. the largest contribution to the production of the gross regional product of the Ural Federal District in 2013 is made by the most populated areas – Tyumen (65.6 %) and Sverdlovsk (20.7 %) regions. The least contribution brings Kurgan region-2.1 % of the UrFO. Nevertheless, in the whole district there is a steady growth of GRP, which is evidence of improvement of the economic situation in the region.

The steady growth of per capita income in all subjects of the UrFO was observed in the period 2000-2008, the decline was recorded only in 2009 in all regions, which was caused by the unstable economic situation both in the world and in the subjects of the Russian Federation. However, the General trend of changes in the volume of per capita income of the population in the UrFO subjects in the period 2000-2012 can be characterized as positive. The population of the Northern raw material regions (Yamal-Nenets, Khanty-Mansi Autonomous districts – 52 and 36 thousand rubles) has the largest per capita income. accordingly, the Tyumen region-33 thousand rubles), as well as the industrial-oriented Sverdlovsk region – 27.7 thousand rubles.the High level of per capita monetary income in the framework of the need to counter external threats can serve as a prerequisite for containing social tension from changes in the functioning of the regional economy.

Consumer spending is an indicator of the ability of the population of the region to Finance their own consumption of goods and services. Based on the data presented in table 3, we can distinguish the regions with the highest level of population spending – Yamal-Nenets (52 thousand rubles in 2012), Khanty-Mansi (36 thousand rubles in 2012) Autonomous districts, as well as the Tyumen region (33 thousand rubles in 2012), i.e. the regions with the highest per capita income. In dynamics in the period from 2000 to 2012 it is possible to distinguish two peaks of changes in spending in 2008 and 2011, the Growth in consumer spending during these periods can be explained, on the one hand, increase of population incomes, on the other, rising prices for goods and services.

THREATS ASSESSMENT

To calculate the risks of the economic system, we introduce indicators responsible for taking into account the threats to the development of the socio-economic system. In this case, the parameters taken into account must be normalized and is in the range from 0 to 1. Accounting for these threats should be carried out using the Cobb-Douglas production function, which will assess the degree of influence of threats on the formation of GRP.

We introduce the following notations:

$p_1, p_2, p_3, ..., p_n$ - are the threats, while $0 \le p_1, p_2, p_3, ..., p_n \le 1$;

$(1-p_1), (1-p_2), (1-p_3), ..., (1-p_n)$ – potential sustainability of the system;

y_f – function describing the positive impact of economic factors on the formation of GRP;

y_u – function describing the negative impact of economic factors on the formation of GRP;

y – function describing the formation of GRP in general;

$x_1, x_2, x_3, ..., x_n$ – economic factors influencing the formation of GRP.

The functions describing the formation of GRP take into account the indicators correlated to the main parameters of the classical Cobb-Douglas function, financial and labor resources. In this case, the GRP parameter itself is presented in a normalized form in a dimensionless form. Thus, within the framework of the task, the formation of GRP is described by the following function:

$$y = a \cdot x_1^{\alpha_1} \cdot x_2^{\alpha_2} \cdot ... \cdot x_n^{\alpha_n} . \tag{1}$$

It is also necessary to set the function that forms GRP taking into account the factors describing the positive impact on the system:

$$y_f = a \cdot (x_1 \cdot (1-p_1))^{\alpha_1} \cdot (x_2 \cdot (1-p_2))^{\alpha_2} \cdot ... \cdot (x_n \cdot (1-p_n))^{\alpha_n} . \tag{2}$$

In accordance with the logic of the task, we have $y - y_f = y_u$, which takes into account the mechanism of formation of the GRP function due to the functions of taking into account positive and negative factors. We

introduce a ratio $\frac{y_u}{y}$ that expresses the risk for the formation of GRP by calculating the proportion of adverse factors in the formation of GRP in this approach. We transform these functions:

$$\frac{y_u}{y} = 1 - \frac{y_f}{y} = 1 - \frac{a \cdot (x_1 \cdot (1 - p_1))^{\alpha_1} \cdot (x_2 \cdot (1 - p_2))^{\alpha_2} \cdot \ldots \cdot (x_n \cdot (1 - p_n))^{\alpha_n}}{a \cdot x_1^{\alpha_1} \cdot x_2^{\alpha_2} \cdot \ldots \cdot x_n^{\alpha_n}}. \qquad (3)$$

In this expression, we will reduce the main duplicate parameters, resulting in a formula that allows us to assess the risk to the development of the socio - economic system, expressed as a risk to the formation of GRP:

$$\frac{y_u}{y} = 1 - (1 - p_1)^{\alpha_1} \cdot (1 - p_2)^{\alpha_2} \cdot \ldots \cdot (1 - p_n)^{\alpha_n}. \qquad (4)$$

where $\frac{y_u}{y}$ – is the share of adverse factors in the system of formation of GRP, the risk in the framework of the proposed approach.

CONCLUSION

The degree of influence of control parameters is calculated in function (1). As a result of the transformation, the value of the share of adverse factors in the economic system, calculated on the basis of normalized threat assessment, is obtained. It should be noted that in the development of strategies for the development of regional economies and the calculation of the volume of investment in these regions it is advisable to rely on the results of the calculations based on short-term forecasts because of their greater accuracy and proximity to the real situation. These provisions are of great practical importance under the influence of external factors destabilizing the economy of the region. As a result of this approach, it is possible to obtain a rapid assessment of the impact of economic threats on the development of the economic system and to calculate the economic damage possible in the implementation of these threats. Oil and gas producing entities are the most resistant to external and internal threats, the least resistant is observed in the Kurgan region due to the high demographic burden on the working population.

ACKNOWLEDGEMENTS

The work was supported by Act 211 Government of the Russian Federation, contract № 02.A03.21.0006.

REFERENCES

[1] Ane B.K., Tarasyev A.M., Watanabe C. (2007). Construction of Nonlinear Stabilizer for Trajectories of Economic Growth. Journal of Optimization Theory and Applications. Vol. 134. № 2. pp. 303-320.

[2] Aseev S.M. (2014). On some properties of the adjoint variable in the relations of the Pontryagin maximum principle for optimal economic growth problems. Proceedings of the Steklov Institute of Mathematics. Vol. 287. № 1. pp. 11–21.

[3] Ayres R., Voudouris V. (2014). The economic growth enigma: Capital, labour and useful energy? Energy Policy. Vol. 64. pp. 16–28.

[4] Lambertini L., Tampieri A. (2015). Incentives, performance and desirability of socially responsible firms in a Cournot oligopoly. Economic Modelling. № 50. pp. 40–48.

[5] Palokangas T. (2014). Optimal capital taxation, labour unions, and the hold-up problem. Labour. Vol. 28. № 4. pp. 359–375.

[6] Tarasyev A.A., Krivenko I.A., Pecherkina M.S., Kashina, T.O. (2016). Simulation of the investment attractiveness of science in a region. Economy of Region. Vol.1 pp. 303-314.

Dynamic Modeling of Age-Structured Migration Flows

Alexandr A. Tarasyev [1, a)], Gavriil A. Agarkov[1, b)],
Elena A. Rovenskaya[2, c)], Gui-Ying Cao[2, d)]

[1]*Ural Federal University, 620002, Mira Street, 19, Yekaterinburg, Russia.*
[2]*International Institute for Applied Systems Analysis, A-2361, Schlossplatz 1, Laxenburg, Austria*

[a)] Corresponding author: alextarassiev@mail.ru
[b)] g.a.agarkov@urfu.ru
[c)] rovenska@iiasa.ac.at
[d)] cao@iiasa.ac.at

Abstract. Dynamics of labor migration processes depends on the differentiation and degree of labor market development. Significant difference in the development of socio-economic systems and labor markets is one of the main explanatory factors of increasing migration mobility between developing countries. Provisions of the neoclassical theory of economics, the concept of new economics of migration, the theory of dual labor market, the theory of individual choice, the Lee econometric model and the Massey's synthetic theory of migration, used in our approach, explain this phenomenon. Effective regulation of labor migration implies the need to predict the volume, structure and direction of migration and to estimate the effect of age-structured migration flows on the labor market development. In drawing up the basic dynamic equations of models, it is necessary to consider the situation in the labor markets, characterized by the absence of barriers and boundaries, which will set the socio-economic system with the same initial conditions for all rational individuals and regions, taken into account in the models. This article describes a model that takes into account the feedback of the average wage determined by the supply of labor resources, affecting the migration processes between the countries of origin and destination. The model takes into account the impact of the age distribution of migration flows on the labor market in the country of destination of migration and allows to assess the potential of migration flows and their impact on the socio-economic system. The dynamic model of labor migration is also a model of optimization, which simulates the optimal level of labor resources and their costs, which allows to establish a strategy for the development of migration policy for the regions and countries of migration destination. The main characteristic of this model is that it can cover dynamic mechanisms of interaction of multifactor factors both in sending regions and in receiving countries simultaneously. This model can be used to estimate the outflow of migrants and returning migrants from countries of origin.
Keywords: dynamic modeling, optimization, labor migration, labor market, age structure, human capital export, migration costs, population growth.

INTRODUCTION

Due to the socio-economic problems in Russia during the period since 1992 to 2011 a negative tendency at the labor market was observed, which led to the human potential loss and significant changes it the structure of the labor market. Migration has a significant impact on the labor market development. The complexity of migration processes is due to the interaction of economic, demographic and other social factors that determine the size and age structure of migration flows from the CIS countries to the regions of Russia. In the current state of the socio-economic system, it is necessary to assess the impact of migration on wages and the balance between the supply and demand of skilled labor in the labor market. In Russia, migrants in most cases are employed in jobs that are not claimed by the local population. These are hard, not prestigious and low-paid jobs, temporary or seasonal jobs, informal work in the field of shadow employment. The model design describes the process of external labor migration for migrants of different age groups. The model is based on the interaction of economic and demographic factors and is used both for the analysis and modeling of migration flows between the sending and receiving regions [4].

LABOR MIGRATION MODEL DESCRIPTION

The model takes into account the provisions of the synthetic theory of migration in terms of the impact of migration networks on the decisions of the migrant and the new economic theory of migration in the transition from individual migration planning to group interdependence to maximize the benefits of households [6]. In accordance with the new economic theory of migration, the decision to migrate is made in accordance with the coherence of actions at the household level, while the rest of the household members do not change their place of residence. At the same time, the living standard of the household environment is singled out, which has a direct impact as a social incentive for migration. In this case, migration solves the issue of satisfaction of the individual with his/her social position and income level of the household [1].

According to the model design, when migrating, a rational individual decides to migrate from the country of origin to the region of the country of attraction, comparing the expected income level of w_i with the current w_j. Thus, the decision on migration will be made if the difference between earnings in the country of origin and the region of destination of the migrant is positive, i.e. $w_j-w_i>0$. The model is based on the assumption that there are no barriers to migration of labor, respectively; with its help, it is possible to describe migration between countries with visa-free regime. Taking into account the specifics of the functions describing the dynamics of wages depending on the influx of migrants, this model simulates an increase in the level of competition in the centers of attraction of migration and reduction of competition in the countries of departure. Accordingly, the individual's decision to move to another region or country positive if the expected benefits due to the earning gap is positive, i.e., if $w_h(t_k)-w_s(t_k)>0$. If $w_h(t_k)-w_s(t_p)<0$ a person with certain probability will make a decision on return migration from the host region h to source country s or a decision to move to another host region l for which $w_l(t_p)-w_s(t_k)>0$.

When choosing a destination region, each participant in the migration process, in addition to maximizing the expected income, will seek to minimize their costs, including the direct costs of moving. As a result, when considering the case of migration to regions with identical levels of expected income and a comparable level of development of regional socio-economic systems, a rational individual will choose for migration a region closer to the country of origin, or a region in which he can go to work with the least cost of movement. Information on regional labor markets obtained through migration networks will also have a significant impact on the decision to migrate [2]. Taking into account the above main criteria, a dynamic equation describing the process of migration from the country of departure i to the region of attraction j at time t:

$$x_{ij}(t_{p+1}) = x_{ij}(t_p) + \Delta\alpha x_{ij}(t_p)\big(M_i - x_i(t_p)\big)\big(w_j(t_p) - w_i(t_p)\big), i = 1,\dots,m;\ j = 1,\dots,n \quad (1)$$

where α – is the calibration factor for region j.

To obtain the state of Nash equilibrium in the model, functions describing the dynamics of changes in the wages of migrants depending on the level of competition for jobs were developed. The prediction of the wage dynamics in the region of attraction j at the migration flow $x_i(t_p)$ [3] at the time t is made in accordance with the equation:

$$w_j\big(x_j(t_p)\big) = w_j(t_0)\frac{E_j(t_p) + V_j(t_p)}{E_j(t_p) + U_j(t_p) + x_j(t_p)}, \quad (2)$$

where $w_j(t_0)$ – is the average salary of migrants in the region of attraction j at time t_0;

$E_j(t_0)$ – the number of people employed in the region of attraction j at time t_0;

$V_j(t_0)$ – the number of vacancies in the region of attraction j at time t_0;

$U_j(t_0)$ – the number of unemployed in the region of attraction j at time t_0;

$x_j(t_p) = \sum_{i=1}^{m} x_{ij}(t_p)$ – the number of labor migrants from m countries of origin in the region of attraction j.

Model forecasting of wage dynamics in the country of origin i at $x_i(t_p)$ at time t is performed according to the function:

$$w_i\big(x_i(t_p)\big) = w_i(t_0)\frac{E_i(t_p) + V_i(t_p)}{E_i(t_p) + U_i(t_p) - x_i(t_p)}, \quad (3)$$

where $w_i(t_0)$ – is the average wage in the country of origin i at time t_0;

$E_i(t_0)$ – number of employees in country of origin i at time t_0;

$V_i(t_0)$ – number of vacancies in the country of origin at time t_0;

$U_i(t_0)$ – the number of unemployed in the country of origin at time t_0;

$x_i(t_p)=\sum_{j=1}^{n} x_{ij}(t_p)$ – number of labor migrants from country of origin *i* going to *n* regions of attraction.

TRANSITION BY AGE GROUPS IN THE MODEL

The developed model of labor migration takes into account 3 age groups [5] allocated among the able-bodied population: youth (Y), average (M) and senior (O). The value $x_{ij}^{\alpha}(t_k)$ represents the number of labor migrants by age groups, where *α=Y,M,O* corresponds to the type of age group from the country of departure *i* to the region of attraction *j* at the time t_k. Accordingly, the upper index *α* denotes all the variables in the model to simplify the breakdown into age groups. As a result, we get the functions of wages, depending on age groups. The wage level in the host region is described by the equation:

$$w_j^{\alpha}(t_p)=w_j^{\alpha}\left(x_j^{\alpha}(t_p)\right)=w_j^{\alpha}(t_0)\frac{E_j^{\alpha}(t_p)+V_j^{\alpha}(t_p)}{E_j^{\alpha}(t_p)+U_j^{\alpha}(t_p)+a_j x_j^{\alpha}(t_p)}, \quad (4)$$

where w_j – is the basic wage rate in case of no migration and full employment;
E_j – presents the number of employed;
U_j – is the number of unemployed;
V_j – presents the number of vacancies in host region *h*;
$x_j^{\alpha}(t_p)=\sum_{j=1}^{N_j} x_{ij}(t_p)$ – is the total number of migrants in host region *h*.

The wage level in the source country is described by the equation:

$$w_i^{\alpha}(t_p)=w_i^{\alpha}\left(x_i^{\alpha}(t_p)\right)=w_i^{\alpha}(t_0)\frac{E_i^{\alpha}(t_p)+V_i^{\alpha}(t_p)}{E_i^{\alpha}(t_p)+U_i^{\alpha}(t_p)-a_i x_i^{\alpha}(t_p)}, \quad (5)$$

where w_i – is the basic wage rate in case of no migration and full employment;
E_i – describes the number of employed;
U_i – presents the number of unemployed;
V_i – is the number of vacancies in source country *i*;
$x_i^{\alpha}(t_p)=\sum_{i=1}^{N_i} x_{ij}(t_p)$ – is the total number of migrants that have left source country *i*.

The method of moving ages is taken into account in the model as follows:

$$x_{ij}^{\alpha}(t_{p+1})=x_{ij}^{\alpha}(t_p)+\Delta q_{ij}^{\alpha}x_{ij}^{\alpha}(t_p)\left(P_i-x_i^{\alpha}(t_p)\right)\left(w_j^{\alpha}\left(x_j^{\alpha}(t_p)\right)-w_i^{\alpha}\left(x_i^{\alpha}(t_p)\right)\right)+\Delta F_{ij}^{\alpha}(t_p), \quad (6)$$

where $x_{ij}(t_k)$ – is the migration flow;
$w_j^{\alpha}\left(x_j^{\alpha}(t_p)\right)-w_i^{\alpha}\left(x_i^{\alpha}(t_p)\right)$ – describes the wage gap between regions;
$P_i-x_j^{\alpha}(t_p)$ – describes the decreasing potential of migrant workers in the host region;
$F_{ij}^{\alpha}(t_p)$ – are the transport flows for the age groups;
q_{ij} – is the coefficient of migration attractiveness of the host region.

In this case, the dynamic model of labor migration for *m* countries of origin and *n* regions of attraction is presented as a system of dynamic equations:

$$\begin{cases} x_{ij}^{y}(t_{p+1})=x_{ij}^{y}(t_p)+\Delta\left(q_{ij}^{y}x_{ij}^{y}(t_p)\left(P_i-x_i^{y}(t_p)\right)\left(w_j^{y}\left(x_j^{y}(t_p)\right)-w_i^{y}\left(x_i^{y}(t_p)\right)\right)+I_{ij}(t_p)-\beta_{ij}^{y}x_{ij}^{y}(t_p)+R_i^{y}x_{ij}^{y}(t_p)\right) \\ x_{ij}^{m}(t_{p+1})=x_{ij}^{m}(t_p)+\Delta\left(q_{ij}^{m}x_{ij}^{m}(t_p)\left(P_i-x_i^{m}(t_p)\right)\left(w_j^{m}\left(x_j^{m}(t_p)\right)-w_i^{m}\left(x_i^{m}(t_p)\right)\right)+\beta_{ij}^{y}x_{ij}^{y}(t_p)-\delta_{ij}^{m}x_{ij}^{m}(t_p)+R_i^{m}x_{ij}^{m}(t_p)\right), \\ x_{ij}^{o}(t_{p+1})=x_{ij}^{o}(t_p)+\Delta\left(q_{ij}^{o}x_{ij}^{o}(t_p)\left(P_i-x_i^{o}(t_p)\right)\left(w_j^{o}\left(x_j^{o}(t_p)\right)-w_i^{o}\left(x_i^{o}(t_p)\right)\right)+\delta_{ij}^{m}x_{ij}^{m}(t_p)-\mu_{ij}^{o}x_{ij}^{o}(t_p)+R_i^{o}x_{ij}^{o}(t_p)\right) \end{cases} \quad (7)$$

RESULTS ANALYSIS

The number of foreign labor force in the Sverdlovsk region from the CIS countries with visa-free regime is at the level of – 165 thousand people. The potential salary of migrants will be 9.7 thousand rubles for the younger age

group, 10,8 thousand rubles for the middle age group, 10,5 thousand rubles for the older age group in the Sverdlovsk region. The model was tested and tested on panel data for the regions of Russia and CIS countries and gives reliable results. The dynamics of migration flows, directed into the Sverdlovsk region, are on figure 1.

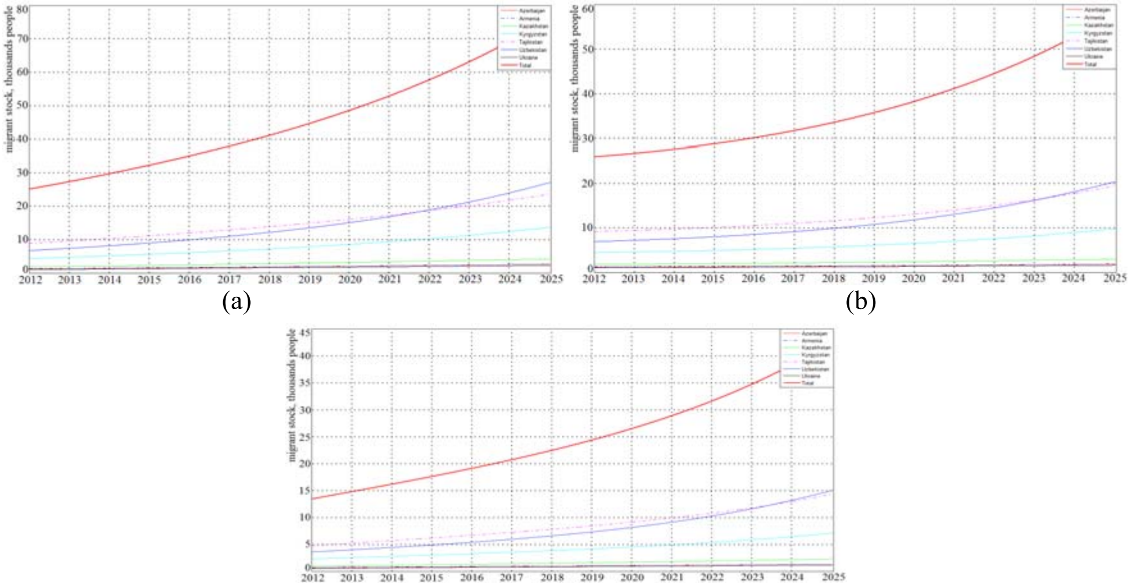

(a) (b)

(c)

FIGURE 1. Migration flows into the Sverdlovsk region, differentiated by age groups
(a) – younger age group (15-29), (b) – middle age group (30-44), (c) – older age group (45-59)

CONCLUSION

The labor market of migrants in the developed model reacts to the influence of external parameters, which is carried out by setting the dynamics of natural growth and population decline, which increases the permissible limit of the model forecast. In accordance with the proposed model, the main factor of push and pull is the level of income, the values of which are converging in the countries of origin and the region of destination with the increase in migration flows.

ACKNOWLEDGEMENTS

The work was supported by Act 211 Government of the Russian Federation, contract № 02.A03.21.0006.

REFERENCES

[1] Borjas G.J. (1987). Self-Selection and the Earnings of Immigrants. The American Economic Review. Vol. 77. Is. 4. pp. 531–553.

[2] Dustmann C., Preston I. (2011). Estimating the Effect of Immigration on Wages. Northface Migration. Discussion Paper No. 26.

[3] Massey D. A. (2002). Synthetic theory of international migration. World in the mirror of international migration. Vol. 10. pp. 143-153.

[4] Stark O., Bloom D.E. (1985). The New Economics of Labor Migration. The American Economic Review. Vol. 75. Is.2. pp. 173–178.

[5] Tarasyev A., Cao G.-Y., Rovenskaya E. (2016). Migration Flows and Effects in the CIS Countries-Dynamic Modelling. Modern Economy. Vol. 7, pp. 799-814.

[6] Todaro M.P. (1969). A Model of Labour Migration and Urban Employment in Less Developed Countries. American Economic Review. Vol. 59. pp. 138–148.

Dynamic Game Model for Finding the Equilibrium Level of Migration Flows

Alexandr A. Tarasyev [1, a)], Gavriil A. Agarkov[1, b)],
Tatyana V. Tarasyeva[1,2, c)], Jeenat B. Jabbar[3, d)]

[1]*Ural Federal University, 620002, Mira Street, 19, Yekaterinburg, Russia*
[2]*Institute of Economics of the Ural Branch of the Russian Academy of Sciences, 620014, Moskovskaya Street, 29, Yekaterinburg, Russia*
[3]*The University of Dhaka, Sattar Bhaban (4th Floor), 179, Shahid Syed Nazrul Islam Sarani, Bijoynagar, Dhaka-1000, Bangladesh*

[a)] Corresponding author: alextarassiev@mail.ru
[b)] g.a.agarkov@urfu.ru
[c)] tataponomaryova@mail.ru
[d)] jeenat.jabbar@gmail.com

Abstract. Effective regulation of labor migration implies the need to predict the volume, structure and direction of migration. Model description and forecasting of migration processes is necessary to optimize the flow of labor resources between labor markets that arise as a result of new trends in migration and reform of society. Weak regulation of labor migration in the absence of a complete information base necessary for migrants to decide on the optimal choice of the region of destination of migration, leads to an increase in the share of labor migrants employed in the informal sector of the economy, which as a result reduces the potential of human capital in the regions. The analysis of migration processes shows the need to simulate the dynamics of migration flows, which allows to describe the trends in the redistribution of labor in the current period and to make forecasts for the short-term long-term perspective. In this regard, a number of existing types of models of population migration were considered and dynamic models of population migration were based on them. We developed a model tool based on a dynamic game model of labor migration, which determines the value of migration flows in the conditions of uneven distribution of income levels of the population in the regional labor markets. In accordance with the proposed model, migration flows tend primarily to regions with more attractive working conditions, in our case – to regions with higher wages. Based on the data obtained in the simulation, we can talk about a significant decrease in the average wage level in the sectors of the labor market occupied by migrants in the regions of attraction.
Keywords: dynamic modeling, optimization, labor migration, labor market, equilibrium level, migration costs.

INTRODUCTION

The assessment and modeling of migration processes are necessary to enable the improvement of public planning policies aimed at the provision of services and the stabilization of regional labor markets through the impact on the levels of migration flows. When modeling social and economic processes, there is a need for complete, reliable information about the processes under consideration, otherwise there is a decrease in the predictive accuracy of the main model parameters [1].

In the construction of dynamic models for the description and prediction of migration processes, it is necessary to note the debatable nature of the consequences of migration, and therefore it is difficult to make the optimal management decision to improve the quality of life in the region. Traditionally, when drawing up models of migration of the population as the resulting factors of attraction and expulsion of migration [3]. Data on the unemployment rate in the regions, the total number of vacancies, the average monthly wage and the annual number

of migrants are used. Most of the models are based on the position of behavioral economics - rational economic behavior of the individual.

In accordance with the provisions of general economic theory, we can assume that the economically active population will migrate from countries with low wages in a country with high wages as long as the levels are not equal. Thus, to describe this dynamics, the method of potential difference, which is the potential of labor migrants and the potential of wages in the regions taken into account, is optimally suited [2].

GAME MODEL OF LABOR MIGRATION

The cosmopolitan model of development is focused on General democratic values, which in the Western liberal tradition are associated with the principles of market economy. This model is based on the paradigm of human rights, which affirms the priority of human rights over the rights of citizens, through the allocation of the right to free movement for migration [4].

To predict the flows of labor migrants within the framework of the concept of liberal development model, the author developed a dynamic game model of labor migration, which determines the value of migration flows in the conditions of the general labor market through the introduction of two types of functions to assess the level of wages of migrants [5]. The migration flow from country i to the region of attraction A according to this model is determined by the equation:

$$\frac{\partial x_i(t+1)}{\partial t} = \frac{1}{r_i} \cdot x_i(t) \cdot \left(M_i - x_i(t)\right) \cdot \left(-S_i\left(x_i(t)\right) + SA\left(x(t)\right)\right), i = 1,...,m, \quad (1)$$

where $x_i(t)$ – is the number of migrants to the region of attraction from the country of departure i at time t;

r_i – distance from the capital of the country of departure i to the regional center of gravity;

M_i – number of potential migrants in country i;

$x=(x_1,...,x_n)$ – full vector of migration flow to the region of attraction;

$S_i(x_i(t))$ – function of income level in the country of departure i at outflow of migrants $x_i(t)$;

$SA(x(t))$ – is a function of the income level in the region of attraction in the influx of migrants $x(t)$.

In accordance with (1) migration outflow from country i will continue until the level of income in the country does not exceed the level of income in the region of attraction A. At the same time, the level of income in both the region of attraction and the country of origin depends on the number of migrants. The outflow of population from the country creates a shortage of labor resources, which, with a decrease in the level of competition, leads to an increase in wages, and the influx of population to the region, on the contrary, creates a surplus of labor resources, which leads to a decrease in wages. In this regard, we developed separately the income level function for the country of departure (2) and the income function for the region of departure (3):

$$S_i\left(x_i(t)\right) = S_{i_av} \cdot \frac{E_i(t)}{E_i(t) + U_i(t) - \sum_{j=1}^{n} x_j(t)}, \quad (2)$$

where S_{i_av} – is the average of the average monthly nominal wage in country i;

$\sum_{j=1}^{n} x_j(t)$ – the flow of labor migrants from the country of origin j to the regions of attraction at time t;

$E_i(t)$ – number of employed population in the region of departure;

$U_i(t)$ – number of unemployed in the region of departure.

The income level function for the region of attraction is:

$$SA\left(x(t)\right) = SA_{\max} \cdot \frac{E_j(t)}{E_j(t) + U_j(t) + \sum_{i=1}^{m} x_i(t)}, \quad (3)$$

where SA_{max} – is the maximum size of the average monthly nominal wage in the region of attraction;

$\sum_{i=1}^{m} x_i(t)$ – flow of labor migrants to the region of attraction from countries of departure i at time t;

$E_j(t)$ – employment in the region of attraction;

$U_j(t)$ – the number of unemployed in the region of attraction.

The result of the substitution of data by country of origin in the model are dynamic trajectories of migration flows, changing over time depending on the level of income of the population. The model was tested using data from Sverdlovsk region, Moscow, and St. Petersburg. When modeling, the CIS countries are the countries of

departure. The lag between their and Russia's economic development for a long time reproduces the reasons for labor migration. Among them, countries characterized by stable migration flows of labor migrants sent to the regions of the Russian Federation were selected for modeling: Tajikistan, Uzbekistan, Kyrgyzstan, Kazakhstan, Armenia, Azerbaijan and Ukraine.

The result of the substitution of donor country data in the model is the dynamic trajectories of migration flows, which vary over time depending on the level of income of the population. The model dynamics saturate when the incomes of the population in the donor countries and the region of attraction stabilize at the same level for all countries and regions involved into migration (figure 1).

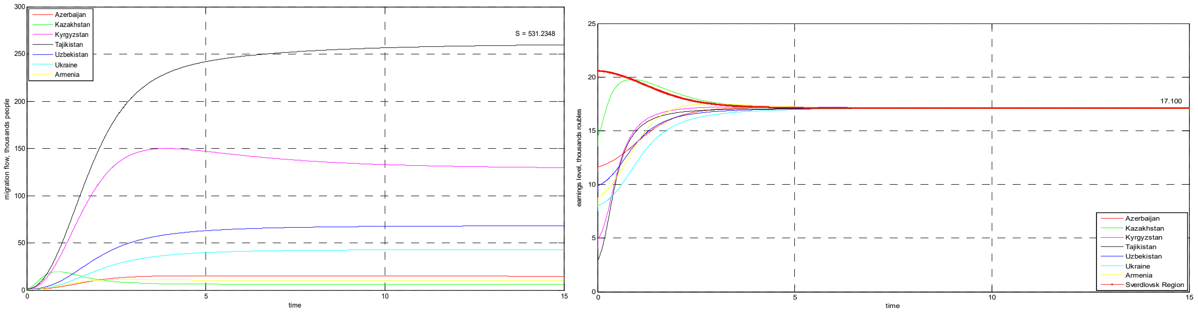

(a) (b)

FIGURE 1. Convergence of the model on the infinite horizon for the Sverdlovsk region
(a) – migration flows, (b) – salary level

FINDING THE EQUILIBRIUM LEVEL OF MIGRATION FLOWS

The main idea of the author's model is that the inhabitants of the territory *i* want to move to the territory *A* only if they are guaranteed to receive a higher salary in the territory *A*. Each territory seeks to maximize its utility function, in which the average monthly nominal wage in the territory is correlated with the average monthly nominal wage in territory *A*, taking into account the likelihood of employment [6].

The model involves *n* players, which may be municipalities (with the exception of the regional center), solving the problem of reducing the outflow of population to the regional center. Each territory *i* controls its own flow of migrants $x_i(t) \geq 0$. The labor market in region *i* is interested in maximizing its own utility function w_i, the derivative of which is:

$$w_i'(x) = -S_i + SA \cdot \frac{E+V}{E+U+\sum_{i=1}^{m} x_i}, \tag{4}$$

where $x=(x_1,\dots,x_n)$ – is the full vector of migration flow to the territory *A*;
S_i – size of average monthly nominal accrued wages in the territory *i*;
SA – the average monthly nominal accrued wages in the territory *A*;
E – the number of employed people in the territory *A*;
V – number of employees required for vacant jobs;
U – number of unemployed.

By specifying different options, it is also possible to determine the average monthly wage in territory *i*, which would make its inhabitants indifferent to moving to territory *A*:

$$w_i'(x) = -S_i(x_i) + SA\left(\sum_{i=1}^{m} x_i\right) \cdot \frac{E+V}{E+U+\sum_{i=1}^{m} x_i}, \tag{5}$$

where $S_i(x_i)$ – is a function of the average monthly nominal wage in territory *i* at outflow of migrants x_i;
$SA\left(\sum_{i=1}^{m} x_i\right)$ - the function of the average monthly wage in territory a with the total outflow of migrants.

A graphical representation of migration flows to Sverdlovsk region, calculated based on the proposed model, is on figure 2. In accordance with the obtained results, the number of migrants engaged in labor activities on the territory of Sverdlovsk region, can be 532 thousand people subject to the operation of the migration flows based on

market laws without the constraints of quotas. In addition, according to the results, the inflow of labor migrants from Kazakhstan will be the shortest.

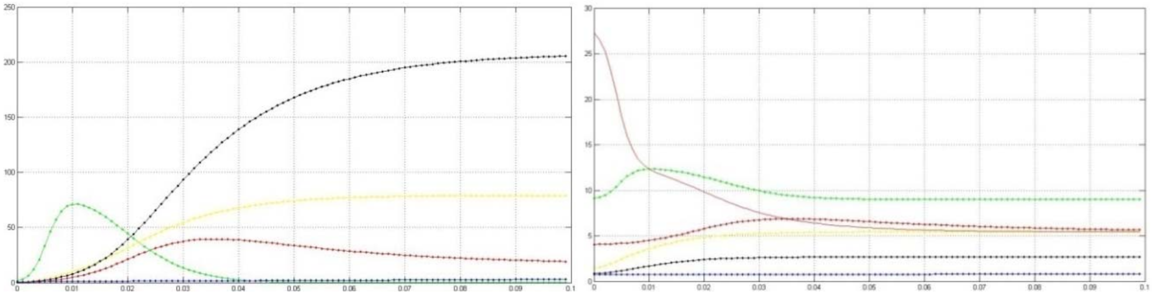

(a) (b)

FIGURE 2. Interdependent dynamics of migration flows and wages in the model of finding the equilibrium level of migration flows

(a) – migration flows, (b) – salary level

The labour market of migrants in the developed model responds to the impact of external parameters, which is in determining the dynamics of natural growth and the decline of the population, which increases the permissible limit of model forecasting. In accordance with the proposed model, the main factor for emissions and attraction is the income level, the values of which come in the countries of origin and the target region with the increase of migration flows in more detail.

CONCLUSION

In accordance with the proposed model, migration flows tend primarily to regions with more attractive working conditions, in our case – to regions with higher wages. The model is based on the interaction of economic and demographic factors and is used for both the analysis and modeling of migration flows between the sending and receiving regions. Based on the data obtained in the simulation, we can talk about a significant decrease in the average wage level in the sectors of the labor market occupied by migrants in the regions of attraction. Model dynamics comes to saturation at a synthetic time when the incomes of the population in the countries of origin and regions of attraction in the given branches of the labor market are as close as possible to each other. When we compare the results of the simulations for individual countries of departure with the number of registered labor migrants from these countries in the Sverdlovsk region, we can then estimate latent migration by country of origin.

ACKNOWLEDGEMENTS

The work was supported by Act 211 Government of the Russian Federation, contract № 02.A03.21.0006.

REFERENCES

[1] Borjas G.J. (1987). Self-Selection and the Earnings of Immigrants. The American Economic Review. Vol. 77. Is. 4. pp. 531–553.

[2] Dustmann C., Preston I. (2011). Estimating the Effect of Immigration on Wages. Northface Migration. Discussion Paper No. 26.

[3] Herr H. (2008). The Labour Market in a Keynesian Economic Regime: Theoretical Debate and Empirical Findings. Cambridge Journal of Economics. Vol. 3. Is. 5. pp. 949-965.

[4] Lewis W.A. (1954). Economic Development with Unlimited Supplies of Labor. The Manchester School. Vol. 22. No. 2. pp. 139-191.

[5] Massey D. A. (2002). Synthetic theory of international migration. World in the mirror of international migration. Vol. 10. pp. 143-153.

[6] Stark O., Bloom D.E. (1985). The New Economics of Labor Migration. The American Economic Review. Vol. 75. Is.2. pp. 173–178.

Assessment and Forecasting of Regional Economic Systems Sustainability

Tatyana V. Tarasyeva[1,2, a)], Alexandr A. Tarasyev [1, b)], Gavriil A. Agarkov[1, c)]

[1]Ural Federal University, 620002, Mira Street, 19, Yekaterinburg, Russia
[2]Institute of Economics of the Ural Branch of the Russian Academy of Sciences, 620014, Moskovskaya Street, 29, Yekaterinburg, Russia

[a)] tataponomaryova@mail.ru
[b)] Corresponding author: alextarassiev@mail.ru
[c)] g.a.agarkov@urfu.ru

Abstract. The functioning of the regional system is associated with a constant change in the internal and external conditions of development, among which it is necessary to highlight the economic situation, social factors and the political situation. The dynamic nature of the environment could have a negative impact on the ability of the regional system to maintain stability and to strive for better development. Sustainable development is therefore a priority for all regional systems. Based on the position, that the sustainable development of the regional economic system depends on economic growth, and given the importance of forecasting this indicator to determine the vector of development of the territory, we consider the theoretical and model approaches to the economic growth of regional systems. In order to obtain the best result in forecasting the dynamics of macroeconomic indicators, we used the model of optimal economic growth, which is a modification of the Solow economic growth model. Both representatives of the authorities and representatives of the scientific environment solve the task of ensuring sustainable development of the economic system. The region's ability to maintain reliability of operation of the system and to ensure economic growth in the unstable conditions of global economic conditions determines the execution of the main purposes of any of the territory: increase of competitiveness of the economic system at various levels of interaction as well as improve the quality of life of the population. This modification of the model of economic growth allows us to forecast the dynamics of GRP, to calculate the optimal level of investments, required for the sustainable development of the regional economy. Using this model, it is possible to identify the trend of the labor force and predict its dynamics.
Keywords: dynamic modeling, optimization, economic growth, production function, Pontryagin maximum principle.

INTRODUCTION

During the recent years, we observe an unstable economic situation in the world. Since the possibility of maintaining and improving the competitiveness of the region at various levels, as well as improving the quality of life of all spheres of the population, largely depends on the undiminished pace of development of economic parameters special importance should be given to the economic component of the overall sustainability of regional systems. Thus, it is necessary to introduce the concept of "sustainable development of the economic system of the region". This concept has a bidirectional nature: preservation of stability of functioning of system and economic growth. Analyzing the works, containing clarification of the term "stability of the economic system", we can distinguish four main approaches to its definition, which relate to any areas of stability of the system.

Thus, within the framework of the study of theoretical approaches to the concepts of "sustainable development of the economic system" and "sustainability of the economic system" we determine that the stability of the economic system is to maintain the reliability of the links between its elements and ensure the qualitative development of its functions. Therefore, the sustainable development of the regional economic system is to maintain the quality development of the elements of the system and ensure quantitative economic growth of the parameters of the system.

Economic science at the present stage has two theories of economic growth: neo-keynesian and neoclassical, which determines the use of two types of models that characterize these theories. The basis of neo-keynesian theory (the founder George.M. Keynes) are the ideas of relative instability of the market economy, as well as macroeconomic equilibrium. The neo-Keynesian direction [3] considers the factors that determine, first, the volume and dynamics of national income, and second, the volume of consumption and savings. The increase in consumption and accumulation in Keynes' theory was associated with the level of national income, in addition, the theory considered the problem of income distribution and achieving full employment.

The main problem in the process of ensuring the sustainability of economic growth, but at the same time the possibility of improving the production process, is to find the optimal match of consumption savings. The excess of savings over investment contributes to the incomplete realization of growth potential. The nature of the ratio of savings and investment is inherent in all models developed under the neo-keynesian theory: the rate of savings and the degree of efficiency of investment determine the growth of national income [4].

OPTIMAL ECONOMIC GROWTH MODEL

The most widespread were the models of the keynesian direction of Roy Harrod (1900-1978) and Evsey Domar. The models presented by these economists are similar: namely, they are designed to analyze the process of economic growth in the long-term situation, provided by the equality of savings and investment. In the case of a long-term review, there is a difference between savings and investment. The private – property economy in which the capital of firms belongs to consumers-represents their assets is considered. Each of the consumers in continuous time maximizes utility under dynamic budget constraint [1]. The task of a representative firm is to maximize profits. The model also considers a representative household. It is assumed that the decisions, taken by the household, will be equivalent to the decision of the individual, which takes into account the levels of current and future well-being. The utility function of this individual will have the form (1):

$$U = \int_0^\infty u(c_t)^{-\rho t}\, dt \,, \tag{1}$$

where c_t – is per capita consumption at time t,

ρ – is a positive discount coefficient reflecting intertemporal preferences of an individual.

The utility function $u(c_t)$ depends only on the consumption at this point in time. In addition, it is assumed that the marginal utility (derivative $u'(c)$) is a positive and decreasing function. At the same time, when the consumption tends to zero, the marginal utility tends to infinity, and when the consumption tends to infinity, the marginal utility tends to zero. The income of the individual consists of w_t wages and $r_t a_t$ income from at assets owned by him and having a yield of r_t (assets can be negative, which implies a net debt situation, while the rate of borrowings is assumed to be equal to the yield of positive assets). Revenues are spent either on consumption or on increasing assets. Thus, the increase in assets per unit of time is $w+ra-c$. It should also be noted that the population is growing at the rate of n, so the assets per person are reduced at the same rate, that is, the rate of change of assets at each time reduced by na. Hence, the individual's budget constraint in this model would be as follows (2) [2]:

$$\dot{a} = w + ra - c - na \,. \tag{2}$$

Also in the neoclassical direction of great importance for the development of the theory of economic growth are the works of Robert Solow. In his research, R. Solow modified the Cobb-Douglas function by taking into account an additional factor in the model-the level of technology development. At the same time, Solow assumed that some change in the level of technology development contributes to the same increase in K and L (3) [5]:

$$Q = T \cdot F(K, L) \,, \tag{3}$$

where Q – is output,

K – fixed capital,

L – labor invested (in the form of wages),

T – level of technology development,

$F(K,L)$ – Cobb-Douglas production function.

The share of capital in output is determined through the capital-labor ratio, capital productivity and the share of labor, while the contribution of technological progress is expressed as the balance of the difference between the increase in output of the share of products obtained from the increase in labor and capital. This balance (Solow balance) reflects the share of economic growth due to technological progress. In the context of a constant volume of capital, population growth contributes to a decrease in the capital stock. The attracted investments should not only

cover the capital outflow, but also provide the capital of new workers in the same volume. In order to ensure the constancy of the values of the capital-labor ratio with the growth of the population, it is necessary to increase the capital at the same rate as the population (4):

$$\frac{\Delta Y}{Y}=\frac{\Delta L}{L}=\frac{\Delta K}{K}, \tag{4}$$

where Y – GRP,

L – number of employees,

K – is the stock of fixed assets.

In the Solow model, technological progress is the main condition for achieving a constant improvement in the standard of living of the population, since only with continuous technological progress the growth of the capital-labor ratio and output per employed person is recorded [6]. Nevertheless, the growth of capital-labor ratio increases the number of products per employee to a lesser extent than the capital-labor ratio, as the productivity of capital decreases. If we express production per employee as *(Q/L)q*, and the amount of capital per employee *(K/L)* through *k* (capital-labor ratio), the production function is as follows (5):

$$q=T\cdot F(k). \tag{5}$$

The model of optimal economic growth, developed by Robert Solow, is used to simulate the dynamics of the main economic indicators. This model aims to analyze the dynamics of growth of the gross regional product (*GRP*) of the country, defined as the market value of all goods and services produced in the region during the year. The model considers three factors used in production. Parameters *K(t)*, *L(t)* denote the size of capital and labor at time *t*. The volume of output *Y(t)* is given by the equation *Y(t)=F(K(t),L(t))=aKα(t) L(1-α)(t)*, the production function of the exponential Cobb-Douglas type is denoted through *F(K(t),L(t))*. The transition to relative variables will get the value of the capital (t)=K(t)/L(t) and GRP y(t)=Y(t)/L(t), per worker. The production function is (6):

$$y(t)=\frac{Y(t)}{L(t)}=\frac{F(K(t),L(t))}{L(t)}=F\left(\frac{K(t)}{L(t)},1\right)=f\big(k(t)\big)=ak^{\alpha}(t)\,. \tag{6}$$

This model considers a closed economic system, which is characterized by output aimed only at consumption and investment. Due to this premise, a balance sheet ratio is required, which is expressed in equation (7):

$$Y(t)=C(t)+I(t)=C(t)+u(t)\cdot Y(t)\Rightarrow c(t)=\frac{C(t)}{L(t)}=y(t)\cdot\big(1-u(t)\big). \tag{7}$$

where *C(t)* – is the level of consumption,

I(t) – fixed capital investments at time t,

c(t) – s the consumption level of one worker,

u(t) – share of GRP invested in fixed capital.

Thus, $I(t)=u(t)\cdot Y(t)$. From the balance equation, we obtained limits on the volume of investment (8), (9):

$$0\le c(t)=y(t)\cdot\big(1-u(t)\big)<y(t), \tag{8}$$

$$0\le u(t)\le\overline{u}<1. \tag{9}$$

In this modification of the economic growth model, it is assumed that changes in the capital *K(t)* occur in accordance with Solow dynamics (10):

$$\dot{K}(t)=u(t)\cdot Y(t)-\mu\cdot K(t),\quad K(0)=K_0,\quad \frac{\dot{L}(t)}{L(t)}=n,\quad L(0)=L_0, \tag{10}$$

where μ – is the rate of capital depreciation,

n – is the relative level of change in the labor force *L(t)*.

In the transition to the relative values we obtained the dynamics of *k(t)* (11):

$$\dot{k}(t)=u(t)\cdot f\big(k(t)\big)-\delta\cdot k(t),\quad k(0)=k_0=\frac{K_0}{L_0}, \tag{11}$$

where $\delta=\mu+n$ – is the degree of capital erosion due to its depreciation and increase in the volume of labor.

The problem of optimal capital investment management is considered, where the target functional is presented as an integral of the logarithmic consumption index discounted at an infinite time interval (12):

$$J(\cdot)=\int_0^{\infty}e^{-\rho t}\ln c(t)dt=\int_0^{\infty}e^{-\rho t}\big(\ln f\big(k(t)\big)+\ln\big(1-u(t)\big)\big)dt, \tag{12}$$

where ρ – is the discounting factor.

In utility theory, the logarithmic function describes the relative increase in consumption per unit of time. Under uncertainty, this function sets a constant relative risk aversion. It is necessary to describe an investment strategy that satisfies the restrictions (8), (9) and maximizes the target functionality on the trajectories of the dynamic system. This optimal control problem corresponds to a modification of the Pontryagin maximum principle for unlimited time. There is the only optimal strategy stabilizing at a stationary point with coordinates (k^*, u^*):

$$k^* = \begin{cases} \left(\dfrac{a\alpha}{\delta+\rho}\right)^{\frac{1}{1-\alpha}}, & u^* = \dfrac{\alpha\delta}{\delta+\rho} < \bar{u} \\ \left(\dfrac{\bar{u}\alpha}{\delta}\right)^{\frac{1}{1-\alpha}}, & u^* = \bar{u} \end{cases}, \quad y^* = a\left(k^*\right)^{\alpha}, \; c^* = y^*\left(1-u^*\right). \tag{13}$$

In conditions, where fixed capital investment satisfies the restriction $u^*<u$ over time, its level decreases to u^*. In another case, the level of investment will remain as high as possible for the entire period until the moment when the dynamic system stabilizes. The solution of the system has a pronounced *S*-shape regardless of the development scenario, which is provided by the parameter u, limiting the investment $u(t)$. In addition, optimal trajectories have a tendency of growth saturation.

CONCLUSION

Thus, the task of ensuring sustainable development of the economic system is a priority for all territorial entities and is solved by both the authorities and representatives of the scientific environment. The region's ability to ensure the reliability of functioning of system and economic growth in conditions of instability of global economic conditions determines the execution of the main purposes of any of the territory: increase of competitiveness of the economic system at various levels of interaction as well as improving the quality of life of the population. The urgency of the stated problems determines the necessity of forecasting economic growth on all time horizons as an important component of sustainable development of the region. In order to obtain the best result in forecasting the dynamics of macroeconomic indicators, it is necessary to use the model of optimal economic growth, which is a modification of the Solow economic growth model.

ACKNOWLEDGEMENTS

The work was supported by Act 211 Government of the Russian Federation, contract № 02.A03.21.0006.

REFERENCES

[1] Ane B.K., Tarasyev A.M., Watanabe C. (2007). Construction of Nonlinear Stabilizer for Trajectories of Economic Growth. Journal of Optimization Theory and Applications. Vol. 134. № 2. pp. 303-320.

[2] Aseev S.M. (2014). On some properties of the adjoint variable in the relations of the Pontryagin maximum principle for optimal economic growth problems. Proceedings of the Steklov Institute of Mathematics. Vol. 287. № 1. pp. 11–21.

[3] Lambertini L., Palestini A. (2014). On the feedback solutions of differential oligopoly games with hyperbolic demand curve and capacity accumulation. European Journal of Operational Research. Vol. 236. № 1. pp. 272–281.

[4] Lehmijoki U., Palokangas T. (2009). Population growth overshooting and trade in developing countries. Journal of Population Economics. Vol. 22. № 1. pp. 43–56.

[5] Solow, R.M. (1970). Growth Theory: An Exposition. NY, Oxford Univ. Press.

Labor Market Regulation: A Dynamic Model

Anastasiya E. Sudakova[1, a)], Andrei F. Shorikov[1, b)]

[1]*Ural Federal University, Mira Street 19, Yekaterinburg, Russia, 620002*

[a)]Corresponding author: a-chusova@mail.ru
[b)]afshorikov@mail.ru

Abstract. The article discusses issues of labor market regulation; the authors put forward the hypothesis that the labor market is a self-regulating system, with some assumptions that are unemployment rates and GDP. The article also presents a theoretical overview of the self-regulation of the labor market, taking place in the studies of other authors. In the second part of the article, the dynamic model of optimal management of specialists training formed by the authors is presented.

INTRODUCTION

The problem of unemployment and its rate is a relevant issue in the modern world. Often the unemployment is one of the main economy's performance indicators of a particular country. The higher the unemployment rate goes, the poorer the country's economic performance and standards of living of the citizens are; the higher the unemployment rate goes, the higher the crime level goes. Employment of young professionals strongly correlates with the problem of unemployment. In the last decade both in Russia and abroad (in particular in European countries), the issue of young professionals' employment has acquired particular relevance.

In the speech of the government of Russia, the imbalance in the structure of training young professionals was repeatedly mentioned. Thus, the share of graduates with university degrees increases, while the share of those holding secondary vocational degrees declines every year. In 1990 Russia had 4.8 times more graduates with secondary and basic vocational qualifications than those with university degrees, whereas in 2017 there were 1.6 times more of the latter than the former: the shift is mainly due to the growth in the number of university graduates with degrees in humanities, social sciences and economics.

Elias and Purcell [1] note the increase in the number of university graduates: 3 times for men and 2 times for women [2]; the researchers also point out that since 1960s a programme has been in place in the UK intended to facilitate access to higher education, which has proved to be rather controversial, as the share of unemployed among those with university degrees has been on the increase. The growth in the number of university graduates out of employment has also been registered in the European Union: since the start of the recent recession about 1/6 of young university graduates in Greece and Spain are unemployed [3], with the lowest unemployment rate among graduates registered in Germany in 2015 (8%). The main reasons for the imbalance between the labour market and the higher education system noted in most papers are the mismatch between the market demands and the specialisms provided by universities [4], excess of supply over demand: there are more graduates than the market needs [5]. According to some estimates, Europe's economy loses about 1% of GDP as a result of unemployment among young professionals [6]. There is one more indicator in the Russian government statistics – the share of Russian people, who work in a sphere different from their first specialty – that is about 60-73% of the economically active population in Russia; meanwhile, according to the Russian statistics service the unemployment rate in Russia in September 2018 was 4.7% (in 2009 – 8.3%).

A very different situation prevailed in the planned economy of the Soviet Union - back at that time after having graduated from an educational institution a Soviet student had to work for at least three years at a particular place, which the State chose itself. Forced distributions were introduced back in 1933 by the Council of People's

Commissars – initially the idea was to work for 5 years, and the deviants were at risk of facing the trial; all those young professionals in the USSR, who got their higher education, were to be distributed.

In summing up, please note that the research dedicated to the labor market covers the issues of labor migration, unemployment, economy's demand for personnel, as well as specific questions such as accordance of graduates' competence with the requirements of the labor market, monitoring of their employment and starting salary amount.

However, the question of the labor market self-regulation remains understudied. In this regard, the following hypothesis was made by the authors of the article: the labor market is a relatively self-regulated economy sector; professionals choose a work place and obtain employment according to their competence, desires and needs with a slight adjustment due to the labor market demand. Whereas educational institutions (higher and secondary vocational education) act as a link in the process of employment (for example, in a pair "desires – competence", acquisition of initial competence).

So, our hypothesis is superficially supported by the following information: about 60% of the economically active population in Russia do not work in a sphere related to their specialty, i.e. they either changed their sphere of activity (retrained) or moved into other spheres, which do not require higher education. Meanwhile the unemployment rate in the country is decreasing, having hit historic lows in 2018.

Under this hypothesis, two questions arise at once: what role does the higher education play in this case and what is the measure of self-regulation? The labor market self-regulation is present unless the unemployment rate does not hit a critical value and the economy has a positive trend within the given balance on the labor market.

Among the few models designed to solve the problem focused on by the authors, one can note the econometric model developed by Gottschalk and Hansen [7], the main idea of which is the balance between sector 1, where professionals with university degrees are employed, and sector 2, which employs those with secondary vocational education; university graduates can be employed in both sectors.

The equilibrium condition depends on the sector-specific wage premium offered to graduates and the relative wage between sectors. Gottschalk and Hansen's model is merely an adaptation aimed at finding the balance between professionals with degrees of different level; the main postulate of the wage equation was used in earlier models [8].

DYNAMIC MATHEMATICAL MODEL

The quality of management for the process of training is estimated by vector functionality, which estimates the costs of training, the level of training and the volume of output. On the basis of the ratio (1-4) in work the economic and mathematical model for considered process of preparation of specialists is formed and within the formed model (2-4) the problem of optimum management of preparation is formed. To solve this problem of optimal software modeling, we consider a linear discrete model of complete information and a control vector of the proposed technique based on [9].

The formation of a dynamic mathematical model to optimize the process of managing the training of specialists with higher education in a particular University, based, for example, on the results of [10-11] can be formalized as follows.

We introduce the following notation: n – the number of key parameters describing the state of the process of training specialists with higher education in a particular university (number of educational programs, number of training places, indicators of the material base, indicators of the social sphere, etc.), $n \in \mathbf{N}$ ($\mathbf{N}$ – set of all natural numbers); p – the number of technologies for organizing and implementing the process of training specialists with higher education at a higher education institution (taking into account various methods of training specialists, various methods of financing, etc.), $p \in \mathbf{N}$; each j-th technology of organization and implementation of training specialists with higher education at a higher education institution ($j \in \overline{1,p} = \{1,2,\dots,p\}$) in a period of time $t \in \overline{0,T-1}$ ($t \in \mathbf{N};\ T > 1$) (t, for example, semester, academic year) is characterized by a vector ($(b_{1j}(t), b_{2j}(t), \dots, b_{nj}(t))' \in \mathbf{R}^n$ hereinafter, for $k \in \mathbf{N}$, $\mathbf{R}^k$ – is the k-dimensional vector space of wind-columns); if $b_{ij}(t) < 0$, that $b_{ij}(t)$ determines the cost of the i-th parameter ($i \in \overline{1,n}$) in the j-th technology ($j \in \overline{1,p}$) organization and implementation of training specialists with higher education at the university during the period of time t; if $b_{ij}(t) > 0$, that $b_{ij}(t)$ determines *the volume of issue of the i-th parameter* ($i \in \overline{1,n}$) in the j-

th technology ($j \in \overline{1, p}$) organization and implementation of training of specialists with higher education in the university in a period of time t; if $b_{ij}(t) = 0$, that $b_{ij}(t)$ determines *no issue or cost i*-th parameter ($i \in \overline{1, n}$)in the j-th technology ($j \in \overline{1, p}$) organization and implementation of training of specialists with higher education in the university in a period of time t.

Denote: $u_j(t)$ – *intensity of use of j-th technology* ($j \in \overline{1, p}$) intensity of use of j-th technology ($u_j(t) \in \mathbf{R}^1$); $s_i(t)$ – the amount of demand for specialists of the i-th specialty ($i \in \overline{1, n}$), produced by the university in the period of time t ($s_i(t) \in \mathbf{R}^1$). It is assumed that the capabilities of the university are such that they can meet the emerging demand, i.e. Inequality always holds: $\forall t \in \overline{0, T-1}$; $\forall i \in \overline{1, n}$: $\sum_{j=1}^{p} b_{ij}(t)u_j(t) - s_i(t) \geq 0$.

Denote: $x_i(t+1)$ – the number of the i-th parameter ($i \in \overline{1, n}$), describing its state in a period of time (t+1) (reserves in a period (t+1)), which is formed from stocks in the volume $x_i(t)$ of the previous period and the resulting surpluses in this period of time using the formula: $x_i(t+1) = x_i(t) + \sum_{j=1}^{p} b_{ij}(t)u_j(t) - s_i(t)$; or in vector form

$$x(t+1) = x(t) + B(t)u(t) - s(t), \ t \in \overline{0, T-1}, \tag{1}$$

$x(t) = (x_1(t), x_2(t), \ldots, x_n(t))' \in \mathbf{R}^n$ – the vector of parameters of the state of organization and implementation of training of specialists with higher education in the university in a period of time t or the phase vector of the system; $u(t) = (u_1(t), u_2(t), \ldots, u_p(t))' \in \mathbf{R}^p$ – vector of intensity of use of technology organization and implementation of training of specialists with higher education at the university in a period of time t or vector control action (control) system; $s(t) = (s_1(t), s_2(t), \ldots, s_n(t))' \in \mathbf{R}^n$ – vector of demand volumes for specialists trained by the university, during the period of time t; $B(t) = \left\| b_{ij}(t) \right\|_{\substack{i \in \overline{1,n} \\ j \in \overline{1,p}}}$ – *"technological matrix" of training specialists in higher education institutions of dimension* $(n \times p)$.

Note that if at the beginning of the period of time t $(t \in \overline{1, T})$ at the university there were reserves of parameters (number of educational programs, number of training places, indicators of the material base, indicators of the social sphere, etc.) of the process of preparing specialists at the university in the number of x(t), then by the end of this period for the implementation of the considered process of training specialists, only their part equal to $A(t)x(t)$, where $A(t) = \left\| a_{ii}(t) \right\|_{i \in \overline{1,n}}$ – is the diagonal matrix of dimension (nxn), which characterizes the “aging” of parameters during this period of time. Then the vector equation (1), describing the process under consideration, will have the following form:

$$x(t+1) = A(t)x(t) + B(t)u(t) - s(t), \ x(0) = x_0, \ t \in \overline{0, T-1}, \tag{2}$$

where $x_0 \in \mathbf{R}^n$ – is the specified initial value of the phase vector. It is assumed that in the considered process of managing the training of specialists the values of the phase vector $x(t) = (x_1(t), x_2(t), \ldots, x_n(t))' \in \mathbf{R}^n$ for each time period *t* ($t \in \overline{1, T}$) must satisfy the following given geometric constraint:

$$x(t) = (x_1(t), x_2(t), \ldots, x_n(t)) \in \boldsymbol{X}^*(t) \subset \mathbf{R}^n, \tag{3}$$

where the set $\boldsymbol{X}^*(t)$ sets the technical and economic restrictions on the main parameters of its state that are available in the process of training specialists in a higher school and can be described, for example, in the form:

$$X^*(t) = \{x(t):\ x(t) = (x_1(t), x_2(t), \dots, x_n(t))' \in \mathbf{R}^n, \forall i \in \overline{1,n} : 0 \le x_i(t) \le x_i^*\},$$

where $\forall i \in \overline{1,n} : x_i^* \in \mathbf{R}^1$, $x_i^* > 0$. It is also assumed that in this process of management training specialists, the values of the control vector $u(t) = (u_1(t), u_2(t), \dots, u_p(t))' \in \mathbf{R}^p$ for each time period t ($t \in \overline{0, T-1}$) must satisfy the following given geometric constraint:

$$u(t) = (u_1(t), u_2(t), \dots, u_p(t)) \in U^*(t) \subset \mathbf{R}^p, \tag{4}$$

where the set $U^*(t)$ describes the limitations on the intensity of technology for its implementation, i.e. defines the control resource and can be described, for example, in the following form:

$$U^*(t) = \{u(t):\ u(t) = (u_1(t), u_2(t), \dots, u_p(t))' \in \mathbf{R}^p, \forall j \in \overline{1,p} : u_{j*}(t) \le u_j(t) \le u_j^*(t)\},$$

где $\forall j \in \overline{1,p} : u_{j*}(t) \in \mathbf{R}^1$, $u_{j*}(t) > 0$, $u_j^*(t) \in \mathbf{R}^1$.

CONCLUSION

The labor market may have the makings of self-regulation: in Russia, the level of the economically active population, which works not received the primary specialty 60-70%, while reducing the unemployment rate. We assume that self-regulation of the labor market is possible under certain conditions: the unemployment rate, the growth rate of the economy. In this regard, we have proposed a dynamic model of optimal management of training.

ACKNOWLEDGEMENTS

The work was supported by Act 211 Government of the Russian Federation, contract № 02.A03.21.0006

REFERENCES

[1] Elias P., Purcell K. Measuring Change in the Graduate Labour Market, IER/ESRU Report № 1 (2003).
[2] Elias P., Purcell K. Seven Years On: Graduate Careers in a Changing Labour Market. London: The Higher Education Careers Service Unit (2004).
[3] Kačerová Eliška. "Risk Factors of Young Graduates in the Competitive E.U. Labour Market at the End of the Current Economic Crisis". Journal of Competitiveness. Vol. 8, Issue 3, 38 – 51 (2016).
[4] Němec, J. "Ze školní lavice na židli státního úřadu". Ekonom. 15, 35-39 (2013).
[5] *Research of Long-Term Forecasting System of the Labour Market Demand and Analysis of Improvement Options*, (2007).
[6] *The Economist. Generation jobless. The global rise of youth unemployment.* (2013).
[7] Gerard J. van den Berg, Geert Ridder. "An Empirical Equilibrium Search Model of the Labor Market". Econometrica. Vol. 66, No. 5, 1183-1221 (1998).
[8] Albrecht, James W & Axell, Bo. "An Equilibrium Model of Search Unemployment. Journal of Political Economy", University of Chicago Press, Vol. 92(5), 824-840 (1984).
[9] Sudakova A.E., Shorikov A.F., Agarkov G.A. "Optimizing university training structure: a deterministic dynamic model". 17th IFAC Workshop on Control Applications of Optimization (CAO 2018) (Yekaterinburg, 15-19 October, 2018.): Conference Proceedings. Yekaterinburg: IFAC, 2018, p. 401-406.
[10] A. Shorikov. *Minimax estimation and control in discrete dynamical systems*. Yekaterinburg. Ural university (1997).
[11] Aksyonov K., Bykov E., Aksyonova O., Nevolina A., Goncharova N. "The Multi-agent Resource Conversion Processes Model Design and Implementation". Proceedings of the International Conference on Computer Science and Applications 2016 (ICCSA 2016) - part of the World Congress on Engineering and Computer Science 2016, WCECS 2016, October 19-21, 2016, San Francisco, USA. Vol. I. p. 219-223.

Development of Decomposition Methods for Auction Games

Nikolay A. Krasovskii[1, a)] and Alexander M. Tarasyev[1, 2, b)]

[1]*Krasovskii Institute of Mathematics and Mechanics UrB RAS, 620990, S. Kovalevskaya Street, 16, Yekaterinburg, Russia.*
[2]*Ural Federal University, 620002, Mira Street, 19, Yekaterinburg, Russia.*

[a)]nkrasovskiy@gmail.com
[b)]Corresponding author: tam@imm.uran.ru, a.m.tarasyev@urfu.ru

Abstract. The paper addresses the problem of searching maximum Pareto points which possess special decomposition characteristics, that inherits the properties of the competitive Nash equilibrium. Such point is called market equilibrium. First, the competitive Nash equilibrium is constructed for the auction game of three players and its properties are analyzed. Then the set of Pareto points is described analytically on the basis of convolution method. The main task is to construct a path from the competitive Nash equilibrium to the point of market equilibrium in the Pareto set. This path is generated by the shift algorithm which is based on analytical calculation of the players' best replies with respect to auction prices. The auction mechanism of the search algorithm is expressed as a system of nonlinear differential equations, precisely they describe formation of auction prices and players' best replies to these prices. Trajectories of the generated dynamic system are constructed and their properties of convergence to the market equilibrium are examined. The proposed algorithm is applied to the model of the auction game of fast growing economies and its efficiency is shown particularly for the emissions reduction problem.
Keywords: optimal control, dynamic games, competitive equilibrium, cooperative solutions, shifting trajectories
PACS: 02.30.Yy

MODEL DESCRIPTION

A game model is considered, which goal is to shift players from a non-cooperative equilibrium to a cooperative maximum. The prototype of this problem is the model of emissions reduction trade [9]. The model involves n players, which can be countries - participants of the agreement, solving the problem of reduction of greenhouse gas emissions. It is assumed that the agreement is reached in the step-by-step auction process managed by the auctioneer. Each country i controls own amount of emission reduction $x_i \geq 0$. The country i is interested in the maximization of its own utility function w_i, which is given by the formula:

$$w_i(x) = -C_i(x_i) + B_i\left(\sum_{j=1}^{n} a_{ji} x_j\right). \qquad (1)$$

Here the symbol $x = (x_1, \ldots, x_n)$ - is the full vector of emissions reduction; $C_i(x_i)$ - is the cost function of the country i on the emissions reduction x_i; $B_i\left(\sum_{j=1}^{n} a_{ji} x_j\right)$ - is the function of ecological benefit, which country i receives due to the total emissions reduction $\sum_{j=1}^{n} a_{ji} x_j$ on its territory; and a_{ji} - is the transboundary transport coefficient, that is, a part of the industrial emissions of the country j transferred to the territory of the country i. It is assumed that $a_{ji} > 0$ and $\sum_{i=1}^{n} a_{ji} \leq 1$.

The model is specified for a game situation between three players: China, India and Dynamic Asian Economies Countries. For them, we identify the quadratic cost functions [3] and the logarithmic ecological benefit functions [11]:

$$C_i(x_i) = \frac{e_i}{2} x_i^2 + c_i; \;\; B_i\left(\sum_{j=1}^{n} a_{ji} x_j\right) = d_i \ln\left(\sum_{j=1}^{n} a_{ji} x_j\right). \tag{2}$$

The utility function is the combination of the cost function and the ecological benefit function.

Without loss of the generality of reasoning, we assume that the free terms of the cost functions are equal to zero.

The coefficients for quadratic terms in the cost functions have the following values calibrated in the econometric analysis:

$$e_1 = 0.024(China), \;\; e_2 = 0.079(India), \;\; e_3 = 0.377(DAE). \tag{3}$$

Such difference in the cost function coefficients is explained by the fact that in the Dynamic Asian Economies Countries the emissions reduction is more expensive than in India and China.

Coefficients for the ecological benefit functions have the values $d_1 = 1, \; d_2 = 1, \; d_3 = 1.$ The equal values of these coefficients show that all countries are equally interested in improving the environmental situation as a result of the emissions reduction.

For the case of carbon dioxide CO_2 the emission reduction transport coefficient can be considered as: $a_{ji} = 1.$

NASH EQUILIBRIUM

We study the model within the constructions of the dynamic games theory [1, 2,6,8,10,12]. In this research, we essentially use the approaches and methods proposed in [4,5,7,9].

Definition 1. The vector of emission reduction $x^N = \left(x_1^N, \ldots, x_n^N\right)$ is the Nash equilibrium, if the system of equilibrium conditions is fulfilled:

$$\max_{x_i \geq 0} w_i\left(x_1^N, \ldots, x_i, \ldots, x_n^N\right) = w_i\left(x_1^N, \ldots, x_i^N, \ldots, x_n^N\right), \;\; i = (1, \ldots, n). \tag{4}$$

Since the functions w_i are strictly concave, the relations (4) are equivalent to the fact that all partial derivatives $\partial w_i\left(x^N\right) / \partial x_i$ in the equilibrium are equal to zero:

$$\frac{\partial w_i}{\partial x_i}\left(x^N\right) = 0, \;\; i = (1, \ldots, n). \tag{5}$$

Analytical calculations for (5) provide the following values for coordinates of the Nash equilibrium:

$$x_1^N = 5.52, \;\; x_2^N = 1.68, \;\; x_3^N = 0.35. \tag{6}$$

THE SET OF PARETO MAXIMUM POINTS

Definition 2. The vector of the emissions reduction $x^P = \left(x_1^P, \ldots, x_n^P\right)$ is the Pareto maximum, if for any other vector $x \neq x^P$ there exists the component j, for which $w_j(x) < w_j\left(x^P\right).$

By Germeyer's theorem for strictly concave functions w_i the set of Pareto points coincides with the set of all solutions of the parametric maximization family:

$$\text{maximize } w(x, \alpha), \;\; x_i \geq 0, \tag{7}$$

where the symbol $w(x, \alpha)$ denotes the convolution function:

$$w(x, \alpha) = w(x_1, \ldots, x_n, \alpha_1, \ldots, \alpha_n) = \sum_{k=1}^{n} \alpha_k w_k(x). \tag{8}$$

The convolution coefficients should be non-negative and belong to the simplex:

$$\alpha_k \geq 0, \;\; \sum_{k=1}^{n} \alpha_k = 1. \tag{9}$$

According to the fact that functions w_i are strictly concave, the maximizer in (7) is described by the equation:

$$\sum_{k=1}^{n}\alpha_k \frac{\partial w_k}{\partial x_i}\left(x\right)=0,\ \ i=\left(1,\ldots,n\right). \qquad (10)$$

MARKET EQUILBRIUM

Definition 3. Let us call market equilibrium a vector of positive emissions reduction $x^M=\left(x_1^M,\ldots,x_n^M\right)$, if for each player i the function $w_i\left(\lambda x^M\right)\left(\lambda>0\right)$ reaches its maximum when $\lambda=1$,

$$x^M=\arg\max\left\{w_i\left(\lambda x^M\right):\lambda x^M,\left(\lambda>0\right)\right\}, \qquad (11)$$

which is equivalent to the relation:

$$\frac{dw_i\left(\lambda x^M\right)}{d\lambda}\Big|_{\lambda=1}=0\ \ \left(i=1,\ldots,n\right). \qquad (12)$$

It is worth to note, that an analogous definition is given in the paper [9]. This definition means that maximum of the payoff functions for all players is reached at the point of the market equilibrium x^M when searching on the direction generated by this equilibrium.

The definition of the market equilibrium combines properties of two previous definitions: the Nash equilibrium and Pareto maximum. From the definition of the Nash equilibrium we take the structure of optimization of each function separately, and the definition of points of Pareto maximum is reflected in the joint direction of searching the maximum.

Let us note that in the definition of the market equilibrium we can assume that the base point is placed at the origin. Such a base point can be the current state or equilibrium of the system. The case when this role is played by the point of the Nash equilibrium is of the special interest. In this situation, we can talk about shifting the system from the Nash equilibrium to the new equilibrium position - the point of the market equilibrium. It is namely this shift that is being studied in the considered model.

Let us present the system of equations for the shift:

$$\begin{cases} y_1\dfrac{\partial w_1}{\partial y_1}\left(y_1,y_2,y_3\right)+y_2\dfrac{\partial w_1}{\partial y_2}\left(y_1,y_2,y_3\right)+y_3\dfrac{\partial w_1}{\partial y_3}\left(y_1,y_2,y_3\right)=0,\\ y_1\dfrac{\partial w_2}{\partial y_1}\left(y_1,y_2,y_3\right)+y_2\dfrac{\partial w_2}{\partial y_2}\left(y_1,y_2,y_3\right)+y_3\dfrac{\partial w_2}{\partial y_3}\left(y_1,y_2,y_3\right)=0,\\ y_1\dfrac{\partial w_3}{\partial y_1}\left(y_1,y_2,y_3\right)+y_2\dfrac{\partial w_3}{\partial y_2}\left(y_1,y_2,y_3\right)+y_3\dfrac{\partial w_3}{\partial y_3}\left(y_1,y_2,y_3\right)=0.\end{cases} \qquad (13)$$

This system can be resolved as best replies equations:

$$\begin{cases} F_1\left(y_1,y_2,y_3\right)=-f_1(y_1)+y_2+y_3=0,\\ F_2\left(y_1,y_2,y_3\right)=-f_2(y_2)+y_1+y_3=0,\\ F_3\left(y_1,y_2,y_3\right)=-f_3(y_3)+y_1+y_2=0,\end{cases} \qquad (14)$$

where $f_i(y_i)=y_i\times\left(\dfrac{\left(e_i\left(x_1^N+x_2^N+x_3^N\right)\left(x_i^N+y_i\right)\right)}{\left(d_i-e_iy_i\left(x_i^N+y_i\right)\right)}-1\right),\ i=\left(1,\ldots,3\right).$

The dynamics of best replies has the following form:

$$\begin{cases} \dfrac{dy_1}{dt}=-f_1(y_1)-y_1+p_1y_1=0,\\ \dfrac{dy_2}{dt}=-f_2(y_2)-y_2+p_2y_2=0,\\ \dfrac{dy_3}{dt}=-f_3(y_3)-y_3+p_3y_3=0,\end{cases} \qquad (15)$$

where prices p_i are given by the equation: $p_i=\left(y_1+y_2+y_3\right)/y_i,\ i=(1,\ldots,3).$

The system of equations of the auction (15) is integrated by the Runge-Kutta method.

The obtained results are demonstrated on Fig. 1, where we depict the location of the Nash equilibrium (*NE*), the set of Pareto maximum points (*PM*) and trajectories of the proposed algorithm (TR_1, TR_2, TR_3) starting from different initial points and converging to the point of the market equilibrium located on the set of Pareto maximum. Thus, the proposed algorithm provides the shift from the competitive Nash equilibrium to the cooperative market equilibrium on the Pareto set.

The numerical experiments implemented in the MATLAB program shows that trajectories of the algorithm are stabilized at the equilibrium point with the following coordinates:

$$x_1^M = 7.5254, \quad x_2^M = 3.1380, \quad x_3^M = 1.1715. \tag{16}$$

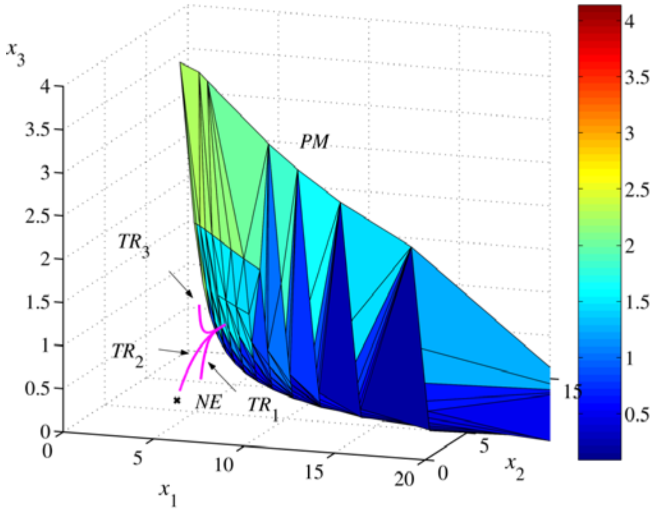

FIGURE 1. Trajectories of the Dynamic Auction.

ACKNOWLEDGMENTS

The first author Nikolay A. Krasovskii is supported by the RFBR project No. 18-01-00221a.

REFERENCES

[1] Bagno A., Tarasyev A.A., Tarasyev A.M. (2017). Value function in economic growth model. AIP Conference Proceedings. 1906, 070009.

[2] Basar T., Olsder G.J. (1982). Dynamic Noncooperative Game Theory. Academic Press, London.

[3] Ellerman A.D., Decaux A. (1998). Analysis of Post-Kyoto CO2 Emissions Trading Using Marginal Abatement Curves. MIT Joint Program on the Science and Policy of Global Change, vol. 40.

[4] Klaassen G., Kryazhimskii A.V., Tarasyev A.M. (2004) Multiequilibrium Game of Timing and Competition of Gas Pipeline Projects. Journal of Optimization Theory and Applications, vol. 120 (1), pp. 147-179.

[5] Krasovskii A.A., Taras’ev A.M. (2007). Dynamic Optimization of Investments in the Economic Growth Models. Automation and Remote Control, vol. 68 (10), pp. 1765-1777.

[6] Krasovskii A.N., Krasovskii N.N. (1995). Control Under Lack of Information. Birkhauser, Boston etc..

[7] Krasovskii N.A., Tarasyev A.M. (2015). Decomposition Algorithm of Searching Equilibria in a Dynamic Game. Automation and Remote Control, vol. 76 (10), pp. 1865-1893.

[8] Krasovskii N.N., Subbotin A.I. (1988). Game-Theoretical Control Problems. Springer, New York, Berlin.

[9] Kryazhimskii A., Nentjes A., Shybaiev S., Tarasyev A. (2001). Modeling Market Equilibrium for Transboundary Environmental Problem. Nonlinear Analysis, vol. 47 (2), pp. 991-1002.

[10] Kryazhimskii A.V., Osipov Yu.S. (1995). On Differential-Evolutionary Games. Proceedings of Math. Institute of RAS, vol. 211, pp. 257-287.

[11] Tol R. (2005). The Benefits of Greenhouse Gas Emission Reduction: an Application of Fund”, Hamburg University Working Paper FNU-64.

[12] Vorobyev N.N. (1985). Game Theory for Economists and System Scientists. Nauka, Moscow.

Piecewise Constant Control Approximations in the Problem on Effective Resource Consumption

Alexander M. Tarasyev[1, 2, a)] and Anastasiia A. Usova[1, b)]

[1] *Krasovskii Institute of Mathematics and Mechanics of Ural branch of Russian Academy of Sciences (16 S. Kovalevskaya street, Yekaterinburg, Russia, 620990)*
[2] *Ural Federal University (19 Mira street, Ekaterinburg, Russia, 620002)*
[a)] Corresponding author: tam@imm.uran.ru
[b)] ausova@imm.uran.ru

Abstract. The paper proposes the piecewise constant control approximations in the control problem in the infinite time interval that is based on the growth model of effective resource consumption under the condition on resources' exhaustibility. The problem is analyzed within the Pontryagin maximum principle for the problems in the infinite time interval. We investigate the behavior of the dynamic system under different control regimes and search for the stationary levels of the Hamiltonian system. The paper constructs a piecewise constant control as an approximation of an optimal control that takes into account the condition on limited resources. The obtained approximate solutions are compared with the solutions derived using the non-linear stabilizer technique that is widely applied for the considered class of optimal control problems.
Keywords: optimal control, growth models, piecewise constant controls

INTRODUCTION

The paper studies the problem on optimization of resource productivity by means of an investment policy aimed at the dematerialization of the economy. The problem statement is based on the conventional approaches borrowed from the economic growth models [2, 3, 6, 7, 8, 10], and methods presented in the work [9]. The model includes the price-formation mechanism that indicates the inverse proportionality of the cost of the natural resources to their stock. The price-formation mechanism can be considered as the natural fine for violating the phase constraints in the optimal control problems. Simultaneously, raising cost of natural resources negatively affects the consumption index that estimates the quality of the control process [10].

According to the statistical data [5], the rate of resource consumption is rapidly increasing, and therefore, an optimization problem of resource productivity is highly important. The main goal is to find such a distribution of investment flows that the utility function in the form of integral logarithmic consumption index discounted at the infinite time interval, takes the maximum value along the trajectories of a dynamic system. The problem is investigated within the Pontryagin maximum principle [1, 6]. The qualitative analysis of the Hamiltonian system allows for deriving the conditions on model parameters that guarantee an existence of a steady state. Moreover, the paper offers another approach for constructing an approximate problem solution that is based on the properties of the system under the constant controls. The developed approach considers the phase constraints imposed by the condition of resources' exhaustibility. An approximate solution is compared with the stabilized trajectories that are constructed by the algorithm presented in [10].

The rest of the paper is organized as follows. Next section describes the model of the resource consumption and formulates the optimal control problem. Further, the problem analysis is conducted within the Pontryagin maximum principle, and the piecewise constant controls are constructed. Finally, we compare the approximate and stabilized solutions and discuss the obtained results.

CONTROL PROBLEM ON OPTIMIZATION OF THE RESOURCE PRODUCTIVITY

The main phase variables of the model are presented by the current production *y(t)*, the resource use *m(t)* and the cumulative resource consumption *M(t)*, where variable t stands for the time $t\in[0,+\infty)$. The cumulative resource consumption *M(t)* is introduced as the integrated material use *m(t)* and upper-bounded by the initial stock $\overline{M}$ of the natural resources

$$M = M(t) = \int_0^t m(\tau)d\tau \le \overline{M} = \int_0^{+\infty} m(t)dt \,. \qquad (1)$$

The initial consumption level $m(0)=m_0$ is known. The resource productivity *z(t)* is determined by the formula

$$z(t) = y(t) / m(t) \,. \qquad (2)$$

In the definition of the price formation mechanism the basis is provided by the concept of raising prices *p(t)* on natural resources in the case of their limitation or exhaustion:

$$p(t) / p_0 = M_0 / (M_0 M(t)). \qquad (3)$$

It is assumed that prices are growing according to the inversely proportional rule of resources exhaustion. Formula (3) envisages that price *p(t)* can grow rapidly to infinity according to the hyperbolic law when the integrated material use *M(t)* reaches its limitation $\overline{M}$. Under the assumption on closedness of the economy, the **balance equation** takes place

$$y(t) = c(t) + p(t)m(t) + u(t)y(t) \,, \qquad (4)$$

i.e. the production *y(t)* in period *t* is shared between consumption *c(t)* and the growing cost of the natural resources *p(t)m(t)* plus investment *u(t)y(t)* in increasing the resource productivity *z(t)*. The balance relation (4) allows for deriving the current consumption level *c(t)* of the form

$$c(t) = y(t)\big(1 - p(t)m(t) / y(t) + u(t)\big) \qquad (5)$$

and for indicating the constraints for the control parameter *u(t)*

$$0 \le u(t) \le \overline{u} < 1 \,. \qquad (6)$$

The Cobb-Douglas **production function** describes the dependence of the output *y(t)* from the resource use *m(t)*

$$y(t) = ae^{bt} m^{\alpha}(t), \;\; a > 0, \;\; b \ge 0, \;\; 0 \le \alpha < 1 \,, \qquad (7)$$

where parameter a is a scale factor, symbol b stands for the growth rate of the output *y(t)* due to the development of the production factors (*i.e.* resource use *m(t)*), and the constant α is an elasticity coefficient. Let assume that the relative raise in the resource productivity *z(t)* is proportional to the portion of the assigned investment *u(t)* (see [2]):

$$\dot{z}(t) = \beta u(t) z(t), \;\; \beta \ge 0 \,, \qquad (8)$$

where parameter β indicates an effectiveness of the investment process *u(t)*. The equality (8) together with the formulae (2) and (7) provides the dynamics of the material use

$$\dot{m}(t) = \big(b - \beta u(t)\big) m(t) / (1 - \alpha). \qquad (9)$$

For the model analysis, we introduce new phase variables of the form

$$x_1(t) = m(t) / \big(\overline{M} - M(t)\big), \;\; x_2(t) = p(t)m(t) / y(t) \,. \qquad (10)$$

The first variable $x_1(t)$ means the share of the current stock of natural resources that is used in the current period *t*, and the second variable $x_2(t)$ is the share of the output that is spent on the purchase of the natural resources. The dynamic relations for the new variables $x_1(t)$ and $x_2(t)$ can be derived using equalities (1), (3), (7) - (9).

$$\begin{aligned} \dot{x}_1(t) &= f_1\big(x_1(t), x_2(t), u(t)\big) = x_1(t)\big(x_1(t) + \big(b - \beta u(t)\big)/(1 - \alpha)\big), \qquad & x_1^0 &= m_0 / \overline{M} \\ \dot{x}_2(t) &= f_2\big(x_1(t), x_2(t), u(t)\big) = x_2(t)\big(x_1(t) - \beta u(t)\big), & x_2^0 &= p_0 m_0^{1-\alpha} / a \end{aligned} \,. \qquad (11)$$

In variables $x_1(t)$ and $x_2(t)$ (10), the logarithmic consumption index can be found by the formula

$$\ln c(t) = \ln x_1(t) - \ln x_2(t) + \ln\big(1 - u(t) - x_2(t)\big) + \ln\big(p_0 M_0\big) = w\big(x_1, x_2, u\big) + \ln\big(p_0 M_0\big). \qquad (12)$$

The quality of a control process is determined by the integral consumption index discounted in the infinite time interval

$$J\big(x(\cdot), u(\cdot)\big) = \int_0^{+\infty} e^{-\rho t} \omega\big(x_1(t), x_2(t), u(t)\big) dt \,. \qquad (13)$$

The optimal control problem is to maximize the utility function (13) along the trajectories ($x_1(t)$, $x_2(t)$, *u(t)*) of the dynamic system (11) that satisfy the initial conditions x_1^0, x_2^0 in phase variables $x_1(t)$ and $x_2(t)$, respectively, and the constraints (6) on control variable *u(t)*.

PROBLEM ANALYSIS

The problem analysis is conducted within the Pontryagin maximum principle [5] generalized for the optimal control problems in the infinite time interval [1]. The stationary Hamiltonian function has the form

$$\hat{H}(x_1,x_2,\psi_1,\psi_2,u)=\ln w(x_1,x_2,u)+\psi_1 f_1(x_1,x_2,u)+\psi_2 f_2(x_1,x_2,u). \qquad (14)$$

Where ψ_1, ψ_2 are conjugate variables, and $f_1(\cdot)$, $f_2(\cdot)$ are the right-hand parts of the dynamics (11). For the analysis, it is convenient to introduce the adjoint variables of the form $x_3=\psi_1 x_1$, $x_4=\psi_2 x_2$ and denote by symbol x the vector of phase and adjoint variables, *i.e.* $x=(x_1, x_2, x_3, x_4)^T$. The Hamiltonian function $\hat{H}(\cdot,u)$ (14) as a function of variable u takes the maximum value $H(x):=\max_{u\in[0,\bar{u}]}\hat{H}(x,u)$ at $u=u^0(x)$, where

$$u^0=\begin{cases}0, & x\in D_1:=\{x:\nu(x)\geq 1-x_2\}\\ 1-x_2-\nu(x), & x\in D_2:=\{x:1-\bar{u}-x_2\leq\nu(x)\leq 1-x_2\},\ \nu(x)=-\dfrac{1-\alpha}{\beta(x_3+(1-\alpha)x_3)}\\ \bar{u}, & x\in D_3:=\{x:\nu(x)\leq 1-\bar{u}-x_2\}\end{cases}. \qquad (15)$$

The obtained control u^0 maximizing the Hamiltonian function $\hat{H}(\cdot,u)$ (14) splits the task space in 3 domains. In each domain, the Hamiltonian system can be derived by the formula

$$\dot{x}_i=\partial H(x_1,x_2,\psi_1,\psi_2)/\partial\psi_i,\ \dot{\psi}_i=\rho\psi_i-\partial H(x_1,x_2,\psi_1,\psi_2)/\partial x_i,\ i=1,2. \qquad (16)$$

The dynamics of the conjugate variables x3 and x4 can be found from (16) due to their definitions, i.e. $\dot{x}_3=\dot{x}_1\psi_1+\dot{\psi}_1 x_1$ and $\dot{x}_4=\dot{x}_2\psi_2+\dot{\psi}_2 x_2$. Qualitative analysis of the Hamiltonian system (16) reveals that a steady state may exist only in the domain D_2 of the transient control regime $u_0=1-x_2-v(x)$, if the model parameters belong the set Ω depicted at Fig.1. The steady state coordinates analytically expressed by the formulae (17). The control u^* corresponding to the steady state takes the value $u^*=b/(\alpha\beta)\leq\bar{u}<1$.

$$x_1^*=b/\alpha,\ x_2^*=(\alpha\rho-b)((1-\alpha)\rho+\alpha\beta-b)/\alpha\beta\rho,\ x_3^*=(1-\alpha)(1-\alpha\rho/(\alpha\beta-b))x_4^*,\ x_4^*=-(\alpha\beta-b)/(\alpha\rho(1-\alpha)(\beta-\rho)+b(\alpha\beta-b)). \qquad (17)$$

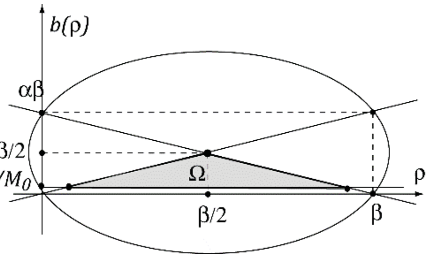

FIGURE 1. Steady state domain, Ω

PIECEWISE CONSTANT CONTROLS

The piecewise constant control $\hat{u}(t)$ has the structure

$$\hat{u}(t)=u_1,\ t<T;\quad \hat{u}(t)=u^*,\ t\geq T, \qquad (18)$$

where u_1 is a constant control satisfying the restriction (6). For estimating the time instant T, we substitute (18) in the dynamics of the resource use (9)

$$m(t,\hat{u})=m_0 e^{\frac{b-\beta u_1}{1-\alpha}t},\ t<T;\quad m(t,\hat{u})=m_0 e^{\frac{b-\beta u_1}{1-\alpha}T}e^{-\frac{b}{\alpha}(t-T)},\ t\geq T, \qquad (19)$$

and find the cumulative resource use at the infinite time interval

$$\overline{M}=\int_0^{+\infty}m(t,u_1)dt=\frac{m_0(1-\alpha)}{b-\beta u_1}\left(e^{\frac{b-\beta u_1}{1-\alpha}T}-1\right)+\frac{m_0\alpha}{\beta}e^{\frac{b-\beta u_1}{1-\alpha}T}, \qquad (20)$$

Solving the equation (20) with respect to the time T, we estimate the switching time instant $T=T(u_1)$ of the form

$$T(u_1)=\begin{cases}\dfrac{1-\alpha}{b-\beta u_1}\ln\left(\dfrac{b\overline{M}}{\alpha m_0}\dfrac{\eta-u_1}{u^*-u_1}\right), & \beta u_1\neq b\\ \overline{M}/m_0-\alpha/b, & \beta u_1=b\end{cases},\ \eta:=\frac{1}{\beta}\left(b+\frac{m_0}{\overline{M}}(1-\alpha)\right). \qquad (21)$$

Noteworthy, there exists such a level η of control u_1 that $\lim_{u_1 \to \eta} T(u_1) = +\infty$, and for any $u_1 > \eta$, the switching time instant T does not exist. Hence, the condition (1) of the natural resources' exhaustibility is fulfilled if the constant control value u_1 does not exceed the level of η. According to the qualitative analysis of the Hamiltonian system (16), there exists the steady state satisfying (17). We use this fact to estimate the initial constant control u_1 by assuming that at the switching instant $T(u_1)$ the approximate solution $x_2(t, u_1)$ achieves the stationary level of x_2^*, i.e. $x_2(T(u_1), u_1) = x_2$. Using the formulae (1)-(4), (7), (10) and (17), we find the initial control u_1 numerically.

STABILIZED AND APPROXIMATE SOLUTIONS

Numerical experiments were conducted under the following values of model parameters (see [4,8]): $m_0=0.09847$, $M=1.81*10^6$, $u=0.12$, $a=64.34$, $b=0.069$, $\alpha=0.4091$, $\beta=1.523$, $p_0=100$. By the formulae (17), we find the steady state $x^*=(0.14, 0.03, 6.21, -2.22)^T$, and the steady state control value $u^*=0.11$. Eigenvalues of the Jacobian evaluated at the steady state of the Hamiltonian system (16) evidence the saddle character of the steady state, since eigenvalues are real numbers, and two of them are negative $\lambda_1=-1.832$, $\lambda_2=-0.011$, and two others are positive $\lambda_3=0.203$, $\lambda_4=2.0$. As is shown in [3], the stabilized solutions, constructed by the algorithm provided in [7], approximate the optimal trajectories with the quadratic precision around the steady state. Therefore, we compare an approximate solution described in the paper with the stabilized trajectories at a vicinity of the steady state. Figures 2 (a), (b) illustrate phase trajectories $x_1(t)$ and $x_2(t)$ constructed by the algorithm developed in [7] and in the present paper. The trajectories have similar behavior. Approximation accuracy is not sufficient, especially for the first phase component $x_1(t)$. Therefore, in the future work, it is reasonable to construct a piecewise constant control with several intermediate control regimes.

ACKNOWLEDGMENTS

The second author Anastasiia A. Usova is supported by the RFBR project No.18-01-00264a.

REFERENCES

[1] Aseev S.M., Kryazhimskiy A.V. (2007). The Pontryagin Maximum Principle and Optimal Economic Growth Problems. Proceedings of the Steklov Institute of Mathematics. Pleiades Publishing. Vol. 257.
[2] Bagno A., Tarasyev A.A., Tarasyev A.M. (2017). Value function in economic growth model. AIP Conference Proceedings. 1906, 070009.
[3] Grossman G.M., Helpman E. (1991). Innovation and Growth in the Global Economy. MIT. Press. Cambridge. Massachusetts.
[4] Hartman Ph. (1964). Ordinary Differential Equations. J. Wiley & Sons. NY.
[5] Pontryagin L.S., Boltyanskii V.G., Gamkrelidze R.V., Mishchenko E.F. (1962). The Mathematical Theory of Optimal Processes. Interscience. NY.
[6] Shorikov A.F., Sudakova A.E., Agarkov G.A., Tarasyev A.A. (2018). A deterministic dynamic model of optimizing university training structure. IFAC PapersOnLine. Vol. 51-2. pp. 121–125.
[7] Solow R.M. (1970). Growth Theory: An Exposition. NY, Oxford Univ. Press.
[8] Tarasyev A.A., Agarkov G.A. (2018). Dynamic modeling of scientific migration in terms of proportional economic growth. AIP Conference Proceedings. 2040, 050006.
[9] Tarasyev A. M., Usova A.A. (2012). Stabilizing the Hamiltonian System for Constructing Optimal Trajectories. Proceedings of the Steklov Institute of Mathematics. Vol. 277. pp. 248-265.
[10] Tarasyev A., Zhu B. (2012). Optimal Proportions in Growth Trends of Resource Productivity. IFAC-PapersOnline. 45(25). pp. 182-187.

Methods for Predicting the Production of Natural Resources

Alexander M. Tarasyev[1,2, a)], Julian A. Vasilev[3, b)], Victoria F. Turygina[2, c)], Svetlana V. Kravchuk[2, d)], Alyona E. Strelchuk[2, e)]

[1]*Krasovskii Institute of Mathematics and Mechanics UrB RAS, S. Kovalevskay, 16, Yekaterinburg, Russia, 620990*
[2]*Ural Federal University, Mira 19, Yekaterinburg, Russia, 620002*
[3]*Varna University of Economics, bul. "Knyaz Boris I-st " 77 9002, Varna, Bulgaria*

[a)]Corresponding author: tam@imm.uran.ru
[b)]vasilev@ue-varna.bg
[c)]v.f.volodina@urfu.ru
[d)]svetlana.kr.98@mail.ru
[e)]st-a-ed@yandex.ru

Abstract. Sverdlovsk region is the oldest mining region of Russia and is one of the largest in Russia in terms of explored reserves and forecast resources of various minerals. Therefore, the relevance has the ability to predict mining. In this article, two forecasting methods will be compared and recommendations on their use will be given.
Keywords: natural resources, mineral raw materials, statistical analysis, correlation analysis, regional economy, trend line method, correlation method, forecasting.

INTRODUCTION

One of the most important questions in the use of natural resources is analysis of data and elaboration of forecasting trends for the production of mineral resources. This article discusses several methods that solve such important problems for the entire mining system.

It should be noted that, at present, the mining waste is actually used in the production of building materials and only a small amount of waste is exploited for the production of the target products: gold, copper, zinc, chromium, due to the lack of technology.

The main methods investigated in the article are based on mathematical modeling in combination with correlation analysis and forecast with trend lines. These statistical studies are new and can make a significant contribution to the theory and practice of efficient use of natural resources on the regional level. The studied tools can also form the basis of the business trends of enterprises, thus facilitating the process of work planning and resources allocation.

The purpose of the article is to engage in a qualitative comparison of several selected methods for forecasting the use of natural resources in order to identify the most accurate of them and then implement it in the production processes.

DESCRIPTION OF THE METHODS

Trend Line Analysis Method

In this study, based on data for the period from point 0 to point 10, the forecast is established based on the trend line analysis using the MS Excel software graph. This tool is most often used to build a trend line [1-4].

Correlation method

Our study adopts the correlation analysis using the SPSS Analysis / Correlation / Two-dimensional tool. All variables are included into the correlation matrix. We assume that positive and negative correlations in the extraction of various ores are plausible [4].

Calculations and comparison of selected methods

To compare the methods and their accuracy, we use the data set, which is presented in Table 1. The data set is a summary table with information on the amount of mineral resources extracted for 10 (0-10) years in the Sverdlovsk region [5-7].

TABLE 1. Extraction of mineral raw materials in the Sverdlovsk region

	0	1	2	3	4	5	6	7	8	9	10
Iron	50449	52676	51885	58113	59161	53610	50746	55504	59891	62122	62112
Chromium	14	18	16	30	55	87	40	41	54	33	34
Bauxite	3342	3173	3072	3068	3054	2853	2942	2861	2980	2500	2500
Copper	49,7	52,8	96,4	72,2	65,8	71	74,6	84,7	86,3	75,3	75,3
Nickel	9,2	6,8	11,2	13,5	12,2	9,5	6,5	10,9	7,3	9,8	9,8
Gold	7,5	8,8	10	10,7	11,1	10	10,5	13,2	12,2	11,6	12,8

The result of the comparison of methods is given on the graph reflecting three lines, two of which are the predicted amount of raw materials in each year, and the third line is the real level of raw materials, which can be traced from relatively new data.

We consider iron ore mining as an example of calculations, since the Sverdlovsk region has significant reserves of this mineral, which consequently increases the demand for forecasting its production.

Using the first methodology and based on data for the period from point 0 to point 10, a forecast can be made as part of analysis of the trend line on the graph of MS Excel software.

To predict the iron ore production for years 11 and 12, it is necessary to use the following equation of the trend line function:

$$-10{,}608 * X \wedge 4 + 311{,}88 * X \wedge 3 - 2989{,}1 * X \wedge 2 + 11300 * X + 40768 \quad (1)$$

The value of X in the formula is replaced by point 12 and point 13 for 2014 and 2015, respectively.

Based on the results obtained, it is expected that the iron ore production in 2014 amounts to 64899 thousand tons, and in 2015 - 64735 thousand tons. It is necessary to take into account that this prediction lies in the confidence interval, the size of which is determined by Student's t-statistics.

Let us apply the second method. The correlation analysis is performed for the data in Table 2 using the MS Excel Data / Data Analysis / Correlation tool. All variables, except the variable "Year", are included in the correlation matrix.

TABLE 2. Correlation matrix of mineral resources extraction

	Iron	Chromium	Bauxite	Copper	Nickel	Gold
Iron	1,000					
Chromium	0,217	1,000				
Bauxite	-0,691	-0,295	1,000			
Copper	0,240	0,159	-0,400	1,000		
Nickel	0,313	-0,006	-0,031	0,204	1,000	
Gold	0,717	0,335	-0,726	0,649	0,201	1,000

The correlation between iron ore and gold is positive and close in value to one (0.717). This means that the degree of connection between the production volumes of these types of resources is quite high, and, consequently, the increase in iron production is associated with an increase in gold production. This can be explained by the fact that iron-containing ores also contain gold.

To predict the iron production, it is necessary to create a regression equation based on the correlation between gold and iron. The equation is made up of the Y and X values using the Data / Data Analysis / Regression tool. The resulting function is as follows:

$$35824{,}2 + 1876{,}7 * Z \quad (2)$$

Here, the variable Z is the value of the amount of gold production for a particular year.

The forecast for 2014 according to this formula gives the result 59798 thousand tons = 35824,2 + 1876,7 * 12,8.

The forecast for 2015 gives the result of 60195 thousand tons = 35824,2 + 1876,7 * 13,0.

COMPARISON OF TWO FORECASTING METHODS

For a visual representation of the advantages of a particular method of forecasting, for each of them the corresponding trend line is depicted on the graph.

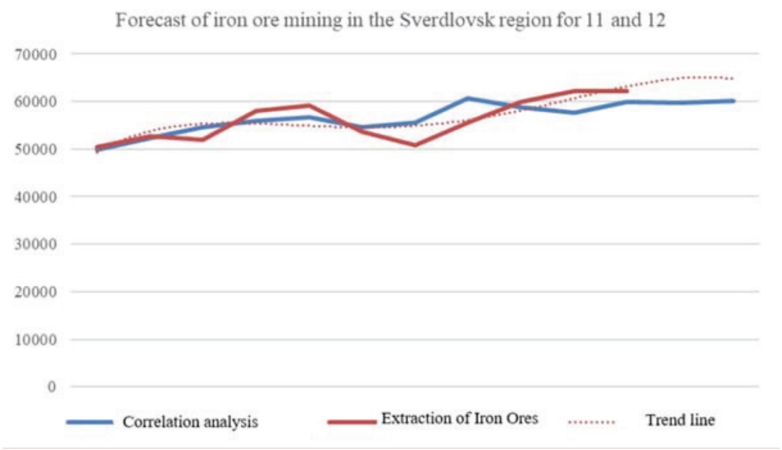

FIGURE 1. Linear graph of the iron production forecast.

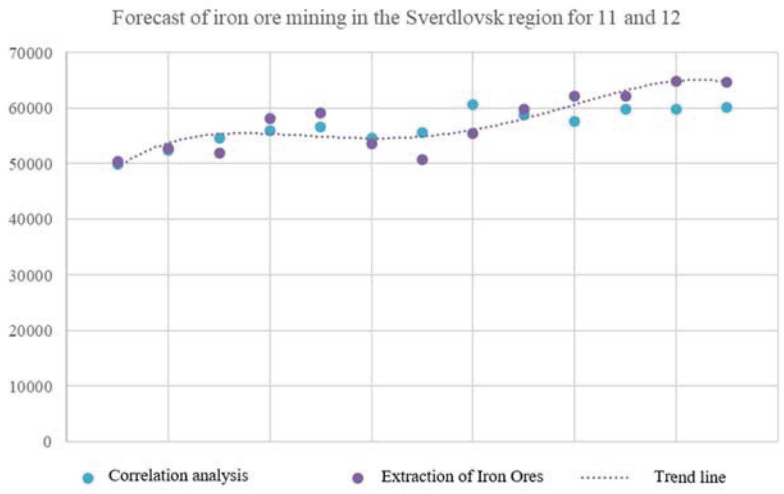

FIGURE 2. Point graph of the iron production forecast.

On the graph obtained, one can see that the trend line and the correlation line approximately coincide until the point 6. In the period from point 6 to point 8, the first method shows a smoother increase in iron ore production, while the correlation analysis yields a sharp jump from 55,530 thousand tons to 60,597 thousand tons. This phenomenon can be explained by the fact that the second method is based on the relationship between gold and iron mining, and during this period of time, there is an increase in the gold production from 10.5 thousand tons to 13.2 thousand tons, which leads to a sharp increase in the iron ore production. Similarly, the situation in the period from point 8 to point 10 can be explained.

As for the predicted values in the period 11-12, they are significantly different. The trend line shows a slight increase in production volumes from 62,112 thousand tons to 64,899 thousand tons at point 11, and then a slight drop to 64,735 thousand tons at point 12. This is due to the fact that the average value of the iron ore production for previous years is equal to about 56,024 thousand tons and indicators each year are gradually reduced to this value in order to balance the level of reserves of this resource in the region.

In addition, the correlation analysis shows for the forecast period values of 59 798 thousand tons for point 11 and 60 195 thousand tons for point 12. This is explained by a slight increase in the gold production during this time period.

After analyzing these graphs, one can say that a universal method of forecasting is the way to build a trend line, because the forecast relies only on previous indicators and does not depend on third-party factors.

The method of the correlation analysis for obtaining the accurate result requires additional information (in our case, the amount of the gold production for the forecast period). And also, a sufficiently high degree of correlation of the correlated features is needed. Therefore, the method of forecasting the output of the iron ore production depending on the gold production, considered in the article, is applicable only to the Sverdlovsk region, while for other regions and countries this indicator may differ significantly.

In conclusion, our comparison analysis demonstrates that both methods, one way or another, provide realistic trends in their calculations. For the clarity, we conduct this analysis on the same data, taking a small fragment from the whole analysis of forecasting the natural resources production.

Both considered methods are suitable for forecasting the exploitation of raw materials in various regions of Russia and other countries. However, there are some differences in the application of these methods, so it is advisable to use them carefully for particular problems.

The trend line analysis shows the specific scale of the resources extraction for a certain year in the future. In parallel, the correlation analysis characterizes only the dependence of the size of the production of one resource with respect to the production of another one, i.e. it demonstrates correlation of growing and decreasing trends in the output of both natural resources.

Therefore, the method for analyzing the trend line is more suitable for forecasting the resources extraction, while the correlation method is aimed mostly at increasing the efficiency of the extraction and the use of natural resources.

REFERENCES

[1] Atanasova, T., Kasheva, M., Sulova, S., Vasilev, J. "Analysis of the possible application of Data Mining, Text Mining and Web Mining in Business Intelligent Systems". MIPRO 2010 - 33rd International Convention on Information and Communication Technology, Electronics and Microelectronics, Proceedings, pp. 1294-1297.

[2] J. Vasilev, V.F. Turygina, A.I. Kosarev, Y.Y. Nazarova. "Mathematical Optimization in Environmental Economics. Algorithm of Gradient Projection Method". 16th International Multidisciplinary Scientific GeoConference SGEM 2016, Conference Proceedings, Book 5, Vol. 3 (2016), pp. 349-356.

[3] Alexander M. Tarasyev, Julian Vasilev, and Victoria F. Turygina. "Statistical analysis and forecasting of extraction and use of natural resources". AIP Conference Proceedings 2040, 050011 (2018).

[4] Tarasyev, A.M., Vasilev, J., and Turygina, V.F. "Quantitative analysis of raw materials mining of Sverdlovsk region in Russia". AIP Conference Proceedings 1738, 110009 (2016).

[5] On the state of the environment of the Sverdlovsk region in Russia 2015. State Report. Yekaterinburg. The Ministry of Natural Resources and Ecology of the Sverdlovsk Region.

[6] On the state of the environment of the Sverdlovsk region in Russia 2010. State Report. Yekaterinburg. The Ministry of Natural Resources and Ecology of the Sverdlovsk Region.

[7] On the state of the environment of the Sverdlovsk region in Russia 2013. State Report. Yekaterinburg. The Ministry of Natural Resources and Ecology of the Sverdlovsk Region.

Descriptive Statistics of Air Particulate Matter Size Distribution in Industrial City

Elena Baglaeva[1, 2, a)], Alexander Buevich[1, 2, b)], Alexander Sergeev[1, 2, c)], Andrey Shichkin[1, 2, d)], Irina Subbotina[2, e)]

[1]Ural Federal University, Mira str., 19, Ekaterinburg, RUSSIA 620002
[2]Institute of Industrial Ecology UB RAS, S. Kovalevskoy str., 20, Ekaterinburg, RUSSIA 620990

[a)]elenbaglaeva@gmail.com
[b)]bagalex3@gmail.com
[c)]Corresponding author: aleksandrpsergeev@gmail.com
[d)]and@ecko.uran.ru
[e)]iesub@mail.ru

Abstract. The mass concentration, size-distribution, height stratification and season variability of atmospheric particulate matter (PM) were researched in residential quarters of the industrial city in Ekaterinburg, Russia. The air dust samples were collected from March to May 2016. The particle size distribution in Ekaterinburg showed that most particles had diameters in the range of 0.5–2.5 μm. The particulate matter size distributions had dominant pattern with right tail and maximum was near 1 μm.

INTRODUCTION

The particulate matter (PM) is Europe's most problematic pollutants (WHO, 2016; Guerreiro et al, 2014) [1-3]. Urban air PM is a heterogeneous mix of various particles originating from the different sources: soot emissions from fuel combustion, organic compound, mineral particles from the road wear and the soil dust and other (Chung et al., 2008 (Alfaro-Moreno et al., 2002; Soukup and Becker, 2001)). The characteristics of urban air PM are changed with the season, weather conditions, the chemical processes in atmosphere and other (AQI, 2017; He) The deposition of PM in the respiratory system are described in ICRP Publication 66 (ICRP66, 1994), but health effects are depended of characteristics and origin of the particles [Amato et al., 2017; Rovelli et al., 2017; Lehtomäki et al., 2018; Pipal et al., 2014]. Monitoring of PM level are limited PM2.5 and/or PM10 in the cities [Krasnov]. The knowledge of detailed particulate matter size distributions is useful for understanding health effects and modelling of air dust pollution on a smaller scale and various parameters.

In this work the frequency particulate matter size distributions is built for residential quarters of industrial city (on the example of Ekaterinburg).

MATERIALS AND METHODS

Ekaterinburg is the fourth-largest city of Russia and industrial center located on the eastern side of the Ural Mountains (N56.5°, E60.4°). There is humid continental climate (Dfb) (Kottek et al., 2006). It is characterized by sharp variability in weather conditions, with well-marked seasons: 65–70 days of short summer with an average temperature at about +18°C and 180–190 days of winter temperatures below. Ekaterinburg is an important transport and logistic hub on the Trans-Siberian Railway, the large industrial center of the machinery, metal processing, and ferrous and non-ferrous metallurgy. The sampling area of PM monitoring is located on the lawns within a residential area and far from the highways in Ekaterinburg (Fig. 1).

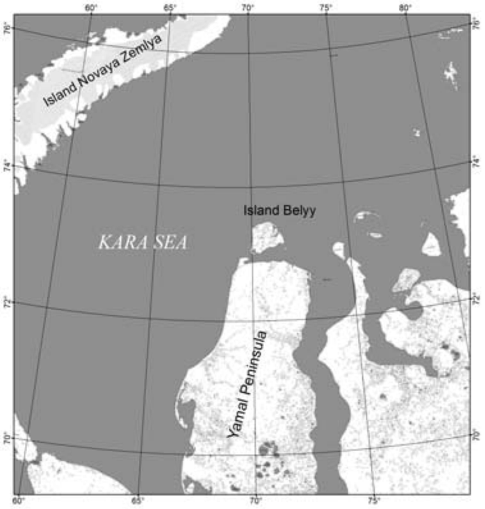

FIGURE 1. Sampling area location.

The mobile atmospheric dust sampling post with a height stratification designed to extract air samples for absorption filters AFA-VP-10 (diameter 4.5 cm) was used for atmospheric dust sampling. This device was constructed from the air pump with a volume flow rate up to 10 m3, a power source (the standard car battery capacity depending on the monitoring tasks from 40 to 90Ah), six gasometer with volume flow regulators and filter holders (alonges) on the different heights: 0.5 m, 1.0 m, 1.5 m, 2.0 m, 3.0 m and 4.0 m. Before sampling, the filters AFA-VP-10 were dried, weighed and placed in numbered envelopes. The volume pumped through the filter, the sampling time and the meteorological data were recorded after pumping. After sampling, the dirty filters were again dried, weighed, and the air dust weight concentration on the filter was given by (1):

$$C = (m_2 - m_1)/V_0, \tag{1}$$

where C - air dust concentration, mg/m^3, m_2 – dirty filter mass after pumping, mg; m_1 – net filter mass before pumping, mg; V_0 – pumping volume for the standard conditions as temperature of 20°C (293.15 K) and an absolute pressure of 1 atm (101.33 kPa), m^3.

The air particulate matter size distribution was determined by counting, the filters were examined under the microscope MBI-15 (Russia) with the calibration slide. Linear limit resolution I s near 0.25 µm, dust particles less than 2.5 µm are invisible. Experimentally it was determined five fields of vision are enough to build the dust particle size empiric distribution. The number of visible grains visually was counted by five fields of vision for each filter. The dust was distributed at 11 intervals: less than 1 µm, 1-2 µm, 2-3 µm, 3-4 µm, 4-5 µm, 5-6 µm, 6-7 µm, 7-8 µm, 8-9 µm, 9-10 µm, more than 10 µm. The number of dust particles was summed in each interval over the five fields of vision for every filter. The mean dust diameter was calculated (3) to compare the filters of different sites.

$$\bar{d} = (\textstyle\sum_{i=1}^{11} d_i \cdot n_i)/\sum_{i}^{11} n_i, \tag{2}$$

where $\bar{d}$ - mean dust diameter on the filter, µm; d_i – mean dust diameter in i-interval, µm (for example, for particle size is less than d_1 = 0.5 µm and for particle size is from 1 µm to 2 µm than d_2 = 1.5 µm); n_i – number of particles seen on the filter under the microscope in i-interval.

Mean dust diameter, standard deviation, median dust diameter, mode dust diameter and coefficient of variation were used for description of the dust particle size empiric distribution. The median and the mode were defined as midpoint of the correspond intervals.

RESULTS AND DISCUSSION

The sampling was covered three seasons in 2015. Season I was in March (Snow), II – in April (The snow melted, no grass, no foliage), III – in May (There are the grass and foliage). 180 samples were taken in 30 measurements in three seasons with stratification at altitudes of 0.5 m, 1.0 m, 1.5 m, 2.0 m, 3.0 m and 4.0 m.

The results of dust weight concentration determining the dust content were presented in Table 1.

TABLE 1. Results of determining the dust content in Ekaterinburg

Heights, m	I season		II season		III season	
	Number of filter count	Mean air dust concentration ± SD*, mg/m^3	Number of filter count	Mean air dust concentration ± SD, mg/m^3	Number of filter count	Mean air dust concentration ± SD, mg/m^3
4.0	10	0.05±0.02	11	0.15±0.07	9	0.07±0.02
3.0	10	0.06±0.03	11	0.16±0.08	9	0.08±0.03
2.0	10	0.05±0.02	11	0.16±0.08	9	0.08±0.02
1.5	10	0.05±0.02	11	0.16±0.08	9	0.08±0.02
1.0	10	0.04±0.02	11	0.12±0.06	9	0.05±0.02
0.5	10	0.05±0.02	11	0.17±0.08	9	0.09±0.02

*) SD - the standard deviation.

Analysis of dust weight concentration in residential quarters of Ekaterinburg showed the following. I season is the cleanest with the mean air dust concentration near 0.05 mg/m^3, which is caused by snow cover. II season is the dirtiest with the mean air dust concentration near 0.16 mg/m^3, which is associated with dusting surface without snow or grass cover. The highest dust concentrations were detected at 0.5 m and 3.0 m in each season. Above 3.0 m, the dust content apparently begins to decrease. The lowest concentrations were at height 1.0 m in each season. The feature requires additional studies.

Some descriptive statistics for the dust particle size distribution are shown in Table 2. Median dust diameter was 2.5 µm, in other words, more often particles are less than 2.5 µm.

TABLE 2. Descriptive statistics of dust diameter for the dust particle size distribution for I season in Ekaterinburg

Height, m	Mean ± SD, µm	Median ± RE*, µm	Mode ± RE*, µm	Coefficient of Variation
4.0	2.9±1.9	2.5±0.5	1.5±0.5	0.7
3.0	2.8±1.9	2.5±0.5	1.5±0.5	0.7
2.0	3.0±2.1	2.5±0.5	1.5±0.5	0.7
1.5	3.1±2.0	2.5±0.5	1.5±0.5	0.6
1.0	2.9±1.8	2.5±0.5	1.5±0.5	0.6
0.5	3.0±2.0	2.5±0.5	1.5±0.5	0.7

*) RE – Readability Error is 1/2 of the grating period of the instrument's measurement capability.

Totally 20 filters in I season were used to build air dust particle size distributions. Every filter was explained under a microscope. The number of the dust particles was summed within 11 intervals over five fields of vision. The average pattern of dust particle size distribution in March is presented at Fig. 2.

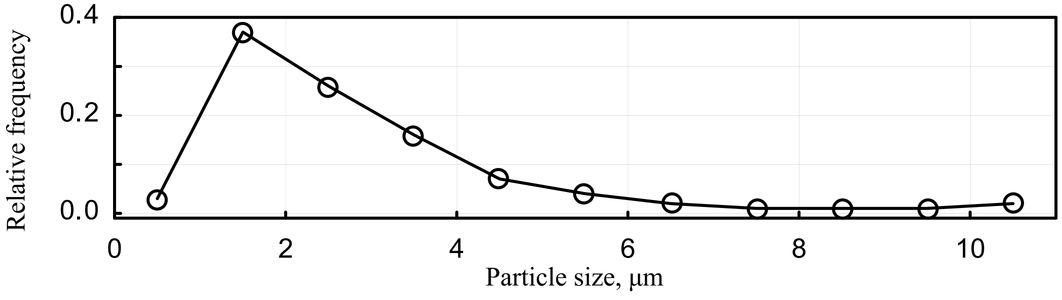

FIGURE 2. The air dust particle size distributions in March

The pattern had a heavy tail like to the dust size distribution for landlocked area [9]. For average dust particle size distribution in I season the mean dust diameter was 2.9 μm. PM2.5 comprises more than 65 % at the same time. The particles with a diameter larger than 10 μm were accounted for only 2 %.

CONCLUSION

In Ekaterinburg, 180 air dust samples were collected in one location at six different heights (from 0.5 m to 4 m) within three seasons. Mean air dust concentrations were calculated from 0.04 to 0.17 mg/m3 by various heights in different seasons. The mean dust diameters of the dust particles found on the filter was from 2.9 to 3.1 μm at all heights in I season. These detailed data may be useful in modeling the PM pollution of industrial cities for the objective of evaluating the effects in the environment and public health.

REFERENCES

[1] Amato, F., Bedogni, M., Padoan, E., Queroll, X., Ealo, M., Rivas, I. "Characterization of Road Dust Emissions in Milan: Impact of Vehicle Fleet Speed". Aerosol and Air Quality Research. 17, 2438-2449. doi: 10.4209/aaqr.2017.01.0017 (2017).

[2] WHO, 2016. Health risk assessment of air pollution general principles. Copenhagen. WHO Regional Office for Europe. http://www.euro.who.int/__data/assets/pdf_file/0006/298482/Health-risk-assessment-air-pollution-General-principles-en.pdf?ua=1.

[3] Pipal, A.S., Jan, R., Satsangi, P.G., Tiwari, S., Taneja, A. "Study of surface morphology, elemental composition and origin of atmospheric aerosols (PM2.5 and PM10) over Agra, India". Aerosol Air Qual. Res. 14, 1685-1700 (2014).

[4] EEA, 2013. Air Quality in Europe – 2013 Report European Environment Agency, Copenhagen. Report No 9/2013.

[5] Galloway, J.N., Thornton, J.D., Norton, S.A., Volchok, H.L., McLean, R.A. "Trace metals in atmospheric deposition: a review and assessment". Atmos. Environ. 16, 1677 - 1700 (1982).

[6] Mohanraj, R., Azeez, P.A., Priscilla, T., "Heavy metals in airborne particulate matter of urban Coimbatore". Arch. Environ. Contam. Toxicol. 47 (2), 162-167 (2004).

[7] Krasnov, H., Kloog, I., Friger, M., Katra, I., "The Spatio-Temporal Distribution of Particulate Matter during Natural Dust Episodes at an Urban Scale". PLoS ONE. 11 (8) e0160800. https://doi.org/10.1371/journal.pone.01608002016 (2016).

[8] He, J., Mao, H., Gong, S., Yu, Y., Wu, L., Liu, H., Chen, Y., Jing, B., Ren, P., Zou, Ch. "Investigation of Particulate Matter Regional Transport in Beijing Based on Numerical Simulation". Aerosol and Air Quality Research. 17, 1181-1189 (2017).

[9] Yue, W., Li, X., Liu, J., Li, Y., Yu, X., Deng, B., Wan, T., Zhang, G., Huang, Y., He, W., Hua, W., Shao, L., Li, W., Yang, Sh., "Characterization of PM2.5 in the ambient air of Shanghai city by analyzing individual particles". Sci. Total Environ. 368, 916-925 (2006).

Statistical Characteristics Calculation of the Natural Dust Size Distribution in the Air Surface Layer of Belyy Island

Elena Baglaeva[1, 2, a)], Alexander Buevich[1, 2, b)], Alexander Sergeev[1, 2, c)], Andrey Shichkin[1, 2, d)], Irina Subbotina[2, e)], Yuriy Markelov[2, f)], Pavel Petrov[3, g)]

[1]*Ural Federal University, Mira str., 19, Ekaterinburg, RUSSIA 620002*
[2]*Institute of Industrial Ecology UB RAS, S. Kovalevskoy str., 20, Ekaterinburg, RUSSIA 620990*
[3]*University of Economics, 77 Knyaz Boris I Blvd., Varna, Bulgaria 9002*

[a)]elenbaglaeva@gmail.com
[b)]bagalex3@gmail.com
[c)]Corresponding author: aleksandrpsergeev@gmail.com
[d)]and@ecko.uran.ru
[e)]iesub@mail.ru
[f)]markelovgm@gmail.com
[g)]petrov@ue-varna.bg

Abstract. To studying variability of atmospheric particulate matter (PM), dust content measurements in location without industrial air pollution are very useful. The first time the air dust content and the size distribution were studied at 73.1° North latitude. This research presents data of the mass concentration and size-distribution of PM in the surface layer of atmospheric air on the Arctic island Belyy, Russia. The data was collected in Belyy Island, Yamal Peninsula, Siberia, Russia, in July of the same year. The mean air dust concentration was lower instrument limit of detection. The particle size distributions had two dominant Land Breeze and Sea Breeze patterns associated with the wind direction.

INTRODUCTION

Air pollution of particulate matter (PM) is a problem for some industrial cities [1-3]. The health effects of PM are associated with the particle size, morphology, composition and their complex combination [4-6]. Most of studies are focused on PM2.5 and/or PM10 with legal air quality thresholds and limited to the cities with PM monitoring stations [7]. The composition of urban air PM can vary meteorological conditions, pollutant emissions, the chemical processes in atmosphere and the removal process [8]. The identification and quantification of the differences in PM (natural and anthropogenic) pollution levels on a smaller scale and different parameters may lead to a better understanding of the PM distribution and exposure.

The aim of this work is to get features of the frequency particle size distribution of the air dust in area free from any industrial activity.

MATERIALS AND METHODS

Measurements of air dust were made on Bely Island (Fig.1) near the Russian Hydrometeorological Station (N73.1°, E71.2°), YNAO, Russia in summer 2015. The island is located in the Kara Sea 5-10 km north of the Yamal Peninsula (Fig.1). Bely Its area is over 1900 km^2. It is covered by tundra, but some dwarf shrubs also grow on this island. Bely is free from any modern settlements and industrial activity.

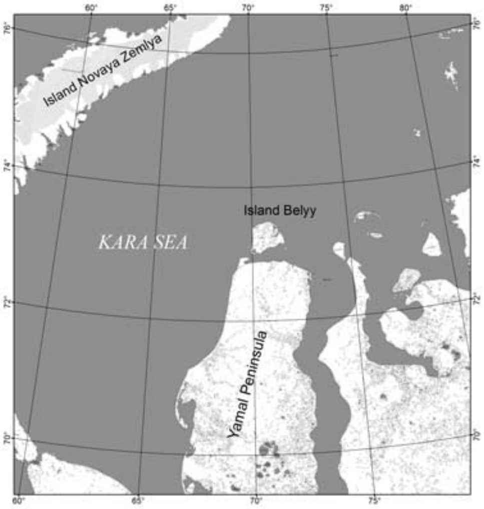

FIGURE 1. Sampling area location

The atmospheric dust sampling post was used to extract air samples on absorption devices (filters AFA-VP-10 with diameter 4.5 cm). AFA-VP-10 may applied to estimate the weight concentration of dust in a gaseous medium at a temperature from -200°C to 60°C from perchlorovinyl fiber filter material. Before sampling, the filters were dried, weighed and placed in numbered envelopes. Prior to the start of the measurement, the filters were re-weighed to eliminate the influence of the humidity in the filter holders, registered meteorological data and inflated air. After pumping, the volume pumped through the filter, the sampling time, and the meteorological data were recorded. After sampling, the filters were again dried, weighed, and the mass of the settled dust was calculated.

The post consists of the air pump with the volume flow rate up to 10 m^3, the power source (the standard car battery capacity depending on the monitoring tasks from 40 to 90Ah), gasometer with the volume flow regulators and the filter holder (alonge). The alonge was on the heights 1.5 m.

The air dust weight concentration on the filter was determined by (1):

$$C = (m_2 - m_1)/V_0, \tag{1}$$

where C - air dust concentration, mg/m^3, m_2 – dirty filter mass after pumping, mg; m_1 – net filter mass before pumping, mg; V_0 – pumping volume for the standard conditions as temperature of 20°C (293.15 K) and an absolute pressure of 1 atm (101.33 kPa), m^3.

The air particulate matter size distribution was determined by counting, the filters were examined under the microscope MBI-15 (Russia) with the calibration slide. Linear limit resolution is near 0.25 μm, dust particles less than 2.5 μm are invisible. On the filter, five fields of vision were selected and the number of visible grains visually was counted. The dust was distributed at 11 intervals: less than 1 μm, 1-2 μm, 2-3 μm, 3-4 μm, 4-5 μm, 5-6 μm, 6-7 μm, 7-8 μm, 8-9 μm, 9-10 μm, more than 10 μm. The number of dust particles was summed in each interval over the five fields of vision for every filter.

The mean dust diameter was calculated (3) to compare the filters of different sites.

$$\bar{d} = (\sum_{i=1}^{11} d_i \cdot n_i)/\sum_{i}^{11} n_i, \tag{2}$$

where $\bar{d}$ - mean dust diameter on the filter, μm; d_i – mean dust diameter in i-interval, μm (for example, for particle size is less than d_1 = 0.5 μm and for particle size is from 1 μm to 2 μm than d_2 = 1.5 μm); n_i – number of particles seen on the filter under the microscope in i-interval.

The descriptive statistics (mean dust diameter, standard deviation, median dust diameter, mode dust diameter, coefficient of variation) were used for the dust particle size empiric distribution. The median and the mode were defined as midpoint of the correspond intervals.

RESULTS AND DISCUSSION

11 air dust samples were collected from 16 to 29 July, 2015. The snow has melted on island. The temperature was from 4 to 15°C, the wind regime was highly unstable, north-northeast and northeast-east winds were dominant.

Table 1 presents the results of dust weight concentration determining the dust content and some descriptive statistics for the dust particle size distribution.

TABLE 1. Results of determining the dust content

Sampling Site	Number of filter count	Mean air dust concentration, mg/m³	Mean dust diameter, µm	Standard Deviation, µm	Median dust diameter, µm	Mode dust diameter, µm	Coefficient of Variation
Bely Island (Sea Breeze)	5	< LOD*)	2.01	2.22	1.5±0.5	0.5±0.5	1.11
Bely Island (Land Breeze)	6	< LOD*)	4.71	3.26	3.5±0.5	1.5±0.5	0.69
Bely Island (All**))	11	< LOD*)	3.38	3.11	2.5±0.5	0.5±0.5	0.92

*) Mean air dust concentration is lower instrument limit of detection (LOD). LOD of the weigh scales is 0.5 mg.

**) Pattern "All" corresponds calm wind conditions.

The mean air dust concentration on filters was lower instrument limit of detection (LOD is 0.5 mg). The filters were not completely white. The dust particles were visible through the microscope. Belyy island is "clean" area without human activity.

Totally 11 filters were viewed to build dust particle size distribution. Two pattern of dust particle size distribution is detected: Sea and Land breezes (Fig. 2). The Land breeze pattern had a heavy tail with high relative frequency of the particles bigger than 10 µm. It can be explained by the wind transfer of the coarse particles from the land. The Sea Breeze pattern was with a significant fraction of the particles with a diameter less than 1 µm. The Sea Breeze brings more fine particles. These patterns can be associated with the wind regime. Pattern "All" noted in Table 1 is averaging by the total sampling set. These conditions correspond to calm and are never realized on Bely Island.

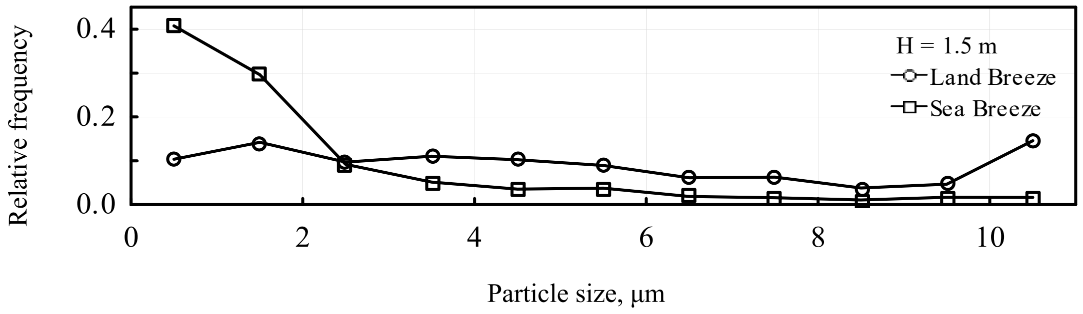

FIGURE 2. The air dust particle size distributions on Bely Island.

The obtained Land Breeze pattern (Fig. 2) was similar to the dust size distribution for landlocked area [9]. Mode dust diameter for island was 0.5 µm, in other words, more often particles are less than 1 µm.

CONCLUSION

The air dust particle size measurements were first carried out depending on the wind direction near 73.1° north latitude in the almost complete absence of the human activity. The air particle size distributions were built for this "clean" territory. The obtained data may be useful in modeling the PM pollution of industrial cities.

REFERENCES

[1] Amato, F., Bedogni, M., Padoan, E., Queroll, X., Ealo, M., Rivas, I. "Characterization of Road Dust Emissions in Milan: Impact of Vehicle Fleet Speed". Aerosol and Air Quality Research. 17, 2438-2449. doi: 10.4209/aaqr.2017.01.0017 (2017).

[2] WHO, 2016. Health risk assessment of air pollution general principles. Copenhagen. WHO Regional Office for Europe. http://www.euro.who.int/__data/assets/pdf_file/0006/298482/Health-risk-assessment-air-pollution-General-principles-en.pdf?ua=1

[3] Pipal, A.S., Jan, R., Satsangi, P.G., Tiwari, S., Taneja, A. "Study of surface morphology, elemental composition and origin of atmospheric aerosols (PM2.5 and PM10) over Agra", India. Aerosol Air Qual. Res. 14, 1685-1700 (2014).

[4] EEA, 2013. Air Quality in Europe – 2013 Report European Environment Agency, Copenhagen. Report No 9/2013.

[5] Galloway, J.N., Thornton, J.D., Norton, S.A., Volchok, H.L., McLean, R.A. "Trace metals in atmospheric deposition: a review and assessment". Atmos. Environ. 16, 1677-1700 (1982).

[6] Mohanraj, R., Azeez, P.A., Priscilla, T., Heavy metals in airborne particulate matter of urban Coimbatore. Arch. Environ. Contam. Toxicol. 47 (2), 162-167 (2004).

[7] Krasnov, H., Kloog, I., Friger, M., Katra, I. "The Spatio-Temporal Distribution of Particulate Matter during Natural Dust Episodes at an Urban Scale". PLoS ONE. 11 (8). e0160800. https://doi.org/10.1371/journal.pone.01608002016.

[8] He, J., Mao, H., Gong, S., Yu, Y., Wu, L., Liu, H., Chen, Y., Jing, B., Ren, P., Zou, Ch. "Investigation of Particulate Matter Regional Transport in Beijing Based on Numerical Simulation". Aerosol and Air Quality Research. 17, 1181–1189 (2017).

[9] Yue, W., Li, X., Liu, J., Li, Y., Yu, X., Deng, B., Wan, T., Zhang, G., Huang, Y., He, W., Hua, W., Shao, L., Li, W., Yang, Sh. "Characterization of PM2.5 in the ambient air of Shanghai city by analyzing individual particles". Sci. Total Environ. 368, 916–925. 2006.

Using Autoregressive Neural Network with External Input for Calculation of Expected Carbon Dioxide Surface Concentration for Different Time Intervals

Alexander Sergeev[1, 2, a)], Elena Baglaeva[1, 2, b)], Andrey Shichkin[1, 2, c)], Alexander Buevich[1, 2, d)], Anna Rakhmatova[1, 2, e)], Alexandra Kosachenko[1, f)], Anastasia Moskaleva[1, g)], Marina Sergeeva[2, h)]

[1]Ural Federal University, Mira str., 19, Ekaterinburg, RUSSIA 620002
[2]Institute of Industrial Ecology UB RAS, S. Kovalevskoy str., 20, Ekaterinburg, RUSSIA 620990

[a)]Corresponding author: aleksandrpsergeev@gmail.com
[b)]elenbaglaeva@gmail.com
[c)]and@ecko.uran.ru
[d)]bagalex3@gmail.com
[e)]anya_rahmatova@mail.ru
[f)]alleshch7@gmail.com
[g)]amoskalyova03@gmail.com
[h)]marin@ecko.uran.ru

Abstract. The results of the prediction of a model based on an artificial neural network were compared to predict the concentration of carbon dioxide (CO_2) in the surface layer of the atmosphere for different time intervals. Measurements were taken on the Arctic island of Belyy, Russia. For comparison, three time intervals were used, which differed in the dependence of carbon dioxide concentration on the time of day. A non-linear autoregressive neural network with external input (NARX) was used. The model based on NARX successfully coped with the prediction. The smallest error was for the time intervals with a strong dependence of CO2 concentration on the time of day.

INTRODUCTION

In various areas of knowledge, time series research is an important task. This includes research in the field of ecology and, in particular, climate change [1-5]. Of great importance is the identification of patterns of the changes in the content of the greenhouse gases. This is especially true for the Arctic regions of the planet [6, 7].

In our study, the change in carbon dioxide content in the surface layer of the atmosphere is predicted for three different periods. We use the approach based on the ANN, which had well proven itself in many previous works [7-18].

MATERIALS AND METHODS

Measurements of the carbon dioxide were made on the Arctic Island, Belyy, YNAO, Russia. (Fig.1). Concentrations of greenhouse gases were measured by a cavity ring-down spectrometer Picarro G2401.

The time series consisted of hourly measurements of carbon dioxide concentrations in the surface layer of atmospheric air. In total, three time intervals of 168 hours each were selected.

FIGURE 1. Place of measurements (Google Earth)

The first (I) - the dependence of the CO_2 on the time of day was absent.

The second (II) - had the dependence of the CO_2 content on the time of day (during the day CO_2 concentration is higher than at night), the average carbon dioxide concentration was grown within the selected interval.

The third (III) - had the dependence of the CO_2 content on the time of day (during the day CO_2 concentrations are higher than at night), the average carbon dioxide concentration was about the same within the selected interval.

Each interval was divided into two subsets. The first one with a duration of 144 hours was used for training, the second one, with a duration of 24 hours, was used only for the forecasting.

For comparison, the recurrent dynamic multi-level feedback network NARX was used. The number of neurons in the hidden layer in NARX was selected using the minimum mean square error (RMSE). The number of neurons ranged from 5 to 25. Each network was trained 500 times. Then the best of them was selected.

Indices RMSE (1) and a root mean squared relative error (RMSRE) (2) was used to verified the predictive accuracy.

$$RMSE = \sqrt{\frac{\sum_{i=1}^{n}(z_{mod}(x_i) - z(x_i))^2}{n}} \quad (1)$$

$$RMSRE = \sqrt{\frac{1}{n}\sum_{i=1}^{n}\left(\frac{z_{mod}(x_i) - z(x_i)}{x_i}\right)^2} \quad (2)$$

where $z_{mod}(x_i)$ is a predicted concentration, $z(x_i)$ is a measured concentration, and n is a number of points.

RESULTS

The Levenberg-Marquardt training algorithm was used. The final neuron number in the hidden layer was 20. Table 1 shows that the forecast errors for all intervals are small. The most accurate forecast for all indicators was for the III interval (**in bold**). Figure 2 shows the forecast results for all intervals.

TABLE 1. Accuracy assessment indices of the CO_2 concentration for the different time intervals

Interval	RMSE, ppm	RMSRE
Training interval		
I	1.00	0.003
II	0.54	0.001
III	**0.32**	**0.0008**
Test interval		
I	2.15	0.006
II	1.11	0.003
III	**0.90**	**0.002**

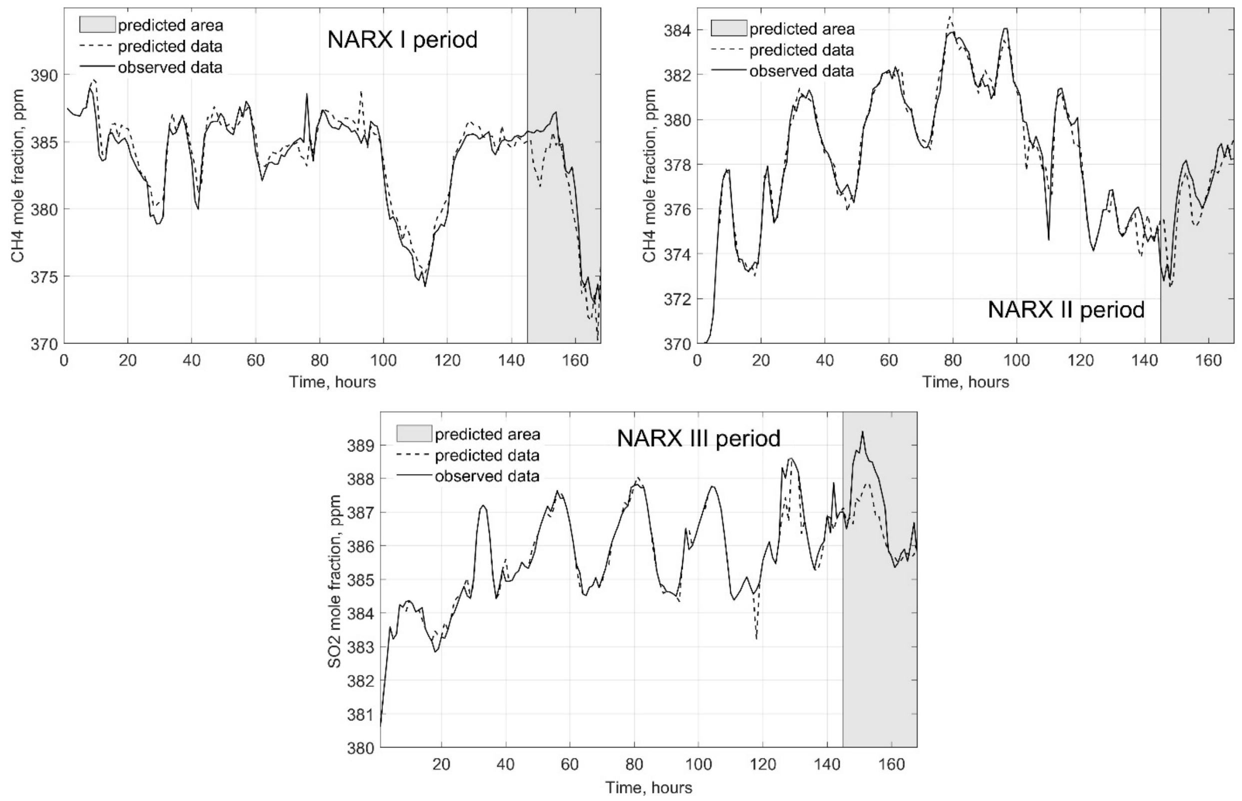

FIGURE 2. Comparison of the forecast results for different intervals.

CONCLUSION

Based on hourly measurements, a forecast was made of a change in CO2 concentration in the atmospheric surface layer for three time intervals. Within the selected time intervals, there was a different degree of dependence of the CO2 content on the time of day, as well as different dynamics of changes in the average gas concentration. ANN type NARX showed an acceptable result for all intervals. The most accurate was the prognosis for the II interval with the most pronounced dependence between the time of day and the concentration of CO2.

ACKNOWLEDGMENTS

The work is supported by the project of the Ural Branch of Russian Academy of Sciences No. 18-9-2-25. The analyzed data were obtained using the equipment of "Collective Use Center of Arctic Environmental Research of IIE UB RAS".

REFERENCES

[1] M. Ardalani-Farsa and S. Zolfaghari, "Chaotic time series prediction with residual analysis method using hybrid Elman–NARX neural networks". Neurocomputing, 73, 2540–2553 (2010).
[2] A.V. Dmitriev, "Time series prediction of morbidity using artificial neural networks". Biomedical Engineering, 47, 1, 43–45 (2013).
[3] J.M. Jr. Menezes and G.A. Barreto, "Long-term time series prediction with the NARX network: An empirical evaluation". Neurocomputing, 71, 3335–3343 (2008).
[4] E. Pisoni, M. Farina, C. Carnevale and L. Piroddi, "Forecasting peak air pollution levels using NARX models". Engineering Applications of Artificial Intelligence, 22, 593–602 (2009).

[5] G. Zhang, "Time series forecasting using a hybrid ARIMA and neural network model". Neurocomputing 5, 159–175 (2003).
[6] C. Nullis, *Provisional WMO Statement on the Status of the Global Climate in 2016* (World Meteorological Organization, 2016).
[7] M.C. Serreze and R.G. Barry, "Processes and impacts of Arctic amplification: A research synthesis". Global and Planetary Change 77, 85–96 (2011).
[8] G. Dimitrov, G. Panayotova, I. Garvanov, O. Bychkov, P. Petrov and A. Angelov, "Performance analysis of the method for social search of information in university information systems", in 3rd International Conference on Artificial Intelligence and Pattern Recognition (AIPR), (Lodz, Poland, IEEE, 2016), pp. 149-153.
[9] A. Erdil and E. Arcaklioglu, "The prediction of meteorological variables using artificial neural network". Neural Computing & Application, 22, 1677–1683 (2013).
[10] K. Mohanty and T. J. Majumdar, "Using artificial neural networks for synthetic surface fitting and the classification of remotely sensed data". International Journal of Applied Earth Observation and Geoinformation, 1(1), 78–84 (1999).
[11] G. Panayotova, G. Dimitrov, P. Petrov and O. Bychkov, "Modeling and data processing of information systems", in 3rd International Conference on Artificial Intelligence and Pattern Recognition (AIPR), (Lodz, Poland, IEEE, 2016), pp. 154-158.
[12] Z. Polkowski, J. Vasilev, D. Zajac and A. L. Florina, "A content analysis of existing educational portals for teaching data warehouse and business intelligence", Proceedings of the 8th International Conference on Electronics, Computers and Artificial Intelligence, ECAI 2016, 7861146 (2017), pp. 420-437.
[13] A. Russo, F. Raischel and P. Lind, "Air quality prediction using optimal neural networks with stochastic variables". Atmos. Environ., 79, 822–830 (2013).
[14] A.P. Sergeev, A.G. Buevich, E.M. Baglaeva and A.V. Shichkin, "Combining spatial autocorrelation with machine learning increases prediction accuracy of soil heavy metals", Catena 174, 425–435 (2019).
[15] S. Stojadinovic, "Prediction of fly rock launch velocity using artificial neural networks". Neural Computing & Application 27, 515–524 (2016).
[16] D.A. Tarasov, A.G. Buevich, A.P. Sergeev and A.V. Shichkin, "High Variation Topsoil Pollution Forecasting in the Russian Subarctic: Using Artificial Neural Networks Combined with Residual Kriging", Applied Geochemistry 88(B), 188-197, (2018).
[17] J. Vasilev, V.F. Turygina, A.I. Kosarev and Y.Y. Nazarova, "Mathematical optimization in environmental economics. Algorithm of gradient projection method", in International Multidisciplinary Scientific GeoConference Surveying Geology and Mining Ecology Management, SGEM (2016), pp. 349-356.
[18] Q. Zhou, H. Jiang, J. Wang and J. Zhou, "A hybrid model for PM2.5 forecasting based on ensemble empirical mode decomposition and a general regression neural network". Sci. Total Environ., 496, 264–274 (2014).

Application of Random Forest Algorithm to Predict the Average Issued Amounts In ATMs

T.A. Malysheva[1, a)], A.A. Panachev[1, b)], M.A. Medvedeva[1, c)], E.I. Kazakova[2, d)]

[1]*Ural Federal University, Mira 19, Yekaterinburg, Russia, 620002*
[2]*Department of Economic Cybernetics, Donetsk National Technical University, Artema Street 131, Ukraine, 83015*

[a)]T.A.Malysheva@yandex.ru
[b)]panachev1@mail.ru
[c)]Corresponding author: marmed55@yandex.ru
[d)]kazakova_donetsk@mail.ru

Abstract. The article deals with the problem of predicting changes in the average dispensed amounts, which is the important factor not only for planning the optimal route scheme for the Bank's cash logistics units, but also for ensuring uninterrupted ATM operation. It is proposed to use the Random Forest algorithm to analyze the data, build and select the best model. The best developed model predicts the amount of the average daily cash withdrawals with a pretty high probability of 79.8%. Based on the results obtained it is concluded that the model built on the basis of a Random Forest algorithm (Random Forest Regressor) can act as an efficient tool that improves the quality of logistics of cash in ATMs.
Keywords: Prediction, machine learning, random forest, regression, ATM.

INTRODUCTION

The problem of forecasting the dynamics of the average daily amount of cash withdrawal from ATMs is particularly relevant today, since the regular lack of cash in ATMs indicates a low quality of services provided and can form a judgment about the Bank's unreliability. Thus, timely encashment of ATMs directly affects the quality of the services provided by the Bank.

In a market economy, the purpose of operating a commercial Bank is to make a profit. To maximize profits, it is necessary to optimize costs, including cash logistics expenses.

In order to improve the quality of services offered to bank customers, it is necessary both to increase the number of ATMs availability to the public and to optimize their working mode. And on the part of the bank itself, the problem lies in timely cash logistics of ATMs, as well as determination of the minimum allowable cash balance in ATMs [1, 2].

The optimal cash logistics plan is based on the parity of the amount loaded and the period of encashment. If the funds are overloaded, the Bank will incur additional alternative costs due to diverted funds. At the same time it is necessary to choose the optimal cash logistics period and minimize its cost.

The main problems of predicting the average daily amount of cash dispensed by ATMs are:

1. Isolation of ATMs from the Bank's network infrastructure;
2. Encashment finds out the availability of cash in the ATMs upon arrival.

Thus, often the routing scheme of the cash logistics units is not optimal, since encashments are not necessary at this time.

Currently, this problem is solved by statistical analysis of cash flow in ATMs, identifying regularity of expenditure. There are also automated management systems that optimize the process of managing cash logistics and funding.

The main algorithms for solving regression problems are Decision tree; Random forest; Gradient boosting; Multiple linear regression [3-5], and they are widely used in different spheres [6-9]:

$$y = \beta_0 + \beta_1 x_1 + \beta_2 x_2 + \cdots + \beta_m x_m + \varepsilon \quad (1)$$

where y - is the target variable,

m - is the number of considered variables,

$x_1, x_2, \ldots, x_m$ - are independent variables,

$\beta_1, \beta_2, \ldots, \beta_m$ – are coefficients for dependent variables, calculated by the least squares method,

β_0 – is free coefficient of the model,

ε – is random model error.

Within the framework of this research, it was decided to use the Random Forest Regressor algorithm to analyze the data to build and select the best model.

The purpose of this research is to select such a model that will accurately predict changes in the average daily amount issued, optimizing the route scheme of the Bank's cash logistic units. It will increase uninterrupted operation of ATMs, eliminate the problem of cash availability, and minimize the Bank's expenses for cash logistics.

METHODS

For the practical implementation of the task were used the programming language Python 3, the Scikit-Learn and Pandas libraries [10, 11].

In the course of the study the search for optimal values of model parameters was carried out by using the grid search method GridSearchCV (Scikit-Learn library), which finds the most optimal parameters for the model.

The following parameters were considered [11]:

- The maximum depth of the tree (max_depth);
- The number of features to consider when looking for the best split (max_features);
- The minimum number of samples required to split an internal node (min_samples_split);
- The minimum number of samples required to be at a leaf node (min_samples_leaf);
- The number of trees in the forest (n_estimators).

MODEL BUILDING

Training and testing ATM data sets were used to predict the dynamics of the average daily amount of cash withdrawal from ATMs, which contain such features as:

- Dispenser status; Money counting by spray-dispenser;
- Card reader status; Finishing payment preparation on the payment server (quantity);
- Card capture event; Check print event (quantity); Logical error of the client session (quantity);
- Type of transaction; Codes of authorization requests; and etc.

As a result of feature engineering, the original data was converted to 790 features.

The following data sets were used to build the model:

- training data set consisted of 6285 records;
- testing data set consisted of 351 records.

DATA PROCESSING

To assess the quality of the models, the following metrics were selected:

1. The mean square error (MSE) was chosen as the loss function.
   MSE error is described as follows:

$$MSE = \frac{\sum_{i=1}^{n}(y_i - \hat{y}_i)^2}{n} \quad (2)$$

   where y_i- is the observed value,
   $\hat{y}_i$- is corresponding predicted value,
   n - is the number of observations.

2. As a metric for prediction quality was chosen the coefficient of determination (R2):

$$R^2 = 1 - \frac{\sum_{i=1}^{n}(y_i - \hat{y}_i)^2}{\sum_{i=1}^{n}(y_i - \bar{y})^2} \quad (3)$$

   where y_i- is the observed value,
   $\hat{y}_i$- is corresponding predicted value,

$\bar{y}$ - is arithmetic average of the predicted values,

n - is the number of observations.

Table 1 presents the simulation results.

TABLE 1. The effect of algorithms on the model's predictive accuracy.

Algorithm	R^2 for training dataset	R^2 for testing dataset	MSE
Random Forest Regressor (without selection of parameters)	0.971	0.706	11359912707
Random Forest Regressor (selection of parameters using GridSearchCV)	0.968	0.798	7808370263

Thus, the model of the Random Forest Regressor with selected parameters using the grid search (GridSearchCV) has the best predictive abilities.

The considered variations of the model parameters values constructed by using the Random Forest Regressor algorithm and optimal model parameters values found with the using the grid search are presented in Table 2.

TABLE 2. Search for optimal model parameters values by using the GridSearchCV method.

Model Parameters	Considered parameter values	Optimal value
The maximum depth of the tree	20, 40, 60, 80, 100	60
The number of features to consider when looking for the best split	auto, sqrt, log	auto
The minimum number of samples required to split an internal node	2, 5	5
The minimum number of samples required to be at a leaf node	1, 4	4
The number of trees in the forest	10, 30, 60, 90	90

The Random Forest algorithm is a set of decisive trees. The visualized fragment of the decision tree Random Forest Regressor t is shown in Fig. 1.

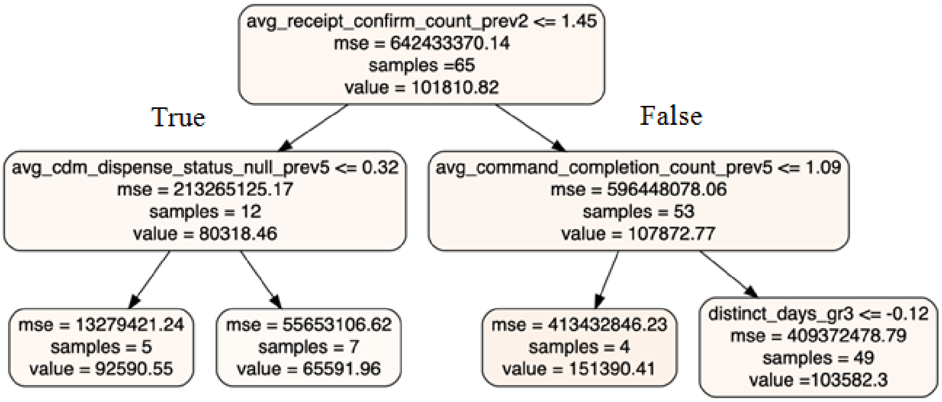

FIGURE 1. Fragment of the decision tree Random Forest Regressor.

The tree is built from top to bottom, from more significant parameters to less significant ones. In each block there is a value of its splitting condition indicated at the end of the first line. Each level also indicates: splitting criteria (the average square of the error - MSE) and the number of objects in the leaf (samples). The goal of the tree is to get the final answer (value). In the regression task solved by using the Random Forest Regressor algorithm, all final values of trees are averaged.

The obtained correlation between actual and predicted values is presented in Fig. 2.

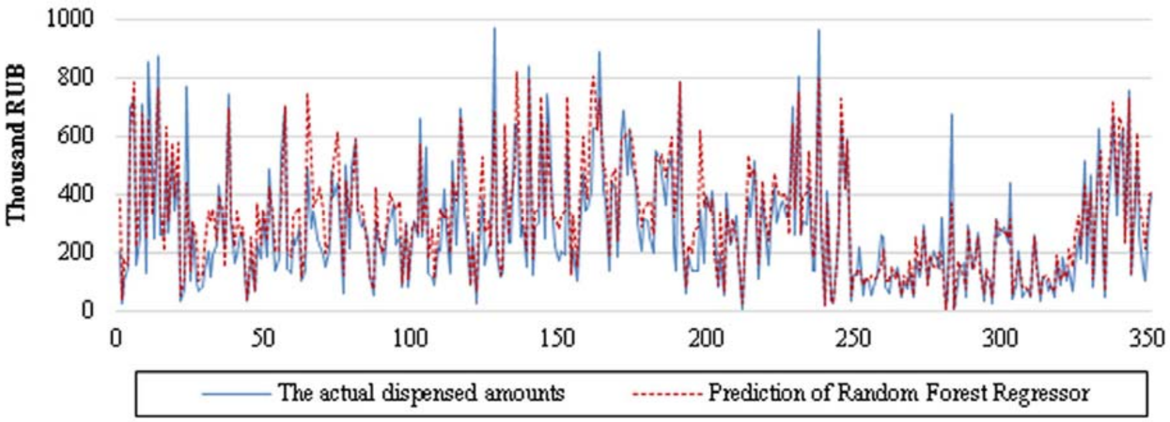

FIGURE 2. Correlation between the actual daily average cash withdrawal amount in ATMs and predicted by the Random Forest Regression model.

Usage of this model made it possible to achieve the indicator R^2 in 0.968 and 0.798 for the training and testing samples, respectively. Thus, the model with the best parameters predicts the amount of the average daily cash withdrawals by 79.8%. The obtained result is a threshold, being just below the 80% level. Nevertheless, the result of this work shows that we can predict the amount of the average daily cash withdrawal with a high degree of probability. Based on the final result, we can also conclude that the model built on the basis of a Random Forest algorithm (Random Forest Regressor) can act as a tool that improving the quality of logistics of cash in ATMs.

REFERENCES

[1] T.S. Vanina, "Encashment management problems," in *Kazan Science, No. 5,* ("Kazan Publishing House", Kazan, 2010), pp. 34–39.

[2] T.S. Vanina, "Optimization of the encashment service routing and determination of the optimal cash balance in ATMs and cash desks of the bank," in *Kazan Science, No. 2,* ("Kazan Publishing House", Kazan, 2010), pp. 88–91.

[3] S.P. Chistyakov, "Random Forests: Overview," in *Proceedings of the KarRC of RAS. No. 1*, (2013), available at https://cyberleninka.ru/article/n/sluchaynye-lesa-obzor (Date of access: 10.01.2019).

[4] Andreas C. Müller, Sarah Guido, *Introduction to machine learning with Python* (O'Reilly Media, USA, 2016).

[5] V.V. Voronin, A.V. Mikheev, N. G. Yarushkina, K.V. Svyatov, *Theory and practice of machine learning: a tutorial* (Ulyanovsk State Technical University, Ulyanovsk, 2017).

[6] S.M. Borodachev and M.A. Medvedev, "Optimization of the bank's operating portfolio", AIP Conference Proceedings 1738, 110012 (2016).

[7] Mujahed A. Saif, Alexander N. Medvedev, Maxim A. Medvedev, and Todorka Atanasova, "Classification of online toxic comments using the logistic regression and neural networks models", AIP Conference Proceedings 2048, 060011 (2018).

[8] Ivan A. Berg, Oleg E. Khorev, Arina I. Matvevnina, Alexey V. Prisjazhnyj, "Machine Learning in Smart Home Control Systems - Algorithms and New Opportunities", AIP Conference Proceedings 1906, 070007 (2017).

[9] A. Medvedev, D. Taushankova, M. Medvedeva, A. Varaksin, A. Sergeev, "Snow Pollution Regression Model for Karabash City of Russia", in *14th GeoConference on Ecology, Economics, Education and Legislation. Conference Proceedings, Volume 1. Ecology & Environmental Protection. SGEM2014* (Published bySTEF92 Technology Ltd., 2014), pp. 601-606.

[10] NumPy, available at http://www.numpy.org. (Date of access: 10.01.2019).

[11] Scikit-learn: machine learning in Python, available at https://scikit-learn.org. (Date of access: 10.01.2019).

On the Prediction of Dispenser Status in ATM Using Gradient Boosting Method

V.V. Shcherbitsky[1, a)], A.A. Panachev[1, b)], M.A. Medvedeva[1, c)], E.I. Kazakova[2, d)]

[1]*Ural Federal University, Mira 19, Yekaterinburg, Russia, 620002*
[2]*Department of Economic Cybernetics, Donetsk National Technical University, Artema Street 131, Ukraine, 83015*

[a)]tutamob96@yandex.ru
[b)]panachev1@mail.ru
[c)]Corresponding author: marmed55@yandex.ru
[d)]kazakova_donetsk@mail.ru

Abstract. The purpose of this study is to solve the problem of determining the status of an ATM to increase its resiliency, which will reduce the reputational and financial losses of banking structures. The tools for the goal achieving were machine learning methods such as gradient boosting model (on the example of Russian Sberbank ATM data). The study showed good enough accuracy in the problem of binary classification of the status of ATM dispensers, and also revealed the importance of time characteristics of the occurrence of errors and transactions. The methodology has practical value; it is possible to use it outside the banking sector due to the flexibility of the chosen model.
Keywords: Gradient boosting, machine learning, ATM, classification.

INTRODUCTION

The malfunction of ATMs and its important part - the dispenser, can lead to a number of serious problems for the bank. This happens due to the fact that the economy and society highly depend on financial instruments and banking services [1]. Bypassing with enclosing machines at the moment in Russia is taking place on a strict schedule without regard to the state of the ATM (the ATM outside the bank's branches is not connected to the banking network for security reasons). Also, a non-working device leads to customer dissatisfaction.

The use of machine learning methods in this case is advisable because of their high efficiency in solving wide range of problems in different fields [2-9]. The solution of the considered problem is reduced to the problem of binary classification, for which logistic regression and decision trees are suitable. This is confirmed in [10] and [11], where the examples of positive experience of using machine learning models in bankruptcy predicting and solving some other tasks of banking sector.

This study focuses on the gradient boosting model, which demonstrates high performance, accuracy and predictive ability (over 70%, higher than random guessing) at the Kaggle Championships (including regression tasks).

METHODOLOGY

Gradient booting is a variation of the classifier and in a general sense it is the aggregation of arbitrary machine learning algorithms to achieve higher accuracy [12]. In this case, it is an ensemble of decision trees, formed iteratively with preservation of the previous state to improve the subsequent one.

In the GBM algorithm, firstly, the statement of problem (1) made, the solution of which should lead to minimization of the chosen loss function (maximum likelihood method):

$$\hat{f}(x) = \arg\min \mathrm{E}_{x,y}[L(y, f(x))] \tag{1}$$

Next, due to the infinity of the functional space, the task is simplified by reducing to the optimization of values of the parameters (2), which are approximated iteratively:

$$\hat{f}(x) = f(x, \hat{\theta}), \hat{\theta} = \arg\min E_{x,y}[L(y, f(x, \theta))] \tag{2}$$

For each iteration, the gradient of the loss function is calculated at the current approximation (3):

$$\nabla L_{\theta}(\hat{\theta}) = [\frac{\partial L(y, f(x, \theta))}{\partial \theta}]_{\theta = \hat{\theta}} \tag{3}$$

At the last iteration steps, the current approximation is set on the basis of the calculated gradient (4) in the opposite direction of the gradient direction, and the approximation of the parameters is updated (5):

$$\hat{\theta} \leftarrow -\nabla L_{\theta}(\hat{\theta}) \tag{4}$$

$$\hat{\theta} \leftarrow \hat{\theta} + \hat{\theta}_t = \sum_{i=0}^{M} \hat{\theta}_i \tag{5}$$

This technique is used in many other problems of machine learning and neural networks. For example, in the article [13], gradient boosting successfully solved task of analyzing survival (predicting death or machine breakdowns).

The "sklearn" library, the "pandas" library and "numpy" for working with data and the Python programming language were chosen as tools. During the research process, the following hyper parameters were changed:

- learning_rate (gradient step size in the direction of the global minimum),
- iterations (the number of iterations of the boosting, forms one decision tree, only in CatBoost),
- n_estimators (the number of booster stages produced by the algorithm is only in Xgboost).

Accuracy metrics and f1-score [14] were used to measure prediction ability of the model.

MODEL BUILDING

Building the model, based on the tools selected above, is based on the following elements:

1. Sberbank's ATM datasets: 6638 observations divided into training and test samples in the ratio of 95 to 5 with 70 initial features in 18 different states.
2. The initial parameters include the device characteristics for transactions (date, time, volume frequency, etc.), module status (start, shutdown, etc.) and technical data (identifier, model, age, etc.). The table below is provided the data (Table 1).

TABLE 1. Data features groups.

Features groups	Examples of features	Features value data type	Percentage in the total sample
ATM transactions	Cash delivery status, operation type, notes count, client session, last working time	Time, Number	54.3%
ATM moduls statuses	Dispancer status, check printer status, EPP status, service start time	Time, String	34.3%
ATM tech. data	Atm ID, age, model, cash in and out, display type	Time. Boolean, String	11.4%

3. The target variable is binary and equal to 0 or 1, the inactive and active status of the ATM dispenser respectively.

DATA PROCESSING

The stage of data preparation for use in the model consists of: feature engineering, data normalizing, interpolation and feature elimination. At the last stage, the use of RFE (recursive feature elimination) algorithm and / or correlation matrix is possible.

Thus, at the first stage 909 features were singled out, and then 204, among which there were: the number of days elapsed since the last shutdown, the average number of errors during work and in the process of carrying out transactions, as well as other time and quantity signs of ATM's sessions.

The model Xgboost with the standard library settings showed an accuracy of 78% after a thorough cleaning of the original data from correlating features. However, this result was slightly increased with the help of the CatBoost library. The final results can be seen below (Fig. 1, Fig. 2 for CatBoost and Fig. 3 for Xgboost).

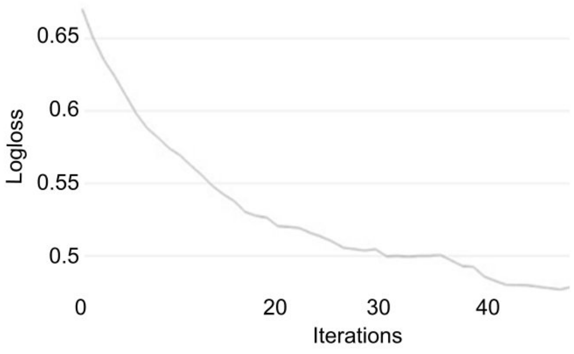

FIGURE 1. CatBoost Logloss function movement.

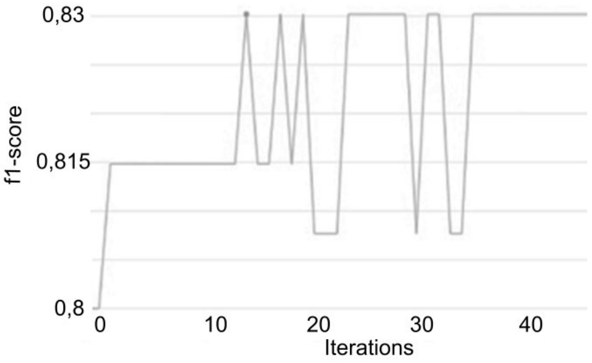

FIGURE 2. CatBoost **f**1-scrore movement of prediction.

In the Figure 1 there is Logloss plot that demonstrates loss function value during training process. The best value is slightly bellow 0.5. Figure 2 shows f1-score that sharply jumps during training process - the best value is 0.83 or 83%. It is important to say that the model prediction accuracy highly depends on features and feature preprocessing in particular.

Also, Figure 3 shows a confusion matrix of Xgboost prediction results. Model with 0.01 learning_rate and 350 n_estimates gave result of 148 truly positive and 120 truly negative values.

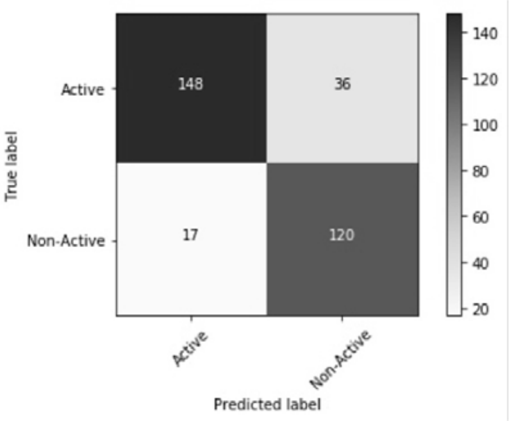

FIGURE 3. Xgboost confusion matrix plot.

Compared to other similar models, CatBoost and Xgboost show approximately the same result, differing only by a few percent. The CatBoostClassifier still appears with the best classification accuracy of 84% on the test sample, the second model also has a figure above the average. In some sources, an experiment was made with a static criterion, but the accuracy there does not exceed 69%. A similar result was at the initial stage of the model, without taking into account the correlation, but this approach was not applied. The predictive ability of the algorithm is at an acceptable level, there are sharp jumps in the learning process that do not affect the final result [15].

CONCLUSION

As a result of the study it can be concluded that the use of CatBoost and Xgboost is appropriate for the following values of hyper parameters: iterations - 50, learing_rate - 0.1. The accuracy of the model was about 83% with the selected 204 features. The greatest importance was shown by time series features. In the context of further work on the issues it is possible to change the model in the direction of building dispenser shutdown periods, determining the current status of the device and taking into account the probability of these periods occurring in the future.

REFERENCES

[1] Anisoara Niculina, Apetri. Role of importance of banking system in economy (2007), available at https://www.researchgate.net/publication/227364445_ROLE_AND_IMPORTANCE_OF_THE_BANKING_SYSTEM_IN_ECONOMY.

[2] A.V. Berdishev, AI as technical background for banking development (2018), available at https://cyberleninka.ru/article/n/iskusstvennyy-intellekt-kak-tehnologicheskaya-osnova-razvitiya-bankov.

[3] Ivan A.Berg, Oleg E. Khorev, Arina I. Matvevnina, Alexey V. Prisjazhnyj. "Machine Learning in Smart Home Control Systems - Algorithms and New Opportunities", AIP Conference Proceedings 1906, 070007 (2017);

[4] A. Panachev, E. I. Komotskiy, D. B. Berg, T. B. Atanasova, and O. E. Khorev. "Prediction of ferrous scrap price: Neural network model application", AIP Conference Proceedings 2040, 050013 (2018);

[5] Anastasia Chirkina, Marina Medvedeva, and Evgeny Komotskiy, "CIN classification and prediction using machine learning methods", AIP Conference Proceedings 1836, 020010 (2017);

[6] Alexander G. Buevich, Alexander N. Medvedev, Alexander P. Sergeev, Dmitry A. Tarasov, Andrey V. Shichkin, Marina V. Sergeeva, and T. B. Atanasova. "Modeling of Surface Dust Concentrations Using Neural Networks and Kriging", AIP Conference Proceedings, 1789, 020004 (2016)

[7] Shichkin, A. V., Buevich, A. G. & Sergeev, A. P. "Comparison of artificial neural network, random forest and random perceptron forest for forecasting the spatial impurity distribution", Mathematical Methods and Computational Techniques in Science and Engineering II. American Institute of Physics Inc., Vol. 1982, 020005.

[8] Tarasov, D. A., Buevich, A. G., Sergeev, A. P. & Shichkin, A. V. "High variation topsoil pollution forecasting in the Russian Subarctic: Using artificial neural networks combined with residual kriging", Applied Geochemistry 88, pp. 188-197.

[9] Mujahed A. Saif, Alexander N. Medvedev, Maxim A. Medvedev, and Todorka Atanasova, "Classification of online toxic comments using the logistic regression and neural networks models", AIP Conference Proceedings 2048, 060011 (2018).

[10] A.U. Korablev, R.B. Bulatov, Machine learning in business (2018), available at https://cyberleninka.ru/article/n/mashinnoe-obuchenie-v-biznese.

[11] Taha Zaghdoudi, Bank failure prediction with logistic regression (2013), available at http://www.academia.edu/3639881/Bank_Failure_Prediction_with_Logistic_Regression.

[12] V.V. Kitov, Accuracy analisys of the gradient boosting method with random rotations (2016), available at https://cyberleninka.ru/article/n/issledovanie-tochnosti-metoda-gradientnogo-bustinga-so-sluchaynymi-povorotami.

[13] Yifei Chen, Zhenyu Jia, Dan Mercola, Xiaohui Xie, A gradient boosting algorithm for survival analysis via Direct Optimization of Concordance Index (2013), available at https://www.hindawi.com/journals/cmmm/2013/873595/.

[14] Metrics in machine learning tasks, OpenDataScience blog post, available at https://habr.com/company/ods/blog/328372/.

[15] K.I. Salakhitdinova, I.S. Lebedev, I.E. Krivcova, Gradient boosting trees method in task of software identification (2018), available at https://cyberleninka.ru/article/v/algoritm-gradientnogo-bustinga-dereviev-resheniy-v-zadache-identifikatsii-programmnogo-obespecheniya.

Structural Analysis of Network Transactions between Economical Agents of a Municipality

A.A. Panachev[1, a)], D.B. Berg[1, b)], M.A.Medvedeva[1, c)], A.O. Kolomytseva[2, d)]

[1]*Ural Federal University, Mira 19, Yekaterinburg, Russia, 620002*
[2]*Department of Economic Cybernetics, Donetsk National Technical University, Artema Street 131, Ukraine, 83015*

[a)]panachev1@mail.ru
[b)]bergd@mail.ru
[c)]Corresponding author: marmed55@yandex.ru
[d)]anniris21@rambler.ru

Abstract. The main goal of the research is to compare two local entrepreneurial networks which are based on municipal operations and banking transactions. The method of comparisons is based on Social Network Analysis which consists of calculation density, neighborhood properties, dyadic parameters, density of system and etc. The main difference between networks is located in density and centrality of agents. The municipal network consists of «city-formed» organizations and there are no «external» agents. The density of such networks is higher and the «main» companies locate in the center of the system. In the second network, which is built on banking transactions, there is a classical «market competition» system. The agents can join or leave from system any time. The density is much lower in the second case than in the first one, and the network is not based only on central agent.
Keywords: Social Network Analysis, Experimental economic models, Institutional models, Self-organization mechanism.

INTRODUCTION

The economical situation on the local market can change due to world political instability or macro-economic changes in country economy. Both situations can provoke the local society of entrepreneurs to feel a lot of threats. The laws of our history showed that instability on the market leads to unite single entrepreneurs into local networks [1]. There are two main forms of local industrial cooperation: cauterization and entrepreneurial networks. Both variants can be used to reach the goals of an industrial group. They can use all kinds of their resources together. The main reason of collaboration and association is to feel safer in instable time [2].

Economic clustering of entrepreneurs can be formed on temporary or permanent basis. The first one can be used to get the goal, which can be reached only together [3]. The second one can be formed in local areas, for example in small towns. It can be a non-formal conglomerate of industrial entrepreneurs. The networks located in the same area are called clusters.

Joint activities suggest exchange of goods or facilities (energy, materials, information, resources, etc.) through their trade relations [4]. These flows of resources begin to circulate in the network according to certain laws.

A Part of financial and goods flows circulate only in a local area between entrepreneurs in one network. It is a good reason to start using clearing in the system, which companies can start using through specialized clearing center or through the modern digital system. Also the system can start to use the local complementary currency which can be represented through tickets, talons or electronical forms of non-cash payment [5]. In context of using alternative systems of payment the main governance currency can be used in external developing of company and in other investment projects.

The main goal of the study is to compare two local networks of entrepreneurs. They will be compared by their structural analysis.

STRUCTURAL ANALYSIS

The industrial networks used in the research were formed in two different ways. The first industrial cooperative network was taken from the municipal economy's model published in [6-9]. It is based on the set of the 12 real business entities, which consume their goods and services for 10000 residents. This entrepreneurial network has its own industry-specific structure that is diversified and provides production of different commodities and services. The matrixes of the commodity flow between the municipal enterprises were generated based on the statistical data and the actual economic data of similar enterprises. The enterprises are based on different industries: 1– agricultural production cooperative, 2 – farm, 3 - poultry farm, 4 - meat factory, 12 – population and etc. These flows, denominated in rubles, show the production of network agent's communications and reflect the movement of commodities and services between the enterprises located in the production area.

The graph with municipal entrepreneur network is shown in Fig. 1. The graph shows that most population is in the main agent in scheme. It's a typical situation, because the industries in this graph are based in b2c (business-to-customers) sector.

The second network was received from the real banking transactions during 1 month. It is based on data from 3 bank branches in little town. The first dataset, which was processed for this research, consists of more than 15 thousand transactions between more than 600 entrepreneurs. In process of data engineering and building the final model was found that in this area there are 9 closed networks which are based on 70 organizations. The industries are diversified; in the result network organizations provide goods and facilities in the following areas of economy: 1 – wholesale of timber, construction materials and sanitary equipment; 3 – production of dry mixes; 4 – flat-leasing and etc.

In total, it consists of more than 45 industries which represent all kind of industrial facilities from flat-leasing and ending the roads and houses building areas. And all of them are linked in one closed network of entrepreneurs.

The graph with network, which based on banking transactions, is shown in Fig. 2.

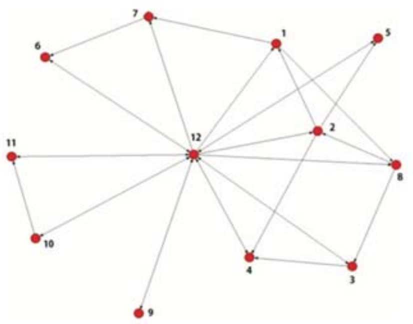

FIGURE 1. Graph of municipality network.

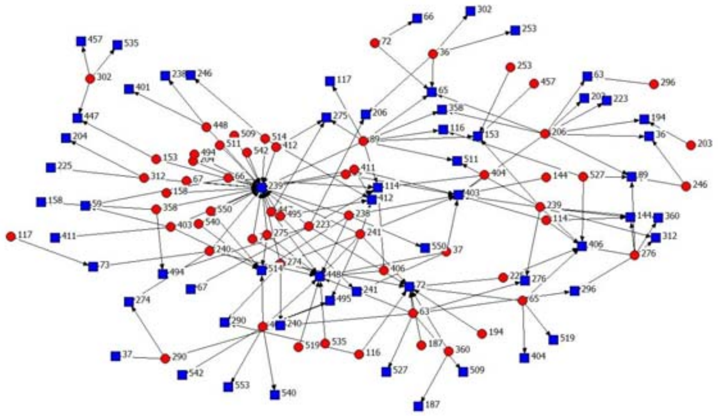

FIGURE 2. Graph of banking transactions network.

The main difference between the first and the second networks is that it is shown without population. From one point of view, citizens are the main consumers of goods, but on the other side in industrial sector of economy such as metallurgical industry b2b (business-to-business) relations cam be seen more often.

Networks are defined according to the following parameters:

Nn - number of nodes (agents, actors);

Ne - number of edges (relations, communications, ties);

D - density is simply the proportion of all possible links they actually present, D = Ne/Nn(Nn-1);

Sum - total amount of transactions/payments (in rubles);

AvrCost - average cost of transaction in rubles, AvrCost = Sum/Ne

Ng - number of different types of goods and services produced and consumed in the network;

Var - variety of products of network, Var = Ng/Nn.

Values of networks parameters are listed in Table 1.

The networks cover not similar periods of time, but this factor can't influence the comparativeness. The graphs of each one look the same. The first table demonstrates that the matrix of municipality network is based on few numbers of agents and the result matrix is smaller, but the amount is bigger.

The approach to indexing the network quantitative characteristics is focused on four types of parameters: the whole network parameters, ego network (neighborhood) properties, dyadic parameters, and single actor parameters. Calculations were performed according to common formulas [10, 11], which are shown at the Table 2.

TABLE 1. Industrial entrepreneurial networks parameters.

Parameters	Network of Municipality	Network of Bank clients
Nn	12	59
Ne	28	169
D	0,212	0,049
Sum	3 673 560	63 562,18
AvrCost	131 198	376,11
Ng	14	43
Var	1,27	0,73

The main goal of this research is to compare graphs of municipal and based on banking transactions networks. Investigation of network structure was performed according the following techniques: calculations network parameters of both graphs; comparison of graph parameters between municipal and based on banking transactions networks; estimation of their relative deviations. Relative deviation (RD) of graphs is calculated as follows:

$$RD = \frac{\Delta}{BT}, \tag{1}$$

where $\Delta = |\mathrm{BT} - \mathrm{M}|$, BT – network based on banking transactions, M – network of municipality.

Calculations were carried out utilizing the framework UCINET 6 for Windows, which supports SNA (Social Network Analysis) methodology.

TABLE 2. Industrial entrepreneurial networks parameters for structural analysis and their calculations.

Parameters	Formula	Explanation
D	$D = \max\limits_{i,j=1,..,n}(d(n_i, n_j)),$	$d(n_i, n_j)$ – the shortest (geodesic) path n_i – actor I; n_j – actor j
Re	$Re = \frac{\sum L_p}{\sum L},$	L – dyadic tie L_p – reciprocated dyadic tie
Tr	$Tr = \frac{N_t}{N_d},$	N_t – number of non-vacuous transitive ordered triples N_d – number of triples in which ties go from actor n_i to actor n_j and from actor n_j to actor n_k
CC	$CC = \frac{1}{N}\sum\limits_{i=1}^{N} C_i,$	C_i – density of the i-th actor's neighbourhood
IDCenz	$\frac{\sum_{i=1}^{n}(IDC^* - IDC_i)}{\max\limits_{i,j=1,..,n}\sum_{i=1}^{n}(IDC^* - IDC_i)},$	IDC^* – in-degree centrality of the most central actor IDC_i – in-degree centrality of the i-th actor
ODCenz	$\frac{\sum_{i=1}^{n}(ODC^* - ODC_i)}{\max\limits_{i,j=1,..,n}\sum_{i=1}^{n}(ODC^* - ODC_i)},$	ODC^* – out-degree centrality of the most central actor ODC_i – out-degree centrality of the i-th actor
BCenz	$\frac{\sum_{i=1}^{n}(BC^* - BC_i)}{\max\limits_{i,j=1,..,n}\sum_{i=1}^{n}(BC^* - BC_i)},$	BC^* – betweenness centrality of the most central actor BC_i – betweenness centrality of the i-th actor

Results of calculation are shown in Tab. 3. The table shows that there are a lot of differences between networks in the research. The first difference is the density. Network, which is based on municipal relations, consists of «city-forming» organizations. The agents of this cluster collaborate and exchange the goods with more density, because the system is closed from the other «external» agents. In the network, which is based on banking transactions the situation is different. Agents cover almost all of industries and there is «market competition» system.

TABLE 3. Values of industrial entrepreneurial networks parameters

Parameters	Network of Municipality	Network of Bank transactions	Relative Deviation
D	4	11	0,64
Re	0,33	0,454	0,27
Tr	0,15	0,126	0,19
CC	0,52	0,025	19,80
IDCenz	0,46	0,4414	0,04
ODCenz	0,86	0,1082	6,95
BCenz	0,77	0,23	2,35

CONCLUSION

Two models of entrepreneurial networks were compared in the present research. Both of them are based on transactions and economic relations between organizations. The period of research is not the same and number of companies of each system is not the same either, but the methods of Social Network Analyses allow to compare it correctly. The research shows that the networks have some differences. The first one is density. Municipal network is based on «city-formed» organizations and has the main agent in the center of this system. The system of second matrix illustrates classical «market competition» system without central agents.

ACKNOWLEDGEMENTS

Present study was carried out under financial support of the Russian Fund of Fundamental Research grant № 19-010-00974 "Experimental institutional models of the autonomy of local communities finances in context of public confidence decreasing in forms of participation in the budget process".

REFERENCES

[1] A. N. Asaul, M. P. Voynarenko, P. Y. Yerofeyev, *Organization of business. Tutorial*, edited by A.N. Asaul (Gumanistika, Spb., 2004).

[2] S. G. Svetunkov, M. G. Svetunkov, "Patrimonial business networks and competition", Modern Competition 1, 7-17 (2012).

[3] A. N. Asaul, E. G. Skumatov, G. E. Lokteeva, *Methodological aspects of formation and development of enterprise networks. Textbook*, edited by A.N. Asaul (Gumanistika, Spb., 2004).

[4] D. B. Berg, O. M. Zvereva, "Features of communication between functional coupling agents of the production network", Herald SibSUTI 1, 82-97 (2015).

[5] V.V. Popkov, D.B. Berg, E.A. Ulyanov, N.A. Selezneva, "Simulation as a tool for the formation of commodity and financial network in the regional economy", Economy of the Region 2, 236-246 (2015).

[6] V.V. Popkov, D.B. Berg, E.A. Ulyanova, N.A. Selezneva, "Commodity and Financial Networks in Regional Economics", R-Economy 1, issue 2, 305-314 (2015).

[7] Dmitry B. Berg and Olga M. Zvereva, "Identification of Autopoietic Communication Patterns in Social and Economic Networks", in *Analysis of Images, Social Networks and Text*, 4th International Conference AIST 2015 (Yekaterinburg, 2015), 286-296.

[8] G.K. Shevchuk, O.M. Zvereva, M.A. Medvedev, "Imbalance Detection in a Manufacturing System: An Agent-Based Model Usage", AIP Conference Proceedings 1906, 070013 (2017).

[9] Berg D.B., Davletbaev R.H., Nazarova Y.Y., Zvereva O.M. "The Detailed Structure of Local Entrepreneurial Networks: Experimental Economic Study", in: Ignatov D. et al. (eds) Analysis of Images, Social Networks and Texts. AIST 2016. Communications in Computer and Information Science, Vol. 661. (Springer, 2017).

[10] M. E. J. Newman, "The structure and function of complex networks", SIAM Review 45, -256 (2003).

[11] L. da F. Costa, F. A. Rodrigues, G. Travieso and P. R. Villas Boas, "Characterization of complex networks: A survey of measurements", Advances in Physics, Vol. 56, No. 1, 167–242 (February 2007).

System-Dynamic Model of Managing the Budgetary Financial Resources in Targeted Programs

A.O. Kolomytseva[1, a)], M.A. Medvedeva[2, b)], V.I. Kolomiets[1, c)]

[1]*Department of Economic Cybernetics, Donetsk National Technical University, Artema Street 131, Ukraine, 83015*
[2]*Ural Federal University, Mira 19, Yekaterinburg, Russia, 620002*

[a)]anniris21@rambler.ru
[b)]Corresponding author: marmed55@yandex.ru
[c)]kolomiietsv.i@yandex.ru

Abstract. The article presents a variant of solution of the task of managing budgetary financial resources and controlling their use. A system-dynamic model is presented, which provides management of budget spending and eliminates the possibility of manipulating reports and financial assets. The model includes levels, flows and variables in the architecture of information links between the main components of the regional financial management system. The model provides two contours for analyzing the dynamics of budget spending: basic and optimized. This allows, based on a series of simulation experiments, obtaining a forecast of the budgetary, social and economic efficiency of the implementation of the targeted financial program.
Keywords: system dynamics, simulation experiment, targeted financial program, efficiency.

INTRODUCTION

The problem of adequate allocation of resources, as well as control and improvement of the effectiveness of public investment in the economy is one of the key issues in public administration.

One of the most popular instruments for the implementation of state regional policy is long-term targeted programs that allow solving problems of reducing the differences in the level of regional development and ensuring the sustainability of regional development.

In this regard, an urgent task is the development of modern scientific approaches and computer tools for managing the resources of financial programs, monitoring of their sustainability [1, 2], the effectiveness and legality of using funds, as well as eliminating the manipulation of financial reporting.

In the literature, there are many methods of identifying the manipulation of financial reporting, in particular: M. Benish model (M-Score, 1999), D. Piotroski model (F-score), Benford's law. The most famous is the M-score model by Messod Benish (Kelly School of Business, 1999), which is based on the assumption that companies predisposed to manipulation have similar internal conditions that push the company's management to the manipulation [3, p. 632]. Based on a study of the financial statements of a number of organizations and companies, he calculated eight ratios, as well as weights for indicators, and proposed an equation, called the Benish M-score. If the result of the equation is more - 2.22, then we can assume that the company has signs of fraud. However, this technique is applicable only if there is an overstatement of financial performance. In the case of understating financial results, the predictive power of the M-score is rather low [4]. Alekseev M.A. [4] showed that the F-score index can be used to assess the financial statements of Russian companies, but this index does not allow determining the direction of the distortion of financial statements.

In this paper, it is proposed to use a system-dynamic simulation model as a tool for preliminary strategic planning of the allocation of financial resources [5, 6]. Such a model will allow more fully taking into account the high complexity of the studied economic systems [7-11]. The dynamic component makes the system dynamics

method an attractive tool for predicting the results of using financial program resources in a complex and uncertain environment [5-7].

The purpose of this study is the development and implementation at the experimental level of a simulation system-dynamic model for evaluating the effectiveness of the financial program (on the example of the subprogram of socialization of small business in the system of regional entrepreneurship). The results of the use of the model will make it more reasonable to make management decisions on the volume of allocated budgetary funds, as well as to assess the rationality and legitimacy of their use.

METHOD AND EMPIRICAL RESULTS

To implement the model, the PowerSim system-dynamic modeling platform was chosen. According to the system-dynamic approach, all indicators of the resource management process of the targeted program were divided into controlled and unmanaged variables, levels of accumulation of results and rates (intensities) of accumulation. The main hypothesis is that state-controlled financial regulation is the basis for managing the resources of the targeted program. The program should be cost-effective, as well as transparent, so that one can assess its budgetary and social efficiency in the region.

The formalization of causal relationships for the proposed system-dynamic model is presented in Table 1. The algorithm developed is based on the assumption that the set of data under study can be modeled using a linear combination of multidimensional normal distributions. The purpose of the algorithm is to estimate the distribution parameters that maximize the log likelihood function used as a measure of the model quality.

TABLE 1. Basic formulas of a system-dynamic model for predicting the effectiveness of a regional small business development program.

Name of the main indicators of the model	Description of variables and parameters
Non-normalized integral performance indicator of the targeted financial program: $$P_I(t) = \frac{1}{3} \times \left[\alpha_1 \int_{t0}^{tn} I_B dt + \alpha_2 \int_{t0}^{tn} I_E dt + \alpha_3 \int_{t0}^{tn} I_C dt\right] + Em$$	I_E – integral indicator of economic efficiency of business activities at the regional level; I_B – integral indicator of budgetary efficiency of business at the regional level; I_C – integral indicator of the social efficiency of businessat the regional level; α_i – weighting factor (importance of the indicator for the integral assessment of efficiency); Em – em-algorithm for preparing data for modeling.
Non-normalized indicator of economic efficiency: $$P_E(\mathrm{t}) = \int_{to}^{tn} V_P dt - \int_{to}^{tn} S_Z dt$$	V_P – volume of products produced in small enterprises of the region; S_Z – the sum of all costs in enterprises.
Non-normalized indicator of budgetary efficiency: $$P_B(\mathrm{t}) = \int_{to}^{tn} V_{NP} dt - \int_{to}^{tn} V_{GZ} dt$$	V_{NP} – volume of tax payments of small businesses; V_{GZ} – amount of government spending to support small businesses.
The level of social efficiency: $$P_c(t) = \frac{1}{2} \times \left[\int_{t0}^{tn} H_{MZ} dt + \int_{t0}^{tn} H_{ZR} dt\right] + \int_{t0}^{tn} C_{SA} dt$$	H_{MZ} – share of workers employed in small businesses in the total number of workers in the region; H_{ZR} – unemployment rate in the region; C_{SA} – analysis of population responses to evaluating the effectiveness of small business development projects.
Volume of products manufactured at the enterprises of the region: $$\frac{dV_P}{dt} = \frac{2Q}{\sqrt{\frac{Qt}{P} * (\delta_3 k_{VGZ} + \delta_4)}}$$	k_{VGZ} - coefficient of regulation of the volume of financing production of small businesses; $\frac{Qt}{P}$ - dynamics of changes in demand for materials and raw materials for production.
The amount of funding for the program (costs of development) $$P_I(\mathrm{t}) = V_{GZ} \times \int_{t0}^{tn} V_{GZ}^B dt$$	V_{GZ} – amount of government spending to support small businesses; V_{GZ}^B – base public spending.
The sum of all the costs of managing small business	S_{OF} – cost of fixed assets of small business;

TABLE 1. Continued

Name of the main indicators of the model	Description of variables and parameters
development in the region: $\Delta S_Z(\mathrm{t}) = S_{OF}(\mathrm{t}) + S_{OS}(\mathrm{t}) + S_{KV}(\mathrm{t}) + S_{FI}(\mathrm{t}) + S_{II}(\mathrm{t})$	S_{OS} – cost of small business working capital; S_{KV} – small business capital investment; S_{FI} – financial investments; S_{II} – intellectual investment.
Share of workers employed in small businesses: $\Delta H_{MZ}(\mathrm{t}) = \frac{H_M(\mathrm{t})}{H_Z(\mathrm{t})}$	H_M – the total population of the region employed in small business; H_Z – the total employed population of the region.
Employment rate: $\Delta H_{ZR}(\mathrm{t}) = \frac{H_Z(\mathrm{t})}{H_R(\mathrm{t})}$	H_Z – The total employed population of the region; H_R – The total population of the region.
Profit for the study period in the region (criterion for the comparison of funding results): $\Delta NI(t) = V_{NP}(t) - P_E(t)$	V_{NP} – volume of tax payments of small businesses; P_E – non-normalized indicator of economic efficiency.
Balance of cash flows from current operations: $\Delta CFO(t) = V_P(t) - S_{OF}(t)$	S_{OF} – cost of fixed assets of small business/

The experimental data included input information on the main elements of the financial program in the form of a table of weights - internal tuning coefficients, the magnitude of which corresponds to the vectors of social, budgetary or economic efficiency of the program. These weights function in the model as adaptive control components.

The following assumptions were made for the experiments: population growth in the region is subject to the normal distribution law; weights are used to evaluate the effectiveness of the component parts of the program; investments and other contributions are subject to the normal law of distribution; the value of the em-algorithm is taken from the information system as a correction factor.

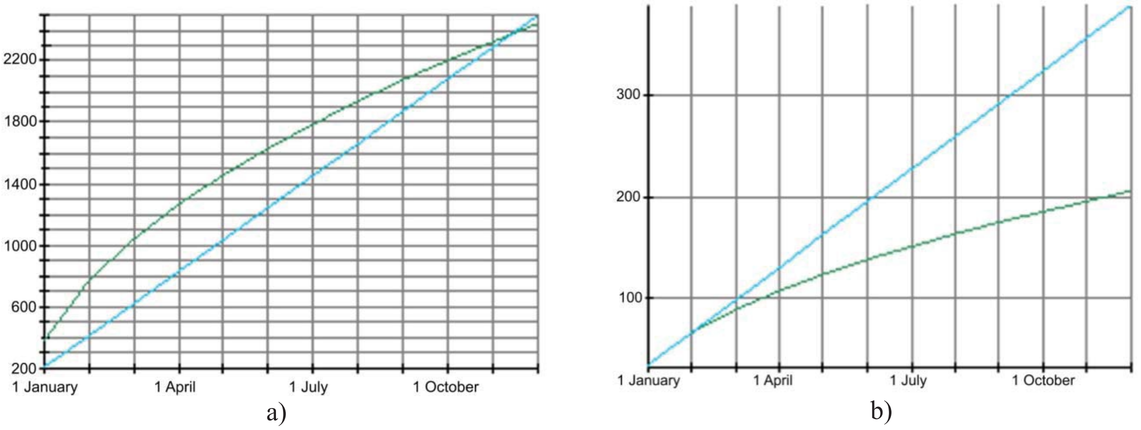

FIGURE 1. Schedule of financial costs and tax revenues (conventional units) when the value of the funding regulator is: a) 150%, b) 200% of the base funding in the region. The green line - budget costs, the blue line - tax revenues.

The model for assessing the effectiveness of resource management of targeted state programs is implemented in the PowerSim Express modeling environment. The simulation period was 1 year with 1 month increments.

Figure 1 shows how the values of budget expenditures and tax revenues change at different levels of the funding regulator of government spending on small business development programs in a particular region.

With an increase in the cost of supporting small businesses, the point of equality of financial costs and tax revenues (the payback point of the regional financial program) shifts forward in time that indicates the efficient use of financial resources. For this simulation experiment, the best efficiency is observed at the level of financial costs of about 150-160% of the base volume of current financial expenses in the region (Fig. 1, a). With an increase in the amount of program funding to 200% of the base funding, the payback point shifts in the opposite direction, which indicates a decrease in the budget efficiency of this targeted program (Fig. 1, b).

CONCLUSION

It is developed and implemented at the experimental level a simulation system-dynamic model for evaluating the effectiveness of a regional targeted financial program.

The model makes it possible to evaluate the expected indicators of the social and economic efficiency of the targeted program, as well as to determine the ratio of financial costs and tax revenues for various values of the control action (changing the amount of targeted program financing from regional budget).

Based on the simulation results, one can determine the optimal amount of financial resources needed to achieve the best result. This allows making informed decisions on the management of resources of targeted financial programs at the regional level, taking into account the objectives and priorities.

REFERENCES

[1] Zvereva, O.M., Berg, D.B. & Kondratyev, A., "Structural patterns for system sustainability: Experimental study", CEUR Workshop Proceedings 1975, 326-333 (1 January 2017).

[2] Alina Bodnar, D.B. Berg, Maxim Medvedev, Nikolay Medvedev, "Functional Algorithm of Information and Communications Management Based on the Models of Fuzzy Logic", AIP Conference Proceedings 1978, 440020 (2018).

[3] L.P. Aliyeva, K.I. Kirgizov, "Using the method of M. Benish (M-Score) to manipulate the financial statements of companies in the Russian reality", *Regulation of economic activity and business environment: problems, prospects and solutions: A collection of scientific papers on the materials of the International Scientific and Practical Conference* (Togliatti, December 22, 2016), pp. 630-636.

[4] M.A. Alekseev, M.S. Tyuzhina, "Verification of approaches to identify directions of distortion of financial statements", Siberian Financial School, No. 3, 69-75 (2017).

[5] Berg, D.B., Kolomytseva, A.O., Apanasenko, A.V. & Isaichik, K.F., "Modelling of the Municipality Entrepreneurial Community Functioning Using the Methods of System Dynamics", IFAC-PapersOnLine, Vol. 51, Issue 32, 61-66 (2018).

[6] O.A. Iskra, E.A. Sizonenko, Marina Medvedeva, "Imitation Model of Decision Support for Mobile Applications Lifecycle Management", AIP Conference Proceedings 1978, 440012 (2018).

[7] D.Yu. Katalevsky, Management of Organizational Growth Based on a System-Dynamic Approach, Moscow University Bulletin, Ser. 21 Management (state and society), № 4 (2007).

[8] A.A. Akayev, "The derivation of a general macroeconomic dynamics equation that describes the joint interaction of long-term growth and business cycles", Reports of the Russian Academy of Sciences, Vol. 417, No. 4, 439-441 (2007).

[9] J.W. Forrester, "Counterintuitive behavior of social systems", Technology Review, Vol. 73, Issue 3, 52-62 (1971).

[10] D. Novikov. *Theory of Control in Organizations*. (Nova Science Publishers, N.-Y, 2013).

[11] A.S. Akopov, L.A. Beklaryan. "Simulation of Human Crowd Behavior in Extreme Situations", International Journal of Pure and Applied Mathematics, Vol. 79, No. 1, 121–138 (2012).

Development of Information Model and Methods of Data Analysis on Land Taxation Objects for Yekaterinburg City of Russia

V.V. Kalinin[1, a)], A.S. Ilyin[1, b)], A.V. Ilyina[1, c)], N.A. Demin[1, d)],
A.N. Medvedev[1, e)], Yu.E. Kharitonov[2)]

[1]Ural Federal University, Mira 19, Yekaterinburg, Russia, 620002
[2]Department of Economic Cybernetics, Donetsk National Technical University, Artema Street 131, Ukraine, 83015

[a)]kalinin_valeryi@mail.ru
[b)]ias@snufo.ru
[c)]a.v.ilina@urfu.ru
[d)]na.demin@snufo.ru
[e)]Corresponding author: alnikmed52@gmail.com

Abstract. The work is devoted to the use of information technology in the taxation system at the municipal level. As a result of the study, an information model was created and the characteristics of the land taxation objects of Yekaterinburg, Russia were analyzed. It has been proposed to use Shewhart control chart to single out a group of objects, the amount of land tax for which ones is formed for special reasons of non-random and non-market character. It was shown that for the city of Yekaterinburg, in the aggregate of land taxation objects, fractal structures with different fractal dimension can be distinguished. It was proposed to divide and group objects of taxation using the fractal dimension to optimize the procedure for calculating the tax sizes.
Keywords: Information model, land taxation, Shewhart control chart, fractal dimension.

INTRODUCTION

Due to the change in the tax legislation of Russia, from January 2020 the amount of property tax and land tax will be calculated as a percentage of the cadastral value of real estate [1].

For effective management of these types of taxation at the municipal level, it is necessary to develop a methodology for calculating taxes, taking into account the individual characteristics of taxable items. Such an approach can be implemented on the basis of the information model, which will provide analysis of data on taxable objects and obtain quantitative estimates of the parameters characterizing each object. Such information models and systems are currently widely used in the field of economics, management, ecology and other social sciences, as well as in decision-making support systems at different levels [2-6].

This paper presents an information model and some approaches to analyzing data on land taxation objects for the city of Yekaterinburg.

METHODS AND RESULTS

During the study, a database of land taxation objects of the city of Yekaterinburg was formed, which contains about 130,000 lines. The database includes information on the following individual features of the objects: name, type (land, property) location, permitted use, actual use, area, cadastral value, residual value, as well as some additional indicators.

It was revealed that the city of Yekaterinburg has a heterogeneous structure. In this regard, the management of the process of taxation of land and property must take into account the heterogeneity of these objects.

In the context of the study, it is necessary to define the following concepts: system - the territory on which the land tax is collected; process - the determining of land tax with taking into account the parameters that characterize it. The state of the system is the state of the territory at a given point in time of the tax calculation process.

We assume that real estate objects were formed as a result of some process and their characteristics (in this case, the area) can be represented as Shewhart Control Charts (SCC) [7]. Some objects will have characteristics above the upper specification level (upper specification level USL), part below the lower specification level (LSL).

$$USL = \bar{X} + \sigma_x$$
$$LSL = \bar{X} - \sigma_x$$
$$\sigma_x = \sqrt{\frac{\sum(X-\bar{X})^2}{n}}, \quad (1)$$

where σ - is the standard deviation, $\bar{x}$ - arithmetic mean value.

In this case, one can make an assumption that exit of the chart line out the SCC corridor indicates the presence of some heterogeneity of data objects of taxation (Fig. 1 - Shewhart Control Chart for the size of the area of retail activity objects). Therefore, on the basis of the SCC, it is possible to distinguish objects whose land tax size is formed under the influence of special causes, that is, non-random and non-market ones. Accordingly, in a heterogeneous statistical data set one can distinguish the main array of objects, which is created formed under the influence of the reasons determined by the system variability of the process of forming an array of land taxation objects.

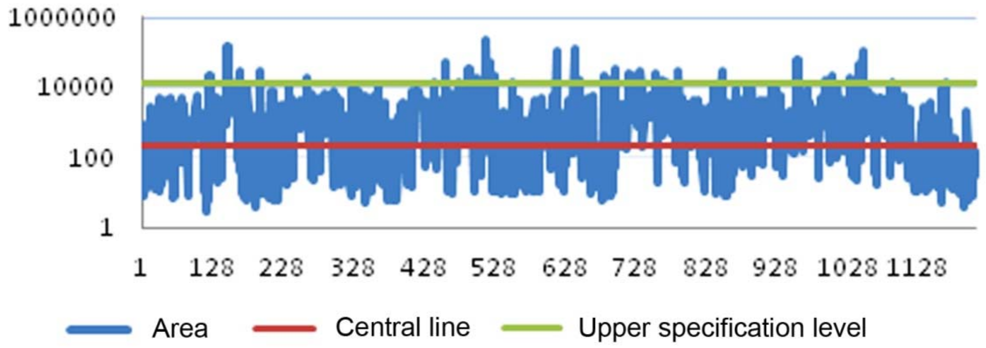

FIGURE 1. Shewhart Control Chart - size of the area of retail activity objects.

The homogeneity of objects in statistical analysis is of great importance, since it has a direct impact on the accuracy of the calculation of indicators and the quality of analytical conclusions. The more homogeneous the data, the more reliable are the results of statistical analysis.

The main measures of homogeneity of the data are such indicators as: variance, standard deviation, average linear deviation. However, they are all related to the scale of the source data and do not provide an independent (relative) characteristic of the measure of dispersion. The relative characteristic of homogeneity is the coefficient of variation, which is calculated as the ratio of the standard deviation and the average value of the parameters of the objects under study. To assess the homogeneity of the statistical set of the retail spaces, the coefficient of variation V was calculated [7]:

$$V = \frac{\sigma}{\bar{x}}, \quad (2)$$

As can be seen from Table 1, the variation coefficients for different types of retail space in Yekaterinburg differ significantly (from 1.10 to 5.33 in terms of area and from 0.80 to 5.17 in terms of tax), which indicates the heterogeneity of this data.

In accordance with [8], systems similar to the Yekaterinburg city system considered here are subject to power laws and have fractal properties, as is observed in many environmental and economic problems [9, 10]. Therefore, it can be assumed that the set of land taxation objects of Yekaterinburg may also have fractal properties that maybe evaluated and taken into account.

TABLE 1. Coefficients of variation for the area of retail activity objects of Yekaterinburg city.

Kind of objects	Coefficient of variation (V)	
	On area size	On tax size
Land under high-rise buildings	1,10	1,19
The land under the houses of individual residential buildings	1,35	1,29
Lands of gardening associations of citizens	2,54	2,11
Lands under garages and parking lots	1,23	0,80
Lands under shopping centers and buildings of service companies	1,45	1,49
Lands under educational institutions and organizations	1,17	1,42
Lands under industrial objects	3,23	2,10
Lands under administrative, managerial and public facilities	1,61	1,80
Lands under military objects	4,29	2,62
Lands under the objects of medical and recreational purposes	1,81	1,46
Agricultural land	3,41	2,78
Lands under urban forests	5,33	5,17
Lands under water bodies	4,99	4,67
Other land of settlements	2,20	1,37

To assess the fractality of the objects of the database under study, it is necessary to determine the fractal dimension of the objects D. The ratio of the exponent of the rank power distribution β and the fractal dimension of Hausdorff D for the fractal structure formed of the elements, which dimensions are characterized by the integer characteristic dimension Dc, has the following view:

$$\beta = \frac{D_c}{D}, \tag{3}$$

For three groups of the retail activity objects of Yekaterinburg city (low, medium and big sizes) rank power distribution coefficient equal correspondingly: $\beta 1 = 0{,}911$; $\beta 2 = 2{,}156$; $\beta 3 = 8{,}535$.

We assume that the characteristic dimension for the retail space is 2. Then the Hausdorff dimension for these groups of the retail spaces is: D1 = 2,195; D2 = 0,928; D3 = 0,234.

Thus, the objects of commercial real estate in Yekaterinburg of different area size may be devided in 3 groups with different fractal dimension from 0.2 to 2.2 (Fig. 2). The coefficients of variation for these groups are: V1 = 200%, V2 = 16%, V3 = 76%.

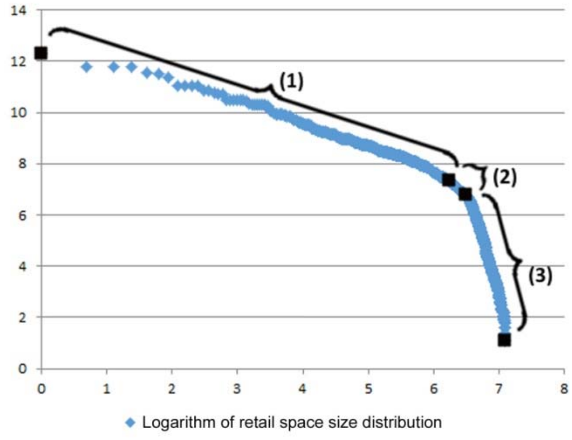

FIGURE 2. Groups of the objects with different fractal dimensions: 1, 2, 3 - objects of small, medium and large area, respectively.

It can be concluded that to analyze the information on the second group, which is homogeneous, one can apply the standard means of statistical data processing. The first and third groups are substantially non-uniform, so to calculate the value of the tax for these group's objects additional information is required that takes into account the individual characteristics of these objects.

CONCLUSION

As a result of the study, a database of land taxation objects of the city of Yekaterinburg was created. The data analysis has shown that in most cases the data sets, characterizing the objects of study, are heterogeneous. It has been proposed to use Shewhart Control Charts for identifying objects, the amount of land tax of which is formed taking into account non-random and non-market reasons. Accordingly, a homogeneous array of land taxation objects was selected in the common base, which is formed under the influence of market factors determined by the system variability of the process under study.

It was made an assumption that in Yekaterinburg it is possible to mark out fractal structures with different values of the Hausdorff dimension in the aggregate of land taxation objects. Based on the conducted fractal dimension calculations, three groups of objects was determined for the further calculation of the land tax amount.

REFERENCES

[1] Ilyina A.V., Ilyin A.S. "Balanced application of new property tax collection mechanism", Problems of the modern economy, № 2 (54), 237-240 (2015).

[2] M. Medvedeva, S. Parusheva. "Application of Information Technologies in Management of Greenhouse Gases and Wastes", in *6th International Multidisciplinary Scientific GeoConference SGEM 2016, Conference Proceedings, Book 2, Vol. 1* (2016), pp. 49-54.

[3] Yu.E. Kharitonov, D.B. Berg, Maxim Medvedev, Nikolay Medvedev. "On a Relational Model of the Production Nomenclature Information Management", AIP Conference Proceedings 1978, 440022 (2018).

[4] O.A. Iskra, E.A. Sizonenko, Marina Medvedeva. "Imitation Model of Decision Support for Mobile Applications Lifecycle Management", AIP Conference Proceedings 1978, 440012 (2018).

[5] Dmitry B. Berg, Igor L. Manzhurov, Konstantin L. Antonov, Ayapbergen Taubayev, Victoria F. Turygina "Decision-making in waste management: scenarios evaluation", IFAC-PapersOnLine Vol. 51, Issue 32, 125-129 (2018).

[6] Ayshan Gasanova, Alexander N. Medvedev, and Evgeny I. Komotskiy. "he assessment of corruption impact on the inflow of foreign direct investment", AIP Conference Proceedings 1836, 020011 (2017).

[7] *General Theory of Statistics: a Textbook*, ed. Yefimov E.V. (INFRA-M, Moscow, 2009).

[8] Gushchina E.S., Smogunov V.V. "Fractal dimension in the evaluation of the planning structure of a large city", Electronic scientific and practical journal "Modern Scientific Research and Innovation", № 2 (2016), available at: http://web.snauka.ru/issues/2016/02/63202 (visited 23.09.2018).

[9] D.B. Berg, A.N. Medvedev, I.L. Manzhurov, and A.A. Taubaev. "Use of Fractal Models in the Earth's Remote Sensing of the Arctic Zone", AIP Conference Proceedings 1789, 020007 (2016).

[10] T.O. Zagornaya, M.A. Medvedeva, V.L. Panova, K.F. Isaichik, A.N. Medvedev. "Possibilities of fractal analysis of the competitive dynamics: approaches and procedures", AIP Conference Proceedings 1906, 070011 (2017).

Analysis of the Learning Curve in a Foreign Language Study: The Methods Development

Zh.A. Mukanova[1, a)], D.B. Berg[1, b)], M. Kit[2, c)], E.B. Berg[3, d)], A.N. Medvedev[1, e)]

[1]*Ural Federal University, Mira 19, Ekaterinburg, Russia, 620002*
[2]*Language Interface Inc., 1st Ave. 1221, Seattle, USA, 98101*
[3]*Ural State Law University, Komsomolskaya Street 21, Ekaterinburg, Russia, 620137*

[a)]zhanna.mukanova.83@mail.ru
[b)]bergd@mail.ru
[c)]clodpool@gmail.com
[d)]elenabkct@gmail.com
[e)]Corresponding author: alnikmed52@gmail.com

Abstract. This article describes the outcome of the studies aimed at development of methods for obtaining the learning curve (LC) for foreign language learning. It also suggests ways for the use of the learning curves. Two types of LC were obtained: short-term and medium-term memorization. Comparative analysis of the two curves suggests that the subject continues learning for up to 14 hours after the completion of a flash memory session since medium-term memorization tests readings are consistently higher than those for the short-term memorization. The paper presents various approximations of the learning curve and the functions that fit best the LC for foreign language learning. Based on a comparison of the results of the approximations of the experimental LC by functions of various types a conclusion has been drawn that all of them provide satisfactory results, with logarithmic and polynomial approximations slightly better than the others. Based on these findings, forecasts for subsequent learning achievements and proposals for further studies are made.
Keywords: Learning curve, LexSite dictionary, foreign languages, learning efficiency.

INTRODUCTION

Any human activity is preceded by a learning phase. The learning curve shows the relationship between human performance and time spent for learning. Learning Curve (LC) is a graphic image of the student's achievements in learning the assigned subject. LC models are an important technique for making predictions on how long it will take to complete future tasks. One of the most widely used forms of monitoring and assessment of the knowledge of a foreign language today is testing, as shown in [1] and [2] and it is advisable to use it to build a learning curve.

Learning curves are widely used in various branches of human activity. In particular, for the industry, Argote [3], Morgunov [4], they call LC one of the most effective tools for monitoring the workers' productivity when performing repetitive tasks, which leads to a reduction in technological losses due to the inexperience of workers in the first production cycles. In Wahab and Jaber's research [5], the authors used LS to analyze and control production operations. And Grahame [6], Nembhard and Uzumeri [7], in their studies, examined LC for the distribution of tasks among workers in accordance with their training profiles. The analysis presented in the researches above, was carried out using various mathematical models.

Table 1 shows two examples of learning curve formation: in an industrial enterprise and in a medical practice.

Modern changes in society set new challenges for the educational system. One of these tasks is the development and introduction of new approaches to the organization and improvement of the learning process of a foreign language. This, in turn, increases the quality requirements of the organization of testing and evaluating learning

outcomes in order to obtain reliable objective information on the status and quality of educational achievements [10].

Thus, the purpose of this study is to develop a methodology for constructing and analyzing a learning curve when learning a foreign language.

TABLE 1. Examples of the learning curve.

№	Research object	Independent variable	Dependent variable	The formula for the analytical dependence of these variables
1	Production activity of an industrial enterprise	Cumulative production volume	Unit costs of an industrial enterprise	$y_t = ax_{t-1}^{-\gamma}$, where x_t — actual total production in the period t; y_t – agent labor time t; a - first production cost; γ - learning process constant (labor intensity reduction agent's rate [8].
2	People (healthy and with various psychological dependencies)	Session sequence number	Number of the memorized words	$y = B2e^{-B1(x-1)} + B3(1 - e^{-B1(x-1)})$, where x — training session number; y – number of the memorized words; B2 — the initial state of learning, i.e. number of words known before the start of training; B3 — the asymptotic value of the learning degree, i.e. maximum number of words memorized for the entire training period; B1 – system characteristic [9].

METHODS

To conduct an experiment on the LC formation when studying a foreign language, an English-Russian dictionary was compiled containing 50 words-terms on the subject of the "learning curve". The study of vocabulary was carried out using flash cards daily (2 sessions per day) for 20 minutes in the English-Russian dictionary mode with simultaneous sound reproduction of the words studied. Thus, 2-3 demonstrations of each flash card were carried out for each session. Verification of the obtained knowledge was carried out using testing, which also consisted of flash cards. Each flash card shows the word in English and the proposed translations; you had to select one correct translation. It was given 10 seconds to answer. Testing took about 9 minutes. Taking the test daily allowed us to obtain a comprehensive assessment of the acquisition of the vocabulary contained in the dictionary.

Figure 1 shows the timing diagram for the training. To analyze the short-term memorization of the words, a session was conducted in the evening using the algorithm "first study vocabulary using flash cards, then test knowledge with a test". To analyze the mid-term memorization of words, the session was conducted in the morning. At the beginning of each session, testing was conducted, then they worked with flash cards. A total of 5 periods of study were conducted.

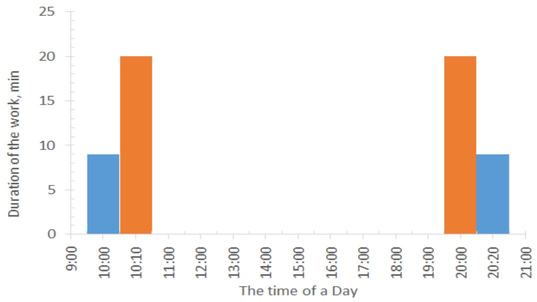

FIGURE 1. Experiment scheme (- test; - work with flash cards).

So this scheme allowed us to construct two types of the learning curve: the learning curve of medium-term memory, i.e. verification of memorization 14 hours after learning (morning data), and the learning curve of short-term memory, i.e. verification of memorization immediately after training (evening data).

When conducting a study of the learning curve when learning a foreign language, the LexSite reference and training system [11] were used, which incorporates tools that allow translators, engineers, teachers, researchers, students - everyone for whom inter-language communication, to learn foreign vocabulary in the English-Russian language pair is relevant [12]. To track the effectiveness of the word learning process, the LexSite system provides analysis tools for building a learning curve.

RESULTS

Table 2 shows the results of tests conducted during the experiment.

TABLE 2. Test results.

Period of study	1	2	3	4	5
Medium term LC, %	78	81	89	89	91
Short term LC, %	68	81	80	87	89

The obtained experimental data were approximated by four different functions (Table 3). To assess the quality of the approximation, the coefficient of determination R2 and the standard deviation (SD) were calculated.

TABLE 3. Approximation of experimental data.

Function	Formula	LC	A	B	C	SD	R2
logarithmic	$y = A + B\ln x$	Short term	69,1	12,4		7,9	0,9257
		Medium term	77,3	8,6		5,6	0,9183
Power-mode	$y = Ax^B$	Short term	69,2	0,2		8,0	0,9215
		Medium term	77,5	0,1		5,5	0,9210
polynomial	$y = Ax^2 + Bx + C$	Short term	-1	10,8	59,6	5,5	0,9052
		Medium term	-0,7	7,7	70,4	7,8	0,9355
exponential	$y = Ae^{Bx}$	Short term	67,2	0,1		7,8	0,8327
		Medium term	75,725	0,0402		5,4	0,8778

The analysis of the values of the standard deviation and R2 showed that the most accurate data were obtained when making a logarithmic approximation for analyzing short-term memory and polynomial approximation in the case of analyzing medium-term memory. Figure 2 shows the learning curves resulting from the experiment.

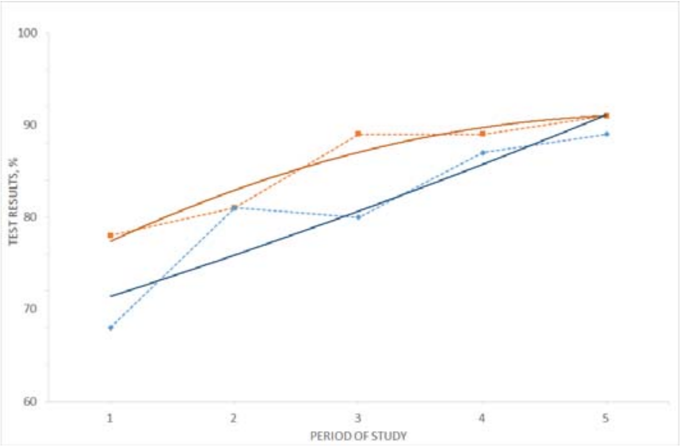

FIGURE 2. Learning curves obtained as a result of the experiment.
(- accurate data (LC short-term); - approximated data (LC short-term);
- accurate data (LC medium-term); - approximated data (LC medium-term)).

The results of the experiment as a whole show a practically monotonous increase in the memorization of foreign words from one session to another, which is consistent with all known data on LC.

A comparison of the two curves clearly shows that the subject keeps learning for 14 hours after the flash memory session since the test results for the medium-term memory are consistently better than those of the short-term memory.

On the basis of a comparison of the results of approximation of an experimental LC to functions of various types, it can be concluded that all of them give satisfactory results, and the logarithmic and polynomial approximations turn out to be more accurate.

The approximation of test results with analytical functions allows us to predict and calculate the number of days required to study this dictionary in full, so that a 100% test result would be obtained. The calculations showed that in order to fully memorize all 50 words of the dictionary (obtaining a 100% test result), it would be necessary to spend 12 days.

DISCUSSION AND CONCLUSIONS

The result of this work is the methods development for learning foreign languages and tracking results through the LC formation. For data analysis, several ways of data approximation were considered, which allows making a forecast of learning foreign languages. The data on the dynamics of the learning process, obtained as a result of the experiment, suggest that the developed technique can be applied in the study of foreign languages in various educational institutions.

To continue the experiment on the development of methods and study of the application of the learning curve in the study of foreign language in the future requires a set of statistics on the construction of the forgetting curve.

REFERENCES

[1] V.V. Vonog, E.A. Ponomareva, T.V. Zhavner, "Testing as an efficient means for controlling the level of foreign language acquisition among students of engineering majors", Problems of socio-economic development of Siberia. Bratsk State University (Bratsk), No. 2 (24), 148-151 (2016).

[2] L.V. Yarotskaya, *Control in the productive paradigm of linguodidactics* (Saarbrüchen: LAP, 2011).

[3] L. Argote, *Organizational learning: Creating, retaining and transferring knowledge*. (Springer, NewYork, 1999).

[4] V.M. Morgunov, "The effect of the learning curve as a result of iterative learning", *in 15th International Scientific Practical Jubilee Conference: Conference proceedings. Karlik A.E., E.H. Lokshina. Innovation and Marketing Center "Science of Higher School - St. Petersburg"* (2015), pp.230-235.

[5] M.I.M. Wahab, M.Y. Jaber, "For quality, different holding costs", Computers & Industrial Engineering, No. 58 (1), 186–190 (2010).

[6] S. Grahame, "The learning curve. The key to future management?", Chartered Institute of Management Accountants, No. 6 (12) (2010).

[7] D.A. Nembhard, M.V. Uzumeri, "An individual-based description of learning within an organization", IEEE Transactions on Engineering Management, No. 47 (3), 370–378 (2000).

[8] O.V. Pavlov, "The dynamic task of maximizing the profits of the enterprise, taking into account the demand and the effect of the learning curve", ECONOMIC SCIENCES: LLC "Economic Sciences" (Moscow), No. 133, 26-29 (2015).

[9] I.I. Stepanov, O.M. Efremov, N.B. Suvorov, M.M. Danilovskiy, N.P. Maidanov, S.P. Shklyaruk, "Informativeness of the mathematical model of the learning process", Information management systems, No. 1 (50), 34-40 (2011).

[10] E.B. Berg, M. Kit, "Formation of control materials for assessing the qualifications of an interpreter: the cognitive aspect", Scientific journal "Modern linguistic and methodological-didactic research", Voronezh: Voronezh State. tech. university, No. 4 (40) (2018).

[11] E.B. Berg, M. Kit, "Lexicography in networks", *in Crossing Borders: Intercultural Communication in a Global Context: Collection of materials I Intern. scientific-practical conf. Moscow. A.S. Pushkin State IRA* (2018), pp. 129-131.

[12] E.B. Berg, M. Kit, "LexSite Personal Learning Dictionary as an interactive learning tool", *in Problems of modernization of modern higher education: linguistic aspects. Linguistic and methodological problems and trends in the teaching of foreign languages in a non-linguistic university: Proceedings of the IV Intern. scientific conference* ("Ippolitova" Publishing house, Omsk, 2018).

Regression Model of Sales Manager Behavior: Forecast and Experimental Confirmation

A.A. Polozov[a)], M.V. Kraev[b)], A.V. Rolis[c)], A. Noyakshev[d)], A.N. Medvedev[e)]

Ural Federal University, Mira 19, Ekaterinburg, Russia, 620002

[a)]A.A.Polozov@mail.ru
[b)]kraev-antooz@ya.ru
[c)]al.v.rolis@gmail.com
[d)]nojakschevsascha@mail.ru
[e)]Corresponding author: alnikmed52@gmail.com

Abstract. The aim of our study was to create a rapid computer test for the selection of a sales manager with a prognostic estimate of the expected turnover. The methodology of such testing assumed the selection of the most significant criteria of employers, the formation of an adequate typological model of the manager's personality (personality type, character, and intelligence), the search of the inflection point in the test results and the formation of the regression equation of the expected turnover on their basis. Formed from 82% of employers' requirements, a regression equation based on 5 short tests 72 sales managers gave an expected turnover of a manager who had a correlation coefficient with a real turnover of r=0.89. This indicator turned out to be high due to the fact that in each studied characteristic they found an inflection point in the test results which was taken as 100%. The typological model of the structure of personality based on the Myers-Briggs personality types, character and intelligence types allows solving the problem of selecting a sales manager economically and efficiently. However, the difficulties of self-identification of the person being tested make it difficult to automate this process.
Keywords: personnel, personality type, type of character, turnover, sales manager.

INTRODUCTION

Sales managers are the most sought-after category in the Russian labor market. However, in the first year more than half leave this job. The high turnover of staff creates significant difficulties for the employer, is unfavorable for working with clients in general. Selection of a new sales manager becomes an ongoing task. At the same time, the construction of a selection methodology that would allow achieving a sustainable solution to the problem is possible from various considerations.

In [1] considered that for a sales manager, sociability, responsibility, initiative, emotional stability, organizational skills, and purposefulness are necessary. To assess these qualities, the authors used the R. Kettel test, the questionnaire KOS-2, questionnaire O.F. Potemkina, the method of "style of self-regulation of behavior." D.K. Dikova [2] considers it sufficient for the evaluation of the personnel manager to test the motivation to succeed and avoid failures of T. Ehlers, and to assess the communicative and organizational skills of B.A. Fedorshina (CBS). Evaluation of Communicative and Organizational Propensities (CBS) B.A. Fedorishina suggest an assessment of communication and organizational skills by the percentage of expected answers from their maximum value. This technique allows the subject to easily determine what is expected of him. It does not imply the specifics of the work. In his book, S. Ivanov [3] itemizes at least 30 different aspects of the sales manager's work: adaptability, active listening, ambition, activity, analytical thinking etc. That they list so many positive qualities at once is bad. The essence of the work of the manager remains unclear. However, part of this list coincides with the strengths of the individual. Mark K. [4] compared the experience and training of sales managers. Experiences with the seller, and to

a lesser extent, preparation are the basis of sales presentation skills. The professionalism of the seller when using adaptive sales techniques is associated with increased productivity [5].

THEORETICAL BACKGROUND AND HYPOTHESES

Authors [6] and [7] set out the modular typological structure of the personality in relation to the field of sports. In theses we recall its content. The majority of psychologists of the past favored a three-component personality structure: Z. Freud - Conscious (ego), unconscious (moral norms, instincts of life and death); S.L. Rubinstein - orientation, ability, temperament and character; R. Cattel - interests, abilities, temperament; A.G. Kovalev - ability, focus, character; K.K. Platonov - socially determined inclinations, experience, biologically determined inclinations, individual characteristics. Based on the foregoing, the author in 2005 proposed to "place" the types known to all in each of the three spheres: in the sphere of "orientation of interests" - 16 TL (Myers-Briggs, Jung K); in the sphere of "will and feelings" - 8 TX (V. Talanov and others.); in the "associative-intellectual" - 7 types of intelligence (Gardner G.). If THB (ENTP, ISFP, etc.) are well known, the types of character are still under discussion. The types of character influence on the relationships of people to the greatest degree. Of the many works gradually outlines the 8 types of character. McWilliams (1998), Naranjo (1998), Popov, Weed (2000), Lowen (2000), Horney (1995) identified: 1. Schizoid 2. Paranoid 3. Narcissistic 4. Psychopathic 5 Compulsive 6 Hysterical 7 Depressive 8. Masochistic.

Most manager selection formulas have a KPI rating format:

$$KPI = \sum_{I=1}^{n} \delta_I \times \frac{Fact\ i}{Plan\ i}$$

Where i - directions of work with the formation of the planned results Plan i are distinguish from the manager. However, there are innovations. As is known, the index values in the UN rating are calculated according to the formula proposed in 1990 by Pakistani economist Mahbub ul-Haq:

$$IRHP = \frac{F - min}{\max - min}$$

By analogy with this indicator, some formulas for the effectiveness of a sales manager have changed:

$$Index\ KPI = \sum_{i=1}^{n} \delta i \times \left(\frac{Fact\ i - \min i}{\max i - \min i}\right)$$

The authors [1] went further. They identified all the mentioned qualities of a manager in the literature and made up a matrix, where each selected manager property in the matrix had an upper (b1) and lower bound (w1):

$$x = \begin{bmatrix} [w_{11}; b_{11}] & \cdots & [w_{1n}; b_{1n}] \\ \vdots & \ddots & \vdots \\ [w_{n1}; b_{n1}] & \cdots & [w_{nn}; b_{nn}] \end{bmatrix}$$

An interesting formula for assessing the professional viability of an employee was suggested by N Yagunova N.:

$$K = Oobr \times \left(1 + \frac{C}{4} + \frac{B}{18}\right)$$

Oobr - assessment of the level of education (0.15-1); C - work experience in the specialty; B - age.

THE METHOD AND THE EMPIRICAL RESULTS

Objective: to create a rapid test for the selection of sales managers with a prognostic estimate of the expected turnover.

Step 1. Requirements of employers. 130 of the most typical ads on the sales market in Yekaterinburg (Russia) were taken which list the requirements for applicants. These opinions are grouped and summarized.

Step 2. Tests meeting the requirements of employers and the typological model of the personality structure. If you summarize all the requirements of 130 employers who advertised for a sales manager, they are looking for a 24-year-old girl with hysterical TX, TL ESFP, with 5 years of experience, who is able to determine the most significant motivation of the interlocutor, and to show the benefit in the interlocutor's priorities and knowledgeable in enterprise technology.

Step 3. Forming the necessary test base. As to type of person, testing of THB consisted of two different tests: the traditional MBTI and the good test of Weissband I. D. (1992) living in Germany. As to type of character, the test was familiarity with the annotation of TX and the phased reduction of their number at the expense of obviously not suitable for testing. The description was based on Talanov V. (2003).

Step 4. Logistic nature of dependence. In the tests intellectual abilities were measured among other things. It is useful to see their evolution from age. Figure 1 can be interpreted as a graph of two combined logistic curves: ascent and degradation. An inflection point can be obviously seen in any graph of dependence of the test result.

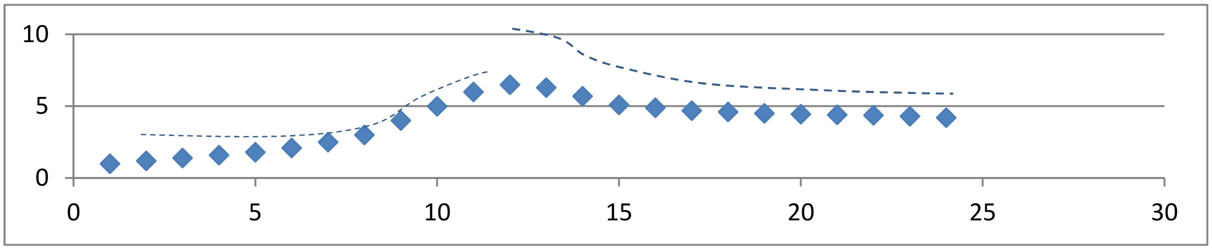

FIGURE 1. Schematic division of the schedule into two combined logistic curves: ascent and degradation.

In biology, logistic dependence is:

$$P(t) = \frac{K \times Po \times e^{rt}}{K + Po \times (e^{rt} - 1)},$$

where K is the strategy of slow population growth, r is the strategy of rapid population growth, P is the population size. However, another formula is more common in management where N is the number of product consumers, x is consumers familiar with advertising:

$$x = \frac{N}{1 + (\gamma - 1) \times e^{Nkt}}$$

Step 5. Experimental part. Testing was performed on the basis of the "Sales Expert" (headed by Dmitry Gubin), 2GIS and Abak Press companies (all companies from Ekaterinburg, Russia). 134 managers of these companies were tested. Only 72 managers went through the procedure for dual testing of TL and TX. They indicated the same TL, TX in two different tests. The remaining participants were eliminated. The criteria for the work of the manager were considered the total value of the goods ordered by his clients (Table 1).

Types of character. For TX, a turnover averaging procedure was performed for each TX. According to the results of testing, the following deviation from the average turnover value was received: Schizoid -20, paranoid +25, narcissus -11, Psychopathic -40, compulsive +20, hysterical +44, depressive +2, Masochistic +4

The correlation coefficient with a turnover of 0,47. Range of values -20: +20 = 40

Sex of manager. The average turnover of women is 100, men - 73, with an average turnover of 83. The correlation coefficient with turnover is r = 0.4. Accordingly, in the case of a woman being tested, the intended turnover was increased by 17, and in the case of a man it was reduced by 10.

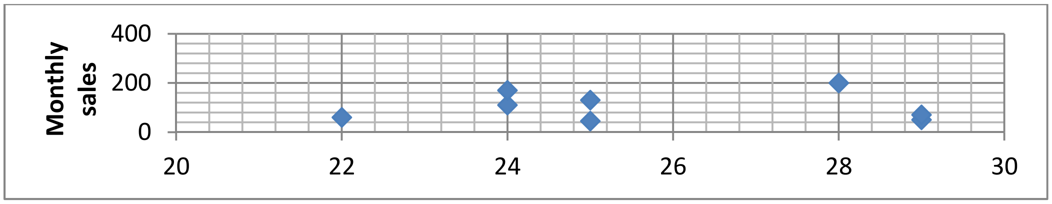

FIGURE 2. Age of sales managers, men GIS, materials after averaging.

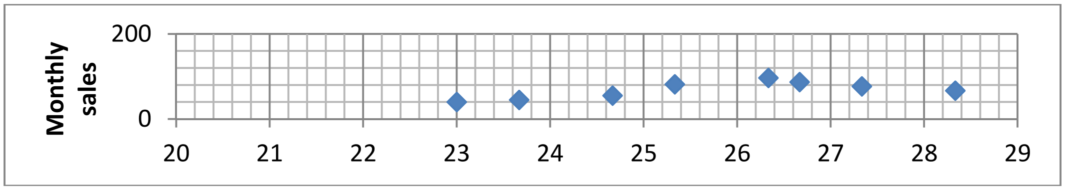

FIGURE 3. Age of sales managers, women, GIS direction building, the direction of transport services without data.

As to age of manager, for 100%, a girl was 24 years old, men were 26 years old (Fig. 2, 3). Since the turnover in the companies under consideration differed, it is more correct to take data for each separately. For each year below girls of 24 were reduced to the expected estimate by 26.8 units of conditional turnover.

As to work experience, the correlation coefficient is a turnover of 0.81. The average work experience left 1.6 years. Each year, the length of service gives a gain of 32 in turnover.

Marketing test. The inflection point is 8 correct answers from 15. A deviation of 1 answer gives a decrease of 10 units of turnover. The expected turnover of the manager P in arbitrary units is equal to the sum of the average for all existing employees of Pcp, the significance of TL (P (TL)), TX (P (TX)), Pexp experience, age of Page, test result for understanding the motivation of the interlocutor Ppsy, the result of the marketing test P:

$$P = P_{average} + P_{TL} + P_{TX} + P_{m/w} \pm 32 \times \left(P_{exp} - 1{,}6\right) \pm 27 \times \left(P_{age} - 24\right) + 40 \times \left(P_{psy} - 4\right) + 10 \times \left(P_{\$} - 8\right)$$

TABLE 1. Algorithm for calculating the expected turnover of the manager.

Name	Man/ woman	Type of personality	Type of character	Work experience	Age	turnover	Man/ worman	Type of personality	Type of character	Work experience	Age	Interperson al test	Marketing test	Estimated turnover	Turnover actually
Ив	ж	ISTj	7	2	24	98	14	-13	-2	12.8	0	0	0	109.8	**110**
Пл	м	ESFJ	4	1	23	98	-14	-8	-44	-19.2	0	0	0	12.8	**40**
Кр	м	ESTJ	8	1	26	98	-14	-8	0	-19.2	14.3	0	0	71.1	**70**
Ти	м	ENFP	3	1	28	98	-14	-15	-15	-19.2	-14.3	-10	30	40.5	**80**
То	ж	ESFP	8	4	28	98	14	22	0	76.8	-12.4	0	0	198.4	**200**
Ви	м	ESTJ	3	0.5	22	98	-14	-18	-15	-35.2	-32.6	0	6	-10.8	**50**
Да	ж	INFP	2	4	24	98	14	33	21	76.8	0	20	-24	238.8	**170**
Чи	ж	ESTJ	8	0.75	22	98	14	-18	0	-27.2	40.2	-10	6	22.6	**60**
Ку	м	ISTP	8	0.5	24	98	-14	-16	0	-35.2	0	-10	-24	-1.2	**30**
Ко	м	ESFJ	2	1	27	98	-14	-8	21	-19.2	0	-10	21	88.8	**110**
На	ж	ISFJ	8	1	29	98	14	12	0	-19.2	-18.6	-10	6	82.2	**50**
Же	ж	ESFJ	8	2.25	29	98	14	-8	0	20.8	-18.6	20	-24	102.2	**70**
Correlation coefficient with turnover							0.46	0.69	0.52	0.81	0.24	0.39	0.1	0.89	

CONCLUSIONS

The use of the typological model of the structure of the personality made it possible to solve the daily task of selecting a sales manager. The expected and actual values of turnover for existing managers were obtained. Their correlation coefficient is r = 0.89. Of the parameters used, the greatest correlation with the result of the work was shown by TL and experience. The difference from the well-known tests is that the test does not rely on the subjective assessment of a specialist, but forms the expected turnover from the job of the applicant for the position. For each area of the sales manager, you need to create similar simple equations that retain high accuracy in specific conditions. To obtain an adequate model, it is necessary to adhere to the dome-shaped behavior of most of the patterns.

REFERENCES

[1] O.A. Chadenkova and D.S. Mishchenko, Bulletin of the Samara Humanitarian Academy. Series: Psychology, № 1, 57-61 (2007).

[2] D.K. Dikova, Bulletin of the Samara Humanitarian Academy. Series: Psychology, № 1, 67-81 (2007).

[3] S. Ivanova, *How to find your people* (Publishing house Alpina Publisher, Moscow, 2013).

[4] V. Vertogradov, *Sales management*, 2nd ed. (Peter, SPb, 2005).

[5] M.K. Johke, Journal of Business and Industrial Marketing, Vol. 21, Issue 5, 311-319 (2006).

[6] Yagunova N.A. Improving the system of personnel performance assessment at industrial enterprises, Ph.D. thesis, Saratov, 2004.

[7] E.K. Zavadskas, Z. Turskis, J. Tamosaitiene, V. Marina, Computer Modelling and New Technologies, Vol. 12, No. 3, 22–28 (2008).

Calculation of the Social Laziness Syndrome Level Indicators in the Game of Top-Level Sport Teams

A.A Polozov[a)], M.V. Kraev[b)], I. Kovyazina[c)], A.V. Rolis[d)], A.N. Medvedev[e)]

Ural Federal University, Mira 19, Ekaterinburg, Russia, 620002

[a)]A.A.Polozov@mail.ru
[b)]kraev-antooz@ya.ru
[c)]inna12.03@yandex.ru
[d)]al.v.rolis@gmail.com
[e)]Corresponding author: alnikmed52@gmail.com

Abstract. The aim of the study was to calculate instrumentally available indicators of reducing the level of results of highly professional top-level teams in football (1,458 matches), hockey (1,551 matches) and basketball (274 matches) in 2016-18 due to social laziness syndrome. Using the method of determining the rating of the team from the previous results the difference in the ratings of two participants in the upcoming match and the proportion of actually won victories was compared. Comparing the proportion of matches won with the advantage in the ranking it was found that the dynamics of compliance of these indicators begins to distort considerably with a significant advantage of one of the teams. In contrast to other works where the amount of social laziness could not be established experimentally, in the present work it is found that a team cannot expect more than 85% of the winning probability even with a huge advantage over an opponent. The effect of social laziness syndrome is quantified. It indicates itself in the games of unequal teams and allows a weaker team to gain an additional 10-17% of the won matches of professional teams of the top level.
Keywords: indicators, rating, social laziness, sport, top-level team.

INTRODUCTION

The Ringelmann effect was discovered in 1913 and means the individual contribution C of each of the K members of a group in common result:

$$\mathrm{C} = 100 - 7 \times (K - 1)$$

Social laziness is the tendency of people to make less effort when they unite their efforts for a common goal than in the case of individual responsibility. This phenomenon is studied in social psychology. In the literature one can find several names of this phenomenon: Ringelmann effect [1], social relaxation [2], social laziness [3], social parasitism [4], the effect of a parasite, or parasite ("sucker effect") and a "free rider effect". The phenomenon in question was called the Ringelmann effect in honor of the scientist who recorded it. In 1913 French agrarian M. Ringelmann found that the labor productivity of students in the performance of group tasks decreased as the group size grew.

THEORETICAL BACKGROUND AND HYPOTHESES

It can be assumed that conscientiousness can be the opposite of social laziness. The more conscientious a person is, the less inclined he is to be socially lazy. The study by Yut-Christine Klee and Neil Anderson found that conscientiousness is not related to the degree of social laziness. In the studies of other authors, a negative relationship was found between this personal characteristic and social laziness.

Several studies have been devoted to the problem of the connection between conviction in one’s own uniqueness and the expression of social laziness. The results of these studies indicate that the participants in the experiment who

considered themselves unique in the academic field showed social laziness (when performing a task of brainstorming), while in subjects with low indices for this characteristic social laziness was not detected [5]. However, in further studies it was found that people convinced of their uniqueness in a situation of collectively performing an assignment can show social compensation, that is, intensify their efforts in group performance of the assignment due to the expectation of low productivity of other group members [6].

THE METHOD AND THE EMPIRICAL RESULTS

Research methodology. By rating, the authors understand the result of the participant in the global hypothetical macro tournament among all participants for the year (1). The result of the game is Z - goals and P - goals conceded. The difference between Z and P during the season splits into differences in each match separately.

$$Z - P = Z_1 - P_1 + \cdots . + Z_N - P_N$$

$$\frac{(Z-P)}{(Z+P)} = \frac{(Z_1+P_1)}{(Z+P)} \times \frac{(Z_1-P_1)}{(Z_1+P_1)} + \cdots + \frac{(Z_n+P_n)}{(Z+P)} \times \frac{(Z_n-P_n)}{(Z_n+P_n)}$$

$$\Delta = \delta_1 \times \Delta_1 + \cdots + \delta_n \times \Delta_n \ (2)$$

By definition, rating is a positive number. Therefore, it is necessary to shift upwards on a numerical scale by such a value at which the rating of the weakest of the participants will be a positive value:

$$2200 + \Delta = 2200 + \delta_1 \times \Delta_1 + \cdots + \delta_n \times \Delta_n$$

$$Rt = \delta_1 \times Rt_1 + \cdots + \delta_n \times Rt_n$$

$$Rt_i = \sum_{i=0}^{n} (\delta_j \times Rt_j) + \Delta_i$$

The authors forget that when they write the equation for determining the rating of a competitor they form a system of linear equations (hereinafter referred to as CASE) n.

$$\begin{cases} Rt_i = \sum_{i=0}^{n} (\delta_j \times Rt_j) + \Delta_i \\ Rt_{average} = (\sum_{i=1}^{N} Rt_i)/N \end{cases}$$

Participant rating during the season may significantly change. Therefore, it is advisable to consider both the rating for the entire season and the current value. The latter should most closely match the expected result of the next match. We can compare the interval in the form of the number of last rounds for the calculation of the rating and the accuracy of the forecast. Too small an interval results in a large error due to a lack of results. Too much spacing yields a lot of stale data. The interval between these segments is the interval with the greatest accuracy, but its boundaries are blurred due to the asynchrony in the dynamics of different participants. The best accuracy of the prediction for the upcoming match from the rating will be when receiving the SLN by the latest 8 results in football, 9 - in hockey, 5 - in basketball.

The following results were taken:

- 1458 matches of the championships of Italy, Spain, England, Germany, Russia in football in the 16/18 season.
- 1551 Continental Hockey League 2016-2018 games
- 274 VTB United League basketball games 2016-18.

We considered the teams rating through the decision of SLN by the latest 8 results in football, 9 - in hockey, 5 - in basketball. They compared the advantage in such a rating of two teams meeting in the next round and in fact the result obtained. In the course of the study, a form of logistic dependence with the smallest dispersion with experimental points was selected. General view of this form of logistic dependence:

$$\% = \text{Co} \times \text{Bo} \times \exp(-\Delta/\text{Ao})/(\text{Co} + \text{Bo} \times (\exp(-\Delta/\text{Ao}) - 1)),$$

where % is the proportion of matches won by teams with the advantage Δ = Rt (1) -Rt (2). The averaging was carried out over 100 points — the games with the closest value to the advantage of the home team at Δ = Rt (1) -Rt (2). For different performance in hockey (Z + P <4 washers, Z + P = 4-6 washers, Z + P> 6 washers):

$$\% = 0{,}7 \times 0{,}4 \times \exp(-\Delta/433)/(0{,}7 + 0{,}4 \times (\exp(-\Delta/433) - 1))$$

$$\% = 0{,}8 \times 0{,}47 \times \exp(-\Delta/327)/(0{,}8 + 0{,}47 \times (\exp(-\Delta/327) - 1))$$

$$\% = 1 \times 0{,}37 \times \exp(-\Delta/315)/(1 + 0{,}37 \times (\exp(-\Delta/315) - 1)).$$

Co coefficient plays the role of a "maximum" in this dependence. It can be seen that as the result of the match (Z + P) increases, the "maximum" also grows.

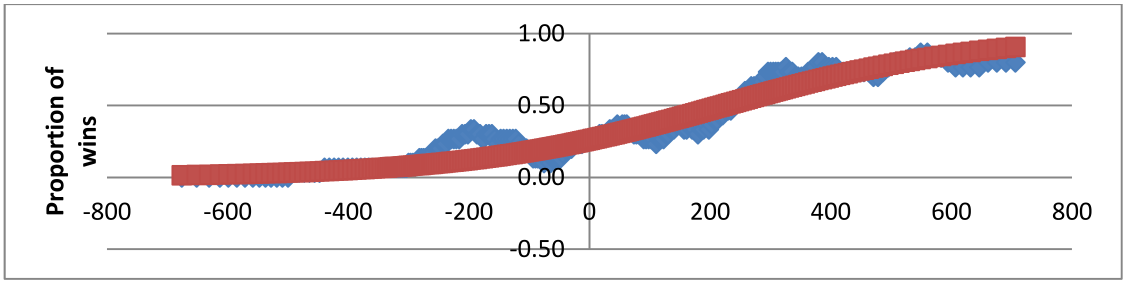

FIGURE 1 The probability of winning the home team for 574 games of the five leading football championships in 2016-18. The behavior of experimental points (blue line) and the overall view (red line).

The behavior of the logistic curve (Football, G + P <2, 574 games of the leading championships 2016–18) averaged over 50 values of experimental points and the least squares constructed by the least squares method is far from a perfect match.

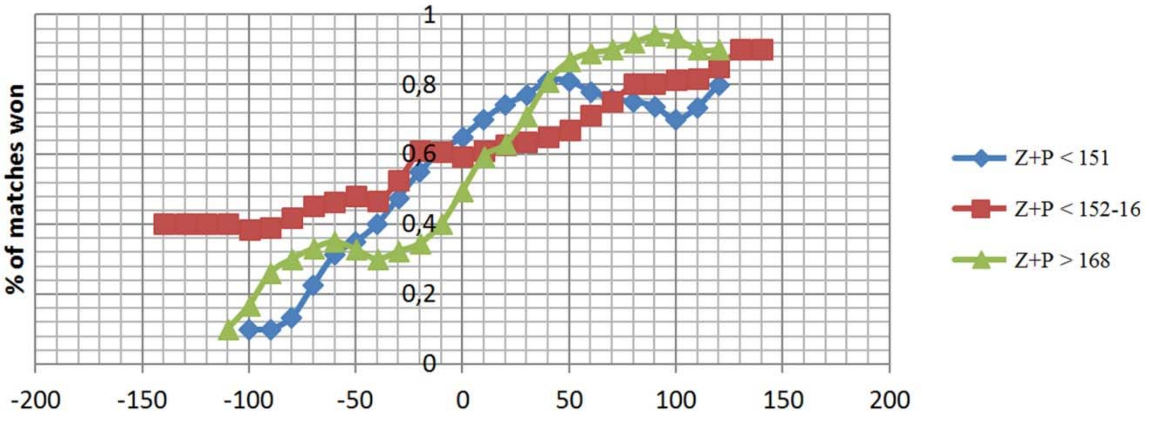

FIGURE 2 Dependence of the won matches proportion on the advantage in the ranking of the home team VTB 16/18.

A large number of points determines the type of dependence, which, given a certain advantage of one of the parties, gives a 100% probability of winning a match. However, we do not see this on real graphs No 6-8. On the contrary, as can be seen from graphs No 6-8 of three different and the most popular game sports the probability of winning the match practically never rises above 85%. This is the observed phenomenon of "social laziness." Schematically, this phenomenon can be represented as in Fig. 3.

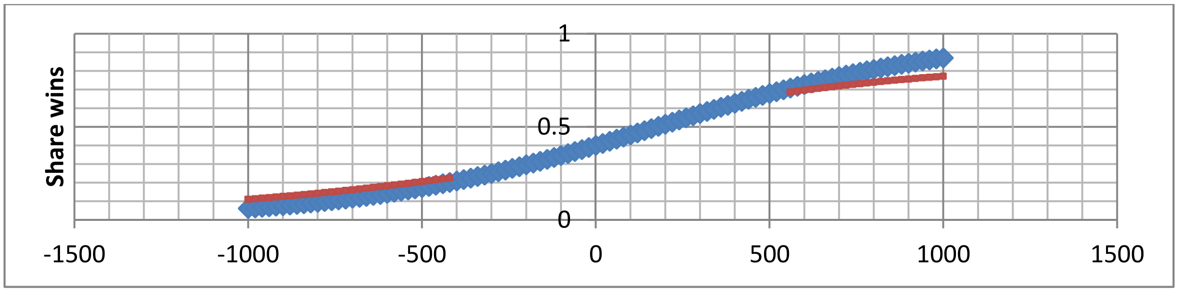

FIGURE 3. Schematic representation of the social laziness phenomenon in the game of top-level teams.

Since we are talking about teams playing in the same tournament of the highest level, then there is no reason to see the meeting of very different opponents. In the vast majority of games, the chances of the teams to win are 40% - 60%. This dominant mass of points on the graph is near to zero level of advantage in the rating. The same group of points forms the entire graph to a greater extent which is obtained by the method of least squares. However, we

visually observe a departure from this graph at the boundaries of the interval. This deviation makes it almost impossible to exceed the chances of winning a match of one of the teams above 85%.

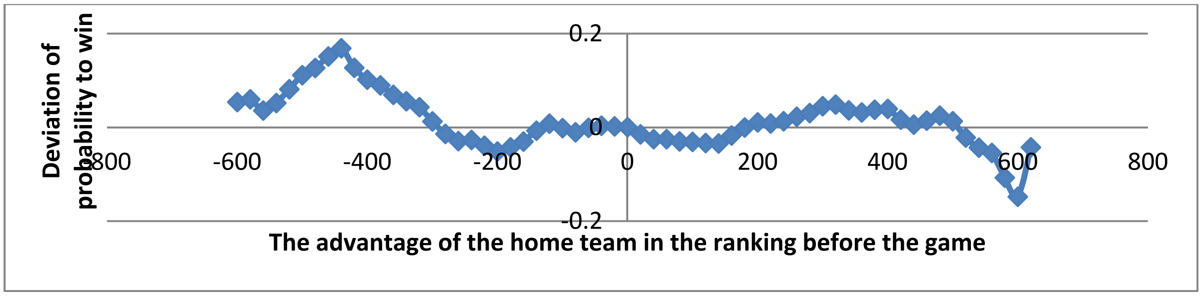

FIGURE 4. Deviation of experimental points from the generalized schedule for 670 games of the KHL 2017-18.

The same statement is presented in a different form (Figure 5). All games of the 2017-2018 KHL season formed the dependence % = F (Rt (1) - Rt (2)) graph. All the results of the games were aggregated by points of the rating scale taken at intervals of 20 p. That is, % of wins were determined for all games that were closest to this level of advantage in the rating Δ = Rt (1) - Rt (2) (-1000, -980, -960, etc.). Further, the coefficients of the logistic equation A, B, C were calculated. The values of the probability of winning the match in each of the fixed points of the advantage in the experimental rating and from a generalizing logistic dependence were obtained. It was expected that a relatively uniform deviation in both directions throughout the entire interval would be found, but it turned out that this is not the case. Weaker teams with values of Δ = 500p scored 17% more points than expected. Accordingly, they were not received by the stronger teams.

CONCLUSION

1. The phenomenon of social laziness in the games of top-level teams is a decrease in the level of play of individual players or the team as a whole, with a big advantage in the level of play of the team in a match with another opponent. This decrease is always uneven for each player individually. The effect indicates itself to the greatest extent in the more numerous sports in terms of the number of players on one team. The largest deviation values are obtained for hockey. Relatively small variations for football can be explained by a higher level of competition in football and a higher level of public attention.
2. The syndrome of social laziness in games of top-level teams in football, hockey and basketball is that a team cannot expect more than 85% of the probability of winning even with a huge advantage over the opponent.
3. The average deviation at the edges of the interval (-1000 p and 1000 p) is 10-17% in favor of weaker clubs, wherein we are talking about professional teams of the highest level.

REFERENCES

[1] Platonov Yu.P., (2008), available at URL: http://elitarium.ru/2008/05/23/gruppovye_jeffekty.html.
[2] A.L. Sventsitsky, *Social psychology* (Prospect, Moscow, 2005).
[3] M. Hunt, *History of psychology* (AST, MOSCOW, 2009).
[4] B.G. Meshcheryakova, V.P. Zinchenko, *Big psychological dictionary* (Prime-Evroznak, Moscow, 2003).
[5] A. Karminsky, A. Polozov, *Handbook of Ratings. Approaches to Ratings in the Economy, Sports, and Society* (International Publishing House "Springer", 2016).
[6] D.A Kravitz and Martin B., Journ. of Personality and Social Psychology, Vol. 50, No. 5, 936-941 (1986).

Preface of the International Symposium on Computer Science and Information Technology (ISCSIT 2019)

Martin Kotyrba[1,a)], Eva Volna[1,b)], Vladimir Bradac[1,c)], Martin Zacek[1,d)], and Bogdan Walek[1,e)]

[1]University of Ostrava, 30. dubna 22, 70103 Ostrava, Czech Republic.

[a)]Corresponding author: martin.kotyrba@osu.cz
[b)]eva.volna@osu.cz, [c)]vladimir.bradac@osu.cz, [d)]martin.zacek@osu.cz,[e)]bogdan.walek@osu.cz
URL: http://www.osu.cz

Computer science is the study of the theory, experimentation, and engineering that form the basis for the design and use of computers. It is the scientific and practical approach to computation and its applications and the systematic study of the feasibility, structure, expression, and mechanization of the methodical procedures (or algorithms) that under lie the acquisition, representation, processing, storage, communication of, and access to information. Information science and EDU is to mediate new findings and approaches of experts in the field of ICT application not only in Education

Martin Kotyrba

Martin Kotyrba is an assistant professor at the Department of Computer Science at University of Ostrava, Czech Republic. His interests include artificial intelligence, formal logic, soft computing methods and fractals. He is an author of more than 50 papers in intenational journals and proceedings of conferences.

Eva Volna

Eva Volna is an associate professor at the Department of Computer Science at University of Ostrava, Czech Republic. Her interests include artificial intelligence, artificial neural networks, evolutionary algorithms, and cognitive science. She is an author of more than 70 papers in technical journals and proceedings of conferences.

Vladimir Bradac

Vladimír Bradáč is an assistant professor at the Department of Computer Science at University of Ostrava, Czech Republic. His interests include language education, e-learning and adaptive systems for personalised e-learning support. He is an author of more than 20 papers published both at international conference proceedings and journals.

Martin Zacek

Martin Žáček is an assistant professor at the Department of Computer Science at University of Ostrava, Czech Republic. His interests include artificial intelligence, formal logic, knowledge representation, software engineering, and education. He is an author of more than 50 articles and papers in international journals and proceedings of conferences.

Bogdan Walek

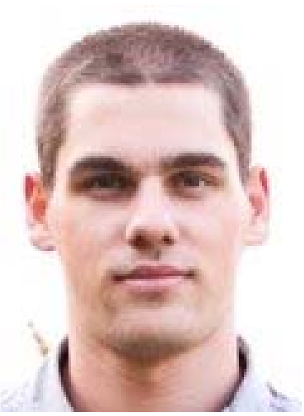

Bogdan Walek is an assistant professor at the Department of Computer Science at University of Ostrava, Czech Republic. His current research interests are fuzzy modeling tools, expert systems, decision support systems. He is an author of more than 60 articles and papers in intenational journals and proceedings of conferences.

Introduction to Digital Circuits Based Logical Programming (DCBLP) - the Multiparadigmatic Way of Logical Based on Programming

Lukáš Hapl[1,a], Hashim Habiballa[1,b]

[1]*Dept. of Informatics and Computers, Faculty of Science, University of Ostrava, 30. dubna 22, 70103 Ostrava 1, Czech Republic*

[a] lukas.hapl@roznovskastredni.cz, [b]hashim.habiballa@osu.cz

Abstract. This article brings an overview and at the same time the very first introduction of possibly new way of programming based together on multiple programming paradigms, Boolean logic/combinational logic/sequentional logic and finite state machines principles. We will focus on the basics and fundamentals of such programming, its possible advantages and possible usage in real life using current programming languages without the needing to develop a new one.

INTRODUCTION TO DCBLP

We are able to use various programming paradigms with the rise of high-level programming languages and more efficient processors. It is also possible for teaching based on multi-paradigm programming with overlap to other disciplines, not only Informatics. These alternative paradigms in teaching programming enable to utilize non-standard paradigms and their common combinations (standard is for example structured programming with object oriented programming).

One of these non-standard paradigms is programming based on digital circuits and boolean logic, with combination of structured programming, object oriented programming and flow-based programming (FBP) [1]. Our presented approach is derived from the mentioned combination and we call it DCBLP – Digital Circuits Based Logical Programming.

The main principle of this programming paradigm lies in direct translation of hardware, physical principles and internal logic of digital circuits into software representation. In real world we are able to design logic based digital circuits, its interconnection, data flow by the means of electric signals [2].

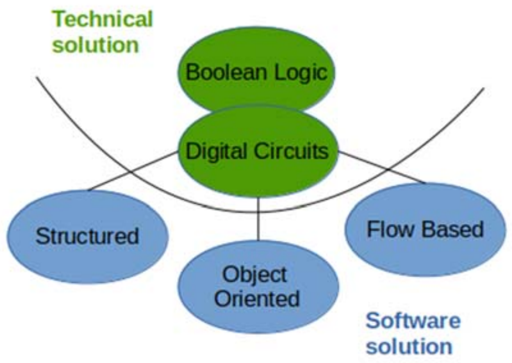

FIGURE 1. DCBLP bridge between HW and SW world

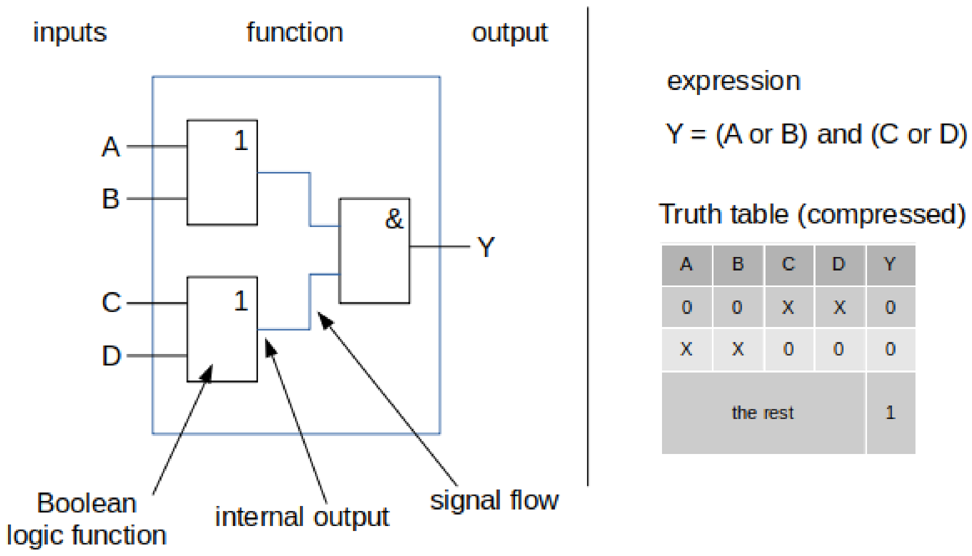

FIGURE 2. The description of basic logic functions interconnection

With present technologies we can simulate these circuits by function, which is not implemented on hardware level (HDL languages), but on software level on CPU of certain platform. Functions and properties of digital circuits we can model as classes and their instances are particular digital circuits. This enables us to use principles of object oriented programing. Their interconnection is performed through inputs and outputs (in instance methods), conductors are implemented by variables, pipes or queues. Electric signals are implemented by numerical values of inputs and outputs. In this model we use FBP principles – FBP uses black box objects with input and output data (details can be found in [1, 3]). We can use special instances of classes containing all other instances and their methods constituting logical network. The main method of this special instance is executed in its own thread with predefined period for repeating content, in order to simulate real world which is not only sequential. This leads us also into multithreading programming, which is mentioned not only in FBP [3], but also in texts based on structured programming [4].

TABLE 1. Paradigms comparison of implementation elements

Physical world of technical digital logic solutions	**Programming world**	**Paradigm used**
Digital Integrated Circuit parameters & function & logic	Class	Object Oriented
Real physical Digital Integrated Circuit	Class Instance	Object Oriented
Internal Combinational or Sequential logic	Function (method) in Class	Procedural, Object Oriented
Circuits Inputs, Outputs, n-bit bus	Variables, Queues, Pipes	Data Flow principles with Object Oriented
BreadBoard, CircuitsBoard	Class instance + thread	Object Oriented with multithreading

The basic idea for program design is logical network in DCBLP, truth or state table (depending on particular system) without the need to create UML diagram as a common programming base. It is not common top-down method, but combined form [4] with engineering approach to problem solving [3].

All relations in a DCBLP system are based on the principles of boolean algebra. Classes defining methods and object properties include basic logical functions and rules (binary values) and this could be related to Logic Programming paradigm [5].

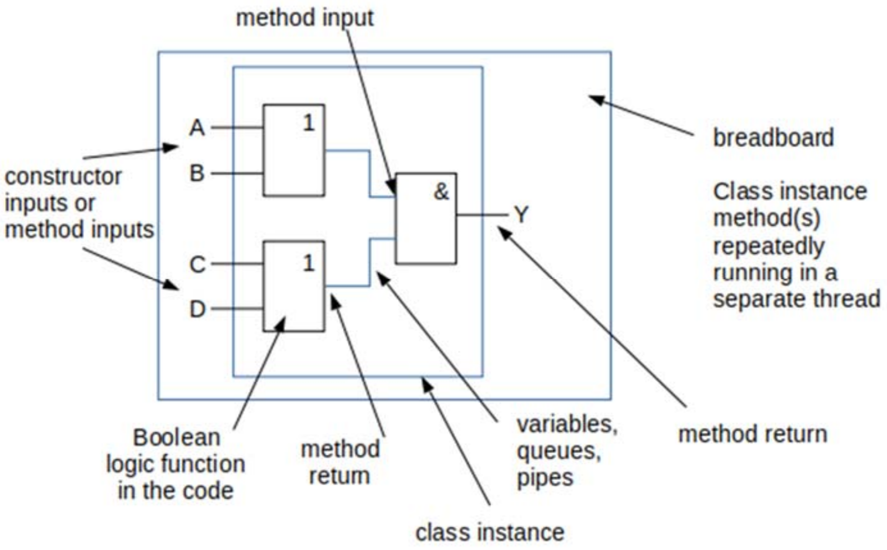

FIGURE 3. Usage of the logical network principles in object and flow based principles

CHARACTERISTICS OF DCBLP

Advantages of using DCBLP paradigm in teaching could be summarized as follows:

- It is possible to use the code to describe the function of simple digital circuits.
- Ït can enhance the way of multiparadigm programming.
- It can be possibly used by the technicians to better read the code.
- Possibility in education using programming languages to learn the Bool funcs.
- Possibility to create the code without using „if“ statements.
- Alternative way of programming without establishing a flow chart.
- Possibility to use technical, logical, digital circuits principles in programming.

The main properties of code for DCBLP include the following rules:

- Code describes the system, which can be represented on digital level.
- Resulting logic consists of basic logical functions (not blackbox).
- Truth and state tables are essential elements with digital circuits functions.
- Code does not contain common conditional constructs (if), loops are used only for better understanding the code. Multithreading is mandatory for complex circuits.
- Code can be based both on structured and object oriented programming.
- Code is not based on simulation particular states, but it is based on internal functions logic and it includes FBP elements, i.e. data flow between I/O.
- It can be directly bound to digital inputs and outputs.

Use of DCBLP is further limited by computational power of implementation technology and also by complexity of logical network or state automaton.

PROGRAMMING LANGUAGES SUITABLE FOR DCBLP

Suitable programming language for DCBLP has to fulfill several prerequisites:

- Support for structured and object oriented programming.

- Support for multithreading.
- Native implementation of basic logical functions.
- Usage of flow based principles.
- Usage for IoT platforms with GPIO interface for input/output peripherals connection.

One suitable possibility is the Python language. FBP paradigm was successfully used in JavaScript of Java as well as Python. Examples of Python's usage could be found for projects Pyperator or Pypes [6]. Brief examples of our tasks for DCBLP teaching that demonstrate control of dynamic peripheral ouput devices connected to GPIO by the DCBLP-based code. It can substantially improve the learning process with the help of modern technologies and activating methods [8].

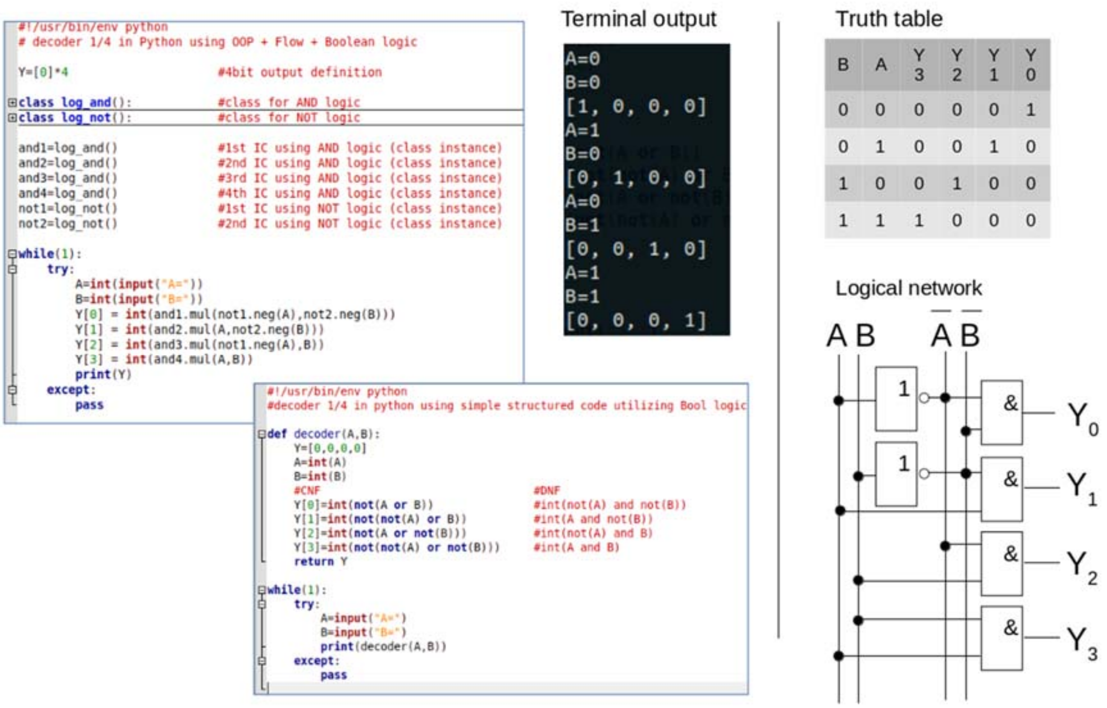

FIGURE 4. Combinational circuit as decoder 1/4 described by DCBLP principles adapted in Python

CONCLUSIONS

There is possibility to enhance the way Boolean logic is used in programming and at the same time taught at schools. It is possible to use high level programming languages suitable for Internet of Things platforms (at least some of them) to support the case. This paper showed up the idea of creating Boolean logic based components in general and in Python language utilizing programming multiparadigms. All can be possibly used in education area with the practical outputs on IoT. We also demonstrated the DCBLP usage in the case of simple combinational logic. The research and meaningful implementation in the field of education will follow.

REFERENCES

1. J. P. Morrison. Flow-Based Programming. [online] http://www.jpaulmorrison.com/fbp/
2. A. Bindal. Fundamentals of Computer Architecture and Design. Springer International Publishing, 2017.
3. J. P. Morrison. Flow-Based Programming: A New Approach to Application Development. New York: Van Nostrand Reinhold, 1994. ISBN 0-442-01771-5.
4. S. P. Dandamuni. Fundamentals of Computer Organization and Design. Springer-Verlag: New York, 2003.

5. M. Gabbrielli and S. Martini. Programming Languages: Principles and Paradigms, pp. 369-378, London: Springer, 2010, ISBN 978-1-84882-913-8.
6. J. P. Morrison. Flow-Based Programming: Links to External References (as of Sept. 2015), 2015, [online] <http://www.jpaulmorrison.com/fbp/links_external.html>
7. L. Hapl. Potential of Raspberry minicomputer in teaching (in czech). In: Perspektivy elektroniky. Rožnov pod Radhoštěm: SŠIEŘ Rožnov pod Radhoštěm, 2018. pp. 1-10 . ISBN 978-80-270-5415-1.
8. H. Habiballa and R. Jendryščík. Constructivistic Mathematical Logic Education. In: International Conference of Computational Methods in Sciences and Engineering 2017: AIP Conference Proceedings 2018 AIP Conference Proceedings. MELVILLE, NY USA: AIP Publishing Inc., 2018. ISSN 0094-243X.

DCBLP - Applications and Education

Lukáš Hapl[1,a], Hashim Habiballa[1, b]

[1]*Dept. of Informatics and Computers, Faculty of Science, University of Ostrava, 30. dubna 22, 70103 Ostrava 1, Czech Republic*

[a] lukas.hapl@roznovskastredni.cz,[b]hashim.habiballa@osu.cz

Abstract. Article describes combinational and sequential logic principles adopted by Digital Circuits Based Logical Programming (DCBLP) based on Python scripting language. The usage of the principles will be demonstrated on ARM Cortex-A based minicomputers Raspberry Pi 3 in education. Simple peripherals will be included to demonstrate the functionality.

DCBLP PRINCIPLES OVERVIEW

DCBLP is the unusual way of imperative languages usage, especially in the education process dealing with the areas of digital circuits and Boolean logic [1]. At the same time the teaching of carefully selected high level programming/scripting language can be supported as well [2]. First of all the scope of functionality must be set, principles and methods established and usable programming/scripting language libraries must be developed.

The scope is to take the digital circuits logic [3] and transform that logic as good as possible into the code. Boolean logic is mainly used in this transformation. After the transformation the classes with (let's call them DCBLP primitives) will be made (more details can be found at [1]). DCBLP primitives can be used later to create larger and advanced flow based interconnections to fulfill the requirements (aka the problem that needs to be solved).

An algorithm for structured programming languages can be based on a classic flowchart diagram as well as on an unusual and untypical and not widely used truth tables, state tables and logic network (circuit) design [1]. It's just another point of view how to use the structured or object-oriented languages differently (meaning using the different paradigm or go against its nature philosophy). Here we create the code the same way as we create the logical circuit design. The code is then executed on the processor of the selected platform (in contrast to HDL, where the code interpretation leads to hardware creation) – Figure 1.

In basics the principles also lay on Boolean logic. All parts of the code are based on Boolean functions. There are no "if" statements although structured based languages are used. To better reflect the real world the object-oriented programming paradigm and principles can be used as well. "For" statements can be used just to shorten the visual interpretation of the code. Multithreading can and for advanced solutions should be used to support sequential logic.

An advantage of this solution is in how it deals with digital inputs and outputs. There is no type conversion needed inside the functions if we use Boolean logic from the beginning (inputs) until the end (outputs).

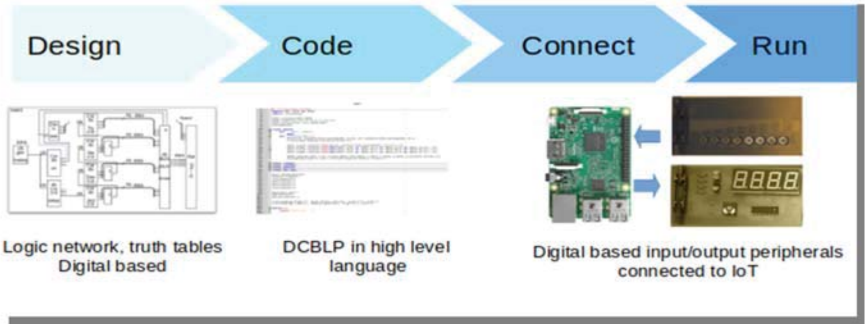

FIGURE 1. Simplified workflow philosophy for DCBLP usage and implementation on IoT [4]

EXAMPLES OF DCBLP IN COMBINATIONAL AND SEQUENTIAL LOGIC

In this paper we introduce two DCBLP examples utilizing Python programming (scripting) language supporting digital logic education. The first example summarized on Figure 2 represents simple structure programming based binary to 7- segment display decoder. It consists of 1/16 decoder connected to small memory array (only 10 decoded addresses are used). In the real world the memory itself can be designed as an array of individual mechanical switches or ROM holding one of two possible states. Logical structure of the memory cell array is represented by the loop (for statement) using only indexes and Boolean logic. Loop is used just to simplify the code, not as a workaround to achieve the goal. It can be coded without loop as well and still not affecting the final solution yet. It can be seen that there are no "if" statements at all, inputs and outputs are Boolean logic based and so do the functions themselves. The inputs and outputs can be easily connected to available GPIO libraries necessary to run peripherals on IoT (such as on Raspberry Pi mentioned earlier).

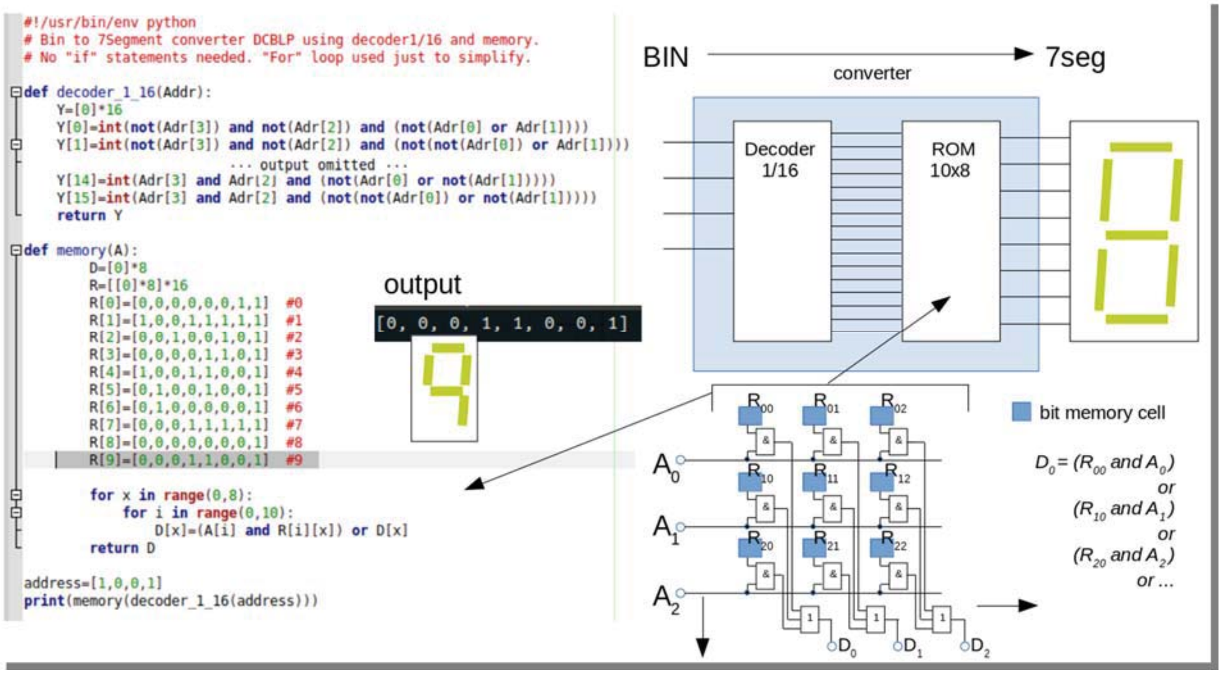

FIGURE 2. Combinational circuit decoder 1/16 connected to ROM used as bin to 7-segment converter

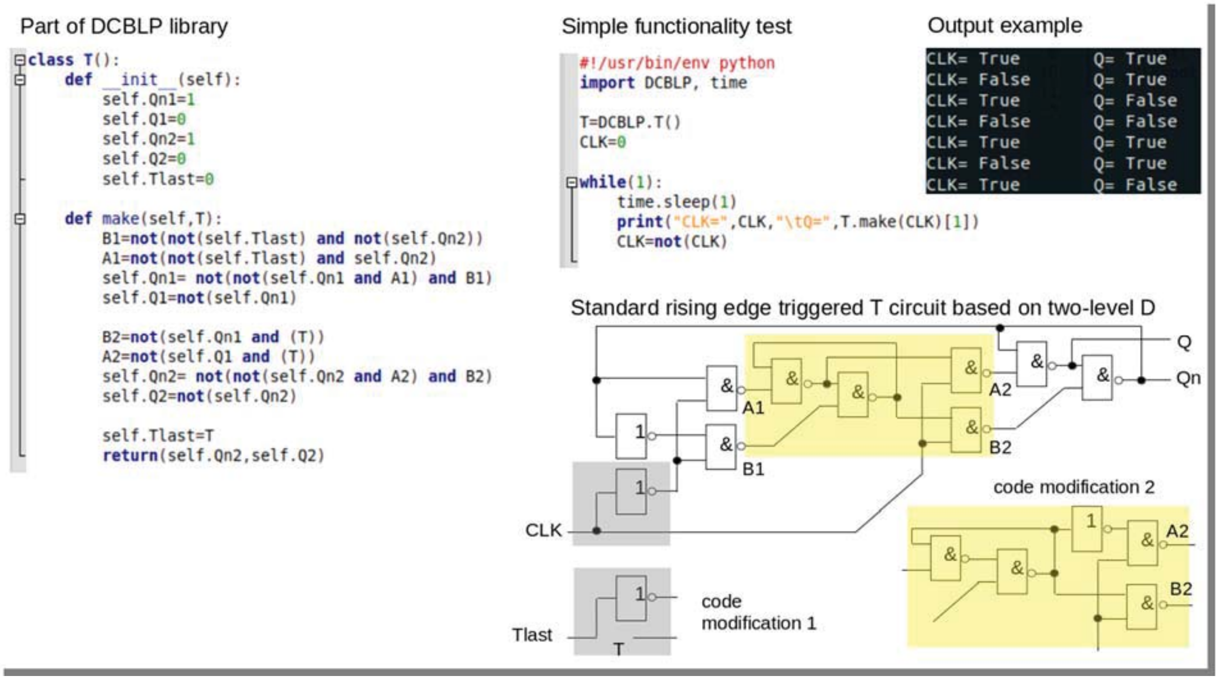

FIGURE 3. Sequential circuit of "T-type" (toggle, flip-flop) based on standard edge triggered "D" circuit

The second example on Figure 3 shows classes and sequential logic altogether. The class named T has got one function that establishes (makes) the logic of T-type circuit. It was necessary to modify slightly the circuit design described by the code (yellow and grey highlighted parts) because the nature of sequential circuits (the physical principles) and the nature of the programming language Python differ. One has to understand that the code is executed instruction by instruction (that affects some transitions and states), but an electric signal that spreads through the real circuit occurs everywhere in every occasion (omit the delay). Hence the state machines cannot be converted to code as simple as the combinational circuits can be converted into the functions. However, once it is done the function of circuit remains the same and the class can be used. Very simple example has been prepared (right part of the code on Figure 3) to demonstrate the function of T-type circuit [5].

```
#!/usr/bin/env python
import DCBLP, time, RPi.GPIO as GPIO
GPIO.setmode(GPIO.BCM)
LED=21
GPIO.setup(LED, GPIO.OUT)
T=DCBLP.T()
CLK=0
while(1):
    time.sleep(1)
    GPIO.output(T.make(CLK)[1])
    CLK=not(CLK)
```

FIGURE 4. LED toggle using T-type on Raspberry Pi 3

When the LED is connected to selected IoT GPIO pin (on Raspberry Pi 3 with RPi.GPIO) [6], it turns ON and OFF continuously with the frequency of 0.5 Hz (1 second ON, 1 second OFF). The modified code enhanced for Raspberry Pi 3 is observable on Figure 4. The best usage of sequential based circuits can be achieved with multithreading and timer approach however, but these parts are beyond the scope of this brief review.

DCBLP USAGE IN EDUCATION

DCBLP must be seen as the domain specific programming (where Boolean logic can be used) with the high applicability for (and during) the secondary professional education process. It can support integration of programming languages into technical area of digital circuit education and enhance the methods and content of this area. This can lead the students to better understanding this field of study. There is also possibility that using such an approach can meaningfully enhance and support teaching of high level imperative programming languages just because of usage of the logical level based tasks/examples very suitable to maintain structured and object-oriented languages.

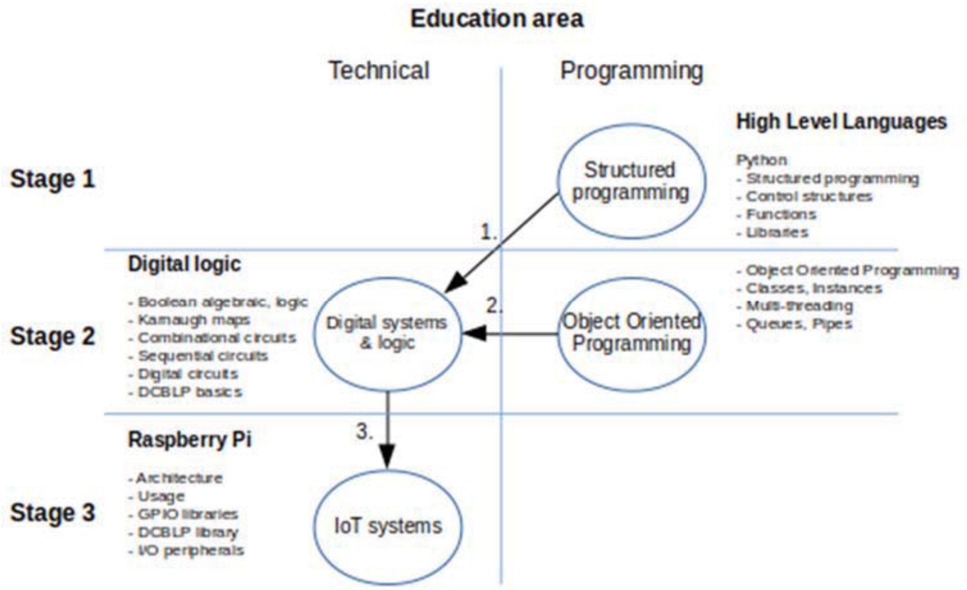

FIGURE 5. Stages of possible DCBLP implementation in education.

Figure 5 is a proposing of a possible way of basic DCBLP implementation into the secondary professional (technical oriented) education. The first stage expects the students to learn some of the high level programming languages and the classic structured way of programming principles (Python seems to be the usable one). This is something usual and needs no special attention. During the second stage the knowledge acquired in the previous stage is used to support the education in the area of digital based systems, especially in matters of combinational functions. The education of the object-oriented programming approach must continue in parallel or right after in the worst case. Creating the classes representing the logic and its function as well as diving into the multithreading is mandatory in most cases dealing with the sequential logic. The final stage expects verification, practicing and usage of an acquired knowledge on IoT such as Raspberry Pi.

Applications suitable for education can consist of registry, generators of hashes, controllable PWM, digital clocks; basically the applications using 7-segment displays, buttons, matrix keyboards, matrix display, (step) motors, LEDs and so on. Some of these applications have been introduced already [2].

The necessity of such approach comes along with an unpleasant situation showing that some of IT students are losing an interest to learn technical based subjects/content and dive more into deep. Young IT students are nowadays more focused on programming than understanding the principles of other important IT related disciplines. There is a possibility they can see the Boolean logic area from the different point of view using proposed approach. They can mix something they are interested in (programming) with something they rather refuse to learn (logic based systems) - without the necessity to learn an additional language. Integration and bounding can be tried and experiments dealing with the cognitive and affect aspects of education can be made. There is an ongoing research and experiments focused on this area covered by the University of Ostrava. There an effort has already existed to support theoretical education of formal Boolean logic (and the theory itself) by constructivist teaching methods [7]. DCBLP

approach can also be a part of it or perhaps a whole new branch supporting this educational initiative. The questions regarding the DCBLP in education are as follows:

1. We realized this part is attractive for some students. What is the main reason of such attractiveness?
2. Is this approach of teaching digital logic systems more beneficial in cognitive area compared to standard?
3. What method should be developed for DCBLP integration to digital logic and programming?
4. Is this approach somehow beneficial for teaching I/O digital peripherals on IoT such as Raspberry Pi?
5. What would be the final recommendation regarding the integration of DCBLP or similar intentions?

CONCLUSIONS

DCBLP is a domain specific programming technique that mixes more programming paradigms altogether. It deals with the digital inputs and outputs in a natural manner using appropriate code functions based on Boolean logic and operations. Structured based programming languages can be used, however, there can be no branch visible in the code at all. This approach is very simple to use in the area of combinational logic, helping students learn binary logic in more attractive way. It is not so straightforward for sequential logic but the goals can be achieved as well. The big benefit is in the simple integration with some I/O peripherals on appropriate IoT as mentioned in the review. The next research and developments will focus on improvement of the DCBLP classes for selected combinational and sequential IC instances. Experiments on secondary education level will be made to answer the given questions.

REFERENCES

1. L. Hapl. Introduction to Digital Circuits Based Logical Programming (DCBLP) -the multiparadigmatic way of logical based programming. Ph.D. projects, University of Ostrava, Ostrava, 2019.
2. L. Hapl. Potential of Raspberry minicomputer in teaching (in czech). In: Perspektivy elektroniky. Rožnov pod Radhoštěm: SŠIEŘ Rožnov pod Radhoštěm, 2018. pp. 1-10 . ISBN 978-80-270-5415-1.
3. Ch. H. Roth. *Fundamentals of logic design. 5th ed*. Belmont, CA: Thomson/Brooks/Cole, 2004. ISBN 978-0534378042.
4. "File:Raspberry Pi 3 Model B.png." *Wikimedia Commons, the free media repository*. 28 Jan 2018. 14 Jan 2019, https://commons.wikimedia.org/w/index.php?title=File:Raspberry_Pi_3_Model_B.png.
5. Sequential-logic-circuits: Toggle-flip-flop. *Electronics-tutorial* [online]. [cit. 2019-01-14]. [online] http://www.electronics-tutorial.net/sequential-logic-circuits/toggle-flip-flop/index.html.
6. B. Croston,. *RPi.GPIO - PyPi. Pypi.org* [online]. Python Software Foundation, 2019 [cit. 2019-01-15]. https://pypi.org/project/RPi.GPIO/
7. H. Habiballa and R. Jendryščík. Constructivistic Mathematical Logic Education. In: International Conference of Computational Methods in Sciences and Engineering 2017: AIP Conference Proceedings 2018 AIP Conference Proceedings. MELVILLE, NY USA: AIP Publishing Inc., 2018. ISSN 0094-243X.

Application to Train Short-Term Memory According to the CHC Intelligence Model

Klara Smiskova[1,a], Martin Kotyrba[1,b], Eva Volna[1,c], Martin Austynek[2,d], Petr Nilius[3,e]

[1]*Department of Informatics and Computers, University of Ostrava, 30 dubna 22, Ostrava, Czech Republic*
[2]*Technical University of ostrava, 17. listopadu 2172/15, 708 00 Ostrava-Poruba, Czech Republic*
[3]*Ambulance of clinical psychology, Spojů 835/2, Ostrava Poruba, 708 00, Czech Republic*

[a]klara.smiskova@osu.cz, [b]martin.kotyrba@osu.cz,[c]eva.volna@osu.cz, [d]martin.augustynak@vsb.cz,
[e]petr.nilius@amkp.cz

Abstract This paper deals with a proposal of an application designed to train short-term memory according to the Cattell-Horn-Carroll (CHC) model of intelligence. This application is one of the parts in the project called „Intelligent neuro-rehabilitation system for patients with acquired brain damage in early stages of treatment", whose aim is to develop a smart neuro-rehabilitation system to increase the effectivity of the acute phase of neuro-rehabilitation of patients with brain damage. Following the project's requirements, the application is prepared as a web application built on the .NET technology.

MEMORY

Memory is an ability of the central nervous system to keep and use information on previous experience [1]. It concerns a process of *coding*, *storing, and retrieving* of experience. Memory divides according to the length of storing of the remembered into *sensory, short-term, intermediate,* and *long-term*; in addition, it divides according to the information form into *visual, acoustic, semantic* (storing the meaning), etc. Another alternative is its division into *mechanical* and *logical*.

Sensory memory is a conscious memory holding information from senses. Those are kept for a period necessary to process and decide if the information is suitable for further processing or not. If yes, it then continues to short-term and long-term memory.

Short-term memory is a conscious, active part of memory, where most mental processes are performed (e.g. solving current problems). It processes information supplied by sensory memory and information recalled from long-term memory. Short-term memory is limited to 5-9 items, which are stored for c. 15-20 s. When repetition is blocked. In order to keep information in short-term memory, it must be repeated. Sometimes *intermediate* memory is stated, which holds the information for the period of c. 20 minutes.

Long-term memory is a relatively passive part of memory stored in unconscious mind. Its capacity is hypothetically unlimited. It stores important experience and findings. Coding information into long-term memory takes c. 30 minutes. The brain stores information into long-term memory during sleep which should be at least 6 hours long.

THE CATTELL-HORN-CARROLL THEORY

The first factor analysis of intelligence was described by British psychologist Charles Spearman (1863–1945). According to him, all abilities to solve tasks in intelligence tests can be simplified to a single factor, which he called

g (general intelligence factor). The Cattell-Horn-Carroll theory recognises the existence of factor *g* and divides it into 10 cognitive abilities, which further divide into 70 subgroups [2]:

1. Fluid intelligence – ability to logically reason, abstractly think, and solve new problems.
2. Crystallised intelligence – gathered knowledge and vocabulary.
3. Quantitative reasoning – ability to handle numbers and relations between them.
4. Reading and Writing – factor including both of these abilities.
5. Short-term memory – ability to keep information conscious for a period necessary to use it.
6. Long-term memory and recalling stored information when needed.
7. Auditory processing – ability to handle auditory impulses.
8. Visual processing – ability to perceive and process visual impulses.
9. Processing speed – ability to quickly perform automated or very simple cognitive tasks which require concentrated attention.
10. Decision/Reaction speed – promptness which is used by a human to react to impulses or to solve a problem.

This paper will be focused on the development of an application designed to train short-term memory according to the CHC intelligence model.

PROPOSAL OF THE APPLICATION

The project entitled "Intelligent neuro-rehabilitation system for patients with acquired brain damage in early stages of treatment", which is in the focus of the research, will serve as an intelligent neuro-rehabilitation system. The proposed web application is designed to train short-term memory according to the Cattell-Horn-Carroll model of intelligence. The basic requirement for this application is modularity as other training games will be added to it as independent modules on application's background. The created main gaming module is in a form of a fictitious town Eddie (Fig. 1), where other games can be added. The town of Eddie is managed by a postman (i.e. user), who delivers letter to selected houses, where games are held. At the end of each game, there is information concerning the place in the town where the postman has to deliver another letter to play another game.

FIGURE 1. Town of Eddie in an interactive presentation.

The application is divided into three parts. The first one is the application itself, the second one is the gaming module (town of Eddie), and the games are in the third part, which sends the data to the first part as this part communicates with the server and the database. Each training game is then created in dependence on this module. After a user logs in, data from played game begins to be sent to the server to be analysed. The scheme in fig. 2 represents the communication between the created modules – web application, the main gaming panel of the town of Eddie, and individual game. All training games include an adaptation rule, which enables to adapt individual levels

according to the user results' success rate [4]. It then functions based on the principle of checking user results after each played game level. If a user is found to have made a mistake, the difficulty level is then set to the same or lower level, without user's awareness. If a user is correct, the difficulty remains the same.

When creating the application, the following technologies have been used [3]:

- *.NET*: is a roofing term for a set of technologies in SW products creating a comprehensive platform available for Web, Windows and Pocket PC. The basic component is Microsoft .NET Framework, the environment needed to run applications and offering the launching interface and necessary libraries.
- *Microsoft Visual Studio*: is an environment to develop console applications and applications with a graphic user interface together with other applications. It is not limited concerning platforms and programming languages.
- *ASP.NET*: is part of .NET Framework for the creation of web applications and services. It includes a wide range of libraries created in C#.
- *ASP.NET MVC Framework*: is a web application framework, which implements pattern Model-View-Controller and enables to create web applications as an assembly of three components: model, view, and controller.
- *JavaScript:* is a multiplatform, object-oriented, event-driven scripting language.
- *jQuery:* is a JavaScript library with wide support of browsers, which emphasises interaction between JavaScript and HTML.
- *Ajax* (Asynchronous JavaScript and XML): is a general term for technologies of developing interactive web applications which change their content without the need of their complete re-reading using asynchronous web page processing by using a library written in JavaScript.
- *Pixi.js*: is a publically available gaming 2D engine. It uses modern technologies for game creation. It is based in *JavaScript* and uses HTML technologies.
- *HTML 5:* is a version of HTML used for web page creation.
- *CSS* (Cascading Style Sheets): is a language to describe the way of displaying elements on pages written in HTML, XHTML, or XML.
- *JSON* (JavaScript Object Notation): is a simplified format for data exchange. It is easy to read and write by a human and easy to analyse and generate by a machine.
- *Mobirise:* is a web editor enabling to easily create web pages without coding.
- *Adobe Illustrator:* is a program to create vector graphics.

Short-Term memory Training

Topics and structure of all games have been consulted with a psychologist and the results of users will be passed to appointed medical workers.

The proposed game to train short-term memory is also an introductory training game in the town of Eddie. This training game is called *Zapamatuj si obrazce (Remember the Shapes).* Using simple geometric shapes, the player learns to engage working memory. The objective is to remember a certain number of shapes in a limited time. This game includes three difficulty levels – easy, medium, difficult, altogether six levels. Each difficulty has two levels. These levels differ in the time limit and the number of displayed shapes to be remembered (see Fig. 3). The time limit is only for shapes to be remembered. In each level, the shapes change. The minimum number to be remembered is one.

The first and second level (difficulty easy) contains only one shape to be remembered and is limited for the time of five seconds. Then the shape is hidden and another three shapes appear from which the user selects. If the selection is correct, the user advances to the next difficulty.

The third and fourth level (medium difficulty) includes two shapes for seven seconds. Then, the same as in the previous levels, the shapes are hidden and five shapes are displayed. Having answered correctly, the user advances to the next difficulty.

The fifth and sixth level (difficult difficulty) includes three shapes for ten seconds. Having reached the time limit, six shapes appear from which the user selects.

FIGURE 3. Graphical basis for game *Remember the Shapes*.

(a) (b)

FIGURE 4. The first level of *Remember the* Shapes. (a) Remember this shape. (b) Select the correct shape.

At the end of the game, the player's final evaluation is displayed. This evaluation shows the average time of identifying the shapes and the number of correct and wrong answers. The results are stored in a JSON file. Two files are stored: a JSON file with monitored data and a text file with the user's data, such as user name and the IP address.

CONCLUSION AND FUTURE WORK

The created game *Remember the Shapes* have been verified on a set of 30 users. The created application is designed to train short-term memory according to the CHC intelligence model. The application is part of the project entitled “Intelligent neuro-rehabilitation system for patients with acquired brain damage in early stages of treatment”, whose aim is to develop a smart neuro-rehabilitation system to increase the effectivity of the acute phase of neuro-rehabilitation of patients with brain damage.

ACKNOWLEDGMENTS

The research described here has been financially supported by The Technology Agency of the Czech Republic (TA CR) Project No. TL02000313, it was also supported by the University of Ostrava grant SGS/PrF/2019.

REFERENCES

1. Piaget, J., and Inhelder, B. *Memory and intelligence (psychology revivals)*. Psychology Press (2015).
2. Schneider, W. J., & McGrew, K. S. The Cattell-Horn-Carroll theory of cognitive abilities. *Contemporary intellectual assessment: Theories, tests, and issues*, pp. 73-163 (2018).
3. Smiskova, K. Creating an application designed to train short-term memory by the CHC model of intelligence. *Bachelor thesis*. University of Ostrava 2018.
4. Staddon, J. E. *Adaptive behavior and learning*. Cambridge University Press (2016).

Application to Train Cognitive Skills According to the CHC Intelligence Model

Tomas Prorok[1,a], Robert Jarusek[1,b], Pavel Smolka[1,c], Martin Cerny[2,d]

[1]*Department of Informatics and Computers, University of Ostrava, 30 dubna 22, Ostrava, Czech Republic*
[2]*Technical University of ostrava, 17. listopadu 2172/15, 708 00 Ostrava-Poruba, Czech Republic*

[a]tomas.prorok@osu.cz, [b]robert.jarusek@osu.cz, [c]pavel.smolka@osu.cz, [d]martin.cerny@vsb.cz

Abstract This paper deals with a proposal of an application designed to train quantitative abilities of thinking according to the CHC intelligence model. This application is one of the parts in the project called „ Intelligent neuro-rehabilitation system for patients with acquired brain damage in early stages of treatment", whose aim is to develop a smart neuro-rehabilitation system to increase the effectivity of the acute phase of neuro-rehabilitation of patients with brain damage. Following the project's requirements, the application is prepared as a web application built on the .NET technology.

COGNITIVE FUNCTIONS

Cognitive functions are a tool to process information as they enable us to be aware of ourselves and the environment where we are. Thus, we gradually create a value orientation, which helps us solve problems which we encounter throughout our life – and therefore live and survive [1]. Cognitive functions can be classified into two categories: *Basic Cognitive Functions* can be described as a lower functional layer covering attention, perception, and memory. *Higher Cognitive Functions* can be described as a higher functional layer, which is dependent on the lower layer (although virtually all cognitive functions are mutually dependent). This higher layer covers speech, language, and executive functions. The activity of all cognitive functions can be measured by neuro-psychological tests and neuro-psychological batteries, where the achievements can be compared with others of peers or with own over the time. The research area dealing with cognitive functions is called *cognitive psychology*.

CHC MODEL INTELLIGENCE

The Cattell-Horn-Carroll theory of cognitive abilities (hereinafter as CHC intelligence model) is currently the most complex and empirically supported psychometric theory of the cognitive functions structure [2]. An important feature is that the CHC intelligence model is not static, but rather dynamic. It is still reorganised and there are continuously done changes adapted to the permanent research. The model works with elements representing a given ability (or factors), which can be measured by various psychological tests. One of the elements describes the area of quantitative abilities of thinking, whose training is described in this paper.

Quantitative abilities of thinking are, according to the CHC intelligence model, characterised as a quantitative element which represents the depth and width of individual's knowledge related to mathematics and mathematical symbols; they are typically measured by performance tests (e.g. mathematical calculations). The *quantitative element* represents a set of acquired mathematical knowledge of an individual, including performing mathematical operations, whereas *quantitative reasoning* represents only the ability of induction and deduction when solving quantitative problems. The quantitative element is the most obvious when the task requires the use of mathematical abilities (e.g. addition, subtraction, multiplication, division) and general mathematical knowledge (generally work with mathematical symbols). On the other hand, quantitative reasoning is required when solving typical tasks where a missing number (symbol) in a sequence is to be added.

Measuring the “quality” of the quantitative element is done by the *Woodcock-Johnson tests* [3]. These tests focus on individual cognitive elements and their abilities which divide into test areas (clusters). Individual clusters divide into categories (battery). Batteries are usually of two types: standard battery and extended battery. All batteries create one complete version of the Woodcock-Johnson test.

PROPOSAL OF THE APPLICATION

Firstly, it is necessary to explain the basic terms to understand the following text [1].

Cognitive training is exercising cognitive functions in healthy persons, who are activated by this activity. It does not mean a remedy of a deficit but strengthening current abilities.

Cognitive rehabilitation expresses a remedy for damaged cognitive functions. The aim is not only compensation of disorders by learning new strategies, but the support of mental settling up with functional deficits in a way that an individual can further plan his/her life. It is supervised by an experienced therapist and the individual has his/her own rehabilitation individual plan.

Neuro-rehabilitation expresses a complex care of persons with severe brain damage. It uses activation techniques as well as physiotherapy, physical therapy, etc. Neuro-rehabilitation is supervised by an experienced therapist and the individual has his/her own rehabilitation individual plan.

The project called „Intelligent neuro-rehabilitation system for patients with acquired brain damage in early stages of treatment”, for which the application is proposed, will serve as an intelligent neuro-rehabilitation system including tools and mechanisms from cognitive training to neuro-rehabilitation. The final application will perform cognitive training focused on quantitative abilities of thinking according to the CHC intelligence model.

Concept of the Training Game

With regard to the future extension of the training games, it was necessary to adapt the concept to be scalable and modular. All games will be made as one independent module, yet roofed by a central gaming module. This will act as one big game, as a "drive" of all functions, which will use individual parts making up the training games, and as a communication mediators with the web application. After a consultation with a psychologist, a training game was proposed to train numerical abilities, where the user can train understanding numbers on counting geometric shapes. This proposed game is divided into nine levels, which are further divided into difficulties: *easy, medium, difficult*. The difficulty level is given by the number of displayed shapes at the given level and by the aspect, such as random rotation or simple animation. This training game includes an adaptation rule [5] so the levels can be adapted to the user’s results’ success rate. A scheme of the application concept is given in Fig. 1 [4]. The internal structure is divided into two parts. The first part is the web application, which ensures the central functionality of the unit; the second one is the gaming module, which ensures the functionality of the gaming unit (one big game). Each training game is then created in dependence on this gaming module.

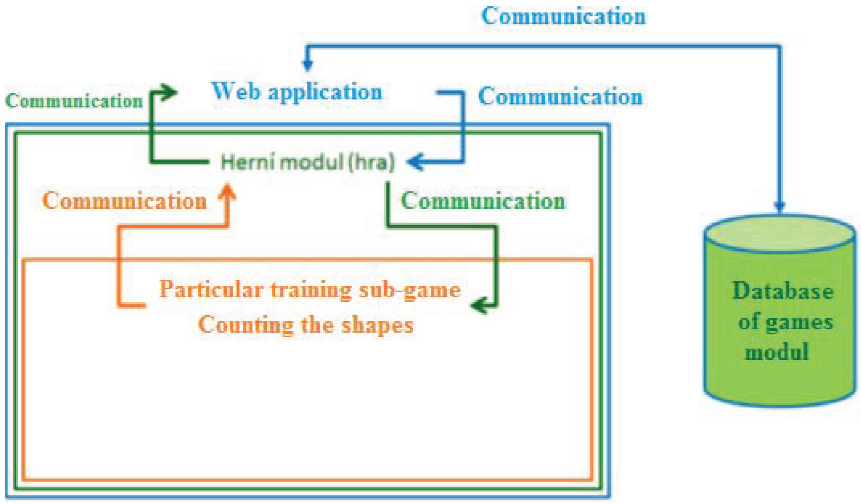

FIGURE 1. Scheme of the application concept.

Architecture of the Application

The proposed web application is built on architecture Model-View-Controller (MVC), which stems from the MVC pattern and is implemented using the ASP.NET MVC Framework. The principle of MVC consists in dividing the application logic into three parts: *Model, View,* and *Controller*. *Model* is represented by classes and represents the application logic and the data part. *View* represents a processed output, usually in a form of a generated web page. A particular view to be displayed is determined by the controller. *Controller* ensures communication of all units, processes user's requests, works with a given model, and selects a given view to be displayed. From the AJAX requirements design point of view, each AJAX requirement has its own fixed controller. If the concept is maintained, the MVC pattern cannot be disrupted as AJAX always sends the request to the corresponding controller which immediately responds.

The gaming module and the training game are created as an independent jQuery plugin, which is created according to the pattern for jQuery plugins. Each functional part is created as one independent JavaScript file.

Graphics of the Web Application

The graphics is adapted to be responsive. Responsivity is solved using so-called *media queries* in CSS, which are easy conditions whose block of rules is applied only to the defined distinguishing in their condition. The whole stylesheet of the web application look is divided in *.scss files (file of SASS pre-processor), which then serve to generate the final CSS file of the web application look connected to the web pages.

The graphic bases for training games were created in Adobe® Illustrator®. These graphic bases are used by engine Pixi.js to create textures which are used to create Sprites drawing into scenes.

The stylesheet of the training game is written in two variants. The first variant is written in one root *.scss file, the second one is written directly in the source code of the gaming module, which assigns each created HTML element a CSS identifier (id) or CSS class identifier (class). This is done to be able to style dynamic elements without the need to interfere into the source code of the gaming module. The only thing created dynamically are textures for individual graphic objects serving as buttons in given levels of the training game. Those are created on the basis of drawing rectangles by gaming engine Pixi.js. They are used to create Sprite representing a button.

TRAINING GAME OF COUNTING SHAPES

This training game *Counting Shapes* is divided into nine levels, which are further divided into difficulties: *easy, medium, difficult*. The difficulty level is given by the number of displayed shapes, different symbols, different size, random rotation, or simple animation. Each level has one solution, which is processed by the server side and is stored into a *session* (i.e. a mechanism to store data on the server). Based on server's evaluation, the response is sent back with a sign UseAdaptive; whether the adaptation rule is to be used or not.

The *Adaptation rule* adapts to the results from currently finished level and is used if the answer for a given level is evaluated as wrong. The proposed adaptation rule acts on the following principle: if the answer is evaluated as wrong, the adaptation rule finds out the level of the previously played game and based on that, it will select all games with the same level. One game is then selected and presented to the user. The user does not know that he/she has made a mistake and goes on playing. The aim of the adaptation rule is to prevent the user from advancing to more complicated levels before he/she is trained well not to make mistakes. If the level is evaluated as correct, the adaptation rule is idle and the predefined sequence of the training game levels is followed.

Testing and Experimental Verification

The training game collects data, such as *total time, number of generated symbols, solutions selected by the user*. Having evaluated this data on the server side, it is supplemented with facts, such as how many answers were correct and wrong, in which game, level, difficulty, etc. it is highly important to store the data so that it is always accessible. There was a requirement to use a universal data format, which was met by the JSON format used not only for data exchange (e.g. by technology AJAX), but to store data in a form legible by the user. This format has support in jQuery, C# as well as in many other analysis tools. From the point of view of data exchange though the AJAX technology, the JSON format is also used to store solutions in a database and individual data is sent to the server and back in this format.

Having launched the training game, the time is counted for each level separately. The user must click on one possible answer, which he/she considers correct. The training game (its module) communicates on the background with the main module, which ensures background communication with the web application, such as sending data from the training game and processing answers for a currently running training game module. Fig. 2 shows an example of the first and last level of the training game *Counting the Shapes*.

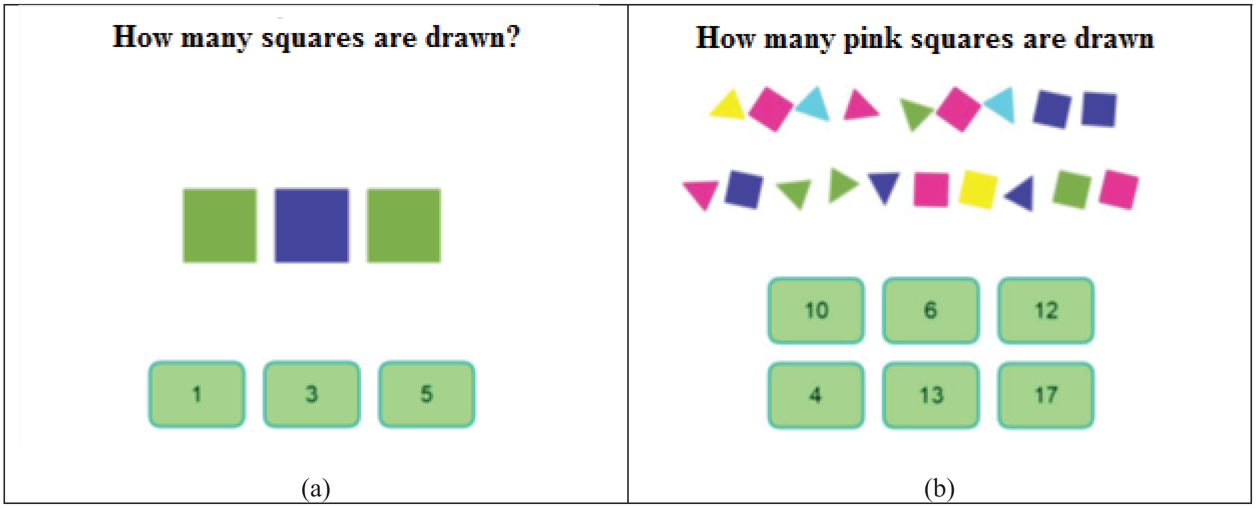

FIGURE 2. (a) The first level of *Counting the Shapes* (b) The last level of *Counting the Shapes*.

Having played the training game, the user can see a well-arranged screen with the total score and its graphical interpretation. The graph shows the time necessary to click on the answer button in each level. The graph is drawn by the module of the game itself and is interactive. Once displayed, the data is already stored on the server in the JSON format and the user can finish the game. Two files are stored: a JSON file with monitored data and a text file with the user's data, such as user name and the IP address.

CONCLUSION AND FUTURE WORK

The created training game *Counting the Shapes* has been verified on a set of 50 users. The created application is designed to train cognitive abilities of thinking according to the CHC intelligence model. This application is one of the parts in the project called „ Intelligent neuro-rehabilitation system for patients with acquired brain damage in early stages of treatment", whose aim is to develop a smart neuro-rehabilitation system to increase the effectivity of the acute phase of neuro-rehabilitation of patients with brain damage.

ACKNOWLEDGMENTS

The research described here has been financially supported by The Technology Agency of the Czech Republic (TA CR) Project No. TL02000313, it was also supported by the University of Ostrava grant SGS/PrF/2019.

REFERENCES

1. R. Näätänen, *Attention and brain function*. Routledge, 2018.
2. W. J. Schneider and K. S. McGrew, The Cattell-Horn-Carroll theory of cognitive abilities. *Contemporary intellectual assessment: Theories, tests, and issues*, pp. 73-163, 2018.
3. N. Mather and L. E. Jaffe, Woodcock-Johnson: Reports, recommendations, and strategies. Wiley & Sons 2016.
4. T. Prorok, Creating an application designed to train quantitative skills by the CHC model of intelligence. *Bachelor thesis*. University of Ostrava 2018.
5. E. Volna, M. Janosek, M. Kotyrba and V. Kocian, Pattern recognition algorithm optimization. In *Modern Methods of Prediction, Modeling and Analysis of Nonlinear Systems* (pp. 251-260). Springer, 2013.

Using Messenger and Factory Design Patterns for Real-Time Information System Development

Filip Hardt[a], Martin Kotyrba[b], Vladimir Bradac[c]

Department of Informatics and Computers, University of Ostrava, 30 dubna 22, Ostrava, Czech Republic

[a]filip.hardt@osu.cz, [b]martin.kotyrba@osu.cz, [c]vladimir.bradac@osu.cz

Abstract This paper deals with the use of Messenger and Factory design patterns to design and implement a real information system focused on business intelligence (BI). The whole development was implemented in the .NET platform in C# using modern programming techniques and tools. The substance of the paper is to show how it can be useful to use particular design patterns when developing information systems.

INFORMATION SYSTEMS AND BI

Organisation's information system (IS) is a system of information technology, data, and people that aims at effective support of information and decision-making processes at all levels of organisation's (company) management. The development and operation of an IS are affected by numerous aspects. An information application is a relatively independent IS (including HW, SW, and data), which is created or embedded into an IS by one project (e.g. email, assets management, bookkeeping). Our developed IS will consist of two modules/applications [1]:

- Stock – it will collect and analyse data on spare parts taking
- Maintenance – it will collect and analyse data on the number of failures in individual production lines

Business Intelligence is part of an IS focused on a particular activity, such as data collection and analysis. This is the activity of the mentioned BI. BI is used to monitor, collect, analyse, and process data about the company as a whole, not only about the customers, market, or competitors. The same term is used in relation to management, analysis, and evaluation of large data volumes, mostly in relation to storing raw data, its management, and data mining [2].

DESIGN PATTERNS

In object-oriented programming, there is a frequent need to solve programming procedures which can be addressed as best practices, i.e. such procedures that are long-term verified and which secure both better legibility of the code and elimination of the need to rewrite the code after some time due to bugs in the design. It concerns design patterns. There is a large number of design patterns and, of course, new still emerge. Object-oriented design patterns typically represent relations and interactions between classes and objects without determination of particular class implementation. Algorithms are not considered design patterns as they solve particular problems, not design problems.

Implementation of individual design patterns relies on the programmer who can modify them if necessary [3].

There are several types of design patterns according to the domain they solve:

- Creational Patterns – related to the creation of individual objects
- Structural Patterns – related to the arrangement of classes into functional units
- Behavioural Patterns – related to the behaviour of individual objects

When developing our information system, two design patterns were used, namely Messenger and Factory.

MESSENGER PATTERN AND ITS USE IN REAL DEVELOPMENT

Design pattern Messenger (Fig. 1) is a special class which serves to transfer several attributes. It concerns a normal class with several special attributes. As mentioned above, it enables us to work with more values as well as with only one, and it enables us to transfer it between classes. This pattern has three main principles of its use:

- Each value is defined as own attribute
- Attributes are declared as public
- Attributes are simple or object-data types

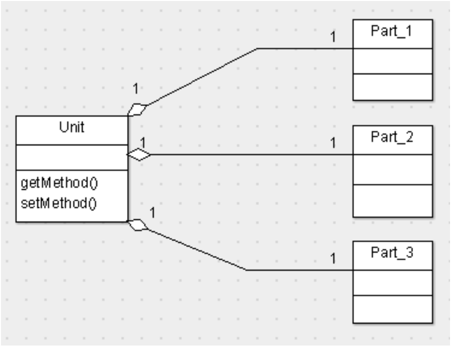

FIGURE 1. Architecture of design pattern Messenger

During development, Messenger was used to transfer attributes in statistical calculations into a window which draws graphs in order to avoid calling window drawing from public methods. We used two classes of Messenger. The first was AnonymousMessenger, which is a modification of design pattern Messenger and its combination with design pattern Strategy. This class is an abstract class, and instances are created in the program run. The programs select which descendant to call according to the input value, data type respectively, see Fig. 2.

```
using System;
using System.Collections.Generic;
using System.Linq;
using System.Text;
using System.Threading.Tasks;

namespace ITT.Global_classes
{

    abstract class AnonymousMessenger
    {
        public List<double> Values { get; set; }
    }
    /// <summary>
    /// Abstract class contains properties
    /// </summary>
    abstract class GenericAnonymousMessenger<T>: AnonymousMessenger
    {
        virtual public IEnumerable<T> Keys { get; set; }
    }
    /// <summary>
    /// Messenger,transfer matrix of values(List) date type DateTime
    /// </summary>
    class AnonymousMessengerTime : GenericAnonymousMessenger<DateTime>
    {
        public override IEnumerable<DateTime> Keys { get; set; }
    }
    /// <summary>
    /// Messenger, transfer matrix of values(List) date type string
    /// </summary>
    class AnonymousMessengerString : GenericAnonymousMessenger<string>
    {
        public override IEnumerable<string> Keys { get; set; }
    }
}
```

FIGURE 2. Sample of transferring two attributes using class AnonymousMessenger

Class AnonymousMessenger is abstract and contains one attribute, namely Values. Class AnonymousMessenger passes down to GenericAnonymousMessenger, and this class adds attribute Keys, for the time being only as a generic data type. Keys is a generic data type for now as more kinds of data types are transferred, string and datetime respectively. AnonymousMesseneger passes down to two classes, namely:

- **AnonymousMessenger time** – transfers time and overlays List<**T**> keys to List<**datetime**>
- **AnonymousMessenger string** – transfers stringy and overlays List<**T**> keys to List<**string**>

We call static method TimeSeries (Fig. 3) which is entered by class AnonymousMessengerString as a parameter, which goes against an interface. We can then call methods with data collections of various data types. Notice that the method is marked, instead of a data type, with letter T, which is sufficient to know that it is a generic data type.

```
//create messenger and call algorythm
var messenger = StatisticMethods.TimeSeries(new AnonymousMessengerString()
{ Keys = listPom.Select(x => x.Key.Value.ToShortDateString()).ToList(),
Values = listPom.Select(x => Convert.ToDouble(x.Sum)).ToList() });
messenger.Description = "Time serie - repair count";
messenger.Title = "Repair count";
```

FIGURE 3. Sample of Code 1

The second used class of Messenger was GraphsMessengerPattern, see Fig. 4. This class serves to transfer more attributes between windows drawing graphs and methods analysing data. The purpose is to separate individual calculations from drawing windows. The values are calculated in class statisticMethods.cs, which was already mentioned and analyses data. The analysed data is then sent to window **Graphs**, which draws individual graphs. The figure depicts all attributes included in Messenger. Notice that each attribute is represented by one so-called property and at the same time it is public. The use of the class will be demonstrated in the following figure. As mentioned above, the class is closely related to data analysis and graph creation. In this given case, there is a need to return several values from the method at once, which will be served by Messenger. The figure shows the use of design pattern Messenger and its attributes when we need to return several values from the method that analyses the data.

```
var graphs = new GraphsWindow(
                  new GraphsMessengerPattern() {
                        Labels = labels.Take(100).ToList(),
                        Description = "Histogram repair count",
                        Points = lines.Take(100).ToList(),
                        Title = "Repair count"}, "Histogram");
```

FIGURE 4. Sample of Code 3

FACTORY PATTERN AND ITS USE IN REAL DEVELOPMENT

This design pattern is frequently used and primarily deals with the creation of individual objects – classes. It concerns a design pattern dealing with object creation, so-called **Creational Pattern**; design pattern division is stated above. It defines an interface for the creation of individual objects, and it does not create objects itself, this operation is performed by interface descendants. Factory thus uses basic characteristics of OOP, i.e. inheritance [4].

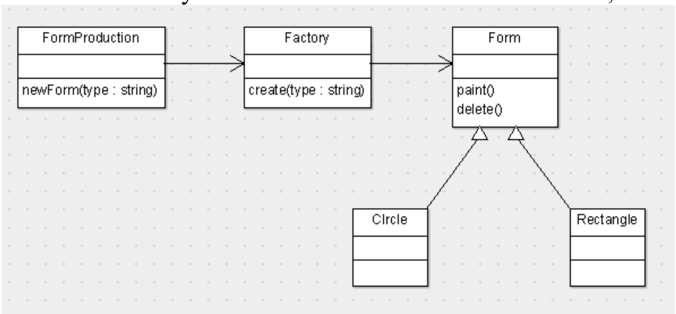

FIGURE 5. Architecture of pattern Factory

Within the research, design pattern factory is used to create individual groups to define failures. Our class is called Factory and is a modification of design pattern Factory. It concerns an abstract class which other classes will use to inherit from. Figure 5 shows a so-called Class diagram describing classes constructed according to design pattern Factory. The code uses so-called programming against an interface. As can be seen, class Factory contains virtual methods, which do not have a body and will be overlaid by descendants, and one static method to define descendants, which will overlay class Factory. For now, all switches nodes are default set to class CategoryFactory1 since other classes are not defined yet. More precisely, the process of defining a business process when individual workers on individual types of devices must define their internal structure. This process is very demanding and time-consuming. Statistical method GetFactory is entered by an integer value representing the number of the given factory, and the method returns an individual class which overlays the abstract Factory.

```
///<summary>
///Category 1 for choosen device
///</summary>
public override List<string> Category1
{
    get
    {
        return new List<string>() { "Conveyor", "UL", "MIX",
"Manipulators", "Gain SPT", "Table", "Aggregate", "Preparation SPT",
"Station", "Safety", "Switchboard" };
    }
}
```

FIGURE 6. Factory properties of class CategoryFactory1

The figure 6 shows a code from class categoryFactory1, which inherits from class Factory and overlays its properties. Property Name represents the name of a given Factory and another two properties Category1 and Category23Dictionary represent categories of individual fixings. Let's move on to methods featured by class CategoryFactory1. Each method is entered by a string representing selected category 1, inside the method body there is a switch, which decides, based on the input value, which branch to perform while branches contain constructors for individual libraries. If a user selects, for instance, Manipulator as category 1, manipulator constructor is called and as Category23DIctionary properties, a library for manipulators is initialised. This enables to "break down" all devices and define all categories of fixings on individual devices. It enables us to define in detail individual failures in order to analyse and understand the given problem by the managing staff. Individual devices are divided into groups. Each group of devices will represent own Factory.

CONCLUSION

The main objective was to point out the fact that a possible development of an information system oriented on BI cannot do without the implementation of real design patterns. The whole information system was created according to the principles of iterative development and the use of the UML language. In addition, it will be described in a separate paper, which is currently in the state of preparation. It is necessary to mention that the developed IS is currently implemented in a corporate company branch with the main office in the Czech Republic. It is daily used by dozens of people and manages more than 10 thousand items.

ACKNOWLEDGMENTS

The research described here has been financially supported by the University of Ostrava grant SGS/PrF/2019.

REFERENCES

1. A. D. Nerkar. Business Analytics (BA): Core of Business Intelligence (BI). International Journal of Advanced Engineering, Management and Science, 2(12), 2016.
2. Li, L., Chou, W., Zhou, W., & Luo, M.. Design patterns and extensibility of REST API for networking applications. IEEE Transactions on Network and Service Management, 13(1), 154-167, 2016.
3. J. W. Cooper. Design Pattern Java Companion. Addison Wesley, 2017.
4. E. Volna. Recommender systems in knowledge-mining. In *AIP Conference Proceedings* (Vol. 1863, No. 1, p. 070003). AIP Publishing, 2017.

DEMO Methodology and its Potential for Collaboration

Frantisek Hunka[a)], Jiri Matula[b)]

University of Ostrava, Department of Computer Science, Dvorakova 7, Ostrava 1, Czech Republic

[a)]frantisek.hunka@osu.cz, [b)]jiri.matula@osu.cz

Abstract: DEMO (Design Engineering Methodology for Organization) has its foundation in Enterprise Ontology and provides a strong theoretical foundation for business process modeling. Thanks to its theoretical background, the DEMO methodology has a good body of empirical appropriateness for many different areas of enterprise modeling. On the other hand, the DEMO methodology provides generic framework for business process modeling and doesn't deal with domain specific artifacts. The aim of the paper is to contemplate and propose some ways how to utilize the DEMO potential for collaboration with other business process modeling methodologies.

INTRODUCTION

The DEMO methodology is based on the theory of Enterprise Ontology and provides a generic platform for business process modeling, and much more [1, 4]. DEMO is based on a generic ontology e.g. enterprise ontology, which is an ontology that meets the strictest requirements provided by conceptual modeling theories. DEMO is further based on social communication and language theories of Habermas [1] and others, general systems theory, the design science paradigm [3], conceptual languages, native executing software engines [5] and strong formal foundations. DEMO is a modeling methodology that provides four so-called aspect models of an enterprise. These four DEMO models are propositions in a formal language, each with a precisely defined grammar and vocabulary. Its strong formal foundation enables the design and implementation of a software engine that directly executes DEMO models. This approach eliminates any programming; the model is the executable specification. The practical value for business process modeling in a professional environment is high. DEMO model execution in production provides many valuable capabilities; complete workflow(-like) control of the actors in the enterprise; total knowledge of each atomic communication act of each actor with complete audit trails and process-mining(-like) analysis of daily business process execution.

DEMO modeling has a good body of empirical appropriateness for many different areas of enterprise modeling in the professional world; "it works well for many areas and many projects in real life".

Enterprise Ontology is a generic ontology in the formal sense [1] which means that it captures strictly and exclusively the generic theoretical concepts within the domain ontology. These concepts are defined by the DEMO operation axiom [1]: i) "there is world of human actors that fulfill actor roles"; ii) "there is a world of communication, of communicative acts and facts between actors"; and iii) "there is a world of productions delivered by actors". In addition, the DEMO transaction axiom [1] states that actors communicate with each other follow a specific transaction pattern.

DEMO – MAIN FEATURES

According to DEMO (Design & Engineering Methodology for Organizations) methodology [1], an organization is composed of people (social individuals) that perform two kinds of acts, production acts and coordination acts. The result of successfully performing a production act is a production fact. An example of a production fact may be that the payment has been paid and accepted, or the offered service has been accepted. All realization-specific details are fully abstracted out. Only the acts and facts as such are relevant, not how they are achieved. The result of successfully performing a communication act is a communication fact. Examples of coordination acts are requesting and promising a production fact, which essentially constitutes a mutually binding contract. The subsequent communication acts and facts "state" and "accept" of the production constitute the fulfilment of that contract, agreed by both actors.

A fact is a proposition that can be either false or true, to be validated by empirical observation. A fact may encompass a single object, or may encompass more objects. Depending on the number of objects that are involved in a fact, we speak of unary, binary, ternary, etc., facts. An example of unary fact is that Vendor is a Person. Another example of binary fact is that a Customer receives a Pizza.

In DEMO modeling enterprises are represented by discrete deterministic systems that may exist in a set of precisely defined allowed states. For each state there is a set of allowed transitions to another state, the so-called state transition space. All other state transitions are forbidden and cannot occur. In general, a state is determined by the set of facts that exist at that moment. A state change or state transition consists of one or more facts starting or ending to exist. The occurrence of a transition at some moment is called an event.

Events are widely defined as "things that happen in the real world", and that cause some effects. In DEMO there exist only i) communication acts - one actor communicating with another actor, following the transaction pattern; ii) production facts that describe the production of a specific actor; and iii) facts, that are caused by acts in the real world that may become true or false. Example i): the pizza has been requested by the customer and promised by the pizza baker, a contract has come into existence. Example ii): the production fact of the pizza baker is a pizza margarita. Example iii): the exchange rate between the US dollar and the EURO is 1.234. By empirical observation of the real world this fact is either true or false.

The simplest application of value modeling can consist of two exchange processes. In the first process the purchase of goods is made whereas in the second process the sale of goods is made. So the initial activity of the first process is purchase accompanied by cash disbursement and the initial activity of the second process is sale accompanied by the payment for goods. For better understanding, the goods may be represented by artist's artifacts which can be sold in auction. It can be concluded from the previous description that the simplest REA process is composed of two transactions (give and take).

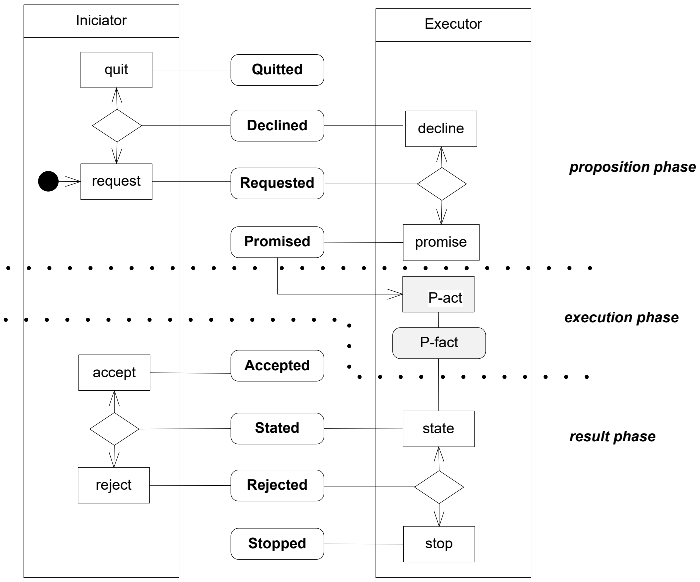

FIGURE 1. The Transaction axiom, the standard pattern source: [1]

The diagram in Figure 1 shows the standard pattern of the DEMO transaction axiom, which is a hypothesis about phenomena in the real world. It assumes that any transaction in the real world follows this pattern. It contains interrelated acts and facts and the transaction is in one of the allowed discrete states. The partition of the Initiator contains the coordination acts and the decisions, represented by diamonds in the diagram. The partition of the executor contains the corresponding coordination acts, the decisions and the production act and production fact. The production act and the production fact, depicted in grey color, are performed by the Executor. The coordination facts are situated in the middle of the figure as states in bold format. The complete transaction pattern can be extended by revokes of communication acts, since we observe these patterns also in the real world.

COLLABORATION ANALYSIS

A DEMO transaction represents a precisely defined state machine with states and state transitions. In case of DEMO, transactions are organized in a tree structure utilizing production facts aggregation (DEMO composition axiom) to form a business process. To express transaction dependence, the dependent transaction is enclosed within an 'independent' transaction in the context of a business process.

When thinking about different methodologies collaboration, the first thing that one may occur is a top-down concept mapping from one methodology to another. Direct mapping a different methodology to DEMO would require expressing each different methodology concepts in DEMO primitives. This approach would bring about a lot of incompatibilities because precisely defined DEMO primitives would be not properly defined and the benefits of the DEMO approach, strong ontological foundations, would be lost.

A bottom-up conceptual mapping is the alternative way:

Use DEMO to capture the phenomena in the real world, after all, we must understand and represent this as good as possible. The strong ontological foundations of DEMO are an advantage. The result is a DEMO model, supported by shared reasoning, validated and verified, that exhibits the phenomena we want to capture. This DEMO model will be used to identify all the phenomena that are needed for the different methodology. In fact, we try to construct different methodology concepts using DEMO concepts. The only way to realize this is empirical investigation and analysis; we must simulate and study DEMO models to identify the necessary other methodology concepts.

The only possible way to design some way of collaboration is to start from the common area of both frameworks. Majority of standard business process methodologies address only the production world. These methodologies do not properly and precisely capture social communication between the actors. The DEMO's Object Fact diagram is exclusively aimed at the world of production and its elements are depicted in the form of object classes and their property types and attribute types, which are arranged according to facts. These facts represent production facts.

In DEMO, actors communicate about some production fact. DEMO "says" nothing about production facts, except there is a hierarchical structure (DEMO composition axiom). Human actors commit themselves to a production fact (DEMO Request and Promise) and agree by communication (DEMO State and Accept) that the production fact exists in the real world. So, by analyzing the communication acts and facts it is possible to derive factual propositions about production facts such as "actors agree that a product has to be delivered" which is a mutually binding contract. The production facts "product X has been produced and accepted", "payment Y has been made" are the fulfilment of a contract. Since every atomic communication act and fact is precisely known and recorded at production time, it must be possible to provide complete and correct information about all events that occur in the real world.

The other modeling methodology works only with "production" activities. Its crucial concepts have the following meaning. An event usually reflects changes in the resources which may be expressed by e.g. utilizing the value of resource with regards to different partaking actors. It stands for a production act and production fact in DEMO. An agent that denotes a human being or an organization has its counterpart in DEMO actor, more specifically in its actor role. A resource is a concept of a domain specific ontology that is closely connected with production activities. DEMO as a generic methodology is able to capture the resource value changes in its coordination facts but it does not further record or processed them. The ability to capture a production activity by means of coordination activities is possible because the DEMO production fact comes into existence when it passes successfully through the accepted coordination fact. In DEMO, coordination facts have the following structure:

<performer> <intention> <addressee> <product>

Meaning of the individual parts of the coordination fact is following:

<performer> and <addressee> represents actor roles involved in the coordination fact,

<intention> marks the phase of the coordination act within the scope of transaction pattern,

<product> represents the result of the transaction. It includes production fact and property types (attribute types) of the product.

More precisely the structure of coordination act/fact is depicted in Figure. 2. The coordination act/fact comprises both performer and addressee in the for of subject and specific actor role. Intention represents specific coordination act such as request, promise, decline, state, accept, reject. Request, accept and reject communication acts are issued by the performer and promise, decline and state communication acts are issue by the addressee. In this way, one can obtained six different figures representing a standard transaction pattern. A product item can be captured either as an entity, which is represented by individual entity attributes (such as article type, number of items, price per unit,

delivery date) or by production facts. Examples of production facts are as follows: article type is pizza margherita, number of items is 2, price per unit is 9 €, delivery date is today at 18:30. As can be seen from the figure, each coordination act/fact includes production act/fact. This can be also seen in figure 1 but figure 2 provides a different view, which can be considered in a sort of way to be more related to collaboration analysis. The remarkable feature of the production is that it remains the same form the beginning to the end of the transaction, except for declining and rejection transaction steps.

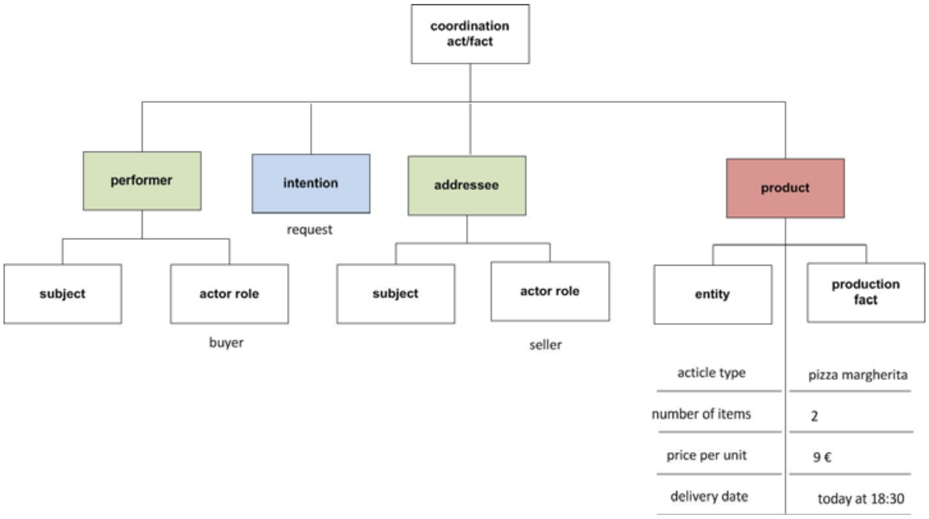

FIGURE 2. Coordination act/fact and its structure source [2]

A tree structure in which the DEMO transactions are arranged forms Bill of Material that can be used for DEMO model to capture all details.

CONCLUSION

The paper deals with the idea of different business processing methodologies collaboration. As a feasible way for different methodology collaboration with the DEMO methodology was proposed collaboration based on the conceptual facts which may be provided to the other methodology. These facts can cover all production facts but in many case even coordination facts. The validity of coordination facts may differ and strongly depends on the modeling domain. The DEMO transaction pattern is a generic pattern which captures all artifacts in social world. This pattern also covers revoking (cancelation) operations. It can be concluded that the DEMO methodology provides all necessary infrastructure for business process modeling.

ACKNOWLEDGMENTS

This paper was supported by the grant No. SGS06/PRF/2019 provided by Ministry of Education, Youth and Sports of the Czech Republic.

REFERENCES

1. J. L. G. Dietz, *Enterprise Ontology Theory and Methodology*. Springer-Verlang, Berlin Heidelberg .2006
2. J. L. G. Dietz, *The Essence of Organization. An Introduction to Enterprise Engineering.* Sapio bv, 2012
3. A. Hevner, A three cycle view of design science research. Information systems and Decision Sciences, Scandinavian Journal of Information Systems, 2007, 19(2): 87-92. University of South Floria, USA.
4. S. J. H. van Kervel, Ontology driven Enterprise Information Systems Engineering. (Doctoral dissertation) SIKS Dissertation series nr. 2012-50 Delft University of Technology. 2012
5. S. J. H. van Kervel, J. L. G. Dietz, J. Hintzen, T. Meeuwen, B. van Zijlstra, Enterprise Ontology driven Software Engineering. Proceedings of ICsoft 2012 – 7th International Conference on Software Paradigm Trends. SciTePress. 2012

Derivation of the Concepts in Data Modelling

Zdenka Telnarova

University of Ostrava, Faculty of Science, Department of Informatics and Computers, 30. dubna 22, Ostrava, Czech Republic.

Corresponding author: Zdenka.Telnarova@osu.cz

Abstract. Theoretical development in the area of databases systems has been keeping its dynamics. One of its directions is unfolding the conception of derived data. Models based on derived data are the outcome of the combination of logic programs and databases. They can potentially solve many problems in analysis, design and implementation of databases and information systems and add semantics to the databases. We can use deductive rules for derivation of classes/relations, derivation of attributes, views, for design of query, for expressing integrity constraints.

THE RECENT DEVELOPMENT IN THE AREA OF DATABASES SYSTEMS

Hardly any other area of informatics has undergone such an extensive development of theoretical conceptions as database systems. The first commercial software applications of database systems were available to users already at the end of the 60s (IMS and IBM firms). It might seem that enough time has passed and that the entire theoretical development has already reached its accomplishment. Yet, after more than fifty years that is not true, and the current development still brings a number of new views and conceptions the only aim of which is more exactly to seize a reality to be modelled.

The recent development in the area of database systems has progressed from the oldest hierarchical conception characterized by a quite rigid structure of hierarchic relations among data elements of entity nature, through network conception that was actually the improvement, generalization of hierarchical conception, to relation conception. Database modeling is also influenced by fuzzy theory [1] and current trend leans to NoSQL databases like document-oriented, graph oriented, etc. Into the group of graph-oriented approaches we can include RDF models and OWL [3], [4]. Many other concepts can be seen for example with connection to LMS systems [2]. In all these models deductive approaches play important role.

DERIVED DATA IN DATABASES

This contribution will at least briefly concentrate on the problem of modelling of derived data in databases. The pure relational theory does not deal with derived data. There is a notion that derived data will always come into existence only on the basis of selection of atomic data from the database and that they are presented by users as a reflection of the immediate state of the database. In practice, however, the application of such approach brings a considerable set of problems. At frequent selections of the same nature from extensive databases, the overall efficiency of processing is decreasing. An ordinary requirement from the area of business is a requirement for the derived data to be filed in some way and analyzed later (time series, overall surveys and the like). A data model may contain objects/relations and attributes whose instances or values are derivable from other instances and thus they are obtainable from the data stored in the database. Derived instances can be represented as additional information. Rules for derivation of additional information are being created in the phase of designing the information system.

Analogically object or compromise object-relational conception by comprising methods to object-classes easily solves the creation of derived data defined by the method. Another, probably more sophisticated, but also more

specifically orientated conception modelling the derived data is a conception of semantic data models. This conception will be later dealt with in greater detail.

Semantic data models are based on the support of theory of proving and they are able to deduct additional facts from the database. Specified deductive axioms and deductive rules have been built in them.

DEDUCTIVE RULES

Conventional database systems do not work with a term deductive rules and its partial function is exercised by queries. In semantic database systems the rules are the basic concepts used in order to obtain information from the database. In addition to it, the rules are used as means for maintaining database consistency. From a formal standpoint, the rules are declarative expressions. By their evaluation (or an appropriate interpretation) it is possible to obtain additional information from the database.

Introduction to deductive rules

Deductive rule is an expression in the form:

$$\text{Conclusion} \leftarrow \text{Premise}$$

where conclusion is an atomic formula (head of the rule) and premise is a formula (body of the rule). Theory of deductive rules is based on deductive axioms; deductive axiom is a rule by which we are able to deduce additional facts from the given facts.

Deductive rules can be used to express the subsumption relationship between concepts, to define intentional predicates, to express different types of knowledge, to represent causal relationship between causes and effects.

In terms of analysis, design and implementation of information system we can use deductive rules for derivation of classes/relations, derivation of attributes, views, for design of query, for expressing integrity constraint.

Deductive rules for data derivation

As it has already been mentioned, deductive rules can serve as a powerful tool for data derivation on the basis of extensional data stored in the database and for defining of requirement for database consistency. Creator of database system should weigh which classes/relations and attributes must be the part of extensional database, and which can be derived.

Rules for derivation of attributes

Concrete examples will be focused on students environment. Let us have, for example, a class Student:

```
Individual Student in Class with
attribute
    id_num : String;
    name : String;
    year : Integer;
    st_results : Results
End
```

where Results are also a class:

```
Individual Results in Class with
attribute
    semester : Integer;
    course: String;
```

```
    branch: String;
    credits_requested: Integer;
    credits_gained: Integer
End
```

Rules for deduction of recursive attributes

For derivation of the attribute prerequisites a recursive deductive rule for the transitive closing of relation will be applied (the attribute prerequisites is a set of all courses that have to have been completed by a student so that they could enter their names for a given course):

```
Define implementation for Course
attribute
    X in Self.prerequisites ← Course(X), X in Self.requisite;
    X in Self.prerequisites← Course(X), X in Self.requisite.prerequisites
End
for a class Course:
Individual Course in Class with
attribute
    course_no: Integer;
    c_name: String;
    g_member: Group;
    requisite : Course
End
```

Rules for derivation of classes

On the basis of concrete values of the given attributes it is possible to define classes. Example can be a class Inf_branch_student that represents all students for which the value of attribute branch = Informatics.

```
Define implementation for class Student
population
    Inf_branch_student(X) ←  Student(X), X.branch = ,Informatics´
End
```

Rules for inversion relation

Let us have such classes Course and Group so that there is an inversion relation between them. Attribute g_member of the class Group and attribute g_member of the class Course are then inversion attributes. From the view of database integrity maintenance it is more convenient to define one of these attributes as derivated by applying a deductive rule:

```
Define implementation for Course
attribute
    X in Self.g_member  ←  Group(X), X.g_member= Self
End
```

Class Group will be defined:

```
Individual Group in Class with

attribute

    group_no: Integer;

    students: Student;

    g_member: Course

End
```

CONCLUSION

Semantic databases score a fast progress at present. It is mainly because of their ability to model reality more precisely, to process complex data more efficiently and to ensure better the independence of data both on users´ applications and on their implementation. In connection with semantic databases we talk about a so called knowledge independence that can be considered as another step to flexibility of databases and their applications. Therefore, the field of analysis and design of IS with a database by employing deductive approaches is certainly a topical theme mainly in connection to RDF and OWL as well as to graph orientation in general.

REFERENCES

1. P. Smolka and V. Bradac, " Fuzzy Queries above Relational Database," in Proceedings of the international conference of computational methods in sciences and engineering 2017 (ICCMSE-2017), *AIP Conference Proceedings* 1906, DOI: 10.1063/1.5012350
2. P. Smolka, "Concept of Outcomes Evaluation Model in LMS Moodle Conditions Working in a Vague Background," in *Proceedings of the international conference on numerical analysis and applied mathematics 2016 (ICNAAM-2016)*.
3. A. Lukasova, M. Vajgl and M. Zacek, "Knowledge Represented Using RDF Semantic Network In The Concept of Semantic Web," in *Proceedings of the international conference on numerical analysis and applied mathematics 2015 (ICNAAM-2015*). DOI: 10.1063/1.4951895
4. A. Lukasova, M. Zacek and M. Vajgl, "Building a Non-monotonic Default Theory in GCFL Graph-Version of RDF," in *Modern trends and techniques in computer science (CSOC 2014),* pp. 455-465, DOI: 10.1007/978-3-319-06740-7_38.

NoSQL Databases for Large Volumes of Data

Zdeňka Telnarová [1, a)], Martin Žáček[1, b)], and Pavel Smolka[1, c)]

[1] *University of Ostrava, Faculty of Science, Department of Informatics and Computers, 30. dubna 22, Ostrava, Czech Republic.*

[a)] Corresponding author: Zdenka.Telnarova@osu.cz
[b)] Martin.Zacek@osu.cz
[c)] Pavel.Smolka@osu.cz

Abstract. The paper is devoted to the issue of NoSQL databases and their application in gradually increasing volumes of data in databases. Concerning approaches, three are covered: key-value databases, column-oriented databases, and document databases.

INTRODUCTION

In the present days, it seems that most large enterprises minimally take care about the maintenance of their current enterprise systems. It results in the use of incorrect database schemes and the databases degrade [1]. The authors of this statement take grounds in the discussion with more than twenty databases administrators (DBAs) from three large enterprises. The database change according to conditions in the business, commonly once per quarter or more. Heterogeneous and dynamic data environment leads to a frequent disappearance of the central administrator. A more frequent is rather a decentralised approach with more groups of DBAs, who deal with enterprise databases. (Pokorný)

Databases are usually relational. Since the introduction of the data relational model, there have been several additional databased models introduced, such as object-oriented (OO), object-relational, (OR), XML, or RDF. OO and OR DBMSs reacted to object approaches in software engineering from the 90's. Such means, however, have never been really competitive. The reasons could have been in the lack of their theoretical bases and limited performance.

Simultaneously, there is an explosion of database technologies. In order to secure such a massive increase of data, it is necessary to develop other approaches which resign to strict structural requirements. Storing and processing large collections of data is often done by the use of NoSQL databases. NoSQL means "not only SQL" or "non SQL", which makes this database category very diverse and not much clearly specifiable. NoSQL databases, whose development started in the late 90's, offer easier scalability and higher performance compared with relational databases. The first generation of NoSQL systems represented only elementary interface, i.e. key-value. It mostly concerned systems without a scheme which do not require a definition of the type associated with the value stored in the database. Currently, there are hundreds of so-called NoSQL databases, the most popular are MongoDB, HBase, and Cassandra. Mongo DB is based on the document model. HBase and Cassandra are based on the column model.

CONSISTENCY, AVAILABILITY, TRANSACTION

The basic dilemma of NoSQL databases is consistency versus availability as well as ensuring transaction processing (ACID transaction properties).

NoSQL databases support various levels of consistency

- Strong consistency. This system ensures that the data provided to the user reflect all updates accepted by the system.
- Timeline consistency. In such a case, the system ensures all data updates, although reading operations in progress do not have to provide updated data accepted by the system.
- Eventual consistency. In such a case, the system does not guarantee update of all system replications.

NoSQL databases are known for an existing contradiction between consistency and availability. A highly available system also needs to have operations allowed in a case of one unavailable system node. This could result in doubts whether the system stays consistent after the operation has been terminated.

ACID guarantee

- Traditional relational databases ensure ACID properties.
- Atomicity: Operation which creates a transaction creates an atomic unit which must be performed as a whole. If a transaction cannot be performed, the database must be restored to the state before transaction initiation.
- Consistency: Operations transfer the database from one consistent state to another consistent state. It is impossible for the database to be inconsistent after a transaction.
- Isolation: Operations which must be restored after an incomplete transaction must not affect the result of other, already confirmed transactions.
- Durability: ensures that data changes after a successfully performed transaction will be permanently retained.
- NoSQL databases differ from relational databases in this support. Most of NoSQL do not support the ACID guarantee.

CAP theorem

The CAP theorem, also called Brewer' theorem, is related to distributed systems. It concerns properties to ensure the operation of a distributed database system. It includes three requirements: Consistency, Availability, and Partitioning tolerance. In addition, it also states that it is not possible to meet all of them at 100%.

CAP in connection with NoSQL databases was understood with the following properties:

- Consistency means that the same data is available at a certain moment in all nodes of a distributed system.
- Availability means that each client sending a request receives a response about the operation being successful of not.
- Partition tolerance states that if there is a failure on a part of the network, the system must still be able to respond to requests.

Scalability

The volume of data stored on the Internet is increasing and thus it is necessary to ensure more premises. If it concerned only data not intended to be read, we would get along with a mere extension of disk capacities on web servers. Yet, it does not make sense to store data not intended to be read, higher capacities go hand in hand with the response of applications which work with such data (either for reading, writing, or updating) because these applications must search through the data and organise it. Scalability is primarily discussed in [4].

André Bondi from AT&T Labs states that "Scalability is a desirable attribute of a network, system, or process. The concept connotes the ability of a system to accommodate an increasing number of elements or objects, to process growing volumes of work gracefully, and/or to be susceptible to enlargement." And that scalability is the ability "(1) to function well as it is changed in size or volume in order to meet a user need; and (2) not only to function well in the rescaled situation, but to actually take full advantage of it."[2]

Increasing disk capacity in relational and non-relational systems is not usually sufficient. Therefore, it is the system performance that is increased, which can be achieved by two methods:

Vertical scaling

Performance increase of a physicals server is done, for instance, by adding memory and replacing the processor for a more powerful one. This way of scaling is, however, limited. The limitations are compatibility and primarily financial demands as this method requires high-performing, thus expensive, hardware. Frequently, the server itself must be replaced.

Horizontal scaling

On the other hand, horizontal scaling takes a different way. It does not attempt to improve one server, but it distributes the data to more servers which mutually cooperate. It does not have to seem at first sight, but this approach is cheaper as less powerful machines are required. An undoubtable advantage is also the fact that there is no theoretical limit for the capacity increase.

BASIC APPROACHES TO NOSQL DATABASES

Key-value databases

Associative fields or HashMap are the simplest data structures that can hold a key/value pair. The key is a unique value, which can be used to search data. The key-value databases can be of different types. Some of them store data in memory and others enable to store the data on a disk.

The most known databases of the key-value system are:[3]

Redis
Official website – http://redis.io/
The project was initialised in 2009 as an independent project. VMware became the sponsor of Redis.

Voldemort
Official website – http://project-voldemort.com/
Created by LinkedIn in 2008.

Cassandra
Official website – http://cassandra.apache.org/
Developed by Facebook. In 2008, the project became an open source. Apache Cassandra was then donated to Apache Software Foundation. It is used by Facebook, Twitter, etc.

Column-oriented databases

Column-oriented databases store data in a column form, not in a row one known in relational databases. For example, let's have a two-dimensional table storing data about products

Id	category	code	price
1	5	101	5,000
2	3	250	800
3	5	102	2,000

In a table database, data would be stored as follows:

Id	category	code	price
1	5	101	5,000
2	3	250	800
3	5	102	2,000

Column-oriented databases, however, join all values in columns together.

1,2,3;

5,3,5;

101,250,102;

5.000,800,2.000;

Column-oriented databases are more powerful when we need to perform an aggregation function over many rows, but on a limited number of columns. This powerfulness also become evident if we want to change column values in all rows at once.

The most common representatives are:

HBase

Official website – http://hbase.apache.org

Created by Powerset in 2007. The project later became a part of the Apache Software Foundation. Use: Facebook and others.

Document databases

Document databases are not systems to manage documents. The term “document” in document databases means freely structured key-values in documents. The basic element here is a document where data is stored and which is marked with a unique identifier and a set of key-values. Storing data is usually done by means of JSON.

The most common representatives are [3]:

MongoDB

Official website – www.mongodb.org.

Created by 10gen, which develops it as an open source. Use: FourSquare, and others.

CouchDB

Official website – http://couchdb.apache.org a www.couchbase.com

In 2005, Damien Katz started to write it, but after two years he released it as an open source. In 2008, the project was incorporated under the Apache Software Foundation. Use: BBC, Apple, CERN, and others.

CONCLUSION

In the conclusion, we would like to express our opinion on the usability of NoSQL. We would choose a NoSQL product in case of tens or hundreds of millions of records or if the data structure changed frequently. Then, NoSQL advantages would prevail. In other cases, we would rather keep to SQL systems, whose language is powerful with high expressivity and can use semantics of data. Concerning a shift from a relational database to a NoSQL database, MongoBD would be the choice as we suppose it to be the most sophisticated with well-elaborated documentation, and materials are very easily accessible.

REFERENCES

1. M. Stonebraker, D. Deng, M. L. Brodie, “Database decay and how to avoid it”. In: *Proc. of 2016 IEEE Int. Conference on Big Data*, IEEE Explore (2016), pp. 7-16.
2. A. B Bondi, Characteristics of Scalability and Their Impact on Performance [online]. [cit. 2019-02-03]. Available at: https://www.win.tue.nl/~johanl/educ/2II45/2010/Lit/Scalability-bondi%202000.pdf
3. Professional NoSQL. Indianapolis, Indiana: John Wiley & Sons, Inc., 2011. ISBN 978-0-470-94224-6.
4. J. Pokorný, NoSQL Databases: a step to databases scalability in Web environment. *Inter-national Journal of Web Information Systems*, 9 (1) (2013) 69-82.

Smart Building with Loxone System

Martin Žáček[1, a)]

[1]University of Ostrava, Faculty of Science, Department of Informatics and Computers, 30. dubna 22, Ostrava, Czech Republic.

[a)]Corresponding author: Martin.Zacek@osu.cz

Abstract. The article focuses on Smart Building and its realization. The Smart Building uses Loxone for home control. The article aims to describe the house, describe the Loxone system and its components (hardware). Next show distribution point - the intelligence of the Smart Building. In conclusion, the article deals with other possibilities of expanding the intelligent house and its vision.

INTRODUCTION

The definition of a Smart Building will take into account the recognized need for holistic and integrated design, taking into account both the current themes described in the literature, the drivers for building progression and the methods through which these can be achieved [1]:

"*Smart Buildings are buildings which integrate and account for intelligence, enterprise, control, and materials and construction as an entire building system, with adaptability, not reactivity, at the core, in order to meet the drivers for building progression: energy and efficiency, longevity, and comfort and satisfaction. The increased amount of information available from this wider range of sources will allow these systems to become adaptable, and enable a Smart Building to prepare itself for context and change over all timescales.*" [1]

Figure 2 shows the diagrammatic representation of the authors' Smart Building definition [1].

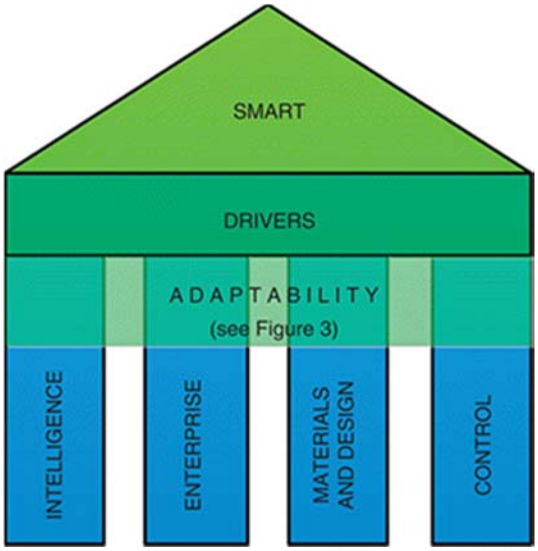

FIGURE 1. Definition of the Smart Building [1].

BASIC DESCRIPTION OF THE HOUSE

Installation of intelligent management was in a passive house, which is situated mainly on the south side. Basic description of the passive building:

- bungalow with a gable roof,
- roof insulation - blown cellulose,
- building size: 4kk + garage (kk = open-plan kitchen),
- French windows in the living room.

Current equipment of the passive building:

- a regenerative brake with a heat pump,
- a hot water boiler with a heat pump,
- photovoltaics,
- an outdoor blind,
- a light control - outdoor and indoor,
- a building heating - resistance wires,
- fire alarms (not yet connected).

The connection (see Figure 2) of all sockets, lights, appliances, and technology is wasted into the distribution box.

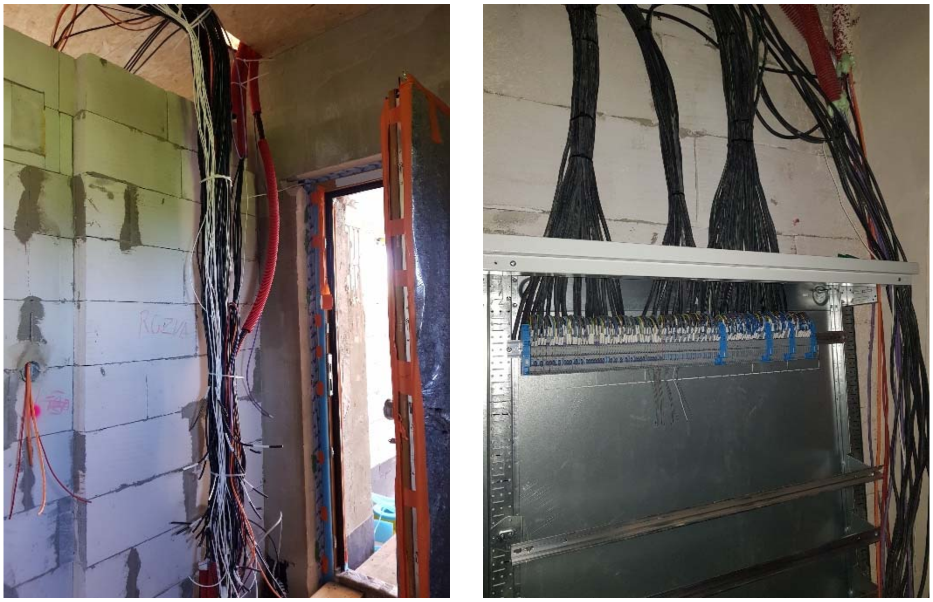

FIGURE 2. The wire distribution box.

SYSTEM LOXONE FOR CONTROL BUILDING

Countless systems on the market can be used in a building (such as iNels, Insight Home, Siemens, and now Google).

The intelligent control installation can be applied in any room or building. We have to choose the right technology we want. If one is a new building, I recommend everything to lead by cable. If the building is already built or it is an apartment, we can use wireless technology without interfering with the house construction.

Given that my building was new chose the system Loxone with cables for my building, which was at the time of construction of the house available. Loxone is not a closed system for users - each user can program this system with active elements completely alone.

"Loxone Smart Home" works just like the nervous system of animals. It connects all devices with sensors (senses) to the central unit (brain) – Miniserver (see Figure 3). This central system (unit) is located in the distribution box. The purpose of the smart building is the monitoring of essential things for us, on which then reacts without our interaction.

FIGURE 3. The Miniserver of the Loxone system [2].

The Miniserver evaluates available sensor data and makes intelligent decisions. It learns by the intelligence it contains and takes care of things, which we can't. For example: turns the heater on well before we come home; it simulates the presence in the building even when we are on vacation; uses shading technology to control temperature; monitoring water leakage - in time when we are not at home.

FIGURE 4. The distribution box with Loxone system.

Figure 4 shows a distribution box that contains the following components: Miniserver, Extension, Dimmer, Relay, Modbus Extension, RS 232, Tree, RGBW Tree.

EXPANDING SMART BUILDING AND VISION

The suggestion of hardware extension

The smart building is not complete. The plan is to extend the intelligence using the alarm system (motion sensors, cameras, and recording technology). In the building, there will be and electronic valve of the main water pipe and sensors for water leakage in the kitchen, bathroom, toilet and utility room.

It is planned to place on the roof of a weather station to measure wind speed (more than the maximum speed Loxone system pulls outdoor blinds), measuring the intensity of sunlight (in the summer period leads to shielding the building before overheating by outdoor blinds).

The suggestion of software extension

Many scientific articles are dealing with software expansion of a smart building, such as using any database [3]. On a higher level of abstraction, we can use the ontology [4] (representing a logical model [5]) for the intelligent building, which is very widespread today. Here, an ontology contains a complete description of the whole smarts building. An example is the authors' ontology [6].

The basis of any ontology is concept [7, 8] and relationship. The concept in the house can be, for example sensor, heating, blinds. In my case, the Loxone system uses its software.

CONCLUSION

The paper introduces the implementation of intelligent control to a new building. The output is the Smart Building that is controlled by the Loxone system. The Smart Building is not yet complete; some components are missing, as it was written in the article. As we can see in the article, for a house to be intelligent, it is not enough to use only intelligent elements, but mainly the house has to learn itself, but it must be properly programmed.

REFERENCES

1. A. H. Buckman, M. Mayfield and S. BM Beck, "What is a smart building?" in *Smart and Sustainable Built Environment*, 3(2), 92-109 (2014).
2. Loxone Smart home, http://www.loxone.com
3. P. Smolka and V. Bradac, "Fuzzy Queries above Relational Database," in *Proceedings of the international conference of computational methods in sciences and engineering* 2017 (ICCMSE-2017), DOI: 10.1063/1.5012350.
4. Z. Telnarova and J. Schenk, "The Logical Model for Pattern Representation," in *Proceedings of the international conference on numerical analysis and applied mathematics 2015 (ICNAAM-2015)*, DOI: 10.1063/1.4951892
5. Z. Telnarova, "Transformation of Extended Entity Relationship Model into Ontology," in *Intelligent information and database systems, ACIIDS 2018*, PT II, Lecture Notes in Artificial Intelligence 10752, pp. 256-264, DOI: 10.1007/978-3-319-75420-8_24
6. M. Žáček and M. Janošek, SBOnto: Ontology of Smart Building. *Far East Journal of Electronics and Communications*, 2017, pp.1101-1109. DOI: 10.17654/EC017051101
7. P. Smolka, "Concept of Outcomes Evaluation Model in LMS Moodle Conditions Working in a Vague Background," in Proceedings of the international conference on numerical analysis and applied mathematics 2016 (ICNAAM-2016), DOI: 10.1063/1.4992231.
8. Janosek, M., Volna, E., & Kotyrba, M. Knowledge discovery in dynamic data using neural networks. *Cluster Computing*, *18*(4), 1411-1421, (2015).

Methods and Algorithms Computer Reading Text for Czech Language

Martin Žáček[a], Zdeňka Telnarová[b]

University of Ostrava, Faculty of Science, Department of Informatics and Computers, 30. dubna 22, Ostrava, Czech Republic.

[a]Martin.Zacek@osu.cz, [b]Zdenka.Telnarova@osu.cz

Abstract. The article aims to process methods and algorithms of computer reading. The authors follow up on the previous work of the authors and describe the synthesis of Text to speech and show the possibilities of using libraries for the future intonation reader with a focus on the Czech language. The result of this study is an understanding of the methodology of reading the Czech text.

INTRODUCTION

On the market, there are countless ways to help blind people (people with special needs). The first option is to use the Braille font but in the case of a printed version. Another option is to use a special program that reads the text in electronic form. In an article [1], the authors focused on several programs for reading texts. Among the most interesting special programs are the authors describe programs: Balabolka, CIT Reader, Text to Speech Reader Windows. These readers of the text but monotonously read the text, so it becomes for people with specialized needs quite difficult in the text often confess.

Language synthesis is an artificial reproduction of natural speech. A computer creates speaking terms. They are not played from a pre-recorded set of expressions but are currently created.

This sound material is divided into small parts, called units. It can be individual vowels (i.e. phonemes), e.g. “A” and “E,” but also diphthongs, such as “OU” or “IA,” or even whole syllables. This is very important because the same letter can always be different depending on the surroundings. For example, in the word “melodie” (melody) in the Czech language, the letter E appears twice, but it is always different.

The units are then assembled with extremely sophisticated algorithms into a new, fluent audio text. These algorithms use their own synthesis; in the strict sense it means “compilation.” It requires some understanding of the text to read as a result as possible as naturally as possible. There is a simple rule that voice with a question mark has to increase; at the end of the sentence marks a decline. However, for a natural intonation of the voice (prosody) to exist within a sentence, the program must know where the subject is in the sentence because there is a stronger accent on that word. Naturally, these analytical procedures are much more complex. This program must proceed as Latin students!

TEXT-TO-SPEECH (TTS) SYNTHESIS

Text-To-Speech Synthesis is performed in several stages:

1. TTS receives text as input
2. The text is analyzed (text analysis)
3. Subsequently, the transformation is made to phonetic transcription
4. The output is a spoken output.
5. Then prosody is created.

These existing information can produce spoken output.

Text analysis for the Czech language

The text analysis consists of several steps:

1. Suppose we have the following texts: "č."(No.), "12" and the year "1997." For the token "č." is created by orthographic expansion form "číslo" (number), the token "12" gets the orthographic "dvanáct" (twelve), and "1997" will be transformed into " devatenáctsetdevadesátsedm " (nineteen-ninety-seven). As we can see, this expansion is not easy under certain circumstances. We can give an example of the number "1" in the Czech language. This example must be expanded according to what it indicates. If it indicates a numeral, so we get "jedna," in the expression "1 kilogram" will be "jeden," in the phrase "1 kočka honí 1 psa" must be "1" is expanded as the first "jedna," and the second as "jednoho."

It is very simple in English, as we can see in the following table (Table 1).

TABLE 1. The number "1" in Czech language and English language.

Number "1"	Czech language	Englich language
"1"	jeden jednoho jednomu jedna jedna jedne jednou	one

2. Also around the token is analyzed during text analysis: Abbreviation "den."(day) cannot determine without context analysis whether it should be expanded as "denně," "denní," "denního," "denním," "denních" etc. Contextual analysis is also needed in German, for example: to remove ambiguities from accents. eg "modern" and "modern" which cannot be distinguished based on the method of writing [2].

The rules of pronunciation

After completion of textual analysis can be applied rules of pronunciation. After completion of textual analysis [5] can be applied rules of pronunciation. An individual character under certain circumstances may not correspond to any or more phonemes. Also, a single phoneme can respond to more letters.

Two strategies are used to determine the pronunciation of words:

- In solutions with morphological components based on the dictionary is stored the largest amount of morphemes in a single dictionary. Full shapes are created by flexural, derivative, and compositional rules. Alternatively, the full-form dictionary is constructed so that all existing word forms are stored therein. The pronunciation of those words that are not stored in the dictionary is made up of pronunciation rules.
- In rule-based solutions, pronunciation rules are created from phonological knowledge of dictionaries. Only words are included in the exception dictionary if the pronunciation is an absolute exception [2].

The two approaches differ in the size of their dictionaries, whereby a dictionary-based solution is many times greater than the exception dictionary solutions based on rules. Solutions based on a dictionary or there may be more accurate than solutions based on the rules if they have a large enough phonetic dictionary.

3. Once the pronunciation is established, then generating the prosody follows. The degree of naturalness of a TTS depends on prosodic factors such as modulation of intonation (phrasing and accenting), modulation of amplitude, and length of modulation (this includes voiced time and voiceless time, thereby determining the length of the syllable and speech rate).

Prosodic features have different functions:

- With their help can be discerned sentence focus, i.e. emphasizes the important or new constitution.
- Besides, the prosodic qualities are responsible for splitting the sentence.
- They can create relationships between parts of sentences or sentences and determine the type of sentence (the sentence notification - the sentence interrogative).

Syntactic information has particular importance in creating prosody. Thanks to the knowledge of the syntactic structure of sentences can be calculated prosody for most sentences.

In some sentences are important semantic and pragmatic information:

- Sentences that are ambiguous in their structure often get a different meaning according to the highlighted element.
- The position of the focus is particularly important in negative sentences: folders that relate to negative should be emphasized by an accent (for example: "Marie nejela autem do Hamburku."(Marie did not go to Hamburg by car.)).

Semantic and pragmatic knowledge is available only a few TTS [2].

4. Data from the speech processing module is passed to the output processing module. Here performs the actual synthesis where the audio output is generated. The units are selected and chained in the case of flotation synthesis. For each audio unit are selected the best candidates from the database (if more suitable candidates are available) and ranked behind each other [2].

SPEECH SYNTHESIS IN C

The speech synthesis (also known as Text-to-speech) is used to generate human speech by computer. A program that does this is called a synthesizer. The best option for the Czech language is Speech API (SAPI), which is integrated into Windows. The whole API resides in the System.Speech.dll library, which also contains five important namespaces:

- tSystem.Speech.Audio format
- System.Speech.Recognition
- System.Speech.Recognition.SrgsGrammar
- System.Speech.Synthesis
- System.Speech.Synthesis.TtsEngine

To access the capabilities of the API, we must first do a new project (Console, WinForms, WPF, ...) to add a reference to System.Speech.dll (Fig.1) [3].

Speech Synthesizer class

This class handles text-to-speech itself. The most important classes are Speech and SpeechAsync. The first one will spell the text in sync (the application will lock until the computer speaks) and the other (SpeechAsync) will start speaking asynchronously, using another thread [3].

The Speech Synthesizer [4] class provides four properties - Rate, State, Voice, and Volume:

- Rate - sets the speed of speech, ranges from -10 to 10.
- State - returns the current state of the SpeechSynthesizer (if it is ready or just talking, etc.).
- Voice - returns the currently used voice as VoiceInfo object.
- Volume - adjusts the volume of the voice, ranging from 0 to 100.

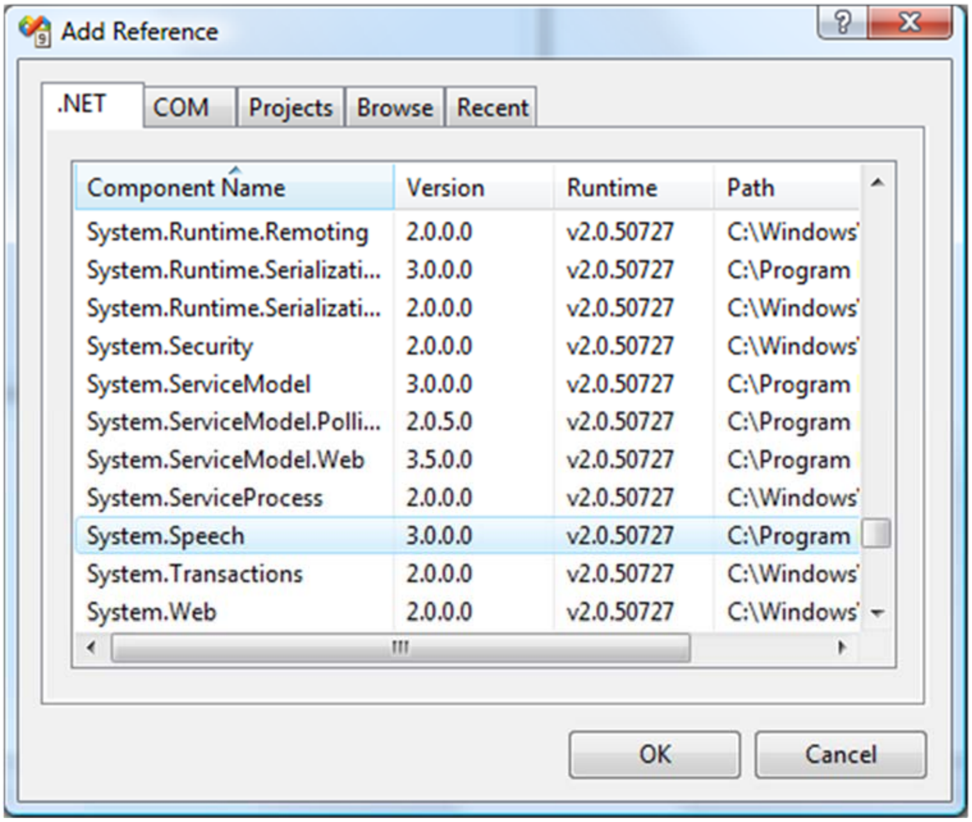

FIGURE 1. Adding a reference speech to Visual Studio.

CONCLUSION

The output of this article is an analysis of options for an intonation reader that will focus exclusively on the Czech language.

In the introduction, the authors describe the ways and pitfalls of the Czech language for pronunciation and intonation. As we can see in the table, for example, one word in the Czech language has up to 7 expressions, and each expression is different.

We currently have several options that are mentioned and discussed in the article: text-to-speech, text analysis, pronunciation rules. In conclusion, the authors focused on the C # library for the intonation reader.

REFERENCES

1. D. Kiculis, M. Žáček and Z. Telnarová, "Overview and research of intonation readers for students with specific needs," in *Proceedings of the international international conference of computational methods in sciences and engineering 2018* (ICCMSE 2018), DOI: 10.1063/1.5079077
2. LinguaTexh, "Text-to-Speech Technologie." Online: https://www.linguatec.de/text-to-speech/tts-technologie/
3. Programujte.com, "C# Speech Synthesis." Online: http://programujte.com/clanek/2009020100-synteza-reci-v-c/
4. K. Tokuda, T. Yoshimura, T. Masuko, T. Kobayashi and T. Kitamura, "Speech parameter generation algorithms for HMM-based speech synthesis." IN 2000 IEEE international conference on acoustics, speech, and signal processing. PROCEEDINGS, (Cat. No. 00CH37100) (Vol. 3, pp. 1315-1318). IEEE.
5. Janosek, M., Volna, E., & Kotyrba, M. Knowledge discovery in dynamic data using neural networks. *Cluster Computing*, *18*(4), 1411-1421, (2015).

Optimization Techniques for Scientific Computation in C/C++

Tomáš Botor[1], Hashim Habiballa[1,a]

[1]*Dept. of Informatics and Computers, Faculty of Science, University of Ostrava, 30. dubna 22, 70103 Ostrava 1, Czech Republic*

[a] hashim.habiballa@osu.cz

Abstract. The need of highly optimized code is important issue especially for scientific computations. While using parallelization for target code is an usual way for code optimization, we can also use vectorization or unrolling loops for efficient code. In the article we present our experiments utilizing these methods.

INTRODUCTION

Finding the most effective C++ compiler and using parallelization are possibly most important factors in optimization of source code [3]. However there are even more contemporary optimization techniques, which should speed up execution of our code like the means of vectorization or unrolling loops [4]. Code optimization is especially important for big data scientific computations like evolutionary computation [1].

VECTORIZATION IN C++

Microprocessors have vector instructions that allow us to perform the same operations over multiple blocks of data simultaneously. This could be applied to image processing, sound processing and math operations over vectors and matrices. In contrast, vector operations are not suitable for standard sorting algorithms [2].

Vector operations use special vector registers. The maximum size of each vector register is 128 bits (XMM) for SSE2 instruction set, 256 bits (YMM) for support of the AVX instruction set. There is also an AVX512 instruction set that allows us to store elements in a 512-bit vector [2].

We can briefly describe how to use automatic vectorization in source code. This is achieved by selecting either the Streaming SIMD Extension or the Advanced Vector Extension in the release mode. The above described options are dependent on the particular processor and its specific instruction designated. We can search for exact instructions on possible instructions on the ark.intel.com website or easily read them from CPU-Z program. In our case, we have both SSE and AVX variants.

Let's do a more detailed analysis of the code in the sample and compare automatic vectorization with the compiler, using both SSE, AVX instructions, and without them. We achieved the following results. The entire algorithm is measured by the *rdtsc* method [5]. In the following three tables, it is possible to see in the columns the maximum extreme values that have a strong influence on their average observations. Pay attention to the minimum column that most likely reflects real values. Measured algorithm is very simple. It contains two arrays and for loop. In this loop we store elements from first array to the second one.

TABLE 1. Automatic vectorization – no optimization

number of repetition	min	average	max
64	432	866	46 060
128	850	1 429	46 818
256	1 650	2 892	56 322
512	3 254	5 146	71 756
1024	6 636	10 067	59 074

TABLE 2. Automatic vectorization – SSE2

number of repetition	min	average	max
64	62	163	36 602
128	140	280	36 876
256	252	466	43 028
512	470	909	38 654
1024	914	1 485	68 236

TABLE 3. Automatic vectorization – AVX2

number of repetition	min	average	max
64	20	143	3 606
128	22	254	48 068
256	42	794	44 600
512	82	867	48 520
1024	208	1 345	43 345

If we take the results of the minimum values, interpret them in a separate table, and then draw them to the chart, we get the following table and display.

TABLE 4. Comparison of automatic vectorization

number of repetition	AVX2	SSE2	no optimization
64	20	62	432
128	22	140	850
256	42	252	1 650
512	82	470	3 254
1024	208	914	6 636

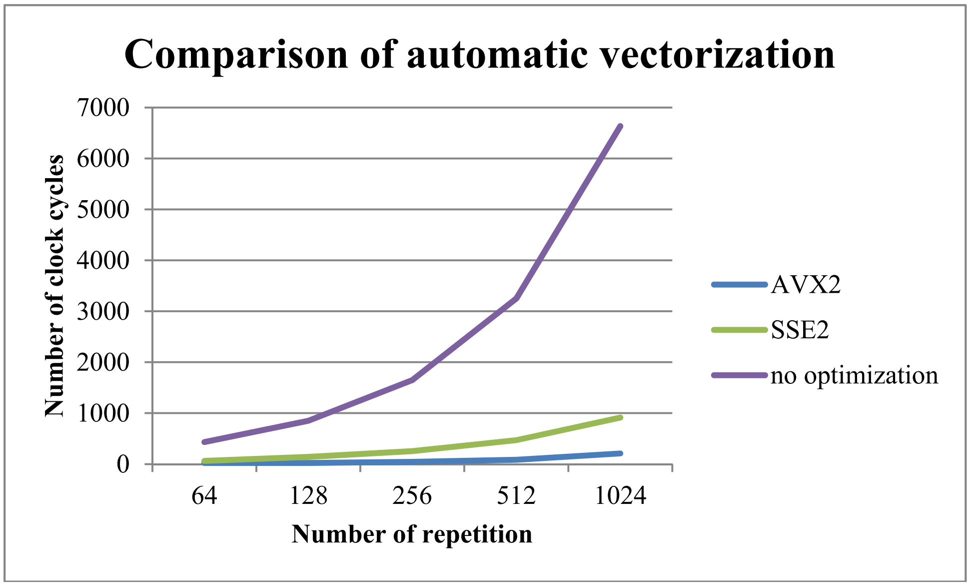

FIGURE 1. Comparison of automatic vectorization

UNROLLING LOOPS

The critical part of the program is often a loop sequence. The clock frequency of modern computers is so high that even the most time-consuming instructions are executed during a fraction of a microsecond. Therefore the delays caused by the inefficient code are only observable when a large amount of repetitions occurs. For loops the instruction is needed to jump back to the beginning of the loop, and it is up to you to decide when the loop needs to be terminated. Optimizing these instructions is a relatively general technique that can be used in many situations. Unrolled loops are a way of optimizing code when the number of loop iterations is reduced [2].

Take into account the following simple example. We have one variable that will be incremented by one in one iteration of the cycle and number of iterations in the loop is equal to 1200. Table 4 shows results of the experiment. The values are given in units of clock cycles measured by the rdtsc method.

TABLE 5. Unrolling loops

Number of unrolls	Number of repetitions	Minimum	Average	Maximum
1	1200	6092	7952	187764
2	600	7172	7452	99788
3	400	7164	7326	88556
4	300	7176	7363	65612
5	240	7180	7270	58015
6	200	7176	7265	41676
8	150	7168	7295	33458
10	120	7164	7301	8716

If we compare the first two lines, we can notice that if we design the loop by writing two commands inside, we get an average value instead of 7952 clock of cycles of only 7452 clock cycles, which is 500 clock cycles less than in the first case.

The table also shows that there is no point in unrolling the loop to infinity. It is necessary to find the right ratio in which the loop is still effective. In our case, we could say that if we unroll the loop by 5, the source code accelerates by approximately 700 clock cycles. With greater unrolling, the average values stop around the number 7290. We have accelerated the entire code by about 10% of the clock cycles. It can also be noticed that the clock cycles are more stable when unrolling loops. There are no significant differences between the average, minimum, and maximum values.

CONCLUSIONS

In this article we present some optimization techniques, that are also important for optimization our source code. The loop unrolling technique can be used when we have a large number of iterations in loop. If there are simple commands in the loop, it is possible to unroll the loop. By duplicating commands, the code becomes less readable, but on the other hand, we can save hundreds to thousands of clock cycles.

We recommend using the vectorization rather than compiler optimization. Nowadays, there should be no problem that the processor does not support at least the SSE2 instruction set. Of course, if the processor has a more recent version of the instructions, it is much more efficient to use the AVX2 instruction set. This allows more efficient use of vectoring thanks to larger registry capacities.

REFERENCES

1. H. Habiballa and T. Botor. Compiler Optimization for Scientific Computation in C/C++. In: International Conference of Computational Methods in Sciences and Engineering 2017: AIP Conference Proceedings 2040 2018 Rhodes, Greece. MELVILLE, NY USA: AIP Publishing Inc., 2018. pp. 0300041-0300044. ISBN 978-073541766-3.
2. A. Fog. Optimizing software in C++ An optimization guide for Windows, Linux and Mac platforms [online]. 2004, 168 [cit. 2018-06-08]. Online: http://www.agner.org/optimize/optimizing_cpp.pdf
3. R. Allen and K. Kennedy. Optimizing Compilers for Modern Architectures. Morgan Kaufmann Publishers, 2001.
4. A. V. Aho, R. Sethi, J.D. Ullman. Compilers: Principles, Techniques, and Tools (1st ed.). Addison-Wesley, 1986.
5. INTEL, Corp. Using RDTSC instruction for Performance Monitoring. [cit. 2017-10-10]. Online: https://www.ccsl.carleton.ca/~jamuir/rdtscpm1.pdf

Survey on the Usage of Public Cloud Services with Copyrighted Contents

Tomas Sochor[1,2,a)], Pavel Smolka[1], Zuzana Priscakova[2], Petr Jedlicka[2] and Dita Dlabolova[2]

[1]*Department of Informatics and Computers, University of Ostrava*
30. dubna 22, 70103 Ostrava, Czech Republic
[2]*Institute of Informatics, Mendel University in Brno*
Czech Republic

[a)]Corresponding author: tomas.sochor@osu.cz

Abstract. As the importance of public cloud services for sharing various files including copyrighted contents increases, a poll was organized among Czech university students focusing on their usage of such services so that to reveal their habit in usage of such services. The results from more than 750 respondents showed that there are certain typical usage patterns. The most significant conclusions showed that female usage of interactive cloud services differ, e.g. in more frequent usage of Uloz.to and Facebook and less frequent usage of LinkedIn.

INTRODUCTION

Together with the increasing availability of broadband internet connection for individuals, both in households and on mobile devices, the number of users and usage frequency of public cloud services have been increasing recently. The increase in could services usage was also facilitated by the rapid improvement of an average QoS in the internet [1]. This increasing usage trend includes primarily cloud services providing on-line content of various types with major role played by multimedia content [2].

There are just rare publications focusing on cloud computing usage, e.g. [3] or [4]. Nevertheless, their focus differs significantly from the poll presented here. In addition, there are some papers that served as inspiration for polling method applied here, e.g. [5]. In addition, also the security aspect of cloud services should be taken into account like in [6]. This aspect was beyond the scope of our study, primarily because of wide range of fields in the target group. It seems that the only relevant source providing at least partly comparable result is [7] but still significant differences exist.

There is a significant issue associated to providing multimedia content, namely the copyright protection of most of such files [8]. Among providers of cloud services providing (at least potentially) copyrighted content, there are various approaches towards such content. Some of them (like Youtube with their ContentID service [9]) try to avoid uploading of protected contents (both via legal and technical measures) and removing it when detected. Others (like Dropbox) try to leave the responsibility on the user with an option to have the right to remove it when detected. On the opposite, some of them (like uloz.to) do not perform almost any check of the contents and their service seems to provide incentives for users to share copyright-violating contents.

Bearing in mind previous results confirming that the major share of multimedia contents available on-line is somehow protected by copyright laws [10], and because students are often mentioned a one of major groups of potential offenders of copyright laws, a decision was made to collect data for verification of such hypotheses. As a verification means, a poll survey was organized among students in two universities in the Czech Republic.

METHODOLOGY

As the first step, the classification of the services provided has to be determined. So far, only few classification attempt were published (e.g. [11]). Here, a slightly different classification was used, primarily because the authors developed their own classification before the study [11] was finished. The prevailing type of provided service (namely data storage cloud storages, multimedia portals and streaming services, social media) was chosen as the main classification criterion. The inclusion of social media could seem inorganic at glance but after some initial investigations a conclusion was made that the major social media (including Facebook, Twitter, Instagram and LinkedIn) have become a platform form massive sharing of multimedia contents during recent years and they deserve to be included in the poll.

Questionnaire

The initial hypothesis was formulated that the cloud service usage pattern would be correlated to the users demographic data. Therefore, several questions asking for anonymous demographic data (like the region of residence and the average population size of the village/town/city) were added to the questionnaire to the main portion of questions focusing on various cloud services usage frequency. The survey was decided to be performed as an anonymous online poll. For this purpose, a questionnaire was composed in Google Forms and distributed among students via e-mail. To avoid discouraging users to pass the questionnaire, the total number of questions was kept below 10. No external motivation for participation in the poll was applied. Therefore, the return rate close to 10 % could be indicates that the addressing of the target group was relatively successful.

The respondents were asked about the usage frequency and habits in using specific cloud services in each of the three categories defined in advance. For the sake of clarity, the respondents were offered common manes of several major services in each category (with optional adding other service names). Based on known recommendation on the survey research e.g. [12]), the necessary demographic questions (here, asking about the size of the place and the region of residence) were located at the end of the questionnaire.

RESULTS

In total, 762 respondents filled in the questionnaire in May and June 2018. All of them were university students, i.e. their age ranged approx. from 19 to 28. Among the respondents, 257 men and 505 women took part. The majority of respondents (above 39%) lived in cities (above 100,000 inhabitants), next 28,5% lived in towns (between 10,000 and 100,000 inhabitants), and the rest in villages. The majority of respondents live in northern and central Moravia, only few in the rest od the Czech Republic and Slovakia.

Summary results

Several interesting results were obtained from the responses. First, it was observed that female respondents tend to use the cloud services significantly less than male ones. For data storage services, female user use them in average at 1.7 services/pers. while men at 2 services/pers.. This is true for multimedia cloud services, too (1.14 for female and 1.22 for male). On the other hand, differences among users according to the place of residence size were less significant (maximum 1.88 services/pers. in towns, minimum 1.75 in small villages but in cities the value as almost as low (1.78).

Only few respondents identified their own (not offered) name of a cloud service. Also the number of users not using any service in any of the three categories was very low. Nevertheless, this fact cannot be overvalued. This should not be interpreted in a way that significant majority of youngsters use the services. Certain part of students is expected to decide rather not to respond if they do not use such services often or at all and they are not present in results therefore.

Service–specific results

When focusing solely on data storage cloud services (i.e. excluding stream and other multimedia services), the usage of the most popular services can be seen in Tab. 1. In the table, some figures are significantly exceptional, namely the very high usage of Uloz.to and Leteckaposta.cz among female respondents comparing male ones. The statistical significance of these differences was confirmed by the statistical t-test.

TABLE 1. Data storage cloud service usage frequency (for the selected most frequently used services)

	Google drive	OneDrive	Dropbox	Uloz.to	iCloud	Letecka posta.cz	Not used at all
Male	140	81	66	97	34	61	33
Female	244	96	89	209	86	137	93

In multimedia and streaming service category, the significant dominance of Youtube (580 users) and Spotify (174 users) was observed unsurprisingly, with iTunes (89 users) in the third place. No other competitor service reached considerable number of users, except SoundCloud (42 users). Here, no significant exception in usage patterns between male and female users was detected.

In social media category, the results could seem relatively expectable at first glance. The more detailed view on them revealed some less predictable observations. The results for this category (only the selected most popular social media) are shown in Fig. 1. Not surprisingly, Facebook dominated in the poll results, followed by Instagram (with less than half number of users). Behind them, the triad formed by LinkedIn, Google+[1] and Twitter had quite balanced results. As one can see partly from Fig. 1, the most significant gender differences were observed here. On one hand, the domination of Facebook among female users (410 users) is significantly stronger than for male users (191). This is true for Instagram as well (186 female vs. 70 male users). On the other hand, the situation differs in LinkedIn (41 female and 38 male users) and primarily in Twitter where male users dominated (34 male vs. 24 female users). However, it must be admitted that the numbers for both LinkedIn and Twitter are low and therefore the significance of such difference is limited.

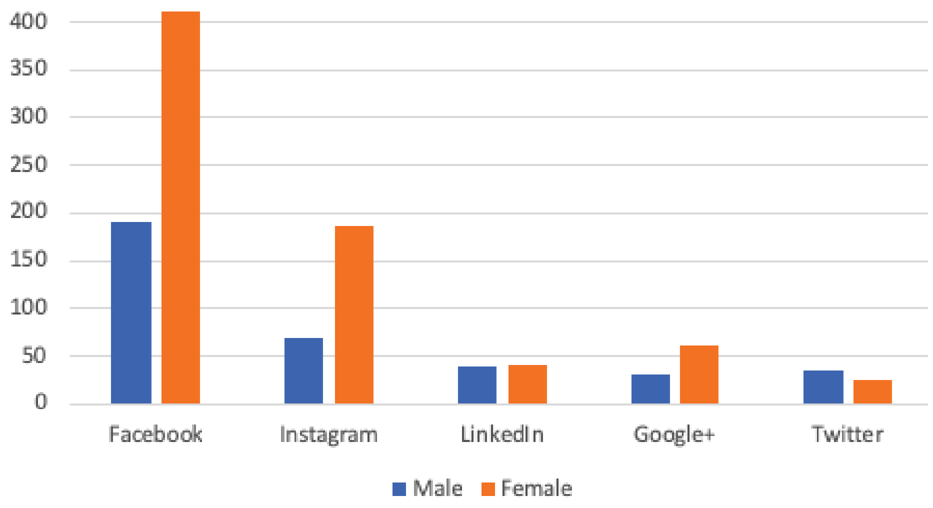

FIGURE 1. The number of users of social media in the poll for female and male users

Usage frequency

The frequency of intentional use of the cloud services covered b the poll was included in the questionnaire. Unlike major data storage cloud services whose usage is often silent (the client installed in the device does not need a user intervention), other services (streaming, multimedia, social media) typically require a user interaction. Therefore, those results can be considered valid only for services of the latter type. The result on usage frequency are summarized in Tab. 2. It is clear that the no significant differences in usage frequency among the residence size can be found. The highest share of daily users should be accounted in favor of social media. The usage frequency of other services could differ significantly and would deserve further investigation.

[1]In this context, the recent announcement about Google+[13] end of life seems even more surprising despite the fact that security aspects seemed to be the decisive factor here.

TABLE 2. Usage frequency of cloud services vs. residence size

	Daily	Several times in a week	Once a week	Once a month	Not used/ No answer
Villages (up to 10 K inhab.)	118	27	20	13	68
Towns (10-100 K inhab.)	111	25	15	11	55
Cities (above 100 K inhab.)	164	43	18	13	61

CONCLUSIONS

Partly in accordance with other publications ([11] and [7]), there are always identical most popular services in each category. What extends the previously published results, however, are certain significant differences in usage patterns of cloud services observed, primarily different habits in certain cloud services. Namely, Uloz.to and Leteckaposta.cz as Czech–specific cloud data storage services and Facebook was significantly more popular among female users while LinkedIn was more popular among men. The observation from this study could help in considering the new European regulation on quick removal of copyrighted contents as announced recently. However, the generalization of the presented results should be done with care because the only single age group (university students) and region (Czech Republic) was subject to the poll.

REFERENCES

[1] P. Zach, M. Pokorny, and J. Balej. Quality of experience of voice services in corporate network. *Procedia Economics and Finance*, 12, 771-779 (2014)

[2] How essential is cloud storage for global consumers? (by gender). *Statista.com: The Statistics Portal*. [online]. [quot. 2019-03-15]. Available from: https://www.statista.com/statistics/552738/worldwide-cloud-storage-survey-importance-by-gender/

[3] H. T. Dinh et al. A survey of mobile cloud computing: architecture, applications, and approaches. *Wireless communications and mobile computing, 2013* 13.18: 1587-1611.

[4] P. Pina. File-Sharing of Copyrighted Works, P2P, and the Cloud: Reconciling Copyright and Privacy Rights. *Handbook of Research on Emerging Developments in Data Privacy*. IGI Global, 2015. p. 51-68.

[5] H. Sochorova and I. Zavacka. Special Educational Needs and the Study at the Field of Medicine. *Creative Education.* 2018, Vol. 9, No. 8, pp 1258-1276. ISSN 2151-4755.

[6] S. Lysenko et al. Information technology for botnets detection based on their behaviour in the corporate area network. *Communications in Computer and Information Science. Vol. 718*. pp.167-181 (2017)

[7] A. Asaro. Stay Tuned: Whether Cloud-Based Service Providers Can Have Their Copyrighted Cake and Eat It Too. *Fordham L. Rev.*, 2014, 83: 1107.

[8] C.J. Millard (ed.). *Cloud computing law*. Oxford: Oxford University Press, 2013.

[9] L. Solomon. *Fair Users or Content Abusers: The Automatic Flagging of Non-Infringing Videos by Content ID on Youtube.* Hofstra L. Rev., 2015, 44: 237.

[10] SEN J. Security and privacy issues in cloud computing. In: Cloud Technology: Concepts, Methodologies, Tools, and Applications. IGI Global, 2015. p. 1585-1630.

[11] Ministry of Industry and Trade of the Czech Republic. Study of providers of selected services of the information society in the Czech Republic as a part of Society 4.0 (in Czech, Studie poskytovatelÅ vybranch sluÅeb informan spolenosti v esk republice v rmci Spolenosti 4.0) [online]. [quot. 2019-03-15]. Available from: https://www.mpo.cz/cz/e-komunikace-a-posta/postovni-sluzby/sluzby-informacni-spolecnosti/studie-poskytovatelu-vybranych-sluzeb-informacni-spolecnosti-v-ceske-republice-v-ramci-spolecnosti-4-0–241166/ (2018)

[12] H. Rezankova, T. Loster and D. Husek. Evaluation of categorical data clustering. *Advances in Intelligent Web Mastering–3*. Springer, Berlin, Heidelberg, 2011. p. 173-182.

[13] Google Plus Will Be Shut Down After User Information Was Exposed, *New York Times* Oct. 8, 2018. [online]. [quot. 2019-03-15]. Available from: https://www.nytimes.com/2018/10/08/technology/google-plus-security-disclosure.html

Analysis of Tools for Input Diagnostics in LMS Moodle

Pavel Smolka[1, a)], Vladimír Bradáč[1, b)]

[1]*University of Ostrava, Faculty of Science, Department of Informatics and Computers, 30. dubna 22, Ostrava, Czech Republic.*

[a)] Corresponding author: pavel.smolka@osu.cz
b) vladimir.bradac@osu.cz

Abstract. The paper focuses on an analysis of tools that are at the disposal in LSM Moodle in the context of the input diagnostics of the educated persons – students in the e-learning environment. The input diagnostics is viewed from two aspects. The first aspect is student's prerequisites, which are necessary for further education as it affects the speed of student's progress through a learning unit – course. The second aspect then considers student's preferences, i.e. the form of the educational sources.

INTRODUCTION

Current trends in the development of modern society significantly accentuate the meaning of education. It becomes obvious both in the initialisation phase, when a human enters an economic process, and in the course of human's life in a form of further education. These principles form a fundamental stone of the concept of knowledge economy.

From the organisational point of view of an educational process, e-learning systems seem to be crucial. They are crucial for educational organisation in the phase of further education, primarily for their relation with IT and the flexibility towards student's possibilities. These systems feature a various level of complexity. In addition, there is always a tool to publish study materials, a different level of supporting educational activities aiming at fixing and deepening acquired knowledge with its subsequent diagnostics. From the point of view of organisation, the key factor component of an e-learning system is a learning unit.

One of favourite e-learning systems is LMS Moodle. It achieved its popularity for its licensing policy and high modularity of this environment. This system, similarly to many others, primarily focuses on the area of realising educational event and achieving a certain level of knowledge and skills. From the point of view of realising each educational event, the key is student's input level and their preferences. It is the mapping of such diagnostics tools at the input level that is in the focus of this paper.

KOMPLEX SCHEME OF LMS MOODLE

If complex break-down of the LMS Moodle system is to be done from the abovementioned perspective, we can identify several blocks which ensure realisation of the educational process. Among these key block belong user and course. A user is an entity that encompasses all relevant information on the system user and using this entity, it puts the user into the position of a student in particular cases.

The second key entity is a course, which is a general unit for providing a framework of the educational process. The course is then equipped with a range of individual components which enable to publish study materials of various character. It also covers educational activities and communication management with the student and their testing as well as recording study results.

Quite a key component is the entity of competency, which can very complexly described the area of the output in the context of the whole LMS Moodle environment. In practice, this entity enables to define individual competency frameworks, their taxonomy, and output. These competency frameworks are then projected to all individually

evaluated activities in the course on one hand. On the other hand, they are projected to a user – student, where complex evaluation is provided based on the definition of these competency frameworks. This concept is depicted in the following diagram.

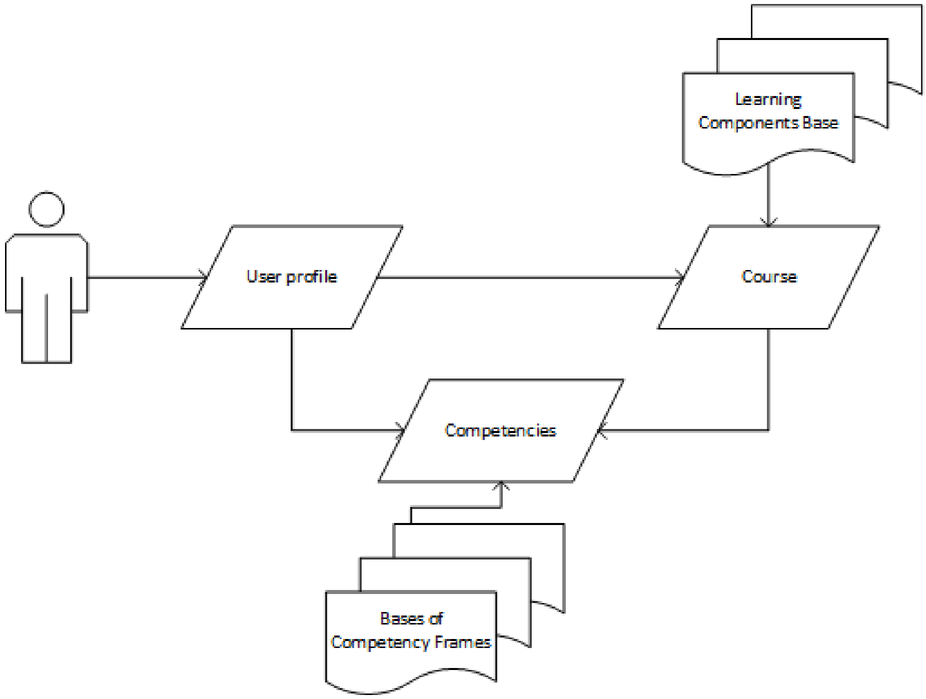

FIGURE 1. Key components of LMS Moodle

From the text above and the diagram, it is obvious that current conception of the LMS Moodle structure primarily focuses on the issue of achieving a certain standard, for which it provides a wide range of tools how to describe and achieve this standard within partial activities in the course.

DIAGNOSTICS OF STUDENT'S INPUT LEVEL

From the point of view of analysing the tools of LMS Moodle, which will enable us to perform the input diagnostics of a student, it is necessary to describe the objective of such a diagnostics and what is should record. It is highly important to work with the term of the student's input profile P_{in} , see (1), which means unification of two parts: a global student's profile within the instance of LMS Moodle, which reflects a stable preference part P_g and a local (course) student's profile P_c, which relates to a particular content of a course and is significantly influenced by the process of studying the particular course and by other study activities.

$$P_{in} = P_g \cup P_c \qquad (1)$$

The global part of profile P_g reflects student's preferences in a form of offered study materials, their mixture respectively. It is advisable to take grounds in already existing VARK model published in 1992 [3], which classifies student's preferences from the viewpoint of the form of the study materials divided into four categories:

1. Visual (V) – students prefer work with maps, diagrams, schemes. They prefer symbolic representation and hierarchical structures.
2. Auditory (A) – students prefer spoken word and heard information. It also includes discussions of any form.
3. Read / Write (R) – students prefer written text and they are performing in writing within the feedback mechanisms.
4. Kinaesthetic (K) – students prefer simulations, experiments, and knowledge acquired in practice.

In real world, it is relevant to have a mixture of the above-listed preferences, where it is interesting to define the ratio of individual components. This model is often used when designing adaptive platforms to realise e-learning [2].

The local (course) part of profile P_c reflects the level of prerequisites after the course completion and is closely related to the content of the given course. The level of these prerequisites affects, to a certain extent, the ability to understand the studied subject matter and significantly affects the time progress through a course as well as acquisition of the required competencies.

The objective of designing the student's input profile is an effort for controlled progress through a course and its adjustment from the point of view of the form of offered study materials. From this perspective, the group of tools enabling to realise the above-described approach in LMS Moodle is fragmented.

Application of the preferences according to the VARK model can be implemented in LMS Moodle using a modification of the user's profile. This modification enables to introduce new fields whose values can be either a numerical value or a linguistic value. This approach was verified in foreign language education in 2017 [1]. Regarding the conception of the presented student's input profile, this is an eligible implementation as it manifests throughout all courses of the LMS Moodle instance.

Regarding the local (profile) part, the situation is different and no individual tool to catch the input state – values exists. At this positon, one can use primarily input tests, which, however, do not have to suit everyone. Their advantage is automated grading of results. Potentially, open questions can also be used, but there is a higher ratio of author's work when evaluating. In order to be able to aggregate them in the case of combined diagnostics tools, it is suitable to use a grade category. Potentially, it would be advisable to define individual competencies considered as input competencies. Competencies, however, cannot be used for a conditioned progress for now, as depicted in the following figure.

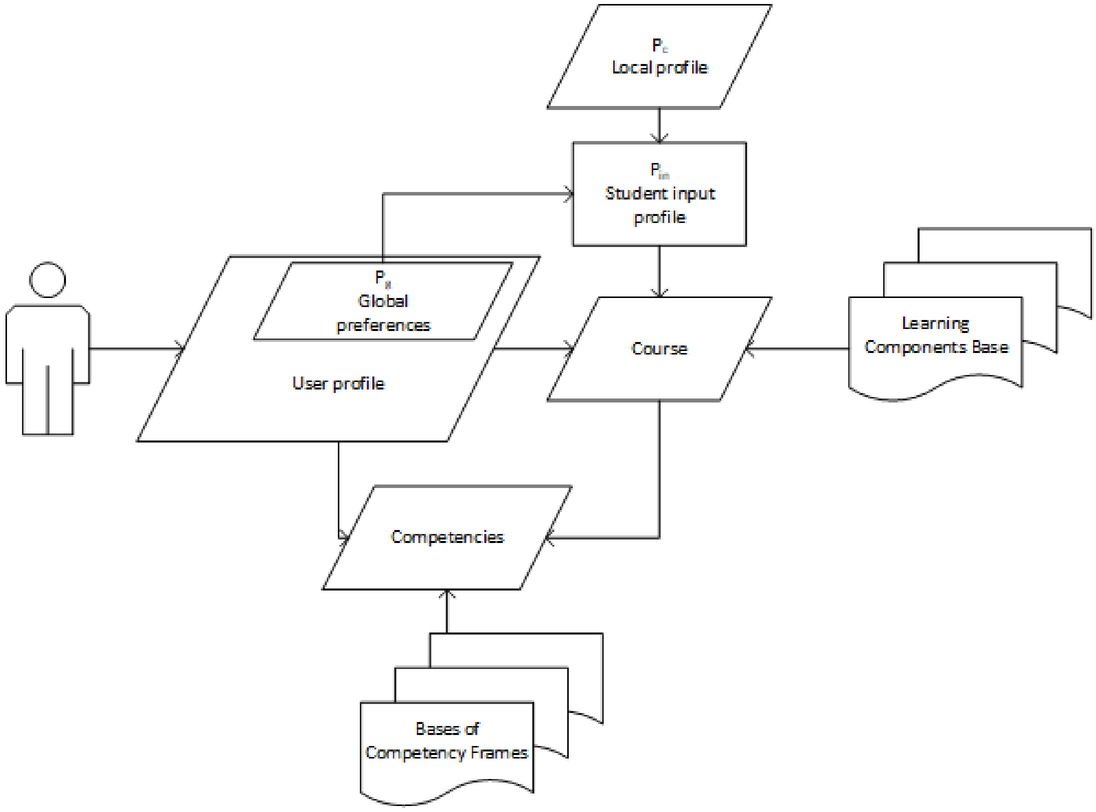

FIGURE 2. Modifying an existing model

The role of grade category can also take advantage of the possibilities to set the method of a summary calculation for a category. Each newly created grade category in the course is considered a subcategory of the category. Thus, a hierarchical system is created, where it is possible to set weights of individual subcategories having an effect on the final score in the course. This aspect is interesting not only from the diagnostics point of view, but from the viewpoint

of a complex education management in the LMS Moodle environment. Despite this contribution, the data in the student's input profile still remains fragmented.

Although the LMS Moodle disposes of a wide range of development base, which produces quite a high number of extension modules for the standard environment, the above-mentioned issues are not solved in any of them.

SUMMARY

The above-mentioned description and analysis of the issue reveals that a systematic solution is to extend the standard data structure with structures treating both the preferential part of profile P_g, with its impact on the whole LMS Moodle instance, and the local part of profile P_c, with its impact on a particular course. In the case of P_c, the definition must be encompasses very flexibly so that this part could be used in all areas of education and the user would only define these input parameters. It is worth considering classification of the level of the partial parameters by a linguistic expression with its subsequent relation to an expert part controlling the progress through the course. This approach stems from the knowledge of natural language morphology and its possibilities when designing information systems [5]. Concerning the structure, we reckon that it would be possible to take rounds in the following model.

Extending the structure, which is primarily realised in the area of a database, takes advantage in already defined patterns and the whole approach stems from a logic already described in [4]. When modifying the previous module, the structure of the standard module has been extended. It newly accepts preferential selection according to the VARK model. Each course has a newly define structure P_c, which locally identifies the level of prerequisites. The complex student's input profile P_{in} is the result of unification aiming at interpreting both groups of characteristics as one unit.

REFERENCES

1. V. Bradac and B. Walek, A comprehensive adaptive system for e-learning of foreign languages, *Expert systems with applications*, volume 90, pp. 414-426, 2017.
2. F.S. Diaz, T.P. Rubilar, C.C. Figueroa and R.M. Silva, An adaptive e-learning platform with VARK learning styles to support the learning of object orientation, *2nd IEEE World Engineering Education Conference – EDUNINE*, University CAECE, Buenos Aires, pp. 152-157, 2018.
3. N.D. Fleming and C. Mills, Not Another Inventory, Rather a Catalyst for Reflection, To Improve the Academy, 11, pp. 137-155, 1992.
4. Z. Telnarová, Modeling and Language Support for the Pattern Management, *Pattern Recognition and Classification in Time Series Data*, pp. 86-106, 2017.
5. M. Zacek and D. Homola, Analysis of the English Morphology by Semantic Networks, *International Conference of Computational Methods in Sciences and Engineering*, Thessaloniki, 2017.

MicroLearning Approach to e-Learning Course Creation and Reasons for it

Radim Polasek[1, a)] Tomas Javorcik[1, b)]

[1]*Department of Information and Communication Technologies, Faculty of Education, University of Ostrava, Dvorakova 7, 701 03 Ostrava, Czech Republic.*

[a)]Corresponding author: radim.polasek@osu.cz
[b)]tomas.javorcik@osu.cz

Abstract. The paper describes creation of e-Learning course using so called MicroLearning (ML). MicroLearning is not so new theoretical way of creating courses and study materials (processing subject matter) but maybe due to its limitations was not used much in university e-Learning course creation. Some authors see MicroLearning as one of trends in e-Learning, we look at reasons why MicroLearning can be suitable solution and which basic rules are with it connected. Presented is experience we gained when creating MicroLearning course for our students and pitfalls connected with this approach. Literature says that ML is not suitable for use with complex skills and creation of small learning units can lead to loosing general overview in specific subject matter. Described are students' opinions on MicroLearning course we have created. Opinions were generally positive although just small sample of respondents was questioned.

EVOLUTION OF E-LEARNING AND MICROLEARNING

Information and communication technologies (ICT) are being used in education already for some time. They are also used quite often as needed tool for use of e-Learning in its various possible versions. E-Learning itself evolved first from mail based distant learning [11] to various types of computer supported or assisted learning [5] and is today unconditionally connected with use of ICT.

E-Learning is, as nearly every aspect of our society and education, under almost constant development and is influenced by changes around us. We can say that not only learning is shaping people and society but also the way we are living is affecting effectivity of learning and so retrospectively changing learning and e-Learning.

MicroLearning (ML) as a term is around already for some time, as it was used for the first time in 2004 [7]. Since then this term, its definition and examples from real life and educational environment have been defined and discussed many times.

Some authors consider MicroLearning as next step in evolution of e-Learning [5, 9], at least we can consider it as a one way which can be named when talking about innovative approaches to e-Learning. Other worth mentioning are gamification, mobile learning, personal learning environments, MOOCs and open education [20, 30].

Reasons behind the fact that MicroLearning is considered as one of the today's e-Learning trend lies in a way we live now. We live our lives fast, people are almost constantly in a hurry, not having time or distracted by more activities at once. Mainly in retail and marketing is mentioned so called overchoice [10, 16, 23, 28], when we are overwhelmed by so many possibilities then it is hard to choose just one – or we are changing our attention so often that it is hard to talk much about focus on what we are doing. Another today's trend is so called information overload [17, 24] which creates literally flood of information we have to face every day. Then it is hard to choose what information to "consume" or time spent with one activity is limited.

Ability to adapt to changes is mainly in business considered as new important quality needed for success [1]. This is important mainly for employees. But if we accept that, it logically has its implications in a field of education too. Learning should be ready to offer solutions for both theory and practice and for lifelong and work-based

learning. These days MicroLearning is mentioning as almost miracle amongst work-based learning professionals [21].

If we look at mentioned issues at least some reaction from educational approach would be appropriate. MicroLearning is approach that offers solution that with its nature address many negative effects of above mentioned features of modern way of living. It is probably not so effective or without negative qualities as described by commercial-based e-Learning solutions suppliers but we should take ML into account.

MICROLEARNING AND ITS RULES

Term MicroLearning was first coined by Gassler in 2004 [7], as mentioned earlier. In connection with Webpages and trends which appeared in around 2009, rather short, concise small Webpages started to appear. They are called microsites [3] and were predominantly connected with advertising and marketing. To other causes that supports reasons for use of MicroLearning we can add text messages that inherently are short and are shaping ways of writing of younger generations [8]. Question is why short texts, use of "crazy" abbreviation would not affect or if it do affect also other domains (as learning, thinking, attention). Social media and their specific concise language in connection with almost nonstop stream of information that catches attention of almost every youngster waiting at the bus stop can also be possible catalyst that cause changes. Changes that may not be fully described now but are visible. Some researches already shows that there are notable limits of attention of both children [26] and students [29].

MicroLearning's basic characteristics in a nice way summed Hug [13]. Mainly ML content should be short (not to waste time consuming it), divided into small parts, curriculum-wise is focused on just one part of large chapter, subject. Small parts, small learning objects, in connection with ML (called MicroLearning units) resonate with researches focused on short-term memory and learning [6, 19].

As to the definition of MicroLearning, we can look at ML from wider perspective as Lindner [18] who says that ML is „what people are doing, knowingly or not, when they face the challenge to find new information and build new knowledge in new networked digital media environments. With e-mails, mobile phones, Google and the Web 2.0, professional and private users increasingly have to deal with small chunks of "microcontent", loosely joined, permanently changing, re-arranging and circulating". But this doesn't focus so much on educational dimension of use of ML. Alqurashi [4] takes into account also pedagogical use saying that ML is „learning strategy designed using a series of short learning content and short activities that makes a mini course." We understand ML as mean of processing teaching material in the form of small separate units which endeavour at one moment to represent information without unnecessary connections beyond that unit. This form of processing teaching material allows for one of its parts (MicroLearning Unit, MLU) to be consumed over a relatively short time period (5-7 minutes). In choosing the form, emphasis is also placed on interactivity, multimediality and learners self-testing, which require the choice of a suitable technical solution. In this, we consider MicroLearning to be a form of e-Learning

Students opinions on learning

Before start of the winter semester 2018/2019 (where we tested created ML e-Learning course) we conducted survey amongst students of Faculty of Education (237 questionnaires send by email, 58 received; respondents aged 19-41 or more) focused on their learning preferences. Results showed us that students rather enjoy learning (more than 50%), they do not prefer short text (67%), rather like short pieces of subject matter (53%) [14]. Results showed that ML is promising way for creating new e-Learning courses. To get feedback from students, at the end of semester we surveyed those how went through newly created course.

COURSE CREATION FOLLOWING MICROLEARNING RULES

For e-Learning course creation we chose LMS Moodle, but we do think that future learning content creators don't have to feel bound by this specific software. LMS Moodle provides classic division of subject matter into topics (chapters) which is used in classic styled e-Learning courses. Many so far described applications of MicroLearning used some kind of special software/environment (eg. mobile application) [2]. LMS Moodle offers in contrast very robust (maybe even complicated) system with many possibilities, features etc., some not needed for ML. But with realistic approach even LMSs as Moodle can be used to create ML based e-Learning course.

Course was created for subject Computer Architecture and Operating System Basics. When building ML course structure, we used division into topics, but subdivided each topic into small units, as requires rules of ML. We tried to use as much as possible interactive or multimedia content in these units, to create engaging learning units. Possible pitfalls connected with creation of similarly designed courses are that creation is toilsome. Creation of small content units need its time and preparation.

In total was created 120 ML units that we divided into 10 topics. Smallest number of MLUs in one topic was 8, the highest 18, average per topic was 12. MicroLearning Units were content-wise separated, not connected, only latter units could make use of knowledge already mentioned in previous units. Each ML unit also included at least simple quiz to give students opportunity to test and reinforce newly acquired knowledge.

Generally, negatives connected with ML are paradoxically linked with granularity which is their key feature. In connection with complex skills and problems, ML is not suitable solution [15]. Similarly there is pitfall that small steps would result only in a sum of piled isolated information [12].

Students opinions after finishing ML course

MicroLearning course was made accessible to 12 students. They were questioned after finishing this course. 41% of them saw ML course different in comparison to classic e-Learning courses. All students liked the ML course. 91,7% of them would welcome similarly designed courses also in other subjects. 83,3% of respondents says that ML adaptation of course was more suitable for that in comparison to classic e-Learning courses and 91,7% agrees that because of course design they learned more. 89,7% of respondents assessed ML course with 1 and 2 marks (on five-point scale; 1 = best).

CONCLUSION

Decision to create newly designed e-Learning course was made to try to deliver subject matter in different, hopefully better way. MicroLearning was identified as the one with potential to improve “classic styled” e-Learning courses. Created course was tested on small sample of students, so we should be careful in interpretation of results. But students’ feedback showed generally positive acceptance. What we find as disadvantage connected with course creation is that it is time demanding. Generally speaking MicroLearning approach to course creation complies with short-time memory theory [22]. On the other hand, there are pitfalls in granularization and choosing ML for the right subject matter (subject), so that subject is not very complex or doesn’t require complex skills.

REFERENCES

1. Adapting to Change in a Rapidly Changing Business Environment [WWW Document], n.d. . FMLink. URL https://fmlink.com/articles/adapting-to-change-in-a-rapidly-changing-business-environment/ (accessed 3.19.19).
2. S. Aigerim, Z. Azamat, Microlearning based mobile application for preparation to CCNA examination. IEEE, pp. 1–3, 2014. https://doi.org/10.1109/ICECCO.2014.6997558
3. All About Microsites [WWW Document], 2019. Microsite.com. URL https://microsite.com/microsites/ (accessed 3.19.19).
4. E. Alqurashi, Microlearning: A Pedagogical Approach for Technology Integration. The Turkish Online Journal of Educational Technology 2017, 942–947, 2017.
5. Z. Bezhovski, S. Poorani, The Evolution of E-Learning and New Trends. Information and Knowledge Management 6, pp. 50–57, 2016.
6. A. Conway, M. Kane, M. Bunting, D. Hambrick, O. Wilhelm, and R. Engle, Working memory span tasks: A methodological review and user’s guide. PSYCHONOMIC BULLETIN & REVIEW 12, pp. 769–786, 2005.
7. G. Gassler, Integriertes Mikrolernen (Diploma theses). University of Innsbruck, Innsbruck, 2004.
8. S. Geertsema, C. Hyman, and van Deventer, C., Short message service (SMS) language and written language skills: educators’ perspectives. *South African Journal of Education* 31, (475–487) 2011. https://doi.org/10.15700/saje.v31n4a370
9. L. Giurgiu, Microlearning an Evolving Elearning Trend. Buletin Scientific 22, pp. 18–23, 2017.

10. R. Greifeneder, B. Scheibehenne, and N. Kleber, Less may be more when choosing is difficult: Choice complexity and too much choice. Acta Psychologica 133, pp. 45–50, 2010. https://doi.org/10.1016/j.actpsy.2009.08.005
11. W. K. Horton, Leading e-learning. ASTD, Alexandria, VA, 2001.
12. T. Hug, MicroLearning. Encyclopedia of the Sciences of Learning, 2012.
13. T. Hug, Microlearning: A New Pedagogical Challenge (Introductory Note), in: *Microlearning: Emerging Concepts, Practices and Technologies after e-Learning*. Presented at the Microlearning 2005, Innsbruck university press, Innsbruck, pp. 7–11, 2006.
14. T. Javorcik, and R. Polasek, The Basis for Choosing Microlearning Within the Terms of E-Learning in the Context of Student Preferences, in: 2018 16th International Conference on Emerging ELearning Technologies and Applications (ICETA). Presented at the 2018 16th International Conference on Emerging eLearning Technologies and Applications (ICETA), IEEE, Starý Smokovec, pp. 237–244, 2018.
15. O. Jomah, A. K.Masoud, X.P. Kishore and S. Aurelia, Micro Learning: A Modernized Education System. BRAIN: Broad Research in Artificial Intelligence & Neuroscience 7, pp. 103–110, 2016.
16. B. A. Kaplan, and D. D. Reed, Decision processes in choice overload: A product of delay and probability discounting? Behavioural Processes 97, pp. 21–24, 2013.
17. S. Khalid, M. Saeed, and S. Syed, Impact of Information Overload on Students' Learning: An Empirical Approach. FWU Journal of Social Sciences 10, pp. 58–66, 2016.
18. M. Lindner, What is Microlearning?, in: Micromedia and Corporate Learning. Proceedings of the 3rd Microlearning 2007 Conference. Presented at the Microlearning 2007, innsbruck university press, Innsbruck, pp. 52–62, 2007.
19. F. Mathy, and J. Feldman, What's magic about magic numbers? Chunking and data compression in short-term memory. Cognition 122, pp. 346–362. 2012.
20. M. Matteo, E-learning: new strategies and trends. Tecnología, Ciencia y Educación, Vol 6, Iss 6, Pp 75-87 (2017) 75 2017.
21. MicroLearning: The Modern Solution for Employee Development [WWW Document], 2018. . The Customer Service Institute of America. URL https://www.serviceinstitute.com/2018/05/21/microlearning-the-modern-solution-for-employee-development/
22. G.A. Miller, The magical number seven, plus or minus two: some limits on our capacity for processing information. Psychological Review 63, pp. 81–97, 1956.
23. J. Y Park and S. Jang, Confused by too many choices? Choice overload in tourism. Tourism Management 35, pp. 1–12, 2013.
24. L.E. Pilli, and J. A. Mazzon, Information overload, choice deferral, and moderating role of need for cognition: Empirical evidence. Revista de Administração 51, pp. 36–55, 2016.
25. S. Salomonsen, Microlearning: The Modern Strategy for the Modern Workplace, 2018.
26. C. E. Schaefer and H. L. Millman, How to help children with common problems. J. Aronson, Northvale, N.J, 1994.
27. The Microlearning Company | Grovo [WWW Document], n.d. URL https://www.grovo.com/ (accessed 1.23.19).
28. V. A. Vieira, The Moderating Role of Involvement on the Overchoice Effect in Retail Decision Making. Journal of Relationship Marketing 16, pp. 99–118, 2017.
29. K. Wilson and J.H. Korn, Attention During Lectures: Beyond Ten Minutes. Teaching of Psychology 34, pp. 85–89, 2007.
30. H. H. Yang, New World, New Learning: Trends and Issues of E-Learning. Procedia - Social and Behavioral Sciences 77, pp. 429–442, 2013.

Tasks to Develop Spatial Imagination and Creativity with 3D Graphics

Marek Pytlik[a] and Kateřina Kostolányová[b]

Pedagogical Faculty, Department of Information and Communication Technologies, Fráni Šrámka 3, 709 00 Ostrava – Mariánské Hory, Czech Republic

[a]marek.pytlik@osu.cz, [b]katerina.kostolanyova@osu.cz

Abstract. The article focuses on the way of obtaining positive effects with 3D graphics (3D objects) in a three-dimensional environment. The paper describes the genesis and application of tasks that help to improve, for example, spatial imagination and creativity in cooperation with 3D software or applications with the lowest technical demands and with great education efficiency. The authors of the article want to highlight the benefits and positive effects of the ever-evolving area of 3D graphics and technology. The article is a direct follow-up to the previous contribution by the authors entitled "3D Graphics in Education".

INTRODUCTION

With the rapid development of technology (hardware and software), 3D graphics and three-dimensional virtual objects are used for various benefits and its capabilities in many previously difficult to implement areas. Interacting with digital contents in 3D is an essential task in various applications such as modelling packages, gaming, virtual reality, etc [1].Study Reduced mental load in learning a motor visual task with virtual 3D method proved learners benefit from interacting with a 3DS realistic human avatar compared with a 2D video in a spatial ability task, suggesting a central role of bottom-up processing in visual perception. The higher level of ambiguity due to the lack of depth cues in 2D format requires extended processing time for object/dynamics recognition. [2]. Working with 3D graphics appears even in the cultural area of architectural monuments. Case study Augmented Reality to preserve hidden vestiges in historical cities „Our software provides a support for different multimedia con- tents, which can be displayed from an approximate location in an interactive and ludic way. Disseminated remains and the lack of historical information about the archaeological site are two important issues to provide a reconstruction of the current state at the end of the Roman Empire“. [3].

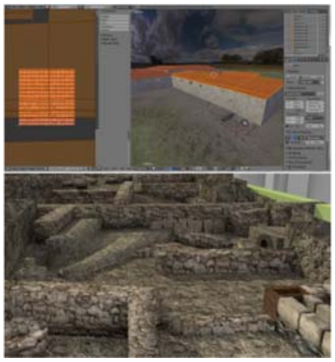

FIGURE 1. Augmented Reality to preserve hidden vestiges in historical cities

It is therefore clear that 3D graphics can be beneficial in many different industries. Thanks to technological development, the obstacle to software unavailability or insufficient performance of computers or workstations was eliminated. So it is easy to create tasks that could effectively develop for example spatial orientation. Spatial skills as cognitive skills can be learnt and taught formally to students using appropriately designed tools, technologies, and curricula [4]. There is still a lack of specific knowledge concerning how spatial skills may be best spread across curricula and how to optimally incorporate new technologies in order to provide better results for children [5].

CURRENT STATE

Research from Czech Republic „ Influence od Game Application Usage on Spatial Skills by Preschool Children", proves that Training with the help of ICT seems to be faster. There may be several reasons:

1) Educational applications are able to display environments in 3D. The entire area a child needs to move within, according the instructions provided, is shown on the screen and the child is able to observe the various movements and directions. It is a new experience compared to moving oneself in space (which must be the first natural experience and activity of a child). At the age of 6, children are able to perceive and understand things from a different perspective.
2) There are rotations of a subject, which the child can observe and combine repeatedly. They can also try new combinations.
3) The tasks are often connected to the narrated instructions. Voices and instructions are linked with movements inside the space of the game.
4) Children are solving multiple logical sequences and playing out the individual steps of a solution in their logical order. In an ordinary game the possibilities of those tasks are very limited and children learn repeating patterns relatively fast. The variation of tasks in this game is a significant benefit.
5) Children are able to perceive the concept of spatial orientation and perception thanks to different play environments in the game.
6) In the narrated instructions concerning spatial skills, there are many abstract words referring [6].

V China was developed EZ-Manipulator, a new 3D manipulation interface using smartphones that supports mobile, fast, and ambiguity-free interaction with 3D objects. Our system leverages the built-in multi-touch input and gyroscope sensor of smartphones to achieve 9 degrees-of-freedom axis-constrained manipulation and free-form rotation. Using EZ-Manipulator to manipulate objects in 3D is easy. The user merely has to perform intuitive singleor two-finger gestures and rotate the hand-held device to perform manipulations at fine-grained and coarse levels respectively. We further investigate the ambiguity in manipulation introduced by indirect manipulations using a multi-touch interface, and propose a dynamic virtual camera adjustment to effectively resolve the ambiguit [1].

In research "How 3D Interaction Metaphors Affect User Experience in Collaborative Virtual Environment" we learn The results demonstrate that there is a significant difference by changing the interaction metaphor on the copresence, awareness, involvement, collaborative effort, satisfaction usability, and preference. The results confirm our overall working hypothesis, that the choice of 3D interaction metaphor affects significantly user's experience in CVE [7].

TASK DESIGN

This paper describes the genesis of tasks for working with 3D graphics and three-dimensional objects to reach positive effects on solvers (students, students) and develop skills:
Expected positive effects and abilities that can be developed with the created tasks: Spatial imagination; Spatial orientation; Creativity; Logic; IT competence.

Specifically, spatial ability has recently been recognized as a crucial area in children's education, one which might have a broad positive or negative impact on the further learning, education and even future career of a child [8].

In order to be able to develop certain aspects of human capabilities in the most effective way, proposed tasks must be compatible with several criteria. These criteria are designed in such a way that tasks are practicable in almost all circumstances and that could prevent barriers, prolong or complicate their processing are eliminated.
Key Criteria and Task Features:

- must be resolved in any 3D graphics software or application
- must be simple to understand, not contain many complex instructions
- compatible with users with low IT skill
- Correct solution of tasks must not exceed a maximum of 5 minutes
- must respect the basics of logic and algorithmization
- must be suitable for solvers from 7 to 60 years old

Certain criteria must also be met by the tools (software or applications); Again, the unwanted effects that should be addressed need to be eliminated

Key criteria and features of software tools:

- Available for pupils and students (preferably free or very low cost)
- Simple installation, possibly without installation
- User-friendly and simple interface
- Possibility to insert and manipulate basic objects (primitives) such as: cube, sphere, cone

The student, pupil or person who will perform the tasks must be free to choose the software or application in which they will work. Below is a PC software that meets the above specifications.

Recommended PC software application to solve these tasks:

- Blender
- Paint 3D
- SketchUp

It is also important to choose whether the solution will work on a classic PC or mobile device. See the table in the previous article entitled "3D Technology in Education" for information on suitable applications.

TASKS

Suggested tasks are inspired and based on already conducted researches that combine geometric puzzles in combination with spatial imagination and three-dimensional space. It has been clearly shown that spatial skills are critical for mathematical performance [9].

Research "Enumerating 3D-Sudoku Solutions over Cubic Prefractal Objects" proves, that in this enumeration, at first he used a computer with a simple backtracking search algorithm, but finally he derived all of them by hand. His experiences show that the six-ways Sudoku constraint is so strong that there are only a small number of solutions. Therefore, a simple backtracking search algorithm works in a realistic time, and one can even enumerate them by hand. [10].

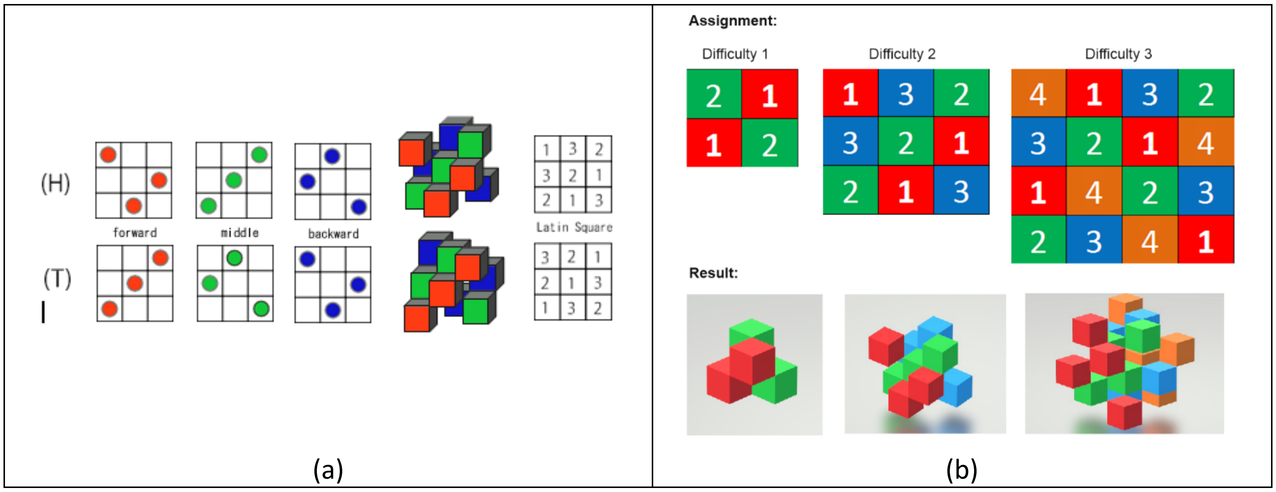

FIGURE 2. (a) Jigsaw-Puzzle-Like 3D Glyphs for Visualization of Grammatica. (b) Enumerating 3D-Sudoku Solutions over Cubic Prefractal Objects

Another inspiring research The Ougi system (visual programming system) enables a user to edit and execute a program by direct hand manipulation and to visualize the program in 3D. Immersive and visual programming systems such as Ougi require appropriate 3D visualization of programs and relationships of elements. This is one of

the motivations for this research. The use of 3D diagrams to represent both syntactical and semantic constraints in a programming language is proposed. The diagrams are created by using jigsaw-puzzle-like 3D glyphs, or shapes, to represent the grammatical constraints. The glyphs have convex, concave, and/or wire-frame parts, and an inclusive match between glyphs represents the satisfaction of a constraint. The, proposed glyphscan represent polymorphism clearly. Examples of representations are used to illustrate polymorphic constraints in an assignment. The polymorphic constraints have not been re-presented by other graphical representations using glyphs or icons [11].

Task for working with 3D objects: 3D Sudoku, Difficulty: 5/10

Assignment:

- Create 3D Sudoku by 2D input (Picture 4).
- Number specifies the nesting level of an individual cube (block). The higher is the number, the more nesting level. Time and precision are evaluated.
- Submit a JPEG image and source composition file from your software.
- Design and develop your own 3D Sudoku.

Evaluation criteria:

- Solving time (evaluated and compared separately for each difficulty)
- The design of your own Sudoku is evaluated separately.
- Precise elaboration

Awaited positive effects:

- Spatial orientation and imagination
- Ability to work with 3D graphics
- Creativity (Design your own 3D Sudoku)
- IT competence
- Logical thinking

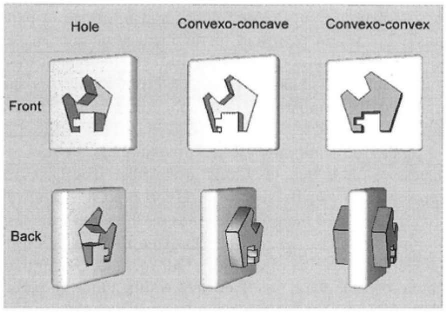

FIGURE 3. Task for working with 3D objects: 3D Sudoku

CONCLUSION

Based on the knowledge of using 3D graphics in other industries, puzzles have been created to help develop students' skills and have positive effects on them. These tasks can be measured and the results analysed.
Several other tasks are currently underway, which together will form a comprehensive set of tasks for working with 3D graphics in order to develop students' abilities.

REFERENCES

1. P. Tseng, S. Hung, P. Chiang, Ch. Yao, & H. Chu, EZ-Manipulator: Designing a mobile, fast, and ambiguity-free 3D manipulation interface using smartphones. National Tsing Hua University", Taiwan, China, 2018.
2. A. Dan & M. Reiner. Reduced mental load in learning a motor visual task with virtual 3D method. Technion, Israel Institute of Technology, Israel, 2017.
3. J. L. Martineza, S. A. lvareza, J. Finatb, F. J. Delgadoa & J. Finata, Augmented Reality to preserve hidden vestiges in historical cities. Universidad de Valladolid Paseo de Belen 11, Valladolid, Spain, 2015.

4. National Council of Teachers of Mathematics, Curriculum focal points for prekindergarten through Grade 8 mathematics. (on/line: https://www2.bc.edu/solomon-friedberg/mt190/nctm-focal-points.pdf).
5. S. N. Newcombe, A. Frick. Early Education for Spatial Intelligence: Why, What and How,
6. S. Pekárková, Influence od Game Application Usage on Spatial Skills by Preschool Children (UHK, 2019)
7. H. Hrimech, L. Alem & F. Merienne, How 3D Interaction Metaphors Affect User Experience in Collaborative Virtual Environment . Arts et Metiers ParisTech, France, 2011.
8. J. Gustafsson. Hierarchical models of individual differences in cognitive abilities . Advances in psychology of human intelligence. Vol. 4, pp. 35-71.1988.
9. D. H Uttal, D. I Miller & N. S Newcombe, Exploring and Enhancing Spatial Thinking: Links to Achievement in Science, Technology, Engineering, and Math?. Current Directions in Psych. Sci., 2013.
10. H. Tsuiki & Y. Yokota, Enumerating 3D-Sudoku Solutions over Cubic Prefractal Objects. Kyoto, 2011.
11. N. Osawa. Jigsaw-Puzzle-Like 3D Glyphs for Visualization of Grammatica. University of Tokyo, 2008.

How to Develop Computational Thinking in Pre-School Children

Tatiana Havlásková[1, a)], Zuzana Homanová[1, b)], Kateřina Kostolányová[1, c)]

[1]*Pedagogical Faculty, Department of Information and Communication Technologies, Fráni Šrámka 3, 709 00 Ostrava – Mariánské Hory, Czech Republic*

[a)]Corresponding author: tatiana.havlaskova@osu.cz
[b)]zuzana.homanova@osu.cz
[c)]katerina.kostolanyova@osu.cz

Abstract. The paper is aimed at using modern technology, specifically the programmable toy Bee-Bot, to teach pre-school children, helping them develop their computational thinking as well as logic and abstract thinking and pre-mathematical concepts. Moreover, it also introduces an activity which uses the aforementioned programmable toy to help children develop not only their computational thinking, but also their problem-analysis and problem-solving skills.

PRE-SCHOOL CHILDREN AND ALGORITHMIZATION

Is there a relationship between pre-school education and computational thinking? Most certainly there is. However, it all depends on how computational thinking is taught to pre-school children, i.e. what methods are chosen, how the teacher organizes class work and what teaching aids they use.

Pre-school education is a vague term. It is the most crucial and sensitive period in a child's life, a period of their psychological development. Children at this age learn a lot on their own – by imitating, playing, exploring and simply by being curious. However, a tutor (a parent or a teacher) is still the most important factor. Pre-school education can be understood as targeted action aimed at supporting and motivating pre-school children, helping them develop competencies they will need in school. Moreover, pre-school education is also an educational process which should help make children's life easier and prepare them for further education [1].

Kindergarten children learn a lot of new information which – depending on their age – they unconsciously absorb. Moreover, they also develop key competencies which are crucial for their future lives. So why not expand their education to include the development of their *problem-solving skills* (one of the essential key competencies)? Children face problems which they try to solve every day. Therefore, it is extremely important to map children's thought process when solving a problem (finding new and non-standard solutions) and expand these findings using appropriate methods, i.e. helping them develop their computational thinking, abstract thinking, logical thinking and pre-mathematic concepts in a natural way.

Pre-school children are already familiar with numbers. However, they have yet to understand their meaning. Even older children have difficulty understanding relations between numbers and their relative numerical significance (sometimes five can be more and other times less). Children need to understand that the result does not depend on what we count, i.e. that the result is always the same (it does not matter whether it is apples, pears, etc.) [2].

Logical thinking of pre-school children is specific. Basically, it is based on finding the path which leads to the correct answer (i.e. to solving a problem). Logical thinking is the ability to draw a conclusion from a premise or to prove the correctness of a solution. The following tasks are used to aid the development of logical thinking: which of the following does not belong to the group, logical pairs, relations between symbols, riddles, quizzes and codes [3].

The problem-solving competence is vital to computational thinking. Everyone solves problems all the time; they need to solve problems and solve them correctly. As far as pre-school education is concerned, problem solving needs to be divided into two parts [2]:

- Defining a problem and its interpretation – a pre-school child often pays attention to unimportant details which prevents them from understanding the situation and solving the problem.
- Finding correct solutions and their realization – when it comes to pre-school children, creating a systematic plan is difficult. Their plans are often situational and difficult to realize. These unrealistic solutions result from children's optimistic self-assessment, i.e. they think that they can do more than they are capable of.

INCORPORATNG TECHNOLOGY INTO PRE-SCHOOL EDUCATION

Since we live in a digital age, many institutions, including kindergartens, use digital technology, which creates an opportunity to incorporate this technology into pre-school education and use it to help children develop basic digital competencies and the aforementioned computational thinking. Framework educational programs (not only for pre-school education) are constantly being updated, with the topics of digital literacy, computational and algorithmic thinking becoming more and more relevant. Therefore, it is important to incorporate these ideas into education – using games and involuntary learning, but most of all knowing that pre-school children's perception of the world and facts is very specific. Developing computational thinking from an early age is key to being successful in the next stages of life – compulsory education, further education, personal life. Problem-solving skills, logical thinking, creativity and originality are the most appreciated skills today. Therefore, starting to develop these skills as early as kindergarten is a logical conclusion.

The Framework Educational Program for Pre-School Education only touches on the use of digital technology (and technology in general), introducing possible risks. In her paper, [4] focuses on this topic, stating that psychomotor development of children needs to be considered as it is important to understand the mental development of a pre-school child. The teacher needs to use technology in order to achieve an educational goal. The time the child spends with technology should also be specified.

In order to be able to use technology (not only in pre-school education), teachers need to be familiar with it. If the teacher is not able to use technology in an effective manner, they cannot possibly incorporate computational and algorithmic elements into instruction and help children develop their digital competencies. That is why the TPCK model should be mentioned. In the beginning, there was Shulman's theory that defined the so-called PCK (Pedagogical Content Knowledge). It is based on the notion that professional content should be taught together with methods suitable for teaching a particular curriculum. The development of technology made this model popular. Mishra and Koehler expanded it by adding a technological aspect, thus creating TPCK (Technological Pedagogical Content Knowledge) [5].

The model defines today's teacher who should not only be an expert in their field, but who should also use appropriate didactic and methodical approaches and be able to incorporate technological elements into them. A pre-school teacher should be a college graduate who is familiar with pre-school education methodology and didactics. Moreover, they should also understand children's psychology, development and behavior, and also be able to sing, lecture, read fairy tales to children, etc. The teacher should also be technologically educated, i.e. be able to use basic technological equipment such as the computer, mobile phone, Internet. In kindergarten these tools could be effectively used to help develop perceptual skills, transparency, etc. Interactive whiteboards, digital aids and robotic toys are extremely beneficial if the teacher can use them properly.

BEE-BOT

Bee-Bot is a programmable robotic toy, an interactive digital tool for developing logical thinking, spatial imagination, planning and pre-mathematical concepts. It appears to be a perfect tool for developing computational thinking and basics of programming, informatics and mathematics.

FIGURE 1. Bee-Bot

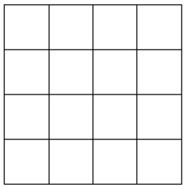

FIGURE 2. Worksheet

Bee-Bot works by remembering and storing individual steps/commands in the order chosen by the user. Children are immediately faced with abstraction as the toy does not have a display or screen on which they could see the selected commands. Therefore, it is important to plan the individual commands in advance (e.g. using a record sheet). The upward arrow allows us to make the bee move forward by 15 centimeters (forward means in the direction of the bee's eyes). The downward arrow allows us to make the bee move backward by 15 centimeters (backward means in the direction of the bee's "buttocks"). The right/left arrow makes the bee turn 90 degrees to the right/left. The "X" button is used to delete the commands stored in the bee's memory. Children should keep this in mind to make the bee carry out only the current commands, and not the past ones. The "II" button is used to stop the toy during the execution of a command. The "GO" button starts the bee and makes it execute the proposed sequence of commands. When creating Bee-Bot activities, the teacher should use a worksheet with 15x15cm squares. It is entirely up to the teacher how many squares there will be. If the worksheet is transparent, the teacher can put pictures under the individual squares, creating obstacles and/or stops on the bee's way.

Proposed Activity

Daily activities

This activity is aimed at developing children's learning, social, personal and professional competencies. Children will learn how to use commands to achieve the expected result, determine and justify the sequence of commands and understand that if they change the sequence of commands, they might not be able to reach the finish line (i.e. to solve the problem). Moreover, they will also learn how to control a programmable toy.

Required tools:

- Programmable bee
- 75x75cm worksheet (Figure 3) with 15x15cm squares – the first column contains numbers (representing the correct order of commands) while the last column contains pictures which describe the activity (in a randomized order)
- Record sheet (optional)

Activity: The teacher divides the children into smaller groups (of 3 or 4), with each group having their own worksheet and programmable toy. First of all, the children need to find out what the pictures represent (what kind of activity). Then they need to determine why the pictures are in a randomized order (and which pictures are not in the correct order). Their next task is to assign the numbers on the left side of the worksheet to the pictures on the right side. The bee always starts from the square representing a particular number (1 to 5), to which the children need to assign the correct picture. The teacher can also use the so-called record sheet to write a program (using arrows) which would make the bee assign the correct pictures to the individual commands (steps). Only then can each group try and program the bee and check whether or not they assigned correct pictures to the individual steps.

Problems that may occur are related to children's not knowing how to properly control the programmable toy, not being familiar with the arrow symbol or a lack of spatial orientation (to the left/right). The activity can be modified by changing the task as well as the worksheet, i.e. to replace the current daily activity with another (grandmother baking a cake, crossing an intersection controlled by traffic lights, how a plant grows, which season follows which, etc.).

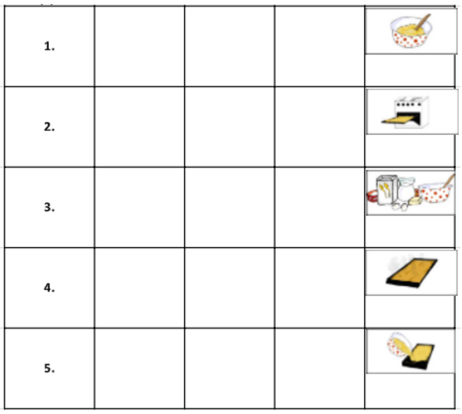

FIGURE 3. Activity worksheet

CONCLUSION

Pre-school education should teach children to be "fully functional", i.e. when they leave kindergarten, children should be able to live a proper life and cooperate. They should leave kindergarten having mastered the following competencies: the coordination of movement and the movement itself, fine and gross motor skills, the ability to complete basic tasks and perform basic commands and operations, self-sufficiency, psychomotor and mental development, communication and socialization, social skills and habits, basic behavior patterns, social norms and principles, moral values, general knowledge of the world and many others. Early exposure to activities aimed at the development of algorithmic thinking, solving problems based on real-life scenarios and the use of technology puts children in a good starting position which serves as a springboard for other efforts.

REFERENCES

1. E. Opravilová, *Preprimární pedagogika* (Grada, Praha, 2016).
2. M. Vágnerová, *Vývojová psychologie: dětství a dospívání* (Karolinum, Praha. 2012).
3. J. Fořtíková, *Rozvoj rozumových schopností u dětí v MŠ: pracovní listy pro předškolní děti* (Portál, Praha, 2014).
4. H. Splavcová, *Informační Technologie V Mateřské Škole – Úvod* (Metodický portál RVP, 2015). Available at: https://clanky.rvp.cz/clanek/c/p/20585/INFORMACNI-TECHNOLOGIE-S-MATERSKE-SKOLE-I.html/.
5. B. Brdička, *Integrace technologií podle modelu TPCK* (Metodický portal RVP, 2009) Available at: https://spomocnik.rvp.cz/clanek/10641/INTEGRACE-TECHNOLOGII-PODLE-MODELU-TPCK.html

Using Video as a Tool for the Improvement of Teachers' Abilities and Skills

Zuzana Václavíková

Department of Mathematics, University of Ostrava, 30. dubna 22, Ostrava, Czech Republic

zuzana.vaclavikova@osu.cz

Abstract. Although video or streaming is currently widespread in all areas of everyday life, its use as a tool for improving the teaching process is still not fully implemented. While software is already available in English for utilizing video to analyze lessons, there is only limited experience with its use in the Czech Republic. Our experience with the substitution of classical sit-in class observation for recorded lessons followed by a detailed analysis will be described in this paper.

INTRODUCTION

One of the most integral parts of teacher training is observation during lectures. It means that future teachers are present in class during real lessons and are able to monitor how classes are taught in a specific subject.

This allows them to observe which learning methods are used, how active the teacher is, who is the leader of the lesson, and the general interaction with students [1].For future teachers, sitting in on lectures is a great opportunity to get involved in observing the primary experience of a teacher's professional life. It is often the starting point of their own thinking about teaching methods, and about the future direction of their didactic activities. To fulfill the educational goal of lesson observation it is important to carefully prepare beforehand, monitor carefully during the course of the lesson, and follow up with a detailed analysis and discussion. Usually for teacher training programs, there is a group of 5 students together in a class with one teacher of didactics for the monitored subject during a lesson observation. Class observations are also often used by active teachers to improve learning. In this case, the presence of experts for the subject's didactics, general didactics and experts of pedagogy and psychology are required. It means that there are 10-15 people watching the lesson at any one time. Sometimes it is not possible to authorize the presence of such a large number of "strangers" in the class. This is where the development of IT can be put to better use, by utilizing video as a support tool. Video can also help teachers learn to notice, that is, to develop new ways of "seeing" what is happening in their classrooms. It is claimed that this ability to notice is critical in the context of current reforms that require teachers to make pedagogical decisions in the midst of instruction [4].

OBSERVATION OF LECTURES USING VIDEO

According to project Příroda (supported by the European Social Fund between 2017-2019), where the main outcomes were learning materials for secondary school children in four subjects – physics, chemistry, geography and biology, we used class observation as the starting point of research. The research was focused on mapping current teaching methods of the selected topics in each mentioned subject and developing the teaching methods. This included the preparation of supporting educational and learning materials that take into account the needs of gifted, intact (average) and special needs students. The base point at the beginning of the research was the selection

of the topic from the subject and the mapping of its current educational approach in elementary schools. The target groups of students were 12-13 year old and 14-15 year old children at secondary school (ISCED 2A). Learning materials were prepared for 45 minutes, including the time for reading, based on the inquiry-based learning method.

The classical lesson observation, i.e. being present in class, carries one negative. If we would like to monitor the class, usually the presence of many experts in the class disturbs the atmosphere, and the class behaves differently than it would normally. Additionally, the fact that the project is run by the University of Ostrava with two partners – the first being Palacký University in Olomouc and the second one is the institution of informal education, called Korunka, it was necessary to gather lots of experts at a given time in one place. Therefore, experts for the evaluation of the teaching methods were from all three of these institutions. Therefore, we decided to use video as a tool for monitoring the class instead of sitting in on the class, similarly as [7]. Streaming the lesson using a videoconference didn't use the simultaneous transmission of sound, image and data between two or more participants, but it was strictly one-sided. Respectively, it was only between the teacher and the group of experts who were watching the lesson from another place, with minimal interference from the experts in the process. Each lesson was recorded and so it was possible to return to certain parts repeatedly and analyze them after its conclusion. In particular, as Sherin has described [5,6], video analysis affords teachers an opportunity to engage in a set of practices that are very different from what they do in the classroom. Video offers a permanent record of classroom interaction [3, 4]. It can be paused and rewound so segments can be re-viewed on multiple occasions, with different perspectives each time if one desires.

TECHNICAL BACKGROUND

The easiest way to record the lessons is using Accordent Technology [2, 8] or a similar solution for creating presentations that synchronize streaming video with PowerPoint slides. Accordent reduces demands on time, which are usually associated with creating audio and video recordings of lectures using synchronous presentations or other components such as interactive boards, etc. The entire device is permanently set up in a specialized classroom in our university building. In line with the projects' requirements we needed to analyze at least 4 lessons for each of the four scientific subjects, so we had to complete at least 16 class observations using the streaming method. It wasn't possible to achieve this only in this specialized classroom. Fundamentally, because the transport of pupils became problematic (time-consuming), some topics had to be carried out in laboratories, and we needed and wanted the lessons to take place in a normal, authentic environment for pupils. Therefore, we decided to use the mobile camera system directly in the schools.

We used 2 cameras (Hikvision IP WebCam) for recording. They were placed so that first one occupied the space of the teacher and the board and the second one covered all the pupils from the front, as Figure 1 shows. The recordings were taken at a resolution of 1280x960 pixels and then merged into a single 2560x960 image. The aspect ratio of 4:3 was chosen instead of 16:9 with respect to the required outputs of both of the cameras. The files were made in the mkv format of the H264 codec due to the ability of the cameras to record directly in that format, also to enable a wide variety of supported formats in players, and finally, the ability to create smaller capacity files than older formats. The projector was set up in the room reserved for streaming.

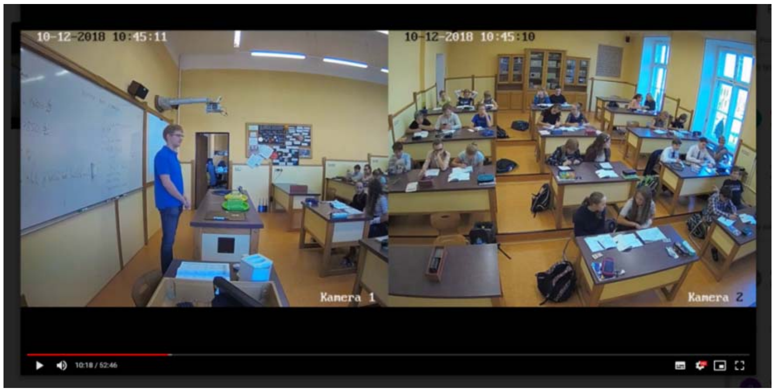

FIGURE 1. The final format of the video – both of the cameras in one single 2560x960 image.

ANALYSIS OF THE VIDEO

In the first phase of the project, we analyzed 8 lessons in this way, in the second phase, which is currently underway, we will analyze an additional 8 hours. During every stream, there was a group of approximately 10 experts and if necessary, in another place additional observers were watching on-line (Fig. 2). During the streaming, the experts only made notes, or even remarked on the moments they felt were important. Immediately after the lesson, the recording was discussed, notes were compared and the discussion with the teacher was conducted. During the following week, the recording was scripted separately by the experts and by the teacher of the lesson. We used a similar model to the software tool, Video Analysis Support Tool (VAST)[5], to support teachers in developing their ability to notice and interpret aspects of classroom practice. The experts lead the teacher to think about the teacher's role, students thinking, and the connection between the intention of the teacher and the teaching itself. The final step is the discussion between the teacher and experts, where the lesson is reviewed again and new methods are suggested.

(a) (b)

FIGURE 2. Pictures of the biology lesson stream (a) and the room for experts watching it on-line (b).

BENEFITS AND NEGATIVES OF USING VIDEO FOR OBSERVATION

The main benefit of using streaming as a tool for monitoring the class instead of the classical sit-in observation was that the lesson could be watched by any number of people without disturbing the lesson. In addition, the recording of the whole lesson itself facilitated the creation of analysis and reports, which is an integral part of the subsequent discussion. To evaluate the entire delivery of the lecture, the teaching methods used, work with the pupils and the work of the teacher, it is possible to return to the recording and to watch the key moments repeatedly and in detail. Because monitoring each individual pupil's work was not the main goal for analyzing the lessons, we didn't need to use a third camera for recording the details (for example how the students work with the learning worksheets). So the environment in the classroom was not disturbed by any extra external influences.

The negatives were linked to two facts – the first one was that we had to use the mobile camera system, and the second was that teachers at the chosen school do not have any experience with streaming. Selecting a suitable position for the classroom cameras was not a problem except for some classes (usually in a laboratory) where recording the teacher and multimedia boards at the same time was problematic, because they were too far apart. In this case the presentation on the multimedia boards was unreadable. Although the cameras contained a microphone, the sound was almost unintelligible. It was necessary to transfer the sound from an external microphone wirelessly using the smartphone communications application. Unfortunately the sound and video weren't synchronized, however the quality of the audio was more important than being synchronized. The problems with the teachers' inexperience with the recording of the lecture resulted in them often being stood in the wrong place – they obstructed the multimedia board, or the microphone did not record them. We also had a problem with the willingness of teachers to participate with the recording itself. Their active interest in analyzing the lesson requires

a great deal of courage and patience. Because there is no career progression or other complex assessment system for this profession in the Czech Republic, they often have no interest and no reason in improving their teaching.

CONCLUSION

As has been described, utilizing video as a tool for learning development could be useful for the improvement of the education process as a more efficient substitute for the classic sit-in lesson observation. Video offers more in depth feedback opportunities for teachers than just the reflection of experts in the classic model of sitting in on a class. It will also provide a much more detailed insight into a number of mistakes that experienced teachers may not be able to notice or recognize. We hope that in the future software like VAST will exist using the Czech language, which will help teachers analyze their methods more effectively.

ACKNOWLEDGMENTS

This research was supported by a grant of the ESF named PŘÍRodovědné Oborové Didaktiky A praktikující učitel, CZ.02.3.68/0.0./0.0/16_011/0000669. I thank our colleagues from the expert teams and school teachers who provided insight and expertise that greatly assisted the research, although they may not agree with all of the interpretations/conclusions of this paper.

REFERENCES

1. Z. Bochníček, J. hališka, Z. Kobíková, O. Šimoník, P. Krupka, O. Rotreklová, T. Papírník, A. Mareček, V. Herber and J. Herman, *Na pomoc pedagogické praxi.* 1. vyd. Brno: Masarykova Univerzita (2013)
2. https://en.wikipedia.org/wiki/Accordent_Technologies
3. B. Latour, *Drawing things together*, In M. Lynch & S. Woolgar(Ed.), Representations in scientific practice, pp. 19-68, Cambridge,MA: MIT Press, (1990)
4. M. G. Sherin, E. van Es, *Using video to support teachers‘ ability to notice classroom interactions*, Journal of Technology and Teacher Education, pp. 475–491(2005)
5. E. van Es and M. G. Sherin, *Learning to Notice: Scaffolding New Teachers' Interpretations of Classroom Interactions,* Jl. of Technology and Teacher Education 10(4), 571-596 (2002)
6. M. G. Sherin, *New Perspectives on the Role of Video in Teacher Education*, in Jere Brophy (ed.) Using Video in Teacher Education (Advances in Research on Teaching, Volume 10) Emerald Group Publishing Limited, pp.1 – 27 (2003)
7. N. Stehlíková, "*Využití videozáznamů pro rozvoj didaktických znalostí obsahu budoucích učitelů matematiky*", in T. Janík and kol. Možnosti rozvíjení didaktických znalostí obsahu u budoucích učitelů, Paido, Brno (2009)
8. Z. Václavíková, *Metodická příprava výuky a tvorby prezentací s využitím moderních technologií*, Ostravská univerzita v Ostravě, Ostrava(2013)

Eye-Tracker Technology in Didactic Research

Zuzana Václavíková

Department of Mathematics, University of Ostrava, 30. dubna 22, Ostrava, Czech Republic

zuzana.vaclavikova@osu.cz

Abstract. Eye-tracking, i.e. the measurement of eye activity as a technology is used in many different areas. The most useful is for example using an eye-tracker as a tool for controlling a computer, as a diagnostic tool, as well as a tool for scientific research in many different subjects (marketing, education, medicine, and so on). Our experiences with using eye-tracker technology for research into the effectiveness of learning materials and learning outcomes will be described in the paper.

INTRODUCTION

Although eye-tracker technology is mostly used in other areas (marketing, medicine, etc.), it was and is used also in didactic research (often for the detection of talents [see 2 and 3] or specific learning disorders, etc.). Using this technology, the changing position of the eye is recorded and compared with a task assignment, which makes it possible to understand the student's strategy of solving the problem [see 1 and 5]. Eye-tracker technology gives researchers the opportunity to test pupils' learning outcomes as well as their strategies for solving problems, to differentiate and compare pupils' approaches, and to trace their way of thinking.

According to project Příroda (supported by the European Social Fund during the years 2017-2019), where the main outcomes were learning materials for secondary school children in four subjects – physics, chemistry, geography and biology, we tested the quality of outcomes using the eye-trackers. The research in the above mentioned project is focused on the individual potential of each student - methodological outputs of the project take into account the needs of gifted, intact (average) and special needs students. So we are also able to compare the solutions from different groups of students. The target groups were 12-13 year old and 14-15 year old children at secondary school (ISCED 2A). Learning materials were prepared for 45 minutes including the time for reading, based on the inquiry-based learning method. There were questions about the learned topics for evaluating the education process by the student at the end of each worksheet. We have decided to test the pupils' knowledge after the piloting of a newly designed lesson using the eye-tracker technology. For testing we used the questions from the prepared learning materials and adapted them into a form suitable for the eye-tracker system.

TECHNICAL BACKGROUND

For our research we use the Gazepoint system GP3 [see 4], the measuring set was completed with the HP 250 G5 laptop and an external 19" LCD AOC (280 x 1024 pixels). Together with the eye tracker, the original Gazepoint Analysis Professional Edition (v4.2.0) x64 and Gazepoint control x64 full license software are used to collect data and calibrate the eye tracker. Subsequent analysis of the measured data is provided by OGAMA version 5.0 due to a wider range of analytical tools.

Measurements took place directly at the schools involved in the project. The preparation of the eye-tracker system at the school took about 15 minutes, with regards to the spatial possibilities, the appropriate layout and the necessary lighting. Measurements were performed in parallel on three sets, which allowed a larger group of pupils to be tested.

For each set, the technician was available throughout the measurement. The eye-tracker set is shown in Fig. 1 (a), the calibration in Fig 1. (b).

Although the system works perfectly, a major problem was that looking away from the monitor is recorded as an error, and the eye-tracker does not receive a signal. So we had to discuss how to prepare the tests if students needed to read the input from the monitor, to follow the drawings and pictures, to choose from the solutions offered, or especially verbally answer and record the answer – as we do during the classical learning process. To ensure the correct function of the eye-tracker it is necessary to

- maintain a certain distance between the student and the monitor, as there is no proper reading of student movements when zoomed in,
- be careful that no objects interrupt the signal between the students and the movement analyzer,
- remember that for eyelashes the students are monitored from the bottom of the monitor.

(a)

(b)

FIGURE 1. Installation of the eye-tracker set at school (a) and calibration of respondent's eyes (b).

HOW TO PREPARE THE TASKS FOR EYE-TRACKER TESTING

One of the basic questions in research with eye-trackers is the preparation of the materials. We decided to prepare one test for each target group from one of the mentioned subjects. The student's time for solving was not limited but the tests were designed to be no longer than 20 minutes, this was due to the concentration required to view the monitor being demanding. Setting the eye tracker to the respondent and its calibration (used with all nine calibration points) takes 5 minutes on average. This time depends mainly on the lighting conditions in the room, the possibilities of their regulation and the needs of a particular respondent (dioptric glasses, contact lenses, eye defects, etc.).

Because we had four scientific subjects for testing and there are significant differences between the working sheets from biology, geography, chemistry and physics, our approaches were different with regards to the needs of every subject. There are also significant differences between the needs of gifted, intact and special needs students so the tests were prepared in three modified versions.

Firstly we needed to understand if just viewing the monitor is sufficient for students or if writing is necessary as well. From this point of view, we discussed the possible options of setting up the eye-tracker measuring set and preparing the tests for students. In the situation where just viewing the monitor is sufficient, we can prepare questions so that the solutions are offered. The students choose the right one and stay for 3-5 seconds on the answer they believe is correct. This approach is the easiest from the point of view of solving, but the most complicated for preparing the tests. The intermediate case is viewing the monitor combined with clicks. However, care should be taken to ensure that the answers offered/place to be clicked are far enough apart so that any inaccuracies of the eye recording are not interpreted as a wrong answer. In general, it is better to place answers side by side with sufficient space, rather than line by line. The example of this testing task is shown in Fig. 2 (a).

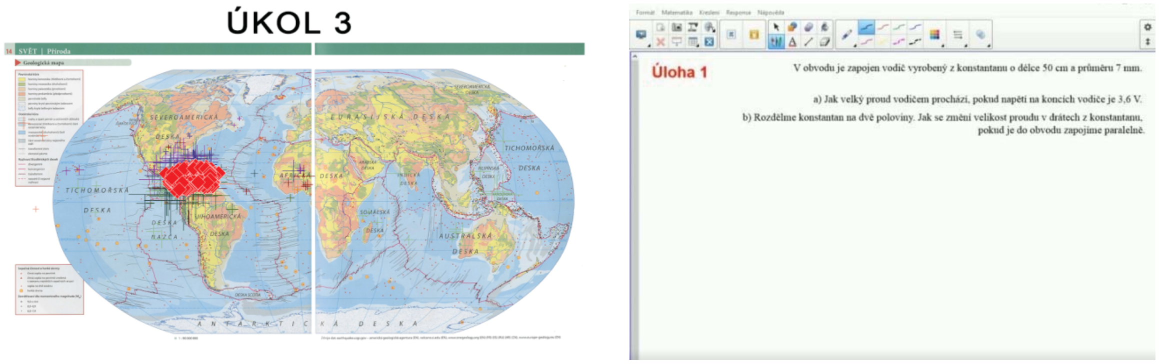

(a) (b)

FIGURE 2. Example of tested question using eye-tracker viewing the monitor and clicks (a) and example of tested question using eye-tracker with Smart tablet for writing (b).

In the second case, in order to record responses or shifts in the test, each eye-tracker measuring set can be equipped with a wireless keyboard and mouse or an electronic pen and tablet can also be used. The tablet is connected to the computer via the USB connector and the e-pen software is used. A SMART Notebook was used in our research. If the students are able to write on the tablet and looking only at the monitor, then there is no eye-averting and signal interruption between the eye-tracking device and the person. Questions in the test can be more open, requiring a calculation or sketch, and then better demonstrate a strategy for the solution, in this case (see Fig.2 (b)). Students can also use the calculator implemented on the computer. The drawback is that writing on a tablet and looking at the monitor is a matter of practice and experience; and in the early stages pupils had a problem with this new way of writing (see Fig. 3). It was observed that the handwriting and sketches are poor due to the difficulty of coordinating writing on tablets and viewing on the monitor at the same time. In the case of using the SMART Notebook for writing, time for understanding how to use it was needed for each respondent. It was between 5-10 minutes on average.

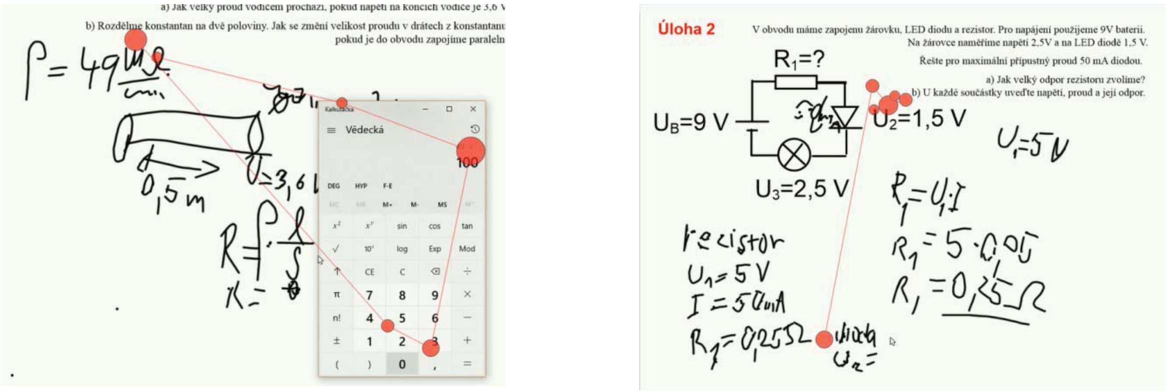

(a) (b)

FIGURE 3. Example of students solving – the questions from the physics required sketching, calculation and writing (a) and required reading the sketch and computing/writing (b).

It is also possible to write notes directly and solve a task on the monitor using the tablets or touchscreens. In order to use this method, a miniaturized eye-tracking device must be used that is placed directly on the bottom of the tablet or laptop. When solving a problem, it is necessary to be careful not to interrupt the hand signal that draws and writes on the monitor. We did not implement this method because the University of Ostrava does not own such facilities.

RESULTS

During the year 2018 we prepared the tests focused on physics at two levels - Density and its measurement (12-13 year old children) and Direct current (14-15 year old children), one test focused on geography – Natural hazards and disasters(14-15 year old children) and one test focused on chemistry – Water (12-13 year old children). The first and the last one were prepared exclusively for pupils with specific needs; they were given an example for each task according to which they should subsequently solve the task. By tracking the areas of interest, the number of vision fixations, the fixation duration and the changes between the areas of interest in time, it was clearly proven that the pupils used the example and found solutions exactly according to the pattern. The second and third one subjects were created and piloted on all three groups of students (gifted, intact and special needs students).It was possible to interpret each student's problem-solving sequences and differences in the individual potential of each student. From the data we were also able to evaluate the student's ability to concentrate throughout the solution, to discover the imperfections of the prepared materials (font size, page breaks, etc.) and the ability to co-ordinate between writing and looking at the monitor. Based on the pilot verification, we then modified the materials for real testing. At this moment we are in the process of testing the rest of the subjects and the general data and conclusions are not available currently. However, from the partial data obtained we can conclude that there are significant differences between the gifted students and others, and we have many interesting insights. For example changing strategies during a solving (check and delete), incorrect working with a calculator (missed queues), repeated reading of the tasks (often reading only a part of task).

CONCLUSION

In any situation, the use of eye-tracker technology is very beneficial for didactic research. However, producing a large amount of data means it is also difficult for drawing complex conclusions, as it is necessary to cooperate not only with teachers and subject's didactics, but also with statisticians, technicians and pedagogical psychologists. Undoubtedly, such measurements offer a whole range of challenges that can not only help upgrade learning materials, but also improve the educational process itself.

ACKNOWLEDGMENTS

This research was supported by grant of ESF named PŘÍRodovědné Oborové Didaktiky A praktikující učitel, CZ.02.3.68/0.0./0.0/16_011/0000669. I thank our colleagues from expert teams and school teachers who provided insight and expertise that greatly assisted the research, although they may not agree with all of the interpretations/conclusions of this paper.

REFERENCES

1. S. Popelka, *Eye-Tracking (Nejen v kognitivní kartografii), Praktický průvodce tvorbou a vyhodnocením experimentů.* Olomouc: Palacky Univeristy Olomouc (2017)
2. J. Škrabánková, L.Laš and P. Bujok, *Visualisation and interpretation of student strategies in solving natural science-based tasks using the eye-tracker,* inJournal of Eye Movement Research. 11(4) (2018)
3. J. Škrabánková and E. Trnová. *Researching Students Gifted in Science Using the Method of Eye Tracking*, e-Pedagogium, roč. 2015, pp. 79-93 (2015)
4. EyeTracking. [cit. 13.3.2019]. Available from: http://www.eyetracking.com/About-Us/What-Is-Eye-Tracking
5. Gazepiont. . [cit. 13.3.2019]. Available from: https://www.gazept.com/

Preface of the "3rd Symposium on Computational Simulation and Experimental Analysis of Hygrothermal Phenomena in Building Envelopes"

Zuzana Hlaváčová [1,a)]

[1]*Department of Physics, Faculty of Engineering, Slovak University of Agriculture in Nitra, Tr. A. Hlinku 2, 949 76 Nitra, Slovak Republic*

[a)]Corresponding author: zuzana.hlavacova@uniag.sk

The overall degradation of a building material or structure can be expressed, in the simplest way, by a qualitative or numerical indicator of the global condition level which determines the loss of performance of the considered material, building part or the whole building under its climatic environment over time. Hygrothermal phenomena are responsible for a substantial part of degradation processes particularly in the cold regions, where water condensation and freezing belong to the main deterioration mechanisms. The load-bearing structures and surfaces are parts of a building where the assessment of the degradation level is most significant. The interface between structure and surface layer is another important point because if the adhesion of both layers is compromised, whole parts of surface layer can be detached. Computer simulation is a powerful tool for an assessment of the degradation level of a particular material or structure. However, the quality of input data presents a critical factor for the achievement of reliable results. Therefore, in any analysis of the environmental impact on degradation of building envelopes computational simulations and experimental measurements are supposed to be done together.

The symposium brings together mathematicians active in numerical analysis and applied mathematics on one side, and experimental physicists and materials engineers working in the field of hygrothermal analysis and degradation of materials on the other. The main topics include but are not limited to:

- Characterization of environmental impact on buildings
- Computational modeling of hygrothermal processes in building envelopes
- Determination of input parameters for computational analyses
- Experimental investigation of hygrothermal processes
- Computer-aided service life estimates

Zuzana Hlaváčová

is a lecturer on the Department of Physics, SUA in Nitra. Professional training: The Comenius University in Bratislava – M.Sc., RNDr., Faculty of Engineering SUA – Ph.D., Assoc. Prof. Courses: Physics, Applied Physics, Selected Chapters from Physics, Biophysics, and Physical Properties of Food. Research interests: Moisture content metrology, Electrical properties of materials, Electrical properties utilization in industry and agriculture. Member of Editorial Board of scientific journals: Acta Technologica Agriculturae (SCOPUS), Journal on Processing and Energy in Agriculture (Serbia), Agricultural Engineering (Poland), Asian Network for Scientific Information. Member of Scientific Board of International Conferences – BioPhys Spring, Conference of Food Physics, Processing and Energy in Agriculture, Biosystems and Food Engineering, …

Verification of Computational Model for the Assessment of Interior Thermal Insulation Systems Using a Laboratory Critical Experiment

Václav Kočí[1, b)], Jiří Maděra[1, c)], Zbyšek Pavlík[1, d)], Miloš Jerman[1, e)] and Robert Černý[1, a)]

[1]*Department of Materials Engineering and Chemistry, Faculty of Civil Engineering, Czech Technical University in Prague, Thákurova 7/2077, 166 29 Prague 6, Czech Republic*

[a)]Corresponding author: cernyr@fsv.cvut.cz
[b)]vaclav.koci@fsv.cvut.cz
[c)]madera@fsv.cvut.cz
[d)]pavlikz@fsv.cvut.cz
[e)]milos.jerman@fsv.cvut.cz

Abstract. Unlike exterior thermal insulation systems, the interior ones require specific treatment as they might expose masonry to frost damage, mold growth, salt efflorescence, or other damage patterns that can limit the service life. Computational modeling belongs to effective tools which can be used for assessment of building segments performance without necessity of the segments to be built. However, a verified mathematical model is a key factor that ensures the results obtained will be accurate enough. In this paper, a verification procedure of a mathematical model for description of coupled heat and moisture transport is presented. Comparing temperature profiles obtained using a laboratory critical experiment and its computational representation, the applicability of the model is demonstrated. Two segments of masonry with and without thermal insulation system are selected for the analyses. In both cases, the root mean square error is less than 0.325 °C which confirms a high level of the model's accuracy and enables its possible application at the assessment of performance of interior thermal insulation systems.

INTRODUCTION

Thermal protection of buildings is an important task of today's civil and materials engineering. Better thermal insulating properties of building envelopes substantially reduce operational costs as heating may account for 42-45 % of operational costs during residential buildings' life cycle [1-2]. Lesser demands on energy spent on heating have also environmental benefits [3]. Load bearing materials with excellent thermal insulation properties, e.g. autoclaved aerated concrete or highly perforated ceramic bricks, have been developed for this purpose. Anyway, single layer masonry is not typical and thermal insulations, more likely, have therefore become an integral part of most building envelopes [4], especially those in cold regions.

The position of thermal insulation in a composition of external wall may vary. The mostly preferred solution is an application on exterior side of walls which goes along with an easier handling, elimination of thermal bridges and protection of masonry against weather conditions. However, this application makes buildings monotonous as it denies diversities of particular facades' appearance. This solution is therefore not acceptable in case of historical buildings or even buildings under preservationists' surveillance [5].

Keeping an original facade's appearance, interior thermal insulation systems have been developed as an alternative to exterior ones. On the other hand, several disadvantages have been found which make their application less favorable. Insufficient elimination of thermal bridges, risks of interstitial condensation, frost damage, mold growth, or salt efflorescence belong to the most frequently mentioned negatives in that respect [6-7]. To ensure a

proper hygrothermal function of the systems, these issues must be assessed and eliminated within a design stage using advanced techniques.

A laboratory critical experiment (LCE), a representative of above mentioned techniques, makes it possible to study a hygrothermal performance of selected construction details. Using set of probes, moisture and temperature fields can be studied in detail and corresponding modifications can be proposed. Exploiting these results, computational modeling goes far beyond LCE capabilities: verified computational models are able to predict a hygrothermal performance of any construction detail even without a necessity to be built. Therefore, it makes computational modeling a powerful tool for the assessment of hygrothermal performance of materials and constructions as it is able to provide practically immediate and cheap results which can result to an improvement of building construction performance.

LABORATORY CRITICAL EXPERIMENT

The laboratory critical performance was carried out using NONSTAT system consisting of two climatic chambers and a connecting tunnel with a specimen placed in it of dimensions up to 0.72 m × 0.72 m × 0.60 m. The boundary conditions on the exterior side corresponded to winter weather data for Olomouc, Czech Republic, covering December/March period of the test reference year (TRY) [8]. TRY contains long-term average hourly values of temperature, relative humidity, precipitation, wind characteristics and sun radiation data. Standard conditions (21 °C, 55 % of RH) [9] were applied on the interior side.

Two variations of the construction detail were investigated. Var. 1: Solid brick masonry (0.29 m) provided with lime-cement plaster from exterior (0.02 m) and interior (0.03 m) side. It was further assumed (Var. 2) that this construction was retrofitted by means of attaching a thermal insulation made of wood fiberboard (0.08 m) to the interior side and provided with interior finish (0.02 m). The construction details were mounted by a set of Ahlborn probes for continuous monitoring of temperature and relative humidity in selected positions. The data was subsequently used for the model verification. A scheme of the detail is depicted in Fig. 1. Properties of the materials involved are summarized in Table 1 [10-11].

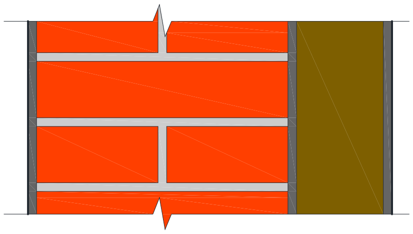

FIGURE 1. Scheme of construction detail.

TABLE 1. Material properties.

	Solid brick	Wood fiber board	Plaster
Bulk density [kg·m^{-3}]	1831	147	1244
Porosity [%]	27.9	90.1	49.8
Thermal conductivity [W·m^{-1}·K^{-1}]	0.59 – 1.74	0.07 – 0.69	0.30 – 0.94
Specific heat capacity [J·kg^{-1}·K^{-1}]	825 – 1254	2088 – 3855	1054 – 1592
Water vapor diffusion resistance factor [-]	8.8 – 22.1	4.11 – 5.12	5.52 – 7.52
Apparent moisture diffusivity [m^2·s^{-1}]	1.08×10^{-6}	5.53×10^{-6}	3.27×10^{-8}
Hygroscopic moisture content [m^3·m^{-3}]	0.0036	0.0259	0.0144

COMPUTATIONAL MODELING

A diffusion-type mathematical model for description of coupled heat and moisture transport in porous building materials was used in the verification procedure [12]. The balance equations of heat (1) and moisture (2) can be written as

$$\frac{dH}{dT}\frac{\partial T}{\partial t} = div\left(\lambda \,\mathrm{grad}\, T\right) + L_v div\left[\delta_p \,\mathrm{grad}\, p_v\right] \tag{1}$$

$$\left[\rho_w \frac{dw}{dp_v} + \left(n - w\right)\frac{M}{RT}\right]\frac{\partial p_v}{\partial t} = div\left[\left(B \cdot D_w \rho_w \frac{dw}{dp_v} + A \cdot \delta_p\right)\mathrm{grad}\, p_v\right] \tag{2}$$

where following symbols stand for: H [J·m^{-3}] enthalpy density, T [K] absolute temperature, λ [W·m^{-1}·K^{-1}] thermal conductivity, L_v [J·kg^{-1}] latent heat of evaporation of water, δ_p [s] water vapor diffusion permeability, p_v [Pa] partial pressure of water vapor in porous space, ρ_w [kg·m^{-3}] density of water, w [m^3·m^{-3}] moisture content by volume, n [-] porosity, M [kg·mol^{-1}] molar mass of water vapor and R [J·K^{-1}·mol^{-1}] the universal gas constant. The coefficients A and B in Eq. (2) denote the membership functions defining the transition between particular phases of water. All the calculation was prepared and run using the computer code Temp-Moist 2D [13].

RESULTS AND DISCUSSION

The verification of the model was done using temperature profiles before and after the application of the interior thermal insulation in the 15th day of the experiment which corresponded to December 15 of the reference year. The boundary conditions defined on the exterior and interior surface require also quantification of heat and moisture transfer coefficients. These values are strongly dependent on other parameters, such as temperature, air flow or surface roughness and absorbance, so their values cannot be estimated precisely in advance. They were therefore set as free parameters and their values were fitted to reach the highest agreement between computationally and experimentally obtained temperature profiles.

The results of the model verification are shown in Fig. 2. It can be clearly seen that a very good agreement between experimental and computational outputs was reached for both details solved. The root mean square error accounted for 0.325 °C for the insulated detail and only for 0.175 °C in case of the unprotected wall.

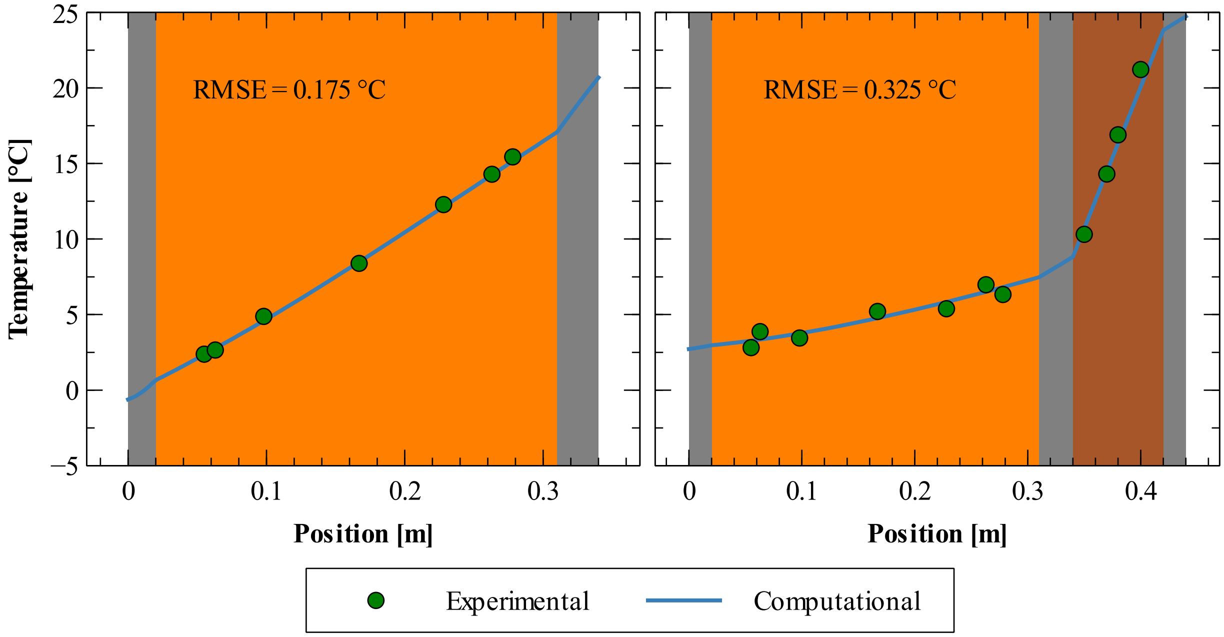

FIGURE 2. Results of model verification: unprotected wall (left), interior thermal insulation (right).

The computational outputs were obtained using heat and moisture transport coefficients summarized in Table 2, where the values found are compared to those prescribed in standards [14].

TABLE 2. Transfer coefficients.

		Standard value	**Identified value**
Exterior	Heat transfer coefficient [$W \cdot m^{-2} \cdot K^{-1}$]	25	32
	Moisture transfer coefficient [$s \cdot m^{-1}$]	not defined	7.765×10^{-7}
Interior	Heat transfer coefficient [$W \cdot m^{-2} \cdot K^{-1}$]	8	10
	Moisture transfer coefficient [$s \cdot m^{-1}$]	not defined	7.939×10^{-7}

One can see some differences, but the standard values presented in form of constant numbers cannot be assumed to be accurate as there are lots of affecting factors that cannot be covered by only one value for all cases. Since this problem is much more complicated, a separate research should be conducted in order to identify precise transfer coefficients, which is beyond the scope of this paper. Anyway, regarding the number of affecting factors, the found values differ only marginally, so the computational model could be considered as verified.

CONCLUSIONS

A computational model for description of coupled heat and moisture transport in building constructions with interior thermal insulation systems was verified in the paper. The verification was done by means of comparison of computational outputs (temperature profiles) with data measured in laboratory critical experiment where the whole construction segment was built. Since the root mean square error in case of insulated and noninsulated segment was very small, accounting for only 0.325 °C at maximum, it can be concluded that the model is able to provide precise results and can be used for the assessment of construction segments provided with interior thermal insulation systems.

ACKNOWLEDGEMENT

This research has been supported by the Ministry of Culture of the Czech Republic, under project No DG16P02H046.

REFERENCES

1. European Comission, *An EU strategy on Heating and Cooling* (Brussels, 2016).
2. U.S. Energy Information Administration, *Residential energy consumption survey (RECS)* (Washington, 2009).
3. J. I. Levy, M. K. Woo, R. D. Tebbens, Y. Nishioka, Int J Life Cycle Ass **23**, 1723-1734 (2018).
4. D. D. Tingley, A. Hathway, B. Davison, Build Environ **85**, 182-189 (2015).
5. J. Straube, C. Schumacher, A. Webb, Renew Sust Energ Rev **77**, 748-759 (2017).
6. M. Abuku, H. Jannsen, S. Roels, Energ Build **41**, 101-110 (2009).
7. D. I. Kolatis, E. Malliotakis, D. A. Kontogeorgos, I. Mandilaris, D. I. Katsourinis, M. A. Founti, Energ Build **64**, 123-131 (2013).
8. ČSN ISO 15927-4 *Hygrotermal performance of buildings - Calculation and presentation of climatic data - Part 4: Hourly data for assesing the annual energy use for heating and cooling* (Czech Office for Standards, Metrology and Testing, Prague, 2005).
9. ČSN 73 0540-2 *Thermal Protection of Buildings – Part 2: Requirements* (Czech Office for Standards, Metrology and Testing, Prague, 2011).
10. V. Kočí, M. Čáchová, D. Koňáková, E. Vejmelková, M. Jerman, M. Keppert, J. Maděra, R. Černý, Int J Thermophys **39**, 63 (2018).
11. V. Kočí, J. Maděra, M. Jerman, J. Žumár, D. Koňáková, M. Čáchová, E. Vejmelková, P. Reiterman, R. Černý, Clean Technol Envir **18**, 1725-1733 (2016).
12. J. Kočí, J. Maděra, M. Jerman, M. Doleželová, R. Černý, IOP Conf Ser-Mat Sci **364**, 012009 (2018).
13. J. Maděra, J. Kočí, V. Kočí, Temp-Moist 2D (software available at http://tpm.fsv.cvut.cz/naki2.php, 2017).
14. ČSN 73 0540-3 *Thermal Protection of Buildings – Part 3: Standard value quantities* (Czech Office for Standards, Metrology and Testing, Prague, 2005).

Hygric and Thermal Properties of Selected Materials Suitable for Interior Thermal Insulation Systems

Miloš Jerman[1, a)] and Robert Černý[1, b)]

[1] *Department of Materials Engineering and Chemistry, Faculty of Civil Engineering, Czech Technical University in Prague, Thákurova 7, 166 29 Prague, Czech Republic*

[a)]Corresponding author: milos.jerman@fsv.cvut.cz
[b)]cernyr@fsv.cvut.cz

Abstract. The properties of three thermal insulation wood fiber boards suitable for the application on the interior side of historical building envelopes are studied in the paper. Water absorption coefficient, apparent moisture diffusivity, thermal conductivity, and specific heat capacity of all materials, as fundamental hygric and thermal parameters, are measured in a dependence on moisture content. The measured data will be used as input parameters in computer simulation studies which will provide moisture and temperature fields necessary for an appropriate design of interior thermal insulation systems.

INTRODUCTION

In the building sector there is a considerable potential for saving energy, the main challenge is to find ways to reduce energy for heating of the existing buildings. The most effective way to reduce energy consumption of building construction is to insulate building envelope. The outer appearance is the best technical solution but for heritage buildings it is unacceptable and interior insulation is the only acceptable solution. However, interior thermal insulation systems have some weaknesses, the main problem is increased moisture level and condensation risk on the cold side of construction, often between the construction and thermal insulation. Condensed water promotes mould growth in buildings, it can also have negative effects on health, comfort, and durability of construction. Therefore, before the application of this kind of systems, every case should be always carefully analyzed in order to find the most suitable solution. There are two main possibilities how to build an interior insulation system, either it can be tight or it can be based on a capillary active material. For both systems, it is important to limit the risk of damage, so it is very useful to reduce the amount of moisture entering the wall from the outdoor environment through exterior render. Capillary active insulation may not be feasible without an additional protection of the façade against driving rain, since there is a high risk of moisture accumulation behind the insulation [1,2].

In capillary active system such materials are utilized which are able to absorb condensed water and transport it back to the interior. The most important material parameter for capillary active materials is high water absorption coefficient. Representatives of these materials are, e.g., calcium silicate [3] or hydrophilic mineral wool [4]. For interior thermal insulation also organic materials like flax, hemp, sheep wool can be utilized. Organic materials are generally water vapor permeable and can accumulate moisture by adsorption from the air.

This paper is focused on capillary active wood fiber boards which may be utilized for interior thermal insulation systems. Generally wood board is a renewable environmentally friendly material with very low embodied energy compared to mineral wool or calcium silicate which are commonly utilized in the insulation systems. The properties

of wood fibers can be modified by admixtures, e.g., hydrophobic or hydrophilic. Wood fiber boards studied in this paper are designed especially for interior insulation and improved by hydrophilic admixture. The interior thermal insulation system should be carefully evaluated by computer simulation. However, the quality of simulation results highly depend on input parameters. As input parameters serve materials characteristics of all components of the system. Therefore, the knowledge of hygrothermal properties is crucial for reliability assessment of the system. In this paper, the key hygric and thermal properties like water absorption coefficient, moisture diffusivity, thermal conductivity, and specific heat capacity of three different wood fiber boards are measured in a dependence on moisture content.

EXPERIMENTAL METHODS

Bulk density ρ_V [kg·m^{-3}], matrix density ρ [kg·m^{-3}] and open porosity ψ [-] were determined by water saturation method [5]. The water absorption coefficient A [kg·m^{-2}·s$^{-1/2}$] and apparent moisture diffusivity κ [m^2·s^{-1}] were measured using a water sorptivity experiment [6]. The specimens were water and vapor-proof insulated on four lateral sides and the face side was immersed 1–2 mm into water. The automatic balance allowed recording the increase of mass. The measurement was done on the samples with square cross sectional area with dimension of 100 × 100 mm. The water absorption coefficient A was then calculated using the formula:

$$i = A \cdot t^{1/2} \tag{1}$$

where i is the cumulative water absorption [kg·m^{-2}], t is the time from the beginning of the suction experiment [s]. The water absorption coefficient was then employed for the calculation of the apparent moisture diffusivity in the form [6]

$$\kappa = \frac{A^2}{w_c^2} \tag{2}$$

where w_c is the saturated moisture content [kg· m^{-3}].

Thermal conductivity λ [W·m^{-1}·K^{-1}] and specific heat capacity c [J·kg^{-1}·K^{-1}] were measured using the commercial device Isomet 2104 (Applied Precision, Ltd.). The measurement is based on analysis of the temperature response of the analysed material to heat flow impulses. The heat flow is induced by electrical heating using a resistor heater having a direct thermal contact with the surface of the sample. The measurement of soft wood fiber board was done by needle probe on the samples with the dimensions of 70 × 70 × 300 mm. Pavatex and hard wood fiber wool were measured by surface probe.

EXPERIMENTAL RESULTS

Basic physical properties are summarized in Table 1. The lowest bulk density ρ_V exhibited wood fiber CIUR Soft, the highest CIUR Hard. All materials had a high open porosity.

TABLE 1. Basic physical properties

Material	ρ_V kg·m^{-3}	ψ %	ρ kg·m^{-3}
Pavatex	147	90.1	1474
CIUR Hard	178	87.95	1480
CIUR Soft	53.7	96.37	1480

The average cumulative curves of moisture content as functions of square root of time are shown in Fig. 1. The calculated water absorption coefficient and apparent moisture diffusivity are shown in Table 2.

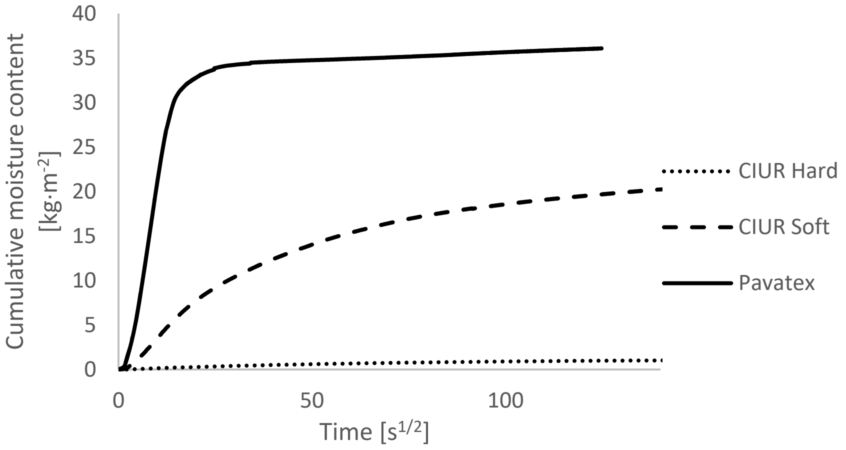

FIGURE 1. Cumulative moisture content as a function of square root of time

The highest water absorption coefficient achieved the board Pavatex. This material exhibited also the highest apparent moisture diffusivity, as it can be seen in Table 2. The lowest absorption coefficient achieved wood fiber Ciur Hard.

TABLE 2. Water absorption properties

Material	A $kg\cdot m^{-2}\cdot s^{-1}$	κ $m^2\cdot s^{-1}$
Pavatex	2.12	5.53 E-6
CIUR Hard	0.0103	1.37 E -10
CIUR Soft	0.41	1.87 E-7

Values of thermal conductivity and specific heat capacity in dry state are summarized in Table 3.

TABLE 3. Thermal properties in dry state

Material	λ $W\cdot m^{-1}\cdot K^{-1}$	c $J\cdot kg^{-1}\cdot K^{-1}$
Pavatex	0.062	2088
CIUR Hard	0.067	1966
CIUR Soft	0.047	2130

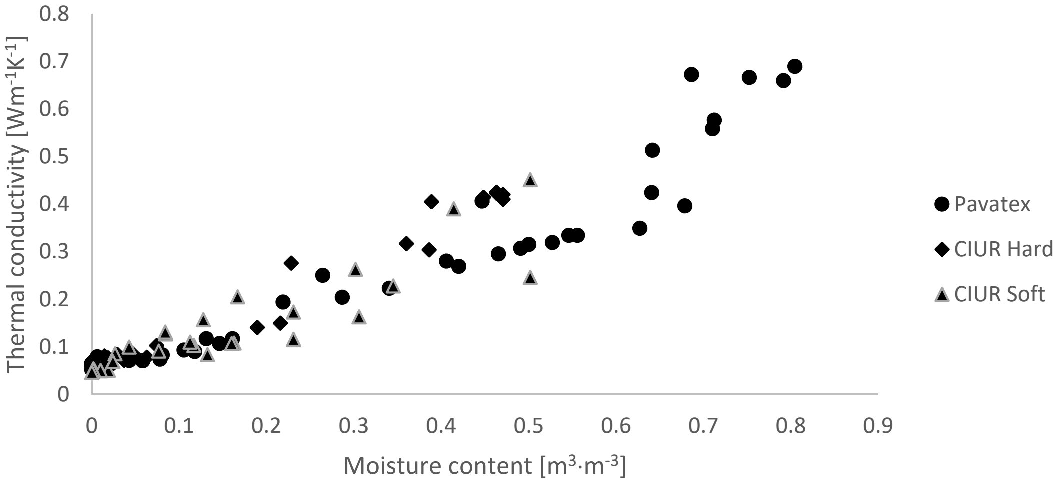

FIGURE 2. Thermal conductivity in dependence on moisture content

The lowest thermal conductivity in dry state achieved wood fiber board CIUR Soft which was in a good agreement with bulk density. Thermal conductivity of material CIUR Hard was about 30% higher than CIUR Soft. Specific heat capacity of all materials was higher in a comparison with other thermal insulation materials like polystyrene or mineral wool.

Results of the measurement of thermal properties in dependence on moisture content are shown in Figs. 2, 3. Due to hydrophobic admixture inside CIUR Hard is the maximal moisture content only 0.28 [$m^3 \cdot m^{-3}$]. The values of thermal conductivity increased rapidly with increasing moisture content. They were slightly higher than for conventional thermal insulators but still able to improve thermal properties of building envelopes. The specific heat capacity as a function of moisture content was calculated according to the theoretical procedure described in [7] and increased fast with increasing moisture content.

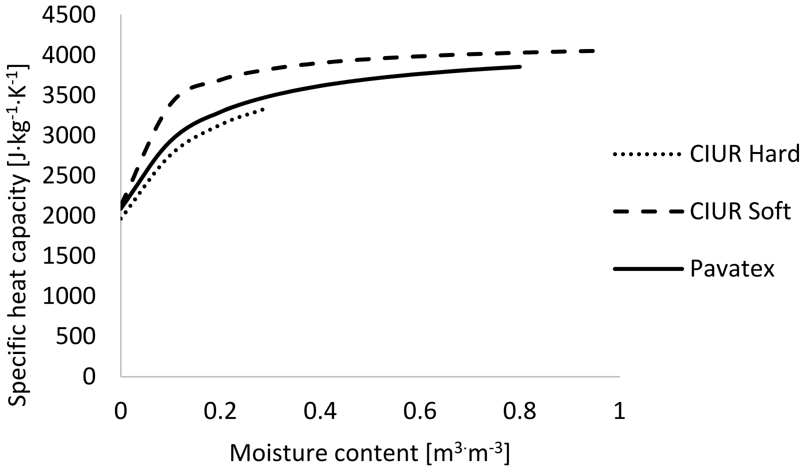

FIGURE 3. Specific heat capacity in dependence on moisture content

CONCLUSIONS

Three different wood fiber board materials were studied. The measured basic physical properties, hygric and thermal properties of studied materials can be used as input parameters of computational models of heat and moisture transport. The lowest bulk density showed the board CIUR Soft which also exhibited the best thermal conductivity. However, the most promising results for the interior thermal insulation systems achieved the board Pavatex which was capable of very fast transport of liquid water.

ACKNOWLEDGMENT

This research has been supported by the Ministry of Culture of the Czech Republic, under project No DG16P02H046.

REFERENCES

[1] G. R. Finken, S.P. Bjarløv, R. H. Peuhkuri, Construction and Building Materials **113**, 202–214 (2016).
[2] E. Vereecken, S. Roels, Materials and Structures **48**, 3009–3021 (2015).
[3] P. Klošeiko, E. Arumägi, T. Kalamees, Journal of Building Physics **38**, 444–464 (2015).
[4] Z. Pavlík, R. Černý, Applied Thermal Engineering **29**, 1941-1946 (2009).
[5] S. Roels, J. Carmeliet, H. Hens, O. Adan, H. Brocken, R. Černý, Z. Pavlík, C. Hall, K. Kumaran, L. Pel, R. Plagge, Journal of Thermal Envelope and Building Science, **27**, 307-325 (2004)
[6] M. K. Kumaran, Journal of Thermal Envelope and Building Science, **22**, 349-355 (1999)
[7] M. Jerman, M. Keppert., J. Výborný, R. Černý, Cement Wapno Beton, **16/78,** 18-29 (2011)

Computer-Aided Assessment of Critical Details of Interior Thermal Insulation Systems for Historical Masonry

Václav Kočí[1, a)], Jiří Maděra[1, b)] and Robert Černý[1, c)]

[1]*Department of Materials Engineering and Chemistry, Faculty of Civil Engineering, Czech Technical University in Prague, Thákurova 7/2077, 166 29 Prague 6, Czech Republic*

[a)]Corresponding author: vaclav.koci@fsv.cvut.cz
[b)]madera@fsv.cvut.cz
[c)]cernyr@fsv.cvut.cz

Abstract. Interior thermal insulation systems represent in some cases the only admissible form of wall retrofitting. Having different impact on masonry than commonly used exterior systems, application of interior insulation requires a special treatment that consists in an assessment of hygrothermal performance within a pre-design stage. In this paper, computational modelling is used to make the assessment of wall segment with wooden beam laid in it. The assessment is done for unprotected as well as retrofitted wall and the results are compared. It was revealed that presence of interior thermal insulation system may result in deterioration of hygrothermal performance of the wall as the relative humidity content in a reference year is higher by up to 2.5 % after retrofitting. Such a change may speed up degradation processes due to colonization of the beam, e.g. by fungi. Additional measures should therefore accompany this kind of wall retrofitting, which would improve the hygric performance and prevent creation of suitable conditions for the wall segment degradation.

INTRODUCTION

Even if interior thermal insulation systems are not as frequently applied as the exterior ones, some cases permit only this solution when a building envelope is retrofitted [1]. When interior systems are designed, one must deal with specific issues related to this type of thermal insulation. Being placed on the interior side, the insulation leaves the load bearing masonry unprotected against weather conditions which may result in several damage patterns such as excessive hygric straining, frost damage, salt efflorescence, mold growth or presence of thermal bridges [2-3].

Based on that, an interior thermal insulation design requires a special treatment incorporating advanced techniques for assessment of hygrothermal performance. Computational modelling is one of optimal tools that can carry out the assessment already in a pre-design stage, i.e. without the construction being built. Beside relatively fast and cost efficient results, this method provides also a valuable feedback which can help to adjust construction details properly and thus overcome possible shortages in a hygrothermal function.

Wooden beam ends laid in the masonry represent a typical critical detail that may suffer from the disadvantages of interior thermal insulation systems. Increased moisture content that can occur in masonry during its life time can significantly contribute to wood decay [4-5]. In this paper, the computational modelling of coupled heat and moisture transport is therefore used to reveal possible risks of such a critical detail.

COMPUTATIONAL MODELLING

Hygrothermal performance of wooden beam laid in brick masonry was investigated. The details were analyzed without thermal insulation as well as retrofitted using interior insulation system (see Fig. 1). The properties of materials involved are summarized in Table 1 [6-7].

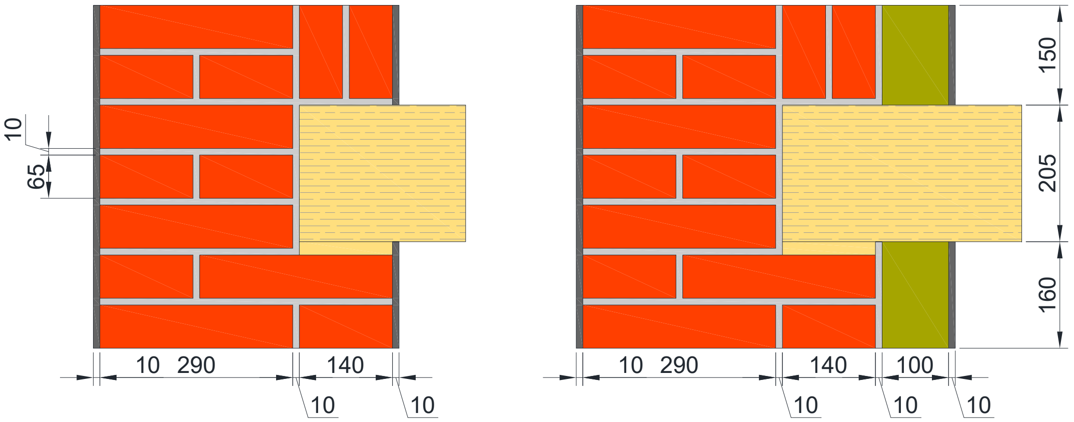

FIGURE 1. Analyzed critical details

TABLE 1. Material properties.

	Solid brick	Wood fiber board	Mortar/Plaster	Wood
Bulk density [kg·m^{-3}]	1831	147	1244	417
Porosity [%]	27.9	90.1	49.8	35.5
Thermal conductivity [W·m^{-1}·K^{-1}]	0.59 – 1.74	0.07 – 0.69	0.30 – 0.94	0.13 – 0.29
Specific heat capacity [J·kg^{-1}·K^{-1}]	825 – 1254	2088 – 3855	1054 – 1592	1501 – 2733
Water vapor diffusion resistance factor [-]	8.8 – 22.1	4.11 – 5.12	5.52 – 7.52	31.99 – 134.85
Apparent moisture diffusivity [m^2·s^{-1}]	1.08×10^{-6}	5.53×10^{-6}	3.27×10^{-8}	1.04×10^{-9}
Hygroscopic moisture content [m^3·m^{-3}]	0.0036	0.0259	0.0144	0.0342

The material properties were applied as one of input parameters in a mathematical model for description of coupled heat and moisture transport. A diffusion type of the model was selected which put emphasis on precise distinguishing between particular water phases. The model was verified within a previous research [8].

In order to achieve accurate results, dynamic climatic conditions in form of reference year (TRY) were applied on the exterior side of the detail. The reference weather data set is constructed based on long term observation of weather conditions accommodating hourly values of temperature, relative humidity, rainfalls, wind velocity, wind direction and direct and diffusion type of sun radiation [9]. Olomouc, Czech Republic was selected as the studied location. Due to history of this city, it is characterized with an increased historical building density which, when retrofitted, must be treated considerately, preserving an original appearance of facades. Standard boundary conditions were applied on the interior side (21 °C, 55 % of relative humidity) [10].

The simulated period took three years which is according to our experience long enough to achieve some kind of a dynamic equilibrium. The results presented further in this paper were related to the last year of the simulations.

RESULTS AND DISCUSSION

The main objective of the computations is to assess an influence of application of interior thermal insulation on hygrothermal performance of the analyzed segment of construction. The wood beam end is assumed to be the most critical point in the analyzed detail because wood, as an organic material, is the most prone to be damaged at even lower moisture content. Some fungi are able to colonize wood at 81 % of RH and cause decay at 90 % of RH [11]. In Figure 2, relative humidity of the beam end is compared when the wall is either retrofitted or thermally unprotected. It can be seen that the wall retrofitting by the application of the interior thermal insulation system resulted in deterioration of moisture conditions, as moisture content increased by up to 2.8 percentage points of RH. In winter months, the relative humidity can reach up to 75 % when the wall is retrofitted which is very close to the colonization threshold.

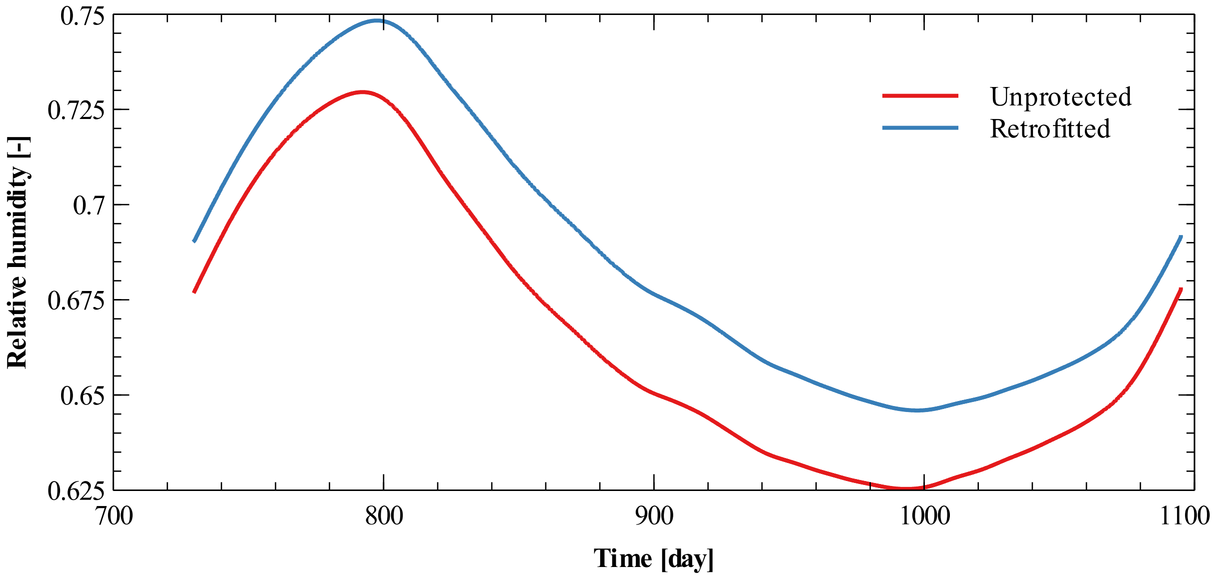

FIGURE 2. Relative humidity in the beam end, the second year of simulations

Such a behavior can be easily explained: thermal insulation on the exterior side substantially decrease the temperature in the masonry which makes it more vulnerable to moisture condensation. It also slows down the vapor transport through the wall from the exterior to the interior. The moisture is therefore accumulated in the masonry in a higher extent. Such phenomena are demonstrated in Figures 3 and 4 comparing the temperature and relative humidity distribution in a selected time.

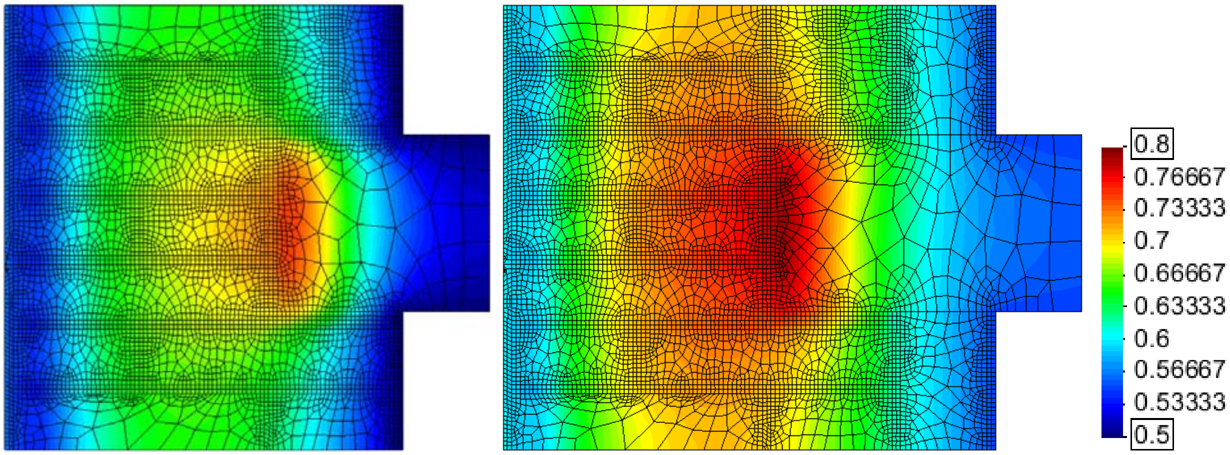

FIGURE 3. Distribution of relative humidity of unprotected (left) and retrofitted (right) wall, March 11 of the reference year

The results revealed, special treatment of the wall after retrofitting is necessary to achieve a proper hygrothermal function. It comprises e.g. an application of capillary active or hydrophilic insulation materials, water vapor barriers, exterior plasters with hydrophobic agents etc. Otherwise, the energy savings can be balanced by increased risks of deterioration of wall constituents such as bricks, mortar or wood.

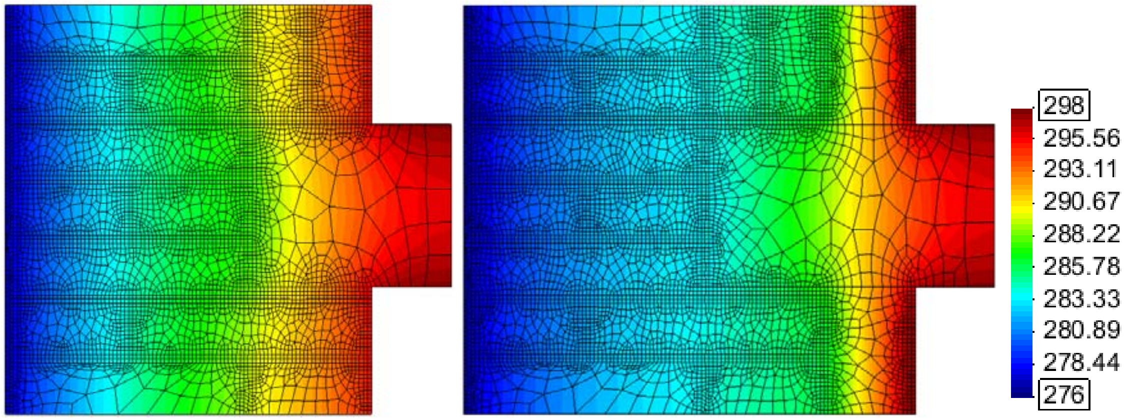

FIGURE 4. Distribution of temperature of unprotected (left) and retrofitted (right) walls, March 11 of the reference year

CONCLUSIONS

Hygrothermal performance of a wall detail comprising of masonry with mortar and a wooden beam end was analyzed within this paper. Using computational modelling, the performance was compared when unprotected and retrofitted using an interior thermal insulation system which is usually applied in case of traditional/historical buildings or, in general, buildings under preservationists' surveillance.

The results of computational modelling revealed that presence of the interior thermal insulation resulted in deterioration of hygrothermal performance of the masonry as is led to decrease of temperature and increase of moisture content. It means that after retrofitting in this manner, the walls require additional measures that must enhance their hygric performance in particular, in order to prevent possible degradation risks. Such research will be conducted within the future work.

ACKNOWLEDGEMENT

This research has been supported by the Ministry of Culture of the Czech Republic, under project No DG16P02H046.

REFERENCES

1. J. Straube, C. Schumacher, A. Webb, Renew Sust Energ Rev **77**, 748-759 (2017).
2. M. Abuku, H. Jannsen, S. Roels, Energ Build **41**, 101-110 (2009).
3. D. I. Kolatis, E. Malliotakis, D. A. Kontogeorgos, I. Mandilaris, D. I. Katsourinis, M. A. Founti, Energ Build **64**, 123-131 (2013).
4. E. Vereecken, S. Roels, Enrgy Proced **132**, 664-669 (2017).
5. J. Y. Wang, R. Stirling, P. I. Morris, A. Taylor, J. Lloyd, G. Kirker, S. Lebow, M. E. Mankowski, H. M. Barnes, J. J. Morrel, Wood Fiber Sci **50**, 110-127 (2018).
6. V. Kočí, M. Čáchová, D. Koňáková, E. Vejmelková, M. Jerman, M. Keppert, J. Maděra, R. Černý, Int J Thermophys **39**, 63 (2018).
7. V. Kočí, J. Maděra, M. Jerman, J. Žumár, D. Koňáková, M. Čáchová, E. Vejmelková, P. Reiterman, R. Černý, Clean Technol Envir **18**, 1725-1733 (2016).
8. V. Kočí, J. Maděra, Z. Pavlík, M. Jerman, R. Černý, Verification of Computational Model for the Assessment of Interior Thermal Insulation Systems Using a Laboratory Critical Experiment, AIP Conf Proc, **in press**
9. ČSN ISO 15927-4 *Hygrotermal performance of buildings - Calculation and presentation of climatic data - Part 4: Hourly data for assesing the annual energy use for heating and cooling* (Czech Office for Standards, Metrology and Testing, Prague, 2005).
10. ČSN 73 0540-2 *Thermal Protection of Buildings – Part 2: Requirements* (Czech Office for Standards, Metrology and Testing, Prague, 2011).
11. O. Schmidt, Mycol Prog **6**, 261-279 (2007).

Experimental and Theoretical Analysis of Acoustic Properties of Building Materials

Lukáš Fiala[1, a)], Petr Konrád[2, b)], and Robert Černý[1, c)]

[1]*Department of Materials Engineering and Chemistry, Faculty of Civil Engineering, Czech Technical University in Prague, Thákurova 7, 166 29 Prague 6, Czech Republic*

[2]*Experimental Centre, Faculty of Civil Engineering, Czech Technical University in Prague, Thákurova 7, 166 29 Prague 6, Czech Republic*

[a)]Corresponding author: fialal@fsv.cvut.cz
[b)]petr.konrad@fsv.cvut.cz
[c)]cernyr@fsv.cvut.cz

Abstract. It is undisputable that constantly increasing acoustic deterioration of environment is affecting more and more people. It is especially noticeable in urban areas, near to the places with heavy traffic, or in areas close to the airports. Since high level of ambient noise negatively influences well-being and health of people, it should be decreased in building constructions by selection of building materials with good acoustic performance. The very first step of building structures acoustic performance evaluation lies in experimental determination of materials parameters necessary for acoustic modeling, e.g. displacement, sound velocity, amplitude of input and propagated wave. In this paper, a measurement based on acoustic excitation of fired brick sample by one period of 1000 Hz and 4000 Hz sine wave and subsequent analysis of data measured by two accelerometers is introduced. The first accelerometer is used for detection of the sine wave entering the sample, whereas the second one for detection of the attenuated wave that was propagated through the sample. Sound velocity in fired brick is calculated from time shift between the first voltage peaks detected by accelerometers and amplitudes (1st voltage peaks) are compared in terms of their decrease.

INTRODUCTION

Acoustic properties of building materials are currently getting on higher importance. It is due to an increasing noise deterioration of environment that negatively affects health and well-being of people exposed to a high level of acoustic pressure [1, 2]. Therefore, materials with good acoustic performance should be utilized in constructions to prevent such adverse effects. The first step in the selection of suitable materials lies in identification of their acoustic or acoustically dependent properties. For that purpose, several methods are widely used, e.g. measurements in reverberation rooms [3, 4], reverberation chambers [5], or Kundt's tube [6, 7]. Only after proper determination of acoustic parameters of a particular building material or building element it is possible to optimize it in terms of its acoustic properties, e.g. by utilization of bulk materials used in a role of filler [8].

In this paper, an experiment based on excitation of the sample by a period of the sine wave was designed and two examples of measurement at different frequencies were analyzed in terms of voltage amplitude and time shift between the signals detected by accelerometers.

MATERIALS AND METHODS

The measurements were conducted on fired brick sample of dimensions (209.5 × 98.5 × 48.4) mm^3 and mass 1979 g. The sample was excited by one period of a sine wave at frequency 1000 Hz and 4000 Hz, respectively, generated by GW Instek AFG-3051 function generator. Two accelerometers were mounted into central position of the sample opposite lateral sides to detect mechanical excitation. Measured data were collected by datalogger PCB Piezotronics 482C and analyzed by GW Instek GDS-2104A oscilloscope and DIADEM software installed on a supporting computer. To ensure good contact of an excitation speaker with surface of the sample, steel adaptor connecting the sample with the speaker was glued to those two parts by two-component superglue X60. The sample was suspended on steel supports that were covered by acoustically insulating polyurethane boards in order to reduce noise and vibrations from the environment. Diagram of the measuring apparatus is presented in Fig. 1. The fired

brick sample ready for acoustic measurements and involved measuring devices are presented in Fig. 2 and Fig. 3, respectively.

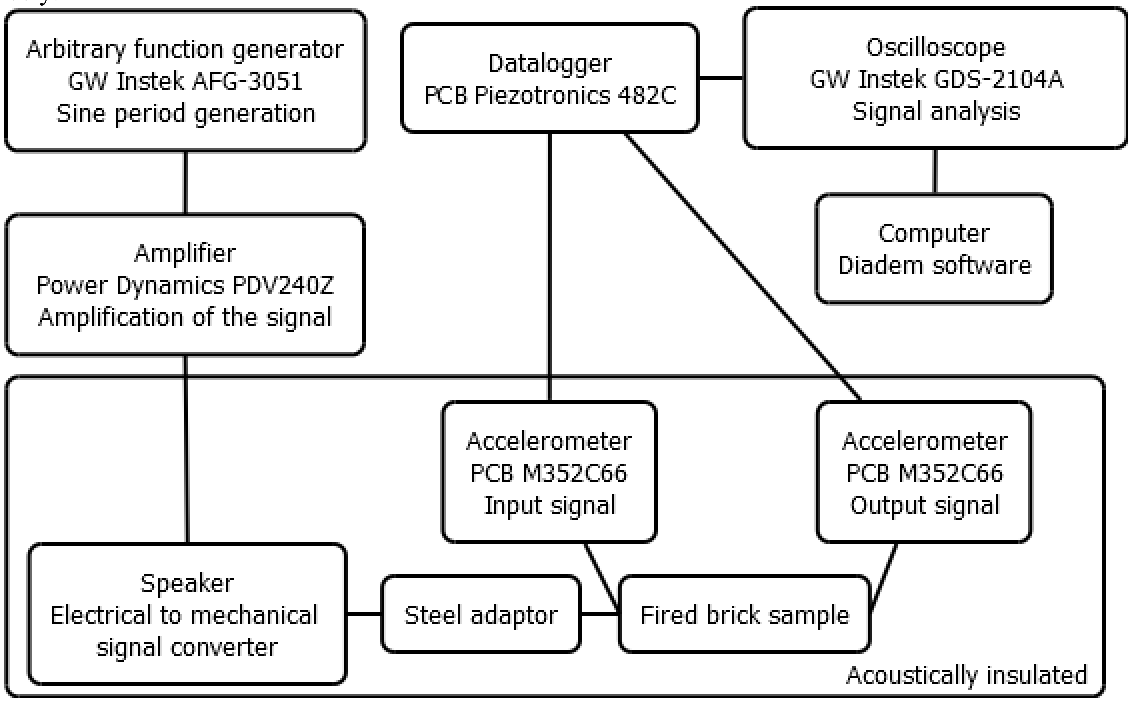

FIGURE 1. Diagram of the measuring apparatus

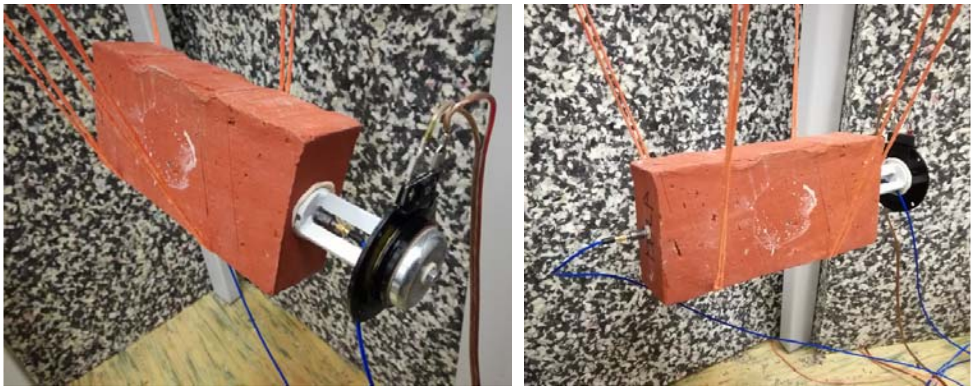

FIGURE 2. Fired brick sample prepared for the acoustic measurement

FIGURE 3. Measuring devices used in experimental part

RESULTS AND DISCUSSION

In the experiment, the fired brick sample was subjected to excitation of one period of a sine wave at frequency 1000 Hz and 4000 Hz, respectively. In Fig. 4 and Fig. 5, voltage dependence on time measured by accelerometers is presented. The time shift between the first amplitude peaks is proportional to the sound velocity in the material. Propagation of one period of the sine signal through the distance between accelerometers (length of the sample - 0.2095 m) lasted 1.01×10^{-4} s (1000 Hz) and 9.94×10^{-5} s (4000 Hz), so the sound velocity was therefore equal to 2074 $m \cdot s^{-1}$ and 2108 $m \cdot s^{-1}$, respectively. Results were compared to those obtained by measurements of elastic properties of illitic brick clay heated to sinter at different temperatures [9]. The calculated sound velocity was approximately of 1750 $m \cdot s^{-1}$, 2050 $m \cdot s^{-1}$ and 2300 $m \cdot s^{-1}$ with respect to the measured dynamic modulus of elasticity of the samples treated by 900 °C, 1000 °C and 1100 °C. Taking into account temperature used for production of fired bricks that is typically around 1000 °C, the presented results were in good agreement.

In case of 1000 Hz excitation, input and output amplitude (1^{st} peak) was of 3.58×10^{-2} V and 1.78×10^{-2} V, whereas for 4000 Hz sine wave, input and output amplitude (1^{st} peak) was of 1.36×10^{-1} V and 6.33×10^{-2} V, respectively. The 1^{st} amplitude peak measured on output accelerometer was about 50 % lower than the 1^{st} amplitude peak measured on input accelerometer for both frequencies.

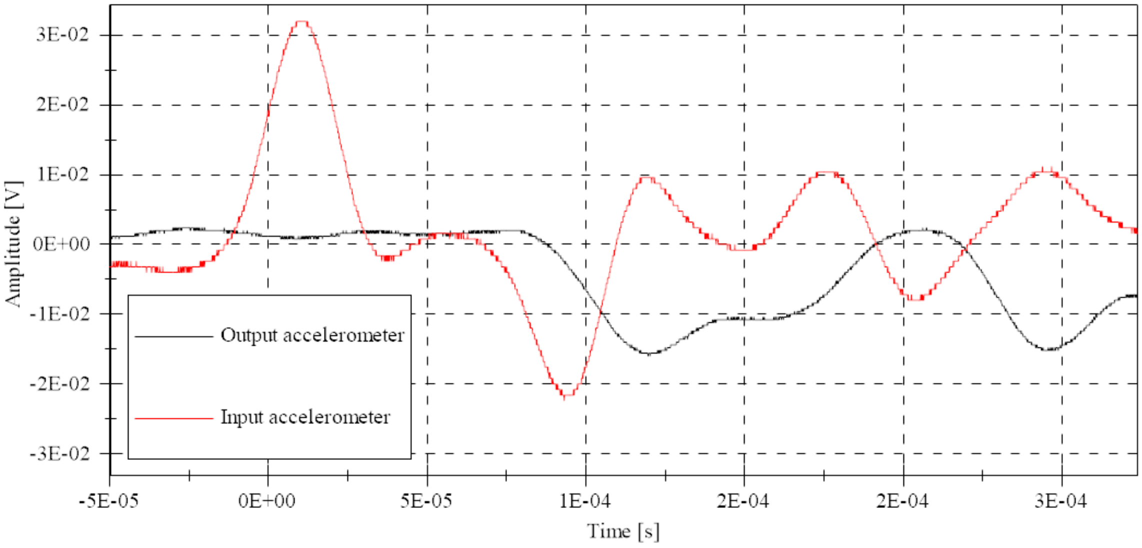

FIGURE 4. Voltage response (1 period of sine wave, 1000 Hz) on accelerometers – fired brick sample

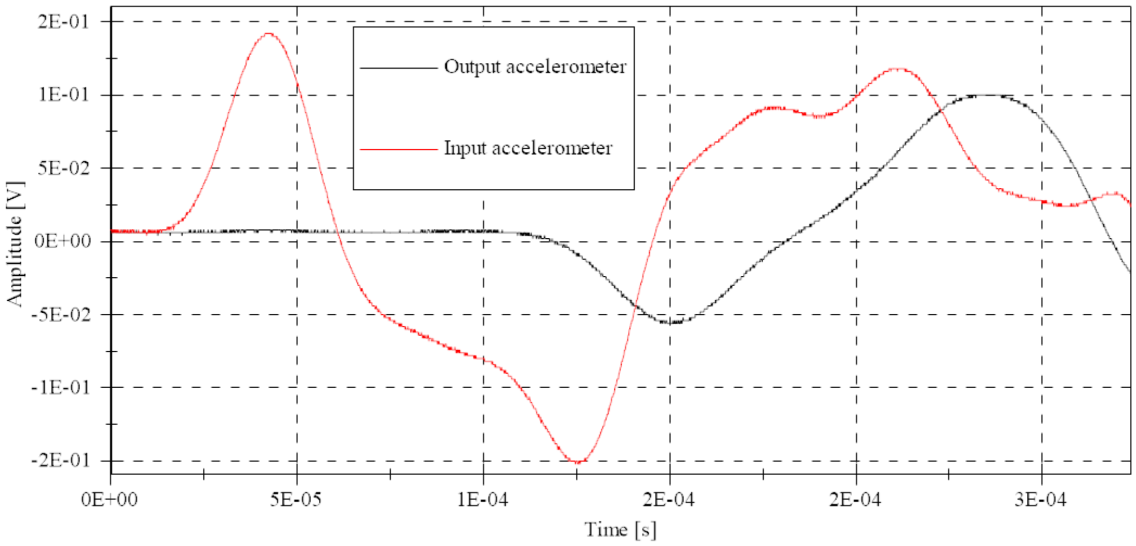

FIGURE 5. Voltage response (1 period of sine wave, 4000 Hz) on accelerometers – fired brick sample

CONCLUSIONS

In this paper, acoustic behavior of fired brick sample was studied. The sample was excited by an amplified signal (one period of 1000 Hz and 4000Hz sine wave) generated by a function generator, and two accelerometers placed into the defined positions on the sample were used for monitoring.

The sound velocity in the fired brick calculated from the wave propagation time between the known distance was: 1000 Hz - 2074.26 $m \cdot s^{-1}$ and 4000 Hz - 2107.65 $m \cdot s^{-1}$. With respect to the typically applied temperatures used for sintering of clays in fired brick production, one can conclude that the measured data were in good agreement with the data presented in literature.

For both frequencies, the 1^{st} peak voltage amplitude of the output signal was about 50%, compared to the input one.

Future work will be focused on acoustic measurements conducted on various building materials and small-scale building constructions. Furthermore, an important task lies in detailed analysis of the data measured by accelerometers and identification of wave reflections occurring due to the attached steel adaptor that lead to superposition of involved waves.

ACKNOWLEDGMENTS

This research has been supported by the Ministry of Industry and Trade of the Czech Republic under Project No. FV10036.

REFERENCES

1. M. Oh et al., "Influence of noise exposure on cardiocerebrovascular disease in Korea" in *Science of the Total Environment*, 2019, Vol. 651, pp. 1867-1876.
2. K. M. Paiva et al., "Exposure to road traffic noise: Annoyance, perception and associated factors among Brazil's adult population" in *Science of the Total Environment*, 2019, Vol. 650, pp. 978-986.
3. E. Fraile-Garcia et al., "Acoustic Behavior of Hollow Blocks and Bricks Made of Concrete Doped with Waste-Tire Rubber" in *Materials*, 2016, Vol. 9, No. 12, 962.
4. A. Y. Zverev and V. V. Chernyh, "Experimental Determination of Acoustic and Vibroacoustic Characteristics of Multilayer Composite Panels" in *Acoustical Physics*, 2018, Vol. 64, pp. 750-759.
5. K. Baruch et al., "The effect of changes in atmospheric conditions on the measured sound absorption coefficients of materials for scale model tests" in *Applied Acoustics*, 2018, Vol. 141 pp. 250-260.
6. D. Caballol and A. P. Raposo, "Analysis of the measurement of transmission loss in rigid building materials with a standing wave tube" in *Construction and Building Materials*, 2018, Vol. 182, pp. 242-248.
7. A. Danihelova et al., "Acoustic Properties of Selected Thermal Insulation Materials and their Contribution to Pollution of Environment" in *Akustika*, 2018, Vol. 30, pp. 35-41.
8. L. Fiala et al., "Methodology of Sealing Plugs Development for Brick Block with Enhanced Acoustic Properties" In *AIP Conference Proceedings 1988, 23rd International Meeting of Thermophysics*, Smolenice, 2018, 020014.
9. M. Jankula et al., "The influence of heat on elastic properties of illitic clay Radobica" in *Journal of the Ceramic Society of Japan*, 2015, Vol. 123, pp. 874-879.

Bending Characteristics of Fiber-reinforced Composite with Plywood Balsa Core

Martin Böhm[1, a)], Viktor Brejcha[2], Miloš Jerman[1], Robert Černý[1]

[1]*Department of Materials Engineering and Chemistry, Faculty of Civil Engineering, Czech Technical University in Prague, Thakurova 7, 166 29 Prague, Czech Republic*
[2]*Department of Wood Product and Wood Constructions, Faculty of Forestry and Wood Science, Czech University of Life Sciences, Kamycka 129, 165 00 Prague, Czech Republic*

[a)]Corresponding author: martin.bohm@fsv.cvut.cz

Abstract. The purpose of the research was to evaluate the bending characteristics of sandwich composite material based on balsa plywood reinforced with flax and glass fibers with epoxy resin. For manufactured composites with a thickness of 12 mm, the basic physical properties were determined and a mechanical three-point bending test according to EN 310 was carried out. Reinforcement of the balsa plywood with both types of fibers significantly increased the modulus of elasticity and bending strength. However, there are significant differences between both types of fibers. Whilst for flax fibers the flexural modulus was 7.5% higher than for glass fibers, the bending strength values of glass fibers were 26.5% lower compared to flax fibers. The experiment confirmed that in the production of composites, flax fibers with less of an environmental impact may be a material that is used as an adequate replacement of glass fibers.

INTRODUCTION

The selection of a composite material for the design of a specific product or construction is particularly influenced by its mechanical and physical properties, as well as by its cost and environmental impact.

In order to improve the properties of fiber composites, either organic or inorganic fibers are used. Examples of products that have very good mechanical properties include widely used carbon or aramid fibers. Although glass fibers do not achieve high strength, they are more affordable and cheaper and are therefore also widely used [1, 2]. However, problematic recycling of composite materials from these types of fibers is one of the main causes of efforts to develop new types of reinforcement from natural fibers.

Unlike glass fibers, natural fibers indicate the low energy coefficient values needed to produce one kilogram of raw fiber for production - MJ/kg, and their cost is also more favorable. For example, the current price of raw processed glass fibers with a density of 2.6 $g \cdot cm^{-3}$ is approximately 2-4× greater than that of flax fibers with a density of 1.5 $g \cdot cm^{-3}$[3]. On the contrary, the disadvantage of natural fibers is high moisture absorption, lower heat resistance and high variability of their properties [4]. The properties of fiber composites are also influenced by the type of used matrix and the surface finish of the fibers, which affects their surface wettability [5, 6].

Various foams, honeycombs or balsa are used for the central layer of sandwich composite materials. The purpose of the center layer is to provide greater material thickness, reduce density, ensure sufficient stiffness, ideally all whilst reducing costs. Although Balsa has a relatively high density for this type of application, it also has very low processing energy demands [7]. Therefore, in terms of the ecological aspect, its use for the central layer may be advantageous.

For the purposes of research, a sandwich construction with a balsa core of reinforced fiber on both sides with epoxy matrix was designed. Fiber reinforcement is symmetric on both sides to avoid differences in the properties

between both sides of the material, as is the case with some particle composites, particleboards or oriented strand boards [8].

The use of composite material is assumed, for example, on partitions or ribs inside the hull of a ship, for the construction of the partition walls of a caravan or rail vehicles, for visual parts of interiors, etc., all while maintaining the appearance of natural material embedded in clear resin.

EXPERIMENTAL METHODS

Three groups of test samples, i.e. a total of 45 pieces with dimensions of 50 × 290 × 12 mm were manufactured for the bending test. Untreated balsa plywood (Balsa) was used as a reference sample group. In the second group of samples, the balsa plywood surface was reinforced on both sides with flax fiber with epoxy matrix (Flax), and in the third group, glass fibers with epoxy matrix (E-glass) were on the surface. The core of the composite material was made of three-layer balsa plywood. In the middle layer, the direction of the fibers was perpendicular to the longer side of the test sample. Phenol-formaldehyde adhesive Lignofen G/3/D (LERG SA, Pustkow, Poland) was used to bond individual plywood layers. The balsa plywood samples intended for reinforcement were sanded after bonding by 1 mm to ensure the same thickness after application of the fibers.

Flax fibers in the form of 2×2 twill 400 g/m^2 fabric was used to make the outer layers of the composite material, and glass fibers with their surface treated with oxidation were used in the form of roving fabric with a weight of 390 g/m^2. The matrix consisted of thermosetting epoxy resin SAP CLR (Entropy Resins EU, Spain). Lamination was carried out using press SCM GS 6 at a pressure of 300 kPa.

The samples for measuring density and moisture samples had dimensions of 50×50×12 mm, and 6 pieces were made for each group. The preparation of the test specimens and all laboratory measurements were carried out at 23 °C and 55% air humidity. The bending characteristic were evaluated on test machine TIRA test 2850 according to EN 310 (1995). The modulus of elasticity in bending and bending strength were determined by applying a load to the center of a specimen supported at two points (Fig. 1).

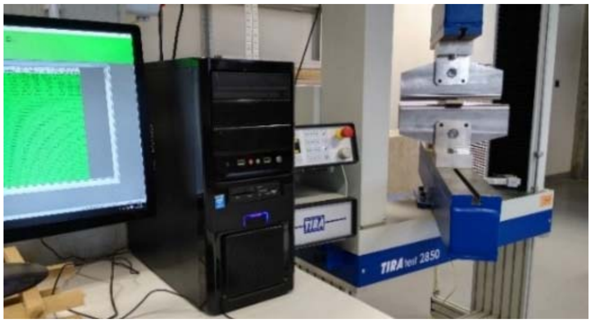

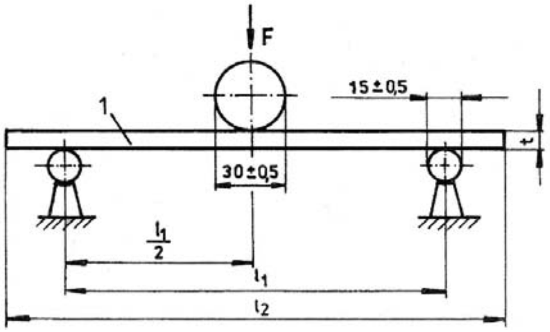

FIGURE 1. Arrangement of the bending apparatuses

The modulus of elasticity in bending (E_m) and bending strength (f_m) were calculated using the following equations:

$$E_m = \frac{(F_2 - F_1)l_1^3}{4bt^3(a_2 - a_1)} \qquad f_m = \frac{3F\max l_1}{2bt^2} \tag{1, 2}$$

where l_1 is the distance between the centers of the supports [mm], b is the width of the test piece [mm], t is the thickness of the test piece [mm], $F_2 - F_1$ is the increment of load on the straight line portion of the load-deflection curve [N]; F1 shall be approximately 10% and F2 shall be approximately 40% of the maximal load, $a2 - a1$ is the increment of deflection at the mid-length of the test piece [m], corresponding to load increment $F_2 - F_1$ and F_{max} is the maximum load [N].

An analysis of the surface of the flax and glass fibers was carried out using electron microscope MIRA 3 (Tescan-Orsay holding). The instrument was set to an acceleration voltage of 15,000 V, magnification of 1000x and a working distance of 22 mm. A secondary electron detector was used to display the surface of the samples. After

visual evaluation of the fiber surface images, an analysis of the resulting mechanical tests was carried out using Statistica 13 software (TIBCO Software Inc.) via the ANOVA method with a post-hoc Tukey HSD test.

EXPERIMENTAL RESULTS

Table 1 shows the basic physical properties of the produced composites, measured at a relative air humidity of 55% and temperature of 23 °C.

TABLE 1. Basic physical properties

Material	Density [kg·m^{-3}]	Coef. Var. [%]	Moisture content [%]	Coef. Var. [%]
Balsa	163	4.72	7.51	4.94
Flax	311	4.34	5.36	5.85
E-glass	262	2.85	5.61	3.19

In the table can be seen the higher moisture and density of the composites reinforced with flax fiber. The moisture absorption from the environment is one of the main disadvantages of natural fibers. The higher density of composites reinforced with flax fibers was due to their uneven surface (see Fig. 2) as well as the higher water absorption of fibers whose surfaces were untreated. For this reason, during the production of samples, the application of the epoxy resin had to be increased by 50% compared to the recommended technical procedure and compared to the sample group with glass fibers.

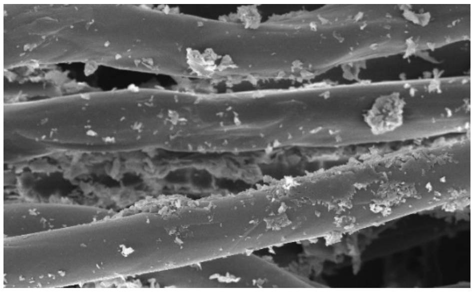

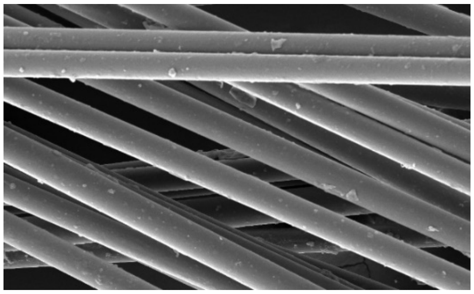

FIGURE 2. SEM images of flax fiber surfaces (left) and glass fiber (right) surfaces at the same magnification

The average cumulative load-deflection curves of different materials during the bending test are shown in Fig. 3.

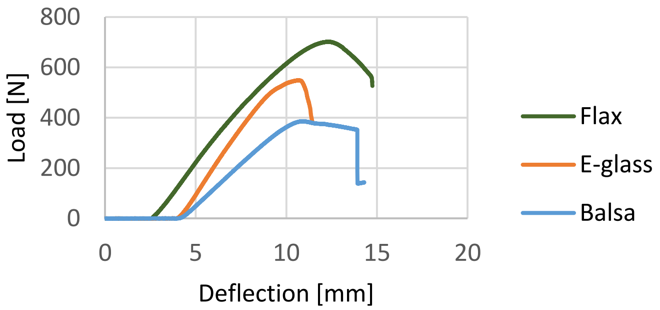

FIGURE 3. Cumulative load-deflection curves of individual materials

The slope of the load-deflection curve of the samples reinforced with glass fibers corresponds to a higher modulus of elasticity; adversely, the samples reinforced with flax fiber achieve greater strength. During the bending test, there was a pressure breach at the location below the loading head. Delamination caused by insufficient saturation of fibers by epoxy resin only occurred in two of the samples reinforced with flax fiber.

The values of the modulus of elasticity and bending strength are summarized in Table 2 and Table 3.

TABLE 2. Modulus of elasticity in bending

Material	Mean [MPa]	Min. [MPa]	Max. [MPa]	Std. Dev.	Coef. Var. [%]
Balsa	2200.2	1703.5	2691.8	276.3	12.6
Flax	3822.7	3651.5	4132.2	105.7	2.8
E-glass	4131.2	3171.1	4589.2	334.4	8.1

TABLE 3. Bending strength

Material	Mean [MPa]	Min. [MPa]	Max. [MPa]	Std. Dev.	Coef. Var. [%]
Balsa	15.8	11.9	19.4	2.3	14.6
Flax	33.9	29.4	39.5	3.5	10.3
E-glass	24.9	10.0	34.5	5.8	23.2

Reinforcement of balsa plywood with both types of fibers led to a significant increase in the modulus of elasticity in bending and bending strength values. Samples reinforced with glass fiber achieve the highest modulus of elasticity values. Their average value is 4131 MPa, which represents an increase in the modulus of elasticity of balsa plywood by almost 88%. Samples reinforced with flax fiber have the highest bending strength. Their average value is 33.9 MPa, which is more than double (115%) the strength increase of balsa plywood.

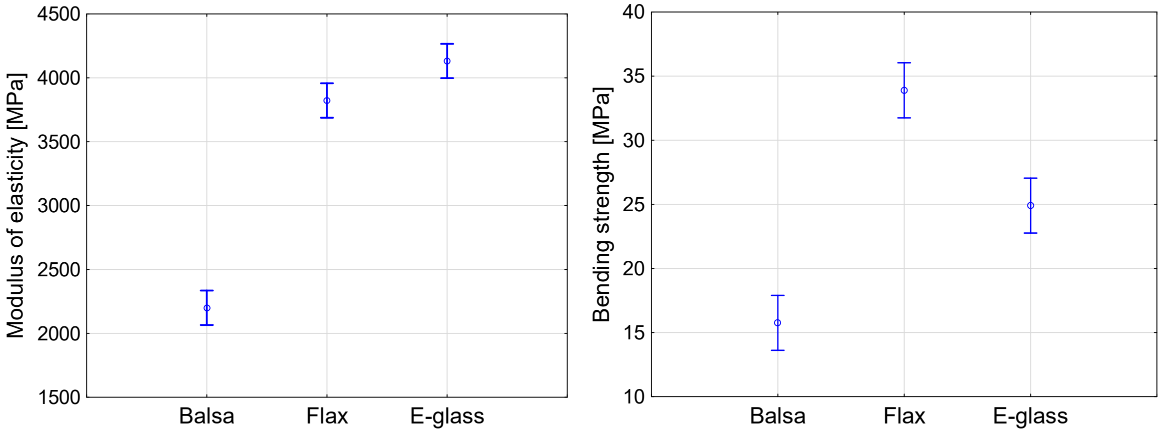

FIGURE 4. ANOVA results for modulus of elasticity and bending strength. Vertical bars denote 0.95 confidence intervals.

The outputs of analysis of variance are shown in Figure 4. The results of the multiple comparison test showed statistically significant differences between all of the sample groups ($p<0.01$). Significant differences between the two types of fibers were also confirmed. While the flexural modulus is 7.5% lower for flax fibers than for glass fibers, the bending strength values for glass fibers are 26.5% lower than flax fibers.

Compared to glass fibers, the bending strength for flax fibers was higher despite the fact that the flax surface had not been treated before the epoxy was applied; however, the flax fibers absorbed more resin, and therefore the epoxy application had to be increased.

CONCLUSIONS

It can be concluded from the performed experiment that in terms of mechanical properties, flax fibers may be an adequate substitute for commonly used glass fibers in the production of composite materials with a sandwich structure. In the future, due to their lower production costs and significantly lower CO_2 emissions, flax fibers can be expected to increase their share in composite materials structures at the expense of glass fibers.

ACKNOWLEDGMENT

This research was supported by the Czech Technical University in Prague, under project No. SGS19/143/OHK1/3T/11 – Analysis of interactions between composite building materials and the environment.

REFERENCES

[1] C. Stevens and J. Mussig, *Industrial applications of natural fibres: structure, properties and technical applications*. John Wiley & Sons, pp. 560 (2010).
[2] P. Šedivka, J. Bomba, M. Böhm, A. Zeidler. BioResources **10(3)**, 4674–4685 (2015).
[3] S. V. Joshi, L. T. Drzal, A. K. Mohanty, S. Arora, S. Composites Part A: Applied science and manufacturing **35(3)** 371–376 (2004).
[4] F. Ahmad, H. S. Choi, M. K. Park, Macromolecular materials and engineering, **300(1)** 10–24 (2015).
[5] A. Arbelaiz, B. Fernandez, G. Cantero, R. Llano-Ponte, A. Valea, I. Mondragon, Composites Part A: applied science and manufacturing **36(12)** 1637–1644 (2005).
[6] X. Li, L. G. Tabil, S. Panigrahi, Journal of Polymers and the Environment **15(1)** 25–33 (2007).
[7] D. B. Miracle, S. L. Donaldson, S. D. Henry, C. Moosbrugger, G. J. Anton, B. R. Sanders, W. W. Scott, Vol. 21: Composites, in *ASM Handbook*, ASM international, pp. 107–119 (2001).
[8] M. Böhm, P. Šedivka, J. Bomba, J. Reisner, Drvna industrija **62(2)** 123–127 (2011).

Analysis of In-Diffusion of ^{241}Am In Concrete by an Inverse Technique

Igor Medveď[1, 2, a)] and Robert Černý[1, b)]

[1]Department of Materials Engineering and Chemistry, Faculty of Civil Engineering, Czech Technical University in Prague, 16629 Prague, Czech Republic
[2]Department of Physics, Faculty of Civil Engineering, Slovak University of Technology, 81005 Bratislava, Slovakia

[a)]Corresponding author: igor.medved@fsv.cvut.cz
[b)]cernyr@fsv.cvut.cz

Abstract. Apparent diffusion coefficients of decaying radionuclides transported in saturated porous media can be evaluated by an inverse technique based on the Boltzmann-Matano method. Here this technique is applied to obtain concentration dependences of the apparent diffusion coefficient of ^{241}Am for which the corresponding concentration profiles were measured for two types of concrete. These general results are compared with those from the original study in which the diffusivity was constant. Three types of simple functions are used to approximate the experimental concentration profiles, and the corresponding dependences of the diffusion coefficient on concentration are given via quite simple formulas. Although being different at low and high concentrations, they all provide similar results within the intermediate range.

INTRODUCTION

Fick's laws of diffusion of species, including radionuclides, in saturated porous media may be formulated as [1]

$$\frac{\partial C}{\partial t} = D_a \, \Delta C \qquad \text{and} \qquad \mathbf{j} = -D_e \, \nabla C \,, \tag{1}$$

where C is the species concentration in the non-sorbed form, **j** is the diffusive flux, and D_a and D_e are called the apparent and effective diffusion coefficients, respectively. In this formulation D_a and D_e are constants and the adsorption isotherm of the species is linear, $C_s = \rho k C$, where ρ is the matrix density, k is a constant called the distribution coefficient, and C_s is the concentration in the adsorbed state. There is a simple relation between the two diffusion coefficients, $D_a = D_e/(\varepsilon + \rho k)$, where ε is the material porosity [1]. Thus, D_a includes the role of adsorption, contrary to D_e.

Perhaps the most frequent method to calculate D_a or D_e is by fitting data from 1D diffusion experiments with analytical or numerical solutions to Eq. (1) with appropriate initial and boundary conditions [2–5]. In many cases, however, D_a has a rather strong dependence on concentration [6–8]. Then a single value of D_a cannot interpret experimental profiles correctly and the approach in which the diffusion coefficients are constants is inadequate.

The Bolztmann-Matano method is one the inverse approaches from which varying diffusion coefficients can be determined [7, 9]. We modified it in [10] to include radioactive decay of species; i.e., for the case of radionuclides. The technique was applied to the concentration profiles of an S shape that could be approximated by the error function and for which we were able to obtain the resulting concentration dependence $D_a(C)$ as a formula. In this approach, there are no problems with reliability assessment (the back-calculation of the original profile), numerical errors when evaluating the profiles' derivatives (the profile is smooth), and final smoothing and removal of illogical jumps or spikes.

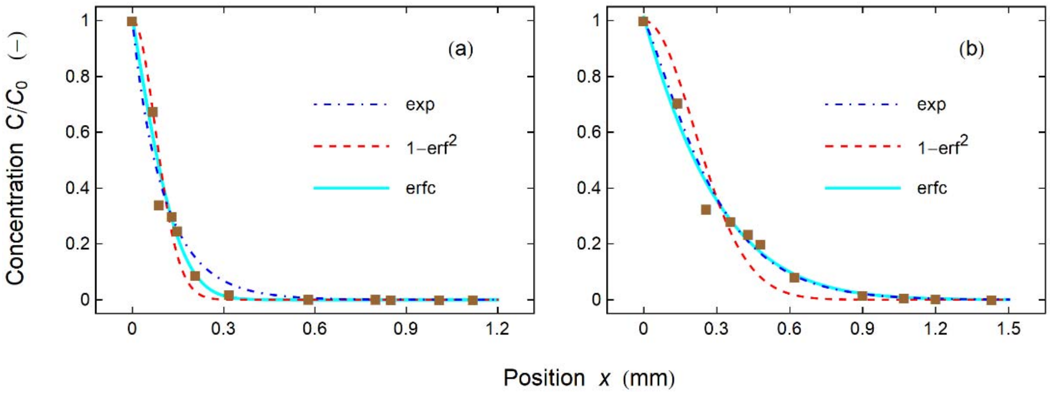

FIGURE 1. The concentration profiles for the diffusion of ^{241}Am in (a) silica concrete and (b) blast-furnace slag concrete. Experimental data are represented by squares and their theoretical fits with Eqs. (5) – (7) are shown as curves.

In this paper we extend the approach from [10] to two more concentrations profiles of decreasing shapes and provide the associated formulas for $D_a(C)$. We use all three cases to calculate $D_a(C)$ for the diffusion of ^{241}Am in two types of concrete, using the experimental data obtained in [11]. The three cases are compare mutually as well as with the constant values of D_a calculated in [11].

EXPERIMENTAL DATA AND THEORETICAL BACKGROUND

We shall use the experimental data obtained by Albinsson and co-workers in [11]. They studied diffusion of ^{241}Am in concrete samples by in-diffusion laboratory experiments. One type of the samples was from came from silica concrete (denoted as SC) and the other one from blast-furnace slag concrete (denoted as BC); both were based on Portland cement in which different solids were added. The samples were of cylindrical shape (the diameter of 20 mm, length of 25 mm), covered with a thin layer of resin on all sides except at one end that was in contact with a reservoir of water spiked with Am of concentration C_0. After the diffusion time of t_0 = 912 days the samples were ground, removing a layer of (0.1 – 0.7) mm in each grinding. The radioactivity of Am was measured by a scintillation detector, the corresponding profiles being shown in Fig. 1. Notice that the penetration of Am into the samples is very small in spite of a rather long diffusion time.

In the case of a varying D_a, it is necessary to modify Eq. (1) to a more general form as [12, 13]

$$\frac{\partial C}{\partial t} = \frac{\partial}{\partial x}\left(D_a(C)\,\frac{\partial C}{\partial x}\right) - \lambda C\,. \qquad (2)$$

In addition to 1D diffusion, radionuclide decay with a decay constant λ is included. Applying the standard procedure [7], the apparent diffusion coefficient can be calculated as

$$D_a(C(x,t_0)) = \frac{1}{\frac{dC(x,t_0)}{dx}}\left(\frac{1}{2t_0}\int_x^{\infty} x' \frac{dC(x',t_0)}{dx} dx' - \lambda \int_x^{\infty} C(x',t_0)\,dx' \right), \qquad (3)$$

where t_0 is the time at which the concentration profiles were measured. Equation (3) yields the concentration dependence $D_a(C)$ from $D_a(C(x, t_0))$ and $C(x, t_0)$.

Rather than evaluating Eq. (3) numerically, we shall approximate experimental profiles $C(x, t_0)$ by the following three functions [14]

$$\frac{C(x,t_0)}{C_0} = \frac{h}{2}\,\mathrm{erfc}\,[a(x-x_0)], \quad \frac{C(x,t_0)}{C_0} = 1-\mathrm{erf}^2(ax), \quad \frac{C(x,t_0)}{C_0} = \exp[-(ax)^b] \qquad (4)$$

(here erfc = 1 – erf, where erf is the Gauss error function). The first function is convenient when profiles are of S shapes, while the last two are convenient for profiles of decreasing shapes. For each of them the right-hand side of Eq. (3) can be evaluated, yielding the formulas

TABLE 1. The values of the fitting parameters in the theoretical profiles from Eqs. (5) – (7).

Type of concrete	Profile erfc			Profile 1 – erf²	Profile exp	
	h (–)	a (mm⁻¹)	x_0 (mm)	a (mm⁻¹)	a (mm⁻¹)	b (–)
SC	2.09	5.71	– 5.2 10^{-3}	8.33	9.46	0.95
BC	12.1	1.20	– 0.81	3.01	3.37	1.22

$$D_a(C) = \frac{1}{2a^2}\left[\frac{1}{2t_0} + \lambda + \frac{\sqrt{\pi}}{h}\left(\frac{a\,x_0}{t_0} - 2\lambda\,E_C\right)\frac{C}{C_0}\,e^{E_C^2}\right], \qquad E_C = \mathrm{erfc}^{-1}\frac{2C}{h\,C_0}, \tag{5}$$

$$D_a(C) = \frac{1}{2a^2}\left\{\frac{1}{2t_0} + \lambda + \frac{1}{4y_C}\left[\sqrt{2}\left(\frac{1}{t_0} + 2\lambda\right)\mathrm{erfc}(\sqrt{2}E_C) - 2\sqrt{\pi}\lambda\frac{C}{C_0}E_C\right]e^{E_C^2}\right\}, \qquad E_C = \mathrm{erf}^{-1}y_C, \tag{6}$$

$$D_a(C) = \frac{L^{1/b-1}}{2b^2 e^{2a/b}}\left[\frac{b}{t_0}L^{1/b} + \left(\frac{1}{t_0} + 2\lambda\right)\frac{C_0}{C}\,\Gamma(1/b, L)\right], \qquad L = \log\frac{C_0}{C}. \tag{7}$$

The first formula, Eq. (5), was already obtained in [10]. Here erf^{-1} and erfc^{-1} are the inverse functions to erf and erfc, respectively, $y_C = (1 - C/C_0)^{1/2}$, and Γ is the incomplete gamma function. Notice that the concentration appears in Eqs. (5) – (7) only via the ratio C/C_0, so that we actually have the dependence of D_a on this ratio.

RESULTS AND DISCUSSION

We begin with the fitting of the experimental concentration profiles of ^{241}Am with the theoretical formulas from Eqs. (5) – (7), adjusting their parameters to get the best fit. Table 1 gives the values of these parameters following from a least-square regression analysis. The corresponding statistical error (in relative terms) in the determination of the parameters is rather high for the erfc profile, but it does not exceed 8.2% for the remaining two profiles; the smallest coefficient of determination for all three profiles is still quite high, R^2 = 0.9652. Therefore, the theoretical profile from Eqs. (5) – (7) are reasonable good approximations of the experimentally measured concentration profiles, with the erfc profile having rather large uncertainty in its parameters' values.

We may now use the values of the profiles' parameters from Table 1 and plug them into the formulas from Eqs. (5) – (7) to obtain the concentration dependences of D_a (see Fig. 2). While the so calculated D_a(C) could be somewhat inaccurate near the low and high concentrations (i.e., when C is near 0 or near C_0), it should be rather plausible for intermediate concentrations, say, for C between 0.2 C_0 and 0.8 C_0. Within this range, it is clear from Fig. 2 that D_a has values (0.5 – 2) × 10^{-16} m²s⁻¹ for concrete SC and (3.5 – 10) × 10^{-16} m²s⁻¹ for concrete BC. Note that the D_a(C) calculated from the erfc profile is almost constant for concrete SC, lying in the interval (0.93 – 0.97) × 10^{-16} m²s⁻¹. All these values of D_a are extremely low, as should be expected for such a slow the penetration of Am into the studied concrete samples. In the original study [11] they obtained a constant value of D_a by fitting the measured profiles with the analytical solution of the 1D diffusion equation in semi-infinite porous media with appropriate initial and boundary conditions. Their results were 1 × 10^{-16} m²s⁻¹ for concrete SC and 9 × 10^{-16} m²s⁻¹ for concrete BC, in good agreement with our results. It is obvious, however, that our results indicate that D_a can

change by a factor of three or four as the concentration changes from 0.2 C_0 to 0.8 C_0. Thus, quite imprecise predictions may be concluded when a constant value of D_a is assumed. It should be also noted that some of the three calculated dependences D_a(C) are increasing and some are decreasing. Rather than their shapes, it is therefore their range of values that is physically interesting.

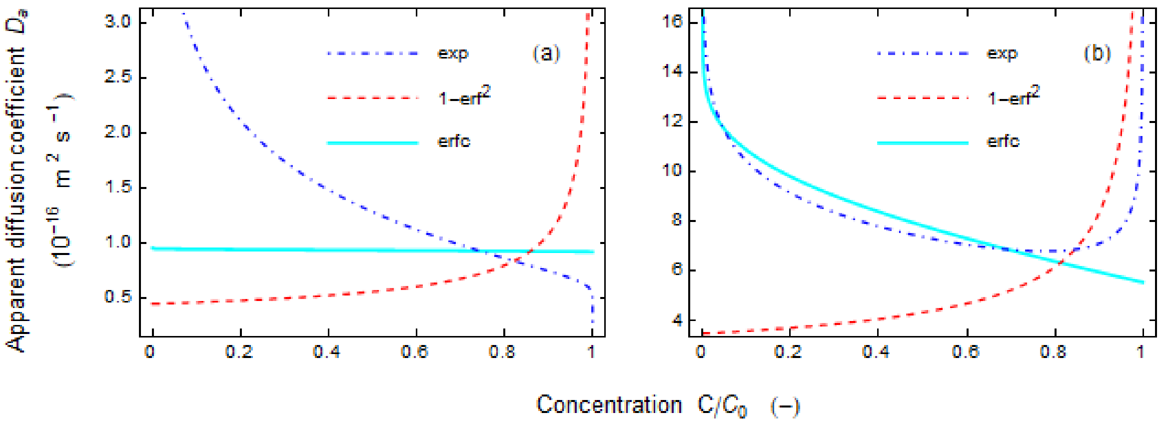

FIGURE 2. The concentration dependence of the apparent coefficients of diffusion of ^{241}Am in (a) concrete SC and (b) concrete BC obtained from Eq. (5) – (7). The decay constant λ for ^{241}Am is 5.08 × 10^{-11} s^{-1} [15].

CONCLUSIONS

We estimated concentration dependences of the apparent diffusion coefficient D_a for the in-diffusion of ^{241}Am into two types of concrete based on Portland cement. We first found the best fits to the concentration profiles that were experimentally measured in Ref. [11], using three types of suitable approximating functions. We then applied a version of the inverse Boltzmann-Matano method in which sorption and radioactive decay are included. We argued that reliable values of D_a were obtained at intermediate concentrations. It was pointed out that D_a may be imprecisely estimated by a factor of two or three when it is considered to be constant.

ACKNOWLEDGMENTS

The research in this paper was supported by the Czech Science Foundation, Project No. 17-11635S.

REFERENCES

1. C. D. Shackelford and S. M. Moore, Eng. Geol. **152**, 133–147 (2013).
2. J. L. Cormenzana, M. Garcia-Gutierrez, T. Missana, A. Junghanns, J. Contam. Hydrol. **61**, 63–72 (2003).
3. L. R. Van Loon, J. Eikenberg, Appl. Rad. Isotop. **63**, 11–21 (2005).
4. M. Molera and T. Eriksen, Radiochim. Acta **90**, 753–760 (2002).
5. L. R. Van Loon, P. Wershin et al., Radiochim. Acta **92**, 757–763 (2004).
6. R. Černý, Z. Pavlík, P. Rovnaníková, Cement Concrete Comp. **26**, 705–715 (2004).
7. Z. Pavlík et al., J. Frankl. Inst. **348**, 1574–1587 (2011).
8. I. Medveď, R. Černý, Transport Porous Med. **105**, 597–610 (2014).
9. J. Carmeliet et al., J. Therm. Environ. Bldg. Sci. **27**, 277–305 (2004).
10. I. Medved', R. Černý, AIP Conference Proceedings **1978**, 080007 (2018).
11. Y. Albinsson, K. Andersson, S. Börjesson, B. Allard, J. Contam. Hydrol. **21**, 189–200 (1996).
12. C.-T. Chen and S.-H. Li, Waste Manage. **17**, 53–64 (1997).
13. J. Bear and Y. Bachmat, *Introduction to Modelling of Transport Phenomena in Porous Media* (Kluwer, Dordrecht, 1990).
14. I. Medved' and R. Černý, Met. Mater. Int. **21**, 907–912 (2015).
15. W. M. Haynes, *CRC Handbook of Chemistry and Physics* (Taylor & Francis, Boca Raton, 2016).

Determination of Pore Size Distribution of Porcelain Samples Using Water Thermoporometry

Anton Trník[1, 2, a)], Omar Al-Shantir[2, b)], Magdaléna Doleželová[1, c)], Jiří Maděra[1, d)], and Zuzana Hlaváčová[3, e)]

[1]*Department of Materials Engineering and Chemistry, Faculty of Civil Engineering, Czech Technical University in Prague, Thakurova 7, 16629 Prague, Czech Republic*
[2]*Department of Physics, Faculty of Natural Sciences, Constantine the Philosopher University in Nitra, A. Hlinku 1, 94974 Nitra, Slovakia*
[3]*Department of Physics, Faculty of Engineering, Slovak University of Agriculture in Nitra, A. Hlinku 2, 94976 Nitra, Slovakia*

[a)]Corresponding author: anton.trnik@fsv.cvut.cz
[b)]omar.alshantir@ukf.sk
[c)]magdalena.dolezelova@fsv.cvut.cz
[d)]madera@fsv.cvut.cz
[e)]zuzana.hlavacova@uniag.sk

Abstract. The pore size distribution of porcelain samples is studied using thermoporometry. Thermoporometry is a calorimetric method where the pore structure is described from the melting or freezing point depression of a liquid confined in pores. The pore size distribution is derived from differential scanning calorimetry during the melting process of ice in the pores. As a probe, water is used. The thermal analysis is performed in the temperature interval from –20 °C to 5 °C with a heating rate of 0.1 °C/min. The results are compared with mercury intrusion porosimetry. It is found that the pore distributions depend on equations which are used for its calculation. It is also confirmed that water thermoporometry and mercury intrusion porosimetry of porcelain samples are in good correlation up to the pore size of 40 nm.

INTRODUCTION

Porosity of ceramic materials is very important because it influences many properties, such as thermal conductivity and diffusivity, heat capacity, and thermal expansion. Porosity is the ratio of the void of a material to its volume. The pores may be open or closed. Pores can be divided according to their sizes. Micropores have pores below 2 nm in diameter, mesopores have pores with diameters between 2 and 50 nm, and finally macropores have pores greater then 50 nm [1].

Mercury intrusion-extrusion (MIP) or nitrogen adsorption-desorption manometry are the most used methods for measurement of material porosity. The total pore volume, mean pore size, and pore size distribution are determined from pore-filling methods. The principle of both techniques is to derive porosity using the surface tension, capillary forces, and pressure. A gas adsorption porosimetry is based on the principle of capillary condensation. It requires the knowledge of gas-liquid phase transition of the gas (usually nitrogen) inside pores. On the other hand, if mercury porosimetry is used, mercury is added to an evacuated cell and forced into pores by defined pressure. This method has several disadvantages. One is that samples must be dry. So, this method is problematic for hydrophilic samples. Another disadvantage is the application of high pressures, which may crush or deform pores [1].

Thermoporosimetry (TPM) is a calorimetric method for the determination of the porosity from the melting or freezing point depression of a liquid confined in pores. This is possible due to the added contribution of surface

curvature to the phase-transition free energy [1]. The physical basis is as follows: the temperature equilibrium for a solid–liquid phase transition is determined by the radius of curvature of the interface between the solid and liquid phases [1]. Usually, water is used as a common liquid probe. Water is confined in pores so that it freezes at a lower temperature than in the bulk. The freezing temperature depends on the size of the pores [2, 3]. Differential scanning calorimetry (DSC) is appropriate for a precise measurement of the small temperature deviation due to particular sensitivity to exothermic or endothermic transitions (freezing/melting). TPM with water as a liquid probe is not able to detect pores with sizes larger than 200 nm. This is due to the influence of the freezing point depression and the ink-bottle effect in the freezing process [1, 2, 4]. The main disadvantage of TPM is that this method is nontraditional and is not used as widely as the gas adsorption or mercury intrusion method [1].

TPM has been used to determine porosity for different building materials, such as hardened concrete [5, 6], hardened cement pastes [4, 7], calcium sulfoaluminate cements [3], calcium phosphate cements [8], mortars [9], Portland cement [10], mesoporous silicas [11, 12], and aerated autoclaved concrete [13].

The aim of this study is to determine the pore size distribution of two different porcelain samples using thermoporometry and to compare the so obtained results with MIP.

EXPERIMENTAL

Samples and measurement method

The studied samples were made from the porcelain mixture C130 which was produced by the company PPC Cab from Slovakia. It contains mainly illitic clay, kaolin, feldspar, and alumina. This mixture was dry-compressed with two compression pressures (70 MPa and 110 MPa). From the compressed mixture, the samples were prepared using a grinder. Then the samples were preheated at 1000 °C. We denote them as C130/70(1000) and C130/110(1000).

To measure the porosity of samples by TPM, the final size of samples was ∅5 × 2 mm. The samples were drying 12 hours at 80 °C. Then, the masses of samples were measured. Subsequently, samples underwent backfilling with demineralized water by boiling for 2 hours and were left in water for 24 hours. The saturated samples were placed in sealed aluminium crucible of 100 μl.

Differential scanning calorimetry was performed by DSC 822^e apparatus (Mettler Toledo) equipped with cooling device Julabo FT 900. DSC measurements were carried out during heating in the temperature interval from –20 °C up to 5 °C with a heating rate of 0.1 °C/min. Before heating, the samples were kept at –20 °C with a soaking time of 20 min. At this temperature, both bulk and confined water freezes. So, the pore size distribution is determined from DSC curves during the solid to liquid transition.

To obtain the pore size distribution from a DSC signal, the temperature ΔT must be expressed in terms of a pore diameter R_p (in nm) and the heat flow in terms of the differential pore volume. The former can be done using several equations. In this study, three equations for melting of water from different authors will be used. Landry [1] derived the following equation for melting of water in controlled-pore glass samples,

$$R_p = -\frac{19.082}{\Delta T + 0.1207} + 1.12. \quad (1)$$

Brun et al. [2] determined the equation for the melting of water in hypothetical cylindrical pores as

$$R_p = -\frac{32.33}{\Delta T} + 0.68. \quad (2)$$

Finally, Ishikiriyama et al. [14] obtained the equation for the melting of water in silica gels as

$$R_p = -\frac{33.30}{\Delta T} + 2.52. \quad (3)$$

Generally, the heat flow ($\mathrm{d}Q/\mathrm{d}t$) is expressed via the differential pore volume ($\mathrm{d}V_p/\mathrm{d}R_p$) according to the equation [1]

$$\frac{\mathrm{d}V_p}{\mathrm{d}R_p} = \frac{\mathrm{d}Q}{\mathrm{d}t}\frac{\mathrm{d}t}{\mathrm{d}(\Delta T)}\frac{\mathrm{d}(\Delta T)}{\mathrm{d}R_p}\frac{1}{m\rho(T)\Delta H_f(T)}, \quad (4)$$

where t is time, m is a mass of a dry sample, and $\Delta H_f(T)$ and $\rho(T)$ is the heat of fusion and density of water, respectively. The value of the heat flow for water should be determined from following equation [1, 14]

$$\Delta H_f(T) = 334.1 + 2.119\Delta T - 0.00783\Delta T^2. \quad (5)$$

Similarly, the density of water is calculated according the equation [1, 14]

$$\rho(T) = 0.917(1.032 - 1.17 \times 10^{-4}\Delta T). \quad (6)$$

The pore size distribution was also measured by the mercury intrusion porosimetry (Pascal 140+440Evo, Thermo Fisher Scientific) for comparison of results. This method detects pores smaller than 100 µm in diameter.

RESULTS AND DISCUSSION

The bulk density, matrix density, and open porosity of the studied samples are presented in Table 1. The bulk density was calculated from the mass and dimensions of samples. It is smaller for sample C130/70(1000) and its value is 2041 kg/m^3. On the other hand, the matrix density is almost the same for both studied samples. It was determined using He-pycnometry. From the bulk and matrix densities, the open porosity was obtained. It was found that the open porosity is smaller for sample C130/110(1000), having a value of 30.7 %.

TABLE 1. Basic properties of porcelain samples preheated at 1000 °C

Material	Bulk density [kg/m^3]	Matrix density [kg/m^3]	Open porosity [%]
C130/70(1000)	2041	3003	32.0
C130/110(1000)	2082	3004	30.7

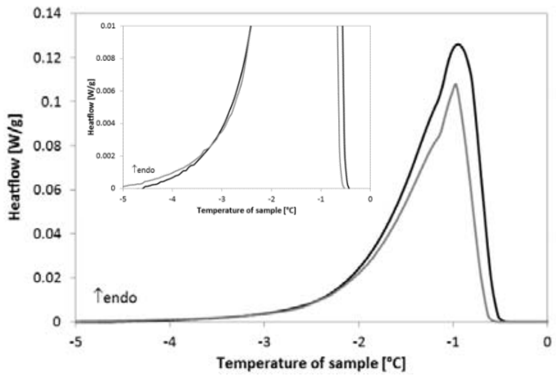

FIGURE 1. Heatflow of studied samples C130/70(1000) (black line) and C130/110(1000) (grey line) in the temperature interval from –5 °C to 0 °C.

The results of DSC measurements for both types of the studied samples C130/70(1000) and C130/110(1000) are shown in Fig. 1. The peaks correspond to the melting of the confined water. So, the ice crystals melt in the mesopores. This process fully depends on the dimension of pores in a sample. The melting process in the mesoporeses starts slightly earlier for sample C130/110(1000). Namely, for sample C130/110(1000) it starts at –5 °C and for sample C130/70(1000) it starts at –4.5 °C. The melting is finished at the temperatures of –0.47 °C and –0.37 °C for samples C130/110(1000) and C130/70(1000), respectively. At these temperatures, all ice crystals in the pores are completely melted.

The pore size distributions were determined from the DSC curves (see Fig. 1) according to Eqs. (1)–(3) and the differential pore volume was calculated according to Eq. (4). The pore size distributions of samples C130/70(1000) and C130/110(1000) obtained using TPM are shown in Fig. 2. The results depend on the model equation which was used for the calculation. For both types of the studied samples the smallest pores were detected from Eq. (1), then from Eq. (2), and finally from Eq. (3). Pore sizes are in the interval from 5 nm up to 65 nm for sample

C130/70(1000) and from 5 nm up to 55 nm for sample C130/110(1000). So, it can be concluded that the pore size decreases with the compression pressure. The differential pore volume is higher according to Landry then the other two equations.

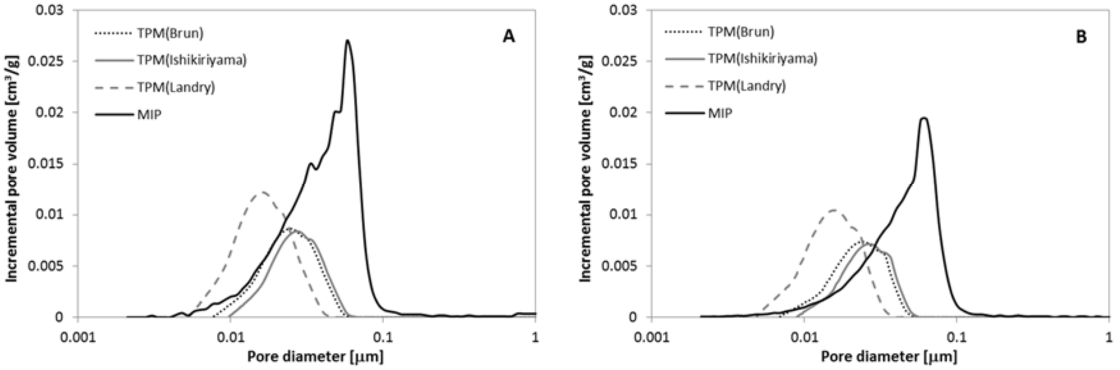

FIGURE 2. The comparison of pore size distribution of porcelain samples (A – C130/70(1000) and B – C130/110(1000)).

The results obtained from MIP are also in Fig. 2 (black lines). The pore size distributions of both studied samples are from 4 nm to 160 nm and from 3 nm to 130 nm, respectively. So, their difference is about 20 % and they are higher than from TMP results. The comparison of both results (TPM and MIT) shows that the determination of pore diameters up to 30 nm using Eq. (2) and Eq. (3) are in good agreement (differences are up to 10 %).

CONCLUSIONS

The pore size distributions of porcelain samples were studied using thermoporometry. The obtained results according to three different equations were compared with those received from mercury intrusion porosimetry. It was found that

- the pore size calculated from different equation varied,
- the pore size decreased with compression pressure,
- the pore distributions calculated from Eq. (2) or Eq. (3) were in good agreement with the results from MIP up to 30 nm.

ACKNOWLEDGMENTS

This research has been supported by the Czech Science Foundation, under project No. 17-01365S.

REFERENCES

1. M. R. Landry, Thermochim. Acta **433**, 27–50 (2005).
2. M. Brun *et al*., Thermochim. Acta **21**, 59–88 (1977).
3. S. Irico *et al*., Cem. Concr. Res. **53**, 239–247 (2013).
4. K. Kurumisawa, Constr. Build. Mater. **101**, 926–931 (2015).
5. M. Wu and B. Johannesson, Thermochim. Acta **580**, 66–78 (2014).
6. M. Wu, B. Johannesson, and M. Geiker, Thermochim. Acta **589**, 215–225 (2014).
7. J. J. Valenza and J. J. Thomas, Cem. Concr. Res. **42**, 440–446 (2012).
8. D. Pastorino, C. Canal, and M. P. Ginebra, Acta Biomater. **28**, 205–214 (2015).
9. Z. Sun, G. W. Scherer, Cem. Concr. Res. **40**, 740–751 (2010).
10. E. Robens *et al*., J. Therm. Anal. Calorim. **62**, 435–441 (2000).
11. D. Majda *et al*., J. Therm. Anal. Calorim. **127**, 207–220 (2017).
12. D. Majda *et al*., Microporous Mesoporous Mat. **222**, 33 – 43 (2016).
13. A. Trnik *et al.*, AIP Conf. Proc. **1978**, 080008 (2018).
14. K. Ishikiriyama *et al*., J. Colloid Interface Sci. **171**, 92 – 102 (1995).

Thermal and Energy Performance of AAC Exposed To Low Temperatures in the Computational Simulation with Advanced Input Parameters

Jan Kočí[a)] and Jiří Maděra[b)]

Department of Materials Engineering and Chemistry, Faculty of Civil Engineering, Czech Technical University in Prague, Thákurova 7, 166 29 Prague 6, Czech Republic.

[a)]Corresponding author: jan.koci@fsv.cvut.cz
[b)]madera@fsv.cvut.cz

Abstract. This paper analyses the performance of advanced mathematical model aimed for description of heat and moisture transport in porous materials including phase change of transported moisture. The objective of the research is to investigate the effect of two types of thermal input parameters. First, the model is performed with the standard thermal properties determined for the room temperatures. Then, the same simulation is performed with the properties determined in the range of subzero to room temperature. The results are compared against each other and the thermal and energy performance of studied element is analyzed. The results showed there is a difference about 5 °C in temperature distribution and about 6 % in energy performance.

INTRODUCTION

A proper description of hygrothermal and energy response of building materials exposed to the effect of the environment is important in many engineering fields [1-4]. In order to describe those responses properly, it is necessary to involve computational modelling with advanced physical models [5]. In case the studied material or building component are exposed to low temperature, it is essential that the computational model takes into account phase changes of the moisture that is retained within the material's pore structure. However, considering the phase changes inside that material, there is not only a necessity for advanced computational model, but also for advanced input material parameters as well. Those parameters should include changes of material properties during freeze/thaw cycles that may appear during material's service life [6].

In this paper, a computational analysis of thermal and energy performance of autoclaved aerated concrete (AAC) exposed to low temperature is presented. For the computational modelling, an advanced hygrothermal model is used allowing for modelling phase changes of liquid moisture that may appear in the material. The main objective of this paper is to investigate the effect of material thermal input parameters that are used in that model. First, the model is performed with the standard thermal properties determined for the room temperatures. Then, the same simulation is performed with the properties determined in the range of subzero to room temperature. The results of both simulations are evaluated and the model outputs are discussed.

COMPUTATIONAL MODEL

For the testing of model performance with various input parameters a computational model that is based on a fixed-domain method was used [7]. The model is based on modified Künzel's mathematical model [8] with the

effective specific heat capacity feature for a description of water/ice phase change [5]. Balance equations are given below

$$c_{eff}\rho_v \frac{\partial T}{\partial t} = \text{div}\left(\lambda \text{grad} T\right) + L_v \text{div}\left(\delta_p \text{grad}\, p_v\right), \tag{1}$$

$$\left[\rho_w \frac{dw}{dp_v} + \left(n - w\right)\frac{M}{RT}\right]\frac{\partial p_v}{\partial t} = div\left[D_g \,\text{grad}\, p_v\right], \tag{2}$$

where c_{eff} (J·kg^{-1}·K^{-1}) is the effective specific heat capacity, ρ_v (kg·m^{-3}) is the bulk density, T (K) is the absolute temperature, λ (W·m^{-1}·K^{-1}) is the thermal conductivity, L_v (J·kg^{-1}) is the latent heat of evaporation of water, δ_p (s) is the water vapor diffusion permeability, p_v (Pa) is the partial pressure of water vapor in the porous space, ρ_w (kg·m^{-3}) is the density of water, w (m^3·m^{-3}) is the moisture content by volume, n (-) is the porosity of the porous body, M (kg·mol^{-1}) is the molar mass of water vapor, R (J·K^{-1}·mol^{-1}) is the universal gas constant, and D_g (s) is the global moisture transport function. More information on the modified model can be found in [8], description of effective specific heat capacity is given in [5].

Boundary conditions for interior were kept constant at 21 °C and 55 % of relative humidity during the simulation. The exterior conditions were represented by hourly weather data from the Test Reference Year for the location of Šerák, Czech Republic that can induce very severe conditions to the constructions.

STUDIED MATERIAL

The investigation of model performance was done on a testing sample made of AAC having thickness 500 mm. The basic material parameters are shown in Table 1. The advanced material parameters determined at low temperatures were taken from [6]. Namely the thermal conductivity, specific heat capacity, moisture diffusivity and water vapor diffusion resistance factor taken in the range from subzero to room temperatures.

TABLE 1. Material parameters of AAC in dry state at 20 °C

Parameters	AAC P 1.8-300
Bulk density ρ (kg·m^{-3})	289
Open porosity ψ (%)	86.9
Specific heat capacity c (J·kg^{-1}·K^{-1})	1090
Water vapour diffusion resistance factor μ_{dry} (-)	15.61
Water vapour diffusion resistance factor μ_{sat} (-)	6.17
Thermal conductivity λ_{dry} (W·m^{-1}·K^{-1})	0.092
Thermal conductivity λ_{sat} (W·m^{-1}·K^{-1})	0.769
Apparent moisture diffusivity κ (m^2·s^{-1})	7.02 10^{-8}

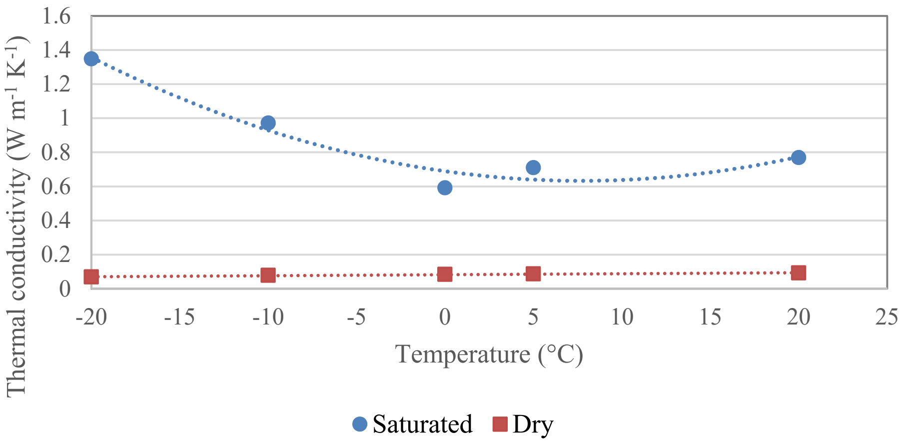

FIGURE 1. Thermal conductivity of dry and saturated sample as a function of temperature

Thus, those parameters were interpolated as a function of both temperature and moisture content. For illustration, the thermal conductivity of dry and saturated sample as a function of temperature is shown in Fig. 1.

RESULTS AND DISCUSSION

The objective of the paper was to investigate the effect of two different input parameters on thermal and energy performance of the studied material. First, the material parameters were considered as a function of moisture content at room temperatures only, second, the same parameters were determined as both function of moisture content and temperature in the range from subzero to room temperatures. The outputs were compared in two ways. First, the temperature distributions in winter and summer periods were compared (see Fig. 2). And second, the thermal performances in form of annual heat fluxes were compared (see Table 2). The quantification of thermal performance of the studied walls was done on the basis of calculation of time development of heat flux density $q(t)$ on the interior surface of the construction during a year. The heat flux densities were determined as

$$q(t) = \lambda_{ip}(w,t)\frac{\Delta T_e(t)}{\Delta x_e}, \tag{3}$$

where $\lambda_{ip}(w,t)$ ($W \cdot m^{-1} \cdot K^{-1}$) is the moisture-dependent thermal conductivity of the interior plaster, Δx_e (m) is the thickness of the element adjoining to the face side of the wall in the main direction of the heat flux, and ΔT_e (K) is the temperature difference between the opposite sides of the element adjoining to face side of the wall in the main direction of the heat flux.

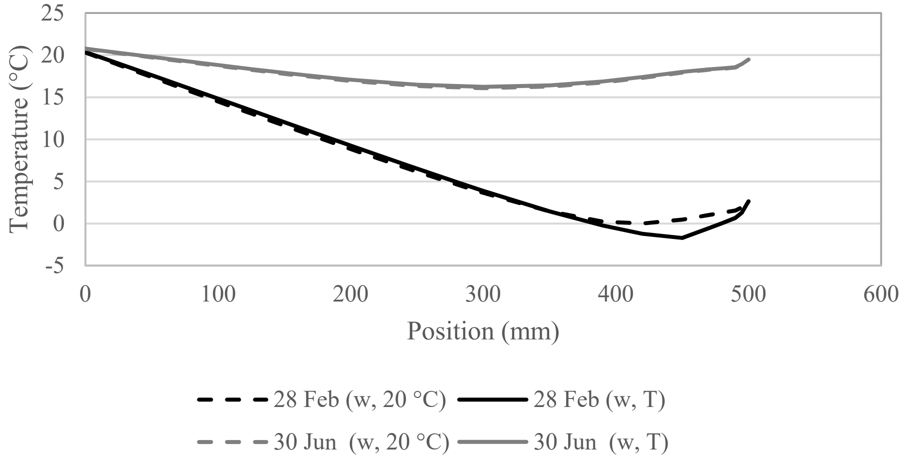

FIGURE 2. Temperature distribution in the studied material on February 28 and June 30

TABLE 2. Energy performance of studied material

Input parameters	Heat transmission per unit area of the wall (kWh m^{-2} a^{-1})		
	Loss	**Gain**	**Total**
$f(w, 20\ °C)$	31.301	0.0000	31.301
$f(w, T)$	29.501	0.0000	29.501

It is obvious from Fig. 2 that treating thermal conductivity as both function of moisture content and temperature as well as including material properties during phase change brings significant differences when compared to the standard values. The differences in temperature distribution were up to 5 °C and were apparent mostly in the winter period when the phase change of moisture takes place together with affected material properties by low temperatures. In overall energy performance during whole year, there was difference about 6 % between the two simulations. Surprisingly, the better performance was observed for the input parameters that were measured as a

function of temperature. Despite the fact, that thermal conductivity is generally rising with decreasing temperature, this phenomenon can be explained by slight decrease of thermal conductivity in the range between 5 and 20 °C, which is typical the temperature range typical for major part of the year. As the freezing occur in small part of the construction for limited period only, the change of material properties has not determinative effect on overall energy performance.

CONCLUSIONS

In this paper an advanced hygrothermal model was tested with two different thermal input parameters. First, the model was performed with the standard thermal properties determined for the room temperatures. Second, the same simulation was performed with the properties determined in the range of subzero to room temperature. The results showed impact of advanced input parameters. The differences in temperature distribution in the construction were up to 5 °C. The highest differences were observed in winter period, which was caused by water/ice phase change inside the material and change of material properties under low temperatures. From the point of view of energy performance, the differences between standard input properties determined at 20 °C and properties determined in the range from subzero to room temperature (including the phase change of liquid moisture) were about 6 %. The simulation results proved the necessity for utilization of advanced numerical models with advanced input parameters in order to obtain more accurate results.

ACKNOWLEDGEMENT

This research has been financially supported by the Czech Science Foundation, under project No 17-01365S.

REFERENCES

1. Y.F. Pan, G.J. Xian, and H. Li, J. Compos. Constr. **22**, 04018011 (2018)
2. A. Abdul Hamid, and P. Wallentén, Build. Environ. **123**, 351 (2017)
3. H. Maljaee, B. Ghiassi, P.B. Lourenço, and D.V. Oliveira, Compos. Struct. **147**, 143-154 (2016).
4. H. Xin, Y. Liu, A. Mosallam, Y. Zhang, and C. Wang, Constr. Build. Mater. **127**, 237 (2016)
5. J. Kočí et al. „Formulation of a Hygrothermal Model for Description of Ice-forming Process in Porous Building Materials, AIP Conference Proceedings **XXXX**, XXXXX (2018).
6. J. Kočí, J. Maděra, M. Jerman, and R. Černý, Int. J. Thermophys **40**, https://doi.org/10.1007/s10765-018-2464-2 (2019).
7. J. Crank, *Free and moving boundary problems* (Calverdon Press, Oxford, 1984).
8. J. Maděra, J. Kočí, V. Kočí and J. Kruis, Adv. Eng. Softw. **113**, 47-53 (2017).

Energy Performance of the Building Envelopes Provided with Interior Plasters with Moisture Buffering Effect

Jan Kočí[a)], Jiří Maděra[b)] and Jan Fořt[c)]

Department of Materials Engineering and Chemistry, Faculty of Civil Engineering, Czech Technical University in Prague, Thákurova 7, 166 29 Prague 6, Czech Republic.

[a)]Corresponding author: jan.koci@fsv.cvut.cz
[b)]madera@fsv.cvut.cz
[c)]jan.fort@fsv.cvut.cz

Abstract. In this paper, three different plasters are investigated in order to study their effect on whole building envelope energy performance. As the studied plaster contain various amount of super absorbent polymers, they are primarily intended to control relative humidity levels in both building envelopes and interior environments. However, influencing moisture levels in the envelopes will have certain impact on energy performance as well. In order to investigate that effect, the material parameters of all studied plasters were determined and then, series of computational simulations was carried out. The results showed, that even a thin layer of interior plaster may have significant impact on overall building envelope performance. The studied plaster contributed to the reduction of energy consumption from 4 to 6 %.

INTRODUCTION

Moisture level significantly affects durability of constructions, their thermal performance, quality of indoor air as well as energy performance of buildings [1-3]. The building envelope is exposed to the effect of numerous sources of moisture and water vapor from both interior and exterior side. Therefore, a proper design may significantly increase the performance of the construction. However, there exists some advanced types of materials, which designers and engineers try to incorporate into building enclosure in order to enhance the primary functions of those envelopes. In this respect, for example addition of vermiculite, perlite or super absorbent polymers (SAP) to the mixture of interior plasters increases the absorption capacity of those plasters [4-6], which can significantly help to control moisture levels in both construction and interior space. On the other hand, affecting of moisture levels in the envelopes, may significantly influence the energy performance of the envelope, which is often ignored.

In the proposed paper, the newly developed plasters with enhanced moisture accumulation capability are analyzed by the computational simulation. First, the necessary material parameters are determined in the series of laboratory experiments. Those parameters are then used as input data in the computational model. The objective of the computational simulation is to study energy performance of building envelope provided with advanced interior plasters. Based on the simulation results, it is shown that even thin layer of interior plaster may have an impact on whole envelope energy performance.

MATERIALS

The investigation of energy performance was done on brick wall (450 mm) provided with three types of modified plasters on both exterior and interior surfaces (20 mm). The ceramic brick was marked as CB, and the plasters were marked as P-ref, P-2%, and P-3%. The P-ref refers to a reference plaster, while P-2% and P-3% refer to the modified reference plaster by adding 2 wt% or 3 wt% of SAP (Favor PAC 300 by Evonik Ltd.), respectively.

The basic physical, thermal and hygric properties are summarized in Table 1, where following symbols are used: ρ_v is the bulk density, ρ_{mat} is the matrix density, ψ is the total open porosity, λ is the thermal conductivity, c is the specific heat capacity, μ is the water vapor diffusion resistance factor, κ_{app} is the apparent moisture diffusivity, and *w/c* is the water-cement ratio. The sorption and desorption isotherms are shown in Fig. 1. Other material parameters determined within the frame of this research were moisture diffusivity and water retention curves. All the material parameters were obtained in the laboratories of the Department of Materials Engineering and Chemistry, FCE CTU Prague. The material parameters of ceramic brick were measured in the same laboratories in previous research [7].

TABLE 1. Basic material parameters of studied materials.

Parameter/Material	CB	P-ref	P-2%	P-3%
ρ_v (kg·m^{-3})	1389	1593	1225	1203
ρ_{mat} (kg·m^{-3})	2581	2548	2574	2563
ψ (-)	0.279	0.375	0.524	0.531
λ (W·m^{-1}·K^{-1})	0.59	0.53	0.38	0.36
c (J·kg^{-1}·K^{-1})	825	920	1087	1099
μ (-)	22.1	16.8	9.8	7.3
κ_{app} (m^2·s^{-1})	$2.15\cdot10^{-9}$	$9.93\cdot10^{-8}$	$6.80\cdot10^{-7}$	$1.02\cdot10^{-6}$

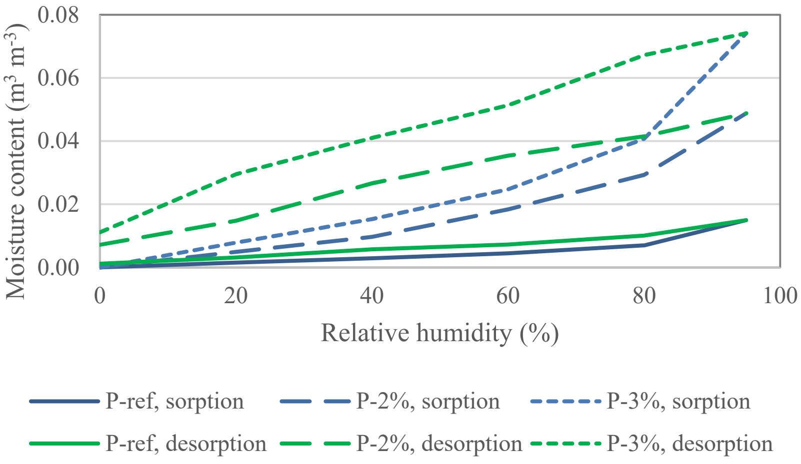

FIGURE 1. Sorption and desorption isotherms of studied plasters.

COMPUTATIONAL MODEL

For the investigation of the effect of weather data on hygrothermal performance of building materials, a modified Künzel's mathematical model was used [8] to describe heat and moisture transport through porous body. The model is described by following balance equations

$$c_{\mathrm{eff}}\rho_{\mathrm{v}}\frac{\partial T}{\partial t} = div\left(\lambda \mathrm{grad} T\right) + L_{\mathrm{v}} div(\delta_{\mathrm{p}} \mathrm{grad}\, p_{\mathrm{v}}), \tag{1}$$

$$\left[\rho_w \frac{dw}{dp_v} + \left(n - w\right)\frac{M}{RT}\right]\frac{\partial p_v}{\partial t} = div\left[D_g \,\mathrm{grad}\, p_v\right], \tag{2}$$

where c_{eff} (J·kg^{-1}·K^{-1}) is the effective specific heat capacity, ρ_v (kg·m^{-3}) is the bulk density, T (K) is the absolute temperature, λ (W·m^{-1}·K^{-1}) is the thermal conductivity, L_v (J·kg^{-1}) is the latent heat of evaporation of water, δ_p (s) is the water vapor diffusion permeability, p_v (Pa) is the partial pressure of water vapor in the porous space, ρ_w (kg·m^{-3}) is the density of water, w (m^3·m^{-3}) is the moisture content by volume, n (-) is the porosity of the porous body, M

(kg·mol^{-1}) is the molar mass of water vapor, R (J·K^{-1}·mol^{-1}) is the universal gas constant, and D_g (s) is the global moisture transport function. More information on the modified model can be found in [9].

The quantification of thermal performance of the studied walls was done on the basis of calculation of time development of heat flux density $q(t)$ on the interior surface of the construction during a year. The heat flux densities were determined as

$$q(t) = \lambda_{ip}(w,t)\frac{\Delta T_e(t)}{\Delta x_e}, \quad (3)$$

where $\lambda_{ip}(w,t)$ (W·m^{-1}·K^{-1}) is the moisture-dependent thermal conductivity of the interior plaster, Δx_e (m) is the thickness of the element adjoining to the face side of the wall in the main direction of the heat flux, and ΔT_e (K) is the temperature difference between the opposite sides of the element adjoining to face side of the wall in the main direction of the heat flux.

Boundary conditions for interior were kept constant at 21 °C and 55 % of relative humidity during the simulation. The exterior conditions were represented by hourly weather data from the Test Reference Year for the location of Šerák, Czech Republic that can induce very severe conditions to the constructions.

RESULTS AND DISCUSSION

The objective of the paper was to investigate the effect of various interior plasters on the whole building envelope energy performance. Since the plasters may significantly influence the moisture distribution in the wall, it is believed that also their effect on energy performance could be important. Fig. 2 shows distribution of relative humidity in the studied envelope in 1 July. The presented results clearly show that even thin layer of exterior and interior plaster may significantly affect the moisture distribution in the entire building envelope.

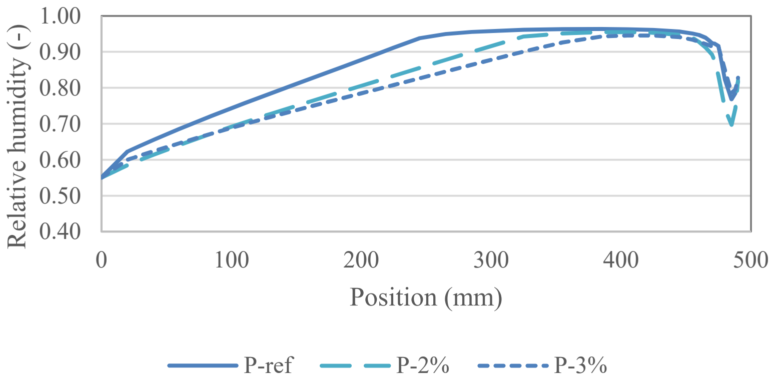

FIGURE 2. Relative humidity distribution in the studied element on July 1

The analysis of energy performance of studied walls is shown in Table 2.

TABLE 2. Energy performance of studied building envelopes

Plaster	Heat transmission per unit area of the wall per year (kWh·m^{-2}·a^{-1})		
	Loss	**Gain**	**Total**
P-ref	154.5128	0.0033	154.5161
P-2%	148.1960	0.0011	148.1971
P-3%	145.2664	0.0023	145.2687

It is obvious from Table 2 that adding SAP to the interior plaster influences the total energy performance. After adding 2 % and 3 % of SAP, the heat losses decreased by 4.1 % and 6.0 %, respectively. The heat gains were in this case negligible, which is given by the boundary conditions, which were quite severe. Nevertheless, the best performance in this case was observed for P-2%, which even outperformed P-3% with better thermal properties.

When the plaster would be tested in more hot conditions that induce more significant heat gains through the building envelope, this could be an interesting feature of those plasters which should be worth of further investigation. We would like to also note, that the tested building envelope was not provided with thermal insulation. When the thermal insulation is applied, the differences would be almost negligible.

CONCLUSIONS

In this paper a hygrothermal model was used to investigate heat and moisture transport in the building envelopes provided with different plasters with enhanced moisture accumulation properties. The enhanced properties of the plasters were achieved by adding various amount of super absorbent polymers. Based on the simulation results, the energy analysis was performed. The results showed, that adding SAP in to plasters may contribute to reduction of energy performance of whole building envelope. The heat losses through the envelope were reduced by (4 – 6) %. Adding SAP may contribute to reduction of heat gains as well, but as the applied weather data were quite severe, it is ambiguous to make any conclusion in this respect. Therefore, further investigation in various weather conditions and various envelope composition is suggested.

ACKNOWLEDGEMENT

This research has been financially supported by the Czech Science Foundation, under project No 18-03997S.

REFERENCES

1. H. Maljaee, B. Ghiassi, P.B. Lourenço, and D.V. Oliveira, Compos. Struct. **147,** 143-154 (2016).
2. A.J. Lohonayi and Y. Korany, Energ. Buildings **66,** 143-153 (2013).
3. A. Abdul Hamid, and P. Wallentén, Build Environ **123**, 351-362 (2017).
4. J.C. Gonzáles, M. Molina-Sabio, and F. Rodríguez-Reinoso, Applied Clay Science **20(3)**, 111-118 (2001).
5. T. Hasegawa, H. Iwasaki, Y. Shibutani, and I. Abe, Journal of Porous Materials, Springer **16(2)** 129-134 (2009).
6. H. Yang, Z. Peng, Y. Zhou, F. Zhao, J. Zhang, X. Cao, and Z. Hu, Energy and Buildings, 43(2-3) 386-392 (2011).
7. M. Čáchová, D. Koňáková, E. Vejmelková, M. Keppert, K. Polozhiy, and R. Černý, Advanced Materials Research **982**, 104-107 (2014).
8. J. Maděra et al. „Influence of weather-affected material characteristics on appereance of freeze/thaw cycles in building envelopes, in *Thermophysics 2017*, AIP Conference Proceedings **1866**, 040023 (2017).
9. V. Kočí et al., J Build Phys **41**, 497-520 (2018).

Material Selection in Order to Minimize the Heat Loss of Piping Based on Measurements and Calculations

Ákos Lakatos[1, a)], Ferenc Kalmár[1,b)] and Imre Csáky[1, c)]

[1]*Department of Building Services and Building Engineering, Faculty of Engineering, University of Debrecen, Debrecen, Ótemető str 2-4. 4028, Debrecen, Hungary*

[a)]Corresponding author: alakatos@eng.unideb.hu
[b)]fkalmar@eng.unideb.hu
[c)]imrecsaky@eng.unideb.hu

Abstract. In this paper a laboratory test completed with caclulations will be presented in order the designate a possible material to be used as an insulation for a pipe system. Four different types of insulation materials (fibrous aerogel, mineral wool, armaflex and polyurethane) will be tested. Once their thermal conductivity will be measured with a Holometrix lambda heat flow meter apparatus. Afterwards, sorption measurements will be carried out under two different states, furthermore, the results will be completed with optical microscope images to visualize the surface structure of the probes. The laboratory measurements results will be used for heat transfer calculations in the function of the varying surface temperature differences. Subsequently, the measurements will be used for calculations with respect to the pipe system of the "ALTAIR" advanced personalized ventilation system.

INTRODUCTION

Nowadays the use of thermal insulations both on the external surface and inside buildings is essential. By applying thermal insulation materials on the external surface of the buildings both the energy consumption and the CO_2 emission can be reduced [1]. Piping are mainly used for domestic hot and cold service water systems as well as for HVAC systems in buildings. When a temperature of a system is higher or lower than room temperature, there will be exchanges of heat [2], which may change its temperature and still result in a loss of energy.

As piping, the dominant materials are the plastics and metals. For thermal insulating of pipes, the mainly used materials are the closed cell types e.g.: armaflex and the polyurethane (PUR) foam. However, the use of the fibrous insulations is also possible. In this paper heat transfer calculations through pipes will be presented by using measured thermal conductivities. Surface heat transfer coefficient (inside the pipe) will be also estimated by varying the temperature and the air velocity. Besides humidity measurements optical microscope photographs taken from the insulations will be presented either. Nowadays, personal ventilation systems (PV) seem to be one of the energy conscious solutions providing appropriate indoor air quality and thermal sensation around the occupants in the occupation zone [3, 4]. At the University of Debrecen a novel PV equipment was developed, which can lead to important cooling energy savings., [5, 6]. The novelty of this system is that the air flow jet is provided alternately from different directions around the head (see Fig. 1). However, proper control of the air temperature is extremely important, because in the case of PV"s draught may create discomfort. Thus, air ducts have to be provided with proper thermal insulation in order to avoid heat gains or losses, which may lead to the increase or decrease of the air flow temperature.

FIGURE 1. The novel personalized ventilation equipment developed at the University of Debrecen

MATERIALS AND METHODS

In Figure 2 one can see the optical microscope photographs of the tested samples with about 20x magnification. Namely, (a) belongs to the armaflex with 40 kg/m^3 density), (b) belongs to the aerogel with 150 kg/m^3 density, (c) belongs to the PUR with 50 kg/m^3 density, and (d) belongs to the mineral wool with 100 kg/m^3 density.

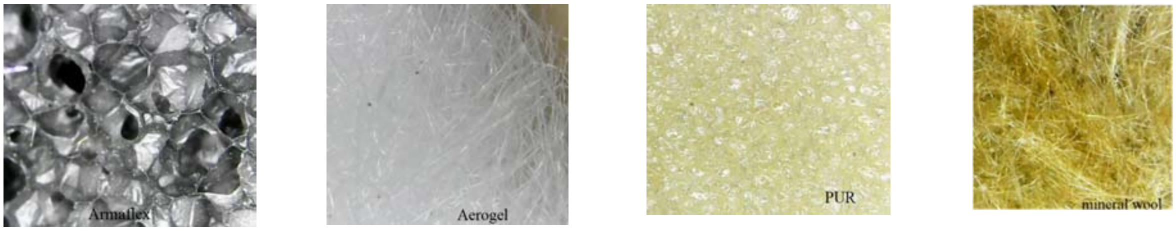

(a) (b) (c) (d)

FIGURE 2. The optical microscope photographs of the tested samples (~20x)

Sorption and thermal conductivity measurements

Both the humidity and the thermal conductivity measurements were carried out after drying the samples in a VentiCell drying instrument. After drying the samples, they were treated in a climatic chamber (ClimaCell 111) at 22 ºC and 25 ºC under 50% relative humidity for one week. For measuring the thermal conductivity of the samples, Lambda 2000 Heat flow meter (HFM) was used. For the thermal conductivity measurements, samples with 30 cm x 30 cm base area and with 2 and 5 cm thicknesses were used, while for the humidity measurements besides the same thicknesses samples with 10 cm x 10 cm base area were used. The measurement order and the detailed parameters of instruments are presented in Ref. [7].

Calculation method

Heat loss and convective surface heat transfer coefficient calculations

Firstly, the heat loss through the pipes were calculated for two cases. Once the shape of the piping was supposed to be cylindrical, secondly it was supposed to have square face area. The heat losses (in watts) were calculated from the conductive thermal resistances (R, (m^{2}K)/W, reached from Eq.1.), both in un-insulated and in insulated cases, by using the measured thermal conductivities (λ, W/(mK)) of the four different types of insulations.

$$R = \frac{1}{2\,\pi L\lambda} ln(\frac{d_e}{d_i}) \quad (1)$$

where d_i and d_e are the diameters of the pipe (internal and external), while L is the length of the pipe and λ is the thermal conductivity.

By using Eq. 1 the thermal resistances as well as from the thickness of the pipe or insulation (t) were calculated in the case of square shaped tunnel, too.

$$R = \frac{t}{\lambda} \quad (2)$$

$$\mathrm{R_T} = \mathrm{R_p} + \mathrm{R_i} \quad (3)$$

In order to reach the heat loss surface temperatures and total resistance were used, too. The heat losses were obtained by the ratio of the temperature difference and the resistances.

In this case, besides the length the covering surface area was taken into account either. For the calculation of the forced flow, some assumptions should be taken into account: steady operating conditions exist, radiation effects are negligible; air is an ideal gas with constant properties (the properties only depend from the temperature); smooth pipe, frictionless flow. The calculation method was followed as the one presented in Ref. 8. However, for the forced flows, both for the flow in the square shaped tunnel (Eq. 4) and in the cylindrical shaped pipe (Eq. 5) the following Nusselt numbers were applied in function of the Reynolds (Re) and the Prandtl (Pr) numbers.

$$Nu = 0.018Re^{0.8} \tag{4}$$

$$Nu = 0.023Re^{0.8}Pr^{0.3} \tag{5}$$

RESULTS AND DISCUSSION

From thermal conductivity measurements the following results were reached: 0.0171±0.0005 (W/mK) for the aerogel, 0.0293±0.001 W/(mK) for the armaflex; 0.0387±0.0007 (W/mK), for the PUR, and 0.0317±0.0002 (W/mK) for the mineral wool. These values were used for the calculations in order to reach the heat loss values, presented in Fig.3. The tested pipe system in real is partially metal partially plastic. For these thermal conductivities with 46 and 0.2 W/(mK) values were used. The length of the metal section is 0.57 m, while the length of the plastic section is 1.69 m. The heat losses were calculated for both parts and were added to each other. The diameter of both pipe sections were d_e/d_i=0.055/0.05 m/m, moreover the external diameter of the insulated pipe was 0.095 m. For the calculations of the case of the flow in the tunnel, the equivalent diameters were used.

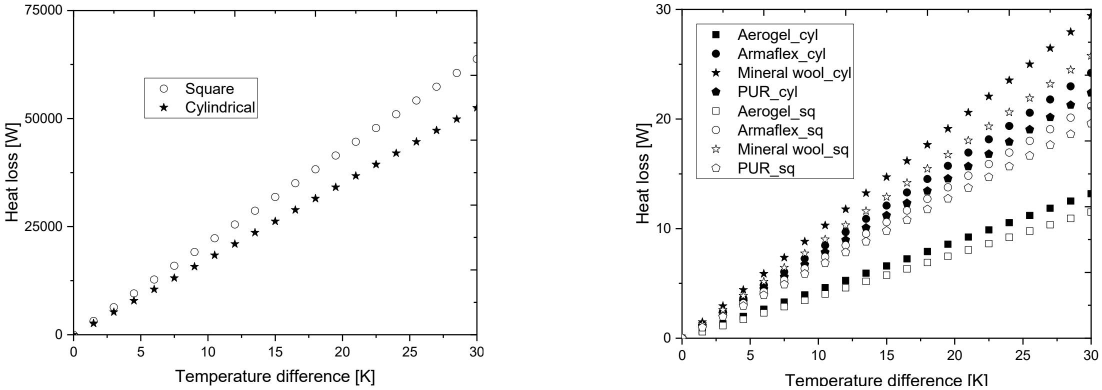

(a) (b)

FIGURE 3. The results of the calculations for the uninsulated case (a) and for the insulated case (b).

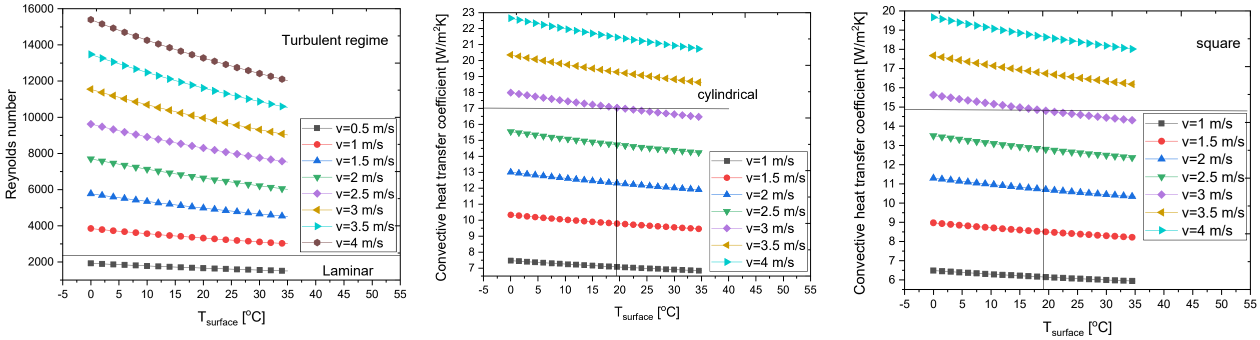

(a) (b) (c)

FIGURE 4. The results of the calculations for the Reynolds number and for the convective surface heat transfer coefficients

As results of the calculations, we can declare, that the greater heat loss is expected through the tunnel without insulation compared to the heat loss of the cylindrical shape, while greater reduction was reached after insulating the tunnel. The best insulation capability belongs to the aerogel, properly to the measured thermal conductivities presented above. To see the changes in the convective surface heat transfer coefficient as well as in the type of the flows, calculations were executed regarding Eq. 1-5. Previously in the pipe system the air velocities were measured

with a Testo 445 type wing anemometer and the air velocities were determined. The results were ranging between 0.8 and 4 m/s. Since these results were used for calculations. (see Fig. 4 a, b and c.) We stated that by using smaller than 1 m/s for the velocity the type of the flow was purely laminar. Greater surface heat transfer coefficient was reached for the same temperature and velocity in the case of a cylindrical shape.

FIGURE 5. The Testo 445 anemometer

Three samples from each types were wetted in a climatic chamber for one week after drying them to changeless weight. Two air conditions were fixed to 22 ºC 50 %, and 24 ºC 50 % temperature and relative humidity (rh). The test results are presented in Table 1. The air conditions were chosen as the directions of MSZ CR1752 standard, for lecture halls, and category "B".

TABLE 1. The results of the sorption investigations

	Aerogel	±	Armaflex	±	PUR	±	Mineral wool	±
Moisture content at 22 ºC 50 % rh. (m/m%)	1.16	0.022	0.33	0.013	0.97	0.009	0.1	0.004
Moisture content at 24 ºC 50 % rh. (m/m%)	1.21	0.012	0.283	0.012	1.11	0.011	0.12	0.0006

From Table 1 we can state that the moisture up-taking capability of the insulations is increasing with the temperature of the environment, except the armaflex. It is promising that the mineral wool has the lowest moisture contents.

CONCLUSIONS

All current building energy codes and standards require pipe insulation on service hot water and HVAC piping. Requirements vary, but none of the model codes differentiates pipe insulation requirements based on pipe material. In this paper the comparison of effectiveness of different types of insulation as possible pipe covering is presented. As a result, of the thermal conductivity measurements the best insulation capability was reached for the case of the aerogel, while for the moisture up-taking case the mineral wool performed better. After the calculations regarding the surface heat transfer coefficients we found higher values for the cylindrical shapes.

ACKNOWLEDGMENTS

The research was financed by the Higher Education Institutional Excellence Programme of the Ministry of Human Capacities in Hungary, within the framework of the Energetics thematic programme of the University of Debrecen.

REFERENCES

1. Verbai, Z., Csáky, I., Kalmár, F. En. and Build. **135**, 1-9 (2017)
2. L. L. L. Costa, J. U. L. Mendes, Y. R. Paiva, G. P. Oliveira, D. L. Sous, "*Manufacture and analysis of thermophysical properties of thermal insulation for pipes*", 23rd ABCM International Congress of Mechanical Engineering December 6-11, Rio de Janeiro, RJ, Brazil, (2015)
3. A. K. Melikov. R. Cermak, M. Majer, En. and Build.;, **34**: 829-836. (2002)
4. Q. Zeng, R. Zhao, Tsin. Sci. and Techn., **10**, 2: 227-232.(2005)
5. F. Kalmár. J. of Build. Phys. **42** : 2 173-193. , (2017)
6. F. Kalmár, T. Kalmár. En. and Build., 65: 37–44. (2013)
7. Á. Lakatos. En. and Build. **139** 506-516. (2017)
8. F. Szodrai, Á. Lakatos. Int. Rev. Appl. Sci. Eng. **8** 1, 67–73. (2017)

Diagnostics of Health through Prism of Physical Activity Prevention

Elena Bendíková [1,a)] and Mirosława Szark-Eckardt[2)]

[1]*Matej Bel University, Faculty of Arts, Department of physical Education and Sport, Tajovského 40, 974 01 Banská Bystrica, Slovak Republic, EU,*
[2]*Faculty of Physical Education, Health and Tourism at the Kazimierz Wielki University in Bydgoszcz, Sportowa 2, 85-091 Bydgoszcz, Poland*

[a)]Corresponding author: Elena.Bendikova@umb.sk

One of priority tasks, which every person has in a life, is a care for his/ her health. Unlike the past, an emphasis is now increasingly on a personal responsibility for one's own health. While in a past, the health has been determined predominantly by an influence of biological patterns, it is now more and more clearly conditioned by social factors. For the last two decades, we have witnessed an increase in civilization diseases, both in children and adult populations, where early and proper diagnostics with appropriately selected physical activity can be starting point and prevention of the listed situation.

Assoc. Prof. Dr. Elena Bendíková, PhD.

She works at the Department of Physical Education and Sports, Faculty of Arts, Matej Bel University, (Slovakia), where she held the position of associate professor from the year 2013 in the field of Sports Educology as a co-guarantor. She is a lecturer in the Bachelor's and Master´s Degree Programmes with the intension on: Health Physical Education, Methodology and Sports Medicine. Among other she concentrates on Physical Education and Sport at School through the prism of Didactics of Physical Education and Teaching Practice.

Her scientific and research area is focused on improving health and lifestyle, especially in school and adult population through the implementation of physical intervention programmes with preventive and stabilizing character. She has authored and co-authored several books monographs, university textbooks and scientific studies presented and published at national and international level as well as in international indexed journals.

Dr. Mirosława Szark-Eckardt

Master of pedagogy and physical education. Doctorate in Physical Science. Deputy Dean for Didactics of the Faculty of Physical Education, Health and Tourism at the Kazimierz Wielki University in Bydgoszcz.

For over 20 years she has been involved in physical activity in both theoretical and practical terms. The author of more than 130 articles and five publications focusing on physical culture, health and recreation (with particular emphasis on people with different dysfunctions). She has been advocating the idea of a healthy lifestyle on numerous international conferences and national workshops. A member of several national and international scientific societies (i.e. the Polish Association of Anthropological Societies, Fédération Internationale D'Écation Physique).

Measuring Body Composition among Junior Section Schoolchildren in Slovakia

Beáta Dobay

J. Selye University, Faculty of Education,
Bratislavská 3322, 945 01 Komárno, Slovak Republic

Corresponding author e-mail: dobayb@ujs.sk

Abstract: The importance of physical activity is one of the distinguished challenges of the 21st century. Even in kindergarten age, it is very important to get the children to become fond of movement in a playful way. Numerous surveys show obesity among children. Sport, movement is not only a problem for public health but also for education. It contributes to the change in character, which can be positive, and at the same time it can have an effect on the learning skills (Vári, Balázs, Győri 2016). To do so, well qualified Physical Education teachers are needed who promote children to develop habits and healthy self-image and motivate the weak, overweight children (Németh, Költő 2010). In junior section, in Hungary, one of the most important aims is to achieve the proper performance of the movement to be acquired in a playful way. An important element is the pleasurable activity and forming a positive attitude towards movement (http://keretttanterv.ofi.hu). By the end of the junior section the schoolchildren have to be aware of their fitness state and the assessment of their development. In Hungary, this is assured by the introduction of everyday Physical Education lessons and the accompanying testing methods which are aimed at the children's health- and skill centred fitness (Kaj et al. 2014). The Slovakian State Education Program sets out the principles within the Sport and Physical Education subject in the following way - divided into three main parts: health and healthy lifestyle, physical capability and the development of movement skills, sport activity in the lifestyle (state education program - ŠVP). Within the themed units the aim is the acquisition of basic motor skills which include natural movements and fine motor skills. In Slovakia schoolchildren have two Physical Education lessons a week and besides the choice of choosing a sport activity is provided by the school clubs. Nonetheless, the number of obese children has grown significantly for the past few decades. According to Slovakian data the 6-9-year-old children's is 28% (2015/2016, WHO 2017). In Hungary this data is 26, 5% (2015/2016, WHO 2017). In the background of the problem you can find inactivity, low sport activity and besides bad eating habits. Surely, the problem is much more complex there are other determiners to obesity such as environment and genetic makeup. This is why Physical Education in schools has a very important role in prevention meanwhile this is only one among the many possibilities which can help solve the problem in the long term. In the junior section familiarization to motor tests in a playful way is very important (Kaj et al. 2014). It should establish motivating curiosity for tests. They should see the interpretation of the results and the simplified interpretation of the results. In our work out of health centred fitness state we focus on measuring the body composition. By body composition we mean the proportion of fat, water, protein and minerals in the body (Dishman, Heath, Lee 2013). In case of body composition mostly fat mass and lean fat mass is measured (Kenney, Wilmore, Costill 2012). In our case we show the result in body fat percent (%). The unfavourable changes in the results of body composition measuring correlate closely with lower physical activity and malnutrition (Tremblay et al. 2011). Numerous researches point out the fact that high body fat increases the development of heart- and cardiovascular diseases, cancer, type 2 diabetes and can contribute to the development of certain psychological diseases (Katzmazyk, Church, Craig, Bouchard 2009). Obesity can result in numerous cardiovascular problems even in childhood. Body composition has an effect on our state of health the same way as physical fitness. This is the reason why it is important that body composition tests be included in school Physical Education. The NETFIT® test introduced in Hungary show a good example where there are body composition tests as every school is provided with the proper measuring instrument children can be measured with. On this basis we started using a simpler measuring instrument which can be used by any Physical Education teacher. There are several methods to be used for measuring body composition. Out of these Ultra Sound, CT and MRI scanners can give the most accurate results but you need special qualification to use them. You can measure body density under water (densitometry) to define the water content of the body (hydrometrics). To make anthropometrical estimation they use measuring skin fold thickness, the proportion of waist and hip and the determination on the basis of bio impedance theory (Kaj et al. 2014). Naturally, the application of these methods is impracticable on Physical Education lessons this is why we turned to an instrument which is handy. This apparatus is OMRON BF 511. With BMI results we used IOTF limits (Cole, Lobstein 2011) on the basis of which they define age and gender categories in NETFIT® (Joubert 2006). BMI and body fat percentage categories were divided into lean, healthy, development needed and increased development needed zones. The body fat is measured with bio impedance analyser which works on the principle of determining electrical resistance. The electrodes of the device

deliver small so physiologically safe currents into the body. The water content of the body conducts electricity impedance can be measured with OMRON BF511 apparatus so you can estimate what percentage of the body weight is made up of fat (Kyle et al.2004). The first year schoolchildren (aged 6-7) of two Komárno primary schools attended the measuring, the number of schoolchildren was n=108, 83,3% of the parents approved of their children's measurement. Out of this number, this way we managed to measure n=90 (boy n=33, girl n=57). During the measurement we weren't able to measure the body fat percentage or body muscle percentage of n=8,8% unfortunately, the device couldn't defy the data in most cases because of the schoolchildren's low weight but there were cases when the schoolchild couldn't keep the proper static position. Methods: height measurement (stadiometer), weight, BMI, body fat and body muscle (OMRON BF511). The obtained results are as follows (n=90): height: 123cm±13cm, weight: 37.55kg± 19.65kg, BMI: 21.8kg/m^2±8.2kg/m^2. The measuring apparatus was not able to measure 8 children (boy n=3, girl n=5) so n=82, the body fat percentage is 25.7%±17.5%, the body muscle percentage is 25.6%±10.3%. On the basis of BMI 70% (n=63) of the schoolchildren belongs to healthy zone. 21% (n=19) needs improvement and 8.8% (n=8) needs increased improvement. In the case of body fat 45.1% (n=37) of the schoolchildren belongs to the healthy zone, 36.6% (n=30) needs improvement and 18.3% (n=15) needs increased improvement. In BMI and body fat percentage we found the biggest difference in healthy zone where in body fat percentage we got 24.9% (n=26) lower result than that of improvement needed where it is 15.5% (n=11), in increased improvement needed zone it is 9.5% (n=7). Even the obtained results show that regular body composition tests should be included even among junior section schoolchildren. The analysis of the information can help parents and teachers to detect the development of risk factors in children on time. The results obtained during measuring can be the basis of personalized counsel. Our recommendation is that every school have such a simple and handy apparatus we can serve the health of rising generation with the analysis of specific data with.

Key words: physical activity, OMRON BF511, body fat, BMI, healthy zone

INTRODUCTION

Children of the 21st century get a great number of stimuli from their environment during their development. Unfortunately, the technology that is valuable for the mankind discourages exercising at the same time. This is not different with children. From education in kindergarten as exercising and healthy lifestyle must begin to be taught even at this age group in a very conscious way. This is followed by school environment where our research aimed at first grade schoolchildren (aged 6-7). The earlier we pay attention to our children's healthy development, the sooner we can start the conscious education to exercising. Obesity cannot only be seen as aesthetic fault but it is considered to be a promoting factor of developing a disease posing a serious threat to our children (Zuzda et al., 2017a, 2017b). These diseases may occur years later. Obesity increases the risk of the following diseases: heart attack, stroke, fat metabolic disorders, type 2 diabetes, musculoskeletal disorders, sleep disorders and scoliosis. Some of these diseases such as type 2 diabetes, high blood pressure, sugar- or fat metabolic disorder and malignant tumour can more often occur in childhood (Must, Tybor 2005, Gaál-Rodé, 2013; Kurková, Nemček, 2015, 2016; Nemček, 2016). We find it important that emphasis be put on prevention in time, in childhood. In this it can help if teachers are prepared to apply a technical device that can help them with preventing children from obesity. The analysis of the results of BMI and body fat percentage guides us in choosing the adequate movement and getting children to like movement in support of the children's health.

AIM

Our aim is to present the potential of a handy body composition measuring instrument within Physical Education in schools. Another aim is to show how these results help teachers with the health conscious education of children.

METHOD

The review of specialized literature.

Document analysis.

Measuring body height (body height measuring instrument – stadiometer).

OMRON BF511 body composition measuring instrument, measuring weight, BMI, body fat and body muscle. n=90 (boy n=33, girl n=57), age group: 6-year olds.

Preparing charts and tables with Excel program and the analysis of the results.

Subject characteristics

According to Makszin (2014) school changes the child's lifestyle and poses unfamiliar challenges. The development plays a role in formation of intellectual ability and skills. The body proportions change, the age of the first metamorphosis finishes. The growth of the head slows down, the shoulders are broadening, the spinal curvature takes shape and the nascent muscles can be seen. The movement of children is becoming more coordinated. This age is widely called the 'golden age' of motoric skills. The reason for this is that the physiological processes take place in a balanced way (Makszin 2014). We did the measurements in Komarno, Slovakia. The town is located in the south of Slovakia, with its 38,228 population it is considered a medium sized town in the country. The research was made with first year schoolchildren in two primary schools in October 2018. In the measurement 6-7-year old schoolchildren attended with the consent of the institutions and parents. This measurement will be repeated twice: in March and October 2019. The total number in the two schools n=108, the parents consented to the measurement of n=90 children. This is 83.3% of the total number. So n=90 schoolchildren (boys n=33, girls n=57) took part in the research. (Tab. 1). In the school number 1 there are n=53 schoolchildren in the first grade out of whom n=48 children's parents gave consent to the measurement (boys n=16, girls n=32). In the school number 2 there are 55 schoolchildren (out of whom 13 children's parents didn't give their consent to the participation in the research) in the first grade so n=42 schoolchildren (boys n=17, girls n=25) took part in the research.

TABLE 1. The distribution of schoolchildren by school (my own edition)

	School number 1	School number 2	Summer
Boy	16	17	**33**
Girl	32	25	**57**
Total	**48**	**42**	**90**

Measurement Organisation.

Within a week after having been given the institutions' and parents' consent, we carried out the research in mid-October between 15th and 19th in the morning hours. We began with height measurement with the stadiometer fixed on the wall beforehand. We followed with measuring body composition, BMI, body fat percentage and body muscle percentage with OMRON BF511. Each child stood on the measuring instrument in gymnastic clothing barefoot. After each child's measurement the instrument was disinfected. Each schoolchild had a data recording form we recorded the results obtained on (as the research will be resumed twice we will record those results on this form too). This was followed by recording the data with a data management program in a computer

Measurement Taking

With the measurement we introduce the application of OMRON BF511 body composition measuring instrument. We are talking about a handy instrument that can be used on PE lessons in any school. The body composition analysers do not only measure body composition but they also show whether the child's body composition is appropriate to his/her age, sex, weight and height. The simpler so called two-electrode body fat percentage measuring instruments only measure relative fat amount. The instrument gives a result about body fat percentage by measuring the bioelectrical resistance (it leads 50 kHz frequency and weaker than 500 μA electric current through the body). The more serious four-electrode InBody instruments besides defying body composition can diagnose obesity (body mass index and hip to waist ratio) too. They defy basal metabolic energy demand (*BMR basal Metabolic Rate)*, the total water and mineral content of the body and lean body mass. The more modern InBody models defy body composition data not only for the whole body but also separately for the four limbs and the trunk. The software presents the ideal weight and body composition data stored according to the specialized literature specified by sex, age and height and can even suggest an exercise program to reach the ideal data. The everyday application of such more complex instruments is not feasible in schools. This is why we use the easily applicable OMRON BF511 type instrument. Before measuring the instrument was put on hard, flat, level surface. In order to get precise data, we had to enter some data into the display of the instrument. After entering the schoolchild's height, sex and age, the measuring instrument showed 0.0 kg. Then the schoolchildren stood on the sole sensors of the instrument barefoot without any metal objects. Their soles had to be located precisely on the sensors we drew their attention to beforehand. While the instrument defied the weight of the child, we prepared the mobile function

unit we put into the children's two hands after defying their weight. They had to hold their arms forward motionless. This had to be done until the instrument finishes the definition of values. We managed to record weight and then body mass index and body fat percentage and finally resting metabolism on the data recording form. The instrument can measure visceral fat too but as the children didn't have enough weight for the instrument to defy this we couldn't record this data. If the schoolchildren did everything the way they had been instructed beforehand, the measurement didn't last longer than 1 minute. However, there were cases when the instrument sent an error message. Some margins of error can occur: the child's weight is not enough (less than 20 kg), his/her sole is dry (we wet the child's sole), he/she cannot hold the arms forward motionless with the mobile function unit for 20 seconds. In these cases the measurement had to be repeated (Csányi 2014).

Data Analysis

To analyse the results, we used Excel program. We chose this program as nowadays all the teachers can apply this program in their work so it is easy for them to process the results. These result contribute significantly and provide information to the development of their teaching standards. The results of the schoolchildren (n=90) participating in the research are: height: 123cm±13cm, weight: 37.55kg± 19.65kg, BMI value: 21.8kg/m^2±8.2kg/m^2. The measuring instrument couldn't measure 8 schoolchildren (boys n=3, girls n=5) so n=82, body fat percentage: 25.7%±17.5%, body muscle percentage: 25.6%±10.3% (Tab. 2).

TABLE 2. The core values of the schoolchildren

	Height	Weight	BMI	BF%	M%	RM kcal
n=90	123cm ± 13cm	37.55kg ±19.65kg	21.8 kg/m2 ± 8.2kg/m2	25.7%±17.5%	25.6%±10.3%	1213.5kcal±295.5kcal

RESULTS

We begin the presentation of the research results with the results gained from body composition and nutritional profile tests. In our case the average height was 124cm (n=90). In the 1998-1999 academic year they measured 6-year-old children (n=806) in Hungary. The average height with boys was 115.94 cm, with girls 115.39 cm. In 2002, the measured 6-year-old children's (n=819) height was 118.29 cm of boys and 117.75 cm of girls (Farmosi, Gaál 2007 a, b). The difference between the average height of boys and girls was only 0.55-0.54 cm. In the case of schoolchildren participating in our research, the average height of boys (n=33) is 125.7 cm, that of girls (n=57) is 2.7 cm less than that of boys', on the basis of the mean it reached 3 cm. It is clear from the data measured in three different periods that the height rate increased at the given age group. The average weight (n=90) was 26.7 kg, boys 28.1 kg, girls 25.9 kg which is 2.2 kg more. On the basis of the mean the difference between the two sexes is 1.1 kg. As the boys' height is higher, their weight is higher too. On the basis of the measured data by Farmosi, Gaál (2007 a, b) in 1998-1999 the average weight of boys was 20.92 kg, that of girls was 20.89 kg which is 0.03 kg less. In 2002 the average weight of boys was 22.13 kg, that of girls was 21.71 kg (Farmosi, Gaál 2007 a, b). In 2018 the average weight of boys was 28.1 which establishes a link between the increase in height but with physical inactivity too (Table 3).

TABLE 3. The data of the measured schoolchildren's height and weight (own edition)

TOTAL n=90	HEIGHT		WEIGHT	
	BOY n=33	GIRL n=57	BOY n=33	GIRL n=57
AVERAGE	125.7cm	123cm	28.1 kg	25.9kg
MAXIMUM	138cm	136cm	57.2kg	43.1kg
MINIMUM	115cm	112cm	19.5kg	17.9kg
MEDIAN	126cm	123cm	25.7kg	26.8kg

On the basis of the schoolchildren's BMI values 70% of them (n=63) belongs to the healthy zone, 21% (n=19) needs improvement and 8.8% (n=8) needs increased improvement. If we divide these results into sexes, 63.6% of the boys (n=21) while 59.6% of the girls (n=34) belong to the healthy zone which we classified according to NETFIT® (Joubert 2006) categories. Thereafter we had a look at the body fat data. It is surprising that only 41.1% of the children (n=90) fell into the healthy zone, 36.6% of the boys and 40.3% of the girls (Tab. 4). What is interesting is that 5.3% of the girls fell into category slim. The measuring instrument didn't measure 8 children as they didn't reach the required weight. This may occur with 6-year-old children.

TABLE 4. BMI and body fat values divided by sex

CATEGORY	BMI		CATEGORY	BF%	
	BOY n=33	GIRL n=57		BOY n=33	GIRL n=57
UNDERWEIGHT	3 (9%)	5(8.8%)	UNDERWEIGHT		3 (5.3%)
HEALTHY ZÓNE	21 (63.6%)	34(59.6%)	HEALTHY ZÓNE	12 (36.3%)	23 (40.3%)
DEVELOPMENT NEEDED	5 (15.2%)	14 (24.6%)	DEVELOPMENT NEEDED	13 (39.4%)	17 (30%)
INCREASED DEVELOPMENT NEEDED	4 (12.1%)	4 (7%)	INCREASED DEVELOPMENT NEEDED	6 (18.2%)	9 (15.7%)
NO MEASURED DATA			NO MEASURED DATA	3 (9%)	5 (8.7%)

It seems to be interesting that while 70% of BMI results fall into healthy zone, only 41.1% of body fat results is in the same zone. (Chart 1). This is why body fat measuring is becoming more and more widespread. We are trying to bring these simple measuring instruments closer and more available for teachers as this way they can get a more accurate picture of the children's body composition, which can contribute significantly to improve quality in planning Physical Education. The biggest difference in BMI and body fat results was in healthy zone where body fat results were 24.9% (n=26) smaller results comparing it with improvement needed zone where it is 15.5% (n=11) and in increased improvement needed zone it is 9.5% (n=7).

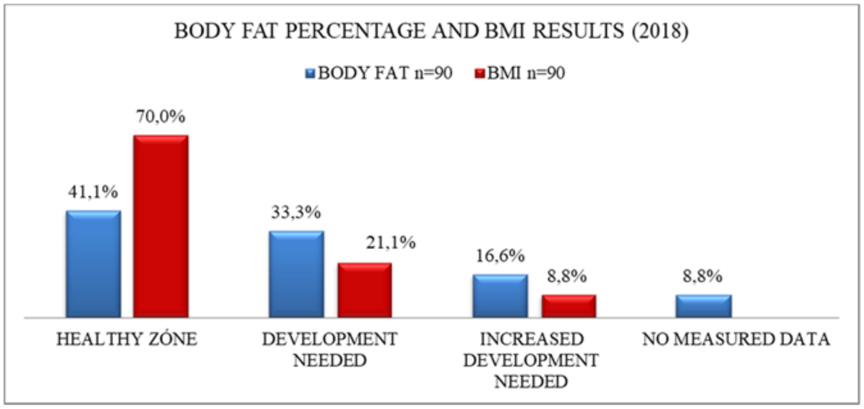

Chart 1 Body fat percentage and BMI results (own edition)

38.8% (n=35) of the measured children's BF (Body Fat) fell into healthy zone, 33.3% (n=30) fell into improvement needed zone and 16.6% (n=15) belonged to increased improvement needed zone. The body fat on average (n=90) was 21.9%, the minimum value was 8.2%, the maximum was 43.2% (Table 5). The maximum value is very high, which can draw the teacher's attention and find a suitable solution together with the parents. The

body muscle average is 27.7%, the maximum value was a girl's 35.9%, which is considered very good, the minimum value was also a girl's 15.3%, which draws the attention of teachers that sports activities should be highlighted and they should take advantage of the sports facilities given by schools (Tab. 5).

TABLE 5. Presentation of BMI and Body Fat Values (own edition)

	BF%			M%			RM kcal		
	School 1 n=48	School 2 n=42	Total n=90	School 1 n=48	School 2 n=42	Total n=90	School 1 n=48	School 2 n=42	Total n=90
average	22.4%	21.3%	21.9%	28.0%	27.3%	27.7%	1082 kcal	1075 kcal	1079 kcal
maximum	43.2%	40.5%	43.2%	35.9%	31.6%	35.9%	1320 kcal	1509 kcal	1509 kcal
minimum	8.2%	8.4%	8.2%	15.3%	21.1%	15.3%	918 kcal	926 kcal	918 kcal
median	21.9%	21.1%	21.7%	28.2%	27.5%	27.8%	1083 kcal	1069 kcal	1071 kcal

DISCUSSION

We would like to draw the attention to a simply applicable measuring instrument which can help not only teachers (Szőköl, 2017) and schoolchildren. It can trigger educational forms that spark the children's interest in their own health. Within the State Education Program one of the main principles of Sport and Physical Education subject tends to health that is health and healthy lifestyle (Ihász, 2013; Szököl, 2015a, b; Bendiková 2016, 2017, 2019) physical capability and motor skills. Moreover, the information can be useful for the parents too (ŠVP, 2014). As it is a very complex matter, parents should be involved in interpreting the results as this way they can follow the changes in their child's body composition. The results can encourage more care to healthy lifestyle. They can ensure more physical activity, proper eating and prevention for their children. The results indicate well that BMI and body fat results are different this is why it would be important that measuring body composition be introduced even in primary schools. In our case 70% of the schoolchildren's BMI belonged to healthy zone but body fat results are not so promising as only 41.1% of the children belonged to healthy zone.

CONCLUSIONS

During our measurement we presented a simply applicable method and instrument for measuring body composition which is available for every school. In education interpreting the results of such measurements helps teachers with their professional educational work (Szőköl, Horváth 2016, Puskás, 2017; Fobel, Fobelová, 2017). This has a model in Hungary as everyday Physical Education was introduced gradually since 2011-2012 academic year (Domokos, 2014) and at the same time NETFIT® measurements (for senior section in primary schools and grammar schools), whose part is measuring body composition. During our research we would like to point out that it is worth focusing on a simple but informative measurement of junior section schoolchildren's body composition with a handy OMRON BF511 instrument. It is noticeable that they detected a correlation between sports activity habits and BMI in the results of both kindergarten (Müller et. al., 2017) and primary school children (Herpainé et. al., 2017). The BMI of children doing sports is more favourable than that of those who do not do any sports activity. In our research we do not cover this topic but in the continuation we would like to observe the coherences. Therefore, measurements are considered important in this process while: "The decisive moment is not the fact that the birth value arises in the centre or on the periphery, but whether it moves with the world. It is about transferring the issue from geographic to socio-psychological soil." (Šenkár, 2017). And that in our case also leads to the student's physical disposition.

REFERENCES

1. Bendíková, E. (2016). *Curricular Transformation of Education in the Field of Physical and Sport Education in Slovakia,* European Journal of Contemporary Education, 18/4, pp.410-417.
2. Bendíková, E. (2017). *Theory of Health, Movement and Lifstyle of Human Beings,* Publisher: University of Debrecen, ISBN 978-963-473-219-8, 42-55.p.

3. Bendíková, E. et al. (2019). Effect of 4-Week Physical Program on Musculoskeletal System in Adolescent Sport Class Students with Focus on Ice Hockey *Physical Activity Review.* 7(1), p. 63-70.
4. Cole, T.J., Lobstein, T. (2012). *Extended international (IOTF) body mass index cut-offs for thinness, overweight and obesity.* Pediatric Obesity. 7. (n4.), 284-294.p.
5. Csányi, T. (2014). *Kézikönyv a Nemzeti egységes Tanulói fittségi teszt (NETFIT) alkalmazásához.* Budapest: Pátria Nyomda Zrt. 2014.,9- 105.o. ISBN: 978-963-08-8654-3
6. Dishman, K., Heath,W.G., Lee,I. (2013). *Physical Activity Epidemiology*. (second edition) Human Kinetics, Champaign, Illionis.
7. Domokos M. (2014) *A testnevelés és sport tanításának módszertana*, ISBN 978-963-306-366-8 http://www.jgypk.hu/tamop13e/tananyag_html/testnevtan/a_mindennapos_testnevels_bevezetse.html
8. Farmosi, I., Gaál, S. (2007a). *Óvodások testi fejlettsége és motorikus teljesítménye*,In. Az óvodai testnevelés alapjai –második bővített kiadás, Valuer Kft., Dunaszerdahely, ISBN 978-80-89234-25-7, 47-76.p.
9. Farmosi, I., Gaál, S. (2007b). *Óvodások kisiskolások testi és mozgásfejlődése*, Dialóg Campus Kiadó, ISBN978 963 7296 88 8,21-35.p.
10. Fobel, P., Fobelová, M. (2017). Happiness as an indicator of social prosperity and sustainability of life, In. *Globálne konteksty poszanowania praw I wolności czlowieka*, N9, 2017, Katedra Stosowanych Nauk Spolecznych WOIZ PŚ, Zabrze. pp. 71-81,
11. Herpainé, L.J.; Simon, I. Á.; Nábrádi, Zs.; Müller, A. (2017) *Családok sportolási szokásainak szocioökonómiai hátterére*, Képzés és gyakorlat: Training and practice 15 : 4 , pp.37-52. , 16 p.
12. Ihász, F. (2013). Egészségmegőrzés, Prevenció, Terheléslélettani alapismeretek, Kiadó: Magyar Sporttudományi Társaság, ISBN 978-963-08-5981-3, 62-68.p.
13. Katzmazyk, P.T., Church, T.S., Craig, C.L., Bouchard, C. (2009). *Sitting time and mortality from all causes, cardiovascular disease, and cancer.* Medicine & Science in Sports & Exersice. 41. N. 5. 998-1005.p.
14. Kaj, M., Csányi,T., Karsai,I., Marton,O. (2014*). Kézikönyv a Nemzeti Egységes Tanulói Fittségi Teszt (NTFIT®) alkalmazásához*, Kiadó: Magyar Diáksport Szövetség, ISBN 978 963 08 8654 3, 14-20 p.
15. Kenney, W.L., Wilmore, H.J., Costill, L.D. (2012). *Physiology of Sport and Exercise*. (fifth edition) Human Kinetics, Champaign, Illionis.
16. Kurková, P., Nemček, D. & Labudová, J. (2015). Pupils with sensory disabilities in Physical Education classes: Attitudes and preferences. *Acta Gymnica, 45*(3), 139–145.
17. Kurková, P., Nemček, D. (2016). Attitudes of students with disabilities towards physical education lessons: Reasons for their indifference and preference for leisure time activities. *Journal of Physical Education and Sport*, *16*(1), 222–229.
18. Kyle, U.G., Bosaeus, I., De Lorenzo, A.D., Deurenberg, P., Elia, M., Gómez, J.M., Heitmann, B.L., Kent-Smith, L., Melchior, J.C., Pirlich, M., Scharfetter, H., Schols, A.M.W.J., Pichard, C. (2004). *Bioelectrical impedance analysis – part I: review of principles and methods.* Clinical Nutrition. 23. N.5, 1226-1243.p.
19. Makszin, I. (2014). *A testnevelés elmélete és módszertana.* Budapest-Pécs: Dialóg Campus Kiadó. ISBN 963931076x, 282.p.
20. Must, A., Tybor,D.J. (2005)Physical activity and sedentary behavior: a review of longitudinal studies of weight and adiposity in youth. International Journal of Obesity. 29. 84-96p.
21. Müller, A.; Bíró, M.; Boda, E.; Herpainé, L. J. (2017) *Az óvodások testtömegének és sportolási szokásainak összefüggései egy egri kutatás tükrében*, Acta Academiae Paedagogicae Agriensis Nova Series: Sectio Sport, 44 pp. 191-203., 13 p.
22. Németh, Á. and Költő,A. (2010). *Serdülőkorú fiatalok egészsége és életmódja* 3: 26. Online http://www.ogyei.hu/anyagok/HBSC_2010.pdf.
23. Nemček, D. (2016). Life satisfaction of people with disabilities: A comparison between active and sedentary individuals. *Journal of Physical Education and Sport*, *16*(2), 1084–1088.
24. 51/2012. (XII.21.). számú EMMI rendelet a kerettantervek kiadásának és jogállásának rendjéről, 1. melléklet: Kerettanterv az általános iskola 1-4.évfolyam. számára, http://keretttanterv.ofi.hu/index.html, letöltve 2014.03.26.

25. Puskás, A. (2017). *Assessing Young Learners in the ELT Classroom*, The Challenges of Alternative Assessment, In: 20. Apáczai-napok Tudományos Konferencia. - Győr : Széchenyi István Egyetem, 2017. - ISBN 978-615-5391-97-2, P. 176-182.
26. Rodé M.., Gaál, A. (2013). *Elhízás és rosszindulatú daganatok,* Magyar Tudomány, ISBN: 978-6155207884, 802-810.p.
27. Šenkár, P. (2017). The Cultural-Pedagogical Aspects of the Regional and the Global (Also Based on the Example of the Slovaks in Romania). In: AD ALTA : Journal of Interdisciplinary Research. 2017, volume 7, issue 2, pp. 191. ISSN 1804-7890.
28. Štátny pedagogický ústav Telesná a športová výchova – pre primárne vzdelávanie – Štátny vzdelávací program Slovenska, 2014 http://www.statpedu.sk/files/sk/svp/inovovany-statny-vzdelavaci-program/inovovany-svp-1.stupen-zs/zdravie-pohyb/telesna-sportova-vychova_pv_2014.pdf
29. Szököl, I. (2015a). Quality management system in educational process. In Gómez Chova, L., López Martínez, I., CandelTorres, I. (eds*.): 8th International Conference of Education, Research and Innovation*. Seville (Spain) : IATED Academy, 2015, p. 7282-7285.
30. Szököl, I. (2015b). Modern elképzelések, szemléletmódok alkamazása a tanításban. In Juhász, GY., Nagy, Á., Stredl, T., Tóth-Bakos, A. (eds.). *Inovácia a kreativita vo vzdelávaní a vede.* Komárno : UJS, 2015, p. 158-162.
31. Szőköl, I. (2017). *The Concepts of Evaluation in Relation to the Concepts of Education* , In: ICERI 2017: Conference Proceedings. - ISBN 978-84-697-6957-7. - ISSN 2340-1095, 7517-7522.p.
32. Szőköl, I., Horváthová, K. (2016) *The dimensions of educational evaluation*, In: Képzés és Gyakorlat - Neveléstudományi folyóirat = Training & Practice - Journal of Educational Sciences. - Évf. 14, n. 3-4, online, p. 247-256. http://www.trainingandpractice.hu/?q=hu/issues/677778735
33. Tremblay, S.M., Leblang, G.A., Kho, E.M., Saunders, T.j., Larouche, R., Colley, R.C., Goldfield,G., Connor Gorber,S. (2011). Systematic review of sedentary behaviour and health indicators in schol-aged cildren and youth.International Journal of Behavioral Nutrition and Physical Activity, 8., 9.n. (89.pub.)
34. Vári, B., Balázs, K., Győri, F. (2016). Mindennapos testnevelésben résztvevő és nem résztvevő általános iskolások koordinációs képességeinek összehasonlító vizsgálata, In. Sports Science Kaleidoscope, Studies and abstracts from the area of sports science research, László Ferenc Sporttudományi Kutatóműhely III.kötet, ISBN 978 963 306 499 3, Szeged 2016, 110-125.p.
35. World Health Organisation (1998). Obesity-preventing and managing the global epidemic. Report of a WHOconsultation on obesity. WHO. Genf.
36. World Health Organisation onlina (2017)http://apps.who.int/gho/data/view.main.BMIPLUS1CREGv?lang=en
37. Zuzda, J.G., Poljanowicz, W., Latosiewicz, R., Borkowski, P., Bierkus ,M., Moska,O., (2017a). Innovative E-Portal for Prevention and Therapeutic Programme for Treatment of the Obesity and Overweight in Health-Tourism. (W:) Proceedings of the International Conference of Computational Methods in Sciences and Engineering 2017 (ICCMSE-2017)(ed.) Simos, T.E., Zacharoula Kalogiratou, Z., Monovasilis T. New York: American Institute of Physics, Book Series: AIP Conference Proceedings Volume: 1906 Article Number: UNSP 180005-1 DOI:10.1063/1.5012458.
38. Zuzda, J.G., Borkowski, P., Poplawska, J., Latosiewicz, R., Moska, E. (2017b). Computer Methods in Designing Tourist Equipment for People with Disabilities,(W:) Proceedings of the International Conference of Computational Methods in Sciences and Engineering 2017 (ICCMSE-2017) (ed.) Simos, T.E., Zacharoula Kalogiratou, Z., Monovasilis T. New York:American Institute of Physics, Book Series: AIP Conference Proceedings Volume: 1906 Article Number: UNSP 180 006-1 DOI: 10.1063/1.5012459.

The Future (Industry 4.0) is Closer than We Think.Will it also be Ethical?

Pavel Fobel[1,a], Aleksandra Kuzior [2,b]

[1]University of Matej Bel in Banská Bystrica, Slovakia
[2] Silesian University of Technology in Gliwice, Poland
[a)]Pavel.Fobel@umb.sk, [b)]aleksandra.kuzior@polsl.pl

Abstract: We live in an era when we are significantly confronted with new social trends which affect the living environment, sustainable life, migration processes, global social changes, and economic innovations, as well as new technologies and more efficient use of artificial intelligence. We perceive the future not only as a scientific and technological challenge, but also as an issue of ethical importance and potential ethical risks. Therefore the civilisation changes, such as the adaptation to the parameters of a new society under Industry 4.0, call for ethical caution and moral sensibility in order to reduce, or even eliminate, potential negative impacts on humans and their existential conditions. The use of robotics and artificial intelligence in various areas, such as in the field of law, education, construction of smart cities or public administration, gene technologies, housing, productivity, social services, industry, and the like also poses a new requirement. For example, the demand will grow for creative people, professionals having understanding for a human in a new environment, in everyday contact with artificial intelligence, new functioning of institutions, business transformation, and the entire social systems. They should be individuals able to response, in a creative manner, to specific situations and needs, new forms of self-realization. There will be a radical change in the area of personalisation, this including both the education and the personalised and individualised service, responses to individual requirements of a citizen, client, or consumer. Modern era was based on mass production and social revolutions. The social changes and shifts in values are mirrored by intellectual authorities, such as G. Lipovetsky who emphasises the necessity to adopt new ethical approach in relation to the new social paradigm. "Postmodern age is obsessed with information and self-expression" (Lipovetsky, 1998, p. 19). Individual ethics will gain its momentum, the ethics of other (third) type will be necessary, e.g. the ethics as presented by G. Lipovetsky: "Our era does not restore the rule of the "good old morality", it abandons it. In this sense, it is not possible to expect any changes of laws, any exploration of new moral values. Its ambition is to participate in solutions and changes, implement mechanisms of ethical prevalence, or the instruments of ethical supervision within social plans being prepared or already implemented.

Its mission is to enrich the dialogue in the area of new trends with ethical questions, to extend the interdisciplinary discourse, to enter the dialogue within innovative projects and be an active player in such dialogues. Each change affects human and human's integrity. Underestimation of professional opinions of ethical nature may generate an irreversible or dangerous situation which could put humans under threat. Solution of consequences without setting responsibilities, assessment of ethical risks may lead to serious social issues and delayed responses which would rather stem from searching of conscience.

What is more, it needs to be emphasised that new technologies are the outcome of scientific production, implementation of science, and are associated with the activities of research teams. And this is the aspect that is pointed out by the representatives of the Technology Assessment concept[1], the importance of applying ethical criteria to technology assessment. The significance and risks of contemporary science are also addressed by Ulrich Beck in his *Risk Society*. It is evident that the issue deserves wide interdisciplinary discourse across all areas aiming to overcome particularised approaches to understanding and solutions of dilemmas. In this interdisciplinary discourse, it is necessary to emphasise the ethical context and value and contextual parameters. Initiatives associated with the transformation to the new paradigm *Industry 4.0* start emerging also in Slovakia. The initiative originated at the Ministry of Economy and was approved by the Slovak Government in October 2018. Action Plan was prepared in cooperation with the representatives of individual departments, industry, associations, and the academic circles. This national concept perceives the process in conjunction with other social components and stakeholders. National strategies and conceptions tend to underestimate the ethical aspect, not taking it as an important part of innovative approaches, mitigation of risks, or prevention. We hold the opinion that Industry 4.0 constitutes a fundamental turning point that deserves ethical appreciation and solutions. The peculiarities of this paradigm should also be explored within ethics and enter, in a constructive manner, the discourse in the area of science and research, both within professional socialisation and within the area of institutionalisation of ethical instruments in order to minimise, to a maximum possible extent, the ethical risks and potential negative consequences of new technologies and use of digital data in relation to customers and partners.

Key Words: Future, Industry, Ethical aspect.

---

[1] *Technology assessment* is a scientific, interactive, and communicative process that aims to contribute to the formation of public and political opinion on societal aspects of science and technology. It is based on the conviction that new developments within, and discoveries by, the scientific community are relevant for the world at large rather than just for the scientific experts themselves, and that technological progress can never be free of ethical implications. As active participants in this dialogue and through coordination of ITAS Karlsruhe (Germany), significant events and specialised interdisciplinary discourses take place within international network.

INTRODUCTION

We live in an era when we are significantly confronted with new social trends which affect the living environment, sustainable life, migration processes, global social changes, and economic innovations, as well as new technologies (Bendíková, 2017) and more efficient use of artificial intelligence. We perceive the future not only as a scientific and technological challenge, but also as an issue of ethical importance and potential ethical risks. Therefore the civilisation changes, such as the adaptation to the parameters of a new society under Industry 4.0, call for ethical caution and moral sensibility in order to reduce, or even eliminate, potential negative impacts on humans and their existential conditions. Discussions about future are vigorous and it's positive that optimistic outlooks and expectations prevail. Representatives of positive and optimistic view of the future also include, for example, the visionary Peter Diamendis who develops initiatives to change sci-fi to reality supporting 20 organisations focusing on future and space colonization, or his cooperation with Elon Musk, Larry Page (Google). Similar attention deserve their existing projects, such as launching the SpaceX Falcon Heavy rocket test or implementation of the intelligent tunnel initiated by E. Musk to be opened in Los Angeles at the end of 2018. This indicates that we are already confronted with future, are going through a thoroughly new experience, and a world of new values.

Industry 4.0 as a New Civilisation and Value Paradigm

It is necessary to emphasise that humans are truly experiencing a new situation and will be (and already is) confronted with these changes and new visions on a daily basis. The adaptation of humans to these changes calls for ethical reflection, ethical preparedness, dispositions to be able to assess social and ethical risks, development of preventive mechanisms to eliminate these risks. The ethical side should not be underestimated when it comes to such changes. On the contrary, it should be beneficial in the context of these changes.

The use of robotics and artificial intelligence in various areas, such as in the field of law, education, construction of smart cities or public administration, gene technologies, housing, productivity, social services, industry, and the like also poses a new requirement. For example, the demand will grow for creative people, professionals having understanding for a human in a new environment, in everyday contact with artificial intelligence, new functioning of institutions, business transformation, and the entire social systems. They should be individuals able to response, in a creative manner, to specific situations and needs, new forms of self-realization. There will be a radical change in the area of personalisation, this including both the education and the personalised and individualised service, responses to individual requirements of a citizen, client, or consumer. Modern era was based on mass production and social revolutions. The social changes and shifts in values are mirrored by intellectual authorities, such as G. Lipovetsky who emphasises the necessity to adopt new ethical approach in relation to the new social paradigm. "Postmodern age is obsessed with information and self-expression" (Lipovetsky, 1998, p. 19). Individual ethics will gain its momentum, the ethics of other (third) type will be necessary, e.g. the ethics as presented by G. Lipovetsky: "Our era does not restore the rule of the "good old morality", it abandons it. In this sense, it is not possible to expect any changes of laws, any exploration of new moral values. They have basically remained the same for centuries and millennia. However, this long-lasting continuity should not wipe away the new relationship to values, new methods of regulation of morality which are so unfamiliar that they represent a totally new period in the history of modern ethics". (Lipovetsky, 1999, p.13)

If we continue to prefer humanity in the new civilisation paradigm, then the question of accessibility and exploitation of technical achievements should remain the same, stemming from imaginative sympathy. This is why it is possible to also agree with the views of P. Staněk and P. Ivanová that the fourth industrial revolution is based "particularly on cognitivity, communicative ability, creativity, humanity, and adaptability. If we take these parameters as qualitative parameters, the humanity itself and also in relation to the human history, neurological system, etc. implicates solidarity, empathy, self-knowledge, individuality, and collectivity." (Staněk, Ivanová, 2017, p.135)

In spite of many positive features of digital society which is described as a society of abundance and better life (P. Daimondis, Michio Kaku), we also need to realise other risks which may gain momentum and have a negative impact on the quality of life. Experts believe that in the new, digitalised community we will be confronted with, for example, a loss of natural ability to interact, with cyber addiction, cyber stress, digital depression, digital insomnia, manipulation or even a massive suicide wave affecting young people (Japan), monitoring of messages by artificial intelligence (Huawey affair), etc. Also the danger of anonymity on social media networks, and blogs will grow, not forgetting the risk of loss of identity. It is probable that they will transform to digital forms of bullying,

cyber harassment, and the like. Therefore we take the initiatives of the European Union to adopt legislative measures in this area as a positive step. Even the ethical attitude to the issue of Industry 4.0 leads us toward adopting an opinion that the "crucial step to making this dream come true lies in the inevitable transformation of ourselves". (Staněk, Ivanová, 2017, p.167)

We have to accept the fact that both the robotics and artificial intelligence are, on one hand, a positive trend and irreversible process of social transformation and, on the other hand, they generate new risks related to new mechanisms of their operation. What is more, the state-of-the-art smart technologies may be used both for good and evil ends; information and technology can be easily misused. This is evident with the use of drones or military technology, protection of information and confidential data. This is also why, besides other important questions, ethical question of security, setting (formulation and control) of ethical limits at development and use of new technologies are one of the key topics in discussions about artificial intelligence. These questions should constitute a prevention algorithm of behaviour of entities.

In this regard, the initiative of Stephen Hawking and Elon Musk, who proposed and implemented 23 principles in association with the development and use of artificial intelligence, principles 6 - 18 directly relating to ethics and values, may be taken as ethically positive. Preferred are such requirements as e.g. security, responsibility, non-subversion, and adherence to human values and needs. The discussions concerning the presentation of Sophia, personalised artificial intelligence, also opened the ethical question of human rights, gender role of robots, or their cultural identity.

It is positive that the ethical side of robots and their integration into various social areas attracts permanent attention. It is also evidenced by e.g. the opinion of James Hughes, Executive Director of the Institute for Ethics and Emerging Technologies who pointed out three most important threshold values in ethics which are purely social and troublesome when talking about robots. For the time being, robots are not able to simulate and show, individually, such human attributes as the ability to perceive pain, they don’t have any conscience, or an ability to be a responsible moral actors.[2]

Ethical Risks in the New Civilisation Paradigm

From its very beginnings, ethics headed towards practical direction and has managed to hold until present the ambition to support and address actual problems, play an active role in ethically disputable ideas, point out unethical behaviour, and ethically troublesome solutions. Its ambition is to participate in solutions and changes, implement mechanisms of ethical prevalence, or the instruments of ethical supervision within social plans being prepared or already implemented.

Its mission is to enrich the dialogue in the area of new trends with ethical questions, to extend the interdisciplinary discourse, to enter the dialogue within innovative projects and be an active player in such dialogues. Each change affects human and human’s integrity. Underestimation of professional opinions of ethical nature may generate an irreversible or dangerous situation which could put humans under threat. Solution of consequences without setting responsibilities, assessment of ethical risks may lead to serious social issues and delayed responses which would rather stem from searching of conscience.

What is more, it needs to be emphasised that new technologies are the outcome of scientific production, implementation of science, and are associated with the activities of research teams. And this is the aspect that is pointed out by the representatives of the Technology Assessment concept[3], the importance of applying ethical criteria to technology assessment. The significance and risks of contemporary science are also addressed by Ulrich Beck in his *Risk Society*. As a renowned diagnostician of the contemporary era, he emphasised the fact that sciences play a central role in the process of modernization and innovation. Unlike in the first modernity, sciences in the risk society (that U. Beck also refers to as "second modernity") are confronted with their own products, results, and deficiencies. Science has thus become the cause of risks and should now assume new responsibility, the

---

[2] Refer to SHOULD WE GIVE AIS THE SAME RIGHTS AS HUMANS? OUR DEFINITION OF “PERSONHOOD" WILL DEFINE FUTURE CIVILIZATION. Available on the Internet on 10/12/ 2018: https://futurism.com/should-we-give-ais-the-same-rights-as-humans

[3] *Technology assessment* is a scientific, interactive, and communicative process that aims to contribute to the formation of public and political opinion on societal aspects of science and technology. It is based on the conviction that new developments within, and discoveries by, the scientific community are relevant for the world at large rather than just for the scientific experts themselves, and that technological progress can never be free of ethical implications. As active participants in this dialogue and through coordination of ITAS Karlsruhe (Germany), significant events and specialised interdisciplinary discourses take place within international network.

responsibility for finding solutions to these risks. While he designates the first wave as "simple scientisation", the second one should go hand in hand with "reflexive scientisation", critical thinking, and ability to identify, critically assess, and address complex issues. The issue of modernisation must be perceived in new relations, within "hyper-complexity", and the risks should be taken as poly-causal phenomena. Therefore our moral mission in science is to overcome resortism, narrow specialisation, and address risks in a wider context. Otherwise, we remain within the boundaries of previous scientific production and generation of more and more risks. An isolated way of thinking remains as important as ever, but it is not able to respond to the adequate risks of modernity anymore. These risks need to be accepted within production of new technologies, we have to realise their impact both on the nature and the humanity.

It is evident that the issue deserves wide interdisciplinary discourse across all areas aiming to overcome particularised approaches to understanding and solutions of dilemmas. In this interdisciplinary discourse, it is necessary to emphasise the ethical context and value and contextual parameters. The application of ethics, its professional and appropriate institutionalisation is a precondition for elimination and minimisation of ethical risks. The implementation of the strategy of smart technologies may be characterised by various dynamics, as well as by social or ecological consequences. Penetration of foreign investors, globalisation in information technologies, application of economic and technological standards in the EU, strengthening of social communication and value environment, implementation of common research projects, and application of new model of companies and institutions indicate that the issues are taking an in-debt form and deserve compatibility of policies and strategies, participatory efforts of stakeholders in these changes, and specific application efforts which allow for the particularities of individual cultures and environments.

From the perspective of ethics, research calls for an analysis of relations between technical, social, and ethical aspects of this process laying emphasis on the specific value and cultural contexts of our society. These qualitative changes will significantly affect humans, their life style, changes at work, but also the communications, health-care and education systems, science and business. Therefore it is important for the research to focus on the assessment of ethical limits of such social changes and propose solutions to eliminate potential risks.

The integration of ethical, value and cultural aspects, and implementation strategies create a prerequisite for a long-lasting responsibility going hand in hand with the idea of responsible innovation which, as a regulatory idea, should accompany production technologies, operation of information networks, economic and social effects. This issue is perceived at an interdisciplinary level and the discourse should take the form of permanent efforts at mastering the complexity of the area.

National Strategy of Smart Industry as an Ethical Challenge?

Initiatives associated with the transformation to the new paradigm *Industry 4.0* start emerging also in Slovakia. The initiative originated at the Ministry of Economy and was approved by the Slovak Government in October 2018. The action plan of Smart Industry of the Slovak Republic[4] introduces a set of 35 measures which should be taken until the end of 2020.

The action plan aims at supporting industrial undertakings, undertakings providing services and trading businesses irrespective of their size focusing on creating better conditions for implementation of digital solutions, innovative solutions, and improving competitiveness by reducing administrative burden, adaptation of legislation, defining standards, change of education programmes and the labour market, by co-funding the research, and the like. It is positive that the Action Plan was prepared in cooperation with the representatives of individual departments, industry, associations, and the academic circles. This national concept perceives the process in conjunction with other social components and stakeholders.

In order to attain these strategic objectives, it set up certain priority areas, research, development and innovations, basic principles of IT security of smart industry implementation, labour market and education, reference architecture, standardisation and development of technical standards, framework European and national legal conditions, including information and propagation.

[4] The entire draft is presented on the official web site of the Slovak Government. Refer to: http://www.rokovania.sk/Rokovanie.aspx/BodRokovaniaDetail?idMaterial=27835

In 2018, a survey was conducted to establish how much has the *Industry 4.0* penetrated into the Slovak undertakings. The survey shows that the proportion of businesses which apply the *Industry 4.0* initiative is growing. However, businesses have not managed to build the organisational and personnel structure for innovation management and implementation of changes. The philosophy of transformation is gradually penetrating also into the corporate culture of businesses and a majority of them takes transformation as an important aspect. On their way, they will also be supported by the action plan of smart industry approved by the Government.
The poll surveying how businesses look at the application of Industry 4.0:

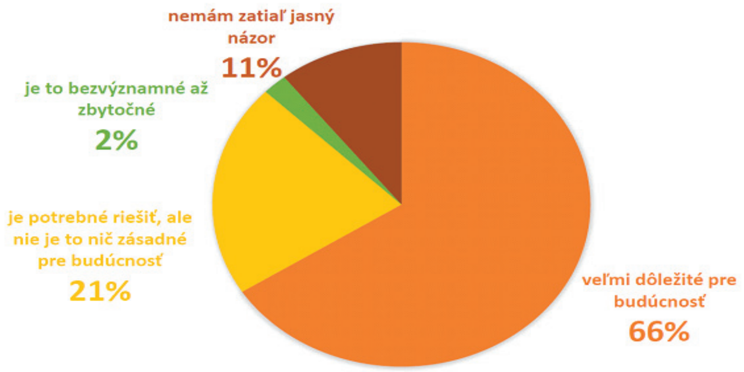

SOURCE: http://www.quark.sk/industry-4-0-na-slovensku/

Legend: *No opinion yet 11%; It is not important and useless 2%, It needs to be addressed, but it's not essential for the future 21%, Very important for the future 66%*

Two thirds of businesses realise the significance of Industry 4.0 applications for their future development. However, a relatively large part of respondents considers the Industry 4.0 applications to be less significant for the future of the company. The Industry 4.0 is still subject to myths and doubts coming from all sides, which also bring attitudes that its importance and impact is not very big for businesses. This is related to the understanding and interpretation of the concept itself, as well as to the failure to capture trends, and to the interpretations in the media and superficial presentations of the topic.

14% of businesses in Slovakia started applying the Industry 4.0 elements. However, more businesses have declared the need for changes. Their proportion changed from the last year's 15% to 31% in this year. This category covers particularly businesses with the Slovak capital. On the contrary, the number of businesses which have not started with the application yet dropped to a half and their proportion changed from 25% in 2017 to 11% in this year. Based on the survey, one third of businesses already have the Industry 4.0 strategy in place; however, the businesses with foreign capital prevail in this category. Businesses are implementing the strategy using predominantly their own resources without external cooperation (60%), only 11% cooperate with external suppliers.[5]

According to the Slovak experts at Industry4UM *"Industry 4.0 is a topic for a majority of businesses, but the stage of its implementation varies. All in all, we may say that businesses gradually start entering the first phases of Industry 4.0 application. Majority of businesses is rather in the phase of implementation of isolated measures focusing on individual optimisation objectives without a more complex strategy."*[6] The survey showed that, on one side, implementation has a progressive trend but, on the other hand, small and medium businesses continue to feel quite uncertain about what the Industry 4.0 implementation truly requires and how to approach it.

National strategies and conceptions tend to underestimate the ethical aspect, not taking it as an important part of innovative approaches, mitigation of risks, or prevention. So far, ethical competence is not perceived as a component part of education, research, implementation processes of smart industry or smart cities.

---

[5] In: PODIEL SLOVENSKÝCH FIRIEM APLIKUJÚCICH INDUSTRY 4.0 RASTIE, ZAVEDENIE FINANČNE PODPORÍ AJ VLÁDA (*SLOVAK BUSINESSES APPLYING INDUSTRY 4.0 STILL GROWING, GOVERNMENT TO PROVIDE FINANCIAL SUPPORT FOR IMPLEMENTATION*). Analytik Industry 4 UM Martin Morháč., Available ont he Internet on 10/12/2018: http://dennikpolitika.sk/archiv/46339
[6] Ibid.

Ethically appropriate could also be, for example, professional cooperation between the private and the academic sectors in research, development and innovations oriented to the Industry 4.0 parameters. It should include assessment and addressing of ethical risks, adoption of ethical standards or formulation of ethical limits (trainings by way of case studies and solution of potential moral dilemmas, searching for and adoption of best practices models based on experience of businesses which were confronted with dilemmas, implementation of ethical prevention and ethical audit, application of ethical instruments in foreign or cutting-edge smart businesses - operation of codes of ethics, commission, methods of human resources activities at selection and adaptation of workers, etc.).

CONCLUSION

We hold the opinion that Industry 4.0 constitutes a fundamental turning point that deserves ethical appreciation and solutions. The peculiarities of this paradigm should also be explored within ethics and enter, in a constructive manner, the discourse in the area of science and research, both within professional socialisation and within the area of institutionalisation of ethical instruments in order to minimise, to a maximum possible extent, the ethical risks and potential negative consequences of new technologies and use of digital data in relation to customers and partners. New ethical responsibility will have to be defined in relation to employees, stakeholders, and the environment. In order to implement these plans, it will be necessary to develop and form new dispositions and new approaches. Our approaches must be innovative, coherent, and appropriate in the context. The participatory role of the applied ethics, ethical consulting, and ethical expertise should be compatible with such unusual requirements and new mission.

ACKNOWLEDGMENTS

The authors would like to thank Agency APVV for their support of the *APVV-17-0400 project „Enhancing the Ethical Environment in Slovakia (Institutional Procedures, Actors, Risks, Strategies)“*. This article was created as part of the project.

REFERENCES

1. Action plan of the intelligent industry of the Slovak Republic. Available on the internet: 10.12.2018: http://www.rokovania.sk/Rokovanie.aspx/BodRokovaniaDetail?idMaterial=27835.
2. Bendíková, E. 2017. Application of multimedia-based exercise programmes focused on improvement of the schoolgirls' musculoskeletal system during breaks between classes. In *ICCMSE-2017 : AIP proceedings of the international conference of computational methods in sciences and engineering 2017*, Thessaloniki, Greece, 21–25 April 2017. Vol. 1906. - 1. ed. - New York : American institute of physics, 2018. - ISBN 978-0-7354-1596-6.
3. Beck. U. (2011). Risk Society. On the way to another modern. Second edition. Sociologické nakladatelství, Praha, 2011.
4. Fobel, P., Banse, G., Kiepas, A. (2001). *Ethics and Information Society*. 2001. B. Bystrica: FHV UMB; 2001. p. 145.
5. Historical moment for humanity. Robot was citizien in South Arabia and the mountained debate wronged on the internet. Available on the internet: 10.12. 2018: https://fontech.startitup.sk/robot-s-umelou-inteligenciou-dostal-obcianstvo/
6. Values, communication, middle. Ladislav Tondl's Selection of Applied Ethics. Compiler: P. Fobel. Vydavateľstvo Univerzity Mateja Bela - Belianum, 2014.
7. Industry 4.0 in Slovakia. 19. Október 2017. In.: QUARK. Magazín o vede a technike. Available on the internet: 10.12. 2018: http://www.quark.sk/industry-4-0-na-slovensku/
8. Lipovetsky, G. (1998). *Era of emptiness. Reflections on contemporary individualism*. Praha: PROSTOR 1998.
9. Lipovetsky, G. (1999). *Dawn of duty*. Praha: Prostor, 1999.
10. Mařík, V. et. al. (2015). *Industry 4.0. Call for the Czech Republic*. Praha: Management Press, 2015.
11. Should we give ais the same rights as humans? Our definition of "personhood" will define future civilization. Available on the internet: 10.12. 2018 : https://futurism.com/should-we-give-ais-the-same-rights-as-humans
12. Staněk, P., Ivanová, P. (2017). *Company 5.0. Economics of the Future?* Bratislava 2017, Wolters Kluwer.

Taking Care of Health in a Society Focused on Productivity and Self-Optimisation - Ethical Values of the Environment

Daniela Fobelová[1,a], Monika Klimentová Fobelová[1,b]

[1]*University of Matej Bel in Banská Bystrica, Slovakia*
[a)]Daniela.Fobelova@umb.sk, [b)]monika.fobelova@gmail.com

Abstract: The paper deals in one of the most important ethical values - health, care for health in a society which focuses on productivity and self-optimisation. Health is not only an invaluable value, but also a moral duty of a post-modern man. In this context, societies have at least two concepts of care for the health of an individual and population: it is the Michel Foucoult's concept of biopower and the Ulrich Beck's concept of risk society. Michel Foucoult perceives health as a technology of disciplined power. Within anatomic politics forming one of the aspects of biopower, Foucoult draws attention to the the creation of docile body as an object of clinical interest under massive assistance of all kinds of examination, testing, monitoring technologies in order to diagnose, create new therapeutic technologies or instruments. In the biopolitics - the other side of biopower - attention turns to the health of the nation, population and, thereby, e.g. to governmental healthcare programmes and social policy. According to M. Foucoult, the state should assume co-responsibility for the health of population and the individual. All of this in exchange for the individual's loss of freedom to care for her own health alone. An opposite trend is represented by the concept of U. Beck of risk society in which author emphasises personal responsibility of the individual for her health without participation of the state. The progress of society goes hand in hand with technological, ecological, and social risks which affect every single individual without exception, these risks are egalitarian, democratic. Health thus becomes a project for the life of each one of us. If we want to accomplish this project, we have to combine it with prevention and, consequently, also with education. Such projects may also fully engage applied ethicists in such sub-disciplinary applied ethics as is social ethics (sports ethics, human rights ethics), or professional ethics (medical, teacher's ethics, ethics of a public or state administration worker, etc.), or the ethics of science and technology, or media (advertising). Health has a human object - body that is the product of genes, i.e. of nature. However, culture pushes it towards perfection, productivity, capability. This dependence of body on culture may also have shady sides e.g. in the form of doping. We are living hyper-consumption times pushing humans not only to massive consumption e.g. of food and subsequent prevention of obesity and cardiovascular diseases, but also to heroic productivity that we aim for in order to touch perfection - simply, we want to be fit. Such behaviour and conduct focuses on attainment of happiness, good or quality life, satisfaction, and better future. This way, we are developing values which could serve as a background for building the ethical environment of a 21st century society. In order to institutionalise ethics in real life, the case study seems to be an appropriate method as a form of qualitative research affecting both education and trainings. One of the grave objectives of case studies in ethics is the increase in ethical sensitivity and, of course, the skills in solving moral dilemmas by way of alternatives with moral justification. Basis for such thinking should be taken from well-balanced (coherent) thinking within some of the generally recognised ethical approaches - normative ethical theories. This method was applied for the presentation of the significance of the bonds between health and the environment.
Key words: Health, Ethical Values, Enviroment.

INTRODUCTION

In the contemporary global world, the focus on health becomes more and more widespread and intensive. Care for health became the main topic of both professional and lay discussions, TV shows, advertisements, sports events, and free-time activities. The topic touching the health is present everywhere and at any time (Dobay, 2015; Bendíková, 2016, 2017; Zuzda et al., 2017). It affects all age groups. It needs to be emphasised that it does not relate to activities which are governed solely by state institutions. The theme of health is penetrating more and more into the industrial sphere, i.e. into the health business. Some are trying to heal people, others bet on prevention getting them only a step from the notion of a healthy life style, good life, quality of life Aristotle used to praise. Health is not only an invaluable value, but also a moral duty of a post-modern man. As G. Lipovetsky says: "The ideal of self-overcoming and victory is not restricted to only some areas of social life, but penetrates the society as a whole and absorbs both the domain of consumption and life styles, both the intimate sphere and the state of mind. Everyone is encouraged to compete, take risks and get to the lead; the trend of productivity is spreading in all directions and the rationality of competitiveness and heading for perfection for the sake of perfection itself are in the lead both in stadiums and in business, both in free time and at schools, both in the sphere of beauty and nutrition, in sex and in

health." (Lipovetsky, 2007, p. 288) It is the cult of health as a duty which emerges before the contemporary individual (Superman, Superwoman) and the society.

Biopower vs. Risk Society in Health Management

The approach to care for health does not have to necessarily depend only on an individual. This may be demonstrated on two well-known concepts - the M. Foucault's concept of biopower and the U. Beck's concept of risk society. M. Foucault presents a concept in which health is viewed as a technology of disciplinary power. M. Foucault refuses classical definition of power that would be held by someone or that would be denied to someone. Power is, in his view, dispersed in the society and we may see it as a network of relationships. Biopower is a modern form of power oriented on life. One side (pole) is formed by anatomic politics, the role of which is to create a docile body as an object of clinical interest. It constitutes a form of various techniques of examination, testing, monitoring in order to diagnose, develop new therapeutic techniques or instruments (from stethoscope to magnetic resonance) on an individual body. In biopolitics (the second pole of piopower), attention concentrates on the health of a nation, population. It monitors therapeutic and administrative methods of health care in a state (governmental programmes of health-care and social policy - vaccination, care for newborns, senior people, homeless individuals, etc.). The goal of biopolitics is to create a society of prosperity and security (welfare society) with a system of general public health care. Another side of such care, safety, and certainty is the loss of freedom, because the society must be controlled. Safety is conditioned by docility, subordination to disciplinary power. It deprives an individual of her autonomy and freedom to play an active role in her own life. In the M. Foucault's concept, biopower relies on the responsibility of the individual for her health under full co-responsibility of the state for the health of population she is a part of. In the 1980s, Ulrich Beck introduces his concept under the title of risk society, meaning a society which threatens itself. "The supranational nature of impossibility to cope with modernisation risks corresponds to the method of their spreading. Their invisibility hardly leaves an open space for decision, at least for the consumer. They are "products carried as burdens" that we co-swallow and co-inhale. They are "free riders" of normal consumerism. They travel with the wind and water. They may be hidden in anything and with that which is the most important for life - with air that we breath, with food, clothes, furniture, etc. - they penetrate into all otherwise so strictly controlled protection zones of modernity." (Beck, 2004, p. 53) Success (progress) of society goes hand in hand with technological, ecological, and social risks. Such risks affect everyone without exception, they are egalitarian, democratic. They do not respect social structures. "Poverty is hierarchical, while smog is democratic. Spreading of modernisation risks - threat to nature, health, nutrition, etc. - makes the social differences and boundaries relative." (Beck, 2004, p. 47) Forced individualisation in the risk society indicates that an individual is a specific product of social development. Freedom of choice is understood as an individual strategy of life. Infrastructures of education, health care, social law, etc. support freedom of choice of the members of the society. The management or risks and crises depends on setting the boundaries - limits. Risk society is a society which supports free market, deregulation of all areas of the life of humans and society, trying to get free from responsibility (co-responsibility) for the life of people. An individual is challenged to assume responsibility for herself (and for her health) and thus also take power over herself. The state gets rid of co-responsibility, at least until the moment when the population is exposed to a health risk (e.g. in the event of pandemic). If we assume that individuals (we cannot say what percentage of the citizens of a society it will be!?) are the ones who hold the responsibility relation to their health, because this is the imperative of our times - cult of health, then we have to say that we will witness the development, creation of strong self-discipline. Health, being healthy is a factor that is supposed to be in our hands, provided that we live a healthy life style, eat healthy, move, work out, but also extend our knowledge in this field. Health is becoming our life-long project. We can already monitor on our own, without the need to consult specialists, e.g. pressure, sugar, using our own instruments.

The responsibility or co-responsibility for health is bound up with prevention, that is with education. As many specialists point out, this is the space for those who co-participate in the creation of a good life, quality of life, healthy life - applied ethicists by way of sub-disciplines of applied ethics (sports ethics, human rights ethics as part of the social ethics, medical ethics as part of the professional ethics, ethics of science and technology, or ethics of media). Our healthy body is what we have inherited, a product of genes and not the society. What influences our body is the pressure of the society that declares that which is to be considered to be the correct healthy model of our body. In order to have a healthy body, we have to look at it as at a task in the sense of everyday care for the body. At certain stage of the evolution of society when norms for the desirable "form" of body and conduct (not just election of miss) were established, we do see a motivation to make our bodies perfect in the sense of a duty. Being fit. Those

who do not do their best to approach this "perfection" are condemned, discriminated, pushed away by the society. This may arouse a feeling of shame, humiliation.

"While everything else is changing, our bodies will remain with us until the end of our days." (Bauman, 2004, p. 122) As Z. Bauman asserts, the care for health must not be confused with the fitness of body. "Taking care of health means that we maintain the body in a normal and functional condition...
The ideal of fitness is a body as a means to gain experiences which make life joyful, entertaining, exciting or, to put it simply, pleasant." (Bauman, 2004, p. 126) However, fitness needs to be showed, e.g. by wearing sports clothing and running shoes, or cycling clothing, or by working out in a gym. Such articles need to be purchased in brand stores.

Much more arguable are the discussions on the topic when: "Superman changes to a "mobile pharmacy". Superman is shining in glory on stadium tracks as a celebration of physical balance and perfect health, although, in real life, it is equally vulnerable, shaking and left at the mercy of addictions just like Narcissus." (Lipovetsky, 2007, p. 301) The performance which drives the athlete is so strong that if the athlete wants to keep the step she has to turn to doping (unpermitted will to victory"). As Lipovetsky says, one of the major features of hyper-consumer society and the related hyper-individualism is the desire to physical performance and Stakhanov-like activism in direct relation to a puritan scales of values.

Author argues with these well-known theses and evidences it referring to huge campaigns to prevent obesity and cardiovascular diseases. Rather, he draws attention to the motives that lead people to doing sports for fun or to live healthy, such as the efforts to keep fit, hygiene of life, joy of discovering one's own body, relax, contact with nature and other people. "A hyper-modern athlete is obsessed with attainments, her primary goal is to be fit and feel good or better. What is decisive here are not the values of heroism, but dispersion, the effort to keep up one's strength and achieve inner balance." (Lipovetsky, 2007, p. 305) It is an expression of social ideal of satisfaction in compliance with the WHO's definition of health - as a condition of thorough physical, mental, and social satisfaction. A. Kuzior emphasises that in the contemporary global world "the quality of life is based on the health of ecosystems, but the quality of human life is also influenced by other aspects, such as: providing for basic needs (life, food, hygiene, housing, efficient law, transfer of science and innovative technologies, access to information, access to culture and education, participatory model of decision-making, securing fundamental rights and freedoms. High quality of life of a particular human is conditioned by personal safety." (Kuzior, 2014, p. 76-77) The "health" of human and of the living environment constitute necessary conditions of good life.

The "life" of human and nature, i.e. good vs. hyper-consumer society, i.e. rich life?

In connection with institutionalisation of ethics in real life, the case study seems to be an appropriate method as a form of qualitative research both for education and trainings. The stakeholders in the case study must concentrate on the understanding of the case at hand, analyse the relationships, as well as foresee the probability of the result of various solutions of the relevant case and the moral choice with the corresponding argumentation as an optimum solution for ethical decision. This should result in a paradigmatic situation of the relevant case study. Paradigm cases become paradigms when there exists certain link between them and generally valid values; when the link is maintained during transition from one case to another, then individual cases must be related through one or several values. What is more, if someone identifies the case as a paradigm, it means that she accepts any of the principles or values which allow paradigms to be transferred also to other cases." (Fobel, 2011, p. 13)

A story of a young family unfolds in a distant corner of a country with a picturesque natural scenery. A young couple, Adam and Eva, decided to move to and live at the Silver Lake due to the reasons that start tormenting civilised communities. They were looking for clean natural environment for their new family situation - raising of their 6-months old daughter Theresa. They took out a mortgage to buy a new apartment. Little Theresa's father, a biochemist, found employment in a nearby small business dealing in chemical production of cleaning agents. Adam is satisfied with his family and his job. Adam's wife takes care of little Theresa until she, as a graduate teacher, will be able to replace the teacher at the day care. Everything goes as planned and they live a peaceful life. However, this perfect picture of a happy life comes to an end when Theresa is diagnosed a kidney cancer. All their plans suddenly collapse. Hopeless parents try to find a cause in family history. But doctors give them, as if by the way, some information about the situation at the Silver Lake. And that situation takes them aback. During the past three years, little Theresa has not been the only one to fall ill with cancer, there is a much greater group of both children and adults who were diagnosed similar disease. Also increased numbers of miscarriage and birth defects have been reported. The young couple, Adam and Eva, were not satisfied with the passivity of doctors and the entire medical

staff. They could do nothing but use elimination method to identify the causes. Whereas there is a larger number of "victims", it seems that the cause of the disease is external. Adam, a graduate of biochemistry, searched for causes in air, in soil, and in water. His colleagues from the university helped him, and the Silver Lake, and particularly its ground water, unveiled horrible secrets. Water, the drinking water, contained mercury. The results of his investigations led him to the only possible polluter - it was the chemical plant in which he worked. There he quite easily found out, to his horror, that the employees responsible for transport of waste have made their work simpler by taking the waste to an illegal dump close to the drinking water source. And they have been doing it only to save money of the plant! At this moment, Adam faces a moral dilemma. What should he do now? He consults the findings with his wife Eva. They found out that it is not just about them and their Theresa, but that the threat potentially applies to everyone living at the Silver Lake. The first step led to the responsible Environment Management of the plant who did not deny anything, but neither did he plan to howsoever address the issue. And he gave advice to Adam to do it the same way, in order to be able to repay the mortgage. If he lost his job, that would be a great trouble.

Hypothesis: Let's assume that Adam, with the help of his wife Eva, does not give up and will continue to argue with the plant that employs him about a just solution of the dangerous situation at the Silver Lake, a solution that would not harm the health of people or the nature and will fight the battle for everyone else.

Alternatives:

1. Adam gives notice of termination of his employment and then files an action against the plant with a court due to violation of the waste act.
2. Adam gives notice of termination and moves with his family away to a different region.
3. Adam, after his discussion with the environment manager, leaves things as they are in fear of the loss of employment.
4. Adam does not get scared, he does not terminate his employment, and reports the plant's illegal practices.

Moral consequences of individual alternatives:

The first alternative is a solution which is more lawful than moral. From the perspective of ethics of responsibility, the young family with Adam in the lead would act irresponsibly (who, for what, to whom, according to which criteria), because they would lose the source of subsistence, mortgage and, eventually, also the treatment for their little daughter. This solution would neither be in line with the virtues ethics, because Adam would not have finance to cover court costs. From the perspective of utilitarianism, this solution would not be to the benefit of anyone.

The second alternative is contrary to the hypothesis, because it is absolutely egoistic and does not take into consideration other children and adults, and so it is neither in line with the virtues ethics, nor the ethics of responsibility (who, for what, to whom, according to which criteria), or utilitarianism, because no one would benefit from it.

The third alternative demonstrates cowardice, fear, and retreat in contrast with the value ethics, and would lead Adam to, on one hand, personally and, on the other hand, to locally unacceptable situation, which would be irresponsible in the sense of the ethics of responsibility. The aspect of the rules of duty-based ethics - the categorical imperative of unconditional action, would not be fulfilled.

The fourth alternative represents Adam's active conduct in line with the norms of the virtue ethics (courage, justice). The same also applies to the components of the ethics of responsibility or the utilitarian ethics.

Solution of the moral dilemma:

From the perspective of normative ethical theories, we consider the fourth alternative as an optimum solution of this dilemma. It is also known as whistleblowing, which is an ethical instrument to remedy injustice, harmful conduct, unlawful behaviour (whistleblower is a person who exposes an activity that is deemed unfair). In order to accept whistleblowing as an ethical instrument, it must meet five moral requirements which will make it morally justified for taking action.

The situation which takes place once the information is published will change the plant's approach to the solution of ground water pollution caused by waste generated in production. The next step will lead to dump removal and cleaning of the site. It is clear that also the financial side of the activity would be covered by the plant. It is very probable that the finance used may (but do not have to, if the plant meets CSR) result in the need for lay offs. In such event, it should be emphasised that Slovakia has passed a law to protect whistleblowers, and so Adam

should not worry that he could lose his job. This story indicates that citizens always have a choice to take care of their health by protecting the environment. We have to have a lot of courage to be able to process the direct proportion - decrease in job positions as a consequence of the finance used - but in exchange for a huge achievement - restoration of a clean, healthy environment for people, animals, vegetation. From the perspective of utilitarian ethics, this solution will benefit everyone in the plant as well as the environment, by which we mean not only people, but also the fauna and flora. It is the duty of people to embrace norms which will contribute to the maximisation of happiness with respect to future generations.

From the perspective of the duty-based ethics, it is Adam and his wife who are obliged to take this step in order to prevent pollution of the environment and safeguard health for citizens. It was the duty of the affected environment managers to act, from the very beginning, in line with CSR (social responsibility) and the ISO quality standards. Adam and Eva (who is responsible) should take responsible action in relation to the health of both their child and other citizens (to whom are they responsible?). Responsible conduct is triggered by irresponsible response of environment managers in the plant which pollutes ground water (for what?) and affect thus the healthy life of people under certain standards (responsibility criteria). The choice to inform the public is in line with the ethics of responsibility also because some of the employees at the plant were influenced and acted in an illegal way by dumping the waste in nature. It is most difficult to assess this situation from the perspective of virtues ethics, because it concerns mainly the process of acquiring a habit to do good for all and refuse evil in the form of pollution of the environment. Adam's justification of his position started with the ethics of discourse, i.e. even though this ethical norm was not successful at the beginning, communication was gradually renewed and the situation got better.

The hypothesis was proved true by way of using normative ethical theories.

CONCLUSION

In spite of prevailing economic indicators of social dynamics and performance of businesses, a society focused on productivity and self-optimisation sees gradual assertion of other than just economic indicators... "Happiness is one of the main goals of the life of every human, but also a means to find balance between the economic growth and its impact on the society and the environment." (Fobel, Fobelová, M., 2017, p. 72)

Only in this society may human reach satisfaction, harmony and good conditions for development of an ethical environment. "We may agree with the assertion that application of this indicator (happiness) in human life may mobilise us to create better future, better quality of life and its sustainability." (Fobel, Fobelová, M., 2017, s. 77)

Ethical values to create better life and moral environment need a lot of time to form.

ACKNOWLEDGMENTS

The authors would like to thank Agency APVV for their support of the *APVV-17-0400 project „Enhancing the Ethical Environment in Slovakia (Institutional Procedures, Actors, Risks, Strategies)"*. This article was created as part of the project.

REFERENCES

1. Bauerlein, M. (2010). The brightest generation. As a diginat, it frightens young Americans and threatens our future or never anyone under 30, Bratislava, the SSS edition looks horizontally.
2. Bauman, Z. (1995). Postmodern Body Accidents, In: Reflections on Postmodern Time, pp. 61-88.
3. Bauman, Z., May, T. (2010). Think sociologically. Unconventional testimony to sociology, 2010, Prague, Slon.
4. Beck, U. (2004). Risk, Risk Society. On the way to other modern, 2004, Prague, Slon.
5. Bendíková, E. (2016). Curricular transformation of education in the field of physical and sport education in Slovakia. *European Journal of Contemporary Education*, *18*(4), p. 410 -417.
6. Bendíková, E. (2017). Application of multimedia-based exercise programmes focused on improvement of the schoolgirls' musculoskeletal system during breaks between classes. In *ICCMSE-2017 : AIP proceedings of the international conference of computational methods in sciences and engineering 2017*, Thessaloniki, Greece, 21–25 April 2017. Vol. 1906. - 1. ed. - New York : American institute of physics, 2018. - ISBN 978-0-7354-1596-6.
7. Dobay, B. 2015. *Az iskolai sporttanfolyamok motivációs hatása a felnıttkori rekreációs sporttevékenységekre Dél-Szlovákiában*. Komárom: Kompress kiadó.

8. Fobel, P., Fobelová, M. (2017). Happiness as an indicator of social prosperity and sustainability of life, pp. 71-81, In. *Globálne konteksty poszanowania praw I wolności czlowieka*, N9, 2017, Katedra Stosowanych Nauk Spolecznych WOIZ PŚ, Zabrze.
9. Fobel, P. (2011). The importance of caseality for applied ethics, pp. 7-29. In. Case - application - ethics. Banská Bystrica, Matej Bel University, Faculty of Humanities.
10. Fobelová, D. (2011). Case Study as Learning Methods in Applied Ethics, pp.83-101. In. *Case - application - ethics.* Banská Bystrica, Matej Bel University, Faculty of Humanities.
11. Fobelová, D. (2011). The importance of caseality in the preparation of applied ethics, In. Applied ethics and professional practice, 2011, Banská Bystrica, Matej Bel University, Faculty of Humanities.
12. Foucault, M. (2000). Power, subject and sexuality, Bratislava, Kalligram, 2000.
13. Kuzior, A. (2014). *Axiology of sustainable development*. Bellianum, Banská Bystrica, Matej Bel University, Faculty of Arts.
14. Lipovetsky, G. (2007). Paradoxical Happiness, Essay on Hyperconsuming Society, 2007, Prague, Prostor.
15. Zuzda, J.G., Borkowski, P., Poplawska, J., Latosiewicz, R., Moska, E. (2017). Computer Methods in Designing Tourist Equipment for People with Disabilities,(W:) *Proceedings of the International Conference of Computational Methods in Sciences and Engineering 2017* (ICCMSE-2017) (ed.) Simos, T.E., Zacharoula Kalogiratou, Z., Monovasilis T. New York:American Institute of Physics, Book Series: AIP Conference Proceedings Volume: 1906 Article Number: UNSP 180 006-1 DOI: 10.1063/1.5012459.

Selected Time Space Characteristics in Female Pole Vault

Peter Krska

Faculty of Education, Catholic University, 034 01 Ruzomberok, Slovakia

Corresponding author: peter.krska@ku.sk

Abstract: This research is stressed at time and space characteristics (centre of gravity movements) in female pole vault. Kinetic parameters were gained by two-dimension analyser Consport Motion Analysis System (CMAS). There are involved 19 female pole vault jumpers with sport performance 380 – 483 cm, divided on 2 different groups; higher and lower level from the point of sport performance. We found that in time parameters reached better results high performance level jumpers in phases hanging and lifting. It is coursed by better transmission on pole after take-off and by better work on the pole. As for the centre of gravity the jumpers of higher performance reached higher growth in all phases. The most significant difference can be seen in phase of lifting. Comparison of time and space characteristics enable to show the way for technique improvement in female pole-vault.
Key words: female pole vault, rhythm of the jump, centre of gravity height, two-dimension analysis

INTRODUCTION

Pole vault is the only athletic event in which the performance is reached with use of tool. The pole use put this event away from fundamental locomotion and adjoins it to complex athletic events. The movement activity is realised in two basic parts; the first is approach ended with take-off and the second is the movement of jumper on the pole. The approach has cyclical movement structure and it is influenced with both arm holding, bearing and displacing pole. The movement activity on the pole has on the contrary acyclic character and it represents the structure of shifting movements in front and upside position at parallel rotation round horizontal and vertical body axes and round pole and that is performed at optimal time sequence – rhythm Bojko - Nikonov, 1989; Grabner, 1997; Mcginnis, 1997; Krška – Koštial, 2000; Krška, 2008; Vespalec, 2013.

Pole vault sport performance structure is relatively very complicated from the point of view of biomechanical parameters. On the bases of two-dimension (2-D) analyse of group of female pole vault jumpers, Krška (2008) prepared by multiple correlation and regression analysis, where 76 variables were entering into process, the model of sport performance structure (fig 1).

We can see that 1st level is formed by two decisive variables: absolute grip (distance between bottom of the pole and hand grip of upper arm) and standing over (it means distance of the centre of gravity over hand grip). In the 2nd and 3rd level we can find mostly speed, angle, time (duration of single jump phases) and centre of gravity movement (space) parameters (tab 1). Those are the most usable factors from the point of technique improvement in training process.

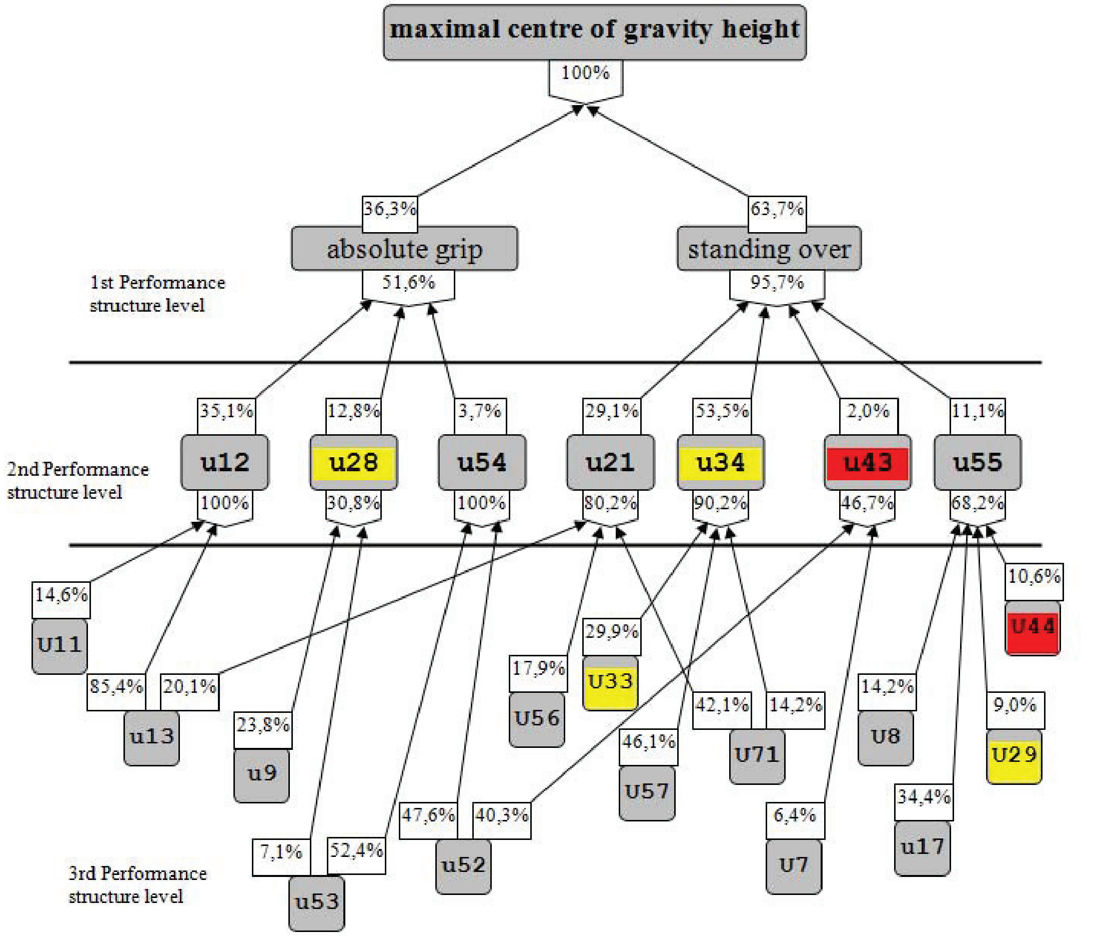

FIGURE 1 Female pole vault sport performance structure (KRSKA, 2008)
Legend: Time parameters Space parameters

TABLE 1. Selected speed, angle, time and centre of gravity movement parameters in sport performance structure

Horizontal speed of centre of gravity at moment of	
u11	Tread-down on take-off
u12	End of take-off
u13	Speed lost during take-off
Vertical speed of centre of gravity at the end of	
u17	Hanging position
u21	Pull with turn
Angle Parameters	
u52	angle of tread-down of take-off
u53	angle of take-off
u54	operating angle during take-off
u55	climb angle

TABLE 1. Continued

u56	angle between body and vertical line at moment of straightening up end
u57	angle between body and vertical line at moment of pull with turn end
Centre of gravity height at moment of end of	
u28	Take-off
u29	Hanging
u33	Pull with turn
u34	Lifting
Time duration of	
u43	Take-off
u44	Hanging

In this contribution we will analyse parameters of time duration and centre of gravity movements of single jump phases.

OBJECTIVES

In this contribution we want to analyse selected time and space female pole vault characteristics on two different sport performance level groups and thus reveal relations between sport performance and technique mastery.

MATERIAL AND METHODS

This research was performed in on the meetings Golden spiked shoes in Ostrava, Czech Republic. Our kinematic parameters were gained by two-dimension analyser Consport Motion Analysis System (CMAS). There are involved 19 female pole-vaulters with the sport performance 380 – 483 cm. All watched top-level female pole-vaulters (group S) were divided on 2 smaller groups; lower sport performance group (S1) and higher sport performance group (S2). Fundamental statistical characteristics can be seen in table 2.

TABLE 2. Statistical characteristic of kinetic parameters of involved groups S, S1 ans S3

Whole group S; sport performance 380 – 483 cm; n=19		[unit]	x	x_{max}	x_{min}	s
u1	Maximal centre of gravity height	[cm]	448.03	490.50	408.10	23.07
u2	Absolute height of upper arm grip	[cm]	403.11	420.00	385.00	10.86
u3	Standing over (peak height)	[cm]	44.92	70.50	11.20	16.24
Lower sport performance group S1; 380 – 430 cm; n=9		[unit]	X	x_{max}	x_{min}	s
u1	Maximal centre of gravity height	[cm]	428.36	441.14	408.10	12.28
u2	Absolute height of upper arm grip	[cm]	395,89	406.00	385.00	6.81
u3	Standing over (peak height)	[cm]	32.47	49.10	11.20	10.83
Higher sport performance group S2; 440 – 483 cm; n=10		[unit]	x	x_{max}	x_{min}	s
u1	Maximal centre of gravity height	[cm]	465.73	490.50	449.30	13.98
u2	Absolute height of upper arm grip	[cm]	409.60	420.00	395.00	9.79
u3	Standing over (peak height)	[cm]	56.13	70.50	33.30	11.35

In this contribution we analyse all technique pole-vault phases (take-off, hanging, swinging, roll up, straitening up, pull with turn, lifting and bar crossing) that were assessed from the point of their time durations and of centre of gravity (CGv) motions. For better clearness we used bar charts in absolute eventually in relative values with distinctive colours. In order to be able to follow all decisive phases we also use illustrative figures with border positions (fig 2 – 9).

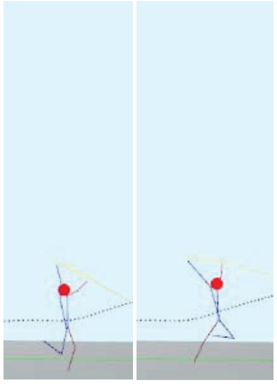

FIGURE 2. Border positions of take-off phase

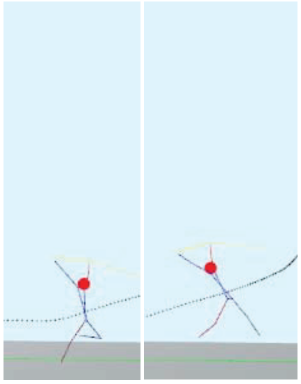

FIGURE 3. Border positions of hanging phase

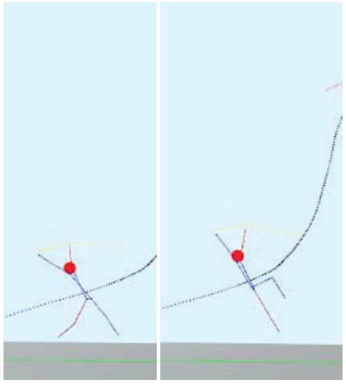

FIGURE 4. Border positions of swinging phase

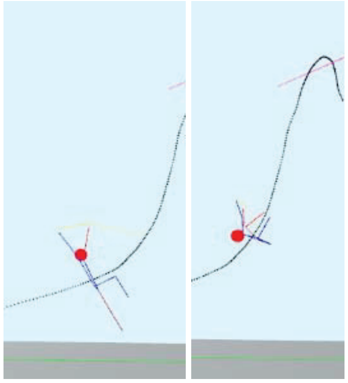

FIGURE 5. Border positions of roll up phase

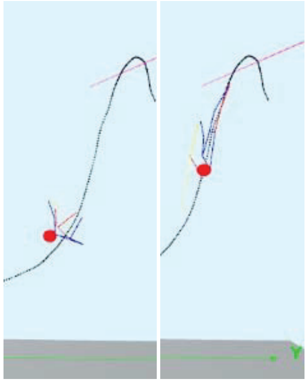

FIGURE 6. Border positions of straitening up phase

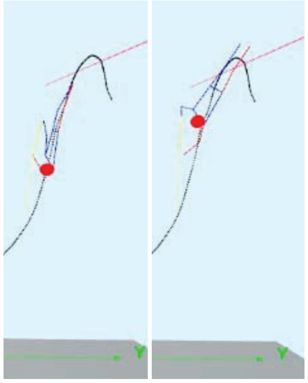

FIGURE 7. Border positions of pull with turn phase

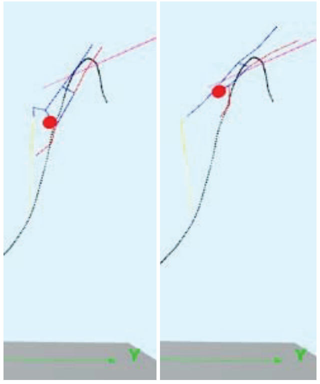

FIGURE 8. Border positions of lifting phase

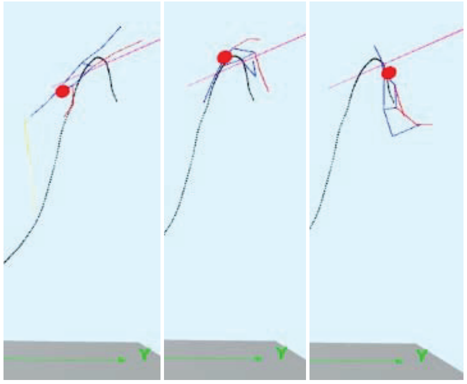

FIGURE 9. Border positions of bar crossing phase

For pedagogical interpretation we used logical methods, mostly analyse, comparison, deduction and generalisation.

RESULTS AND DISCUSSION

Absolute and relative time duration of single phases can be seen in fig 10 and 11.

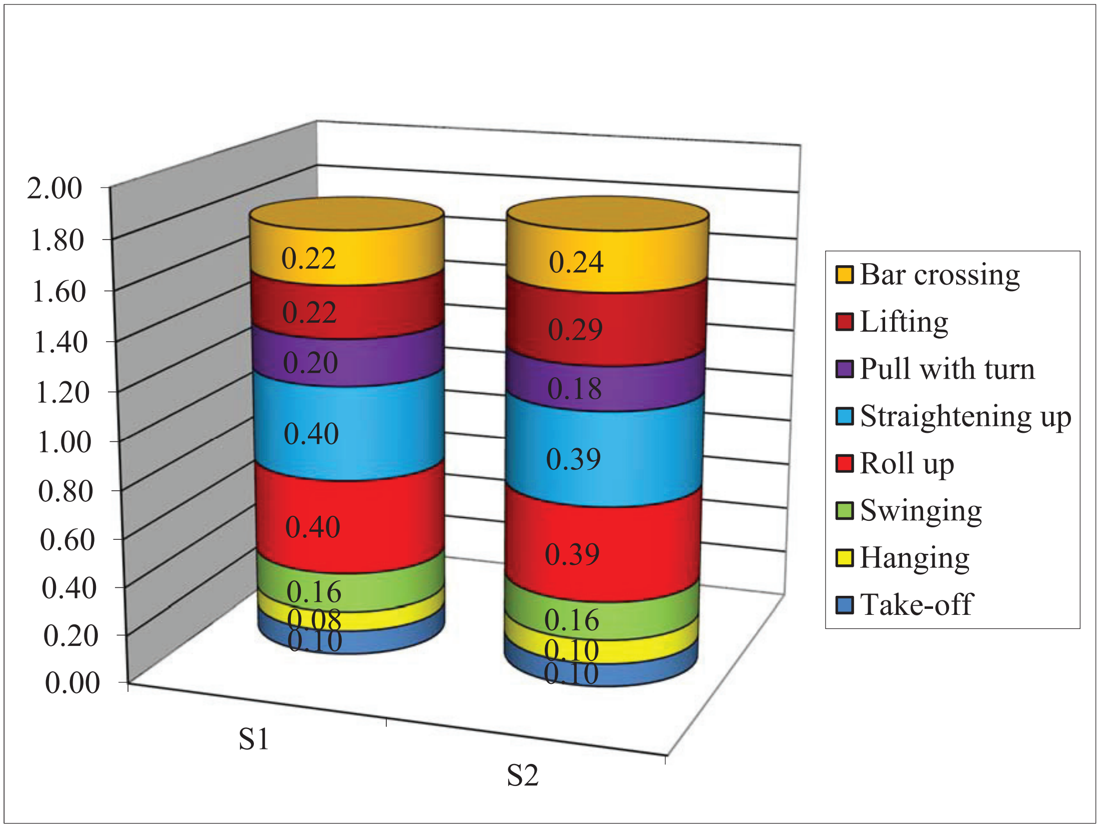

FIGURE 10 Comparison of single phases during jumps

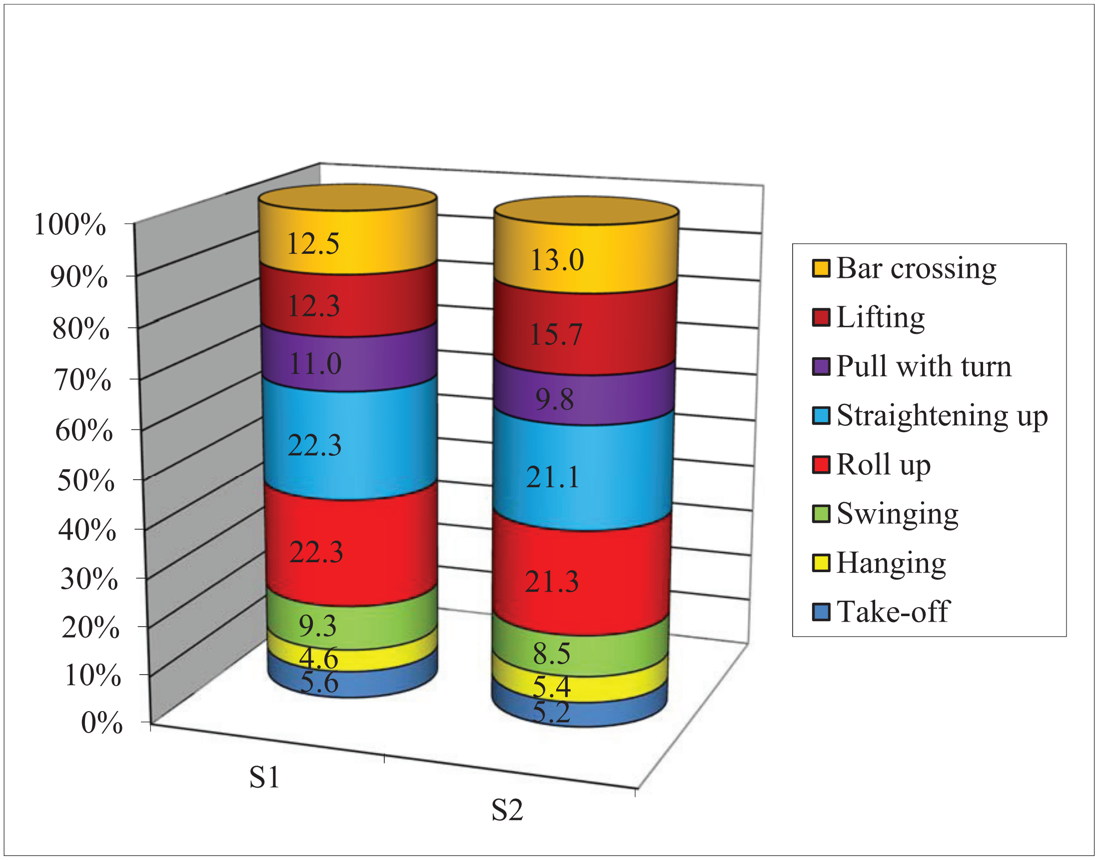

FIGURE 11. Percentage comparison of time phases duration during jumps

Our female pole-vault jumpers needed in average 1.68s in S1 and 1.75s in S2 group, in order to perform movement activity on pole from the end of take-off till crossing bar plane with the whole body. The average total time was slightly different in favour higher sport performance level group – S2. The total time is up to certain level also influenced with suitable stands setting.

Comparison of single phases of our two groups S1 and S2 shows that there are only few differences, though the average sport performance difference is relatively great – over 37 cm. The first substantial difference according our view is in the phase of hanging, in which the difference is 0.02 s (relatively 0.08%) in favour of S2 group. These 0.02s of longer duration in hanging phase enables to bend over the pole stronger and thus use better the potential of pole elasticity and accumulate in this phase more kinetic energy in pole bending that can be availed during following phases of jump.

Further differences are watched mainly in phases pull with turn, lifting and bar crossing. In the phase pull with turn we can see that S1 group has longer duration time; together with the lower centre of gravity increase (CGv) in this phase (fig 13) we can state that here in this phase is already manifested faster and stronger pole straightening that courses faster centre of gravity vertical speed (KRSKA – SEDLACEK – KOSTIAL, 2014) of S2 group; higher CGv speed courses shorter pull with turn phase duration. The greatest difference in time duration can be seen in the phase of lifting in favour of S2 group. The average difference is 0.07 s. This longer time phase duration we consider like positive for longer and higher centre of gravity standing over (CGv gets over upper arm hand grip); the longer you are lifting your CGV, the higher you can get it. Also in the latest phase there is a difference in favour of S2 group – 0.02 s. Mainly in these two last phases lifting and bar crossing the group of higher sport performance level (S2) shows their higher technique mastery for they are able to use better accumulated energy in pole, when pole straightens and this enables to work longer on it, mainly during these two phases.

From the point of jump rhythm we can state that the most important phases from the point of view of sport level difference are phases of hanging and lifting. Higher sport performance group (S2) here shows better transmission on pole and higher use of kinetic energy accumulated in the pole.

In the fig 12 can be seen centre of gravity changes during jump phases of S1 and S2 groups.

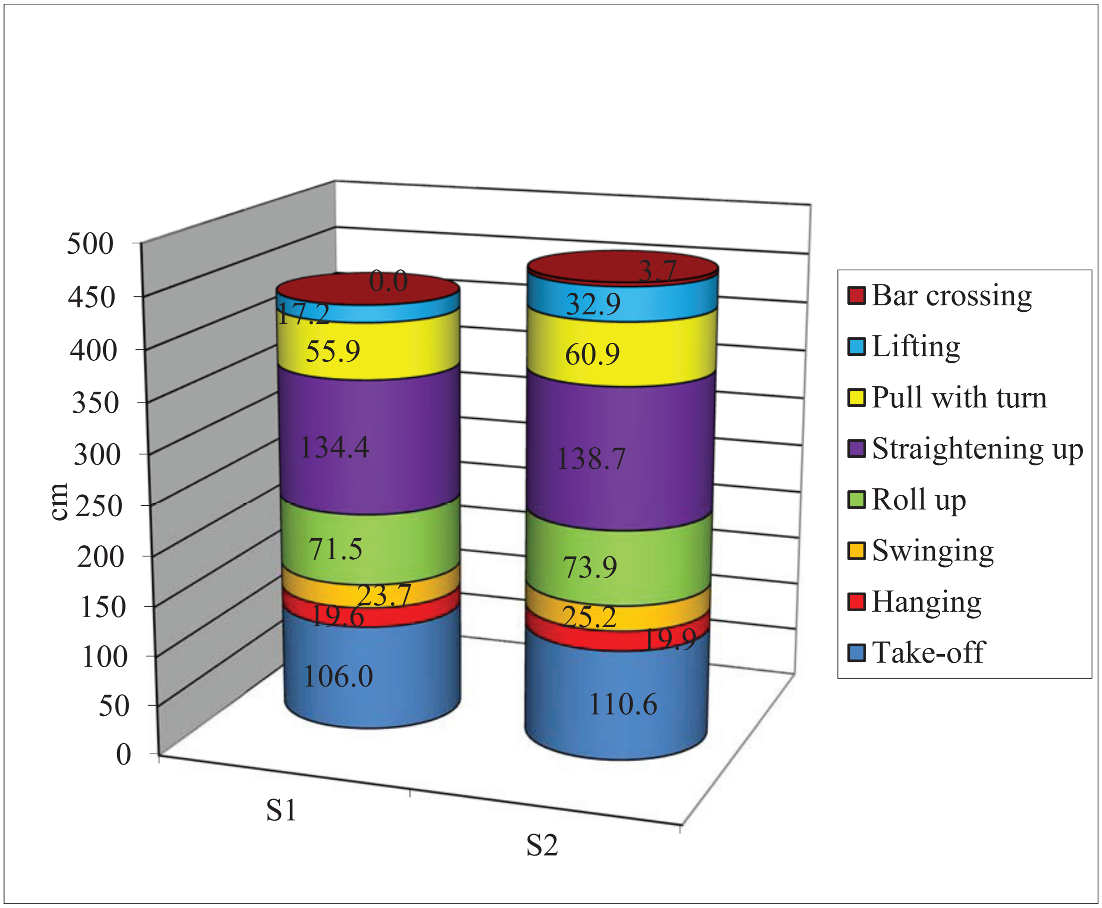

FIGURE 12. Comparison of centre of gravity growth during phases

We can state that in average can be seen the same increase tendency of centre of gravity height in both watched groups; with higher increase of higher performance level group (S2) in all phases. At take-off end is average CGv height 106.0 cm in group S1and 110.6 cm in group S2; it is more likely coursed by higher body height of S2 like by technique mastery. In the phase of hanging we measured nearly identical CGv growth (19.6 cm resp. 19.9 cm). In the phase of swinging reached jumpers of S2 1.5 cm more in CGv height like S1 group. In the phase of roll up gained S2 jumpers another 2.4 cm comparing S1 group. After pole bending end and its next straitening the CGv difference in vertical direction between both groups increase in favour of S2 group; this is also coursed by better S2 group work on pole (higher technique mastery) during following phases. In the phase of straitening reached S2 more 4.0 cm like S1 group. In the phase pull with turn more about 5,0 cm; in the phase lifting again more about 15.7 cm and in phase bar crossing more about 3.7 cm, while S1 jumpers here in this last phase did not reach any increase.

CONCLUSIONS

1. In female (just like male) pole vault technique assessment plays biomechanical analyse decisive role. Sport performance structure contains mostly kinetic parameters of speed, angle, time and space characteristics.
2. Time parameters show that mostly in phases hanging and lifting is manifested technique mastery of higher sport performance female jumpers; while during hanging phase, which them lasts longer this S2 group better transmit on pole, then during lifting phase they are able to use more pole elasticity and reach higher vertical CGv growth.
3. Centre of gravity increase during single phases shows that higher performance group (S2) reaches higher gains comparing S1 mostly in second part of jump, in more vertical CGv jump direction. This is of course connected with technique mastery and better use of pole elasticity.

4. We recommend in technique training improvement to use regularly 2-D or if possible also modern 3-D analysis systems. This enables to precise technique details, which can be decisive from the point of sport performance level increase.

REFERENCES

1. ADAMCZEWSKI, H. - PERLT, B. 1997. Run - up velocities of female and male pole vaulting and some technical aspects of women′s pole vault. In: New studies in athletics. Monaco : IAAF, roč. 12, 1997, č.1, s 63 – 77.
2. BOJKO, V. - NIKONOV, I. (1989): Novoe v prižke c šestom [New of pole vault]. In: Legkaja atletika, no. 10, p. 30 - 31.
3. GRABNER, S. (1997): Kinematic analysis of the Women pole vault. In: New studies in athletics. Monaco : IAAF, 12, 1997, no. 1. p. 47 – 61.
4. KOŠTIAL, J. – DOBIÁŠOVÁ, K. 2004. The Kinematic Indicators Changes in a Contest Kinetic Activity of a High Level Performance Woman Pole Vault Jumper. In: Kościoł w służbie człowiekowi. Lublin: Norbertinum, 2004, s. 54 – 65. ISBN 83-7222-207-X
5. KRŠKA, P. – KOŠTIAL, J. (2000): Somatické a motorické faktory štruktúry športového výkonu v skoku o žrdi žien [Somatic and motor factors of sport performance structure in female pole vault]. In: Zborník vedeckých prác katedry atletiky FTVŠ UK. Bratislava : SVŠ TVŠ, p. 46 – 49. ISBN 80-89057-00-2.
6. KRŠKA, P. (2008): Vývoj modelu kinematickej štruktúry športového výkonu v skoku o žrdi žien. In: Elektronický zborník z medzinárodnej konferencie: Atletika. Nitra: UKF PF KTVŠ, 2008, s. 68 – 73. ISBN 978-80-8094-373-8, EAN 9788080943738
7. KRSKA, P. – SEDLACEK, J. – KOSTIAL, J. (2014): Influence of Selected Kinetic Parameters in Female Pole Vault on Sport Performance. In Cluj-Napoca (Rumunsko) 5.-6.12.2014. The 7th international konference Education for health and performance. In: Studia Universitatis Babes-Bolyai Educatio Artis Gymnasticae, č.4, roč.LIX,2014, s.5-16. ISSN 2065-9547; ISSN-L 1453-4223
8. McGINNIS, P. M. (1997): Mechanics of pole vault take-off. In: New studies in athletics. Monaco : IAAF, 12, no. 1, p. 43 - 46.
9. VESPALEC, T.- ZVONAR, M. -PAVLIK, J. -PAVLIK, J. (2013): Balance Abilities of Adult Population in Relation to Their Physical Activity. In: 9th International Conference on Sport and Quality of Life. Masaryk University, Faculty of Sports Studies, Brno, p. 190 – 199.

Comparison of Differences of Czech Teenagers with Sensory Disabilities in Physical Education Classes

Kurková Petra[1,a], Nemček Dagmar[2], Bendíková Elena[3]

[1]*Department of Anthropology and Health Education, Faculty of Education, Palacký University Olomouc, Olomouc, Czech Republic*
[2]*Department of Sport Educology and Sport Humanities, Faculty of Physical Education and Sports, Comenius University in Bratislava, Bratislava, Slovakia*
[3] *Department of Physical Education and Sports, Matej Bel University, Faculty of Arts, Banská Bystrica, Slovakia*

[a]Corresponding author: petra.kurkova@upol.cz

Abstract: Aim: The purpose of this study was to describe and analyse the attitudes among teenagers with sensory disabilities in physical education classes. Materials and Methods: The sample was based on the following features: a) a participant had to be deaf and hard of hearing, b) a participant had to have a visual impairment, and c) had to have been educated in special educational settings. Both absolute and relative frequencies including mean and standard deviation were used to describe the data. Results The differences between teenagers who are deaf and hard of hearing and teenagers with a visual impairment were assessed using the non-parametric Mann-Whitney U-test. Tests were performed at a level of = 0.05. In this study participated 24 teenagers who are deaf and hard of hearing (16 boys and 8 girls, an average age of 14.3±1.2 years) and 26 teenagers with a visual impairment (16 boys and 10 girls, an average age of 14.1±1.2 years). Statistical tests did not prove any difference in responses in all explored indicators between participants who are deaf and hard of hearing and participants with a visual impairment. The item concerning the importance of physical education as a school subject was the only one that approached statistical significance. Conclusion: Both teenagers who are deaf and hard of hearing and teenagers with a visual impairment perceive physical education and leisure physical activities in almost the same way and have a similar opinion towards this issue.
Keywords: blind and partially sighted; deaf and hard of hearing; leisure time; physical activity; special education.

INTRODUCTION

Physical education (PE) is considered essential for helping children and youth to develop the knowledge, skills, and dispositions they need to build a physically active life (Ministry of Education, Youth and Sports of the Czech Republic, 2016).

The education of students with sensory disabilities in schools that have been specifically established for these students takes place under specific conditions that emerge over time as the facilities develop. Students who do not find it convenient to study at mainstream schools for whatever reason mostly attend schools for the deaf or blind. While the schools especially established for students with sensory disabilities feature the possibility of accommodation in a hostel and provide quality leisure time management for the students, schools in mainstream education have other positives, the main one being the close proximity to the student's home (Bendíková, 2016; Kurková et al., 2010; Dobay, 2015). Research has demonstrated that responsible and concentrated programming of PE classes can help develop fundamental motor and balance skills needed for students with sensory disabilities to maintain a physically active lifestyle (Fobelová, Fobel, 2008; Bendíková & Dobay, 2017; Ciolca & Mogaldea, 2013; Haegele et al., 2015; Haegele & Porretta, 2015; Nemček, 2017). Research focusing on the PE experiences of students with sensory disabilities, has focused on the different topics, such as parents (e.g. Ellis et al., 2014; Kurková, 2015; Perkins et al., 2013; Štěrbová & Kudláček, 2014), typically developing peers (e.g. Grenier et al., 2014; Lieberman et al., 2000), PE teachers (e.g. Best et al., 2002; Haegele & Lieberman, 2016; Perkins et al., 2013; Schultz et al., 2013; Zaccagnini, 2005) or para/deaf professionals (e.g. Bryan et al., 2013; Kurková et al., 2011). Findings from this line of research suggest that students with sensory disabilities tend to experience a number of barriers to participation in physical education. These barriers can include: (a) reduced physical fitness including motor skills of these students (Hartman et al., 2011; Levesque et al., 2014); (b) school type and curricular focus (Butterfield et al., 1993; Fobel, 2002; Fobelová, 2004; Perkins et al., 2013); c) the personality of the PE teacher (Stuart et al., 2006; Zaccagnini, 2005).

There has been published increased research investigating the experiences of the children with sensory disabilities in PE classes. In the field of qualitative research are many studies provide more insight into how experience different aspects of life (e.g. Haegele et al., 2017; Haegele & Sutherland, 2015; Haegele et al., 2016; Kurková et al.,

2010; Kurková et al., 2011; Štěrbová & Kudláček, 2014; Zitomer & Goodwin, 2014). On the other hand, there are only a few studies, which have utilized quantitative research methodology related to experiences of students with sensory disabilities in PE classes (e.g. Kurková, 2015; Kurková et al., 2015; Lieberman et al., 2002; Lieberman et al., 2006).

AIM

The purpose of this study was to describe and analyse the differences in opinions among teenagers with sensory disabilities in PE classes.

METHOD

Participants

The research sample comprised a total of 50 teenagers with sensory disabilities from the second stage of four elementary schools in Olomouc and Prague, the Czech Republic (Table 1). Twenty four teenagers who are deaf and hard of hearing (D/HH) (16 boys and 8 girls, an average age of 14.3±1.2 years) and twenty six teenagers with a visual impairment (VI) (16 boys and 10 girls, an average age of 14.1±1.2 years) participated in the questionnaire survey. The study included only teenagers who had not been diagnosed with a combined disability. Students were informed of the purpose of the research and the procedure for filling out the questionnaire, which was to be completed in the presence of their head teacher and the researcher. At the schools for students who are D/HH, we set up a procedure that ensured that teenagers who are D/HH and used Czech sign language properly understood all the questions in the questionnaire. Upon previous agreement and explanation of the purpose of the questionnaire, the actual questions were signed via video format of Czech sign language and with whom the teenagers were familiar. We proceeded by asking each item individually and then fact-checking to make sure that the teenagers individually understood the questions. Teenagers with a VI had the use of a questionnaire with enlarged letters and the head teacher read the questions out loud to the teenagers. Teenagers with partial sight completed the questionnaire with the help of special aids. The research was approved by the Ethics Committee of the Faculty of Education, Palack University Olomouc (ref. no. 1/2016).

Data collection

A structured questionnaire was used to collect the data, of which six questions were selected. Those questions were related to opinions or feelings towards PE classes and assessed: a) the popularity of PE (Question 1: For me, PE as a school subject is: very popular; popular; neither popular nor unpopular; unpopular; very unpopular); b) the importance of PE (Question 2: For me, PE as a school subject is: very important; important; neither important nor unimportant; less important; unimportant); c) the demandingness of PE (Question 3: For me, PE as a school subject is: very demanding; demanding; neither demanding nor easy; easy; very easy); d) effort in PE classes (Question 4: In PE classes: I am: very assiduous; assiduous; sometimes assiduous, sometimes not; less assiduous; not assiduous at all); e) emotionality in PE classes (Question 5: In PE classes I feel: always good; mostly good; sometimes good, sometimes bad; mostly bad; always bad); f) emotional response if a PE class is cancelled (Question 6: If a PE class is cancelled: I am always happy, I am often happy, I am indifferent about it, I usually get upset, I always get upset). For scale questions, students gave only one reply (1 was the highest level and 5 was the lowest level). The lower the average value of the replies, the PE is for students more popular, more important, and more demanding, students are more assiduous and they have better feeling during PE classes or express the lower level of emotional response if a PE class is cancelled.

Data analysis

Statistical analysis was undertaken using IBM SPSS Statistics 23.0 (Armonk, NY, USA). The data were differentiated from the point of view of the type of school or, as the case may be, the type of disability. Both absolute and relative frequencies including mean and standard deviation were used to describe the data. The differences between teenagers who are D/HH and teenagers with a VI were assessed using the non-parametric Mann-Whitney U-test. Tests were performed at a level of $p = 0.05$. If the p-value was less than 0.5, we considered the differences to be statistically significant.

RESULTS AND DISCUSSION

Demographics of the participants

The demographics of the participants concerning the type, degree and time of onset of disability are shown in Table 1. In terms of demographic data, a statistically significant difference between teenagers who are D/HH and

teenagers with a VI was found in the time of onset/diagnosis of the disability. Teenagers who are D/HH have more often been disabled since birth (n = 20; 83.3%). Most respondents used disability aids. Teenagers who are D/HH wore a hearing aid (n = 12; 63.2%) or a cochlear implant (n = 7; 36.8%). Teenagers with a VI used a white stick (n = 5; 23.8%) or a different aid such as a magnifying glass or glasses (n = 16; 76.2%). None of them had a guide dog. Most participants said that their parents had no hearing or visual impairments. For more information on the analysed sample, see Table 1.

Table 2 present the intergroup comparison of teenagers in PE classes by type of a disability. Both teenagers who are D/HH and teenagers with a VI consider PE classes to be very popular or popular (teenagers who are D/HH 66.7%, teenagers with a VI 76.0%). In the Importance indicator, the p-value is at the limit of statistical significance (p = 0.061). Here, we can observe a trend where PE is more important to teenagers who are D/HH. It is important or very important to seventy five per cent of the respondents. Among teenagers with a VI, it is only important to half of the respondents. In the question concerning to demandingness of PE, one third of teenagers who are D/HH rated the subject as easy or very easy, the same opinion was expressed by more than a half of teenagers with a VI (teenagers who are D/HH 33.3%, teenagers with a VI 53.8%). In the Emotionality 1 indicator, both teenagers who are D/HH and teenagers with a VI stated that PE makes them feel always good or mostly good (teenagers who are D/HH 83.4%, teenagers with a VI 80.8%). On the other hand, in the Emotionality 2 indicator, when a PE is cancelled, more than a half teenagers who are D/HH and one third of teenagers with a VI expressed indifference (teenagers who are D/HH 58.3%, teenagers with a VI 30.8%).

TABLE 1. Sample demographic information

	Teenagers who are D/HH (n = 24)		Teenagers with a VI (n = 26)	
	n	%	n	%
Gender				
Boys	16	66.7	16	61.5
Girls	8	33.3	10	38.5
Onset of disability				
Since birth	20	83.3	13	50.0
Since age 1	1	4.2	13	50.0
Since age 2	1	4.2		
Since age 3	2	8.3		
Degree of hearing loss/VI				
Light to moderate HL/B3	7	29.2	19	73.1
Severe HL/B2	5	20.8	4	15.4
Deaf/B1	12	50.0	3	11.1
Disability aid usage				
Yes	19	79.2	21	80.8
No	5	19.2	5	20.8
Type of disability aid				
Hearing aid	12	63.2		
Cochlear implant	7	36.8		
White stick			5	23.8
Glasses, magnifying glass			16	76.2
Communication				
Czech language	1	4.2	26	100.0
Czech sign language	7	29.2		
Combination	16	66.7		
Parents – father				
Without a disability	18	78.3	23	88.5
With a disability	5	21.7	3	11.5
Parents – mother				
Without a disability	17	70.8	26	100.0
With a disability	7	29.2		

Note: D/HH – deaf and hard of hearing; VI – visual impairment; HL – hearing loss.

TABLE 2. Intergroup comparison of absolute (relative) frequencies and mean values of teenagers opinions towards physical education, by type of a disability

	Teenagers who are D/HH (n = 24)		Teenagers with a VI (n = 26)		
	n(%)	Mean±SD	n(%)	Mean±SD	Z (p)
Popularity		1.83±0.92		2.12±1.11	
Very popular	12(50.0)		8(30.8)		
Popular	4(16.7)		12(46.2)		–0.821 (0.412)
Normal (neutral)	8(33.3)		2(7.7)		
Unpopular	0		3(11.5)		
Very unpopular	0		1(3.8)		
Importance		1.96±0.95		2.54±1.14	
Very important	9(37.5)		5(19.2)		
Important	9(37.5)		8(30.8)		–1.872 (0.061)
Normal (neutral)	4(16.7)		9(34.6)		
Less important	2(8.3)		2(7.7)		
Unimportant	0		2(7.7)		
Demandingness		3.04±1.04		3.46±0.95	
Very demanding	1(4.2)		0		
Demanding	7(29.2)		5(19.2)		–1.468 (0.142)
Normal (neutral)	8(33.3)		7(26.9)		
Easy	6(25.0)		11(42.3)		
Very easy	2(8.3)		3(11.5)		
Effort		2.00±0.83		2.23±1.07	
Very assiduous	6(25.0)		6(23.1)		
Assiduous	14(58.3)		13(50.0)		–0.662 (0.508)
Normal (neutral)	2(8.3)		3(11.5)		
Less assiduous	2(8.3)		3(11.5)		
Not assiduous at all	0		1(3.8)		
Emotionality 1		1.79±0.83		1.77±0.76	
Always good	10(41.7)		11(42.3)		
Mostly good	10(41.7)		10(38.5)		–0.010 (0.991)
Normal (neutral)	3(12.5)		5(19.5)		
Mostly bad	1(4.2)		0		
Always bad	0		0		
Emotionality 2		2.92±0.83		2.85±1.38	
I am always happy	2(8.3)		6(23.1)		
I am often happy	3(12.5)		4(15.4)		–0.286 (0.774)
I am indifferent about it	14(58.3)		8(30.8)		
I usually get upset	5(20.8)		4(15.4)		
I always get upset	0		4(15.4)		

Note: Z – the value of the test statistic for the Mann-Whitney *U*-test, p – value of statistical significance; D/HH – deaf and hard of hearing; VI – visual impairment; SD – standard deviation.

PE turned out to be a popular, important and relatively easy school subject, which proved to be demanding mainly for teenagers who are D/HH. At the same time, however, these teenagers seem to make more effort. Similar results were found by Kurková et al. (2015), where more than sixty per cent of Slovak students who are D/HH considered this subject to be easy. As part of an intergroup comparison of the mean values in the demandingness indicator, minimal differences were found, where students of mainstream schools rated PE as an easy school subject (a score of 3.55) and students from Czech mainstream schools reached even higher values (a score of 4.23) (Hrabal & Pavelková, 2010). In comparison with our sample, Slovak students who are D/HH reached a mean score of 3.78 points. On the other hand, the mean value of the subject's demandingness, was higher among Czech and Slovak teenagers with a VI (a score of 3.46 and 3.48). These intergroup differences may be due to the personnel, financial and spatial possibilities of the given school, where – in the case of teenagers with sensory disabilities – it is necessary to adopt an individual approach and make use of modifications within physical activities. Without consistent opportunities and goals for PE, these individuals may not attain the appropriate skills to participate in physical activity or sports and

games with their peers. Lack of appropriate skills, therefore, may limit opportunities for the positive relationships with peers that could result from the positive involvement in physical activity (Lieberman et al., 2006; Schultz et al., 2013).

In a comparison of Czech and Slovak teenagers, the same study produced opposite results for making effort in PE, i.e. Slovak students with a VI had higher percentage values, while Slovak students who are D/HH made little effort or expressed a neutral attitude. In our study, the rating of feelings in PE classes was mostly highly positive, with the exception of one teenager who is D/HH and who said he felt mostly bad. According to a Slovak study by Kurková et al. (2015), teenagers who are D/HH experienced different feelings, where positive responses were balanced, including a neutral attitude. Similarly, in intergroup comparisons, only slight differences were found in the indicators of effort and feelings (Hrabal & Pavelková, 2010; Kurková et al., 2015), where the mean score for effort ranged between 1.92 and 2.30 and the mean score for emotionality in PE classes ranged between 1.52 and 2.14. These differences in the effort made by teenagers in PE classes may have been affected by the activities that are currently being done. In individuals with sensory disabilities, participation in physical activities may also be affected by climate change, fear of injury, current health condition or, if relevant, being overweight (Bendíková, 2011; Bláha, 2010; Jaarsma et al., 2014; Nemček, 2016; Tsai & Fung, 2005). However, those factors in our study were not examined.

Interestingly, Kurková et al. (2015) found out that none of the students with a VI who were interviewed in Slovakia replied that PE was an unpopular or very unpopular school subject, while even these responses were received in the Czech Republic. Neither teenagers who are D/HH in the Czech Republic nor teenagers in Slovakia expressed an outright negative opinion towards the popularity of the subject. By comparing the mean values for responses of Czech and Slovak students with sensory disabilities in special education (Kurková et al., 2015), it was found that PE was the most popular among Slovak teenagers with VI (a score of 1.64). However, a mutual comparison showed that the value was higher for Czech teenagers who are D/HH than for Slovak teenagers (a score of 2.08). Having compared the mean values for the responses of Czech students of the second stage of mainstream elementary schools in the given indicator (Hrabal & Pavelková, 2010), we can conclude that Slovak students with a VI indicate the same degree of popularity (a score of 1.65 vs 1.64) (Kurková et al., 2015). For Slovak students without disabilities, the students achieved a similar score (1.92). Furthermore, in the study carried out by Vašíčková et al. (2015), students who considered PE a popular school subject showed a higher degree of physical activity – expressed as the number of steps – and a more positive attitude to implementing PE.

In terms of assessing the importance of PE, there is a clear trend for teenagers who are D/HH to perceive PE as more important. Similar results were found in a study by Kurková et al. (2015), where Slovak students who are D/HH considered PE to be a very important or important school subject. However, in a comparison between Czech and Slovak teenagers with a VI, the values for Slovak students were higher. By comparing our results with the responses of Czech and Slovak teenagers in the importance indicator within the same studies, we have found slight differences in the mean values. Teenagers with a VI consider the school subject to be the most important (a score of 1.73), teenagers of Czech and Slovak schools rate the importance of the subject similarly (a score of 1.96 vs 2.05). The worst mean values were found among Czech and Slovak students of mainstream elementary schools (a score of 2.80 and 2.31).

Although teenagers with sensory disabilities showed interest in PE, and PE was one of their favourite school subjects, a relatively large proportion of them were happy when PE was cancelled. On the other hand, one third of teenagers with a VI were upset when PE was cancelled, and more than a half of teenagers who are D/HH expressed indifference. Similar results have been published in other studies, both for Slovak students of mainstream schools and for students with sensory disabilities (Kurková & Nemček, 2016).

CONCLUSION

Statistical tests did not prove any difference in responses to questions 1 to 6 between participants who are D/HH and participants with a VI. The item concerning the importance of PE as a school subject was the only one that approached statistical significance. Both teenagers who are D/HH and teenagers with a VI perceive PE in almost the same way and have a similar opinion towards this issue. This may be due to the fact that the conditions that are provided by elementary schools for these teenagers do not differ significantly. However, the curricular focus of PE may be somewhat different, which may – in turn – lead to differences in the evaluation of the various parameters in PE classes. In PE classes, the feelings of teenagers with sensory disabilities may also be influenced, among other things, by the personality of the teacher and the assistant teacher, the classmates, the school environment, as well as the current health of the teenager.

The results cannot be generalized, they only attest to the schools within the given region. This study was limited due to the low number of participating schools and the number of teenagers with sensory disabilities, as well as due to the lack of knowledge of the level of current fitness and overall health condition of the teenagers under this study.

ACKNOWLEDGEMENTS

This paper was supported by the grant project VEGA No. 1/0409/19.

REFERENCES

1. Bendíková, E. (2011). The current health status and reasons for student absence in physical and sports education classes. *Physical Education and Sport, 21*(1), 6–10.
2. Bendíková, E. (2016). Changes in the posture of students due to equipment-aided exercise programs that are applied in physical and sport education. *Journal of Physical Education and Sport, 16*(2), 281–286.
3. Bendíková, E. & Dobay, B. (2017). Physical and Sport Education as a Tool for Development of a Positive Attitude toward Health and Physical Activity in Adulthood. *European Journal of Contemporary Education, 6*(1), 14–21.
4. Best, C.; Lieberman, L. & Arndt, K. (2002). Effective use of interpreters in general physical education. *Journal of Physical Education, Recreation and Dance, 73*(8), 45–50.
5. Bláha, L. (2010). *Pohybové aktivity a zrakově postižení: problémy a možnosti* [Physical activities and visual impaired: problems and possibilities] (1st ed.). Banská Bystrica, Slovensko: Univerzita Mateja Bela.
6. Bryan, R.R.; McCubbin, J.A. & van der Mars, H. (2013). The ambiguous role of the paraeducator in the general physical education environment. *Adapted Physical Activity Quarterly*, *29*(2), 164–183.
7. Butterfield, S.A.; Van der Mars, H. & Chase, J. (1993). Fundamental motor skill performances of deaf and hearing children ages 3 to 8. *Clinical Kinesiology, 47*(1), 2–6.
8. Ciolca, C. & Mogaldea, C. (2013). Types of communication in kinetotherapy classes involving students with hearing impairments. *Procedia Social and Behavioral Sciences*, 117, 610–615.
9. Dobay, B. 2015. *Az iskolai sporttanfolyamok motivációs hatása a felnıttkori rekreációs sporttevékenységekre Dél-Szlovákiában*. Komárom : Kompress kiadó.
10. Ellis, M.K.; Lieberman, L.J. & Dummer, G.M. (2014). Parent influences on physical activity participation and physical fitness of deaf children. *Journal of Deaf Studies and Deaf Education*, 19(2), 270–281.
11. Fobelová, D. (2004). O aplikacji etyki w procesie pedagogicznym i wspolczesnych trendach w pedagogidze moralnej. I*Auxilium sociale. Wsparcie spoleczne*, (1), pp. 82-91.
12. Fobel, P. 2002. *Aplikovaná etika : teoretické východiská a súčasné trendy.* Martin: Honner, 2002, 135 p.
13. Fobelová, D. & Fobel, P. (2008). The Applied Ethics and the Moral Value of Mentally Handicapped. *Terapia pedagogiczna w rehabilitacji osób niepelnosprawnych* : praca zbiorowa pod redacja Ktrysztofa Kucypera i Adama *Stankowskiego*. Bielsko-Biala: Wyžsza Szkola Administracji, 2008, pp. 33-34.
14. Grenier, M.; Collins, K.; Wright, S. & Kearns, C. (2014). Perceptions of a Disability Sport Unit in General Physical Education. *Adapted Physical Activity Quarterly*, *31*(1), 49–66.
15. Haegele, J.A.; Brian, A. & Goodway, J. (2015). Fundamental motor skills and school-aged individuals with visual impairments: A review. *Review Journal of Autism and Developmental Disorders, 2*(3), 320–327.
16. Haegele, J.A. & Lieberman, L.J. (2016). The Current Experiences of Physical Education Teachers at Schools for Blind Students in the United States. *Journal of Visual Impairment*, *110*(5), 323–334.
17. Haegele, J. A. & Porretta, D. (2015). Physical activity and school-age individuals with visual impairments: A literature review. *Adapted Physical Activity Quarterly, 32*(1), 68–82.
18. Haegele, J.A. & Sutherland, S. (2015). Perspectives of students with disabilities toward physical education: A qualitative inquiry review. *Quest, 67*, 255–273.
19. Haegele, J.A.; Sato, T.; Zhu, X. & Avery, T. (2017). Physical education experiences at residential schools for students who are blind: A phenomenological inquiry. *Journal of Visual Impairment and Blindness*, *111*(2), 135–147.
20. Haegele, J.A.; Zhu, X & Davis, S. (2016). The meaning of physical education and sport among elite athletes with visual impairments. *European Physical Education Review, 23*(4), 375–391.
21. Hartman, E.; Houwen, S. & Visscher, C. (2011). Motor Skill Performance and Sports Participation in Deaf Elementary School Children. *Adapted Physical Activity Quarterly*, *28*(2), 132–145.

22. Hrabal, V. & Pavelková, I. (2010). *Jaký jsem učitel* [What type of teacher I am] (1st ed.). Portál, Czech Republic: Prague.
23. Jaarsma, E.A.; Dekker, R.; Koopmans, S.A.; Dijkstra, P.U. & Geertzen, J.H.B. (2014). Barriers to and Facilitators of Sports Participation in People with Visual Impairments. *Adapted Physical Activity Quarterly*, *31*(3), 240–264.
24. Kurková, P. (2015). Emotions in the physical activities of Czech students who are deaf or hard of hearing in general and special education. *Journal of Physical Education and Sport, 15*(4), 823–828.
25. Kurková, P. & Nemček, D. (2016). Attitudes of students with disabilities towards physical education lessons: Reasons for their indifference and preference for leisure time activities. *Journal of Physical Education and Sport*, *16*(1), 222–229.
26. Kurková, P.; Nemček, D. & Labudová, J. (2015). Pupils with sensory disabilities in Physical Education classes: Attitudes and preferences. *Acta Gymnica, 45*(3), 139–145.
27. Kurková, P., Scheetz, N. A., & Stelzer, J. (2010). Health and physical education as an important part of school curricula: A comparison of schools for the deaf in the Czech Republic and the United States. *American Annals of the Deaf*, *155*(1), 78–87.
28. Kurková, P.; Válková, H. & Scheetz, N. A. (2011). Factors impacting participation of European elite deaf athletes in sport. *Journal of Sports Sciences*, *29*(6), 607–618.
29. Levesque, J.; Theoret, H. & Champoux, F. (2014). Reduced procedural motor learning in deaf individuals. *Frontiers in Human Neuroscience*, *8*(343), 1–6.
30. Lieberman, L.J.; Dunn, J.M.; Van Der Mars, H. & Mc Cubbin, J. (2000). Peer tutors' effects on activity levels of deaf students in inclusive elementary physical education. *Adapted Physical Activity Quarterly*, *17*(1), 20–39.
31. Lieberman, L.J.; Houston-Wilson, C. & Kozub, F.M. (2002). Perceived barriers to including students with visual impairments in general physical education. *Adapted Physical Activity Quarterly, 19*(3), 364–77.
32. Lieberman L.J.; Robinson, B.L. & Rollheiser, H. (2006) Youth with visual impairments: Experiences in general physical education. *RE:view 38*(1), 35–48.
33. Ministry of Education, Youth and Sports of the Czech Republic. (2016). *Rámcový vzdělávací program pro základní vzdělávání* (třetí verze) [*Framework Education Programme for Basic Education* (with amendments as at January 1st 2016)]. Retrieved from http://www.nuv.cz/uploads/RVP_ZV_2016.pdf
34. Nemček, D. (2016). Life satisfaction of people with disabilities: A comparison between active and sedentary individuals. *Journal of Physical Education and Sport*, *16*(2), 1084–1088.
35. Nemček, D. (2017). Self-esteem analyses in people who are deaf or hard of hearing: A comparison between active and inactive individuals. *Physical Activity Review*, 5, 95–104.
36. Perkins, K.; Columna, L.; Lieberman, L. & Bailey, J. (2013). Parents' perceptions of physical activity for their children with visual impairments. *Journal of Visual Impairment & Blindness, 107*(2), 131–142.
37. Schultz, J.L.; Lieberman, L.J.; Ellis, M.K. & Hilgenbrinck, L.C. (2013). Ensuring the success of deaf students in inclusive Physical Education. *Journal of Physical Education, Recreation*, *84*(5), 51–56.
38. Stuart, M.; Lieberman, L. & Hand, K. (2006). Beliefs about physical activity among children who are visually impaired and their parents. *Journal of Visual Impairment & Blindness, 100*(4), 223–234.
39. Štěrbová, D. & Kudláček, M. (2014). Deaf-blindness: Voices of mothers concerning leisure-time physical activity and coping with disability. *Acta Gymnica, 44*(4), 193–201.
40. Tsai, E. & Fung, L. (2005). Perceived constraints to leisure time physical activity participation of students with hearing impairment. *Therapeutic Recreation Journal*, *39*(3), 192–206.
41. Vašíčková, J.; Neuls, F. & Svozil, Z. (2015). Popularity of school physical education and its effect on performed number of steps. *Journal of Physical Education and Sport*, *15*(1), 40–46.
42. Zaccagnini, K.J. (2005). How physical education teacher education majors should be prepared to teach students with hearing loss: A national needs assessment. *American Annals of the Deaf, 150*(3), 273–282.
43. Zitomer, M.R. & Goodwin, D. (2014). Gauging the quality of qualitative research in adapted physical activity. *Adapted Physical Activity Quarterly, 31*(3), 193–218.

Application of "Propriofoot Concept" in Training Process of Female Athlete in Long Jump

Šárka Tomková[1)], Elena Bendíková[2)], Stanislava Lajčáková[1)] Michal Marko[2, a)], Ingrid Palaščákova Springrová[3)]

[1]*St. Elisabeth University of Health Care and Social Work, Bratislava, Slovak Republic*
[2]*Matej Bel University, Faculty of Arts, Banska Bystrica, Slovak Republic*
[3]*Rehaspring Physiotherapy and Education Centre, Celakovice, Czech Republic*
[a]Corresponding author: Michal.Marko@umb.sk

Abstract: The aim of the pilot study was to verify the possibilities of improving the jumping abilities of the female athlete in the long jump by applying the method of the Propriofoot Concept. The monitored group consisted of one female student (n = 1) (17 years old, 57 kg and 170 cm) of the second year of the Secondary Technical School in Banská Bystrica, Slovakia. The monitored group has been active for seven years with focus on the long jump and sprints (60 m and 200 m). At the time of input and output testing, the state of health was without injuries and subjective difficulties. In terms of data acquisition methods, we used standardized methods, which are applicable in the physiotherapy practice, with focus on the muscular system in the areas of the pelvis and lower limbs. The obtained results, which were processed in the form of clinical case, reported to positive changes of the observed factors of the proband's motor tests (female athlete in the long jump). During the indoor season, she advanced her personal indoor maximum in the long jump of 12 cm (from 535 cm to 547 cm), which we evaluated positively. *The listed study is the part of the research project: VEGA 1/0519/19 "Physical activity as prevention of health of school population in Slovakia".*

Key words: Female athlete, foot, jumping abilities, "Propriofoot Concept".

INTRODUCTION

A long jump is one of the oldest technical athletic disciplines. It belongs to group of horizontal jumps. It is mixed speed and strength athletic discipline, which involves combination of cyclical activity in run-up and acyclical activity in taking off and flight through an air. The overall performance in this discipline depends on the linking of the run-up speed with the exact timing of the taking off, coordination of the flight through the air and completion of it by the landing into the sandbox. The important role is reflected in phase of taking off (take-off force). The take-off board helps the jumper in the long jump in the phase of taking off, in which is needed touching it by the heel, then through the entire foot, even the thumb. The thumb is the last taking off impulse. Therefore, the attention should be paid to the most obvious part of the lower limb, which is the foot. Adamec (2005) claims that the foot is developed until the 6th - 7th year of life. The main role of the foot is to reduce the energy expenditure, required for symmetrical movements during walking and to reduce the impact of the foot on the pad. The basic role of the foot is static and dynamic function. The static foot function represents the right leg support to provide the postural stability of the human body in the standing position (Hodges, Richardson, 1996; Psalman, Zvonař, 2007). The dynamic function ensures locomotion. It allows us to move, what is based on allowing the foot from the pad. At the same time, it represents the basic connection of the body with the terrain, which can be adapted to. The contact of the leg with the pad is the source of proprioceptive and extroceptive stimuli, which are going into the central nervous system (CNS). It is the control system of all movements (Vařeka, Vařeková, 2009; Véle, 2006).

The important role is played by pressure receptors of the foot, which are applied in the standing position, even in the dynamic walking (Brozmanová, 2015). Through them, the body acquires information about the change of the

center of gravity and subsequent disturbance of the balance, by which it is able to respond adequately in preventing the fall.

For static and dynamic foot function is necessary proper body weight distribution, which is ensured by the arch of the foot (Véle, 2006). The foot arch protects the soft tissues, is important for the flexibility of the foot, and thus for the proper walking (Kolář et al., 2009; Vařeka, Vařeková, 2009). On the proper posture of the foot are engaged bones by shapes and positions, ligaments, tendons, calf muscles and foot muscles. The activity of these three main components is controlled by the CNS (Vařeka, Vařeková, 2009). The most important ligament, which supports the correct posture of the longitudinal arch is the lig. plantare longum. M. peroneus longus, m. peroneus brevis a m. abductor digiti minimi are the muscles, which aw supporting the lateral arch of the longitudinal arch. Among the muscles, which keep the dynamic arch of the foot include m. tibialis posterior, m. flexor digitorum longus, m. flexor hallucis longus, m. peroneus longus, m. abductor hallucis longus and short superficial muscles of the foot. The transverse arch is supported by m. tibialis posterior, m. peroneus longus a m. adductor hallucis (Hamill et al., 2009; Vařeka, Vařeková 2009; Čihák, 2011). Fallen arch may be the cause of various pathological conditions in the whole human body (Vařeka, Vařeková 2009; Čihák 2011,). Flat foot often occurs as a symptom of incorrect posture (Kolář et al., 2009). Lewitová (2016) claims that the flat foot in children belongs to the most common diagnoses in orthopedics and physiotherapy.

Nowadays, the sensorimotor stimulation (SMS) is used in the therapy of various functional disorders of the locomotor system. The main tasks of the SMS include improving coordination and balance, correcting the incorrect posture, influencing the proprioceptive disorder, improving postural stabilization of the torso and combining of the learned motor programs with activities in everyday life. For practice, it is usable in wide range of disorders of the muscular system. The Propriofoot Concept belongs to the physiotherapeutic concepts, which use sensorimotor activation of the foot (Kim, Kim, 2016; Palaščáková Špringrová, 2016, 2017).

The aim of the research was to find out the effect of the applied exercises of the Propriofoot Concept on proband's jumping ability who was the female athlete in the long jump.

METHOD

Participants

The monitored group consisted of one female student (n = 1) (17 years old, 57 kg and 170 cm) of the second year of the Secondary Technical School in Banská Bystrica, Slovakia. The monitored group has been active for seven years with focus on the long jump and sprints (60 m and 200 m). At the time of input and output testing, the state of health was without injuries and subjective difficulties.

Procedure

The realized research was carried out in the period of 21.10.2017 - 07.03.2018. The listed physical program, the Propriofoot® Concept according to Baicry, Paris (2017) was realized for 4 months. The 1st and the 2nd month (7x/ week, 6 minutes/ 20 exercises). In the 3rd and the 4th month, it was done 3 x/ week, 6 minutes/ 20 exercises). The recommended approach of the Propriofoot® Concept was maintained, with the emphasis on managing all exercises (in number of 20, from the easiest to the most difficult). The correct realization of the positions (fixation and starting) has acted as the targeted, specific factor in the development of the monitored research indicators.

The listed time period included the input (I1) and output (O2) diagnosis with focus on the personal anamnesis and objective examination of the muscular and skeletal system by the physiotherapist.

Firstly, we evaluated by aspection the standing position and walking (author, year). Subsequently, we examined by palpation the position of the pelvis, as we evaluated the stability of the pelvis with the Trendelenburg test. The symptom of the sacroiliac shift in the pelvis was observed by the "Spinning Phenomenon" (author, year). The examination of the extent of mobility of the hip, knee and ankle joint was performed by using the goniometry method (recorded by the SFTR method, which means that the movement was performed in all planes). The method of the anthropometry was measured by the dimensions of the foot (Janíková, 1998).

The examination of the motor stereotypies of the lower limbs was realized according to Janda (2004). We observed the movement of extension and abduction in the hip joint. We compared the performed movement with the motor stereotype of extension and abduction in the hip joint according to Janda (2004).

While evaluating the foot arch, we used the non-invasive imaging method of PodoCam. This is a device for diagnosing footprints with polarized light, where the proband is standing on a glass pad during the evaluation. The proband´s foot is monitored by 2 cameras from the rear and bottom (the area of the heel and the Achilles tendon and area of the foot). We realized the evaluation in the following positions: standing, standing in squat on both lower limbs

and also follow by the intensification on one lower limb and in standing in squat. Subsequently, the obtained images were evaluated by using the Chippaux-Smirak (CSI) method. To calculate the index, we used the ratio of the widest point to the lowest point of the middle part of the footprint, which was obtained from the PodoCam evaluation. The measured distances are always perpendicular to the outer tangent of the plantogram. The index is expressed by percentage. The higher CSI values indicate presence of longitudinal flat foot. In the case of high foot arch, we measured the distance between the front and back of the foot (Vařeka, Vařeková, 2009) (fig. 1).

As complement to the area of the foot, we used 4 tests: The Véle test (Lewit, 2003), helps to reveal the transverse flat foot. The Hubscher test (Jack's test) was a test evaluating the flexibility of the foot arch (Kollář, et al., 2009). The Navicular Drop Test (Charlesworth, Johansen, 2010) and LAA - Longitudinal Arch Angle were the third and the forth tests.

FIGURE 1. Evaluation of foot by Chippaux-Smírak on podoscope

In order to determine the effectiveness of the Propriofoot® Concept application in the training process of the proband, we used motor tests with focus on the jumping ability (long jump).

Myotest test

A diagnostic device designed to diagnose speed and strength components of the performance. Using the device, we performed the jump tests. The first test was to make three jumps in a row. The height of the jump was averaged at the end of the test. The second test was to jump and reach the maximum height (Video Analysis, 2018).

Standing long jump and 10 jumps

To test the horizontal distance, we used the standing long jump test, in which the proband from the zero speed exerted the maximum strength. The second test was the 10 jumps, which consisted of 10 multiple jumps, which were realized with both lower limbs. The tests were applied at the beginning (I1) and the end of the evaluation (O2). In each test, the proband performed three attempts and we selected the best test result for the evaluation.

Data analyses

While processing the obtained qualitative and quantitative data we used clinical case report (Vojtaššák, 2000). We also used methods of logical analysis and synthesis, inductive and deductive approaches, comparison and generalization.

RESULTS

Based on the partial aim and research tasks, we present results, which are the subject of further accurate monitoring and processing within the project. These results cannot be generalized, but it is necessary to understand them in general contexts as indicative, in consideration of the health of adolescent age of the proband. From the characterizing data of the monitored group, we selected those, which were relevant to the target. At the same time, the results should be seen in broader contexts.

Clinical case report

Case history

*FCH: parents in the past were actively engaged in sports, father was involved in football and mother was involved in athletics, brother played active football and floorball during high school, more serious illnesses in the family are not stated.

*PCH: overdone common childhood illnesses, wristed elbow (right upper limb - 2012), broken wrist (BW) (right upper limb - 2016), resurgery - removal of support material from the right BW (2017).

*SCH: lives in flat with parents, older brother who studies at university (lives at home rarely), has a dog.

*PhCH: the second year secondary school student.

*SCH: actively devoted to sport, firstly to swimming, the last 7 years to athletics.

Does not smoke or drink.

Dominant LL: take off lower limb for long jump - left.

Subjective examination: does not have any pain or other difficulties.

*Note: FCH – family case history, PCH – personal case history, SCH – social case history, PhCH – physical case history, SCH – sports case history, DLL – lower limb.

Objective examination

Standing.

Forward: slight rotation position of the left foot, fingers are loosely laid on the mat, without bilateral deformities, valgosity of the ankle and knee joint on the right, contours of foreleg and thighs are bilaterally in norm, symmetric height of both patella, pelvis is levelled, upper limbs are without significant pathology, left shoulder is slightly increased, head in extension of spine axis.

Side: no bilateral knee joint hyperextension is presented, increased dorsal lordosis, pelvis in anteversion, arms and head are forward.

Behind: valgus position of the right ankle and knee joint, significant Achilles tendons, symmetrically shaped calf muscles and back muscles of the thigh, pelvis is levelled, paravertebral muscles at elevated tension, symmetrical position of the shoulders, increased tension of m. trapezius on the left, head position in spine extension.

Walking: rhythmical, the same length of steps, symmetrical cooperation of the upper limbs, which are correctly placed in the walking process, steady load on both lower limbs, hip joint extension at moderate limitation, narrow base, unwinding of the foot from the pad, more load on the lateral side of the foot, modifying the walking without difficulty.

Palpation examination of pelvis: palpation without pain, pelvis in symmetrical position, pelvis is levelled (frontal plane), anteversion of the pelvis (sagittal plane) with increased tension of paravertebral muscles.

Trendelenburg test: negative on both sides. Standing on one leg was done correctly without any decrease or compensation mechanisms of the pelvis.

Goniometry: in proband, we did not expect significant limitation of mobility due to the absence of any injury. The test confirmed our expectations. The joints of the lower limb are symmetrically movable without significant limitation (tab. 1).

TABLE 1. Range of joint mobility of lower limb (n=1)

Joints of lower limb/ planes	Sides/ degrees° of angles in joints	
Hip joint	dx.	sin
Sagittal plane (ext/ fle)	10° – 0° – 130°	10° – 0° – 130°
Frontal plane (abd/ add)	40° – 0° – 20°	40° – 0° – 15°
Plane of rotations (ero/ iro)	40° – 0° – 35°	40° – 0° – 35°
Knee joint	dx.	sin.
Sagittal plane (ext/ fle)	0° – 0° – 150°	0° – 0° – 150°
Plane of rotations (ero/ iro)	20° – 0° – 30°	20° – 0° – 30°
Ankle joint	dx.	sin.
Sagittal plane (dor. fle/ pl. fle)	20° – 0° – 60°	20° – 0° – 60°

Dynamic evaluation of the spine revealed mild hypermobility of the spine. Using the Thomayer, Stibor, Schober and Otto tests, we found that the development of the spine of the proband was carried out in separate sections without significant pathology (tab. 2).

TABLE 2. Clinical case report: Dynamic evaluation of spine (n=1)

Tests of dynamic function of spine	Values (cm)
Thomayer test (Th)	-5 cm
Stibor test (St)	12 cm
Schober test (Sch)	5,5 cm
Otto index (bending forward/ backward) (Ot)	33 cm/28 cm
Lateroflexion (L)	17.5 cm (dx.)/17 cm (sin.)

Anthropometry. Measuring length of both limbs without any differences. The measurement confirmed the position of the pelvis, which was levelled (tab. 3).

TABLE 3. Clinical case report: Measuring length of lower limbs (n=1)

Length of lower limbs/ sides	dx.	sin
Anatomical length	82.5 cm	82 cm
Functional length	87.5 cm	87 cm
Length of lower limb	96 cm	95.5 cm
Length of thigh	41 cm	41.5 cm
Length of foreleg	41.5 cm	40 cm

The measurement of the circumference did not show significant difference; the left lower limb used the athlete in the long jump as taking off lower limb, which may be the reason for the deviation in our measurement (tab. 4). The last measurement of the lower limb dimensions was anthropometry of the foot - the feet are symmetrical without the presence of deformities (tab. 5).

TABLE 4 Clinical case report: Measuring circumferences of lower limb (n=1)

Circumference of lower limbs/ sides	dx.	sin
Thigh at rest – prox. (20cm)	48.5 cm	49 cm
Thigh at rest – dist. (8cm)	38.5 cm	39 cm
Foreleg (15cm)	34 cm	34.5 cm
Ankle joint	25.5 cm	26 cm
Instep	22 cm	22 cm

TABLE 5 Clinical case report: Anthropometry of foot (n=1)

Foot/ sides	dx.	sin
Length of foot	25 cm	25 cm
Distance: heel – I. metatarsal head	19.5 cm	19.5 cm
Distance: heel – V. metatarsal head	15.5 cm	15 cm
Distance: head of the I. – V. metatarsal	8 cm	8.5 cm
Width of heel	5.5 cm	5.5 cm

Evaluation of shortened muscles. We investigated the shortened muscles of the entire lower limb. The most striking tension and painfulness proved us m. illiopsoas - degree 2, during the examination.

Muscle strength - the proband was without injuries, in the performance of active training. No significant weakening of lower limb muscles was found. The movement was carried out against great resistance without any difficulties on both lower limbs. The muscle strength in all the examined muscles was in degree 5.

Evaluation of stereotypes of lower limbs

Extension in the hip joint: motor stereotypes to the extension of the hip joint were carried out equally on both limbs. In the areas of the lumbar spine, we saw increased activity of paravertebral muscles, the muscular groups were engaged in the right order, the movement was started by the activity of m. gluteus maximus, followed by ischiocrural muscles and finally contralateral and homolateral paravertebral muscles were involved, movement stabilization was sufficient, it was performed without raising the pelvis.

Abduction in the hip joint: due to increased muscle tension and shortening of m. iliopsoas we were able to follow a slight tensor mechanism during abduction in the hip joint, the movement was not performed in "pure" abduction and the leg went forward into a slight flexion on both lower limbs.

Special tests

Véle test: while the weight of the body was transferred to the tiptoes, a protective reaction of finger flexion on both lower limbs was induced as a symmetrical.

Jack's test: by passive test was not a noticeable change in the foot arch. The foot arch remained in a slightly high position. While exercising (standing on tiptoes), after increasing the load on the front of the foot, the foot arch slightly decreased. The foot arch was flexible to the specified load.

Navicular drop test: in sitting position we noticed a higher left foot arch on the left lower limb by 0.5 cm. With the gradual increase of the load (standing, squat position) the foot arch decreased. In the final phase of the test, the difference between the lower limbs was reduced by 0.3 cm. The difference between os naviculare in sitting position and squat position was 0.5 cm (right foot) and 0.7 cm (left foot). The foot is in the norm.

LAA: measured values were identical to the upper limit of the physiological status range. The measured angle between the I. metatarsal head, os naviculare and medial extension of the ankle was 150°.

PodoCam examination:

Using the Chippaux-Smirak method for the flat feet, we evaluated the images from the PodoCam (tab. 6) at the input (fig. 2) and the output evaluation (fig. 3).

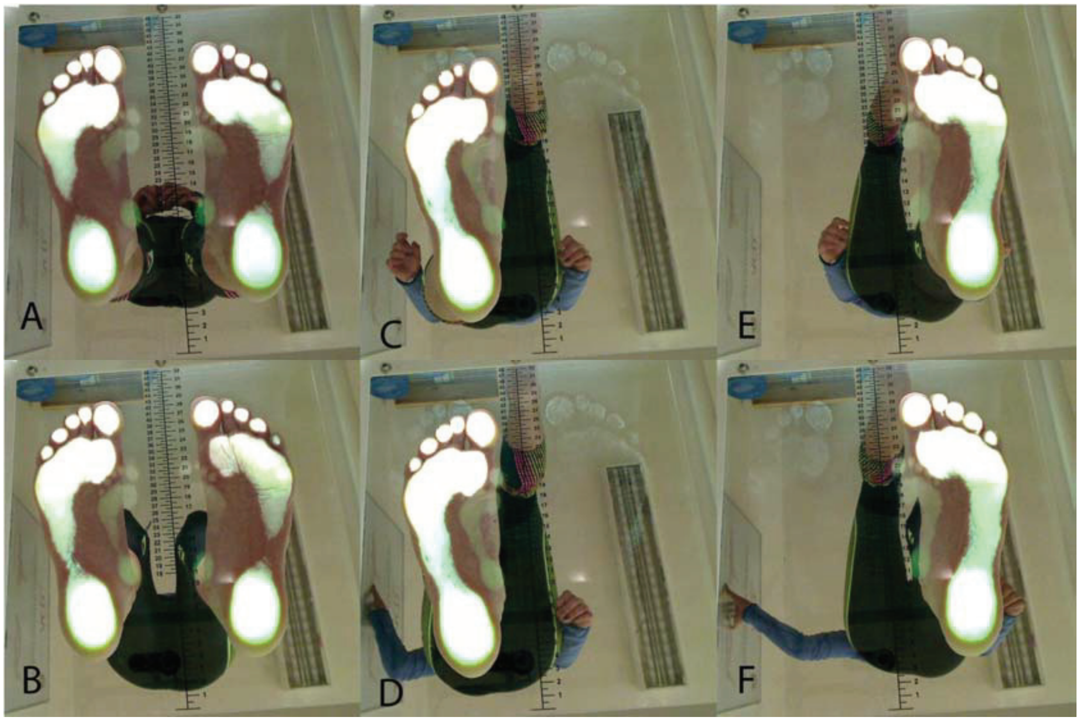

FIGURE 2. Input evaluation of proband´s foot by PodoCam (n=1)

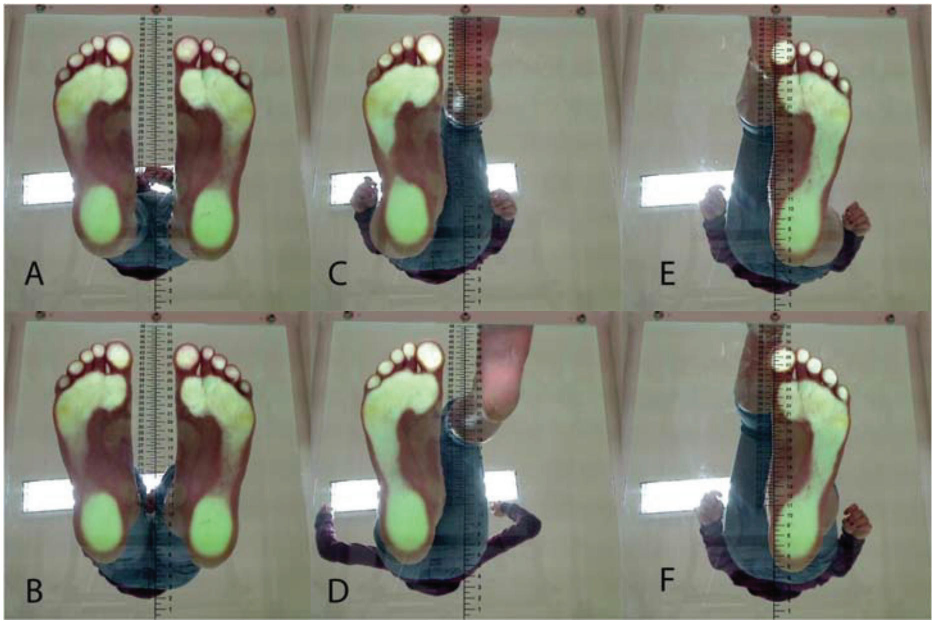

FIGURE 3. Output evaluation of proband´s foot by PodoCam (n=1)

TABLE 6. Clinical case report: Evaluation of PodoCam images of proband (n=1)

Position	Input evaluation (I1)	Output evaluation (O2)
Standing	High foot – 1. degree (0.8cm) The highest load – toe side, medial side of the heel Slightly valgus position of AJ	Connection of footprints - more significant on the right LL Steady load on the foot The slightly valgus position of the AJ
Squat	Left LL – connected Right LL – stays in high position	Steady layout of weight Left LL is upright to mat
Standing – Left LL	Decrease of FA The highest load - the entire lateral area of the foot 33.3% - 2. degree of the normally arched foot, the varous position of the foreleg	High foot – 1. degree (1cm) The highest load – toe Varous position of foreleg
Squat – Left LL	Decrease of FA The highest load - the entire lateral area of the foot Fingers evenly loaded 35% - 2. degree of normally arched foot Impaired stability	Decrease of FA The highest load - toe 34% - 2. Degree of normally arched foot Perpendicular position to foreleg
Standing – Right LL	Decrease of FA The highest load - the front part of the foot, toes and medial side of the heel 32.5% - 2. degree of normally arched foot Varous position of foreleg	Steady layout of weight The highest load - fingers 33.3% - 2. degree of normally arched foot Slightly varus position of foreleg
Squat – Right LL	Decrease of FA The highest load - the front part of the foot, fingers and medial side of the heel 35.3% - 2. degree of normally arched foot Impaired stability	Steady layout of weight 33.3% - 2. degree of normally arched foot Stability - good

Note: LL – lower limb, AJ – ankle joint, FA – foot arch.

By PodoCam evaluation, we assessed the changes in the position of the foot, which we took into account in the results of the motor test to find out to what extent the Propriofoot® Concept influenced the jumping abilities. PodoCam evaluation showed that proband improved stability. There was a significant change in foot load. After our therapy, the body mass was evenly distributed without significant overload of the individual parts of the foot. At the beginning, the proband had a high arch at standing. With an increased load, the FA managed to set itself in an almost ideal position. In most of the movement tests performed, the proband was able to improve. During the indoor season, her personal maximum also moved by 12 cm, from 535 cm to 547 cm (tab. 7). From the point of view of the discipline that the athlete devotes to, we consider this move to be significant. Just the fingers and thumbs give the last pulse to take off of the foot from the pad.

TABLE 7. Movement tests with focus on jumping ability of LL of proband (n=1)

Tests	Input evaluation (I1)	Output evaluation (O2)
Myotest – 3 jumps	1. attempt – 41.2 cm/134 ms **2. attempt – 41.3 cm/139 ms** 3. attempt – 39.8 cm/123 ms	1. attempt – 41.5 cm/127 ms **2. attempt – 43.0 cm/115 ms** 3. attempt – 41.5 cm/109 ms
Myotest – 1 jump	1. attempt – 41.3 cm 2. attempt – 42.0 cm **3. attempt – 43.4 cm**	1. attempt – 39.1 cm 2. attempt – 39.1 cm **3. attempt – 41.3 cm**
Standing long jump	1. attempt – 2.17 cm 2. attempt – 2.23 cm **3. attempt – 2.24 cm**	**1. attempt – 2.30 cm** 2. attempt – 2.25 cm 3. attempt – 2.27 cm
10 jumps	**1. attempt – 23.10 m** 2. attempt – 22.90 m 3. attempt – 22.50 m	1. attempt – 24.90 cm **2. attempt – 25.48 cm** 3. attempt – 25.3 cm
Long jump – personal record	535 cm	**547 cm**

CONCLUSION

We consider the obtained results as very important for both clinical and sports practice. In a relatively short time, positive changes in the area of the foot were achieved. The weight of the body has spread evenly over the entire length of the foot, thereby improving the stability of the body, due to a steady constructed exercise unit containing the lability of the forefoot and hindfoot. It follows from the above that the use of the Propriofoot Concept in the training unit had its justification.

It was showed to activate and strengthen the muscles of the entire lower limb and to influence the jumping ability of the proband. Significant improvement was seen in motor tests, especially in the case of horizontal type of taking off, which is more important for long jump, as performance does not take into account the height of the take off. These changes in motor tests need to be seen and understood as a guideline and a basis for creating training content for athletes in the long jump.

In the end, correctly chosen, realized exercises and physical programs positively influence and create a prerequisite for the posture as a manifestation of the functioning of the muscular system. The sketched "intensity factor" is a knowledge and a basis for sports theory and practice. It is necessary to perceive it as an adjunct therapy in the correction of functional disorders of the foot, in order to activate the foot arch.

ACKNOWLEDGEMENT

The listed study is the part of the research project: VEGA 1/0519/19 "Physical activity as prevention of health of school population in Slovakia“.

REFERENCES

1. Adamec, O. (2005). Plochá noha v dětském věku – diagnostika a terapie. *Pediatrie pro praxi*, (4), 194-196
2. Brozmanová, B. (2015). Ako sa dá znížiť riziko plochonožia u detí? In *teória a prax- farmaceutický laborant,* (4), 34-35.
3. Čihák, R. (2011). *Anatomie 1.* Třetí, upravené a doplněné vydání. Praha: Grada Publishing, a.s,
4. Hamill, J., Knutzen, K.M., Derrick, T.R. (2015). *Biomechanical Basis of Human Movement.* 4th edition. Library of Congress Cataloging-in-Publication Data,
5. Hodges, P. W, Richardson, C. (1996) Inefficient muscular stabilization of the lumbar spine associated with low back pain. A motor control evolution of transversus abdominis. *Spine*, (21), 2640-2650.
6. Charlesworth, S.J., Johansen, S.M. (2010). *Naviculare Drop Test.* [http://kennisbank.hva.nl/document/225653].
7. Janda, V. (2004). *Svalové funkčné testy.* Praha: Grada Publishing.
8. Janíková, D. (1998). *Fyzioterapia: funkčná diagnostika lokomočného systému I.* Martin: Osveta.
9. Kim, E., Kim, J. (2016). The effects of short foot exercises and arch support insoles on improvement in the medial longitudinal arch and dynamic balance of flexible flatfoot patients. *Journal of Physiacal Therapy Science,* 11(28), 95.
10. Kolář, P. et al. (2009). *Rehabilitace v klinické praxi*. Praha: Galén.
11. Lewit, K. (2003). *Manipulační léčba v myoskeletální medicíně.* Praha: Zdelovací technika, Česká lekářská společnost J.E.Purkyňe.
12. Lewitová, C. (2016). O dětských nohách. In *Umění fyzioterapie,* 1(1), 5-7.
13. Palaščáková Špringrová, I. (2016). *Propriofoot, preventivně – terapeutická balanční pomůcka,* Čelákovice: Rehaspring centrum s.r.o.
14. Palaščáková Špringrová, I. (2017). *Studijní materiál pro kurz Propriofoot Concept.* Čelákovice: Rehaspring Centrum s.r.o.
15. Psalman, V., Zvonař, M. (2007). Three dimensional biomechanical analysis as a mean for diagnostics of dynamic balance abilities. *4th FIEP European Congress Physical Education and Sports*, Bratislava, Slovakia, p.111.
16. Sarl Propriofoot Associées. (2007). *Propriofoot.* [online]. 2007. [cit. 2018-02-20]. Dostupné na internete: http://www.propriofoot.com/proprioception-cheville/#page7 .
17. Vařeka, I., Vařeková, R. (2009). *Kineziologie nohy*. Olomouc: Vydavatelství UP.
18. Véle, F. (2006). Kineziológie, Přehled kineziologie a patokineziologie pro diagnostiku a terapii poruch pohybové soustavy. Praha: Triton.
19. Vojtaššák J. (2000). Ortopédia. Bratislava: SNP.
20. Videoanalyza.cz. (2018). *Myotest.* [online]. 2018. [cit. 2018-03-08]. http://www.videoanalyza.cz/myotest/testy.

Active Exercise to Affect Sole of Foot by "Physiotherapy Function"

Michal Marko[1,a)], Šárka Tomková[2)], Elena Bendíková[1)]

[1]Matej Bel University, Faculty of Arts, Banska Bystrica, Slovak Republic
[2]St. Elisabeth University of Health Care and Social Work, Bratislava, Slovak Republic

a) Corresponding author: Michal.Marko@umb.sk

Abstract. The aim of the study was to identify active exercise to affect sole of foot by "Physiotherapy Function". The monitored group (n = 2) consisted of female pupils (n = 2) (11 years of age, 38 kg, 150 cm and 16.6 Bmi) in pubescence who have attended public elementary schools in Banská Bystrica, Slovak Republic. The testing (input and output) was done within the monitored group (n = 2) whose health situation was without any illnesses or subjective difficulties. In terms of data acquisition methods, the standardized methods were used, which were based on evaluation of body posture, foot according to "Physiotherapy Function" and by podoscope. Moreover, the obtained results of the study were processed in form of clinical case reports, which after eight weeks reported positive changes of all listed evaluations. The presented results, which were processed in forms of the clinical case reports, reported to positive changes in both female pupils (n = 2), in method of Klein and Thomas modified by Mayer and tests of Trendelenburg, elevation of contralateral upper and lower extremities and forearm-supported side lying. In female pupil 1 (n = 1) was recorded slightly positive changes in ability of relaxation and grip strength, while in female pupil 2 (n = 1) was recorded in reaction of the foot at stimulus. *The listed study is the part of the research project: VEGA 1/0519/19 "Physical Activity as Prevention of Health of School Population in Slovakia".*

Key words: body posture, female pupils, foot, "Physiotherapy Function".

INTRODUCTION

A prevalence of current level of muscular and skeletal system significantly differs, as an occurrence of various disorders (functional and structural) increases yearly, even doubles (Bendíková, 2012). It starts in period of preschool (Erick, Smith, 2011), younger school age/ pubescence (Mitova, 2015; Azabagic, 2016) and adolescence (Marko, Bendíková, 2018; Bendíková et al., 2019). However, it occurs in adulthood (Singh et al., 2014) and old age (Gheno et al., 2012). What is more, the increased occurrence of listed disorders is associated with foot (sole) and its influence and functionality. It occurs in all of the periods of human development, starting with childhood (Arya, 2014), continues with adulthood (Menz, 2013) and finishes in old age (Malanga, Ramirez, 2008).

The standards of society, in which we live, are based on wearing the shoes with thick sole. It depletes us of valuable information from proprioceptors (Schmidt, Gúth, Hrdý, 2010; Palaščáková Špringrová, 2016, 2017) and these factors negatively affect body posture. Zambojová (2013) adds that the foot is the first source of information for postural stabilization and developing foot deformities resulting in changes of the muscle tension, which are connected to muscular and skeletal system. The mentioned system causes muscular imbalances (Thurzová, 1998; Bendíková, 2011, 2017a), which lead to the different functional and structural disorders (White, Mencio, 1995; Buran, 2002; Čihák 2011; Lubkowska, 2015; Lubkowska, Zdeb, Mroczek, 2015).

The muscular and skeletal system, within the area of foot, especially sole is tight pack of forma and function. The mentioned area consists of 26 bones and 19 muscles (Dungl, 1988; Gross, 2005; Kolář, 2010) and forms acral part of the lower extremity and mediates the body's contact with the terrain, on which we move. Similarly the monkey's foot grabs the branches; the human foot is adapted to grasp the ground (Véle, 2006). It is masterpiece of the human evolution. It possesses significant features such as: arch architecture, biomechanical interplay, strength, flexibility or damping (Pročková, 2016). According to "Physiotherapy Function", the foot forms the root of the body and ensures the connection within the earth's surface. The foot arch is very significant, as it forms the basis for other structures of muscular and skeletal system (Rozkydal, Chaloupka, 2001).

If the object is stable, it must be supported at the three points and the center of gravity must be between them. The foot has also three supportive points; the heel bone, the head of the first metatarsus and the head of the fifth metatarsus. There are two arches between these points - the transverse and longitudinal (Dylevský, 2000). The both arches are filled with the strips of soft tissues from the plantar side, which act as dampers (Gross, 2013).

The sole of the foot is very flexible; the heel segment is variable and has its axis. An important fact is that the foot support function ends in the diaphragm. In children, the most natural manifestation of joy is movement (Dobay, 2015; Müller, Bácsné, 2018) and therefore is needed flexible muscular and skeletal system (Bendíková, 2017; Bendíková, Marko, Šmída, 2018). The resulting shape of foot is determined by the interaction of the structure of the individual bones, storage and mutual situation. The position of bones in the proximal row is decisive (Šmondrk, 1995; Hamill, Knutzen, 2015).

"Physiotherapy Function" is an approach based on the teaching of Clara Lewitová, in which a physiotherapist from a structure of the body, the tension of the soft tissues, and the reactivity of a patient reads about the function, movement, behavior, its state and possibilities of change in the sense of optimum. The Lewitová´s approach involves two basic components, namely examination and therapy. The examination starts with an observation, in which we determine the basic characteristics of the patient and describe the form according to the seven criteria. The basic point is the overall description of the patient. We briefly try to describe him at most by three words and try to find his main deficit. We conduct dialogue with the patient during the examination, and after the therapy, we try to prepare the tissue for its active work. The therapy involves affecting tension and regulating sensitivity, in the terms of decreasing and increasing sensitivity, stabilizing, mobilizing and patient education (Lewitová et al 2017).

The aim of the study was to identify the active exercise to affect the sole of foot by "Physiotherapy Function", within monitored group (n = 2) who have attend public elementary schools in Banská Bystrica, Slovak Republic.

METHOD

Participants

In accordance with the aim of the study, the monitored group (n = 2) of the selected elementary schools (Elementary School of Ján Bakoss/ Elementary School of Štefan Moyses) in Banská Bystrica, Slovak Republic. The selection was focused on foot and spine deformities of the female pupils (n = 2) (12 years of age, 38 kg, 150 cm and 16.6 Bmi) in pubescence. The testing (input and output) was realized in the period of the health situation, which was without any illnesses of subjective difficulties. The primary characteristics of the monitored group (n = 2) is presented in table 1.

TABLE 1. The primary characteristics of monitored group (n = 2)

Measured values	Monitored group	
	Female pupil 1	Female pupil 2
Age [years]	12	12
Body weight [kg]	39,5	36,5
Body height [m]	153	147
Body mass index [kg/m^2]	16,6	16,6

Legend: kg - kilogram, **m -** meter, **kg/m^2 -** kilogram per square meter.

Procedure

The research was realized within the interval of 07 January 2019/ 01 March 2019. The approach "Physiotherapy Function" by Clara Lewitová was realized 8 weeks/ 2 x/ 20 minutes (Monday/ Friday) in private clinic - TaoFyzio Centrum in Banská Bystrica, Slovak Republic. The female pupils (n = 2) proceed according to references of listed approach - "Physiotherapy Function", as we prepared exercises (in number of 20, from the easiest to the most difficult), which were applied to improve the function of foot and spine. The realization of the specific exercises acted in development of the monitored research indicators. The research consisted of three stages:

1. Input testing/ clinical case reports (07 January 2019),
2. Realization of "Physiotherapy Function" (07 January 2019/ 01 March 2019),
3. Output testing (01 March 2019).

In terms of the data acquisition methods, several of them were applied, as the research was realized. The first data acquisition method, which was applied, was method of studying literary sources. It was used in the introduction; however some authors and their methods are stated in section method/ procedure.

The characteristics of the monitored group (n = 2) were completed by the method of somatometry (Hošková, Matoušová, 2005; Bendíková, 2011).

The observation (aspection) and palpation methods are divided; within the body parts they were applied:

1. Evaluation of body posture (Klein and Thomas modified by Mayer, Crampton′s test, Matthias′s test, Trendelenburg′s test, tests of elevation contralateral upper & lower extremities, forearm-supported side lying) (Janíková, 1998; Labudová, Vajcziková, 2009).
2. Evaluation of foot by "Physiotherapy Function" (standing and lying foot description mobility indicative evaluation, standard of sensitiveness, grip strength, tri-flexion) (Holubcová, Maryška, 2017).
3. Evaluation of foot by podoscope (rehabilitation plan/ program) (Volf, 2005) (fig. 1).

FIGURE 1. Evaluation of foot by podoscope

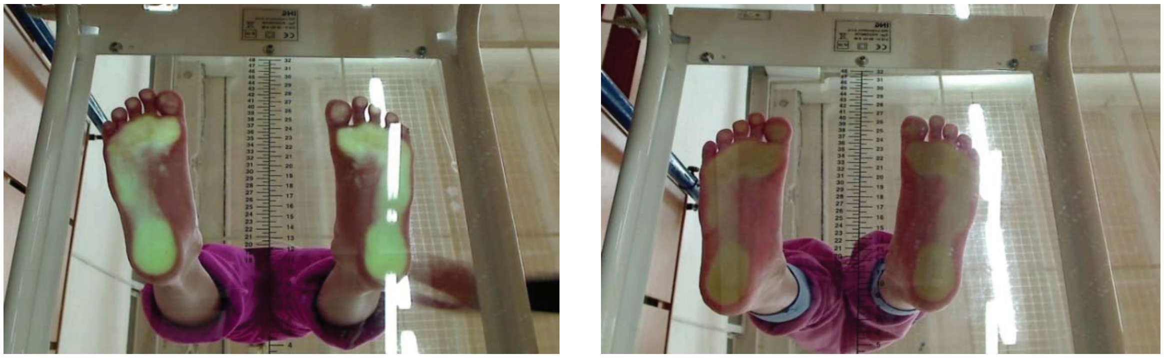

FIGURE 2. The input and output testing of female pupil 1 (n = 1) on podoscope

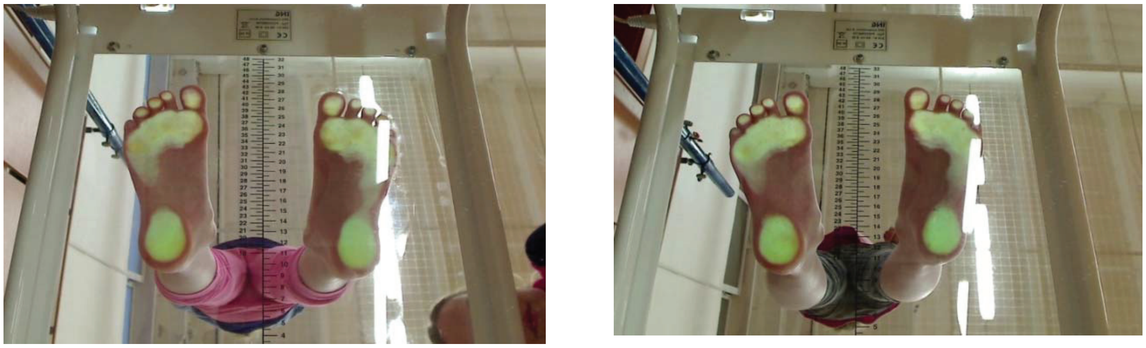

FIGURE 3. The input and output testing of female pupil 2 (n = 1) on podoscope

Data analyses

The obtained qualitative and quantitative information were processed by clinical case reports. What is more, analysis, synthesis, inductive and deductive approaches, comparisons and generalizations were applied (Vojtaššák, 2000).

RESULTS

Based on the aim and below presented results which are subject to accurate monitoring and processing, the listed results cannot be generalized, but it is necessary to understand them in the overall context, in relation to health, through the prism of muscular and skeletal system, namely in areas of foot and spine.

The sections of the results are based on the clinical case reports, in which we studied the monitored group (n = 2). Both female pupils (n = 2) are presented in the tables (2, 3, etc.), but subsequently are presented final reviews of the clinical case reports as conclusions.

TABLE 2. The clinical case reports of monitored group (n = 2)

Measured values	**Monitored group**	
	Female pupil 1	**Female pupil 2**
Family	* Father - Soccer/ mother - handball; ° Brother - Soccer	* Father - Soccer/ mother - athletics; ° Sister - Judo
Personal	Childhood illnesses, without broken bones	Childhood illnesses, without broken bones
Social	Lives in flat with parents and + brother	Lives in house with parents and + sister
Physical	Not playing any sports, more devoted to studying	Not playing any sports, more devoted to studying

Legend: * Used to play, ° Still playing, + Studies at universities.

TABLE 3. The results of Klein and Thomas modified by Mayer of monitored group (n = 2)

Quality levels	**Monitored group**			
	Female pupil 1		**Female pupil 2**	
	Input testing	**Output testing**	**Input testing**	**Output testing**
I.	2	1	1	1
II.	1	1	2	2
III.	2	1	4	3
IV.	2	2	1	1
V.	2	2	2	2
Total	9	7	10	9

Legend: I. Head and neck posture, **II.** Shape of chest, **III.** Shape of abdomen and pelvic inclination, **IV.** Overall curvature of spine, **V.** Height of shoulders and scapulae position.

TABLE 4. The results of Crampton′s and Matthias′s tests of monitored group (n = 2)

Measured values	**Monitored group**			
	Female pupil 1		**Female pupil 2**	
	Input testing	**Output testing**	**Input testing**	**Output testing**
Crampton′s test 1	Chest touches wall, nose is 4 cm away	Without changes	Chest touches wall, nose is 1 cm away	Without changes
Crampton′s test 2	Heels, butt and chest touch wall	Without changes	Heels, butt and chest touch a wall	Without changes
Matthias′s test	Decreased shoulders, upper extremities and increased lumbar lordosis	Increased lumbar lordosis, without decreased shoulders	Increased lumbar lordosis	Without changes

TABLE 5. The results of Trendelenburg′s test of monitored group (n = 2)

Measured values	Monitored group			
	Female pupil 1		Female pupil 2	
	Input testing	Output testing	Input testing	Output testing
Right lower extremity	Vibration of lower extremity, pelvic elevation of examined lower extremity	Vibration of lower extremity	Elevation and rotation of pelvis after 15 s. of examined lower extremity	Vibration of lower extremity after 10 s.
Left lower extremity	Pelvis remains leveled for 10 s., pelvic elevation and vibration of lower extremity	Pelvis remains leveled 20 s., vibration of lower extremity	Vibration of lower extremity after 10 s.	Pelvis remains leveled 20 s.

Legend: s. Seconds.

TABLE 6. The results of test of elevation contralateral upper and lower extremities of monitored group (n = 2)

Measured values	Monitored group			
	Female pupil 1		Female pupil 2	
	Input testing	Output testing	Input testing	Output testing
Right side	Position is correct, vibration of body	Position is without problems	Cannot hold position after 5 s., decreased lower extremity	Without changes
Left side	Cannot hold position, incorrect chest stability and rotation	Correct holding of position for 10 s., decreased lower extremity	Cannot hold position, rotation of chest, decreased lower extremity	Correct holding of position for 5 s., decreased lower extremity

Legend: s. Seconds.

TABLE 7. The results of test of forearm-supported side lying of monitored group (n = 2)

Measured values	Monitored group			
	Female pupil 1		Female pupil 2	
	Input testing	Output testing	Input testing	Output testing
Forearm-supported side lying	Correct holding of position for 8 s., weakened abdominal wall, vibration of body	Correct holding of position for 13 s., weakened abdominal wall, vibration of body	Increased thoracic kyphosis, weakened abdominal wall	Increased thoracic kyphosis after 5 s., weakened abdominal wall

Legend: s. Seconds.

Evaluation of foot by "Physiotherapy Function"

Standing and lying foot description

Standing - Female pupil 1 (n = 1)

Input testing- While comparing dorsal side of the foot with the plantar side; the dorsal side of the foot has increased muscle activity. The medial edge of the foot, basically on both feet, is slightly fallen through, the thumbs and toes are close to each other.

Output testing- Without changes.

Standing - Female pupil 2 (n = 1)

Input testing- The medial edge of the foot is weakened on both sides, the thumbs and toes are apart, while the fourth and fifth toes are not active and the foot is relaxed.

Output testing- Longitudinal arch is slightly falling medially on both feet, the thumbs and toes are apart, the fourth and fifth toes and foot in generally are more active than in input testing.

Lying - Female pupil 1 (n = 1)
Input testing- Increased muscle activity on dorsal side, the feet are in position of tiptoes.
Output testing- The feet are in slight tension; in position of tiptoes are able to relax better.

Lying - Female pupil 2 (n = 1)
Input testing- The foot is in natural position, orientated in 80° flexion in ankle joint.
Output testing- Without changes.

Mobility indicative evaluation
Female pupil 1 (n = 1)
Input testing- Flexion, extension supination and pronation are without limitation; the rotation of the foot is looser at right lower extremity than at left lower extremity.
Output testing- Without changes.

Female pupil 2 (n = 1)
Input testing- The flexion and extension are adequate and same at both feet; bigger extension of movement towards supination and pronation of right lower extremity; rotation of the foot is looser at right lower extremity than at left lower extremity.
Output testing- Without changes.

Standard of sensitiveness
Female pupil 1 (n = 1)
Input testing- The reaction at stimulus is slight; it comes to slight twitch of the foot.
Output testing- The reaction at stimulus is slight; stronger at right lower extremity.
Female pupil 2 (n = 1)
Input testing- The reaction at stimulus is featureless; it comes to slight twitch of the foot.
Output testing- The reaction at stimulus is strongly on both feet; adequate twitch of the foot.

Grip strength
Female pupil 1 (n = 1)
Input testing- The moderate grip strength.
Output testing- The high grip strength.

Female pupil 2 (n = 1)
Input testing- The high grip strength on both feet.
Output testing- Without changes.

Tri-flexion
Female pupil 1 (n = 1)
Input testing- The movement of the ankle, knee and hip joints was realized correctly.
Output testing- Without changes.

Female pupil 2 (n = 1)
Input testing- The movement of the ankle, knee and hip joints was realized correctly.
Output testing- Without changes.

Evaluation of foot by podoscope
Rehabilitation plan
Female pupil 1 (n = 1) and female pupil 2 (n = 1)
According to approach "Physiotherapy Function" we increased feet support, regulated muscle tensions, strengthen the sole of feet and built adequate foot response to stimulus. Thereby, we improved overall feet functions.

Rehabilitation program

Female pupil 2 (n = 1) and female pupil 2 (n = 1)

Facilitation of the foot sole, inhibition of dorsal foot, mobilization of peripheral joints of feet and activation of the feet by method “Big Foot” was realized correctly.

CONCLUSION

Final reviews of the clinical case reports

Female pupil 1 (n = 1)

While evaluating the body posture by method of Klein and Thomas modified by Mayer, we noticed two-point overall improvement. It changed the head position, pelvic inclination and abdominal shape. The total number of points almost positively changed the body posture from good to perfect body posture. Crampton′s tests came out without any pathological changes within the input and output testing. The tests of Trendelenburg and elevation of contralateral upper and lower extremities positively pointed to improvement of both, right and left lower extremities. The slight improvement was also recorded in forearm-supported side lying. While examining the foot, we evaluated better ability of relaxation and grip strength on both feet.

Female pupil 2 (n = 1)

While evaluating the body posture by method of Klein and Thomas modified by Mayer, we noticed one-point overall improvement. It changed pelvic inclination and abdominal shape. The total number of points stayed at good body posture. The first Crampton′s test pointed to incorrect body posture and the second Crampton′s test came out without aby pathological changes within the input and output testing. The Trendelenburg′s test positively pointed to slight improvement in both the right and left lower extremities. However, the elevation of contralateral upper and lower extremities was recorded with worse chest stability on left side, but slight improvement of the right side. While examining the foot, we evaluated the better activity of the fourth and fifth finger in standing position and the better foot response to the stimulus from the outside.

To sum up, the presented results, which were processed in forms of the clinical case reports, reported to positive changes by using approach of “Physiotherapy Function” in both female pupils (n = 2), in method of Klein and Thomas modified by Mayer and tests of Trendelenburg, elevation of contralateral upper and lower extremities and forearm-supported side lying. In female pupil 1 (n = 1) was recorded slightly positive changes in ability of relaxation and grip strength, while in female pupil 2 (n = 1) was recorded in reaction of the foot at stimulus.

ACKNOWLEDGEMENT

The listed study is the part of the research project: VEGA 1/0519/19 "Physical activity as prevention of health of school population in Slovakia“.

REFERENCES

1. Arya, R. (2014). Low Back Pain - Signs, Symptoms and Management. *Journal, Indian Academy of Clinical Medicine*, (15), 30-41.
2. Azabagic, S. et al. (2016). Epidemiology of Musculoskeletal Disorders in Primary School Children in Bosnia and Herzegovina. *Materia Socio-Medica*, (28), 164-167.
3. Bendíková, E. (2011). *Oporný a pohybový systém, jeho funkcia, diagnostika a prevencia porúch*. B. Bystrica : Univerzita Mateja Bela v Banskej Bystrici.
4. Bendíková, E. (2012). Oslabený oporný a pohybový systém žien a jeho úprava pohybovým programom. B. Bystrica : Fakulta humanitných vied, Univerzita Mateja Bela v Banskej Bystrici.
5. Bendíková, E. (2017a). Theory of Health, Movement and Lifstyle of Human Beings. Publisher : University of Debrecen, Debrecen.
6. Bendíková, E. (2017). Application of multimedia-based exercise programmes focused on improvement of the schoolgirls’ musculoskeletal system during breaks between classes. In ICCMSE-2017 : AIP proceedings of the international conference of computational methods in sciences and engineering 2017, Thessaloniki, Greece, 21–25 April 2017. Vol. 1906. - 1. ed. - New York : American institute of physics, 2018. - ISBN 978-0-7354-1596-6.
7. Bendíková, E. et al. (2019). Effect of 4-Week Physical Program on Musculoskeletal System in Adolescent Sport Class Students with Focus on Ice Hockey. Physical Activity Review, 7(1), 63-70.

8. Bendíková, E., Marko, M., Šmída, L. (2018). Influence of Change in Content of Physical and Sport Education as Case Study on Level of Dynamic Function of Spine among Secondary School Female Students. *European Journal of Contemporary Education*, (7), 633-641.
9. Buran, I. (2002). *Vertebrogénne algické syndrómy*. Bratislava : S+S.
10. Čihák, R. (2011). *Anatomie 1*. Praha : Grada Publishing.
11. Dobay, B. (2015). Az iskolai sporttanfolyamok motivációs hatása a felnıttkori rekreációs sporttevékenységekre Dél-Szlovákiában. Komárom : Kompress kiadó.
12. Dungl, P. (1988). *Ortopedie a traumatology nohy*. Praha : Avicenum.
13. Dylevský, I. (2000). *Funkční anatomie člověka*. Praha : Grada Publishing.
14. Erick, P., Smith, D. (2011). A Systematic review of Musculoskeletal Disorders among School Teachers. *Muscular and Skelelat Journal,* (2), 120-130.
15. Gheno, R. et al. (2012). Musculoskeletal Disorders in the Elderly. *Journal of Clinical Imaging Science*, (2), 131-139.
16. Gross, J. (2005). *Vyšetření pohybového aparátu*. Praha: Triton.
17. Gross, J. (2013). *Vyšetrení pohybového aparátu.* Praha : Portál.
18. Holubcová, J., Maryška, J. 2017. *Fyzioterapia funkcie 1*. Dobřichovice : Centrum komplexní péče.
19. Hošková, B., Matoušová, M. (2005). *Kapitoly z didaktiky zdravotní tělesné výchovy pro studující FTVS UK*. Praha : Karolinum.
20. Janíková, D. (1998). *Fyzioterapia*. Martin : Osveta.
21. Kolář, P. (2010). *Rehabilitace v klinické praxi*. Praha : Galén.
22. Labudová, J., Vajcziková, S. (2009). *Športová činnosť pri poruchách orgánov opory a pohybu*. Bratislava : Slovenský zväz rekreačnej telesnej výchovy a športu.
23. Lewitová, A. et al. (2017). Prevence a rehabilitace ploché nohy u dětí a mládeže. *Rehabilitace*, (54), 164-173.
24. Lubkowska, W. (2015). The concept of treatment of scoliosis employing asymmetrical aquatic exercises. *Cent Eur J Sport Sci Med.*, 9(1), 55-64.
25. Lubkowska, W., Zdeb, T., Mroczek, B. (2015). Assessment of physiological spine curvature in girls who trained competitive swimming versus non-swimming girls. *Family Medicine & Primary Care Review,* 17(3), 189 - 192.
26. Malanga, G., Ramirez, J. (2008). Common Injuries of the Foot and Ankle in the Childhood and Adolescent Athlete. *Physical Medicine and Rehabilitation Clinics of North America*, (19), 347-371.
27. Marko, M., Bendíková, E. (2018). Level Changes of Musculoskeletal System in High School Female Students by Physical Program within Physical and Sport Education. Istanbul : Marmara University.
28. Menz, H. (2013). Foot Pain and Mobility Limitations in Older Adults. *The Journal of Gerontology*, (68), 1281-1285.
29. Mitova, S. (2015). Frequency and Prevalence of Postural Disorders and Spinal Deformities in Children of Primary School Age. *Research in Kinesiology*, (43), 21-24.
30. Müller, A., Bácsné, B. É. (2018). *Az egészséges életmód és a sport kapcsolata*. Létavértes, Magyarország : Létavértes SC '97 Egyesület, 2018, 96 p.
31. Palaščáková Špringrová, I. (2016). *Propriofoot, preventivně – terapeutická balanční pomůcka,* Čelákovice : Rehaspring centrum s.r.o.
32. Palaščáková Špringrová, I. (2017). *Studijní materiál pro kurz Propriofoot Concept.* Čelákovice : Rehaspring Centrum s.r.o.
33. Pročková, P. (2016). Barefoot obuv pro déti. *Umění fyzioterapie*, (1), 11-15.
34. Rozkydal, Z., Chaloupka, R. (2001). *Vyšetrovací metódy v ortopédii*. Brno : Masarykova univerzita.
35. Schmidt, F., Gúth. A., Hrdý, J. (2010). Postura- jej zložky a ich terapeutické ovplyvnenie komplexnou kúpeľnou liečbou. *Lekársky obzor*, (59), 276-281.
36. Singh, V. et al. (2014). Epidemiology of Low Back Pain. *Neuromodulation*, (2), 123-131.
37. Šmondrk, J. (1995). Balneofyzikálna liečba plochej nohy. *Rehabilitácia*, (28), 220-223.
38. Thurzová, E. (1991). Funkčné svalové poruchy u detskej populácie. *Telesná výchova a šport*, (14), 23-28.
39. Véle, F. (2006). *Kineziológie, přehled kineziologie a patokineziologie a diagnostiku a terapii poruch pohybové soustavy*. Praha : Triton.
40. Vojtaššák, J. (2000). *Ortopédia*. Bratislava : Slovak Academic Press.
41. White, G., Mencio, G. (1995). Genu Valgum in Children: Diagnosis and Therapeutic Alternatives. *Journal of the American Academy of Orthopaedic Surgeons*, (3), 275-283.
42. Zambojová, I. (2013). Úloha nohy pri chôdzi posturálnej stabilizácií. In *Physiotherapia Slovaca*, (20), 24-30.

Health Status Differences in Perceived Satisfaction with Health of Active and Inactive Population

Dagmar Nemček [1)], Elena Bendíková [2a)], Petra Kurková [3)]

[1]*Comenius University, Faculty of Physical Education and Sports, Nábr. Arm. Gen. L. Svobodu 9, 814 69 Bratislava, Slovak Republic*
[2]*Matej Bel University, Faculty of Arts, Tajovského 40, 974 01 Banská Bystrica, Slovak Republic*
[3] *Palacký University, Faculty of Education, Žižkovo nám. 5, 771 40 Olomouc, Czech Republic*

a) Corresponding author: dagmar.nemcek@uniba.sk

Abstract: The aim of our investigation was to find out the differences in perceived satisfaction with health within three evaluated groups with different level of health status: healthy people, people with noncommunicable diseases (NCDs) and people with disabilities. Two main groups of people were recruited for the study: (1) active people (n=607; regularly participating in sport activities) and (2) inactive people (n= 494; not participating in sports activities). We used second part of S.QUA.L.A. questionnaire where participants evaluated perceived satisfaction with 23 indicators using the 5-point rating scale. The lower mean score meant the higher perceived satisfaction. For our investigation we analysed perceived satisfaction with only one indicator "overall health". Statistical analysis was performed using IBM SPSS version 23.0. The data were statistically tested by the Kolmogorov-Smirnov test of the sample distribution normality. One-way ANOVA was used to determine the differences in perceived satisfaction with health within three evaluated groups based on their health status. Post-hoc Bonferroni test was used to examine the differences in satisfaction with health between two groups of population based on their health status. Student's two-sample t test was used to examine the differences between active and inactive people within each population group based on their health status. We found the highest level of perceived satisfaction with overall health in the group of healthy actively living population and the lowest perceived satisfaction with overall health in the group of inactive people with NCDs. In the group of active as well as inactive people we found significantly higher perceived satisfaction with health in the group of healthy people comparing people with NCDs and people with disabilities. No significant differences were found in the comparison of perceived satisfaction with overall health between people with NCDs and people with disabilities nor in the group of active neither inactive population. In all groups of people related to their health status the significantly higher perceived satisfaction with health was demonstrated by actively living populations comparing inactive population.
Key words: satisfaction with overall health, healthy people, people with noncommunicable diseases, people with disabilities, actively living and inactive population.

INTRODUCTION

Perceived satisfaction with health can be defined as the overall assessment of the various positive and negative experiences and outcomes that result overall health. Perceived satisfaction is theorized to be a critical predictor of health behaviour change maintenance. Sports and recreational activities can be targeted to affect somatic, motor and functional aspect of man to improve overall health as well as physical and mental condition, and subjective well-being (Bendíková et al., 2019).

Human health is interconnected throughout the life span from conception to fatal life to early childhood and adolescence and on into adulthood and the senior years. Each stage presents its own unique health needs and problems, yet each of them is interconnected. There is compelling evidence that early life may have a profound impact on health and disease in later life (Barker, 1992; Bhargava et al., 2004; Gluckman et al., 2008; Müller & Bácsné, 2018). The emerging pandemic of non-communicable diseases (NCDs) is creating major health challenges globally. NCDs are currently the leading cause of mortality causing 68 % of all deaths globally. Cardiovascular diseases, cancer, chronic obstructive pulmonary diseases and diabetes have been identified by the World Health Organization as the four major NCDs occurring worldwide (WHO, 2014). Many of the NCDs can cause permanent disabilities in later life.

Many people with NCDs (WEF, 2017) and disabilities (Rimmer et al., 2004) have poor general health, limited community participation, and low quality of their life. Promotion of health and quality of life for disabled people is one of the World Health Organization's objectives. Few investigations have shown that participation in regular physical activities has a positive effect on overall health and overall quality of life (Tomková & Palaščáková Špringrová, 2013; Kurková & Maertin, 2014; Bendíková, 2014; 2017; Dobay, 2014, 2015; Lubkowska, 2015; Łubkowska et al., 2014, 2015, Zuzda, 2017), quality of psychological health (Pačesová et al., 2018), quality of physical

health (Bendíková, 2011; Müller, 2013; Müller et al., 2018), quality of family life (Dobay & Bendíková, 2014) and quality of social life (Fobel et al., 2001; Kurková, Válková & Scheetz, 2011) among people with NCDs and those with disabilities. On the other hand, leisure time sedentary behaviour has been found to have stronger associations with all-cause mortality than total daily sitting time, possibly because it might be accompanied by unfavourable eating behaviours (Hagger-Johnson et al., 2016; Shaw et al., 2017). Individuals who stay sedentary over longer periods of their life represent the most important target for interventions since they have the highest risk of health problems that decreases their own life quality. There is evidence for associations with mortality (Katzmarzyk et al., 2009; Biswas et al., 2015; Hagger-Johnson et al., 2016), cancer incidence (Biswas et al., 2015), diabetes (Wilmot et al. 2012), bone density (Chastin et al., 2014) and falls (Nemček, 2009; Jefferis et al., 2015).

AIM

The aim of our investigation was to find out the differences in perceived satisfaction with health within three evaluated groups with different level of health status (healthy people, people with noncommunicable diseases and people with disabilities) regularly participating in sport (active people) and not participating in sport (inactive people) in their leisure time.

METHOD

Participants

Two main groups of people (n=1101) were recruited for the study. The research sample comprised (1) 607 people who are regularly participating in their leisure time in different sports and physical activities (active people) at least two times per week for 30 minutes minimum duration and (2) 494 people who are not participating in any sport and physical activities in their leisure time (inactive people). In the research participated 334 healthy people (74.6 % active; 25.4 % inactive), 308 people with NCDs (55.2 % active; 44.8 % inactive) and 459 people with disabilities (40.9 % active; 59.1 % inactive) (Table 1). Active people participated mostly in football and other sport games at the professional and recreational level, afterwards they participated in different group/team physical activities with music accompaniment like different types of aerobics and dances, performed strength work out in the gyms and fitness centres, etc.

TABLE 1 Descriptive characteristic of participants (n; %)

		Sport Participation (n; %)		Gender (n; %)	
Health Status	Total	Active	Inactive	Men	Women
Healthy people	334 (30.4)	249 (74.6)	85 (25.4)	199 (59.6)	135 (40.4)
People with NCDs	308 (27.9)	170 (55.2)	138 (44.8)	141 (45.8)	167 (54.2)
People with disabilities	459 (41.7)	188 (40.9)	271 (59.1)	228 (49.7)	231 (50.3)
Total	1101 (100)	607 (55.1)	494 (44.9)	568 (51.6)	533 (48.4)

Participants procedure

Active people were contacted through representatives of selected national sport organisations (associations and federations), sport universities located in Slovakia and through different sport facilities intended for recreational athletes. Some questionnaires were sent electronically, and some were filled out during meetings organised by sport organisations, after exercise classes in fitness centres and students of sport universities filled out the questionnaires during their classes with university teacher permission. The data of inactive people were collected mostly through students attending regular universities located in Slovakia and they were asked to give the same questionnaire to their inactive friends, peers and relatives (parents, grant parents, siblings, etc.). Students filled out the questionnaires during their classes with university teacher permission and questionnaires of their friends, peers and relatives brought to seminars within the span of two months. All data were collected during year period 2017. All participants with disabilities agreed participate in the study and gave their written informed consent.

The Subjective Quality of Life Analysis (S.QUA.L.A)

S.QUA.L.A. is a multidimensional instrument. This multidimensional self-assessment method was created by Mathieu Zannotti in 1992 (Zannotti & Pringuey, 1992). This scale includes 23 items (indicators) of life. It covers traditional areas (food, family relation etc.), and more abstract aspects of life (politic, justice, freedom, truth, beauty and art, love). We used second part of S.QUA.L.A. where for each indicator, participants were asked to evaluate their degree of perceived satisfaction using the 5-point rating scale. Score 1 (high satisfaction) meant the highest satisfaction and in the same time the highest level and score 5 (total disappointment) expressed the absolute insignificance of the indicator in life. The lower mean score meant the higher perceived satisfaction. For this study we analysed one quality of life indicator "overall health". In this study a Slovak version of the S.QUA.L.A. was used (Nemček et al., 2011).

Data analyses

Statistical analysis was performed using IBM SPSS version 23.0. Qualitative variables are presented as proportion (n) and percentage (%). Quantitative variables are presented as mean ($\bar{x}$) and standard deviation (SD). The data was statistically tested by the Kolmogorov-Smirnov test of the sample distribution normality. One-way ANOVA was used to determine the differences in perceived satisfaction with health within three evaluated groups based on their health status (healthy people, people with NCDs and people with disabilities) both in two main groups of active and inactive populations. Post-hoc Bonferroni test was used to examine the differences in satisfaction with health between two groups of population based on their health status in both two main groups of active and inactive populations. Student's two-sample t test was used to examine the differences between active and inactive people within each population group based on their health status. In current study, only one measurement has been made and two main groups formed the study. The level of statistical significance was set at $p<.05$.

RESULTS AND DISCUSSION

Analysing the subjective satisfaction with health we found the highest satisfaction demonstrated by the lowest mean score (1.827±0.689 points) in the healthy group of population regularly participating in sport. Actively living population with NCDs presented the subjective satisfaction with health by achieving 2.476±0.924 points of the mean score and people with disabilities who regularly participating in sport revealed the health satisfaction value 2.628±0.907 of the mean score. These differences were significant at 1 % of statistical significance [$F(2.80) = 58.08$; $p=0.00$; $\eta^2 = 0.16$] (Table 2).

In the group of people who are not participating in any sport and physical activities in their leisure time we found that healthy people from three evaluated groups presented the highest satisfaction with health achieving 2.153±0.824 points of the mean score. People with disabilities who are not participating in sport followed the group of healthy inactive people by achieving 2.849±0.849 points of the mean score and the lowest level of satisfaction with health demonstrated the inactive group of people with NCDs with 2.964±0.962 points of the mean score. These differences were also significant at 1 % of statistical significance [$F(2.39) = 25.41$; $p=0.00$; $\eta^2 = 0.09$] (Table 2).

TABLE 2 Satisfaction with health comparison within three groups with different health status

Sport Participation	Health Status	$\bar{x}$/SD	F	Sign
Active	Healthy people	1.827±0.689		
	People with NCDs	2.476±0.924	58.08	0.000
	People with disabilities	2.628±0.907		
Inactive	Healthy people	2.153±0.824		
	People with NCDs	2.964±0.962	25.41	0.000
	People with disabilities	2.849±0.849		

In the pair comparisons we found significant differences in satisfaction with health between the two comparisons in the group of active either inactive populations. Concretely active healthy people are significantly more satisfied with their health than actively living people with NCDs and actively living people with disabilities and on the other hand healthy inactive people are significantly more satisfied with their health than inactive people with NCDs and inactive people with disabilities (Table 3). A comparison of health satisfaction further revealed no significant

differences between the active people with NCDs and active people with disabilities as well as between inactive population with NCDs and inactive population with disabilities. The mean score of satisfaction with health revealed a higher satisfaction of active individuals with NCDs (2.476±0.924 points) compared to active individuals with disabilities (2.628±0.907 points) and on the other hand the mean score of satisfaction with health in the group of inactive individuals showed higher satisfaction with health in individuals with disabilities (2.849±0.849 points) versus inactive population with NCDs (2.964 ± 0.962 points) (Table 2).

TABLE 3. Satisfaction with health pair comparison in the groups of active and inactive people

Sport Participation	Health Status	Mean Difference	Std. Error	Sign.
Active	Healthy people vs People with NCDs	-0.649**	.083	0.000
	Healthy people vs People with disabilities	-0.800**	.080	0.000
	People with NCDs vs People with disabilities	-0.151	.088	0.260
Inactive	Healthy people vs People with NCDs	-0.811**	.121	0.000
	Healthy people vs People with disabilities	-0.696**	.109	0.000
	People with NCDs vs People with disabilities	0.115	.092	0.630

The results further revealed significantly higher satisfaction with health in actively living populations comparing inactive populations with the same health statuses at the 1 % level of statistical significance (Table 4). Concretely active healthy people declared significantly higher satisfaction with health than inactive healthy population [t(126)=-3.3; p=0.00; d=0.043]. Results show significantly higher satisfaction with health in active people with NCDs comparing inactive people with NCDs [t(288)=-4.5; p=0.00; d=0.052] and also significantly higher satisfaction with health in actively living population with disabilities comparing inactive people with disabilities [t(384)=-2.7; p=0.00; d=0.025].

TABLE 4. Satisfaction with health comparison between active and inactive people with different health status

Health Status	Sport Participation Active $\bar{x}$/SD	 Inactive $\bar{x}$/SD	df	t	Sign.
Healthy people	1.827±0.689	2.153±0.824	334	-3.275**	0.000
People with NCDs	2.476±0.924	2.964±0.962	308	-4.499**	0.000
People with disabilities	2.628±0.907	2.849±0.849	459	-2.666**	0.000

The aim of our investigation was to find out the differences in perceived satisfaction with health within three evaluated groups with different level of health status regularly participating in sport (active people) and not participating in sport (inactive people). We found the highest level of perceived satisfaction with overall health in the group of healthy actively living population and the lowest perceived satisfaction with overall health in the group of inactive people with NCDs. In the group of active as well as inactive people we found significantly higher perceived satisfaction with health in the group of healthy people comparing people with NCDs and people with disabilities. Interestingly no significant differences were found in the comparison of perceived satisfaction with overall health between people with NCDs and people with disabilities nor in the group of active neither inactive population. In all groups of people related to their health status (healthy people, people with NCDs and people with disabilities) the significantly higher perceived satisfaction with health was demonstrated by actively living populations comparing inactive population.

As we see, our investigation confirmed that participation in regular physical activity and sport positively affected perceived satisfaction with health. There are some scientific papers that reveal the opposite results. Nemček's (2016a) investigation revealed no significant differences in perceived satisfaction with overall health between active and inactive people with physical disabilities (n=150; χ^2=4.042; p=0.374), neither in physical health (χ^2=2.909; p=0.513) nor psychological health (χ^2=4.132; p=0.388). Another investigation also did not confirm significant differences in life satisfaction between active and inactive healthy people (Bendíková & Nemček, 2016). On the other hand, the investigation of Nemček (2016a) confirmed significantly higher perceived satisfaction with overall health in the group of actively living people who are deaf and hard of hearing comparing inactive people with hearing impairments (χ^2=11.79; p=0.045). Author further demonstrated significantly higher satisfaction with physical health

(χ^2=42.14; p=0.000) and psychological health (χ^2=31.78; p=0.000) in the group of active people who are deaf and hard of hearing comparing inactive individuals with the same disability (Nemček, 2016a; Nemček, 2017). Bendíková & Nemček (2016) showed significantly higher life satisfaction in actively living population with NCDs comparing inactive people with similar chronic diseases.

Another investigation (Nemček, 2016b) even declared significant differences in perceived satisfaction with health between active people with physical disabilities (n=73) and active people who are deaf and hard of hearing (n=52) where significantly higher perceived satisfaction with health was presented by actively living people who are deaf and hard of hearing comparing actively living people with physical disabilities (χ^2=13.51; p=0.008). Active people who are deaf and hard of hearing showed significantly higher perceived satisfaction with physical health (χ^2=22.07; p=0.000) as well as with psychological health (χ^2=18.55; p=0.000) comparing active people with physical disabilities. On the other hand, inactive people with physical disabilities (n=77) in the same study demonstrated significantly higher satisfaction with physical health comparing inactive people who are deaf and hard of hearing (n=113; χ^2=50.57; p=0.000). Significantly higher perceived satisfaction with overall health was showed by the group of inactive people who are deaf of hard of hearing comparing inactive people with physical disabilities ((χ^2=10.66; p=0.034) (Nemček, 2016b).

Nemček & Kručanica (2014) assessed perceived satisfaction with health in the group of 152 participants who are deaf and hard of hearing and found that those who are involved in sport show significantly higher satisfaction with physical health, psychological health and presented significantly higher satisfaction with overall health comparing the individuals who lead sedentary lifestyle. The study further revealed that the individuals who are deaf and hard of hearing are more satisfied with physical health than with psychological health (Nemček & Kručanica, 2014).

CONCLUSION

The current study revealed the highest level of perceived satisfaction with overall health in the group of healthy actively living population and the lowest perceived satisfaction with overall health in the group of inactive people with NCDs. In the group of active as well as inactive people we found significantly higher perceived satisfaction with health in the group of healthy people comparing people with NCDs and people with disabilities. No significant differences were found in the comparison of perceived satisfaction with overall health between people with NCDs and people with disabilities nor in the group of active neither inactive population. In all groups of people related to their health status (healthy people, people with NCDs and people with disabilities) the significantly higher perceived satisfaction with health was demonstrated by actively living populations comparing inactive population. On the base of the results we recommend that all people not matter if they are healthy or have some chronic diseases should participate in different physical activities according to their abilities and health status (Labudová, Nemček & Kraček, 2015). Wattanapisit (2016) says that for people with NCDs and with disabilities, participation in physical activity under the care of healthcare providers and professional trainers of adapted physical activities and adapted physical education is safe and needed.

ACKNOWLEDGEMENT

The study was supported by grant projects VEGA No. 1/0726/17, VEGA No. 1/0519/19, VEGA No. 1/0409/19, VEGA No. – The projects of The Ministry of Education, Science, Research and Sport of the Slovak Republic.

REFERENCES

1. Barker, D.J.P. (1992). The Fetal and Infant Origins of Adult Disease. *British Medical Journal*, *301*(6761), 1111.
2. Bendíková, E. & Nemček, D. (2016). Life satisfaction of healthy people and people with non-communicable diseases: differences between active and inactive individuals. *Sport Science*, 9 (suppl. 2), 19-23.
3. Bendíková, E. (2011). The current health status and reasons for student absence in physical and sports education classes. *Physical Education and Sport, 21*(1), 6-10.
4. Bendíková, E. (2014). Lifestyle, physical and sports education and health benefits of physical activity. *European researcher: International Multidisciplinary Journal*, *69*(2-2), 343-348.

5. Bendíková, E., & Stackeová, D. (2015). Effect of exercise programme with compensatory aim targeting on spine mobility in school girls of secondary high school. *Hygiena, 60*(1), 4-9.
6. Bendíková, E. (2017). Application of multimedia-based exercise programmes focused on improvement of the schoolgirls' musculoskeletal system during breaks between classes. In *ICCMSE-2017 : AIP proceedings of the international conference of computational methods in sciences and engineering 2017*, Thessaloniki, Greece, 21–25 April 2017. Vol. 1906. - 1. ed. - New York : American institute of physics, 2018. - ISBN 978-0-7354-1596-6.
7. Bendíková et al. (2019). Selected determinants of seniors' lifestyle, *Journal of Human Sport and Exercise, 10*(3), 805-814.
8. Bhargava, S.K., Sachdev, H.S., Fall, C.H., Osmond, C., Lakshmy, R. et al. (2004). Relation of serial changes in childhood body-mass index to impaired glucose tolerance in young adulthood. *The New England Journal of Medicine*, *350*(9), 865–875.
9. Biswas, A., Oh, P.I., Faulkner, G.E. et al. (2015). Sedentary time and its association with risk for disease incidence, mortality, and hospitalization in adults: a systematic review and meta-analysis. *Annals of Internal Medicine, 162*(2), 123–132.
10. Dobay, B. 2014. Az iskolai sporttanfolyamok hatása a nyári üdülési szokásokra = The influence of school sport courses on summer recreational habits. In *27. Didmattech 2014 : New methods and technologies in education and practice*, international scientific and professional conference, Olomouc: Palacký university, 2014, p. 112-118.
11. Dobay, B. 2015. *Az iskolai sporttanfolyamok motivációs hatása a felnıttkori rekreációs sporttevékenységekre Dél-Szlovákiában*. Komárom : Kompress kiadó.
12. Dobay, B. & Bendíková, E. (2014). Športové a rekreačné aktivity v životnom štýle dospelých [Sports and recreational activities in the adults lifestyle]. *Slovak Journal of Sport Science*, *6*(2), 19-31.
13. Fobel, P., Banse, G., Kiepas, A. (2001). *Ethics and Information Society*. 2001. B. Bystrica: FHV UMB; 2001. p. 145.
14. Gluckman, P.D., Hanson, M.A., Cooper, C. & Thornburg, K.L. (2008). Effect of in utero and early-life conditions on adult health and disease. *The New England Journal of Medicine*, *359*(1), 61–73.
15. Hagger-Johnson, G., Gow, A.J., Burley, V. et al. (2016). Sitting Time, Fidgeting,and All-Cause Mortality in the UK Women's Cohort Study. *American Journal of Preventive Medicine, 50*(2), 154–60.
16. Chastin S.F., Mandrichenko, O., Helbostadt, J.L. & Skelton, D.A. (2014). Associations between objectively-measured sedentary behaviour and physical activity with bone mineral density in adults and older adults, the NHANES study. *Bone, 64*, 254–62.
17. Jefferis, B.J., Merom, D., Sartini, C.et al. (2015). Physical activity and falls in older men: the critical role of mobility Limitations. *Medicine and Science in Sports and Exercise, 47*(10), 2119–2128.
18. Katzmarzyk, P.T., Church, T.S., Craig, C.L. et al. (2009). Sitting time and mortality from all causes, cardiovascular disease, and cancer. *Medicine and Science in Sports and Exercise, 41*(5), 998–1005.
19. Kurková, P. & Maertin, J.J. (2014). The benefits of square dancing as a means of physical activity for Czech dancers with hearing loss. *Acta Gymnica, 44*(4), 223–230.
20. Kurková, P., Válková H. & Scheetz, N. (2011). Factors impacting participation of European elite deaf athletes in sport. *Journal of Sports Sciences, 29*(6), 607–618.
21. Labudová, J., Nemček, J. & Kraček, S. (2015). *Šport na každý deň,* [Sport for every day]. Bratislava, END.
22. Łubkowska, W., Zdeb, T. Mroczek, B. (2015). Assessment of physiological spine curvature in girls who trained competitive swimming versus non-swimming girls. *Family Medicine & Primary Care Review* 17(3), 189 - 192.
23. Lubkowska, W. (2015). The concept of treatment of scoliosis employing asymmetrical aquatic exercises. In: *Cent Eur J Sport Sci Med.* 9(1), 55-64.
24. Lubkowska, W., Paczyńska-Jędrycka, M., Eider, J. (2014).The significance of swimming and corrective exercises in water in the treatment of postural deficits and scoliosis. *Cent Eur J Sport Sci Med.* 6(2), 93-101.
25. Müller, A. et al. (2013). Fitnesz trendek a rekreációban. *Acta Academiae Agriensis*. *XL*., p. 25-35.
26. Müller, A.; Bácsné, B. É. (2018). *Az egészséges életmód és a sport kapcsolata*. Létavértes, Magyarország : Létavértes SC '97 Egyesület, 2018, 96 p.
27. Müller, A.; Pfau, C.; Gabnai, Z.; Bácsné, B. É; Borbély, A.; Pető, K. (2018). A gyógy-wellness- és sportszolgáltatások fejlesztési lehetőségei a gyógyturizmusban egy hazai kutatás tükrében. *International Journal of Engineering and Management Sciences* / Műszaki és menedzsment tudományi közlemények, 3(4), 101-114.
28. Nemček D. & Kručanica, L. (2014). Satisfaction with health status in people with hearing impairments. *International Scientific Conference Sports, Physical Activity and Health 2014,* Bratislava, Slovakia, Comenius University, 185–191.

29. Nemček, D. (2009). Level of motor abilities determine risk of falls in elderly women, *Physical education and Sport in Research 2009: Aging and Physical activity*, Leszno, Państwowa wyźsza szkoła zawodowa.
30. Nemček, D. (2016a). Quality of life of people with disabilities: differences in satisfaction with indicators and domains between active and inactive individuals. *Physical Activity Review*, 4, 62-71.
31. Nemček, D. (2016b). Quality of life of people with disabilities from sport participation point of view. *Acta Facultatis Educationis Physicae Universitatis Comenianae*, *56*(2), 77-92.
32. Nemček, D. (2017). Self-esteem analyses in people who are deaf or hard of hearing: a comparison between active and inactive individuals. *Physical Activity Review*, 5, 95-104.
33. Nemček, D., Labudová, J., Peráčková, J., Bendíková, E. et al. (2011). *Kvalita života seniorov a pohybová aktivita ako jej súčasť* [*Quality of Life in Seniors and Physical Activity as a Part of It*]. Prešov, Slovakia: Michal Vaško
34. Pačesová, P., Šmela, P., Kraček, S. & Plevková, L. (2018). Women's Well-Being, State and Trait Anxiety Regarding their Sport Activity. *Sport Mont Journal*, *16*(2), 33-38.
35. Rimmer, J.H., Riley, B., Wang, E., Rauworth A. & Jurkowski, J. (2004). Physical activity participation among persons with disabilities: barriers and facilitators. *American Journal of Preventive Medicine*, *26*(5), 419-425.
36. Shaw, R.J., Čukić, I., Deary, I.J., Gale, C.R., Chastin, S.F.M. et al. (2017). Relationships between socioeconomic position and objectively measured sedentary behaviour in older adults in three prospective cohorts. *BMJ Open, 7*(6), 1-10.
37. Tomková, Š.; Palaščáková Špringrová, I. (2013). Kinesiotape a jeho vplyv na korekciu päty u adolescentov. In *Fyzioterapia, Regenerácia a Šport,*recenzovaný zborník vedeckých prác. Trenčín : TUAD, Fakulta zdravotníctva, p. 124 - 127.
38. Wattanapisit, A. (2016). A Review of the Current International Physical Activity Guidelines for Various Age Groups to Prevent and Control Noncommunicable Diseases. *Songkla Medical Journal*, *34*(1), 39-49.
39. Wilmot, E.G., Edwardson, C.L., Achana, F.A. et al. (2012). Sedentary time in adults and the association with diabetes, cardiovascular disease and death: systematic review and meta-analysis. *Diabetologia, 55*(11), 2895–905.
40. World Economic Forum, (2017). *Human Centric Health: Behaviour Change and the Prevention of Non-Communicable Diseases,* Switzerland: WEF.
41. World Health Organisation, (2014). *Global Status Report on Noncommunicable Diseases 2014*, Switzerland: WHO.
42. Zannotti, M. & Pringuey, D. (1992). A method for quality of life assessment in psychiatry: The S-QUAL-A (Subjective QUAlity of Life Analysis). *Quality of Life News Letter*, *4*(6).
43. Zuzda, J.G., Poljanowicz, W., Latosiewicz, R., Borkowski, P., Bierkus ,M., Moska,O., (2017a). Innovative E-Portal for Prevention and Therapeutic Programme for Treatment of the Obesity and Overweight in Health-Tourism. (W:) Proceedings of the International Conference of Computational Methods in Sciences and Engineering 2017 (ICCMSE-2017)(ed.) Simos, T.E., Zacharoula Kalogiratou, Z., Monovasilis T. New York: American Institute of Physics, Book Series: AIP Conference Proceedings Volume: 1906 Article Number: UNSP 180005-1 DOI:10.1063/1.5012458.

Comparison of Hand Arches in Athletes

Ingrid Palaščáková Špringrová[1], Monika Ballyová[2], Šárka Tomková[3], Elena Bendíková[4,a]

[1]Rehaspring Physiotherapy & Education Centre, Čelákovice, the Czech Republic
[2] Orthotes, s.r.o., non-state health institution, the Czech Republic
[3]St. Elisabeth University of Health Care and Social Work, Bratislava, Slovakia
[4]Matej Bel University Faculty of Arts, Banská Bystrica, Slovakia

[a]Corresponding author: palascakova@rehaspring.cz

Abstract: Aim: Finding out the state of hand arches in press-up positions in a selected sample of participants in relation to their sporting activities. Method: 29 participants took part in the study. The group of athletes consisted of 14 participants i.e. 12 men and 2 women, age 27 ± 4.4, BMI 22 ± 2kg, frequency of training: 5 ± 1 per week. The control group included 15 participants from the general population, i.e. 8 men and 7 women age 23 ± 2.3, BMI 21.9 ± 2.2 working out no more than once a week without ambition to become professional athletes. The data was analysed in Microsoft Excel 2016 and in Control Freak programme (developed by Contchart Software company), particularly assessment by Shapiro -Wilk test. Results: The average value measured at PodoCam during initial examination was 0.88 ± 0.9 in the group of athletes and 1.92 ± 1.18 in the control group. **Conclusion**: The results of our study confirmed assumption concerning statistically significant incidence of standard hand arches in climbers. The character of climbing activity supports assumption about impact of the character of daily activities on the musculoskeletal system of climbers. Some physiotherapeutic methods use maintenance of hand arch in press-up position in order to improve techniques and performance of athletes.

Keywords: hand arch, visual scale, climbing, athletes, the Acral Coactivation Diagnostics, PodoCam

INTRODUCTION

Motor learning is a process accompanying our motor behaviour throughout life and it leads to changes in our motor skills. Motor learning, accompanying us from birth to the end of life, is not only about quantity but also about quality when evaluating movement and improvement in motor skills. Improvement is a matter of motor training, which is successful on the basis of plasticity of the central nervous system (Levin et al., 2014). Motor skills are maintained until we use them. If an individual does not use a learnt motor skill, it is overlapped by a new skill (Nemček, 2009, 2016a, b). It is a common matter that individuals tend to recall newly mastered and automated skills in their daily lives than the older ones, which can be recollected only by means of a conscious activity (Censor, 2012; Dayan, 2011; Seidler, 2010). Medical fields as well as the sport sector deal with motor learning. From the perspective of sports training motor learning is often divided into two categories: implicit and explicit (Dragounová, 2013), or into motor learning phases: gross coordination, fine coordination, stabilization and variable creativity (Dovalil, 2002). For people their hands are a sensitive instrument allowing a wide range of activities from gross to the finest motor skills. Hands perform not only motor function but also stereognosis. Kapandji describes a dome-shaped hand grip made by arches at three various levels (Kapandji, 1982; Tubiana, 2009). Press-up exercises work also with functional setting of dome-shaped handgrip position. Palaščáková Špringrová describes this functional setting as maintenance of transverse and longitudinal arch during press-up exercises. If hand arch is flat, then the entire surface of the palm touches the mat when pressing up on heels of the hands (Palaščáková Špringrová, 2014). Athletic training exploits working out in closed kinetic chains when all muscles are engaged in coordination and neurosmuscular stabilisation is optimized (Latasch, 1993). Closed kinetic chains are useful in training aimed at gaining appropriate joint stability, thus more efficient movement (Dvořák, 2005), and they have an effect on spine straightening and respiratory function (Měrková

et al., 2015). The Acral Coactivation Diagnostics tests positions of hands when pressing up. Typology of the acral parts of upper limbs is assessed on a visual scale (Vagner et al., 2017).

AIM

Finding out the state of hand arch in press-up positions in a selected sample of participants in relation to their sporting activities.

METHOD

Participants

Measuring was held in the functional laboratory of the Department of Rehabilitation and Sports Medicine in Motol University Hospital in Prague. All examined participants were made aware of the course of measuring in advance. 29 participants took part in the study. They had to meet the following criteria: age 20-40, dominant right upper limb and absence of acute myoskeletal affection during the measuring. On the day of measuring all participants were asked about difficulties in upper limbs, articulatio humeri and back. The third degree of pain on the Visual Analogue Scale was the inclusion condition of the study. All participants met this condition. On the basis of filled out anamnestic questionnaires the examined participants were divided into two groups: a group of athletes and a control group. The group of athletes consisted of 14 participants and the control group of 15. Selection of participants in the group of sportsmen followed these criteria: performance of a regular sporting activity at least four times per week with dominant involvement of upper limbs and a sporting activity at the top level (at least within the Czech Republic). 14 participants pursuing climbing (on artificial climbing walls) or rock climbing met these criteria. 12 men and 2 women were involved in the study. Characteristics of the group of athletes is described in the Table 1.

TABLE 1. Characteristics of the group of athletes (n=14)

Factors	Average value ± SD
Age (years)	27±4.4 years
Body height (m)	1.81±0.08 m
Body weight (kg)	71±7.6 kg
BMI (kg/m^2)	22±2 kg/m^2
Frequency of trainings (per week)	5±1 training per week

The control group included 15 participants meeting the following selection criteria: a sporting activity performed no more than once a week without ambition to become professional sportsmen in the relevant sport sector. Based on the above mentioned criteria 15 participants were classified in this group, i.e. 8 men and 7 women. Characteristics of the control group is described in the Table 2.

All examined participants provided basic anamnestic data in the form of an electronic questionnaire filled out several days before measuring. The anamnestic data included information from the following spheres: personal, professional and sport history and current difficulties, plus confirmation that the right upper limb is dominant. Participants´ body weight and height were necessary for calculation of body mass index (BMI).

TABLE 2. Characteristics of the control group (n=15)

Factors	Average value ± SD
Age (years)	23±2.3 years
Body height (m)	1.74±0.1 m
Body weight (kg)	67±11 kg
BMI (kg/m^2)	21.9±2.2 kg/m^2

On the day of measuring the participants were asked about difficulties in their right upper limb and trunk, which was evaluated on the Visual Analogue Scale. They were also scanned by PodoCam device. Initial examination was carried out in the kneeling position when the participants were facing PodoCam, with both palms resting on the upper plate of the device. The participants got the following instructions: “kneel down and rest on both knees on the designated line, put both palms on the upper plate of the device, look ahead at the designated point, lift both knees simultaneously 2 cm above the mat, hold the position, then relax and put both knees back to the mat.” Another test: kneeling on one knee, the left foot is put forward, the right hip is next to PodoCam, the right palm is resting on the upper plate of the device. The participants got the following instructions: “kneel down and rest on both knees, put your right hip very close to PodoCam, put your left foot forward in front of your body, put your right palm on the upper plate of the device, look ahead at the designated point, lift your right knee 2 cm above the mat, hold this position, then relax and put the knee back to the mat.” The present examiner gave no more information to the participants.

Data Collection

Data collected from the examinations were assessed according to the methodology of the Acral Coactivation Diagnostics (ACD). Assessment was performed by three independent physiotherapists who were trained in the ACD aimed at typology of acral parts of upper limbs.

Hand types are assessed in two situations: as “a natural strategy” (i.e. assuming position including hand arch spontaneously) and then under loading, i.e. when the acral part is bearing greater weight than the adjacent body segments.

Palaščáková Špringrová (2015) describes 4 types of hand arches as follows: standard – the acral part is pressing against the mat at the spot of thenar, hypothenar and the heel of the hand (i.e. area of proximal row of carpal bones) and palmar surface of distal phalanges of 1st up to 5th finger. Flat hand – type I: the acral part and the heads of 4th and 5th metacarpus touch the mat. Flat hand – type II: the acral part and the head of 3rd metacarpus touches the mat. Flat hand– type III (“flat hand”): the acral part is pressing against the mat at the spot of thenar, hypothenar, palmar surface of distal phalanges of 1st up to 5th finger as well as the heads of 1st up to 5th metacarpus touch the mat. Our study assessed data relating to the dominant right upper limb under loading when both knees, or only one of them, were lifted from the floor.

Data Analysis

Technical specification of the used PodoCam device (Hadrava, 2010): full metal construction with two cameras, resolution of 1600 x 1200 pixels, PC software. Microsoft Excel 2016 was used for statistical data processing and the following quantities were calculated: arithmetic mean, median, modus, dispersion and standard deviation. Next, Control Freak programme (developed by Contchart Software company) was used particularly for assessment by Shapiro-Wilk test (i.e. test for normal distribution of initial data).

RESULTS AND DISCUSSION

Results of right hand arches were evaluated on the basis of this scale: 0 – standard (normal hand arch), 1- flat hand of type I, 2- flat hand of type II, 3- flat hand of type III. The Chart 1 shows the results of the control group and the Chart 2 the results of the group of athletes. Typology of arches of hand acral parts was assessed by individual assessors and subsequently the values were averaged. These results were used for data processing. First, Shapiro-Wilk test was used for data distribution. It was found out that this data distribution was different from the standard one. For this

reason the nonparametric Mann-Whitney U-test was applied then. Statistical significance level α = 0.05 was selected for testing.

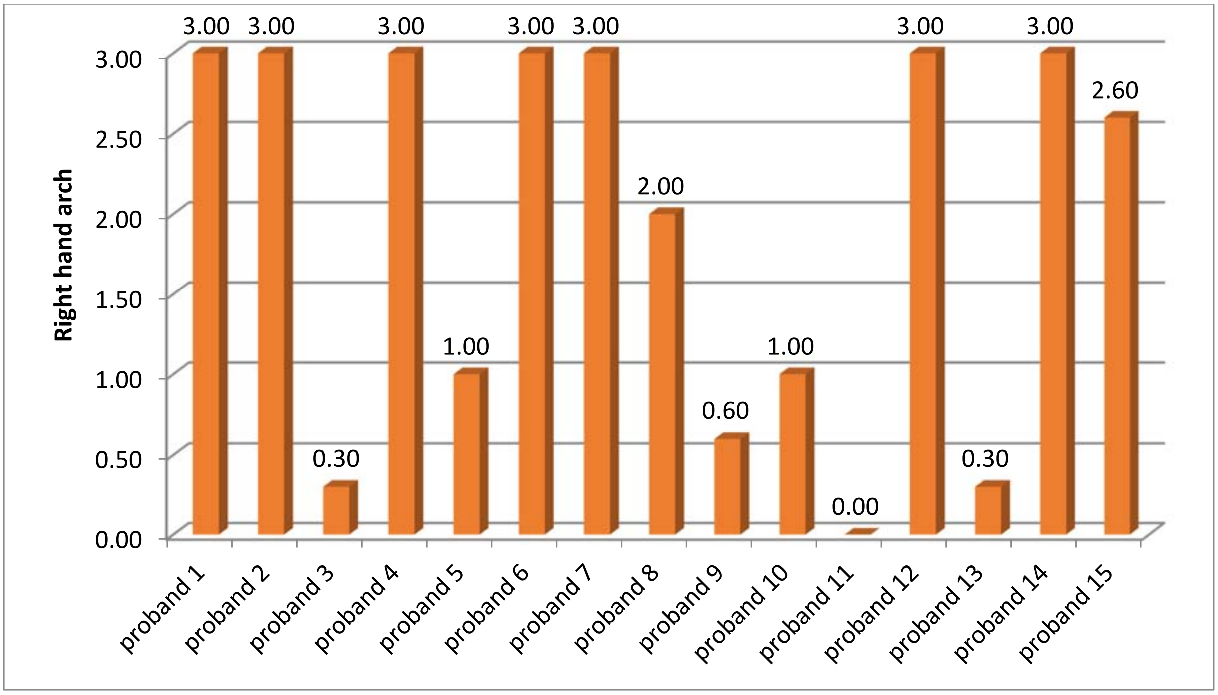

FIGURE 1. Initial examination at PodoCam under loading – the control group

The average value measured by PodoCam was 1.92 ± 1.18 during the initial examination of the control group. The group of athletes showed the value 0.88 ± 0.9.

The group of athletes consisted of sport climbers who climb both on rocks and on artificial climbing walls. Climbing is a sporting activity during which climbers use functional setting of hand arch which is very similar to the setting of acral parts described in the Acral Coactivation Therapy (Palaščáková Špringrová, 2011). Spine straightening is absolutely essential for climbing and the functional hand setting in arch supports it. During initial examination PodoCam recorded statistically more significant incidence of standard arch of the supporting upper limb in the group of athletes than in the control group. These results confirm our assumption that climbers use functional hand setting in arch when climbing. Regular repetition of this physical activity results in hand arch also in other postural positions, not only the one when climbers widely use this setting of the acral part.

The Acral Coactivation Diagnostics was used for the purposes of this study. Three independent physiotherapists trained in both the Acral Coactivation Diagnostics and treatment conducted assessment. The assessors demonstrated compliance in more than 70%, which is a relatively high level of reliability. The assessors made the most mistakes in the lowest degrees of flat hand arches – type I and II.

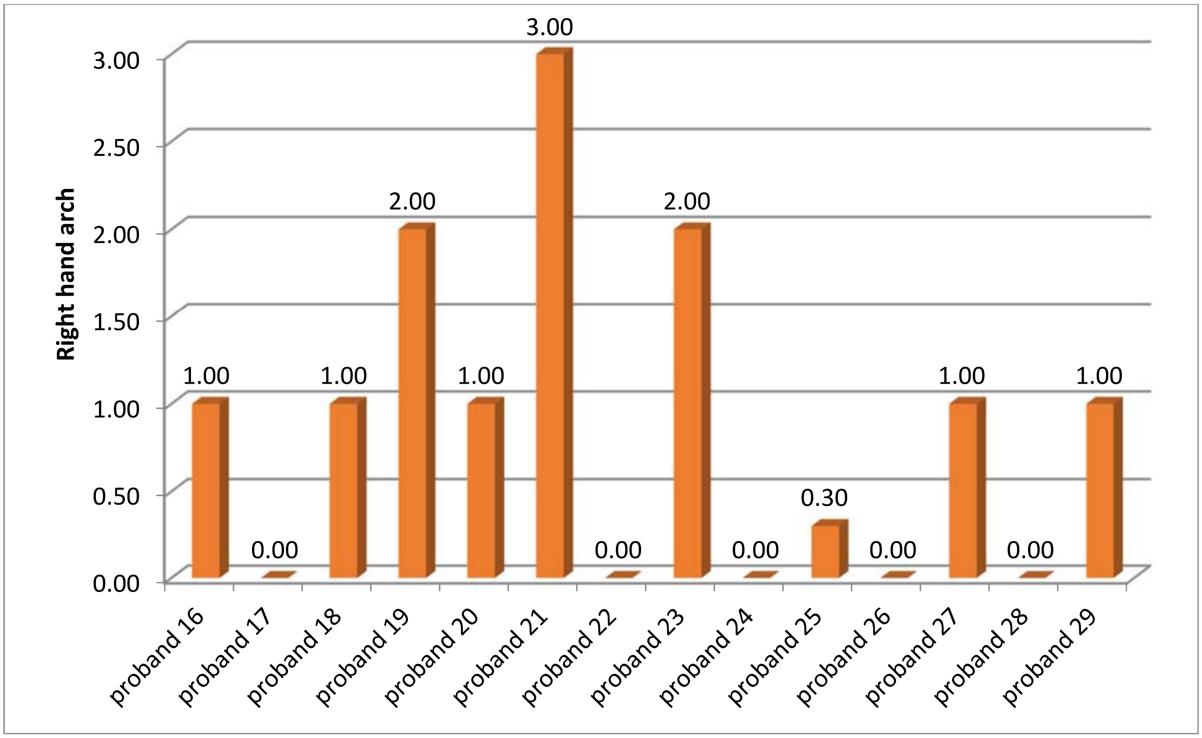

FIGURE 2. Initial examination at PodoCam under loading – the group of athletes

Palaščáková Špringrová et al. (2018) describes incidence of flat hand arch of type III in 60% of tennis players, while only 3% of them had standard hand arch. Athletes aged 13 on average were subjects of the study, which confirms the claims on motor learning and automation of motor patterns when an individual repeats them regularly. The assumption of Brügger claiming that an organ is formed by its function must not be forgotten (Valihrach, 2003; Véle, 2006).

Setting of acral parts in arch can be caused also by shortened muscles in arms and forearms. Then greater incidence of standard hand arch in athletes practising sports connected with hand grip function can be assumed. In her study Bínová describes changes in muscle chains during pressing up against acral parts of upper limbs, which was measured by means of electromyography (Bínová, 2008).

The group of athletes consisted of sport climbers who climb both on rocks and on artificial walls. Climbing is a sporting activity during which climbers use hand arch as a functional hand setting, which is very similar to the setting of acral parts described in the Acral Coactivation Therapy (Vagner et al., 2018). Spine straightening is absolutely essential during climbing and functional hand setting in arch supports it. This functional setting of acral parts as well as spine straightening can be observed in climbers directly during climbing, but also just before getting started when they virtually go through the route they will take.

The control group consisted of participants from the general public. Differences in types of hand arch depending on participants´ profession were observed during the measuring. The participants working with computers and using a computer mouse had a different state of acral parts of their upper limbs. The hands using computer mouse had greater incidence of standard hand arch in comparison with the second hand where flat hand arch of 2nd degree was determined.

From a constructive point of view PodoCam is standardized for examination of acral parts of lower limbs, which is its primary use in clinical practice, so several drawbacks result from its construction in terms of examination of hands. Identification of the type of acral parts of upper limbs depends on somatic constitution of participants. Unfortunately, the upper plate of PodoCam is not height-adjustable. When participants are kneeling on both knees the upper plate is too high, while when they are kneeling on one knee with a palm resting on the floor the plate is too low. Due to these circumstance participants get in positions which are not physiological for some of them, thus the right muscle coactivation and optimal spine straightening is impossible. Height-adjustable construction would be useful. The size of the plate, which does allow sufficiently wide position of upper limbs when pressing up, is another

disadvantage. Some participants have large palms, so assessment of their acral parts as well as change in maintenance of position and reaction is impossible due to the narrow supporting base.

Subsequent assessment based on visual evaluation is subjective. For the purposes of this study assessment was done by means of the Acral Coactivation Diagnostics described by Palaščáková Špringrová (2011). Application of similar principles of examination as those used for evaluation of lower limb arches in orthopaedics can contribute to objectification of typology of upper limb arches. In the future it would be useful to apply Denis scale of flat feet and imprint analysis of acral parts of upper limbs described by Adamec (2005) in plantogram typology.

The position of kneeling on both knees appeared more favourable during the measuring because subjectively it was better accepted by the participants and objectively it was more suitable for both static and dynamic coactivation.

CONCLUSION

The character of a sporting activity of climbers supports the assumption that musculoskeletal system is influenced by daily activities of an individual. However, the pilot study brought other outputs significant for clinical practice. A simple screening of a dominant hand showed that the typology of right hand arch described in the above mentioned study was standard in the group of climbers compared to the control group of non-climbers whose dominant hands were flat.

REFERENCES

1. Adamec, O. (2005). Plochá noha v dětském věku – diagnostika a terapie. *Pediatrie pro praxi*, No. (4), 194-196.
2. Bínová, A. Špringrova Palaščáková, I. (2008). Nové aspekty v metodě Roswithy Brunkow sledováním aktivity vybraných svalů pomocí povrchové EMG. *Rehabilitace a fyzikální lékařství*, No.(2), 74-81.
3. Censor, N.; Sagi, D. & Cohen, L.G. (2012). Common mechanisms of human perceptual and motor learning. *Nature Reviews Neuroscience*. No. (9), 658-664.
4. Dayan, E. & Cohen, L.G. (2011). Neuroplasticity Subserving Motor Skill Learning. *Neuron*, No. (3), 1057-1066.
5. Dovalil, J. (2002). Výkon a trénink ve sportu. 1st ed. Praha: Olympia, pp. 331.
6. Dragounová, Z.; Perič, T. & Dovalil J. (2013). Implicitní motorické učení – možnosti ve sportovním tréninku. *Česká kinantropologie*. No. (3), 11-22.
7. Kapandji, A., I. (1982). The physiology of the joints: annotated diagrams of the mechanics of the human joints. 2nd ed. Edinburgh: Churchill Livingstone, pp. 283.
8. Latash, M. (1993). Control of human movement. 1st ed, Champaign: Human Kinetics Publisher, pp. 392.
9. Levin, M. F.; Weiss, P. L.; Keshner, E. A. et al. (2014). Emergence of Virtual Reality as a Tool for Upper Limb Rehabilitation: Incorporation of Motor Control and Motor Learning Principles. *Physical Therapy* No (3), 25 – 46.
10. Měrková, H.; Neumanová, K. & Dvořák, R. (2015). Vliv akrální koaktivační terapie na sílu výdechových svalů a na rozvíjení hrudník, *Rehabilitace a fyzikální lékařství*, No.(2), 51-56.
11. Nemček, D. (2009). Level of motor abilities determine risk of falls in elderly women, *Physical education and Sport in Research 2009: Aging and Physical activity*, Leszno, Państwowa wyźsza szkoła zawodowa.
12. Nemček, D. (2016a). Quality of life of people with disabilities: differences in satisfaction with indicators and domains between active and inactive individuals. *Physical Activity Review*, 4, 62-71.
13. Nemček, D. (2016b). Quality of life of people with disabilities from sport participation point of view. *Acta Facultatis Educationis Physicae Universitatis Comenianae*, *56*(2), 77-92.
14. Palaščáková Špringrová, I. (2014) Straight back with Acral Dynamic- Support Exercises. 1nd ed. Čelákovice: ACT centrum s.r.o., pp.82
15. Palaščáková Špringrová, I. (2011). *Akrální koaktivační terapie: vycházející ze základních principů metody Roswithy Brunkow*. 1st ed. Čelákovice: Rehaspring, pp. 142
16. Palaščáková Špringrová, I.; Santariová, A.; Dvořák, R.;Tomková, Š. & Bendíková, E. The Impact of the Acral Coactivation Therapy on Sports Performance in Professional Tennis Players. Physical Activity, Health and Prevention III. International Scientific Conference Conference Textbook, Banská Bystrica 2018
17. Seidler,R. (2010). Neural Correlates of Motor Learning, Transfer of Learning, and Learning to Learn. *Exercise and Sport Sciences Reviews*. No.(1), 3-9.

18. Tubiana, R. ; Thomine, J.-M. & Mackin, E. (2009) Examination of the hand and wrist. 2nd ed., New York: Informa Healthcare. pp. 408
19. Vagner, J.; Palaščáková Špringrová, I.; Přikryl, P. ;Tomková, Š. & Rafi , M. (2018). Physical Therapy Based on Closed Kinematic Chain Patterns for Patients after Total Hip Replacement. In Total Hip Replacement. IntechOpen ed.by Vaibhav Bagaria
20. Valihrach, J. (2003) Bolesti při funkčních onemocněních pohybového aparátu dle konceptu Dr. Brüggera. *Neurologie pro praxi*. No.(4), 197-199.
21. Véle, F. Kineziologie (2006). Přehled klinické kineziologie a patokineziologie pro diagnostiku a terapii poruch pohybové soustavy . 2nd Prague Triton, 375.
22. Hadrava,M. PodoCam [online].2010,[cit.2015-07-08]. http://www.medsport.cz/podocam.html .

Diagnosis, Surgery Treatment and Post-Surgery Process at Vertebrectomy (Spinal Disease)

Jan Ciencala[1], Vladimir Psalman[2*], Martin Zvonar[3]

[1]Department of Ortopaedical Surgery, Faculty Hospital, Masarykova University, Brno, Czech Republic
[2]Faculty of Education, University of South Bohemia, Czech Republic
[3]Faculty of Sport Sciences, Masarykova University, Brno, Czech Republic
[*]Corresponding author: vpsalman@pf.jcu.cz

Abstract. There are several reasons how to damage spine and how to come to serious spinal disease. One of them is spinal column tumor, others are caused by local weakness, column ruptures from car accident, sport injures, long term human overloading, inflammations, etc. The first reason, spinal tumor, is probably the most serious and the correct treatment depends on factors unique to the individual patient and their individual tumor. There are a lot of therapies available to treat spinal tumors, ranging from observation to total vertebrectomy. Both, undertreatment and overtreatment as well, can lead to difficulties. A successful surgical plan is consisted of step-wise investigational algorithm. When conservative therapy failed to control metastatic disease, medicine doctors must determine whether surgery is likely to improve the body functions of patient, his quality of life, or longevity. Vertebrectomy of damaged spinal column is a very rare but serious and very complicated solution of health problem. Because of wide range of the body parts like skin, muscles (especially latissimus dorsi), heart, aorta, lungs, nerves, spinal columns, spinal cord, arm joint, rib and removement of the fifth rib and due to possible postoperative infection and pains requires surgical treatment with antibiotics and narcotics. Therefore, there is a difficult position and access in thoracic space next to vital organs, then a very high risk of massive bleeding from different ruptures and resections/cuttings can appeared. During post-surgery time the first period is in Intensive care department. All vital functions were continuously checked and treatment together with the pain were positively influenced by the correct use of drugs. On the day 3, there was the first trial to walk a few meters with the support equipment. On the day 7, the transport to the normal bed in orthopaedic clinic was realised. Starting on the day 10, normal walking began, hand in hand with improving of body posture and reactivate the rest of the body. On the day 15 after surgery, the patient was released from the hospital and went to the home health care, where treatment with the help of drugs and specific exercises continued. The pain lost approximately three months after the surgery and walking and breathing improvements progress from day to day. Forty days after vertebrectomy the treatment started to be supported by chemotherapy. Also biological treatment by using of new drug product – Tivozanib was added. Specific strengthening with the own body, breathing exercises, stretching, walking and swimming after post-surgery day 90 were applied. Progress was significant, body was more powerful, weight went up in 6 kilograms, tumor inactivity was confirmed by CT scans, range of tumor is smaller, back pain is very light or light (depends on the daily loading and rest in lying position) and health status is stabilised. Walking quality after six month is very close to the pre-surgery level and we report here the successful result of this case.
Keywords: vertebrectomy; Th 6 replacement; metastases; adenocarcinoma of the rectum; surgery; post-surgery treatment

INTRODUCTION

Changes in body stability are seen in everyday life aging and its progress and regress in all body functions. But much more worse it is in case if the body is damaged unexpectable and body alone (organism) can not solve this situation itself. Those serious impacts and dysfunctions connected with pains need only solution: surgery operation. Based on the knowing that human organism is very complicated and many systems have cooperate together (Krška, Koštial, 2001; Psalman et al., 2014). In case of damaged innervation, there is a need to create reinnervation which takes months or years. This has influence body posture, quality of movement and also for elimination of pain (Malátová et al, 2013; Krška et al., 2016). Spinal problems appear if the spinal area is in disorder, muscles have dysfunction and spine is not stabilized (Bendíková et al., 2018a, b, 2019). All this mentioned above was studied by following authors: Cresswell et al. (1992), Cresswell et al. (1994), Deyo (2004), Gracovetsky et al. (1985), Hides et al. (1996), Hodges and Richardson (1996), Hodges and Gandevia (2000), Philips et al. (2008) and others.

PURPOSE

The purpose of this work was to realize succesful thoracic surgery operation and post-surgery treatment. Also analyse motor learning process of walking and describe it by kinematic characteristics after surgery operation and during following treatment and describe it.

TASKS

From the purpose formulation following tasks were established:

1. Choose the type of human movement.
2. Choose the handicaped person.
3. Choose kinematic charactertics – displacement, trajectory, angles and velocities regarding to the specific time (moment) or time period (duration).
4. Realise three tests with the same standard laboratory conditions but in different times after the surgery operation.
5. Understand the possibilities of three dimensional (3D) software SIMI Motion for kinematic analysis of gait cycle.
6. Raw data processing and tracking all recorded videos.
7. Analyse the obtained characteristics.
8. Compare achieved results in different attempts.
9. Recommend the conclusions.

BACKGROUND

Current disease:

Beginning of the orthopedic examination was realized on 16.11.2012. But firstly, we have to move back to December 2007, when adenocarcinoma of the rectum was found and a month later (January 2008) followed the surgical operation - excision of the tumor on the surface of the colon. The operation was successful and the subsequent cancer treatment, according to most members of the medical committee was not considered necessary. The stricter observations in intervals not exceeding 3 months were established. In July 2012, through a CT scan found in the retroperitoneal lymph node. Three months later, in October 2012 PET (Positive electron transmission) examination diagnosed metastases in the lymph nodes in the mediastinum and retroperitoneum and also the sixth thoracic vertebrae Th6. The surgery (12/11/2012) removed lymph nodes from the retroperitoneum. At that time still had minimal spine palpation and percussion pain between the shoulder blades, neurological examination was normal. MRI diagnosed osteolysis Th6 to prominence in the spinal canal. Diagnosis of metastases of spinal column Th6 after rectal cancer was established.

The patient was admitted to the orthopedic clinic for surgery, during hospitalization were carried out X-ray of the spine and side-long format. MRI is necessary to supplement the cross sections and prepare the patient for surgery at the earliest time because after contacting the crumbling vertebrae with spinal cord, there is paralysis of the patient in the lower body. Patient has no pain, because regularly used analgesics. Problems with urination does not exist. Neurological examination showed that the patient is without pathological findings.

METHODS

The submitted work is a type of case study, in which patient – tested person was in age of 51,7 years. The intention for this choice was that there were a possibilty of regular testing and serious surgery operation and treatment which are really unusual. Based on MR diagnostics the tested person had to underwent surgery transplantation of thoracic column Th6 which appeared to be damaged. The only possible solution was its removal and change for the titan one (figure 1). For surgery management were very usefull scientific informations regarding surgeries in thoracic area which were submitted by Atik et al. (2006), Garisto et al. (2010), Malvindi et al. (2010), Reyes et al. (2009) and Sulllivan et al. (1988).

Method for analysis of walking quality after surgery operation was established – Three dimensional kinematical analysis by using Simi Motion software. Three tests – 1, 2 and 3 months after the surgery operation

were done in standard laboratory conditions - in the same daily time and with the same testing team, using the same testing protocol. Each testing started with three practice attempts for warming up and afterwards three attempts were recorded by two synchronized video cameras. This creates three dimensional space which is real and very clear for understanding basic human movement like walking (Psalman, Zvonar, 2007; Krška et al., 2014). Three dimensional kinematical analysis with the help of software Simi motion 3D allows to find exact values of kinematic parameters. They are trajectories, angles, velocities and accelerations of each body segment. These main segments (joints) were taken into the consideration: head, left arm, right arm, left elbow, right elbow, left wrist, right wrist, left hip, right hip, left knee, right knee, left ankle, right ankle. But for the purposes of our study we prefered center of gravity – its trajectory, vertical movement measured in meters, velocity in meters per second, length and width of steps.

For footwork analysis we recorded right and left ankles. Monitoring of all kinematic parameters can be realized in axis x, y, z directions and as absolute value. In sport testing then axis x represents forward – backward movement, axis y represents lateral movement and axis z represents vertical movement.

Name of operation:
Phase I - partial vertebrectomy of spinal columnTh6 (vertebrae) from behind and link Th5 and Th7.
Phase II - vertebrectomy of Th6 from the front and compensation by Hydrolift (titanium cage). During this phase of surgery the stomach tube was used and the patient was positioned on the abdomen (down the face). Blood loss was measured and the final value established on 600ml.

RESULTS AND DISCUSSION

Operating findings:

Phase I is quiet in general anesthesia, the surgeon leads a cut above the thoracic spine and connect spinal columns Th5 and Th7 with surrounding segments. There now follows a laminectomy (removal) Th6 with resection of the transverse processes, joint inter-process pedicles of Th6 and release the spinal cord. Samples of tumorous masses are sent for histological laboratories for analysis.
Status and location stabilize bars and crosslink. Drainage is led to a depth and suture of the injured body is done in layers. Blood loss from behind (posterior) part is 250 ml.

Phase II begins by turning the patient into position on the right side. The surgical incision is made over the fifth rib, crosses the subcutaneous tissue and muscle mass to the fifth rib. It is then resect and arc - side parts removed. This is given access to the thoracic spine. Furthermore, crosses the pleura and depth of penetration is verified by X-ray amp. Vertebral (column) body of Th6 is resected together with the adjacent discs (plates), the spinal cord is relaxed (released) and between the vertebral bodies of Th5 Th7 expands (widen/open) by titanium cage - Hydrolift. Position of the patient is stable. Tissue is removed and sent for histological analysis. The following operations are suture of the pleura (pleural sowing) and chest wall by layers. This creates a double thoracic drainage, which is aseptically covered. Total blood loss was stabilized on level of 550ml. Fixation was not necessary. The total duration of surgery was 390 minutes.

With its high risk of rupture, disturbing spinal cord and nerves in Th 6 area, vertebrectomy was required as an immediate operation when diagnosed due to the high possibility of immobility. The important assumptions were: precise diagnostics by using CT, PET (positive electron transmission), X-ray, MRI and their evaluation by top medicine experts, perfect surgery plan in very short time, immediate surgery – vertebrectomy, post-surgery treatment (biological treatment, chemotherapy every two weeks from post-surgery week 7 and rehabilitation process (stretching, specific exercises, soft massage, walking, swimming), repeated post-surgery diagnostics - scans from CT and X-ray. After doing this properly and avoiding any mistakes, the surgery and post-surgery process was very successful and patient has six months after surgery normal quality of life. One exception appeared - increased daily fatigue which was caused by chemotherapy effect.

TABLE 1. Characteristics of slow, normal and fast walking in adult population in age from 20 to 59 years (Waters et al., 1988)

	Velocity (m/min)			**Pace (steps/min)**			**Length of 2 steps (m)**		
	SW	**NW**	**FW**	**SW**	**NW**	**FW**	**SW**	**NW**	**FW**
Women	37	78	99	68	118	137	0,89	1,32	1,24
Men	48	82	110	76	108	125	1,03	1,51	1,67
Average	43	80	106	72	113	131	0,97	1,42	1,47

Legend: SW – slow walking, NW – normal walking FW – fast walking

The whole activity of the lower extremities during the gait cycle is described by authors Perry, Burnfield (2010) in their publication „Gait analysis. Normal and Pathological Function."

Initial phase of left step (Phase 1, P1)

Initial phase is the first contact phase where is the left heel touching the ground. At the same time right lower extremity should be upright and in this case is reaching the proper angle which is 166 degrees (figure 1).

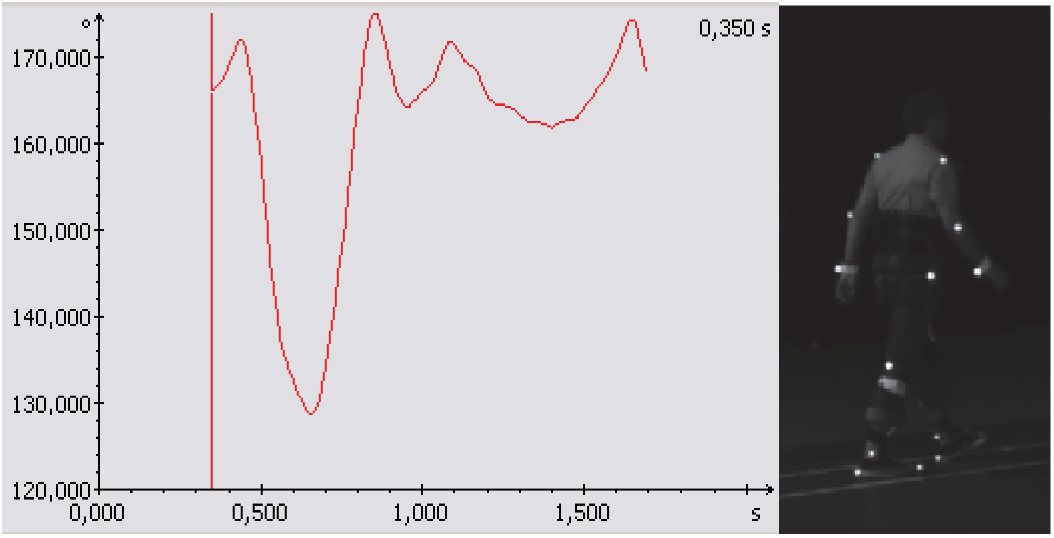

FIGURE 1. Angle in right knee joint (left) and real picture (photo) in initial phase (right) – pre-surgery status

Selected (chosen) phases (P1 - P4) during the left step (real pictures 2a,2b,2c,2d)

FIGURE 2. (a) – real picture in time 0,305s, (b) – real picture in time 0,440s, (c) – real picture in time 0,650s, (d) – real picture in time 0,849s

Height of the body changes: minus 4 cm immediately after the surgery. Plus 2 cm in the next twelve weeks. Weight changes: we recorded the decrease of 18 kilograms during the first 3 months, then weight was stabilized for ten weeks and afterwards came very slow increase in range half to one kilogram per two weeks. Body composition changes: much weaker all muscles, less body fat – decrease at about 11 %. Blood pressure changes - hypertension started from post-surgery week 10, treatment with Agen 10 mg daily. Origin blood pressure was normal 120/80 mg Hg, later on achieved even maximal value 144/121 mg Hg.

Arm joint range:

- right arm achieved the pre-surgery range (100%) in post-surgery week 21,
- left arm achieved only 80% of the pre-surgery range in post-surgery week 21.

Lower extremities – sensitivity:

- Zaldiar 100 mg daily was applied for the first 14 weeks.
- Lyrica 300 mg daily replaced Zaldiar from week 15.
- Feet massages were applied once a week.
- Feet exercises – rolling the small ball (8 cm diameter) with the bare fee.t

By using 3D kinematic analysis we could obtain very precise kinematic characteristics in chosen key phases of gait cycle in three different tests: T1 – 1 months after surgery operation, T2 – 2 months after surgery operation and T3 – 3 months after surgery operation.

Immediately after this serious operation – transplantation of thoracic column (vertebrae Th6) was the start of new motor learning process because all innervation in trunk area was disconnected and muscles of trunk and upper extremities were damaged. From the reason mentioned above, also the lower extremities were out of order, that means without any sensitivity (neuropathy of feet areas). The very strong different drugs against the pain disturbed the correct function nearly in all body system and brought the muscle weakness and loss of equilibrium. Weak muscles and insufficient static and dynamic balance abilities lead to incorrect posture. There appeared the neck kyphosis and thoracic lordosis with the arm bending forward and downward.

TABLE 2. Length and width of steps during 16 weeks (average values in centimeters)

Week	**1**	**2**	**3**	**4**	**5**	**6**	**7**	**8**	**9**	**10**	**11**	**12**	**13**	**14**	**15**	**16**
Length	1,9	7,5	26,7	31,3	33,5	38,2	38,5	40,3	43,8	44,3	51,1	58,4	63,6	64,5	65,2	75,2
Width	61,2	51,1	48,6	47,5	45,9	43,8	43,6	42,9	42,8	42,0	41,7	41,5	39,7	37,7	37,3	34,1

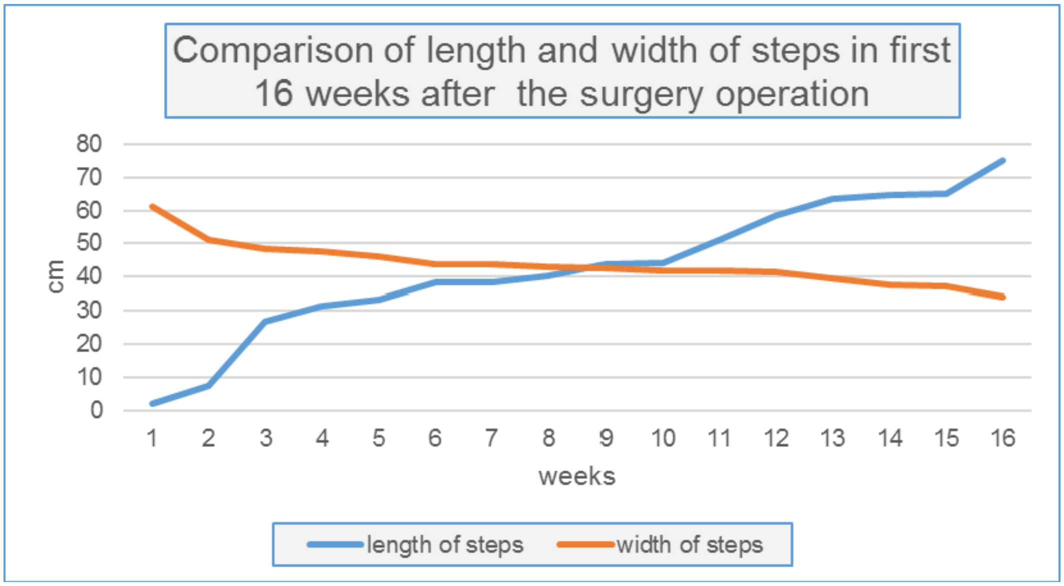

FIGURE 3. Comparison of length and width of steps in first 16 weeks after the surgery operation

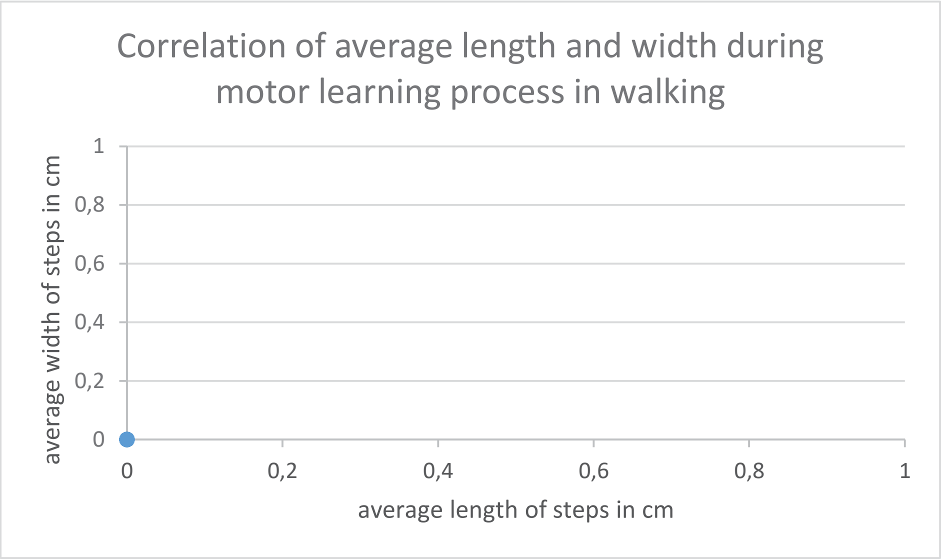

FIGURE 4. Correlation of average length and width during motor learning process in walking

Post-surgery changes in COG (center of gravity)

T1 – 1 month after surgery operation (SO)

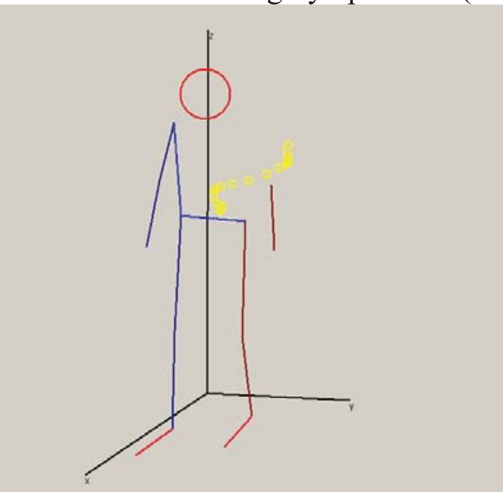

FIGURE 5. Trajectory of COG (yellow curve)

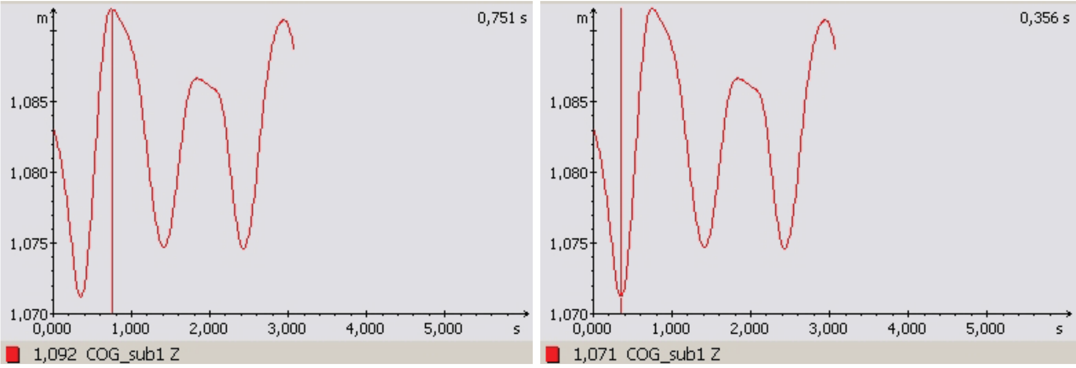

FIGURE 6. Maximal and minimal vertical movement of COG

There is a difference 2.1 cm.

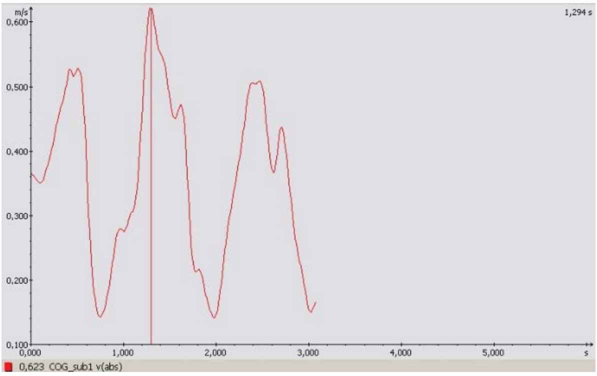

FIGURE 7. Maximal velocity of COG (0.623 m/s)

T2 – 2 months after surgery operation (SO)

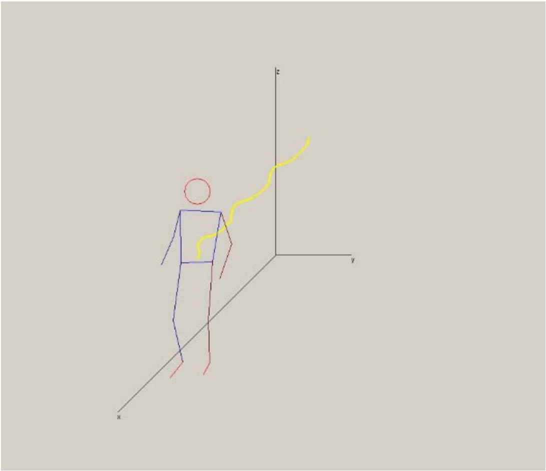

FIGURE 8. Trajectory of COG (yellow curve)

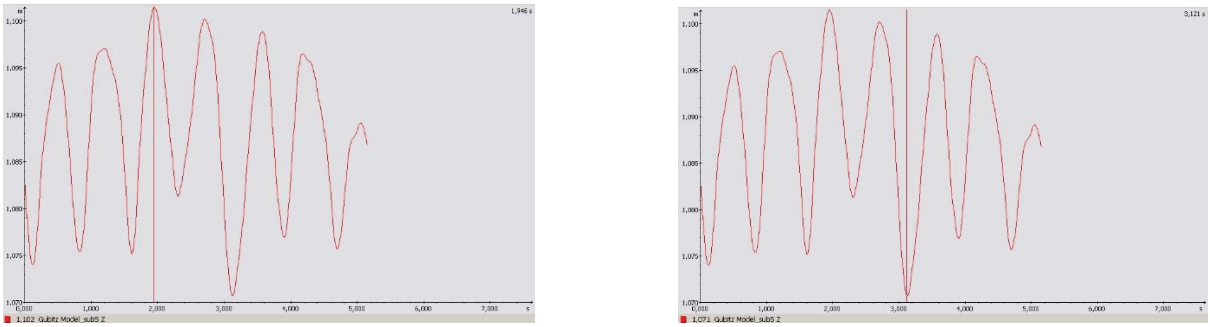

FIGURE 9. Maximal and minimal vertical movement of COG

There is a difference 3.1 cm.

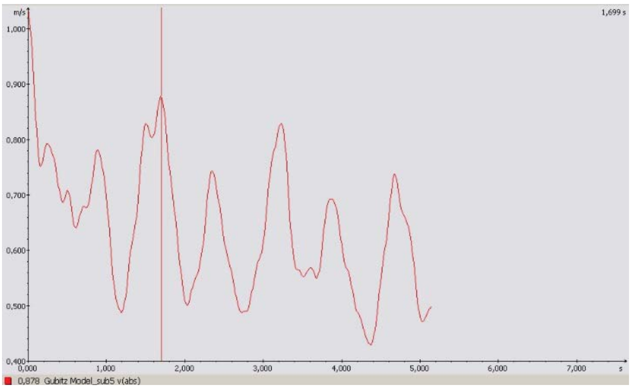

FIGURE 10. Maximal velocity of COG (0.878 m/s)

T3 – 3 months after surgery operation (SO)

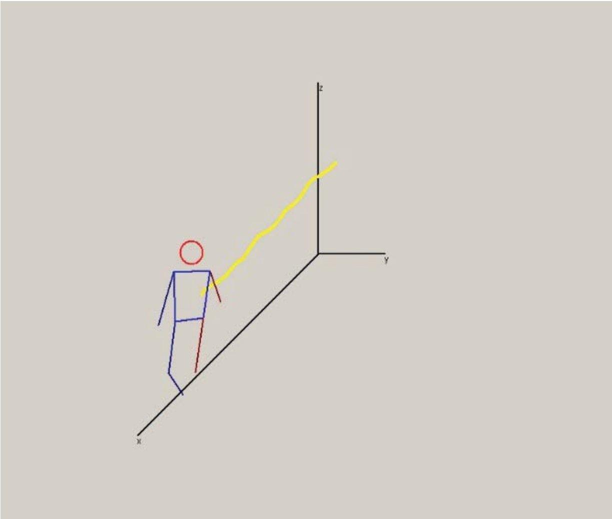

FIGURE 11. Trajectory of COG (yellow curve)

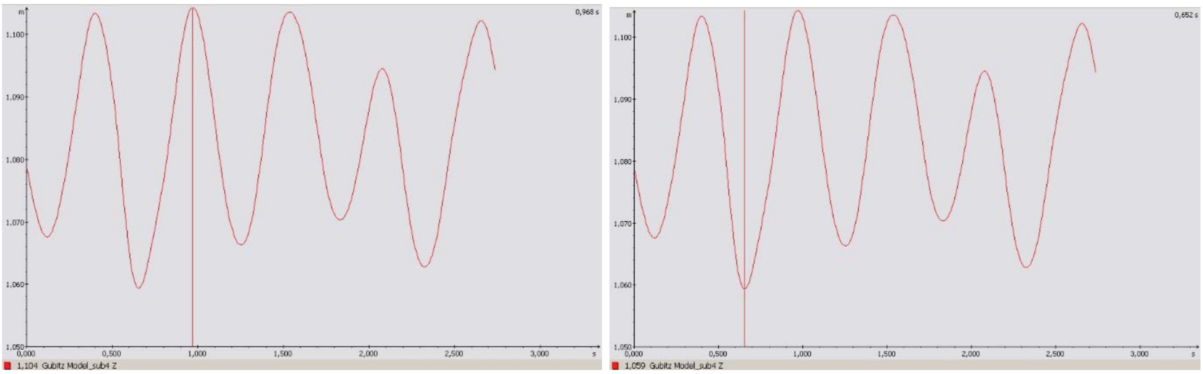

FIGURE 12. Maximal and minimal vertical movement of COG

There is a difference 4.5 cm.

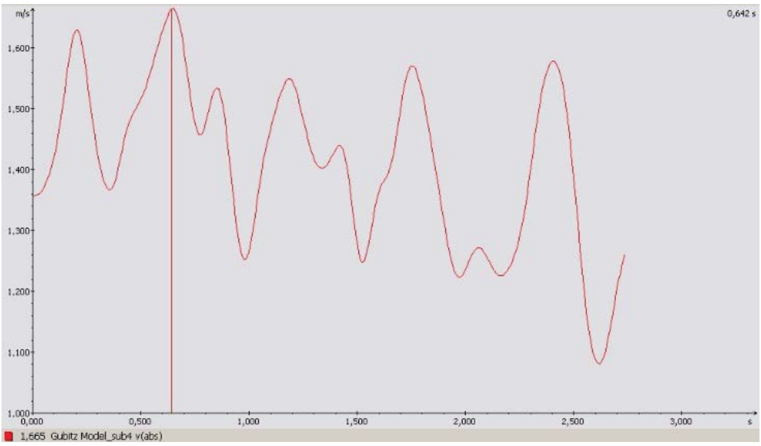

FIGURE 13. Maximal velocity of COG (1,665m/s)

Trajectory – we can compare trajectories in T1, T2 and T3 and we can see that in case T1 – only 1 month after surgery operation the trajectory looks very curvy. These big lateral movements indicate very poor stability and coordination during the whole gait cycle. Test T2 – 2 months after SO we can see less curvy trajectory than in case T2, so quality of walking improved. Test T3 – 3 months after SO the trajectory of COG represented by yellow curve is more straight than in cases T1 and T2 with minimal unuseful lateral movements.

Maximal and minimal vertical movement of COG – regarding to this we can observe gradual higher differences between maximum and minimum. In T1 it was only 2,1 cm where maximal value achieved 1,092 m and minimal 1,071 m). In T2 is difference 3,1 cm and max vertical movement went up to 1,102 m (higher than in T1) and min was 1,071 which is the same like in case T2. In T3 appeared the biggest difference between max and min and is 4,5 cm. This can confirm better quality of walking, more active where maximum is the highest from all 3 tests – 1,104 m and minimum is only 1,059 cm which is the lowest value from T1, T2 and T3.

Maximal velocity of COG. Regarding velocities, there is evident that better quality in walking is represented by faster velocity which went gradually up. T1 started with velocity 0,623 m/s, then T2 had 0,878 m/s and finally velocity in case T3 was 1,665 m/s.

CONCLUSIONS

If a large damage of spinal column is located in the thoracic space, then there is a very high risk of other disadvantages, dysfunctions and human being is quite handicapped. All functions have to start again after the proper innervation which happened in this case and surgery operation and following rehabilitation treatment brought the successful result and motor learning of walking was effective and lead to the pre-surgery status.

Evaluation of gait cycle can be done very precisely and sufficiently by using 3D kinematic analysis. This study brings also specific values of time intervals, trajectory, angles and velocities.

The kinetic chain is a coordinated activation of the all body segments where each segment should has some optimal trajectory, velocity and there should be optimal angles between segments located next to each other. Based on this biomechanical analysis we have the proof that it is possible to improve individual walking technique which requires special individual training.

Vertebrectomy of damaged spinal column was very serious and complicated health problem. Wide range of the body parts like skin, muscles, heart, lungs, nerves, spinal columns, spinal cord, arm joint and rib were treated day by day for many months but we can confirm that treatment was successfully finished in May 2014. All post-surgery periods achieved sufficient quality and all vital functions were saved and now they are working without any problems. One exception is neuropathy of both feet but there is still the process of inervation. The treatment supported by chemotherapy and biological product – Tivozanib took fifteen months and was completely finished. Specific strengthening with the own body, breathing exercises, stretching, walking and swimming after post-surgery day 90 were applied. Progress was significant, body was more powerful, weight went up in 6 kilograms, tumor inactivity was confirmed by CT scans, range of tumor is smaller, back pain is very light or light (depends on the daily loading and rest in lying position) and health status is stabilised. Walking quality after six month started to be similar to the pre-surgery level and we report here the successful result of this case.

REFERENCES

1. Atik, F.A., Navia, J.L., Svensson, L.G., Vega, P.R., Feng, J, Brizzio, M.E., Gillinov, A.M., Pettersson, B.G., Blackstone, E.H., Lytle, B.W.: Surgical treatment of pseudoaneurysm of the thoracic aorta. *J Thorac Cardiovasc Surg* 2006, 132:379-385.
2. Bendiková, E., Palaščaková Špringrová, I., Tomková, S., Vagner, J. 2018a. Effects of an exercise program on the dynamic function of the spine in female students in secondary school. *J Phys Educ Spor*t. 18(2), p. 831-839.
3. Bendíková, E., Marko, M., Šmída, L. 2018b. Influence of Change in Content of Physical and Sport Education as Case Study on Level of Dynamic Function of Spine among Secondary School Female Students. In: *European Journal of Contemporary Education.* 7(4), p. 633-641.

4. Bendíková, E., Marko, M., Rozim, R. Martinský, L. 2019. Effect of 4-Week Physical Program on Musculoskeletal System in Adolescent Sport Class Students with Focus on Ice Hockey. *Physical Activity Review*. 7(1), p. 63-70.
5. Cresswell, A.G, Grundstrom, H., Thorstensson, A. Observations on intra-abdominal pressure and patterns of abdominal intra-muscular activity in man. Acta Physiol Scand. 4, 1992, p. 409-418.
6. Cresswell, A.G, Oddsson, L, Thorstensson, A. The influence of sudden perturbations on trunk muscle activity and intraabdominal pressure while standing. *Experimental Brain Research*. 2, 1994, p. 336-341.
7. Deyo, R. A. Treatments for back pain: can we get past trivial effects? *Ann Intern Med*. 12, 2004, p. 957-958.
8. Garisto, J.D., Medina, A., Williams, D.B., Carrillo, R.G: Surgical Management of a Giant Ascending Aortic Pseudoaneurysm. *Tex Heart Inst J* 2010, 37:710-713.
9. Gracovetsky, S., Farfan, H., Helleur, C. The Abdominal Mechanism. *Spine*. 4, 1985, p. 317-324.
10. Hides, J.A., Richardson, C.A., Jull G.A. Multifidus muscle recovery is not automatic after resolution of acute, first-episode low back pain. *Spine* 21, 1996, p. 2763-2769.
11. Hodges, P.W., Gandevia, S.C. Activation of the human diaphragm during a repetitive postural task. *Journal of Physiology*. 1, 2000, p. 165-175.
12. Hodges, P. W, Richardson, C. Inefficient muscular stabilization of the lumbar spine associated with low back pain. A motor control evolution of transversus abdominis. *Spine*. 21, 1996, p. 2640-2650.
13. Krška, P., Koštial, J. *Štruktúra a modelovanie kinematických ukazovateľov techniky v skoku o žrdi žien.* In: Zborník vedeckých prác. Bratislava: FTVŠ UK a SVŠ TVŠ, 2001, p. 39 – 47. ISBN 80-89075-06-1.
14. Krška, P., Sedláček, J., Koštial, J. Influence of Selected Kinetic Parameters in Female Pole Vault on Sport Performance. In Cluj-Napoca (Rumunsko) 5.- 6.12.2014. The 7th international konference Education for health and performance. In: Studia Universitatis Babes-Bolyai Educatio Artis Gymnasticae, 2014, roč. LIX (4): 5-16.
15. Psalman, V., Hubinák, A., Krška, P. Hodnotenie chôdze dospelej populácie prostredníctvom kinematografie a trojrozmernej kinematickej analýzy. In: Disputationes scientificae Universitatis catolicae in Ružomberok. Ružomberok: VERBUM - vydavateľstvo KU, 2014, 14(2): 90-99.
16. Krška, P., Sedláček J. Koštial J.: Influence of selected kinetic parameters in female pole vault on sport performance. In: *Sport şi Societate* = Sport and Society: Revista de Educaţie Fizică, Sport şi Ştiinţe Conexe = Interdisciplinary Journal of Physical Education and Sport, 2016, 16(1): 57-60.
17. Malátová, R., Rokytová, J., Štumbauer J. The use of muscle dynamometer for correction of muscle imbalances in the area of deep stabilising spine systém. *Proc Inst Mech Eng H.* 2013. August;227(8):896-903.
18. Malvindi, P.G., van Putte, B.P., Heijmen, R.H., Schepens, M.A., Morshuis, W.J.: Reoperations for aortic false aneurysms after cardiac surgery. *Ann Thorac Surg* 2010, 90:1437-1443.
19. Perry, J., Burnfield, J.M. Gait analysis. Normal and Pathological Function. Second Edition. SLACK Incorporated, USA, 2010, 551p. ISBN: 978-1-55642-766-4.
20. Psalman, V., Zvonař, M. (2007): Three dimensional biomechanical analysis as a mean for diagnostics of dynamic balance abilities. In: 4th FIEP European Congress Physical Education and Sports, Bratislava, Slovakia, p.111.
21. Reyes, K.G., Pettersson, G.B., Mihaljevic, T., Roselli, E.E.: A strategy for safe sternal reentry in patients with pseudoaneurysms of the ascending aorta using the PORT-ACCESS EndoCPB system. *Interact Cardiovasc thorac Surg* 2009, 9:893-895.
22. Sullivan, K.L., Steiner, R.M., Smullens, S.N., Griska, L.: Meister SG, Pseudoaneurysm of the ascending aorta following cardiac surgery. *Chest* 1988, 93:138-143.
23. Waters,R.L., Lunsford, B.R., Perry,J., Byrd, R. Energy-speed relationship of walking: standard tables. *Journal Orthop Res.* 1988, 6(2), p. 215-222.

Is there any Effect of Step Aerobics Training on Physical Fitness of Female Students?

Jolanta Grażyna Zuzda[1,a)], Marcin Pasek[2,c)] , Robert Latosiewicz[3,b)], Mirosław Bierkus[4,d)]

[1]Bialystok University of Technology, Faculty of Management, Faculty of Tourism and Recreation,, Ojca Tarasiuka 2, 16-001 Kleosin, Poland
[2] Gdansk University of Physical Education and Sport, Faculty of Tourism and Recreation, K. Górskiego 1, 80-336 Gdansk, Poland
[3] Medical University of Lublin, Faculty of Rehabilitation and Physiotherapy, Al. Racławickie 1, 20-059 Lublin, Poland
[4] Gdansk University of Physical Education and Sport, Faculty of Physical Education, K. Górskiego 1, 80-336 Gdansk, Poland

[a)] Corresponding author: fitness2004@wp.pl
[b)] r.latosiewicz@umlub.pl
[c)] marcin.pasek@awfis.pl
[d)] miriano@wp.pl

Abstract: Physical fitness testing provides information on biological characteristics of individuals and of whole populations. The objective of this study was to evaluate the influence of Step Aerobics Training (SAT) on physical fitness of sixty-two female students 21.18(±1.25) years old. **Methods:** The Physical Work Capacity 170 (PWC_{170}) test was used for estimation of aerobic capacity. To evaluate the long-term effects of training, the coefficient of restitution effectiveness (CRE), BMI index and waist circumference WC) were measured. The SAT was applied over 30 weeks. The evaluation was performed three times: before the SAT, after 15 weeks of the SAT and after 30 weeks of the SAT. **Results**: Training decreased BMI (22.21 vs 21.88) and WC (76.34 vs 75.45), increased cardio–respiratory efficiency (VO_2max:39.93 vs 40,57), but had no effect on the CRE (71.64 vs 71.74) of participants. **Conclusion:** The results suggest that SAT can be sufficient to increase aerobic capacity and decrease body mass in females. Physical fitness programs, including SAT, should be encouraged at universities promote students` health.
Keywords: Physical work capacity, Step Aerobics Training, Physical Fitness, Health

INTRODUCTION

Physical activity (PA) is a fundamental means of improving people's physical and mental health. PA has major beneficial effects on most diseases of the population worldwide [1]. PA is a significant factor in decreasing weight and tackling obesity and other metabolic diseases [2, 3]. Physical Fitness (PF) is a separate concept to PA, although the two are often related. Physical exercises are a subset of PF, defined as planned, structured and repetitive bodily movements performed to improve or maintain one or more components of health [4]. One of the most popular collective forms of fitness is SAT. SAT is a low impact PA recommended for the improvement of cardio respiratory and muscular fitness. It is one of the most popular collective forms of fitness using a step, or platform. SAT, invented by Gin Miller, became a major trend in aerobics in the 1990s [5]. The majority of female university students are sedentary and do not achieve sufficient levels of PA. Universities should organize information sessions about the benefits of physical activity PA on health and, at the same time, it should promote the practice of all forms of PA in students' free time.

The aim of this study was to evaluate the influence of SAT on physical fitness in female in order to demonstrate the potential of SAT in developing positive health-related outcomes.

MATERIALS AND METHODS

The research was conducted with the approval of the Bioethics Committee of the Medical University of Bialystok. Before training sessions commenced, all subjects were informed about the testing and training protocol and gave their informed consent to the procedures of the study. The effects of SAT exercises in the cardiovascular system were evaluated on the basis of maximal oxygen consumption (VO_2max). For this purpose, the Physical Work Capacity 170 (PWC_{170}) test was used [6]. To evaluate the long-term effects of training, the coefficient of restitution effectiveness (CRE) was used [7]. To determine CRE the HR was measured prior to PWC_{170}, one minute after completion of PWC_{170} and 5 minutes after completion of PWC_{170}. CRE was calculated according to following equation:

$$CRE=\frac{(C2-C3)}{(C2-C1)}\cdot 100\%, \qquad (1)$$

where:
C1 – HR prior to PWC_{170}
C2 – HR one minute after completion of PWC_{170}
C3 – HR 5 minutes after completion of PWC_{170} [8]

Body weight, BMI were measured by using scale and stadiometer WPT 100/200 OW (Radwag Wagi Elektroniczne, Poland). BMI was automatically calculated using manufacturer's software. Circumferences of waist were measured using centimeter tape.

The evaluations were performed 3 times: before starting the SAT programme, after 15 weeks of the programme and after 30 weeks of the programme. Each training session of SAT consisted of the following parts: warm-up, main training activity and cool-down (with stretching exercises). The intensity of SAT was controlled by and adjusted to the rhythm of background music. The rate of the music oscillated between 118 BPM and 132 BPM.

Means and standard deviations were calculated for the demographic data of all participants. For basic data characteristics, the Shapiro-Wilk test was used for the analysis of normal distribution. Basic descriptive statistics, Wilcoxon test was applied for dependent variables. A value of $p<0.05$ was considered significant. Computer software Statistica 12.5 (StatSoft Polska, Poland) was used for analysis.

RESULTS

Sixty–two female students 19–26 years old (mean: 21.18 y) were recruited for the study with their voluntary consent. Anthropometric characteristics of the study group are shown in Table 1.

TABLE 1. Anthropometric characteristics of the study group prior to SAT (n = 62)

Parameters	Age [years]	Height [cm]	Body weight [kg]	BMI [kg/m^2]	Waist circumference [cm]
Mean	21.18	1.67	62.12	22.21	76.34
SD	1.25	0.06	7.11	2.26	7.04
Min.	19.00	1.52	46.12	18.10	63.00
Max.	26.00	1.78	80.00	27.59	99.00

After 15-weeks of SAT statistically significant changes occurred in BMI, WC and the VO_2max index (Table 2)

TABLE 2. The effects of SAT on VO_2max, CRE, WC and BMI index between pre-SAT and 15-weeks SAT (n = 62)

Variable	Pre-SAT Mean ± SD	15-weeks SAT Mean ± SD	*Z*	*P*
BMI [kg/m^2]	22.21 ± 2.26	21.99 ± 2.42	3.51	0.000*
WC [cm]	76.34 ± 7.04	75.69 ± 7.11	2.37	0.01*
VO_2max [ml/kg/min]	39.93 ± 4.36	40.59 ± 4.44	3.26	0.001*
CRE [%]	71.64 ± 8.95	72.29 ± 9.17	0.84	0.398

Statistically significant changes occurred in BMI between 15-weeks and 30-weeks of SAT (Table 3). Even no statistically significant changes occurred in VO2max, WC and CRE (Table 3).

TABLE 3. The effects of SAT on VO_2max, CRE, WC and BMI index between 15-weeks SAT and 30-weeks SAT (n = 62)

Variable	15-weeks SAT Mean ± SD	30-weeks SAT Mean ± SD	Z	*P*
BMI [kg/m^2]	21.99 ± 2.42	21.88 ± 2.39	2.79	0.005*
WC [cm]	75.69 ± 7.11	75.45 ± 6.93	0.80	0.42
VO_2max [ml/kg/min]	40.59 ± 4.44	40.57 ± 4.44	0.34	0.73
CRE [%]	72.29 ± 9.17	71.74 ± 8.93	0.81	0.414

Statistically significant changes occurred in BMI, WC and the VO2max index after 30-weeks of SAT as compared to initial values (Table 4).

TABLE 4. The effects of SAT on VO_2max, CRE, WC and BMI index between Pre-SAT and 30-weeks SAT (n = 62)

Variable	Pre-SAT Mean ± SD	30-weeks SAT Mean ± SD	Z	*P*
BMI [kg/m^2]	22.21 ± 2.26	21.88 ± 2.38	4.65	0.000*
WC [cm]	76.34 ± 7.04	75.45 ± 6.93	2.96	0.003*
VO_2max [ml/kg/min]	39.93 ± 4.36	40.57 ± 4.44	0.34	0.000*
CRE [%]	71.64 ± 8.95	71.74 ± 8.93	1.13	0.9

After 30 weeks of SAT, the mean value of participant BMI declined to 21.88 kg/m^2 as compared to 21.99 kg/m^2 after 15 weeks of SAT ($p<0.05$). The mean value of waist circumference (WC) also reduced to 75.45 cm as compared to 75.69 cm after 15 weeks of SAT ($p<0.05$). The mean value of VO_2max increased from 39.93 ml/kg/min to 40.57 ml/kg/min after 30 weeks ($p<0.05$). The mean value of the CRE before SAT was 71.64%, increasing to 72.29% after 15 weeks of SAT and falling from 72.29% to 71.74% after 30 weeks of SAT. These changes were not statistically significant ($p>0.05$).

DISCUSSION

Regular PA improves health and reduces contributory factors of development-related diseases, which often occur in physically inactive people [9,10,11,12]. Thus it is very important to educate society about the importance of regular PA. The right choice of a suitable form of PA is significant and adds a kind of mental pleasure to participation. One form of activity that has a positive impact on cardiorespiratory is SAT [5]. One of the main findings of our study is that 30-weeks-long SAT may be an effective way to increase participants' aerobic power and to improve their overall oxygen efficiency. The VO_2max average result obtained before training (39.93 ml/kg/min) was below the average for that age group [13]. 30 weeks of SAT raised this value to 40.57 ml/kg/min compared with pre-training, which was statistically significant ($p<0.05$), though still remaining below average limits. Similar findings were reported by Williford et al.[14], showing that SAT produced minor changes in VO_2max as compared to running. Porcari et al. [15] study on the effects of ten weeks of SAT on participants' aerobic power demonstrated improvements of 11.7% in peak oxygen consumption and 6.7% in maximal minute ventilation. Kraemer et al. [16] showed significant improvement of peak VO_2max in groups of women participating in SAT and a combination of SAT and resistance exercises training.

There are numerous data suggesting that aerobic-type exercises, like SAT, improve lipoprotein lipid profiles and body composition in healthy young women [17,18]. Our study shows the beneficial effect of SAT in lowering the BMI values of participants: after 30 weeks of training this value decreased significantly ($p = 0.000$) from 22.21 kg/m^2 to 21.88 kg/m^2. In contrast, the 2013 study of Drobnik–Kozakiewicz et al. [18] showed that 10 weeks of SAT produced

no statistically-significant changes in BMI. However, in this case the subjects were students of a Sports University and their physical fitness was rated as above average.

Waist circumference (WC) can be used as a health risk indicator, as abdominal obesity results in increased risk of type 2 diabetes, hypertension, dyslipidaemia, coronary artery disease and non-insulin-dependent diabetes mellitus. In our study, participating woman were within normal WC values (the normal range being between 70 and 89 cm, according to Dancy et al. [19]). 15 weeks of SAT significantly reduced WC (p=0.01) from 76.34 cm to 75.69 cm. We believe this was mainly caused by the caloric requirements of SAT, which was an adequate effect in study group due to the duration and frequency of training. Moreover, the WC reduction can also be attributed to the toning of the abdominal area.

To evaluate the long-term effects of training the Coefficient of Restitution Effectiveness (CRE) is often used [7]. Normally CRE values are higher in trained persons than in untrained persons. Nevertheless, this method is not quite error-free. For instance, changes in heart rate can have emotional causes. In our study, this could be the reason that, despite the improvement in VO_2max, changes of CRE were not statistically significant (p>0.05). For this reason, we cannot judge the positive effect of SAT on the ability of the body to rest after physical training. Mirek et al. [20] show that PA should be considered an important factor in the development of students' physical fitness and that compulsory physical education classes can be a very important factor in its maintenance, and thus on students' health [21, 22, 23, 24].

According to our results and previous findings [5] SAT is effective for improving total physical fitness and a woman's health profile, not only among full-time students but also their part-time colleagues. Physical education classes would be a very important factor in shaping the cardiorespiratory fitness and stimulating changes in body composition of young people. In our opinion, physical education programmes in universities should include recreational forms of fitness, including SAT. Such a state of affairs would certainly help to increase students' interest in various forms of fitness and thereby improve the health of those young people. Participation in SAT classes may also develop students' knowledge and skills, enabling proper health behaviour and encouraging active participation in other forms of recreation.

CONCLUSION

Our evidence has demonstrated that regular PA protects against non-communicable diseases including cardiovascular diseases, cancer, type 2 diabetes, chronic lung disease, and musculoskeletal disorders. 30-weeks-long SAT in female undergraduate students decreased students' body mass (BMI) and waist circumference (WC) and increased their cardio respiratory efficiency (VO_2max), but had no effect on the restitution ability (CRE) of participants.

It can be seen that the positive changes in the BMI and WC were more dynamic in the first, 15-week training cycle. The same applies to the increase in the level of VO_2max. There was statistically significant difference between the initial test result and the result of the measurement carried out in the 15th week of the cycle, but no difference when comparing VO_2max resulted between 15 and 30 weeks of the cycle. Thus, the subjects reacted more effectively to the initial load, and in the further part of the cycle their reactions to training stimuli became less spectacular.

SAT classes should be conducted in universities due to their positive effects on VO_2max and body composition, and therefore health, of students. Participation in SAT classes may result in physical skills that will change behavior and encourage active participation in different forms of recreation. It should be a necessary component of human lifestyle. Further investigation should be done to evaluate other markers of body composition: FAT-mass and Fat Free Mass.

REFERENCES

1. WHO. *2008-2013 Action plan for the global strategy for the prevention and control of noncommunicable diseases*. Geneva; 2008. Available from: http://www.who.int/nmh/publications/ncd_action_plan_en.pdf ISBN: 978-92-4-159741-8
2. WHO. *Global strategy on diet, physical activity and health;* 2004. Available from: http://www.who.int/dietphysicalactivity/strategy/eb11344/strategy_english_web.pdf ISBN: 92-4-159222-2

3. Hand GA, Blair SN. *Energy Flux and its Role in Obesity and Metabolic Disease, US Endocrinology* 2014; 10(1): 59–63, DOI: http://doi.org/10.17925/USE.2014.10.01.59
4. Caspersen CJ, Powell KE, Christensen GM. *Physical activity, exercise, and physical fitness: definitions and distinctions for health-related research. Public Health Reports 1985*; 100, 2: 126–131, PMCID: PMC 1424733, PMID: 3220711
5. Zuzda JG and Latosiewicz R. *An Innovative Method of Conducting Recreational Classes Using the System of Reebok Step Exercises.* Bialystok: University of Technology; 2010. https://www.researchgate.net/profile/Jolanta_Zuzda2/publication/281148580_An_Innovative_Method_of_Conducting_Recreational_Classes_Using_the_System_of_Reebok_Step_Exercises/links/55d87cd008ae9d65948f9016/An-Innovative-Method-of-Conducting-Recreational-Classes-Using-the-System-of-Reebok-Step-Exercises.pdf
6. Gorski J. Fizjologiczne podstawy wysiłku fizycznego. Warszawa: PZWL; 2006, ISBN: 83-200-3250-4
7. Fortuna M. *Podstawy ksztaltowania i kontroli zdolnosci wysilkowej tlenowej i beztlenowej.* Jelenia Gora: Kolegium Karkonowskie; 2008. Available from: doi: 10.1249/MSS.0b013e318213fefb ISBN: 978-83-926801-4-7
8. Klonowicz S. *Metody badan fizjologicznych w zakładzie przemysłowym*. Warszawa: PZWL; 1970.INDEKS: 2721/66/0009, TIN: T00143623
9. Warren JM, Ekelund U, Besson H et al. *Assessment of physical activity – a review of methodologies with reference to epidemiological research: a report of the exercise physiology section of the European Association of Cardiovascular Prevention and Rehabilitation*. Eur J Cardiovasc Prev Rehabil. 2010; 17(2): 127–139. Available from:doi: 10.1097/HJR.0b013e32832ed875, PMID: 202115971
10. Ribeiro JM, Rodrigues L, Santos L et al. *Physical and sport activities in school and community context: what impaction health indicators? 2nd IP Leiria International Health Congress: Challenges & Innovation in Health: Leiria*; 2014, ISSN: 0034-8910, ISSN online: 151887-87
11. Bendíková, E., Dobay, B. 2017. Physical and sport education as a tool for development of a positive attitude toward health and physical activity in adulthood. European journal of contemporary education, 6(1), 14-21. ERIC Number: EJ1137901
12. Bendíková, E., Palaščáková Špringrová, I., Tomková, Š., Vagner, J. 2018. Effects of an exercise program on the dynamic function of the spine in female students in secondary school. Journal of Physical Education and Sport, 18(2), 831 – 839. DOI:10.7752/jpes.2018.02123
13. Morrow JR, Jackson A, Disch J et al. *Measurement and Evaluation in Human Performance 4th*. Human Kinetics. Champain, IL: Human Kinetics; 2010, ISBN-13: 978-1450470438, ISBN-10: 1450470432
14. Williford HN, Richards LA, Scharff-Olson M et al. *Bench stepping and running in women. Changes in fitness and injury status*. J Sports Med Phys Fitness 1998; 38(3): 221–226. Available from: https://www.ncbi.nlm.nih.gov/pubmed/9830829 PMID:9830829
15. Porcari JP, Chapek CL, Huntley EL, Elizabeth L. Huntley, Glenn A. Brice & Sandra Price. *Effects of a 10-week step aerobics training program on the aerobic power and body composition of college age w*omen. Sports Medicine Training and Rehabilitation 1995; 5(4): 321–329. https://doi.org/10.1080/15438629509512028
16. Kraemer WJ, Keuning M, Ratamess NA et al. *Resistance training combined with bench-step aerobics enhances women's health profile.* Med Sci Sports Exerc. 2001; 3(2): 259–269. Available from: https://www.ncbi.nlm.nih.gov/pubmed/11224816 PMID:11224816
17. Sanal E, Ardic F, Kirac S. *Effects of aerobic or combined aerobic resistance exercise on body composition in overweight and obese adults: gender differences*. A randomized intervention study. Eur J Phys Rehabil Med. 2012; 49(1): 1–11. https://www.ncbi.nlm.nih.gov/pubmed/22569489 PMID:22569489
18. Drobnik - Kozakiewicz I, Sawczyn M, Zarebska A. et al. *The effects of 10 weeks Step Aerobics Training on VO2max isometric strength and body composition of young women*. Central European Journal of Sport Sciences and Medicine 2013; 4(4), 3–9, p-ISSN: 2300-9705, e-ISSN-2353-2807
19. Dancy PJ. *ACSM's guidelines for exercise testing and prescription. Philadelphia*: American College of Sports Medicine; 2010, ISBN: 978-1-60913-605-5
20. Mirek W, Mleczko E, Januszewski J. Motor activity of Cracow students and their Physical fitness. Antropomotoryka 2008; 41: 49–68. https://e-antropomotoryka.pl/api/files/view/16091.pdf

21. Dobay, B. 2014. Az iskolai sporttanfolyamok hatása a nyári üdülési szokásokra = The influence of school sport courses on summer recreational habits. In 27*. Didmattech 2014 : New methods and technologies in education and practice, international scientific and professional conference*, Olomouc: Palacký university, 2014, p. 112-118.
22. Dobay, B. 2015. *Az iskolai sporttanfolyamok motivációs hatása a felnıttkori rekreációs sporttevékenységekre Dél-Szlovákiában*. Komárom : Kompress kiadó.
23. Fobel, P., Fobelová, M. (2017). Happiness as an indicator of social prosperity and sustainability of life, pp. 71-81, In. *Globálne konteksty poszanowania praw I wolności czlowieka*, N9, 2017, Katedra Stosowanych Nauk Spolecznych WOIZ PŚ, Zabrze.
24. Nemček, D. (2016a). Quality of life of people with disabilities: differences in satisfaction with indicators and domains between active and inactive individuals. *Physical Activity Review*, 4, 62-71.

Preface of the "Symposium on Computational Data Analysis and Numerical Methods"

Luís Miguel Grilo

Instituto Politécnico de Tomar (IPT), Quinta do Contador-Estrada da Serra, 2300-313 Tomar, Portugal.
Centro de Matemática e Aplicações (CMA), FCT, UNL, Portugal.
Centro de Investigação em Cidades Inteligentes (Ci2), IPT, Portugal.
CIICESI / ESTG – P. Porto, Portugal.

lgrilo@ipt.pt
URL: http://www.aim.estt.ipt.pt/~lgrilo/PagPessoal/

The papers of the symposium on Computational Data Analysis and Numerical Methods are essentially applications on different statistical methods (such as Survival Analysis, Time Series and Structural Equation Modeling). All but one theoretical paper in Statistical Inference, used real data in the areas of Social and Health Sciences, Education, Management and Economy, Engineering/Industry and Tourism.

Luís Miguel Grilo

Luís Miguel Grilo (PhD in Mathematics and Statistics, Technical University of Lisbon, 2006) is currently Adjunct Professor and Director of the Department of Mathematics and Physics of the Polytechnic Institute of Tomar (PIT), Portugal.
Has been collaborating, as invited Professor, in some Portuguese Universities and also in some international projects, namely in Arizona State University, USA.
As an integrated member of the Center for Mathematics and Applications of the Faculty of Sciences and Technology of the New University of Lisbon (CMA-FCT-UNL), develops scientific research in Distributions Theory (exact and near-exact distributions of some statistics used in Multivariate Analysis) and Applied Statistics (with special interest in Engineering and Health). Currently is also a collaborating member of the Smart Cities Research Center of the Polytechnic Institute of Tomar and in the Center for Innovation and Research in Business Sciences and Information Systems of the Polytechnic Institute of Porto, Portugal. Regularly publishes papers in international scientific journals and has made several presentations in national and international meetings of Statistics, namely as Plenary Speaker.
At the moment, is one of the editors of the Special issue "Advances in Computational Data Analysis", in the Journal of Applied Statistics (JAS), Taylor & Francis, and member of the board of CLAD (Portuguese Association of Classification and Data Analysis).
As a member of Scientific and Organizing Committees, has participated in several national and international meetings of Mathematics and Statistics. In particular, in the PIT has been the Local Chair of some International Conferences and the Chair of the annual Workshop on Computational Data Analysis and Numerical Methods.

Survival Analysis of Portuguese SMEs: a Preliminary Approach

Ana Borges[1,a)], Marco Machado[1,b)] and Fabio Duarte[1,c)]

[1]*CIICESI/ESTG - P.Porto, Margaride 4610-156 Felgueiras, Portugal.*

[a)] Corresponding author: aib@estg.ipp.pt
[b)]8130341@estg.ipp.pt
[c)]fdd@estg.ipp.pt

Abstract. A high rate of corporate bankruptcy can be devastating to economic and entrepreneurial ecosystem, especially among countries with a high concentration of Micro, Small and Medium Sized Enterprises (SMEs). Most bankruptcy studies focus on large companies, ignoring the fact that SMEs play a key role in achieving the objectives of job creation and economic growth, which are particularly relevant in the peripheral countries of the European Union. Considering the relevance of these companies to the Portuguese economy and the scarcity of empirical studies, in this paper we offer a preliminary study about the determinants of survival of SMEs operating in Portugal. Unlike to the traditional models (i.e., static models tending to ignore the longitudinal factor of time to predict corporate bankruptcy) this study applies the Cox proportional risk model in order to predict, based on historical data taken from SABI, the probability whether a SME will be in financial distress. Using data between 2008-18 and controlling for spatial effect (*Region*), *Size* and *Activity Sector*, we found evidences on the negative relation between ownership concentration and financial distress.

INTRODUCTION

Corporate bankruptcy in recent years has become one of the most discussed topics in corporate finance investigations, seeking to define the best predictive model on the topic [2]. In an attempt to predict the risk associated with stress events linked to financial health of companies, investigations carried out by several academics around the world use different techniques of modeling, each of them with different assumptions and complexities. Classical statistical methods, such as multiple discriminant analysis and logistic regression, are the most common approaches adopted to predict bankruptcy. Investigations conducted on this topic are generally focused on the development of predictive models that predict bankruptcy on the basis of financial ratios [6]. Additionally, most of them focus on large firms, and only a few researchers study SMEs. SMEs are particularly important for the economy of the European Union countries, specifically Portugal, where they account for 99.6% of the total of the business sector, which attests to their relevance to the country's employment and economic growth [22]. After the global crisis of 2008 several SMEs were on the verge of bankruptcy, and others still suffer from the consequences of the crisis. Nonetheless, despite its importance to the economy and the importance of the topic on corporate risk management, the heterogeneous characteristics of SMEs and the constraint in access to financial data have justified the scarcity of studies on these companies [6]. The timely identification of imminent failure of firms is desirable to ensure the stability of financial markets and overall economic prosperity [11]. Considering its relevance to the economy this study aims to be an introductory analysis to identify the main determinants of survival of SMEs in Portugal, starting to explicitly analyze the role of ownership concentration, based on Capital Structure Theories' insights. For this, in our survival analysis we apply a model that reflects the longitudinal factor of time, considering that this type of model has a superior performance comparing to most of the static models that ignore the fact that a company changes along the time [24], a particularly notable feature in the case of younger and smaller companies. The proportional hazards model of Cox [5] has been one of the most models because it is less restrictive in the assumptions of the model comparing to linear regression models [16]. The application of the Cox model to a sample of Portuguese SMEs will make it possible to determine the probability of these companies closing in a certain time interval, based on historical events of their survival. In this preliminary study

we test if ownership concentration has a significant effect on firm survival in terms of financial distress, controlling for spatial effect (region), firm size and industry sector, using a sample that covers different periods: a period pre-crisis; a period of crisis and; a period of financial adjustments and economic growth in Portugal.

Data

The data used in this work were obtained from the Bureau van Dijk SABI (Iberian Balance Sheet Analysis System) database for the period 2007-2017. The sample comprises 18 145 Portuguese SMEs from the manufacturing sector. Companies are considered SMEs when they meet two of the following three criteria: (1) less than 250 employees; (2) a turnover of less than 50 million euros; and (3) total assets less than 43 million euros. Through the date of the current situation of the company it was possible to identify that only a small number of firms (< 1%) left the market in the period from 2007 to 2017. In this way, and despite the exit of a company from the market and financial difficulties are different events [12], the model will be considered that the financial difficulties have the consequence of the exit from the market. Thus, following the study of [12], we consider that a company is in financial distress when its EBITDA (Earnings Before Interest, Taxes, Depreciation and Amortization) is less than financial expenses for two consecutive years, and general liquidity (current assets over current liabilities) is less than 1 for two consecutive years. Although [12] use solvency (equity over total liabilities) instead of general liquidity, the use of the latter ratio shows the ability of a company to meet its short-term obligations. When this ratio is less than 1 the company's short-term debts (ie, debts to be settled within one year or less) are higher than the value of the assets with the highest liquidity, such as cash and cash equivalents and others that can be converted into money within a year or less. The choice of variables for this study is based on literature review, and some control variables such as *Size*, *Region* and *Activity sector* were introduced. The variable *Ownership concentration* is a proxy for the management characteristics of the company distinguishing firms owned at least in 50% by its largest shareholder from other ones (based on [10], [19], [21], [25].). This distinction finds support on literature on Capital Structure studies, namely in some studies addressing the performance of family firms versus nonfamily firms (e.g., [20]). Variable *Ownership concentration* takes value 1 if a firm is owned at least in 50% by its largest shareholder, and 0 otherwise. We built the variable *Size* based on [17]: a categorical variable that takes the value 1 if Micro-sized firm; 2 if Small-sized firm; 3 if Medium-sized firm. To control for spatial and industry effects, i.e. to capture different geographic regions and economic activities' idiosyncratic influence on SMEs' survival, we included the variables *Region* and *Activity sector*, respectively. *Region* is a categorical variable controlling seven regions according to NUTS II (Nomenclature of Territorial Units for Statistics): North, Algarve, Center, Lisbon, Alentejo, Azores and Madeira. *Activity sector* is a categorial variable controlling 309 diferent economic activities among the Manufacturing Sector to NACE Rev.3.

Methodology

In order to estimate the relative risk of financial distress, we will first explore the non-parametric Kaplan-Meier estimates [15], for *Ownership concentration* stratified by categories, comparing them by their graphical representation. The Kaplan-Meier estimator is a non-parametric maximum likelihood estimator (MLE) of the survival function, $S(t) = P(T > t)$. T is a non-negative random variable that represents the life time of a company from a given homogeneous population. This estimator is a step function with jumps at observed times of the event of interest (company financial distress). In order to evaluate the statistical significance of the differences between the survival curves of each category of the variable, the log-rank test or the Mantel-Haenszel test will be used, where the null hypothesis to be tested is the existence of no difference between the (true) survival curves. Since the Kaplan-Meier estimator is a non-parametric procedure and does not allow the simultaneous study of the effect of several covariates on the life time, nor to adjust this effect to eventual combinations of other variables, we will make use of the Cox proportional hazards model [5]. This model is the appropriate choice for this type of analysis as it is able to capture the characteristics of Portuguese SMEs as reported by [17] and [18]. Also, it allows us to consider data right censorship (i.e., partial observation of the response, since we do not observe the total life time of a company in the analyzed time window) and explains the time dependence on the risk function $h_i(t)$. The model is expressed as follows:

$$h_i(t) = h_0(t) exp(x_i \beta) \tag{1}$$

This model assumes that the risk rate of any firm i at time t is the product of two factors: a baseline risk function $h_0(t)$, and an exponential linear function of covariates $x_i\beta$. A particularity of this model, which can be viewed as one

of its advantages, is that the estimation of the coefficients does not require the formulation of the baseline cumulative survival function as it gets absorbed when the coefficients are estimated by the method of partial log likelihood. However, there are some restrictions on the application of this type of model such as the assumption of proportional risk. This assumption can be validated through a graph $\log(-\log(t))$ *versus* t, where the curves obtained must be parallel. Thus, the proportional hazards model is inadequate when the curves intersect.

Main Results

Throughout the period under study, 43.47% of the 18145 firms analyzed registered financial distress. Of the 8423 firms with ownership concentration above 50%, we registered 43.9% firms in financial distress and 43.9% for the firms with ownership concentration below 50% (9722). Subsampling by firm size, we accounted for 44.14% of micro-sized firms (of a total of 10868 firms), 40.47% of small-sized firms (of a total of 5580 firms) and 49.09% of medium-sized firms (of a total of 1697 firms) presenting financial stress. Analyzing the differences on survival probability (with financial distress as our event of interest), by means of a non parametric estimator of Kaplan Meier, by *Ownership concentration* categories (Fig: 1), the Log Rank Mantel-Cox test ($\chi^2 = 16.39$; $p - value < 0.001$) confirms statistical significant differences between risk curves, with firms with higher ownership concentration the ones that present a higher risk of financial distress. In fact, fitting a multivariated Cox proportional hazard model (Table1) considering

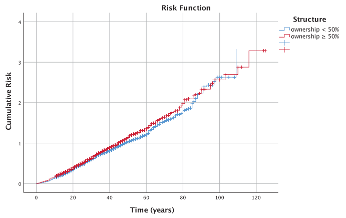

FIGURE 1. Kaplan Meier Risk Function by *Ownership concentration*.

Ownership concentration as explanatory variable and *Size*, *Region* and *Activity sector* as control variables, we confirm that firms with higher ownership concentration are the ones that present a higher hazard ratio for financial distress (HR=1.126, $p - value < 0.001$) comparatively to others. The proportional hazards assumption was validated through

TABLE 1. Cox Propotional Hazard Ratios Estimates

Variable	**HR 95% CI**	**p-value**
Ownership concentration ≥ 50%	1.126 [1.076; 1.179]	< 0.001
Control Variables		
Region	*Included*	*Included*
Size	*Included*	*Included*
Activity Sector	*Included*	*Included*

$\log(-\log(t))$ versus t graphs for both size and structure variables[1].

Discussion

Considering the relevance of SMEs companies to the Portuguese economy and the scarcity of empirical studies on corporate bankruptcy in this paper we aim to contribute to the study about the determinants of survival of these companies. In particular we tests if ownership concentration has a significant effect on firm survival in terms of financial distress, controlling for spatial effect (*region*), *firm size* and *activity sector*. The attention to the relation between

[1]Graphs are not presented for space limitation but available under request

ownership structure and firm performance dates back to [4]. [7], [14] and [8] amplified the interest on the subject by approaching this relation based on agency costs arguments. Literature on agency costs hypothesized that different ownership structures are related with different levels of risks that firms take [3]. [14] suggests that high ownership concentration is typically efficient: to provide managers with incentives to work and; to provide to large investors incentives to monitor the managers. Accordingly, traditional agency models argue that private firms with low fractionated ownership may alleviate agency costs [26] which may increase firm performance. Nonetheless, making use of a Cox Proportional Hazard model we found that firms with higher ownership concentration are the ones that present a higher hazard ratio for financial distress comparatively to others. Thus, founding evidences on the negative relation between ownership concentration and financial distress. Hence, contrary to above agency costs arguments, our results reject the idea that firms with undiversified shareholders face a higher probability of survival. Future research might go further addressing this finding taking in account not only the ownership structure but also corporate governance characteristics. Additionally, capital structure should be included in future research based on [14]' arguments on the value of debt to mitigate agency costs.

ACKNOWLEDGMENTS

The authors thank the support by the Center for Research and Innovation in Business Sciences and Information Systems (CIICESI), ESTG - P.Porto.

REFERENCES

[1] Altman, E. I., & Sabato, G. (2007). *Abacus*, 43(3), 332–357.
[2] Balcaen, S., & Ooghe, H. (2006). *British Accounting Review*, 38(1), 63–93.
[3] Berger, A. N., & Udell, G. F. (1995). *Journal of business,* 351-381.
[4] Berle, A., & Means, G. (1932). *New York*, 2(3), 45-53.
[5] Cox, D. R. (1975). *Biometrika*, 62(2), 269–276.
[6] Cultrera, L., & Brédart, X. (2016). *Review of Accounting and Finance*, 15(1), 101–119.
[7] Fama, E. F., & Miller, M. H. (1972). *The theory of finance*. Holt Rinehart & Winston.
[8] Fama, E. F., & Jensen, M. C. (1983). *The journal of law and Economics*, 26(2), 301-325.
[9] Fitzpatrick, P. J. (1932). *Accountants Publishing Company*.
[10] Gonzalez, M., Guzman, A., Pablo, E., & Trujillo, M. A. (2019). *Research in International Business and Finance*, 48(November 2018), 169–186.
[11] Gordini, N. (2014). *Expert Systems with Applications*, 41(14), 6433–6445.
[12] Gupta, J., Barzotto, M., & Khorasgani, A. (2018). I*nternational Journal of Finance & Economics*, (March), 571–605.
[13] Holmes, P., Hunt, A., & Stone, I. (2010). *Applied Economics*, 42(2), 185–195.
[14] Jensen, M. C., & Meckling, W. H. (1976). *Journal of financial economics*, 3(4), 305-360.
[15] Kaplan, E. L., & Meier, P. (1958). *Journal of American Statistical Association*, 53(282), 457–481.
[16] Kim, M. H. Y., Ma, S., & Zhou, Y. A. (2016). *Journal of the Asia Pacific Economy*, 21(3), 418–443.
[17] Mata, J., & Portugal, P. (1994). *The Journal of Industrial Economies*, 42(3), 227–245.
[18] Mata, J., Portugal, P., & Guimarães, P. (1995). *International Journal of Industrial Organization*, 13(4), 459–481.
[19] Miller, D., Le Breton-Miller, I., Lester, R. H., & Cannella, A. A. (2007). J*ournal of Corporate Finance*, 13(5), 829–858.
[20] Miralles-Marcelo, J. L., del Mar Miralles-Quirós, M., & Lisboa, I. (2014). *Journal of Family Business Strategy*, 5(2), 156-168.
[21] Montoro-Pons, J. D., & Cuadrado-García, M. (2018). J*ournal of Cultural Economics*, 42(2), 287–307.
[22] Nunes, P. M., & Serrasqueiro, Z. (2012). *Applied Economics Letters*, 19(9), 849–855.
[23] Pérez, S. E., Llopis, A. S., & Llopis, J. A. S. (2004). *Review of Industrial Organization*, 25(3), 251–273.
[24] Shumway, T. (2001). *The Journal of Business*, 74(1), 101–124.
[25] Steijvers, T., Voordeckers, W., & Vanhoof, K. (2010). *Small Business Economics*, 34(3), 243–259.
[26] Voordeckers, W., & Steijvers, T. (2006). *Journal of Banking & Finance,* 30(11), 3067-3086.

Time Series Forecasting using Holt-Winters Exponential Smoothing: an Application to Economic Data

Susana Lima[1,b)], A. Manuela Gonçalves[2,a)] and Marco Costa[3,c)]

[1]*Department of Mathematics, University of Minho, Portugal.*
[2]*Department of Mathematics and Center of Mathematics, University of Minho, Portugal.*
[3]*Águeda School of Technology and Management and Center for Research and Development in Mathematics and Applications, University of Aveiro, Portugal.*

[a)]Corresponding author: mneves@math.uminho.pt
[b)]susanamrlima@gmail.com
[c)]marco@ua.pt

Abstract. This study deals with forecasting economic time series that have strong trends and seasonal patterns. How to best model and forecast these patterns has been a long-standing issue of time series analysis. In this work, we propose a Holt-Winters Exponential Smoothing approach to time series forecasting in order to increase the chance of capturing different patterns in the data and thus improve forecasting performance. Therefore, the main propose of this study is to compare the accuracy of Holt-Winters models (additive and multiplicative) for forecasting and to bring new insights about the methods used via this approach. These methods are chosen because of their ability to model trend and seasonal fluctuations present in economic data. The models are fitted to time series of e-commerce retail sales in Portugal. Finally, a comparison is made and discussed.

INTRODUCTION

Time series forecasting is an important area of forecasting in which past observations of the same variable are collected and analyzed to develop a model describing the underlying relationship. The model is then used to extrapolate the time series into the future. Forecasting methods are a key tool in decision-making processes in many areas, such as economics, management and finance, or environment. Much effort has been devoted over the past several decades to the development and improvement of time series forecasting models. The main propose of this work is to compare the accuracy of the additive and the multiplicative Holt-Winters Exponential Smoothing models for forecasting economic time series; both models can increase the chance of capture different patterns in the data and improve forecasting performance.

According to the GfK study ”European Retail 2016” that analyzes 33 countries in Europe, the retail segment in private consumption, in Portugal, in the year 2015, accounted for 33.4%. The study of the economic variables associated with this area is essential and quite useful both to characterize the recent past and to anticipate trends. Obtaining empirical results from several real data sales forecasting is one of the most important issues behind all strategic and planning decisions in any retail business. The objective of the turnover index is to show the development of the market for goods and services. Turnover comprises the totals invoiced by the observation unit during the reference period, and this corresponds to market sales of goods or services supplied to third parties. Turnover also includes all other charges (transport, packaging, etc.) passed on to the customer, even if these charges are listed separately in the invoice. Turnover excludes VAT and other similar deductible taxes directly linked to turnover, as well as all duties and taxes on the goods or services invoiced by the unit. The data used in this study, available on the Eurostat platform, corresponds to monthly indexes of turnover (total, TOVT) in the context of retail sales via internet (e-commerce) observed between January 2000 and February 2018 (Fig. 1). Note that this index should be compared with the base year, in this case 2015, which correspond to the index 100.

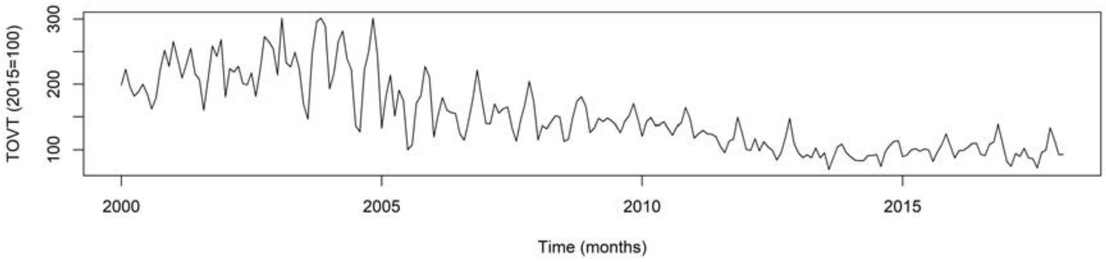

FIGURE 1. E-commerce retail sales time series of Portugal.

METHODS

The Holt-Winters (HW) method is an extension of the Holt method, and is applied whenever the data behaviour is trendy and is seasonal [2]. Relatively to the seasonal type, it can be additive or multiplicative, depending on the oscillatory movement along the time period. In both versions, forecasts will depend on the following three components of a seasonal time series: its level, its trend and its seasonal coefficient. In addition, both are implemented in the *HoltWinters()* function of the *forecast* package in R [3]. The additive version ought to be considered whenever the seasonal pattern of a series has a constant amplitude over time. In the additive case, the series can be written by $Y_t = T_t + S_t + \epsilon_t$, where T_t represents the trend (the sum of the level and slope of the series at time t), S_t is the seasonal component, and ϵ_t are error terms with mean zero and constant variance. In the multiplicative case, the series can be represented by $Y_t = T_t \times S_t + \epsilon_t$. The recursive equations of the multiplicative and additive HW methods, for level, trend, seasonal factors and forecast, with $h_s^+ = [(h-1) \ \ mod \ s] + 1$, are presented in Table 1, where Y_t is the observed data at time t, s is the length of seasonality (number of months in a season), h is the number of forecast ahead, and $\theta = (\alpha, \beta, \gamma)^T$ is the vector of smoothing parameters [4].

TABLE 1. Holt-Winters method recursive equations.

Additive HW method	**Multiplicative HW method**
Level: $l_t = \alpha(Y_t - s_{t-s}) + (1-\alpha)(l_{t-1} + b_{t-1}),\ 0 \leq \alpha \leq 1$	Level: $l_t = \alpha \frac{Y_t}{s_{t-s}} + (1-\alpha)(l_{t-1} + b_{t-1}),\ 0 \leq \alpha \leq 1$
Trend: $b_t = \beta(l_t - l_{t-1}) + (1-\beta)b_{t-1},\ 0 \leq \beta \leq 1$	Trend: $b_t = \beta(l_t - l_{t-1}) + (1-\beta)b_{t-1},\ 0 \leq \beta \leq 1$
Seasonal: $s_t = \gamma(Y_t - l_t) + (1-\gamma)s_{t-s},\ 0 \leq \gamma \leq 1$	Seasonal: $s_t = \gamma \frac{Y_t}{l_t} + (1-\gamma)s_{t-s},\ 0 \leq \gamma \leq 1$
Forecast: $\hat{Y}_{t+h} = l_t + hb_t + s_{t-s+h_s^+}\ ,\ \ h = 1, 2, \ldots$	Forecast: $\hat{Y}_{t+h} = (l_t + hb_t)s_{t-s+h_s^+}\ ,\ \ h = 1, 2, \ldots$

To initialize these methods, the R environment uses the *decompose* function to perform a decomposition of the series in its components – trend and seasonality– through a moving average process, and thus determine the initial values for l_s, b_s and s_i, $i = 1, \ldots, s$ ($\hat{l}_s$ e $\hat{b}_s$ are determined by means of the trend of a simple linear regression by using the initial observations).

Computing prediction intervals is an important part of the forecasting process, intended to indicate the likely uncertainty in point forecasts. The forecast intervals are usually based on the Mean Square Error (MSE) that denotes the variance of the h-step-ahead forecast errors. Empirical forecast intervals (if a normality assumption is verified) at h-step-ahead and the time series presents a seasonal component with period s are given by the following expression

$$\left(\hat{Y}_{t+h} - z_{1-\alpha/2}\sqrt{\mathrm{MSE}_{(h)}}, \hat{Y}_{t+h} + z_{1-\alpha/2}\sqrt{\mathrm{MSE}_{(h)}}\right), \tag{1}$$

where z is the appropriate quantile for the standard Normal distribution, and $\mathrm{MSE}_{(h)} = \frac{1}{n-h-s+1}\sum_{t=h+s}^{n}(Y_t - \hat{Y}_{t|t-h})^2$ denotes the variance of the h-step-ahead errors. In order to compare the predictive accuracy of both methods, we considered five forecasting performance criteria: Mean Square Error (MSE), Root Mean Square Error (RMSE), Mean Absolute Percentage Error (MAPE), Mean Absolute Scaled Error (MASE), and Theil's U-statistics.

RESULTS AND DISCUSSION

The methods considered in this study are applied to two sets: training data (in-sample data) and testing data (out-of-sample data) in order to testify the accuracy of the proposed forecasting models. The selected training data from January 2000 to December 2016 (first 204 months) was used in order to fit the models to the data, and the test period from January 20017 to February 2018 (last 14 months) was used to forecast. The smoothing constants estimates and the values used for the initialization of both multiplicative and additive methods can be found in Table 2 and Table 3, respectively.

TABLE 2. Initialization of level, trend, seasonal and exponential smoothing parameters of the multiplicative HW model for the e-commerce retail sales time series of Portugal.

Multiplicative model		MSE= 420.3237		
$\hat{\alpha} = 0.1823$	$\hat{\beta} = 0.0589$	$\hat{\gamma} = 0.6781$	$\hat{l}_1 = 203.2920$	$\hat{b}_1 = 2.2286$
$\hat{s}_1 = 1.1915$	$\hat{s}_2 = 1.0632$	$\hat{s}_3 = 0.9320$	$\hat{s}_4 = 1.0118$	$\hat{s}_5 = 1.1139$
$\hat{s}_6 = 0.9367$	$\hat{s}_7 = 0.8972$	$\hat{s}_8 = 0.7744$	$\hat{s}_9 = 0.8494$	$\hat{s}_{10} = 1.0460$
$\hat{s}_{11} = 1.1568$	$\hat{s}_{12} = 1.0271$			

TABLE 3. Initialization of level, trend, seasonal and exponential smoothing parameters of the additive HW model for the e-commerce retail sales time series of Portugal.

Additive model		MSE = 452.3238		
$\hat{\alpha} = 0.1765$	$\hat{\beta} = 0.0648$	$\hat{\gamma} = 0.6588$	$\hat{l}_1 = 203.2920$	$\hat{b}_1 = 2.2286$
$\hat{s}_1 = 42.2531$	$\hat{s}_2 = 13.6990$	$\hat{s}_3 = -15.7135$	$\hat{s}_4 = 2.2865$	$\hat{s}_5 = 25.6698$
$\hat{s}_6 = -14.9552$	$\hat{s}_7 = -21.7302$	$\hat{s}_8 = -47.7510$	$\hat{s}_9 = -32.2427$	$\hat{s}_{10} = 9.2656$
$\hat{s}_{11} = 33.6698$	$\hat{s}_{12} = 5.5490$			

Table 4 shows the results of the accuracy measures calculated for training and testing periods for the two methods applied to the time series under study. As can be seen in the Table 4, according to the five measures of evaluation calculated, the multiplicative model is in fact the one with the best predictive (in the training period from January 2000 to December 2016) and forecast (in the testing period from January 2017 to February 2018) performances of the e-commerce retail sales time series of Portugal. Usually when a series displays a seasonal pattern characterized by an amplitude that varies with the series level, the multiplicative version is a better choice [4], as with the modeling process of this study.

TABLE 4. Forecasting performance evaluation of HW models of e-commerce retail sales time series of Portugal

Model	**MSE**	**RMSE**	**MAPE**	**MASE**	**U-Theil**	
Additive	452.3238	21.2679	9.1284	0.7888	0.6311	training period
Multiplicative	**420.3237**	**20.5018**	**8.4697**	**0.7405**	**0.5866**	training period
Additive	298.9753	17.2909	17.9859	1.1051	1.0825	testing period
Multiplicative	**265.2426**	**16.2863**	**16.7628**	**1.0299**	**1.0215**	testing period

The mean square errors calculated from the 14-step-ahead required for the construction of the forecast intervals are summarized in Table 5. In Fig. 2 are represented the original values of the e-commerce time series, the estimates in the modeling period (training period), the forecasts in the forecasting period (testing period) and the forecast intervals for a confidence level of 95%, applying the additive and the multiplicative model. The models' validation was assessed by means of the residuals analysis. The independency assumption was assessed by estimating the autocorrelation and the partial autocorrelation functions of residuals, by calculating the Durbin-Watson' statistics, and performing the Ljung-Box test and the assumption that the residuals are identically normally distributed were also verified (performing the Kolmogorov-Smirnov test).

It should be noted that the order of magnitude of these errors is big. In fact, this results in prediction intervals with large amplitudes, in terms of the coverage rate: the forecast intervals for the Holt-Winters model include the

TABLE 5. Mean Square Error at h-step-ahead for the multiplicative HW model (the best performance) of e-commerce retail sales time series of Portugal.

h	1 month	2 months	3 months	4 months	5 months	6 months	7 months
$\mathbf{MSE_h}$	420.3237	458.9360	470.3099	500.2939	515.3850	540.0650	616.2973
h	8 months	9 months	10 months	11 months	12 months	13 months	14 months
$\mathbf{MSE_h}$	681.5444	716.6324	749.2076	776.7510	819.6080	1111.9670	1141.6730

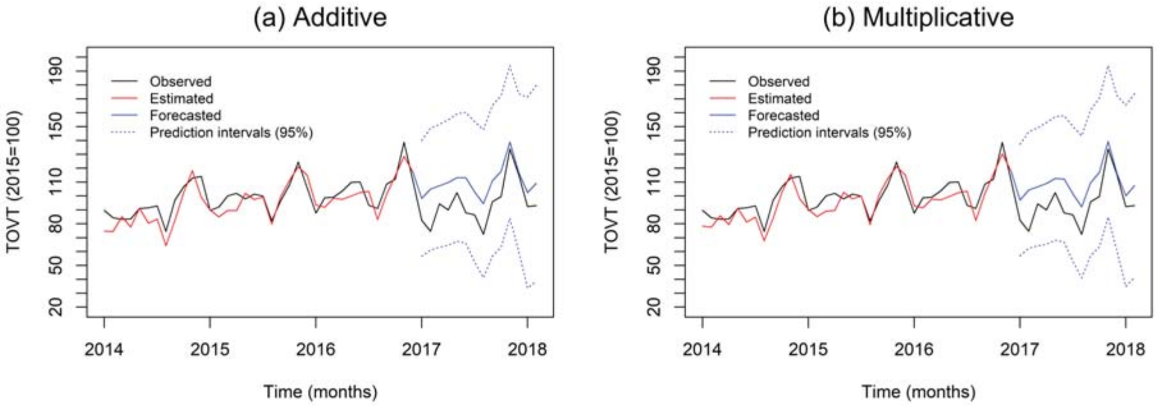

FIGURE 2. Additive HW (left) and multiplicative HW (right) estimates, forecasts, and forecast confidence intervals (95 %) for e-commerce retail sales time series of Portugal.

14 observations of the test time series, hence the coverage rate of 100% (see Fig. 2). However, the normality of prediction errors is, in this case, rejected at a significance level of 5%, for all steps h, with $h = 1, 2, \ldots, 14$. Therefore, it is concluded that the prediction intervals constructed according to the expression (1) are not the most suitable for this type of data, i.e. the HW method is conservative in the construction of forecast intervals. In order to circumvent this failure, as future work an alternative is to study resampling methods for the construction of forecast intervals (an approach already considered in [1]).

ACKNOWLEDGMENTS

This research was partially financed by Portuguese funds by the Center for Research and Development in Mathematics and Applications (CIDMA) and the Portuguese Foundation for Science and Technology (”Fundação para a Ciência e a Tecnologia” - FCT), within project UID/MAT/04106/2019. This research was partially financed by Portuguese funds through Portuguese Foundation for Science and Technology (”Fundação para a Ciência e a Tecnologia” - FCT), within project UID/MAT/00013/2013.

REFERENCES

[1] M. Costa and A. M. Goncalves, “Forecasting time series combining holt-winters and bootstrap approaches,” in *Proceedings of the International Conference on Numerical Analysis and Applied Mathematics 2014 (ICNAAM-2014)*, AIP Conference Proceedings 1648 (T. E. Simos, G. Psihoyios and Ch. Tsitouras, Rhodes, Greece, 2015), pp. 110004–1–110004–4.

[2] P. R. Winters, Management Science **6**, 324–342 (1960).

[3] RCoreTeam, R: a language and environment for statistical computing, `https://www.R-project.org/` (2018).

[4] R. Hyndman and R. Snyder, *Forecasting with Exponential Smoothing. The State Space Approach* (Springer, 2008).

Does Corruption in the Public Sector Reduce Corporate Ethics? – A Panel Data Analysis

Fernanda A. Ferreira[1, a)], Conceição Castro[2, b)] and Cristina Lopes[3, c)]

[1]*Applied Management Research Unit (UNIAG), School of Hospitality and Tourism of P.PORTO, Portugal*
[2]*Porto Accounting and Business School; CEOS.PP/ISCAP/P.PORTO; CEPESE, Portugal*
[3]*Porto Accounting and Business School; CEOS.PP/ISCAP/P.PORTO; LEMA - Mathematical Engineering Lab. , Portugal*

[a)]Corresponding author: faf@esht.ipp.pt
[b)]mariacastro@iscap.ipp.pt
[c)] cristinalopes@iscap.ipp.pt

Abstract. In a globalized world, organizations no longer operate at a national level, which poses challenges for corporate ethics standards. Ethics has gained importance in this competitive business environment. In addition, enterprises face different levels of government ethics and political systems in which they operate and when they face high levels of corruption in the public sector this may lower the standard for corporate ethics. Using regression models for panel-data, the aim of this paper is to assess the effects of corruption in the public sector on corporate ethics, in a sample of 127 countries over the period of 2006–2017.
The results suggest that there is a significant and negative impact of corruption in the public sector on the ethical behavior of firms. In addition, regulatory quality, corporate accountability and internet usage have significant and positive impacts on corporate ethics. This implies that fighting public corruption, promoting the development of policies that are market-friendly, strengthening the standards of auditing and reporting, and increasing the degree of digitalization of a country can improve the ethical behavior of firms.

INTRODUCTION

With globalization, the new environmental challenges, and the need of sustainability, the role of in ethics is enhances in businesses. Business ethics as "an academic field is the systematic study of the morality existing in businesses [1], namely their practices and their values. The standards of corporate ethics may be influenced by the government behavior, since they can play an important role in inspiring the private sector and civil society to have high standards of ethics. When enterprises operate in a country where corruption in the public sector is imbued or there are few efforts to fight corruption, the standards for ethical behavior of firms may be lower. Business ethics can be associated to political structures. Good governance – greater efficiency, transparency and integrity of the public sector – propitiates sound business environment favorable to high standards of ethics. The lack of ethics can also result from a lack of economic freedom [2], since when too much regulation restricts economic freedom, bureaucrats are more likely to adopt rent-seeking behavior and individuals seek to bypass existing barriers. The strength of financial auditing and reporting standards in a country can also influence the corporate ethical behavior as well [3]. The use of Information and Communication Technologies (ICTs) by civil society is a driven force to transparency, enhancing the easiness of disclosure of unethical behaviors at a reduced cost and high speed.

The objective of this paper is to analyze how corruption has an impact on ethical behavior of firms, alongside with other determinants. The paper is organized as follows: first the literature is reviewed. Then the research methodology is defined, followed by the presentation and analysis of the results.

LITERATURE REVIEW

Transparency International defines corruption as the abuse of entrusted power for private gain. According to [4], there is a high correlation between corporate ethics and corruption in the public sector, and [5, 6] emphasize the importance of controlling corruption to improve standards of ethical behavior in firms. Also, [7] investigated the

impact of good governance, measured by the Worldwide Governance Indicators, in a sample of 140 countries. By aggregating countries by region and level of income, the author found for almost all governance indicators a significant impact in the ethical behavior of firms, although with different intensity according to the different regions and level of income. Control of corruption and rule of law were the most influential indicators of corporate ethics for all the considered income groups and regions, and government effectiveness for all regions, except for Africa. Following the study of [7], for 39 African countries [3] found a significant and positive relationship between control of corruption, rule of law and regulatory quality and ethical behavior of firms, but not statistically significant for voice and accountability and political stability.

MODEL, METHODOLOGY AND DATA

The empirical investigation on the impact of corruption on corporate ethics is examined for a panel of 127 countries, for which all the necessary information was available, in a period of 12 years (2006–2017). The model takes the form (1):

$$EBF_{i,t} = \beta_1 CPI_{i,t} + \beta_{2,j} \sum_{j=1}^{k} X_{j,i,t} + \beta_3 EF_{i,t} + \beta_4 ACC_{i,t} + \beta_5 NET_{i,t} + u_i + v_t + \varepsilon_{i,t}. \tag{1}$$

In the model, β_j are the coefficients of the independent variables, u_i and v_t are normally distributed random variables with zero mean and constant variance that represent the specific effects of countries and time, respectively, and $\varepsilon_{i,t}$ is a normally distributed random variable with zero mean and constant variance that represents the error term.

The dependent variable, *EBF*, is the Ethical Behavior of Firms in country *i* (*i*=1, ..., *N*, where *N* denotes the total number of countries) in the year *t* (*t*=1, ..., *T*, where *T* denotes the total number of years). Corporate ethics is measured by the perception about the *Ethical Behavior of Firms* (*EBF*) in their interaction with public officials, politicians and other firms produced by the World Economic Forum (WEF), and is rated from 1- extremely poor to 7- excellent. Corruption is measured by the *Corruption Perception Index* (*CPI*) published by Transparency International and measures the perceived level of corruption in the public sector, according to experts and business people, and ranges from 0 (highly corrupt) to 100 (very clean). The higher the corruption, the lower is CPI. Besides corruption, several indicators (independent variables) were considered for analysis. $X_{j,i,t}$ is the vector of good governance that was measured by the following dimensions of governance: *Regulatory Quality (RQ), Government Effectiveness (GE), Rule of Law (RL), Voice and Accountability (VA)* and *Political Stability and Absence of Violence* (*PS*) included in the Worldwide Governance Indicators of the World Bank (WB), which range from approximately -2.5 (weak) to 2.5 (strong) governance performance. *RQ* captures the perceptions of enterprises, citizens and experts the ability of the government to formulate and implement sound policies and regulations that permit and promote private sector development. *GE* captures the quality of public and civil services, their independence from political pressures, and the quality of policy formulation and implementation. *RL* reflects the perceptions of the extent to which agents have confidence in and abide by the rules of society. *VA* measures the perception of representativeness of the voices of the different social strata, the capacity of the government to provide acceptable justifications for its decisions and actions, and *PS* of the likelihood of political instability and/or politically-motivated violence, including terrorism.

Economic Freedom is measured by the *Economic Freedom Index* (*EF*) published by the Heritage Foundation/Wall Street Journal and includes 12 components, namely business, labour, monetary, trade, investment and financial freedom, on a scale from 0 to 100, where 100 represents the maximum freedom. Corporate Accountability (*ACC*) was gathered from the WEF and is the perception of the strength of auditing and reporting standards, efficacy of corporate boards, protection of minority shareholders' interests and strength of investor protection. *NET* represents the percentage of individuals using the internet, according to the WB, and the internet can be used via a computer, mobile phone, personal digital assistant, games machine, digital TV, etc..

At first, we also used GE, RL and EF variables in the model, but due to strong multicolinnearity we had to remove them, originating the final model in equation (2).

$$EBF_{i,t} = \beta_1 CPI_{i,t} + \beta_{2,1} RQ_{i,t} + \beta_{2,2} VA_{i,t} + \beta_{2,3} PS_{i,t} + \beta_4 ACC_{i,t} + \beta_5 NET_{i,t} + u_i + v_t + \varepsilon_{i,t}. \tag{2}$$

RESULTS AND DISCUSSION

During the period under analysis, the mean value for EBF denotes a decreasing trend. In 2017, New Zealand (6.3) was the leading state in standard ethical behaviour, followed by Finland and Singapore (6.2), and Bolivia, Mauritania

and Venezuela (2.6) have the lowest scores. Figure 1 depicts the distribution of EBF by levels of income, according to the classification of the World Bank, for the countries included in the panel regression. It is noted that high-income countries have a median standard ethical behavior far superior to all other countries, irrespective of their income level. 75% of high-income countries have scores above the 75% of the remaining countries with lower income levels. Analyzing EBF by region (Figure 2), the maximum scores are observed in the WE/EU and AP. It is in WE/EU and MENA that the median standard corporate ethics are higher and in the remaining regions are lower and similar.

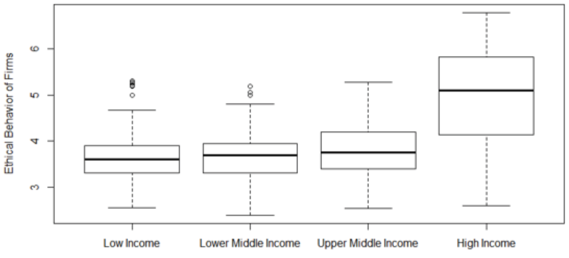

FIGURE 1. EBF by level of income, 2006-2017

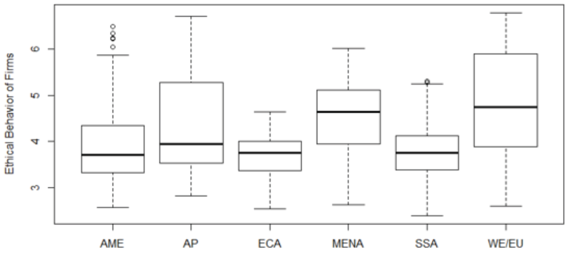

FIGURE 2. EBF by region, 2006-2017

Notes: The line in bold represents the median, framed between the 1st quartile (lower end of the box) and the 3rd quartile (upper end of the box). The lower and upper bars represent, respectively, the minimum and maximum distributions.
Legend: AME – Americas; AP – Asia Pacific; ECA – Eastern Europe and Central Asia; MENA – Middle East & Northern Africa; SSA – Sub-Saharan Africa; WE/EU – Western Europe/European Union

We computed the Spearman correlation matrix across the regressors (Figure 3).

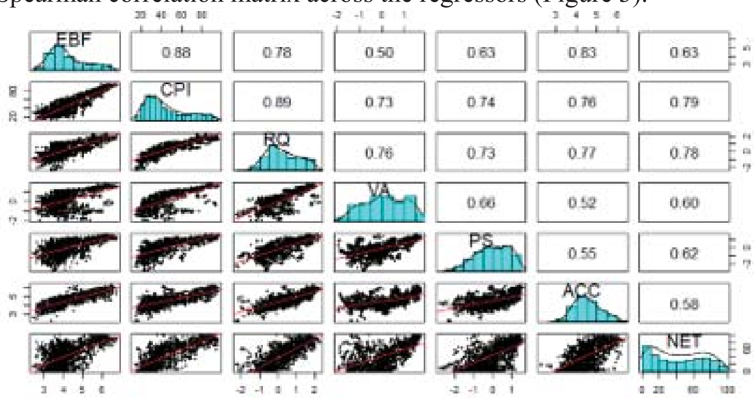

Source: own calculations

FIGURE 3. Correlation matrix and scatterplots between the variables included in the baseline model

In this study, panel data techniques are used to analyze and quantify the impact of explanatory variables on the ethical behavior of firms. The panel data regression is run for pooled ordinary least squares (OLS), fixed effects (FE), and random effects (RE). We performed the Lagrange Multiplier (LM) test to choose between the pooled OLS and panel data regressions. The null hypothesis of LM is that there is no significant difference across countries and across time. The null hypothesis was rejected at $p < 0.0001$ ($\chi^2 = 1141.4$ for countries and $\chi^2 = 242.33$ for time), indicating that pooled OLS would produce inconsistent estimates. So, we concluded that a panel data model is the most appropriate model. Using Hausman test to guide the choice between fixed (within-group) and random effects, the null hypothesis was rejected, implying that the individual effects are correlated with the explanatory variables ($\chi^2 = 347.3$, $p < 0.0001$). So, we concluded that the RE estimator is inconsistent and that the FE estimator is more appropriate. Therefore, we resorted to the fixed-effects (within-group) estimator, allowing us to control for unobserved heterogeneity across countries and across time. A standard assumption in panel-data models is that the error terms are not correlated, both in time and across cross-sections (entities). The discussion of the results is based on the findings of the FE model, which is reported in Table 1.

TABLE 1. Results of panel data regression analysis Model FE for dependent variable EBF considering the robust covariance matrix computed with Arellano method

Independent variables	Coefficients	Standard error			
CPI	0.021	(0.003)	***	N	1524
RQ	0.237	(0.091)	**	R^2	0.997
VA	0.008	(0.148)		Adj. R^2	0.997
PS	-0.038	(0.051)		F-statistic	79.444
ACC	0.314	(0.050)	***	Prob. (F-statistic)	0.000
NET	0.004	(0.002)	*		

, **, and * indicate significance at 5%, 1% and 0.1% levels, respectively*

The R^2 shows that the FE model explains 99.71 percent of the variation in the dependent variable. The independent variables that are significant in the model at the level of 0.05 have the expected sign. We also tested for the presence of multicollinearity by computing the variance inflation factors (VIF), which resulted to be below the threshold of 8. The residuals have a symmetric distribution similar to the normal distribution. The error structure was found to be heteroskedastic (studentized Breusch Pagan Test BP=51.091, $p < 0.0001$) and autocorrelated, therefore we used the standard errors computed from the robust covariance matrix with Arellano method. The coefficient of the CPI is positive and statistically significant at 1% significance level and indicates that an increase in the score of CPI by one point increases the score of EBF by 0.0206 points, *ceteris paribus*. This means that in countries with higher corruption the EBF is lower. The results also suggest that an increase in the score of RQ by one point increases the score of EBF by 0.2373, respectively, *ceteris paribus*. Corporate accountability is an important indicator that influences EBF, meaning that enhancing the standards of auditing and reporting, strengthening the efficacy of corporate boards, the protection of minority shareholders' interests and of investors could improve corporate ethics. In addition, and holding everything else constant, an increase by 1 percentage point in the percentage of individuals using internet increases the EBF by 0.0042 points. There is not a statistically significant relationship between VA and PS and corporate ethics, which is in accordance with [3].

Our results show that, in the countries included in the sample, fighting corruption in the public sector, implementing sound policies to promote the development of the private sector, having high standards of corporate accountability (auditing and reporting) and high levels of internet penetration can be favourable to enhance the standards of corporate ethics.

ACKNOWLEDGMENTS

Fernanda A. Ferreira acknowledges the financial support of UNIAG, R&D unit funded by the FCT – Portuguese Foundation for the Development of Science and Technology, Ministry of Science, Technology and Higher Education, under the Project UID/GES/04752/2019.

REFERENCES

1. R. De George, "A History of Business Ethics", in *Values and Ethics for the 21st Century* (BBVA, Spain, 2012), pp. 337-359.
2. A. Eiras, *Ethics, Corruption, and Economic Freedom* (Washington, The Heritage Foundation, 2003).
3. O. S. Agyemang, G. Fantini and J. Frimpong," Does country-level governance enhance ethical behaviour of firms? An African perspective". International Journal of Law and Management, **57**(6), 582-599 (2015).
4. D. Kaufmann, A. Kraay, and M. Mastruzzi. Measuring corruption: myths and realities. World Bank Paper. Washington, DC (2006).
5. M.M. Khan, The Commonwealth Journal of International Affairs **92** (370), 391-405 (2003).
6. M. Fattah," Professional Ethics and Public Administration in the United States". International Journal of Public Administration, **34** (1-2), 65-72 (2011).
7. C. Boța-Avram, "Effects of Governance on Corporate Ethics: A Cross-Country Investigation". The Romanian Economic Journal, **XVI** (50), 3-25 (2013).

Tracer Experiments with Lithium Chloride to Evaluate the Hydrodynamics of Constructed Wetlands. Comparison of Alternative Analytical Methods

Henrique J. O. Pinho[1,a)], Dina M. R. Mateus[2,b)], Ana Alves[3,c)] and Nuno Graça[3,d)]

[1]*Centro de Investigação em Cidades Inteligentes (Ci2), Instituto Politécnico de Tomar,Portugal*
[2]*Centro de Tecnologia, Restauro e Valorização das Artes (Techn&Art), Instituto Politécnico de Tomar, Portugal*
[3]*Instituto Politécnico de Tomar, Campus de Tomar, Estrada da Serra, 2300-313 Tomar, Portugal.*

[a)]Corresponding author: hpinho@ipt.pt
[b)]dinamateus@ipt.pt
[c)]anampa1906@gmail.com
[d)]nunoajgraca@hotmail.com

Abstract. The characterization of water flow dynamics (hydrodynamics) through constructed wetlands is relevant for optimizing wastewater treatment. Although constructed wetlands consist of simple systems, the water flow is complex and irregular, therefore, the study of hydrodynamics requires the use of experimental technics such as tracer experiments. To evaluate the effects of the use of three different analytical methods to compute the concentration of lithium chloride on the main hydrodynamics parameters, tracer experiments were conducted in ten independent lab-scale constructed wetlands. The concentration of lithium chloride in the output flow of the wetlands was calculated by flame photometry, electrical conductivity using a calibration curve and electrical conductivity using the salt molar conductivity. The paired samples T-test or the non-parametric Wilcoxon's Signed-Ranks test were used to demonstrate that the computed hydraulic retention time and the number of tanks accordingly with the tanks-in-series model were not significantly affected by the selected analytical method.

INTRODUCTION

Constructed Wetlands (CWs) consist in an eco-friendly, affordable and sustainable technology for wastewater treatment. CWs' systems comprise three main components: (i) a basin or a retention structure; (ii) a granular soil media; (iii) macrophyte vegetation. The wastewater is treated by a combination of chemical and physical processes such as assimilation and bioconversion by plants and microbial community, precipitation, filtration and adsorption [1,2].

CWs behave as bioreactors and the treatment efficiency can be optimized using reaction and transport models. Kinetics and equilibrium models for chemical and transport phenomena interpretation are linked to system hydrodynamics, which describe the water flow through the CWs. However, the water path can be very complex due to particle size distribution and uniformities of the granular media packing, the development of biofilms and, particularly, the spread of the plants' roots. As a result, the water flow is usually modeled empirically using tracer experiments [3,4].

Tracer experiments are performed by the injection of a traceable compound in the CWs' inflow wastewater stream and measuring the time-evolution of the tracer concentration in the outflow stream. The monitored tracer concentration over time is used to compute the hydraulic retention time (HRT) and to evaluate the CW's hydrodynamics compared to the theoretical regimes well-mixing continuous stirred reactor or plug-flow reactor types [3,4].

Several substances can be used as tracers as long as they do not affect the CWs' performance, are conservative and can be analyzed by available methods. Examples of usable substances are salts, dyes, fluorescent or radioactive

compounds [3,5]. Inorganic salts, such as sodium or lithium chloride, are cheaper materials and require simpler analytical methods than the referred alternatives. However, common salts may not be conservative as they can be assimilated by the CWs' biota or retained in the granular media by adsorption and precipitation phenomena.

The aim of the present work was to evaluate the use of lithium chloride as a conservative tracer for the hydrodynamics modelling of CWs and to compare three different analytical methods for the quantification of lithium chloride in the outflow stream. The HRT was obtained by numerical integration and the tanks-in-series (TIS) model was fitted to experimental data to obtain the number of equivalent tanks (N). N and HRT, computed from the three different sets of data resulting from the different analytical methods, were compared by paired T-test or by Wilcoxon Signed-Rank test when the compared pairs differences failed the Shapiro Wilk's normality test.

MATERIALS AND METHODS

The tracer experiments were conducted in lab-scale CWs prototypes, whose setup and operative conditions were described in previous works [6]. The experimental set up consisted in five sets of CWs in duplicate. Each set had a different combination of filling material, whose objective was to evaluate the reuse of waste solids as CW's filler. The CWs were operated in continuous mode with regular feed of wastewater. To conduct the tracer trials, a 40 g/l aqueous solution of lithium chloride was injected in the input stream of each CW. The tracer concentration in the outflow stream was quantified at regular time intervals by the three analytical methods.

Analytical methods for lithium chloride concentration evaluation

Method 1 consisted in the evaluation of lithium chloride concentration by flame photometry. Samples of water taken from the outflow stream of each CW were analyzed in a flame photometer (FP910, PG Instruments, UK). The lithium chloride concentration was computed using a calibration curve obtained from standards of known concentrations.

Method 2 consisted in the evaluation of lithium chloride concentration by measuring the electrical conductivity directly in the outflow stream with a multi-parameter meter with data logging capability (HI 98194, Hanna Instruments, US). The electrical conductivity of aqueous solutions depends in the concentration of ionic compounds. The lithium chloride concentration was computed using a calibration curve obtained from measuring the conductivity of standards of known concentrations. As all ionic compounds contribute to the measured electrical conductivity, a baseline was measured before and after the tracer experiments. The accuracy of this method depends strongly on the baseline exactness and precision.

Method 3 is a simplification of method 2. Instead of computing the lithium chloride concentration from a calibration curve, the concentration was computed using equation 1, where Λ_M is the measured electrical conductivity in the outflow streams, Λ_{BL} is the baseline electrical conductivity and Λ_{LiCl} is the molar conductivity of lithium chloride aqueous ions (Li^+ and Cl^-). A value of 114.97 m^2 S mol^{-1} was used for Λ_{LiCl} [7]. As for the method 2, the calculated concentrations depend strongly on baseline accuracy.

$$C = \frac{\Lambda_M - \Lambda_{BL}}{\Lambda_{LiCl}} \tag{1}$$

Numerical methods for CWs' hydrodynamics evaluation

The tracer conservation in each run (T) was evaluated from equation 2, where C_{in} and V_{in} are, respectively, the concentration and the volume of the injected solution, and C is the concentration of lithium chloride in the outflow streams measured in sample extracted at time t, using the analytical method 1. Q is the volumetric flowrate measured in the outflow stream for the corresponding time intervals.

$$T = 1 - \frac{\int_0^\infty QCdt}{C_{in}V_{in}} \tag{2}$$

The observed distribution of residence times was computed from the concentration of lithium chloride measured in the outflow streams over time by each one of the three analytical methods using equation 3.

$$f(t) = \frac{QC}{\int_0^\infty QCdt} \tag{3}$$

The hydraulic retention time (HRT, τ), which represents the mean residence time of tracer in the CWs, was computed from equation 4.

$$\tau = \int_0^\infty tf(t)dt \tag{4}$$

The tanks-in-series (TIS) model, which consists in the Gamma distribution (eq. 5), was fitted to experimental data by non-linear regression to compute the parameter N, which represents the observed number of equivalent tanks.

$$g(t) = \frac{N}{\tau\Gamma(N)}\left(\frac{Nt}{\tau}\right)^{N-1} exp\left(-\frac{Nt}{\tau}\right) \tag{5}$$

Numerical computations were performed using Microsoft Excel® 2016. The HRT and N obtained using the three different methods for the analysis of LiCl concentration were compared using IBM SPPS® version 25.

RESULTS AND DISCUSSION

Figure 1 presents an example of fitting the TIS model to the tracer data obtained by the three different methods. The complete results are presented in Table 1.

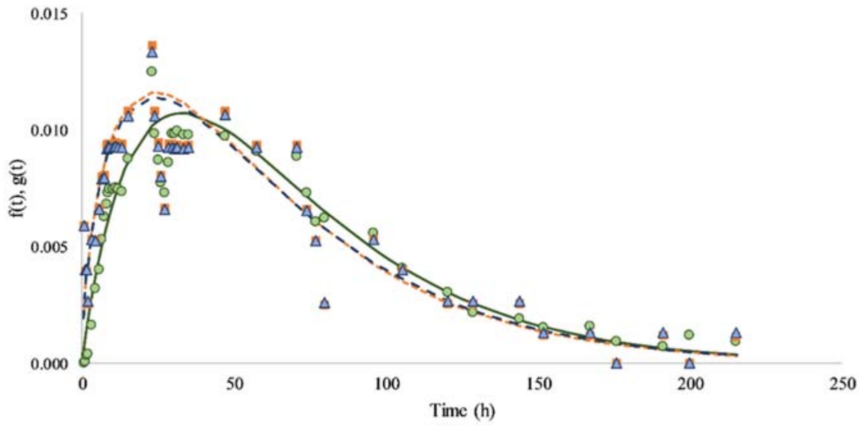

FIGURE 1. Examples of frequency data obtained for dataset 1 by the three analytical methods and respective fittings by the TIS model: Method 1 (● observed; —— fitted); Method 2 (■ observed; ------ fitted); Method 3 (▲ observed; – – – – fitted).

TABLE 1. Hydraulic residence time (τ), fitted number of tanks (N) and r^2 for the 10 experimental datasets by the three analytical methods.

CW (dataset)	Tracer conservation (%)	Method 1			Method 2			Method 3		
		τ (day)	N (-)	r^2	τ (day)	N (-)	r^2	τ (day)	N (-)	r^2
1	96%	68.4	1.93	0.909	62.5	1.62	0.827	63.7	1.61	0.810
2	96%	63.3	1.85	0.816	68.8	1.46	0.803	69.8	1.46	0.790
3	93%	72.4	1.96	0.935	59.4	2.01	0.908	61.0	1.97	0.908
4	96%	74.6	2.16	0.971	65.6	2.26	0.954	67.7	2.19	0.961
5	98%	35.1	2.68	0.876	35.2	2.81	0.849	35.9	2.75	0.849
6	97%	35.7	1.96	0.770	36.5	1.99	0.706	37.1	1.97	0.717
7	91%	75.1	2.23	0.926	73.1	2.51	0.956	74.2	2.44	0.956
8	89%	80.5	2.35	0.878	87.1	2.40	0.891	87.5	2.37	0.887
9	92%	18.8	0.74	0.871	19.5	0.73	0.872	17.1	0.81	0.907
10	97%	22.6	1.12	0.815	19.8	1.19	0.888	17.6	1.30	0.882

Tracer conservation according to Table 1 was always close to or higher than 90%, which is higher than the acceptable value of 80% to validate tracer results [3]. The data scattering observed in Figure 1 is typical and expectable in real and hydrodynamic complex systems like the CWs.

Table 2 presents the results of the statistical tests whose goal was evaluating the hypothesis that any method can be applied to obtain the experimental hydraulic retention time and the number of tanks accordingly with the TIS model. The methods were compared 2 by 2.

TABLE 2. Results of the statistical tests evaluating the significance of the differences between the three analytical methods.

Variable	Test	Method 2 – Method 1	Method 3 – Method 1	Method 3 – Method 2
N	Mean of the differences	0.0036	-0.0104	-0.0140
	95% C.I. of the mean	[-0.1400; 0.1472]	[-0.1497; 0.1289]	[-0.0571; 0.0292]
	Shapiro-Wilk test significance (Statistics)	0.065 (0.854)	0.029 (0.825)	0.070 (0.857)
	Paired t-test significance (Statistics)	0.956 (0.056)		0.483 (-0.732)
	Cohen's d	0.019		0.244
	Wilcoxon test significance (Statistics)		0.432 (-0.866)	
	Matched-pairs rank correlation		0.309	
τ	Mean of the differences	-1.901	-1.505	0.397
	95% C.I. of the mean	[-6.261; 2.459]	[-5.637; 2.627]	[-0.682; 1.476]
	Shapiro-Wilk test significance (Statistics)	0.803 (0.962)	0.883 (0.969)	0.015 (0.802)
	Paired t-test significance (Statistics)	0.349 (-0.987)	0.431 (-0.825)	
	Cohen's d	0.329	0.275	
	Wilcoxon test significance (Statistics)			0.432 (-0.866)
	Matched-pairs rank correlation			0.309

The 95% confidence intervals include the zero for all evaluated paired-differences between the analytical methods. The differences of the paired results for the number of tanks by Method 1 and Method 3 failed the Shapiro-Wilk test for normality. The same non-normality evidence was obtained from the paired results for the hydraulic residence time calculated by Method 2 and Method 3. The Wilcoxon non-parametric test was applied considering the non-normality issue. The results of both parametric and non-parametric tests show that the number of tanks and the hydraulic residence time do not differ significantly across the three implemented analytical methods.

CONCLUSIONS

Constructed wetlands hydrodynamics evaluation using tracer experiments with lithium chloride was not significantly affected by three different analytical methods for tracer quantification. Under the conditions tested, the hydraulic retention time and the number of tanks according to the tanks-in-series model did not differ significantly when the concentration of lithium chloride at outflow streams was quantified by flame photometry or by electrical conductivity. In addition, calculation of tracer concentration using the molar conductivity proved to be acceptable for constructed wetlands hydrodynamics characterization, which represents a fast and affordable experimental technic.

ACKNOWLEDGMENTS

This work has been financially supported by FEDER grant COMPETE-01-0145-023342 to project VALORBIO. Authors acknowledge the support of BIOTEC.ipt and Lab.IPT and the work of Carlos Ferreira, Isabel Silva and Alcino Serras.

REFERENCES

1. A. Gorgoglione and V. Torretta, *Sustainability* **10**, 1-19 (2018).
2. A. Valipour and Y.H. Ahn, in: Singh R., Kumar S. (eds) Green Technologies and Environmental Sustainability. Springer, 1-43 (2017).
3. T. Headley and R. Kadlec, *Ecohydrology Hydrobiology.* **7**, 269-282 (2007).
4. R. Bonner, L. Aylward, U. Kappelmeyer and C. Sheridan, *Ecol. Eng.* **99**, 99-113 (2017).
5. L. Hernández, J. Pérez and M. Gaytán-Martínez, *Powder Technol.* **340**, 274-289 (2018).
6. H. Pinho, A. Alves, N. Graça, D. Mateus, in: Gastescu, P., Bretcan, P. (eds) 4th Water Resources and Wetlands, Tulcea (Romania), 108-113 (2018).
7. P. Vanýsek, in: Haynes, W. (ed) CRC Handbook of Chemistry and Physics, 91th ed., Taylor & Francis, 5.74 (2010).

A Statistical Contribution on the Film Tourism. A Case Study

Hermínia Sol[1,2,3,4,a)], Luís M. Grilo[1,5,6,7,b)] and João Pinto Coelho[1,2,3,c)]

[1]*Instituto Politécnico de Tomar (IPT), Quinta do Contador-Estrada da Serra, 2300-313 Tomar, Portugal*
[2]*Laboratório de Turismo, IPT, Portugal*
[3]*Centro de Tecnologia, Restauro e Valorização das Artes (Techn&Art), Portugal*
[4]*Centro de Estudos Anglísticos da Universidade de Lisboa (CEAUL), Portugal*
[5]*Centro de Matemática e Aplicações (CMA), FCT, UNL, Portugal*
[6]*Centro de Investigação em Cidades Inteligentes (Ci2), IPT, Portugal*
[7]*CIICESI / ESTG – P. Porto, Portugal*

[a)]Corresponding author: hsol@ipt.pt
[b)]lgrilo@ipt.pt
[c)]joao.pinto.coelho@ipt.pt

Abstract. The evaluation of the impact that the images perceived by the spectators have in the destination choices they make as tourists is a growing research field, not only in Tourism and Marketing Management but also among the Behavioural Sciences. Based on a questionnaire previously developed on a Film Tourism sub-project, with qualitative variables in nominal and ordinal scale, a survey was conducted during a number of film screenings hosted by Tomar's (a medium-sized city in Portugal) Film Society. After the characterization of the random sample with the sociodemographic variables, the nonparametric test Pearson chi-square was applied to test the null hypothesis of independence between the variable "Gender" and the variables "Have you ever visited a place by influence of a film?" or "Destination-dream by strong influence of a film". Given that the null hypothesis is not rejected, there is no statistical evidence to consider a dependence/relationship between these variables. Other finding is statistically significant Spearman correlations between some variables, such as "Education level" and "The average number of activities of Film Tourism".

INTRODUCTION

Film Tourism has established itself as a relevant niche market within the tourism industry over the last two decades [1, 2]. Its ability to combine tourism with processes of the imagination makes its success [3]. In essence, the film tourism trend results from the emotional relationship that most consumers of media products (films, TV series, amongst other options) develop with narrative plots and, consequently, with their settings. While not new, this phenomenon has caught the attention of researchers and promoters alike, as more and more people seem to be compelled to undergo trips to film locations. Having proved to be a highly profitable segment, many cities have decided to explore this niche. Moreover, it offers a solution to destinations that wish to diversify their tourism offer in the hope of attracting new markets. With this in mind, and using Tomar – a tourism-driven, medium-sized Portuguese city located in the Médio Tejo region (NUTS3 region) – as basis, this study aims to explore the understanding that moviegoers that regularly attend Tomar's Cinema Society sessions have of this tourism segment. Likewise, it is intended to find out if they identify themselves as Film Tourists. Owner of a well-established Templar identity and the proud host of a Templar Castle and of the Convent of Christ, Tomar has served as the setting for several, mostly European, films and TV series. Nevertheless, its potential as a film tourism destination seems to be yet underexplored. Therefore, taking advantage of the fact that Tomar has a Higher Education Institution – Instituto Politécnico de Tomar – the MOVTOUR project was conceived with the intention of studying how tourist culture influences local development. In this vein, two of its subprojects (Journeying the Screen I & II) were solely devoted to assessing the suitability and feasibility of this tourism trend to the city as an alternative to the Templar-based offers that have been the city's major tourism pull factor. Yet, the overall goal is to assess relationships between some sociodemographic variables and variables related to Film Tourism.

MATERIAL AND METHODS

In order to evaluate the potential importance of this tourism segment a partnership with Tomar's Film Society was established. This was vital in the promotion of six film sessions where six hand-picked road movies were screened. At the end of each session, a survey was conducted amongst a random sample of moviegoers in order to glean information on the impact that those films had as travel instigators and on the individual perception of the respondents regarding the film tourist label. The questionnaire used was previously developed considering only qualitative variables, in both nominal and ordinal scales. From regular moviegoers' of Tomar's Film Society a random sample was obtained and an exploratory analysis of the data was performed. Nonparametric statistical tests and a correlation coefficient were used to evaluate the impact of a film in the moviegoers' choice of travel destinations.

STATISTICAL ANALYSIS

To characterize the respondents of the sample (with size of $n = 103$) the sociodemographic variables available in the questionnaire were considered. "Nationality": although the vast majority were Portuguese (87.4%, 90 moviegoers) nine other nationalities were involved; "Gender": 62.1% (64 moviegoers) were female; "Age": 42.6% (43 moviegoers) were between 18 and 29 years old (Table 1). The mean and standard deviation of the respondents' age were, approximately, 34.7 and 15.4 years old, respectively; "Marital status": 67,6% (69 moviegoers) were single and 12.7% (13 moviegoers) were married; "Education level": 37.6% (38 moviegoers) were graduate and 31.7% (32 moviegoers) were undergraduate (Table 2); "Professional situation": 52.5% (52 moviegoers) were students and 34.3% (34 moviegoers) were employees (Table 3); "Income": 47.6% (40 moviegoers) had an income below 500€ and 25% (21 moviegoers) had an income between 500 and 1000€. Only 9.5% (8 moviegoers) had an income equal or above 2000€ (Table 4). The average and standard deviation income of respondents were, approximately, 791.7€ and 673.1€, respectively. Based on this exploratory analysis, one might say that a considerable number of respondents were single Portuguese women, undergraduate students or recent graduates. Hence, young adults with relatively low income.

TABLE 1. Frequencies of variable "Age".

Age	Frequency	%	Valid %
< 18	4	3.9	4.0
[18, 29[	43	41.7	42.6
[29, 40[	25	24.3	24.8
[40, 51[	12	11.7	11.9
[51, 62[	7	6.8	6.9
≥ 62	10	9.7	9.9
Total	**101**	98.1	100.0
Missing	2	1.9	
Total	103	100.0	

TABLE 2. Frequencies of the "Education level".

Education level	Frequency	%	Valid %
Vocational educat.	8	7.8	7.9
Undergraduate	32	31.1	31.7
Graduate	38	36.9	37.6
Master	13	12.6	12.9
PhD	7	6.8	6.9
Other	3	2.9	3.0
Total	**101**	98.1	100.0
Missing	2	1.9	
Total	103	100.0	

TABLE 3. Frequencies of "Professional situation".

Professional situation	Frequency	%	Valid %
Unemployed	4	3.9	4.0
Retired	9	8.7	9.1
Student	52	50.5	52.5
Employee	34	33.0	34.3
Total	**99**	96.1	100.0
Missing	4	3.9	
Total	103	100.0	

TABLE 4. Frequencies of variable "Income".

Income (€)	Frequency	%	Valid %
< 500	40	38.8	47.6
[500, 1000[	21	20.4	25.0
[1000, 1500[	7	6.8	8.3
[1500, 2000[	8	7.8	9.5
≥ 2000	8	7.8	9.5
Total	84	81.6	100.0
Missing	19	18.4	
Total	103	100.0	

To analyze some of the categorical variables (on nominal and ordinal scales) contingency tables were used. In Table 5 the nominal variables "Gender" and "Are you a Film Tourist?" were considered. Most moviegoers did not

perceive themselves as Film Tourists (87.1% of women and 71.1% of men). However, the percentage of men who considered themselves to be Film Tourists is higher (28.9%) than women's (12.9%).

TABLE 5. "Gender" * "Are you a Film Tourist?" crosstabulation.

Gender		Are you a Film Tourist? Missing	No	Yes	Total
Female	Count	**2**	**54**	**8**	64
	%	3.1	84.4	12.5	100
	Valid %		87.1	12.9	
Male	Count	**1**	**27**	**11**	39
	%	2.6	69.2	28.2	100
	Valid %		71.1	28.9	
Total	Count	3	81	19	**103**

In Table 6 the nominal variable "Gender" and the ordinal variable "Impact of a film on a choice of a tourism destination", with 7 categories, from 1 – "Does not have any impact" to 7 – "High impact", were considered. When comparing the relative percentages obtained by gender, men in the sample gave more importance to the impact of films in the choice of travel destinations (TD). Hence, 57,2% is the cumulative percentage of men who gave, at least, 5 points against 48.9% given by women.

TABLE 6. "Gender" * "Impact of a film on a choice of a tourism destination" crosstabulation.

Gender		Impact of a film on a choice of TD 1	2	3	4	5	6	7	Total
Female	Count	3	3	5	12	8	10	4	45
	%	6.7	6.7	11.1	26.7	17.8	22.2	8.9	100
Male	Count	0	2	1	9	8	5	3	28
	%	0.0	7.1	3.6	32.1	28.6	17.9	10.7	100
Total	Count	3	5	6	21	16	15	7	**73**

The nonparametric test Pearson chi-square was used, when its assumptions were verified, to test the null hypothesis of independence between variables in the population. Thus, the two first variables tested were "Gender" and "Have you ever visited a place by influence of a film?". The differences in the relative percentages by gender are very small (Table 7). The null hypothesis is not rejected, considering the bilateral (2-tailed) or unilateral (1-tailed) test, since the p-values (asymptotic or exact) are higher than the usual significance levels considered, namely 10% (Table 7).

TABLE 7. "Gender" * "Have you ever visited a place by influence of a film?" Crosstabulation and Chi-Square test.

Gender		Have you ever visited a place by influence of a film? No	Yes	Total
Female	Count	44	20	64
	%	68.7	31.3	100
Male	Count	27	12	39
	%	69.2	30.8	100
Total	Count	71	32	**103**

Chi-Square Tests[c]	Value	df	Asymp. p-value (2-sided)	Exact p-value (2-sided)	Exact p-value (1-sided)
Pearson Chi-Square	0.003[a]	1	0.959	1.000	0.569
Continuity Correct.[b]	0.000	1	1.000		
Likelihood Ratio	0.003	1	0.959	1.000	0.569
Fisher's Exact Test				1.000	0.569
N of valid cases	**103**				

a. 0 cells (0.0%) have expected count less than 5. The minimum expected count is 12.12.
b. Computed only for a 2x2 table
c. For 2x2 crosstabulation, exact results are provided instead of Monte Carlo results.

The independence between "Gender" and the "Dream-destination by strong influence of a film" was also tested. Once again, the differences in the relative percentages by gender are small in this sample and the women have a slightly higher percentage of "Yes" (Table 8). For the same reasons mentioned in the previous test, the decision was not to reject the null hypothesis of independence, since all p-values higher than 0.1 (Table 8). Therefore, there is no statistical evidence to consider any dependence between the variables mentioned in the moviegoers' population that regularly attend Tomar's Cinema Society.

TABLE 8. "Gender" * "Dream-destination by strong influence of a film" crosstabulation and Chi-Square test.

Gender		Destination-dream by strong influence of a film: No	Yes	Total
Female	Count	15	46	61
	%	24.6	75.4	100
Male	Count	10	27	37
	%	27.0	73.0	100
Total	Count	25	73	**98**

Chi-Square Tests[c]	Value	df	Asymp. p-value (2-sided)	Exact p-value (2-sided)	Exact p-value (1-sided)
Pearson Chi-Square	0.072[a]	1	0.788	0.814	0.484
Continuity Correct.[b]	0.001	1	0.977		
Likelihood Ratio	0.072	1	0.789	0.814	0.484
Fisher's Exact Test				0.814	0.484
N of valid cases	**98**				

a. 0 cells (0.0%) have expected count less than 5. The minimum expected count is 9.44.
b. Computed only for a 2x2 table
c. For 2x2 crosstabulation, exact results are provided instead of Monte Carlo results.

To assess the association between some variables the Spearman's correlations ($-1 \le r_S \le 1$) were calculated and their significance was also tested (Table 9). The null hypothesis of the correlations being zero in the moviegoers' population (i.e. independence between the variables) is rejected in the two first cases, given that the p-values are < 0.05, and not rejected in the three last cases. In the first case, the correlation is positive which means that when levels of education increase, the activities average on Film Tourism also increase. Likewise, there is a negative correlation between "Professional situation" and "The impact of a film in the tourism destination" (the categories "unemployed" and "retired" are more influenced by Film Tourism than the higher categories "students" and "employed"). This last variable has a negative correlation with both "Age" and "Income", but they are not statistically significant since their p-values are higher than 0.05 (Table 9). Indeed, based on the relative percentages obtained by crosstabulation of these variables, younger (< 29 years old) and lower-income (< 1000€) people give more importance to the impact of a movie on choosing a tourist destination.

TABLE 9. Variables, Spearman correlations and p-values.

Variables	r_S	p-value
"Education level" *versus* "Activities average on Film Tourism"	0.395	0.028
"Professional situation" *versus* "Impact of a film on a choice of a tourist destination"	- 0.289	0.014
"Age" *versus* "Impact of a film on a choice of a tourist destination"	- 0.171	0.151
"Income" *versus* "Impact of a film on a choice of a tourist destination"	- 0.199	0.131
"Income" *versus* "Activities average on Film Tourism"	0.023	0.906

CONCLUSIONS AND FINAL REMARKS

Considering the variables available and based on the results obtained from the survey data, most moviegoers do not consider themselves Film Tourists, but they give a considerable importance to the impact that a film has on the choice of a tourist destination. The variable "Gender" and the variables "Have you ever visited a place by influence of a film?" or "Dream-destination by strong influence of a film" are not statistically dependent, but women who responded to the survey seemed a little more influenced by films when choosing a tourist destination. The benefits of film tourism have been recognized, but by some results they should not be generalized. It seems more like an individual choice. Personal engagement with popular entertainment stories coupled with people's financial resources, education and age, are at the basis of people's decision to travel to a specific destination they might have come across on-screen.

ACKNOWLEDGMENT

This work was supported by the Fundação para a Ciência e a Tecnologia (Portuguese Foundation for Science and Technology) through the project nr. 24068, MOVTOUR – Tourism and Culture with and for Society.

REFERENCES

1. S. Beeton, Film-induced Tourism (Clevedon: Channel View Publications, 2005).
2. J. Connell, *Tourism Management*, 33 (5): 1007-1029 (2012).
3. S. Reijnders, *European Journal of Cultural Studies*, 19 (6): 672-689 (2016).

The Use of Information and Communication Technologies to Overcome Reading Difficulties. Statistical Comparison of Reading Results Through the Use of Letrinhas Software

Célio Gonçalo Marques[1,3,4,a)] António Manso[1,5,b)] Luís M. Grilo[1,5,6,7,c)], Ana Paula Ferreira[1,3,4,d)] and Ana Amélia Carvalho[2,3,e)]

[1]*Polythecnic Institute of Tomar (IPT), Quinta do Contador – Estrada da Serra, 2300-313 Tomar, Portugal*
[2]*University of Coimbra, Faculty of Psychology and Education Sciences, Portugal*
[3]*Educational Technology Laboratory, University of Coimbra, Portugal*
[4]*Centre for Technology, Restoration and Art Enhancement (Techn&Art), IPT, Portugal*
[5]*Research Center in Smart Cities (Ci2), IPT, Portugal*
[6]*Centre for Mathematics and Applications (CMA), FCT, UNL, Portugal*
[7]*Center for Innovation and Research in Business Sciences and Information Systems (CIICESI), IPP, Portugal*

[a)]Corresponding author: celiomarques@ipt.pt
[b)]manso@ipt.pt
[c)]lgrilo@ipt.pt
[d)]anapaula.ferreira@ipt.pt
[e)]anaameliac@fpce.uc.pt

Abstract. Letrinhas is an information system created by the Polytechnic Institute of Tomar (Portugal), in partnership with a School Grouping (Portugal), to give support to elementary school children with reading difficulties. The software can be used on mobile devices, such as a tablet, and allows the evaluation and improvement of reading fluency. By promoting the development of students' reading skills, it contributes to the development of autonomous readers and consequently to the improvement of school results. In order to evaluate the importance of Letrinhas software in the process of reading (children from 2nd and 3rd grade, with a mean age of 7/8 years old), two independent samples were collected, consisting of students from several primary schools. A sample is made up of students who have learned from Letrinhas (experimental group) and the other sample consists of students who have learned to read through the classic process (control group). In the students' learning process there are two essential reading components: fluency and precision. To statistically compare the data gathered for the variables Fluency Index and Precision Index, in both groups (experimental and control), confidence intervals and (non)parametric tests were used. The differences between the two teaching methods of reading, observed in graphs and in the values of some descriptive statistical measures, are statistically significant (also the values obtained for the effect sizes measures are considerable). The positive impact of the Letrinhas software on the fluency and precision of reading, empirically identified by teachers, was statistically confirmed.

INTRODUCTION

Acquiring reading competence is an essential condition for students' academic success [1], as it determines their learning ability in the various subject areas. "Mastery of written language increases our communicative potential and, at the same time, is the great facilitator of school learning, as well as the expansion of individual interests and cognitive growth of the subject-reader" (p. 203) [2].

Learning to read is however a complex process [3, 4]. Nonetheless, it is fundamental in the early stages of schooling and crucial in the creation of competent readers. Given its complexity, the learning process of reading is frustrating for many students, so many authors [5] consider intervention in the context of the difficulties of reading should focus on three main aspects: 1) early identification; 2) prevention; 3) reeducation. The implementation of reading programs should take place in the first two years of schooling [6], because the sooner learning issues are diagnosed, the higher the success rate will be.

Thus, the creation of applications that make it possible to diagnose and act upon students with reading difficulties is extremely important [7, 8], placing Letrinhas in a prominent position in the Portuguese learning landscape, because, in addition to meeting this need, it is also an innovative system that takes advantage of the potential of mobile devices with touch-based interfaces, which promotes not only student motivation but also autonomy. In fact, ICTs provide

students with a more active role in knowledge building [9, 10] and the "studies have found that computer use enhances children's fine motor skills, alphabet recognition, concept learning, numerical recognition, counting skills and premathematical knowledge, cognitive development, and self-esteem or self-concept" (p. 1716) [9].

In this way, the Polytechnic Institute of Tomar in partnership with the School Grouping Artur Gonçalves (Portugal), created Letrinhas, an information system to promote learning and reading development [11]. This system makes use of mobile technologies, providing a more dynamic, interactive and meaningful learning [12].

The main objective of the study is to analyse the impact of Letrinhas software on the development of reading skills in children. For this, the Fluency Index and Precision Index variables were considered and some statistical techniques were applied to compare the available data between the control and experimental groups.

MATERIALS AND METHODOLOGY

In order to evaluate the importance of Letrinhas in the process of children reading, two random and independent samples were collected, consisting of students from 22 primary schools. A sample is made up of students who have learned from Letrinhas (experimental group) and the other sample consists of students who have learned to read through the classic process (control group). The population consisted of students from schools belonging to 9 School Groups from the Center of Portugal (Alvaiázere, Artur Gonçalves, D. Afonso Henriques, Dr. Ginestal Machado, Ferreira do Zêzere, Marrazes, Nuno de Santa Maria, Piscinas Olivais and Templários). The students were between 6 and 10 years old considering both groups (control and experimental). Almost 50% of the students in the sample (n = 65) were 7 years old (more precisely 47.7%) and the average age was 7.45 years (median and mode were equal to 7, and a standard deviation of 0.77 years old, approximately). The control group (with 32 students) had 17 (53.1%) females and 15 (46.9%) males and the experimental group (with 33 students) had 14 (42.4%) females and 19 (57.6%) males. In terms of the school year, in the control group: 18 students (56.3%) attend the 2nd year and 14 (43.7%) attend the 3rd year. In the experimental group: 18 students (54.5%) attend the 2nd year and 15 (45.5%) attend the 3rd year. Each student participated in 13 sessions on average and to analyse the available data some descriptive statistics and graphs were produced for the Fluency and Precision Index variables. To compare the two variables, in both groups, confidence intervals and (non)parametric tests (t-Student test and Wilcoxon-Mann-Withney test) were used. Effect size measures were also used, because they are a simple way of quantifying the difference between the two groups (i.e., they emphasise the size of the difference).

STATISTICAL ANALYSIS

In this section the two Fluency and Precision Index variables were statistically compared in both groups (control and experimental). The Fluency Index allows both the accuracy and the reading time to be taken into account, given by the equation 1. It shows the number of words read per minute and allows a better discrimination of the children, because it considers not only the correctly read words, but also the time spent [13, 14].

$$\text{Fluency index} = (\text{number of words read} / \text{reading time}) \times 60. \quad (1)$$

In Table A1 (Appendix A) are some descriptive statistics of variable Fluency Index in both groups. There are considerable differences between the values of some statistical measures, particularly the mean, median, minimum, maximum and quartiles are relatively larger in the experimental group. In terms of relative variability, the value of the coefficient of variation (ratio of the standard deviation to the mean) of the control group is bigger than the experimental group. The differences between empirical distributions can also be seen on the box-plot of Figure A1 (Appendix A). To apply the t-test for equality of population means of the variable Fluency Index the assumptions of normality (Table 1) and homogeneity variance (Table 2) were verified, since the null hypothesis are not rejected (p-values > 0.05). The null hypothesis of equality of population means is rejected (t-test), given that the p-value = 0.000 < 0.01 (Table 2), and the 95% CI of the difference does not include the zero differences. There is a statistically significant difference in the populations means of the variable Fluency Index of both groups (control and experimental) and the effect size (Choen's d) could be considered strong, since it is bigger than the threshold 0.8 (Table A2 of Appendix A). There is statistical evidence that the presence of the Letrinhas software in the reading process leads to an improvement in the children's Fluency Index (also visualized in the values of the 95% CI for mean of this variable in both groups, on Table A2 and Figure A2 of Appendix A).

TABLE 1. Shapiro-Wilk normality test of the Fluency Index.

Group	**Test of Normality** (Fluency Index)		
	Shapiro-Wilk		
	Statistic	df	p-value
Control	0.975	32	0.651
Experimental	0.942	33	0.076

TABLE 2. Homoscedasticity Levene's test and t-test for equality of means of the Fluency Index.

Levene's Test for Equality of Variances		**Independent Samples Test t-test for Equality of Means** (Fluency Index)						
F	p-value	t	df	p-value (2-tailed)	Mean Difference	Std. Error Difference	95% CI of the Difference	
							Lower	Upper
0.020	0.889	-4.626	63	0.000	-20.674	4.469	-29.605	-11.744

The Precision Index measures the accuracy of the child's reading aloud of a text and is translated in the percentage of correctly read words [13, 14], given by equation 2.

$$\text{Precision Index} = (\text{number of correctly read words} / \text{total of words}) \times 100. \tag{2}$$

In Table A3 (Appendix A) it is possible to visualize the differences in the values of some descriptive statistics for the variable Precision Index. The maximum value is equal to the third quartile (Q_3) and they are equal to each other in both groups. In fact, in the experimental group only 8 students did not have the maximum value 100 and as can be seen in the box-plot there are 5 outliers (2 moderate and 3 severe) in the experimental group (Appendix A, Figure 3). Based on Table 3 the variable Precision Index is not normally distributed, in both groups, since the null hypothesis of normality was not rejected (p-values < 0.01). Thus, the Wilcoxon-Mann-Whitney nonparametric test was used to test the null hypothesis of equality of the population distributions (Tables 4) and it was reject for a level of significance of 1%, whether considering the bilateral (2-tailed) or unilateral (1-tailed) test, the p-values (asymptotic or exact) are approximately zero. The effect size ($-1 \le r_G \le 1$) of - 0.5, approximately, can be considered medium (Table 4). Once again, there is statistical evidence that the presence of Letrinhas software in the reading process leads to an improvement in the children’s Precision Index.

TABLE 3. Shapiro-Wilk normality test of the Precision Index.

Group	**Test of Normality** (Precision Index)		
	Shapiro-Wilk		
	Statistic	df	p-value
Control	0.883	32	0.002
Experimental	0.475	33	0.000

TABLE 4. Ranks, Wilcoxon-Mann-Whitney test for the Precision Index and effect size.

Ranks			
Group	***n***	**Mean Rank**	**Sum of Ranks**
Control	32	24.81	794.00
Experimental	33	40.94	1351.00
Total	65		

Test Statistics[a]	Precision Index
Mann-Whitney U	266.000
Wilcoxon W	794.000
Z	-3.746
Asymp. p-value (2-tailed)	0.000
Exact p-value (2-tailed)	0.000
Exact p-value (1-tailed)	0.000
Effect size (r_G)*	- 0.496

a. Grouping Variable: control, experimental
* Glass rank biserial correlation

CONCLUSIONS AND FINAL REMARKS

According to the statistical results obtained, the differences empirically identified by teachers and also verified in the sample, between the two teaching methods of reading, are statistically significant in terms of the population of children with reading difficulties [15]. The impact of the Letrinhas software on the reading fluency and precision of students in the second and third years of elementary school is considerable, given the magnitude of the effects obtained. In fact, the results clearly point to the importance of the use of Letrinhas in the development of the reading skills of the students involved, with performance levels much higher than students who did not have access to this tool. The students involved in the study were signaled by the teachers, due to their reading difficulties and the activities performed with Letrinhas allowed not only the improvement of their reading skills, but also a high degree of motivation of the different actors involved, students and teachers. Given these results, it would be interesting to extend the scope of use of Letrinhas software to other schools and eventually to other levels of education to enable other students to improve their reading skills, with the impact that this will have on their academic lives [16].

APPENDIX A

TABLE A1. Descriptive statistics for Fluency Index.

Descriptives statistics	**Fluency Index**	
	Control group	Exp. group
n	32	33
Mean	44.75	65.42
5% Trimmed mean	44.63	65.57
Median	40.00	68.00
Std. Deviation	18.12	17.91
CV (%)	40.50	27.40
Minimum	1	34
Maximum	87	97
First quartile (Q_1)	35.25	50.50
Third quartile (Q_3)	59.00	78.50

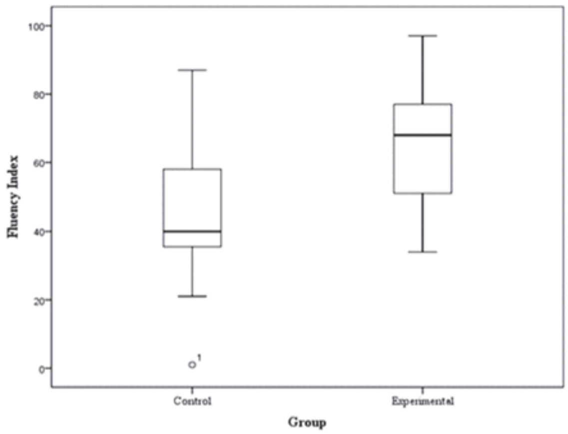

FIGURE A1. Box-plot for Fluency Index.

TABLE A2. 95% CI for mean Fluency Index and effect size.

	Fluency Index	
	Control group	Exp. group
95% CI for mean	(38.22; 51.28)	(59.08; 71.77)
Effect size (Choen's d)	1.166	

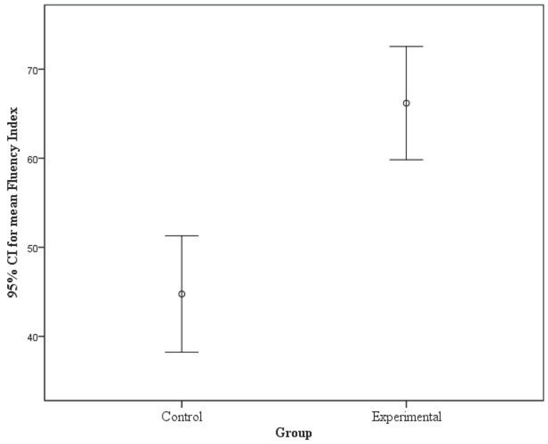

FIGURE A2. 95% CI for mean Fluency Index.

TABLE A3. Descriptive statistics for Precision Index.

Descriptives statistics	Precision Index	
	Control group	Exp. group
n	32	33
Mean	94.88	98.64
5% Trimmed mean	95.26	99.24
Median	95.50	100.00
Std. Deviation	5.12	3.39
CV (%)	5.40	3.40
Minimum	82	84
Maximum	100	100
First quartile (Q_1)	92	99
Third quartile (Q_3)	100	100

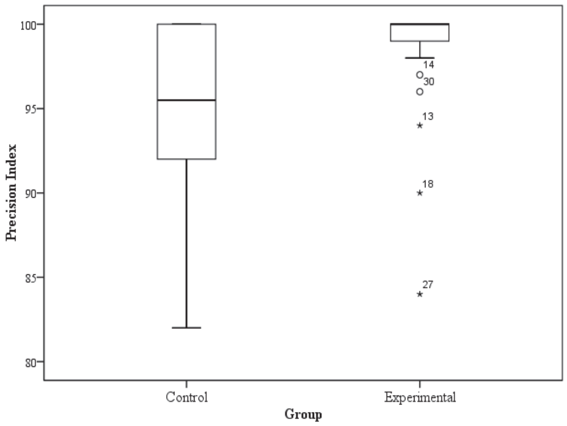

FIGURE A3. Box-plot for Precision Index.

REFERENCES

1. B. Foorman, S. Koon, Y. Petscher, A. Mitchell and A. Truckenmiller, "Examining general and specific factors in the dimensionality of oral language and reading in 4th-10th grades", *Journal of Educational Psychology*, 107(3), pp. 884-899 (2015).
2. I. Sim-Sim, "Desenvolver a Linguagem, Aprender a Língua", A. D. Carvalho and J. Marques (Eds.), *Novas Metodologias em Educação* (Porto Editora, Porto, 1995), pp. 197-226.
3. W. E. Tunmer and W. A. Hoover, "Cognitive and Linguistic Factors in Learning to Read", in P. B. Gough, L. C. E. and R. Treiman (Eds.), *Reading Acquisition* (Routledge, London, 2017), pp. 175-214.
4. L. Verhoeven, P. Reitsma and L. S. Siegel, "Cognitive and linguistic factors in reading acquisition", *Reading and Writing*, 24(4), pp. 387–394 (2011).
5. S. Shaywitz, "Overcoming Dyslexia", (Vintage, New York, 2005).
6. R Foorman, D. J. Francis, B. A. Shaywitz and J. M. Fletcher, "The case for early reading intervention", in B. Blachman (Ed.), *Foundations of reading acquisition and dyslexia* (Erlbaum New Jersey, 1997), pp. 243-264.
7. A. C. Carvalho, "Aprendizagem da leitura: Processos cognitivos avaliação e intervenção" (Psicosoma, Viseu, 2011).
8. T. Nordström, S. Nilsson, S. Gustafson and I. Svensson, "Assistive technology applications for students with reading difficulties: special education teachers' experiences and perceptions", Disability and Rehabilitation: Assistive Technology (Taylor & Francis, 2018).
9. X. Li and M. Atkins, "Early Childhood Computer Experience and Cognitive and Motor Development", *Pediatrics*, 113 (6), pp. 1715-1722 (2004).
10. M. M. Behrmann, "Assistive technology for young children in special education", in C. Dede (Ed.), *ASCD Yearbook 1998: Learning with Technology* (Association for Supervision and Curriculum Development, Alexandria, 1998), pp. 73-93.
11. C. G. Marques, A. Manso, A. P. Ferreira and F. Morgado, "Using Mobile Technologies in Education: A New Pedagogical Approach to Promote Reading Literacy", *International Journal of Technology and Human Interaction*, 13(4), pp. 77-90 (2017).
12. A. Nobre and A. Moura, "Mobile Learning Scenarios in Language Teaching: Perceptions of Vocational and Professional Education Students", in D. René and C. Aubin (Eds.), *Education in a Competitive and Globalizing World* (Nova Science Publishers, New York, 2017) pp. 33-60.
13. A. O. D. C. Carvalho and M. A. M. Pereira, "O Rei: um teste para avaliação da fluência e precisão da leitura no 1º e 2º ciclos do ensino básico", *Psychologica*, 51, pp. 283-305 (2009).
14. A. O. D. C. Carvalho and M. A. M. Pereira, "Teste de Avaliação da Fluência e Precisão da Leitura «O Rei»", *Actas do 7.º Encontro Nacional (5.º Internacional) de Investigação em Leitura, Literatura Infantil e Ilustração* (Universidade do Minho, Braga, 2008), pp. 1-14.
15. C. G. Marques, A. Manso, L. M. Grilo, A. P. Ferreira and A. A. Carvalho, "Statistical analysis of reading results with Letrinhas software. A case study in primary schools in Portugal", in *VI Workshop on Computational Data Analysis and Numerical Methods (VI WCDANM)*, *Book of Abstracts* (Universidade da Beira Interior, Covilhã, 2019), p. 27.
16. H. Küçükoğlu, "Improving reading skills through effective reading strategies", *Procedia - Social and Behavioral Sciences*, 70, pp. 709-714 (2013).

Evaluation of Academic Burnout in College Students. Application of SEM with PLS approach

Luís M. Grilo[1,2,3,4,a)] , Anuj Mubayi[5,6,b)], Katelyn Dinkel[6,c)], Bechir Amdouni[6,d)], Joy Ren[6,e)] and Mohini Bhakta[6,f)]

[1]*Instituto Politécnico de Tomar (IPT), Quinta do Contador-Estrada da Serra, 2300-313 Tomar, Portugal*
[2]*Centro de Matemática e Aplicações (CMA), FCT, UNL, Portugal*
[3]*Centro de Investigação em Cidades Inteligentes (Ci2), IPT, Portugal*
[4]*CIICESI / ESTG – P. Porto, Portugal*
[5]*Simon A. Levin Mathematical, Computational and Modeling Science Center, Arizona State University, USA*
[6]*School of Mathematical and Natural Sciences, Arizona State University, Tempe, USA*

[a)]Corresponding author: lgrilo@ipt.pt
[b)]amubayi@asu.edu
[c)]kdinkel@asu.edu
[d)]bamdouni@asu.edu
[e)]joy.ren18@gmail.com
[f)]mbbhakt1@asu.edu

Abstract. In several academic activities students experience a considerable stress in their daily life. Stressors may affect the mental and physical health of college students, leading some of them to the burnout syndrome. To evaluate this syndrome in students at Arizona State University (ASU), USA, a survey was conducted using a questionnaire previously developed, with ordinal variables. A theoretical Structural Equation Modeling (SEM) was proposed and the estimated model was obtained applying the Partial Least Squares (PLS) approach. Based on the PLS-SEM path coefficients, the latent construct *behavioural stress* has a direct effect on *distress* and *insecurity*, and an indirect effect on both *quantitative demands* and *academic burnout*. Both mediator constructs *quantitative demands* and *distress* have a direct effect on the *academic burnout* in students. A multi-group analysis was also conducted to compare the path coefficients of the estimated model by gender, but the differences are not statistically significant. These results allow a better understanding of burnout syndrome in ASU college students, which can severely limit their psychosocial well-being and performance.

INTRODUCTION

The multifactorial burnout syndrome is considered as a long-term response to chronic interpersonal stressors at workplace. Burnout - a syndrome of occupational exhaustion - has officially entered the International Classification of Diseases (ICD) of the World Health Organization (WHO), but it is not classified as a medical condition (the approval of the 11th revision of this list took place in May 2019 at the 72nd WHO meeting in Geneva). The ICD-11 defines burnout as: "(…) a syndrome conceptualized as resulting from chronic workplace stress that has not been successfully managed". It is characterized by three dimensions: "feelings of energy depletion or exhaustion; increased mental distance from one's job, or feelings of negativism or cynicism related to one's job; and reduced professional efficacy" ([1, 2, 3], among others). According to the WHO, burnout refers specifically to phenomena in the occupational context and should not be applied to describe experiences in other areas of life. In fact, burnout is historically a psychological syndrome associated with high human contact professions, but scientific research on this field has been showing that all occupational groups, including students, could be affected by this syndrome, because they are involved in an organizational structure with mandatory activities (e.g. [4, 5, 6], among others). According to the National Center for Education and Statistics (NCES) [7], the sixth year graduation rate for full time undergraduate students in the USA is around 60%. That is, out of all full time students who entered the class of 2010, only 60% will graduate by 2016 and at some universities, this rate was 32%. "I am exhausted, I am late, I am annoyed, I can't remember, I am irritated, I need a break…" sentences often pronounced by students. Is it a typical expected behavior of young adults, a result of stress, or a sign of a bigger problem? Burnout among college students can affect their performance during their studies, the classes they take, their future relationship with college as an alumni and potential contribution back to that college, and it can taint the college reputation as well [8].

The main objective of this research aims to identify which variables could be considered as sources of *distress* (negative stress) and *academic burnout* and, at the same time, to examine possible differences by gender (female and

male) in students of the Arizona State University (ASU), USA. The Structural Equations Modeling (SEM) was applied to analyze the complex inter-relationships between the indicators or observed variables (directly measured) and the latent constructs (not directly observed), at the observation level (outer/measurement model), as well as among the latent constructs, in the theoretical level (inner/structural model). Partial Least Squares (PLS), a variance-based estimator, was applied because it maximizes the explained variance of the available endogenous latent constructs and because it emphasizes prediction while it simultaneously relaxes the demands on data (like the strong assumption of multivariate normality) and the specification of those relationships [9, 10, 11].

Material and Methods

Although Maslach Burnout Inventory–Student Survey (MBI–SS) [12] has been used in many of the published research about the burnout syndrome in students there is some controversy in the literature about its use [2, 6]. Here a questionnaire ("Precursors to Burnout") with 45 questions was developed by a students' group from the course of Modelling and Simulation in Global Health and Neglected Tropical Diseases (School of Human Evolution and Social Change, ASU) including their own experience as students (no prior analysis of the questionnaire psychometric properties, meaning the scale reliability and validity, was performed to this study). After a previous approval for conducting this survey, from the institutional review board at ASU, flyers were printed and advertised across the campus and then the questionnaire was carried out online at ASU, during the first four months of 2018, in order to collect a representative sample from a population of over 80,000 college students. Some of the questions correspond to ordinal indicators (Table 1), measured on a 10-point scale, which in this case study were considered as operationalizing latent constructs such as *behavioral stress* (state of being happy when dealing with people), *cognitive stress* (problems of concentrating or remembering), *somatic stress* (health issues), *insecurity* (students' worry), *quantitative demands* (number of working hours), *distress* (signs of irritability) and *academic burnout* (feeling tired and hopeless). The categories of indicators were assumed equally spaced and perceived as symmetrical. Thus, they were treated as approximated to an interval-level measurement, allowing to apply PLS-SEM [9, 10].

TABLE 1. Latent constructs, indicators and some questions used on the questionnaire "Precursors to Burnout" (the indicators were coded as 1-2: Never/hardly ever, 3-4: Seldom, 5-6: Sometimes, 7-8: Often, 9-10: Always).

Latent construct	Indicator	Some questions of the "Precursors to Burnout"
Behavioral stress	Bs1	Have you found difficulty in being happy?
	Bs2	Have you not been able to stand dealing with other people?
	Bs3	Have you lacked initiative?
Cognitive stress	Cs1	Have you had problems concentrating?
	Cs2	Have you had difficulty with remembering?
	Cs3	Have you found it difficult to think clearly?
Somatic stress	Ss1	Have you had freq. stomach problems and/or chest pains or tension in some musc.?
	Ss2	Have you had frequent palpitations and/or been short of breath or been dizzy?
Insecurity	Is1	Are you worried about having to give up your courses for health reasons?
	Is2	If a problem arises, how often do you believe you will fail to find a solution to it?
	Is3	Are you worried about not getting a job after finishing your degree?
Quantitative demands	Qd1	How often do you think you work a lot (at a job, internship, or volunteer position)?
	Qd2	How often do you feel you cannot work realistically to reach your goals?
	Qd3	Do you believe you are unable to cope with your workload in this semester?
Distress	Ds1	Do you often feel irritable?
	Ds2	During the current semester, did you ever not have a lot of energy?
Academic burnout	Ab1	Do you feel tired often?
	Ab2	How often do you feel hopeless throughout the semester?

The software G*Power 3.1.9.4 was used to estimate de minimum sample. Thus, a margin error of 5%, 'power of the test' of 0.80, 'effect size' of 0.15 and a maximum of two predictors were considered for assessing the latent construct *academic burnout* [10, 13]. According to the software, the minimum sample should be 68 cases, but in order to have a more consistent model it is usually recommended at least to double this number. A non-probabilistic sample of 374 college volunteer students distributed in more than 30 courses was obtained. The non-parametric Runs test was

performed for several variables and the null hypothesis of "randomness" was not rejected for the usual levels of significance. Thus, there is statistical evidence that the students were answering the questionnaire randomly.

STATISTICAL ANALYSIS AND RESULTS

The socio-demographic variables characterizing each student were: *gender* (80.2% are female); *age* (68.2% have between 18 and 20 years old), with mean and standard deviation of approximately 20.2 and 2.2 years old, respectively; *academic level* (considering "1st semester Freshman", "2nd semester Freshman", "Sophomore", "Junior" and "Senior"), with a relatively balanced students' distribution ("junior" level registered the highest percentage, 25.7%), and *ethnicity* (59.9% are white). Based on a priori authors' perceptions about causal relations among the constructs (Table 1), a theoretical reflective model was proposed. The estimated model in Fig. 1 was obtained using the traditional PLS of the SmartPLS® 3.0 software [14], with the full confidential dataset (where two constructs in Table 1 were not statistically significant). The outer loadings values are between the indicators (rectangles) and the constructs (circles), the estimated path coefficients are between pairs of constructs and the values of coefficient of determination R^2 are displayed only in endogenous latent constructs. The positive signal of the standardized path coefficients between each pair of constructs means that they vary directly. The structural equations of the estimated model can be written as,

$$\left.\begin{aligned} &\textit{Insecurity} = 0.548\ \textit{Behavioral stress}\\ &\textit{Distress} = 0.655\ \textit{Behavioral stress}\\ &\textit{Quant. demands} = 0.625\ \textit{Insecurity}\\ &\textit{Academic burnout} = 0.360\ \textit{Quant. demands} + 0.498\ \textit{Distress}\end{aligned}\right\}\ \textit{Academic burnout} \approx 0.450\ \textit{Behavioral stress}$$

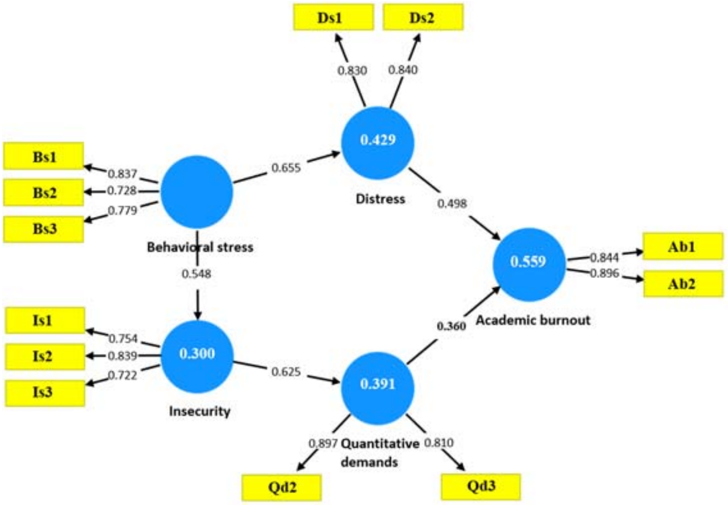

FIGURE 1. PLS-SEM estimates obtained with the SmartPLS® 3.0 software.

Evaluation of the outer and inner models in PLS-SEM

To evaluate the outer and inner submodels some threshold values were verified [9, 10, 13] and in order to test the significance of various PLS-SEM results, once it does not assume that the data is normally distributed, the bootstrap nonparametric procedure (Bias-Corrected and accelerated – BCa), that involves iteratively resampling the dataset with replacement, was applied. Thus, 5000 subsamples with the original sample size, were considered to ensure the stability of the results and *t*-Statistics, p-values and 95% bootstrap BCa confidence intervals (CI) [9, 10, 11]. Firstly, the Standardized Root Mean Square Residual (SRMR) was used as a measure of approximate fit to assess the overall goodness-of-fit (GoF). Since the results obtained with the consistent PLS (PLSc) algorithm indicated poor model fit, which denotes that the data may exhibit the characteristics of a composite model [13], then the traditional PLS was applied giving a SRMR of 0.099 (below the less conservative cut-off threshold of 0.10) which is statistically significant (p-value≈0.000<0.001). To assess the outer model the results on Tables A1 and A2 of Appendix A have to be considered. The outer loadings are bigger than 0.7 (Fig. 1) and about internal consistency (Composite Reliability, CR>0.7), convergent validity (average variance extracted, AVE>0.5) and discriminant validity (Heterotrait-Monotrait ratio, HTMT<0.9) all values of these measures verified the thresholds, except some HTMT values (and the correspondents 95% CI contain the value 1, indicating a lack of discriminant validity), but they are all statistically

significant (p-values≈0.000). To assess the inner model the results on Tables A3, A4 and A5 of Appendix A have to be considered. There is no inner collinearity, as all Variance Inflation Factor (VIF) are less than 3.3, path coefficients (larger than 0.2 in Fig. 1) and also effect sizes f^2 are statistically significant (p-values≈0.000, Table A3). Note that, all effect sizes are strong (>0.35), except one that can be considered moderate. Taking into consideration the research field of the study (in social sciences and behavioral medicine) the endogenous constructs have substantial levels (>26%) of explained variance, with R^2=55.9% for *academic burnout*. The f^2 was also evaluated by the ratio between the part explained and the part no-explained and based on the results of Table A4 all but one (moderate) effect are strong. The blindfolding algorithm was used to obtain the values of Q^2 (at the bottom of Table A5) and because they are all positive it indicates predictive relevance. The values of Q^2 and f^2 are indicative that the model is accurate and the constructs are important for the general adjustment of the model. The values of q^2 were also obtained (Table A5), which is a quasi-effect size measure of the difference in Q^2 (after including and excluding a certain predictor construct from the model), and the relative impacts range from weak (less than 0.02) to moderate (bigger than 0.15).

To test the significance of the differences between the path coefficients of the structural model, by gender (female and male), a multi-group analysis (MGA) with the nonparametric method PLS-MGA was conducted [10]. Despite some differences that might be considered interesting in the light of psychological theory, namely the estimated value between *distress* and *academic burnout* which is higher for females and the estimated value between *quantitative demands* and *academic burnout* which is higher for males, they are not statistically significant. In fact, the null hypothesis, of the absolute difference between the paths coefficients is zero in the population, was not rejected at the 5% probability of error level, since all p-values lie between 0.05 and 0.95 (Table A6 of Appendix A).

CONCLUSIONS AND FINAL REMARKS

Although PLS-SEM is basically an exploratory technique, the use of bootstrap resampling procedure allowed limited but credible forms of inference leading to the conclusion that the main causal hypothesis expressed with the model were supported by data. Bearing in mind that a model is only an approximation to a real-world phenomenon and that some sources of error may exist in this particular project, it is reasonable to admit some bias in the estimated model (it may be possible in a near future to compare these results with those by applying PLS for ordinal categorical indicators [15]). However, it is hoped that the results achieved will at least help to prevent stressful situations for students ASU, by keeping them engaged in order to increase their school performance and thus to reduce dropout.

ACKNOWLEDGMENTS

This work was partially supported by the Fundação para a Ciência e a Tecnologia (Portuguese Foundation for Science and Technology) through the project UID/MAT/00297/2019 (Centro de Matemática e Aplicações).

APPENDIX A

TABLE A1. Composite Reliability (CR), Average Variance Extracted (AVE), p-values and the 95% bootstrap BCa CI.

Latent construct	CR	p_{CR}-value	2.5%	97.5%	AVE	p_{AVE}-value	2.5%	97.5%
Academic burnout	0.862	0.000	0.835	0.885	0.758	0.000	0.717	0.794
Behavioral stress	0.826	0.000	0.797	0.852	0.613	0.000	0.567	0.657
Distress	0.822	0.000	0.787	0.853	0.697	0.000	0.649	0.743
Insecurity	0.816	0.000	0.787	0.842	0.598	0.000	0.553	0.640
Quantitative demands	0.844	0.000	0.807	0.874	0.730	0.000	0.678	0.777

TABLE A2. Heterotrait-Monotrait ratio (HTMT) of original sample (O), *t*-Statistics, p-values and the 95% bootstrap BCa CI.

	HTMT (O)	StDev	*t* (|O/StDev|)	p-value	2.5%	97.5%
Behavioral stress → Academic burnout	0.792	0.056	14.085	0.000	0.675	0.900
Distress → Academic burnout	0.996	0.066	14.999	0.000	0.880	1.215
Distress → Behavioral stress	0.947	0.062	15.280	0.000	0.842	1.171
Insecurity → Academic burnout	0.764	0.057	13.321	0.000	0.647	0.874
Insecurity → Behavioral stress	0.789	0.060	13.262	0.000	0.665	0.901
Insecurity → Distress	0.770	0.071	10.822	0.000	0.624	0.908
Quantitative demands → Academic burnout	0.897	0.057	15.636	0.000	0.776	1.006
Quantitative demands → Behavioral stress	0.790	0.065	12.156	0.000	0.659	0.914
Quantitative demands → Distress	0.823	0.069	11.925	0.000	0.684	0.954
Quantitative demands → Insecurity	0.924	0.065	14.225	0.000	0.787	1.045

TABLE A3. VIF values, path coefficients (with t-Statistics and the 95% bootstrap BCa CI), effect sizes f^2 and p-values of both.

	VIF	Orig. (O)	t (|O/StDev|)	2.5%	97.5%	f^2	p-value
Behavioral stress → Distress	1.000	0.655	20.932	0.587	0.710	0.751	0.000
Behavioral stress → Insecurity	1.000	0.548	14.328	0.463	0.614	0.429	0.000
Distress → Academic burnout	1.334	0.498	12.196	0.416	0.576	0.419	0.000
Insecurity → Quantitative demands	1.000	0.625	17.059	0.546	0.689	0.643	0.000
Quantitative demands → Academic burnout	1.344	0.360	7.766	0.266	0.445	0.218	0.000

TABLE A4. Coefficient of determination R^2 and effect sizes f^2.

Predictor	Endogenous	R^2 included	R^2 excluded	f^2*
Distress	*Academic burnout*	0.559	0.396	0.370
Quantitative demands	*Academic burnout*	0.559	0.464	0.215
Insecurity + Q. Demands	*Academic burnout*	0.559	0.465	0.213
Behavioral stress + Insecurity	*Academic burnout*	0.559	0.395	0.372

R^2 (*Insecurity* = 0.300; *Distress* = 0.429; *Quantitative demands* = 0.391; *Academic burnout* = 0.559)
* $f^2 = (R^2 \text{ included} - R^2 \text{ excluded})/(1 - R^2 \text{ included})$

TABLE A5. Predictive relevance Q^2 and effect sizes q^2.

Predictor	Endogenous	Q^2 included	Q^2 excluded	q^2*
Distress	*Academic burnout*	0.401	0.396	0.008
Quantitative demands	*Academic burnout*	0.401	0.336	0.109
Insecurity + Q. Demands	*Academic burnout*	0.401	0.344	0.095
Behavioral stress + Insecurity	*Academic burnout*	0.401	0.273	0.214

Q^2 (*Insecurity* = 0.168; *Distress* = 0.287; *Quantitative demands* = 0.269; *Academic burnout* = 0.401)
* $q^2 = (Q^2 \text{ included} - Q^2 \text{ excluded})/(1 - Q^2 \text{ included})$

TABLE A6. The non-parametric method PLS-MGA (Path Coefficients-differences and p-values).

	Path Coeff. - diff. (|Female - Male|)	p-value
Behavioral stress → Distress	0.027	0.656
Behavioral stress → Insecurity	0.026	0.622
Distress → Academic burnout	0.042	0.341
Insecurity → Quantitative demands	0.069	0.805
Quantitative demands → Academic burnout	0.128	0.863

REFERENCES

1. W. Schaufeli, M. P. Leiter and C. Maslach, *Career Development International,* 14(3), 204-220 (2009).
2. J. Maroco and J. A. Campos, *Psychological Reports: Human Resources & Marketing*, 111, 3, 814-830 (2012).
3. B. Kim, S. Jee, L. Joungwha, A. Sunghee and M. L. Sang, *Stress and Health,* 34(1), 127-134 (2018).
4. E. C. Chang, K. L. Rand and D. P. Strunk, *Personality and Individual Differences*, 29, 255-263 (2000).
5. H. J. Yang, *International Journal of Educational Development*, 24, 283-301 (2004).
6. G. Yavuz and N. Dogan, *Procedia - Social and Behavioral Sciences* 116, 2453-2457 (2014).
7. U.S. Department of Education, National Center for Education Statistics. *The Condition of Education 2019* (NCES 2019-144), https://nces.ed.gov/fastfacts/display.asp?id=40 (visited it on 11/12/2018).
8. Y. Neumann, E. Finaly-Neumann and A. Reichel, *The Journal of Higher Education*, 61(1), 20-31 (1990).
9. L. M. Grilo, H. L. Grilo and E. Martire, ICCMSE 2018, *AIP Conf. Proc.* 2040 (2018), 110008-1–110008-5.
10. J. F. Hair, G. T. M. Hult, C. M. Ringle and M. Sarstedt, A Primer on Partial Least Squares Structural Equation Modeling (PLS-SEM) (2nd Ed., Thousand Oakes, CA: Sage, 2017).
11. M. Sarstedt, J. F. Hair, C. M. Ringle, K. O. Thiele and S. P. Gudergan, *Journal of Business Research*, 69: 3998-4010 (2016).
12. W. Schaufeli, I. Martínez, A. Pinto, M. Salanova and A. Bakker, *Journal of Cross-cultural Psychology*, 33(5), 464-461 (2002).
13. J.-H. Cheah, M. A. Memon, Francis C., Hiram T. and T. Ramayah, *International Journal of Business and Society*, 19 (1), 139-160 (2018).
14. C. M. Ringle, S. Wende and J.-M. Becker, "SmartPLS 3." Boenningstedt: SmartPLS GmbH 2015, www.smartpls.com.
15. F. Schuberth, J. Henseler and T. K. Dijkstra, *Qual Quant*, 52: 9-35 (2018).

In Enhancing Inference by the STATIS Methodology

Manuela Oliveira[1,a)]

[1] *University of Èvora. Department of Mathematics and CIMA - Center for Research on Mathematics and its Applications.*
Colégio Luís António Verney, Rua Romão Ramalho 59, 7000-671 Évora, Portugal

[a)] Corresponding author: mmo@uevora.pt

Abstract.
The studies in a series may further be considered to have a common structure whenever their corresponding points lie along the first axis. Common structure matched series are modeled in the framework of the STATIS method. For that purpose, the information of each series is summarized in a structure vector and in a sum of square of residues vector. Former models may provide inference capabilities to this overall methodology.

INTRODUCTION

The Analyse Conjointe de Tableaux (STATIS method Structuration des Tableaux a Trois Indices de la Statistique) is an exploratory technique of multivariate data analysis based on linear algebra and especially on Euclidean vector spaces. These methods was introduced by [1], and developed by several authors, in particular by [2] and [3]. The central idea is to compare configurations of the same individuals or variables in different circumstances or moments in time. Therefore, these methods allows us not only to identify the moments in time in which the most significant changes occurred, but also to rank variables and individuals according to their contributions to the total changes. We are also able to draw the trajectory of each individual or variable around its compromise (average) position.

The STATIS methodology

In the STATIS methodology, a study is a statistical triplet (X_i, D_{p_i}, D_n) , where $X_i\, n \times pi$ with $i = 1, \dots, k$ denotes the data table associated to the kth point in time, n refers to the total number of individuals and p_i is the number of variables in the kth data table. D_{p_i} is the metric in the individuals space and, in general, is defined by the identity matrix or by a diagonal matrix whose main elements are the reciprocal of the variance of variables. The metric in the variables space D_n is defined by a diagonal matrix whose elements are the weights associated to the individuals. This methodology have two methods

- the STATIS method, that applies when we have available a set of tables with observations of a group of variables over a set of individuals, the variables possibly being different from table to table ; being: $(\mathbf{X}_i, \mathbf{D}_{p_i}, \mathbf{D}_n),\ i = 1, \dots, k$;
- the STATIS Dual method, that applies when we have available a set of tables with observations of a group of variables over a set of individuals, the individuals possibly being different from table to table; being: $(\mathbf{X}_i, \mathbf{D}_p, \mathbf{D}_{n_i}),\ i = 1, \dots, k$.

and involves different steps. In the first step, termed interstructure, we compare globally the series of studies. In the second step, termed intrastructure, we define a common structure of individuals in all data tables. Finally, we identify which individuals contribute the most (or least) to the observed

differences among the studies. In the interstructure step, we start by defining an object for each data table as the matrix of the scalar products between individuals.

More precisely, we associate to each $\mathbf{X}_i$ a matrix of the scalar products $\mathbf{W}_i$ given by

$$(\mathbf{W}_i, \mathbf{W}_l)_{HS} = tr(\mathbf{W}_i \mathbf{D}_n \mathbf{W}_l \mathbf{D}_n) \;\; i, l = 1, \ldots, k$$

where $\mathbf{X}_i^t$ denotes the transpose matrix of $\mathbf{X}_i$ $n \times p_i$, the array of data and Tr denotes the trace operator of a matrix. This scalar product between operators designated as scalar product of Hilbert-Schmidt to induce a distance between the operators $\mathbf{W}_i$ e $\mathbf{W}_l$, given by the following expression:

$$d_{HS}(\mathbf{W}_i, \mathbf{W}_l) = ||\mathbf{W}_i - \mathbf{W}_l||_{HS} = \sqrt{tr[(\mathbf{W}_i \mathbf{D}_n \mathbf{W}_l \mathbf{D}_n)^2]}.$$

Euclidean geometric representation of the k studies

The $\mathbf{S}$ matrix has the spectral decomposition:

$$\mathbf{S} = \sum_{j=1}^{k} \theta_j \gamma_j^k \gamma_j^{k^t}$$

with $\theta_1 > \theta_2 > \ldots > \theta_k$ eigenvalues of the matrix $\mathbf{S}$ and $\gamma^k{}_1, \gamma^k{}_2, \ldots, \gamma^k{}_k$, their eigenvectors.[3]: "the coordinates of the points representing the j-th study are the j-th components of vectors $\theta_1^{\frac{1}{2}} \gamma_1^k, \ldots, \theta_k^{\frac{1}{2}} \gamma_k^k,\; j = 1, \ldots, k$". The graph obtained by pairs ($\sqrt{\theta_r}\gamma_i, \sqrt{\theta_s}\gamma_j$) whit $r, s\{1, \ldots, k\}$ and $r \neq s$ gives us a representation of the Euclidean k operators in the plan (r, s) of the inter-structure. The common structure exists when, in the representation of the inter-structure, the points representative of the studies lie along the first axis. If the series has a common structure, then

$$||\beta_j^k||^2 = ||\theta_j \gamma_j||^2 \approx 0, \;\; j = 2, \ldots, k$$

[4] present models that may provide inference capabilities to this overall methodology. However, the introduction of errors at the matrices $\mathbf{S}$ level makes these formulations somewhat artificial; so, we now introduce errors at the level of matrices $\mathbf{W}_i \mathbf{D}_n,\; i = 1, \ldots, k$ in the STATIS method and of the matrices $\mathbf{V}_i \mathbf{D}_p$, $i = 1, \ldots, k$ in the Dual STATIS method.

In this paper, a new symmetric model is presented to provide the STATIS methodology with inference capabilities.

Model formulation

Model with random component in S

Let

- $\mathbf{S} = \mathbf{S}_{ij} \,\epsilon\, \Theta_k$ family of symmetric matrices of order k
- $\mathbf{P} = [\gamma_1^k, \ldots, \gamma_k^k]$ diagonalized orthogonal of $\mathbf{S}$
- $\mathbf{D} = (\theta_1, \ldots, \theta_k)$ diagonal matrix whose main elements are the eigenvalues of $\mathbf{S}$

we have

$$\mathbf{S} = \mathbf{P}^t \mathbf{D} = (\theta_1, \ldots, \theta_k)\mathbf{P}$$

so, if there is a common structure, then

$$||\beta_j^k||^2 = ||\theta_j \gamma_j||^2 = \theta_j^2 \approx 0, \;\; j = 2, ..., k,$$

and therefore

$$\mathbf{S} \approx \theta_1 \gamma_1^k \gamma_1^{k^t}$$

[4] assumed the model as

$$\mathbf{S} = \lambda \alpha^k \alpha^k + \overline{\mathbf{E}}$$

where $\overline{\mathbf{E}} = \frac{1}{2}(\mathbf{E} + \mathbf{E}^t)$ is a random matrix such that

$$vec(\mathbf{E}) \sim N(\mathbf{0}, \sigma^2 \mathbf{I}_{k^2}).$$

with $\theta_1, \ldots, \theta_k$ eigenvalues of the matrix $\mathbf{S}$ and $\gamma_1^k, \ldots, \gamma_k^k$ their eigenvectors we can consider the estimators

$$\lambda = \theta_1, \quad \alpha^k = \gamma_1^k, \quad with\ \beta^k = \theta_1 \gamma_1^k,$$

[5], evaluate the accuracy of the estimate of λ and α through simulations. The information contained in the series of studies is condensed in pair:

- $\beta^k = \theta_1 \gamma_1^k$: estimated vector structure;
- $\mathbf{V} = \|\mathbf{S}\| - \|\gamma_1^k \mathbf{S}\|^2$: sum of squared residuals.

Approximate normality

This technique had several developments [6] and is currently based on the asymptotic linearity of statistics $g(\mu + \mathbf{X})$, i.e. $\|\underline{g}(\mu)\|$ dominates, $\forall d > 0$, the supreme of spectral ray of $\underline{\underline{g}}(\mu + \mathbf{z})$ e $\|z\| \leq d$ when $\|\mu\| \to \infty$. So polynomials $P((X) + (\mu))$ of low grade are (very roughly) normal when $\|(\mu)\|$ importantly large.

Models with random component in X

Assumptions and formulation

Having the triplet

$$(\mathbf{X}_i = \mathbf{U}_i + \mathbf{E}_i; \mathbf{D}_p = \mathbf{I}_p; \mathbf{D}_{n_i} = \frac{1}{n_i}\mathbf{I}_{n_i}),\ i = 1, \ldots, k$$

with

$$\mathbf{U}_i = [u_{ilh}], fixed\ matrix\ l, h = 1, \ldots, n$$

and

$$vec(\mathbf{E}_i) \sim N(0, \sigma^2 \mathbf{I}_{n_i p}),\ i = 1, ..., k.$$

Let

- $\mathbf{X}_i = [x_{ijl}] = [u_{ijl} + e_{ijl}],\ i = 1, \ldots, k,\ j = 1, \ldots, n,\ l = 1, \ldots, p$
- $\mathbf{A}_i = X_i^t D_{n_i} X_i D_p$, with $\mathbf{A} = [a_{ilh}],\ i = 1, \ldots, k,\ j = 1, \ldots, n,\ l = 1, \ldots, p$

To build the matrix $\mathbf{S} = [s_{ij}]$, lets determine:

$$S_{ij} = tr(\mathbf{A}_i \mathbf{A}_j^t) = \sum_{l=1}^{n} \sum_{h=1}^{n} a_{ilh} a_{jlh}$$

$$= S_{ij}^{\circ} + \sum_{l=1}^{n} \sum_{h=1}^{n} (e_{ilh}^{\circ} e_{jlh}^{\circ})$$

with

$$S_{ij}^{\circ} \approx \sum_{l=1}^{n} \sum_{h=1}^{n} (\eta_{ilh} \eta_{jlh}) + \sum_{l=1}^{n} \sum_{h=1}^{n} (\eta_{ilh} e_{jlh}^{\circ}) + \sum_{l=1}^{n} \sum_{h=1}^{n} (\eta_{jlh} e_{ilh}^{\circ})$$

so, given the approximate normality, we admit that

$$\mathbf{Z} = vec(\mathbf{S}) \sim N(\eta, \mathbf{W})$$

Inference

If $rank(E(S)) = 1$ we consider the model

$$\mathbf{S} = \lambda \alpha^k \alpha^{k^t} + \mathbf{E}$$

where $vec(\mathbf{E}) \hookrightarrow N(\mathbf{0}^{k^2}, \mathbf{W})$. Let $\theta_1, \ldots, \theta_k$ eigenvalues of the matrix $\mathbf{S}$ and $\gamma_1^k, \ldots, \gamma_k^k$ their eigenvectors we can consider the estimators

$$\lambda = \theta_1,\ \alpha^k = \gamma_1^k,\ \beta^k = \theta_1 \gamma_1^k, \quad ([5])$$

With $\widetilde{\beta}^k = \mathbf{S}\gamma_1^k = (\mathbf{I}_k \otimes \gamma_1^{k^t}) vec(\mathbf{S})$ we take

$$\widetilde{\beta}^k \hookrightarrow N(\beta^k, (\mathbf{I}_k \otimes \gamma_1^{k^t})\mathbf{W}(\mathbf{I}_k \otimes \gamma_1^k))$$

where $\otimes$ represents the kronecker product. Now, with $\mathbf{Y}^{k^2} = vec(\mathbf{S})$, we can obtain a matrix $\mathbf{G}$ such that $\mathbf{G}\mathbf{Y}^{k^2}$ is independent $\widetilde{\beta}^k$ and when the model fits

$$\mathbf{G}\mathbf{Y}^{k^2} \hookrightarrow N(0^g, \sigma^2 \mathbf{I}_g)$$

where $g = rank(\mathbf{G}\mathbf{W}\mathbf{G}^t)$.

Validation

1st Test

H_0: The components $Z_1, ..., Z_g$ of $\mathbf{Z}^g = \mathbf{G}\mathbf{Y}^{k^2}$ are independent and have normal distribution with mean 0 and variance σ^2. With $\delta = \frac{1}{\sigma^2}\beta^{k^t}(\widetilde{\beta}^k)^+\beta^k$ and $l = rank((\widetilde{\beta}^k))$ we have:

2nd Test

$H_0:\ \delta = 0\ v.s.\ H_1 : \delta > 0$

$$\mathcal{F} = \frac{g}{l}\frac{\widetilde{\beta}^{k^t}(\widetilde{\beta}^k)^+\widetilde{\beta}^k}{||\mathbf{G}\mathbf{Y}^g||^2} \hookrightarrow F(\cdot|l, g)$$

ACKNOWLEDGMENTS

Research was partially supported by the Fundacao para a Ciencia e a Tecnologia through the project UID/MAT/04674/2019 (CIMA - Centro de Investigacao em Matematica e Aplicacoes).

References

[1] T. B. L'hermier des Plantes, H., Revue de statistique Appliquée, **XXV, n°2.** (1977).
[2] C. Lavit, *Analyse conjointe de tableaux quantitatifs*, edited by Masson (1988).
[3] Y. Escoufier, Statistique et Analyse des Données **10, n°1.** (1985).
[4] M. Oliveira and J. Mexia, Journal of Statistical Planning and Inference **137** (2007), 10.1016/j.jspi.2006.05.007.
[5] M. M. Oliveira and J. T. Mexia, International Journal of Forecasting **20**, 131–1351 (2004).
[6] A. Areia, M. Oliveira, and J. Mexia, Statistical Methodology **5** (2008), 10.1016/j.stamet.2007.09.001.

Preliminary Reflexion About Waste Management Plan in NRP Ships

José B. Rebelo[1], Joana S. Jerónimo[1], M. Filomena Teodoro[1,2,a)] and Suzana P. Lampreia[1]

[1]*CINAV, Escola Naval, Base Naval de Lisboa, Alfeite, 1910-001 Almada, Portugal*
[2]*CEMAT, Instituto Superior Técnico, Avenida Rovisco Pais, 1, 1048-001 Lisboa, Portugal*

[a)]maria.alves.teodoro@marinha.pt; maria.teodoro@tecnico.ulisboa.pt

Abstract. The waste management and environmental protection have some guidelines, both on land and for ships, followed by all staff from Portuguese Navy (military, militarized and civilian) that cooperate and contribute to the waste management in Navy. Restricting the present study to the residues referred in Marpol 73/78 [1], considering Annexes I, IV and V. To evaluate the procedures how the storage and treatment of ship waste is performed, is necessary to verify the existing equipment, its operational status and whether there is an on-board plan about waste management. To evaluate the knowledge and cooperation of the military on board for the environment was built and implemented a questionnaire to the staff of some selected NRP ships after the permission of the Commander of Portuguese Surface Fleet. We have applied an intermediary level of statistical analysis, so we could identify the major questions contributions, associations and some independents variables that explains the knowledge, attitude and practice about waste management in ships.

INTRODUCTION

Human activity and the rapid economic development have a direct and serious consequence, the pollution of the sea that has increased significantly over the last decades. The marine waste is a major cause of intense human activity [2]. Approximately 80% of the world trade volume is transported by sea [8], causing heavy traffic of ships to be one of the main sources of maritime pollution, which generates solid wastes, sewage and wastes from hydrocarbons, that are also an atmospheric pollutant source [2]. We intend to characterize the profile of waste management in NRP ships. In [3] was compiled specific regulamentation about the theme. Also, in the same monography was implemented a questionnaire to evaluate Knowledge, Attitudes and Practice (KAP) about the waste management during the boarded period in the NRP ships. It was performed a preliminary statistical analysis in [4, 5] using a non complete sample of boarded population, being used as reference in the present work. The author of [6] developed an index about good practices in waste management. In this manuscript, we have continued the statistical approach proposed in [5], but excluding some questions considered statistically similar to others.

The summary of this works consists in an introduction and results and final remarks Sects., Sect. 2 contains some issues about the questionnaire. The sample characterization is done in Sect. 3. The empirical application can be found in Sect. 4. The final remarks can be found in sect. 5.

THE QUESTIONNAIRE

To contribute to an adequate waste management and environmental protection, the Admiral Chief of Staff from the Navy defined a Security and Health Policy in the Work and Environment of the Navy. Some guidelines were established for the units, both on land and for ships. In [7] is done a good description about this effort. Some NRP ships have equipments for waste management. In the present work we perform an analysis of the waste management of the Portuguese Navy's ships, limiting the study to the residues referring in Annexes I, IV and V of Marpol 73/78. For such analysis was built a questionnaire with pertinent questions about knowledge, practice and attitudes of boarded

staff of NRP ships to collect the necessary information about the waste management. After adequate authorization by the Portuguese Surface Fleet Commander, the data collection was carried out through questionnaires and some interviews to the commanders of the selected ships. The questionnaire has two parts, the first part inquires about socio-demographic variables and personal details, the second part is composed with questions that allow to evaluate KAP. The initial part concerns the socio-demographic information about each participant in general: $Q1_1$ - *"'Gender"', "'Age"', "'Grade"', "'Have you ever attended an environmental training course?"', "'If you answered "Yes" in the previous question, it was in Navy"', "'Do you recycle at home?"'.*

The second part of questionnaire consists in questions with open or closed response, giving the possibility of choosing more than one answer in each question or in the form of Likert scale with four levels from 1 to 4 (1 - Totally Disagree, 2 - Partially Disagree, 3 - Partially agree, 4 - Totally Agree; also some questions have a "'yes"' or "'No"' answer; one question has an open answer, where is necessary to identify factors that can contribute for a not proper waste management, this question will have a qualitative, not a quantitative analysis. The questionnaire aimed at evaluating participants' knowledge, attitudes and practices regarding waste management, comprising questions about knowledge issues, other about attitudes and some questions that consider practice details.

SAMPLE CHARACTERIZATION

In a preliminary data analysis of questionnaires taking into account the non-quantitative nature of the involved variables, were calculated measures of association, nonparametric Spearmann correlation coefficient, non-parametric test of Friedman for paired samples, etc. can be found in [4, 5] The participants are composed by 64% men and 36% women. In the selected sample, 46% of people are less than 30 years older, 38% between 30 and 40 years old. The oldest person is 51 years old. About one third (36%) of participants have some training about environmental education. 68% of participants do recycle at home.

EMPIRICAL APPLICATION

To guarantee the reliability of the questionnaire, we computed the alpha of Cronbach indicator. This measure was calculated considering all but socio-demographic questions that conduced to the value is 0.75, indicating that there is an adequate internal consistency of the questionnaire but it is still possible to be improved . It should also be checked whether the questions will have identical answers in terms of statistical distribution. If there are any, the most similar ones may be eliminated, process that generally leads to an increase in alpha of Cronbach indicator. For this purpose we can use various statistical tests. With such idea, we have analyzed each question response frequency distribution 1 as well as the distribution of responses ranks 2. Graphically, we can observe that the responses distributions of each question seems to be distinct. The same issue is conrmed when were performed several tests to compare the answers of questions. The paired T-test, McNemar's test for frequencies comparison, Crochan's Q test for binary variables comparison (agree versus not agree). Also were performed the Friedman test ($p - value < 0.005$) and kendalls coefcient of concordance test ($p - value < 0.005$) (see table 1). All tests conduced to the same conclusion: the distributions of considered questions are not the same. Notice that the Spearmann correlation coefcient conduces to signicant relations between some questions, also Friedman's pairwise test supports such association. In figure 3 is indicated which pair of questions are similar or which questions are distinct ($p - value < 0.005$). After the elimination of the questions which are statistically similar, we have repeated all process described in [5], where it was applied an exploratory factorial analysis (EFA) so it could identify the major questions contributions to the latent variables that explain literacy about waste management in ships.

FINAL REMARKS

After the application of an EFA to the questionnaire only including the questions selected as explained previous paragraph, the results were identical, but it were identified four dominant factors, in the opposite of the three factors selected in [5]. We could identify F_1 as a factor that characterize $Awareness$, F_2 combines variables from $Health\ and\ Safety$, F_3 describes the *Practice* and the fourth factor F_4 is associated as *Knowledge*. These factors were used as dependent variables in an ANOVA approach. The explanatory variables that contribute to explain each factor were selected. The results will be detailed in an extended version of this article.

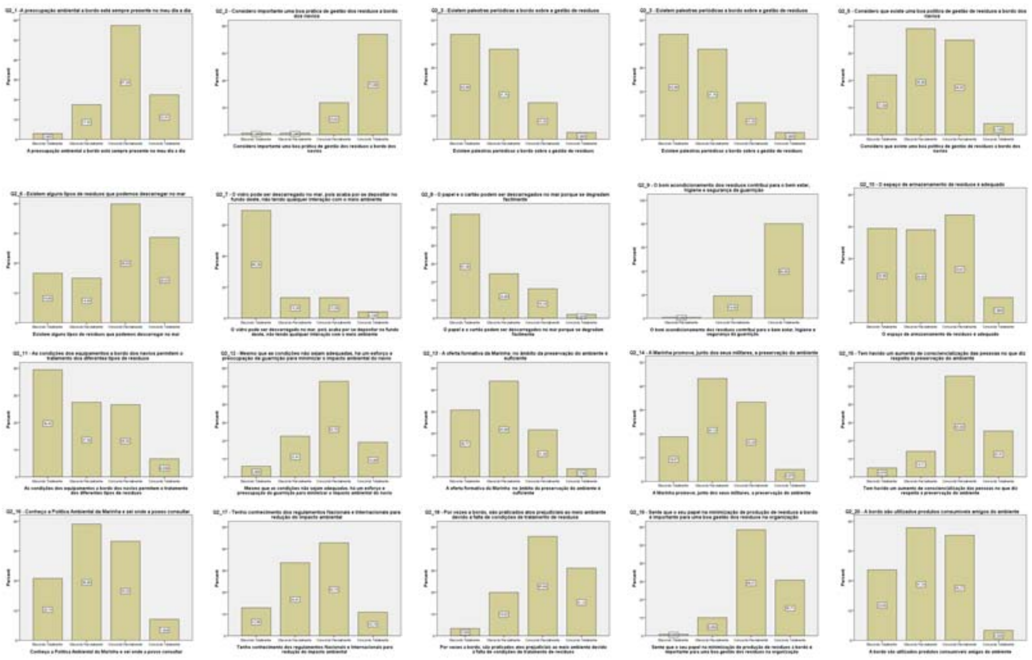

FIGURE 1. Questionnaire responses percentage distribution. Questions $Q2_1$ to $Q2_{20}$. Values: Totally disagree, Partially disagree, Partially agree, Totally agree.

ACKNOWLEDGMENTS

This work was supported by Portuguese funds through the *Center for Computational and Stochastic Mathematics* (CEMAT), *The Portuguese Foundation for Science and Technology* (FCT), University of Lisbon, Portugal, project UID/Multi/04621/2019, and *Center of Naval Research* (CINAV), Naval Academy, Portuguese Navy, Portugal.

REFERENCES

[1] C. Edition, *Marpol 73/78. Regulation*, (2002).

[2] A. Griffin, *Marpol 73/78 and Vessel Pollution: A Glass Half Full or Half Empty*?, Indiana Journal of Global Legal Studies 1(2), 489–513 (1994).

[3] J.B. Rebelo, "'Impacto Ambiental da Marinha Portuguesa. Análise e resolução da Gestão de Resíduos no mar"'. Master thesis. Escola Naval, Almada (2019).

[4] J.B. Rebelo, J.S. Jerónimo, M.F. Teodoro, S.P. Lampreia, "'Modeling the waste management in NRP ships"'. *Regional HELIX 2019, June 26th-29th 2019, Porto, Entrepreneurial Ecosystems and Sustainability. Proceedings of Regional Helix 2019*, 183-188 (2019). ISBN 978-989-98447-7-3.

[5] Rebelo, J.B., Jerónimo, J.S., Teodoro, M.F., Lampreia, S.P. (to appear). "'Literacy about the waste management in boarded staff"'. *Proceedings of EUROGEN 2019*, September, 12nd-14th, Guimarães.

[6] Rebelo, J.B., Jerónimo, J.S., Teodoro, M.F., Lampreia, S.P. (Submitted). *KAP about waste management in a Maritime Environment*.

[7] Monteiro, J. "'Poluição. Marítima; Normas e Controlo nos meios Navais das Forças Armadas"'. Monography, Instituto Universitário Militar. Lisboa (2016).

[8] U.N., United Nations Conference on Trade and Development, (2018). Retrieved from `https://unctad.org/en/PublicationsLibrary/dtl2018d1_en.pdf` Accessed at 25/05/2019.

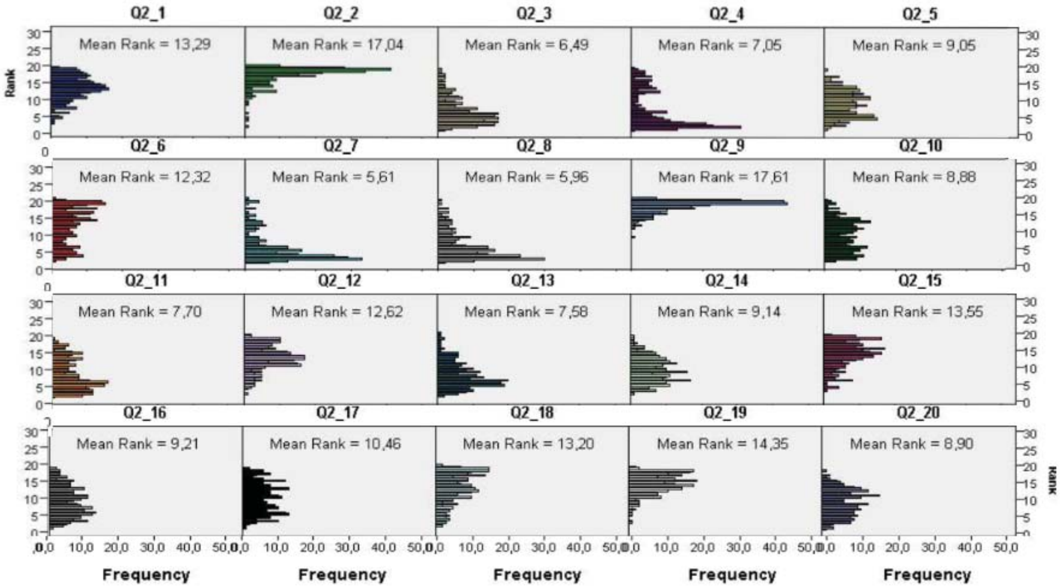

FIGURE 2. Qestionnaire responses ranks frequencies.

TABLE 1. KendalLs test results (left); Friedman test results (on right).

Total N	241
Test Statistic	1.921,606
Degrees of Freedom	19
Asymptotic Sig. (2-sided test)	,000

Total N	241
Kendall's W	,420
Test Statistic	1.921,606
Degrees of Freedom	19
Asymptotic Sig. (2-sided test)	,000

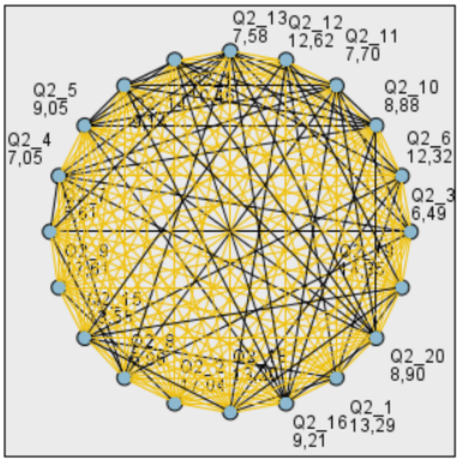

FIGURE 3. Pairwise comparisons: each line represents the two sided test where the null hypothesis considers that the questions at the ends of line have the same distribution. Each node represents the sample average rank. Significance level is 0.05.

Design, Analysis and Retrofitting of Civil Structures and Infrastructures in Seismic Prone Areas

Francesco Clementi[a], Antonio Formisano[b], Gabriele Milani[c,*]

[a] *Polytechnic University of Marche, Via Brecce Bianche, Ancona, Italy*
[b]*Technical University of Milan, Piazza Leonardo da Vinci 32, Milan, Italy*
[c] *University of Naples Federico II, Piazzale Tecchio 80, Naples, Italy*
[*]Corresponding author, e-mail: milani@stru.polimi.it, gabriele.milani@polimi.it, Phone: +39 02 2399 4290.

PREFACE

The Special Session #16 entitled "Design, Analysis and Retrofitting of Civil Structures and Infrastructures in Seismic Prone Areas" was organized within the conference ICCMSE 2019, 15th International Conference of Computational Methods in Sciences and Engineering, held in Rhodes, Greece, 2-5 May 2019 with the aim of continuing a consolidated research stream constituted by five previous classic meetings organized in occasion of ICCMSE conferences, starting from the 2014 edition and ending last year.

Past earthquakes have shown that not only existing structures and infrastructures, but also new constructions may exhibit an insufficient resistance against seismic loads and extreme events, especially if they are for some reasons poorly designed and built with strong money limitations, as it may occur in developing countries.

The numerical and experimental assessment, as well as the mechanical modeling and design practice of existing and new structures when subjected to horizontal loads is undoubtedly an open issue, because of the complexity of the problem itself and because the research involves several different disciplines, fields of expertise and approaches.

Open challenges to tackle a consistent seismic design are more profoundly faced by all those regions where the inadequacy and poor access to advanced technologies, resources, and knowledge constraint the construction of new structures to be still highly vulnerable to horizontal loads.

On the other hand, open issues in industrialized countries are still the mitigation of the seismic vulnerability of the existing structures and infrastructures, with particular attention to traditional materials, especially masonry and timber.

The Special Session was aimed at collecting papers dealing with key issues related to the sound design of new structures and infrastructures, to the effective mitigation of the vulnerability of existing buildings in seismic zone and to paradigmatic case studies.

Several different scientific contributions were collected, favoring information exchange among theoreticians and practitioners active in different fields.

The first paper by Formisano et al. [1] focuses on masonry bell towers, discussing their seismic vulnerability by a parametric study.

Stockdale et al. in [2] concentrate on the prediction of displacements and irrecoverable collapse time for a fixed-hinge dry-stack arch under constant horizontal acceleration.

Grillanda et al. in [3] discuss some preliminary limit analysis results for a masonry arch bridge obtained with a 3D NURBS FE code, whereas in [4] Scacco and co-workers present experimental and numerical analyses on a parabolic tuff arch reinforced with FRCM.

Gazzani et al. in [5] evaluate the effectiveness of different approaches for the seismic vulnerability assessment of RC structures, whereas Giordano et al. in [6] discuss about the nonlinear behavior of unfired dry earth.

Tiberti and Milani in [7] present a novel voxel approach for the homogenized limit analysis of irregular masonry, focusing on the in-plane ultimate homogenized behavior. The procedure allows in principle to deal with multi-leaf masonry under in- and out-of-plane loads in a rigorous way.

Tiberti et al. in [8] present a combined experimental and numerical analysis on an ancient anti-seismic technique used in the past in Mediterranean areas, whereas in [9] Bertolesi and co-workers discuss on the application of homogenization approaches for modeling Fiber Reinforced Cementitious Matrix FRCM-strengthened masonry.

Habieb and co-workers in [10] present preliminary experimental relaxation tests and numerical modeling for rubber pads used for a low cost seismic base isolation system, whereas Milani & Milani in [11] study numerically the optimal vulcanization of the same pads.

Finally, Pingaro & Milani in [12] present a novel 3D CAD approach for the straightforward estimation of the seismic vulnerability of existing masonry towers by means of pre-assigned failure mechanisms.

REFERENCES

[1] Formisano A., Fabbrocino F., Vaiano G. (2019). Parametric analysis on the seismic response of masonry bell towers. In: Proc. 15th International Conference of Computational Methods in Sciences and Engineering, ICCMSE 2019, Rhodes, Greece, 2-5 May 2019 (Editor. Prof. Theodore Simos).

[2] Stockdale G.L., Milani G., Sarhosis V. (2019). Irrecoverable collapse time for a fixed-hinge dry-stack arch under constant horizontal acceleration. In: Proc. 15th International Conference of Computational Methods in Sciences and Engineering, ICCMSE 2019, Rhodes, Greece, 2-5 May 2019 (Editor. Prof. Theodore Simos).

[3] Grillanda N., Milani G., Nale M., Chiozzi A., Tralli A. (2019). Three-dimensional analysis of a damaged masonry arch bridge under horizontal load. In: Proc. 15th International Conference of Computational Methods in Sciences and Engineering, ICCMSE 2019, Rhodes, Greece, 2-5 May 2019 (Editor. Prof. Theodore Simos).

[4] Scacco J., Milani G., Bove M., Castellano A., Fraddosio A., Piccioni M.D. (2019). Experimental and Numerical Analysis of the Effectiveness of FRCM Strengthening on a Parabolic Tuff Barrel Vault. In: Proc. 15th International Conference of Computational Methods in Sciences and Engineering, ICCMSE 2019, Rhodes, Greece, 2-5 May 2019 (Editor. Prof. Theodore Simos).

[5] Gazzani V., Poiani M., Clementi F., Pace G., Lenci S. (2019). Evaluation of different approaches for the seismic vulnerability assessment of RC structures. In: Proc. 15th International Conference of Computational Methods in Sciences and Engineering, ICCMSE 2019, Rhodes, Greece, 2-5 May 2019 (Editor. Prof. Theodore Simos).

[6] Giordano E., Clementi F., Cocchi G., Marcheggiani L. (2019). On the nonlinear behaviour of unfired dry earth. In: Proc. 15th International Conference of Computational Methods in Sciences and Engineering, ICCMSE 2019, Rhodes, Greece, 2-5 May 2019 (Editor. Prof. Theodore Simos).

[7] Tiberti S., Milani G. (2019). Voxel Approach for 3D In-Plane Homogenized Failure Surfaces of Non-Periodic Masonry. In: Proc. 15th International Conference of Computational Methods in Sciences and Engineering, ICCMSE 2019, Rhodes, Greece, 2-5 May 2019 (Editor. Prof. Theodore Simos).

[8] Tiberti S., Scuro C., Porzio S., Olivito R.S., Milani G. (2019). Experimental and numerical analysis on an ancient anti-seismic technique. In: Proc. 15th International Conference of Computational Methods in Sciences and Engineering, ICCMSE 2019, Rhodes, Greece, 2-5 May 2019 (Editor. Prof. Theodore Simos).

[9] Bertolesi E., Ghiassi B., Milani G. (2019). Application of homogenization approaches for modeling of FRCM-strengthened masonry. In: Proc. 15th International Conference of Computational Methods in Sciences and Engineering, ICCMSE 2019, Rhodes, Greece, 2-5 May 2019 (Editor. Prof. Theodore Simos).

[10] Habieb A.B., Milani G., Quaglini V., Milani F. (2019). Relaxation Test and Numerical Modeling of Rubber for Seismic Base Isolation. In: Proc. 15th International Conference of Computational Methods in Sciences and Engineering, ICCMSE 2019, Rhodes, Greece, 2-5 May 2019 (Editor. Prof. Theodore Simos).

[11] Milani G., Milani F. (2019). An integrated kinetic-FE vulcanization model to predict the optimal curing of thick rubber pads for applications in seismic isolation. In: Proc. 15th International Conference of Computational Methods in Sciences and Engineering, ICCMSE 2019, Rhodes, Greece, 2-5 May 2019 (Editor. Prof. Theodore Simos).

[12] Pingaro N., Milani G. (2019). Full 3D CAD procedure for the speedy evaluation of the seismic vulnerability of masonry towers. In: Proc. 15th International Conference of Computational Methods in Sciences and Engineering, ICCMSE 2019, Rhodes, Greece, 2-5 May 2019 (Editor. Prof. Theodore Simos).

Gabriele Milani

Gabriele Milani was born in Cittadella-PD (Italy) in 1977. PhD in Civil and Industrial Engineering, MSc in Civil Engineering, both at the University of Ferrara, Italy.

From 2014: Associate Professor (with habilitation as full professor from 2017), Mechanics of Solids and Theory of Structures, Technical University of Milan, Italy.

Previously, Assistant Professor, Technical University of Milan, Italy (2008-2014), Post Doctoral Researcher, ETH Zurich, Switzerland (2008) and Post Doctoral Fellow, University of Ferrara, Italy (2004-2008).

He has 324 SCOPUS records, he published more than 180 indexed International Journal Papers, 9 Chapters in books, more than 200 Presentations at Conferences. h-index 36 (SCOPUS), more than 3000 total citations.

Reviewer for more than 250 papers in about 70 journals and 10 conferences. EB member in 8 journals and 7 congresses, co-editor of 1 journal, editor of a journal dedicated to masonry (International Journal of Masonry Research and Innovation by Inderscience Publishers), chairman in several congresses.

His scientific interests are: masonry, historical constructions, structural analysis, limit analysis, FEM, homogenization theory, FRP reinforcement, genetic algorithms (GA), rubber vulcanization, elastomeric seismic isolators.
Most Cited Author Years 2006-2010 Diploma, Computers & Structures. Telford Premium Award 2012, by the UK Institution of Civil Engineering. K.J. Bathe Award 2014.

Antonio Formisano

Antonio Formisano was born in Naples in 1977, June 23rd. In July 2003 he graduated cum laude in Building Engineering at the University of Naples 'Federico II', where in 2007 he gained his PhD in Construction Engineering. In the same year he became Assistant Professor of Structural Engineering at the Department of Structures for Engineering and Architecture of the aforementioned faculty. Actually, he is Aggregate Professor of Structural Design at the School of Polytechnic and Basic Sciences of Naples. From 2017 he received habilitation as Associate Professor. Teacher within International Masters "Design of Steel", "Emerging Technologies for Construction" and "Sustainable Constructions under Natural Hazards and Catastrophic Events". He was involved in several national and international research projects. He is editorial board member and reviewer of numerous international journals and conferences. He was lecturer in several national and international Universities, as well as Chairman and Organizer of Mini-Symposium and Special Sessions of many Conferences. He is member of the Eurocode 9 Committees SC 9. T1 Aluminium "Update and Simplification of all parts of EN" and SC 9. T2 Aluminium "New types of Connection". He is author of more than 200 scientific papers, published on national and international journals and conference proceedings, dealing with metal structures, seismic and volcanic vulnerability of constructions, aggregated and monumental masonry structures, robustness and sustainability of buildings.

Francesco Clementi

Francesco Clementi was born in San Severino Marche (Italy) in 1981. He obtains MSc in Civil Engineering (2005), and the PhD Degree in "Architecture, Buildings and Structures" (2009) both at Polytechnic University of Marche. He is Assistant Professor (tenure-track) in "Structural Mechanics" at the Faculty of Engineering of Polytechnic University of Marche since 2012. He has developed research and teaching activities at the Universities of Ancona, Camerino, Lublin and Sao Paulo. He is member of the American Society of Mechanical Engineering (ASME) Technical Committee on "Dynamic and Control of Systems and Structures (DCSS)" since 2015. He was participant in several national and international projects (FP6, FP7, PRIN, Pompei Project, etc.). He is author of more than 80 scientific papers, published on national and international journals and conference proceedings.
Main field of research interest comprises the linear and nonlinear dynamic of structures, the seismic vulnerability assessment, the structural health monitoring. He also studies innovative strategies and techniques for the retrofitting and conservation of historical constructions. Other research interests are the dynamic (linear and nonlinear) of beams and laminates, the computational structural dynamics, mathematical model of curved beams, mathematical model of composites materials, fracture mechanics of earth materials.

Parametric Analysis on the Seismic Response of Masonry Bell Towers

Antonio Formisano[1,a)], Francesco Fabbrocino[2,b)] and Generoso Vaiano[1,c)]

[1]*Department of Structures for Engineering and Architecture, University of Naples "Federico II", Italy*
[2]*Department of Engineering, Pegaso Telematics University, Italy*

[a)] Corresponding author: antoform@unina.it;
[b)]francesco.fabbrocino@unipegaso.it; [c)]generoso.vaiano@inwind.it

Abstract. The Italy is a country rich of historical buildings, often made up of bricks, which were seriously damaged or suffered collapse after recent devastating earthquakes. In this framework the current work shows the results of instrumental researches and structural analysis aiming at the description of the seismic behaviour of masonry belfries or bell towers. Forty case studies belonging to thirteen Italian regions, so to be representative of the different seismic areas of the country, have been herein examined. A global modelling approach based on macro-elements models able to reproduce the seismic behaviour of bell towers with the support of the equivalent frame technique has been implemented through the 3MURI software. This numerical approach has allowed to reproduce the sequence of the main damage mechanisms of structures as horizontal forces increase. Therefore, a parametric analysis has been performed to evaluate the seismic response of investigated structures by changing their geometrical parameters. From the achieved results the individuation of the bell towers most at risk placed in different parts of Italy (North, Centre and South) has been faced. Finally, a new third order polynomial formula is proposed to calculate the principal vibration period of light squared stone towers as a function of their slenderness.

PRELIMINARY REMARKS

In Italy there are plenty of historical masonry buildings which are very sensitive to seismic phenomena. Among these constructions, it is of course recognized the high seismic vulnerability of masonry bell towers. For this reason, a number of studies are available in the technical literature dealing with the numerical/experimental analysis of this structural typology, using non-linear FE codes (Pena et al., 2010; Sahrosis et al., 2017; 2018), also with the use of very specific fibre-element models for the 3-D non-linear dynamics of slender towers (Casolo, 2010), passing through combined eigenvalues and experimental identification studies (Ivorra and Pallares, 2006), to 2D limit analyses performed by means of a no-tension material approach (Heyman, 1992), to experimental in-situ tests (Ubertini et al., 2018), to repairing and rehabilitation proposals (Lourenço, 2005; Modena et al., 2002), etc. In a partial review of the literature, it should be mentioned that the great part of big historical structures has been modelled with a so called macro-modelling strategy, i.e. the heterogeneous masonry is substituted at a structural level through a fictitious material with average mechanical properties (either orthotropic or isotropic) representing globally the response of brickwork under increasing loads (Ivorra and Pallares, 2006; Modena et al., 2002).

Considering the large scientific attention on this topic, in the current paper, a wide parametric analysis on numerous case studies has been done with the final goal to both individuate the bell towers most at risk on the Italian territory and to propose a new formula to assess the main vibration period of light squared stones towers.

FEATURES OF INVESTIGATED MASONRY BELL TOWERS

In the current study a review of masonry bell towers placed on the Italian territory has been made. In particular, forty towers, having medium-low values of slenderness, have been examined and the inspected structures are located in thirteen Italian regions. The geographical distribution of towers is divided into Northern (23 bell towers), Central

(8 bell towers) and Southern (9 bell towers) parts of Italy. In Tables from 1 to 3 the main geometrical properties of towers, namely the longitudinal direction width *B*, the transverse direction width *b*, the height *H* and the thickness *t* are reported. The dimensional variation ranges of examined towers are depicted in Table 4.

TABLE 1. Masonry bell towers in the Northern Italy.

Region	B (m)	b (m)	H (m)	t (cm)
Emilia-Romagna	1.8–12	1.8–12	7-86	30-257
Friuli Venezia Giulia	6.35	6.65	47	200
Lombardia	10	10	54-74	140-200
Piemonte	radius = 4.22		30	200
Veneto	3.7-15	3.7-10	20-58	60-200
Toscana	5.2-10	5.6-9.4	27-55	130-260

TABLE 2. Masonry bell towers in the Central Italy.

Region	B (m)	b (m)	H (m)	t (cm)
Abruzzo	4-10	4-10	20-50	130-150
Lazio	9	8.14	36	115
Marche	2.40-9	2.40-8	4-45	65-120

TABLE 3. Masonry bell towers in the Southern Italy.

Region	B (m)	b (m)	H (m)	t (cm)
Campania	6-13	4.8-13	30-75	60-100
Molise	4.8-6.8	4.8-7.1	20-35	100-200
Puglia	9	8	60	136
Sicilia	6	6	35	88

TABLE 4. Variation ranges of geometrical dimensions of examined towers.

Italian area	H (m)	λ (H/B)	t (cm)
North	20-100	3-13	40-260
Centre	20-60	3-9	60-160
South	20-100	3-11	60-200

NON-LINEAR STATIC ANALYSES

The generation of tower specimens to be investigated under numerical way has been done through the non-linear analysis software 3MURI (S.T.A.DATA., 2016), according to the Italian code (NTC08). Based on the provisions of the Italian M. C. n. 617 (2009), the knowledge level LC1 has been assumed (limited situ checks), and mechanical strength and Young modulus of masonry have been calculated as the lowest value and the average one, respectively, of those reported in the Table C8A.2.1. About the nominal life V_N of towers, 50 years have been considered and the subsoil category of structures has been assumed of type C. Therefore, on the basis of the information collected, average values of tower plan dimensions have been considered for each of the three areas in which Italy is divided. Particularly, plan shapes measuring 7.8 m x 7.8 m (North), 7.0 m x 7.0 m (Centre) and 7.5 m x 7.5 m (South) have been selected as representative dimensions of structures. Starting from these values, the variation of both the height and the thickness of the towers has been considered in order to generate a set of samples to be investigated under numerical way. A summary of main geometrical dimensions of investigated towers is illustrated in Table 4.

For seismic verification it has been considered also the location of towers in different Italian regional capitals: Bologna, Firenze, Milano, Torino,Trieste and Venezia in the North Italy, Ancona, L'Aquila and Roma in the Centre Italy, Bari, Campobasso, Naples and Palermo in the South Italy.

Pushover analysis curves of towers within the three Italian areas are built-up. From these analyses the variation trend of the stiffness *K* with the tower thickness for the three different zones of Italy are illustrated in Figure 1.

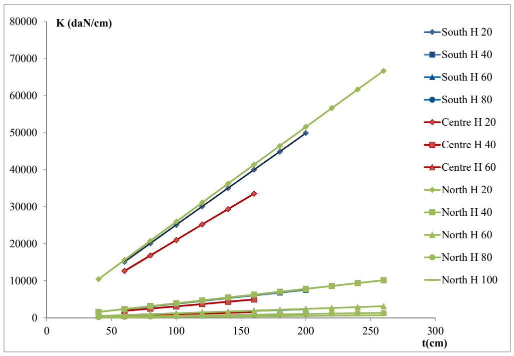

FIGURE 1. Stiffness *K* vs. thickness *t* curves for the investigated towers

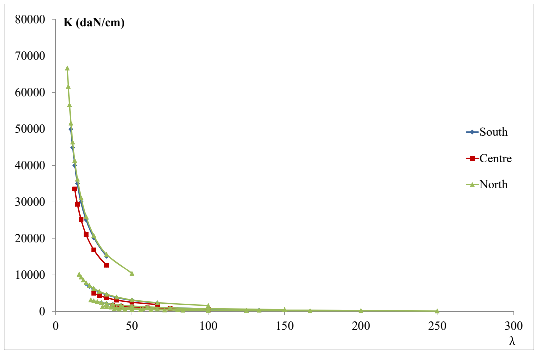

FIGURE 2. Stiffness *K* vs. slenderness *H/t* curves for the investigated towers

From obtained results it appears that the increase of the base shear with the thickness follows more or less the same trend for towers within Northern and Southern Italy, whereas this augment of performance is less marked for Central Italy towers. This is due to the slight difference in terms of plan dimensions of the investigated towers. In Figure 2 also the variation of the pushover curve initial stiffness *K* with the slenderness *H/t* of the towers is plotted.

From these figures it is evident that the increase of stiffness as the thickness increases (or the slenderness decreases) is more pronounced for towers having height of 20 m. Differently, towers with height greater or equal than 40 m have not a significant variation of stiffness with increasing thickness.

The seismic behaviour of towers placed in the three Italian areas has been also investigated in the non-linear static field by evaluating the α_{SLV} parameter, that is the ratio between the capacity acceleration and the demand one. Therefore, α_{SLV} factors greater or equal than one are representative of safety conditions. In the performed analyses, the minimum α_{SLV} factors achieved on the towers sited in the different examined Italian regional capitals are taken into account. The average values obtained are 2.70 in the North Italy (minimum in Bologna α_{SLV} = 1.41 and maximum in Milan α_{SLV} = 4.56), 1.38 in the Centre Italy (minimum in L'Aquila α_{SLV} = 0.81 and maximum in Rome α_{SLV} = 1.95) and 1.43 in the South Italy (minimum in Campobasso α_{SLV} = 0.88 and maximum in Bari α_{SLV} = 2.12). So, the seismic checks, except for the cases of L'Aquila and Campobasso, are always satisfied. Moreover, the average values achieved from recorded safety factors allow to declare that the Northern Italy towers are less susceptible to undergo damages under earthquake. On the other hand, the lowest average safety factor observed has been found in the Centre Italy, with a value similar to that recorded for Southern Italy towers. However, since these average factor values are greater than one, it can be declared that, if towers behave as a unique structural element without showing local failure mechanisms, their seismic behaviour is averagely satisfactory.

LINEAR DYNAMIC ANALYSES

In order to know the seismic linear behaviour of masonry towers, the main vibration periods deriving from the 3MURI analyses have been compared with those achieved from the following relationships: - $T = 0.05 \cdot H^{3/4}$, derived from M.D. 14/01/08 (2008); - $T = 0.013 \cdot H^{1.10}$, provided by Rainieri et al. (2014); - $T = 0.06 \cdot \frac{H}{\sqrt{B}}\sqrt{\frac{2H}{2B+H}}$, derived from the Ministerial Circular of Public Works 24/05/82 n. 22631 (1982); - $T = 0.2 \div 0.25 \cdot \sqrt{\frac{H}{B}}$, provided in Di Gennaro (2010). The comparison among numerical curves and those derived from the previous equations is reported in Figures 3 and 4 as vibration period T vs. tower height H and as vibration period T vs. tower slenderness λ (overall height/width), respectively.

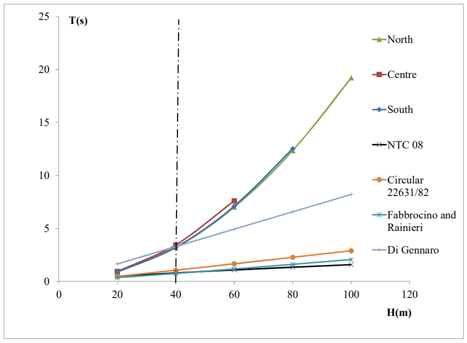

FIGURE 3. Numerical-theoretical comparison of vibration period T vs. tower height H curves

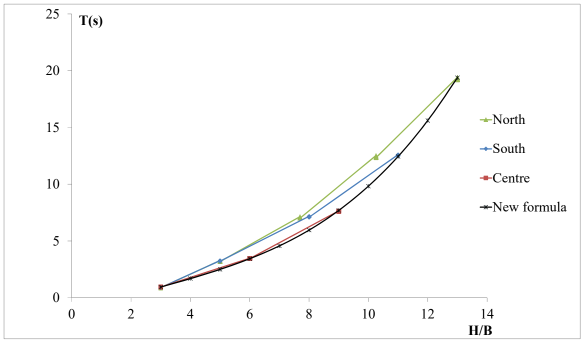

FIGURE 4. Vibration period T vs. tower slenderness λ numerical curves

From this comparison it is seen that the vibration period values calculated with the above formulas are too on the safe side, since they largely underestimate the T values achieved with the 3MURI software. Moreover, the formula that better approaches the trend of the 3MURI curve is the eq. found in Di Gennaro (2010). Nevertheless, for tower height less than 40 m, this relationship provides unsafe results, with vibration periods greater than numerical ones. Contrary, for heights greater than 40 m, the results are better than those provided by the other formulas and are more close to the 3MURI ones.

In conclusion, after this comparative comparisons, a new theoretical third degree polynomial formula (eq. 1) has been proposed to calculate the vibration period T as a function of the tower slenderness λ. This new relationship is able to predict on the safe side the towers vibration period, since it envelopes inferiorly the 3MURI analysis curves.

$$T = 0.0117\left(\frac{H}{B}\right)^3 - 0.1127\left(\frac{H}{B}\right)^2 + 1.109\frac{H}{B} - 1.6902 \quad (1)$$

CONCLUSIONS

In the current paper, an extensive parametric numerical analysis by using the 3MURI software has been performed on some case studies representative of Northern, Central and Southern areas of Italy. Non-linear static and linear dynamic analyses have been carried out on forty specimens of masonry towers having fixed plan layouts and different geometrical properties in terms of total height and thickness.

From non-linear static analyses, it has been found that the base shear increasing with the thickness is similar for Northern and Southern Italy structures, whereas this trend is slightly less marked for Central Italy towers. Moreover, the stiffness of pushover curves strongly increases with the thickness for towers having height of 20 m only, while for larger heights this augment is not considerable. The pushover analysis results have been evaluated also in terms of the ratio between the capacity acceleration and the demand one, which has been evaluated for some towers of several Italian regional capitals. These seismic checks have been always satisfied, except for towers of L'Aquila and Campobasso. Moreover, Central Italy towers have the lowest average safety factors, with values similar to those of Southern Italy ones.

Finally, linear dynamic analyses have been performed by with the purpose to compare the achieved main vibration periods with those deriving from four literature relationships. From this comparison, it has been obtained that literature formulas provide largely on the safe side periods. In addition, the relationship providing the best prediction of periods is that found in Di Gennaro (2010). In conclusion, based on the 3MURI analysis results, a new third order polynomial formula has been proposed to calculate the main vibration period of towers made of light squared stone towers as a function of their slenderness.

REFERENCES

1. S. Casolo, Significant ground motion parameters for evaluation of the seismic performance of slender masonry towers, Journal of Earthquake Engineering **5**(2), 187-204 (2010).
2. A. Di Gennaro, *Approximate relationships of the fundamental vibration period of building structures* (in Italian), Scientific Technical Committee, Engineers Order of the Province of Rome (2010).
3. J. Heyman, Leaning Towers, Meccanica **27**, 153 – 159 (1992).
4. S. Ivorra and F.J. Pallares, Dynamic investigations on a m*asonry bell tower, Eng. Struct.* **28**, 660–667 (2006).
5. P. B. Lourenço, Assessment, diagnosis and strengthening of Outeiro Church, Portugal, Constr. Build. Mater. **19**, 634–645 (2005).
6. Ministerial Circular (M. C.) of Public Works n. 22631, *Instructions related to loads, live loads and criteria for safety checks of constructions* (in Italian), Rome, Italy, 1982.
7. Ministerial Circular (M. C.) of Public Works n. 617, *Instructions for the application of the "New technical codes for constructions"* (in Italian), Official Gazette of the Italian Republic n. 47 published on 2009, February 26th, Rome, Italy, 2009.
8. Ministerial Decree of Public Works (NTC08), *New Technical codes for constructions – M.D. 14/01/08* (in Italian), Official Gazette of the Italian Republic published on 2008 January 14th, Rome, Italy, 2008.
9. C Modena, M.R. Valluzzi, F.R. Tongini and L. Binda, Design choices and intervention techniques for repairing and strengthening of the Monza cathedral bell-tower, Constr. Build. Mater. **16**, 385–395 (2002).
10. F. Pena, P.B. Lourenço, N.Mendez and D. Oliveira, Numerical models for the seismic assessment of an old masonry tower, Engineering Structures, 32, 1466-1478 (2010).
11. C. Rainieri, A. Marra and G. Fabbrocino, On The Estimation of the Fundamental Modal Properties of Italian Historical Masonry Towers. International Journal of Earthquake Engineering **31** (3), 1-15 (2014).
12. V. Sarhosis, F. Fabbrocino, A. Formisano and G. Milani, Seismic vulnerability of different in geometry historic masonry towers, *COMPDYN 2017 - Proceedings of the 6th International Conference on Computational Methods in Structural Dynamics and Earthquake Engineering* 1, Rhodes, 15-17 June 2017, pp. 2519-2532.
13. V. Sarhosis, G. Milani, A. Formisano and F. Fabbrocino, Evaluation of different approaches for the estimation of the seismic vulnerability of masonry towers, Bulletin of Earthquake Engineering **16** (3), 1511-1545 (2018).
14. S.T.A.DATA., *3MURI - Seismic calculation of masonry structures according to the Italian Ministerial Decree 14/01/2008 "New technical codes for constructions"*, Turin, Italy, 2016.
15. F. Ubertini, N. Cavalagli, A. Kita and G. Comanducci, Assessment of a monumental masonry bell-tower after 2016 central Italy seismic sequence by long-term SHM, Bulletin of Earthquake Engineering **16** (2), 775-801 (2018).

Irrecoverable Collapse Time for a Fixed-Hinge Dry-Stack Arch Under Constant Horizontal Acceleration

Gabriel Stockdale[1, a)] Gabriele Milani[1, b)] and Vasilis Sarhosis[2, c)]

[1] *Department of Architecture, Built Environment and Construction Engineering (ABC), Politecnico di Milano, Piazza Leonardo da Vinci 32, 20133 Milan, Italy*

[2] *School of Civil Engineering, University of Leeds, LS2 9JT, United Kingdom*

[a)]Corresponding author: gabriellee.stockdale@polimi.it
[b)]gabriele.milani@polimi.it
[c)] vesilis.sarhosis@newcastle.ac.uk

Abstract. The collapse of dry-stack masonry arches results from the transformation of a static system to a mechanical state through the development of mechanical joints. The traditional failure condition is this mechanization through the formation of four-hinges in a kinematically admissible configuration. The first-order analysis of an arche's seismic capacity is obtained through limit analysis (LA) approaches. One approach is the equilibrium assessment of the kinematic theorem through the use of a kinematic collapse load calculator (KCLC). Utilizing a custom KCLC developed and validated from an experimental arch, with the added control of the single degree-of-freedom rotations, an analytic solution is developed between the applied acceleration and the minimum time duration required for collapse. The collapse multiplier and arch centroid data is recorded for all the admissible conditions that exist in the spatial deformation propagation. From this information, the work required to collapse the arch under kinematic equilibrium is established and utilized to decompose the static and kinematic energy contributions. The time-displacement domain is then defined from the resulting kinematic energy of the overloaded arch and used to evaluate the time where the kinematic energy exceeds the remaining work required for the loss of the kinematically admissible condition. This results in a simple analytical function linking excess static acceleration with a time limit of recovery.

INTRODUCTION

The seismic assessment and understanding of masonry arches is critical for the preservation of existing systems, but it is also vitally important for the reintroduction of dry-stack masonry arches as a modern structural alternative. In the modernization approach, the evaluation and understanding is isolated into two key components. The first component is the ability to design and define the failure, and the second is to quantify that designed failure. For dry stack masonry arches the ability to design and define has been proposed and statically tested [1,2]. In this process of modernization, the development of the Kinematic Collapse Load Calculator has begun, and its ability to efficiently analyze and adapt has been established [3,4]. The KCLC is a calculator that allows the user to define the boundary and load conditions. It then performs kinematic equilibrium-admissibility evaluations and displays the various results such as reactions, collapse value, and coordinates.

The KCLC provides static equilibrium analyses on a geometric configuration of the mechanical arch. Through the incorporation of the failure motion of the arch, the equilibrium analysis is applied to the specially deformed condition of motion. From this condition, the displacement domain of energy and work can be established.

The objective of this research is to establish the first time-domain analysis condition for the failure of a hinge-defined dry-stack masonry arch through the evaluation of excessive horizontal acceleration, kinematic equilibrium and standard arch-failure deformations.

KCLC AND DEFORMATION CAPACITY

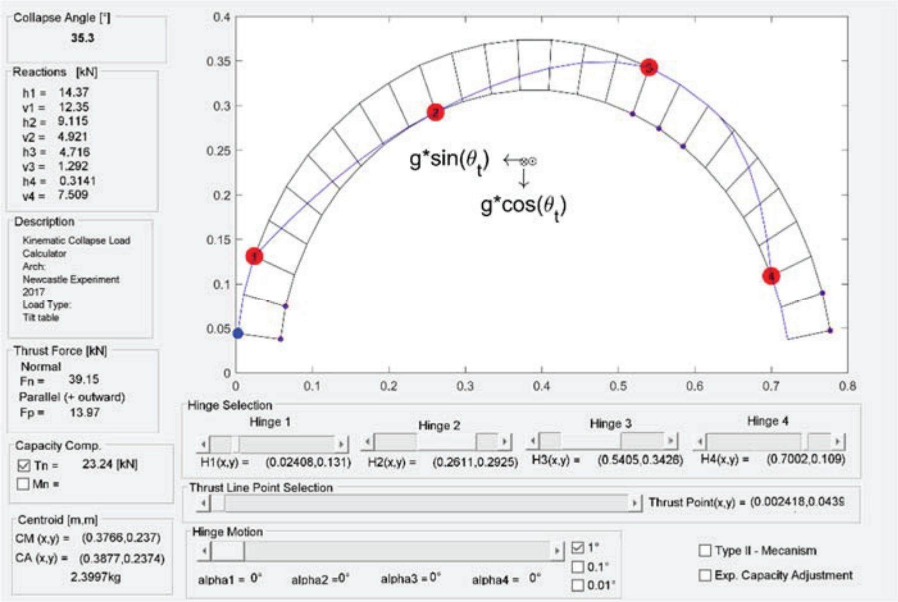

FIGURE 1. The custom KCLC, arch and hinge configuration used in this work.

Figure 1 shows the custom and validated KCLC for an experimental arch with the added hinge motion panel and centroid position display [3,4]. Considering the kinematic motion of rigid elements, the arch-hinge configuration can be represented by three fixed lengths connected by four pins as seen in Fig. 2. The deformation of the system can then be represented by the rotation of the pins and is bound by a SDOF of motion.

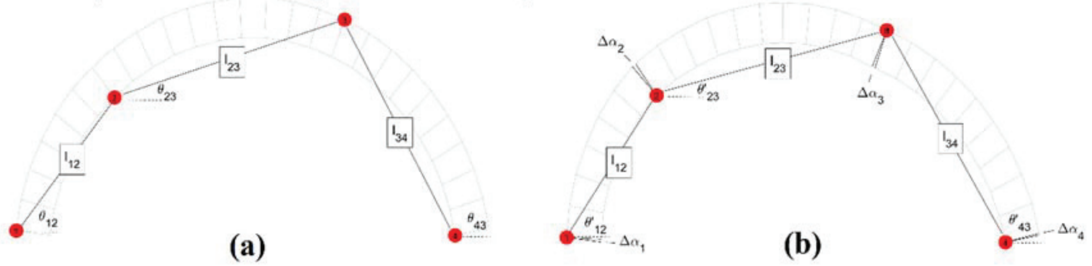

FIGURE 2. Four-pin arch mechanism (a) before and (b) after a SDOF deformation.

For a given rotation, $\Delta\alpha_1$, at H_1 (see Fig. 2) the remaining rotations can be determined by

$$\begin{aligned} \Delta\alpha_4 &= \cos^{-1}\left(\frac{l_{12}}{l_{34}}\left[\cos(\theta_{12}+\Delta\alpha_1)-\cos(\theta_{12})\right]+\cos(\theta_{43})\right)-\theta_{43} \\ \Delta\alpha_2 &= \Delta\alpha_1+\theta'_{23}-\theta_{23} \\ \Delta\alpha_3 &= \Delta\alpha_4+\theta'_{23}-\theta_{23} \end{aligned} \tag{1}$$

For each deformation applied to the arch-hinge configuration, the kinematic equilibrium and admissibility is evaluated, and the results displayed (see Fig. 3)

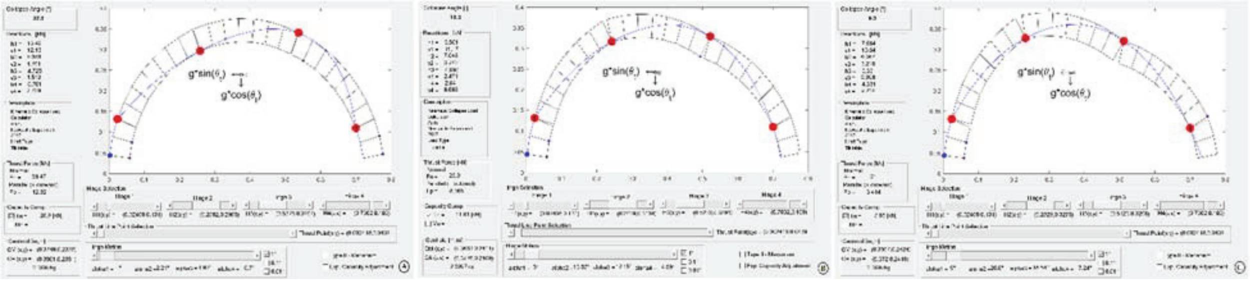
FIGURE 3. A (a) 1°, (b) 6°, and a (c) 9° α_1 rotation applied to the arch-hinge system shown in Fig. 1.

Using the alpha rotation parameter and the added CM coordinate display, the collapse force and center of mass (CM) position was recorded for the range of admissible deformations. The resulting force versus horizontal CM displacement and CM displacement slope verses horizontal displacements are shown in Figure 4.

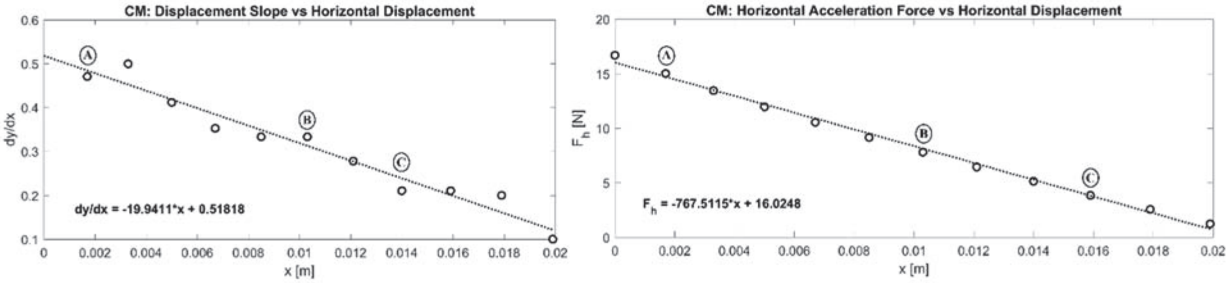

FIGURE 4. CM displacement slope and acceleration force versus horizontal displacement.

WORK AND ENERGY CONSERVATION

From the deformation capacities the work required to deform the arch to collapse can be determined as shown in Fig. 5. From Fig. 5 the required work to maintain equilibrium along the deformed path, W_h, is greater than the change in gravitational potential, U_g. It is postulated that the difference is the result of stored energy required to create and maintain the kinematic state itself. Nonetheless, the required work to maintain kinetic equilibrium establishes a cutoff condition where the conservation of energy dictates that any additional energy added to the system as work is in the form of kinetic energy. Starting from rest the change in kinetic energy becomes

$$\Delta K_E = W_{app} - W_h = \int \left(F_{app} - F_h\right) dx \tag{2}$$

for any applied work, W_{app}, from a horizontal acceleration force, F_{app} that is greater than F_h. Additionally, if at a displacement x' the applied force drops below F_h, with a resulting kinetic energy K_E' then the condition

$$K_E' < \int_{x'}^{x_c} \left(F_{app} - F_h\right) dx \tag{3}$$

will result in a recoverable system.

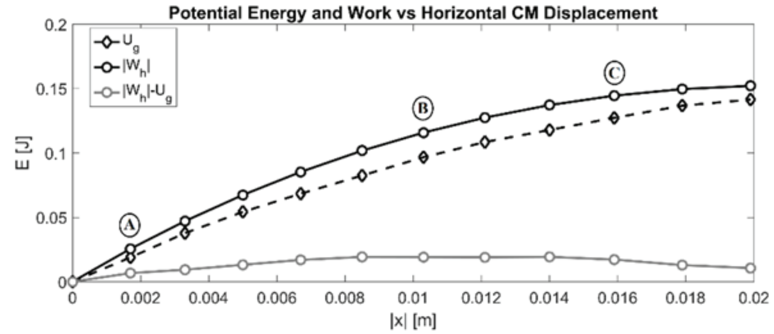

FIGURE 5. Potential Energy and Work required to deform the arch to a non-admissible configuration.

TIME DOMAIN

Starting from rest at time t_0 and a given load/displacement condition that results in a kinetic energy,

$$K_E(x) = \frac{1}{2} m \boldsymbol{v}^{\mathbf{2}} = \int \left(F_{app} - F_h\right) dx \tag{4}$$

the time domain can be introduced,

$$\left(\frac{dr}{dt}\right)^2 = \frac{1}{m} K_E(x) \tag{5}$$

From the linear slope-displacement representation if Fig. 4, and radial-Cartesian vector relations, the relationship between displacement and time becomes

$$\int_0^x \sqrt{\frac{m[A^2x^2 + 2A(1+B)x + (1+B^2)]}{K_E(x)}}\, dx = (t - t_0) \tag{6}$$

where A and B are the slope and constant fits to the linear slope-displacement equation in Fig. 4.

Constant Horizontal Acceleration

Consider a constant horizontal force for a duration of time t_d

$$F_{app} = \begin{cases} C' = C - F_h(0) \geq 0, & 0 \leq t \leq t_d \\ 0, & t > t_d \end{cases} \tag{7}$$

then the root function inside the integral of Eqn. 6 becomes

$$f_{KE}(x) = \sqrt{\frac{m[A^2x^2 + 2A(1+B)x + (1+B^2)]}{(C' - A'x)x}} \tag{8}$$

with A' as one-half the slop constant from the force-displacement linear fit equation. Figure 6 shows the plot of Eqn. 8 for the recorded displacements with the areas identified for the numerical evaluation of the integral in Eqn. 6. The results of the integration are also shown in Fig. 6 and the fitted result establishes a fifth-degree polynomial displacement-time relationship for the condition C' = 0.

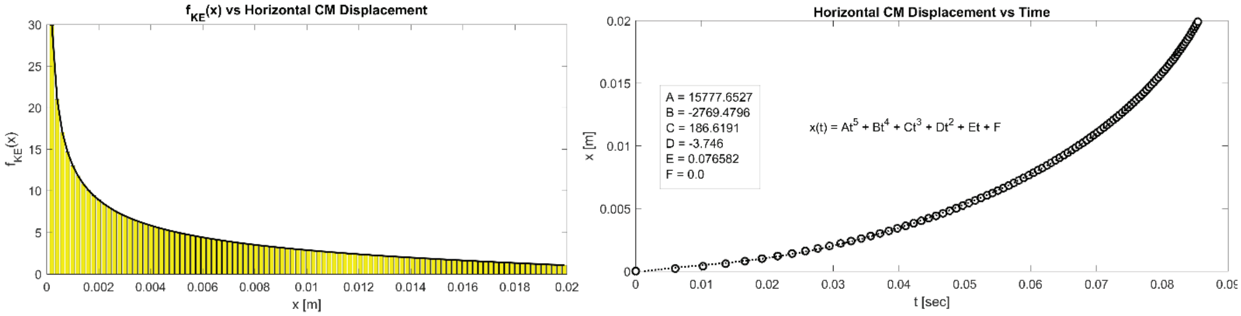

FIGURE 6. Plots of $f_{KE}(x)$ versus horizontal CM displacement and the resulting displacement-time plot for C' = 0.

Figure 7 shows the intersecting plots of kinetic energy and required work, W_{req}, for collapse verses time for variations of C'. This intersection of the energies is identified and establishes the time when the kinetic energy will exceed remaining work. Figure 7 also shows the establish irrevocable collapse time equation for the given arch-hinge configuration in Fig. 1 subjected to a constant acceleration that initiates mechanical deformation. That function is

$$t = 4.651 a_c^{0.7519} \tag{9}$$

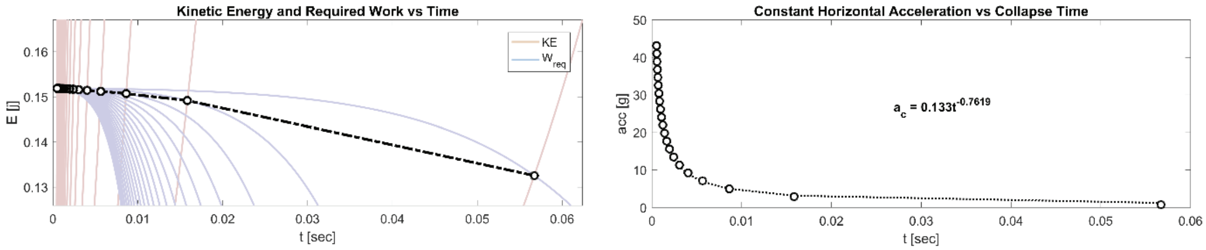

FIGURE 7. Kinematic-required work intersections and the resulting acceleration versus collapse time plot and fit.

REFERENCES

1. G. Stockdale, *Reinforced stability-based design: a theoretical introduction through a mechanically reinforced masonry arch*. International Journal of Masonry Research and Innovation, **1**(2), 101-142 (2016).
2. G. Stockdale, V. Sarhosis, and G. Milani, "Increase in seismic resistance for a dry joint masonry arch subjected to hinge control" in *10th IMC Conference Proceedings*, International Masonry Society, (2018) pp. 968-981
3. G. Stockdale, S. Tiberti, D. Camilletti, G. Papa, A. Habieb, E. Bertolesi, G. Milani, S. Casolo, *Kinematic collapse load calculator: Circular arches*, SoftwareX, **7,** 174-179 (2018)
4. G. Stockdale, V. Sarhosis, G. Milani, *Seismic Capacity and Multi-Mechanism Analysis for Dry-Stack Masonry Arches Subjected to Hinge Control*, Bull Earthq Eng, DOI: 10.1007/s10518-019-00583-7 (2019) pp. 1-52

Three-Dimensional Analysis of A Damaged Masonry Arch Bridge under Horizontal Load

Nicola Grillanda[1, a)] Gabriele Milani[1, b)], Marco Nale[2, c)], Andrea Chiozzi[2, d)] and Antonio Tralli[2, e)]

[1]*Department of Architecture, Built Environment and Construction Engineering (A. B. C.), Polytechnic University of Milan, Piazza Leonardo da Vinci 32, 20133, Milan, Italy.*
[2]*Department of Engineering, University of Ferrara, Via Saragat 1, 44122, Ferrara, Italy.*

[a)]nicola.grillanda@polimi.it
[b)]Corresponding author: gabriele.milani@polimi.it
[c)]marco.nale@unife.it
[d)]andrea.chiozzi@unife.it
[e)]tra@unife.it

Abstract. The aim of this paper is to study the vulnerability to horizontal loads of a severely damaged masonry arch bridge located in the province of Ascoli Piceno (Marche, Italy). The bridge is a traditional single-span masonry arch designated as road bridge. A wide fracture line has been observed along the longitudinal direction. The arch has been studied by applying two distribution of horizontal loads directed in the longitudinal and the transversal directions separately. A new upper bound limit analysis recently developed by the cooperation of the Polytechnic University of Milan and the University of Ferrara has been adopted. For the case of horizontal load acting along the longitudinal direction, the capacity curve and the associated fragility curve are presented.

INTRODUCTION

The theoretical background on the analysis of masonry bridges, or more in general the theory of masonry arches, has been developed essentially by Heyman [1]. In the first studies, a masonry arch was studied by idealizing masonry as a no-tension material [2] adopting the lower bound theorem of limit analysis. Several numerical techniques have been adopted in the year in order to perform analyses of arches even without taking into account the no-tension material (the reader is referred to [3]). Starting from this theoretical background, some practical software has been produced (such as Ring2.0 [4] and ArchNURBS [5]). However, only 2D analyses can be performed through these applications, and eventual damage states cannot be taken into account. The first work focused on a full three-dimensional (3D) analysis on masonry bridges has been proposed by Milani and Lourenço [6,7], in which a FE-based nonlinear approach is adopted. As concern damage, despite it is a typical condition [8], in the past only a few works have been found about damaged masonry bridge [9]. Moreover, in a few works analyses under horizontal load are shown, even if recently seismic event proved the high vulnerability of masonry constructions to this type of actions [10–14]. In this paper, a damaged masonry arch bridge located in Ascoli Piceno (Marche, Italy) is analyzed under horizontal loads. A new method developed by the cooperation of the Polytechnic University of Milan and the University of Ferrara has been adopted. This method, which relies on NURBS geometry, upper bound limit analyses and Genetic Algorithm, allows performing 3D analyses taking into account damage in an easy way. For one of the applied analyses, the capacity curve of the arch and the corresponding fragility curve are presented.

ANALYSIS OF THE BRIDGE

The road bridge of Ascoli Piceno (Marche, Italy) is a traditional single-span semicircular masonry arch composed by arenaceous rock bricks (Fig. 1(a)). The arch is described by an internal span of 6 m, a thickness of 30 cm and a width of 7 m. The backfill is mainly made by gravel and its height is 4.2 m relatively to the center of the arch. All information about materials (and therefore, the applied dead-loads), included parapets (cross section: 1.02 m × 0.4 m), concrete (cross section area: 0.675 m^2) and asphalt (thickness: 0.15 cm), are reported in Table 1.

A certain level of degradation has been observed on the bridge. The worst damage is the wide fracture line (above 2 cm) which involves the whole intrados of the arch along the longitudinal direction (see Fig. 1 (b)). A detailed survey of the damage state has not been provided. However, this fracture is located close to the edge of the arch under the cantilever concrete block (Fig. 1 (c)). It is Author's opinion that the main reason for this damage is a combination of a higher weight applied on this portion of the arch (the concrete block) and repeated traffic loads.

A series of tests aimed at the evaluation of the crushing load of the masonry bricks have been carried out. No data have been provided about the mortar. Therefore, the ultimate compressive stress of masonry has been estimated by combining the obtained ultimate loads of bricks with the properties a low quality mortar, as described in the Italian building code [15]. The final mechanical parameters adopted for the masonry material are reported in Table 1.

The bridge has been analyzed by applying a horizontal acceleration proportional to the vertical weight applied. The procedure has been developed through an adaptive limit analysis approach developed with the cooperation of the Polytechnic University of Milan and the University of Ferrara. This method is based on the representation of the geometry through NURBS surfaces (Non-Uniform Rational B-Spline), the idealization of elements as perfectly rigid with plastic dissipation allowed only along interfaces, an upper bound formulation and the optimization of the kinematic multiplier through a Genetic Algorithm. In this way, the correct failure mechanisms and collapse load multiplier are found. Extended details about this method and applications can be found in the technical literature [16–21]. In this procedure, the fracture line observed along the longitudinal direction has been modeled as "fixed interface" in with lower ultimate stress values have been assigned. Two different limit analyses have been performed, in which the horizontal load has been applied along the longitudinal and the transversal direction separately. Results, in terms of collapse mechanism and load multiplier, are depicted in Fig. 2.

In both cases, the final collapse involves only the portion of the arch in which a higher weight is applied, i.e. the portion which supports the cantilever concrete block. In the case of transversally loaded arch, shear assumes a relevant role in the collapse mechanisms, whereas in the other case a traditional flexural mechanism of the external arch has been obtained (as can be seen in Fig. 2). On the result obtained by considering longitudinal horizontal load, a kinematic non-linear analysis, in which geometry has been modified step by step according to the obtained mechanism, has been performed. In this way, and according to the Italian code prescriptions [15], the capacity curve described by spectral acceleration and ultimate displacement has been determined (see Fig. 3(a)). Moreover, the fragility curve associated with this failure has been determined by adopting a method similar to which described in [22,23]. By adopting the Multiple Stripe Analysis [24], time-history analyses are performed at a specific set of IM levels, i.e. peak ground acceleration (PGA) values, each of which corresponds to one of the 11 ground motions sets considered. The obtained fragility curve is the lognormal cumulative distribution function which best approximates these values (see Fig. 3 (b)). Here, the maximum likelihood has been adopted for the estimation of the central tendency (μ) and the dispersion (β) parameters [25].

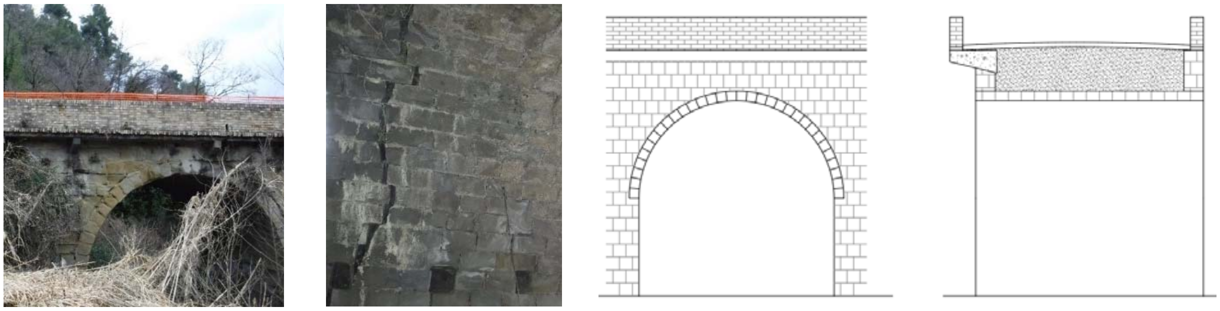

(a) (b) (c)

FIGURE 1. The masonry arch bridge of Ascoli Piceno: (a) perspective view, (b) intrados of the arch, (c) CAD perspective drawing and transversal section at the midpoint.

TABLE 1. Physical and mechanical parameters adopted.

Material	Specific weight [kN/m³]	Tensile strenght [MPa]	Compressive strength [MPa]	Cohesion [MPa]	Friction angle [°]
Masonry of the arch	22	0.2	7.2	0.2	31
Backfill (gravel)	16	-	-	-	-
Parapets	18	-	-	-	-
Concrete	25	-	-	-	-
Asphalt	13	-	-	-	-

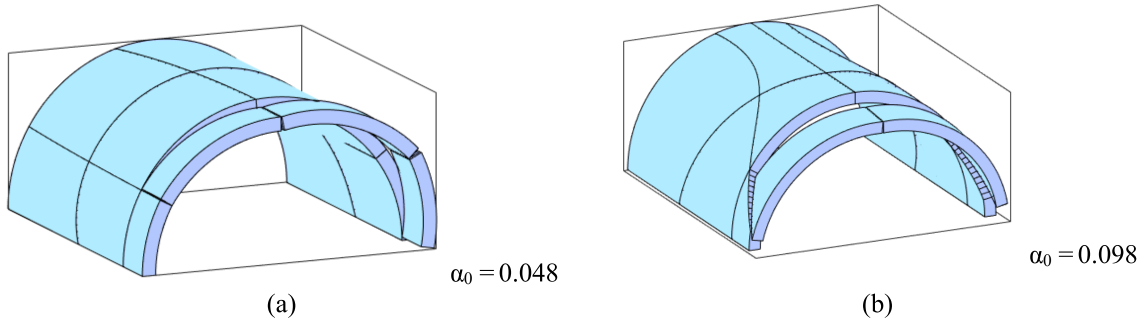

FIGURE 2. Failure mechanisms and horizontal load multipliers α_0 obtained: horizontal load acting along (a) the longitudinal and (b) the transversal direction.

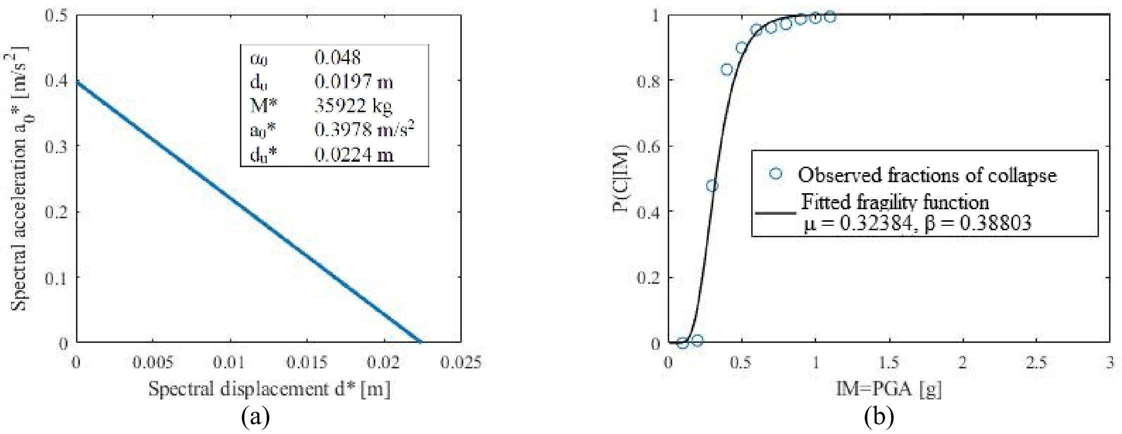

FIGURE 3. Collapse along the longitudinal direction: (a) capacity curve and (b) fragility curve.

CONCLUSIONS

A 3D analysis on a damaged single-span masonry arch bridge has been presented. A new method based on NURBS and upper bound limit analysis has been applied. A collapse in which only the weaker part of the structure is involved has been obtained. The adopted method has proven to more effective than the available software for masonry arches, in which only 2D evaluations can be performed and damage states cannot be taken into account. Moreover, the versatility of this approach allowed obtaining also the capacity curve and the fragility curve for one collapse mechanism under longitudinal horizontal load in an easy way.

ACKNOWLEDGMENTS

The results of the experimental tests on masonry bricks have been provided for us by the AZ Consulting & Commercial Engineering SRL. Their professional help is recognized with gratitude by all Authors.

REFERENCES

1. J. Heyman, *The Masonry Arch* (Horwood, 1982).
2. J. Heyman, "The stone skeleton", Int. J. Solids Struct. **2**, 249–56 (1966).
3. M. Gilbert, "Limit analysis applied to masonry arch bridges : state-of-the-art and recent developments", in ARCH'07 5th International Arch Bridges Conference (2007), pp. 13-28.
4. M. Gilbert, "RING : A 2D rigid-block analysis program for masonry arch bridges", International Arch Bridges Conference, (2001), pp. 459-464.
5. A. Chiozzi, M. Malagù, A. Tralli and A. Cazzani, "ArchNURBS: NURBS-Based Tool for the Structural Safety Assessment of Masonry Arches in MATLAB", J. Comput. Civ. Eng., **30** #401501, 1–11 (2016).
6. G. Milani, P.B. Lourenço, "3D non-linear behavior of masonry arch bridges", Comput. Struct., **110**, 133–50 (2012).
7. E. Reccia, G. Milani, A. Cecchi and A. Tralli, "Full 3D homogenization approach to investigate the behavior of masonry arch bridges: The Venice trans-lagoon railway bridge", Constr. Build. Mater. **66**, 567–86 (2014).
8. B. Harvey, "Stiffness and damage in masonry bridges", Proceedings of the Instution of Civil Engineers-Bridge Engineering, (Tomas Teldford Ltd., 2012), pp. 127–34.
9. T. Kamiński and J. Bień, "Application of kinematic method and FEM in analysis of ultimate load bearing capacity of damaged masonry arch bridges", Proc. Eng., **57**, 524–32 (2013). doi:10.1016/j.proeng.2013.04.067.
10. M. Valente and G. Milani, "Damage assessment and partial failure mechanisms activation of historical masonry churches under seismic actions: Three case studies in Mantua", Eng. Fail. Anal. **92**, 495–519 (2018).
11. M. Valente and G. Milani, "Seismic response and damage patterns of masonry churches: seven case studies in Ferrara, Italy". Eng. Struct., **177**, 809–35 (2018).
12. M. Valente and G. Milani, "Damage survey, simplified assessment, and advanced seismic analyses of two masonry churches after the 2012 Emilia earthquake", Int. J. Archit. Herit., (2018). In press. https://doi.org/10.1080/15583058.2018.1492646.
13. M. Valente and G. Milani, "Damage assessment and collapse investigation of three historical masonry palaces under seismic actions", Eng. Fail. Anal., **98**, 10–37 (2019).
14. M. Valente and G. Milani, "Earthquake-induced damage assessment and partial failure mechanisms of an Italian Medieval castle", Eng. Fail. Anal. **99**, 292–309 (2019).
15. NTC2018. D.M. 17/01/2018 Aggiornamento delle «Norme tecniche per le costruzioni». S.O. alla G.U. n. 42 del 20/02/2018; 2018. n.d.
16. A. Chiozzi, G. Milani and A. Tralli, "A Genetic Algorithm NURBS-based new approach for fast kinematic limit analysis of masonry vaults", Comput. Struct., **182**, 187–204 (2017).
17. A. Chiozzi, G. Milani, N. Grillanda and A. Tralli, "An adaptive procedure for the limit analysis of FRP reinforced masonry vaults and applications", Am. J. Eng. Appl. Sci., **9**, 735–45 (2016).
18. A. Chiozzi, G. Milani, N. Grillanda and A. Tralli, "Fast and reliable limit analysis approach for the structural assessment of FRP-reinforced masonry arches", Key Eng. Mater., **747**, 196–203 (2017).
19. A. Chiozzi, G. Milani, N. Grillanda and A. Tralli, "A fast and general upper-bound limit analysis approach for out-of-plane loaded masonry walls", Meccanica, **53**, 1875–98 (2018).
20. A. Chiozzi, N. Grillanda, G. Milani and A. Tralli, "UB-ALMANAC: An adaptive limit analysis NURBS-based program for the automatic assessment of partial failure mechanisms in masonry churches", Eng. Fail. Anal., **85**, 201–20 (2018).
21. N. Grillanda, A. Chiozzi, F. Bondi, A. Tralli, F. Manconi, F. Stochino, and A. Cazzani, "Numerical insights on the structural assessment of historical masonry stellar vaults: the case of Santa Maria del Monte in Cagliari", Contin. Mech. Thermodyn. 1–24 (2019).
22. G. Tecchio, M. Donà and F. da Porto, "Seismic fragility curves of as-built single-span masonry arch bridges", Bull. Earthq. Eng., **14**, 3099–124 (2016).
23. A. Chiozzi A, M. Nale and A. Tralli, "Fragility assessment of non-structural components undergoing earthquake induced rocking motion", in XVII Convegno ANIDIS-L'ingegneria Sismica in Italia (Pisa, University Press, 2017), pp. 449–58.
24. F. Jalayer, *Direct probabilistic seismic anaysis: implementing non-linear dynamic assessments* (Stanford, Stanford University, 2003).
25. J.W. Baker. "Efficient analytical fragility function fitting using dynamic structural analysis", Earthq. Spectra, **31**, 579–99 (2015).

Experimental and Numerical Analysis of the Effectiveness of FRCM Strengthening on a Parabolic Tuff Barrel Vault

Jacopo Scacco [1, a)], Gabriele Milani [1, b)], Martino Bove [2,c)], Anna Castellano [3,d)], Aguinaldo Fraddosio [2,e)], Mario Daniele Piccioni [2,f)]

[1]Department of Architecture, Built Environment and Construction Engineering ABC, Politecnico di Milano, Piazza Leonardo da Vinci 32, 20133, Milan, Italy
[2]Dipartimento di Scienze dell'Ingegneria Civle e dell'Architettura, Politecnico di Bari, Via Orabona 4, 70125 Bari, Italy
[3]Dipartimento di Meccanica, Matematica e Management, Politecnico di Bari, Viale Japigia 182, 70126, Bari, Italy

[a)]jacopo.scacco@polimi.it, [b)]gabriele.milani@polimi.it, [c)]martino.bove@libero.it, [d)]anna.castellano@poliba.it, [e)]aguinaldo.fraddosio@poliba.it, [f)]mariodaniele.piccioni@poliba.it

Abstract. An experimental and numerical analysis of a tuff barrel vault is here proposed. The work focused on the structural behavior of a vault built in accordance with the traditional buildings of Apulia region. At first, the response of the unreinforced vault was explored under the imposition of a vertical settlement of the abutment. Afterwards, the system has been reinforced at the extrados by means of a Basalt FRCM, in order to define the capacity of the reinforced structure when subjected to an asymmetrical load condition. As the latter experimental stage is still in progress, advanced numerical simulations through Abaqus were carried out in order to reproduce the settlement step and to predict a reliable peak load that may be experienced by the reinforced vault. An heterogeneous micro modeling approach was defined, applying the Concrete Damage Plasticity model to the cementitious matrix and in the mortar joints. The tuff vouissors were assumed as purely elastic, whereas the fibers were modeled with an elastic-brittle behavior.

INTRODUCTION

Barrel vaults, along with arches and other typologies of vaults, stand for the most charming features of historical masonry constructions, as churches, castles and palaces. However, as well known by the evidence and the literature, the marked weakness in tension of masonry may lead to the occurrence of damages, which riskiness is depending on several aspects. For instance, unsymmetrical load and displacement scenario could affect the integrity of the structures, until the extreme condition of a collapse as soon as a sufficient number of "hinges" is reached (Heyman, 1966).

In the context of strengthening of heritage structures, where conservation principles [1] have to be attained, the external application of composites have resulted to be successful. Especially, the use of inorganic matrix in place of an organic one, ensures good performances in terms of mechanical and compatibility properties.

If in literature the behavior of curved masonry elements reinforced by means of FRP has been widely tested, on the contrary, still few experimental analysis [2]–[5] have been carried out on arches and vaults reinforced with TRM (FRCM). The results are still not enough in order to define a typical structural behavior, as the great heterogeneity of variables, including the materials and shape of masonry elements and the wide range of properties of the reinforcement.

The present paper wants to give a further contribution in the field, proposing experimental and numerical approaches. A barrel vault, resembling typical materials and geometrical configuration of Apulia region, has been tested under a vertical settlement of one abutment in order to reproduce the damage induced by foundation settlements, highlighting the weakness points. Subsequently, the reinforcement has been applied on the extrados of the vault with the aim to investigate the increase capacity against further future external actions. The second phase, still in progress, wants to explore the effectiveness of the intervention until the collapse is reached, under the imposition of an unsymmetrical concentrated force. In order to reproduce numerically the settlement test and to predict a probable peak load to be applied on the vault, numerical analysis by means of detailed micro modelling approach have been carried out through commercial software Abaqus.

EXPERIMENTAL INVESTIGATION

a) Frontal view of the barrel vault

b) Lateral view of the barrel vault

FIGURE 1: The experimented barrel vault

The process of constructions was carried out at Laboratorio Ufficiale Prove Materiali "M. Salvati" of Politecnico di Bari. In the realization of the vault, a shape with a polycentric profile was obtained, in order to reproduce the parabolic feature of masonry vaults peculiar to Apulia region **(Fig. 1 a-b**), resulting in a span of 346 cm, a height of 120 cm, and a depth of 72 cm. With a consistent approach, also the material of voussoirs (12x15 cm) is strictly linked to the Apulia territory, being tuff coming from the caves of Gravina in Puglia.

The vault is supported at the base by means of two steel beams, with one of these placed on a hydraulic jack, making possible the application of an asymmetrical vertical displacement. In the final stage of the construction, the filling is simulated though the placement of 40 sandbags with a total weight of 840 kg, taking advantage of their easy removability for the subsequently strengthening.

Afterwards, an experimental campaign has been conducted, involving the settlement analysis on the unreinforced vault and a study of the effectiveness of the reinforcement under an asymmetrical concentrated force. The differential settlement phase was conducted by a gradual adjusting of the pressure in the jack placed under the right support, checking at the end of each step the damage pattern. The test was stopped in correspondence of a global displacement of 17 mm. In fact, at this value, hinges occurred in positions comparable to a collapse mechanism described in [6]. More specifically two extrados cracks appeared at joints between stones 14-15 and 11-10, while one intrados crack at the joint between vouissors 23-24.

The second stage of the experiment, still in progress, will be devoted to the analysis of the increasing of capacity in terms of peak strength and maximum displacement, after the application of FRCM reinforcement. The filling has been removed to allow the application of the strengthening of the FCRM made of two layers of cementitious matrix and a mesh of basalt fibers.

A prediction of a reliable behavior of the reinforced vault is provided by numerical analysis through FEM software Abaqus, as reported in the next section.

NUMERICAL ANALYSIS

Heterogeneous 2D Model: a Micro Modeling Approach

A detailed FE micro modeling approach is selected in order to reproduce properly the settlement stage and to predict the structural behavior of the vault under the imposition of a concentrated force. The heterogonous 2D model involves the separate modeling of the stones, the joints and the strengthening. Idealizing the stones as just elastic, the damage is assumed to spread in the joints and in the FRCM, by means of a constitutive model, already available in Abaqus, the Concrete Damage Plasticity, pretty suitable for brittle and quasi-brittle materials. CDP model assigns a parabolic softening under compression, and a linear softening in tension, where a fracture energy input is preferred to a stress-strain one in order to avoid mesh sensitivity issues. The fibers are modeled assuming an elastic-brittle response, and neglecting any contribute in compression.

In the meshing process, a more detailed discretization is addressed to the mortar joint, where at least two elements across the thickness are ensured. Tuff bricks results to be less defined, having only elastic properties. Linear plane 4-

nodes elements are used for the modeling of the arch. The mortar of the cementitious matrix is modeled in two different layers, of 7.5 mm each. In order to not have an excessively deformed mesh, both layers are modeled with only one element in the thickness, preferring, for this reason, the use of quadratic plane 8-nodes elements. The fibers are idealized as elastic-brittle 2-nodes trusses, with a section of the same amount of the total fibers applied on the extrados of the vault. All the elements are connected each other by means of a tie constrain, renouncing to model the premature debonding from the masonry substrate as its unlikely chance to occur.

Results

All the experimental stages are reproduced, starting from the application of the self-weight, followed by a distributed load simulating the filling. Subsequently the displacement analysis is conducted imposing a gradual vertical displacement at the base of the right abutment. The result in a qualitative way is quite comparable with the one detected during the test, highlighting damages at the intrados around the voussoirs 23-24, and at the extrados around the voussoir 10 (**Fig. 2**).

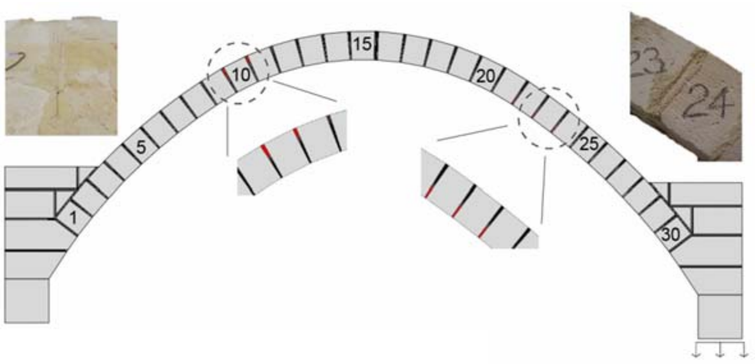

FIGURE 2. Damage pattern after the imposition of the vertical settlement

The reinforcement is then modeled upon the deformed configuration obtained in the previous analysis. In this second step, the behavior of the reinforced vaults is investigated by the application of a concentrate load at ¼ of the span, until the collapse (**Fig. 3**).

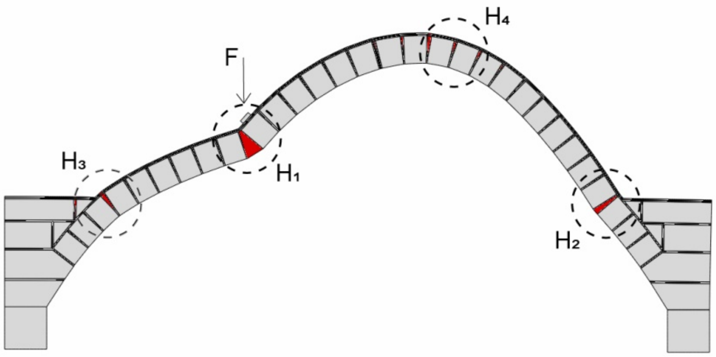

FIGURE 3. Localization of the four hinges in the collapse analysis

As shown in **Figure 4**, the structural behavior of the vault is mainly defined by four branches. An initial elastic response with a stiffness k equal to 10kN/mm is recorded until the occurring of the first hinge H1, in correspondence of the loaded point. Afterwards, the contribute of the fibers starts to be relevant, as it could be noticed in the second (k=4.1 kN/mm) and third branch (1.5 kN/mm). The reduction in stiffness of the global response is due to the opening of the second hinge H2 at the intrados of the right spandrel at 16 kN, and of the third hinge H3 at the extrados of the left spandrel. This latter configuration represents the peak load (22 kN) experienced by the vault with a capacity in displacement of 8 mm. The rupture of fibers starts from this point, involving later also the reinforcement in

correspondence of hinge four H4, leading to the collapse mechanism. Also an estimation of the behavior of the unreinforced model is provided in order to make a comparison in terms of increased capacity.

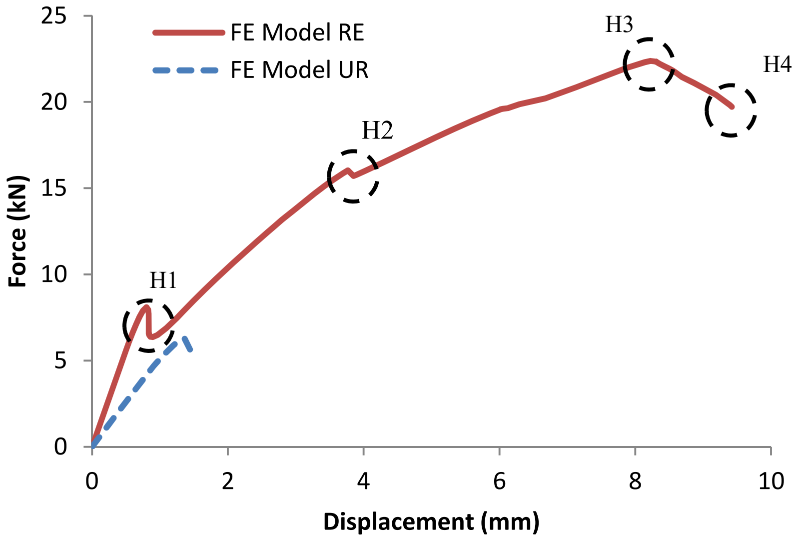

FIGURE 4. Graph Load-Displacement of reinforced and unreinforced vault

REFERENCES

1. The ICOMOS 14th General Assembly, "Icomos Charter- Principles for the Analysis , Conservation and Structural Restoration of Architectural Heritage (2003) Principles," *Archit. Herit.*, pp. 3–6, 2003.
2. L. Garmendia, I. Marcos, E. Garbin, and M. R. Valluzzi, "Strengthening of masonry arches with Textile-Reinforced Mortar: experimental behaviour and analytical approaches," *Mater. Struct. Constr.*, vol. 47, no. 12, pp. 2067–2080, 2014.
3. M. De Stefano, V. Alecci, F. Focacci, G. Stipo, and L. Rovero, "Extrados strengthening of brick masonry arches with PBO–FRCM composites: Experimental and analytical investigations," *Compos. Struct.*, vol. 149, pp. 184–196, 2016.
4. S. De Santis, F. Roscini, and G. de Felice, "Full-scale tests on masonry vaults strengthened with Steel Reinforced Grout," *Compos. Part B Eng.*, vol. 141, no. June 2017, pp. 20–36, 2018.
5. E. Bertolesi, F. G. Carozzi, G. Milani, and C. Poggi, "Numerical modeling of Fabric Reinforce Cementitious Matrix composites (FRCM) in tension," *Constr. Build. Mater.*, vol. 70, pp. 531–548, 2014.
6. P. Zampieri, F. Faleschini, M. A. Zanini, and N. Simoncello, "Collapse mechanisms of masonry arches with settled springing," *Eng. Struct.*, vol. 156, no. October, pp. 363–374, 2018.

Evaluation of Different Approaches for the Seismic Vulnerability Assessment of RC Structures

Valentina Gazzani [1,a)], Marina Poiani [1,b)], Francesco Clementi [1,c)], Giuseppe Pace [1,d)], Stefano Lenci [1,e)]

[1] *Department of Civil and Building Engineering, and Architecture, Polytechnic University of Marche, Via Brecce Bianche, 60131, Ancona, Italy*

[a)] v.gazzani@pm.univpm.it, [b)] m.poiani@pm.univpm.it, [c)] francesco.clementi@univpm.it, [d)]g.pace@univpm.it, [e)]s.lenci@univpm.it

Abstract. The seismic vulnerability of school buildings located in the municipality of Trecastelli (Marche, Central Italy) is evaluated with three different numerical models: the lumped plasticity, the distributed plasticity (fibre) and the 3D Continuum FE approaches. Nonlinear static (pushover) analyses are performed to assess the global seismic behaviour of the structure, and the limitations in the representativeness respect to the reality of different approaches are analysed.

Keywords: Reinforced Concrete, Nonlinear static analyses, 3D Continuum FE model, School building.

INTRODUCTION

The vulnerability assessment of existing public constructions against seismic actions is a crucial issue in seismic prone countries. In seismic regions, several school buildings were built before the development of modern seismic design provisions or not considering seismic provisions at all due to seismic codes and seismic hazard classifications evolved. Also the architectural layouts of school buildings, with their spatial configurations resulting from the distribution of the hosted learning functions, result in irregular structures with intrinsically unfavourable seismic behaviour [1,2].

Nevertheless, the strong earthquakes occurred in the last few decades in Italy, Molise (2002), Abruzzo (2009), Emilia (2012), and Central Italy (2016), confirm the susceptibility of these types of buildings to extensive damage.

The adequate modelling of existing RC frames is studied [3–5] and, during years, researchers proposed several numerical methods to represent the real structural behaviour of buildings best .

According to scientific literature, three different numerical approaches to assess the nonlinear behaviour of RC structures by introducing as few approximations are implemented. Hence refined numerical models are advisable to evaluate the behaviour of RC buildings, to identify their structural weaknesses and to better understand the effects on the whole structure introduced by typical and specific seismic vulnerabilities.

Modelling typologies available to assess the nonlinear response of structural systems in common computational codes follow two different approaches: the lumped and the distributed plasticity. Moreover, numerical models of reinforced concrete (RC) structures within the finite element method (FEM) can be based either on beam elements or 3D continuum elements characterised by a nonlinear material model for concrete in combination with 1D elements for the embedded bars.

THE CASE STUDY

The Primary and Lower Secondary School “G. Marconi” of Monterado (Fig. 1) located in the municipality of Trecastelli (AN) is described. The school complex consists of three independent buildings of different structural and material types: the first construction is realised with masonry walls and one-way hollow block slabs (Unit A in Fig. 1); the second part is 1-storey RC building added to first construction to optimise the functional distribution (Unit B in Fig. 1) and the third building is 2-stories RC framed structure recently built as an extension for teaching functions (Unit C in Fig. 1).

(a) (b)

FIGURE 1. School building complex of Monterado (a) and photographic views and plan of Unit C (b).

For the sake of brevity, only the analyses carried out for Unit C are reported. The case study (Fig. 1) is characterised by a plan consisting of two rectangles (among which there is a misalignment of the structure) and it is made up of RC framed structure with columns (arranged with distances from 2.65 m to 3.92 m in X-direction and 3.85 m and 4.80 m in Y-direction) and beams.

The intermediate floor and the roof are one-way hollow block slabs with a thickness of 20 + 4 cm and 16 + 4 cm cast-in-place with RC joists (i = 50 cm) and they are considered for their characteristics as "rigid floor diaphragms." Double layer hollow blocks make the infill walls with mortar, insulation, and plaster.

The values of material properties used for nonlinear analyses are f_{cm}=34.58 MPa for compressive strength of concrete with an elastic module of 31920 MPa and a f_{ym}=543.49 MPa for steel yielding of reinforcement bars.

DESCRIPTION OF THREE DIFFERENT APPROACHES USED

The global seismic analysis has to use, as far as possible, methods of analysis that allow evaluating both resistance and ductility appropriately, taking into account the possibility of developing resistant mechanisms both "ductile" and "brittle" and adopting material parameters diversified according to the type of verification. National Codes [6,7] and International [8], or Guidelines [9] point out that in existing structures the capacity of elements with both "ductile" and "brittle" resistant mechanisms can be activated.

In Fig. 3 the three different numerical models realised with relative constitutive laws are reported.

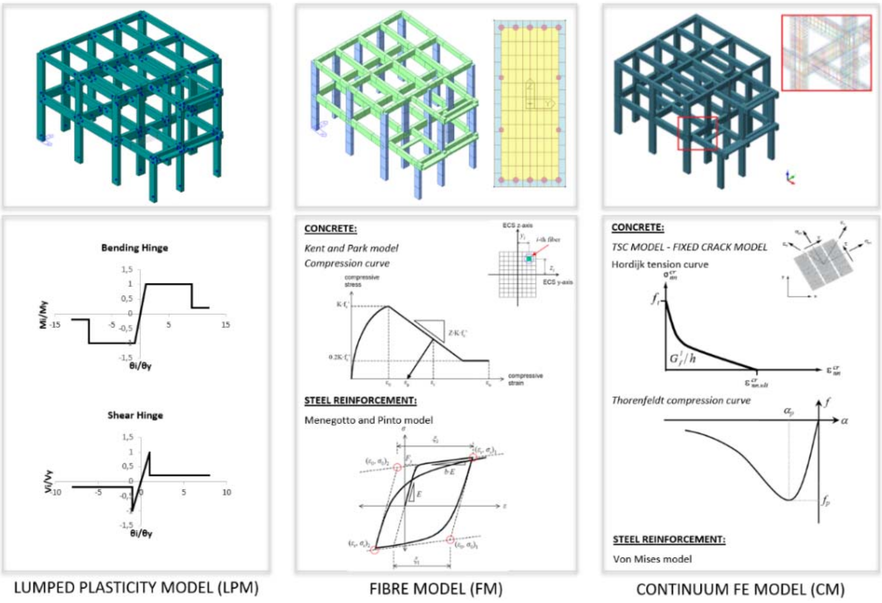

(a) (b) (c)

FIGURE 2. Lumped plasticity (a), Fibre (b) and Continuum FE(c) models [10,11] with the respective constitutive laws.

The first one (Fig. 2a) is lumped plasticity model (LPM) associated with a phenomenological approach where the dissipation areas are located at the end of the element, usually synthesized by a hysteretic behaviour, which differs according to the axial-bending-shear failure.

The frame structure is modelled by beam elements considering the infinite in-plane stiffness of the floors.

Advantages of this modelling are: 1) a meager computational cost; 2) the capacity of depict nonlinear phenomena such as buckling of rebars and bond slip between bars and concrete, poor confinement and shear deformability; 3) the correspondence to the reality with sections rectangular in shape considering that chord rotations of main elements are calculated with trinomial formulation.

On the other hand, the positioning of the plastic hinges requires a specific experience of the operator [12]. The main problem is the absence of interaction between the axial, bending and shear forces during the transversal loading increment that it is purely numerical and delegated to the FE solver.

The classical parabola-rectangle diagram for the concrete under compression is implemented along with an elastic-hardening diagram for the reinforcement steel. The plastic hinges assigned to the elements are axial force and biaxial bending interaction (i.e., PMM 3D status determination with the variation of axial force during the analysis) for columns and pure bending (i.e., M3 pure uniaxial bending) for beams. The hinge nonlinear constitutive laws suggested by the Eurocode 8 provisions [8] are utilised.

The brittle mechanisms (shear failure) are assessed through shear hinges, and the evaluation of shear demand and corresponding capacity at the two ends of each structural member are based on formula proposed in the Italian Seismic Code [13] that considers the resisting model of the classical Mörsch-Ritter truss, different formulation respect Eurocode 8 [8] and CNR-DT 212 [15].

The fibre model (FM) observed in Fig. 2b considers the distributed nonlinearity throughout the structural element, both transversely and longitudinally, unlike the lumped plasticity model; the nonlinearity of the material allows to derive the behaviour of the element through an integration of the response in the section. Structural elements are discretised in "control sections" with a considerable number of fibres (Fig. 2b), which only deform axially, using a force-based element formulation [14]. A fibre model allows to correctly describe the interaction between the axial force and the two components of bending moment.

Actually, in the commercial codes, a fibre model is not suitable to represent nonlinear phenomena such as the buckling of rebars and bond slip between bars and concrete and shear failure, etc.

A distributed plasticity approach suffers the absence of an interaction between bending (M), shear (V) and axial force (N) as the lumped plasticity approach.

The nonlinear properties of sections follow the stress-strain relationship proposed in literature, based on experimental tests, for the behaviour of concrete subjected to cyclic loads [15]. In particular, for the present case study, the Kent and Park model [16] is used for concrete, which is refined to take into account the lateral confinement contribution of the stirrups. Tension strength of concrete is ignored. For the nonlinear behaviour of steel, Menegotto and Pinto model as modified by Filippou et al. [17] is adopted.

In Fig. 2c, the Continuum FE model (CM) used to study the in-plane behaviour of concrete elements is based on a smeared crack approach where the concrete cracks are assumed to be scattered and distributed and not directly modelled. Since smeared crack modelling approaches do not require re-meshing of the Finite Element (FE) model after the occurrence of cracks or a priori definition of possible locations of cracks, they are widely used in FE modelling not only for RC structures but also for masonry structures [18–20].

The Total Strain Crack Model with a fixed crack model is used for the case study.

The numerical model is built to reproduce the geometry of the structure, using 3D mesh elements for the concrete and 1D mesh elements for embedded bars. The adopted mesh size is 150 mm. The hypothesis of rigid floor slab is used, since this is close to the reality, with fixed constraints on the ground floor.

The number of elements realised is 86824 with 88968 degrees of freedom (d.o.f.).

The constitutive models selected for concrete tensile and compressive behaviours are, respectively, the nonlinear tension softening of Hordijk model and the compression curve of Thorenfeldt model (Fig. 2c).

Moreover, the modelling of shear behaviour is necessary for the fixed crack concept where the shear stiffness is usually reduced after cracking with a classical constant value.

The lateral crack effect and the confinement effect are considered by the formulation of Vecchio and Collins [21] and Selby and Vecchio [22]. The required concrete material properties to analyse crack models are defined using CEB-FIP 1990 [23]. The value of fracture energy G_f considered is equal to 0.072 N/mm.

The constitutive model type selected for steel reinforcements is Von Mises model.

The nonlinear analyses are performed assuming the following parameters:

- maximum number of iterations of load increment: 100;
- maximum analysis number of substeps: 500;
- minimum analysis number of substeps: 5;
- initial load factor of 0.1.

The nonlinear system of equations is solved by an incremental nonlinear static analysis with the Arc-length iteration procedure with the Initial Stiffness Method, and an energy norm with a tolerance of 10^{-2} is requested. It is noteworthy to point out that the computing time required by each pushover analysis is heavy.

THE NUMERICAL ASSESSMENT

The nonlinear static analysis is performed following the N2 method, originally proposed by [24], with two distributions, one proportional to the fundamental modes and the other to the mass. In the following, the two distributions will be identified with the labels "PushMode" (proportional to the modes) and "PushMass" (proportional to the mass). The pushover curves obtained by the three models are reported in Fig. 3.

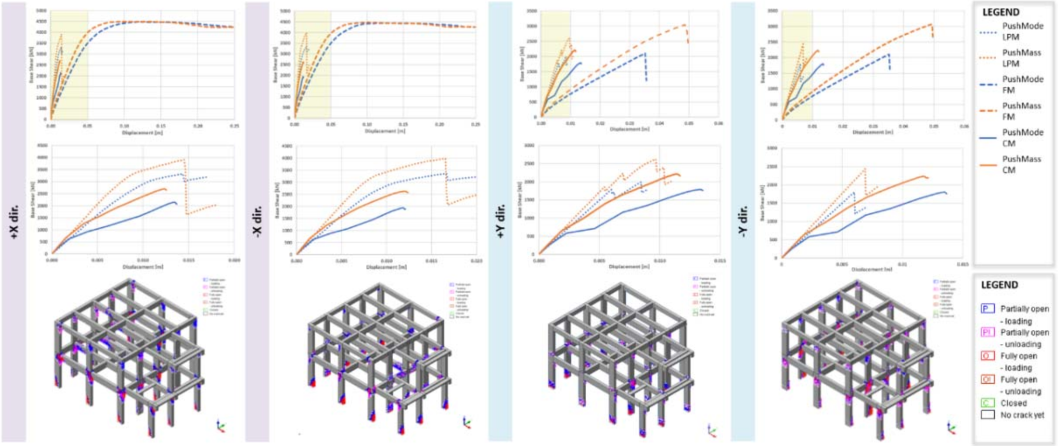

FIGURE 3. Pushover curves for the three models and crack patterns of CM for each direction (PushMode).

The capacity curves highlight a brittle global behaviour (i.e., when the vertical drop in the capacity curve is visible), mainly in -Y/+Y directions. Low building performances are due to the brittle mechanisms localised on the beams of the first floor with misalignments of structural elements. The consistency of the results obtained with the lumped plasticity model is checked by a comparison with the pushover curves of the other models (Fig. 3).

First of all, regarding the global behaviour, the initial elastic stiffness of the capacity curves both for the LPM and the CM is markedly different compared to the corresponding FM curves.

It is known that the stiffness is influenced by choice of the plastic hinge type and location: a stiffer behaviour is observed if the plastic behaviour is concentrated at the end of elements as in the LPM compared to the FM [25,26].

The concomitance of bending (M), shear (V) and axial force (N) and the interaction between them in the inelastic response represent the most relevant phenomena treated approximately and incompletely with lumped plasticity and fibre models. Otherwise, through the continuum model is possible to evaluate together the states of stress (axial bending and shear), offering a realistic representation of the phenomena, as well as stresses on the beam-column joints. Fig. 3 also shows the comparison between the LPM and CM with the cracking patterns.

The displacements in the worst (+ /-Y) directions, very limited in the LPM, tend to increase in the CM model. Also, it is possible to note the variation of the slope of the CM capacity curves, after a first initial elastic part overlapped on the LPM curves. The cracking pattern is developed mainly on the beam-column joints, which are the most stressed elements together with the base of the columns. A proposal of CFRP retrofitting intervention on the beam-column joints is realised [27,28].

CONCLUSIONS

This work investigates the influence of FE modelling on typical and specific vulnerabilities of school buildings belonging to the lower levels of the Italian education system.

To evaluate the effects due to irregularities, functional layouts and inadequate construction details, a case study is presented to consider additional information provided by more accurate modelling approach than a simpler one and three different models are implemented affected by various limitations in the representativeness respect to the reality. The shear is the most critical action for the analysed building. The concomitance of bending, shear, and axial force and their interaction in the inelastic response are the most relevant problems treated approximately and incompletely by both LPM and FM. The FM without elements to account the shear behaviour is unsuitable for structures characterised by shear failure and for representing nonlinear phenomena such as the buckling of rebars and bond slip between bars and concrete and shear failure.

Nonlinear static analyses are performed following the N2 method with two distributions, one proportional to the fundamental mode and the other to the mass. The comparison of pushover curves confirms greater displacement capacities in CM compared to LPM for the worst direction (+Y/-Y).

REFERENCES

[1] M. Dolce, Seismic safety of schools in italy, Proc. Ad Hoc Expert. Gr. Meet. Earthq. Saf. Sch. (2004).

[2] V. Lupo, L'idea di scuola: didattica e tipologia (in Italian), (1996).

[3] & D.S. Elnashai, A. S., Fundamentals of Earthquake Engineering, (2008).

[4] V. Plevris, T. Education, N.D. Lagaros, Structural Seismic Design Optimization and Earthquake Engineering : Formulations and Applications, n.d.

[5] D.N. Grant, J.J. Bommer, R. Pinho, G.M. Calvi, A. Goretti, F. Meroni, A prioritization scheme for seismic intervention in school buildings in Italy, Earthq. Spectra. (2007). doi:10.1193/1.2722784.

[6] Ministero dei Lavori Pubblici, Decreto Ministeriale 14 Gennaio 2008. "Norme tecniche per le costruzioni" (in italian), (2008).

[7] Circolare Ministero dei Lavori Pubblici, Circolare LL.PP. 2 febbraio 2009 , n. 617 "Istruzioni per l'applicazione delle «Nuove norme tecniche per le costruzioni» di cui al Decreto Ministeriale 14 Gennaio 2008 (in italian), (2009).

[8] CEN (Comité Européen de Normalisation), Eurocode 8 - Design of structures for earthquake resistance - Part 3: Assessment and retrofitting of buildings - EN 1998-3, (2005).

[9] CNR, DT 212/2013: Istruzioni per la valutazione affidabilistica della sicurezza sismica di edifici esistenti (in italian), (2013). doi:CNR-DT 212/2013.

[10] Midas GEN, Analysis Manual, (2018).

[11] Midas FEA, Analysis and Algorithm, (2015).

[12] F. Clementi, G. Di Sciascio, S. Di Sciascio, S. Lenci, Influence of the shear-bending interaction on the global capacity of reinforced concrete frame, Performance-Based Seism. Des. Concr. Struct. Infrastructures. (2016) (in press). doi:10.4018/978-1-5225-2089-4.ch004.

[13] Ministero dei Lavori Pubblici, Decreto Ministeriale per aggiornamento delle "Norme Tecniche per le Costruzioni" - NTC 2018 (in italian), (2018) 1–198.

[14] E. Spacone, F.C. Filippou, Fibre beam column model for non linear analysis of RC frames.pdf, (1996).

[15] A. Pierdicca, F. Clementi, D. Maracci, D. Isidori, S. Lenci, Damage detection in a precast structure subjected to an earthquake: A numerical approach, Eng. Struct. 127 (2016) 447–458. doi:10.1016/j.engstruct.2016.08.058.

[16] Dudley Charles Kent and Robert Park, Flexural Members with Confined Concrete.pdf, J. Struct. Div. (1971). doi:10.1017/S000748530002229X.

[17] F. FILIPPOU, E. POPOV, V. BERTERO, Effects of Bond Deterioration on Hysteretic Behaviour of Reinforced Concrete Joints, 1983. doi:https://doi.org/10.1016/j.jad.2016.08.040.

[18] F. Clementi, V. Gazzani, M. Poiani, P. Antonio Mezzapelle, S. Lenci, Seismic Assessment of a Monumental Building through Nonlinear Analyses of a 3D Solid Model, J. Earthq. Eng. (2018). doi:10.1080/13632469.2017.1297268.

[19] F. Clementi, V. Gazzani, M. Poiani, S. Lenci, Assessment of seismic behaviour of heritage masonry buildings using numerical modelling, J. Build. Eng. (2016). doi:10.1016/j.jobe.2016.09.005.

[20] F. Clementi, E. Quagliarini, F. Monni, E. Giordano, Lenci, S., Cultural Heritage and Earthquake: The Case Study of “Santa Maria della Carità” in Ascoli Piceno, Open Civ. Eng. J. (2017). doi:10.2174/1874149501711011079.

[21] F.J. Vecchio, M.P. Collins, Predicting the response of reinforced concrete beams subjected to shear using modified compression field theory, ACI Struct. J. (1988). doi:10.14359/10416.

[22] R.G. Selby, F.J. Vecchio, A constitutive model for analysis of reinforced concrete solids, Can. J. Civ. Eng. (1997). doi:10.1139/cjce-24-3-460.

[23] C.-F.I.F. for Structural, Structural Concrete: Textbook on Behaviour, Design and Performance: Updated Knowledge of the CEB/FIP Model Code 1990, Bulletin. (2009). doi:10.1017/CBO9781107415324.004.

[24] P. Fajfar, P. Gašperšič, The N2 method for the seismic damage analysis of RC buildings, Earthq. Eng. Struct. Dyn. (1996). doi:10.1002/(SICI)1096-9845(199601)25:1<31::AID-EQE534>3.0.CO;2-V.

[25] F. Clementi, A. Scalbi, S. Lenci, Seismic performance of precast reinforced concrete buildings with dowel pin connections, J. Build. Eng. 7 (2016) 224–238. doi:10.1016/j.jobe.2016.06.013.

[26] P.A. Mezzapelle, A. Scalbi, F. Clementi, S. Lenci, The Influence of Dowel-Pin Connections on the Seismic Fragility Assessment of RC Precast Industrial Buildings, Open Civ. Eng. J. (2017) 1138–1157. doi:10.2174/1874149501711011138.

[27] V. Gazzani, Influence of FE modelling on typical and specific vulnerabilities of RC school buildings (PhD Thesis), Polytechnic University of Marche, 2019.

[28] V. Gazzani, M. Poiani, F. Clementi, G. Pace, S. Lenci, Influence of FE modelling approaches on vulnerabilities of RC school building and a proposal of a CFRP retrofitting intervention (submitted), Open Constr. Build. Technloogy J. (2019) 1–22.

On the Nonlinear Behaviour of Unfired Dry Earth

Ersilia Giordano[1,a], Francesco Clementi[1,b)], Giammichele Cocchi[1,c)], Laura Marcheggiani[1,d)]

[1]Department of Civil and Building Engineering, and Architecture, Polytechnic University of Marche, Via Brecce Bianche, 60131, Ancona, Italy

[a)]e.giordano@pm.univpm.it, [b)]francesco.clementi@univpm.it, [c)]g.cocchi@univpm.it, [d)]l.marcheggiani@univpm.it

Abstract. The current work presents the first results on the determination of reliable numerical models of earthen blocks under different loading conditions. Uniaxial compression and 3-points bending tests were performed. Experimental behavior was modelled with a nonlinear model able to describe the cracking behavior. The simplified approach based on macro-modelling shows a satisfactory accuracy and low computational costs. The numerical results are in good agreement with the post-elastic behavior observed in the experimental campaign.

Keywords: Earth block masonry; Experimental test; Numerical modelling; Macro-modelling approach.

INTRODUCTION

The knowledge on the material properties and failure mechanisms of earth block masonry is limited and scattered when compared to the advances in research on stone and brick masonry. Only few systematic investigations into the behavior of earth block masonry under different load conditions are available [1].

Earth has been used for many centuries, together with others natural materials such as stone and wood, in the construction of load-bearing masonry structures, including constructions which are outstanding from a structural point of view, such as the well-known 10-storey buildings in Yemen [2]. Ruins of earth buildings of the Roman imperial age have been found [3,4], but the use of this material is certainly older. The utilized technologies change with the geographical zone and with the historical period. Typically, but not exclusively, earth has been used in the form of blocks, which were readily produced by manual compaction. Theirs constituent phases (clay, sand, etc.) can vary, and are somehow related to the building site.

The production of adequate blocks required an able labor, and this was one of the problems that, after the Roman era and in the middle age, contributed to the marginalization of the construction of earth house in western countries. In fact, they became noncompetitive with respect to other buildings materials (masonry of fired clay bricks first, and then steel and concrete [5–7]), both in terms of costs and of mechanical properties, and because of the impossibility to standardize the composition due to the intrinsic scattering of this material.

Although earth block is a widely utilized building material since prehistoric times, it also represents a type of masonry block that yields the lowest strength values. Typical values for compressive strength of historical unsterilized earth blocks are in a range of 0.6–6.6 N/mm^2 [1]. The modulus of elasticity measured on modern earth blocks with similar compressive strength and particle size distribution as historical earth blocks is in the range of 400–2000 N/mm^2 [1]. Compared to some building stones or fired bricks, earth blocks show a rather moderate to low anisotropic effect towards their mechanical and physical properties [8–12].

An experimental campaign has been performed at the “Laboratorio Prove Materiali e Strutture” of the Polytechnic University of Marche, the results of which are briefly reported in this paper and then numerically assessed to have first results with advanced macro-modelling approach typically used for other types of structures [13–20]. The attention has been paid to other important properties of dry earth, such as damage and fracture. The knowledge of this behavior permits to enlarge the picture of the mechanical behavior, which is particularly needed in the applications where fracture, and not strength, represents the critical event for the structure.

MATERIALS AND PREPARATION

The material used to realize the compressed earth block is made of three different constituents, having the following proportions: 1 volume of "earth," 1/2 volume of "sandstone" and 1/2 volume of fibres straw.

The geotechnical characteristics of the "earth" are reported in Fig. 1a (particle size distribution). According to the ASTM D2487 it can be classified as "lean clay with sand (CL)." The geotechnical characteristics of the "sandstone" are reported in Fig. 1b (particle size distribution). According to the ASTM D2487 it can be classified as "well graded sand (SW)." The fibers straw has a length which varies from 2 to 8 cm, with an average valued of 5 cm.

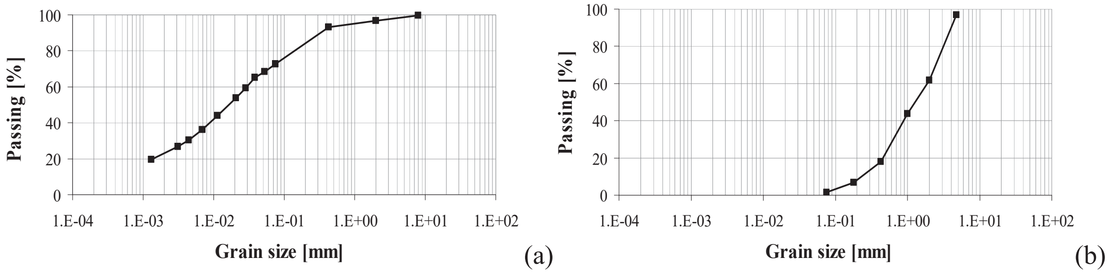

FIGURE 1. Grading curve for the "earth" (a) and the "sandstone" (b).

Material preparation and mixing was carried out manually. 1/3 (on average) volume of water was added to guarantee normal consistency and manual operations. The mixture was manually pressed into formworks of wood of the dimensions of 32×46×13 cm. After removing the boxes, the blocks were cured under stationary thermo-hygrometric conditions (temperature 23-26 °C; relative humidity 45-55%). After about five months, the blocks were cut by saw to obtain the desired specimens. At the end of the tests, it was verified that the moisture content was less than 3-4%, so we have tested a dry material.

COMPRESSION AND 3-POINTS BENDING TESTS

As the compressive strength depends on the dimension of the specimen, and because this matter is still under investigation and it is not definitely established the influence of the aspect ratio [21], we decide to perform compression tests on cubic (Fig. 2a) and prismatic (Fig. 2b) specimens.

To detect the softening branch, we have applied a controlled displacement and measured the force, i.e. a soft device was used. In this paper we report only the monotonic test (Fig. 2), aimed at capturing the general overall behaviour, including the determination of the Young Modulus E, of the maximum stress σ_{max} and of the ultimate strain ε_u, leaving the cyclic tests for future works.

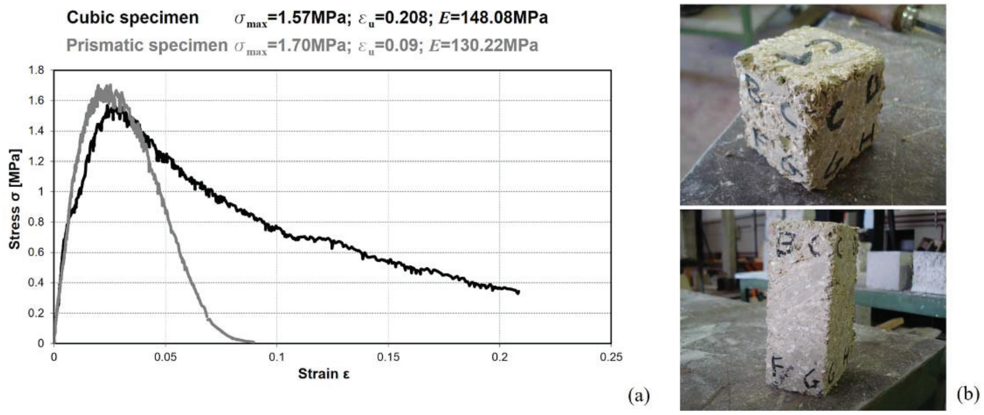

FIGURE 2. Stress-strain relation for the monotonic compression test on prismatic and cubic specimens (a), specimens of the compression tests (b).

The main differences, both qualitative and quantitative, are in the softening branch, that of prismatic sample being much more (approximately one half) shorter. Thus, the “ductility” is lost by the prismatic sample. This can be explained by the different rupture mechanism observed in the two cases. In fact, for the cubic specimen we have a spread cracking at breaking, so that a lot of energy is spent to break the material, while for the prismatic specimen we have seen only one diagonal crack, i.e. a localized rupture requiring less energy and thus developing in an easier way, i.e., for lower values of the strain. This is a noteworthy “size effect” observed in our tests.

Then, tests have been performed on samples obtained from the same block used to make the specimens for the compression tests. So, in addition to the same composition, they have the same content of water after five months of the drying process. The equipment is the same, and we have used also two transducers of horizontal displacement. The specimens of dimensions L' = 355 mm (length), B = 85 mm (width) and W = 112 mm (height) are put on two steel rollers that are free to roll. The distance between the lower rollers is L = 255 mm.

The monotonic test has been done by applying the vertical displacement δ^V in the middle of the upper side of the sample, and by recording the value of the vertical force F by a load cell. The experimental F- δ^V curve is plotted in Fig. 3a, where is shown that the initial elastic range, which can be approximated quite well by a linear path, ends at $F = F^V_{max}$= 2274 N and δ^V= 1.239 mm. After the initial elastic range, an almost vertical crack appeared in the middle of the lower side, for the vertical displacement δ^V = 1.315 mm. It then suddenly propagates toward the upper side. During the crack propagation a relatively long softening branch is observed (Fig. 3a), with a final vertical displacement equal to δ^V_{max}= 10.4 mm.

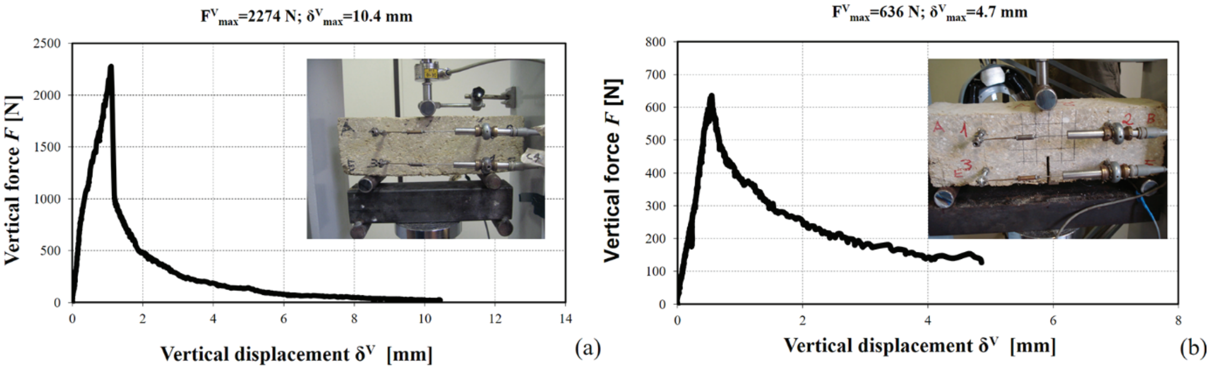

FIGURE 3. The measured vertical force versus the applied vertical displacement δ^V in the monotonic three points bending test for the specimen without (a) and with (b) initial crack.

To further assess the fracture characteristics of the material, we have performed another three points bending test on a specimen with an initial crack (Fig. 3b). Here we have considered a slightly different material composition (1 volume of “earth,” 1/2 volume of “sandstone” and 3/4 volume of fibres straw) and some slightly different geometrical dimensions (L' = 360 mm, L = 320 mm, B = 84 mm and W = 113 mm).

The initial crack length is a_0 = 44 mm, i.e., a_0/W=0.4. The experimental data for the monotonic test are presented in Fig. 3b. From this figure we can see that there is no longer the sudden jump as in Fig. 3b, and the propagation is continuous and starts at $F = F^V_{max}$= 636 N and δ^V = 0.544 mm. Furthermore, the initial crack now induces an almost rectilinear propagation of the crack.

MACRO-MODELLING APPROACH

The experimental results were reproduced considering a macro-modelling approach. Earth blocks were modelled as an equivalent homogeneous material, based on isotropic plasticity. Although regular course masonry generally exhibits an orthotropic behaviour due to the typical arrangement of blocks and mortar joints, and dependent on the relative geometrical and mechanical characteristics of the constitutive materials, in this study given the presence of a single element an isotropic approach was followed for the macro-modelling case. The purpose of this assumption was to keep the equivalent homogenous modelling of this type of masonry as simple as possible and therefore limit the number of mechanical parameters needed to define the material model. The assumed material properties are obtained, in fact, from relatively simple testing procedures aimed at deriving basic information about the masonry. On the

contrary, a thorough characterisation of an orthotropic model would require the determination of a considerably higher number of parameters leading to carrying out expensive testing campaigns. Different material models and constitutive laws were considered for the homogeneous material. A multi-directional fixed crack model was assumed [22]. In this model cracking is specified as a combination of tension cut-off, tension softening and shear retention as also done in [1].

The assumed Young's modulus and Poisson's ratio correspond to the mean values obtained from compression tests. The compressive strength f_c was assumed as the mean value from the tests as well. The coefficient of shear retention β was chosen equal to 0.05 typical of similar brittle or quasi-brittle materials [15]. This parameter allows to describe the post-cracking shear behaviour and was defined in order to provide the sample with a certain value of stiffness after cracking due to interlocking phenomena. The tensile strength f_t was assumed as the as 1/20 of the tensile strength compression one. We have varied the fracture energy in tension and in compression and a lot of analyses, also varying the mesh size, have been done and reported in the Fig. 4 for all the specimens.

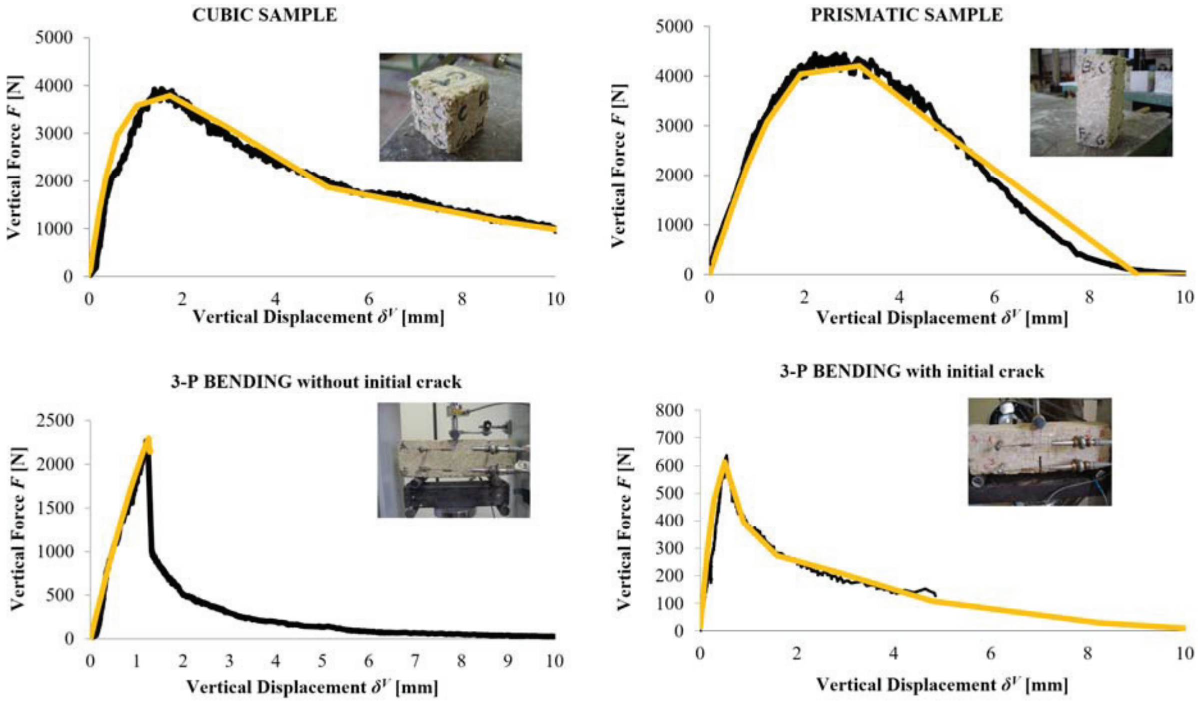

FIGURE 4. Numerical fitting for the four different experimental tests.

As expected, the macro-modelling approach, based on the experimental data, is able to provide results in agreement with the experimental tests in terms of vertical force-displacement behaviour. This is an on-going work and for this reason, waiting to process the cyclic tests that are not listed here, it is possible to estimate a range of variability for the tensile fracture energy between 0.008 N/mm and 0.0085, and for the fracture energy in compression between 0.01 N/mm and 1 N/mm.

CONCLUSIONS

An analysis of the mechanical properties of a traditional earthen construction material is presented based on compressive and 3-points bending results. Displacement-controlled tests were carried out to determine basic mechanical parameters and in particular the post-peak strain behaviour. The experimental results were used to simulate the behaviour of earth specimen by means of nonlinear finite element method based on the macro-modelling approach. Appropriate constitutive behaviour was taken into account and the chosen geometries were in respect with the restraint conditions observed in laboratory testing. A preliminary finite element macro-model calibrated based on

the experimental data was firstly developed, which resulted to a useful prediction of the strength of earth block masonry elements.

REFERENCES

[1] L. Miccoli, A. Garofano, P. Fontana, U. Müller, Experimental testing and finite element modelling of earth block masonry, Eng. Struct. 104 (2015) 80–94. doi:10.1016/j.engstruct.2015.09.020.

[2] E. Quagliarini, M. D'Orazio, S. Lenci, The properties and durability of adobe earth-based masonry blocks, in: Eco-Efficient Mason. Bricks Blocks, Elsevier, 2015: pp. 361–378. doi:10.1016/B978-1-78242-305-8.00016-4.

[3] E. Quagliarini, S. Lenci, M. Iorio, Mechanical properties of adobe walls in a Roman Republican domus at Suasa, J. Cult. Herit. 11 (2010) 130–137. doi:10.1016/j.culher.2009.01.006.

[4] E. Quagliarini, S. Lenci, The influence of natural stabilizers and natural fibres on the mechanical properties of ancient Roman adobe bricks, J. Cult. Herit. 11 (2010) 309–314. doi:10.1016/j.culher.2009.11.012.

[5] G. Maracchini, F. Clementi, E. Quagliarini, S. Lenci, F. Monni, Preliminary study of the influence of different modelling choices and materials properties uncertainties on the seismic assessment of an existing RC school building, in: AIP Conf. Proc., 2017. doi:10.1063/1.4992620.

[6] E. Quagliarini, F. Clementi, G. Maracchini, F. Monni, Experimental assessment of concrete compressive strength in old existing RC buildings: A possible way to reduce the dispersion of DT results, J. Build. Eng. 8 (2016) 162–171. doi:10.1016/j.jobe.2016.10.008.

[7] F. Monni, E. Quagliarini, S. Lenci, F. Clementi, Dry Masonry Strenghtening through Basalt Fibre Ropes: Experimental Results against Out-of-Plane Actions, Key Eng. Mater. 624 (2014) 584–594. doi:10.4028/www.scientific.net/KEM.624.584.

[8] A. Formisano, F. Fabbrocino, E. Dessi, G. Chiumiento, Experimental shear tests on tuff blocks triplets with hemp fibres reinforced lime mortar, in: A.L. Tralli A.M.,Berardi V.P.,Feo L.,Fraternali F. (Ed.), AIMETA 2017 - Proc. 23rd Conf. Ital. Assoc. Theor. Appl. Mech., Centro Servizi d'Ateneo S.r.l., Rome, 2017: pp. 2022–2028.

[9] A. Formisano, E. Dessì, R. Landolfo, Mechanical-physical experimental tests on lime mortars and bricks reinforced with hemp, in: 2017: p. 090006. doi:10.1063/1.5012363.

[10] F. Clementi, S. Lenci, T. Sadowski, Fracture Characteristics of Unfired Earth, Int. J. Fract. 149 (2008) 193–198. doi:10.1007/s10704-008-9239-x.

[11] S. Lenci, F. Clementi, T. Sadowski, Experimental determination of the fracture properties of unfired dry earth, Eng. Fract. Mech. 87 (2012) 62–72. doi:10.1016/j.engfracmech.2012.03.005.

[12] S. Lenci, Q. Piattoni, F. Clementi, T. Sadowski, An experimental study on damage evolution of unfired dry earth under compression, Int. J. Fract. 172 (2011) 193–200. doi:10.1007/s10704-011-9651-5.

[13] F. Clementi, A. Pierdicca, A. Formisano, F. Catinari, S. Lenci, Numerical model upgrading of a historical masonry building damaged during the 2016 Italian earthquakes: the case study of the Podestà palace in Montelupone (Italy), J. Civ. Struct. Heal. Monit. 7 (2017) 703–717. doi:10.1007/s13349-017-0253-4.

[14] A. Pierdicca, F. Clementi, D. Isidori, E. Concettoni, C. Cristalli, S. Lenci, Numerical model upgrading of a historical masonry palace monitored with a wireless sensor network, Int. J. Mason. Res. Innov. 1 (2016) 74–99. doi:10.1504/IJMRI.2016.074748.

[15] F. Clementi, E. Quagliarini, F. Monni, E. Giordano, Lenci, S., Cultural Heritage and Earthquake: The Case Study of "Santa Maria della Carità" in Ascoli Piceno, Open Civ. Eng. J. 11 (2017) 1079–1105. doi:10.2174/1874149501711011079.

[16] F. Clementi, V. Gazzani, M. Poiani, P.A. Mezzapelle, S. Lenci, Seismic Assessment of a Monumental Building through Nonlinear Analyses of a 3D Solid Model, J. Earthq. Eng. (2017) 1–27. doi:10.1080/13632469.2017.1297268.

[17] E. Quagliarini, G. Maracchini, F. Clementi, Uses and limits of the Equivalent Frame Model on existing unreinforced masonry buildings for assessing their seismic risk: A review, J. Build. Eng. 10 (2017) 166–182. doi:10.1016/j.jobe.2017.03.004.

[18] F. Clementi, A. Nespeca, S. Lenci, Seismic behavior of an Italian Renaissance Sanctuary: Damage assessment by numerical modelling, in: Int. Conf. Comput. Methods Sci. Eng. 2016, ICCMSE 2016, Athens, 2016: p. 130004. doi:10.1063/1.4968722.

[19] F. Monni, F. Clementi, E. Quagliarini, E. Giordano, S. Lenci, Seismic Assessment of Cultural Heritage: Nonlinear 3d Analyses of "Santa Maria Della Carità" in Ascoli Piceno, in: Proc. 6th Int. Conf. Comput. Methods Struct. Dyn. Earthq. Eng. (COMPDYN 2015), Institute of Structural Analysis and Antiseismic Research School of Civil Engineering National Technical University of Athens (NTUA) Greece, Athens, 2017: pp. 2533–2541. doi:10.7712/120117.5586.18082.

[20] F. Catinari, A. Pierdicca, F. Clementi, S. Lenci, Identification and calibration of the structural model of historical masonry building damaged during the 2016 Italian earthquakes: The case study of Palazzo del Podestà in Montelupone, in: AIP Conf. Proc., 2017: p. 090013. doi:10.1063/1.5012370.

[21] J.-C. Morel, A. Pkla, P. Walker, Compressive strength testing of compressed earth blocks, Constr. Build. Mater. 21 (2007) 303–309. doi:10.1016/j.conbuildmat.2005.08.021.

[22] F. Clementi, P.A. Mezzapelle, G. Cocchi, S. Lenci, Global analyses of historical masonry buildings: Equivalent frame vs. 3D solid models, in: AIP Conf. Proc., 2017. doi:10.1063/1.4992615.

Voxel Approach for 3D In-Plane Homogenized Failure Surfaces of Non-Periodic Masonry

Simone Tiberti[1, a)] and Gabriele Milani[1, b)]

[1]*Department of Architecture, Built Environment and Construction Engineering, Politecnico of Milan, Piazza Leonardo Da Vinci 32, 20133 Milan, Italy.*

[a)]Corresponding author: simone.tiberti@polimi.it
[b)]gabriele.milani@polimi.it

Abstract. While many historical masonry structures consist of brick masonry where the units display a periodic arrangement (such as stretcher or running bond), there are several examples that instead consist of stone masonry. Here, the blocks present different shapes and dimensions, and are assembled with random arrangements – hence the name "non-periodic masonry". This work presents a Matlab script for the extraction of in-plane homogenized failure surfaces for this type of masonry, and they represent a macroscopic strength criterion for the considered masonry panel. The failure surfaces are obtained through the solution of an upper bound limit analysis problem, formulated as a standard linear programming problem. The 3D finite element mesh used for representing the considered panel is created according to a voxel approach: starting from the rasterized image of the masonry panel, each 2D pixel is extruded to become a 3D voxel, which is subsequently transformed into a finite element. For numerical validation, the in-plane homogenized failure surface is extracted for a sample masonry panel, along with the failure modes for several load conditions, and they are critically commented.

INTRODUCTION

Masonry structures are a prominent part of the cultural heritage in many European countries. These historical buildings are often brick masonry structures, in which the units (in this case the bricks) are assembled according to predetermined regular arrangements: Flemish, English, stretcher bonds are some of the most renowned examples of these arrangements. All these types of masonry go under the name "periodic masonry", since it is possible to identify a periodic cell that is able to represent the whole masonry panel under translation. However, it is not infrequent to find examples of historical masonry structures consisting of stone masonry. It is also not infrequent to observe that the stones present different shapes and dimensions within the same masonry panel; to add even more complexity, the stones are sometimes not arranged in a regular fashion, instead they are randomly assembled within the masonry panel. This type of masonry is known as "non-periodic masonry" or also "rubble masonry", since it is not possible anymore to identify a single periodic cell representing the whole panel. It must be noted that this type of masonry has not so often been addressed in literature, and its mechanical behavior still needs to be fully addressed with the available tools (such as limit analysis).

This paper introduces a script developed in Matlab that enables the extraction of in-plane homogenized failure surfaces for non-periodic masonry. These are obtained by solving a limit analysis problem developed according to the kinematic approach, and formulated as a standard linear programming problem.

VOXEL APPROACH FOR MESH GENERATING PURPOSES

The considered masonry panel is discretized into a 3D finite element mesh that is generated by a Matlab [1] that follows the so-called "voxel approach". This is an evolution of previous works by the authors, where a "pixel approach" was used for creating a 2D finite element mesh [2-3]. The source image for the mesh generator script is the

rasterized picture of the considered masonry panel. Each 2D pixel is evolved into a 3D pixel called “voxel”, which is then transformed into a single finite element. Each voxel/finite element is flagged to signal whether it belongs to a block or to mortar, depending on the “red” value of its related RGB triplet. Hence, the source image must clearly display blocks and mortar with distinct colors: a black-and-white or greyscale source image is preferred. The user must then simply input the dimensions of the considered masonry panel, which determine the reference system for the panel and the XYZ coordinates of the finite elements’ centroid. Solid brick elements are eventually generated from the centroid’s coordinates, and the Matlab script results in two matrices: one list the node numbers and coordinates, the other the element numbers, the 8 adjoining nodes, the block/mortar flag, and the coordinates of their centroid. The transversal layout of the masonry panel is simply derived by extruding the in-plane configuration. Fig. 1a shows the sample of non-periodic masonry test-window chosen for the numerical application, which is extracted from the image taken from the outer wall of a real residential masonry building located in Casola in Lunigiana, in the province of Massa-Carrara, Italy [4]. Its dimensions are 35×35×20 cm^3, and 4 finite elements are used in the transversal direction. Fig. 1b displays the resulting 3D finite element mesh for this example, consisting of 51005 nodes and 40000 elements.

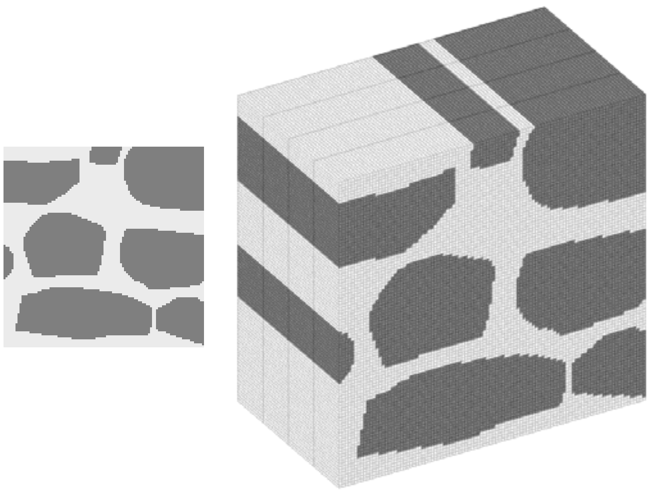

(a) (b)

FIGURE 1. (a) Sample of non-periodic masonry test-window; (b) 3D finite element mesh generated for the sample test-window.

3D IN-PLANE HOMOGENIZED FAILURE SURFACE

The 3D mesh generated from the Matlab script presented in the previous section is later used for extracting the in-plane homogenized failure surface of the considered masonry panel. As mentioned earlier, these result from the solution of an upper bound limit analysis problem, which is aptly formulated as a linear programming problem in a standard form. A homogenization approach is also used, which is enforced by setting periodicity conditions on the elements laying on opposite faces of the masonry panel. Each block and mortar finite elements are considered as rigid elements, but the discontinuities and velocity jumps between block-mortar and mortar-mortar elements are addressed according to a piecewise linear approximation of the 3D Mohr-Coulomb failure surface with 4 linearization planes, combined with a tension and compression cut-offs. The values of cohesion, friction angle, tensile strength, and compressive strength used for this numerical application are listed in Table 1, which come from values proposed in literature [5].

TABLE 1. Mechanical properties of the interfaces.

Cohesion [MPa]	Friction Angle [°]	Tensile Strength [MPa]	Compressive Strength [MPa]
0.15	30	0.1	1.5

Fig. 2 shows the in-plane homogenized failure surface for the considered sample non-periodic masonry test-window. It can be noted that both the shape of the failure surface and its bounding values are consistent with the mechanical properties chosen for the discontinuities. In the tension-tension range, for low values of the horizontal

homogenized stress Σ_{xx} the surface is bounded by the value 0.1, which corresponds to the assigned tensile strength. Conversely, in the compression-compression range the surface is bounded by the value 1.5, which corresponds to the assigned compressive strength. For high values of Σ_{xx}, the test-window experiences an increase in its strength, as it can be expected in these cases. This also proves the reliability of the upper bound limit analysis as formulated in this work.

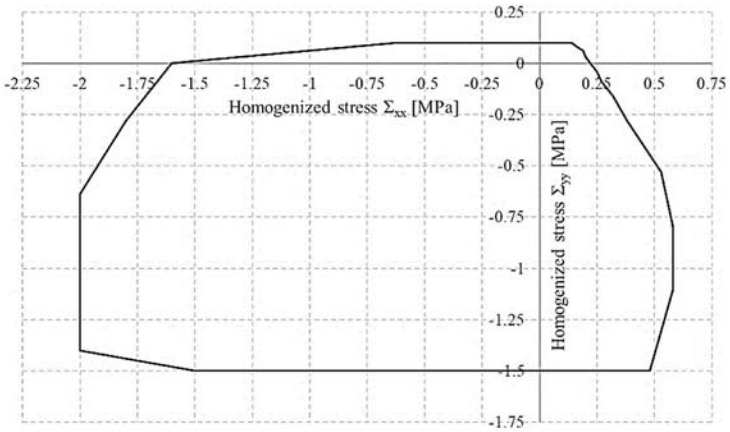

FIGURE 2. In-plane homogenized failure surface for the sample non-periodic masonry test-window.

Fig. 3 shows the failure modes for 8 relevant load conditions. They are all consistent with their respective load conditions: horizontal tension (Fig. 3a) causes widespread cracks in the masonry test-window, while vertical tension (Fig. 3c) originates horizontal cracks, since this test-window – while non-periodic – still displays some distinct bed joints. Other load conditions where vertical tension is prominent (Fig. 3b e Fig. 3d) show similar failure modes. Horizontal compression (Fig. 3e) also originates horizontal cracks – even though they appear different than the previous cases, since they depend on an indirect vertical tension. When horizontal and vertical compression are simultaneously applied, the test-window displays crushing of mortar (Fig. 3f), which is observed also for vertical compression (Fig. 3g). The last case (vertical compression and horizontal tension, Fig. 3h) displays a failure mode that is rather similar to that of pure horizontal tension, which is then the prominent load also for this last case.

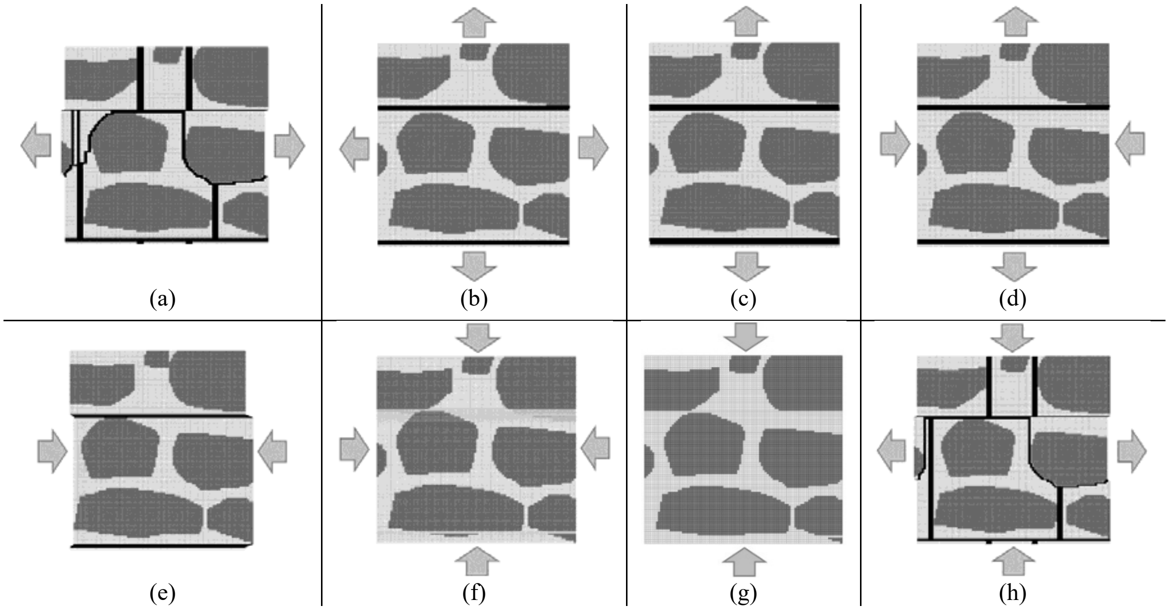

FIGURE 3. Failure modes for 8 relevant load conditions.

CONCLUSIONS AND FURTHER DEVELOPMENTS

A Matlab script for deriving in-plane homogenized failure surfaces of non-periodic masonry panels is introduced. The masonry panel is discretized into a 3D finite element mesh through a "voxel approach" that converts each 3D pixel (the voxel) into a single finite element. The homogenized failure surfaces are extracted as the results of an upper bound limit analysis problem, formulated as a standard linear programming (minimization) problem. The numerical application for the validation of the Matlab script consists in a sample non-periodic masonry test-window, for which the in-plane homogenized failure surface and 8 relevant failure modes are extracted. The failure mode is consistent with the expectations coming from the assigned mechanical properties of the discontinuities across elements, and also the failure modes are consistent with the load conditions here investigated. An incoming work is dedicated to reducing the mesh size of the test-window by adopting a "coarsing" strategy that transforms a square number of voxels into a single finite element, which is sought for also reducing the computational times needed for the numerical analyses. Most importantly, the Matlab script for the extraction of the failure surfaces will be extended to also obtain out-of-plane homogenized failure surfaces, which will express the masonry panel's resistance to overturning moments – a paramount issue when considering the overall structural behavior of a masonry panel. The results will be then compared to those obtained from a simplified approach for assessing the out-of-plane behavior previously proposed by the authors [6-7].

REFERENCES

1. MATLAB and Statistics Toolbox Release 2018b, The MathWorks, Inc., Natick, Massachusetts, United States.
2. S. Tiberti, G. Milani, and L. Macorini, "A novel pixel limit analysis homogenization model for random masonry," in *Proceedings of International Conference of Numerical Analysis and Applied Mathematics (ICNAAM 2017)*, AIP Conference Proceedings 1978, edited by T. E. Simos *et al.* (American Institute of Physics, Melville, NY, 2018), art. no. 450008.
3. S. Tiberti, L. Macorini, and G. Milani, "Homogenized failure surfaces of rubble masonry," in *Proceedings of the International Conference of Computational Methods in Sciences and Engineering 2018 (ICCMSE-2018)*, AIP Conference Proceedings 2040, edited by T. E. Simos *et al.* (American Institute of Physics, Melville, NY, 2018), art. no. 090008.
4. Italian Ministry of Cultural Heritage and Activities and Tourism (MiBACT). Atlante dei tipi costruttivi murari. Italia settentrionale. Schedatura tecniche murarie. Area n° 8 – Lunigiana (internal report).
5. R. van der Pluijm, H. S. Rutten, and M. Ceelen, "Shear behaviour of bed joints," in *12th IB2MaC: Proceedings of the 12th International Brick/Block Masonry Conference*, (2000), pp. 1849–1862.
6. S. Tiberti and G. Milani, "In- and out-of-plane analysis of multi-leaf masonry walls via an elementary homogenized numerical procedure," in *Proceedings of the International Masonry Society Conferences*, (2018), pp. 57–63.
7. S. Tiberti and G. Milani, "Simple homogenized numerical model for the analysis of multi-leaf masonry walls," in *Structural Analysis of Historical Constructions: An Interdisciplinary Approach*, Proceedings of the 11th International Conference on Structural Analysis of Historical Constructions, edited by R. Aguilar *et al.* (Springer, Cham, 2019), pp. 992–999.

Experimental and Numerical Analysis on an Ancient Anti-Seismic Technique

Simone Tiberti[1, a)], Carmelo Scuro[2, b)], Saverio Porzio[3, c)], Renato S. Olivito[3, d)] and Gabriele Milani[1, e)]

[1] *1Department of Architecture, Built Environment and Construction Engineering, Politecnico of Milan, Piazza Leonardo Da Vinci 32, 20133 Milan, Italy*
[2]*Department of Physics, University of Calabria, Via Ponte P. Bucci (cubo 17B), 87036 Rende (CS) Italy.*
[3]*Department of Civil Engineering, University of Calabria, Via Ponte P. Bucci (cubo 39B), 87036 Rende (CS) Italy.*

[a)]Corresponding author: simone.tiberti@polimi.it
[b)]carmelo.scuro@unical.it
[c)]saverio.porzio@unical.it
[d)]renato.olivito@unical.it
[e)]gabriele.milani@polimi.it

Abstract. This work presents an investigation of an ancient aseismic technique developed in Southern Italy. The peculiarity of this technique is the use of a kind of hollow brick called "fictile tubule brick", which is commonly featured in the historical and cultural heritage of several Mediterranean regions. It has been used by Romans since the 2^{nd} century AD to build vaults and domes. After the enormously disastrous earthquake of Messina and Reggio Calabria in late 1908, a Calabrian engineer named Pasquale Frezza patented an anti-seismic construction system which evolved the traditional technology of *casa baraccata*. The main purpose of this work is to investigate this construction technology through experimental and numerical tests. First, an experimental campaign is carried out on beams consisting of mortar and fictile tubules to better understand the rate of adherence that exists between these two constituents. Second, diagonal compressive tests are carried out on scale models of walls made with Frezza's building technique. Eventually, numerical analyses are conducted to validate the results of the experimental tests.

INTRODUCTION

In the Mediterranean cultural heritage, and particularly in the Southern Italian region of Calabria, the term "fictile tubule brick" identifies a peculiar type of brick characterized by a hollow core and a cylindrical shape [1]. This element is identified by many architectural historians as the first hollow brick in history, being used for the first time as a thermal insulator in the *calidarium* of Roman thermal baths. Later, it was used to build vaults and domes in the Roman provinces of Northern Africa where construction timber, traditionally used for the centrings, was scarce [2-3]. In Calabria, this construction system was widely used and different sites, in which there are numerous vaults, domes, kilns and walls made of fictile tubules, have been cataloged [4]. An example is represented by the cross vaults of the Trentacapilli palace in Bisignano, a small village near Cosenza [5-6].

In December 1908 the most disastrous earthquake ever recorded in Italy occurred in the strait between the island of Sicily and Calabria, nearly destroying the two cities of Messina and Reggio Calabria. During their reconstruction many proposals were developed to build anti-seismic buildings: for instance, some builders conceived projects for houses in wood and cork. The most interesting proposal was indeed taken up by a Calabrian engineer named Pasquale Frezza who, observing that structures in fictile tubules hardly collapsed during the earthquake, wanted to create a construction technique with fictile tubules at its very heart as prominent structural elements. Frezza then devised and

patented an anti-seismic construction system which evolved a previous construction technology known as *casa baraccata* [7-8]. Frezza's brainchild heavily featured a specific type of fictile tubule named *carosello* [9], and the structure so conceived alternated *caroselli* with common bricks in masonry walls, which were then to be encased in a timber frame [10].

The main purpose of this work is to carry out a thorough investigation on the construction technique proposed by Pasquale Frezza. The investigation consists of an experimental campaign followed by numerical validation of the results through computational analyses.

EXPERIMENTAL CAMPAIGN

The aim of the experimental campaign is to investigate the interface behavior between fictile tubule bricks and mortar; also, diagonal compressive tests are carried out on scale specimens of walls built according to Frezza's technique. The experimental tests are carried out at the Materials and Structures Engineering Laboratory of Civil Department of University of Calabria.

The interface behavior is investigated using specimens that present the shape of a prism and whose dimensions are 48×16×15 cm^3. These aim at somehow being consistent with the 1:4 ratio between transversal and lateral dimensions of mortar specimens to be used in three-point bending tests. The fictile tubules used in this campaign are labelled NFTs (New Fictile Tubules), with a height of 13 cm, a diameter of about 6 cm, and a thickness of 6 mm [11-12]. Conversely, the mortar is characterized by a compressive strength of about 1.8 MPa and consists of 9 parts of sand, 2 of lime mortar and 1 of cement. Each prism-shaped specimen employs 11 fictile tubules in total.

Three-point bending tests are performed on three specimens so built to assess the rate of adhesion between mortar and fictile tubules. The tests are carried out in accordance with EN 1015/11 [13]. The testing machine employs three steel rollers: one for the application of the top displacement (0.2 mm/min) and other two for supporting the specimen at the base. Fig. 1a shows the final load-displacement graphs for the investigated specimens. All three cases present one single crack developing within mortar on the contact surface between mortar and fictile tubules.

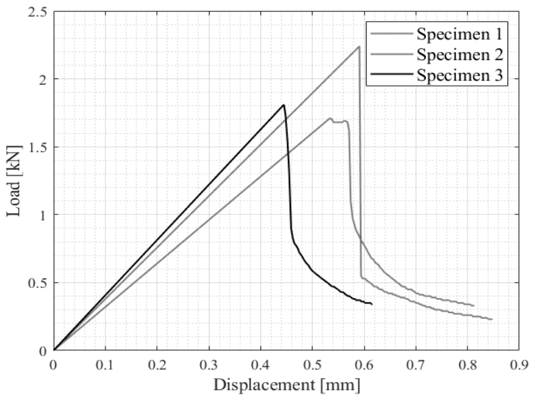

(a)

(b)

FIGURE 1. (a) Load-displacement diagrams for the three specimens; (b) Set-up of diagonal compressive test.

The dimensions of the specimen wall for the diagonal compressive tests are 60×60×15 cm^3. The masonry wall is created within the pre-assembled timber frame using fictile tubules and mortar with the same mechanical characteristics as those previously employed for the prisms. The diagonal compressive test is performed with a dedicated machine, in which the specimen wall is placed after being rotated of 45°; the 0.5 mm/s displacement is applied through a steel cap at the top, while another is placed at the bottom for support (Fig. 1b). Two couples of transducers are applied to the wall to monitor the relative displacements: the couple LVDT0 measures the vertical displacements between two bricks, whereas the couple LVDT1 measures the horizontal displacements between two fictile tubules. The resulting load-displacement diagram shows a decrease in the elastic modulus after 80% of the maximum load is attained: almost immediately after, the peak load is attained and is equal to 51.48 kN.

NUMERICAL VALIDATION

The validation of the experimental results coming from the adherence three-point bending tests is carried out through numerical simulations performed in the commercial finite element software Abaqus. The analytical models of the 11 fictile tubules and the mortar are created and then assembled together. The final finite element mesh consists of about 8600 nodes and 28500 tetrahedral elements, shown in Fig. 2a.

The fictile tubules are modelled with the "brittle cracking model" available in the Abaqus library that is suitable for simulating the mechanical behavior of brittle materials such as clay. This model assumes infinite compressive strength and offers the possibility of replicating the tensile behavior simply by inputting the tensile strength and mode I fracture energy. The Young's modulus used for the fictile tubules is equal to 3900 MPa, the Poisson's ratio is 0.15, the tensile strength is 3 MPa and the mode I fracture energy is 0.087 N/mm [11]. On the other hand, the mechanical model chosen for mortar is the "concrete damaged plasticity model" that is also available in the Abaqus library. Originally conceived for simulating the quasi-brittle behavior of concrete under moderate confining loads, it can be adapted for modelling other similar materials such as mortar. The model requires the definition of separate post-peak constitutive laws in tension and compression, with the former also possibly formulated in terms of the tensile strength and mode I fracture energy. Moreover, this model can also reproduce damage of the material in both tension and compression. The Young's modulus used for mortar is equal to 190 MPa, the Poisson's ratio is 0.2, the tensile strength is 0.6 MPa and the mode I fracture energy is 0.018 N/mm [11]. The interface behavior between mortar and one fictile tubule is addressed by is assessed by considering four distinct configurations that represent different rates of transmission of tangential stresses (0%, 30%, 60% and 100%). These four configurations are properly set as "Interactions" in Abaqus. The three-point bending tests are simulated with analyses performed in the Abaqus/Explicit environment. The load-displacement graphs for the four considered interactions are shown in Fig. 2b, in which they are plotted against the envelope of the experimental results. Only the configuration named "Friction 0.6", which represents a rate of transmission of tangential stresses equal to 60%, grasps the real rate of adherence between mortar and fictile tubules.

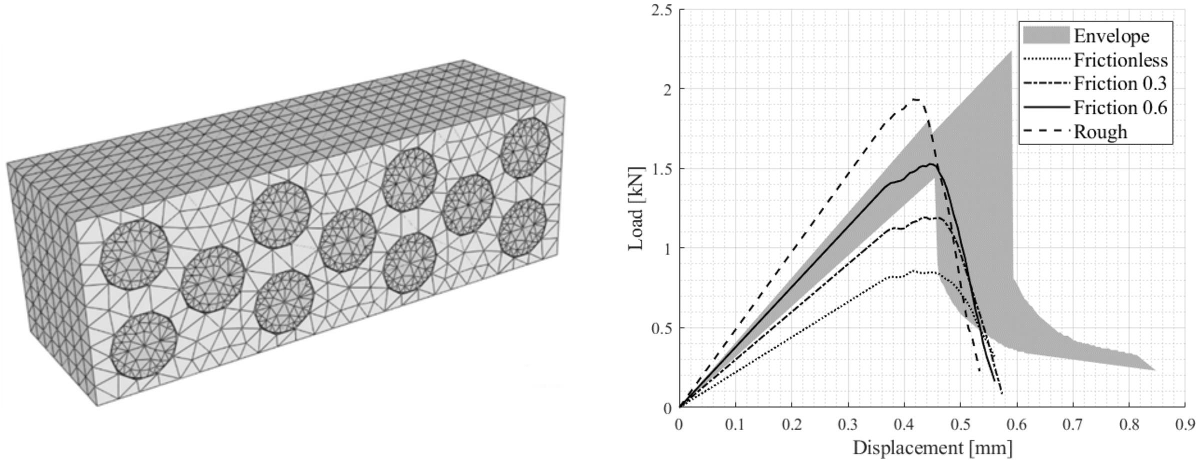

(a) (b)

FIGURE 2. (a) Finite element mesh of the analytical model; (b) Load-displacement graphs of the four interaction configurations.

CONCLUSIONS AND FUTURE DEVELOPMENTS

A thorough investigation of an ancient aseismic technique based on the combination of mortar and peculiar bricks called "fictile tubule bricks" has been presented. This construction technique represents the evolution of a previous technology known as *casa baraccata*, as was developed and patented by Calabrian engineer Pasquale Frezza in the aftermath of the Messina-Reggio Calabria earthquake of 1908. After some historical notes, the results coming from an experimental campaign are reported, which address the rate of adherence between the fictile tubules and the mortar and the mechanical behavior of a specimen wall built according to Frezza's instructions. A numerical validation of the experimental results coming from the adherence investigation is also performed by carrying out computational

simulations in Abaqus. The results prove that there is no perfect adherence between the fictile tubules and the mortar, with the rate of transmission of tangential stresses being about 60% of the expected total.

In a future work, this finding will be implemented in an Abaqus model representing the specimen wall, and the diagonal compressive tests will be replicated via numerical analyses to correctly assess the results coming from the experimental tests carried out on the specimen wall itself.

REFERENCES

1. R. S. Olivito, C. Scuro, and R. Codispoti, "Experimental analysis of typical hollow clay fictile tubules of cultural heritage of Mediterranean area," in *Structural Analysis of Historical Constructions: Anamnesis, diagnosis, therapy, controls*, Proceedings of the 10th International Conference on Structural Analysis of Historical Constructions, edited by K. Van Balen and E. Verstrynge (University of Leuven, Leuven, Belgium, 2016), pp. 1362–1369.
2. S. Tiberti, C. Scuro, R. Codispoti, R. S. Olivito, and G. Milani. "Traditional masonry arches and domes with fictile tubules in Mediterranean seismic areas: advanced numerical models and experimentation," in *Proceedings of 6th International Conference on Computational Methods in Structural Dynamics and Earthquake Engineering*, edited by M. Papadrakakis and M. Fragiadakis (volume 1, 2017), pp. 2431–2448.
3. S. Tiberti, C. Scuro, R. Codispoti, R. S. Olivito, and G. Milani. "Post-cracking FRCM strengthening of an arch composed by hollow clay elements embedded in mortar: experimental investigations and numerical analyses," in *Mechanics of Masonry Structures Strengthened with Composite Materials II*, Key Engineering Materials 747, edited by A. Di Tommaso *et al.* (Trans Tech Publications, 2017), pp. 142–149.
4. R. S. Olivito, C. Scuro, and R. Codispoti, "Static analysis of masonry kilns built with fictile tubules bricks," in *Proceedings of the International Conference of Computational Methods in Sciences and Engineering 2016*, AIP Conference Proceedings 1790, edited by T. E. Simos *et al.* (American Institute of Physics, Melville, NY, 2016), art. no. 130006.
5. R. S. Olivito, R. Codispoti, and C. Scuro, "A seismic analysis for masonry constructions: the different schematization methods of masonry walls," in *Proceedings of the International Conference of Computational Methods in Sciences and Engineering 2017*, AIP Conference Proceedings 1906, edited by T. E. Simos *et al.* (American Institute of Physics, Melville, NY, 2017), art. no. 090007.
6. R. S. Olivito, C. Scuro, R. Codispoti, and S. Porzio, "A seismic analysis for ancient Trentacapilli palace with different schematization methods of masonry walls," in *Proceedings of the International Masonry Society Conferences*, (2018), pp. 2555–2562.
7. G. Vasconcelos, E. Poletti, E. Salavessa, A. M. P. Jesus, P. B. Lourenço, and P. Pilaon, Eng Struct **56**, pp. 1028–1048 (2013).
8. P. Frezza, Construction System of Earthquake-Resistant Houses. Italian Patent No. 103,254 (1909).
9. C. Scuro, F. Lamonaca, R. Codispoti, D. L. Carnì, and R. S. Olivito, Measurement **130**, pp. 246–254 (2018).
10. S. Tiberti, C. Scuro, R. Codispoti, R. S. Olivito, and G. Milani, "Experimental and numerical analysis of historical aseismic construction system," in *Structural Analysis of Historical Constructions: An Interdisciplinary Approach*, Proceedings of the 11th International Conference on Structural Analysis of Historical Constructions, edited by R. Aguilar *et al.* (Springer, Cham, 2019), pp. 910–918.
11. C. Scuro, S. Tiberti, R. Codispoti, G. Milani, and R. S. Olivito, Constr Build Mater **193**, 84–96 (2018).
12. S. Tiberti, C. Scuro, R. Codispoti, R. S. Olivito, and G. Milani, "Masonry structures built with fictile tubules: experimental and numerical analyses," in *Proceedings of the International Conference of Computational Methods in Sciences and Engineering 2017*, AIP Conference Proceedings 1906, edited by T. E. Simos *et al.* (American Institute of Physics, Melville, NY, 2017), art. no. 090010.
13. Ente Italiano di Normazione UNI, UNI EN 1015-11:2007, Methods of Test for Mortar for Masonry – Part 11: Determination of Flexural and Compressive Strength of Hardened Mortar, Rome, Italy, 2007.

Application of Homogenization Approaches for Modeling of FRCM-Strengthened Masonry

Elisa Bertolesi[1, a)], Bahman Ghiassi[2, b)], Gabriele Milani[3, c)]

[1]*ICITECH, Universitat Politècnica de Valencia, Camino de Vera s/n 46022, Valencia, Spain.*

[2]*Centre for Structural Engineering and Informatics, Faculty of Engineering, University of Nottingham, Nottingham, United Kingdom.*

[3]*Department of Architecture, Built Environment and Construction Engineering, Technical University of Milan, Piazza Leonardo da Vinci 32, Milan, Italy.*

[a)]elber4@upv.es
[b)] bahman.ghiassi@nottingham.ac.uk
[c)] Corresponding author: gabriele.milani@polimi.it

Abstract. The creation of an effective, accurate finite element mesh is crucial for running whatsoever numerical analysis on structural models. This is especially true when micro-scale, mesoscale, and homogenization-based approaches are used, since they involve a precise and distinct representation of the constitutive materials. One fitting example is embodied by masonry with irregular bond, where blocks are randomly assembled and often present different shapes and dimensions. This work presents a Matlab script for the generation of a full 3D finite element mesh, which is created directly from a simple rasterized picture of the masonry element under investigation. A voxel approach is here used, where one pixel of the image is turned into one solid finite element. The resulting 3D mesh is employed into a broader Matlab script which derives homogenized failure surfaces for masonry test-windows. In particular, the effectiveness of the 3D mesh is validated by comparing the homogenized failure surfaces obtained for an in-plane loaded masonry panel to those retrieved from the 2D version of the script with a 2D mesh, whose reliability has already been established.

INTRODUCTION

The use of inorganic-based composites such as Textile Reinforced Mortars (TRMs) for strengthening of masonry has become a popular alternative to conventional fiber reinforced polymers, (FRPs) [1-5]. TRMs, also referred as FRCM or FRM, in the literature are composites of a continuous mesh of fibers embedded in a cementitious or lime-based mortar. As a matter of fact, it is obvious that these matrices have a lower tensile strength and elastic modulus (compared to that of epoxies used in FRPs). The mechanical properties of these materials is therefore compatible with masonry.

While experimental characterization of these materials if of critical importance for understanding the mechanics and performance of them in the field, development of suitable numerical models capable of replicating the experimental observations is of critical importance for predicting the performance of structures strengthened with these composites. Application of homogenization techniques is particularly interesting for this purpose. Homogenization allows extraction of the macro properties of the composites system taking into account the mechanisms occurring at a lower scale.

This paper presents a simple two-step homogenization approach for simulation of the numerical response of masonry panels strengthened with TRMs. The suitability and reliability of the proposed modeling approach is shown by comparing the results with a set of experimental tests. The comparisons, show, that the proposed modeling approach is in good agreement both with the experimental results and detailed numerical modeling approach.

TWO STEP HOMOGENIZATION MODEL

A simplified two-step homogenization model is presented here. In the first step, masonry is considered unreinforced and is homogenized at the meso-scale. Then, in the second step, the strengthening material will be applied to the homogenized masonry, at a structural level (macro-scale) by means of rigid elements [6, 7] and homogenized non-linear interfaces, within a Rigid Body and Spring Model (RBSM). TRM is modeled in by means of equivalent trusses with no compressive resistance and limited tensile strength and a fragile behavior. The mechanical properties of the trusses are suitably tuned to take into account the experimental push-pull double lap experimental results. Each truss is assumed perfectly bonded at the extremes to the adjoining rigid elements.

In the first step (homogenization of the unreinforced masonry), the unit cell is discretized with 24 elastic constant stress triangles (bricks) and holonomic interfaces (mortar) where all nonlinearities are lumped. Imposing on the boundary symmetry and anti-symmetry, only ¼ of the RVE is considered, as depicted in Figure 1. Furthermore, it is worth noting that the stress state of elements 4, 5 and 6 is equal to that of elements 3, 2 and 1 respectively, a feature which simplifies further the numerical model. Holonomic constitutive relationships between micro-stresses (normal and tangential) and total jumps of displacements adopted are multi-linear and the homogenization problem path independent, because the interfaces are holonomic and triangular elements elastic. A coupling between normal and shear stresses ruled by a frictional-cohesive law (Mohr-Coulomb criterion) is imposed on interfaces in order to realistically reproduce the actual behavior of mortar joints. Full details of the homogenization model here briefly reviewer can be found in [8, 9].

Imposing different boundary conditions on this unit cell (vertical, horizontal or shear displacement), the equilibrium conditions provides a system of equations in which the solution will lead to the homogenized constitutive laws. The solution can be either graphical or numerical. A detailed description of the solution strategy that can be adopted when a macroscopic tangential deformation is applied to the unit cell is reported in [8, 9], where the reader is again referred.

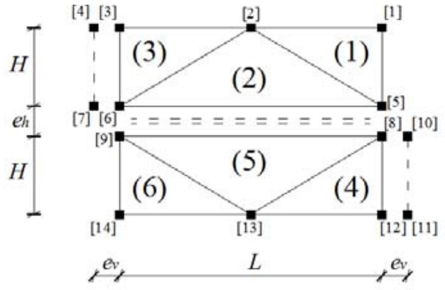

FIGURE 1. Geometry of ¼ of the elementary cell.

The second step is performed at a structural level and relies on implementation of the homogenized stress-strain relationships determined in the first step into a rigid element approach -also known as RBSM, where masonry is discretized by quadrilateral rigid elements interconnected by shear and normal non-linear homogenized springs for in-plane actions. The equivalent force-displacement non-linear relationships to apply for the single trusses/springs characterizing the in- and out-of-plane behavior of the discrete model are classically obtained by properly scaling the homogenized stress-strain relationships obtained at the meso-scale. When dealing with the FRCM reinforcement, a grid of equivalent trusses exhibiting an elasto-fragile behavior is adopted, with very low compressive strength to account for the loss of equilibrium of the system in compression due to internal buckling. The step of the trusses in the homogenized FE model is not related to the real step grid of FRCM and that equivalent areas for the trusses are used. To suitably consider both the possible debonding of the FRCM from the support and the rupture of the grid for axial loads, an idealized bilinear stress-strain curve is generally imposed to trusses.

VALIDATION WITH EXPERIMENTAL RESULTS

The accuracy of the homogenized approach is validated in this section by comparing the numerical predictions with experimental results. The experimental results are reinforced tuff wallettes subjected to standard diagonal compression tests [10, 11]. A cement-based TRM made of bi-directional grids was used for strengthening. The laboratory investigation included four diagonal compression tests on unreinforced tuff panels and eight tests on

strengthened panels considering different reinforcement configurations. Here, for the sake of conciseness, both numerical models (heterogeneous and homogenized) are benchmarked only on walls reinforced with a single grid FRCM disposed on one side. The wallettes had dimensions of 1030×1030×250 mm^3, made with blocks of dimensions 370×120×250 mm^3, laid in a single leaf running bond pattern. Mortar joints thickness is equal to 15 mm. The strengthening system is composed of a bi-directional AR-glass coated open grid, embedded into a fiber reinforced polymer modified cementitious matrix for the application on masonries.

The experimental stress-strain curves obtained during the tests are compared with the numerical predictions in Figure 2. The shear stress τ is calculated as $\tau=0.707\cdot V/A_n$, where V is the experimental applied vertical load, and A_n is the uncracked section area, while the shear strain γ is taken equal to $\gamma=\varepsilon_v+\varepsilon_h$, having indicated with ε_v, ε_h the vertical and horizontal experimental strains indirectly estimated by transducers installed on diagonals. It can be observed that the numerical global stress-strain curves (average tangential stress vs average diagonal strain) obtained (obtained from heterogeneous and the homogenized approach) are in god agreement with the experimental results. The homogenized model show a less stiff response that can be explained by utilization of a regular discretization, which is intrinsically unable to capture the real blocks interlocking behavior well and favors slippage on preferential planes of weakness where shear springs are laid.

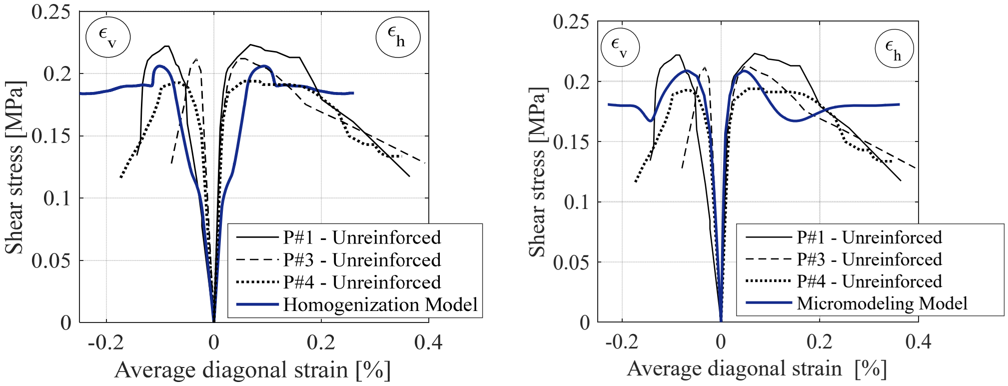

(a) (b)

FIGURE 2. Comparison experimental results and the predictions of the homogenized model for unreinforced masonry: (a) homogenized model; (b) micro modeling approach

The same simulations are replicated for the one side strengthened panels. The global stress-strain curves obtained in this case (both with the homogenized and heterogeneous model) are depicted in Figure 3, where experimental data are also represented. As clearly shown, FRCM presence has the beneficial effect of increasing both strength and ductility of the wall, significantly changing the failure mechanism. Whilst experimental results exhibit a quite wide scatter (around 40% on the peak strength), the agreement obtained with both numerical models can be considered satisfactory, slightly in favor of the homogenized approach, which seems to fit better the experimental lower bound.

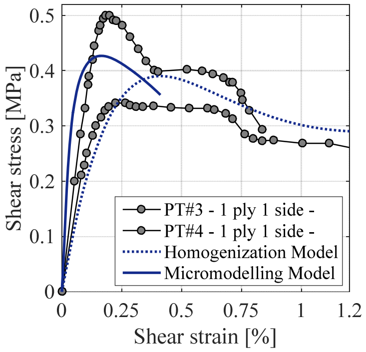

FIGURE 3. Comparison experimental results and the predictions of the homogenized model for strengthened masonry: (a) homogenized model; (b) micro modeling approach

CONCLUSIONS AND FURTHER DEVELOPMENTS

A simplified two step homogenization approach was presented in this study for numerical simulation of masonry components strengthened with textile reinforced mortars. A comparison was made between the predictions of experimental results using the proposed simplified model and detailed numerical modeling approaches. The model was found to be in good agreement with both and found to be a suitable approach for representing the complex behavior of these composites at the structural level. The capability of the model in performing nonlinear simulations at structural scale much faster than detailed numerical models, makes it suitable for engineering applications. In future works, the model will be extended to out-of-plane loading conditions so that it can be used for predicting the three-dimensional seismic response of strengthened structures.

REFERENCES

1. Triantafillou, Tc, and Cg Papanicolaou. 7th International Symposium of the Fiber-Reinforced Polymer Reinforcement for Reinforced Concrete Structures (2005).
2. D'Ambrisi, Angelo, Luciano Feo, and Francesco Focacci. Composites Part B: Engineering, 44(1):524-32 (2013).
3. Razavizadeh A., B. Ghiassi B., D.V. Oliveira. Construction and Building Materials, 16:387-97 (2014).
4. Ghiassi B., D.V. Oliveira, V. Marques, E. Soares, H. Maljaee. Materials and Design, 110(15):903-13 (2016).
5. Dalalbashi A., B. Ghiassi B., D.V. Oliveira, A. Freitas A. Composites Part B: Engineering, 152:43-57 (2018).
6. Bertolesi, E., G. Milani, and C. Poggi. Composite Structures, 158 (2016).
7. Bertolesi, E., G. Milani, and S. Casolo. Meccanica, 53(7):1819-55 (2018).
8. Milani, G., and E. Bertolesi. Construction and Building Materials, 146 (2017).
9. Milani, G., and E. Bertolesi. *AIP Conference Proceedings*. Vol. 1863 (2017).
10. Prota, A, G Marcari, G Fabbrocino, G Manfredi, and C Aldea. Journal of Composites for Construction 10: 223–33 (200).
11. Lignola, Gian Piero, Andrea Prota, and Gaetano Manfredi. Journal of Composites for Construction, 13(4) (2009).

Relaxation Test and Numerical Modeling of Rubber for Seismic Base Isolation

A.B. Habieb[1, a], G. Milani[1], V. Quaglini[1], F. Milani[2]

[1]*Politecnico di Milano, Piazza Leonardo da Vinci 32, 20133 Milan, Italy*
[2]*Chem.Co Consultant, Via J.F.Kennedy 2, 45030 Occhiobello (RO), Italy*

[a)]Corresponding author: ahmadbasshofi.habieb@polimi.it

Abstract. This paper presents a series of experimentations and numerical modeling to evaluate the damping of rubber for seismic isolation purposes. A cyclic shear test is considered as a standard procedure to evaluate the damping of rubber materials. However, there is another method to evaluate the viscous damping of rubber by means of relaxation test that requires only small dumb-bell specimens of rubber, using a uniaxial tensile test device. This method allows an efficient procedure in examining the mechanical characteristic of rubber for seismic isolation purposes. This paper evaluates such a procedure to characterize the mechanical properties of a low damping rubber. The result shows that the proposed procedure presents a good prediction of the mechanical properties of the rubber.

INTRODUCTION

Elastomeric base isolators are widely known as an economical method to mitigate the damage of structures against earthquakes. In the manufacturing of isolator devices, a series of preliminary tests are performed to characterize the mechanical properties of the rubber materials. The main properties of the rubber are shear modulus and damping ratio. To evaluate the shear modulus and damping ratio of rubber for seismic isolation device, a cyclic shear test is considered as a standard method [1,2]. It is performed by bonding a cubic rubber specimen on the testing plates and applying at least three cycles of shear in a frequency around 0.5-1 Hz.

On the other hand, a more efficient method can be considered to determine the damping ratio of the rubber using only small rubber specimens as reported in literature [3]. A relaxation test is performed on the small dumbbell specimens using a similar device for uniaxial tensile tests. Through post data processing, the relaxation data can be used for shear test simulation to estimate the damping ratio of the rubber. This alternative method may reduce significantly the amount of rubber material required for the experimentations of rubber characterization. This paper evaluates such a procedure by performing a series of relaxation tests using different rates of tensile loading. The viscosity curves obtained through the relaxation test are then approached numerically through Prony model. Finally, the results obtained from the proposed procedure are verified through the experimental shear test data.

RELAXATION TEST

Fig. 1 shows the dumb-bell rubber specimens and the dimension according to [4]. The device used is similar to which used for the uniaxial tensile test. In a tensile relaxation test, a dumb-bell specimen is pulled up to desired strain. The device then keeps the strain (see Fig. 2a) and records the evolution of the uniaxial stress up to 600 seconds (see Fig. 2b).

In this work, the relaxation test is performed on one rubber material using different rate of tensile loadings and final strains. As shown in Fig. 2a, the specimen 50%_40mm/s means that the final strain is 50% and the rate of tensile loading is 40mm/s, which is the maximum speed the device can perform. As recommended in the literature [3], for seismic isolation purposes, the rubber specimen should be pulled as quickly as possible to represent the behavior under earthquakes. However, this high speed of tensile loading generates an inertia force that disturbs the relaxation data as

shown in Fig. 3a, the horizontal axis is zoomed-in up to 10 seconds. Thus, some unexpected data should be removed. In the test with low loading speed, see Fig 3b, the inertia effect does not appear. Fig. 4 shows the refined stress-time history curves after post processing.

Fig. 5 shows the normalized stress-time history curves obtained from several relaxation tests using different final strain and loading rate. It is clearly shown that the test using low loading rate (100%_40mm/min), presents a significantly less viscous specimen. The variation of the final strain seems to not affect the evolution of uniaxial stress.

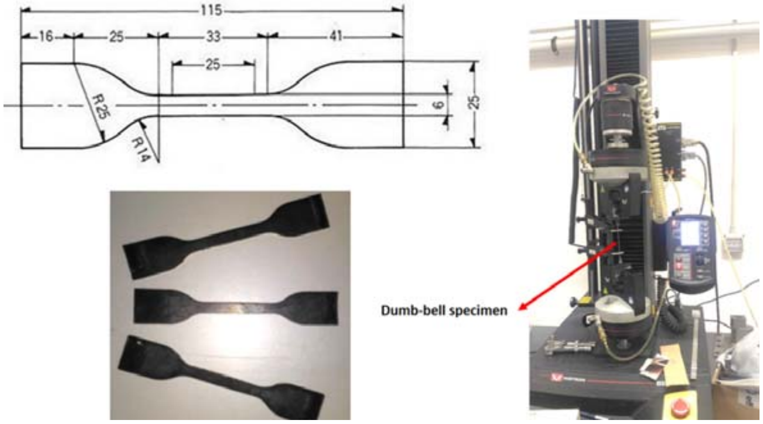

FIGURE 1. Dumbbell rubber specimens and the uniaxial tensile test device

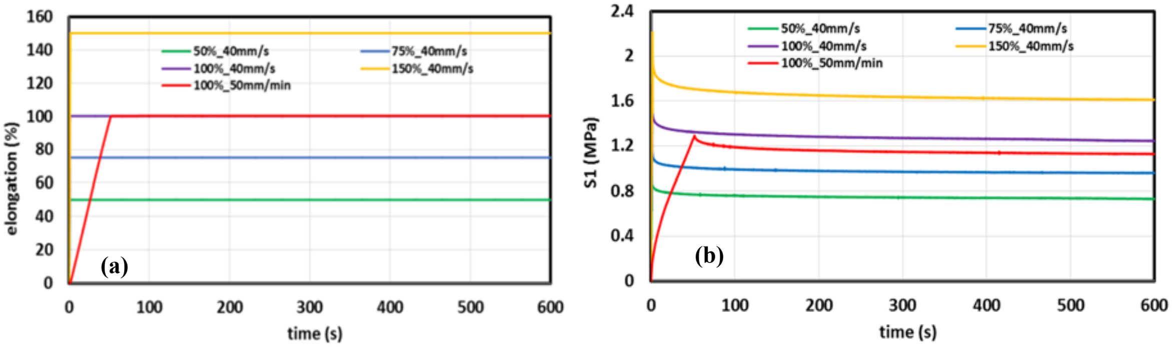

FIGURE 2. (a) Strain-time history and (b) uniaxial stress-time history obtained through several relaxation tests with different loading rate and final strain.

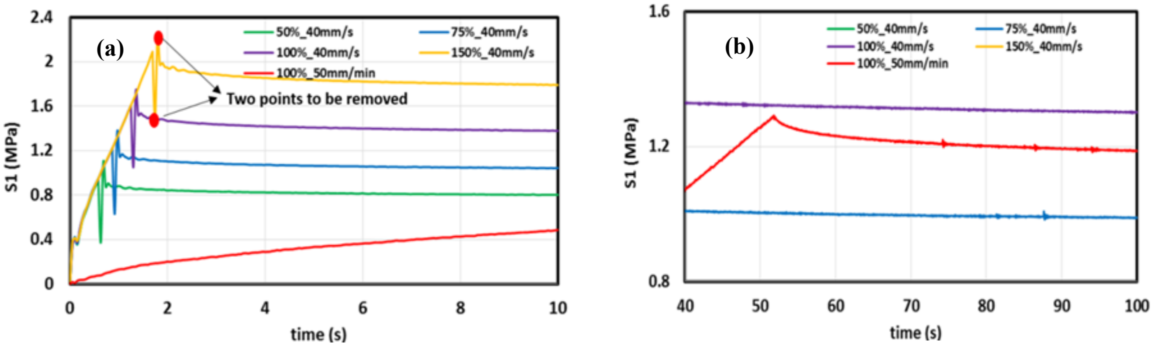

FIGURE 3. (a) Inertia effect due to high loading rate, (b) no inertia effect recorded in the relaxation test with low loading rate.

NUMERICAL MODELING

Prony model is widely used to approach the relaxation curves, see Eq 1, Where G_0 is the normalized initial stress, τ_i are the relaxation times, and g_i are the material constants.

$$\boldsymbol{G_R(t) = G_0(1 - \sum_{i=1}^{N} g_i(1 - e^{-t/\tau_i})} \qquad (1)$$

Fig 5. Presents the normalized stress-time history obtained from Prony model (dashed line). The value of $\boldsymbol{g_i}$ and $\boldsymbol{\tau_i}$ for different tests are also presented in the figure. Using two series of Prony coefficients (i=1, i=2), the curves obtained through experimental test can be well fitted.

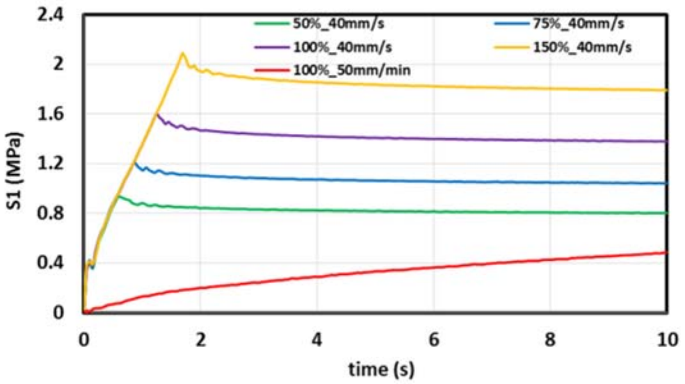

FIGURE 4. The uniaxial stress-time history of several tests after post processing.

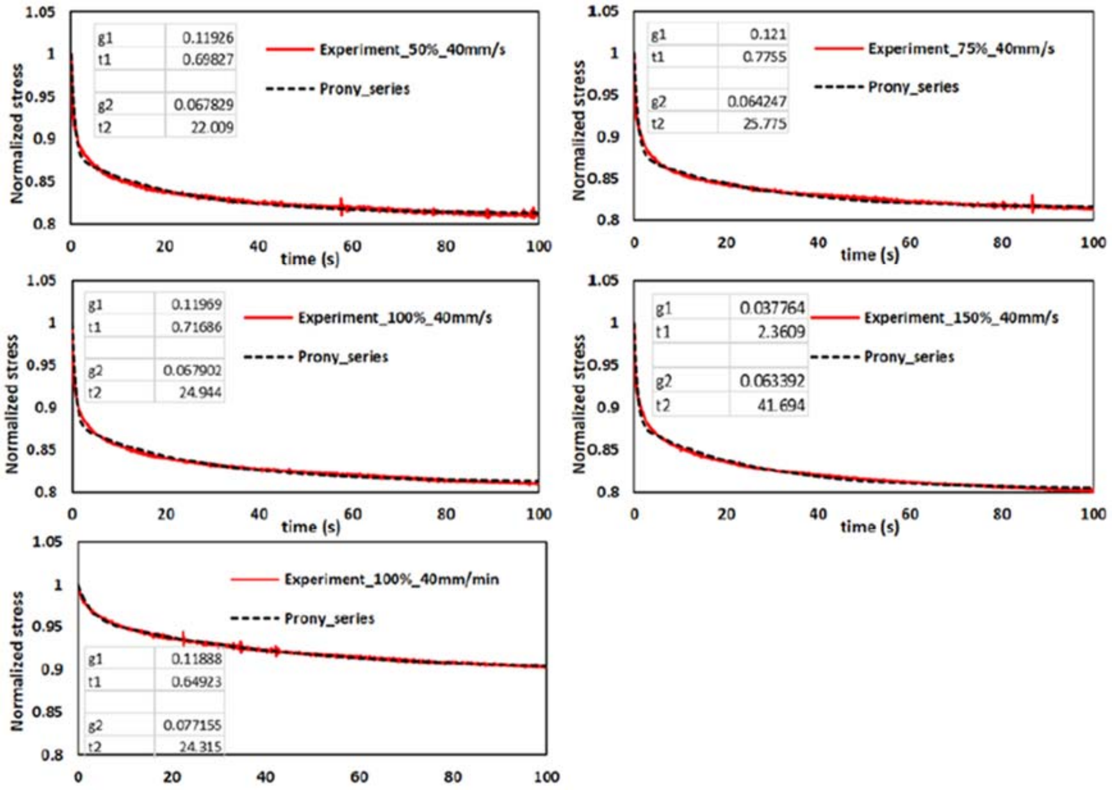

FIGURE 5. Normalized stress-time history of several relaxation tests (red line) and the corresponding Prony model and its coefficients (dashed line)

VALIDATION TROUGH THE EXPERIMENTAL SHEAR TEST

To validate the procedure discussed above, cyclic shear test simulations are performed in Abaqus [5], see Fig. 6. Yeoh hyperelasticity model is used to characterize the nonlinearity of the rubber, while Prony model is implemented to generate the viscosity behavior. Several shear test simulations are performed using different value of Prony coefficients obtained from different relaxation tests. Fig. 7 shows the comparison of the shear force-displacement hysteretic curves obtained from experiments and 3D FE simulations. Only the last cycle of the loop is considered to evaluate the procedure. The value of error represents the difference of damping ratio obtained from the experiment and simulation.

The model using data from relaxation test performed with 100% of final strain and 40mm/s of loading rate (see Fig. 7c) presents the most excellent prediction of the rubber behavior under cyclic shear test. Meanwhile, a large error is depicted in the model using data from the relaxation test with low loading rate, see Fig. 7e.

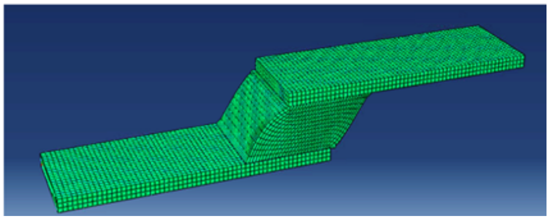

FIGURE 6. Shear test 3D FE simulation of the rubber specimen in Abaqus.

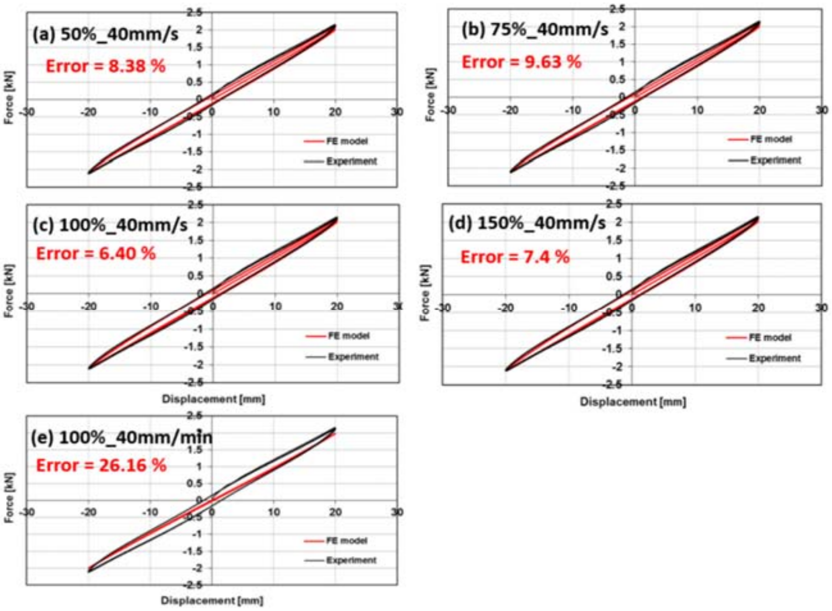

FIGURE 7. Shear force-displacement loop obtained from the experimental test (black line) and from several FE simulations using different relaxation data (red line).

REFERENCES

1. ISO 1827:2011. *Rubber, vulcanized or thermoplastic: Determination of shear modulus and adhesion to rigid plates -- Quadruple-shear methods* (British Standard Institution, London, 2011).
2. ASTM D5992-96. *Standard Guide for Dynamic Testing of Vulcanized Rubber and Rubber-like Materials Using Vibratory Method* (ASTM International, West Conshohocken, 1996)
3. T. Dalrymple, J. Choi, and K. Miller, "Elastomer rate-dependence: A testing and material modeling methodology," in *172nd Technical Meeting of the Rubber Division of the American Chemical Society (ACS),* Cleveland, OH, 2007, pp. 16–18.
4. ISO 37: 2011. *Rubber, vulcanized or thermoplastic: Determination of tensile stress-strain properties* (British Standard Institution, London, 2011).
5. Simulia, D. S. ABAQUS 6.13 User's manual (2013).

An Integrated Kinetic-FE Vulcanization Model to Predict the Optimal Curing Of Thick Rubber Pads For Applications in Seismic Isolation

Gabriele Milani[1, a)] and Federico Milani[2, b)]

[1]*Department of Architecture, Built Environment and Construction Engineering, Technical University of Milan, Piazza Leonardo Da Vinci 32, 20133 Milan, Italy.*
[2]*Chem.Co. consultant, Via JF Kennedy 2, 45030 Occhiobello (RO), Italy.*

[a)]Corresponding author: gabriele.milani@polimi.it
[b)]federico-milani@libero.it

Abstract. Thick rubber pads for cheap isolation of low rise buildings require an optimal vulcanization along the thickness. The present paper is aimed at presenting an integrated three-step approach for the optimization of curing in presence of items exhibiting considerable thickness. It requires a preliminary standard experimental characterization in a rheometer, conceived to tune a simple kinetic steady-state model finally nested into a Finite Element FE heat transmission code, which allows to simulate the curing process in full 3D heat transmission problems. The kinetic model is a phenomenological approach based on 3 kinetic constants, aimed at predicting the initial curing rate, maximum crosslinking and reversion. Kinetic constants are deduced fitting normalized experimental rheometer curves. FE transient curing computations are carried out on a thick rubber pad, used for the production of unbonded low cost seismic isolation devices. The entire 3D geometry is discretized with a refined mesh, in order to realistically reproduce the vulcanization occurring in an industrial mold. From simulation results, interesting design considerations can be drawn, allowing to establish time and temperature of curing as a function of the rubber thickness and chemical composition.

INTRODUCTION

Elastomeric seismic isolation is a classic topic in earthquake engineering. It consists in applying at the foundation level of the structure small devices constituted by rubber pads and steel/fiber laminas which have the property to shift the fundamental period of the structure to large periods, so that the horizontal loads to apply are strongly reduced, according to the reference code spectrum. For new buildings, the application of such devices is quite straightforward because just from the beginning one can conceive the isolation package (i.e. devices, rigid foundation and ring beam of the superstructure) in one step. It remains however a technological solution of protection against earthquakes exhibiting a considerable cost. For developing countries, some researchers have recently proposed (see for instance Habieb et al. 2017, 2018 2019) cheap elastomeric isolation systems based on two distinct concepts, namely the utilization of thick rubber pads with few steel/fiber laminas and the unbonded solution, i.e. the installation of the devices between foundation and superstructure without thick steel plates rigidly bonding the head and the foot of the isolator. As far as the first point is concerned, another key aspect helping to drop down the cost is to use pads made with a blend of natural and artificial rubber (to improve also the mechanical properties) and mix them with exhausted rubber powders or regenerated rubber.

The present paper focuses on the vulcanization of thick rubber pads made by a mixture of different rubbers and is aimed at presenting a computational approach useful to give a quantitative insight into the ingredients to use to maximize the final mechanical properties and the corresponding curing conditions to adopt. In particular, a computational integrated three-step procedure for the optimization of thick rubber pads final mechanical properties useful in civil engineering applications is discussed. The first step is the experimental characterization of the blend,

the second step is a kinetic steady-state model which provides kinetic constants of the blend to implement in the last step into a FE code suitable to solve heat transmission problems in full 3D discretized geometries. Knowing the temperature profile of each node of the mesh in step 3, from the FE kinetic model it is possible to estimate point by point the final degree of vulcanization of each node of the item and provide a reliable information on the local curing. The approach requires a rheometer characterization of the blend at different temperatures and the calibration of a kinetic model directly nested in a FE software. The kinetic model here adopted is characterized by 3 kinetic constants, suitable to predict the initial curing rate, maximum crosslinking and reversion. The experimental characterization has been already presented in Milani & Milani (2018a, b, c), where the reader is referred for further details. It was carried out on two "idealized" blends constituted by Natural Rubber NR and High Cis Poly-Butadiene PB respectively at 70/30 and 50/50 concentrations, with sulfur at 1 phr and two accelerants, namely N-t-butylbenzothiazole-sulphenamide and Di-phenyl-guanidine (TBBS and DPG) at 1 and 3 phr, under standard steady-state vulcanization conditions from 150°C to 180°C. Kinetic constants were then derived fitting normalized rheometer curves through a semi-analytical approach, Milani et al. (2015). The present paper focuses on the numerical simulation of the vulcanization process of a real thick rubber pad, which is suitably discretized into 3D FEs. It is shown how the three-step procedure allows to find the best concentration ratio between rubbers, the optimal balance between strength and elastic characteristics, as well as the optimal time/temperature conditions.

EXPERIMENTAL RHEOMETER CHARACTERIZATION

Experimentation was carried out in Milani & Milani (2018c) on a standard NR with Mn = 1.5x105 g/mol, and a very high cis homo-polymer polybutadiene with Mw = 6.5 x 10^5 g / mol and a % of cis conformation more than 95%. Accelerators used were TBBS (N-t-butylbenzothiazole-sulfenamide) and DPG (di phenyl guanidine) and blends at 50-50% and 70-30% NR-PB were tested at 150, 170 and 180°C. S-TBBS-DPG sulfur/accelerants concentrations respectively at 1-1-0, 1-3-0, 1-0-1, 1-0-3 phr were tested. Experimental rheometer curves are reported in Milani & Milani (2018a, b, c), where the reader is referred for further details. Before any comparison with numerical data, experimental torque $M(t)$ should be normalized (furnishing the experimental vulcanization degree $\alpha_{\exp}$) through Sun & Isayev (2009) approach:

$$\alpha_{\exp} = \frac{M - M_{\min T}}{M_{\max T_0} - M_{\min T_0}} \qquad (1)$$

Where M_{minT} in Eq. (1) is the minimum value of torque at temperature T. Before reaching this minimum value, $\alpha_{\exp}$ is considered equal to zero. M_{minT0} and M_{maxT0} are the minimum and maximum torque values at a curing temperature equal to T_0 low enough to allow neglecting reversion.

SIMPLIFIED KINETIC MODEL OF VULCANIZATION

The basic reaction scheme is classic for NR but can be adapted also in different situations (e.g. Milani & Milani 2017) and is in particular due by Han et al. (1998). Typically, after the initial induction viscous phase which characterizes the uncured rubber at high temperature, curing proceeds through two pathways, with the formation of stable and unstable un-matured cured rubber. The distinction between stable and unstable curing stands in the presence of single or multiple sulfur bonds respectively. Multiple bonds are subjected with higher probability to break and hence they are responsible to macroscopic de-vulcanization (also known as reversion). The kinetic scheme adopted is therefore classically constituted by three reactions:

$$[P]\xrightarrow{K_1}[R_1^*] \qquad [P]\xrightarrow{K_2}[R_2^*] \qquad [R_2^*]\xrightarrow{K_3}[R_r^*] \qquad (2)$$

where $[P]$ is the unvulcanized rubber concentration, $[R_1^*]$ and $[R_2^*]$ the crosslinked rubber, one stable (K_1) and the other (K_2) subjected to reversion, and $[R_r^*]$ is the amount of rubber subjected to de-vulcanization.

Assuming the kinetic scheme of Eq. (2), after suitable mathematical passages not reported here for the sake of conciseness, it is possible to estimate in closed form the crosslinking density $\alpha = \left([R_1^*]+[R_2^*]\right)/[P]$ as follows:

$$\alpha = K_1/\left(K_1+K_2\right)\left[1-e^{-(K_1+K_2)(t-t_s)}\right] + K_2/\left(K_1+K_2-K_3\right)\left[e^{-K_3(t-t_s)} - e^{-(K_1+K_2)(t-t_s)}\right] \qquad (3)$$

Han et al. (1998) suggest to evaluate kinetic constants by means of standard least-squares best fitting on experimental (or regularized) data, but Milani et al. (2017) have recently proposed a more efficient approach where

kinetic constants are estimated in quasi-closed form. In the first step of this latter approach, K_1 and K_2 are evaluated knowing the crosslinking density at the end of the experimental test (α_R) and the vulcanization rate at scorch (α'_0), as $K_2 = \alpha'_0(1-\alpha_R)$ and $K_1 = \alpha'_0 \, \alpha_R$. Assuming the vulcanization degree α_P known at a certain t_P, K_3 is estimated graphically in the second step as the intersection between the following curves:

$$y_1 = \frac{(\alpha_P - C_0)(C_3 - K_3)}{C_2} \quad y_2 = e^{-K_3(t_P - t_s)} - C_1 \quad C_0 = \frac{K_1\left[1 - e^{-(K_1+K_2)(t_P - t_s)}\right]}{K_1 + K_2} \quad C_1 = e^{-(K_1+K_2)(t_P-t_s)} \quad C_2 = K_2 \quad C_3 = K_1 + K_2 \qquad (4)$$

Where t_s is the time at scorch.

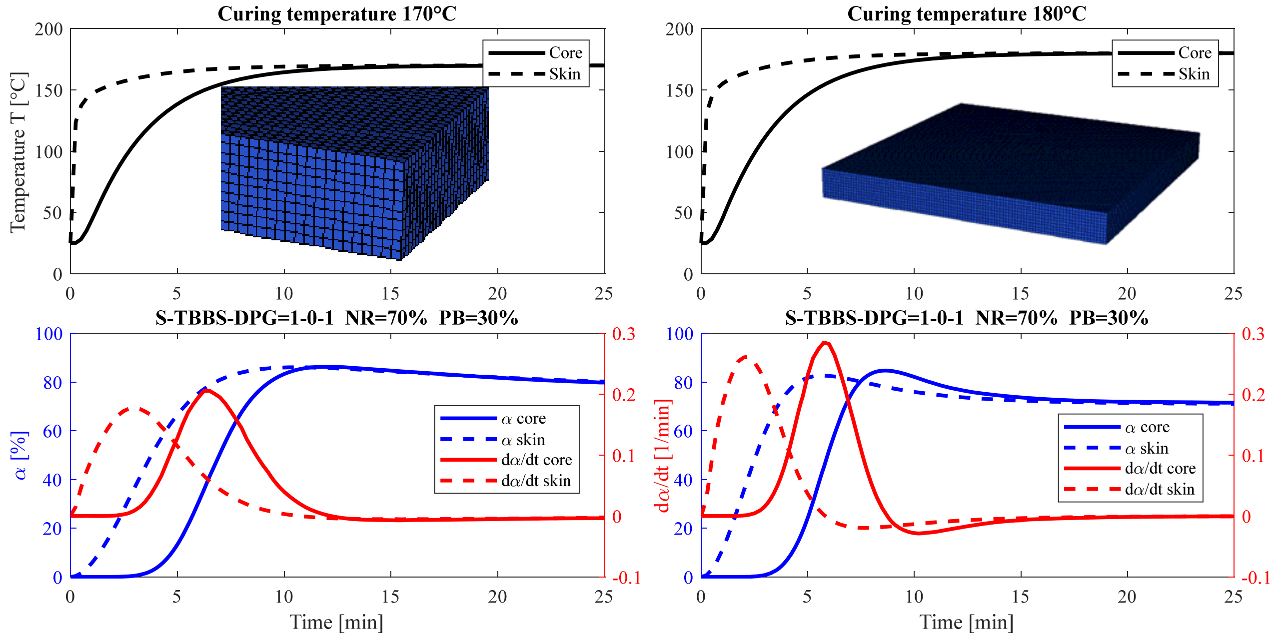

FIGURE 1: Curing of a thick rubber pads simulated with FEs at two different vulcanization conditions

FE VULCANIZATION: NUMERICAL RESULTS

In the most general case of 3D items, temperature profiles for each point of the element are obtained solving numerically Fourier's heat transmission law:

$$\rho_p c_p \partial T / \partial t - \lambda_p \Delta T - r_p \Delta H_r = 0 \qquad (5)$$

where ρ_p, c_p^p and λ_p are rubber density, specific heat capacity and heat conductivity respectively, ΔH_r is rubber specific heat (enthalpy kJ/mol) of reaction (if any and if important for engineering applications), r_p is the rate of cross-linking (mol/m^{3}sec); Δ is the Laplace operator.

Eq. (5) can be easily solved using a Finite Element FE discretization. In this case, FEs must be coupled with the kinetic model previously presented in order to predict point by point the final crosslinking density obtained.

If for a node **P**, the temperature profile T(**P**)=T(t) as a function of time is known from finite elements, then it is possible to show that deriving Eq. (3) the crosslinking rate at an instant t is the following:

$$\frac{d\alpha}{dt} = F_1\left\{1 - e^{-[K_1(T)+K_2(T)]t}\right\} + F_2 e^{-[K_1(T)+K_2(T)]t} + F_3\left\{e^{-K_3(T)t} - e^{-[K_1(T)+K_2(T)]t}\right\} + \frac{K_2(T)}{K_1(T)+K_2(T)-K_3(T)}\left\{F_4 e^{-K_3(T)t} + F_5 e^{-[K_1(T)+K_2(T)]}\right\} \qquad (6)$$

Functions F_1, …, F_5 are not reported here for the sake of conciseness and the interested reader is referred to Milani & Milani (2018b) for further details. Here it is worth noting only that functions F_i depend on the following parameters: dK_i/dt, K_i, dT/dt, T. It is also interesting to point out that $K_i(T)$ is a function analytically defined by Arrhenius relationship, i.e. $K_i(T)=\exp(\ln K_i^\infty - \wp'/T)$, where K_i^∞ is the i-th kinetic constant at an infinite temperature and $\wp'$ is the absolute value of the slope of the Arrhenius law (linear) in the $\ln K_i$-$1/T$ space. Temperature profile first derivative

with respect to time t is again evaluated numerically by finite differences. All quantities appearing in Eq. (6) are therefore known either analytically or numerically: consequently, curing rate is known for each node of the mesh. A final numerical integration allows to determine the crosslinking degree at each instant (including the final curing degree, which is the most important).

NUMERICAL RESULTS

As practical example to analyze, a thick rubber pad with thickness 20 mm and cross section equal to 30x30 cm is considered. The FE discretization is quite refined, as shown in Figure 1 and the heat transmission problem is fully 3D but with the simplifying hypothesis to consider a single pad, with boundary conditions at the vertical surfaces and lower horizontal surface drawn by the contact with the steel walls and the lower lamina. Parameters used to define the heat transmission problem are provided in Milani & Milani (2018c) and they are not repeated here for the sake of conciseness. Here it is only worth noting that data adopted in the simulations are in agreement with general literature indications. Vulcanization is assumed to occur in a chamber filled with nitrogen/air and then cooled at room temperature in air. Two different temperatures of vulcanization are considered, equal to 180°C and 170°C respectively, to simulate both a fast and a slightly slower realistic curing condition. The curing time is assumed equal to 25 minutes in both cases. In Figure 1, the results obtained with a 70-30% NR-PB blend and S-TBBS-DPG=1-0-1 phr are depicted. The first row shows the temperature profiles obtained with FEs for a point in the core and one in the skin of the pad. Left column refers to vulcanization at 170°C, whereas right column at 180°C. The second row shows the curing degree evolution (blue curves) and the curing rate (red curves). Dashed curves refer to the skin and continuous lines to the core. From an analysis of the results it is particularly evident that the skin exhibits a much faster heating with respect to the core node. At 180°C, this feature results into an almost immediate crosslinking (more than 80% in about 5 minutes for all the cases analyzed), but also the early activation of reversion, which induces de-vulcanization and does not allow rubber to exhibit good mechanical properties after the end of the curing process. A vulcanization at 170°C is more effective, but still shows slight vulcanization and in any case it does not exceed 80% at peak. As shown quantitatively in Milani et al. (2018c), using DPG as accelerant is generally associated to suboptimal curing.

REFERENCES

1. A.B. Habieb, G. Milani, T. Tavio, F. Milani "Low cost frictional seismic base-isolation of residential new masonry buildings in developing countries: A small masonry house case study", The Open Civil Engineering Journal, **11** (Suppl-5, M2), 1026-1035 (2017).
2. A.B. Habieb, G. Milani, T. Tavio, "Two-step advanced numerical approach for the design of low-cost Unbonded Fiber Reinforced Elastomeric seismic Isolation systems in new masonry buildings", Engineering Failure Analysis, **90**, 380-396 (2018).
3. A.B. Habieb, M. Valente, G. Milani, "Implementation of a simple novel Abaqus User Element to predict the behavior of unbonded fiber reinforced elastomeric isolators in macro-scale computations", Bulletin of Earthquake Engineering, **17**, 2741–2766 (2019).
4. I.S. Han, C.B. Chung, S.J. Kang, S.J. Kim, H.C. Chung, "A kinetic model of reversion type cure for rubber compounds", Polymer (Korea), **22**, 223-230 (1998).
5. G. Milani, F. Milani, "Closed form numerical approach for a kinetic interpretation of high-ci-polybutadiene rubber vulcanization", Journal of Mathematical Chemistry, **55**, 552–583 (2017).
6. G. Milani, T. Hanel, R. Donetti, F. Milani, "A closed form solution for the vulcanization prediction of NR cured with sulphur and different accelerators", Journal of Mathematical Chemistry, **53**(4), 975-997 (2015).
7. G. Milani, F. Milani, "Rubber blends: kinetic numerical model by rheometer experimental characterization", Journal of Mathematical Chemistry, **56**, 1520–1542 (2018a).
8. G. Milani, F. Milani, "Quasi analytical kinetic model for Natural Rubber and Poly-Butadiene rubber blends. Reaction Kinetics, Mechanisms and Catalysis", **123**, 351–365 (2018b).
9. G. Milani, F. Milani, "Optimal vulcanization of tires: Experimentation on idealized NR-PB natural and poly-butadiene rubber blends, phenomenological smoothed numerical kinetic model and FE implementation", Polymer Testing, **72**, 63-85 (2018c).
10. X. Sun, A.I. Isayev, "Cure kinetics study of unfilled and carbon black filled synthetic isoprene rubber", Rubber Chem. Technol., **82**(2), 149-169 (2009).

Full 3D CAD Procedure for the Speedy Evaluation of the Seismic Vulnerability of Masonry Towers

Natalia Pingaro[1, a)] and Gabriele Milani[1, b)]

[1]*Department of Architecture, Built Environment and Construction Engineering, Technical University of Milan, Piazza Leonardo Da Vinci 32, 20133 Milan, Italy.*

[a)]natalia.pingaro@mail.polimi.it
[b)]Corresponding author: gabriele.milani@polimi.it

Abstract. A very straightforward 3D CAD approach for the speedy evaluation of the seismic vulnerability of existing masonry towers is presented. The procedure requires only the detailed 3D geometric model of the structure and automatically calculates the collapse acceleration on a user defined failure mechanism. In this paper, few pre-assigned mechanisms are tested, as for instance vertical splitting, simple overturning at the base, rocking with inclined yield lines and combined rocking and vertical splitting. The restriction of the possible tower failure within such a few mechanisms grounds on previous numerical research in the field and post-earthquake surveys experience. In any case, any user can define his own mechanisms according to the specificity of the case-study under consideration, directly shaping distinct volumes inside the CAD software. The procedure is automatized and the direct application of the principle of virtual works -assuming that masonry behaves as a no-tension material- allows the immediate evaluation of the horizontal acceleration at collapse. The mechanism associated to the minimum acceleration, in agreement with the kinematic theorem of limit analysis, is that most probably would occur in reality during a seismic event. The approach allows a straightforward evaluation of the seismic vulnerability of a tower and can be used even by practitioners not familiar with advanced FE computations and limit analysis concepts, so adapting well to the heterogeneous community involved in cultural heritage preservation. The automatized procedure is applied in this paper to a historical tower located in central Italy, to show the capabilities of the approach.

INTRODUCTION

Historical masonry towers were typically conceived only for gravity loads and therefore it is not surprising that they usually turn out to be rather vulnerable to earthquakes, a feature demonstrated many times by the catastrophic collapses observed after strong earthquakes (e.g. Acito et al. 2014, Acito et al. 2016).

Italy in particular is a country with thousands of historical towers located in medium/high seismicity zones; some of them have exceptionally high artistic and historical value and need to be preserved. At this aim, the recent Guidelines for the Built Heritage (Guidelines 2011) suggest a simplified procedure based on a cantilever beam approximation to determine towers vulnerability. Primarily, the idea is to obtain a speedy screening of the most dangerous situations, in order to eventually target interventions and funding. Such method is standardized and it is enough simple to be used also by practitioners not familiar with complex concepts of structural analysis. Unfortunately, however, the assimilation of the behavior to a cantilever beam in bending is not always suitable, as proved by post earthquake surveys, which have shown how many times the failure mechanism associated to collapse is not the formation of a plastic hinge in a given position along the height (at the base if the tower is sufficiently regular). The knowledge of the exact mode of collapse is crucial not only for a sound evaluation of the vulnerability, but also to implement an effective strengthening (Milani et al. 2018).

Numerical literature in the field is superabundant and recent trends in the numerical structural analysis of masonry towers include the utilization of sophisticated approaches, such as discretizations with 2D/3D non-linear FE or meshes

constituted by non-linear beams (Casolo 1998, Lucchesi et al. 2004, Milani et al. 2012, Casolo et al. 2013, Valente & Milani 2016). Whilst both families of procedures are appealing, they cannot take into account all the specificities in the different cases and/or require experienced users with a robust theoretical background. As a matter of fact, indeed, in practice the utilization of non-linear methods is still not so common, because commercial codes with advanced material models should be adopted by users that are supposed to have a strong mathematical and mechanical background and deep knowledge on sophisticated non-linear analyses, which is not always the case in the heterogeneous community of historical heritage preservation.

In order to overcome the aforementioned drawbacks, Sarhosis et al. (2018) have recently proposed a kinematic limit analysis where vulnerability can be estimated assuming that a tower fails for the formation of five possible different pre-assigned failure mechanisms, namely vertical splitting, base rocking, Heyman's diagonal rocking (Heyman 1992), combination of splitting+diagonal rocking and base sliding. The final target is similar to that pursued by the Italian Guidelines, i.e. to prefer simplicity, to avoid a discretization into several FEs and to facilitate diffusion at professional level, at the same time providing realistic estimations of the vulnerability and considering the most important features of masonry, as the inability to withstand tensile stresses and the modalities of collapse, characterized by few rigid macro-blocks mutually roto-translating. Adopting a classic limit analysis approach, which is a simple method explicitly suggested in the Italian code, the strong limitation to assimilate a tower to a cantilever can be easily superseded. This notwithstanding, the most important limitation of the procedure proposed by Sarhosis et al. (2018) is the idealization of the towers by means of hollow square cross-sections, a simplification which puts some doubts in its immediate applicability to real cases with complex geometries and irregularities.

This paper is aimed at presenting a new straightforward 3D CAD approach for the speedy evaluation of the seismic vulnerability of existing masonry towers. The procedure requires only the detailed 3D geometric model of the structure and automatically calculates the collapse acceleration on a user defined (or many) failure mechanism(s). In this paper, few pre-assigned mechanisms are tested, as for instance vertical splitting, simple overturning at the base, rocking with inclined yield lines and combined rocking and vertical splitting. The restriction of the possible tower failure to such a few mechanisms grounds on previous numerical research in the field and post-earthquake surveys experience. In any case, user can define his own mechanism according to the specificity of the case-study under consideration. The procedure is automatized and the direct application of the principle of virtual works assuming that masonry behaves as a no-tension material allows the immediate evaluation of the horizontal acceleration at collapse. The mechanism associated to the minimum acceleration, in agreement with the kinematic theorem of limit analysis, is that most probably will occur in reality. The approach allows a straightforward evaluation of the seismic vulnerability of a tower and can be used even by practitioners not familiar with advanced FE computations and limit analysis concepts, so adapting well to the heterogeneous community involved in cultural heritage preservation. The automatized procedure is applied to a historical tower in the central Italy, analyzed to benchmark the procedure. The approach has several advantages, the most important being (1) the possibility to account for the actual geometry of the tower in an extremely detailed manner (so considering openings, irregularities, mass variation along the height, etc.), (2) the drastic reduction of the computational effort needed (only the recursive evaluation of the principle of virtual powers is required), (3) the adaptation of the failure mechanisms to the specificity of the problem treated, (4) the possibility to apply distributions of horizontal loads different from standard ones or specific lateral constraints and finally (5) the easy utilization.

THEORETICAL BASE AND THE CASE STUDY UNDER CONSIDERATION

Let us consider a tower geometrically represented with a 3D CAD model assembled in different volumes with any shape. Such subdivision into different volumes must include the possible activation of all those failure mechanisms that are considered relevant to analyze for the stability of the tower under horizontal loads. Assuming one failure mechanism active, powers dissipated by external loads on a certain volume E are those dependent and independent upon the load multiplier. They are respectively evaluated as follows:

$$P_{\lambda}^{E} = \alpha^{E} V^{E} \lambda \dot{U}_{G} \qquad P_{w}^{E} = \left(W^{E} + F^{E}\right)\dot{V}_{G} \tag{1}$$

In Eq. (1), P_{λ}^{E} is the power dissipated on E by loads depending on the collapse multiplier, α^{E} is a numerical coefficient depending on the actual distribution of horizontal accelerations applied to the structure, V^{E} is the volume, λ is the collapse multiplier, $\dot{U}_{G}$ is the horizontal velocity of the centroid of E , P_{w}^{E} the power expended on E by

loads independent on the collapse multiplier, W^E is E self weight, F^E an eventually present concentrated vertical force (applied on the centroid) and $\dot{V}_G$ the vertical velocity of the centroid. It is worth mentioning that inertia properties of E are typically evaluated in automatic within the most diffused CAD software, by means of consolidated subroutines available in commercial packages. It should be also pointed out that concentrated loads as well as self weight can be applied directly to centroids of the different volumes, so different contributions can be accounted for, as for instance presence of bells, heavy masses or tie rods used as strengthening to reduce vulnerability. Dissipation on interfaces vanishes because the material considered is a no-tension one, in agreement with the Italian code. Quantities $\dot{U}_G$, $\dot{V}_G$ are linear functions in $\dot{\vartheta}$ (the Lagrangian variable defining the motion of the multi-block system in an assigned failure mechanism) and can be re-written as $\dot{U}_G = c_U^E \dot{\vartheta}$ and $\dot{V}_G = c_V^E \dot{\vartheta}$, where $c_{U,V}^E$ are constant values depending on the element E considered. Powers expended must be extended to all volumes, leading to the following expressions (n is the total number of volumes present in the CAD model):

$$P_\lambda = \lambda \dot{\vartheta} \sum_{i=1}^{n} \alpha^i V^i c_U^i \quad P_w = \dot{\vartheta} \sum_{i=1}^{N} \left(W^i + F^i \right) c_V^i \qquad (2)$$

Using the principle of virtual powers (i.e. applying the kinematic theorem of limit analysis), the collapse multiplier is then easily evaluated from Eq. (2) simply by the following expression:

$$\lambda = \sum_{i=1}^{N} \left(W^i + F^i \right) c_V^i \Big/ \sum_{i=1}^{n} \alpha^i V^i c_U^i \qquad (3)$$

For a pre-assigned failure mechanism the collapse multiplier is therefore immediately evaluable interfacing a CAD 3D model with an Excel spreadsheet, as done in the present paper.

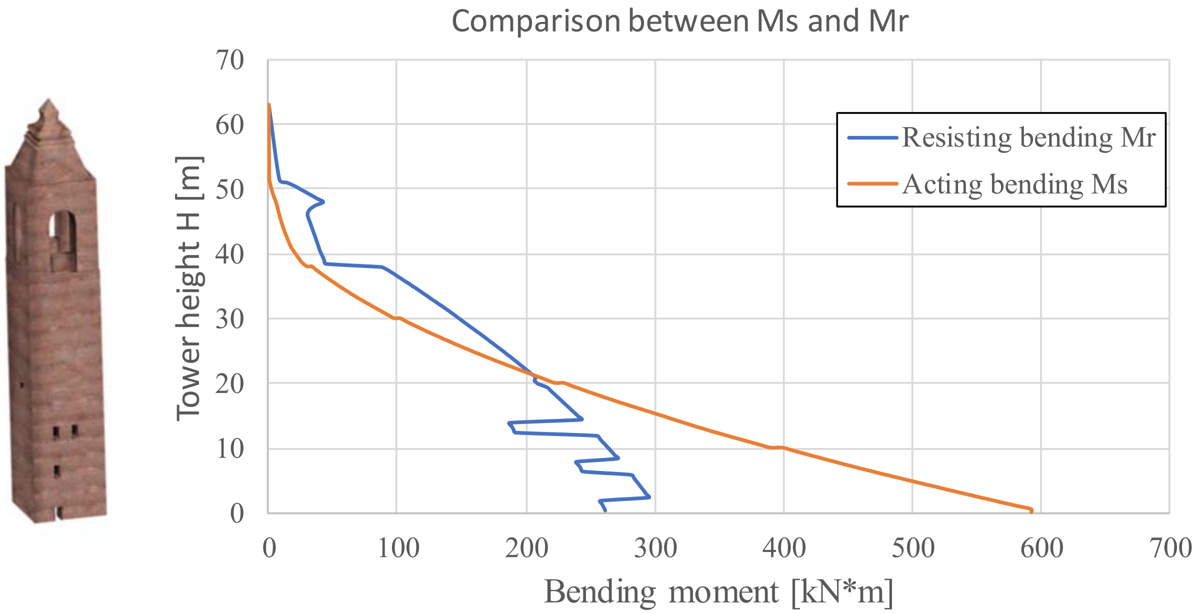

FIGURE 1. Geometry of the tower investigated (left) and comparison between resisting (Mr) and acting (Ms) bending moment

NUMERICAL RESULTS

As practical example to analyze, an existing masonry tower located in central Italy, see Figure 1, is considered. The height of the tower is roughly 60 m; it is globally regular (exception made for the presence of the belfry and the roof between 40 and 60 m), with rectangular cross section of about 8x10 m and small opening in the lower part. A standard verification of the vulnerability made comparing resisting Mr and acting Ms bending moments (see Figure 1), evaluating Mr with the simplified formula provided in Guidelines (2011) and Ms with a PGA=0.25g and constant distribution along the height (to compare with limit analysis results). As can be noted from Figure 1 and as expected,

the tower is vulnerable in the lower 20 m, with a predicted failure due to the formation of a flexural plastic hinge at the base. Kinematic limit analysis results obtained with the present CAD model and reported in Figure 2 confirm the vulnerability index provided by Figure 1, but suggest that most likely failure occurs for the formation of vertical splitting, which is associated to the lowest multiplier. Such outcome is particularly important in light of a future strengthening intervention with tie rods.

a_g/g=0.137 a_g/g=0.146 a_g/g=0.26 a_g/g=0.228 a_g/g=0.288

FIGURE 2. Most relevant failure mechanisms investigated with the CAD procedure proposed and corresponding a_g/g at collapse (from left to right, from smallest to biggest)

REFERENCES

1. M. Acito, M. Bocciarelli, C. Chesi, G. Milani, "Collapse of the clock tower in Finale Emilia after the May 2012 Emilia Romagna earthquake sequence: Numerical insight", Engineering Structures, **72**, 70–91 (2014).
2. M. Acito, C. Chesi, G. Milani, S. Torri, "Collapse analysis of the Clock and Fortified towers of Finale Emilia, Italy, after the 2012 Emilia Romagna seismic sequence: Lesson learned and reconstruction hypotheses", Construction and Building Materials, **115C**, 193-213 (2016).
3. S. Casolo, "A Three Dimensional Model for Vulnerability Analyses of Slender Masonry Medieval Towers", Journal of Earthquake Engineering, **2**(4), 487-512 (1998).
4. S. Casolo, G. Milani, G. Uva, C. Alessandri, "Comparative seismic vulnerability analysis on ten masonry towers in the coastal Po Valley in Italy", Engineering Structures, **49**, 465–90 (2013).
5. Guidelines (2011). DPCM 9/2/2011. Italian guidelines for the evaluation and the reduction of the seismic risk for the built heritage, with reference to the Italian norm of constructions.
6. J. Heyman, "Leaning towers", Meccanica, **27**(3), 153-159 (1992).
7. M. Lucchesi, B. Pintucchi, N. Zani, "Dynamic analysis of slender towers made of no-tension material with limited compressive strength", Structures and Materials, **15**, 323-333 (2004).
8. G. Milani, S. Casolo, A. Naliato, A. Tralli, "Seismic assessment of a medieval masonry tower in northern Italy by limit, nonlinear static, and full dynamic analyses", International Journal of Architectural Heritage, **6**(5), 37–41 (2012).
9. G. Milani, R. Shehu, M. Valente, "Role of inclination in the seismic vulnerability of bell towers: FE models and simplified approaches", Bulletin of Earthquake Engineering **15**, 1707–1737 (2017).
10. V. Sarhosis, G. Milani, A. Formisano, F. Fabbrocino, "Evaluation of different approaches for the estimation of the seismic vulnerability of masonry towers", Bulletin of Earthquake Engineering, **16**(3), 1511-1545.
11. M. Valente, G. Milani, "Non-linear dynamic and static analyses on eight historical masonry towers in the North-East of Italy", Engineering Structures, **114**, 241–270 (2016).

Preface of the session: 'Allometry and Scaling in Medicine, Biophysics and Ecology'

Atanas Todorov Atanasov

Medical Faculty, Trakia University, Department of Physics and Biophysics, Armeiska str. 11, 6000 Stara Zagora, BULGARIA
Corresponding author: atanastod@abv.bg

Small description of the symposium.

Allometry is the study of the relationship of body size to shape , anatomy, physiology, behaviour and ecology first outlined by Otto Snell in 1892, by D'Arcy Thompson in 1917 and by Julian Huxley in 1932. Huge numbers of morphological, anatomical, physiological, medical and biophysical traits of living organisms depend on their mass, size, body mass index, and life expectancy. The relationship between the local parameters and the integral characteristics of the organisms is assumed to be expressed by allometric dependencies of the type: $Y = aX^b$, where a and b are constants, Y reflect the local traits and X reflect the integral characteristics of the organism- mass, volume, surface, BMI, lifespan and others. The power coefficient can have positive and negative values and varied normally in the window from zero to 2.0. The correlation coefficients in these relationships are generally high and reflect statistically significant relationships between variables. Allometric dependencies allow new empirical patterns and statistical links to be found between first-look unrelated characteristics of living organisms. The allometric dependencies are well developed in biology, but are still poorly addressed in the field of medicine, biophysics, biochemistry, bio-technical sciences as well as other scientific areas related to living organisms and systems (ecology, epidemic and climatic dependencies). Allometric scaling is a method for examining the structural and functional consequences of changes in size, mass, lifespan and connection to various unknown regulatory mechanisms. All this expresses the all-time approach as a promising innovative method in all areas of science.

Atanasov AT

SHORT CV- Birth date: 15.01.1954, Trakietz (Haskovo), BULGARIA; **Education**: 1979 MSc, Faculty of Physics, Sofia University "St. Kliment Ohridski", Bulgaria; **First specialty** "Radio-physics and electronics", **Second specialty** "Biophysics", Sofia University, Bulgaria; **Specialization**: 1979-1982, Neurophysiology of brain, Institute of neurobiology, Bulgarian Academy of Sciences; **Work experience**: 2017-Professor of Physics; **Affiliation:** Department of Physics and Biophysics, Medical Faculty, Thracian University of Stara Zagora, Bulgaria; **Teaching Experience:** Medical Physics, Medical Biophysics, Medical Technology and New Technologies in Medicine; **Publications** / full text / - 100; **Basic research interest:** isolation of biologically-active compounds from Bulgarian medicinal plans, study of nasal and sleep cycles, allometry (empiric) laws and relationships in biology and biophysics; transdermal introduction of drugs with pulsed electric field .

Allometric Relationship between Volume to Surface Ratio and Incubation Days in Bird's Eggs

Atanas Todorov Atanasov

Medical Faculty, Trakia University, Stara Zagora, BULGARIA

Corresponding author: atanastod@abv.bg

Abstract. The correlation coefficient between bird eggs volume to surface ratio and incubation time in 28 eggs (from *Struthio camelus* to *Calypte anna*) is R =0.561. The eggs volume (V_{egg}, m^3), eggs surface (S_{egg}, m^2), incubation times (T_{inc}, s) and oxygen permeability coefficient (K_{O2}, m/s) trough inner egg membrane are connected by allometric relationship: $V_{egg} /(S_{egg} \cdot T_{inc}) = K_{O2}$ (for 1 Torr oxygen pressure trough egg shell membranes). This relationship allows calculate dynamics of oxygen permeability coefficient trough inner egg shell membrane during bird embryonal development.

INTRODUCTION

Allometric relationships between volume, surface, lifespan and membrane permeability coefficients of organisms and cells. Between the birds eggs characteristics (eggs mass, volume and surface, eggs density, incubation time, conductance of eggs shell, eggs pore structure, birds embryonal metabolism and others) are found many allometric relationships given in scientific publications of Rahn and Ar [1], Paganelli et all. [2], Hoit [3] and others investigators [4, 5].

In the same direction, in previous studies Atanasov [6] found in all spectrum of living organisms (Unicellular organisms, Poikilotherms, Mammals, Aves), an common allometric relationship between the volume (V, m^3), surface (S, m^2) and lifespan (T_{ls}, s) of organisms :

$$V/S= 8.933\times10^{-11} \cdot T_{ls}^{0.915} \qquad \text{(with } R^2 =0.931) \qquad (1)$$

Especially, for growing Unicellular organisms (from Bacteria to Amoebas) the ratio between the volume to surface to doubling time of unicellulars is equals to membrane permeability coefficients for membrane-potential generating sodium and potassium ions (P_{Na^+, K^+}) [7, 8]:

$$V/(S\cdot T_{dt}) = P_{Na^+,K^+} \quad \text{(in meters per second)} \qquad (2)$$

These two equations express a certain universal relationship between volume, surface, lifespan and permeability of substances that determine the energetic status of given cell or organism [9].

The purpose of the study: is to check the validity of the Eq. 1 and Eq.2 for avian eggs and avian embryonal development.

During bird development the main substances and gases diffusing trough egg shells membranes are oxygen (O_2), carbon dioxide (CO_2) and water vapor (H_2O) [10, 11].

Accordingly to literature data the oxygen permeability coefficient K_{O2} trough external and internal egg shell membranes have relatively low and constant value in order of 1.0×10^{-6} (cm^3 O_2 STP$\cdot sec^{-1}\cdot cm^{-2}\cdot Torr^{-1}$) [10]. The permeability coefficients of H_2O vapor and CO_2 gases are about 2 orders of magnitude higher than that of oxygen, i.e about 1.0×10^{-4} ($cm^3\cdot sec^{-1}\cdot cm^{-2}\cdot Torr^{-1}$).

Working hypothesis: it was taken the working idea that there is an allometric connection between the egg volume (V_{egg}), egg surface (S_{egg}), egg incubation time (T_{inc}) and oxygen permeability coefficient (K_{O2}) trough inner egg shell membranes, accordingly to the formula, similar to Eq.2:

$$V_{egg} /(S_{egg}\cdot T_{inc})=K_{O2} \quad \text{(for 1 Torr } O_2 \text{ oxygen pressure trough egg shell membranes)} \qquad (3)$$

The working hypothesis is demonstrated on Figure 1.

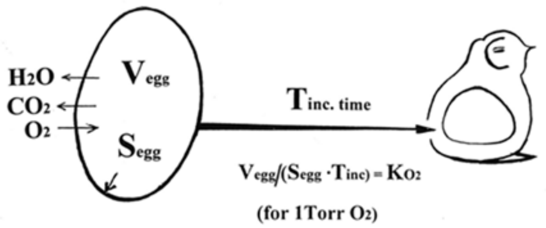

FIGURE 1. Connection between the eggs volume, surface, incubation time and oxygen permeability coefficient across inner egg-shell membrane.

DATA AND METHOD

The data for 28 avian eggs with 10^4 folds difference between their mass were taken from scientific literature. The data for egg volume and egg surface were taken from Hoyt [3]. The data for egg incubation time were taken from Hoyt et al. [4] and Burns [10]. In data set on Table 1 the egg volume to surface ratio from *Struthio camelus* to *Calypte anna* change 14 folds (from 2.116 cm in *Struthio camelus* to 0.15358 in *Calypte anna*). The incubation days change 5 folds only (from *Diomedea nigripes* to *Calypte anna*). All data corresponds to normal and relevant to egg's incubation temperature.

TABLE 1. Bird Egg Volume, Surface, Volume to Surface Ratio and Incubation Days

N	BIRDS	Volume (V) (cm^3)	Surface(S) (cm^2)	V/S (cm)	T_{inc} (days)	$V_{egg}/(S_{egg} \cdot T_{inc})$ (m/s)
1.	*Struthio camelus*	1087.30	513.84	2.116	43.3-45.9	5.49×10^{-9}
2.	*Podilymbus podiceps*	21.53	38.47	0.5596	21	3.084×10^{-9}
3.	*Diomedea nigripes*	299.17	222.14	1.342	65-66	2.39×10^{-9}
4.	*Oceanodroma melania*	10.15	23.17	0.438	50	1.014×10^{-9}
5.	*Morus bassanus*	94.62	104.13	0.9086	43	2.445×10^{-9}
6.	*Phalacrocorax pelagicus*	35.47	54.08	0.6559	31-38	2.169×10^{-9}
7.	*Ardea herodias*	71.09	84.91	0.8372	28	3.460×10^{-9}
8.	*Phoenicopterus rubber*	144.83	139.51	1.0381	28	4.291×10^{-9}
9.	*Olor columbianus*	308.60	228.16	1.3526	30-32	5.05×10^{-9}
10.	*Branta Canadensis*	157.28	145.41	1.0816	28-30	4.317×10^{-9}
11.	*Anas platyrhynchos*	43.41	61.27	0.7085	26-28	3.037×10^{-9}
12.	*Falco peregrinus*	47.61	63.91	0.74495	29-32	1.678×10^{-9}
13.	*Bonasa umbellus*	17.51	33.01	0.53044	21	2.923×10^{-9}
14.	*Phasianus colchicus*	24.26	40.82	0.59431	24-25	2.751×10^{-9}
15.	*Lophortyx californicus*	8.37	20.11	0.4162	24	2.294×10^{-9}
16.	*Meleagris gallopavo*	72.93	86.00	0.8480	28	3.505×10^{-9}
17.	*Numenius americanus*	84.46	94.77	0.8912	27	3.820×10^{-9}
18.	*Calidris alpina*	8.93	21.39	0.41748	21-22	2.197×10^{-9}
19.	*Himantopus mexicanus*	21.63	38.59	0.5605	22-26	2.703×10^{-9}
20.	*Uria aalge*	82.9	97.61	0.8493	33	2.979×10^{-9}
21.	*Aethia pusilla*	15.44	30.81	0.5011	28-36	1.812×10^{-9}
22.	*Coccyzus erythropthalmus*	6.90	17.80	0.3876	14	3.204×10^{-9}
23.	*Tyto alba*	22.49	38.80	0.57964	32	2.096×10^{-9}
24.	*Otus asio*	18.49	33.91	0.54526	21-26	2.685×10^{-9}
25.	*Bubo virginianus*	62.91	76.65	0.8207	28-30	3.275×10^{-9}
26.	*Calypte anna*	0.45	2.93	0.15358	14	1.260×10^{-9}
27.	*Corvus corrax*	30.35	48.81	0.6218	20-21	3.511×10^{-9}
28.	*Corvus brachyrhynchos*	14.40	29.20	0.49315	18	3.171×10^{-9}

In all calculations the statistics packet 'STATISTICA' were used.

RESULTS AND DISCUSSION

1. Calculation of correlation coefficient between volume to surface ratio and incubation days in bird eggs. On Table 1 are given the all data for volume to surface ratio and incubation days for all 28 studied bird eggs, for which an allometric link is looking for. The statistics analyses of data (from *Struthio camelus* to *Calypte anna*) have shown, the correlation coefficient between the eggs volume to surface ratio data and eggs incubation time data is relatively small (R =0.561). Thus, the statistical relationship between volume to surface ratio (V_{egg}/S_{egg} , cm) and incubation days (T_{inc}, days) is low but statistically significant. The confidence level of relationships was determined by Student's t-test and reaches 0.01.). The graphical presentation of this relationship is given on Fig.2.

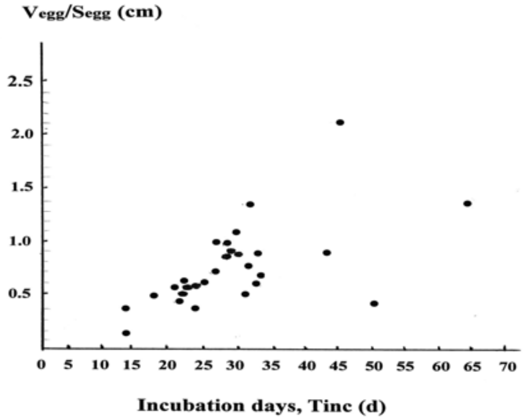

FIGURE 2. Volume to surface ratio *versus* incubation days in 28 bird eggs (R=0.561).

2. Calculation of mean and standard deviation (SD) of volume to surface to incubation day ratio in 28 bird eggs. On Table 1 are given the calculated data for the volume to surface to incubation days ratio: $V_{egg}/(S_{egg}\cdot T_{inc})$ for 1 Torr O_2 pressure gradient trough egg shell membranes. The mean ±SD of this ratio was: $V_{egg}/(S_{egg}\cdot T_{inc}) = 2.9504\times10^{-9}$ m/s $\pm1.0311\times10^{-9}$ m/s. The graphical presentation of mean and SD intervals is given on Fig. 3.

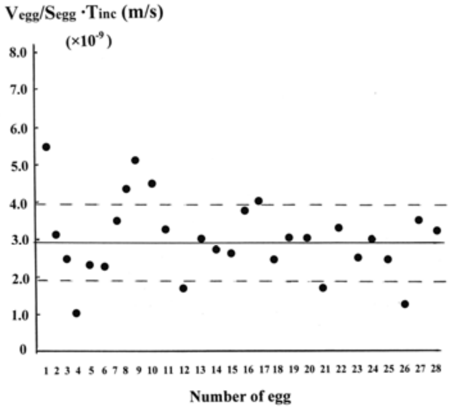

FIGURE 3. The mean value (*continuous line*) and ±SD interval (*dashed line*) of $V_{egg}/(S_{egg}\cdot T_{inc})$ ratio.

On Fig.3 is demonstrated the egg-mass independence of $V_{egg}/(S_{egg}\cdot T_{inc})$ ratio in bird eggs. Indeed, from Table 1 it can see that this ratio for the biggest eggs of *Struthio camelus* is 5.49×10^{-9} m/s. For the smallest eggs of *Calypte anna* the ratio is 1.260×10^{-9} m/s. Thus, these characteristics of two biggest and smallest bird eggs differs only 4.35 folds, in comparison to 10^4 folds difference between egg mass of *Struthio camelus* (~1.4 kg) and *Calypte anna* (~0.13 g). The following allometric relationship may be proposed between V_{egg}/S_{egg} ratio (in meters) and T_{inc} time (in seconds):

$$V_{egg}/S_{egg} = (2.9504 \pm 1.0311)\times10^{-9}\, T_{inc} \quad (4)$$

This equation will include 68.2% of all cases on Fig.3. To include 95% from all cases it need use 2.9504 ±2SD diapasons [10].

3. Calculation of oxygen permeability coefficient trough chicken (Gallus gallus) inner egg shell membrane as function of incubation days to hatching. Egg shell and outer shell membrane O_2 permeability coefficient has constant values (about 1.90×10^{-6} and respectively 1.78×10^{-6} ml O_2 STP·sec^{-1}·cm^{-2}·Torr^{-1}) during entire incubation time of eggs [11, 12 , 13]. The O_2 permeability coefficient of inner egg shell membrane ($K_{inner\ shell\ membrane}$) increases from 0.11×10^{-6} in start of incubation to 1.56×10^{-6} ml O_2 STP·sec^{-1}·cm^{-2}·Torr^{-1} in end of incubation [11, 12 , 13]. The dynamics of calculated $K_{inc(i)}$ trough chicken inner egg shell membrane is graphically presented on Fig.4.

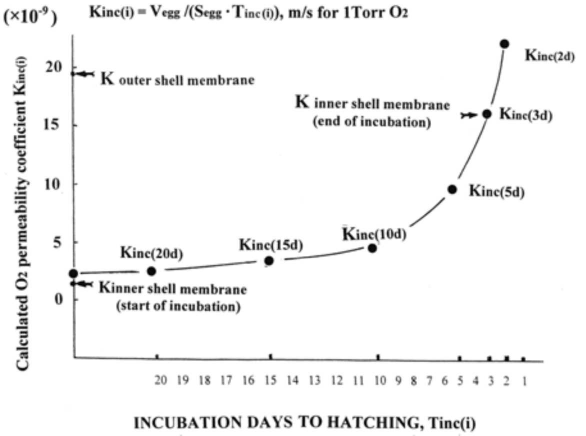

FIGURE 4. Calculation of O_2 permeability coefficient $K_{inc(i)}$ trough inner chicken egg shell membrane by allometric equation: $K_{inc(i)} = V_{egg}/(S_{egg}\cdot T_{inc(i)})$ for i =2, 3, 5, 10, 15, 20 days (all data are recalculated in SI metric system).

On Figure 4, the oxygen permeability coefficient ($K_{inc(i)}$) of inner eggs shell membrane is calculated as function of incubation days (i) to hatching for V_{egg}/S_{egg} = 0.41cm. From Fig. 4 is observed that the calculated O_2 permeability coefficient $K_{inc(i)}$ increases nearly from value of $K_{inner\ shell\ membrane} \approx 2\times10^{-9}$ (m/s) in the start of incubation to nearly the value of $K_{outer\ shell\ membrane} \approx 18\times10^{-9}$ (m/s) in the end of incubation (before hatching). During the entire incubation time the volume to surface ratio of eggs remain constant, while the incubation days decreases linearly from 20d to first incubation days before hatching. During 21 days incubation the calculated $K_{inc(i)}$ increased 9 folds. The coefficient K_{inc}(i) increases as monotonic function: Y(x)=Const/x, where x is the incubation days (in seconds), and Y(x) is the oxygen permeability coefficient (in meters per 1 second).

CONCLUSION

Allometric connection between the egg volume to surface ratio and incubation days allows calculate dynamics of oxygen permeability coefficient trough egg inner and outer shell membranes, as function of incubation days.

REFERENCES

1. H. Rahn and A. Ar, Condor **76**, 147-152 (1974).
2. A. Paganelli, A. Olszowka and A. Ar, Condor **76**, 319-325 (1974).
3. D. F. Hoit, Condor **78**, 343-349 (1976).
4. D. F. Hoyt, R.G. Board, H. Rahn and C. V. Paganelli, Physiol. and Biochem. Zool. **52**, 438 (1979).
5. K. Schmidt-Nielsen. *Scaling.Why is animal size so important?* (Cambridge University Press, 1984).
6. A. T. Atanasov, Trakia Journal of Sciences **10**, 36-47 (2012).
7. A. T. Atanasov, OJBIPHY **3**, 91-98 (2013).
8. A. T. Atanasov, AIP Conference Proceedings **1618**, 942 (2014). doi: 10.1063/1.4897888.
9. A.T. Atanasov, Trakia Journal of Sciences **10**, 134-135 (2012).
10. T.H. Hassard. Understanding Biostatistics. Copyright by Mosby-Year Book., Inc. 1991
11. S.R. Kayar, G. K. Snyder, G. F. Birchard and C.P. Black, Resp. Physiol., **46**, 209-221(1981).
12. S. R. Kayar, G. K. Snyder, G. B. Birchard and C. P. Black, Resp. Physiol. and Neurobiol.**178**, 30 (2011).
13. O.D. Wangensteen, D. Wilson and H. Rahn, Resp. Physiol. **11**, 16-30 (1970-1971).

Statistical Relationship of Malaria in Papua New Guinea and Solar Activity

D. Valev[1], A. Atanasov[2*], R. Werner[1], I. Mindov[2], A. Andonova[2] and R. Martinov[2]

[1]*Space Research and Technology Institute, Bulgarian Academy of Sciences, Stara Zagora, BULGARIA*
[2] *Medical Faculty, Trakia University, Stara Zagora, BULGARIA*

[*]Corresponding author: atanastod@abv.bg

Abstract. We carried out a statistical analysis of the monthly cerebral malaria cases in Papua New Guinea for the period January 1987 - December 1996 and also the analysis of the monthly solar activity and geomagnetic activity for the same period. The solar activity was described by the sunspot numbers and the F10.7 solar flux. As a measure of the geomagnetic activity the aa-indices were used. A close negative correlation between cerebral malaria cases and solar activity indices was found. The correlation of cerebral malaria cases with F10.7 reaches - 0.66, and - 0.70 with sunspot numbers. The confidence level of relationships was determined by Student's t-test and reaches 0.00001. All calculations were performed with raw data without smoothing which supports the correctness of the obtained results. The close correlations of cerebral malaria found in Papua New Guinea with solar activity indices could be important for the prognosis of cerebral malaria in this region.

INTRODUCTION

1. Malaria and cerebral malaria. Malaria is a vector-borne infectious disease affecting humans and other animals, caused by parasitic protozoans (a group of single-celled microorganisms) belonging to the Plasmodium type [1]. The disease is most commonly transmitted by an infected female Anopheles mosquito. Four species of Plasmodium can infect and be spread by humans [2]. Most deaths are caused by Plasmodium falciparum because the rest of the species cause a milder form of malaria [1, 2]. The disease is widespread in the tropical and subtropical regions that exist in a broad band around the equator. This includes much of Sub-Saharan Africa, Asia, and Latin America. In 2016, there were 216 million cases of malaria worldwide resulting in an estimated 731,000 deaths [3, 4]. Approximately 90% of both cases and deaths occurred in Africa [2].

The cerebral malaria (CM) affects the brain and remains one of the most serious complications of Plasmodium falciparum. In particular, this is a rapidly fatal disease characterized by headache, seizures, and coma, with diffuse cerebral oedema and only very rarely by focal neurological symptomatic features such as hemiplegia, aphasia, hemianopia, or cerebellar ataxia. Without treatment, CM is invariably fatal. Despite effective anti-malarial therapy, surviving individuals with CM may develop long-term neurological deficits [5, 6] which indicates that elimination of the parasite does not completely resolve clinical consequences of the infection. It has been registered that despite anti-malarial treatment CM has a mortality rate of 15-20 % [7]. Children and pregnant women, living in endemic areas, and non-immune travelers to these areas are more likely to suffer from CM. Although parasitaemia and CM appear correlated, no causal relationship between degree of parasitaemia and CM has been firmly established.

2. Diseases and solar and geomagnetic activity. There are long-term health effects related to the sunspot cycle. The samples cause some general categories of diseases: autoimmune diseases, tumors and neoplasms, metabolic diseases, neurological, mental and behavior diseases and others. The overall crude death rate is one of the example for relationship between solar activity and mortality rates in Thailand with correlation coefficient higher than 0.5. Besides, there is a strong correlation between neurological mortality and sunspot numbers (R = 0.686), and between hypertension mortality and sunspot numbers (R = 0.66 for females and R = 0.86 for males [8]. The brain is a very sensitive electromagnetic organ with strong dependency on the protective and cellular repair support of melatonin.

The skin cancer is the most common cancer affecting millions people in the world [9]. It has been shown in [10] that strong numerical association with correlation coefficient > 0.5 exist between long term trends in the solar activity and the skin cancer. The studies of the other authors indicate that approximately 90% of non-melanoma skin cancer is associated with ultraviolet exposure [11], while this value is approximately 86% for melanoma skin cancer [12].
According to contemporary scientific ideas, the possible biophysical mechanism of sunspot action on human organism can be melatonin secretion [13, 14]. Melatonin is the primary circadian rhythm neuro-hormone, along with neurotransmitter serotonin. On the other hand the factors that alter human melatonin secretion can influence almost every body organs as heart, brain, nervous system, reproductive system and others. This also covers the sunspots and the recently theory of schizophrenia [15]. Accordingly to that, the incidences of schizophrenia are caused by some factor associated with solar cycles.
It has been shown [16] that solar activity in extremum or ± one year was associated with influenza pandemics and severe Ebola outbreaks in Africa from 1976 to 2014. Recently, it has been found that three grand minima of solar activity on record–the Sporer minimum (1450-1550 AD), Maunder minimum (1650-1700 AD) and the Dalton minimum (1800-1830) have all been marked by a preponderance of pandemics–Small Pox, English Sweats, Plague and Cholera [17].
Surveillance of endemic/epidemic diseases, including early-warning systems, is of prime public health importance. Current and future surveillance efforts should be supported to construct a comprehensive early warning system involving virus monitoring and epidemiology on the ground, solar activity as well as stratospheric sampling for forecasting future pandemics.

DATA AND METHOD

1. Malaria data set. The original data consist of monthly Total CM admissions (hereafter referred to as “Total”) as well as admissions to selected health facilities (referred to as “Facilities”) in Papua New Guinea.The time series dataset was obtained from Cibulskis et al. [18] as originally provided by the Ministry of Health of PNG. The data covered the interval from January 1987 to December 1996. It has been found that CM series in PNG show two clear cycles – seasonal 12 month cycle and multi annual cycle having period about 10 years [19]. The seasonal maximums occurred in May, and the minimums – in September. Clearly, the seasonal malaria cycle is due to seasonal variation in rainfall and temperatures. The period of multi annual cycle is close to the 11-year period of solar and geomagnetic activity. Because of this, we look for statistical relationships of CM data series and solar and geomagnetic activity indices.
2. Solar and geomagnetic data set. In our research we use relative sunspot numbers and F10.7 solar flux as proxy indicators of solar activity, and planetary aa-index as indicator of geomagnetic activity. The relative sunspot number Ri (hereafter referred to as “sunspots”) is obtained using the formula Ri = k (10g + s), where *s* is the number of individual spots, *g* is the number of sunspot groups, and *k* is a factor that varies with location and instrumentation. The relative sunspot numbers have been obtained from [20].
The F10.7 index is a measure of the solar radio flux per unit frequency at a wavelength of 10.7 cm, measured in Sun flux units (SFU = 10^{-22} $W \cdot m^{-2} \cdot Hz^{-1}$). It is an excellent indicator of overall solar activity levels and correlates well with solar UV emissions. The F10.7 index has been found in [21].
The planetary *aa*-index is a global geomagnetic activity index. It is derived from the *K* indices from two approximately antipodal observatories and has units of 1 nT. Current observatories used are Hartland in UK and Canbera in Australia. The main advantages of using aa-indices are that this is the longest time series of geomagnetic activity. The planetary aa-index has been obtained from [22].
3. Statistical methods. The statistical analysis of the examined data series involves linear regression and cross-correlation. The statistical reliability of the obtained correlations is evaluated by Student's t-test. We use monthly mean values of temperature, sunspots and aa-indices for all statistical computations. In all calculations the statistics packet ‘STATISTICA’ were used. We would like to underline that no filtering or smoothing procedures have applied on these values. This enables the correct and unambiguous estimation of the statistical reliability level of the already found statistical relations.

RESULTS AND DISCUSSION

1. Statistical characteristics of CM series in PNG. The series “Facilities” and “Total” were analyzed from January 1987 to December 1996, which are presented in Fig. 1.

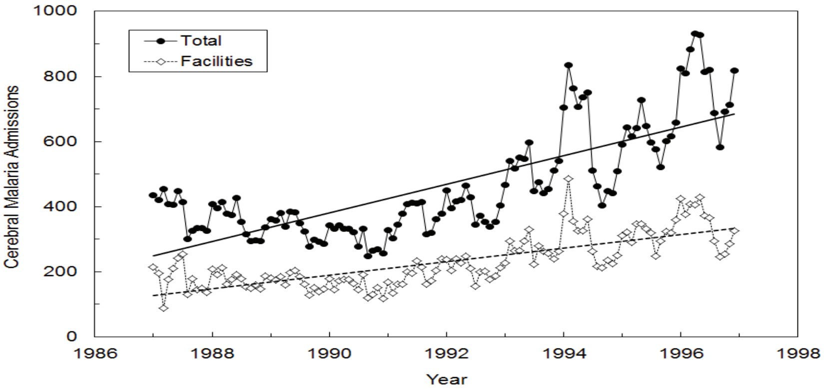

FIGURE 1. CM series in PNG from January 1987 to December 1996.
Linear trend of Total (solid line) and Facilities (dashed line).

It is clearly that during the 10-year study the dynamics of the morbidity is significant. Facilities has changed from 88 cases to 486 cases, i.e. more than 5 times, and Total varied between 247 cases and 932 cases; nearly 4 times. The parameters Facilities and Total are closely related. The linear correlation coefficient of the simple linkage between them (Total = 2.0169 * Facilities) reaches r = 0.94. Therefore, in more of cases we will only present results for Total because the results for Facilities are very close. As shown in [18], in the case of CM in the 1987-1996 period, there is a well-expressed upward trend with a correlation coefficient r = 0.76.

2. Statistical relationships of CM in PNG with solar and geomagnetic indices. Fig. 1 shows that during the course of Total there was a slight downward trend in 1987-1988, which after the local minimum in early 1989. is replaced by an upward trend. These peculiarities in the course of CM have led us to compare them with the course of solar activity since the latter has a pronounced 11-year cycle, the maximum of which in 1989 coincides with the CM minimum in PNG (1987-1996). Fig. 2 shows the Total CM series and the solar activity indices, namely sunspots and F10.7 solar radio flux. The mirrored motion of Total CM in PNG versus sunspots and F10.7 is impressive.

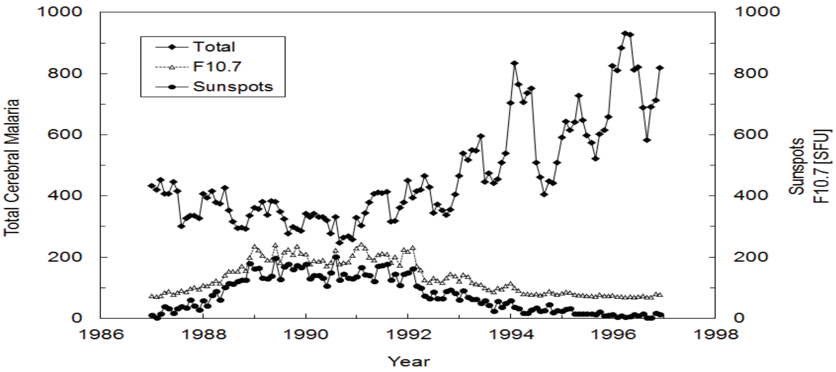

FIGURE 2. Total CM series in PNG versus sunspots and F10.7 solar flux.

It has encouraged us to search linear correlation of monthly CM in PNG and sunspots. We have found a close correlation of Total CM in PNG and sunspots with correlation coefficient reaching r = - 0.70. The negative sign indicates that we have anti-correlation between cases of CM and sunspots. The confidence level of the correlation was determined by Student's t-test and appears very high reaching 0.00001. Therefore, the found correlation of CM in PNG and sunspots is statistically significant and that is an amazing result. The descending linear trend is clearly manifested. In the light of the relationship between CM in PNG and sunspots, the upward trend in Facilities and Total found in [18] is clarified. The majority of the investigated CM series is at the 22nd solar cycle, and due to the anti-correlation of CM and sunspots, an upward trend has been observed in Facilities and Total. The close linear correlation of Total CM in PNG and sunspots is shown on Fig. 3.

After that, we have sought a relationship between Total CM in PNG and the F10.7 solar flux. The linear correlation coefficient r = - 0.66 is slightly lower than the same for CM and sunspots. The p-level determined by Student's t-test

reaches 0.00001 again, therefore the relationship of CM in PNG and the F10.7 solar flux is statistically significant, too. This is not surprising because of very close correlation of 10.7 solar flux and sunspots, reaching r = 0.97. The statistical calculations show the correlation coefficient r <0.1 between CM and aa-index, therefore this relationship is not statistically significant.

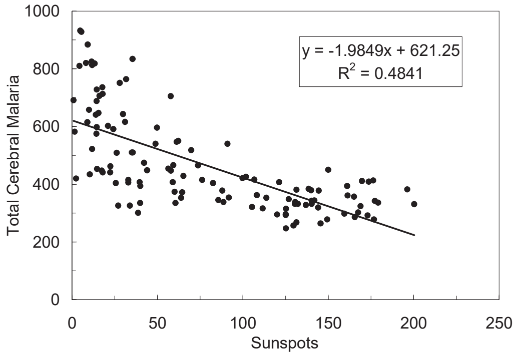

FIGURE 3. Linear correlation of Total CM in PNG and sunspots.

CONCLUSION

It was carried out a statistical analysis of the monthly CM cases in PNG (1987-1996). A high correlation has been found between CM cases and solar activity indices - sunspots and F10.7 solar flux. The correlation coefficient reaches 0.70 and the confidence level 0.00001 is determined by Student's t-test. It has been shown that the minimum of CM cases in PNG coincides with the peak of the 22nd solar cycle in 1989. No statistically significant relationship was found between CM cases in PNG and geomagnetic aa-index. The observed correlations of CM in PNG with solar activity indices (sunspots and F10.7 solar flux) could be important for the prognosis of CM in PNG, and possibly in other regions.

REFERENCES

1. WHO (2014) HTTPS://RELIEFWEB.INT/REPORT/WORLD/MALARIA-FACT-SHEET-NO-94-UPDATED-MARCH-2014
2. *H. Caraballo and K. King, Emergency Medicine Practice* ***16****, 1–23 (2014).*
3. WHO, *WORLD MALARIA REPORT*, PP. 196 (2017).
4. GBD 2015, *LANCET* ***388****,* 1459–1544 *(*2016).
5. M. J. Boivin, J. Develop. & Behav. Pediatrics **23**, 353–364 (2002).
6. M. Kihara, J. A. Carter and C. Newton, Tropical Med. & Int. Health **11**, 386–397 *(*2006).
7. R. Idro, K. Marsh, C. John and C. Newton, *Pediatric* Research **68**, 267**–**274 (2010).
8. N. Cherry, Natural Hazards **26**, 279**–**331 (2002).
9. H. Rogers et al., Arch. Dermatology **146**, 283**–**287 (2010).
10. E. Valachovic and I. Zurbenko, BioMed Res. Int. **Vol. 2014**, Article ID 538574.
11. H, Koh et al., Arch. Dermatology **132**, 436**–**442 (1996).
12. D. Parkin, D. Mesher and P. Sasieni, British J. Cancer **105**, S66**–**S69 (2011).
13. J. Bardasano, S. Cos and M. Picazo, J. Hirnforschung **30**, 639**–**643 (1989) [In German].
14. J. Burch, J. Reif and M. Yost, *Neurosci. Lett.* **266**, 209**–**212 *(*1999).
15. R. Richardson-Andrews, Med. Hypothesis **44**, 16**–**19 (1995).
16. Jiangwen Qu et al., J. Astrobiology & Outreach 4 Article ID154 (2016).
17. N. Wickramasinghe, J. Astrobiology & Outreach 5, Article ID159 (2017).
18. R. Cibulskis et al., *Am. J. Tropical Med. & Hygiene* **77**, 133–137 (2007).
19. B. Dimitrov, D. Valev, R. Werner and P. Atanassova, Epid. & Infection **141**, 2317**–**2327 (2013).
20. NASA, https://solarscience.msfc.nasa.gov/greenwch/spot_num.txt
21.Space Weather Data, https://celestrak.com/SpaceData/SpaceWx-format.php
24. NOAA, ftp://ftp.ngdc.noaa.gov/STP/GEOMAGNETIC_DATA/AASTAR/

Determination of the Sensitivity of Trajectory Log Files Gamma Analysis - a Method Based on Python Scripts

Stanislav Bozhikov[1,a)], Karina Mitarova[1], Filippa Vassileva[1], Bilyana Tacheva[2], Boyana Paarvanova[2] and Miroslav Karabaliev[2,b)]

[1]*Laboratory of Clinical Dosimetry, Department of Radiotherapy, University Hospital St. Ivan Rilski, 15 Alexander Geshov, Sofia, Bulgaria*

[2]*Department of Physics, Biophysics, Roentgenology and Radiology, Faculty of Medicine, Trakia University, 11 Armeiska, Stara Zagora 6000, Bulgaria*

[a)]Corresponding author: bozhikov.stanislav@gmail.com

[b)]miroslav.karabaliev@trakia.uni.bg

Abstract. The aim of the study is to investigate and compare gamma index (γ) results obtained from the Trajectory log (TL) file of linear accelerator (Linac) to γ results obtained by Portal Dosimetry (PD) measurements. The Treatment planning system Eclipse was used to change the Dosimetric Leaf Gap (DLG) in order to study its influence on γ. In this paper, we used the python script API Pylinac (v.2.2.6) to analyze the TL file which stores the performance parameter data of the Linac for radiotherapy, in our case Varian True Beam STX. The results for the gamma passing rate (%GP) obtained from TL tend to be higher from those obtained by PD. We found that the values of %GP obtained by the two methods become comparable when the dose difference criterion used for TL data is 8 to 10 times smaller than the same criterion used with PD data. The methodology described here would allow a verification of the gamma analysis results by using the python script API Pylinac. This could make the verication of the plan before the treatment process more precise and reliable.

INTRODUCTION

Modern radiotherapy uses techniques such as Stereotactic Radiosurgery (SRS) and Stereotactic Body Radio Therapy (SBRT). The increasing demand for this kind of treatments brings higher responsibility for accurate delivery of the dose prescribed to the patient. Therefore, the responsibility for creating a more precise plan relies on the competence of the medical physicist. The Trajectory log (TL) is a file that is generated during the work of the machine and that contains data representing its performance. Analyzing TL can be useful for the planning process in the search of the perfect Radiosurgery plan. By adapting the python API Pylinac we can read the data from Trajectory logs [1] and extract the values of the parameter Gamma index (γ). There are few numbers of papers that concerned the analysis of log files and that used various tests for analyzing gamma index [2]. A different approach was used to verify the leafs positions derived from Electronic Portal Image Device (EPID) and those derived from the trajectory log [3]. The aim of this study is to investigate the influence of Dosimetric Leaf Gap (DLG) values on the results for gamma index (γ) obtained by EPID and the results for gamma index (γ) derived from the Trajectory log.

MATERIALS AND METHODS

The measurements and evaluations of the gamma index (γ) for different DLG were performed using a Varian True-Beam STX machine equipped with HD 120 leaf MLC (Multileaf collimator) system and a flat panel MV (Mega Volt Image) system. The EPID attached to the Linac is Portal Vision aS1000 (Varian Medical System, Palo Alto, CA, USA) amorphous silicon portal image device.

Trajectory log

The TrueBeam control system generates Trajectory log files for every field which is delivered. Every Trajectory log contains data of the expected values and the actual values collected during delivery of the beam such as monitor units (MU), position of the table coach, position of the MLC leaves, collimator rotation, gantry angle, and so on.

Experimental Measurements

Before the actual measurement was done we performed EPID calibration as described in the Manual of Varian. It was done by delivering ”dark” and ”flood” fields until the imaging device sensitivity map was found to be correct. All measurements were analyzed with the Dosimetry module of the Treatment planning system (called Portal Dosimetry). The Algorithm of the Portal Dosimetry (PD) was calibrated using measurements and following the steps provided from the Manual. The energy and maximum dose rate were obtained by using 6 flattening filter free (FFF) and 600 MU/min.

Gamma analysis method of comparison of two dose distributions

The gamma index (γ) analysis is the most commonly used way to verify the dose distribution of a radiotherapy fields used in techniques such as volumetric modulated arc therapy (VMAT) and intensity modulated radiotherapy (IMRT). The gamma index analysis combines the two quantities Dose difference and Distance difference. It is used to calculate the matrix of the differences of two dose distributions over the irradiated area or volume, one evaluated distribution (E) and one reference distribution (R). The reference dose distribution is the distribution which was measured with the Detector, in our case the Portal Imaging Device. The evaluated dose distribution is what we compared and was generated from the treatment planning system. The dose difference $\Delta D(\vec{r}_R, \vec{r}_E)$ between two points is calculated using the equation [4]:

$$\Delta D(\vec{r}_R, \vec{r}_E) = D_E(\vec{r}_E) - D_R(\vec{r}_R) \tag{1}$$

where $\vec{r}_E$ is the evaluated point, $\vec{r}_R$ is the reference point, $D_E(\vec{r}_E)$ is the dose from the evaluated distribution and $D_R(\vec{r}_R)$ is the dose from reference distribution.

For each point in the evaluated distribution the value of the quantity $\Gamma(\vec{r}_R, \vec{r}_E)$ is calculated:

$$\Gamma(\vec{r}_R, \vec{r}_E) = \sqrt{\frac{\Delta r^2(\vec{r}_R, \vec{r}_E)}{\delta r^2} + \frac{\Delta D^2(\vec{r}_R, \vec{r}_E)}{\delta D^2}} \tag{2}$$

where $\Delta r(\vec{r}_R, \vec{r}_E) = \left|\vec{r}_E - \vec{r}_R\right|$ is the distance between the two points, δD is the dose difference criterion and δr is the distance difference criterion. The γ for the reference point is taken as the minimum value over the $\Gamma(\vec{r}_R, \vec{r}_E)$ values for evaluated points (eq. 3):

$$\gamma(\vec{r}_R) = min\,\{\Gamma(\vec{r}_R, \vec{r}_E)\}\,\forall\,\{\vec{r}_E\} \tag{3}$$

If for any of the evaluated points $\Gamma(\vec{r}_R, \vec{r}_E) < 1$, then $\gamma(\vec{r}_R) < 1$ and the reference point will meet the criteria and pass the test.

The agreement between the two distributions is expressed by the percentage of points that pass the requirement $\gamma(\vec{r}_R) < 1$ and is referred to as the value ”gamma passing rate” (%GP).

Chair Test

The so-called Chair test is performed to optimize the DLG. The DLG parameter attempts to model the physical difference between the radiation and light field and accounts for inherent leakage between adjoining leaves in the MLC system. The Chair test takes into account specific parameters concerning the MLC system - velocity, transmission and leaf gap. By changing the value of DLG in the Treatment Planning System (TPS) we have obtained certain changes in the values of γ when delivering the test to the system [5]. To check and compare the distributions of the Chair test for both TL and PD we changed consecutively the DLG from the Treatment planning system choosing the values in the range 0.0003 to 0.029.

Developed Software

To derive the values of gamma from the Trajectory log a software API Pylinac (v.2.2.6) was used. Pylinac is library of the python programming language that is intended to analyze images and data generated by linear accelerators. The algorithm for calculating γ in the software is based on Bakai et al. [6]. This algorithm differs from the algorithm of Low (Eq.1 to Eq.3) and uses the calculation of the value χ:

$$\chi = \frac{D_E(\vec{r}) - D_R(\vec{r})}{\sqrt{\delta D^2 + \delta r^2 \left\|\vec{\nabla} D_R\right\|^2}} \tag{4}$$

Here $\vec{\nabla} D_R$ is the local dose gradient for the point from the reference distribution. The value of χ is considered to be approximately equivalent to γ ($|\chi| \simeq \gamma$), so if $|\chi| < 1$ the difference in dose is acceptable and the point passes the test.

The Log Analyser modules configuration file of pylinac, config.yaml, holds the parameters that are needed for the software to function and that the user can manipulate. We were using the criteria for dose difference and distance difference as abbreviated in the configuration file. The dose difference criterion δD is referred to as ”doseTA” (dose-to-agreement) and the distance difference criterion δr is referred to as ”distTA” (distance-to-agreement). The parameter ”Threshold” represents the percentage of the maximum dose, below which gamma was not evaluated and the point is excluded from the calculation. By changing the parameters doseTA, distTA and Threshold we corrected the values of gamma and the value of %GP result.

For every single DLG value that we had chosen in the Chair test, we calculated γ for Threshold 10 % and various pairs of the criteria δD (doseTA) and δr (distTA) - 3%/1mm, 2%/2mm, 1%/1mm.

RESULTS AND DISCUSSION

Figure 1 shows results of the dependence of %GP value on the DLG parameter for three pairs of criteria applied to the Portal Dosimetry (PD) measurements, 3%/1mm, 2%/2mm, 1%/1mm. The Threshold parameter value is 10 %.

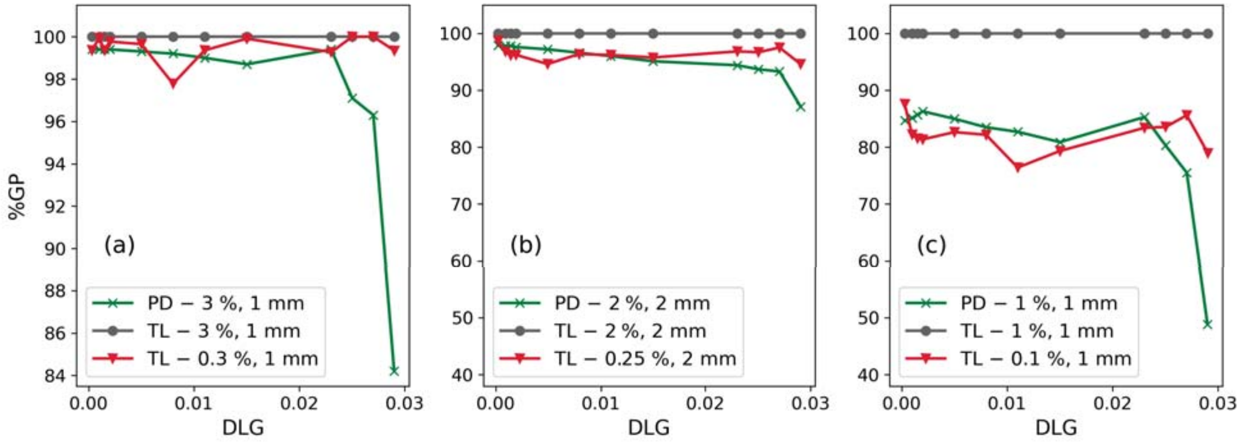

FIGURE 1. Dependence of the gamma passing rate (%GP) on the DLG, obtained from Trajectory log (TL) and with Portal Dosimetry (PD) with fixed criteria. (a) dose difference and distance difference criteria 3% / 1mm; (b) criteria 2% / 2mm; (c) criteria 1% / 1mm. The red curves are TL %GP calculated with different criteria as indicated in the labels.

As can be seen in Fig. 1, for all three pairs of criteria the %GP results obtained from TL tend to be higher than those obtained by PD, and in fact reach a 100 % γ passing. Obviously, the results obtained with TL data need correction in order to become comparable to those from PD. Since the TL %GP results reach 100% for criteria 3%/ 1mm, 2%/ 2mm and 1%/ 1mm we calculated results for harder criteria by changing the dose difference criterion doseTA to smaller values. In Fig. 1abc the red curves represent TL %GP obtained with these smaller values for doseTA compared to the corresponding criterion for the PD measurement. Instead of doseTA = 3% we used criterion

for TL data doseTA = 0.3%, instead of 2% we used 0.25%, and instead of 1% we used 0.1%. It can be seen that the results obtained with these criteria are much more comparable with the PD results for %GP.

Figure 2 shows the dependencies of TL %GP results on either doseTA and distTA when the other criterion is constant. The TL %GP dependence on doseTA is sigmoid in the range 0.1% - 0.4% (Fig. 2a), while the dependence on the distTA criterion is linear in the range 0.01 mm to 1.0 mm for doseTA 0.1%, 0.25% and 0.1% and logarithmic-like for doseTA 0.01% (Fig. 2b). Above doseTA = 0.3% the %GP reaches 100% for all investigated values of distTA (Fig. 2a). That is why at Fig. 2b the green curve for doseTA=0.3% shows almost no dependence on distTA. The question why the TL %GP value is 100% for all doseTA above 0.3% needs further investigation and elucidation. Is this an intrinsic property of the LINAC and the way it generates the Trajectory log and/or is it due to Pylinac and it's algorithm. We also need to establish whether we can rely on some correlation between the results of the Trajectory log and the results of Portal dosimetry.

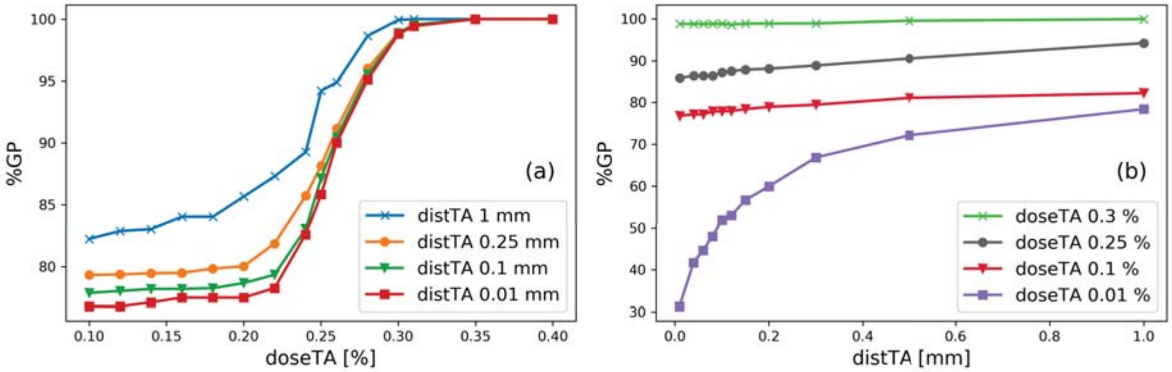

FIGURE 2. (a) Dependence of the Trajectory log (TL) gamma passing result (%GP) on the dose difference criterion doseTA for constant DLG and constant distTA; (b) Dependence of the TL %GP on the distance difference criterion distTA for constant DLG and constant doseTA.

CONCLUSION

Our study results show that if we want to consider the Trajectory log as a secondary tool for quality assurance we have to take into account that the results from the log evaluated by Pylinac (v.2.2.6) differ from those obtained by Portal Dosimetry. The idea to use in a daily routine the data coming from Trajectory log for dose verification is quite appealing. However, the results should be verified and the procedure should be validated, especially if the calculation software is different and uses a different algorithm.

REFERENCES

[1] J. Kerns. Pylinac API Documentation new version 2.2.6, https://pylinac.readthedocs.io/en/stable/, 2019.

[2] J.L. Hudges. *Automated Analysis of Varian Log Files for Advanced Radiotherapy Treatment Verification: A Multicenter Study*. M.Sc. thesis, University of Western Australia, 2015.

[3] R. Kummar, H. I. Amols, M. Lovelock, S. D. Sharma, and D. Datta. *Jurnal of Cancer Research and Therapeutics*, 13:297–303, 2017.

[4] M. Hussein, C.H. Clark, and A. Nisbet. *Physica Medica*, 36:1–11, 2017.

[5] S. Kantz, A.T. McDermott, M. Söhn, S. Reinhardt, C. Belka, K. Parodi, and M. Reiner. *Journal of Applied Clinical Medical Physics*, 18:20–31, 2017.

[6] A. Bakai, M. Albert, and F. Musslin. *Phys. Med. Biol.*, 48:3543–3553, 2003.

Using Trajectory Log Files as Additional Tool for Dosimetry Verification Plan. A Case in Practice

Stanislav Bozhikov[1,a)], Filippa Vassileva[1], Karina Mitarova[1], Boyana Paarvanova[2], Bilyana Tacheva[2] and Miroslav Karabaliev[2,b)]

[1]*Laboratory of Clinical Dosimetry, Department of Radiotherapy, University Hospital St. Ivan Rilski, 15 Alexander Geshov, Sofia, Bulgaria*

[2]*Department of Physics, Biophysics, Roentgenology and Radiology, Faculty of Medicine, Trakia University, 11 Armeiska, Stara Zagora 6000, Bulgaria*

[a)]Corresponding author: bozhikov.stanislav@gmail.com

[b)]miroslav.karabaliev@trakia.uni.bg

Abstract. In this survey, we investigate the usage of Trajectory log data in a single case of a patient undergoing Stereotactic Radiosurgery (SRS) treatment. A dedicated linear accelerator machine Varian TrueBeam STX was used. The software was developed for analyzing the log files which were created by the machine when a certain plan was performed in treatment mode or QA mode. Four plans were created with 7 no-coplanar fields. Additional structures must be added by the physicist in the contouring section in order to optimize the plans. Dosimetry equipment ArcCHECK was used to verify the dose distribution for the created plan. The evaluation of γ passing rate (%GP) from the Trajectory log was done for each field separately using Pylinac v.2.2.6 API (application programing interface) for Machine quality control. It was shown that for one of the plans the values of %GP in some of the fields were very low with about less than 15% passing and at the same time the ArcCHECK shows a good %GP of about 90%. When verifying the plans using the analyzed Trajectory log files it can be detected if there are problems with the rotation of the collimator the positioning of the collimator jaws or with over-modulating of the plan.

INTRODUCTION

To deliver a high quality radiotherapy plan the medical physicist needs to be aware of the limitations of the machine. One common mistake is to over-modulate a plan in which the machine performance in delivering the dose was overestimated. In order to be able to make a plan that the machine can handle with a good performance we need to understand how the over-modulated plan behaves. The use of both the Trajectory log (TL) and a dosimetry equipment for verification of a plan can give the knowledge and the data necessary to decide how well the machine performs on a particular plan. There are many ways to create a treatment plan, but not all of them will perform as good as the machine can handle. The Treatment planning system (TPS) has many tools that can be used for creating a good plan. It is the medical physicist responsibility to use them in a clever way. An understanding of the proper use of the Inverse Planning algorithm is needed to create good plans. With the Inverse Planning optimization additional support structures are created in a proper dimension [1] that serve as a zone around the gross tumour volume (GTV), the clinical target volume (CTV) or the planning target volume (PTV) [2]. In these structures, the behaviour of the dose is controlled in the Optimization process so that the dose is minimized. The delivery of a plan with high prescribed dose brings the need for the creation of a well-developed protocol. The number of fields and its arrangement and the additional structures for the optimization represent Protocol for treatment. In this paper we study all these parameters for such a Protocol, as well as, its behavior from the creation until the decision for whether the plan is over-modulated or not.

MATERIALS AND METHODS

Treatment plans for Radiosurgery were created with linear accelerator (LINAC) TrueBeam STX, Varian with HD Milenium 120 Multileaf Collimator (MLC) system. 19 ”support” structures were added with intention to prevent the irradiation on important healthy organs. The Treatment Planning System used was Eclipse v.13.6. The measurements of the verification plan were done using Sun Nuclear ArcCHECK phantom. All plans were made with 6 MV flattening filter free (FFF) energy.

For each plan a verification process is applied in order to check if the plan can be performed from the machine without over-modulation. The verification relies on the gamma index (γ) analysis based both on the ArcCHECK measurements, and on the data from the Trajectory log files. The workflow of the plan changes during the verification process is shown in Figure 1.

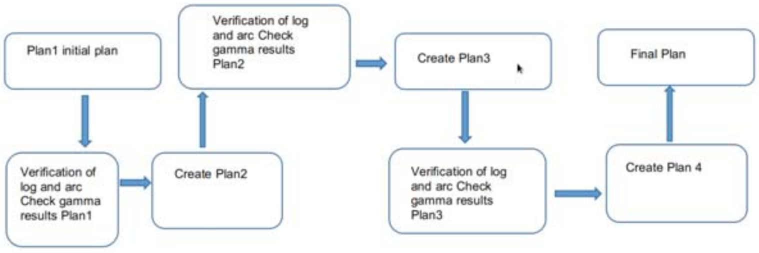

FIGURE 1. The organization of the verification process

The gamma index γ analysis is the most commonly used way to verify the dose distribution of a radiotherapy fields [3]. It is used to calculate the matrix of the differences of two dose distributions over the irradiated area or volume, one evaluated (calculated) distribution (E) and one reference (measured) distribution (R). In our case the reference dose distribution is the distribution which was measured with the Detector (ArcCHECK) or derived from the Trajectory log. The evaluated dose distribution is what we compared and was generated from the treatment planning system. The aim is to identify the regions where the evaluated dose distribution disagree with measurement. The γ analysis combines the two quantities Dose difference ΔD and Distance difference Δr for each point of the reference distribution and the nearest points of the evaluated distribution. The agreement of the two distribution at any reference points ($\vec{r}_R$) is checked against two criteria, the dose difference criterion δD and the distance difference criterion δr. The calculation of γ combines the quantities ΔD, Δr, δD and δr [4]. If $\gamma(\vec{r}_R) < 1$ the reference point meets the criteria and passes the test. The overall agreement between the two distributions is expressed by the percentage of points that pass the requirement $\gamma(r_R) < 1$ and is referred to as the value ”gamma passing rate” in % (%GP).

All measurement with ArcCHECK were done with γ criteria 3%/1 mm with Threshold=10%. The Threshold parameter represents the percentage of the maximum dose, below which gamma was not evaluated and the point is excluded from the calculation. As it was stated in the specification of the MLC system the accuracy of the Leaf position relative to collimator axis, projected at ISO plane (gantry at 0 degrees) is 0.2 mm.

The TrueBeam control system generates Trajectory log (TL) files for every field which is delivered. Trajectory log contains data collected during delivery of the beam such as monitor units (MU), position of the table coach, position of the MLC leafs, collimator rotation, gantry angle, and so on. We are using the logs for every field separately, getting the values of %GP for each of them.

To derive the values of γ from Trajectory log a software API pylinac (v.2.2.6) was used. Pylinac is a library of the python programming language that is intended to analyze images and data generated by linear accelerators [5]. The algorithm for calculating γ in the software is based on Bakai et al. [6]. The %GP is calculated in the Log Analyser (log_analyzer) module of Pylinac. We were using the criteria for dose difference and distance difference as abbreviated in Pylinac [7]. The dose difference criterion δD is referred to as ”doseTA” (dose-to-agreement) and the distance difference criterion δr is referred to as ”distTA” (distance-to-agreement).

The evaluations done with Pylinac and Trajectory log were analyzed with the γ criteria doseTA = 0.03 % and various distTA values in the range 0.01 - 0.2 mm.

RESULTS AND DISCUSSION

Four treatment plans are created till the last plan has good results both for %GP obtained from Trajectory log files and for %GP measurement by the ArcCHECK. The ArcCHECK %GP results for the four plans with γ criteria 3%/1 mm are: for Plan 1 - %GP = 94.1 %, for Plan 2 - %GP = 84.6 %, for Plan 3 - %GP = 89.0 %, for Plan 4 - %GP = 90.5 %. In Table 1 are shown the collimator, gantry, table and dose rate parameters of the fields of the four consecutive plans. In Table 2 are shown the parameters of the "support structures". With the changes of the plan parameters additional changes over the three main "support" structures are done as shown in Table 2.

Figure 2 represents the Trajectory log results for %GP for every field of the four plans.

TABLE 1. The parameters of the four treatment plans. All changes in a plan compared to the previous one are shown as bold numbers.

Field	Plan	Colimator			Gantry	Table	MU
№	№	X	Y	Deg	deg	deg	
1	1	4.1	4.4	327.9	41.0 CW 165.2	296.3	184.2
1	2	**4.0**	**4.7**	**259.6**	41.0 CW 165.2	296.3	**159.1**
1	3	**4.0**	**4.7**	**259.6**	41.0 CW 165.2	296.3	**185.3**
1	4	**5.1**	4.4	327.9	**227.7** CW 165.2	296.3	**157.0**
2	1	4.5	4.5	56.7	162.3 CCW 32.9	312.3	332.1
2	2	4.5	4.5	56.7	162.3 CCW 32.9	312.3	**278.4**
2	3	4.5	4.5	56.7	162.3 CCW 32.9	312.3	**286.3**
2	4	4.5	4.5	56.7	162.3 CCW 32.9	312.3	**274.3**
3	1	4.6	4.7	50.1	280.60 CW 24.7	345.4	265.5
3	2	4.6	4.7	50.1	280.60 CW 24.7	345.4	**251.6**
3	3	4.6	4.7	50.1	280.60 CW 24.7	345.4	**261.4**
3	4	4.6	4.7	50.1	280.60 CW 24.7	345.4	**216.4**
4	1	3.4	5.4	104.6	316.6 CCW 199.3	16.3	224.2
4	2	3.4	5.4	104.6	316.6 CCW 199.3	16.3	**190.2**
4	3	3.4	5.4	104.6	316.6 CCW 199.3	16.3	**203.6**
4	4	3.4	5.4	104.6	316.6 CCW 199.3	16.3	**256.8**
5	1	4.0	4.6	80	210.2 CW 306.7	33.6	211.6
5	2	4.0	4.6	80	210.2 CW 306.7	33.6	**209.4**
5	3	4.0	4.6	80	210.2 CW 306.7	33.6	**209.3**
5	4	4.0	4.6	80	210.2 CW 306.7	33.6	**150.4**
6	1	4.7	3.8	18.4	323.0 CCW 195.3	58.8	110.8
6	2	4.7	3.8	18.4	323.0 CCW 195.3	58.8	**143.1**
6	3	4.7	3.8	18.4	323.0 CCW 195.3	58.8	**149.9**
6	4	4.7	3.8	18.4	323.0 CCW 195.3	58.8	**146.6**
7	1	4.3	4.0	60.6	201.3 CW 338.6	79.7	149.7
7	2	4.3	4.0	60.6	201.3 CW 338.6	79.7	**179.2**
7	3	4.3	4.0	60.6	201.3 CW 338.6	79.7	**206.5**
7	4	**5.4**	**4.9**	**332.0**	201.3 CW 338.6	79.7	**158.0**

According to the ArcCHECK results for %GP we can accept Plan 1 as valid as it passes the criteria of 90% γ passing (Plan 1 - %GP = 94.1 %). We have shown in a previous work that the Trajectory log data evaluated by Pylinac give different results for %GP and have different sensitivity toward the dose difference criterion [7]. It can be seen in Fig. 1a that when this criterion (doseTA) is gradually decreased, the Trajectory log %GP of field 1 in Plan 1 does not pass the 90% criterion. This leads us to do replanning of Plan 1, so we create Plan 2 with the parameters shown in Table 1. In this case we get %GP measured with the ArcCHECK less than 90% (Plan 2 - %GP = 84.6 %) but the Trajectory log's %GP shows better behavior as we can see from Fig. 1b. Continuing that way we reach our final Plan 4 with the Trajectory log results for %GP shown on Fig 2d and %GP = 90.5% from the measurements with ArcCHECK.

TABLE 2. The three main additional ”support” structures and their parameters for Plan 1, Plan2 , Plan 3, and Plan 4. All changes in a plan compared to the previous one are shown as bold numbers.

Number	Name	Type	Plan №	Outer Wall [cm]	Inner Wall [cm]	Volume [cm^3]
1	HD-Inner	wall	1	0.3	0.2	8.5
			2, 3, 4	**0.2**	**0.1**	8.5
2	HD-Outer	wall	1	0.7	0.4	6.8
			2, 3, 4	0.7	0.4	6.8
3	Inner	struct	1	0.0	0.0	0.8
			2, 3, 4	0.0	0.0	**1.2**

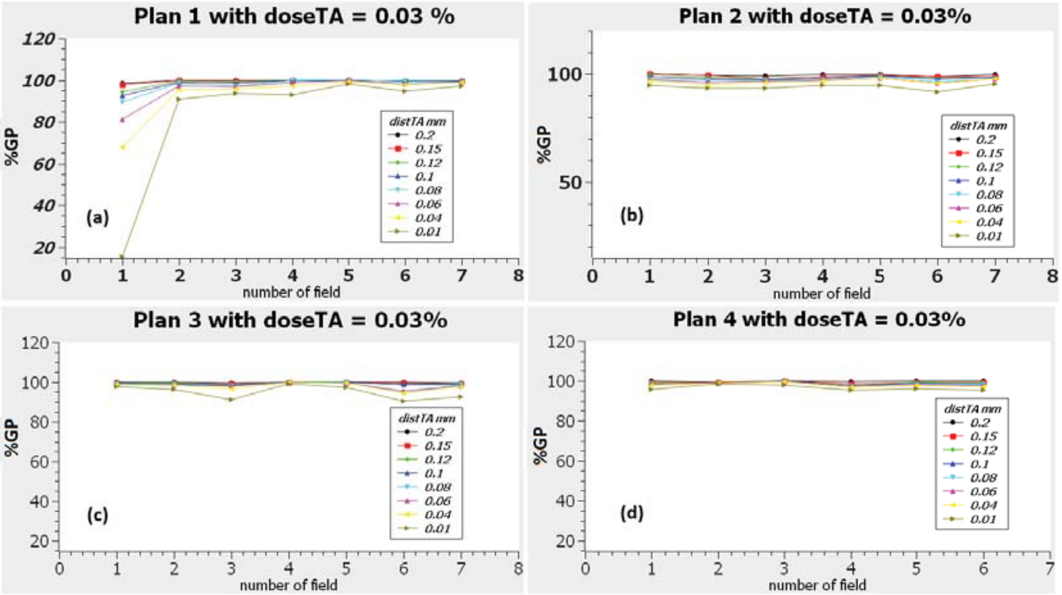

FIGURE 2. Gamma passing rate (%GP) results for the seven fields in the four created plans derived from the Trajectory log by the aid of Pylinac. Different curves represent results obtained with various disTA criteria.

Conclusion

In this work we have try to show the way of applying the Trajectory log data analysis over a particular case. We developed a work-flow which can points out errors in the parameters of the plan. And based on the understanding of the machine capabilities we can get the direction towards High Quality Plan. This kind of approach can help the medical physicist to make a good decision over a complicated plans.

REFERENCES

[1] M. Hartmann and L. Bogner. *Medical physics*, 35(5):2041–2049, 2008.

[2] N.G. Burnet, S.J. Thomas, K.E. Burton, and S.J. Jefferies. *Cancer Imaging*, 4(2):153–161, 2004.

[3] N. Hussein, C.H. Clark, and A. Nisbet. *Physica Medica*, 36:1–11, 2017.

[4] D. A Low, W.B. Harms, S. Mutic, and J.A. Purdy. *Medical physics*, 25:656–661, 1998.

[5] J. Kerns. Pylinac API Documentation new version 2.2.6, https://pylinac.readthedocs.io/en/stable/, 2019.

[6] A. Bakai, M. Albert, and F. Musslin. *Physics in Medicine and Biology*, 48:3543–3553, 2003.

[7] S. Bozhikov, K. Mitarova, F. Vasssileva, B. Tacheva, and M. Karabaliev. Determination of the sensitivity of a trajectory log files gamma analysis - a method based on python scripts. *AIP Conference Proceedings (submitted)*, 2019.

Mild Laboratory-Induced Metabolic Disorder in Rats. Effect on Erythrocyte Membrane According to a Dielectroscopic Study

B.K. Paarvanova [1a)], B. Tacheva [1], A. Tolekova [2], P. Hadzhibozheva [2], K. T. Georgiev [2], M. Karabaliev [1] and I. T. Ivanov [1]

[1] *Department of Physics, Biophysics, Roentgenology and Radiology. Medical Faculty, Thracian University, Stara Zagora 6000, Bulgaria.*
[2] *Department of Physiology, Pathophysiology and Pharmacology. Medical Faculty, Thracian University, Stara Zagora 6000, Bulgaria.*
[a)]Corresponding author: boyana.parvanova@trakia-uni.bg

Abstract. This study concentrates on the effect of mild metabolic disorder (MMD) in fructose-fed rats on the submembrane skeleton MS of their erythrocytes relying on the relationship between membrane structure and its dielectric properties. The segmental flexibility of MS and its attachment to the lipid membrane of erythrocytes is expressed by the MS intrinsic dielectric polarization. The latter was assessed by the difference in dielectric properties of erythrocytes (complex impedance, Z*, and capacitance, C*) prior to and after the thermal denaturation of spectrin assuming the dielectric activity of denatured spectrin nil. The erythrocytes of control (n=4) and fructose-fed (n=5) rats were isolated, washed, suspended in isotonic 10 mM NaCl/mannit solution (hematocrit 0.45) and heated (1.5 °C/min). At the denaturation temperature of spectrin (49°C) the dielectric properties of erythrocyte suspension sustained shreshold changes $\Delta Z^* = \Delta Zre + j\Delta Zim$ and $\Delta C^* = \Delta Cre - j\Delta Cim$. The frequency analysis of ΔZre, ΔZim, ΔCre and ΔCim indicated strongly increased contribution of spectrin to the dielectric properties of erythrocyte membrane. Thus, spectrin contribution to the static capacitance of erythrocyte membrane was 83 % greater and that to the dipole loss of erythrocyte membrane was 38 % greater in erythrocytes from MMD rats, compared to control RBCs. This finding is suggested to be due to the moderate increase in glucose level and related increase in phosphorylation of membrane proteins in MMD rats.

INTRODUCTION

The fructose-fed rats are an animal model displaying numerous features of the metabolic syndrome and are frequently used to study this pathologic condition [1]. The metabolic syndrome predisposes individuals to the development of cardiovascular disease and/or Type 2 diabetes. This study was aimed at elucidating the effect of laboratory-induced mild metabolic disorder (MMD) in rats on the plasma membrane of their erythrocytes which is important determinant of the rheological properties of blood.

The erythrocyte membrane consists of spectrin-based submembrane skeleton, attached to the bilayer membrane directly [2] and via two types of high-affinity protein bridges [3]. Spectrin is a fibrilar protein exhibiting considerable segmental motions which contribute to the mechanical function of erythrocyte membrane [4].

The segmental motions of spectrin skeleton were recently studied applying the method of dielectric spectroscopy on heated suspensions of native erythrocytes and isolated erythrocyte membranes [5; 6]. Threshold changes in the dielectric properties (complex impedance, Z^*, complex capacitance, C^*, dielectric loss) were noted at the spectrin denaturation temperature (49.5°C). Since the spectrin skeleton is considered dielectrically inactive at its denatured state, these changes indicated the contribution of spectrin skeleton to the dielectric properties of native erythrocytes and isolated membranes. The frequency dependence of these changes was processed with the mathematical methods of dielectric spectroscopy [7] revealing two dielectric relaxations on the membrane skeleton. The first relaxation depended on the availability of bridges between the integral proteins and spectrin and was detected at such frequencies whereat the lipid bilayer did not allow penetration of the field into cytosole. It was explained as a direct piezoeffect on the flexible spectrin filaments powered by the electrostriction (beta dispersion) of lipid bilayer. The second relaxation was detected at higher frequencies which allowed direct interaction of alternating field with the spectrin dipoles.

Using thermal dielectroscopy, this study led to the conclusion that MMD in fructose-fed rats resulted in improvement of erythrocyte membrane dielectric properties and markedly increased the contribution of spectrin skeleton to these properties.

MATERIALS AND METHODS

Materials. NaCl and mannitol were purchased from Sigma Chemicals Co, St. Louis, MO, USA.

Laboratory animals. The experiment was conducted according to the institutional and national regulations and European Directive of 22.09.2010 (2010/63/EU) concerning usage of animals for scientific purposes. Used were adult Wistar male rats with weight between 190 - 220 g. The animals had free access to standard lab rat chow. After a habituation period of one week, the rats were randomly divided into two groups:

1) Rats in control group (n = 9) – they received pure tap water;

2) Fructose-fed group of rats (n = 9) – they received tap water with dissolved fructose (150 mg/1000 ml water).

Two weeks from the start of experiment the rats in fructose-fed group were injected intraperitoneally with streptozotocin 20 mg/kg b.w., insufficient to cause diabetes (Sigma, St. Louis MO, USA). The morphometric characteristics (body weight, waist circumference, length from muzzle to tail) of the animals were monitored throughout the experimental period. The amounts of consumed water and fructose solution were measured daily.

TABLE 1. Blood plasma concentrations (in mmol/l) of glucose, triglyceride, uric acid, total cholesterol, creatinine, low-density lipoprotein cholesterol (LDL) and high-density lipoprotein cholesterol (HDL) in control and fructose-fed rats.

	Glucose	Triglyceride	Uric acid	Total cholesterol	Creatinine	LDL	HDL
Control rats	9.83± 2.73	0.81 ± 0.06	74.57 ± 7.70	1.33 ± 0.12	51,22± 5,54	0,43± 0,11	0,54± 0,07
Fructose-fed rats	12.59± 0.62	2.16 ± 0.72	86.62 ± 4.10	1.24 ± 0.22	66,25± 6,23	0,28± 0,13	0,43± 0,11

At the end of the experimental period of 12 weeks the rats were anesthetized with Nembutal (50 mg/kg) intraperitoneally. The thoracic cavity was opened and the blood samples were collected by cardiac puncture.

To establish MMD fasting serum glucose, triglycerides levels, total cholesterol, high-density lipoprotein, low-density lipoprotein, creatinine and uric acid were measured in tested rats using standard laboratory methods.

Dielectric properties of erythrocyte membranes from control and MMD rats. Erythrocytes were isolated from the obtained blood samples and twice washed by centrifugation (250 x g) in isotonic solution of 10 mM NaCl and mannit. The washed erythrocytes were suspended in the washing medium, hematocrit 0.45, and heated (1.5°C/min) in a conductometric cuvette. Complex impedance, $Z^* = Z_{re} + jZ_{im}$, and capacitance, $C^* = C_{re} - jC_{im}$, of erythrocyte suspension at 46ºC and their changes, $\Delta Z^* = \Delta Z_{re} + j\Delta Z_{im}$, and $\Delta C^* = \Delta C_{re} - j\Delta C_{im}$, at 49°C, the denaturation temperature of spectrin [8], were registered by Solartron 1260 Impedance Analyzer as described previously [6,9]. The dielectric loss curves for suspended erythrocytes and for their spectrin skeleton were obtained at 46ºC as described previously [6,9].

RESULTS AND DISCUSSION

Compared to control rats, a MMD was confirmed in fructose-fed rats based on their high triglyceride level, moderately elevated fasting blood glucose and reduced high-density lipoprotein cholesterol (Table 1). Next we studied the effect of this metabolic condition on the plasma membrane of erythrocytes relying on the relationship between membrane structure and its dielectric properties.

At moderate and high hematocrit values, the real capacitance, C_{re}, of an erythrocyte suspension depends mainly on the plasma membrane of suspended cells [7]. The same is valid for the imaginary capacitance, C_{im}, provided its conductive loss component is removed. Further, the symbol C_{im} will designate the remaining pure dielectric loss component of imaginary capacitance. Thus, C_{re} and C_{im} represent the charge accumulation and dipole loss, respectively, of the plasma membrane of tested cells.

The spectrin-based submembrane skeleton of erythrocytes has been shown responsible for substantial portion of C_{re} and C_{im} of erythrocyte suspension [5,6]. Each portion could be determined as a difference between the values of respective dielectric parameter, C_{re} or C_{im}, prior to and after the thermal denaturation of spectrin. The obtained portions, ΔC_{re} and ΔC_{im}, represent the contribution of spectrin skeleton to the charge accumulation and dipole loss, respectively, of erythrocyte membrane. In a recent study [9] the ΔC_{re} and ΔC_{im} have been shown to depend strongly on the phosphorylation status of erythrocyte membrane demonstrating higher values at high phosphorylation and

tending to zero at low phosphorylation. Based on these results we compared the frequency profiles of C_{re} and C_{im} as well as of ΔC_{re} and ΔC_{im} in erythrocytes of rats with and without MMD.

Compared to the plasma membrane of erytrocytes from control rats that from MMD rats demonstrated 23 % greater static capacity (capacitance at low frequency) (Fig. 1A) and 15 % greater dipole loss (Fig. 2A). Much greater differences were measured considering the contribution of spectrin to the dielectric properties of erythrocyte membrane. Thus, compared to control RBCs, in erythrocytes from MMD rats the spectrin contribution to static capacitance of erythrocyte membrane was 83 % greater (Fig. 1B) and to the dipole loss of erythrocyte membrane it was 38 % greater (Fig. 2B). The latter data was statistically significant (standart deviation 12,5 %) and were calculated using the program KORELIA-IDENT [10].

The low frequency (7-20 kHz) resistance of erythrocytes from MMD rats was statistically at the same level as that of control erythrocytes (not shown). This indicates preserved barrier properties of erythrocyte membrane of MMD rats. However, statistically significant differences were established considering the contribution of spectrin to the complex impedance of erythrocyte membrane (Fig. 3). This finding is in line with the above presented capacitance data all indicating that spectrin skeleton of MMD rat erythrocytes had improved phosphorylation and cohesion to the lipid membrane.

Erythrocyte deformability depends on the surface/volume ratio, cytoplasmic viscosity and membrane viscoelasticity which, in turn, depends on cytoskeleton characteristics and on the lipidic composition of the membrane [11]. Erythrocyte deformability has been reported impaired in several anemias [12], and also in metabolic diseases, such as obesity [13], diabetes [14] and metabolic syndrome [15].

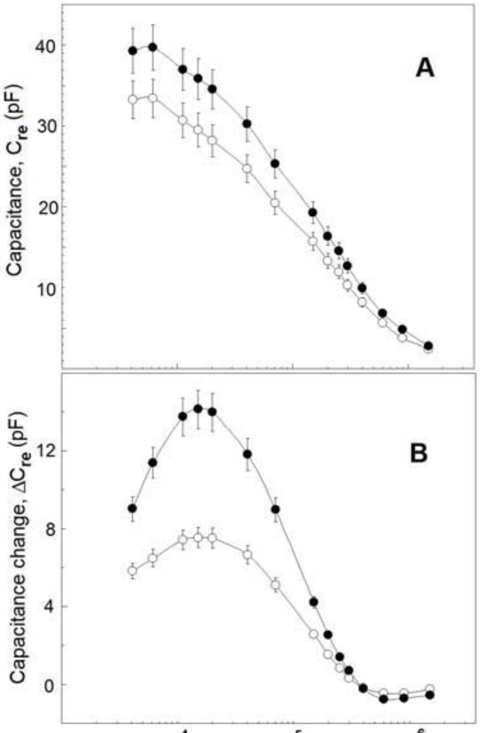

FIGURE 1. Frequency profile of real capacitance, C_{re}, of erythrocyte suspension (A) and its change, ΔC_{re}, at the spectrin denaturation temperature (B). Suspension contains fresh erythrocytes of control rats (o, n=4) and rats with MMD (●, n=5). Vertical bars indicate standard deviation. The hematocrit and suspension medium were 0.45 and isotonic solution of 10 mM NaCl and 280 mM mannitol, respectively.

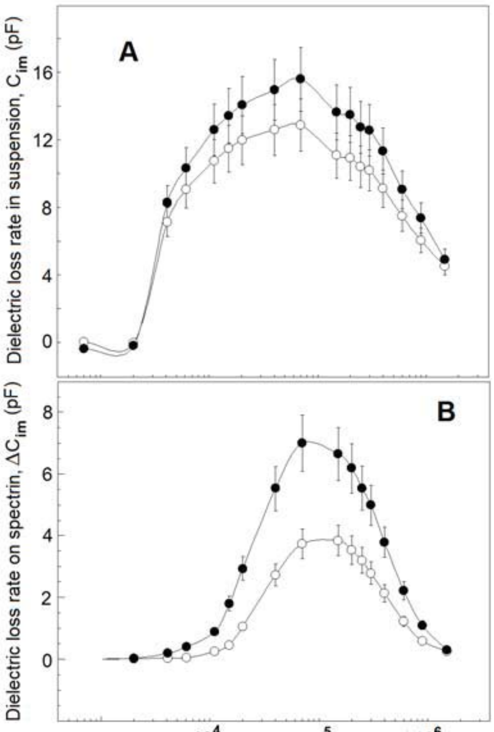

FIGURE 2. Dielectric loss curve for the suspension of rat erythrocytes (A) and for the submembrane spectrin network of suspended erythrocytes (B). Shown is the frequency dependence of the imaginary capacitance, C_{im}, of suspension and its change, ΔC_{im}, at the spectrin denaturation temperature. Other details as for Fig. 1.

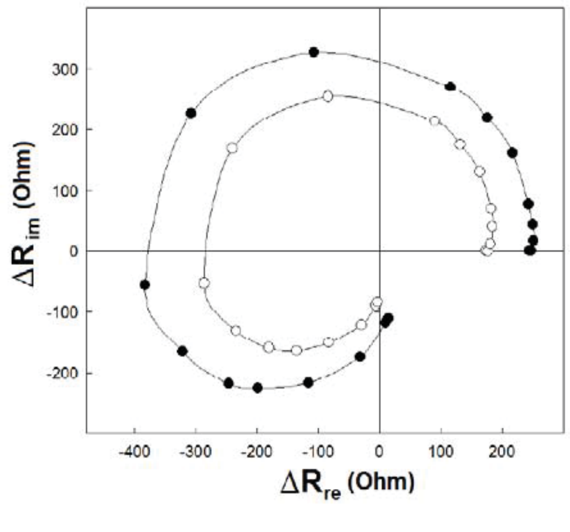

FIGURE 3. Complex impedance change plot for rat erythrocyte suspension at the temperature of spectrin denaturation. Shown is the dependence of the imaginary impedance change, -ΔZ_{im}, on the real impedance change, ΔZ_{re}, measured at the spectrin denaturation temperature. Other details as for Fig. 1.

CONCLUSION

In this study an improvement of the dielectric properties of erythrocytes from MMD rats was established. This outcome is an indication of increased phosphorylation of membrane proteins and consequent improvement of membrane deformability and viscoelasticity. The former outcome is possibly due to the mild increase (28 %) in glucose concentration and assumed low level of free radical oxidation and protein glycosylation, which are known to have high profile in the sever forms of metabolic syndrome.

ACKNOWLEDGMENTS

This work is supported by Trakia University - project № 9/2017 – МФ and project № 5/2018 – МФ

REFERENCES

1. L. T. Tran, V. G. Yuen and J. H. McNeill, *Mol Cell Biochem*., 2009, 332(1-2):145-59.
2. S. Manno, Y. Takakuwa and N. Mohandas, *Proc. Natl. Acad. Sci. U. S. A.,* 2002, 99, 1943–1948.
3. S. de Oliveira and C. Saldanha, *Clinical Hemorheology and Microcirculation*, 2010, 44, 63–74.
4. L. W. M. Fung, B. O. Kalaw, R. M. Hatfield and M. N. Dias, *Biophysical Journal*, 1996, 70, 841-851.
5. I. T. Ivanov, B. Paarvanova and T. Slavov, *Bioelectrochemistry*, 2012,88, 148–155.
6. I. T. Ivanov and B. Paarvanova, *Bioelectrochemistry,* 2016, 110, 59–68.
7. B. Klösgen, C. Rümenapp and B. Gleich, “Bioimpedance Spectroscopy”, in BetaSys: Systems Biology of Regulated Exocytosis in Pancreatic β-Cells. 2, Systems Biology, edited by. B. Booβ-Bavnbek, B. Klösgen, J. Larsen, F. Pociot, E. Renström, (Springer Publishing Company, 2011), pp. 241–271.
8. J. F. Brandts, L. Erickson, K. Lysko, A. T. Schwartz, R.D. Taverna, *Biochemistry,* 1977, 16, 3450–3454.
9. B. Paarvanova, B. Tacheva, M. Karabaliev, and I. T. Ivanov, *AIP Conf. Proceedings,* 2017, 1906, 150004.
10. K. Yankov and D. Ilieva. *Trakia Journal of Sciences*, 2015, 13, 420-425.
11. O. K. Baskurt, M. Hardeman, M. W. Rampling and H. J. Meiselman, *Handbook of hemorheology and hemodynamics,* (IOS Press, Amsterdam), 2007.
12. A. Vaya, J. Iborra, C. Falco, I. Moreno, P. Bolufer, F. Ferrando, et al., *Clin. Hemorheol. Microcirc.,* 2003, 28, 71–78.
13. A. Vaya, A. Hernandez-Mijares, M. Suescun, E. Sola, R. Camara, M. Romagnoli, et al., *Clin. Hemorheol. Microcirc*, 2011, 48, 247–255.
14. Y. I. Cho, M. P. Mooney and D. J. Cho, *J Diabetes Sci Technol,* 2008, 2, 1130–1138.
15. A. Vaya, A. Hernandez-Mijares, E. Bonet, R. Sendra, E. Sola, R. Perez, et al., *Clin Hemorheol Microcirc*., 2011, 49, 493–503.

Kinetics of Hemolysis Induced by Thioridazine

Bilyana Tacheva[1], Boyana Paarvanova[1], Stanislav Bozhikov[2], Ivan T. Ivanov[1] and Miroslav Karabaliev [1,a)]

[1]*Department of Physics, Biophysics, Roentgenology and Radiology, Faculty of Medicine, Trakia University, 11 Armeiska, Stara Zagora 6000, Bulgaria*
[2]*Laboratory of Clinical Dosimetry, Department of Radiotherapy, University Hospital "St. Ivan Rilski", Sofia, Bulgaria*

[a)] Corresponding author: miroslav.karabaliev@trakia-uni.bg

Abstract. The process of hemolysis of erythrocyte suspension induced by thioridazine (TDZ) was investigated by measuring the UV-Vis absorbance spectrum in the range 200 nm – 700 nm. The time needed to obtain the spectrum in this range was 12.5 s, so the spectrum was measured each 15 s. This permitted to follow the changes in absorbance at different wavelengths of the spectra during hemolysis. It was found that at most of the wavelengths measured the absorbance decreased which was related to the decrease of the light-scattering by the intact erythrocytes. In contrast, the absorbance peak of the hemoglobin (Hb) at 416 nm increased significantly during hemolysis. This was attributed to smaller light absorption by Hb when the erythrocytes were still intact and the Hb is still inside the erythrocytes. This phenomenon was due to the forward-scattered light that did not penetrate the erythrocytes and did not interact with Hb. When Hb was released from erythrocytes it could already interact with the light, resulting in increase of the absorption peaks of Hb and especially of the peak at 416 nm. The kinetics of the decrease of light-scattering at 700 nm and 500 nm and the increase of Hb absorption at 416 nm were compared and it was found that they are directly related. The kinetics of hemolysis induced by different concentrations of TDZ were measured. It was found that the time for hemolysis depended on the TDZ concentration as power function with power factor of minus 5.

INTRODUCTION

Interactions of drugs with biological membranes is of primary importance for the drug effectiveness. Red blood cells have been used for decades as a model for the investigation of drug-membrane interactions. One of the most used technique is the hemolytic assay. Hemolytic assays have been used to test the cytotoxicity of various drugs (1-3), phytoextracts (4), surfactants (5) and nanoparticles (6-8). The purpose of this technique is to check whether the compound of interest disturbs the cell membrane and provokes hemolysis when it interacts with the erythrocytes. During the hemolytic assay initially an erythrocyte suspension is incubated with the species investigated for a precise interval of time (usually 10 to 30 minutes). After the incubation period the suspension is centrifuged and the amount of the hemoglobin released from the erythrocytes is measured in the supernatant by spectrophotometry (1-3). Another approach to perform a hemolytic assay is to measure the turbidity of the erythrocyte suspension in real time (9, 10). When the erythrocytes are intact the suspension is turbid due the light-scattering. The scattering itself is due to the fact that in intact erythrocytes the inside of the cell has a different refractive index from the outside of the cell. The reason for this is the high amount of hemoglobin which occupies about half of the volume of the cell. Because of the different refractive indexes when the light reaches the erythrocyte surface it undergoes reflection and refraction thus changing the direction of light propagation, and causing the scattering. When the hemoglobin is released from the erythrocytes their inside becomes similar to the outside, the inside and outside refractive indexes become equal which leads to reduction of the reflection and refraction from the cells' surfaces and hence decrease of the scattering. Thioridazine (TDZ) is a drug from the phenothiazine group. The phenothiazines are used as neuroleptic drugs. It is well known that TDZ interacts with the membrane of erythrocytes, causing stomatocytosis and hemolysis at high enough concentrations (11). The aim of this work is to investigate the kinetics of the process

of hemolysis caused by thioridazine (TDZ) and to develop further the hemolytic assay based on turbidity measurements

EXPERIMENTAL

Human erythrocytes were used as a model to study the interaction of the drug with biological membranes. Venous citrate blood was taken in a clinical laboratory on the day of investigation conducted with the informed consent of patients with normal blood counts and transmitted to the research team without the patient specific data. The blood was centrifuged at 1700× g for 4 min to separate the blood plasma and buffy coat. Erythrocytes were washed initially with physiological saline (154 mM NaCl) at a ten-fold volume dilution (1:10/v:v) and twice washed by centrifugation (250 x g) in isotonic solution of 10 mM NaCl and mannitol. A starting suspension of washed erythrocytes with a hematocrit of 10% was prepared. During the hemolytic assay the erythrocytes were dissolved in a solution of 149 mM NaCl and 5 mM phosphate buffer, pH 7.4 (PBS) to reach hematocrit of 0.5 % or 1 %. Different amounts of thioridazine (TDZ) from 125 μM to 300 μM were added to the suspension in order to follow the kinetics of the hemolysis at different concentrations.

(±) -2-methylthio-10-[2-(1-methyl-2-piperidyl) ethyl] phenothiazine hydrochloride (Thioridazine hydrochloride) is a commercial products of Sigma-Aldrich, St. Louis, MO, USA. Solution of 5 mM thioridazine was prepared in physiological saline (150 mM) of NaCl. Small volumes of this solution was added to the experimental systems to achieve the desired concentrations. The kinetics of hemolysis is followed by measuring the absorbance spectrum of the suspension each 15 seconds with Cary 60 UV-Vis spectrophotometer (Agilent Technolgies). The spectra are measured in the range 200-700 nm, starting from 700 nm, at data interval of 0.5 nm and a scanning speed 2400 nm/min.

RESULTS AND DISCUSSION

The hemolysis induced by TDZ is investigated *in situ* in real time by measuring as many as possible UV-Vis absorbance spectra of the erythrocyte suspension. Representative results are shown in Figure 1, where each fourth spectrum is shown, i.e. the spectra measured each 60 seconds.

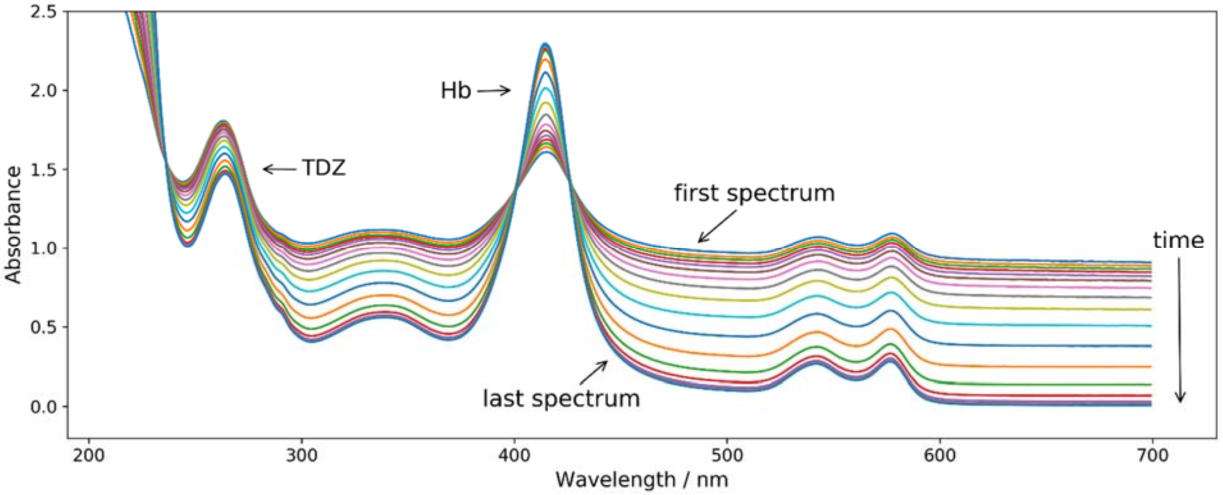

FIGURE 1. Absorbance spectra of erythrocyte suspension measured each 60 seconds during the time course of hemolysis induced by 225 μM TDZ at pH 7.4.. Hematocrit of the erythrocyte suspension was 1%. In total 21 spectra are shown. The peaks of thioridazine (TDZ) and hemoglobin (Hb) are indicated with arrows.

Several peaks can be distinguished in each of the spectra in Fig.1. Three peaks of Hb are clearly observed – a highest peak at 416 nm, and two smaller peaks at 542 nm and 578 nm. The peak of the TDZ present in the suspension can be seen at 262 nm. The first absorbance spectrum in Fig. 1 which is taken at the beginning of the hemolysis assay has the highest background due to the scattering of the intact erythrocytes. During the time course of hemolysis the scattering decreases which results in overall movement of the spectra to lower values of the

absorbance. However, it is interesting to note that all three peaks of Hb are increasing in relative height assumed from the background level. This is especially obvious for the peak at 416 nm, which increases so much that in each subsequent spectrum even the absolute height is bigger than that in the previous spectrum. This results in two apparent points at which all spectra cross each other. These points can be considered to be of the kind of the so called isosbestic points. The isosbestic points are characteristics for spectra taken during a process in which a speciment is undergoing change from one form to another, the two forms having different absorption maxima in the spectrum. In our case the two forms of Hb are Hb inside and Hb outside of the cells. We cannot say that they absorb the light at different wavelength. The difference in the peaks wavelength is hardly noticeable, and this question needs further elucidation. Nonetheless, it is obvious that the absorption is smaller when the cells are intact and Hb is inside the cells. In our opinion this apparent difference in the absorption is due to forward scattering of the light from intact erythrocytes. Portion of the forward scattered light comes from rays of light that undergo multiple reflections from the erythrocyte membranes without penetrating the erythrocytes and without interacting with the Hb inside. In such way the light that reaches the spectrophotometer detector have interacted only with a portion of the Hb present in the suspension. The decrease in the scattering is related to the release of Hb from the cells. The more the scattering decreases, the more there is Hb outside of the cells and the greater is the portion of Hb in the suspension with which the light can interact and hence can be absorbed. In the same time the relative height of the peak of TDZ does not change indicating that the THZ molecules remain outside the cells and on the cell membrane.

The degree of hemolysis can be determined from the absorbance at 700 nm where Hb does not absorb and the overall absorbance is due only to scattering. With the time course of hemolysis the scattering decreases, which results in decrease of the absorbance at 700 nm. Results for the spectra from Fig.1 are shown in Figure 2.

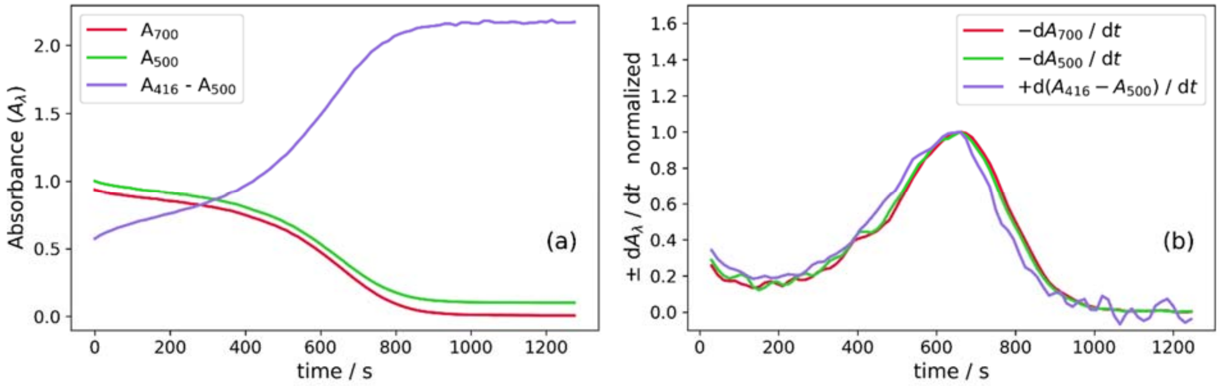

FIGURE 2. (a) The change of the absorbances at three different wavelengths during the hemolysis of erythrocyte suspention with 1 % hematocrit induced by 225 μM TDZ; (b) Normalized derivative curves (dA_λ/dt) of the three curves in in Figure a). The curves are normalized so that their maximum is equal to 1.

Fig. 2a shows the changes in the absorbances at 700 nm and 500 nm where the scattering prevails, and the absorbance at 416 nm, the highest peak of Hb. The height of the peak is corrected for the background, so the difference A(416 nm) – A(500 nm) is plotted in Fig. 2a. It is clearly seen that the shape of all three curves in Fig. 2a is sigmoid. There is an initial period when the hemolysis is slower (or no hemolysis). At some time point the hemolysis speeds up, reaching a "constant speed". After this period of faster hemolysis, the erythrocytes are fully hemolysed. The derivatives of the curves from Fig. 2a are shown in Fig. 2b. These curves are normalized by their maximum value in order to compare them.

$$\frac{dA(\lambda)}{dt}(normalized) = \frac{dA(\lambda)}{dt} / \left(\frac{dA(\lambda)}{dt} \max \right) \quad (1)$$

The three curves in Fig. 2b overlap to a great extent. This means that the release of hemoglobin and the decrease of scattering are directly related and both can be used to follow the hemolysis. The derivative curves are also useful to determine the relative time for the hemolysis, using the prominent maximum in these curves.

Figure 3a represents the hemolysis absorbance curves A(700 nm) for suspensions with hematocrit 0.5 % and different amounts of the hemolysing agent TDZ. Figure 3b shows the dependence of the time of hemolysis on the TDZ concentration. The corresponding times are determined from the derivatives curves (the curves in Figure 3a) as explained for the curves in Figure 2.

It can be seen from Fig. 3a that the time for hemolysis increases faster with the decrease of the TDZ concentration. While at 300 μM TDZ a suspension with hematocrit of 0.5 % hemolyses for 90 s, at 150 μM TDZ more than 3000 s are needed for hemolysis. 125 μM TDZ does not produce any hemolysis. It is interesting to notice the shape of the concentration dependency on the time for hemolysis in Fig. 3b. The points are well approximated with power function. According to this approximation the hemolysis time depends on the TDZ concentrations as the inverse power of 5.

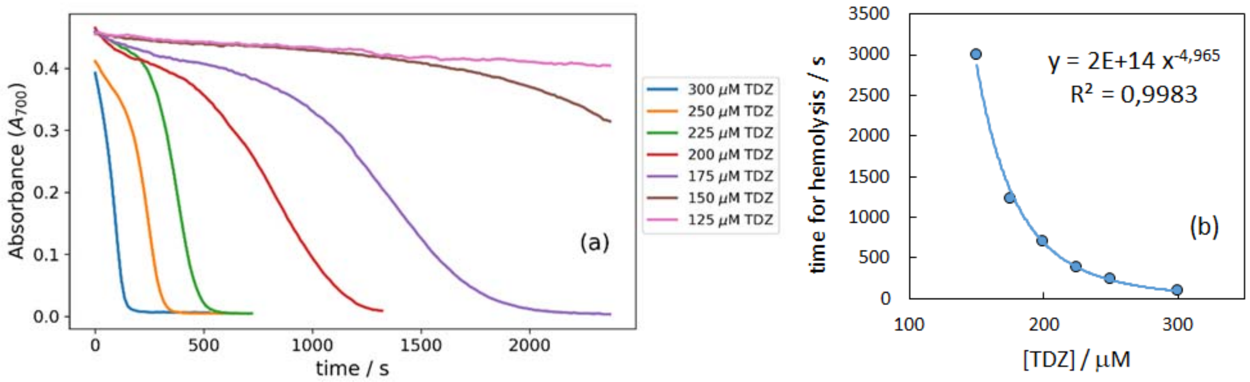

FIGURE 3. (a) Kinetics of the hemolysis of suspensions with 0.5 % hematocrit induced by TDZ with different concentrations in the range 125 μM – 300 μM. The hemolysis is measured by the decrease of the absorbance at 700 nm; (b) Dependence of the time of hemolysis on the TDZ concentration.

CONCLUSION

The modern equipment for spectrophotometry permits the fast cycling measurements of the UV-Vis absorbance spectra of erythrocyte suspension. In such a way the kinetics of hemolysis could be investigated in wide range of wavelengths. During hemolysis the absorption at most of the wavelengths decreases while at 416 nm the absorbance increases due to the release of Hb from the erythrocytes. The kinetics of the decrease of light-scattering at 700 nm and 500 nm and the increase of Hb absorption at 416 nm are directly related. The time for hemolysis depends on the TDZ concentration in a strong way and can be approximated with a power function with a power factor of -5. The presented method could be useful in cytotoxicity studies during development of new drugs and drug delivery systems.

ACKNOWLEDGMENTS

This work is supported by Trakia University - project № 9/2017-МФ and project № 5/2018-МФ

REFERENCES

1. S.V.P. Malheiros, E. de Paula and N.C. Meirelles, Biochim. Biophys. Acta Biomembr. 1373, 332–340 (1998).
2. S.V.P. Malheiros, N.C. Meirelles and E. de Paula, Biophys. Chem. 83, 89–100 (2000).
3. S.V.P. Malheiros, L.M.A. Pinto, L. Gottardo, D.K. Yokaichiya, L.F Fraceto, N.C. Meirelles and E. de Paula, Biophys. Chem. 110, 213–221 (2004).
4. S. Liu and H. Huang, J. Funct. Foods, 18, 1095–1105 (2015).
5. D. Lichtenberg, Biochim. Biophys. Acta Biomembr. 821, 470–478 (1985)
6. C.T.N. Pham, D.G. Thomas, J. Beiser, L.M. Mitchell, J.L. Huang, A. Senpan, G. Hu, M. Gordon, N.A. Baker, D. Pan et al. Nanomed. Nanotechnol. Biol. Med. 2014, 10, 651–660 (2014)
7. C. Chen, Y.C. Cheng, C.H. Yu, S.W. Chan, M.K. Cheung, and P.H.F. Yu, J. Biomed. Mater. Res. Part A, 87A, 290–298. (2008)
8. Y. Zhao, X. Sun, G. Zhang, B.G. Trewyn, I.I. Slowing and V.S.Y. Lin, ACS Nano, 5, 1366–1375 (2011).
9. A.I. Louw and L. Visser, Biochimica et Biophysica Acta (BBA)-General Subjects, 498: 1, 143-153 (1977).
10. P. Maček and D. Lebez. Toxicon 19:2, 233-240 (1981).
11. A.B. Hendrich, K. Lichacz, A. Burek and K. Michalak, Cell. Mol. Biol. Lett. 7, 1081–1086 (2002).

Impact of Waist Circumference on the Relationship between BMI and Hypertension Parameters

Maya Gulubova[1], Koni Ivanova[1, a)], Maria Magdalena Ignatova[2], Emilia Kisiova[2], Dimitur Chonov[1,2,3], Margarit Penev[4], Julieta Gerenova[5], Tatyana Vlaykova[6]

[1]*Dept. General and Clinical Pathology, Medical Faculty, Trakia University, Stara Zagora, Bulgaria,*
[2]*Ungraduated students Medical Faculty, Trakia University, Stara Zagora, Bulgaria.*
[3]*Dept. of Surgery, Medical Faculty, Trakia University, Stara Zagora, Bulgaria*
[4]*Dept. of Cardiology, Medical Faculty, Trakia University, Stara Zagora, Bulgaria*
[5]*Dept. of Endocrinology, Medical Faculty, Trakia University, Stara Zagora, Bulgaria*
[6]*Dept. Chemistry and Biochemistry, Medical Faculty, Trakia University, Stara Zagora, Bulgaria*

[a)]Corresponding author: koni_ivanova@yahoo.com

Abstract. Obesity is an important primary health care problem as it is associated with many other conditions including hypertension. Both obesity and hypertension are important risk factors for cardiovascular diseases. A total of 863 people, 235 males and 628 females in different age (mean 63.00±1,376; from 21 to 92 years old) on the Yambol territory in Bulgaria from 2010 to 2013 year were included in this study. The prevalence of overweight was statistically higher among females as compared with males. ($p=0.001$; $\chi 2=15.693$) Only 40 (18.2%) males and 135 (22.2%) females have obesity. There is significant statistically correlation between sex, age and hypertension. The more positive number with hypertension stage I is in women group in age from 55-74.9 were n=106/157 (67.5%/100%) ($p=0.001$; $\chi 2 = 52.34$), while the male group in same age are n=45/67 (67.2%/100%), ($p=0.032$; $\chi 2 =13.79$). BMI is widely accepted as one of the best indicator of nutritional status in adults. The biological mechanism by which higher BMI increases the risk of developing hypertension is not completely known.

INTRODUCTION

Overweight and obesity are now considered as serious health problems, with an increasing prevalence worldwide. They are related to a number of health consequences, including type two diabetes, coronary heart disease, stroke, hypertension, gallbladder disease, and certain types of cancer, sleep apnea, psychological disturbances and osteoarthritis [1,2]. Studies have demonstrated that obesity is related to elevated systolic and diastolic blood pressure elevation, dyslipidemia, diabetes, etc. [3]. Body mass index (BMI) is defined as the body mass divided by the square of the body height, and is universally expressed in units of kg/m^2, resulting from mass in kilograms and height in meters. The relationship between BMI and blood pressure has also been the subject of epidemiological research [4]. Positive association of BMI and blood pressure has also been reported in different population in the world, like Asia, India, Chinese, Brazil and etc. [5]. The relationship between BMI and blood pressure was for a long time perceived to be strong and a universal finding from the majority of the initial studies that some authors proposed that obesity was central to a common pathway linking risk factors and cardiovascular morbidity. This perception has since changed in the wake of reports of increased blood pressures and hypertension prevalence rates in lean populations [2]. Obesity is an important primary health care problem as it is associated with many other conditions including hypertension. Both obesity and hypertension are important risk factors for cardiovascular diseases [6]. Obesity is generally assessed using BMI which gives information on the distribution of weight with respect to height but fails to give insight into adipose tissue distribution phenotype. Evidence gathered from several

studies shows that central obesity (accumulation of fat in the abdominal area) is a greater risk factor for cardiovascular diseases compared to other types of obesity hence the need to know the distribution of fat in patients to facilitate assessment of patient's risk profile for cardiovascular diseases [7]. Waist hip ratio and waist circumference are commonly used to predict the risk of obesity related morbidity and mortality as they account for regional abdominal adiposity [8]. The aim of this study was to determine the difference in assessment of obesity by BMI and waist hip ratio and to determine the correlation of waist hip ratio and BMI with hypertension, gender and age in a population in an urban area of Yambol region in Bulgaria (Europe).

MATERIAL AND METHODS

Every year in May, the Medical Faculty from Stara Zagora, Bulgaria organizes free prophylactic examinations in the city of Yambol. The examinations included blood sugar measurement, blood pressure, questionnaire and Doppler study. A total of 863 people, 235 males and 628 females in different age (mean 63.00±1,376; from 21 to 92 years old) on the Yambol territory in Bulgaria from 2010 to 2013 year were included in this study. The mean age of male was 59,97±16,25 and for females was 62,22±12,64. For most age-related comparisons, participants were separated into four groups according to age (young <=35 years, 35.1-54.9 years, 55-74,9 years and >=75 years). Height was copied from the ID card of the participants. Weight was measured to the nearest 100 grams, without shoes. BMI (weight/height2) was calculated. BMI was classified according to the proposed criteria of World Health Organization (<19, normal 19-24.9; overweight 25-29.9, and obese >30). In the present study all the subjects having BMI>=30 were taken as obese. Normal blood pressure was taken as <120 mmHg systolic blood pressure (SBP) and <80 mmHg diastolic blood pressure (DBP); 120-139 mmHg (SBP) and 80-89 mmHg (DBP) were classified as prehypertension; stage – I hypertension was taken as 140-159 mmHg (SBP) and 90-99 mmHg (DBP) whereas blood pressure of >160 mmHg (SBP) and >100 mmHg (DBP) were classified as stage – II hypertension (JNC2018). The waist hip ratio was separated in five groups for males and females. This is calculated as waist measurement divided by hip measurement *(W ÷ H).* Normal value for women waist/hip ratio varied from 0.75 to 0.9 Over 0.9 values are indicators for high risk for cardiovascular diseases. Normal value for man waist/hip ratio varied from 0.85 to 1.

Statistical analysis. Continuous variables were presented as mean values and SD. Categorical variables were presented as frequencies. Associations between categorical variables were tested by the use of contingency tables ant the $\chi 2$ test. Comparison between continuous variables was performed by analysis of t test for independent samples. The comparison of the means of three or more continuous variables was made using ANOVA test. The prevalence ratios were calculated using multiple logistic regression analyses. Statistical analysis was performed using SPSS version 16.0 software and values of p<0.05 to indicate statistical significance.

RESULTS

Of the total of 863 adults investigated, 235 were males (59,97±16,25 mean age) and 628 females (62,22±12,64 mean age) from 21 to 92 years old on the Yambol territory in Bulgaria from 2010 to 2013 year were included in this study. We were investigated the correlation between BMI classification in males and females demonstrated on table1. The prevalence of overweight was statistically higher among females as compared with males. (p=0.001; $\chi 2$=15.693) Only 40 (18.2%) males and 135 (22.2%) females have obesity.

TABLE 1. BMI classification in males and females

BMI classification	Males N/%	Female N/%	p value
<19	-	17 (2.8%)	
Normal 19-24.9	63 (28.6%)	213 (35%)	
Overweight 25-29.9	117 (53.2%)	244 (40.1%)	p=0.001
Obese >30	40 (18.2%)	135 (22.2%)	

Age was found to have positive and statistically significant correlation with overweight BMI. On Table 2 is demonstrated the BMI and age of males. From the table there is obviously significantly different between age groups, 53.8% are with overweight BMI in age group from 55-54.9 years old ($p<0.001$; $\chi2=27.618$). The same significant statistically result is demonstrated on Table 3 in females were again the more women's are in age between 55-54.9 years old and are with overweight ($p<0.001$; $\chi2=30.359$).

TABLE 2. BMI and males age groups

Male age groups	BMI N/% < 19	BMI N/% Normal 19-24.9	BMI N/% Overweight 25-29.9	BMI N/% Obese >30
<=35	-	15 (62.5%)	8 (33.3%)	1 (4.2%)
35-54.9	-	12 (25.5%)	24 (51.1%)	11 (23.4%)
55-54.9	-	22 (20.8%)	*57 (53.8%)*	27 (25.5%)
>=75	-	14 (32.6%)	28 (65.1%)	1 (2.3%)

TABLE 3. BMI and females age groups

Female age groups	BMI N/% < 19	BMI N/% Normal 19-24.9	BMI N/% Overweight 25-29.9	BMI N/% Obese >30
<=35	3 (12%)	14 (56%)	3 (12%)	5 (20%)
35-54.9	5 (3.9%)	56 (43.4%)	39 (30.2%)	29 (22.5%)
55-54.9	7 (2%)	104 (29.6%)	156 (44.4%)	84 (23.9%)
>=75	2 (1.9%)	39 (37.5%)	46 (44.2%)	17 (16.3%)

We were compared to BMI with those who have demonstrated hypertension and drink pills every day and people who responded that they don't have hypertension. Table 4 shows that more than those who have hypertension n = 234 (51%) also have an overweight ($p = 0.001$; $\chi2 = 40.779$). From the measured blood pressure at the time of the study only one young person under 35 years have high blood pressure (stage - I hypertension, n=224), in age group from 35.1 to 54.9 n=23 (15.3%) of all persons have hypertension, the more risk group were from 55-74.9 years where they were the most numerous n=151 (32.8%) and in group more than 75 years old they were n=49 (33.3%). In group stage –II hypertension (n=63) were as follows: <= 35 years only 1 person with measured blood pressure more than 160(SBP) / 100(DBP); from 35.1-54.9 years n=4 (2.7%); 55-74.9 n=45 (9.8%), >=75 years n=13 (8.8%). There is significant statistically correlation between sex, age and hypertension. The more positive number with hypertension stage I is in women group in age from 55-74.9 were n=106/157 (67.5%/100%) ($p=0.001$; $\chi2 = 52.34$), while the male group in same age are n=45/67 (67.2%/100%), ($p=0.032$; $\chi2 =13.79$).

TABLE 4. Correlation of BMI classification and persons with hypertension and without hypertension.

BMI classification	Without hypertension	With hypertension	p value
<19	10 (2.7%)	7 (1.5%)	
Normal 19-24.9	164 (44.3%)	112 (24.4%)	
Overweight 25-29.9	127 (34.3%)	234 (51.0%)	p=0.001
Obese >30	69 (18.6%)	106 (23.1 %)	

In the samples studied, Person's correlation coefficient between BMI and waist circumference (WC) was 0.699, significant at 0.0001 (Fig.1a). Similary, Person's correlation between BMI and hip was 0.642 with significant at 0.0001 (Fig.1b).

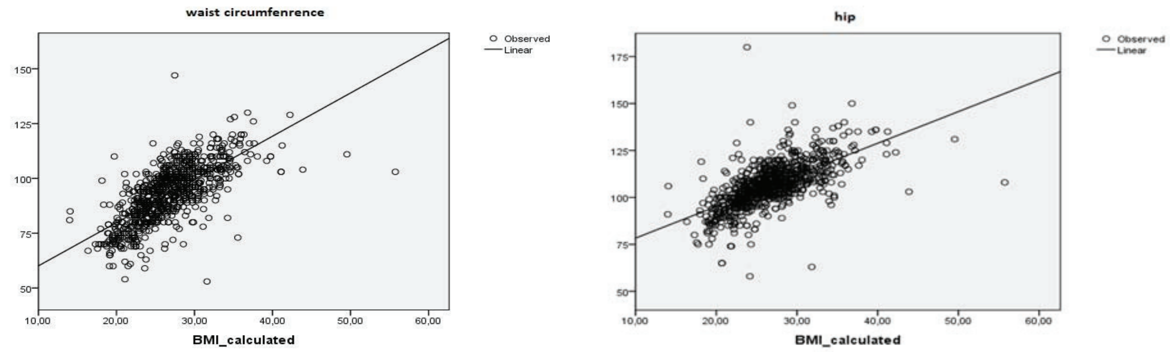

a) (b)

FIGURE 1. Diagram and dispersion between WC (53-150cm) and BMI ($R=0.699$, $p<0.0001$) (a) and Diagram and dispersion between Hip (58-195cm) and BMI ($R=0.642$, $p<0.0001$) (b).

FINAL KEY POINTS TO CONSIDER

Age was positively correlated with blood pressure. The relationship between blood pressure and age was found to be significant and was stronger in women that man in the present study. Many studies have found the relationship between age and blood pressure to be significant among both males and females [6]. In general, blood pressure rises as people get older. Age is known risk factor for high blood pressure [3]. BMI is widely accepted as one of the best indicator of nutritional status in adults [8]. In Japanese rural population the prevalence of combined overweight and obesity was 24% in males and 20% in females [4]. Panagiotakos at al., in study from 2014 in Greece's population they found (overweight 53% in males, and 31% in females, obesity 20% in males, and 15% in females [8]. In our study we found the same risk for both sex but the overweight BMI is prevalence with statistical signification in female population in age from 55-74.9. The waist/hip measurement may be incorporated into life habits, and become an indicator of cardiovascular health for different age population. The biological mechanism by which higher BMI increases the risk of developing hypertension is not completely known. Complex interactions between metabolic and neurohormonal pathways may be the underlying mechanism by which hypertension develops [4]. Insulin resistance, the renin–angiotensin–aldosterone system, and sympathetic tone may be altered by increases in BMI, and these alterations may play a causative role in increasing blood pressure among persons who are overweight and obese [5]. Investigators have reported decreases in plasma renin activity and plasma aldosterone levels after weight loss, which suggests that the renin–angiotensin–aldosterone system may mediate the relationship between BMI and hypertension [2]. Future research is needed to further explore possible biological mechanisms by which higher BMI, especially within the normal range, increases the risk of developing hypertension.

REFERENCES

1. World Health Organization. Obesity: preventing and managing the global epidemic. Report of a WHO consultation of obesity. WHO, Geneva, 1998.
2. Gu D, Reynolds K, Wu X, et al.; Lancet 356:1398-1405, 2005.
3. Pang W, Sun Z, Zheng L, Li J et al. Inter Med 47:893-89, 2008.
4. Marendza M, Hofman KJ, Tollman SM.. South African Heart. 2011;8:48–57.
5. Freedman DS, Goodman A, Contreras OA, DasMahapatra P, Srinivasan SR, Berenson GS. Pediatrics. 2012;130(1):e159–e166.
6. Lui J, Fox CS, Hickson DA, May WD, Hairstoen KG, Taylor HA. J. Clin Endocrinol Metab. 2010;95:5419–5426.
7. Jamison DT, Feachem RG, Makgoba MW, Bos ER, Baingana FK, Hofman KJ, Rogo KO. Disease and Mortality in Sub-Saharan Africa. 2nd Ed. Wahington: World Bank; 2006. pp. 305–328.
8. Panagiotakos DB, Pitsavos C et al., Obes Res 12:1914-1920, 2004

Gender Differences of the Anthropometric Indices of Abdominal Obesity in Individuals with COPD

Maya Gulubova[1, b)], Dimo Dimov[2, c)], Koni Ivanova[1, d)], Atanas Atanasov[3, e)], Tanya Tacheva[4, f)], Tatyana Vlaykova[4, a)]

[1]*Dept. General and Clinical Pathology, Medical Faculty, Trakia University, Stara Zagora, Bulgaria,*
[2]*Dept. Health Care, Medical Faculty, Trakia University, Stara Zagora, Bulgaria.*
[3]*Dept. Physics and Biophysics, Medical Faculty, Trakia University, Stara Zagora, Bulgaria*
[4]*Dept. Chemistry and Biochemistry, Medical Faculty, Trakia University, Stara Zagora, Bulgaria*

[a)]Corresponding author: tvlaykova@abv.bg
[b)]decan@mf.uni-sz.bg; [c)]dmdimov65@yahoo.com; [d)]koni_ivanova@yahoo.com
[e)]atanastod@abv.bg; [f)]tachevat@abv.bg

Abstract. COPD is a chronic inflammatory lung disease which is associated with variety of co-morbidities, as the obesity and cardiovascular diseases (CVDs) are the most frequent. The aim of the current study was to explore the correlations of the age and BMI with the anthropometric indices associated with abdominal obesity in individuals with COPD and to explore the possible difference between the genders. Material and methods: This cross-sectional analysis included 851 citizens from the region of Yambol, Bulgaria. They were interviewed and blood pressure was measured during events organized at the World Diabetes Day, November 14, 2016-2018. One hundred and three of the individuals reported previous diagnosis of COPD. The further statistical analyses were performed only in this group of individuals applying SPSS 16.0 for Windows (SPSS Inc.). Results: Thirty three (32%) of the individuals with COPD were men with a mean age of 58.12 ±13.76 years, while the rest of 70 (68%) persons were women with a mean age of 66.70±10.73 years (p=0.001). The body mass index (BMI) correlated positively with the anthropometric indices associated with central obesity: the waist circumferences (WC, r=0.601, p<0.0001), the hip circumferences (HC, r=0.619, p<0.0001) and waist-to-hip ratio (WHR, r=0.214, p=0.033). The age correlated positively only with the WHR ratio in men (r=0.390, p=0.025), but not in women. When comparing the BMI between genders we did not observed difference (p=0.802). However when classified into groups according to the BMI, women were more frequently with normal weight (30.4%) and obese (33.3%) compared to men (25.8% and 16.1%, respectively), while men were more often with overweight than women (58.1% vs. 36.2%, p=0.091). Men had higher WC (99.23±11.40 cm, p=0.080) and especially WHR (0.922±0.067, p<0.0001) than women (94.17±14.50 cm and 0.855±0.084, respectively). According to the WHR the abdominal obesity was more frequently observed in men with COPD (78.8%) than in COPD women (58.6%. p=0.045). The measured high blood pressure was significantly associated with central obesity both in women (p=0.038) and in men (p=0.035).Conclusions: The results of our study confirm the positive correlation of the BMI with other anthropometric indices associated with abdominal obesity. Based on the results we could conclude that central obesity is more common in men than in women and determines a risk for higher blood pressure in patients with COPD.
Key words: COPD, abdominal obesity, BMI, WHR

INTRODUCTION

According to the Global Initiative for Chronic Obstructive Lung Disease (COPD), it "is a common preventable and treatable disease characterized by persistent respiratory symptoms and airflow limitation due to airways and/or alveolar anomalies commonly caused by significant exposure to harmful particles or gases" [1]. COPD is a lung disease which is however associated with variety of co-morbidities, as the obesity and cardiovascular diseases (CVDs) are the most frequent [2,3]. The other frequent co-morbidities are peptic ulcer, obstructive sleep apnea, diabetes type 2, gastroesophageal reflux and osteoporosis. These pathological conditions contribute significantly to the course of COPD and lead to worsening of the prognosis [3].

Previous studies have shown quite variable prevalence of obesity in COPD patients with no consensus about the effect of obesity on dyspnea or other clinical characteristics and outcome of COPD patients [2,4-6]. Although the obesity is generally associated with restricted pulmonary function in general population and with increased risk of CVD and mortality, in COPD it seems that obesity might have a beneficial effect on dyspnea and on the all-cause mortality. This phenomenon is called "obesity paradox" [6]. Earlier we reported that the increased body mass, particularly obesity is frequent in COPD, especially in less severe diseases and we also suggested that the higher body weight may have a protective effect against the impairment of lung functions [7].

Because of the many inconsistencies in the reported data of the role of obesity in COPD, further studies are encouraged in this area [2]. One of the possible reasons for this disunity might be the differences in methodology for assessing the obesity. Most commonly the obesity is evaluated by the BMI, however it has several limitations. Other indexes are the waist circumferences (WC), the hip circumferences (HC), waist-to-hip ratio (WHR), fat mass index (FMI), suprailiac skinfold measurements and others [8-11].

In the current study we aimed to explore the correlations of the age and BMI with the anthropometric indices associated with abdominal obesity in individuals with COPD and to explore the possible difference between the genders.

MATERIAL AND METHODS

This cross-sectional analysis included 851 citizens from the region of Yambol, Bulgaria. They were interviewed and blood pressure and peripheral blood glucose were measured during events organized by Medical Faculty, Trakia University, Stara Zagora, at the World Diabetes Days, November 14, 2016-2018. One hundred and three (12.10%) of the individuals reported previous diagnosis of COPD, 350 (41.13%) announced some other chronic disease and the rest of 398 (46.77%) persons did not apprise any disease. All individuals were volunteers and after filling in informed consent and a questionnaire, they were interviewed and some anthropometric indices were assessed. The anthropometric indices that were measured were the height, weight, waist circumferences (WC) and hip circumferences (HC) and further the body mass index (BMI) and waist-to-hip ratio (WHR) were calculated using the BMI was following formulas: BMI = weight (kg)/height (m^2); WHC=WC (cm)/HC (cm). The enrolled individuals were categorized on the basis of BMI according to the WHO classification [12]. Overweight was defined when BMI was between 25-29.9, and general obesity was considered when BMI ≥ 30. , blood pressure of the volunteers was also measured.

The statistical analyses were performed only in the group of individuals with COPD by applying SPSS 16.0 for Windows (SPSS Inc.). Factors with $p<0.05$ were considered statistically significant

RESULTS

Thirty three (32%, 33/103) of the individuals with COPD were men and the rest of 70 persons (68%) were women. There was a significant difference between the age of the enrolled men (mean age of 58.12 ±13.76 years) and women (mean age of 66.70±10.73 years, p=0.001). Most of the females were above 55 years old (90.0%), while the men aged above 55 years were 66.7% (p=0.004).

When comparing the BMI between genders we did not observed difference (27.38±3.68 in men vs. 27.63±4.70 in women, p=0.802). However when categorized on the basis of BMI according to the WHO classification [12], women were more frequently with normal weight (30.4%) and obese (33.3%) compared to men (25.8% and 16.1%, respectively), while men were more often with overweight than women (58.1% vs. 36.2%, p=0.091).

In the whole group of COPD volunteers the analysis of the correlations of the BMI with the anthropometric indices associated with central obesity showed statistical significance with the waist circumferences (WC, r=0.601, p<0.0001), the hip circumferences (HC, r=0.619, p<0.0001) and waist-to-hip ratio (WHR, r=0.214, p=0.033). These correlations of BMI remain significant in the groups of females (with WC r=0.628, p<0.0001, with HC r=0.581, p<0.0001 and with WHR p=0.296, p=0.013), while in men BMI correlated only with WC (r=0.609, p<0.0001) and with HC (r=0.764, p<0.0001), but not with the WCR (r=0.051, p=0.783).

The age correlated positively only with the WHR ratio in men (r=0.390, p=0.025), but not in women and with none of the other anthropometric indices.

Men had higher WC (99.23±11.40 cm, p=0.080) and especially WHR (0.922±0.067, p<0.0001) than women (94.17±14.50 cm and 0.855±0.084, respectively) (Fig. 1a and 1b). However, there was no difference in HC between the genders (107.58±9.03 cm in men vs. 110.10±12.52 cm in women, p=0.302).

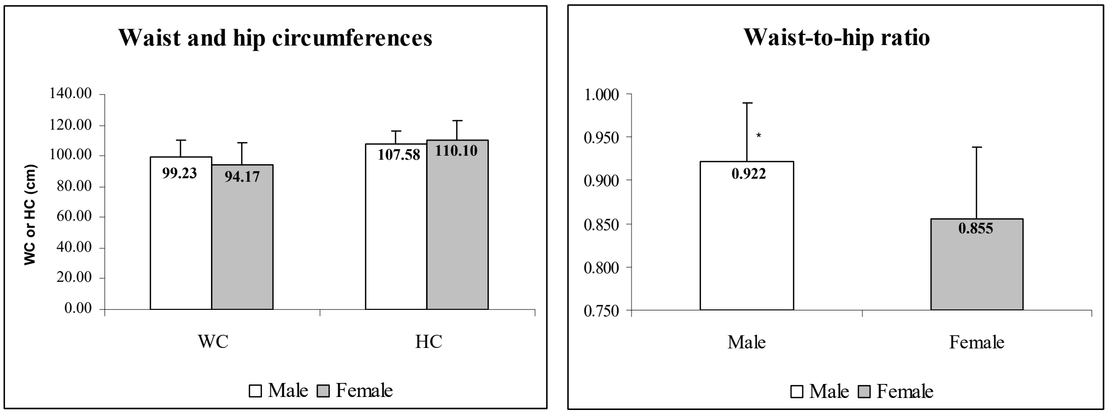

(a) (b)

FIGURE 1. Differences between genders in the anthropometric indices associated with abdominal obesity: Waist circumferences, WC and Hip circumferences, HC (a) and Waist-to-hip ratio, WHR (b). Data are presented as mean ± SD. * - p<0.0001

Applying the WHO criteria for assessing the health status and abdominal obesity based on WHR for men (≥0.90) and for women (≥0.85) the COPD patients were dichotomized into groups with and without abdominal (central) obesity [12,13]. The abdominal obesity was more frequently observed in men with COPD (78.79%) than in COPD women (58.57%. p=0.045).

The measured high blood pressure was significantly associated with higher values of BMI (p=0.001), WC (p<0.0001), HC (p=0.005) and WHR (p=0.019) only in women, but not in men. However when compared the measured blood pressure between individuals with and without abdominal obesity (assessed according WHC) it appeared that there is statistically significant association both in women (p=0.038) (Fig. 2b) and in men (p=0.035) (Fig. 2a).

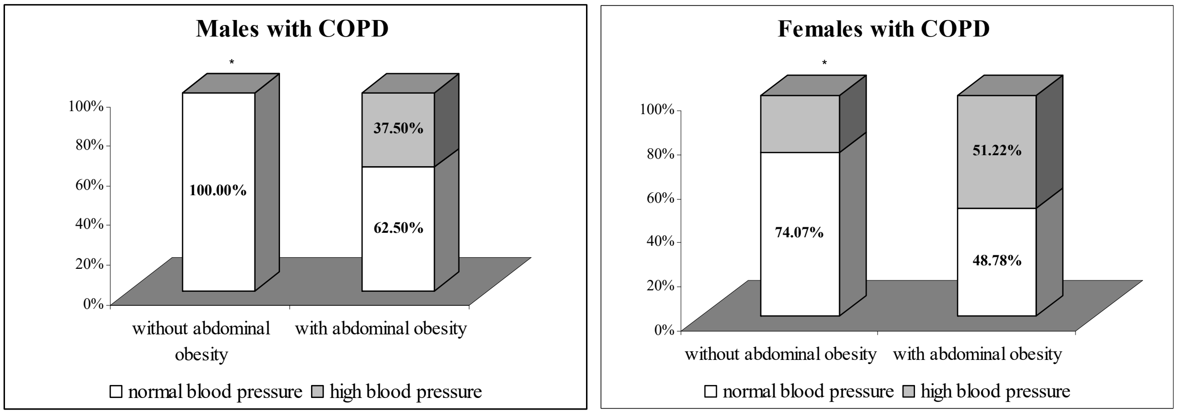

(a) (b)

FIGURE 2. Frequency of the high blood pressure in males with and without abdominal obesity (WHC ≥0.90) (a) and in females with and without abdominal obesity (WHR ≥0.85) (b). * - p = 0.035; ** - p=0.038

The results of the performed interview showed that 51.5% of the men with COPD reported early diagnosed hypertension, while in women these with hypertension were 71.4% (p=0.048). This chronic pathologic condition did not relate to the abdominal obesity, while it was significantly associated with obesity assessed by BMI in women (58.7% in non-obese vs. 95.7% in obese, p=0.001, Fisher's exact test). In men the reported early diagnosed hypertension was significantly associated with BMI above 25 (12.5% in men with normal BMI vs. 69.6% with BMI above 25, i.e. overweight +obese, p=0.011, Fisher's exact test). The BMI above 25 in women was associated with

previous incidence of stroke 22.9% compared to the women with normal BMI (0%) (p=0.015, Fisher's exact test). Similarly, in women with abdominal obesity (WHR ≥0.85), the incidence of stroke tended to be more frequent (22.0%) than in women with WHR < 0.85 (6.9%, p=0.088). No other significant associations were observed between the BMI or WHR with the explored in the questionnaire behavior habits (physical activity, intake of carbohydrates, lipids, applying nutritional diets, intake of alcohol, smoking), other chronic or acute diseases (diabetes, myocardial infarction).

FINAL KEY POINTS TO CONSIDER

The main findings of our cross-sectional study confirm the positive correlation of the BMI with other anthropometric indices associated with abdominal obesity as the waist circumferences, the hip circumferences and the waist-to-hip ratio. Based on the results we could conclude that the abdominal obesity is more common in men than in women and determines a risk for higher blood pressure in patients with COPD. The obtained associations suggest that the indexes related to the abdominal obesity might be more powerful indicators for the risk of development of other co-morbidities as hypertension and cardiovascular diseases than the BMI, the main indicator of general obesity. This notion is in a good agreement with some early reported results displaying the significance of waist circumference and central obesity as risk factors for ischemic heart disease (IHD) even in patients with normal weight [14].

Our study has several limitations; one of the most important is being the lack of assessment of the lung function. In this respect, further studies with more precise questionnaire for the nutritional and behavior habits and spirometric assessment of the lung function are needed and will be conducted.

ACKNOWLEDGMENTS

This work was supported by Trakia University Infrastructural Project 3/2017 and by the National Scientific Program "Young scientists and post-doctors" of Trakia University, Stara Zagora, Bulgaria (K.I. and T.T.).

REFERENCES

1. GOLD: Global strategy for the diagnosis, management, and prevention of chrinic obstructive pulmonary disease. 2017 Report. .(2017)
2. S. Zewari, P. Vos, F. van den Elshout, R. Dekhuijzen, Y. Heijdra *Copd*, **14**, 663-673.(2017)
3. R. Rubinsztajn, T. Przybylowski, M. Grabicki, K. Karwat, M. Maskey-Warzechowska, H. Batura-Gabryel, R. Chazan *Adv Clin Exp Med*, **28**, 319-324.(2019)
4. S. Guerra, D. L. Sherrill, A. Bobadilla, F. D. Martinez, R. A. Barbee *Chest*, **122**, 1256-1263.(2002)
5. C. Hanson, E. P. Rutten, E. F. Wouters, S. Rennard *Int J Chron Obstruct Pulmon Dis*, **9**, 723-733.(2014)
6. F. Spelta, A. M. Fratta Pasini, L. Cazzoletti, M. Ferrari *Eat Weight Disord*, **23**, 15-22.(2018)
7. D. Dimov, T. Tacheva, A. Koychev, V. Ilieva, G. Prakova, T. Vlaykova *Chron Respir Dis*, **10**, 215-222.(2013)
8. S. Popovic-Grle, A. Ladic, B. Butorac-Petanjek, J. Spicek-Macan, B. Cucevic *Acta Clin Croat*, **52**, 69-77.(2013)
9. L. V. Savchenko, I. P. Kaidashev *Wiad Lek*, **71**, 451-459.(2018)
10. M. Emami Ardestani, G. Sajadi, N. Jazayeri *Tanaffos*, **15**, 134-140.(2016)
11. G. Trompeter, M. R. Grigsby, C. H. Miele, R. A. Wise, R. H. Gilman, J. J. Miranda, A. Bernabe-Ortiz, W. Checkley *Lung*, **196**, 277-284.(2018)
12. World Health Organization. *Waist Circumference and Waist-Hip Ratio, Report of a WHO Expert Consultation. Geneva, 8-11 December 2008*. Retrieved March 21, 2012, (WHO Press, Geneva, Switzerland).(2012)
13. N. Ahmad, S. I. Adam, A. M. Nawi, M. R. Hassan, H. F. Ghazi *Int J Prev Med*, **7**, 2008-7802.(2016)
14. Y. Tian, S. C. Yang, C. Q. Yu, Y. Guo, Z. Bian, Y. L. Tan, P. Pei, J. S. Chen, Z. M. Chen, J. Lyu, L. M. Li *Zhonghua Liu Xing Bing Xue Za Zhi*, **39**, 1172-1178.(2018)

Association of Body Mass Index with Helicobacter Pylori Infection in Patients with Chronic Gastritis

Koni Ivanova[1, b)], Rumen Tenev[2, c)], Mehmed Hazhi [1, d)], Julian Ananiev[1, e)], Aleksandra Zdraveska[3, f)], Maya Gulubova[1, a)]

[1]*Dept. General and Clinical Pathology, Medical Faculty, Trakia University, Stara Zagora, Bulgaria,*
[2]*Dept. of Gastroenterology, Medical Faculty, Trakia University, Stara Zagora, Bulgaria*
[3]*Dept. of Social Medicine, Medical Faculty, Trakia University, Stara Zagora, Bulgaria*

[b)]Corresponding author: koni_ivanova@yahoo.com
[c)]rtenev@abv.bg
[d)] bass_hunter@abv.bg
[e)] operation@abv.bg
[f)] dimitrova@abv.bg
[a)] decan@mf.uni-sz.bg

Abstract. Obesity is an important risk factor both for digestive pathology and for cardio-metabolic disease, cancer, respiratory, rheumatologic and dermatological pathologies. Obese patients, already at high cardio-metabolic risk, have higher prevalence of H.Pylori infection. The aim of this study was to examine the association between H. pylori colonization and overweight status in different age groups. The study population comprised 73 patients (38 men and 35 women; mean age, 60.89±13.59 years; from 21 to 84 years old). These patients were gastroscopically biopsy to determine HP and type of gastritis in a period from November 2018 to January 2019 in the University Hospital of Stara Zagora, Bulgaria. The prevalence of overweight shown statistical marginal significant in male patients between 35-54.9 years old ($p=0.052$; $\chi2=16.82$) while higher number were present in female between 55-74.9 years with obesity but without statistically significant ($p=0.110$; $\chi2=14.39$). The present findings suggest that obesity-related gastritis could become increasingly dominant in the near future. Further studies to clarify the role of various factors, including role of endocrine cells and some hormones, in the pathogenesis of obesity-related gastritis are needed.

INTRODUCTION

Helicobacter pylorus (HP) is one of the most common infections affecting the epithelial lining of the stomach, for the first time described by Warren and Marshall in 1984 [1]. Acquisition of the infection will lead to gastritis and the eradication of the bacterium results in healing and final cure of the gastritis [1-2]. Chronic gastritis and HP infection may occur in antrum and/or corpus, and will gradually result in atrophy of the underlying mucosa in a great number of affected persons. Correspondingly, impairments in several important functions of the gastric mucosa are consequences of the atrophy and inflammation [3]. It is correlated with antral gastritis, peptic ulcers and promotes gastric cancer. HP infection is prevalence in development countries and the risk factors including age and socioeconomic status [4]. H. pylori-induced gastritis is an important risk factor in the multifactorial etiology of these diseases. It causes a cascade of reactions that damage the gastric mucosa and epithelium in various ways. The specific mechanisms involved are largely unknown. Some are probably bacterium-related reactions, which are influenced by various virulence factors, and others are consequences of the mucosal inflammation and atrophy [5,6].

Obesity is an important risk factor both for digestive pathology and for cardio-metabolic disease, cancer, respiratory, rheumatologic and dermatological pathologies. Superior digestive tract diseases (gastro-esophageal reflux disease, erosive esophagitis, hiatal hernia,esophageal adenocarcinoma and H. pylori infection) have been

reported as being 2–3 times more frequent in obese persons compared to normal weight [7-9]. The effect of obesity on precursor lesions such as atrophic gastritis or intestinal metaplasia has also been examined in several observational studies, but results are inconclusive [3]. Some studies reported a positive association between BMI and atrophic gastritis or intestinal metaplasia, whereas others reported no association [6,8,9]. However, previous studies used cross-sectional design, limiting their ability to establish the temporal relationship between obesity and atrophic gastritis. In addition, the risk of atrophic gastritis in obese patients can be mediated by insulin resistance and other obesity-associated metabolic abnormalities, but no studies have evaluated whether the association of obesity with atrophic gastritis and intestinal metaplasia is mediated by such metabolic parameters [7].

The aim of this study was to examine the association between H. pylori colonization and overweight status in different age groups.

MATERIAL AND METHODS

The study population comprised 73 patients (38 men and 35 women; mean age, 60.89±13.59 years; from 21 to 84 years old). These patients were gastroscopically biopsy to determine HP and type of gastritis in a period from November 2018 to January 2019 in the University Hospital of Stara Zagora, Bulgaria. For most age-related comparisons, patients were separated into four groups according to age (young <=35 years, 35.1-54.9 years, 55-74.9 years and >=75 years). Height was copied from the ID card of the participants. Weight was measured to the nearest 100 grams, without shoes. BMI (weight/height2) was calculated. BMI was classified according to the proposed criteria of World Health Organization (<19, normal 19-24.9; overweight 25-29.9, and obese >30). In the present study all the subjects having BMI>=30 were taken as obese. The HP infection in this study was characterized like absent or present.

Statistical analysis

Statistical analyses were performed using SPSS 16.0 software package (SPSS, Inc., Chicago, IL, USA). The descriptive statistical tests, including the mean, standard deviation, and median, were calculated according to the standard methods. The associations between BMI and HP were assessed by $\chi 2$ Test, $p < 0.05$ was considered to be statistically significant.

RESULTS

A total of 73 patients, 52.1% males and 47.9% female were included in this study. We were investigated the correlation between BMI classification in males and females demonstrated on Table 1. Nineteen (50%) male patients were with overweight BMI and fourteen (40%) from group of females, therefore a higher percentage of the patients studied are with overweight. The prevalence of overweight shown statistical marginal significant in male patients between 35-54.9 years old ($p=0.052$; $\chi 2=16.82$) while higher number were present in female between 55-74.9 years with obesity but without statistically significant ($p=0.110$; $\chi 2=14.39$). The general characteristic of the study group are demonstrated in Table 2.

TABLE 1. BMI classification in females and males

BMI classification	Males N/%	Female N/%
<19	2 (5.3%)	5 (14.3 %)
Normal 19-24.9	12 (31.6%)	6 (17.1%)
Overweight 25-29.9	19 (50.0%)	14 (40.0%)
Obese >30	5(13.2%)	10 (28.6%)

TABLE 2. General characteristic of the study group

Characteristics	*Unit*	*Total*	*Women (N;%)*	*Men (N;%)*
Age (years)	mean±SD min,;max.	60.89±13.599 18;32	69.09±13.08 27;82	59.79±14.144 22;84
Weight (kg)	mean±SD min,;max.	76.47±15.27 41;118	70.34±13.968 41;99	82.13±14.36 50;118
Height (cm)	mean±SD min,;max.	1.69±9.35 150;187	1.62±5.36 150;172	1.75±7.34 155;187
BMI (kg/m^2)	mean±SD min,;max.	26.85±5.81 15.24;38.46	27.05±5.83 15.24;38.46	26.67±4.36 16.10;37.86
Overweight	N;%	33 (45.2%)	14 (40%)	19 (50%)
Obesity	N;%	15 (13.2%)	10 (28%)	5 (13.2%)
H.Pylori	N;% present	55(75.3%)	26(74.3%)	29(76.3%)
	N;% absent	18(24.7%)	9 (25.7%)	9 (23.7%)

When we analyzed the present of HP we were found that 55 (75.3%) of patient were with HP while only 18 were without infection with HP. We were compared the presence of HP with age of the patients to seen in which age group are more. Thirty patients in age from 55 to 74.9 have HP infection. From total 73 patients histologically had identified a type of gastritis, 55 of them were with chronic atrophic gastritis and HP presence, another 18 were with superficial gastritis and without HP.

FINAL KEY POINTS TO CONSIDER

The discovery of HP infection revolutionized previous concepts regarding chronic gastritis and is currently also under attention as a risk factor for cardiometabolic diseases and cancer. Obese patients, already at high cardio-metabolic risk, have higher prevalence of HP infection [3]. In our study we evaluated the relationship between HP infection and age groups. No significant difference was found when we compared the HP and overweight/obesity. Without statistical significant 26 from the patients with HP infection were with overweight BMI (p=0.151). In other study retrospective study of Torisu et al., 2008 the authors found similar correlation that patients with positive HP infection has decreased BMI more than HP negative patients. The prevalence of overweight was shown statistical marginal significant in male patients between 35-54.9 years old when we correlated them with obesity woman's group.

In other study Kim et al., from 2017 [7] demonstrated that the association between chronic gastritis and Helicobacter pylori HP infection is strong. Clearly more than 80% of cases with chronic gastritis are related to coexistent HP infection. In our study we demonstrated the same results that more than 70% from the investigated group are with HP infection and chronic gastritis.

Available data on H. pylori infection and obesity are still controversial [10]. The present findings suggest that obesity-related gastritis could become increasingly dominant in the near future. Further studies to clarify the role of various factors, including role of endocrine cells and some hormones, in the pathogenesis of obesity-related gastritis are needed.

REFERENCES

1. Weck MN, Stegmaier C, Rothenbacher D, Brenner H. Aliment Pharmacol Ther. 2007;26(6):879–87.
2. Sipponen M. Mater Med Pol. 1992 Jul-Sep;24(3):166-8.
3. Ohata H, Kitauchi S, Yoshimura N, Mugitani K, Iwane M, Nakamura H, et al.. Int J Cancer. 2004;109(1):138–43.
4. Wang Z, Zhang B, Zhai F, Wang H, Zhang J, Du W, et al. Nutr Metab Cardiovasc Dis. 2014;24(8):869–76.
5. Torisu T, Matsumoto T, Takata Y, Ansai T, Soh I, Awano S, et al. J Gastroenterol 2008;43:762–6. 24.
6. Felley C, Bouzourene H, VanMelle MB, Hadengue A, Michetti P, Dorta G, et al. World J Gastroenterol 2012;18:2076–83. 25.
7. Kim N, Youn CH, Kim AS, Ko HJ, Kim HM, Moon H, et al. Korean J Gastroenterol 2017;70:81–8. 26.
8. Park YM, Kim JH, Baik SJ, Park JJ, Youn YH, Park H. Medicine 2016;95:e5351.
9. Choi S, Lim YJ, Park SK. World J Gastroenterol 2006;12:2584–7. 28. Chang Y, Kim BK, Yun KE, Cho J, Zhang Y, Rampal S, et al. J Am Coll Cardiol 2014; 63:2679–86.
10. Pasechnikov Victor D, Sergey Chukov Z, Sergey Kotelevets M, Alexander Mostovov N, Varvara Mernova P, Polyakova Maria. Scand J Gastroenterol. 2005;40:297–301. [PubMed] [Google Scholar]

Performance Evaluation for Social Enterprises in Bulgaria

Darina Zaimova[1, a)] Svetlana Markova[2, b),] Krasimira Benkova[3, c)]

[1] *Darina Zaimova, Dept. Industrial business and entrepreneurship, Trakia University, Stara Zagora, Bulgaria*
[2] *Svetlana Markova, Medical Faculty, Dept. Social activities, Trakia University Stara Zagora, Bulgaria.*
[3] *Krasimira Benkova, Medical Faculty, Dept. Social activities, Trakia University Stara Zagora, Bulgaria.*

[a)] Darina Zaimova, dzaimova@gmail.com
[b)] Corresponding Author:, markova@mf.uni-sz.bg
[c)] Krasimira Benkova , b_enkova@abv.bg

Abstract. The wider recognition of the social enterprises as a hybrid business is solely based on its achievements and impact in spheres where the traditional business has limited interest to invest and operate. This refashioned entrepreneurial model inspired several researches targeted at evaluation and assessment that both account for the economic efficiency and social impact. Our paper estimates and evaluates the efficiency performance of four types of social enterprises in Bulgaria - non-profit legal entities, cooperatives for people with disabilities, specialized enterprises for people with disabilities and other social enterprises (cultural centers – chitalishta).

DEA METHODOLOGY AND EMPIRICAL RESULTS

We use the non-parametric Data envelopment approach (DEA) to optimize on each decision-making unit (DMU) and to calculate a discrete piecewise frontier. Thus, not only efficiency is rated, but also sources and amounts of the inefficiency components in our data set are estimated.

Efficiency coefficients calculations

In our data set we include four types of social enterprises – non-profit legal entities (33), cooperatives for people with disabilities (10), specialized enterprises for people with disabilities (14) and other social enterprises (cultural centers – chitalishta) (12).

TABLE 1. Efficiency coefficients

Type of SE	2017			2018		
	Efficiency CRS	**Efficiency VRS**	**Scale efficiency**	**Efficiency CRS**	**Efficiency VRS**	**Scale efficiency**
Non-profit legal entities	0.985	0.991	0.999	0.987	0.992	1.000
Cooperatives for people with disabilities	0.924	0.984	0.943	0.963	0.987	0.980
Specialized enterprises for people with disabilities	0.963	0.979	0.990	0.971	0.984	0.991
Other social enterprises	0.935	0.966	0.973	0.961	0.972	0.993

Close to 50% is the share of the non-profit legal entities in the total number of the DMUs. They have achieved the highest efficiency scores both under constant and variable returns to scale.

A slight increase we observe in the efficiency levels of the cooperatives for people with disabilities and the cultural centers (chitalishta). Under the assumption for constant returns to scale, their productivity improves by 4% and 3%.

A general overview of the estimated efficiency scores is presented on Graph 1:

GRAPH 1. Efficiency 2017 – 2018

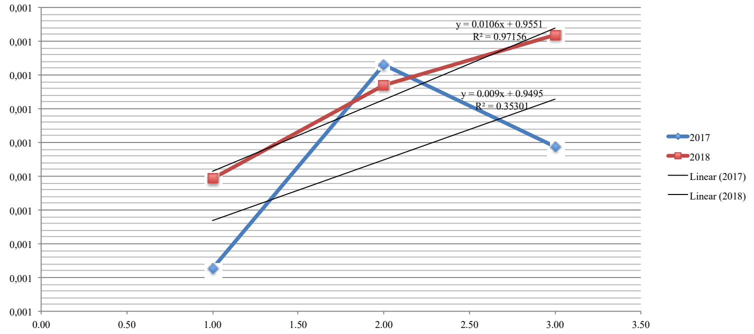

The majority of the DMUs – close to 73% operate under decreasing returns to scale. Having in mind that the scale economies are the flip side of the returns to scale, we would suggest that this majority also operates under diseconomies of scale.

Sensitivity analysis

We calculate the lower and upper bound of the stability regions under VRS for each DMU in the data set (Graph 2) to estimate by how much the inputs (production and labour costs, reinvestments for social purposes and total fixed assets) could be increased without decreasing the efficiency levels.

The indicated bounds identify the input stability regions only for these DMU that keep their efficiency levels even after the increase of their inputs.

GRAPH 2. Stability regions (2017-2018)

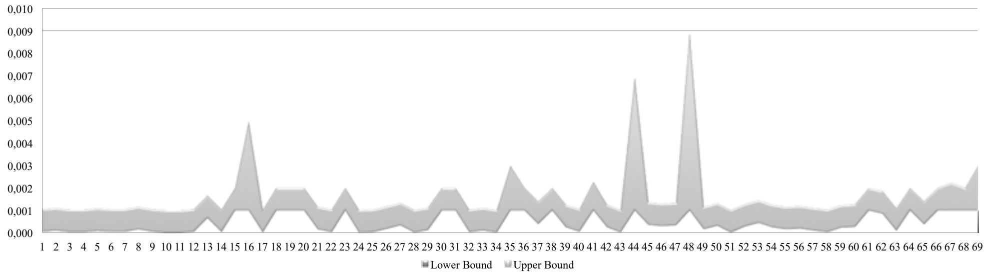

The estimations certify for three sensitivity regions:

- Region I (Increasing Returns to Scale - IRS) – 10% of the DMUs do not explore their optimal production capacity;
- Region II (Constant Returns to Scale – CRS) – 20% of the DMUs operate on the optimal production frontier. Their technical efficiency is 1 and thus they are defined as the benchmark in the data set, belonging to the best-practice frontier.
- Region III (Decreasing Returns to Scale – DRS) – 70% of the DMUs fail to exploit their production capacity.

We perform a sensitivity analysis to calculate the maximum possible increase of each one of the inputs by holding the inputs and outputs unchanged, while changing only the input under evaluation. The results show separately the possible percentage increase of production and labour costs, and reinvestments for social purposes and total fixed assets (Table 2).

TABLE 2. Sensitivity analysis (2017-2018)

Type of inputs	Average change in the data set (%)	Optimal λ (%)	Increase of the efficiency coefficients (%)
2017			
Production costs	98.52	24.22	2.58
Labour costs	26.83	18.59	8.74
Reinvestment in social purposes	36.88	2.17	3.45
Total fixed costs	33.87	30.75	24.81
2018			
Production costs	98.39	18.20	8.33
Labour costs	8.74	31.84	11.86
Reinvestment in social purposes	34.57	40.20	2.22
Total fixed costs	32.96	33.87	20.30

Optimisation of the two cost categories - production costs and reinvestment in social purposes – apparently positively influences the levels of the technical efficiency of the DMUs. An interesting result is the importance of the total fixed costs, which in the third sector is not isolated case.

Slack-based model

We calculate the input slacks to indicate by how much the inputs could be proportionately reduced and still to achieve the same level of output. Under CRS DMUs could on average reduce up to 34% of the labour costs. The contribution of the reinvestment in social purposes could be optimized by 39%. Under the assumption for VRS, DMUs could reduce the labour costs by 15%. The share of the costs related to the fixed assets utilization could be optimized up to 20%, while the reinvestment in social purposes could be reduced with 34%.

The results for the output slacks both under the assumption for CRS and VRS are insignificant – the possibility to increase final outputs is less than 1%.

Context dependent DEA

Theoretically adding or deleting an inefficient DMU or set of inefficient DMUs would not lead to changes in the efficiency levels of the existing DMUs and the best-practice frontier. Such result is possible only when the best-practice frontier is altered. When applying the context-dependent DEA to our data set we calculated three levels of best-practice frontiers. Efficiency coefficients at the Level 1 range between 0.97 - 1 and this level includes 20 DMUs. The second-level frontier includes 33 DMUs and the estimated efficiency scores range between 0.94 - 1. The third-level frontier includes the remaining 16 DMUs and achieves efficiency of 1.

GRAPH 3. Context-dependent DEA (2017-2018)

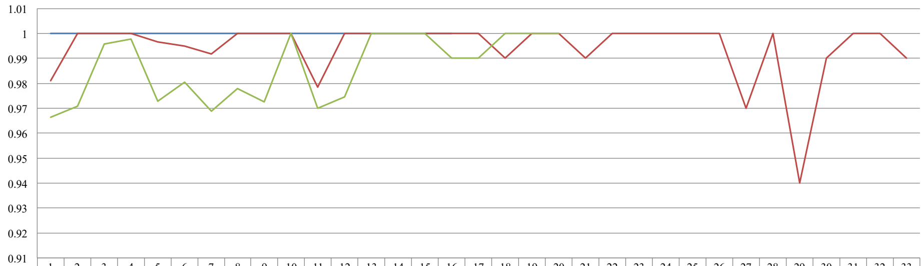

	1	2	3	4	5	6	7	8	9	10	11	12	13	14	15	16	17	18	19	20	21	22	23	24	25	26	27	28	29	30	31	32	33
Level 3	1	1	1	1	1	1	1	1	1	1	1	1	1	1	1	1																	
Level2	0.98	1	1	1	1.00	0.99	0.99	1	1	1	0.98	1	1	1	1	1	1	0.99	1	1	0.99	1	1	1	1	1	0.97	1	0.94	0.99	1	1	0.99
Level 1	0.97	0.97	1	1	0.97	0.98	0.97	0.98	0.97	1	0.97	0.97	1	1	1	0.99	0.99	1	1	1													

Malmquist Index

In our analysis, we used one of the advantages of the DEA to measure the change of the efficiency over time, as well as the change of the efficient frontier. The Malmquist index represents the Total Factor Productivity (TFP)[1].

Our results signify for output increase, but do not favour the innovation effect. The *catch up effect* signifies that there is an increase in the relative efficiency, proven by the average coefficient of the efficiency change – 1.023. The percentage of the DMUs that managed to improve their relative efficiency is significantly high - 65%. Among all DMUs in the data set, 25% showed regress in their efficiency levels, 10% signified for no change.

The average value of the Malmquist index is 0.98. This result is mostly justified by the regress in the frontier technology.

GRAPH 4. Malmquist index

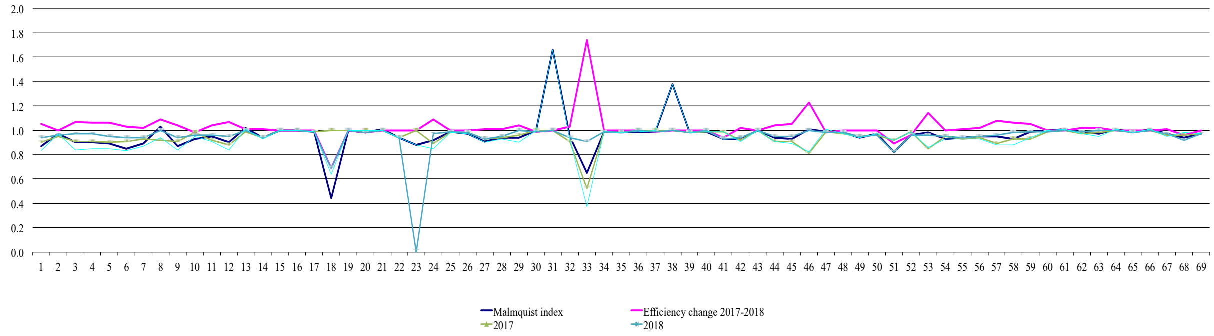

Summary

We performed sensitivity analysis and slack-based model to estimate input utilization and the possibility for optimization. The context-dependent DEA structures new frontiers by translating the inefficient DMUs into relatively efficient ones. The total factor productivity is analyzed through the Malmquist index.

REFERENCES

1. A.I. Ali, C.S. Lerme, L.M. Seford Components of efficiency evaluation in data envelopment analysis, European Journal of Operational Research, 80, pp.462-473, 1995.
2. A.Charnes, W.W. Cooper, B.Golany, L.M. Seford, J.Stutz Foundations of data envelopment analysis for Pareto-Koopman's efficient empirical production functions. Journal of Econometrics, 30, pp.1-17, 1985.
3. L.M. Seiford, J. Zhu Stability regions for maintaining efficiency in data envelopment analysis; European Journal of Operational Research, 108, No. 1, pp.127-139, 1998a.

---

[1] The *"catch up"* effect calculates the degree to which the decision-making unit improves or worsens over time. The progress or regress of the frontier technology between two periods of time under the multiple inputs and outputs is addressed by the *"frontier shift"* effect.

Poverty-Social Exclusion Forecast and the Future of The Social Enterprise

Ruslan Martinov

Medical Faculty, Trakia University, Stara Zagora, BULGARIA
Corresponding author: rmartinov@yahoo.com

Abstract. Mapping poverty at low geographical levels provides information on the heterogeneity of poverty, useful for ranking regions by welfare. It is plausible that $1.25 and $2 global poverty will reduce substantially by 2030. The location of the world's poor people is dependent on changes in inequality as well as on the methods used to estimate poverty. The analyses from ESPAS project showed that the growing inequalities pose a major political, social and economic risk in the years to come. The study of social enterprise (SE) activity in 29 countries leaded to the insights about: the national policy and legal framework for SE; support measures targeting SE; labeling and certification schemes; social (impact) investment markets; factors constraining the development of SE and potential actions to be undertaken to support national initiatives. These characteristics of SE are common also in global aspect and many countries have advanced experience. For many countries (including high-income), and especially for the low-income countries, the social enterprise is a successful model to generate employment and a mean to reduce the poverty and social esclusion, at local and global level. Successful SE is good example of doing business and generates income as well as social impact, and could be considered as a good solution for the future of the enterprise.

INTRODUCTION

World Bank's international poverty rates are based on absolute threshold (reflects how world's poorest countries define minimum threshold of-living standards and national inflation). National line is a function of the income distribution in the year; the international line removes negative welfare values (measured in per capita terms) (1).
An overall decline in global poverty is expected, while inequalities within countries will increase worldwide. By 2030 on present trends inequalities between EU Member States will not diminish. The crisis will continue to affect the most vulnerable members of the society. Thus, 45 % rise in unemployment is expected, an increased risk of poverty for 130 million and exclusion of young people (2).
There is general consensus that the concept of social enterprise (SE) will gain in strength in Europe and that current activity will expand in more new forms of social enterprise. Social enterprises are required across Europe as the basis of future national and European research and policy development.

DATA AND METHOD

In this paper are used data provided from Eurostat, World Bank, National Statistic Institute of Bulgaria (NCI).

1.Data and Forecast Conventions

Data used to prepare country forecasts come from: National Income Accounts, Balance of Payments; fiscal data are from Haver Analytics; the World Development Indicators by the World Bank; the World Economic Outlook, Balance of Payments Statistics, and International Financial Statistics by the International Monetary Fund; Population data and forecasts are from the United Nations World Population Prospects; Country and lending-group classifications are from the World Bank (3).

2.Forecast Process

The forecast process starts with initial assumptions about advanced-economy growth and commodity price forecasts, used for the first set of growth forecasts for EMDEs, produced using macroeconometric models, accounting frameworks, estimates of spillovers from major economies, and high-frequency indicators. World Bank forecasts are updated based on new information and changing global circumstances. The analytical framework used to represent the imperfect transmission of changes in international prices into domestic markets relies on an Error Correction Model (4). The methodology uses a general equilibrium model to generate data for a Monte Carlo simulation to explore the role of estimated coefficients in affecting global and domestic price volatility. Poverty impact is captured through a topdown approach using data set of surveys for 31 countries and 285,000 households. The impact of a

policy shock on poverty depends on price changes, the relative reliance of households on the consumption of individual staple foods and the net food buying status of households in different segments of the distribution (3).

EU-SILC data for EU countries (Eurostat) have been added to ECAPOV database, organized into 6 modules following the Global Monitoring Database (1). Small area estimates of welfare are based on a model using regression analysis, modeling the relationship between household income and its characteristics (data SILC 2012). A two-stage approach (5,6) is used to estimate parameters of a regression equation, with dependent variable income and factors different household characteristics, via ordinary least squares. The household income model is:

$\ln y_{ch} = X`_{ch}\, \beta + u_{ch}$,

where y_{ch} is the adult equivalized income of household *h* in locality *c*, X_{ch} are the household and locality characteristics, and u_{ch} is the residual (7).

Poverty estimates are combining datasets, supplemented by updated data from country-level macro-economic or National Account data (Gross Domestic Product (GDP)). GrIP model facilitates modelling of the growth, inequality and poverty relationship, allowing assessment of future poverty outcomes resulting from growth forecasts (8).

RESULTS AND DISCUSSION

1.Bulgaria

The quality of data for monitoring welfare in Bulgaria is high and surveys are run on a yearly basis. Access to micro data is from EUROSTAT (1,7). The national poverty line in Bulgaria is set at 60 percent of equivalized median disposable income after social transfers, following the European Union standard (1). Bulgaria is among the countries where the risk of poverty rate is above the EU average, but remains relatively stable at about 20 - 22% of the Bulgarian population. The main factor increasing the risk of falling into the group of the poor is the economic activity and participation in the labour market. The social protection system is essential for reducing poverty. The poverty rate will increase to about 50% if pensions and other social transfers are excluded from the household income. Data on the Unemployment rate for EU-28 countries, Romania and Bulgaria are presented on **Figure 1.**

FIGURE 1. Unemployment rate as dependence from the labour force for EU-28, Romania and Bulgaria. Source data: Eurostat.

Poverty mapping results

Estimations of all model parameters allow simulation of income on the census data. Based on simulated incomes, it is possible to produce poverty estimates for each separate territory (region, district, municipality). The calculated relative share of the poor for each territory is the average value of all 100 simulated relative shares, while the standard error is the standard deviation from the respective values (7). The poverty mapping results are based on SILC direct estimates and the poverty line of BGN 3 236 is used to measure the share of the poor. There are districts with high relative shares of poor located in regions with relatively low shares of poor. The relative share of poor is a function of the absolute number of people living below the poverty line and the total number of population. In cities with more than 100 thousand and 36% of the population are concentrated 18.5% of all people at risk of poverty and 38% of all poor in the city districts, leading to two ‘pockets of poverty’ in Bulgaria (7).

2.Global Poverty and income inequality

Low-income countries (LICs)

Per capita Gross Domestic Product (GDP) growth in Low-income countries **(**LICs) is expected to increase modestly from 2.7% in 2018 to 3.1% in 2019, and to 3.5% in 2020-21. Among LICs affected by fragility, conflict, and violence, growth of GDP is expected to be lower: increasing from 0.5% in 2018 to 1.6% in 2020-21. These rates could not lead to a marked reduction in poverty rates, and the number of people in LICs living below $1.90 per day is expected to remain high (3). On **Figure 2** are presented data on the Real GDP for several countries and EU.

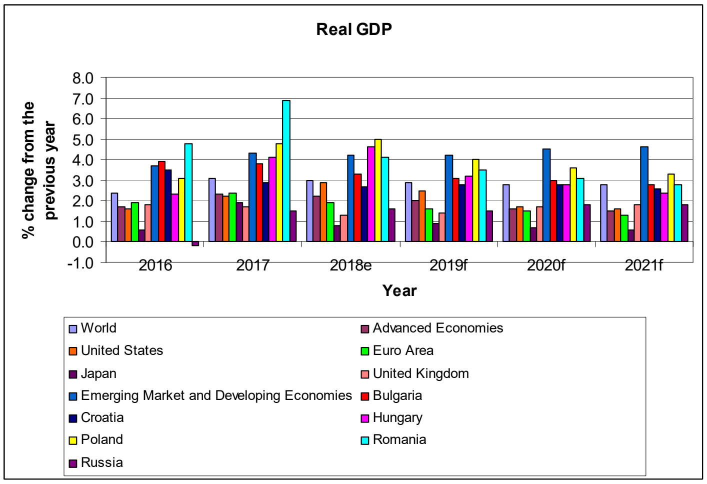

FIGURE 2. Data on the Real GDP as Percent change from the previous year for several countries and EU. Data Sources: World Bank and Haver Analytics. (e-estimated; f-forecast)

Informality, poverty, income inequality

Informal-sector wages are below those in the formal sector. Over the long term, informality may increase income inequality and may contribute to greater poverty in countries with high informality.

Food price shocks. Poverty impact of food price spikes without policy intervention

A high share of net food buyers among the poorest segments of society heightens the adverse effects of food price spikes on poverty and income inequality at microeconomic level. A hypothetical 10 percent surge in rice, wheat, and maize prices raises the number of extreme poor living on less than $1.90% by 0.22% or 2.1 million. Each country's policies can dampen domestic price movements. Thus, the increased food prices combined with government policy responses in 2010-11 raised global poverty by 1 percent or 8.3 million (3).

Poverty estimates using NA means and the costs of ending global poverty

The forecasts using NA means showed that in 2025 global poverty (at $2/day poverty line) will be mainly in fragile and conflict-affected states, focused in LICs. In 2030 most of the world's poor people will live in MICs (8). The total cost of ending global $2 poverty by 2030 could fall to US$250–475 billion if current inequality trends continue (0.2–1.0% of estimated world GDP in 2030). It could fall to US$175–350 billion in 2030 (0.1–0.2% of estimated world GDP in 2030) if growth is strong and countries return to best distribution (8).

3.European Union (EU)

A new vision for 2030. The technological revolution

Education, health social security and public administration account for 50 % of GDP in EU countries. Completion of the single market will facilitate the emergence and growth of flexible organisations by appropriate taxation and regulation. Young people need to be enabled through training and encouragement. New economy could lead to more sustainable, environmentally friendly and low-carbon growth using full the scientific and technological advances. Collaborative work, open sourcing and social innovation might be important components of the future "innovative ecosystems". The technological revolution will have effect on societies, individuals, their working life and their social relationships. Social innovation can provide a better response to social and societal challenges (2).

Unequal societies will be emerging in Europe

New forms of exclusion or marginality are appearing: poor workers, the qualified unemployed, precarious workers. The informal sector or the 'black economy' is growing throughout Europe and the United States following the financial crisis: it offers no up-skilling, no professional recognition, no protection, increases poverty.

Challenge: coping with social and generational inequalities

By 2030 inequalities between EU Member States will not diminish: crisis will continue to affect the most vulnerable members of society. Expected is: 45 % rise in unemployment; increased risk of poverty for 130 million; Young people (one in four is unemployed)*;* vulnerable members of society (young people, women, end-of-career workers and immigrants) will be affected by inequalities. Inequalities within countries will increase and in industrialised countries could weaken the cohesion of middle classes. EU will have high incomes, but lower relative growth (2). Data on the Severely materially deprived people for EU countries are presented on **Figure 3**.

4.Social enterprises and their eco-systems in Europe

The global economic crisis in 2009 resulted in interest in more inclusive and pluralistic economic systems. The social needs created both challenges and opportunities for SE in Europe. There still a lack of availability and consistency of statistical information on social enterprises across Europe (9).

Developing an 'operational definition' of social enterprise: An *entrepreneurial dimension* (engagement in continuous economic activity); A *social dimension* (primary and explicit social purpose); A *governance dimension* (mechanisms to 'lock in' the social goals of the organisation).

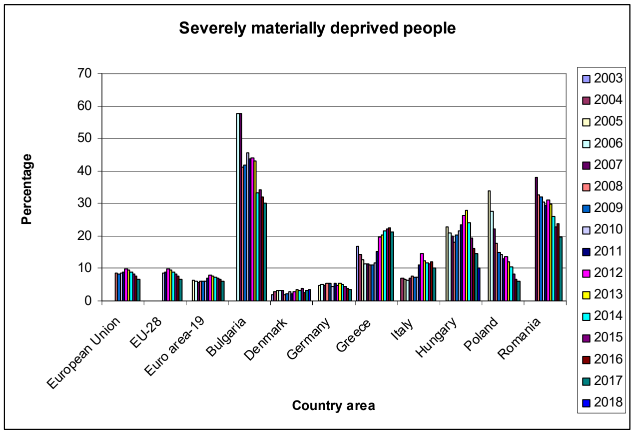

FIGURE 3. Severelly materially deprived people in percentage for EU and European countries with years. Data source: Eurostat.

The national 'social enterprise families' are diverse across Europe, encompassing a range of organisational and legal forms and statuses. European social enterprises are undertaking a growing breadth of activity beyond work integration and social services of general interest.

Social enterprises adopt a variety of legal forms and statuses: existing legal forms (associations, foundations, cooperatives, share companies); new legal forms exclusively designed for social enterprises (adapting or 'tailoring' existing legal forms); legal status that can be obtained by selected or all existing legal forms; new types of legal forms that allow traditional non-profit organisations to undertake economic activity. Social enterprises exploit a range of sources and in most countries, but the majority of their revenue comes from the public sector: *Market sources* (the sale of goods and services to the public or private sector); *Non-market sources* (government subsidies and grants, private donations, non-monetary or in-kind contributions such as voluntary work). The main revenue streams of SE are: Revenue derived from public contracts; Direct grants / subsidies; Market based revenue derived from private sources; Membership fees, donations and sponsorship; Other forms of revenue. *European Structural Funds (ERDF and ESF)* have also played a key role. Development of common social impact measurement systems could result in more transparency, accountability, better recognition of the impact of social enterprises and more interest, from private investors and wider public (9).

These characteristics of the SE are common also in the global world business, where many countries have advanced experience. In low-income countries, the social enterprise is a successful model to generate employment as well as a mean to reduce the poverty.

CONCLUSION

Mapping poverty at low geographical levels provides information on the heterogeneity of poverty, useful for ranking regions by welfare. The poverty mapping results show districts with high relative shares of poor and municipalities affected by poverty or needing social support. The location of the world's poor people is dependent

on changes in inequality. ESPAS project showed that growing inequalities pose a major political, social and economic risk in the years to come that could have an increasing impact on migration and the cohesion of middle classes. SE in Europe is a dynamic and diverse movement for new business models that combine economic activity with social mission. The concept of social enterprise will gain in strength in Europe and current activity will expand in more new forms of social enterprise. SEs are required across Europe as the basis of future national and European research and policy development. Successful SE gives good example of doing business, generate income and social welfare, and could be considered as a good solution to future reduce global poverty and social exclusion.

REFERENCES

1. Bulgaria Poverty & Equity Breaf. Europe & Central Asia. Bulgaria (2018). www.worldbank.org/poverty.
2. Global Trends to 2030: Can the EU meet the challenges ahead? An inter – institutional EU project. (2013).
3. Global Economic Prospects: Europe and Central Asia. Darkening Skies. The World Bank. (2019).
4. M. Ivanic and W. Martin. Journal of International Money and Finance **42**, 272–288 (2014).
5. C. Elbers, J. O. Lanjouw and P. Lanjouw. World Bank Paper 2911 (2002).
6. C. Elbers, J. O. Lanjouw and P. Lanjouw. Econometrica **71** (1), 355 - 364 (2003).
7. Poverty mapping in the republic of Bulgaria. Sofia, NCI (2018).
8. P. Edward and A. Sumner. The future of global poverty in a multi-speed world: new estimates of scale, location and cost. 2013. Working Paper 111 (2013). Brazil. Print ISSN: 1812-108X.
9. A map of social enterprises and their eco-systems in Europe. Luxembourg (2015). doi:10.2767/458972.

Preface of the "GIS, Remote Sensing and Dendrochronology in Geohazards"

Damian Absalon[1,a)] and Ireneusz Malik[1,b)]

[1]*University of Silesia in Katowice, Faculty of Earth Sciences, Będzińska 60, 41-200 Sosnowiec, Poland*

[a)]Corresponding author: damian.absalon@us.edu.pl
[b)]ireneusz.malik@us.edu.pl

The aim of the Symposium is to present results of environmental research conducted with the use of modern methods, i.e. GIS, remote sensing and dendrochronology. The main topics under discussion during the Symposium will be related to geohazards: floods, mass-movements, earthquakes, droughts, etc. These research problems are particularly important from the point of view of the contemporary climate change. Aforesaid geohazards endanger population and infrastructure, thus, studies on natural hazards and risk assessment are particularly welcome.

We would like to invite a wide range of papers presenting current progress in research on geohazards. We believe that the Symposium will be success with presentations providing an inspiration for further joint cooperation and application for research projects. We also hope that results of research presented during the Symposium will gain wide publicity and, thus, will be implemented into spatial panning and economy.

Damian Absalon

Dr. hab. Damian Absalon (PhD, D.Sc.) is vice Director of Silesian Centre of Water, University of Silesia in Katowice and head of Doctoral Studies in Faculty of Earth Sciences, University of Silesia in Katowice, Poland.

He is a geographer, hydrologist and specialist in the field of GIS whose research interests include: Water Resources Management, Water Quality Monitoring, Hydrological Modeling, Environmental Impact Assessment and Geostatistical Analysis. At the University of Silesia he teaches Hydrology, Water Management and GIS. He is an author of more than 150 papers published among others in Science of Total Environment, Geomorphology and Ecotoxicology and Environmental Safety.

Ireneusz Malik

Prof. Dr. hab. Ireneusz Malik is head of the Department for Reconstructing Environmental Change at the Faculty of Earth Sciences, University of Silesia, Poland. He is a geographer, geomorphologists and dendrochronologist whose current research interests include disentangling mixed geomorphic and non-geomorphic signals from tree rings, the impact of air pollution on tree growth, dendrochronological records of various geomorphic processes and hazards among all detecting and dating landslide activity from tree rings. At the University of Silesia he teaches Geomorphology, Dendrogeomorphology and Geomorphic hazards. He is an author of more than 150 papers published among others in Earth Surface Processes and Landforms, Geomorphology, Catena, Geochronometria.

New Inland Waterways in Heavily Invested Areas - Conditions and Hazards

Damian Absalon

University of Silesia in Katowice, Faculty of Earth Sciences, Będzińska 60, 41-200 Sosnowiec, Poland

Corresponding author: damian.absalon@us.edu.pl

Abstract. The planned Silesian Canal is an artificial water conduit connecting the main Polish rivers - the Oder and the Vistula - in the south of Poland. The analysis of conditions and hazards resulting from the creation of a new water conduit in a heavily invested area has been performed. Scarce local water resources and the need to feed the canal with a system of pumps supplying water from the Vistula and the Oder as well as other additional systems were pointed out. Attention has been paid to the course of the canal route through mining areas and through areas with documented hard coal resources. Collisions with environmentally valuable areas that are protected by law were also considered. It was found that due to the complicated conditions and numerous risks at the planning stage, it is necessary to select an optimal direction of the canal route that will have the least negative impact on the environment.

Keywords: inland waterways, environmental hazards, rivers, invested areas

INTRODUCTION

Inland waterways are a part of surface waters on which, due to hydrological conditions and existing water facilities, it is possible to transport people and goods. Establishment of an inland waterway takes place by adapting surface waters (rivers and lakes) for shipping purposes or less often by building a new artificial water conduit. The latter option is much more difficult and more expensive to build and operate.

The aim of the study is preliminary assessment of conditions and hazards resulting from the creation of a new water conduit in the area with a high degree of investment due to urbanization, industrialization and mining of minerals. The considerations were made on the example of the Silesian Canal, which would connect the Vistula and the Oder rivers in the south of Poland (fig.1).

The planned Silesian Canal is an artificial waterway approx. 90 km long, 45 m wide and 3.5 m deep. Connecting the Vistula and the Oder in the south of Poland in a significantly invested area brings about certain consequences and challenges. The development of the inland waterway sector, including the construction of the Silesian Canal, has been included in the Strategy for Responsible Development until 2020 (with a view until 2030). This document was adopted by way of a resolution of the Council of Ministers of the Republic of Poland on 14 February 2017 (Monitor Polski 2017, item 260) - a strategic document indicating the directions of Poland's development in the medium term.

The Water Framework Directive is of the greatest importance for the development of water transport. Other relevant documents include the Floods Directive and the RIS Directive as well as the Trans-European Transport Network TEN-T, the AGN Convention (European Agreement on Main Inland Waterways of International Importance) and the European Action Programme for Inland Navigation NAIADES. One of the ideas of the Water Framework Directive (WFD) is that water management should ensure sustainable development of areas near the rivers, reconciling, among others, various goals related to energy security, flood protection and inland transport.

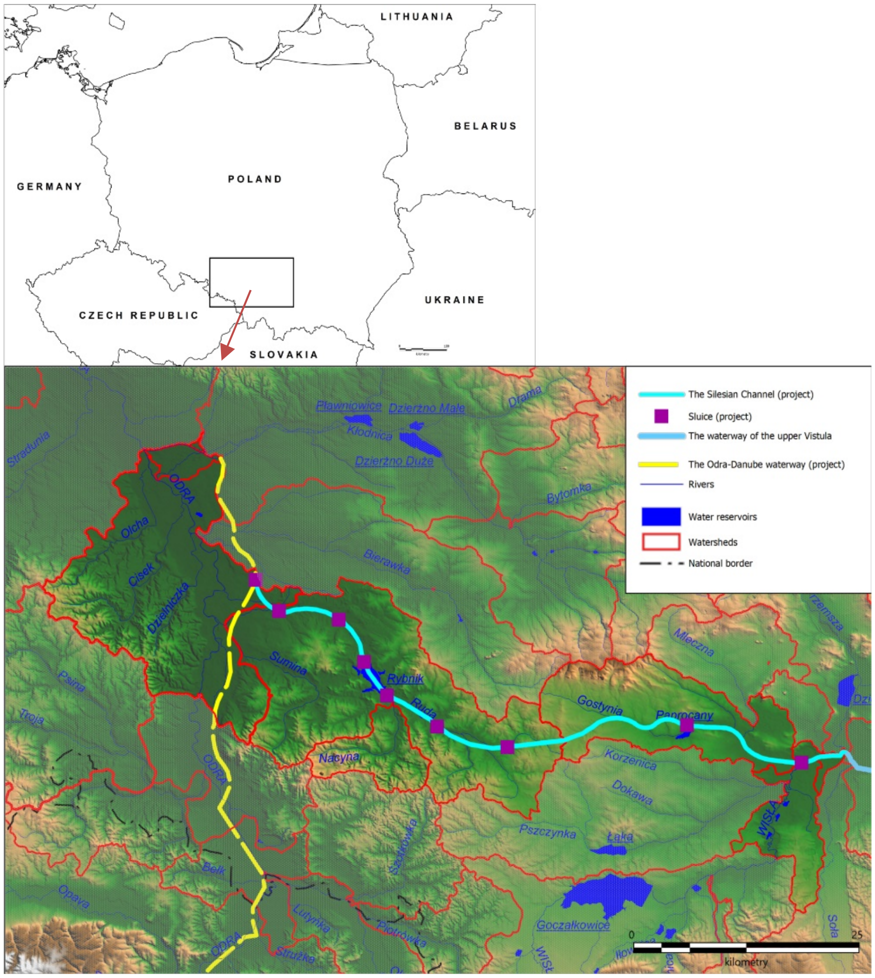

FIGURE 1. Location of study area

METHODS

The course of the most probable route of the Silesian Canal was analyzed. Catchments and bodies of water through which the canal would run were identified. The elevation analysis of the canal route based on the Digital Elevation Model (DEM) was also performed, as a result of which the elevations of higher water levels were determined in relation to the lower water levels of the canal on the Vistula and the Oder rivers. Another element analyzed was the collisions of the Silesian Canal's course with the mining areas of hard coal mines. Final analysis included the hazards resulting from the canal route's crossing the environmentally valuable areas that are protected by law.

RESULTS

The proposed direction of the Silesian Canal is a transport corridor connecting and integrating three important regions located in the south of Poland: Lesser Poland, Silesia and the Opolian Silesia, followed by Lower Silesia. The Silesian Canal, as a complement to the planned Oder-Elbe-Danube Canal, connects the region of Lesser Poland and Silesia with the European waterway system. The first 16 kilometers of the canal will encompass the existing Gliwice Canal to Solarnia near Kuźnia Raciborska, where it will separate itself from the Oder-Danube Canal. After branching off from the Oder-Danube Canal, the proper Silesian Canal will run along the valley of the Ruda River to the east and then to the southeast, all the way to Rybnik. The Silesian Canal will leave the Ruda valley at km 52.0, so that at a distance of about 4 km from Żory it will go through the first-order watershed between the Oder and the

Vistula basins. On the upper level of the canal is the planned Zgoń lock. The route of the Silesian Canal will continue along the valley of the Gostynia River, reaching Bieruń Stary, bypassing it from the south and heading north to enter the Vistula valley. The route of the canal will reach the Vistula and will connect with it about 0.5 km up from the mouth of Przemsza. The total length of the Silesian Canal will be over 90 km, including the existing Kędzierzyn Canal. 9-10 weirs with locks are planned on the canal.

The planned direction of the Silesian Canal is part of 10 surface water bodies (SWB), of which only 3 are natural bodies of water. The remaining SWBs are heavily modified water bodies. According to the Oder and the Vistula River Basin Water Management Plans (Journal of Laws of 2016, item 1967 and Journal of Laws of 2016, item 1911, respectively), all listed SWBs, except for one, are characterized by poor ecological status and are at risk of not achieving environmental objectives. Only the Zgoński Potok SWB (RW200017211829) is characterized by good SWB status and is not threatened by the risk of failure to achieve environmental objectives. The environmental goal of all SWBs is good ecological status/potential and good chemical status. Poor ecological status/potential is in many cases the result of many years of neglect in water management in areas with very strong pressures on deterioration of water quality [1, 2]. Despite many new solutions [3, 4] some of these SWBs are too superficially and too rarely monitored.

Local water resources in catchments are limited, and the condition of the canal's operation will be supplying water to the upper level with the use of a pump system. Feeding from both the Vistula River and from the Oder River should be considered. It is also possible to use water from existing water reservoirs (e.g. the "Łąka" reservoir) and to create a retention and dosing system using less saline waters from the dewatering of neighboring hard coal mines.

The analysis of the course of the route on the basis of the DEM showed that it is necessary to overcome up to 40 m level differences in relation to the bottom level on the Vistula and as much as 70 m in relation to the bottom level on the Oder (Fig. 2).

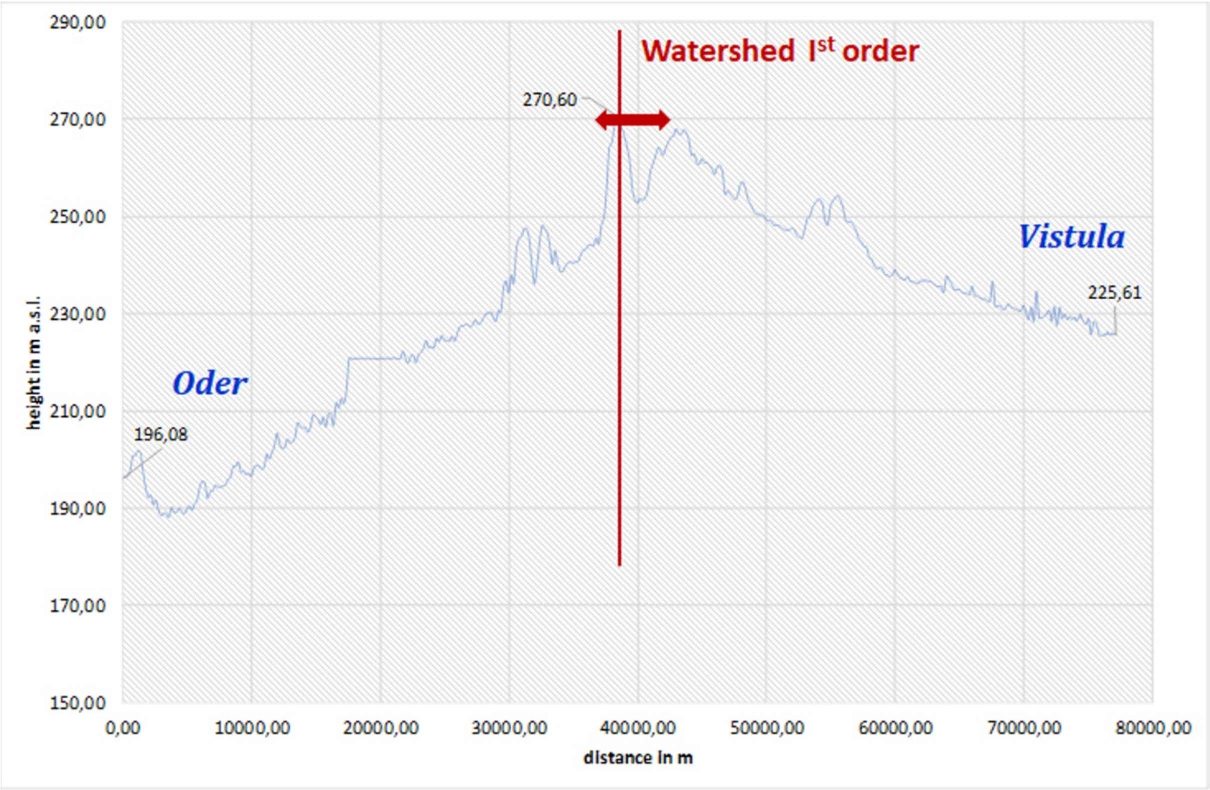

FIGURE 2. Elevation profile of the course of the Silesian Canal route

The planned route of the course of the Silesian Canal does not significantly interfere with the current mining activity of the coal mines of the Upper Silesian Coal Basin. However, on its planned route there are documented deposits of hard coal and applications for concession for its mining are registered, e.g. in the area of Orzesze.

Analysis of the canal location in relation to the existing forms of environmental protection showed the following collisions:
- the western part of the Silesian Canal crosses the valuable areas of the "Cistercian Landscape Compositions of Rudy Wielkie" landscape park;
- in the eastern part, the canal route borders with the Natura 2000 area "Ponds in Brzeszcze";
- in the immediate vicinity of the canal course there are 5 ecological sites: "Jedlin Ponds", "Paprocany", "Kencerz", "Meanders of the Ruda River" and "Oxbow lake near the monastery in Rudy".

In these cases, it is necessary to understand very well the conservation objectives pursued in all forms of environmental protection, so that the canal's infrastructure does not have a negative impact on them.

It should also be noted that the linear infrastructure divides the landscape and populations of terrestrial animals into more or less isolated subpopulations, threatening their protection caused by the so-called barrier effect (Bennett, 1991; Mader, 1984; Trombulak and Frisell, 2000; Forman et al., 2003)

CONCLUSIONS

The main hazard to the operation of the planned Silesian Canal are limited local water resources. In order to secure water needs, it will be necessary to create a supply system for the upper level of the canal with pumps that will draw water from intakes on the Vistula and the Oder rivers. The supplement may be resources from existing water reservoirs and a retention and dosing system using mine water.

Due to the proximity of active mining areas and documented hard coal deposits, work related to hard coal mining and issuing new concessions should be synchronized with activities aimed at canal construction.

The course of the route outside river beds will not affect the hydromorphological conditions of the Ruda and Gostynia rivers. However, collisions and bordering with protected areas require such route selection at the planning stage, which will have the least negative impact on the environment during the construction and operation of the canal.

REFERENCES

1. D. Absalon and M. Matysik, Changes in Water Quality and Runoff in the Upper Oder River Basin, Geomorphology, **92**, 106–118 (2007).
2. D. Absalon, Changes in Water Quality in the Upper Wisła (Vistula) River Basin. Proceedings of the Second International Conference on Environmental and Computer Science in Dubai (IEEE Computer Society Press, Los Alamitos California, Washington, Tokyo, 2009), 29–32.
3. D. Absalon, M. Ruman, M. Matysik, K. Kozioł and Ż. Polkowska, Innovative Solutions in Surface Water Quality Monitoring, APCBEE Procedia 10, 26–30 (2014)
4. M. Ruman, E. Olkowska, K. Kozioł, D. Absalon, M. Matysik and Ż. Polkowska, Reducing Monitoring Costs in Industrially Contaminated Rivers: Cluster and Regression Analysis Approach, Journal of Environmental Quality, 43, 2, 753-762 (2014).
5. A. Bennett, Roads, roadsides and wildlife conservation: a review, Nature conservation 2: the role of corridors, 99-117 (1991).
6. J. H. Mader, Animal habitat isolation by roads and agricultural fields, Biol Conserv, 29: 81-96, 81-96 (1984).
7. S. Trombulak & C. Frissell, Review of Ecological Effects of Roads on Terrestrial and Aquatic Communities, Conservation Biology, 14, 18–30 (2000).
8. R. Forman, D. Sperling, J. Bissonette, and A. Clevenger, Road Ecology: Science And Solutions, Bibliovault OAI Repository, the University of Chicago Press (2003).
9. M. Habel, Effects of flow regulation and river channelization on sandbar bird nesting availability at the Lower Vistula River, Ecological Questions, 29, 4, 43-53 (2018).

The Possibility of Using Personal Weather Station Networks to Verify and Evaluate Local Extreme Phenomena

Radosław Droździoł[1,2 a)] Damian Absalon[1,b] and Ewa Łupikasza[1,c]

[1]*University of Silesia in Katowice, Faculty of Earth Sciences, Będzińska 60, 41-200 Sosnowiec, Poland*
[2]*Institute of Meteorology and Water Management – National Research Institute, Poland*

[a)]Corresponding author: radoslaw.drozdziol@gmail.com
[b)]damian.absalon@us.edu.pl
[c)]ewa.lupikasza@us.edu.pl

Abstract. This paper aims at presenting the possibility of using meteorological data from the Network of Personal Weather Stations (PWS) to monitor extreme meteorological phenomena such as heavy and torrential rain. We analyzed the density of PWS within the Weather Underground network within Górnośląsko-Zagłębiowska Metropolis. After analyzing the maximum daily precipitation totals in 2018, two out of 34 stations were selected which recorded the highest rainfall on May 11, 2018. The rainfall data recorded by the stations was compared with the rainfall data from the stations belonging to the Institute of Meteorology and Water Management of the National Research Institute (IMGW-PIB) in order to check the correctness of data provided by personal weather stations. In addition, the analysis of synoptic situation, meteorological data from IMGW-PIB stations, satellite images and meteorological radar products were used to recognize the area of high rainfall occurrence and describe general weather conditions. We found that the development of convective phenomena in the research area began around noon. From noon towards the evening, the Cumulonimbus capillatus convective clouds developed strongly and caused local storms accompanied by heavy rainfall. This event was registered by, two personal stations and one station belonging to the IMGW-PIB. All three stations recorded similar rainfall totals, and the largest precipitation was recorded at the personal station in Będzin. It was found that data from the networks of personal stations may become an important source of information for the purpose of recording of local extreme meteorological phenomena.

Keywords: Personal Weather Station Network, Automatic Weather Station, meteorological data, meteorological hazard.

INTRODUCTION

In recent years, issues related to extreme meteorological phenomena have become the object of interest of both scientists and ordinary citizens. Thanks to the rapid development of new mass media and social media, in just a few seconds, you can learn about the occurrence of a new (dangerous) meteorological phenomenon around the world. One of such forms of communication is the networks of personal weather stations, which recently have become popular source of information about phenomena occurring in the atmosphere, in particular among amateur meteorologists. In the UK alone, observations and measurements are made by 1700 personal weather stations [1]. For comparison, the English Met Office has 250 professional weather stations in the same area [4]. Depending on the type, personal weather stations make measurements of the following parameters: air temperature, humidity, pressure, wind speed and direction, and atmospheric precipitation. Measurements from the stations (usually of 5 minutes time resolution), are sent to various networks of both commercial and national meteorological services.

The aim of the paper is to check the possibility of using a personal network of weather stations to detect and research heavy precipitation events. Precipitation data from such stations located in the central part of Silesia province were compared with the data from the professional station network of the Institute of Meteorology and Water Management of the National Research Institute (IMGW-PIB). We present an example of the implementing of

data sources from non-national institutions providing meteorological and hydrological services. This is particularly important in the context of the increased frequency of hazards resulting from the occurrence of extreme meteorological phenomena.

MATERIALS AND METHODS

In the initial phase of research the basic problem was the selection of one personal network of weather stations (PWS network). From among three networks, such as: Weather Underground Personal Weather Station Network, Automatisches Wetterkarten System (AWEKAS), Citizen Weather Observer Program (CWOP), a network of personal stations has been selected that has the largest number of registered active users, i.e. Weather Underground (WU). The stations were counted and plotted on a map showing the area of research (Figure 1). Meteorological stations belonging to IMGW-PIB are also included into the map. This allowed for a comparison of the density of personal stations in comparison to IMGW-PIB stations.

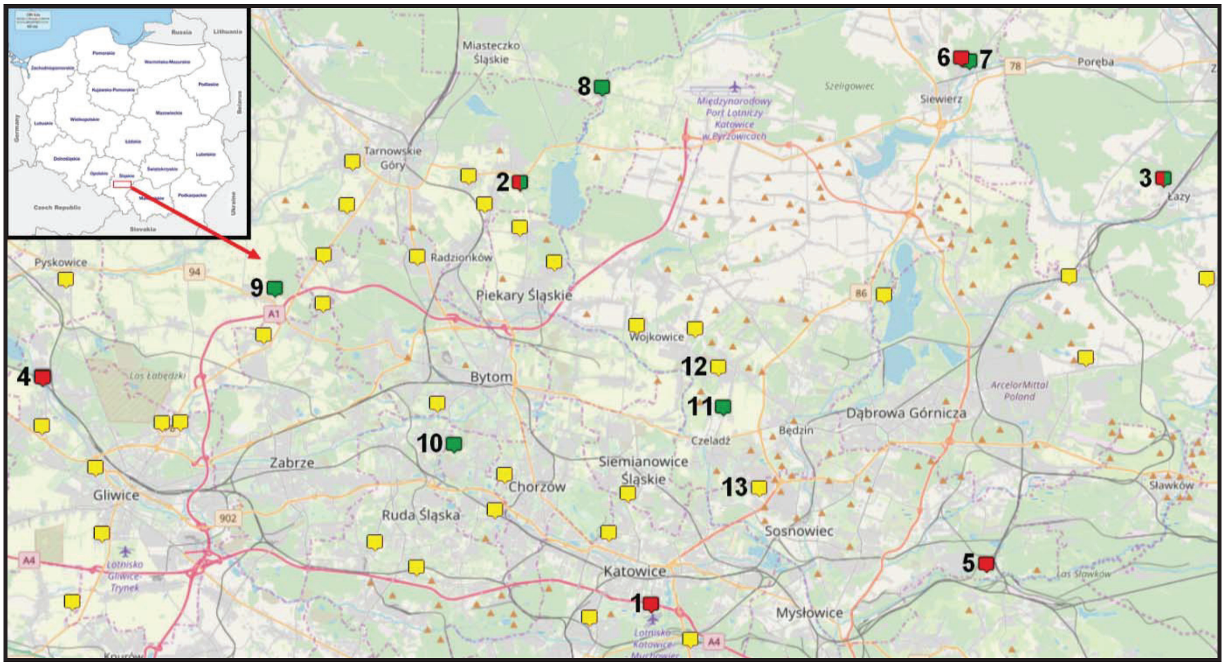

FIGURE 1. Deployment of weather stations in the research area (central part of the Silesia Province). Red points – IMGW-PIB stations with an automatic rain gauge, green points – IMGW-PIB stations with a manual rain gauge, red and green points – IMGW-PIB stations with an automatic and manual rain gauge, yellow points – PWS. Source: Own elaboration on the basis of OpenStreetMap.

Next, the data from 2018 regarding the daily precipitation totals from all 34 personal stations belonging to the WU network were reviewed and two stations were selected with the precipitation significantly higher compared to other stations. This precipitation event occurred on May 11, 2018 and daily total amounted 31 mm in Będzin and 23.6 mm in Sosnowiec. Other personal stations registered precipitation varying between 0.9 and 13.2 mm. The next step was to collect the rainfall data from IMGW-PIB station for that day from 6 stations equipped with the Met One Instruments rain gauge (automatic rain gauge) and from 7 stations with the Hellmann rain gauge (manual rain gauge). Data from automatic rain gauges were calculated, ordered and compiled in the form of a linear graph showing the accumulated precipitation totals within one day. The analysis of the synoptic situation, measurement data and the products of meteorological radars for the region of Będzin and Sosnowiec was also made. In connection with the conducted research, questions arose related to the accuracy of measurements, their regularity and homogeneity in terms of methodology and representativeness for a given area that will be analysed in our future research.

RESULTS

The research area is 1920 km^2. The density of personal stations in this area is 1.7 stations per 100 km^2, and the density of the IMGW-PIB automatic stations is almost 5.5 times smaller and amounts to 0.31 stations per 100 km^2. The personal weather station in Będzin (Fig. 1 - Point 12) is located 12.3 km away from the nearest IMGW-PIB automatic weather station in Katowice (Fig. 1 - Point 1). The distance between the personal station in Sosnowiec (Point 13 in Fig. 1) and the IMGW-PIB station in Katowice is 7.9 km. The distance to the IMGW-PIB weather station in Czeladź (Point 11 in Fig. 1) equipped with the manual Hellmann rain gauge is 2.0 km for the station in Będzin and 4.2 km for the station in Sosnowiec. Both personal stations are separated by a distance of 6.2 km. On May 11, 2018 the largest daily rainfall was recorded on two personal weather stations (Table 1).

Considering MGW-PIB automatic stations, the highest daily precipitation total was recorded in Katowice (Table 1). The precipitation in Będzin was 17.8 mm higher than the rainfall in Katowice, while the rainfall in Sosnowiec was 10.4 mm higher than in Katowice.

TABLE 1. Daily precipitation totals on May 11, 2018 (automatic stations)

Weather station	Type of rain gauge	Precipitation (total) mm
Katowice (Point 1)	Met One Instruments	13.2
Świerklaniec (Point 2)	Met One Instruments	8.5
Łazy (Point 3)	Met One Instruments	10.3
Łabędy (Point 4)	Met One Instruments	0.9
Maczki (Point 5)	Met One Instruments	5.5
Piwoń (Point 6)	Met One Instruments	2.5
PWS Będzin (Point 12)	Davis Vantage Vue	31.0
PWS Sosnowiec (Point 13)	Netatmo Weather Station	23.6

Of the IMGW-PIB stations equipped with the Hellmann manual rain gauge, the biggest daily rainfall occurred in Czeladź (Table 2). It was smaller than the rainfall registered by the personal station in Będzin by 5.3 mm and larger than the rainfall recorded by the personal station in Sosnowiec by 2.1 mm.

TABLE 2. Daily precipitation totals on May 11, 2018. For Hellmann rain gauge daily precipitation total concerns the so-called 1-day precipitation i.e. the period between 6.00 UTC of one day until 6.00 UTC of the next day.

Weather station	Type of rain gauge	Precipitation (total) mm
Świerklaniec (Point 2)	Hellmann	8.8
Łazy (Point 3)	Hellmann	10.2
Piwoń (Point 7)	Hellmann	2.9
Brynica (Point 8)	Hellmann	13.6
Wieszowa (Point 9)	Hellmann	0.8
Lipiny (Point 10)	Hellmann	17.7
Czeladź (Point 11)	Hellmann	25.7

In Będzin precipitation began at 17.00 and from 17.00 to 18.00 its intensity amounted to 27.4 mm/h (Fig. 2a). In Sosnowiec the most intense rainfall reaching 20.8 mm/h occurred from 16.30 to 17.30 (Fig. 2a). In comparison, the highest intensity of rainfall at the Katowice IMGW-PIB automatic station amounted to 10.8 mm/h (from 15.30 to 16.30).

Analysis of radar images indicated that the most intense phase of precipitation occurred in the region of Sosnowiec, Czeladź and Będzin (Fig. 2b). Heavy rainfall occurred from 16.30 to 17.30 with the maximum between 17.00 and 17.20.

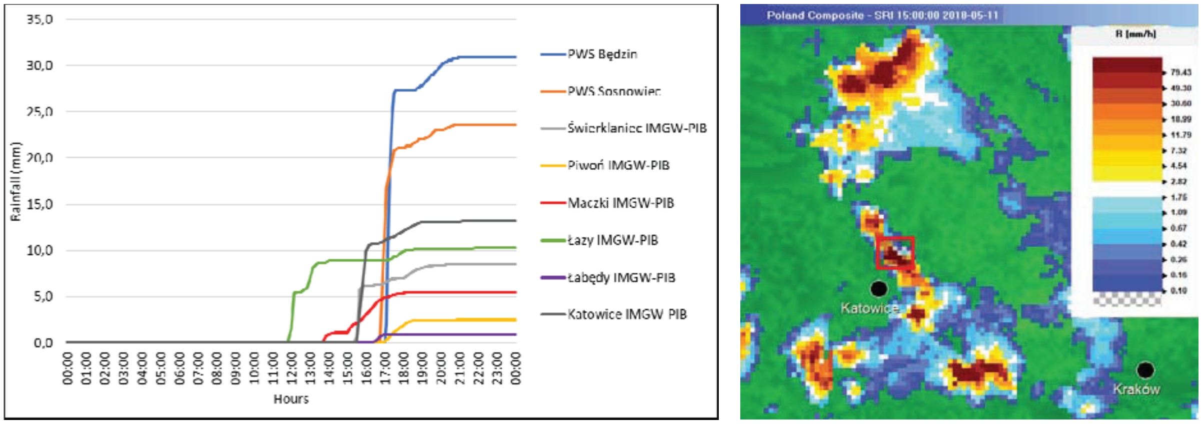

(a) (b)

FIGURE 2. Cumulated rainfall amount recorded by automatic stations (a). Intensity of rainfall on May 11, 2018 at 17.00 DST (15.00 UTC), according to Ramża meteorological radar DPSRI product. Source of graphics (b): DPSRI product of Ramża meteorological radar (IMGW-PIB).

DISCUSSION

Initial analysis of the number and distribution of personal weather stations has shown that data from such stations can become an important source of information to identify locally occurring extreme meteorological phenomena, as the heavy precipitation event discussed as an example. The density of the personal weather station network is almost 5.5 times higher than the density of the IMGW-PIB station network. On May 11, 2018, the research area was under the influence of low pressure system from the North Atlantic and Scandinavia. There was a cold front connected with the low pressure system pushing warm and humid air which caused a convection. In and before the weather front, numerous storm cells were formed with intense rainfall. The largest precipitation totals were registered by three stations. One, in Czeladź, belonging to the Institute of Meteorology and Water Management of the National Research Institute and two personal stations in Będzin and Sosnowiec. The IMGW-PIB station, however, is a station equipped only with a manual rain gauge, from which the observer reads once a day at 6.00 on the next day, whereas the personal stations in Będzin and Sosnowiec operate continuously online with 5 min time resolution. Data from these stations could be monitored on a current basis. Analysis of radar images as well as measurements and observations from the IMGW-PIB station in Czeladź confirmed the heavy rainfall occurrence. According to the Chomicz scale [2.3], the rainfall recorded by the personal weather station in Będzin can be classified as A_4, and the rainfall recorded by the station in Sosnowiec as A_3. Rains categorized as A_3 on Chomicz scale are considered as a potential cause of flood damage.

The results of this study become a stimulus for further research into the use of data from the network of personal weather stations as complementing for IMGW-PIB network.

REFERENCES

1. S. Bell, D. Cornford and L. Bastin, “How good are citizen weather stations? Addressing a biased opinion,” in *Weather*, Vol. 70, No. 3. pp. 75-84 (2015). https://rmets.onlinelibrary.wiley.com/doi/epdf/10.1002/wea.2316
2. K. Chomicz, “Ulewy i deszcze nawalne w Polsce,” in *Wiadomości Służby Hydrologicznej i Meteorologicznej*, t. II, z. 4 (1951).
3. K. Chomicz, „Normy opadowe dla potrzeb kanalizacji miast,” in *Gospodarka Wodna*, r. 13, nr 10 (1953).
4. A. Green, “From Observations to Forecasts - Part 7. A new meteorological monitoring system for the United Kingdom’s Met Office,” in *Weather*, Vol. 65, No. 10. pp. 272-277 (2010). https://rmets.onlinelibrary.wiley.com/doi/epdf/10.1002/wea.649

The Course of Hydrological Drought in the River Drawa Catchment (Northern Poland) as Characterized by the Standardized Runoff Index

Katarzyna Kubiak-Wójcicka

Nicolaus Copernicus University, Faculty of Earth Sciences, Department of Hydrology and Water Management, Lwowska 1, 87-100 Toruń, Poland,

Corresponding author: kubiak@umk.pl

Abstract. The paper presents the course of hydrological droughts in the Drawa River catchment in the period of 1981–2010. The study utilizes daily values of the Drawa's discharge recorded in the Drawiny hydrological station and and daily values precipitation in two meteorological stations (Wierzchowo and Krzyż). Hydrological drought characteristics have been determined on the basis of the Standardized Runoff Index (SRI), which is a common hydrological drought index. SRI values were calculated on the basis of average monthly discharges that were accumulated in 1-, 3-, 6-, 9-, and 12-month periods. The most acute hydrological droughts in the analysed multi-annual period occurred in the years 2003–2007.

INTRODUCTION

Drought is a natural phenomenon associated with a long-term water deficit. There is no universal definition of drought, due to its complex character. The following kinds of drought can be distinguished: meteorological, hydrological, agricultural and socio-economic [1]. Among these classifications, the assessment of hydrological drought is of great importance in the perspective of water management. This paper aims at identifying hydrological drought and assessing its intensity for the River Drawa (northern Poland) using the SRI index. The River Drawa's length reaches 192.08 km, and its catchment covers 3290.93 km^2 [2]. The Drawa catchment has a sizeable percentage of forests (71.06%) and lakes (4.52%). Arable area takes up merely 15.54% of the catchment area and is located primarily in its southern part. The Drawa catchment is located between 220 m above sea level in its northern part, and 30 m above sea level to the south. It is characterised by extremely diversified late glacial landforms with numerous ground depressions, lake basins and predominant permeable formations. Average annual precipitation in the years 1981–2010 was 684.5 mm in Wierzchowo (the northern part of the catchment) and 563 mm in Krzyż (the southern part of the catchment). The highest annual precipitation in Krzyż was recorded in 2007 (750.4 mm) and the lowest - in 1982 (336.8 mm), while in Wierzchowo it was 882 mm in 2010 and 376.1 mm in 1982, respectively. In the period of 1981–2010, the mean annual discharge of the Drawa in the Drawiny station was 21.51 $m^3 \cdot s^{-1}$, while outflow reached 6.53 $dm^3 \cdot s^{-1} \cdot km^{-2}$ and was higher than the Polish average (5.4 $dm^3 \cdot s^{-1} \cdot km^{-2}$) [3,4]. The highest discharge value of the Drawa in the analysed period was 51 $m^3 \cdot s^{-1}$ and occurred on 18 March 1981. The lowest discharge was 7.91 $m^3 \cdot s^{-1}$ and was recorded on 21 September 2004 (Fig. 1). The meteorological and hydrological data come from the Institute of Meteorology and Water Management – National Institute Research.

METHODS

The Standardized Runoff Index – SRI was employed to determine hydrological drought; it is calculated following the same procedure as in the case of SPI [5,6,7]. The two-parameter logarithmic function was adopted as the normalising function [8]. In order to calculate SRI values on different time scales (n months), it is necessary to obtain cumulative sums of runoff for each month and n months. A total of five different time series were analysed: 1-, 3-, 6-, 9- and 12-month. SRI values determine the deviation from the median expressed in standard deviation units calculated by the formula (1):

$$SRI = \frac{f(X) - \mu}{\delta} \quad (1)$$

where: *SRI* – Standardized Runoff Index, *f(X)* – transformed runoff sum, μ – mean value of normalised *X*
δ – standard deviation of *X*

The obtained SRI values formed the basis for classifying drought intensity as indicated in table 1. Hydrological drought occurs when the SRI value is lower than -1.0, and wet periods when it exceeds 1.0. SRI values between -1.0 and 1.0 were described as normal. After [9] it was assumed that in a drought spell the value of the SRI index is negative and, at the same time, in at least one month it is less than or equal to -1.0. The drought is broken when the index value rises above zero [10].

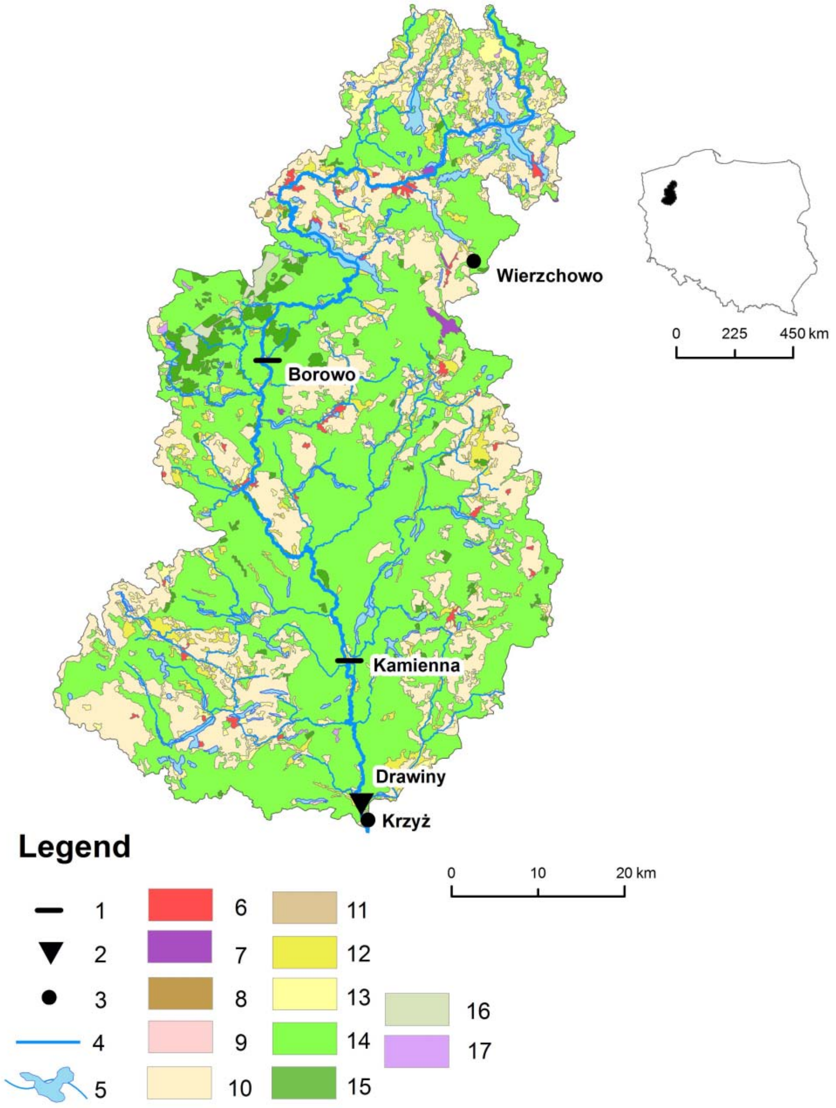

FIGURE 1. Drawa catchment (Corine Land Cover)

Legend: 1- Hydropower station, 2- Hydrological station, 3- Meteorological station, 4- Drawa River, 5- Rivers and lakes, 6- Urban fabric, 7- Industrial, commercial and transport units, 8- Mine, dump and constructions cites, 9-Artifical, non-agricultural vegetated areas, 10- Arable land, 11- Permanent crops, 11- Pastures, 12- Heterogeneous agricultural areas, 13- Forests, 14- Scrub and/or herbaceous vegetation associations, 15- Open spaces with the little or no vegetation, 16- Inland wetlands

RESULTS

In the 1981–2010 period, annual precipitation shows a statistically significant rising trend, while mean monthly discharge is on a downward curve, albeit statistically insignificant. The SRI index was employed to indicate hydrological droughts. It was determined for five different accumulation periods: 1, 3, 6, 9 and 12 months (Tab. 1). The values of the SRI index in individual months of the analysed 1981–2010 period for all accumulation periods ranged between 2.61 and -2.73. In total, wet periods (SRI > 1.0) occurred for 50 to 57 months, which constituted 15–17% of the analysed period. Similarly, dry periods (SRI > -1.0) occurred for between 50 and 55 months, which constituted 14–15% of the period. The extreme values of the SRI index depended on the length of the accumulation period. SRI-1 ranged between 2.34 (April 1988) and -2.73 (September 2004) and it was the largest span among the analysed SRI indices. In longer accumulation periods, the range of values would drop together with increasing length of the cumulation period. Thus, for SRI-3 it stretched from 2.61 (January 1982) to -2.19 (July 2003), for SRI-6 – from 2.39 (February 1982) to -2.17 (July 2006) and for SRI-9 – from 2.23 (March 1981) to -2.29 (November 2006). In the case of SRI-12, the span was somewhat greater and ranged between 2.45 (January 1982) and -2.26 (December 2006). In accordance with the adopted classification most (247–254) of the analysed 360 months populated the -1.0 to 1.0 range, which constituted between 68.6% and 70.6% of the total number of months in the period. In the analysed years, wet periods (SRI > 1.0) last longer than dry periods (SRI < -1.0). Moderately dry spells (-1.5 to -1.0) occurred for between 26 and 35 months (7.2%–9.7% of the whole analysed period). There were fewer severely dry months (-2.0 to -1.5), i.e. between 11 and 19. Extremely dry periods (SRI < -2.0) lasted the shortest – from five to nine months. In comparison with extremely wet periods (SRI above 2.0) which lasted between 8 and 18 months, extreme drought occurred for half as much time.ii) The duration of moderately dry and moderately wet periods were much alike.iii)

TABLE 1. Hydrological drought parameters based on the SRI index in the years 1981–2010 in different timescales

Parameters	SRI-1	SRI-3	SRI-6	SRI-9	SRI-12
N	14	8	5	3	3
D	140	128	126	102	122
T	39	36	35	28	34
maxD	19 (VII2005-I2007)	49 (II2003-II2007)	52 (III2003-VI2007)	54 (III2003-VIII2007)	57 (IV2003-XII2007)
minD	2 (VII-VIII 1995)	4 (I1985-IV1985)	10 (I 2001-X2001)	13 (I 2001-I 2002)	12 (II 1996-I1997)
DM	-125.43	-120.47	-115.98	-105.55	-115.03
I	-0.90	-0.95	-0.92	-1.03	-0.94

Explanations: N – number of droughts in the analyses multi-annual period, D – total drought duration in months, T – percentage share of drought months in the analysed multi-annual period, maxD and minD – duration of the longest and shortest drought, DM – drought magnitude expressed by the sum of SRI values in all drought periods, and drought intensity (I) which is the quotient of drought magnitude and its duration

The highest number of hydrological droughts (14) was recorded for SRI-1; they also lasted the longest, i.e. 140 months, which constituted 39% of the analysed period. Drought magnitude in this shortest discharge accumulation period was higher than in any other timescale, while its intensity was the lowest. The longest drought in the case of SRI-1 occurred between July 2005 and January 2007 (19 months). In the longest accumulation period (SRI-12) this drought lasted for 57 months, began as early as in April 2003 and continued until December 2007. This drought occurred not only on the territory of Poland [8] but also in the whole of central Europe, and was related to scarce precipitation and a heatwave in the year 2003 [9]. It should be noted that the number of droughts and their total duration diminished as accumulation periods grew. Interestingly, as the length of accumulation periods increased, so did the maximum and minimum duration of droughts.

In the case of SRI-1 and SRI-3, extreme hydrological droughts (below -2.0) lasted between one and two months and were marked by high intensity and increased frequency. Extreme droughts which occurred in January 1985 and July 1994 were not indicated already in the 6-month accumulation period. In longer accumulation periods (SRI-6, 9 and 12) such droughts lasted longer, i.e. from two to six months, and were of lower intensity. After the year 2001, hydrological droughts tended to occur more often and were more strenuous for the economy. The years 2003–2007 were a particularly severe time, witnessing the longest and most intensive droughts in the whole study period, regardless of the adopted accumulation period.

SUMMARY

The paper presents the course of hydrological droughts using the SRI index. This requires the author to use accumulated values of mean monthly discharge in different accumulation periods, i.e. 1, 3, 6, 9 and 12 months. The adopted accumulation periods are suggested primarily for small and medium-sized catchments [5,12]. In the case of large river basins, it is recommended to adopt longer discharge accumulation periods, e.g., 12- or 24-month [10,13]. In the analysed 1981–2010 period, the study has identified between 14 hydrological droughts in the shortest accumulation period (1 month) and 3 hydrological droughts in the longest accumulation periods, i.e. 9 and 12 months. In the case of 1- and 3-month accumulation periods, iv)droughts are intensive and short (between one and two months). In longer accumulation periods, hydrological droughts were characterised by low intensity and longer duration (3–6 months), which is especially palpable in the case of SRI-6 and SRI-9. The most acute hydrological droughts in the analysed multi-annual period occurred in the years 2003–2007. Due to the prevalence of permeable formations making up the Drawa catchment and extensive woodland, it seems justified to analyse the relations between meteorological, hydrological and agricultural droughts.v) Once determined, the correlations of time lags between the abovementioned droughts may prove useful in the identification of droughts in that area. The applied index method allows to determine and apply criteria for assessing the duration and intensity of a drought and its comparison with other types of drought.

REFERENCES

1. H. Tabari, J. Nikbakht and P. Hosseinzadeh Talaee, Iran Based on Streamflow Drought Index (SDI). Water Resources Management 27: 137-151 (2013).
2. Atlas podziału hydrograficznego Polski, IMGW, Warszawa (2005).
3. K. Kubiak-Wójcicka, Long-term variability of runoff of Vistula River in 1951-2015. *“Air and Water – Components of the Environment” Conference Proceedings, Clun-Napoca,* Romania, 109-120 (2019). DOI: 10.24193/AWC2019_11
4. K. Kubiak-Wójcicka and B. Bąk, Monitoring of meteorological and hydrological droughts in the Vistula basin (Poland). *Enviromental Monitoring and Assessment,* 190, 11,1-16 (2018). DOI: 10.1007/s10661-018-7058-8.
5. S. Shukla and A. W. Wood, Use of a standardized runoff index for characterizing hydrologic drought. Geophysical Research Letters 35 (L02405) (2008). DOI:10.1029/2007GL032487.
6. I. Nalbantis and G. Tsakiris, Assessment of Hydrological Drought Revisited. Water Resource Management 23: 881-897 (2009). DOI:10.1007/s11269-008-9305-1.
7. L. Gao and Y. Zhang Y., Spatio-temporal variation of hydrological drought under climate change during the period 1960–2013 in the Hexi Corridor, China, J Arid Land, 8(2): 157–171 (2016). DOI: 10.1007/s40333-015-0022-3.
8. B. Bąk and K. Kubiak-Wójcicka, Assesment of meteorological and hydrological drought in Torun (central Poland town) in 1971-2010 based on standardized indicators, Water resources and wetlands. Conference Proceedings, 8-10 September 2016 Tulcea (Romania), ed. P. Gastescu, P. Bretcan, 164-170 (2016).
9. T.B. McKee, N.J. Doesken and J. Kleist J., The relationship of drought frequency and duration to time scales. Proc. of the 8th Conference of Applied Climatology, 17-22 January 1993, Anaheim, California, 179-184 (1993).
10. B. Bąk and K. Kubiak-Wójcicka, Impact of meteorological drought on hydrological drought in Toruń (central Poland) in the period of 1971–2015, Journal of Water and Land Development, 32, 3-12 (2017). DOI: 10.1515/jwld-2017-0001.
11. M. Trnka, J. Balek, P. Štěpánek, P. Zahradníček, M. Možný, J. Eitzinger, Z. Žalud, H. Formayer, M. Turňa, P. Nejedlík, D. Semerádová, P. Hlavinka and R. Brázdil, Drought trends over part of Central Europe between 1961 and 2014. Climate Research, 70, 143-160 (2016). DOI: 10.3354/cr01420.
12. D. Tigkas, H. Vangelis and G. Tsakiris, Drought and climatic change impact on streamflow in small watersheds. Science of the Total Environment 440, 33– 41 (2012). http://dx.doi.org/10.1016/j.scitotenv.2012.08.035.
13. E. Rimkus, E. Stonevičius, V. Korneev, J. Kažys, G. Valiuškevičius and A. Pakhomau, Dynamics of meteorological and hydrological droughts in the Neman river basin. Environmental Research Letters 8: 045014 (10pp) (2013). DOI:10.1088/1748-9326/8/4/045014.

Application of Dendrochronology and Electrical Resistivity Tomography for Studies on Landslide Activity (Southern Poland)

Katarzyna Łuszczyńska[1, a)]

[1]*University of Silesia in Katowice, Faculty of Earth Sciences, Bedzinska 60, 41-200 Sosnowiec, Poland*

[a)]Corresponding author: katarzyna_luszczynska@o2.pl

Abstract. Landslides are a common geodynamic hazard in mountainous regions worldwide, including the Polish part of the Carpathian Mts. Intensive development in this area increases the scale of landslide risk, e.g. landslides pose a threat to infrastructure, cause significant financial losses and even fatalities. Thus detecting landslide activity, hazards and risks became important issue for spatial planning in the area. I applied dendrochronological method and electrical resistivity tomography for estimate landslide activity and identify the geological structure in Kamesznica landslide, in the Beskid Śląski Mts (Western Carpathians, southern Poland). Eccentricity index values were applied to date past landslide events. Dendrochronological results allowed to determine the mean frequency of landsliding at each sampling tree. Obtained results of the dendrochronological study show that the most dynamic landsliding occurred in: 2013-2017, 2005-2006, 2002, 1988-1989 and 1993. Between the episodes of landsliding there were periods of relative stability. The results of measurements using the ERT method allowed to distinguish high and low-resistivity packets and also estimate surface of rupture. Application of dendrochronology and electrical resistivity tomography (ERT) is an attractive solution for studies on landslide activity and can be used in the local spatial planning system.

INTRODUCTION

Landsliding, which is common in the Flysch Carpathians, is a significant problem for local communities [15], [18], 19], [21]. It threatens the infrastructure, including, among others, residential buildings, roads, railway, energy, telecommunications and water supply lines. That is why monitoring of landslides, in particular its activity, is so important. Mapping and displacement monitoring of unstable slopes is crucial for the hazards prevention and assessment [6], [8], [11], [20].

The methodology used to study landslides has often been discussed in the scientific literature both in the world and in Poland [2], [3], [10], [14], [15]. In this work, dendrochronology and the electrical resistivity tomography (ERT) method were used. Dendrochronology allows analysing the activity of landslides in the past, within the last decades and even centuries [7], [9], [17]. Each tree growing on a landslide is a separate sensor of the ground movement, which enables the analysis of the temporal and spatial variability of the course of landslides [4], [20]. Geophysical surveys have also been used in the diagnosis of landslides for years. This method will allow for accurate identification of the structure of colluvium and their substrate [5].

The objective of this study was to analyse the past activity of a landslide in Kamesznica, in Western Carpathians, in the Beskid Śląski Mts (southern Poland) and to investigate the application of resistivity imaging in identifying the geological structure of this landslide.

STUDY AREA

Study area is located in the Beskid Śląski Mts, Western Carpathians, in the southern part of Poland. It is located within the Lower Istebna layers. They belong to the Silesian nappe, a fragment originating from Cretaceous. In the

lithostratigraphic profile for the Beskid Śląski Mts, the Istebna layers are formed mainly as coarse-grained conglomerates, fine-grained conglomerates and sandstones as well as clay gravels [24]. Study landslide is small (270 m long and 110 m wide) and the main scarp was 25 to 30 m height.

Study landslide is covered with forest and belongs to the lower montane vegetation belt, where deciduous beech forests with common beech and Silver fir occur. However, at present the study area is covered with planted, monoculture forests with Norway spruce (*Picea abies* Karst.).

METHODS OF THE STUDY

40 Norway spruce specimens were collected for dendrochronological dating of landsliding on landslide in Kamesznica. Using Pressler borer I took two cores from each tree: one from the upslope side of each stem and the second from the downslope side. Tree-ring widths in samples were measured (with 0.01 mm accuracy) and recalculated into eccentricity index values. Landslide events were dated using reference thresholds (avg. levels of eccentricity typical for a nearby stable slope) [method after 16]. The obtained results of the dendrochronological analyses allowed to determine the mean frequency of landsliding at each sampling tree, it means average number of events occurring per decade.

As part of the work carried out, an ERT profile was also prepared. A geoelectric profile in the area of the landslide was carried with the dipole-dipole arrays by using Terrameter LS. The length of the dipole-dipole profile was 300 m and the electrode spacing was 5 m. The collected data were processed using the RES2DINV software, which automatically generates a 2D resistivity inversion section representing variations in electrical properties of the subsurface features.

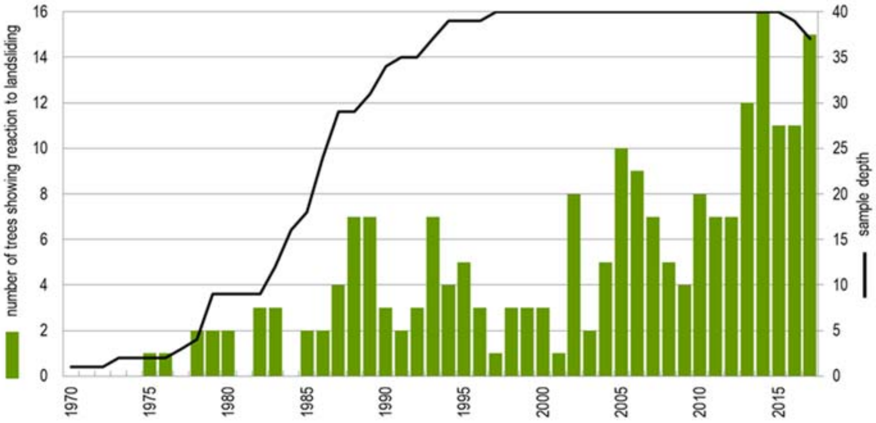

FIGURE 1. Dendrochronological record of landslide activity in Kamesznica landslide

RESULTS AND DISCUSSION

Tree-ring record of landsliding on the studied landslide dates back to 1970. For the period under study I have dated a total of 211 signs of eccentricity indicating landslide movement. Dendrochronological analysis shows that the most dynamic landsliding occurred in: 2013-2017, 2005-2006, 2002, 1988-1989 and 1993. Between the episodes of landsliding there were periods of relative stability, e.g. 1990-1992 or 1996-2001 (Fig. 1). The results obtained suggest that the studied landslide was almost constantly active (Fig. 1).

Spatial activity is varied, it ranges from 0 to 3 events/10 years (Fig. 2). Upper and middle part of landslide body seem to be the most active. In these parts I recorded medium and high level of activity (1 to 3 events/10 years). In down site of the landslide body I recorded mostly low level of activity and in some parts medium activity (Fig. 2).

The geoelectric profile in Kamesznica was conducted for a length of 300 m (Fig. 3). The results of measurements using the ERT method allowed to distinguish high-resistivity packets identified as relatively dry and subjected to erosion, sandstones "in situ" and low-resistivity layers identified as clays, mudstones or sandstones. Locally, there are very high-resistivity lense with resistivity up to 3641 Ωm (Fig. 3). It occurs in the area behind the landslide scarp between 20 and 30 m of the profile's length. Below there is a low resistivity layer which resistivity ranges from 63.5 to 245 Ωm. The colluvium will most probably be a landslide breccia. Symbol 'A" indicates a high-resistivity anomaly

(Fig. 3) that is an artifact of inversion process carried out in the RES2DINV software and could not be eliminated during processing.

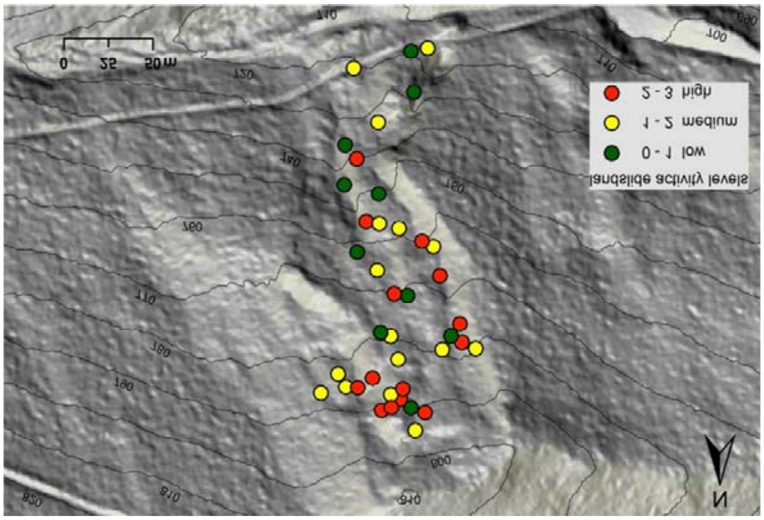

FIGURE 2. Spatial variability of tree-ring record of landsliding in Kamesznica landslide expressed as the mean frequency of landsliding at each sampling tree

The use of dendrochronology for studies on landslide allowed to determine the temporary activity over the last 40 years, but also to determine the spatial variability of landsliding in the study area. Geodethic methods, inclinometers, remote sensing techniques or aerial imagery cannot give us annual resolution data and 40-year long data sets. These methods only provide partial information on landslide history, namely only data after monitoring has started [1], [13].

In the case of the ERT method, accurate qualitative correlation of the resistance layers with the lithological layers in study area was not possible due to the lack of a direct link in the form of boreholes. Due to the applied minimum distance between electrodes of 5 m, the assessment of the thickness of the surface layers cannot be considered as accurate. Despite the above-mentioned disadvantages ERT method is very effective in the monitoring of landslide activity and determination of stable conditions. The advantages of ERT method are relatively easy application in terrain and possibility of repeated measurement. In the ERT method application, right interpretation of results depends on the knowledge of geological structure in the landslide area. A positive result requires relating the results to other, mainly geomorphologic and geologic, information [12]. In study area, literature data and observations made in the area were used for this purpose.

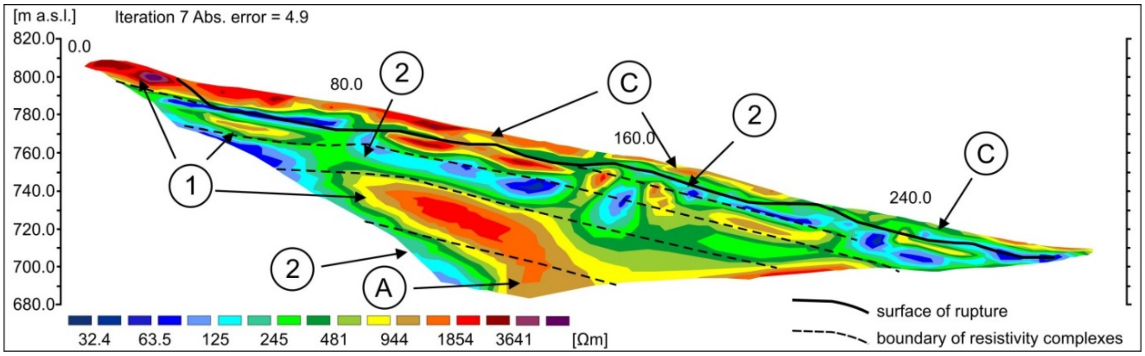

FIGURE 3. Resistivity model of ERT profile carried out on the Kamesznica landslide with the interpretation. Legend: 1 – high-resistivity packets; 2 – low-resistivity packets; C – colluvium; A – an artifact of inversion process.

CONCLUSIONS

Dendrochronolgy has been proved useful in determining temporal and spatial variability of landsliding. Results obtained for the landslide under study indicate mostly medium and high level of activity. Most trees have registered landsliding in the last few years. Also the electrical resistivity tomography proved to be useful for quick and preliminary identification of the landslide structure as well as its flysch substrate.

The combination of the dendrochronological method and the electrical resistivity tomography allowed to obtain comprehensive information on the landslides investigated (including the range, internal landsliding relief, spatio-temporal activity and the structure of the colluvium). These methods are an attractive tool to monitoring landslide activity and recognize the geological structure of the landslides, which can be helpful in early warning system and can be used in local spatial planning.

ACKNOWLEDGMENTS

This study was performed within the scope of the research project no.2017/25/N/ST10/01716 funded by the National Science Centre, Poland (NCN).

REFERENCES

1. M. Béjar-Pizarro, D. Notti,R.M. Mateos, P. Ezquerro, G. Centolanza, G. Herrera, G. Bru, M. Sanabria, L. Solari, J. Duro, J. Fernández, Remote Sensing **9**, 876 (2017).
2. N. Casagli, F. Catani, C. Del Ventisette, G. Luzi, Landslides **7**, 291–301 (2010).
3. L. Cascini, M. Ciurleo, S. Di Nocera, G. Gullà, Geomorphology **241,** 371–381 (2015).
4. A. Demoulin and C.J. Chung, Geomorphology **89**, 391-404 (2007).
5. D. Jongmans, P. Hemroulle, F. Renardy, Y. Vanbrand, Eur. J. Environ. Eng. Geophys. **8**, 75–89 (2000).
6. K. Łuszczyńska, M. Wistuba, I. Malik, M. Krąpiec, B. Szypuła, Geochronometria **45**, 1, 173-184 (2018).
7. P. Migoń, A. Kacprzak, I. Malik, M. Kasprzak, P. Owczarek, M. Wistuba, T. Pánek, Geomorphology **219**, 213-231 (2014).
8. I. Malik, Y. Tie, P. Owczarek, M. Wistuba, W. Pilorz, B. Woskowicz-Ślęza, Geochronometria **40**, 3, 208-216 (2013).
9. I. Malik and M. Wistuba, Geochronometria **39**, 3, 180-196 (2012).
10. I. Malik, M. Wistuba, P. Migoń, M. Fajer, Geochronometria **43**, 1, 24-37 (2016).
11. I. Malik, M. Wistuba, Y. Tie, P. Owczarek, B. Woskowicz-Ślęzak, K. Łuszczyńska, Appl. Geogr. **87**, 54-65 (2017).
12. T. Pánek, J. Hradecký, K. Šilhán, Studia Geomorphologica Carpatho-Balcanica **42**, 57–73 (2008).
13. A. Perrone, V. Lapenna, S. Piscitelli, Earth-Science Reviews **135**, 65–82 (2014).
14. T. Papciak, I. Malik, K. Krzemień, M. Wistuba, E. Gorczyca, D. Wrońska-Wałach, M. Sobucki, Bulletin of Geography. Physical Geography Series **8**, 5-17 (2015).
15. D. Poprawa and W. Rączkowski, Przegląd Geologiczny **51**, 685–692 (2003).
16. M. Wistuba, I. Malik, H. Gärtner, P. Kojs, P. Owczarek, Catena **111**, 41–55 (2013).
17. M. Wistuba, I. Malik, M. Fajer, T. Papciak, Studia Geomorphologica Carpatho-Balcanica **47**, 107-125 (2013).
18. M. Wistuba, "Slope-Channel Coupling as a Factor in the Evolution of Mountains. The Western Carpathians and Sudetes", Springer Verlag, 2014.
19. M. Wistuba, I. Malik, K. Wójcicki, P. Michałowicz, Earth Surf. Process. Landf. **40**, 293-312 (2015).
20. M. Wistuba, I. Malik, K. Krzemień, E. Gorczyca, M. Sobucki, D. Wrońska-Wałach, D. Gawior, Catena **171**, 359-375 (2018).
21. M. Wistuba, I. Malik, M. Krąpiec, Geochronometria **45**, 1, 223-234 (2018).
22. M. Wistuba, I. Malik, J. Badura, Dendrochronologia **53**, 82-94 (2019).
23. R. Unrug, Ann.Soc. Geol. Pol., **33**, 49–92 (1963).

Dendrochronological Assessment of Landslide Hazard For The Purpose Of House Construction (An Example Form Southern Poland)

Ireneusz Malik

University of Silesia in Katowice, Faculty of Earth Sciences, Będzińska 60, 41-200 Sosnowiec, Poland

Corresponding author: irekgeo@wp.pl

Abstract. The increasing number of disastrous mass movements creates a growing threat to buildings, roads, etc. In addition, the growing population, mainly in developing countries, causes the colonization of areas endangered by mass movements. One of the most destructive types of mass movements are landslides. Therefore, new methods of estimating landslide risk are currently being sought. The aim of the study was to assess the landslide hazard for the purpose of house construction in a mountain area. We used dendrochronological methods: the analysis of eccentric tree rings. Trees tilted due to landsliding record information about landslide events in their tree rings with annual resolution. Long series of data obtained from tree rings allow us to assess landslide hazard with great precision. The analysis have shown that the studied building plot in Jaszczurowa (southern Poland) and the slope directly above the plot are a subject of active landsliding. Dendrochronology allowed us to detect numerous small landside events on the analysed area. The hazard is related to heavy rainfall events when landsliding on study area can be triggered or accelerated and the ground can then move at a fast rate and on a larger scale. The study shows that any decision to build up the area under analysis will put new houses under the risk of damage due to landsliding.

Keywords: natural hazards, mass movements, landslide risk, spatial planning

INTRODUCTION

Research conducted in various parts of the world indicate an increase in the activity of mass movements during the last few decades [1], [2]. The most frequent reason for the increase is greater precipitation. In the developing countries the attention is also paid to the growing population and settlement of areas endangered by the occurrence of mass-movement [3]. In such an area many negative effects of human activity are recorded [4], [5], [6]. A lot of buildings, roads and other objects were recently destroyed by mass movements and landslides are particularly dangerous and destructive [7]. The increasing number of landslides and economic losses associated with landsliding are a reason for developing maps of landslide activity, landslide hazard and susceptibility [8]. Methods of protection and early detection of landslides are also expanded and improved [9], [10].

Dendrochronology is one of the methods for dating and assessing landslide hazard [11], [12]. Recently, it has also been used to detect hazard related to initial landslide movements [9], [13]. Dendrochronology is used not only for dating landslide activity, but also in many other fields of geomorphology [14], [15], [16]. In studies on landslide activity we assume that a tree which grows on an active landslide tilts with bedrock instability [17]. After tilting a tree starts to develop eccentric rings (wider on the lower side of a tilted stem and narrower on the upper side – in the case of conifers analysed in this study) [18]. By analysing the width of annual rings developed on opposite sides of tree stems it is possible to check the annual variability of eccentricity and date events of stem tilting by landslide activity (details of the method of dating landslide activity from eccentric growth are described in the paper [19]). The eccentricity of tree growth is also widely applied in other geological and geomorphological studies, e.g. on

dendrochronological record of low-magnitude earthquakes as triggers of landslide activity [20], on dendrochronological record of prevailing winds [21], on coupling between mass movements and bank erosion as a factor of moulding of hillslope-valley topography [22] and on shrubs growing in the high Arctic [23]. The aim of this study was to apply dendrochronological method of the analysis eccentric tree rings to asses landslide hazard on a building plot and for the purpose of constructing new house.

MATERIALS AND METHODS

The building plot for which the analysis of landslide activity was conducted is located in the Jaszczurowa village (Wadowice District, Western Carpathian Mts, southern Poland). In areas adjacent to the plot under study there are slopes with active landslides. Yet, it remains unknown whether the area where the construction of a house is planned is affected by landslide activity or whether it is free of landslide risk.

We have collected 15 cores from 10 trees growing on the tested area. We have sampled silver fir trees (*Abies alba* Mill.). Sampling was conducted with the use of Pressler borers. One or two cores were collected from each tree. One core per tree was collected if the diameter of tree stem was smaller than the length of Pressler borer (40 cm) [24], when diameter of tree stem was bigger we collected two cores per tree, from opposite sides of the tree. Cores were sampled according to the slope inclination because during landsliding rock and regolith slide in this direction and, therefore, wood anatomy disturbances are also most clearly developed in upslope-downslope directions. We avoided sampling of trees which had visible signs of the influence of environmental factors other than mass-movement activity, e.g. in studies on wind or landslides one should not collect samples from trees with large wounds, with significant loss of assimilation apparatus, with strongly asymmetric crowns, with deformed stems.

After collecting cores from trees we glued cores it into wooden holders. After drying, cores were sanded to reveal the structure of wood. For this purpose we use a manual grinder to sand cores with a sequence of sandpapers of grit size 100, 250, 500, 800 and sometimes 1000. To calculate eccentricity index we measured the width of annual rings in cores form opposite sides of stems. Measurements were done using RINNTECH Lintab measuring system and TSAPWin software. After measuring ring widths, ring curves were compared. At the beginning we cross-dated dendrochronological curves from opposite sides of each tree, then the curves between the individual trees were correlated. For dating the landslide activity we used method and formulae described in paper [17].

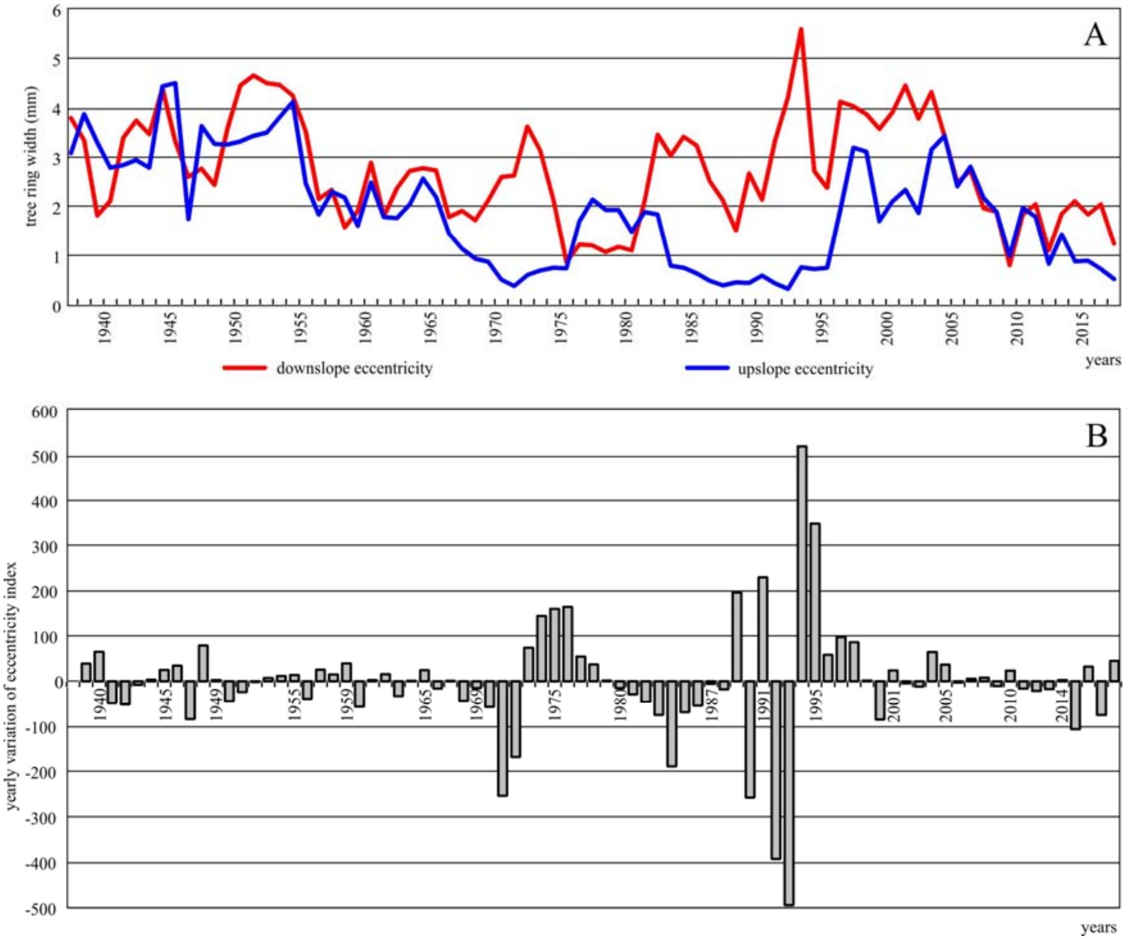

FIGURE 1. Example of the procedure of dating landslide activity from eccentricity record of a single tree: A – downslope tree-ring widths (red curve) compared with upslope tree-ring widths (blue curve). B – yearly variation of eccentricity index.

RESULTS AND DISCUSSION

The analysis has shown that the studied plot in Jaszczurowa and the slope directly above the plot are active and many small landside events were detected there by the means of dendrochronology (Fig. 1). The summary of landslide activity dated from all 10 tested trees (Fig. 2) indicates that since 1955 all trees have developed eccentric tree rings. During the last 62 years material on the examined slope was transported many times by landslide movements of various strength. The analysis of eccentricity index and its annual variability in individual trees also indicates very high landslide activity in some years. Landsliding was particularly intense in 1984-2002. Year 1986 was particularly distinct with 7 of 10 tested trees recording landslide activity. In this year the increase in eccentricity reached 400 percent points compared to the previous year. Among the trees under study eccentricity can commonly increase by 200-300 percent points from year to year. Very high activity was also identified in 2000-2001.

Assessment of landslide activity with the use of dendrochronological method has certain advantages compared to commonly used geodetic methods [25], [26]. Methods such as analysis of DTMs from airborne LiDAR allow to compare changes in the topography (including changes caused by landsliding). Topography changes suggest that certain areas are affected by contemporary landslide movements. However, DTM images for comparison are available only for very recent periods as LiDAR technology is still relatively new. Determining landslide activity based on data covering only several years can be unreliable. Sometimes landslide slope can be inactive for years and then it can suddenly be reactivated. In such cases, the comparison of different DTMs can be an unreliable method if DTM data sets come from the period when the landslide is dormant. On the other hand, dendrochronological studies

can cover periods of past decades-centuries and deliver more reliable data on landslide activity. Other methods used to determine activity and landslide hazard, e.g. inclinometers can also be unreliable. The results obtained from inclinometers are available only since the equipment is installed in the ground. Therefore, one has to wait for the results, while dendrochronology can instantly deliver data on landslide activity during long periods. In addition, the use of inclinometers is expensive. Dendrochronological method, compared to other methods, seems to be effective and inexpensive. However, its basic limitation is the presence of trees in the area for which the determination of landslide activity is to be carried out.

CONCLUSION

Dendrochronological analysis shows that landslide movements occur on the analysed building plot and on the slope directly above the plot. During heavy rainfall, landsliding on this slope can be triggered or accelerated and the ground can then move at a fast rate and on a larger scale. This means that if a decision will be made to build up the plot landsliding will endanger the new house. In the case of house construction it would be necessary to include landslide hazard at the stage of designing the structure of building and to specify construction solutions allowing protection against landsliding.

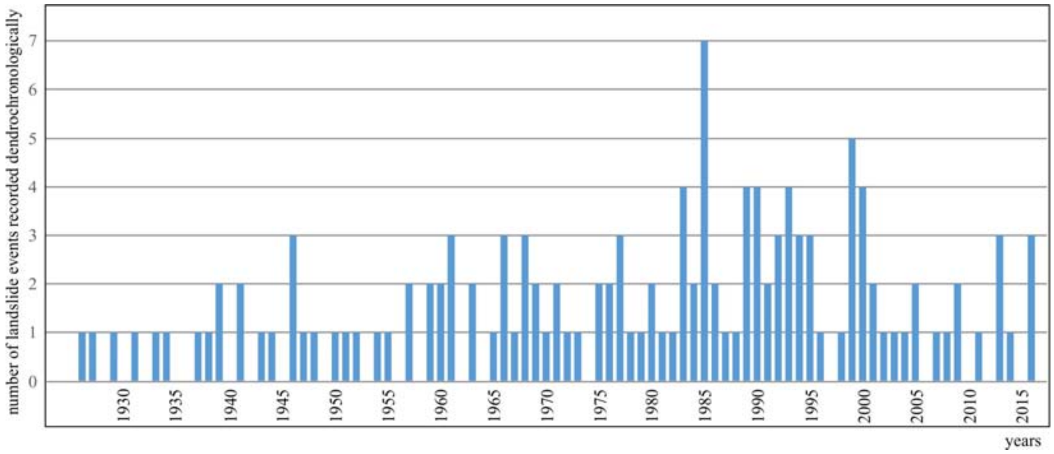

FIGURE 2. Total number of landslide events per each calendar year recorded in trees sampled on the studied building plot.

The study was supported by the National Centre for Research and Development through the project INNOTECH-K3/IN3/58/228202/ NCBR/15.

REFERENCES

1. V. Winchester and R.K, Chaujar, *Geomorphology*, Vol. **47**. pp. 61-74 (2002).
2. D.N. Petley G.J. Hearn A. Hart N.J. Rosser S.A. Dunning K. Oven and W.A. Mitchell, *Natural Hazards,* Vol. **43.** pp. 23-44 (2007).
3. I. Alcántara-Ayala, *Geomorphology*, Vol. **47**. pp. 107-124 (2002).
4. D. Absalon, "Changes in water quality in the Upper Wisła (Vistula) River Basin", 2nd International Conference on Environmental and Computer Science, ICECS, 29-32 (2009).
5. D. Absalon, B. Ślesak, Ecotox Environ Safe. **74** (4), 967-973 (2011).
6. D. Absalon, B. Ślesak, Pol J Environ Stud,. **21** (2), 235-239 (2012).
7. F. Guzzetti F. Ardizzone M. Cardinali M. Rossi and D. Valigi, *Earth and Planetary Science Letters* Vol. **279**. pp. 222-229 (2009).
8. K. Łuszczyńska, M. Wistuba, I. Malik, M. Krąpiec, B. Szypuła, Geochronometria **45**, 1, 173-184 (2018).

9. M. Wistuba, I. Malik, J. Badura, Dendrochronologia **53**, 82-94 (2019).
10. T. Papciak, I. Malik, K. Krzemień, M. Wistuba, E. Gorczyca, D. Wrońska-Wałach, M. Sobucki, Bulletin of Geography. Physical Geography Series **8**, 5-17 (2015).
11. I. Malik and M. Wistuba, Geochronometria **39**, 3, 180-196 (2012).
12. M. Wistuba and I. Malik, Czasopismo Geograficzne **82**, 4, 401-421 (2011).
13. M. Wistuba, I. Malik, M. Fajer, T. Papciak, Studia Geomorphologica Carpatho-Balcanica **47**, 107-125 (2013).
14. M. Wistuba, "Slope-Channel Coupling as a Factor in the Evolution of Mountains. The Western Carpathians and Sudetes", Springer Verlag, 2014.
15. I. Malik, Ł. Pawlik, A. Ślęzak, M. Wistuba, Catena **173**, 264-275 (2019).
16. M. Wistuba, A. Sady, G. Poręba, Catena **160,** 10-23 (2018).
17. I. Malik, M. Wistuba, P. Migoń, M. Fajer, Geochronometria **43**, 1, 24-37 (2016).
18. P. Migoń, A. Kacprzak, I. Malik, M. Kasprzak, P. Owczarek, M. Wistuba, T. Pánek, Geomorphology **219**, 213-231 (2014).
19. M. Wistuba, I. Malik, H. Gärtner, P. Kojs, P. Owczarek, Catena **111**, 41-55 (2013).
20. M. Wistuba, I. Malik, K. Krzemień, E. Gorczyca, M. Sobucki, D. Wrońska-Wałach, D. Gawior, Catena **171**, 359-375 (2018).
21. M. Wistuba, I. Malik, M. Krąpiec, Geochronometria **45**, 1, 223-234 (2018).
22. M. Wistuba, I. Malik, K. Wójcicki, P. Michałowicz, Earth Surf. Process. Landf. **40**, 293-312 (2015).
23. P. Owczarek, A. Latocha, M. Wistuba, I. Malik, Z. Geomorphol. Supp. **57**, 3, 75-95 (2013).
24. P. Migoń, T. Pánek, I. Malik, J. Hrádecký, P. Owczarek, K. Šilhán, Geomorphology **124**, 3-4, 200-214 (2010).
25. I. Malik, Y. Tie, P. Owczarek, M. Wistuba, W. Pilorz, B. Woskowicz-Ślęza, Geochronometria **40**, 3, 208-216 (2013).
26. I. Malik, M. Wistuba, Y. Tie, P. Owczarek, B. Woskowicz-Ślęzak, K. Łuszczyńska, Appl. Geogr. **87**, 54-65 (2017).

Hazards to the Quality of Surface Water from Discharge of Saline Mining Waters in the Upper Oder River Basin

Magdalena Matysik

University of Silesia in Katowice, Faculty of Earth Sciences, ul. Będzińska 60, 41-200 Sosnowiec, Poland

Corresponding author: magdalena.matysik@us.edu.pl

Abstract. Saline mine waters are discharged in Poland, among others, to the Oder river and its right-hand tributaries: Ruda, Bierawka and Kłodnica. Czech mines discharge water to the Oder river and its right tributary, the Olza. In the Upper Oder basin there are 26 discharges of mine water. The discharge of saline waters to rivers causes deterioration of the ecological status of waters and the threat of failure to achieve environmental objectives imposed by the Water Framework Directive 2000/60/EC. The large salinity amplitudes observed in rivers degrade their biological life. In order to protect rivers from excessive salinity caused by the discharging of mine water, it is desirable to build retention and dosing systems, which may lead to the improvement of the ecological potential of surface waters and reduce the threat to ecosystems.

Keywords: water quality, water pollution, mine activity, mining waters.

INTRODUCTION

Water policy in the EU is mainly determined by Directive 2000/60/EC of 23.10.2000 establishing a framework for Community action in the field of water policy. The provisions of the Water Framework Directive (WFD) were incorporated into Polish law in 2011. The WFD's overriding objective is to achieve good water status by 2021. For bodies of water which currently have a very good ecological status/potential, the objective is to maintain this status/potential.

Water quality in the Oder river is affected by many natural factors and powerful anthropogenic influences. The factors, which are particularly noticeable in the studied area, such as extensive urbanization, underground exploitation of hard coal and much industry, have an adverse effect on water quality in [1]. Environmental changes caused by hard coal mining are also manifested in the form of changes in the river network, changes in the course of watersheds, changes in water reservoirs [2].

In the process of hard coal mining, permanent drainage of mining excavations is necessary. Extraction of minerals is accompanied by the outflow of natural groundwater to mine workings. These waters are considered a specific type of waste water, because they are not the result of traditionally understood technological processes.

The impact of hard coal mining on surface water quality is perceived mainly by the introduction of saline waters by mines, which affect the river biocenosis, limiting the possibility of using them for economic purposes [3]. They are very diverse in terms of chemical composition and mineralization values. Mining classification of water quality in mines divides them into four groups [4] taking into account the possibility of utilization and the processes of their utilization. The least saline waters, in particular freshwater and industrial water, occur in the infiltration zone of groundwater. Their chemical composition is very diverse, because they formed in different geological formations. From the chemical point of view, these are mostly HCO_3-Ca, HCO_3-SO_4-Ca, SO_4-HCO_3-Ca-Mg and Cl-HCO_3-Na type waters. On the other hand, waters which are slightly saline are classified as hydrochemical types of Cl-HCO_3-Na and Cl-SO_4-Na. In contrast, the types of Cl-Na and Cl-Na-Ca are characteristic for saline water [5].

High concentrations of chlorides and sulphates in the Oder are affected by hard coal mines in the Czech Republic and Poland. The chemical status of waters in the Upper Oder river basin, which is a receiver of mine waters, depends to a large extent on the chemical composition of these waters.

Polish environmental standards define limit values for chloride and sulphate concentrations, which are: class I (very good ecological status/potential) - Cl^-- 200 mg/l, SO_4^{2}-150 mg/l, class II (good ecological status/potential) - Cl^- - 300 mg/l, SO_4^{2}- 250 mg/l. Exceeding the limit values for class II classifies water below the good status/potential as regards physicochemical elements.

RESULTS

In Poland, saline mine waters are discharged to the Oder and its right-hand tributaries: Ruda, Bierawka and Kłodnica. Czech mines discharge water to the Oder river and its right tributary the Olza.

Coal mining takes place in the entire vertical profile of coal measures. The lowest levels of extraction are located at a depth of about 1000 m below the surface (in the Kłodnica river catchment); the majority of mines located in the Upper Oder basin extract coal from a depth of 600 to 800 m below the surface. In the Upper Oder basin there are 26 discharges of mine water [6].

TABLE 1 Average mine water in 2003–2013.

River	Mine water per year m^3	Mine water in $m^{-3}\cdot s^{-1}$
Oder	19835441	0.629
Olza	5979643	0.190
Ruda	4782052	0.152
Bierawka	5223630	0.166
Kłodnica	36373524	1.153

In the period 2003-2013, on average, 74184100 m^3 (2.35 $m^{-3}\cdot s^{-1}$) of mine water was discharged into these rivers annually. The largest volume of mine water is discharged to the Kłodnica river, the annual average was 36373524 m^3 (1.15 $m^{-3}\cdot s^{-1}$), which accounted for 49% of all discharged mine waters in the Upper Oder catchment. The average annual volume of mine water discharged directly to the Oder in this period was 19835441 m^3 (0.629 $m^{-3}\cdot s^{-1}$), i.e. 27% of all discharged mine waters. For other rivers: Olza, Ruda and Bierawka, the average annual volume of discharged mine water was on a similar level and amounted to 5979643 m^3 (to Olza), 5223631 m^3 (to Bierawka) and 4782052 m^3 (to Ruda). Bytomka, in turn, is characterized by the largest share of mine waters in mean annual flows, which is 30 %. The average mine water discharge to Bytomka is 0.871 $m^{-3}\cdot s^{-1}$ [7].

The average salinity ($Cl^-+SO_4^{2-}$) of mine water discharged in the Upper Oder river catchment is 9308 $mg\cdot dm^{-3}$. Mine waters discharged directly to the Oder river are characterized by the highest concentrations, with the average concentration of $Cl^-+SO_4^{2-}$ in the period 2003-2013 amounting to 20 079 $mg\cdot dm^{-3}$. Mining waters discharged to other rivers are characterized by average salinity not exceeding 9000 $mg\cdot dm^{-3}$. In 1985, the load of $Cl^-+SO_4^{2-}$ transferred to the Oder amounted to 952171 Mg (2609 Mg/Day). In the years 2003-2013, the average annual load of $Cl^-+SO_4^{2-}$ was 603180 Mg (1653 Mg/Day). According to the mines' forecasts, a steady increase in the volume of water and $Cl^-+SO_4^{2-}$ load is predicted - by about 2% per year on average, in 2020 the discharged amount of chlorides and sulphates will amount to about 2475 Mg/Day.

The impact of mine water on surface waters in the Oder basin was confirmed, among others by Drzymała et al. (2013) - hydrogeochemical characterization was performed, chemical type of river waters was determined and analysis of their changes depending on the flows was performed (NQ, SQ, WQ). The surface waters of the Upper Oder catchment are waters of chloride-bicarbonate-calcium-sodium (Cl-HCO_3-Ca-Na) types for high flows and of the chloride-sodium Cl-Na type for low flows. At high flows, they are brackish waters with mineralization of 1.3 $g\cdot dm^{-3}$ and at low flows - brackish waters with mineralization of about 2.2 $g\cdot dm^{-3}$.

Bierawka's waters are characterized by the highest average concentrations of $Cl^-+SO_4^{2-}$ for the period 2003-2013 - 2012 $mg\cdot dm^{-3}$, in Kłodnica the average concentrations of $Cl^-+SO_4^{2-}$ in this period amounted to 1409 $mg\cdot dm^{-3}$. In the Ruda's waters, the average concentration of $Cl^-+SO_4^{2-}$ was 750 $mg\cdot dm^{-3}$. The Olza and the Oder in Krzyżanowice and Miedonia were characterized by average concentrations of $Cl^-+SO_4^{2-}$ at the level of 320 $mg\cdot dm^{-3}$. The lowest mean concentrations of $Cl^-+SO_4^{2-}$ were 167 $mg\cdot dm^{-3}$ and occurred in the Oder in Chałupki. At the Oder site in Zdzieszowice downstream of the mouth of Kłodnica, the average concentration of chlorides and sulphates was 431 $mg\cdot dm^{-3}$. Maximum concentrations of $Cl^-+SO_4^{2-}$ in this period were recorded in the waters of Kłodnica and they amounted to 3419 $mg\cdot dm^{-3}$ and Bierawka 3154 $mg\cdot dm^{-3}$. In the waters of the Ruda, the maximum concentration of $Cl^-+SO_4^{2-}$ was 2600 $mg\cdot dm^{-3}$. This situation is mainly determined by changes in the flow of rivers, with the lowest salinity values recorded in the period of high flows, while at low flows - the highest.

The highest concentrations of $Cl^-+SO_4^{2-}$ are recorded in watercourses just downstream of the discharges of underground water. The highest average concentration in the period 2003-2013 was recorded in the mid-reach Bierawka (downstream of Knurówka) - 4790 $mg\cdot dm^{-3}$ $Cl^-+SO_4^{2-}$, the maximum recorded value was 8185 $mg\cdot dm^{-3}$ $Cl^-+SO_4^{2-}$. High mean concentrations of $Cl^-+SO_4^{2-}$ also occurred in the tributaries of the Kłodnica: Bytomka (2851 $mg\cdot dm^{-3}$), Czarniawka (2666 $mg\cdot dm^{-3}$) and Bielszowicki Stream (2922 $mg\cdot dm^{-3}$). The highest maximum concentration of $Cl^-+SO_4^{2-}$, which was 13486 $mg\cdot dm^{-3}$ occurred in the Bielszowicki Stream, whereas in Czarniawka the maximum concentration of $Cl^-+SO_4^{2-}$ was 12956 $mg\cdot dm^{-3}$. The Vistula river in Bieruń Nowy is also

characterized by high salinity, where waters from mines are also discharged. The recorded annual concentrations of $Cl^-+SO_4^{2-}$ were 2700 mg·dm^{-3} [8].

The impact of saline mine water on the quality of water in the Oder was observed during patrol monitoring conducted on the 40-kilometer section of the Oder between Racibórz and Koźle. There was an increase in conductance downstream of the estuaries of the rivers with saline waters: Ruda, Bierawka and Kłodnica. Chloride concentrations were characterized by high dynamics in the range of 420 to almost 1100 mg·dm^{-3} [9]. Lower concentrations of chlorides in the Oder are the result of inflow of water from watercourses not burdened with such discharges and a marked increase is recorded downstream of the inflows loaded with saline mine waters.

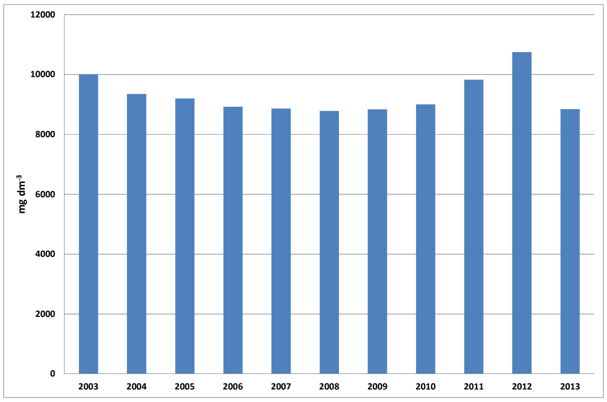

FIGURE 1. Mean concentrations of $Cl^-+SO_4^2$ in mine waters

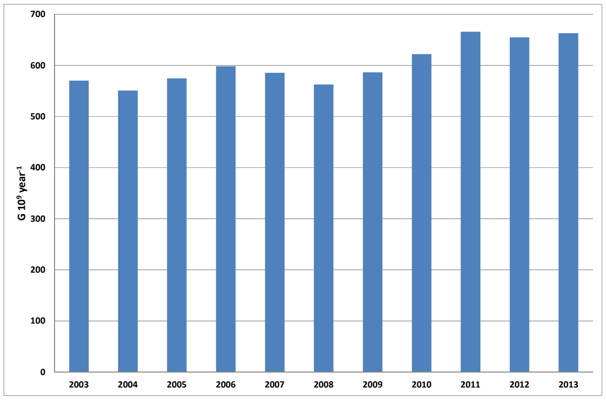

FIGURE 2. Mean loads of $Cl^-+SO_4^2$ in mine waters

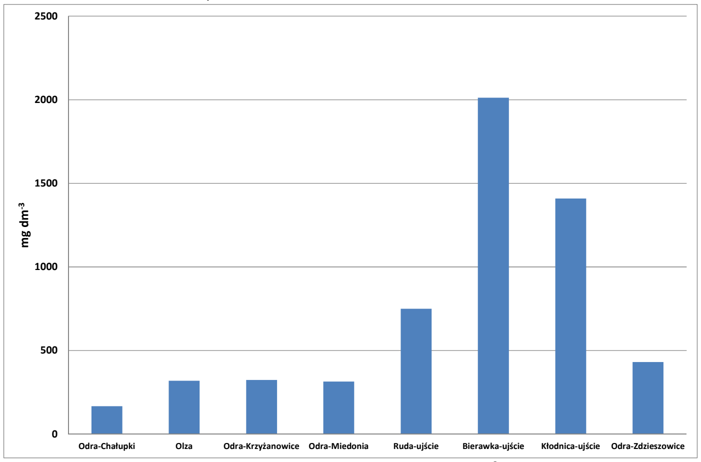

FIGURE 3. Mean loads of $Cl^-+SO_4^2$ in rivers

The most negative impact of mine water discharge was recorded in the period 1986-2003, when mine waters from some of the mines in the volume of 30000 m^{-3} 24h^{-1} were discharged to the Lesznica river, the tributary of Szotkówka (right tributary of the Olza). As a result of the introduction of a large load of chlorides and sulphates to the Leśnica river, the average concentration of chlorides was 8104 mg·dm^{-3}, and sulfates 248 mg·dm^{-3}.

In 2004 mine water discharge to the Oder river has been launched (downstream of the mouth of the Olza). Since 2009, the mine water retention and dosing system has been fully operational in the Upper Oder basin (Olza collector). This system dewaters a total of 6 active and 2 inactive hard coal mines. It is equipped with the monitoring of salinity and the volume of water discharged from individual mines. It ensures mixing of saline mine waters with the Oder river water, which allows maintaining acceptable concentrations of $Cl^-+SO_4^{2-}$. The discharge of saline waters from the Olza collector affected the improvement of the quality of the Oder river water in terms of salinity

Modernization of the "Olza" collector largely contributed to the improvement of the quality of the waters of the Leśnica and the Olza rivers, and the lack of fluctuating ion concentrations has positively influenced their water ecosystem [10].

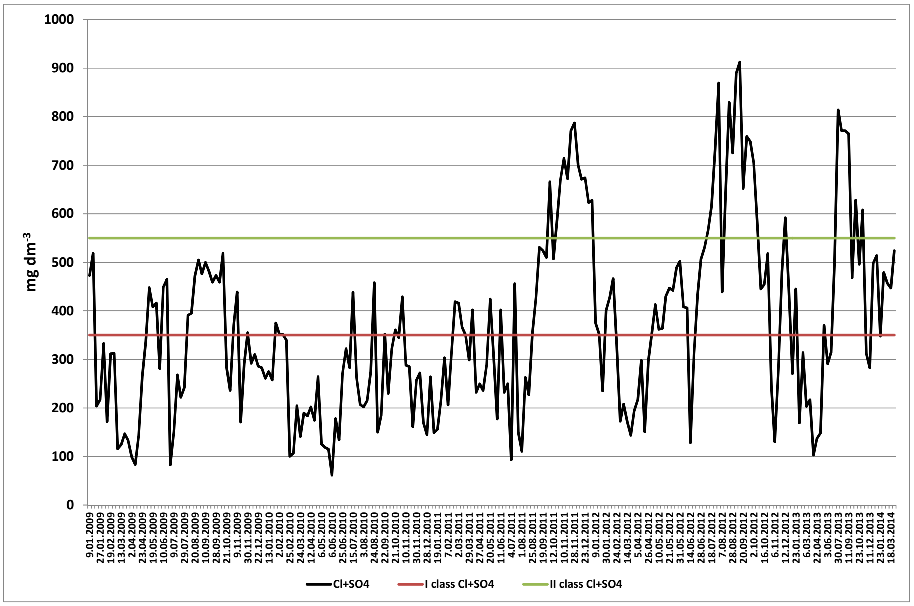

FIGURE 4. Changes in the values of Cl^{-}+SO_4^{2} of the Oder near Olza collector

SUMMARY AND CONCLUSIONS

Mining activity is an important factor modifying the flow and quality of water in the Upper Oder basin. Water quality is extremely important because constant access to good quality water is a condition necessary for biological life and for the economy. The issue of water quality is of particular importance to Poland, which has rather poor water resources compared with many countries of the European Union [8].

Water organisms and their communities have the ability to adapt to the salinity concentration. The more even the concentration of salinity (more stable), the better the adaptation of habitats to dependent waters and aquatic organisms. Large salinity amplitudes observed in the Olza, Ruda, Bierawka and Kłodnica, and especially in their tributaries degrade the biological life of the river. This is confirmed by the observations conducted in the small river Lesznica, where the entire biocenosis has been degraded, and the organisms typical of freshwater have disappeared while others have developed, that are resistant to salinity [10]. The discharge of saline mine water through the "Olza" collector causes a reduction in salinity amplitudes and a significant improvement in the quality of rivers in the Upper Oder basin. In order to protect other rivers from excessive salinity caused by discharging of mine water, it is desirable to build similar retention and dosing systems in other catchments, which may lead to improvement of the ecological potential of surface waters.

REFERENCES

1. D. Absalon, M. Matysik, Changes in Water Quality and Runoff in the Upper Oder River Basin, Geomorphology, 92, pp. 106–118, (2007).
2. D. Absalon, M. Matysik, Effects of renaturalization of the river valley transformed as a result of mining activity - The Szarlejka river case study, AIP Conference Proceedings 1906, 170010 (2017).
3. R. Lach, P. Łabaj, J. Bondaruk, A. Magdziorz, Monitoring wód kopalnianych odprowadzanych do rzek, Prace Naukowe GIG Górnictwo i Środowisko, Research Reports Mining and Environment, 1/2006, pp. 97–115 (2006).
4. I. Pluta, A. Grmela, Odprowadzanie wód kopalnianych do Odry w świetle przepisów prawnych w Polsce i Republice Czeskiej, in: *Conference Proceedings: VI Konferencja naukowo-techniczna „Ochrona środowiska na terenach górniczych“,* AGH Kraków, PS Sosnowiec, GIG Sosnowiec, pp. 377-392 (2006).
5. A. Harat, A. Grmela, Wpływ wód kopalnianych Górnośląskiego Zagłębia Węglowego na zmiany jakości wody w rzece Olza w latach 2000–2007, Monitoring Środowiska Przyrodniczego nr 9, Kieleckie Towarzystwo Naukowe, Kielce pp. 57-62, (2008).
6. M. Matysik, Wpływ zrzutów wód kopalnianych na odpływ rzek Górnośląskiego Zagłębia Węglowego, Wydawnictwo Uniwersytetu Śląskiego, Katowice, p. 162, (2018).

7. M. Matysik, Impact of land development on shaping catchment runoff under the influence of mining activity, AIP Conference Proceedings 1906, 170013, (2017).
8. D. Absalon, Changes in Water Quality in the Upper Wisła (Vistula) River Basin. Proceedings of the Second International Conference on Environmental and Computer Science in Dubai, IEEE Computer Society Press, 29–32 (2009).
9. D. Absalon, P. Kryszczuk and P. Rutkiewicz, Changes in water quality along the course of a river - Classic monitoring versus patrol monitoring, AIP Conference Proceedings 1906, 170011 (2017).
10. J. Swolkień, K. Filek, Wpływ zmian technologicznych w kolektorze „Olza” na skład chemiczny wód rzeki Odry i jej dopływów, Rocznik Ochrona Środowiska, T. 14. R. 2012, pp. 945–959, (2012).

Determination of Selected Parameters/Analytes in Surface Water Samples Collected in the Surroundings of the Capital of Spitsbergen (Longyearbyen)

Marek Ruman[1, a)], Michał Ciepły[1, b)] and Żaneta Polkowska[2, c)],

[1]*University of Silesia in Katowice, Faculty of Earth Sciences, Bedzinska 60, 41-200 Sosnowiec, Poland*
[2]*Gdansk University of Technology, Department of Analytical Chemistry, Faculty of Chemistry, Gabriela Narutowicza 11/12, 80-233 Gdansk, Poland*

[a)]Corresponding author: marek.ruman@us.edu.pl
[b)]michal.cieply@us.edu.pl
[c)]zanpolko@pg.edu.pl

Abstract. Polar regions are extremely sensitive to pollution such as harmful gases, particles or toxic substances which affect the Arctic climate and ecosystems. Spitsbergen, as well as all Arctic region, because of its geographically distant location and lack of industry sector, should be free of chemical pollution. Despite this, many pollutants could be found in the Polar environment, for example in freshwaters. Their occurrence is related with the global distillation process (Grasshopper effect) in which the contaminants from lower latitudes are transferred to the higher latitudes, resulting in the pollution of Arctic area.

The purpose of the research was to determine the selected parameters: TOC (Total Organic Carbon) and formaldehyde, phenols in samples of freshwaterwater (surface water) collected in the area surrounding the capital of Spitsbergen (Longyearbyen). The aim was to investigate the pollution of Arctic freshwater. The obtained results of detected compounds may confirm the role of transport of contaminants over large distances in pollution of Polar regions.

INTRODUCTION

Spitsbergen is the biggest island (39,000 km^2) belonging to the Svalbard archipelago (62,800 km^2) which is located 800 km north from Norway and 1100 km from the North Pole. In turn, Longyearbyen is the biggest settlement of Spitsbergen as well as the greatest administrative center of whole Svalbard. All this region should be uncontaminated, in view of its geographically distant location and lack of industry sector. However, many pollutants could be found in the Polar environment. This is related with global distillation (Grasshopper effect). During this process, the pollutants are carried by the wind from low latitudes towards high latitudes at different distances, depending on their volatility. The greater the volatility of compounds, the further they are shifted, since they are more mobile. The anthropogenic contaminants from hotter equatorial regions are moved to the temperate regions. After condensing and embedding they overwinter, for example in freshwater and soil. Under the influence of the summer sun the chemicals re-vaporize and are transferred by the air currents further to the north, where they fall to the ground once again. The cycle continues until the more volatile pollutants reach the Arctic. In colder polar regions the contaminants could no longer be lifted into the atmosphere. Thus, they remain in the Arctic environment.

The aim of this work was to determine the selected parameters and compounds in the samples of freshwater (surface water) collected in the area surrounding the capital of Spitsbergen (Longyearbyen). The samples were

subjected to the analysis in order to measure: pH, electrical conductivity, TOC parameter, and to detect the concentration of surfactants (anionic, cationic, non-ionic), ions (cations and anions), formaldehyde and phenols. In addition, the extraction of PCBs and PAHs analytes from freshwater was performed to prepare the samples for further detection that would be continued by other researchers. The purpose of the laboratory measurements was to investigate the pollution of Arctic freshwater. Due to the fact, that in Spitsbergen the only branch of the economy is coal extraction, it could be assumed that the pollutants found in Polar region come from remote industrialized countries.

THE LOCATION OF SAMPLING SITES

The freshwater samples were collected in Longyear Valley during two time periods - Spring (the end of May, the beginning of June) and Autumn (September) in 2016. A total of ten samples were gathered, five per each term. Table 1 shows five established sampling sites.

TABLE 1. Sampling sites. The names of samples (abbreviations) with corresponding description.

No.	Name of the sample	Commentary
1	LAR	Larsbreen glacier
2	LYR1	Longyearbreen glacier
3	LYR2	Point no. 1 on Longyear River
4	LYR3	Point no. 2 on Longyear River
5	LYRU	Mouth of Longyear River

A sample called LAR contained water flowing from the Larsbreen glacier, while LYR1 - from Longyearbreen glacier. Water from both glaciers was running down to the Longyear River. Two water samples - LYR2 and LYR3 - were taken at two selected sites on the river. The last one, LYRU, was collected at the mouth of the Longyear River. Figure 1(b) presents a fragment of three-dimensional map of Longyear Valley (South view) on which sampling sites were marked out. Figure 1(a) shows the exact localization of the Valley in Spitsbergen.

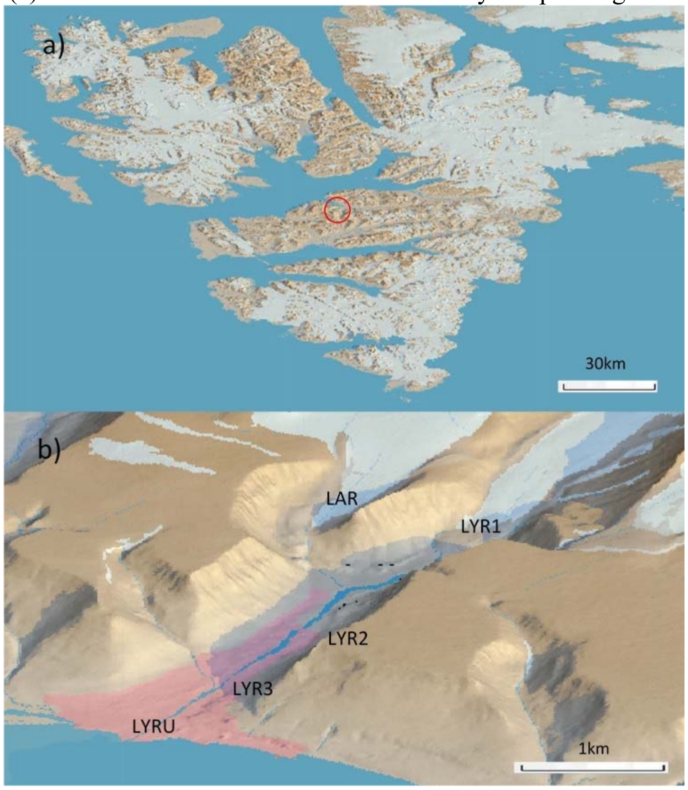

FIGURE 1. Three-dimensional map of Spitsbergen (a) exact localization of Longyear Valley, (b) sampling sites marked out on the three-dimensional map of Longyear Valley in Spitsbergen - South view
(Source: http://toposvalbard.npolar.no, Access: 29.04.2017).

RESULTS AND DISCUSSION

TOC

TOC parameter was measured in order to determine the environmental pollution, since TOC gives a full information about the content of all organic compounds in the sample. The average TOC concentration was higher in freshwater samples collected in September (0.437 mg/L) than in samples collected in May/June (0.211 mg/L). Concerning TOC concentration at particular sampling sites (as shown in the Fig. 2) in samples collected in May/June, the highest value was determined in LYR3 (point no. 2 on Longyear River: 0.367 mg/L). In turn, among samples collected in September, the highest TOC concentration was detected in LYRU (mouth of Longyear River: 0.556 mg/L) and LYR1 (freshwater from Longyearbreen glacier: 0.535 mg/L).

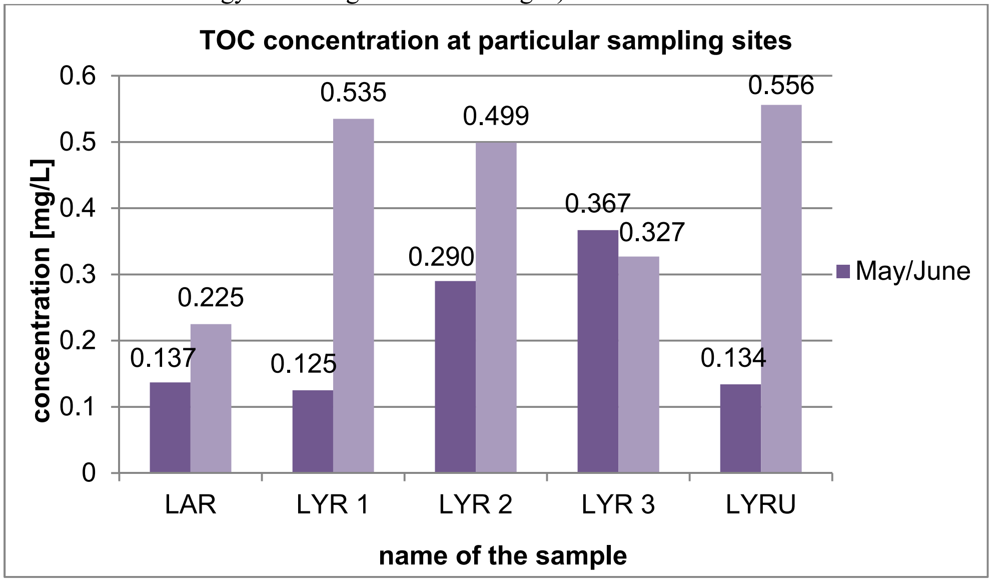

FIGURE 2. TOC concentration at particular sampling sites.

FORMALDEHYDE AND PHENOLS

The collected freshwater was also analyzed to determine formaldehyde and phenols concentration. Figure 3 presenting formaldehyde and phenols concentration at particular sampling sites in samples collected in two seasons, it could be stated that the highest concentration of both formaldehyde and phenols was in LYR1 sample (freshwater from Longyearbreen glacier) collected in September (formaldehyde: 0.710 mg/L, phenols: 0.717 mg/L). Almost the same concentration of formaldehyde as in LYR1 was detected in LYRU sample (mouth of Longyear River: 0.690 mg/L). In case of formaldehyde, its concentration in LYRU sample collected in May/June was also high (0.680 mg/L). Slightly lower results of formaldehyde amount were also obtained in LYR3 samples (May/June: 0.550 mg/L, September: 0.570 mg/L). As for phenols, the second highest concentration was detected in LYR2 sample (point no. 1 on Longyear River: 0.459 mg/L) collected in September, however the result from May/June is comparable (0.402 mg/L).

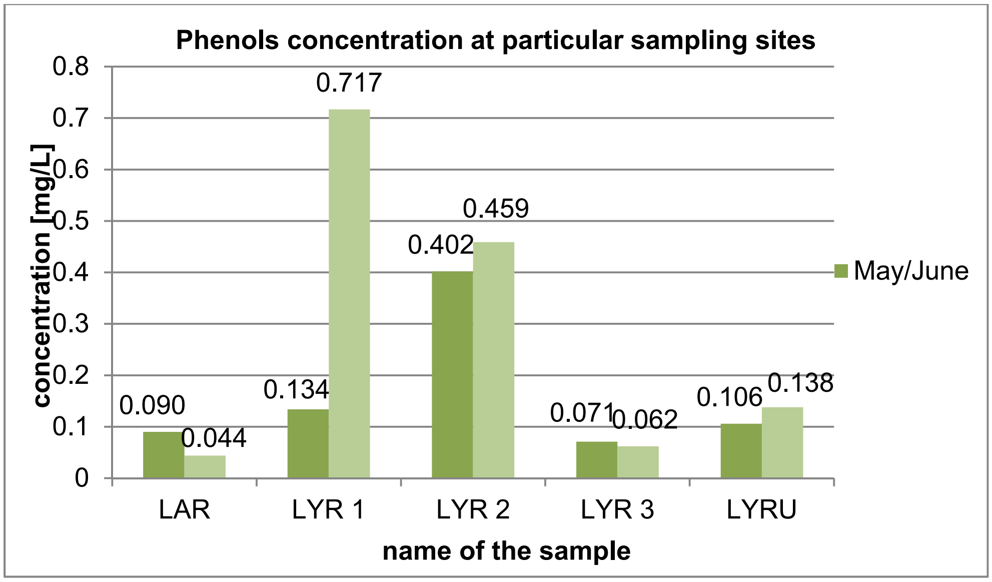

FIGURE 3. Phenols concentration at particular sampling sites.

SUMMARY

The aim of this work was to determine the selected parameters and compounds in the samples of freshwater (surface water) collected in the area surrounding the capital of Spitsbergen (Longyearbyen). Ten samples were subjected to the analysis to measure TOC parameter, and to detect the concentration of formaldehyde and phenols.

The purpose of all laboratory measurements was to investigate the pollution of Arctic freshwater, which because of its distant location far from industrial areas, should be free of chemical pollution. Due to the fact, that in Spitsbergen the only branch of the economy is coal extraction, it could be assumed that the pollutants found in Polar region come from remote industrialized countries. The pollutants are transferred by the global distillation process (Grasshopper effect) from lower to higher latitudes. It also could be established that the global migration of pollutants has adverse effect on the quality of Arctic freshwater, as well as on living organisms (animals).

The TOC parameter was measured additionally for the determination of the degree of environmental pollution. It may be implied that as the level of contamination increases, the concentration of TOC is higher, since TOC gives full information about the sum of all the organic compounds present in the analyzed sample. However it does not provide the detailed information on the type of the individual organic compounds. The maximum value of TOC was determined in LYRU sample (mouth of Longyear River: 0.556 mg/L) collected in September and in LYR1 (freshwater from Longyearbreen glacier: 0.525 mg/L) collected in the same time of sampling.

The highest formaldehyde concentration determined in all freshwater samples was 0.710 mg/L, while the highest concentration of phenols equaled to 0.717 mg/L. The presence of these compounds in tested samples may confirm the role of transport of contaminants over large distances in the pollution of Polar regions. In addition, high concentration of formaldehyde and phenols from sampling site called LYR1 (freshwater from Longyearbreen glacier) may suggest that part of pollution was derived from glacier meltwater.

In general, comparing the two periods of sampling, it could be noticed that the concentration of most of the detected compounds was higher in freshwater samples collected in September than in the samples collected in May/June. The time difference between two seasons of sampling was small, however it could be stated that the tendency of increasing concentration of pollutants occurs. Therefore, it is significant to conduct the research concerning the monitoring of Arctic area. It is also important to develop the analytical techniques serving to study of Arctic environmental samples. The concentration of various contaminants should be regularly detected and the parameters should be measured, since even low levels of contaminants may be an indicator of the pollution of considerable part of the Polar region.

REFERENCES

1. S. R. Arnold, K. S. Law, C. A Brock and J.L. Thomas, Arctic air pollution: Challenges and opportunities for the next decade. *Elem Sci Anth*, **104**, 1-4 (2016).
2. R. Sadler and D. Connell: Chapter 8: Global Distillation in an Era of Climate Change [in]: Organic Pollutants Ten Years After the Stockholm Convention - Environmental and Analytical Update. (InTech, London, 2012) pp. 191-192.
3. K. Kozak, Ż. Polkowska,and Ł. Stachnik, Arctic catchment as a sensitive indicator of the environmental changes: distribution and migration of metals (Svalbard). *Int. J. Environ. Sci. Technol.*, **13**, 2779–2796 (2016).
4. K. Kosek, and Ż. Polkowska, Determination of selected chemical parameters in surface water samples collected from the Revelva catchment (Hornsund fjord, Svalbard). *Monatsh Chem*, **147**, 1401-1405 (2016).
5. Ż. Polkowska, K. Cichała-Kamrowska, M. Ruman, K. Kozioł, W. E. Krawczyk and J. Namieśnik, Organic Pollution in Surface Waters from the Fuglebekken Basin in Svalbard, *Norwegian Arctic. Sensors*, **11**, 8910-8929 (2011).
6. K. Kozak, K. Kozioł, B. Luks, S. Chmiel, M. Ruman, M. Marć and Ż. Polkowska, The role of atmospheric precipitation in introducing contaminants to the surface waters of the Fuglebekken catchment, Spitsbergen. *Polar Research*, **34**, 1-11 (2015).
7. N. Rutter, A. Hodson, T. Irvine-Fynn and M. K. Solas, Hydrology and hydrochemistry of a deglaciating high-Arctic catchment, Svalbard. *Journal of Hydrology*, **410**, 39-50, (2011).
8. B. Etzelmüller, R. S. Ødegård, G. Vatne, R. S. Mysterud, T. Tonning, and J. L. Sollid, Glacier characteristics and sediment transfer system of Longyearbreen and Larsbreen, western Spitsbergen. *Norsk Geografisk Tidsskrift–Norwegian Journal of Geography*, **54**, 157–168 (2000).

Identifying and Dating Remains of Pond Dams in River Valleys (Southern Poland)

Paweł Rutkiewicz[1, a)]

[1]Department of Reconstructing Environmental Change, Faculty of Earth Sciences, Będzińska 60, 41-200 Sosnowiec, University of Silesia in Katowice, Poland.

[a)]Corresponding author: rutkiewiczpawel33@gmail.com

Abstract. The main aim of this study was to identify and determine the age of the former pond dams in river valleys, using GIS tools and radiocarbon dating of organic matter from the dams and then to compare the results with historical sources. Additional goals were to examine the internal structure and morphometry of selected dams. As a first step we studied historic maps. Next, data sheets from aerial laser scanning were obtained. When we had identified the locations of dams damming the bottoms of the valleys, field verification was undertaken and the study sites were designated. During the field studies, each dam was expose. Samples for radiocarbon dating were taken from layers that contained organic matter. Radiocarbon dates of charcoal found in the dams indicate the origin of these structures, in three cases from the Middle Ages, in one case from the Roman period and in one case from the modern period. The radiocarbon dates obtained correspond well with historical data. In some cases radiocarbon dates can serve as indications that the smelting plant may have been established earlier than historical sources suggest. The variability of the layers visible in the dam profiles indicates the modernisation or destruction of these structures.

STUDY AREA AND AIM OF STUDY

The study sites are located in three river basins in southern Poland. The Kalety, Cynków and Koszęcin / Nowy Dwór sites are located in the Mała Panew river basin (Fig. 1), the Furmanów site is located in the Czarna river basin (Fig. 1), while the Bąków site is located in the Stobrawa basin (Fig.1). The Czarna River lies in the River Vistula basin. It is 87.9 km long and the mean annual discharge is 6.04 [m^3/s]. The Czarna is a sand-bedded, meandering river which drains 972.6 km^2 of the Małopolska Upland with a bedrock of Triassic-Jurassic sedimentary rocks (containing iron ores – clayey siderites) that is covered by Quaternary loams [2,10]. The Mała Panew is a right bank tributary of the River Oder. It is 132 km long and the mean annual discharge is 8.97 [m^3/s]. The Mała Panew drains 2037 km^2 of the Silesian Upland and Lowland covered with Quaternary sands. It is a meandering, sand-bedded river flowing through forested areas [6,12], with large amounts of coarse woody debris in the channel, the catchment area has been changed by human activity both past and present [3, 4, 13, 14]. The Stobrawa River is a right bank tributary of the River Oder. It is 80.2 km long and the mean annual discharge is 5.12 [m^3/s]. The Stobrawa drains 1586 km^2 of the Silesian Lowland. The substrate is dominated by sands, glacial and fluvioglacial gravels, and holocene muds as well as aeolian sands in dunes [1].

The main aim of this study was to identify and determine the age of the former pond dams in river valleys, using GIS tools and radiocarbon dating of organic matter from the dams and then to compare the results with historical sources. Additional goals were to examine the internal structure and morphometry of selected dams.

MATERIALS AND METHODS

As a first step we studied historic maps available online and historical literature in order to know the calendar dates or century of origin of the former metallurgical centres and their location. Next, data sheets from aerial laser scanning were obtained as .asc files with LiDAR data (0.2 m spatial resolution). Interpolated airborne laser scanning (LiDAR) data was obtained from the Central Office for Geodetic and Cartographic Documentation (CODGiK) in Poland. DEMs were created based on the LiDAR data. On the basis of the Digital Elevation Models that were prepared,

an analysis was made of the valley bottom and its tributaries including areas from the source of the selected rivers to their outlets. When we had identified the locations of dams damming the bottoms of the valleys, field verification was undertaken and the study sites were designated. In the end, five former pond dams were selected for further study.

During the field studies, each dam was exposed to a depth just below the current level of the valley bottom, depending on the level of the groundwater. Comparison of the current ground level on which the dam is located with the profile of the material in the dam allowed the authors to determine the boundary between the natural sediments and anthropogenic material. From the layers in the dam profile, samples of mineral material were taken. If the thickness of a single layer exceeded 70 cm, two samples were taken from various depths. Sampled material was sifted using a Vibratory Sieve Shaker to determine the basic fraction of the material used for the construction of the dam. Samples for radiocarbon dating were taken from layers that contained organic matter. The charcoal particles available were mostly relatively small (often <1 mm). Radiocarbon dating was undertaken by the Silesian University of Technology, Gliwice, Poland (laboratory code: GdA and GdS) and by the Laboratory of Absolute Dating, Kraków, Poland (laboratory code: MKL). Four organic samples (charcoals) were submitted for 14C AMS (accelerator mass spectrometry) dating and three organic samples were submitted for 14C LSC (liquid scintillation counting) dating. The 14C absolute ages were calibrated with the OxCal v4.2.3 program [19] using the calibration curve IntCAL13 [21].

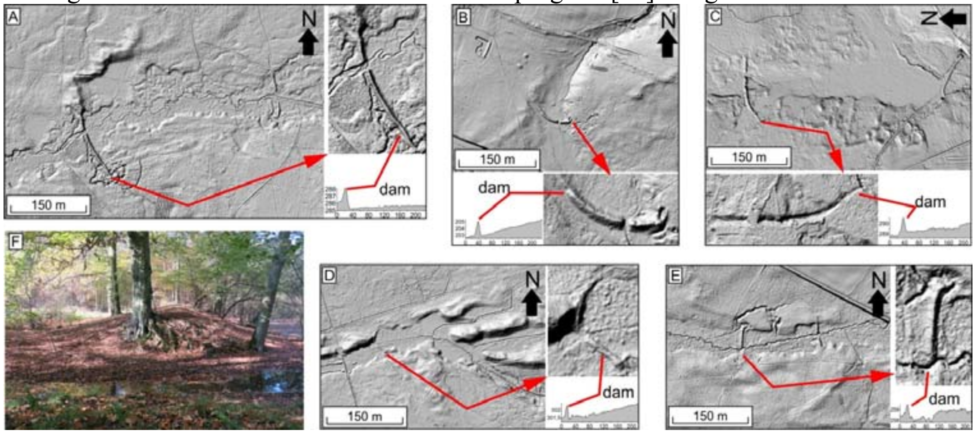

FIGURE 1 Shaded relief models for the following study sites: A - Kalety, B - Bąków, C - Furmanów, D - Cynków, E - Koszęcin / Nowy Dwór; enlarged view of the dam and longitudinal profile through the valley bottom and the selected dam; F - example of dam visible in the field (Bąków study site).

RESULTS AND DISCUSSION

The dam on the Kalety site with a length of 280 m and a width of 20 m, was built on fine sands on the bottom of the Mała Panew river Valley (Fig. 1A). The profile of the dam material is characterised by the occurrence of four main layers of sand of different colour (Fig. 2). The fine-grained sand fraction is dominant. At a depth of 130-140 cm, a layer of fine charcoal is present. The material taken from this layer was dated at 68 – 250 cal AD (95.4 %); (Fig. 2).

The dam at the Koszęcin/Nowy Dwór site is 125 m long and 15 m wide, and was built on medium and fine-grained sands in the valley of a Mała Panew tributary (Fig. 1E). From a depth of 150 cm to a depth of 45 cm there is a layer of light yellow sand, which is separated by a two-centimetre layer of charcoal (149 - 147 cm). This layer composed of charcoal was dated to 1206 – 1276 cal AD (95.4 %). From the depth of 45 cm to 25 cm there is another layer of sands of a light grey colour (Fig. 2). The dam at the Cynków site is 120 m long and 12 m wide and is located on medium and fine-grained sands of the Mała Panew river valley bottom (Fig. 1D). It is made of medium and fine-grained sands, containing small pieces of charcoal (80 – 10 cm). A sample composed of charcoal pieces from a depth of 60-70 cm was dated to 1294 – 1406 cal AD (95.4 %) (Fig. 2). There is a historical reference to dam and iron pond located somewhere in Kalety and Cynków but without precise location and time of construction. Goszyk [8] informs us that, in a document from 1454, ponds which were supposed to function for the needs of iron forges are mentioned in this area. Later they were destroyed as a result of wars and they were not rebuilt. Dating of the dam at the Cynków site at 1294-1406 cal AD (95.4%) correlates well with this information. It can be assumed with high probability, therefore, that the dam was built in the 14th century. In the case of the Kalety site, the dam was dated at 68-250 cal AD (95.4%). This excludes the possibility that it was created for the production and processing of iron using a water wheel. Later, it could be used for the purposes of an ironworks or a mill. The interchangeable use of the same pre-

existing dams for different practices was a common feature in the past. Watermills appeared in Poland in the late 11th and early 12th centuries, and became widespread in the 13th century [7]. However, there are no reports of building dams on the territory of present-day Poland in the late Roman period. The oldest bloomery or other evidence of iron metallurgy in the mouth section of the Mała Panew valley has been documented archaeologically in ten sites of the Przeworsk culture (late Roman period, 2-4 century AD) [16]. The beginnings of metallurgy using water power are noted in the 14th and 15th centuries in a poem on the history and technique of Silesian metallurgy and iron ore mining "Officina ferraria (...)" by Roździeński (1612) [16]. Dating of the dam from the Cynków site at 1294 - 1406 cal AD (95.4%) confirms this information. However, the very accurate result of dating of the dam at the Koszęcin/Nowy Dwór site (1206 - 1276 cal AD (95.5%)) may indicate a slightly earlier moment for the beginning of this type of activity in this area. Unfortunately, this construction is anonymous from the historical point of view.

The dam at the Furmanów site is 270 m long and 18 m wide and was built on the sands on the bottom of the Czarna Valley (175 – 163 cm) (Fig. 1C). The profile can be divided into 7 layers of fine-grained sand. Three of these contained large amounts of charcoal and were dated consecutively to: 1665- present cal AD (95.4%), 1697 – 1930 cal AD (95.4%) and 1695 – 1940 cal AD (95.4%) (Fig. 2). According to the historical description [21], in 1830-1835 a large charcoal blast furnace was built in Furmanów. A reservoir was created in the Czarna Valley and water-power was used to power the metallurgical machinery, production ceased in 1907. The results of the three radiocarbon dates from the Furmanów site suggest the young age of the dam.

The dam at the Bąków site is 145 m long and 18 m wide and was built on sandy sediments with an admixture of silty and clay sediments (Fig. 1B). Four main layers of fine-grained sands of different colours with a significant share of silt-clay sediments can be distinguished in the profile of the material that forms the dam. At a depth of 110 - 100 cm, there is a lens of charcoal (Fig. 2). Dating of this charcoal has allowed the authors to determine its age to 1406 - 1451 cal AD (95.4%). Fragments of slags and green enamel found next to the dam as well as the presence of charcoal hearth remains clearly indicate the functioning of this dam for the purposes of a metallurgical plant. There are no documents or historical records regarding a forge or steelworks in Bąków. However, several kilometres to the northeast of the site investigated, two strongholds have been identified dating back to the 13-14th century [5].

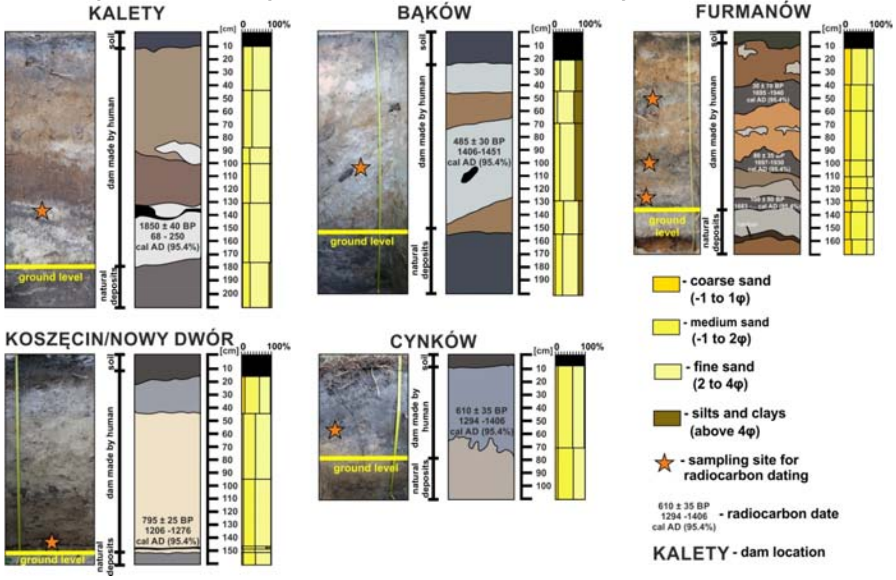

FIGURE 2 Field photographs of the dam exposures with sediment characteristics and interpretations.

According to historical sources, there was intense development of ferrous metallurgy using water power on Polish lands from the 14th century onwards [15, 18]. It is known that charcoal can be used successfully to determine the rate of sedimentation and for sediment dating, as well as for dating old fires [e.g.: 9, 11]. In the case of the dams surveyed, charcoal was found in some layers of the deposits forming the dams. Charcoal could be found inside the dams as a result of the felling of trees and burning the area before the work started. Such a mechanism of human action is presented by Wistuba et al. [17, 22] and Wistuba [23], in her work on Wallachian settlements in the Carpathian area.

CONCLUSIONS

Dating of charcoal samples from the deposits inside the dams allows one to determine the age of these structures. The use of GIS tools in conjunction with field verification made it possible to identify old, sometimes unrecognised, dams. Radiocarbon dates indicate the origin of these structures, in three cases from the Middle Ages, in one case from the Roman period and in one case from the modern period. The radiocarbon dates obtained correspond well with historical data or provide new information on previously unknown structures, as well as supplementing and confirming historical sources. In some cases radiocarbon dates can serve as indications that the smelting plant may have been established earlier than historical sources suggest. The variability of the layers visible in the dam profiles indicates the modernisation or destruction of these structures.

ACKNOWLEDGMENTS

This study was performed within the scope of the research project no. 2017/25/N/ST10/01876 funded by the Polish National Science Centre (NCN).

REFERENCES

1. D. Absalon, A.T. Jankowski, M. Leśniok, "Komentarz do mapy hydrograficznej w skali 1:50 000 Arkusz M-34-37-A Kluczbork", Uniwersytet Śląski, 1998.
2. D. Absalon, "Changes in water quality in the Upper Wisła (Vistula) River Basin", 2nd International Conference on Environmental and Computer Science, ICECS, 29-32 (2009).
3. D. Absalon, B. Ślesak, Ecotox Environ Safe. **74** (4), 967-973 (2011).
4. D. Absalon, B. Ślesak, Pol J Environ Stud., **21** (2), 235-239 (2012).
5. Z. Bagniewski, „Wyniki badań sondażowych na grodziskach w powiecie Kluczbork", Terenowe badania archeologiczne na Opolszczyźnie, rok 1970," Opole, 1970.
6. D. Ciszewski, and I. Malik, Geomorphology, **58**, 161-174 (2004).
7. M. Fajer, Environ. Socio-Econ. Stud. **6**, 25–37 (2018).
8. E. Goszyk, "Miotek i Zielona: zarys dziejów wsi", Miotek, 2016.
9. W. Hubau, J. Van den Bulcke, K. Bostoen, B.O. Clist, A.L. Smith, N. Defoirdt, H. Beeckman, Veg. Hist. Archaeobot., **23**(5), 591-606 (2014).
10. I. Jurkiewicz. "Szczegółowa mapa geologiczna Polski 1:50 000 Arkusz Radoszyce", map, PIG, 1965.
11. K. Kaiser, L. Opgenoorth, W. H. Schoch, G. Miehe, Quaternary Sci Rev. **28**(15-16), 1539-1554 (2009).
12. I. Malik, Dendrochronologia **23**, 29–38 (2005).
13. I. Malik, Earth Surf. Process. Landf. **31**(10), 1227-1245 (2006).
14. I. Malik, M. Danek, E. Marchwińska-Wyrwał, T. Danek, M. Wistuba, and M. Krąpiec, Water Air and Soil Pollut., **223**: 3345-3364 (2012).
15. I. Malik, M. Wistuba, M. Opała, M. Franek, B. Woskowicz-Ślęzak, G. Mańczyk, C. Tyrol, Geochronometria, **42** 79-90 (2015).
16. R. Niedźwiedzki, "Od żelaza do silezaura. Historia górnictwa i odkrycia kręgowców triasowych w Krasiejowie," in *Krasiejów—Palaeontological Inspiration*, editet by E. Jagt-Yazykova, J. W. M. Jagt, A. Bodzioch, D. Konietzko-Mejer, (ZPW Plik, Bytom, 2012), pp. 6-27.
17. T. Papciak, I. Malik, K. Krzemień, M. Wistuba, E. Gorczyca, D. Wrońska-Wałach, M. Sobucki, Bulletin of Geography. Physical Geography Series **8**, 5-17 (2015).
18. P. Rutkiewicz, I. Malik, M. Wistuba, A. Osika Quatern Int., **512**, 133-143 (2019).
19. C. B. Ramsey, Radiocarbon **55**(4), 2021-2027 (2013).
20. P. J. Reimer, E. Bard, A. Bayliss, J.W. Beck, P.G. Blackwell, C.B. Ramsey, P.M. Grootes, Radiocarbon **55**(4), 1869-1887 (2013).
21. F. Sulimierski, B. Chlebowski, W. Walewski, "Słownik geograficzny Królestwa Polskiego i innych krajów słowiańskich," Warszawa, 1895.
22. M. Wistuba, "Slope-Channel Coupling as a Factor in the Evolution of Mountains. The Western Carpathians and Sudetes", Springer Verlag, 2014.
23. M. Wistuba, A. Sady, G. Poręba, Catena **160**, 10-23 (2018).

Examination of Fresh Water Chemistry in Maritime Antarctica during Austral Summer 2017

Małgorzata Szopińska[1, a)], Marek Ruman[2, b)], Robert Bialik[3, c)]
and Żaneta Polkowska[4, d)]

[1]*Gdansk University of Technology, Faculty of Civil and Environmental Engineering, Department of Water and Waste Water Technology, Gabriela Narutowicza 11/12, 80-233 Gdansk, Poland*
[2]*University of Silesia in Katowice, Faculty of Earth Sciences, Bedzinska 60, 41-200 Sosnowiec, Poland*
[3]*Institute of Biochemistry and Biophysics, Polish Academy of Science, Pawińskiego 5a, 02-106 Warsaw, Poland*
[4]*Gdansk University of Technology, Department of Analytical Chemistry, Faculty of Chemistry, Gabriela Narutowicza 11/12, 80-233 Gdansk, Poland*

[a)]Corresponding author: malgorzata.szopinska@pg.edu.pl
[b)]marek.ruman@us.edu.pl
[c)] rbialik@ibb.waw.pl
[d)]zanpolko@pg.edu.pl

Abstract. Due to the fact that Antarctica is one of the least polluted places on Earth, it is a perfect place to observe the spread of global pollution. Therefore, research conducted on this continent is important due to the possibility of investigating the type of pollution and their way of transport. This work considers presence of organic contaminants in Maritime Antarctica in unexplored until now, Lions Rump headland. Qualitative and quantitative analysis of samples were carried out in order to determine the content of analytes such as polycyclic aromatic hydrocarbons (PAHs). Among all determined PAHs in water samples the highest concentrations was observed for naphthalene and anthracene, which is the result of their higher volatility in comparison to the High Molecular Weight PAHs. The presence of PAHs in the water environment may constitute potential negative effect on Antarctic ecosystem and it should be investigated in detail. Moreover, possibility of undertaking various actions reducing contaminants emission are also very important. We hope that improved fossil fuel economy, and not only on the local scale, would help reduce PAH levels in Maritime Antarctica.

INTRODUCTION

Nowadays, it is difficult to indicate a place free of anthropological impact. Depending on the location, the human impact on the environment is more or less intense. Nevertheless, there are still places on Earth with negligible anthropological activity. One of them is Antarctica. This area has not been subjected to significant anthropogenic changes due to the extreme climatic conditions occurring in this area. Such place as Antarctica is an extraordinary source of information about the processes taking place in the environment. However, it should be remembered that it is not possible that those areas would be deprived of anthropological impact due to the occurrence of global anthropression.

Currently, there are many articles about the anthropogenic pollution found in the Antarctica region. The first research and, consequently, articles about pollutants founded in this part of the world come from the second half of the twentieth century. Researches payed attention on abiotic elements such water, snow and air or contaminations found in biotic elements. Researches include both in-organic and organic contaminations. For example, since the 1960s, researches on the presence of pollutants from the group of persistent organic pollutants (POPs) has been undertaken. The presence of pollution in a place like Antarctica is associated with various processes. Thus, for example

semi-volatile and volatile compounds may reach Antarctica together with air masses moving in this direction. This kind of air mass transport is called long-range atmospheric transport (LRAT). However, more attention has been paid to determine of local impact on Antarctic environment associated with the occurrence of many research stations. Due to increasing factors affecting the pollution level, monitoring of different types of pollution has become an important aspect of researches in this region. Special attention in terms of monitoring of the environment merits specially protected areas. There are 72 of Antarctic Specially Protected Areas in Antarctica. These areas have been selected and covered by a special protection for various reasons. Some of them have a rich flora or fauna and they are a valuable place for scientists, others are important for historical or aesthetic reasons. In this study water samples from two protected areas were tested. Both areas ASPA 128 and ASPA 151 are protected for many reasons, but the most important is the presence of many species of birds and penguins in these region.

In this work presence of polycyclic aromatic hydrocarbons (PAHs) found in water samples collected on King George Island, the largest island in the South Shetland, is discussed. These samples of surface water were taken on Lion Rumps headland. Furthermore, this type of study has never been conducted in ASPA No. 151 and its surroundings, hence our findings will have great value for this local Antarctic environment.

SAMPLING

Sampling campaign have been performed during the austral summer 2016/2017. The water samples were collected manually into plastic containers of 1L volume. After collection, all samples were transported to the H. Arctowski Antarctic Station Laboratory and stored frozen at -20°C, and then transported under unchanged temperature conditions to Poland. The specific regions of sampling are shown in Fig.1

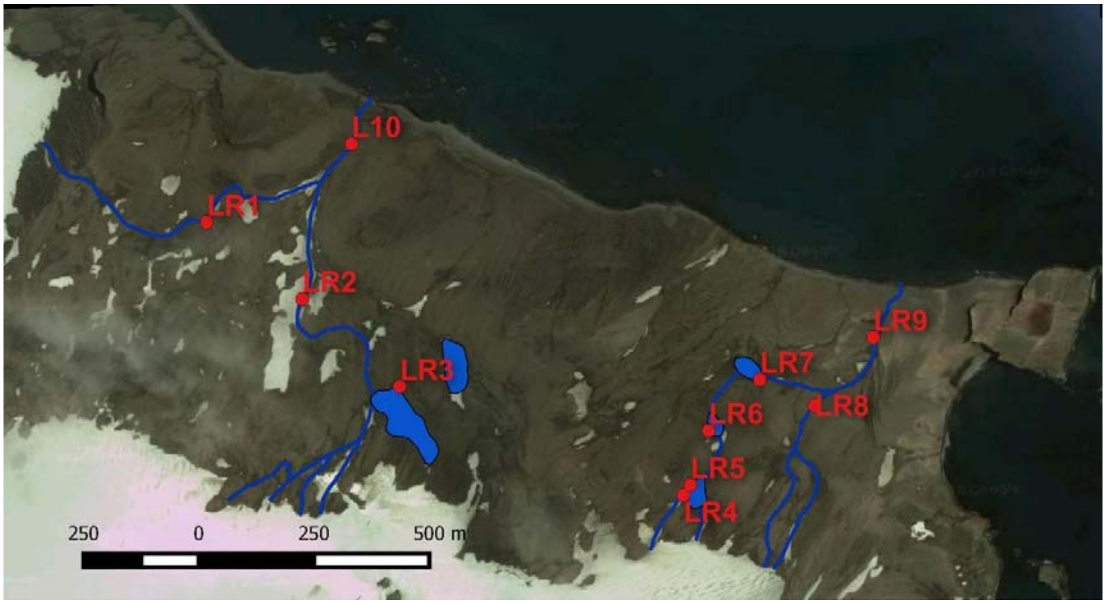

FIGURE 1. Location of sampling points on Lion Rumps headland.

Polycyclic aromatic hydrocarbons (PAHs, ngL^{-1}) were identified and quantified with the use of gas chromatography coupled with single quadrupole mass spectrometer (GC-MS) – Agilent 7890A system (Agilent Technologies, USA). The determination of selected PAHs was performed based on the internal standard calibration method. Before extraction surrogate standards has been added.

RESULTS AND DISCUSSION

Despite its pristine environment, scientific, logistic and touristic activities in the South Shetland Island Archipelago have introduced anthropogenic compounds. Those activities are related to oil storage, fuel combustion, and human waste production. The use of fuel is the main source introducing hydrocarbons into the environment. The principal

Antarctic sources of PAHs are the direct input of fossil fuels and inputs associated with incomplete combustion. Arctic Grade Diesel Fuel is the principle source of energy in Antarctic operations and it consists mainly of semi-volatile aromatic hydrocarbons, including naphthalene and various other non-substituted PAHs containing two or three aromatic rings. However, Arctic Diesel Fuel also has a higher level of complex compounds featuring four or more rings.

The samples were analyzed against the presence of the following compounds, which belong to the PAHs: naphthalene, acenaphthylene, 2-bromonaphthalene, acenaphthene, fluorene, phenanthrene, anthracene, fluoranthene, pyrene, benz[a]anthracene, chrysene, benzo[b]fluoranthene, benzo[a]pyrene, indeno[1,2,3-cd]pyrene, dibenz[a,h]anthracene and benzo[ghi]perylene. The highest concentration was detected in the sample specified by the LR1 and the sample specified by LR4 number. In the first case, a concentration of 18.2 ng/L of anthracene was detected and in sample fourth the same concentration of naphthalene was detected. Whereas, the largest amount of different compounds was detected in the sample described as LR4. Seven of total eight founded compounds are detected in this sample. It is worth to mention, that these above-mentioned samples were collected in the upper part of the watercourse. The most polluted place is the upper part of the watercourse (Fig. 2). As it can be noticed from this figure, the estuaries of the watercourse is also the place where most of the compounds have been detected. On the other hand, lakes and waterfall are the places where the smallest amount of compounds were detected. However, the naphthalene concentration in both lakes and waterfall is similar to concentration of this compound detected in upper part of watercourse and its estuaries.

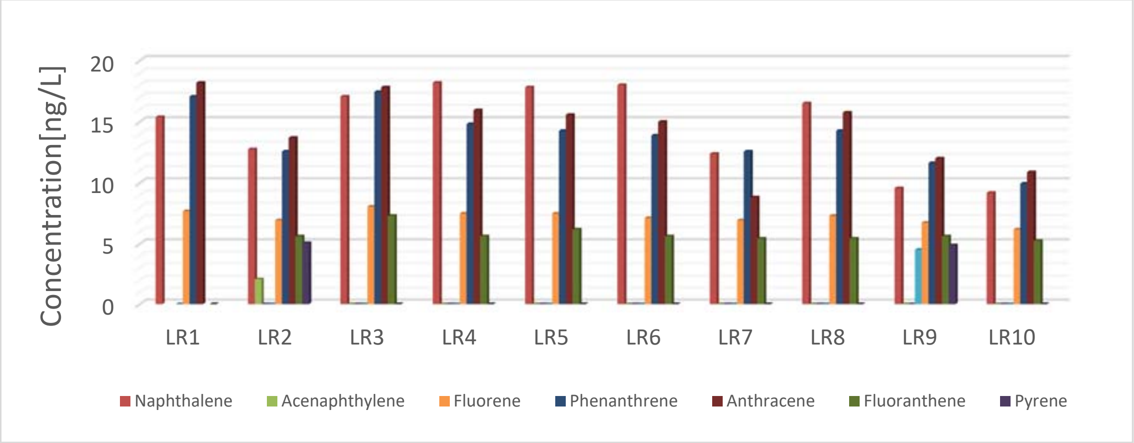

FIGURE 2. Concentration of the individual PAH in the samples taken on Lions Rumps region.

CONCLUSIONS

Antarctica, despite the fact that it is deprived of permanent residents and its localization, which is far away from developed countries, is affected by anthropogenic pollution. Scientists identify pollution across continent that affects biotic elements as well as abiotic elements of Antarctica. Due to the presence of numerous types of pollution in Antarctica, it is necessary to monitor the environment. The issue of monitoring pollution in the Antarctica should be conducted in detail, especially in terms of examination external locations of pollution sources, because they may affect not only Antarctica, but the whole world. Among all determined PAHs in water samples the highest concentrations was observed for naphthalene and anthracene, which is the result of their high volatility. Naphthalene is the most volatile compound of all PAHs, which means that these compounds are relatively easily transported by air (LRAT). It is also worth to noticed that the compounds listed above belong to products of petroleum origin. Thus, their presence may be related to the local activity of a people (the use of fuels on the King George Island). The degradation of compounds from the group of PAH is very difficult due to the low temperature conditions prevailing there. Summer thaws cause release of petroleum products to fresh and marine water. Such products are very dangerous for living organisms that need water to live. Due to the low diversity of flora and fauna in the Antarctica area, PAHs may accumulate in the organisms of such as penguins, fish or fowl. Therefore, their presence may negatively influence indigenous species.

ACKNOWLEDGMENTS

This research has been supported by National Science Centre Poland project (MINIATURA2) entitled: 'Recognition and selection of pollution markers introduced into Admiralty Bay via wastewater discharge: An example from Arctowski Polish Antarctic Station. King George Island. Maritime Antarctica'. Agreement no. DEC-2018/02/X/ST10/01539

REFERENCES

1. Szopińska, J. Namieśnik and Ż. Polkowska, How important is research on pollution levels in Antarctica? Historical approach, difficulties and current trends, Rev. Environ. Contam. Toxicol. **239**, 79–156 (2017).
2. T. Combi , C. C. Martins , S. Taniguchi, J. Leonel, R. A. Lourenço and R. C. Montone, Depositional history and inventories of polychlorinated biphenyls (PCBs) in sediment cores from an Antarctic Specially Managed Area (Admiralty Bay, King George Island); Mar. Chem., **118**, 447-451 (2017).
3. M. Vecchiato, E. Argiriadis, S. Zambon, C. Barbante, G. Toscano, A. Gambaro, R. Piazza, Persistent Organic Pollutants (POPs) in Antarctica: Occurrence in continental and coastal surface snow, Microchemical Journal, **119**, 75-82 (2015).
4. Ż. Polkowska, K. Cichała-Kamrowska, M. Ruman, K. Kozioł, W. E. Krawczyk and J. Namieśnik, Organic Pollution in Surface Waters from the Fuglebekken Basin in Svalbard, Norwegian Arctic. Sensors, **11**, 8910-8929 (2011).
5. J. Potapowicz, D. Szumińska, M. Szopińska, Ż. Polkowska, The influence of global climate change on the environmental fate of anthropogenic pollution released from the permafrost. Part I. Case study of Antarctica, Science of the Total Environment **651**, 1534–1548 (2019).

Climate Change Driven Events and Projects' Vulnerability as Element of the EIA Procedure –Application of the IAEA STE Selection Criteria

Robert Urbaniak[1,2,a)] and Damian Absalon[1,b)]

[1]*University of Silesia in Katowice, Faculty of Earth Sciences, Będzińska 60, 41-200 Sosnowiec, Poland*
[2]*PGE EJ1 Ltd., Mokotowska 49, 00-542 Warsaw, Poland*

[a)]Corresponding author: Robert.Urbaniak@gkpge.pl
[b)]damian.absalon@us.edu.pl

Abstract. There is a clear cause-and-effect interaction at play between environment and the project itself that acts two-way, making the project's suitable site selection of utmost importance. As general public becomes more and more aware of environmental issues that need to be addressed in the course of licensing procedures (Environmental Impact Assessment [EIA]) many aspects that can affect a planned development's site suitability remain hidden from the public view and yet crucial as they can determine investment's not only impact spatial boundaries but even its viability. Determination of a planned development's location, therefore, should be preceded by detailed siting and environmental studies completing of which guarantee removal or at least occurrence probability reduction from a financial equation of significant uncertainties that could impact an investment at either the designing or operating stage. In the paper application of conventional energy sector methodologies as well as site selection criteria of the Safety Standards, International Atomic Energy Agency [IAEA] for nuclear installations as mutually complementing tools are being discussed with a special consideration given to climatic, geological and legislative issues.
Keywords: Siting Process, Environmental Impact Assessment, Climate Change, exclusionary and avoidance criteria.

INTRODUCTION

An interaction between any infrastructural project and the environment, be it negative when a particular environmental quality standard is affected as a consequence of the project's realisation or operation stage or positive when the project's development brings tangible benefits to the environment (e.g. reductions in emission levels of CO_{2eq} or relieving densely populated urban area of heavy traffic) is unquestionably a matter of fact.

This inseparable two-way relationships of human activities and their consequences seen in the environment were known since a long time. However, dwindling natural resources, deteriorating quality of the environmental components (air, water and land), incessant world's population growth and most recently extreme weather events frequency increase consequently disrupting life of millions of people created unprecedented push towards revision of our relationship with nature.

LEGISLATION

A need, however, to address already glaring and no-longer-possible-to-be-ignored issue of negative anthropogenic environmental impacts associated with construction and operation of big infrastructural investments formally appeared in European Union ['EU'] only in 1985 when the first piece of legislation and the most important one at that came into force - the Council Directive 85/337/EEC of 27 June *1985 on the assessment of the effects of certain public and private projects on the environment* [OJ L 175, 5.7.1985, p. 40–48] ['EIA Directive'] [1].

Reasons behind recognizing on the part of contemporary policymakers of a need for formulating legislation that would facilitate standardization of approach in impact assessment of private and public projects on the environment had been a need of transferring and implementation of the relevant technical information into the consecutive stages of the project development, i.e. the site licence and the construction permit.

Introduction of the EIA Directive with its planned developments assessment classification thresholds (Annex 1 and 2 of the Directive) and specific requirements concerning of the Environmental Impact Assessment report's (Annex 3 of the Directive) ['EIA report'] content was preceded by numerous attempts of forming a prevalent EU system enabling an application of uniform methodology throughout EU states in regard to projects' environmental impact assessment.

First United Nations Conference on the Environment in Stockholm were held in 1972 during which Declaration, known as Stockholm Declaration containing 26 principles concerning the environment and sustainable development was agreed upon setting into motion events that eventually lead to creation of the EU Environmental and Consumer Protection Directorate and formation, via the Environmental Action Programme [‘EAP’] as a way of forwarding environmental issues into the mainstream, of so much needed environmental legislation –the EIA Directive.

Subsequently, the European Community adopted several Programmes setting out the principles and priorities that would guide its environmental policies into the future with the most recent, the 7th EAP, guiding environmental policies until 2020, while outlining a prospect of long-term direction for “*a safe and sustainable global society*” [2].

The EIA as a principal instrument of the EU environmental policy to reflect continuously changing marketplace requirements and also to accommodate other legislative changes had to be amended several times–since the adoption of the first EIA Directive in 1985 with the latest codified version amended by Directive 2014/52/EU. The changes, amongst others related to investments weather robustness assessment, brought by the latest amendment were to be transposed into national legal systems of Member States, including Poland, by May, 16th, 2017. Poland fulfilled the requirement. The list of new factors to be considered in EIA reports form now onwards would reflect deeper understanding of interactions between a project and its direct and indirect environmental factors through considerations given particularly to climate change and risk assessment of major accidents and disasters occurrence probability. As much as impact assessment in respect to e.g. air pollution estimates of planned developments through use of appropriate mathematical modelling tools weren’t anything new for EIA practitioners nor involved in the process engineers, existing and planned investments sensitivity assessment to weather conditions and other weather and man induced events turned out to be particularly challenging.

To help develop a common understanding and approach in April 2013, the European Commission adopted the EU *Strategy on adaptation to climate change* [3], which set out a framework for the EU preparation to climatic impacts on infrastructure. In order to facilitate free access to information to support policy-makers at the EU, national, regional, and local levels in this regard the European Climate Adaptation Platform (CLIMATE-ADAPT) as a web-based platform was established. The database comprises a number of documents on every aspect of climate related aspects imaginable from which the Commission Staff working document entitled *Adapting infrastructure to climate change* [4], as well as *Guidelines for Project Managers: Making vulnerable investments climate resilient* (DG Climate Action, Non-paper) [6] in regards to climate change issues are of particular importance.

In regards to impacts related to risks of major accidents and disasters Annex IV of the EIA Directive of 2014 contains direct reference to accidents and disaster risks in two provisions effectively correlating with climatic hazards and their potential impact and its consequences on the project.

The need to build ‘*resilience to natural and man-made disasters*’ [5] and to invest in risk prevention is envisaged in several EU strategies and proposals as well as the Seveso III Directive *on the control of major-accident hazards involving dangerous substances* or the Directive *establishing a Community framework for the nuclear safety of nuclear installations* in a case of which International Atomic Energy Agency [‘IAEA’] Safety Standards are of particular importance.

INVESTMENT VULNERABILITY ASSESSMENT

The [5] provides an instrument enabling assessment of a project’s vulnerability to climatic and other, especially site related hazards. The document puts special emphasis on the site selection process due to climate change site related uncertainties, inter alia in the energy sector. The [5] toolkit comprises 7 modules providing methodologies which can be successfully applied at every stage of project’s development (Fig. 1). Application of modules in conventional asset lifecycle process with other detailed processes and analysis carried out at each stage of project development i.e. feasibility study, site and technology selection, EIA, Front End Engineering Design [FEED] guarantees that climatic aspects are appropriately addressed in the site related design basis -FEED.

A similar approach is applied in the IAEA’s siting process in which through application of a series of activities a suitable site is selected (Stage 1 – Siting Process) that in order to confirm its suitability to host a nuclear installation undergoes a site evaluation process (Stage 2 – Site Evaluation Process) [6].

Application of exclusionary and discretionary criteria at the early stage of the Siting Process in regional analysis and screening leads to the evaluation, comparison and ranking analysis. The analysis outcome is selection of preferred candidate sites (usually one or two) for which an invasive field works will be carried out at the Site Evaluation Process.

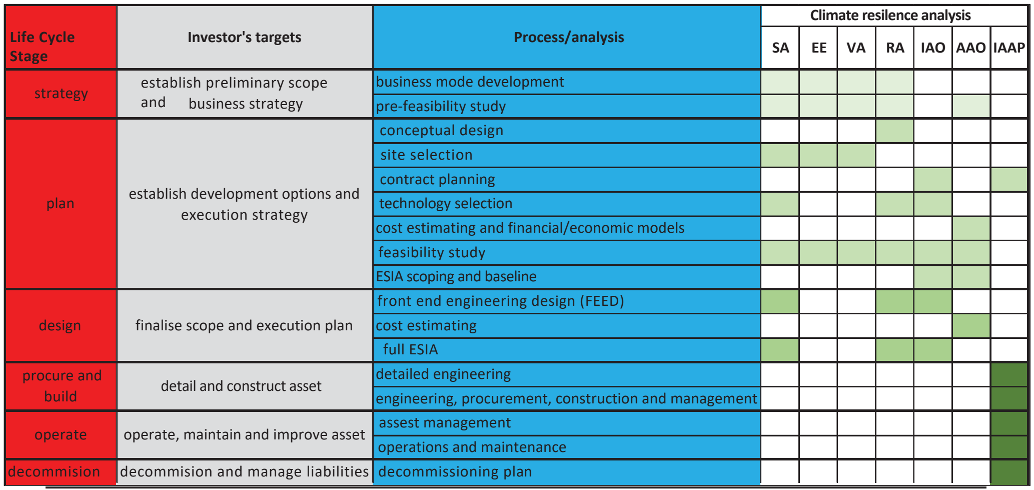

FIGURE 1. Integration of climate resilience into a conventional asset lifecycle

Source: Non-paper Guidelines for Project Managers: Making vulnerable investments climate resilient, EC, 2003, contract no. 071303/2011/650951/SER/CLIMA.C3

The process involves a site verification stage, in which site's suitability is confirmed according to exclusionary criteria and a site confirmation stage, in which site's necessary characteristics for further, safety related analysis and site related design parameters derivation are conducted. Unquestionable importance of this stage is further upheld by the fact that application of exclusionary and discretionary criteria (past, present and potentially future events and phenomena, including meteorological and hydrological causing despite engineering solution in place, unacceptable risk to the installation).

DISCUSSION

Following the [5] (Fig. 1) the first three stages of the asset life cycle, namely strategy, plan and design, identify through SA, EE, VA as well as RA analysis the most crucial aspects of a project's prospective success, one of which will be appropriate site selection that takes into regards site related climatic hazards especially in those locations that are climatically vulnerable-shores, rivers, flood plains i.e. the usual locations of the electricity generating installations.

A need to, via engineering measures, address site-related characteristics among which weather extremes (hurricanes, inundations, blizzards, droughts, storm surges, etc.) and other fixed inputs (capable faults, slope instability, soil liquefaction, subsidence, uplift, collapse, etc.) based not only on historical and purpose-driven (site evaluation/verification and environmental baseline data collection programme) investigated records provides for investments safety and is based on worst case scenario calculations. This safety standpoint is nowhere more apparent that it is in nuclear energy sector where lifelong safe operation of a nuclear power plant is paramount and became a norm.

However, as much as the sensitivity of the project options to different key climate variables as well as other natural and manmade hazards take into regards, to a certain degree, similar factors for both conventional and nuclear projects level of project's exposure and its subsequent vulnerability (modules 2 and 3) the assessment, and especially datasets, are much different. Based on sector standards, well established in the nuclear industry codes of practice as well as legislative requirements, not only past records, be it meteorological, geological or seismological, are gathered and reviewed but in order to accomplish the siting process [6] a use of an increasingly detailed process of field data collection and analysis (deterministic and probabilistic methods alike are used) is necessary. Projects sensitivity to climatic variables, form high (possible significant impact on assets) through medium to having no effect on the project [5] is further developed in module 2 where projects exposure assessment to baseline (regional analysis) and future primary and secondary climatic conditions and related hazards are analysed. Regional analysis carried out in relation to conventional projects that eventually through application of detailed vulnerability and risk assessment tools like: Magnitude of Consequence Table, Risk Register or Risk Matric [5] leads to final stages of the infrastructure climate vulnerability assessment (modules 5-7) of identification, implementation and appraisal of financial and technical feasibility of adaptation options. At European level in different infrastructure sectors standards such as TEN-E Guidelines for trans-European energy infrastructure or Eurocodes are applied to address climate related issues. As much as TEN-E Guidelines focus on application of mitigation as well as adaptation measure in relation to new and existing investments within the energy sector Eurocodes produced by the European Committee for Standardisation

(CEN) constitutes a set of European Standards for the structural design of buildings and civil engineering works that are to provide "*for compliance with the requirements for mechanical strength, stability and safety as basis for design and engineering design specifications"* [5]. Application of technical standards is particularly evident in CEN Guide 4 guidelines "*Guide for the inclusion of environmental aspects in product standards*" which aim to provide a help for professional involved in the environmental licencing processes but are not environmental experts. Special emphasis on the environmental aspects of new- and existing investments' results from the fact that the EIA itself and its place within the licencing procedure is best suited to incorporate relevant aspects of the project design that gives appropriate considerations to climate and natural as well as human made hazards. This particular element is reflected in regards to nuclear installations in the Preliminary Safety Analysis report of the Siting Process [6] a step in which it is demonstrated that the site related design parameters established through field data collection programme and subsequent calculations performed based upon its results have been appropriately taken into account to guarantee a safe operation of the installation.

CONCLUSIONS

The nuclear industry safety record [7] speaks for itself in regards to the fact that application of siting criteria and well established legislative requirements to new-build and as well as retrofitted existing plants results in the safest operating standard imaginable which is left unchallenged by other sectors which are dogged by issues not only related to accidents happening during the operation itself but more fundamental issues reflected in inappropriate site-related design. The CEN developed technical standards that are be applied to different infrastructure projects to make sure their uninterrupted functioning despite even the most extreme weather and other natural conditions don't necessarily hold true when challenged by reality. Based on the author's personal experience within Polish licensing procedures, disproportionate expectations of the Competent Authorities and possibilities of involved engineers and other professionals e.g. performing prognostic calculations, paints a different picture as technical standards and guidelines at the European level haven't cascaded down yet. The most profound argument in relation to the issue at hand concerns finding an answer to a question of how technical standards that do not constitute a legislative requirement can be implemented into a project if they are to add extra weight to it in financial terms. The matter is additionally compounded by the fact that under the EIA Directive's requirements that had been transposed into Polish legislation climate and disaster related hazards are to be addressed in the relevant documentation - Environmental Scoping Report [ERS] or/and EIA report, and any mitigation, adaptation or organization measures that are to be applied in order to make a project less vulnerable are to be listed in the Environmental Permit. The Environmental Permit, on the other hand, will become a blueprint in this regard for the Construction Permit, so e.g. climatic analysis and innate uncertainties associated with assumed in the calculations emission scenarios (e.g. IPCC SRES B1, A1B or A2) [8] based on wishes of the Authority will lend into the project's cost, which especially if it goes into millions of Euros without a solid legislative requirement, is not enough even for Investor's whose risk appetite is very hard to get satiated. In this context suitable location of a planned development if it is to guarantee risk-free operating of an investment needs to consider wider aspects of the environment and the site via application of exclusionary criteria.

REFERENCES

[1] Council Directive 85/337/EEC of 27 June 1985 on the assessment of the effects of certain public and private projects on the environment [OJ L 175, 5.7.1985, p. 40–48];

[2] Decision No 1386/2013/EU of the European Parliament and of the Council of 20 November 2013 on a General Union Environment Action Programme to 2020 'Living well, within the limits of our planet' [OJ L 354/171, 28.12.2013];

[3] Communication from the Commission to the European Parliament, (…), Strategy on adaptation to climate change, Brussels, 16.04.2013, COM(2013) 216 final;

[5] Communication from the Commission to the European Parliament, (…), Adapting infrastructure to climate change (SWD(2013) 137 final);

[6] Guidelines for Project Managers: Making vulnerable investments climate resilient (DG Climate Action, Non-paper), Brussels, EC, Directorate-General Climate Action;

[7] International Atomic Energy Agency, Site Survey and Site Selection for Nuclear Installations, IAEA Safety Standards Series No. SSG-35, IAEA, Vienna (2015);

[8] World Nuclear Association web site, address: http://world-nuclear.org/information-library/safety-and-security/safety-of-plants/safety-of-nuclear-power-reactors.aspx;

Meteorological Triggers of Landslide Activity and Hazard Analysed from Tree Rings (Central Sudetes, Southern Poland)

Małgorzata Wistuba[1, a)]

[1] *University of Silesia in Katowice, Faculty of Earth Sciences, ul. Będzińska 60, 41-200 Sosnowiec, Poland*

[a)] Corresponding author: malg.wistuba@gmail.com

Abstract. The aim of this study is to check which type of precipitation control the activity of Garbatka landslide (southern Poland, Central Sudeten Mts) from a decadal perspective. In order to achieve aforesaid goal dendrochronological methods of reconstructing landslide activity have been applied. The study has revealed dendrochronology to be an efficient method for determining triggering factors of landslide activity as the method provides long data sets on past landslide activity which are suitable for statistical analyses and comparisons with precipitation record. In case of the Garbatka landslide the oldest dated landslide activity event is 1942. Dendrochronological record has been compared with precipitation record from the nearest gauging station which is available since 1951. Correlation of data on landslide activity and precipitation data has shown that the landslide under study is sensitive to high short-term precipitation totals (up to 5-days) and to extremely long-term precipitation totals (60-days and 90-days). The main factor driving the activity of the landslide under study is total annual precipitation which is characterized by the highest level of correlation coefficient. However, the nature of the relation between precipitation and landsliding is complex.

Keywords: landslide, triggering factor, precipitation, dendrochronology
PACS: 92.40.Gc, 92.40.Ha, 92.40.Pb

THE AIM OF THE STUDY

The role of precipitation as landslide trigger depends on its totals as well as on their temporal and spatial distribution [1]. The relation between mass movements and precipitation has been a subject of many analyses (e.g. [2], [3], [4], [5]) as it is important not only for general understanding of slope dynamics and relief development, but also for managing landslide hazard. However, most of threshold levels of precipitation published so far have been defined based on single catastrophic events of landsliding. Thus, established thresholds may not represent actual pattern of the activity of a landslide. Therefore, the goal of this study is to check which type of precipitation control the activity of selected landslide slope from a decadal perspective. In order to achieve aforesaid goal I have applied dendrochronological methods of reconstructing landslide activity (e.g. [6], [7], [8]). Compared to other methods of landslide study and reconstruction, dendrochronology provides long and precise data sets on past landsliding which can be statistically compared to meteorological data. Due to its merits dendrochronology is growing more and more popular in mass-movement studies, including studies on relief development (e.g. [9], [10], [11], [12], [13]), on triggering factors (e.g. [14], [15], [16]) and studies on mass movement hazards (e.g. [17], [18], [19], [20]).

MATERIALS AND METHODS

The landslide under study (the Garbatka landslide) is located in the Kamienne Mts (max 936 m a.s.l.), a part of Central Sudeten Mts., southern Poland (Fig. 1) which is known for the widespread occurrence of landslide-affected areas [21]. The bedrock of the area is composed of igneous rocks prone to landsliding, including rhyolitic tuff at the

site under study, and sedimentary rocks of late Carboniferous and early Permian age (Fig. 1). The Garbatka landslide under study is a slow-moving flowslide [22], [23]. The landslide tongue fills the valley floor with colluvial package probably up to 10 m thick in the proximal part and thinning to a few metres in the distal, fan-like part (Fig. 1). The mean inclination is c. 10°. The total length of the landslide, from the head scarp to the most distant boulders, is nearly 1 km [23]. The climate of the study area is mountain temperate with mean annual temperature of c. 5ºC and mean annual precipitation total of c. 800 mm [22].

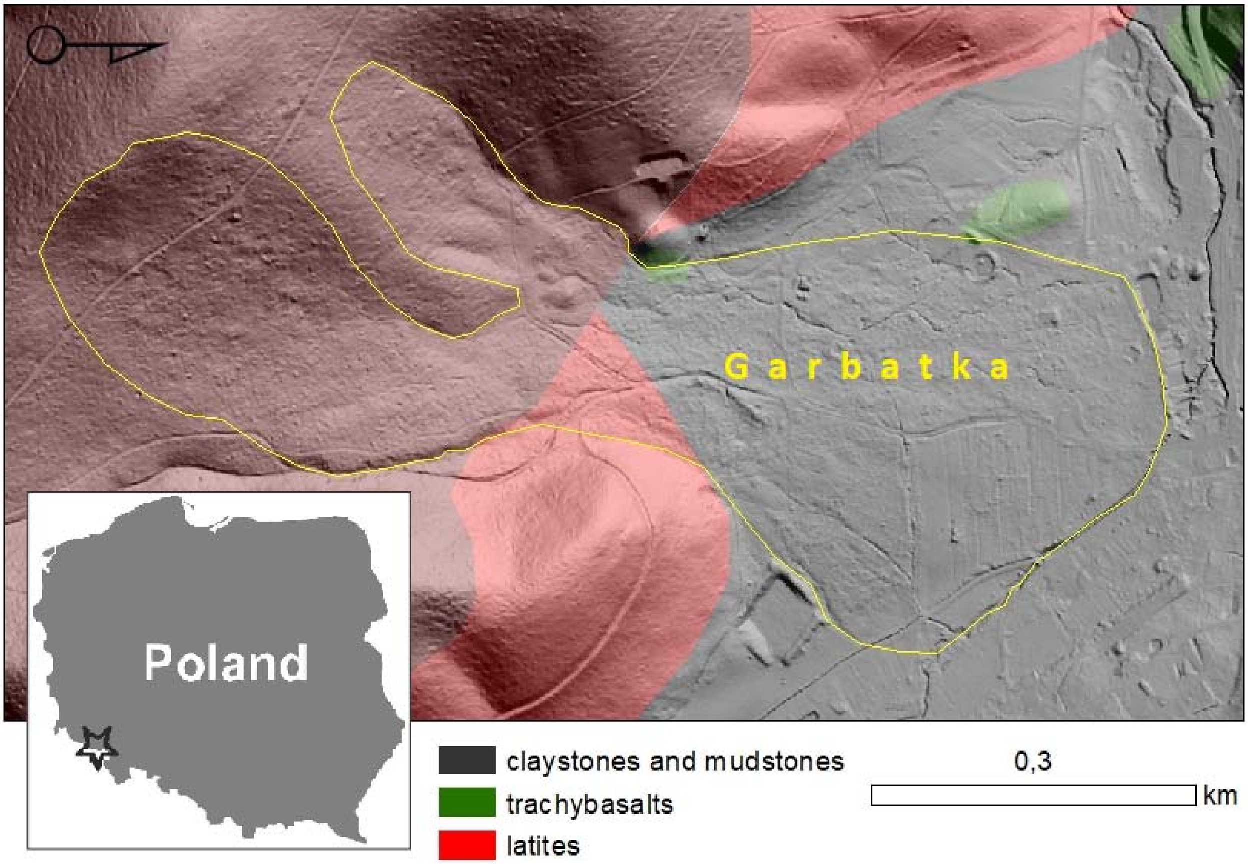

FIGURE 1. Location, relief and bedrock of the landslide under study (landslide outlined in yellow).

For dendrochronological study of landslide activity we have sampled 42 cores from 21 Norway spruce trees (*Picea abies* Karst.) growing on the Garbatka landslide. Two samples were taken from each tree using Pressler borer. Cores were taken at breast height along an axis parallel to slope inclination or to elongation of stem cross-profile (if these were not exactly identical). Only trees without visible loss in assimilation apparatus or stem injuries were sampled. In addition, 20 samples from 10 Norway spruce trees were collected at reference site adjacent to the Garbatka landslide. Altitude, slope inclination, aspect and bedrock of the reference site are similar to the landslide slope, yet it does not show any geomorphic signatures of mass movements.

All dendrochronological samples were glued into wooden holders and polished using sanding paper. Thus, the ring structure of samples was revealed and tree-ring widths in each core have been measured with 0.01 mm precision. Data obtained for the up- and downslope sides of single trees were converted into percent eccentricity index of tree rings and its yearly variation (calculation method after [24]). Samples from the reference site allowed to determine the eccentricity threshold values, i.e. average levels of eccentricity recorded on stable slopes. If the value of a yearly variation index in a given year at the landslide site fell outside the range of reference thresholds, ground disturbance due to landsliding was assumed as the most likely reason for the disturbance in tree growth [24].

Finally, the results of dendrochronological dating have been compared with the precipitation record from Mieroszów weather station available since 1951. Correlation coefficients have been calculated for data sets describing

landslide activity in each year reconstructed from tree rings and precipitation pattern (seasonal totals, max 24-h, 3-day, 5-day, 7-day, 10-day, 20-day, 30-day, 60-day, 90-day totals and number of days with precipitation).

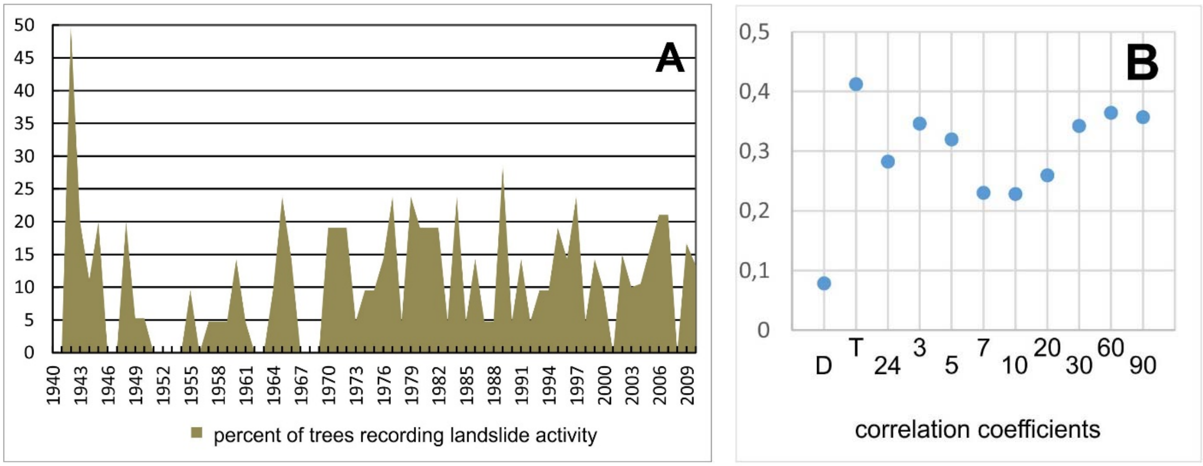

FIGURE 2. The activity of Garbatka landslide reconstructed from tree rings (A) and correlation coefficients calculated for landslide activity and precipitation characteristics (D – number of days with precipitation, T – total annual precipitation, 24 – max 24-h precipitation, 3 – max 3-day precipitation, 5 – max 5-day precipitation, 7 – max 7-day precipitation, 10 – max 10-day precipitation, 20 – max 20-day precipitation, 30 – max 30-day precipitation, 60 – max 60-day precipitation, 90 – max 90-day precipitation).

RESULTS AND DISCUSSION

The oldest dendrochronological indication of landsliding on the Garbatka study site was dated to 1942 (Fig. 2). However, in the detailed analysis of landslide activity we included only the period for which precipitation data are available (since 1951). The greatest per cent of trees disturbed by landsliding in that period was recorded in 1989 (28.60%). Secondary events were recorded in 1965, 1977, 1979, 1984 and 1997 (Fig. 2).

All tested precipitation indicators have positive values which indicates a positive relation between precipitation and landslide activity on the Garbatka study site (Fig. 2), i.e. in general, higher precipitation is connected with more intensive landslide activity. Among precipitation indicators, the highest positive correlation with the activity of the Garbatka landslide has been found for the total annual precipitation (0.41) (Fig. 2). Correlation coefficients 0.35-0.40 were also obtained for: maximum 60-day and 90-day precipitation totals. Correlation coefficients 0.30-0.35 were obtained for maximum 3-day, 5-day and 30-day precipitation. The lowest correlation has been found for the total number of days with precipitation (0.08) (Fig. 2).

The analysis of correlation coefficients calculated for landsliding on Garbatka and 24-h up to 90-day maximum precipitation totals shows that correlation level increases with the length of precipitation from 24-h up to 5-day (Fig. 2). Correlation level decreases for 7-day and 10-day maximum precipitation totals and again increases significantly for 20-day to 90-day maximum precipitation totals (Fig. 2). This indicates that the landslide under study is sensitive to short-term precipitation (up to 5-days) and to extremely long-term precipitation totals (60- and 90-days). Correlation coefficients suggest that both types of precipitation characteristics seem to be important triggers of landsliding on the study site. Results also show that the main factor driving the activity of landslide under study can be the total annual precipitation with the highest level of correlation coefficient. However, due to the fact that several of studied precipitation characteristics present similar correlation with the landslide activity (0.35, 0.36, 0.41) (Fig. 2) determining one dominant trigger is impossible. Also [25] suggests that factors and conditions triggering development of landslides can be complex and include spring thaws, spring and summer precipitation, long-term rainfalls and short, torrential downpours. Even the course of the particular precipitation event is usually complex and it is difficult to determine in an unambiguous manner the thresholds of amount/intensity of precipitation above which geomorphological processes are triggered [1]. The effectiveness of the given precipitation depends also on local relief, vegetation cover, soil type and its humidity in the period immediately preceding the occurrence of the process [26].

CONCLUSIONS

The Garbatka landslide under study is contemporary active showing high frequency of small-scale movements of colluvia. Since 1942 movements of landslide body occurred almost every year but with different strength, affecting different percent of sampled trees.

Increased landslide activity was recorded in tree rings in 1965, 1977, 1979, 1984, 1989 and 1997. The Garbatka landslide under study is sensitive to high short-term precipitation totals (up to 5-days) and to extremely long-term precipitation totals (60- and 90-days). The main factor driving the activity of landslide under study is the total annual precipitation which is characterized by the highest level of correlation coefficient. However, the nature of the relation between precipitation and landsliding is complex.

In addition, dendrochronology has been revealed as an efficient method for determining triggering factors of landslide activity as the method provides long data sets on past landslide activity suitable for statistical analyses and comparisons with precipitation record.

ACKNOWLEDGMENTS

The research was supported by the National Science Centre, Poland through grant no. 2017/26/D/ST10/00792.

REFERENCES

1. T. Papciak, I. Malik, K. Krzemień, M. Wistuba, E. Gorczyca, D. Wrońska-Wałach, M. Sobucki, Bulletin of Geography. Physical Geography Series **8**, 5-17 (2015).
2. N. Caine, Geogr. Ann. A **62**, 1-2, 23-17 (1980).
3. M.T.J. Terlien, Environ. Geol. **35**, 2-3, 124-130 (1998).
4. P. Aleotti, Eng. Geol. **73**, 247-265 (2004).
5. R. Giannecchini, Advances in Geosciences **2**, 21-14 (2005).
6. M. Wistuba and I. Malik, Czasopismo Geograficzne **82**, 4, 401-421 (2011).
7. I. Malik and M. Wistuba, Geochronometria **39**, 3, 180-196 (2012)
8. M. Wistuba, I. Malik, M. Krąpiec, Geochronometria **45**, 1, 223-234 (2018).
9. P. Owczarek, A. Latocha, M. Wistuba, I. Malik, Z. Geomorphol. Supp. **57**, 3, 75-95 (2013).
10. M. Wistuba, I. Malik, M. Fajer, T. Papciak, Studia Geomorphologica Carpatho-Balcanica **47**, 107-125 (2013).
11. M. Wistuba, "Slope-Channel Coupling as a Factor in the Evolution of Mountains. The Western Carpathians and Sudetes", Springer Verlag, 2014.
12. M. Wistuba, I. Malik, K. Wójcicki, P. Michałowicz, Earth Surf. Process. Landf. **40**, 293-312 (2015).
13. I. Malik, Ł. Pawlik, A. Ślęzak, M. Wistuba, Catena **173**, 264-275 (2019).
14. J. Corominas and J. Moya, Geomorphology **30**, 79-93 (1999).
15. D. Germain, E. Dagenais-Du-Fort, P. Lajeunesse, M. Simard, Dendrochronologia **52**, 57-66 (2018).
16. M. Wistuba, I. Malik, K. Krzemień, E. Gorczyca, M. Sobucki, D. Wrońska-Wałach, D. Gawior, Catena **171**, 359-375 (2018).
17. I. Malik, Y. Tie, P. Owczarek, M. Wistuba, W. Pilorz, B. Woskowicz-Ślęza, Geochronometria **40**, 3, 208-216 (2013).
18. I. Malik, M. Wistuba, Y. Tie, P. Owczarek, B. Woskowicz-Ślęzak, K. Łuszczyńska, Appl. Geogr. **87**, 54-65 (2017).
19. K. Łuszczyńska, M. Wistuba, I. Malik, M. Krąpiec, B. Szypuła, Geochronometria **45**, 1, 173-184 (2018).
20. M. Wistuba, I. Malik, J. Badura, Dendrochronologia **53**, 82-94 (2019).
21. P. Migoń, T. Pánek, I. Malik, J. Hrádecký, P. Owczarek, K. Šilhán, Geomorphology **124**, 3-4, 200-214 (2010).
22. P. Migoń, A. Kacprzak, I. Malik, M. Kasprzak, P. Owczarek, M. Wistuba, T. Pánek, Geomorphology **219**, 213-231 (2014).
23. I. Malik, M. Wistuba, P. Migoń, M. Fajer, Geochronometria **43**, 1, 24-37 (2016).
24. M. Wistuba, I. Malik, H. Gärtner, P. Kojs, P. Owczarek, Catena **111**, 41-55 (2013).
25. E. Gorczyca, Przegląd Geograficzny **80**, 1, 105-126 (2008).
26. W. Margielewski, J. Święchowicz, L. Starkel, A. Łajczak, M. Pietrzak, "Współczesna ewolucja rzeźby Karpat fliszowych", in *Współczesne przemiany rzeźby Polski*, edited by L. Starkel L. (Instytut Geografii i Gospodarki Przestrzennej UJ, Kraków, 2008), pp. 57-133.

DEM-based Mapping of the Erosion Processes Spatial Patterns in Forest-Steppe Landscapes of Ukraine

Mykhailo Grodzynskyi[1, 2,a)], Daria Svidzinska[2, b)], Oleksandr Obodovskyi[1, 2, c)] and Anatoliy Melnyk[1, 3, d)]

[1]*Kazimierz Wielki University in Bydgoszcz, Institute of Geography, Poland*
[2]*Taras Shevchenko National University of Kyiv, Faculty of Geography, Ukraine*
[3]*Ivan Franko National University of Lviv, Faculty of Geography, Ukraine*
[a)]Corresponding author: mgrodz@ukr.net
[b)] d.svidzinska@gmail.com
[c)]obodovskiy58@gmail.com
[d)] anatolij.melnyk@gmail.com

Abstract. Spatial dynamics of a landscape is largely controlled by the lateral flows. The methods of geomorphometry, which is rooted in Digital Elevation Models (DEM) automated Geographical Informational Systems (GIS) analysis could be used effectively to study them. The paper presents the method of mapping and classification of landscape spatial dynamics patterns on the basis of lateral flows properties with the use of fuzzy clustering analysis. The analysis is performed using the *k*-means method and is based on the geomorphometric parameters. Topographic indices underlying the study describe both morphosculptural and process-functional components of the moisture and solid matter dynamic redistribution in landscape. The comparative analysis of the results for four sites within the forest-steppe zone of Ukraine indicates that that the classification obtained is meaningful and reproducible.

INTRODUCTION

Studies of the landscape spatial dynamics is a research field of modern landscape science related closely to the geohazards, which are controlled by lateral abiotic flows. These flows define the features of physiographic processes related to the relocation of matter and energy that is reflected on the spatial configuration of landscape [9]. In turn, spatial configuration of lateral abiotic flows depends heavily on the landforms. Therefore, DEM and its geomorphometric analysis using GIS is an appropriate basis for the automated mapping of abiotic flows spatial pattern. The procedure of predictive geomorphological [3], soil [5], and landscape-ecological [1] mapping with the application of geomorphometric analysis has few established stages characterized by the certain methodical features which include DEM preprocessing, DEM geomorphometric analysis, data classification and results interpretation.

MAERIALS AND METHODS

Study Area

Four training sites with diverse physiographic conditions were chosen within the forest-steppe zone of Ukraine (Tab. 1). Every training site is a square of 10×10=100 km^2 area. According to the chosen spatial resolution of 50 m every training site encompasses 40 000 pixels (analytical matrix elements) described by the ten values of geomorphometric variables each. As a result, general data volume assigned with one training site is presented by the set of 400 000 unique values.

TABLE 1. Some characteristic features of the training sites

№	Abs. height, m	Slope, deg.	Dominant type of a landscape
1	133.47-166.24	0-3.95	Mixed coniferous-broad-leaved forests predominate
2	209.03-356.33	0-10.49	Roughly equal shares of forest and steppe
3	69.57-167.75	0-8.11	Meadow-steppe predominates

Geomorphometric Analysis and Fuzzy Clustering

DEM preparation and analysis were performed in the GIS SAGA v. 7.2.0 environment that provides a wide range of raster preprocessing and terrain analysis functions [6]. The procedures of cluster analysis were carried out using the FuzME v. 3.5c software package that is a multipurpose tool for the performance of fuzzy unsupervised data classification (the *k*-means method) with the additional results assessment capabilities (e.g., general uncertainty, partition validity) [4]. The preparation of the SRTM DEM tiles has been performed prior to the analysis. The preparatory procedure encompassed reprojecting joined with the choice of an appropriate spatial resolution [2], filtering [8] and hydrological correction [7].

RESULTS AND DISCUSSION

The output contains cluster allocation of the data points, cluster properties and different statistics describing the clustering performance. To choose the most appropriate number of classes several clustering performance parameters were analyzed, namely Fuzziness Performance Index (FPI), Modified Partition Entropy (MPE), and Separate Distance (S). Generally, the better the clusters are separated, the smaller are the values of FPI, MPE, and S indices. The validity of the performed classification was assessed through the performance indices determined for different number of clusters. Minimal values of FPI, MPE, and S indicate a good (clear, non-fuzzy) grouping of data. Two alternatives of satisfactory partition are identified on the indices' values, namely 3 and 6 classes. This enables to compare the results of classification of different training sites.

In the case of unsupervised classification, we cannot really provide the legend for the final output. We can only try to assign names to extracted classes a posteriori by carefully analyzing their statistical characteristics. Therefore, the semantic interpretation of the obtained classes was done through the statistical analysis of geomorphometric parameters values (Fig. 1).

In the case of 3 classes' partition, morphodynamic units delimited on the basis of morphosculptural features and, consequently, direction, intensity, and migration capacity of lateral abiotic flows, can be interpreted as follows:

Class 1 is autonomous eluvial landscapes (A^E) – flat and convex summit sites. Class A^E represents the independent landscapes that gain matter and energy from the atmosphere; the main process here is leaching of matter and descending flow of water and nutrients; the balance of substances is negative. Secondary topographic attributes that characterize processes of lateral migration approach to minimal values. The exclusion is the training site No1: the class here represented by convex summit sites with the relatively high slope values (0.03–3.95° with the mean value of 1.34°) and with the higher potential for sheet erosion respectively. In this case, the unit can be interpreted as transit-eluvial landscapes (T^E);

Class 2 is subordinate transit landscapes (T^E) – convex and concave slopes of different height position and steepness. These landscapes obtain matter and energy from autonomous (or simply located upslope) units and are responsible for its downslope conduction. Their distinctive feature is parallel to surface (lateral) flow; the balance of substances (in the absence of erosive processes) is close to zero. The landscape of T^E type are mainly characterized by the mean values of secondary topographic attributes that identify the highest (for given area) sheet erosion potential owing to surface flow divergence. For the training sites No1 and 4 this unit can be defined as transit-accumulative landscape (T^A) because it is mainly represented by the footslopes and toeslopes with the mid-height superaquatic position, flat or concave profile, and minimal steepness. Respectively, the T^A units are responsible not for matter conveyance, but for its accumulation due to reduction in surface and intrasoil runoff velocity;

Class 3 is subordinate transit-superaquatic landscapes (Saq^T) – concave interhill depressions and channels. Basically they are represented by erosive network elements, the Saq^T class is responsible for intense conveyance and accumulation of matter in landscape; balance of substances, as a rule, is positive. The class is defined by the maximum TWI values and the highest potential for linear erosion due to prevailing flow convergence. For the

training site No4 this unit can be interpreted as eluvial-accumulative (E^A) because it encompasses mainly closed steppe depressions with deep groundwater bedding.

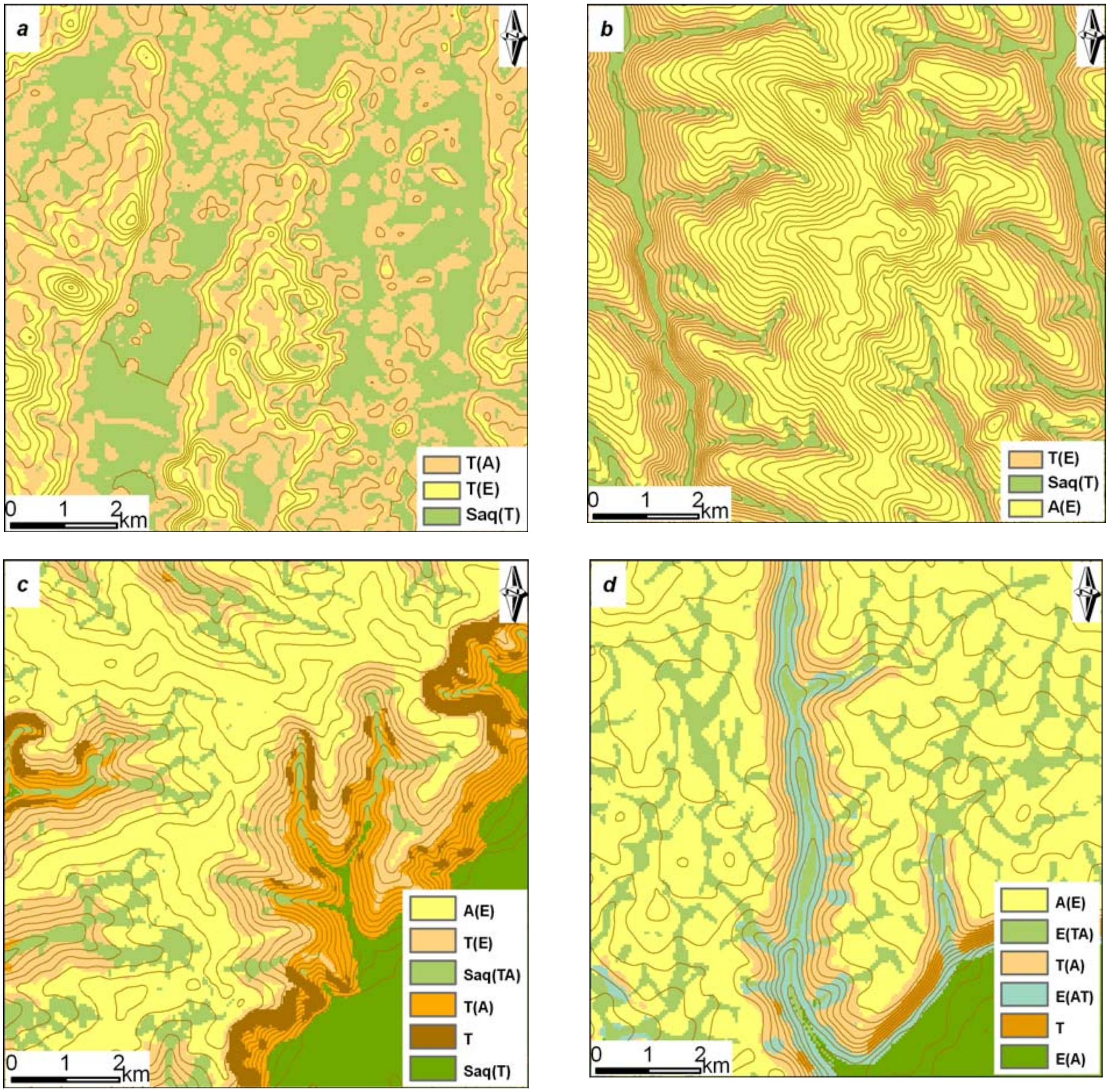

FIGURE 1. The examples of the obtained morphodynamic units classes: 3 classes partition for the training sites 1 and 2 – (a) and (b); 6 classes partition for the training sites 3 and 4 – (c) and (d) respectively.

In the case of 6 classes' partition, the first class of the above-mentioned remains relatively stable, landscapes of transit type are additionally subdivided into three classes, and superaquatic transit landscapes – into two classes with some differences for the training sites No1 and 4:

Class 1 is autonomous eluvial landscapes (A^E) – flat and convex summit sites;

Class 2 is transit-eluvial landscapes (T^E) – shoulder and upper slope (seepage slope and convex creep slope). For these landscapes the sheet erosion potential increases with slope steepness. For the training site No4 class 2 is interpreted as transit-accumulative (T^A) landscapes as they are represented here by the footslopes;

Class 3 is transit-accumulative landscapes (T^A) – free face and transportation midslopes of the moderate steepness. These spatial units play a key role in providing the processes of matter transportation through sheet

surface runoff. For the training site №4 the class is represented by transit landscapes (T) without any additional functions;

Class 4 is transit landscapes (T) – mainly concave steep slopes. For the training sites №1 and No4 the class is defined as superaquatic accumulative-transit (Saq^{AT}) and eluvial accumulative-transit (E^{AT}) landscapes respectively represented by well-defined toeslopes with highly concave profile (-0.01 that is maximum mean for all six classes);

Class 5 is transit-accumulative superaquatic landscapes (Saq^{TA}) – flat and concave interhill depressions and channels. These forms have a tendency to accumulate moisture and characterized by mid-intense, but mostly convergent flow. The exclusion can be done for the training site №4 where the class is defined as transit-accumulative eluvial (E^{TA}) landscapes with prevailing transit function;

Class 6 – transit superaquatic landscapes (Saq^{T}) – flat and concave channels' beds associated with the minimal absolute height values, convergent flow and the highest linear erosion potential. For the training sites No1-3 the processes of transport are prevailing, while for the site No4 the class is associated with closed depression and accumulation, thus, it is defined as accumulative eluvial (E^{A}) landscapes.

CONCLUSIONS

The SRTM DEM after the preprocessing procedures of data filtering and hydrological correction, is proved to be a valid basis for geospatial analysis with the accuracy of 1:100 000 scale.

Since relief is an important driver of the spatial heterogeneity in hydroclimatic conditions, the geomorphometric parameters obtained by DEM automated GIS-analysis can be effectively applied not only for the morphodynamic territorial units delineation and interpretation but for more complex (geoecological) classifications performance as well. The potential for further method improvement is connected with the addition of the geomorphometric parameters assessing warmth redistribution (aspect, incoming solar radiation etc.) or multispectral indices assessing primary productivity (e.g., NDVI).

Multidimensional fuzzy clustering analysis using the k-means method is an objective and reliable procedure of data grouping. It enables to define optimal for given number of parameters number of classes and to analyze features of data redistribution within classes. Moreover, maximal values of confusion index potentially can be used for relief break-lines extraction.

REFERENCES

1. P. Burrough, ,J. Wilson, P. Gaans, A. Hansen, *Landscape Ecology*, 16, 523–546 (2001).
2. T. Hengl, Computers and Geosciences, 32(9), 1283–1298 (2006).
3. R. MacMillan,W. Pettapiece, S. Nolan., T. Goddard, *Fuzzy Sets and Systems*, 113(1), 81–109 (2000).
4. B. Minasny and A. McBratney, FuzME v. 3.5b, *Australian Centre for Precision Agriculture*, The University of Sydney, Australia. Available from http://www.usyd.edu.au/agriculture/acpa/software/fuzme.shtml (2002).
5. M. Möller., M. Volk, K. Friedrich, L. Lymburner, *Journal of Plant Nutr. and Soil S.*, 171(3), 419–430 (2008).
6. V. Olaya., O. Conrad, "Geomorphometry in SAGA," in *Geomorphometry: Concepts, Software, Applications*, edited by T. Hengl and H.I. Reuter (Elsevier, 2009), pp. 293–308.
7. O. Planchon and F. Darboux, *Catena,* 46(2-3), 159–176 (2002)
8. T. Selige, J. Böhner, A. Ringeler, *SAGA – Analysis and Modelling Applications*. Göttinger Geographische Abhandlungen, 115, 97–104 (2006).
9. M. Turner and J. Cardille, J. "Spatial heterogeneity and ecosystem processes," in *Key Topics in Landscape Ecology (Cambridge Studies in Landscape Ecology).* J. Wu and R. Hobbs (eds.). Cambridge University Press, New York, 2007, pp. 62–77.

Evaluation and Mapping of the Hazardous Deflation and Sand Blowing in Volyn Province, Ukraine

Mykhailo Grodzynskyi[1, 2, a)], Anatoliy Melnyk[1, 3, b)], Oleksandr Obodovskyi[1, 2, c)] and Daria Svidzinska[2, d)]

[1]*Kazimierz Wielki University in Bydgoszcz, Institute of Geography, Poland*
[2]*Taras Shevchenko National University of Kyiv, Faculty of Geography, Ukraine*
[3]*Ivan Franko National University of Lviv, Faculty of Geography, Ukraine*
[a)]Corresponding author: mgrodz@ukr.net
[b)]anatolij.melnyk@gmail.com
[c)]obodovskiy58@gmail.com
[d)]d.svidzinska@gmail.com

Abstract. The mathematical reliability theory and landscape mapping were used for quantitative assessment and mapping of the probabilities of hazardous processes caused by the wind for the landscapes of fluvioglacial sandy lowlands of the Eastern Europe. Volyn province serves as a case study area in the research. Calculations and maps show that for a time period of 10 years soil deflation and sand blowing are probable for almost all the province's area, although before the land reclamation works these processes have been observed within arable lands only.

INTRODUCTION

Soil deflation and sand blowing are hazardous processes for the landscapes of fluvioglacial sandy lowlands of the Eastern Europe. Excessive ploughing of sandy soils and land reclamation works in 1960-70-ies have changed the water regime of the landscapes causing intensification of Aeolian processes, including for the areas, where they have not been previously observed. For Volyn province of Ukraine, which lies within the belt of Eastern-European fluvioglacial sandy lowlands (commonly known as Polesie) the area affected by soil deflation is estimated as 1 770 km^2 [7] and about 800 km^2 of post-meliorated peat lands began to suffer from the sand blowing [1]. Other data characterizing current situation with the Aeolian processes in Volyn province are also available [5]. At the same time, for the environmental protection purposes along with the data on current state of the geohazards, the information about their possible development in both space and time is of special interest. From this perspective and in view of climate variability, the evaluation of soil deflation and of sand blowing in probabilistic terms seems appropriate. The evaluation of the probabilities normally requires large data sets, which for geohazards is usually inaccessible. The application of reliability theory to environmental risks assessment proved to be effective in situations where data available are limited [3, 8]. It is also shown that the landscape approach is able to provide comprehensive and systemic basis for dynamic processes evaluation and mapping [6].The aim of the study is to evaluate and then to map the probabilities of soil deflation and sand blowing, using the methods of reliability theory and landscape mapping.

STUDY AREA

Volyn province with the total area of 20 144 km^2 is located in the north-western part of Ukraine within Polesie lowland on Pleistocene sandy fluvioglacial sediments (in the north) and Volynian upland on loess sediments (in the south). The landscapes of Polesie region are represented by sander, alluvial-lacustrine-sander, and moraine-sander lowlands covered with sandy Albeluvisols (Umbric and Gleyic), Arenosols, Histosols (Haplic and Folic) soils.

About 46% of the Polessian lowland is used for agriculture. The Volynian loess upland is covered with loamy soils of Haplic Luvisol and Luvic Phaeozem types. In the land cover arable lands predominate.

METHODS

The values of probabilities of two hazardous processes caused by the wind, namely soil deflation and wind-blown sand movements, were assessed for each type of landscape units of the Volyn province. The probabilities of both these hazardous processes were evaluated using the "loading – resistance" model of the reliability theory [2]:

$$P = \exp\left\{ -\frac{V_{cr}}{\overline{V}_w} + \frac{\sigma_w^2}{2\overline{V}_w^{\,2}} \right\},$$

where V_{cr} – is the critical (threshold) wind velocity sufficient for sand particles translocation (for alluvial sands V_{cr} is equal to 9,6 m/s, and for eolian sands V_{cr} = 4 m/s); V_w is the average for 10 year observation period wind velocity (2.3 m/s is taken as V_w value for Volyn province); σ^2 –is the variance of the wind velocity (for Volyn province σ^2=0.67).

The probabilities of soil deflation occurrence within the microgeochores were calculated using the formula given above with different values for critical for deflation wind velocity V_w: for sandy soils V_w=2.5 m/s, for loamy sandy soils V_w=3.5 m/s, for sandy clay soils V_w=4.5 m/s, for peat soils (Histosols) V_w=1.5 m/s.

To identify the spatial landscape units used for mapping of soil deflation and sand blowing the landscape map was composed. In the map of scale 1: 200 000 the landscape units of taxonomic level of mesogeochores (for criteria see [4]) were delimited and classified. Landscape map and the maps of hazardous processes caused by the wind were composed using ArcGIS v 10.4.1 software. The methods of landscape mapping combines techniques of processing thematic maps (topographic, geological, soil cover, land cover) and techniques of field landscape survey.

RESULTS AND DISCUSSION

The results of calculation the probabilities of sand blowing and of soil deflation are shown in the figures 1 and 2.

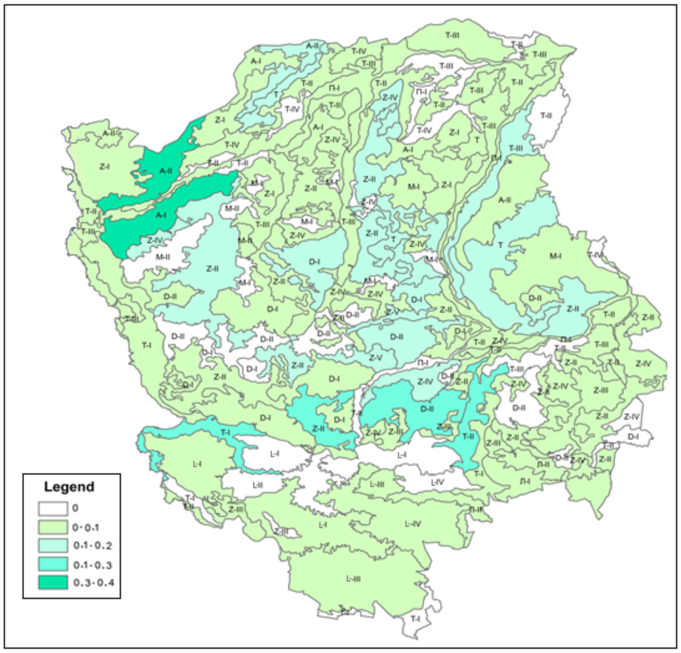

FIGURE 1. The probability of sand blowing during a 10-year period (Volyn province, Ukraine; original scale 1: 200 000)

Map of the sand blowing in Fig.1 shows that for most of the Volyn province the probability of this geohazard does not exceed 0.1. The development of sand blowing needs open sand surfaces or sandy soils covered with grass vegetation only slightly. Such conditions are typical for the mesogeochores of alluvial-lacustrine-sander sandy lowlands with Arenosol soils located in the northwestern part of Volyn province. Mesogeochores of this type are characterized by the highest values of sand blowing probability (*P*=0.3-0.4) throughout all Volyn province. The sand blowing is somewhat less probable (*P*=0.2-0.3) for mesogeochores of the alluvial sandy terraces T-1 and T-II. This type of geohazard could also be originated from the open sand dunes. They are widespread in the central part of Volyn province, especially within the mesogeochores of denudation plains D-II and sander lowlands Z-II. Non-zero probabilities of sand blowing for mesogeochores on loess sediments with loamy soils are also explained by the presence of sand dunes within the loess uplands and sander plains. The risk of sand's deflation is more probable than sand blowing (Fig. 2).

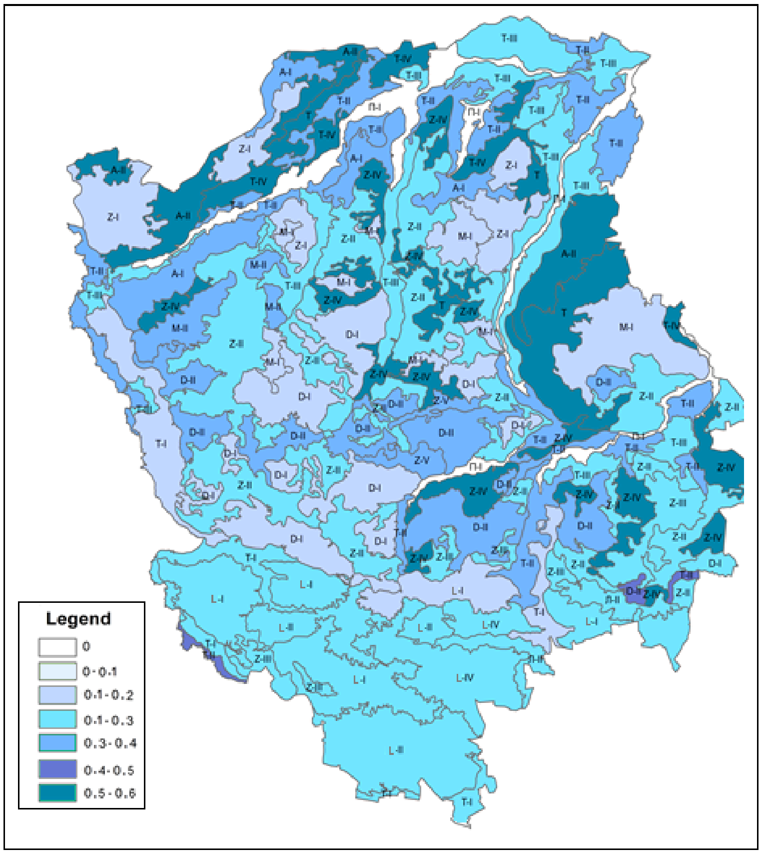

FIGURE 2. The probability of soil deflation during a 10-year period (Volyn province, Ukraine; original scale 1: 200 000)

Fig. 2 shows that, with the exception of some floodplain mesogeochores, the entire territory of the Volyn province is under significant risk of soil deflation. According to the existing estimates, 12.8 per cent of the Volyn province are affected by the deflation [7]. At the same time, our results shows that about 94.7 per cent of its area is under the risk of soil deflation. This process is not taking place currently in most landscapes of Polesie lowland. However, in view of climate change here (in particular, increasing frequency of droughts), transformations in land use and in land management practices (in particular, ploughing using heavy tractors, more row crops in crop rotation schemes, degradation of old forest strips etc.) soil deflation is probable for coming 10 years for almost all the area of Volyn province. This process is especially probable for the mesogeochores Z-IV of sander plains on deep sandy-clay sediments with the soils of Folic Histosol, Gleyic Fluvisol, and Mollic Gleysol types, and for the mesogeochores A-II of alluvial-lacustrine-sander sandy lowlands with the Mollic and Histic Gleysols. In addition to the sander lowlands, the high probability of soil deflation is characteristic feature of all the first floodplain terraces of Volyn

province, especially for mesogeochores of T-IV and T-II types, as well as for mesogeochores D-II of elevated denudation plains with the Rendzic Leptosol soils (rendzinas). It is noteworthy, that for the mesogeochores of the Volyn Upland, where loamy Luvic Phaeozems and Haplic Chernozems are more resistant to deflation than the soils of Polesie lowland, the probability of deflation is lower (P=0.2-0.3). We explain it with the higher moisture of Phaeozems and Chernozems in Volyn Upland than of Polessian sandy soils, which now are over-droughted by land reclamation works.

Massive land reclamation works and construction of drainage systems built mainly in 1960-1970-ies have changed dramatically land cover pattern, water and mineral regimes of landscapes in Polesie lowland. Mesogeochores of pine forests, meadows and peat lands were converted into the arable lands, the groundwater table was declined down to few meters, soil structure was disintegrated. These changes have caused intensification of soil deflation. Each year sandy Umbric Albeluvisol soils lost due to deflation about 0.02 kg/m^2, which is 5 per cent of their humus content, while total amount of fine earth lost from the cultivated ameliorated lands, varies, depending on crop and on agronomic practices, from 0.1 up to 0.25 kg/m^2 during a growing season [1]. The probability of further degradation of meliorated soils due to their deflation is especially high (up to p=0.6) for those mesogeochores where ameliorated peatbogs with Haplic and Folic Histosols occupies more than 30 per cent of the area. Before the land reclamation these geochores were not affected by deflation, but now they became hotspots of landscape desertification in Polesie.

CONCLUSIONS

Soil deflation and sand blowing are hazardous processes that were intensified and spread over vast areas in the Polesie region of Eastern Europe after the land reclamation schemes have been implemented here in 1960-1970-es. These processes continue to develop in the region threatening to its soil productivity and landscapes stability. To elaborate the regional schemes and strategies for preventing soil deflation and sand blowing the maps showing probability of these processes occurrence are of special importance. The “loading-resistance” model of the reliability theory was adopted for the assessment of probability of deflation and sand blowing for Volyn province of Ukraine. The landscape map of the area and calculated values of probabilities of these two hazardous processes occurrences for10 year period of different landscape units (mesogeochores) helped to identify areas where deflation and sand blowing are most probable. In particular, deflation is very probable for ameliorated peat bogs, which before the amelioration have not been affected by the wind erosion.

REFERENCES

1. V. Balkovski, 2009. Soil erosion in post-ameliorated agrarian landscapes of Western Polesie. *Scientific Bulletin of Uzhhorod University. Series "Biology*», Vol. 26. – P. 165-171 (In Ukrainian).
2. R. E. Barlow, Proshan, F., 1974. *Statistical Theory of Reliability and Life Testing: Probability Models*. New York: Holt, Rinehart and Winston. 290 p.
3. M. D. Grodzynskyi, 1995. *Stability of Geosystems to Anthopogenic Pressure.* Kyiv, Likey, 233 p. (In Ukrainian).
4. M. D. Grodzynskyi, 2015. *Landscape Ecology*. Kyiv: Lybid. 550 p. (In Ukrainian).
5. *Regional Report on the state of the natural environment of the Volym Province for 2016 year*. Volyn Province State Administration, Agency for ecology and nature resources. Available from https://menr.gov.ua/files/docs/Reg.report/Доповідь Волинська 2016.pdf (2016).
6. A. Richling, Solon, J. 2011 *Landscape Ecology.* 5th edition. Warsaw: PWN. 464 p. (In Polish)
7. M. Shaguta, Gulay L., 2014. The Current Status of Land Resources of Volyn Region. *Scientific bulletin of Lesya Ukrainka Eastern European National University. Ser. Geographical sciences*. Vol. 11. 48-52 p. (In Ukrainian).
8. D. Szatten, M. Habel, L. Pellegrini, M. Maerker, 2018, *Water (Switzerland),* vol. 10, iss. 11, art. no 1681

Changes in the “Channel-Flow” Hydrodynamic System of the Mountain Rivers in Tisza River Basin (within Ukraine) in Terms of High-Water Conditions

Oleksandr Obodovskyi[1, 2, a)], Vasyl Onyschuk[2, b)], Mikhailo Grodzinskyi[1, 2, c)] and Anatoliy Melnyk[1, 3 d)]

[1] *Kazimierz Wielki University in Bydgoszcz, Institute of Geography, Poland*
[2] *Taras Shevchenko National University of Kyiv, Faculty of Geography, Ukraine*
[3] *Ivan Franko National University of Lviv, Faculty of Geography, Ukraine*
[a)]Corresponding author: obodovskiy58@gmail.com
[b)] willy38@ukr.net
[c)]mgrodz@ukr.net
[d)]anatolij.melnyk@gmail.com

Abstract. This article presents the main results of multi-year laboratory and field studies and researches of channel processes in the mountain rivers of the Tisza River basin. Changes in the “channel-flow” hydrodynamic system (hereinafter referred to as GDS “ch-f”) were monitored by field researches for a period of at least 30 years. By comparative analysis of the results of laboratory and field studies, the methods of determining the channel-formation flow rate and sediments have been developed, the GDS “ch-f” stability levels have been estimated and the floods has been classified in terms of their influence on channel processes and economic activity.

INTRODUCTION

More attention in researches of channel processes has been recently given to the mountain rivers. In this context, the rivers of the Tisza Basin (within Ukraine) are particularly emphasized. The catastrophic floods raise a number of problems regarding the safety of habitation of people in flood plains. For example, catastrophic floods in November 1998 and March 2001, and in August 2008 caused significant damage to the natural and economic complex of the Tisza Basin. With regard to the hydromorphological state of the rivers of this basin, such floods cause significant transformation of channel forms and even changes in the types of channels.

METHODS

The laboratory experiments concerning the study of the stability conditions of the hydrodynamic system “channel-flow” (GDS “ch-f”) of mountain rivers were performed on scour spatial models in compliance with the self-similar quadratic mode of flow of particles of the self-assembling layer of mixtures of sediments different in terms of the fractional composition from the rivers of the Ukrainian Carpathians. Natural surveys of river areas and monitoring surveys were carried out on a permanently installed survey network and during expeditionary work on representative areas of the beds of mountain rivers (Tisza, Teresva, Shopurka, Kosivska, Borzhava, Latorica and Uzh). In this case, the main morphometric (B, h_{cep} , D i d_{cep}) and hydraulic (Q,V,I) parameters of the channels were established. The comparative analysis of laboratory experiments and field observations made it possible to establish conditions for the stability of the GDS “ch-f” based on the allowable critical velocities and to propose new approaches to the classification of floods in the mountain rivers in terms of their influence on the channel processes and economic activity, which is based on the abovementioned provisions.

RESULTS

The periodic changes in the hydromorphological condition of the rivers of the Tisza Basin, and high floods cause significant transformation of channel forms and even changes in the types of channels provided there are mudflow

components. Since the studied sub-basin is transboundary, then any changes in the hydrodynamic system "flow-channel" (hereinafter referred to as GDS "ch-f") of the rivers shall be subject to hydromorphological monitoring in the channel-floodplain complex in a single format with European standards (EU Water Framework Directive - EU WFD) [1,2]. It is established that the first the level of significance in the analysis of mountain river channel processes is occupied by the hydropower indicators - the Froude number $Fr = V_{cep}/(gh)^{0,5}$ and the flow capacity $N = \rho g V_{cep} B h_{cep} I_0 = \rho g\ Q_{p\phi}\ I_0$ (where ρ - density of the substance, kg/m^3, g - acceleration of the earth gravity, m^2/s, B - average width of the channel flow along the free surface of the stream, m, h_{cep} - average depth of the channel flow, m, $Q_{p\phi}$ - the channel-formation substance flow rate, m^3/s, I_0 - longitudinal inclination of the river in the area with three cripples) [3]. The materials of multi-year laboratory and field studies confirmed that the extreme value of the flow capacity is observed with a minimum energy dissipation, which corresponds to the dynamic equilibrium of the GDS "ch-f" in the conditions of the passage of channel-formation flow rate $Q_{p\phi}$ [4-8]. The next factor in this list, with a somewhat less probability of repeating the cause-effect relationship between the elements of the system, is the geomorphological structure of the flow and its reflection in the form of a channel through the parameter B/h_{cep} or relative roughness of the perimeter of the water-carrying corridor of the river - D/h_{cep} (where D is the average weighted coarseness of the particles of the alluvial layer of self-assembling of the channel hollow, m) [9].

Using the functional connection $N = f(B/h_{cep},)$, the channels of mountain rivers are typed. There are 8 types of channels - a rift-waterfall channel, channel with undeveloped alluvial forms, a channel with developed alluvial forms, limited flow, multi-arm channel (midstream sandbank channel), a channeled conduits, incompleted flow, free flow [5,7,9].

It is known that the natural conditions are not the only bearer of spatial-temporal changes in the volume of sediment flow and, accordingly, the intensity of the flow phenomenon development. Economic activity in the water collection areas and river channels results in significant changes in the sediment flow, causing the transformation of the formed types. In some parts of the rivers, especially those that have undergone an open-pit destruction, it is observed that alluvial deposits are washed away with the exposition of rock structures, which in some places act as regulatory groins. The results of field and laboratory studies of river channel processes in mountain rivers [10,11] indicate that the relative dynamic equilibrium of the GDS "ch-f" (large-alluvial channel stability) is expressly determined by the dominant influence of self-assembling channel basin on the development of channel deformations (both the watercourse itself and surface of the channel forms). Consequently, it is recommended for mountain rivers to evaluate their two main states of GDS "ch-f" stability – stable and unstable [3].

The stable channel state is the available pronounced self-assembling layer formed by the natural way after intensive channel re-formations of alluvial sediments, which does not significantly change its structure in case of bed-formation flows. The average flow rate in terms of channel cross section in this state can be taken as non-disrupting for inhomogeneous unbound soil ($V_{н.н}$). In case of slight increase in this watercourse velocity against the background of restricted transit of sediments only the removal of fine particles of sediments from the self-assembling layer may be observed (at $S_0 \approx 0,7$), which is not more than 10% in the total composition of this surface layer. In case of its decrease, a slight washing off (mud accumulation) is possible in the layer of self-immersion is possible. This state of the watercourse can be considered a static equilibrium of the GDS "ch-f", and the value $V_{н.н}$ can be calculated by the formula [12]:

$$V_{н.н} = V_{н.о} S_0^{-0.25}, \tag{1}$$

where $V_{н.о}$ – average non-disrupting flow velocity for homogeneous unbound sediments $d_{cep} = d_{cep\ зв}$ ($d_{cep\ зв}$ –average weighted diameter of the mixture of inhomogeneous unbound sediments; $d_{cep\ зв} \approx d_{60\%}$ - $d_{65\%}$ on the curve of the granulometric composition of channel deposit samples); S_0 - the coefficient of heterogeneity of the channel deposit mixture, which is determined by the formula $S_0 = (d_{25}/d_{75})^{0,5}$, and varies for the channels of the Ukrainian Carpathian rivers nearly in the range from 0,25 to 0,45 (smaller value corresponds to areas of rivers with hydraulic slope I > 0.01).

The unstable state of the channel (critical state) corresponds to the disruption of the self-assembling layer. This state of the GDS "ch-f" is characterized by intense (continuous transportation of bottom bed-formation sediments) washing out and disturbance of the equilibrium of all particles of sediments from the surface layer of the channel bed (self-assembling layer). At the same time, the largest particles of self-assembling sediments, as a rule, remain in place and gradually fail in the thickness of the active layer, where the sediments with smaller coarseness are washed out $d < D_{cep.зв}$ ($D_{cep.зв}$ average weighted diameter of the self-assembling layer). Such a state in the natural environment can be observed only at the peaks of the highest floods (channel- destructive). The average flow

velocity that corresponds to this state can be taken as disrupting $V_{зр.н.}$ for inhomogeneous soils. In this case, the heterogeneity of the surface layer mixture will vary within 0,6 $> S_0 >$ 0,45 (the heterogeneity of the strongly pronounced self-assembling layer corresponds to $S_0 \approx$ 0,7) [9]).

Value $V_{зр.н.}$ can be calculated by the formula [12]:

$$V_{зр.н} = V_{зр.о} S_0^{-0.25}, \tag{2}$$

where $V_{зр.о}$ – disrupting average velocity of flow for the sediments homogenous in terms of granulometric composition $d_{сер} = d_{сер\ зв}$.

The ratio between Vн.н. and Vзр.н for the sediments with nonuniform composition [12], as well as for homogeneous sediments [13] is equal to 1,41, i.e. Vзр.н, = 1,41 Vн.н.

Between stable and unstable states, one can distinguish three intermediate states, which are not less typical in practical terms, namely:

- *control state* of the GDS "ch-f" ($V_к$=1,2 $V_{н.н}$) - close to the dynamic equilibrium;
- *boundary state* of the GDS "ch-f" ($V_{г.р}$=1,1 $V_{н.н.}$) - close to the static equilibrium;
- *dynamic equilibrium* of the GDS "ch-f" ($V_{д.р.}$*=1,3* $V_{н.н.}$).

The dynamic equilibrium of the GDS "ch-f" of the particular area of the mountain river is the optimal state for self-organization, which is observed after the passage of the bed-forming flows and sediment within the structural organization of the channel relief (floods that pass, as a rule, within the gullies).

The state of the GDS "ch-f" dynamic equilibrium is divided into two qualitatively different groups of five floods of the proposed classification (Fig. 1) [4,7]. The first two floods (channel-preserving and channel-controlling) are relatively passive, correspond to the channel formation stages at the lower structural levels (the formation and movement of micro - and mesoforms). During these floods, only reverse channel deformations can occur, which, as a rule, do not significantly affect the GDS "ch-f" capacity and the hydro-environmental conditions of the adjacent basin. Two catastrophic floods (channel-destructing and channel-destructing with catastrophic consequences) are extremely active, depending on the sediment transportation mode. These floods cause irreversible processes of channel formation and occurrence of emergency situations of ecological, social and socio-economic nature. A brief evaluation of these floods proves the following.

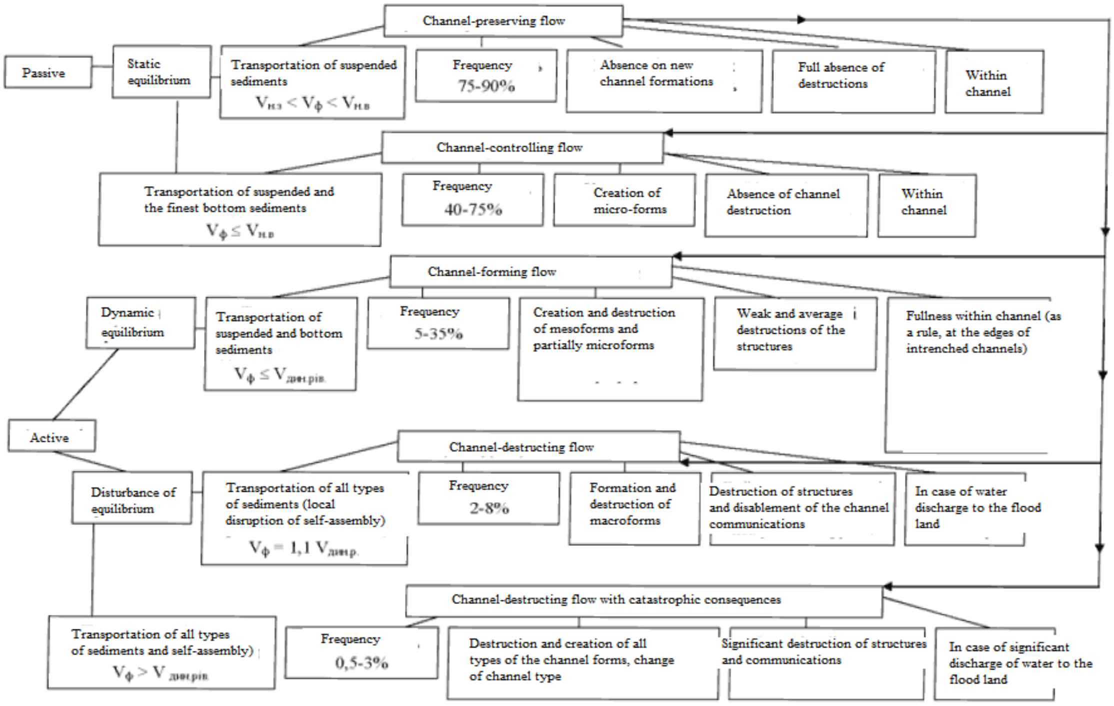

FIGURE 1. Classification of floods on mountain rivers in terms of their influence on channel processes and economic activity.

The channel-preserving flood causes only transportation of suspended sediments, which indicates a passive (passive manifestation of channel processes in the presence of a pronounced layer of self-assembling of the channel bottom) adaptation of flood flow to previously formed channel forms, i.e. without any noticeable transformations. It corresponds to the stable state of the GDS “ch-f”.

The channel-controlling flood is characterized by the state of the “flow-channel” system, when the flow velocity does not exceed the critical non-disrupting velocity. The channel thus also controls the structure of the flow, but at the microform level the dynamics of channel formations is already observed, and there is a slight destruction of the concave shores of the meandering channels. During these floods, there is a “preparatory” moment for active interaction in the “flow-channel” system. This flow corresponds to the control and boundary states of the GDS “ch-f”.

Both listed floods are classified as passive with a static equilibrium in the “flow-channel” system. In terms of their hydraulic parameters, they can not significantly affect the forms of manifestation and intensity of channel deformations.

The channel-destructing flood is characterized by the transportation of all types of sediments (including the disruption of the self-assembling layer) with active channel horizontal and vertical deformations at the level of macroforms and the destruction of various engineering structures in some areas of the channel. Taking into account the fact that in a mountainous environment the flood land may be absent or its width is insignificant and does not exceed tenfold breadth of the channel, then when the stream flows to its surface, the “dynamic-kinematic effect” associated with the sharp decline of its transportation capacity has no clear manifestation. At the same time, the dynamic axis of the flow is almost not shifted, and under these hydraulic conditions the destructive action of the flow increases. This is evidenced by its turbulent state caused by advanced growth of kinetic energy. In case of such floods, there is unstable state of the GDS “ch-f”.

The channel-destructing flood with catastrophic consequences takes place in the conditions of continuous transportation of sediments (including self-assembling layer), active channel and flood land deformations, change of direction of channel processes, types of channels and significant destruction of various structures. This flood also meets the unstable state of the GDS “ch-f”.

The given classification has one more important aspect - ecological. The different types of floods have quite differentiated affect on the environmental situation not only in the river channel, but also on its catchment area. The formation of active floods results in changes in the living conditions of people in the riverfront zones and flood land. And floods with catastrophic consequences, which have a significant destructive force, can significantly affect the human living conditions and management and change the various elements of the river ecosystem.

Thus, from the point of view of the channel formation the most environmentally dangerous are active floods (especially channel-destructing and channel-destructing flood with catastrophic consequences), which cause significant channel deformations and erosive-accumulative phenomena in the river channels.

The application of the main provisions of the given classification in practice will make it possible to systematize approaches to the implementation of a number of flood control measures on the mountain rivers and categorization, designing and erection of the shore protection and protective-regulating structures, as well as assessment of the potential loss in case of catastrophic floods. In this context, compliance with the provisions of the EU Water Framework Directive [1] is particularly important in preserving or improving the hydromorphological status of mountain and piedmont water bodies.

It has been established that over the past 30 years, floods on the rivers of the Tisza Basin, which are classified as channel-preserving and channel-controlling, have been observed almost every year and are mostly rainy by the type of supply. 9 channel-forming floods were recorded (1990, 1995, 1998, 2000, 2002, 2004, 2005, 2010, 2013), 6 channel-destructing (1992, 1993, 1995, 2006, 2010, 2015) and 3 channel-destructing floods with catastrophic consequences (1998, 2001, 2008).

CONCLUSIONS

This article presents the main results of multi-year laboratory and field expeditionary studies of the GDS “ch-f”. Two main states of this system are identified - stable and unstable; as well as three intermediate states- control, boundary and state of dynamic equilibrium. On the basis of the comparative analysis of the main parameters of the GDS “ch-f”, five typical states of the channel basin stability have been identified, which made it possible to classify the floods. The proposed five categories of floods make it possible to standardize the legislation as to reaction to

floods varying in terms of water content of floods and develop managerial decisions to improve the hydromorphological status of rivers in urbanized channel-floodplain complex areas.

ACKNOWLEDGMENTS

Studies on this publication were partly funded by the State Water Resources Agency of Ukraine (No. 0106U008964) and the Ministry of Education and Science of Ukraine (No. 0111U005047).

REFERENCES

1. Water Framework Directive 2000/60/EC: Basic terms and definitions / [prepared by: Aliyev K. et al.]. – Official publication - K., 200. – 240 p.
2. Humen Impact on the Fluvial Processes of Erosion Rivers. (Edited by M.Habel. Wielki University in Budgoszcz, Budgoszcz, 2012, - 240 p.
3. Iu. Obodovskyi, O. Obodovskyi, V. Onyschuk, *Journal of Education, Health and Sport*. - Bydgoszcz, Poland, 2016. – Vol. 6 – No.13. – P. 307-316.
4. O. G. Obodovskyi V.V. Onyschuk and Konovalenko O.S., *Bulletin of the University of Kyiv*, Faculty of Geography - 2002. - Issue 48. - p. 42-47.
5. V. V. Onyschuk, A.C. Bilchuk, Kozytsky O.N., *Land reclamation and water management.* - 1989. - p. 60-65.
6. O. G. Obodovskyi, V.V. Onyschuk, Grebin V.V. et al. River processes of Limnytsa river / Edited by O.G. Obodovskyi - K.: Nika-Center, 2010. - 256 p.
7. O. G. Obodovskyi, V.V. Onyschuk, Rozlach Z.V. et al. Latorica: hydrology, hydromorphology, channel processes / Edited by O.G. Obodovskyi - K.: Publishing and printing center “University of Kyiv”, 2012. - 319 p.
8. O. G. Obodoskiy, Y.O. Obodoskiy, V.V. Onishchuk., *Geography and Tourism*. – Bydgoszcz, Poland, 2016. – Vol. 4 – No.2. – P. 89-98.
9. O. G. Obodovskyi. Chanel Processes: Textbook / O.G. Obodovskyi - K.: Publishing and printing center “University of Kyiv”, 2017. - 511 p.
10. M. N. Bukhyn, Onyschuk V.V. Experimental investigations of the self-assembling of the channels of the piedmont rivers. - Reclamation and water management. - K.: Urozhay, 1976. - Issue 38. - p. 44-50.
11. V. A. Bazylevych, Bukhyn M.N., Onyschuk V.V., *Reclamation and water management*. - K.: Urozhay, 1984. - Issue 52. - p.53-66
12. V. V. Onyschuk, Determination of nonerosive velocity for inhomogeneous unbound soils // Erosion and mud processes and their control. M: VNIIGiM, 1978. - Issue 6. - p. 19-26.
13. V. N. Goncharov, Dynamics of channel flows. - L.: *Gidrometeoizdat*, 1962. - 376 p.

Modern Approaches to Constructing Maps of the Minimum Flow of the Mountain Rivers (the Case of the Tisza Rivers Basin within Ukraine)

Oleksandr Obodovskyi[1, 2, a)], Olena Pochaievets[2, b)], Mikhailo Grodzinskyi[1, 2, c)] and Anatoliy Melnyk [1, 3, d)]

[1]*Kazimierz Wielki University in Bydgoszcz, Institute of Geography, Poland*
[2]*Taras Shevchenko National University of Kyiv, Faculty of Geography, Ukraine*
[3]*Ivan Franko National University of Lviv, Faculty of Geography, Ukraine*
[a)]Corresponding author: obodovskiy58@gmail.com
[b)] po4aevets@gmail.com
[c)]mgrodz@ukr.net
[d)]anatolij.melnyk@gmail.com

Abstract. Information on the water flow, which for the entire Tisza basin is formed in particular in the Ukrainian Carpathians, is important for the regions located in the middle and lower currents. During the period of climate change and intensification of droughts, the necessity of study of dangerous hydrological phenomena. The period of minimal runoff can also be attributed to dangerous hydrological phenomena. According to the normative documents [13], the basic calculation characteristics of the minimum flow of rivers are the 30-days minimum flow for the summer-autumn and winter periods. However, the river flood type of the Tisza river basin influences the determination of continuous periods of 30-days minimum flow. Taking into account other studies , it was proposed to use the value of 7-days minimum flow for mountain rivers. As a result of the calculations a set of thematic layers and multi-layered maps of the 7-day minimum flow was obtained.

INTRODUCTION

The minimum flow of the rivers in the Tisza river basin is insufficiently studied, because due to excessive humidity of the area, much attention was paid to the maximum drainage of this region. However, recently there were extremely low flow periods on the indicated rivers, which even reached historical minima. Therefore, the research of minimum flow of the river is extremely important in water management.

One of the methods for determining the minimum flow of the rivers with no regular hydrometric observations is the use of distribution maps of the modules of minimum flow. Depending on the needs, in Ukraine there are different requirements for calculating the minimum water flow in rivers. For the functioning of the river ecosystem, the ecological water flow is used - the amount of water that should remain in the channel. For water management calculations are used maps of the module of the 30 days minimum flow with exceedance probability of 80% separately for the summer-autumn and winter low flows periods [13]. Taking into account the foregoing, one can conclude that in Ukraine, still, there is no uniform requirements for estimating the minimum low flows. There are different conditions in different spheres [4,5,6]. In view of this, it was decided to analyze also the experience of foreign scientists and specialists in the field of water management [8-12]. According to the requirements of the Water Framework Directive [1], one of the most important conditions is the observance of the status of a water facility suitable for the functioning of ecosystems, that is, for the life of fish. Thus, it is necessary to take into account not only the quality of water, but also its quantity.

METHODS

According to [8-12], one of the values of the calculation of minimum flow is the mean annual 7 day minimum flow with different exceedance probability consumption (10 years, 20 years - depending on water management needs). To determine 7 days minimum flow of water consumption, average daily water consumption at 29 hydrological stations in the basin of the Tisza River was used (of which 22 within Ukraine and 7 beyond its borders). The period of observation ranged from 30 to 70 years. The data was analyzed for this period until 2015 inclusive. Daily data on water discharge at 29 hydrological stations in the Tisza basin (of which 22 within Ukraine and 7 outside it) were used to determine the 7-days minimum flows of water. The period of observation ranged from 30 to 70 years. Data was analyzed by 2015 year. The mean annual values of the 7 days minimum water flow for the summer-autumn and winter period, as well as their statistical parameters were determined using the IHA software (Indicators of Hydrologic Alteration) [2]. Also, the amounts of daily rainfall in the meteorological stations, located directly near the hydrological posts were used. On the basis of these data, a hydrograph and precipitation curves were constructed, which confirmed the calculated values of the minimum 7-days minimum flow of water.

To construct maps of the spatial distribution of the minimum flow, it was necessary to exclude the influence of the catchment area of the rivers. For this purpose, the values of the water flow of the rivers, which are presented in the form of layers (Y, mm) or modules of water flow (q, l · s-1 · km-2), were used. These values were assigned to the points - the catchment centers of the catchment, which, thus, reflect the average conditions for the formation of a runoff for the water catchment [5]. The collection, systematization and visualization of the results of spatial information evaluation was carried out using GIS [14]. It should be noted that in mountainous areas it is important to take into account the features of the relief when interpolating between the points. For this purpose, dependences of the module of the minimum flow of rivers from the height of their catchment areas are constructed. Usually, the mapping is not applied to data on water runoff from a small watershed. Because this small watersheds depends on azonal factors, first of all, on the areas of catchments. Also large rivers (more than km^2) are not included in the construction of maps as occurring in several geographic areas [3,5-7]. However, in the case of a map for the Tisa basin, data from small and medium-sized catchments has been taken into account. The location of isolines takes into account all general geographic trends in changes in hydrological characteristics, relief, climate and other physical and geographical features of the territory.

RESULTS

Database. To constructing the maps of the module 7-days minimum flow, 22 hydrological stations located on the rivers Tisa basin within Ukraine and 7 hydrological stations outside the basin were used. All data on water discharge were attributed to the median centers of catchment. Points outside the Tisza river basin were taken as additional, with local refinements of interpolation between the median centers of catchments, because the observation period is different in duration. For all hydrological station exceedance probability of the 80% of the 7-days minimum flow was calculated. Estimation of the accuracy of the definition of the mean annual value of the 7-day minimum flow for constructing a map of modules was carried out. The relation between water flow and the orographic characteristics of the catchment was also carried out. The relationship among water flow and the orographic characteristics of the catchment was also were defined.

For the estimation of reliability of values of 7-days minimum flow the mean square error has been used. It`s depends on the values of the coefficient of variation and the number of years of observations of the water flows on hydrological stations. The results show that the mean square errors are varied from 3.3% to 9.3% for summer-autumn and from 3.75% to 8.57% for winter minimum season. The largest value of mean square error values has observed on hydrological stations with the highest values of coefficients of correlation. The average values of the mean square error of the calculation of the 7-day minimum flows are ± 5.9% for summer-autumn and ± 5.81% for the winter minimum season. The obtained values of the average quadratic error of the 7 days minimum flow do not exceed ± 15%, which makes it possible to use them for mapping the modules of the minimum flow of the Tisza river basin. Taking into account the above, maps of modules of the 7 days minimum flow for winter minimum period (Fig.1) and summer-autumn minimum period (Fig.2) for the rivers were constructed.

An assessment of the reliability of mapping the modules of the 7-day minimum flow was defined. The comparison between the actual values in the hydrologic stations and the values taken from the map was accomplished (Fig.3).

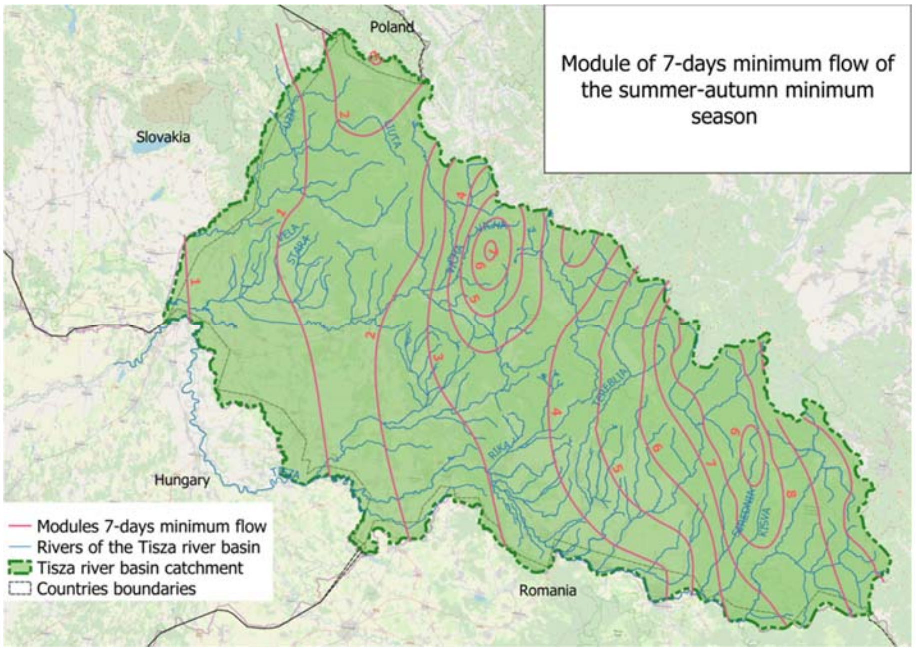

FIGURE 1. 7-days mean annual low flow of the winter minimum season of the Tisza river basin

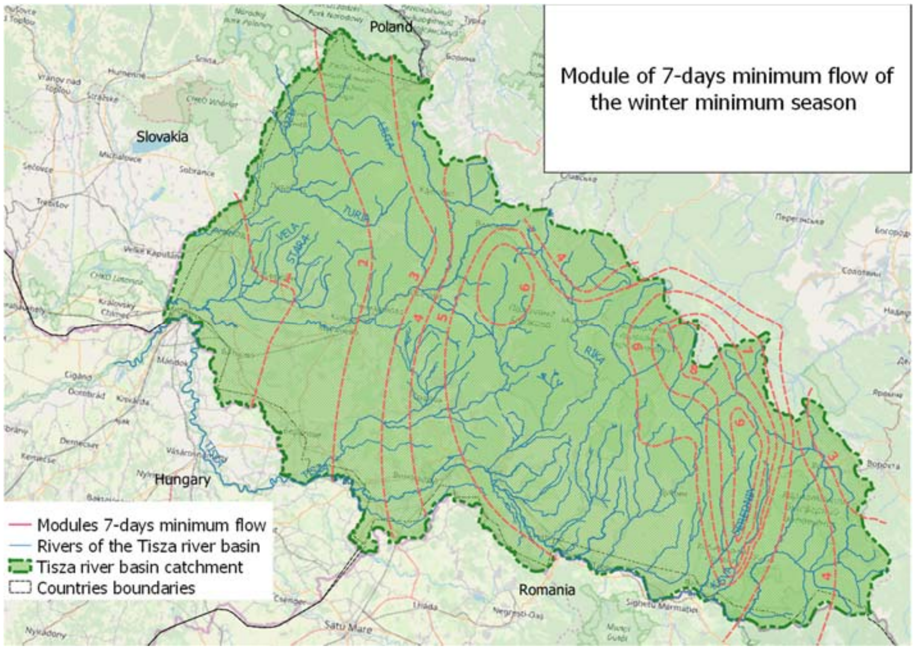

FIGURE 2. 7-days mean annual low flow of the summer-autumn minimum season of the Tisza river basin

The points chart shows a close relationship between the calculated values from the map and the observed values of 7-days minimum flow. The function is characterized by the determination coefficient, which equal R2 = 0,93 та 0,94 for winter and summer-autumn minimum season. The communication line coincides with the line of equal values. Deviations of the calculated and input values of the flow modules are within the limits of the relative error of calculation.

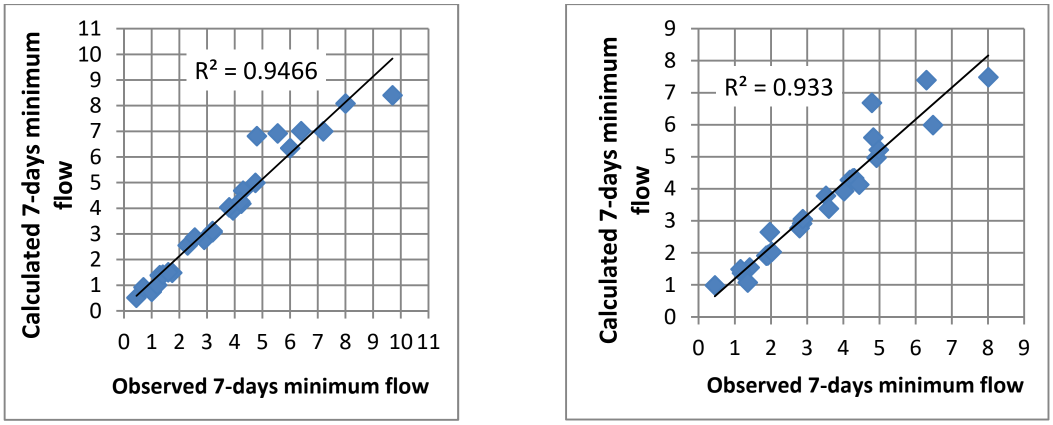

FIGURE 3. The relationship between the calculated values from the map and the observed values of 7-days minimum flow

CONCLUSIONS

Maps of the modules of the 7-days minimum flow based on indicators of 22 hydrological stations located on the rivers of the Tisza basin within Ukraine, and 7 hydrological stations outside the basin were constructed using GIS. Estimation of the accuracy of determining the long-term value of the module of the 7-days minimum flow was conducted. The average values of the mean square error of the calculation are ± 5.9% for summer-autumn and ± 5.81% for the winter minimum season, which makes it possible to use them for mapping the modules of the minimum flow of the Tisza river basin. The accuracy and reliability of mapping was confirmed by the close relationship between the calculated and the input values. The determination coefficient R2 = 0,93 та 0,94 for winter and summer-autumn minimum season.

ACKNOWLEDGMENTS

The research was conducted out as part of the implementation of the topic №14BP050-01 at Taras Shevchenko National University of Kyiv for funding the Ministry of Education and Science of Ukraine.

REFERENCES

1. Directive 2000/60/EC of the European Parliament and of the Council of 23 Oct 2000 establishing a framework for Community action in the field of water policy / Official Journal L 327, 22/12/2000 P. 0001
2. Indicators of Hydrologic Alteration Version 7.1. User`s Manual. The Nature Conservancy, 2009.
3. O. I. Luk'ianets', T.P. Kamins'ka, Naukovyj visnyk Chernivets'koho universytetu: zbirnyk naukovykh prats'. Chernivtsi: Chernivets'kyj nats. un-t. Vyp. 744–745: *Heohrafiia*. 2015. S. 18-24.
4. K. A. Lysenko, Trudy UkrNYHMY. 1976. Vyp. 149. p. 130-142.
5. O. Obodovskyi, O. Lukianets, Konovalenko O., Korniienko V. *Nauk. zbirnyk. Hidrolohiia, hidrokhimiia i hidroekolohiia. Kyiv*: VHL Obrii. 2016. №44. S. 25-32.
6. O. O. Obodovskyi, M.A. Pochaievets, *Nauk. zbirnyk. Hidrolohiia, hidrokhimiia i hidroekolohiia*. Kyiv: VHL Obrii. 2016. №40. S. 60–69.
7. O. H. Obodovskyi, Suray K.S., Pochaievets O.O. *Hidrolohiia, hidrokhimiia i hidroekolohiia*, 2018. № 2(49). S. 6–15.
8. J. Opperman, (2006). Preliminary IHA analysis for the Middle Fork Willamette River at Jasper OR.
9. C. Reilly, Estimation of 7-day, 10-year low-streamflow statistics using baseflow correlation / C. Reilly, N. C. Kroll. // *Water resources research*. – 2003. – №30. – С. 1–10.
10. B. D. Richter, J.V. Baumgartner, Braun, D.P., and Powell, J. (1998). *Regulated Rivers: Research & Management*, 14, 329-340.
11. B. D. Richter, J.V. Baumgartner, J. Powell., and Braun, D.P., (1996) *Conservation Biol.*, 10(4), 1163-1174.
12. B.D. Richter, J.V. Baumgartner, Wigington, R., and Braun, D.P. (1997). *Freshwater Biology*, 37, 231-249. SNyP 2.01.14-83 Vyznachennia rozrakhunkovykh hidrolohichnykh kharakterystyk. Hidroproekt. Leningrad. 1984. p.448
13. U. Gandhi. QGIS Tutorials and Tips [Electronic resource] – Resource access mode: http://www.qgistutorials.com/uk/docs/introduction.html

Hazardous Hydro-Meteorological Phenomena in the Skole Beskyds National Park (Ukrainian Carpathians)

Anatoliy Melnyk[1, 3, a)], Mykhailo Grodzynskyi[1, 2, b)], Oleksandr Obodovskiy[1, 2, c)] and Olesya Buryanyk[3, d)]

[1]*Kazimierz Wielki University in Bydgoszcz, Institute of Geography, Poland*
[2]*Taras Shevchenko National University of Kyiv, Faculty of Geography, Ukraine*
[3]*Ivan Franko National University of Lviv, Faculty of Geography, Ukraine*

[a)]Corresponding author: anatolij.melnyk@gmail.com
[b)]mgrodz@ukr.net
[c)]obodovskiy58@gmail.com
[d)]olesya.buryamk@lnu.edu.ua

Abstract. The natural background of hazardous processes and phenomena in the Skole Beskyds National Park, Ukraine are characterized using the Rybnik Majdansky river basin covering 25% of the park's area. The spatial regularities of floods, coastal erosion, earth flows, landslides, avalanches, and windbreaks are shown. On the basis data from Maidan hydrological station the dynamics of thunderstorms for the period from 2002 to 2012 is analyzed as well as the set of hydrological parameters for the Rybnik Majdansky experimental basin were calculated. The estimates were used to find the time intervals (years and months) of the highest activity of hazardous hydro-meteorological processes and events.

INTRODUCTION

The Skole Beskyds National Park is located in the Beskydnyj District of Ukraine. Its area is made up of flysh sediments, characterized by a mild continental relatively humid climate. Due to these natural conditions such hazardous hydro-meteorological processes as thunderstorms, river floods, surface and coastal erosion, earth flows, landslides, and avalanches. Strong winds cause windbreaks that in their turn influence on the spreading of plant's diseases and the dieback of the forest stands. These processes became active few times during the year causing economic damages and threats to human life both in Carpathian Mountains and in its foothills. The basins of small montane rivers having the hydro-meteorological stations are the most relevant sites to study the abovementioned processes and relations. The Rybnik Majdansky river basin served as the case study area to study the spatial extent and temporal regularities of hazardous processes within the Skole Beskyds National Park. The basin belongs to the Skolivski Beskyds microregion, which is the part of Eastern Bieshchady mesoregion, Forested Beskyds macroregion, subprovince of Exterior Eastern Carpathian of the Eastern Carpathian Province [3].

MATERIAL AND METHODS

To study the natural drivers and spatial distribution of the hazardous hydro-meteorological processes the methodology of the field landscape surveying and mapping was applied [5]. In addition, the methodology of geological and geomorphological field surveying was used. To study the actual vegetation cover of the basin the schemes of forest stands of Majdansky [8] and Zavadkivskiy [9] forestry enterprises of the Skole Beskyds National Park. The satellite images from the SAS Planet program were also used. The raw data for the period from 2002 to 2012 of Maidan hydrological station of the Hydro-meteorological State Service of Ukraine were applied to study the

temporal regularities of the hazardous processes and events [2]. The software Arc GIS 9.3.1 Spatial Analyst was used to process the data.

RESULTS

The area of the Rybnik Majdansky river basin is 80.85 km², 5.46 km wide, its longest axis is 14.8 km long, the compactness coefficient is 0.49, the average elevation is 847 m above sea level, 89% of the basins area are forested. The landscape pattern of the basin is typical for the Skole Beskyds Mountains and since the 1999 it belongs to the strictly protected area of the Skole Beskyds National Park. From the geological point of view, the Rybnik Majdanskiy river basin belongs to the Skyby tectonic zone within three folds, namely Parashka, Zelemyanka and Rozhanka each of 2 km wide [7]. The landforms are mainly steep slopes, the density of horizontal erosional dissection of the area is 1.6, vertical dissection – 10 m, the maximum relative elevation is 690 m.

The climate of the Rybnik Majdansky river basin is mild continental. Its area lies within the moderate climatic belt (499-850 m above sea level) and cool climatic belt (850-1250 m) [1]. The average January temperature is -4.5 °C, while the average July temperature raises up 18 °C, the annual precipitation varies from 800 to 1000 mm, and the average wind velocity is 1.8-2.7 m/s [6]. The thunderstorms are the most frequent hazardous events within the Rybnik Majdansky river basin. They stimulate the development of the earth flows, river floods, coastal and channel erosion, landslides. Data from Majdan hydrological station [2] shows that for the 2002-2012 period 37 days with thunderstorms within the river basin were recorded.

The amount of precipitation influence heavily on the surface and subsurface flows, which in their turn are connected with the hazardous hydro-meteorological processes [10]. Using the data of Majdan hydrological station we have calculated and analyzed the principal parameters of the river flow for the 2002-2012 year period such as water level, water discharge, volume and modulus of flow. The calculations served as the basis for finding out the temporal regularities of the hazardous hydro-meteorological processes and events.

Forests dominate in the vegetation cover of the basin. Using the maps of forest stands of Majdansky [8] and Zavadkivsky [9] forestry of the Skole Bekids National Park we analyzed the species and age structure of forests within the basin of the Rybnik Majdansky River. Spruce and beech forests in the brown mountain forest soils predominates min the basin. Coniferous forests comprised 53.7% of the area with *Picea abies, Abies alba, Pinus sivestris, Larix decidua.* Deciduous forests occupy 43,1% of the area with *Fagus sylvatica, Acer pseudoplatanus, and Alnus incana* as dominant tree species. In the age composition of the forests the middle aged species predominate (42.2%), the overgrown occupies 26.4% while young trees occupies 9.4% of area, only [8, 9]. Such age composition of the forests is unfavorable in view of the development of hazardous processes on slopes and rivers.

The human activity in the Rybnik Majdansky river basin in the past was associated with intensive tree cutting. As a result, the native beech tree stands were replaced by the secondary fir spruce stands. The network of dirt roads within the basin dissected the forest cover which is also the negative factor causing surface erosion.

The landscape map illustrates the spatial distribution of hazardous hydro-meteorological processes. Three types of landscape geocomplexes, that compose the landscape structure of the Rybnik Maidansky river basin, correspond to landforms of particular morphology, genesis and elevation. Landscape surveying in the Rybnik Maidansky river basin revealed that hazardous hydro-meteorological processes have strong tendency to occur with particular types of landscape geocomplexes. This spatial correspondence is shown in Fig.1.

Among the dangerous hydro-meteorological processes the greatest damage to humans is caused by floods. Together with the coastal erosion, they are typical for geocomplexes of terraced bottoms of the river valleys. The flood happened in July 2008 was the most hazardous. During July 25-26, 179 mm of rain fell and as a result, residential buildings, agricultural lands, roads, bridges were damaged. Coastal erosion is common in the downstream of the Rybnik Maidansky River.

The earth flows within the studied area are not widespread and tend to happen in the bottoms of steep mountainous streams developed within the sandy-clay flysh. The landslides are characteristic feature of the geocomplexes of the eroded and denudated steep slopes of the forested low-mountains composed of sandstone-argillite flysh and mainly are developed on slopes along the river beds. The landslide processes happen predominantly on the slopes of the southwest exposure is facilitated by the monoclinal folding of the flysh rocks.

Avalanches within the studies basin are distributed locally and correspond to the very steep deforested slopes of the northeastern exposition of the Mount High Upper in mid-mountains. The effects of meteorological factors are associated with windbreaks and windfalls, which corresponds to the wooded steep slopes in mid-mountains and are especially typical for the slopes of the crests covered with pure spruce forests.

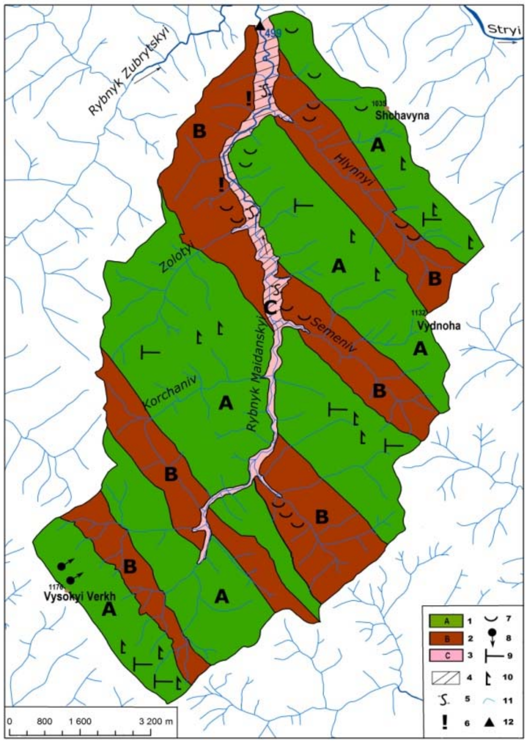

FIGURE 1. Hazardous hydro-meteorological processes in the landscape geocomplexes of the Rybnik Majdansky river basin. Landscape geocomplexes: 1- eroded and denudated steep slopes of the forested mid-mountains; 2 - the same in low-mountains; 3 - river bottoms with terraces. 4- areas affected with the floods. Hazardous hydro-meteorological processes: 5 - coastal erosion; 6 - earth flows; 7 - landslides; 8 - snow avalanches. 9 - windbreaks. 10 - windfalls.. 11- rivers and streams. 12 - Maidan hydrological station

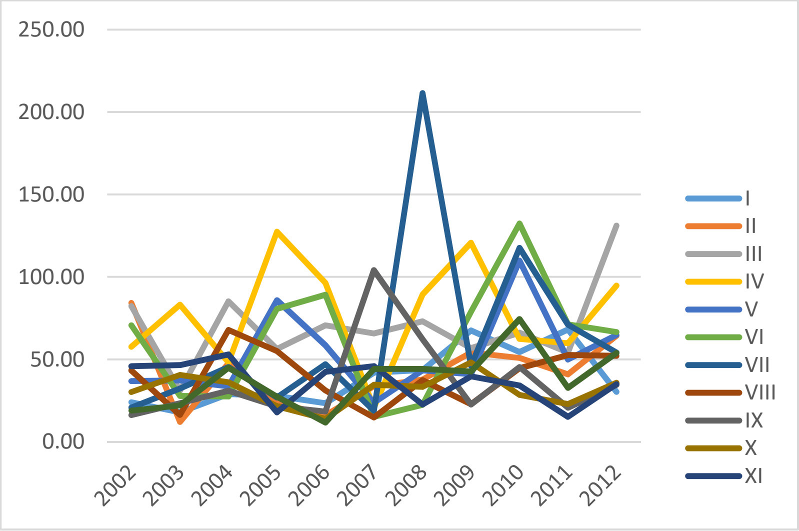

FIGURE 2. Average monthly values of the flow modulus (m³/s from 1 km²) in the Rybnik Majdansky river basin for the 2002-2012 period (calculated on the data from Maidan hydrological station [2])

The temporal features of the hazardous meteorological phenomena (storm rainfall) and processes (flood, coastal erosion, earth flows, and landslides) for the investigated period from 2002 to 2012 are correlated with the dynamics

of thunderstorms [2] and of flow modulus (Fig. 2). The unusual activity of these processes took place in 2008-2012, when the water level, runoff coefficient and other hydrological characteristics exceeded the norm.

During the year, hazardous hydro-meteorological processes and events are distributed unevenly. Generally, in the Rybnik Maidansky basin and in the Skole Bekyds National Park they occur during the spring and summer months, when spring floods and most intensive rainfalls are happens as well. The largest amounts of precipitation occurred in May, June and July 2008, 2009 and 2010. In particular, 383 mm of precipitations were recorded in July, 2008; 180 mm – in June, 2009; 173 mm – in May, 2010; 222 mm –in June, 2010, and 218 mm – in July, 2010. At that, the values of flow modulus exceeded 100 m^3/s from 1 km^2, in particular in July 2008 it was 210 m^3/s from 1 km^2, while the standard value for the flow modulus is equal to 63 m^3/s with 1 km^2.

CONCLUSIONS

Rainstorms is the main factor of the hazardous hydro-meteorological processes in the Skole Bekyds National Park. They occur in 2 – 5 days every year. The domination of secondary coniferous forest stands in vegetation cover as well as vast areas of steep slopes composed of sandstone-argillite play an important role in the development of hazardous processes. They demonstrate clear spatial distribution in accordance with the landscape geocomplexes of particular type: floods and coastal erosion are common in the terraced bottoms of the river valleys, the earth flows and landslides are typical for geocomplexes of slopes in low-mountains, while avalanches and wind-breaks develop in mid mountainous steep slopes. The activation in time of hazardous processes is quite high - five of the 11 analyzed years are characterized by an increase in the rate of precipitation and, consequently, hydrological parameters correlated with the frequency of hazardous hydro-meteorological processes. At the same time, every 11 years it has catastrophic consequences, as it happened in July 2012.

REFERENCES

1. M.S. Andrianov, 1957. *Geographic Almanac of the Lviv University*. Series Geography, Vol.4. – P.189 – 199.(in Russian)
2. *Hydrological Yearbooks* of the Central Geophysics Observatory of the Hydro-meteorological State Service of Ukraine, 2002 – 2012.
3. J. Kondracki, 1993. *Regional delimitation of Carpathians* (map of scale 1:2 000 000). Warsaw, 1993 (In Polish).
4. K.T. Logvinov, A.N. Rayevskij, M.M. Ajzenberg, 1973. *Hazardous hydro-meteorological phenomena in Ukrainian Carpathians*. Leningrad, - 199 p. (In Russian)
5. G.P. Miller, 1974. Landscape studies of the mountains and foothills. Lviv, - 202 p. (In Russian)
6. *Records of the Natural Environment.* Skole Beskids Nature National Park, 2000. Vol. 3. – 172 p. (In Ukrainian).
7. Report of Lviv geological prospering expedition on the results of complex geological field survey in scale 1:50 000 within Pidgorodci, Skole, Turka areas, 1960–1982. Funds of the State geological enterprise "Zahidukrgeologiya". Lviv. (In Ukrainian).
8. *Scheme of the forest stands of Majdanske forestry* of the «Skole Bekids» NPP., 2003. Lviv. (In Ukrainian).
9. *Scheme of the forest stands of Zavadkivske forestry* of the «Skole Bekids» NPP., 2003. Lviv. (In Ukrainian).
10. D. Szatten, M. Habel, L. Pellegrini, M.Maerker, 2018., *Water (Switzerland),* vol. 10, iss. 11, art. no 1681, DOI:10.3390/w10111681

Altitudinal Differentiation of Snow Cover in the North-Eastern Sector of Chornohora Massive In Ukrainian Carpathians

Anatoliy Melnyk[1, 3, a)], Mykhailo Grodzynskyi[1, 2, b)], Oleksandr Obodovskiy[1, 2, c)], Lydmyla Kostiv[3, d)], Mykola Karabiniuk[3, e)] and Roman Prytula[3, f)]

[1]*Kazimierz Wielki University in Bydgoszcz, Institute of Geography, Poland*
[2]*Taras Shevchenko National University of Kyiv, Faculty of Geography, Ukraine*
[3]*Ivan Franko National University of Lviv, Faculty of Geography, Ukraine*

[a)]Corresponding author: anatolij.melnyk@gmail.com
[b)]mgrodz@ukr.net
[c)]obodovskiy58@gmail.com
[d)]ludmyla.kostiv@lnu.edu.ua
[e)]mykola.karabinyuk@lnu.edu.ua
[f)]roman.prytula@lnu.edu.ua

Abstract. was carried out o For the explanation of snow cover formation and spatial distribution on the north-eastern macro-slope of Chornohora, the highest mountain range of Ukrainian Carpathians, the methodology of physical-geographical analysis was applied. The temporal pattern in distribution of the snow cover in its dependence on elevation and the landscape pattern in the upper Prut river catchment was found. In our investigation we used data collected during our field measurements of the snow cover along the profile from 928 m a.s.l. up to 1749 m a.s.l. as well as data from Pozhyzhevska weather station of Hydro-meteorological Service of Ukraine (1450 m a.s.l.) and Chornohora Geographical Research Station of the Ivan Franko National University of Lviv (998 m a.s.l.).

INTRODUCTION

According to the physical-geographical zoning of J. Kondracki Chornohora is a separate mesoregion within the Eastern Beskyds macroregion, External Eastern Carpathians Sub-province, Eastern Carpathians Province [7]. It is the highest mountain range in the Ukrainian Carpathians, occupying the area of 630 km^2. The range is18 km wide and stretches from north east to south west on 40 km. Its absolute elevations exceed 2000 m a.s.l. with Mount Hoverla, 2061 m a.s.l. as its summit. Considering history of development, geological structure and relief, some differences between the north- eastern and southwestern macro-slopes (landscape sectors) of Chornohora are reported [8].

The Northeastern landscape sector is characterized by steep slopes, which are formed on the upper parts of the parent rocks, and has cooler climate. Northern aspects of the slopes and its steep inclination in the North-eastern sector caused the expansion of glaciation in Pleistocene and formation of glacial land forms (cirques, carlling, trough valleys). Northeastern sector of Chornohora is divided among several river basins – Lazeshchyna (the tributary of the Chorna Tisza), Prut, Bystrets, Dzembronia and Pogorilets (right tributaries of the Chorny Cheremosh river). The information on spatial and temporal differentiation the snow cover in Chornohora is important for the prediction of spring floods on above-mentioned rivers as well as for analysis of avalanche risk.

MATERIALS AND METHODS

The research transect is located within the Upper Prut river basin, where three stations are running long-term hydro-meteorological observations, including monitoring of the snow cover, namely Pozhyzhevska snow-avalanche weather station, Vorokhta gauging station, both belong to the Ivano-Frankivsk regional center for hydrometeorology of the Ukrainian Hydro-meteorological Emergency Services of Ukraine [4, 5] and the Chornohora research station of the Ivan Franko National University of Lviv established in1978 [1]. Landscape geocomplexes of two taxonomic levels were used in our study, namely landscape mesogeochores– geocomplexes occupying a certain altitude position and characterized by a combination of landforms of common genesis and landscape microgeochores — geocomplexes associated with one particular landfrom [8]. Landscape map with geochore of both these types is shown in Fig. 1.

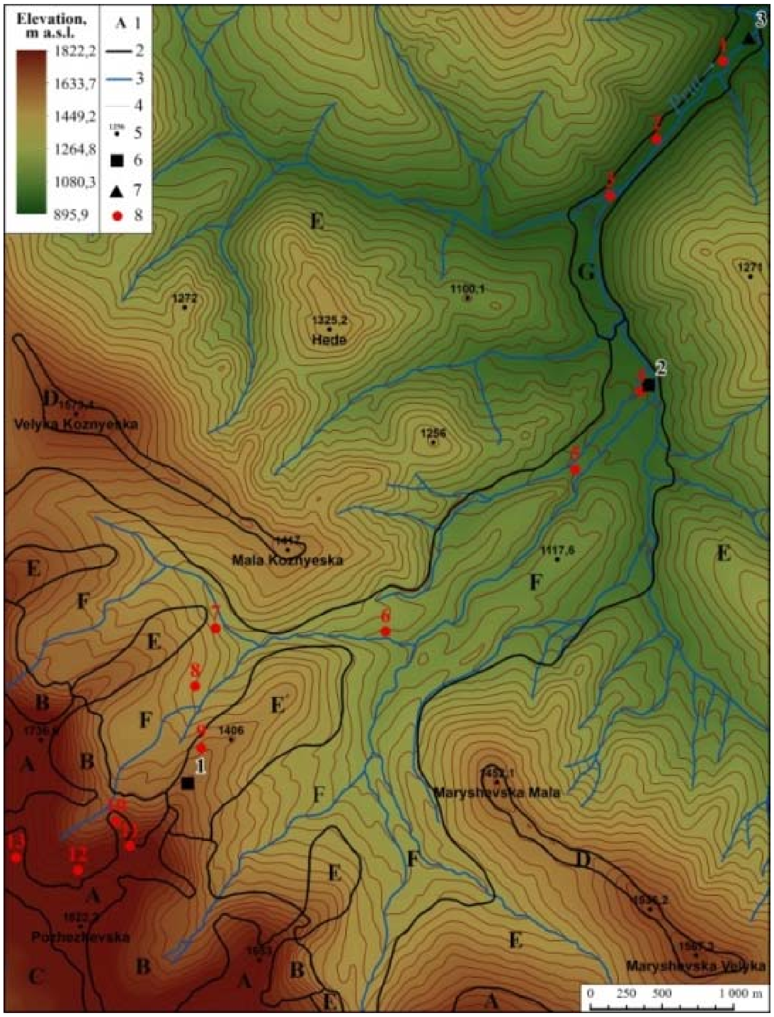

FIGURE 1. Observation sites and landscape map of the Upper Prut river basin in Chornohora mountain range, Ukraine. Landscape mesogeochores [6]: A. Slightly convex denudated surfaces of supalpine-alpnie high-mountain meadows of very cold and wet climate (average temperature of the coldest month -12 °C; and of the warmest months + 7 °C; annual precipitation up to 2000 mm) on mountainous brown meadow soils and mountainous brown peat bog soils. B. Concave old-glacial subalpine high-mountain surfaces of very cold and wet climate (January - 12 °C; July +8 °C, precipitation over 1500 mm) with deciduous and coniferous shrubs on mountainous brown peat bog soils and stony talus. C. Nival-erosional subalpine high-mountain surfaces of very cold and wet climate (January – -10°C; July +10-12 °C, precipitation over 1500 mm) with mountain-pine forests and elfin woodlands with *Alnus viridis* on mountainous brown meadow soils. D. Gentle slightly convex denudation surfaces of mid-mountains of cold (February -12 °C, July - 8 °C), humid (over 1000 mm) climate with spruce forests on brown soils. E. Steep eroded and denudated slopes of mid-mountains of cold (February -10° C; July - 10 °C); humid (over 1000 mm) climate with

spruce and fir-beech-spruce forests on brown soils. F. Old-glacial-accumulative plains in mid-mountains of moderately cold (February -10 °C; July - 10 °C) humid (over 1000 mm) climate with spruce forests on brown soils. G. Bottoms of river valleys in mid-mountains of cool (February -8°C, July- 14°C), moist (near 1000 m) climate and flood regime rivers, with spruce and willow forests and secondary grass herb meadows on brown and turf-brown soils. 1 - Pozhizhevska hydrological station, 2- and Chornogirsky geographical station, 3- Vorokhta gauging station, 1-13 – points of snow-cover observations

According to long-term meteorological observations at the Chornohora research station (998 m a.s.l.), which have been run systematically since 2001, the formation of a stable snow cover in the wooded mid-mountainous mesogeochore of Chornohora begins mainly in mid-November and lasts until the end of March and early April [3]. In this regard, snow surveys were carried out in the middle of the winter period. Mapping of the snoe cover was performed in the northeastern sector (macroslope) of the Chornohora massif on February 15, 2019 by routing snow measuring on the transect covering heights from 928 m a.s.l. up to 1749 m a.s.l., according to the methodology commonly used in the Hydrometeorological service of Ukraine, using the BC-43 tool [6]. For high-mountain mesogeochore (altitude 1570-1749 m a.s.l.) data from Pozhyzhevska snow-avalanche weather station were used [4, 5].

RESULTS AND DISCUSSION

The characteristics of snow cover (height, density and water reserves in snow) depend, on the one hand, on weather conditions and elevation above sea level, as well as on the properties of landscape complexes of the local level on the other. We analyzed weather conditions for the formation of snow cover in the winter season of 2018-2019 on the basis of meteorological observations carried out at two meteorological sites of the Chornohora research station [2]. The sites are located at an altitude of 998 m. in the landscape microgeochore of a floodplain in fluvio-glacial cone covered with the forest composed with *Vaccinium myrtillus, Luzula sylvatica, Oxalis acetosella, Polytrichum, and Picea abies*. Two landscape facies were chosen as experimental sites: meadow facies of the gently slope of the floodplain terraces with secondary vegetation and forest facies of the surface of floodplain terraces with wet forest where *Oxalis acetosella* and *Picea abies* dominate [1].

A steady snow cover on a meadow site began to form after insignificant precipitation, therefore in mid-November its height was only 4 cm, while on forested site such height of the snow was reached only in the third decade of November. The alternation of short periods with positive and negative average daily temperatures with their gradual decrease, as well as abundant precipitation at the end of November, formed snow cover with a clearly expressed differentiation into horizons. On the treeless site, its height reached 19 cm at a snow density of 0.10 g/cm^3, while on the forested site the snow height was 12 cm with its density of 0.09 g/cm^3.

In the first decade of December, as a result of a short-term thaw (with a maximum temperature of 4 °C), the snow depth in the meadow area decreased to 9 cm, on the forested area to 6 cm only. The difference is explained with the fact that under the forest canopy the temperature amplitudes were not as significant as those on the treeless area. This contributed to the saturation of snow moisture. Intensive snowfall and negative temperatures caused a repeated increase in snow thickness and compaction with a significant decrease in temperature. Particularly, in the second decade of December the snow depth increased from 34 cm in the meadow area and 14 cm, and in the forested area to 26 cm and 13 cm, respectively; In the third decade - from 46 cm and 23 cm to 40 cm and 22 cm, and in the first decade of January - from 59 cm and 29 cm to 50 cm and 28 cm. The average density of snow varied within 0.19-0.22 g/cm^3 in the meadow area and 0.15-0.21 g/cm^3 – in the forested area.

From mid-January, short-term thaws alternated with cold frost periods, which were accompanied by precipitation, which led to a periodic increase in the thickness of snow cover, its partial melting, water saturation, and further compaction and crystallization of the lower horizons. At the time of conducting snow surveys on transects (February 15), the height of snow cover at the meadow site was 60 cm, and at the forested site – 36 cm.

Snow measurement sites were located at different heights in four landscape mesogeochores (Fig. 1): the terraced bottom of the Prut River valley (points 1, 2 and 3); long-glacial-accumulative wooded mid-mountains (points 4-8); erosion-denudation slopes of the wooded mid-mountains (point 9); denuded alpine-subalpine highlands (points 10,13,14) and old-glacial subalpine highlands (point 12). Figure 2 shows the difference in snow cover and snow attributes between these mesogeochores. In the terraced bottom of the Prut river valley, with slight changes in altitude of its sites, the snow depth has low spatial variation – from 30 to 34 cm. A noticeable change in the density of snow in points 2 and 3 from 0.18 g/cm^3 to 0.25 g/cm^3 and content of water in the snow from 55.8 to 85.0 mm is not so much associated with a change in height, but with the nature of the river valley. In point 3 it expands considerably to the south causing considerable transformation of snow cover under the direct influence of the sun's

rays. For the wooded mid-mountains (points 4–9) the increase in elevation causes gradual increase in the height of snow cover (from 36 to 95 cm) and in water content in snow (from 97, 2 mm to 199.5 mm). High values of snow density (0.27 g/cm^3) in the areas at the heights lower than that of points 4 and 5 (0.20 g/cm^3) are explained, as mentioned above, by a significant expansion of the bottom of the Prut River valley.

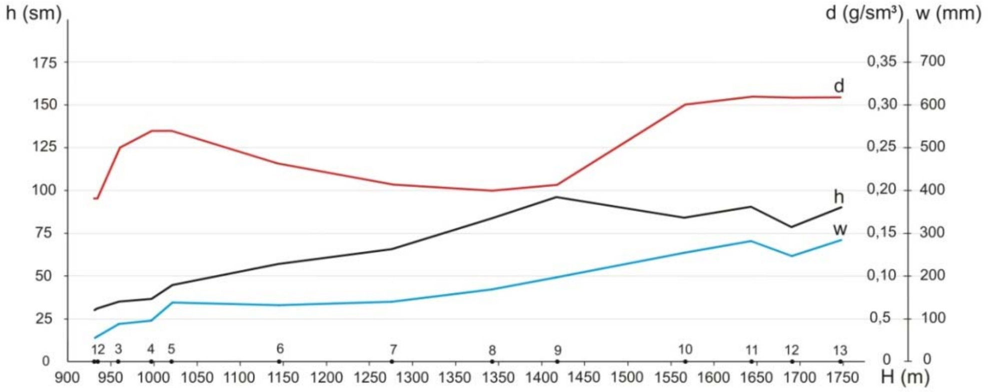

FIGURE 2. Distribution of snow properties in the basin of the Prut River with height (as of 15.02.2019) (data for stations 10-13 are calculated using the dada from the Pozhyzhevska snow-avalanche weather station) [2,3]; H - height in m a.s.l., h - snow cover, d - snow depth, w - water reserves in the snow

In the sub-alpine and alpine highlands, the study of snow cover was carried out on four points with meadow vegetation. The height of the snow cover varied from 84 to 90 cm with a relatively identical density (30-31 g/cm^3), and the water content in the snow ranged from 248 to 279 mm. The structure of the snow is also similar and is characterized by a well-twisted strata feature with four crusts.

CONCLUSIONS

The increase in snow cover in the northeastern sector of Chornohora in the Prut river basin with a height from 30 to 90 cm and, consequently, an increase in water content in snow from 54 to 279 mm is explained by the increase in winter precipitation, lowering of temperature with the elevation in mountains and, accordingly, less distinct thaws. More intense thaws in the broad bottom of the Prut River resulted in a significant increase in the density of snow by 0.5-0.7 g/cm^3 compared to those located above mentioned sites, which will lead to an increase in the amount of water in it.

REFERENCES

1. *Chornohora geographic station*, 2003. Lviv University Press. - 132 p.1.
2. *Data Records* of the Chornohora geographic research station of the Ivan Franko National University of Lviv. Observation journal “Meteorological data”, 2001-2019. Vorohta
3. *Data Records* of the Chornohora geographic research station of the Ivan Franko National University of Lviv. Observation journal “Snow Cover”, 2001-2019. Vorohta
4. *Data Records* of the Ivano-Frankivsk regional hydro-meteorological center. Data on the depth of snow cover in the remote racks in Pozhyzhevska snow-avalanche weather station. 2019. Ivano-Frankivsk,.
5. *Data Records* of the Ivano-Frankivsk regional hydro-meteorological center. Observation journal of the Pozhyzhevska snow-avalanche weather station, 2019. Ivano-Frankivsk.
6. *Guidelines for hydro-meteorological stations and sites*. Part 1. Meteorological observations on the stations. State Hydro-meteorological service, 2011. Kyiv: Nika-Centre, 280 p.(In Ukrainian).
7. J. Kondracki, 1993. *Regional delimitation of Carpathians* (map of scale 1:2 000 000). Warsaw, 1993 (In Polish).
8. G.P. Miller, 1974. *Landscape studies of the mountains and foothills*. Lviv, - 202 p. (In Russian)

Preface of the "VI - International Symposium of Computational and Mathematical Modeling of Biologic and Medicine Targets"

Dilson Silva and Sotiris Missailidis

Instituto de Tecnologia em Imunobiologicos – Biomanguinhos / FIOCRUZ
Av Brasil, 4365 - Pavilhão Rocha Lima
Rio de Janeiro / Brazil. Phone +55 (21) 3882-7210

Corresponding authors: sildilson@gmail.com; sotiris.missailidis@gmail.com

We have been organizing the symposium along the last six years as an adequate space to join students and scientists interested in discussing modeling and the use of mathematical tools and computational methods applied to biologic and medicine targets, specially focusing on interactions of ligands to proteins, modeling neurobiology, and methods to bio-monitoring ecosystems health, among others. Our expectation is to bring together researchers working in the study of molecular interactions of a wide range of systems, from natural products to synthetic pharmaceutics, with an emphasis to novel biological therapeutics, specially aptamers and other oligo-nucleotides, and proteins with diagnostic potential. Organizers are reviewers for most of important journals in the field and have been actively publishing papers in this research scope. We are kindly grateful to all who attended the present and past editions, and strongly encourage you to gather the next symposium and take the occasion to change experiences.

Topics:

- Advancing in Ligand Binding Models;
- Developing Pharmaceutics
- Biomarkers of Environmental Contamination;
- Modeling in Neurobiology.

Dr. Dilson Silva

Professor Dilson Silva has graduated in Biology, with MSc and PhD in Biological Sciences at the University of the State of Rio de Janeiro (Brazil). Post-graduating studies has been focused on the molecular approach of ligands binding to proteins. Post-doctoral studies were conducted at the University of São Paulo, Department of Physics and Informatics (2005) granted by the "Human Frontier Science Program" within a project led by the Salk Institute and the Wien University. After that he has awarded a Visiting Research position at the Molecular and Structural Biophysics Laboratory, still in the University of São Paulo. In 2009/2010 he has developed projects as Visiting Research Fellow at the Department of Chemistry and Analytical Sciences, The Open University, UK (2009-2010). He is now Professor at the Department of Applied Mathematics and Professor of the graduating courses of Computational Sciences and Medical Sciences, both at the University of the State of Rio de Janeiro. His focus points to new tools and modeling techniques to better understand the mechanisms of drug interaction, identifying binding sites and calculating binding constants of a wide class of ligands and proteins. Since 2014 he organizes the symposium at the ICCMSE.

Dr. Sotiris Missailidis

Sotiris Missailidis has graduated in Biology from the American University of Athens (1991) and has completed his MSc (1993) and DPhil (1997) in Chemistry at the University of York (UK). Following that, he has completed post-doctoral studies at the University of Nottingham, Department of Pharmaceutical Sciences (1996-2000) and University of Cambridge, Laboratory of Molecular Biology and Department of Chemistry (2000). He was subsequently awarded a Leverhulme career fellowship, which he undertook at the Open University (2000-2002), where he was subsequently awarded a permanent post (2002-2012), leading his own aptamer group. During this period, he has also been awarded visiting professorships at the University of Paris 13 and the University of Lisbon, as well as a Mike Price European Fellowship in Cancer to develop aptamers against ovarian cancer with the University of Patras. Whilst in the UK, he has been awarded funding from Cancer Charities (Breast Cancer Campaign, Cancer Research UK, and European Association for Cancer Research) and Industry for his aptamer work. He moved to Brazil as a senior visiting researcher at the Institute Oswaldo Cruz developing novel diagnostic assays for rickettsial diseases and hantaviruses and is currently the Vice-Director of Technology Development at Biomanguinhos plant of the institute, responsible for the R&D development of biologics, vaccines and diagnostics. He is one of the leading authorities on aptamers with publications on high impact journals, edited books, chapters in books, and various conference participations as an invited speaker. He has also got patents granted and has been the founder and CEO of Euzoia Limited in the UK and Scientific advisor of Naxos DNA Serv in Brazil.

Scientific and Technological Research on the use of Molecular Markers in Turtles

Alana Lislea de Sousa[a,*], Lígia Almeida Pereira[b] , Helmara Diniz Costa[c], Ana Lúcia Abreu Silva[d], Ligia Tchaicka[b].

[a]*Departament of Veterinary Clinics, Maranhão State University, Brazil;*
[b]*Department of Chemistry and Biology, Maranhão State University, Brazil.*
[c]*Biodiversity and Biotechnology of the Legal Amazon – BIONORTE, Maranhão , Federal University, Brazil.*
[d]*BIONORTE Network Program, Maranhão State University, Brazil.*
[*]alislea@hotmail.com

Abstract. The objective of this prospection was to study the use of molecular markers in turtles. For this, information was obtained on scientific articles in Science Direct, Web of Science and SCOPUS databases as well as on patent documents in INPI, WIPO and EPO databases. Thus, a large number of published studies involving molecular markers were found, although this number is lower when associated with use in turtles. Regarding patents, only one was filed (in 2011), indicating research opportunities in this area.
Keywords: Molecular markers, turtles, technological prospecting.
PACS: 00 - 06

INTRODUCTION

In recent years, there has been a significant advance in molecular genetic techniques, using molecular markers, which are applicable in different areas of knowledge as useful tools, safe and capable of providing an accurate diagnosis. Comparative studies of genetic variation described through molecular markers and regional morphometric patterns have been performed for several wild species [1, 2, 3]. Among vertebrates, turtles occupy a worrying position regarding their conservation, being very vulnerable to extinction, since more than half of the species are threatened. The percentage of threat of these animals is higher than the rates verified for birds (13%), mammals (25%) and amphibians (41%) [4].

The molecular markers allow the knowledge of important genetic data, complementing ecological and morphological data and allowing design of conservation strategies. Thus, the objective of this study was to know and map the already developed and patented researches regarding the use of molecular markers in turtles from the scientific and technological perspective.

MATERIALS AND METHODS

This research was carried out from October to November of 2015. The scientific analysis was developed from the published articles in the bases Science Direct, Web of Science and SCOPUS. In order to verify the registration of patents, the INPI (National Institute of Industrial Property), EPO (European Patent Office) and WIPO (World Intellectual Property Organization) were surveyed. The descriptors used were: molecular marker, turtle, chelonian, molecular marker and turtle * and marker * and turtle *. The terms in English were used for the international bases, while the terms in Portuguese for the national base where the descriptors were part of the title and / or abstract. In the mentioned research, no date range were determined for the search, and all articles and patent documents available by the end of the research (November 30, 2015) were consulted.

RESULTS AND DISCUSSION

The results of the search of scientific articles indexed in international databases evidenced the high number of researches using molecular markers (Table 1), which generically covers studies on animals and plants, confirming its application in several lines of research. However, when we related the markers to turtles, this number decreased significantly. Such results can be explained by the fact that many species are not yet studied or even sufficiently

studied. Specifically in the case of Brazil, the country is considered atypical when it comes to species conservation, despite its size and biological diversity, when compared to the United States, Russia, Australia, China and Canada; because, unlike these, it has few resources to conserve them [5].

TABLE 1 - Number of scientific articles by keywords and grouping of words, retrieved from Science Direct, Web of Science and SCOPUS databases from October to November 2015.

Keywords	Science Direct	Web of Science	SCOPUS
Molecular marker	593.630	300.512	160.194
Turtle	32.743	31.914	18.229
Chelonian	1.660	850	1.219
Molecular marker and turtle	2.753	205	110

The results of the technological prospection presented below (Table 2) refer to all applications for patent deposits made by analyzing the keywords and their combinations in the INPI, EPO and WIPO databases. It can be observed in the three databases that the proportion of patent applications related to molecular markers was much higher than the other searches, confirming the scientific interest in the applicability of this tool. It is also observed that the results decrease significantly in the research for the term "turtle" and that only one patent was located in all bases with the term "chelon". In the search for associated keywords, it was found that technological production is still scarce, with 02 patents found in EPO and 04 in WIPO, evidencing a gap for this animal group. This gap occurs partly because of patenting legislation, which varies among countries. Statistical data shows that the United States continues to be the country that focuses the most on international patent registration, ahead of China, while emerging countries need to stimulate technological innovation more strongly [6].

Regarding to patents related to turtles, only one record was found for conservation purposes, referring to the species *Chinemys reevesii* (CN 102146382 A) which invention was the provision of microsatellite markers, showing availability of ten new informative loci and respective amplification methods. According to the inventors, it may be applied in studies on genetic diversity of different geographic populations and identification of paternity.

TABLE 2. Number of patents for keywords, truncation and grouping of words searched in INPI, EPO and WIPO databases from October to November 2015.

Keywords	INPI		EPO	WIPO
	Title	**Abstract**	**Title or Abstract**	**All fields**
Marcador* molecular* or molecular marker*	1596	4886	5190	5058
Tartaruga* or turtle*	13	08	3686	3530
Quelônio* or chelonian*	01	01	13	08
Marcador* molecular* e tartaruga*/molecular and marker* and turtle*	0	0	02	04

The International Patent Classification (IPC) is an important tool to expedite searches on the patent bases [7]. According to this classification [8], patents are distributed according to their application. The documents of this research were analyzed according to the CIP (Figure 1) where it was verified that two patents are referred to section C12N (C12N 15/10 and C12N 15/11) and the other two to C01B.

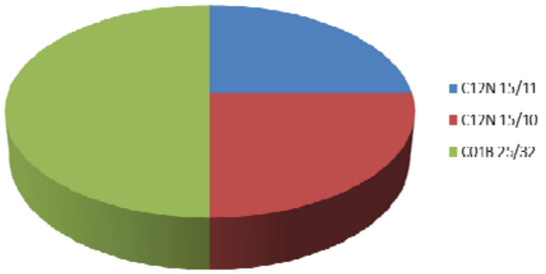

FIGURE 1. Distribution of patent applications by IPC.

The IPC section C12 (biochemistry, beer, alcohol, wine, vinegar, microbiology, enzymology, genetic or mutation engineering) covers microorganisms or enzymes; their composition, propagation, preservation or the maintenance of microorganisms or tissue; genetic or mutation engineering; and culture media, which are framed in subclass C12N. The patent applications belonging to this subclass were deposited in C12N 15/10 (mutation or genetic engineering, DNA or RNA concerning genetic engineering, vectors such as plasmids or their isolation, preparation or purification; the use of their hosts; recombinant DNA technology *DNA or RNA fragments* or *modified forms thereof*), as well as C12N 15/11 (mutation or genetic engineering; DNA or RNA concerning genetic engineering, vectors such as plasmids or their isolation, preparation or purification; the use of their hosts, recombinant DNA technology *DNA or RNA fragments* or *modified forms thereof*).

Section C01 (inorganic chemistry) involves non-metallic elements and their compounds (CO1B) in the subclass; classification of C01B 25/32 refers to phosphorus, its phosphorus oxyacid compounds, and its phosphate salts. Two (2) patents are classified in this section under the same main inventor's name: Bruce A. Keizer.

Scientific articles and patents are respectively ways of dissemination of scientific and technological knowledge [9]. When analyzing the correlation between scientific articles and patents in this research, there was a disproportion between them. A factor to be considered to justify the low technological production on the use of molecular markers in turtles would be its applicability, which is directed especially for conservationist purposes, not arousing economic interest in the protection of these technologies, unlike therapeutic discoveries, where scientific investment is encouraged, considering the possibility of medicinal application.

ACKNOWLEDGMENTS

We would like to acknowledge the Technological Development – FAPEMA, for financial support.

REFERENCES

1. M. Weksler, C. R. Bonvicino, I. B. Otazu, J. S. S. Junior. J Mamm**.** **82**:109-122 (2001)
2. J. F. Vilela, C. A. M. Russo, J. A. Oliveira. Zootaxa. **2646** 26–42 (2010).
3. J. D. Ross, J. L. Bouzat. The Auk, **3**, (131), 298-313 (2014).
4. V. P. Páez, M. A. Morales-Betancourt, C. A. Lasso, O. V. Castaño-Moura, B. C. Brock. (Instituto de Investigación de Recursos Biológicos Alexander Von Humboldt) 528 pp. (2012).
5. E. Rodrigues. (Semina: Ciências Agrárias, Londrina) **23**(2): 261-272 (2002).
6. R. Freire. Número de patentes internacionais e a economia global. Disponível em: http://www.clarkemodet.com/pt_BR/actualidade/blog/2016/10/brasil-analise-numero-de-patentes-internacionais-e-a-economia-global.html. Acesso em 06 ago. 2017. (2016).
7. M. R. Serafini, S. L. Russo, A. E. Paixão, G. F. Silva (2011). Rev. Geintec,1:1-11 (2011).
8. Patentes on Line. Classificação de Patentes. Disponível em: <htttp://www.patentesonline.com.br/classificacoes/> (2015).
9. S. P. M. Mueller, V. Perucchi. Perspectivas em Ciência da Informação, **19**(2):15-36 (2014).

Fluorescence Spectroscopy Study of Single-Stranded Nucleic Acid Aptamer Species Against NS5 Zika Virus

A. A. Abalo[1], A.P.C. Argondizzo [2], L.M. Morais [3], L.N. Alves [4], D. Silva [1], E.C.N. Valdez [5], S. Missailidis [6, a)]

[1]*Laboratório de Tecnologia em Anticorpos Monoclonais, Pavilhão Rockfeller, Bio-Manguinhos/Fiocruz, Av. Brasil, 4365-Manguinhos, Rio de Janeiro, RJ, CEP 21040-900, Brazil*
[2] *Laboratório de Tecnologia Recombinante, Pavilhão Rockfeller, Bio-Manguinhos/Fiocruz, Av. Brasil, 4365-Manguinhos, Rio de Janeiro, RJ, CEP 21040-900, Brazil*
[3]*Laboratório de Tecnologia Virológica, Edifício Rocha Lima, Bio-Manguinhos/Fiocruz, Av. Brasil, 4365-Manguinhos, Rio de Janeiro, RJ, CEP 21040-900, Brazil*
[4] *International Centre for Genetic Engineering and Biotechnology, ICGEB, Località Padriciano, 99 – Trieste, TS, CEP 34149, Italy.*
[5] *Programa de Pós-Graduação em Ciências Médicas, UERJ, R. São Francisco Xavier, 524, Maracanã, Rio de Janeiro,- RJ, CEP 20550-900, Brazil*
[6] *Vice Diretoria de Desenvolvimento Tecnológico, Edifício Rocha Lima, Bio-Manguinhos/Fiocruz, Av. Brasil, 4365-Manguinhos, Rio de Janeiro, RJ, CEP 21040-900, Brazil*

[a)] Corresponding author. E-mail: sotiris.missailidis@bio.fiocruz.br

Abstract. Zika virus (ZIKV) belongs to the *Flaviviridae* family and its recent outbreak and association with human diseases (e.g. neurological disorders) have raised global health concerns. The viral NS5 protein is the most conserved ZIKV protein, and is comprised of two domains, an N-terminal methyltransferase domain and an RNA-dependent RNA polymerase (RdRP) domain at the C-terminal end. The fact that viral NS5 is essential for viral replication but lacks a human counterpart makes NS5 an important target to be studied. Single-stranded DNA oligonucleotides aptamers can fold into unique three-dimensional conformations that recognize targets with high-specific and –affinity. This work aims to study single-stranded DNA aptamers displaying high affinity and specificity generated against ZIKV NS5 protein to be used in diagnostic platforms.

INTRODUCTION

ZIKV was isolated in 1947 in the Ziika Forest in Uganda and remained a footnote among neglected tropical diseases until November 2015, when accumulating cases of microcephaly in Brazil were associated with a ZIKV epidemic several months prior[1]. Zika is usually asymptomatic, and most symptomatic infections are mild and resemble those observed with dengue: rash, fever, arthralgia, conjunctivitis, myalgia, headache and retro-orbital pain. Multiple *in vivo* and *in vitro* infection models demonstrated that ZIKV infection can disrupt neuro-development, and is the first of the widely distributed arboviruses to be considered as a significant risk factor for human congenital malformations[2]. Although most infections are likely mosquito transmitted, ZIKV can spread directly from person to person through sexual contact or vertically from mother to fetus, and this sets ZIKV apart from other pathogenic flaviviruses and creates significant and unexpected public health concerns. There have been reports of hematospermia and symptoms resembling prostatitis following infection and viral RNA and infectious virus have been detected in the semen of men weeks after clearing of acute symptom. Moreover, Zika has been strongly associated with neurological sequelae, most commonly Guillain– Barré Syndrome, but also meningo–encephalitis and myelitis[3]. Most symptomatic ZIKV infections are self-limited and resolve in less than a week; however, there are documented cases of severe Zika in patients with other underlying conditions[4].

The flaviviral genome is a positive-strand RNA that encodes a single polyprotein that is co- and post-translationally cleaved by viral and host proteases into three structural (C, prM, and E) and seven nonstructural proteins (NS1, NS2A, NS2B, NS3, NS4A, NS4B, and NS5)[5]. The RdRp and the mRNA capping methyltransferase activities are provided by the viral NS5 protein, which synthesizes viral genomic RNA via a *de novo* initiation mechanism and it is mainly localized in the nucleus[6]. Aditional functions were found for NS5, such as regulation of the gene splicing process in host cells and proteassome activity and degradation of the INF-regulated transcriptional activator STAT2 from humans, evading ZIKV infection from IFN signaling, which is important for host antiviral innate immunity[7]. Another function of NS5 was also recently described in the regulation of NLRP3 inflammasome, which leads to activation of Interleukin 1-β (IL-1 β) secretion and induction of agressive host inflammatory

responses that are major determinants of ZIKV pathogenicity[8]. Additionally, as NS5 protein is a major target for CD4+ and CD8+ T lymphocytes, the whole antigen has been proposed as a promising strategy in the development of a vaccine against zika, in order to induce a significant celular immune response in different human populations in the world[9].

Aptamers are *in vitro* selected nucleic acid molecules that bind to a broad range of targets with high affinity and specificity. The basic isolation process, termed "systematic evolution of ligands by exponential enrichment" (SELEX) utilizes a large initial pool of randomized nucleic acids from which high affinity binders are isolated and enriched through subsequent rounds of selection[10]. The host–viral interface has become an increasingly popular target for aptamers because interactions between nucleic acids and proteins are critical to viral replication. Although not a pre requisite, targeting nucleic acid binding proteins by aptamers has a high probability of success due to the presence of basic surface charges on most of these proteins[11].

OBJECTIVE

To study aptamers displaying high affinity and specificity generated against ZIKV NS5 protein to be used in diagnostic platforms.

METHODOLOGY

ZIKV NS5 recombinat protein obtainment and SELEX

The purified recombinant protein NS5 ZIKV (rNS5z) was obtained based on the *Escherichia coli* (*E.coli*) expression system, as described by Alves *et al.*[12]. A random DNA library was used to select sequences that recognize rzNS5 through the method of Systematic Evolution of Binding by Exponential Enrichment (SELEX). For the selection of aptamers against NS5, we used the protocol described by Simmons *et al.* (REF), with the purified recombinant protein ZIKV NS5 immobilized on ELISA plate or using the HiTrap NHS columns (GE).

Briefly, the aptamer library was incubated with rNS5z in a Top Yield PCR tube for one hour at room temperature and eluted using a salt step gradient. Eluates were desalted using Microcon filters and amplified by PCR. Aptamers were detected by agarose gel electrophoresis in all salt fractions. The 1.0 M and 1.5M NaCl, and 3.0 M NaSCN elutions were selected for cloning, as they were expected to contain aptamers with the highest affinity for the target. After sequencing and cloning, the homologous aptamer sequences from both 1.5 M NaCl and 3.0 M NaSCN elutions were analysed using the Mfold program, which predicts three-dimensional structures by calculating their minimum Gibbs free energies as well as the free energy of folding of each base pair at 37°C. Both the variable and primer regions were analysed, as the primer regions often help to confer stability upon the aptamer and are therefore frequently implicated in their structure.

Fluorescence Quenching Experiments

Experiments were performed using a Jasco FP-6500 (ESP060) fluorimeter, with the sample in a 1 mL fluorescence cuvette. Emission spectra were acquired between 300 and 400 nm with an excitation wavelength of 280 nm and integration time of 1s, at 5 nm increments and at room temperature. After performing the acquisition on 2 μM rNS5z in potassium phosphate buffer 10 mM (pH7,4), aptamer was titrated to the following final concentrations in the cuvette, mixed and an acquisition taken immediately: 0.3 μM, 0.6 μM, 0.9 μM, 1.2 μM, 1.5 μM, 1.8 μM, 2.1 μM, 2.7 μM, 3.3 μM. Results were analysed using Microcal Origin 6 and the equilibrium association constant (KA) determined using the equation described by Missailidis and Brady[13].

RESULTS

Selection Generated Aptamer Species Against rNS5z

In a preliminary screening, we have managed to identify sixteen aptamer species. The aptamers sequences were aligned and had its secondary structure predicted using mfold analysis. From five aptamer species that suggested proeminent species, based on sequence homology and secondary structure analysis, three are shown in Figure 1 in their predicted structures.

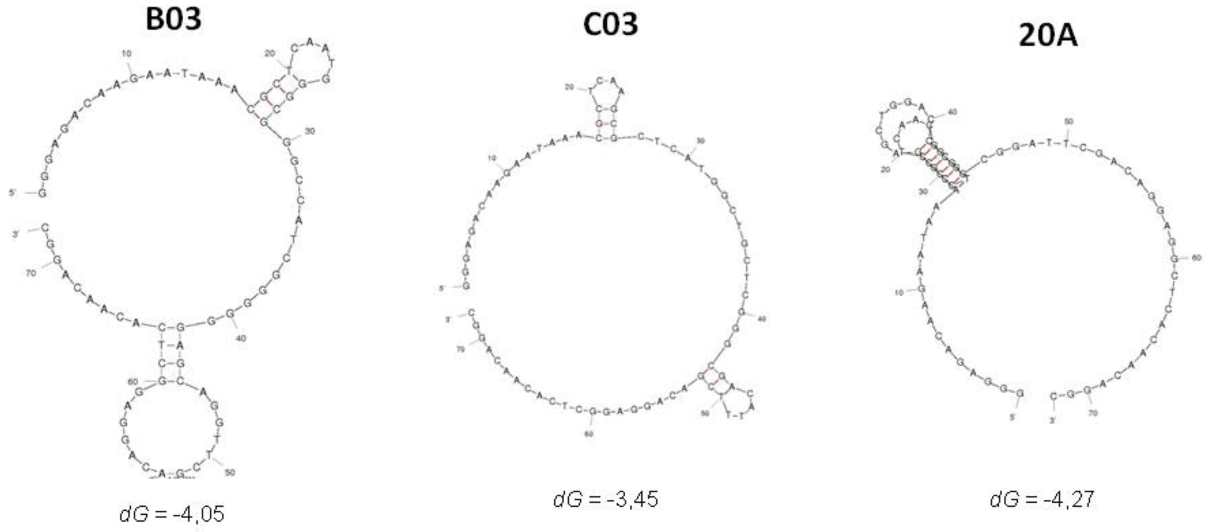

FIGURE 1: Mfold predicted structures of three selected aptamers species generated against rNS5z.

Aptamer Species Bind to rNS5z

A total of sixteen aptamers were obtained and analyzed using fluorescence spectroscopy and modelled their binding. We have identified Stern-Volmer constants for the selected aptamers, which have shown affinity for rNS5z (Tabel 1).

TABLE 1. Sequence Consensus and Stern Volmer constant values (Ksv) obtained for aptamer species with high affinity to rNS5z.

Aptamers	Sequence 5' - 3'	Ksv M^{-1}
A04	GGGAGACAAGAATAAACGCTCAAGGCAGGTGGTGGGGGAGGGTGGAAGTTCGACAGGAGGCTCACAACAGGC	1,5416E+05
A07	GGGAGACAAGAATAAACGCTCAAACTGCGGGGCGGAGGGGGGCGGCTATTCGACAGGAGGCTCACAACAGGC	2,4627E+05
B03	GGGAGACAAGAATAAACGCTCAATGGGCGGGCCATCGGGGGGAGCAGGTTCGACAGGAGGCTCACAACAGGC	4,9412E+05
B08	GGGAGACAAGAATAAACGCTCAACGCATTGATCAGGTACTAGCTGCTATTCGACAGGAGGCTCACAACAGGC	1,3352E+05
C03	GGGAGACAAGAATAAACGCTCAAGCGCTCATGGCTGCTCGGGCGACATTTCGACAGGAGGCTCACAACAGGC	3,5943E+05
C09 (D09)	GGGAGACAAGAATAAACGCTCAATCTTCCTGTTCACCGCAACTCGTTCGACAGGAGGCTCACAACAGGC	1,5263E+05
D04	GGGAGACAAGAATAAACGCTCAAGTTGTAGAGTCTCATTCCCTGGTAATTCGACAGGAGGCTCACAACAGGC	1,3228E+05
E03	GGGAGACAAGAATAAACGCTCAATGATCTGAATTAGCTTAGGCACGAGATTCGACAGGAGGCTCACAACAGGC	1,3127E+05
H06	GGGAGACAAGAATAAACGCTCAAACAACGCCGGGCGCTTGGTGCTGCTTTCGACAGGAGGCTCACAACAGGC	2,7300E+05
H08	GGGAGACAAGAATAAACGCTCAAGCCTCATACACACCATCTCCGCGAATTCGACAGGAGGCTCACAACAGGC	1,4114E+05
15_16	GGGAGACAAGAATAAACGCTCAACCGTTTCAGATTCACGGAATACCTATTCGACAGGAGGCTCACAACAGGC	1,5529E+05
13_19_20	GGGAGACAAGAATAAACGCTCAAGTGTCAGGGCGTTCTGCCCCCGCGTTCGACAGGAGGCTCACAACAGGC	1,3395E+05
13	GGGAGACAAGAATAAACGCTCAATTCGGCGGTGTACACCGCGCTGCCCTTCGACAGGAGGCTCACAACAGGC	1,4070E+05
20A	GGGAGACAAGAATAAACGCTCAACGCGTCCCGAGCTGGACCGGGCGGATTCGACAGGAGGCTCACAACAGGC	3,8761E+05
25A	GGGAGACAAGAATAAACGCTCAACTTTCCAGGCTGTATCCTGGTAAGGTTCGACAGGAGGCTCACAACAGGC	1,2991E+05
18C	GGGAGACAAGAATAAACGCTCAATGATATGCGAGTCACAGGGCTCAGGTTCGACAGGAGGCTCACAACAGGC	1,4127E+05

Fluorescence quenching titrations were carried out using the natural intrinsic fluorescence of rNS5z, due to the solvatochromic emission peak of tryptophan, to determine the binding interactions of the sixteen species of aptamers, analysed by a quadratic equation[14]. Aptamer binding to rNS5z was characterized using fluorescence quenching experiments and aptamers were found to interact with protein with equilibrium association constants with a very similar pattern, in the range of 10^5 M^{-1}, and could detect rNS5z at 2 μM in phosphate buffer. Current studies are now underway to further investigate the effect of the temperature variation on aptamer binding.

REFERENCES

1. Fauci, A. S. & Morens, D. M. Zika Virus in the Americas--Yet Another Arbovirus Threat. *N. Engl. J. Med.* 374, 601–604 (2016).
2. Plourde, A. R. & Bloch, E. M. A Literature Review of Zika Virus. *Emerging Infectious Diseases* 22, 1185–1192 (2016).
3. Rasmussen SA, Jamieson DJ, Honein MA & Petersen LR. Zika virus and birth defects – reviewing the evidence for causality. *N Engl J Med* 374: 1981-1987 (2016).
4. Petersen LR, Jamieson DJ & Honein MA. Zika Virus. *N Engl Med* 374: 1552-1563 (2016).
5. Hou W, Cruz-cosme R, Armstrong N, Obwolo LA, Wen F, Hu M & Tang Q. Molecular cloning and characterization of the genes encoding the proteins of Zika virus. *Gene* 628, 117-128 (2017).
6. Barrows N, Campos R, Liao KC, Prasanth KR, Soto-Acosta R, Yeh SC, Schott-Lerner G, Pompon J, Sessions OM, Bradick SS & Garcia-Blanco MA. Biochemistry and Molecular Biology of Flaviviruses. *Chemical Reviews* 118: 44484482 (2018).
7. Grant A, Ponia SS, Tripathi S, Balasubramaniam V, Miorin L, Sourisseau M, Schwarz MC, Sanchez Seco MP, Evans MJ, Best SM & Garcia-Sastre A. Zika virus targets human STAT2 to inhibit type I interferon signaling. *Cell Host Microbe* 19: 882–890 (2016).
8. Wang W, Li G, Wu D, Luo Z, Pan P, Tian M, Wang Y, Xiao F, Li A, Wu K, Liu X, Rao L, Liu F, Liu Y & Wu J. Zika virus infection induces host inflammatory responses by facilitating NLRP3 inflammasome assembly and interleukin-1β secretion. *Nature Communications* 106: 1-16 (2018).
9. Franco LS, Vidal PO & Amorim JH. In silico design of a Zika virus non-structural protein 5 aiming vaccine protection against zika and dengue in different human populations. *Journal of Biomedical Science* 24: 88–97 (2017).
10. Sun, H., Sun, Y. A Highlight of Recent Advances in Aptamer Technology and its application. Molecules 20: 11959-11980 (2015).
11. Zhou, J. & Rossi, J. Aptamers as targeted therapeutics: current potential and challenges. *Nat Rev Drug Discov* doi:10.1038/nrd.2016.199 (2016).
12. Alves LN, Abalo AA, Argondizzo APC, Rocha HF, Silva D, Cortez CM & Missailidis S. Selection and evaluation of the binding of aptamers against NS5 Zika virus using fluorescence spectroscopy . *American Institute of Physics* (AIP Conference Proceedings) 2040, 100005, doi: 10.1063/1.5079160 (2018).
13. Missailidis S & Brady K. Characterization of antibody-antigen interactions by fluorescence spectroscopy. *Methods Mol Biol* **248**: 431–441 (2004).
14. Simmons SC, McKenzie E.A., Harris L,K., Aplin J.D., Brenchley D.E, Velasco-Garcia M.N. & Missailidis S. Development of Novel Single-Stranded Nucleic Acid Aptamers against the Pro-Angiogenic and Metastatic Enzyme Heparanase (HPSE1). *Plos One* **7**, e37938 (2012).

Fish Larval Distribution in a Macro-tidal Regime: an in Situ Study in São Marcos Bay (Brazilian Equatorial Margin)

Rômulo de Araújo Soares[a] , Audalio Rebelo Torres Junior[a,*] , Raimunda N. Fortes Carvalho Neta[b]

[a]Marine Sciences Institute, Federal University of Maranhão, Brazil

[b]Chemistry and Biology Department, State University of Maranhão, Brazil

[*]audalio.torres@gmail.com

Abstract. The distribution of Ichthyoplankton is directly related to the hydrodynamics of a region. In this study we aim to map the privileged zones of highest occurrence of Ichthyoplankton from the densities observed in situ in São Marcos Bay (Brazil), that has one of the highest amplitudes of tides of Brazil. Ichthyoplankton was collected using horizontal drag technique in the surface layer (layer 0 to 0.5 m), using a conic roller net with mesh of 300 micrometers which was coupled a flow meter to estimate the volume of filtered water. The density was calculated from the ratio between the total number of eggs and larvae in each sample and the filtered water volume. For spatial interpolation we used the technique of Voronoi polygon. Results showed that in the two sampling periods of the year (rainy season and dry season) were collected 4,934 eggs and fish larvae, and 60% were recorded in the dry season. The location of the largest Ichthyoplankton densities vary with the highest concentrations closer to the south-east channel of the CESM in the dry season, moving to the center in the rainy season. The South-East channel of the CESM is therefore a nursery area for many species of fish, requiring priority actions for environmental protection..

Keywords: Ichthyoplankton, São Marcos Bay, Larval transport

PACS: 92.05.Fg - Diurnal, seasonal and annual cycles.

INTRODUCTION

São Marcos Bay (Complexo Estuarino de São Marcos - CESM, Maranhão) has one of the highest amplitudes of tides of Brazil (Souza Filho 2005). This region has a dynamic that has been studied for the generation of energy (González-Gorbeña et al. 2015). This is one of the most representative estuaries of northeastern Brazil (Pereira and Harari 1995), which is currently installed the second public port that handles more cargo in Brazil with pollution potential for the aquatic organisms (Carvalho-Neta et al. 2012; Carvalho Neta and Abreu-Silva 2013). Moreover, in this region there is an environmental protection area that has the largest continuous stretch of mangrove in Maranhão (Carvalho Neta and Castro 2008).

The distribution of Ichthyoplankton is directly related to the hydrodynamics of a region (Chia et al. 1984), which affects on the Ichthyoplankton accumulation process (Rumrill 1990; Sfakiotakis et al. 1999) and larval dispersion of several species (Chia et al. 1984; Cowen et al. 2000; Shima and Swearer 2010; Green et al. 2014). The knowledge about where is the accumulation and larval retention of fish is important for biological conservation and the establishment of protected areas (Warner et al. 2000). However, few studies have shown direct evidence that protected areas successfully seed unprotected areas with larvae of fish species (Christie et al. 2010). In this study we aim to map the privileged zones of highest occurrence of Ichthyoplankton from the densities observed *in situ* in São Marcos Bay (Brazil).

MATERIALS AND METHODS

The CESM is located in the central coast of the Maranhão State, the equatorial margin of Brazil (Amazon coast). This estuarine system extends from the division of Mearim river by the Caranguejos island until his departure to the continental shelf (MMA 1999). The average depth of the region is 10 meters and has an area of approximately 3.000m² with tidal amplitudes in the region range from 3.3 meters to 7 meters height in times of spring tide. (Souza Filho 2005). The CESM has a strong hydrodynamics, with velocity of tidal flow above $4 m.s^{-1}$ (Teixeira Bonecker et al. 2009). The climate is tropical with only two well defined seasons: the rainy season (January to June) and dry season (July to December) (INMET 2015).

Quantitative data of Ichthyoplankton were acquired during the period of one year. Sampling occurred in November 2014, March 2014, June 2015 and September 2015. Sampling stations were distributed in four cross sections (Fig. 1).

FIGURE 1 - Identification of sampling sections in São Marcos Bay, Maranhão, Brazil.

Ichthyoplankton was collected using horizontal drag technique in the surface layer (layer 0 to 0.5 m), following the traditional method proposed by (Smith and Richardson 1977). For this, we used conic roller net with mesh of 300 micrometers which was coupled a flow meter mark Hydro Bios® model 438-115 to estimate the volume of filtered water.

The nets were hauled in three minutes duration and executed with 2 knots. The material was fixed in 4% formalin and its screening and quantification was carried out with the magnifying aid Brand Style Zeiss Stemi DV4 model with focal resolution of 8-32x.

The density (individuals $100m^{-3}$) was calculated from the ratio between the total number of eggs and larvae in each sample and the filtered water volume (Barkley 1964). In this study, spatial distributions of Ichthyoplankton were considered continuous and were organized to represent the asynchronously sampled distribution conditions. For spatial interpolation we used the technique of Voronoi polygon (Aurenhammer 1991; Fortune 1992).

RESULTS AND DISCUSSION

In the two sampling periods of the year (rainy season and dry season) were collected 4,934 eggs and fish larvae, and 60% was recorded in the dry season.

In the rainy season the highest density of Ichthyoplankton was observed in the region near the Section 03, and obtained maximum concentrations 1100-$100m^{-3}$ individuals in the first sampling (November 2014). In the second sampling (March 2015) of the same rainy season, the maximum concentration of Ichthyoplankton observed was 661-$100m^{3}$ individuals, 30% lower than the previous sample (Fig. 2).

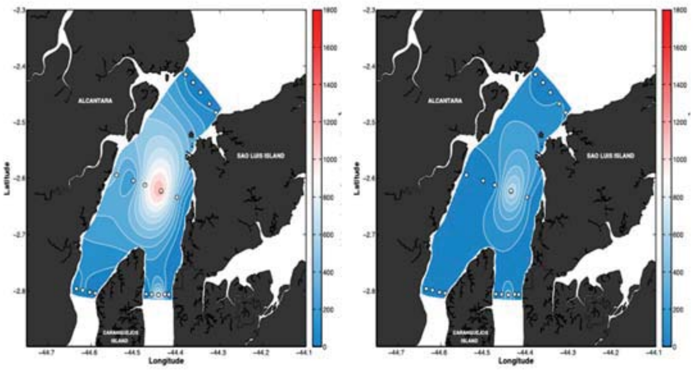

FIGURE 2 - Spatial distribution of Ichthyoplankton in the rainy season in São Marcos Bay. A) sampling carried out in Novem-ber 2014; B) sampling carried out in March 2015.

In the first sampling of the dry season (June 2015) was observed density of 906 individuals 100m^{-3}, 17% lower than the first sampling of the rainy season. We can also worth noting that the region with the highest density of Ichthy-oplankton occurred in the center of Section 03.

Most Ichthyoplankton density that occurred throughout the analyzed area was observed in sample carried out in the dry season (September 2015). The highest density point of larvae (1727 individuals 100m^{-3}) was also different from the already observed above, focusing on section 02 (Fig.3).

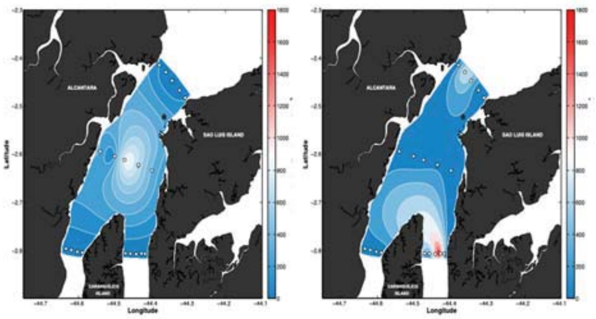

FIGURE 3 Spatial distribution of Ichthyoplankton in the dry season. A) sampling conducted in June 2015; B) sampling con-ducted in September 2015.

The location of the largest Ichthyoplankton densities vary with the highest concentrations closer to the south-east channel of the CESM in the dry season, moving to the center in the rainy season.

The highest densities of Ichthyoplankton on the south-east channel of section 02 of CESM could indicate a spawn point in the region. This region (Caranguejos Island) is directly part of an environmental protection area established by the Government of the State of Maranhão in 1991. The Caranguejos Island (in the area with the greatest influence of the Mearim river) appears to be an exporter of fish larvae to the center of CESM. In a survey of the fish assemblage of the Caranguejos Island it was observed that the number of species, Margalef's richness and Sanders' rarefaction curves showed higher values on the side with the greatest influence of the river Mearim River and the large proportion in the samples of juveniles of all taxa of fishes suggests that this area is mainly used for feeding and breeding activities of the fishes (Carvalho Neta and Castro 2008). Studies indicate that the protected marine / estuarine areas are important because they provide the conditions for feeding and reproduction of many fish species (Pauly et al. 2002). In addition, the protected areas are important because they can function as an exporter of eggs and larvae to unprotected areas

(Pauly et al. 2002; Christie et al. 2010). Observations of larval connectivity provide direct evidence of marine protected areas successfully seeding unprotected areas with larval fish (Christie et al. 2010).

The accumulation of Ichthyoplankton observed in CESM is influenced by seasonality, since the highest percentage (60%) of Ichthyoplankton was recorded at the end of the dry season on the east bank of the CESM. This larval retention was greater in the area of greater influence of Mearim River (1727 individuals100m^{-3}) near of the Caranguejos Island. These data suggest that the fish spawn in Caranguejos Island a few months (September) before the rains start in the region (November) and macrotidal regime occurring in the region contributes to the dispersion of the larvae to the center of the CESM. Research indicates that several species of fish have restricted spawning periods (Lowe-McConnell 1987b), usually at the end of the dry season so that the larvae are active during the rainy season (Araujolima 1994). This strategy ensures feeding conditions (Nikolskii 1963), reduction of predators (Lowe-McConnell 1987a; Lowe-McConnell 1987b) and dispersal of larvae in subsequent periods (Wootton 1990; Helfman et al. 2009). This occurs especially in river environments, because rains allow the flooded areas to provide additional shelters (Puebla 2009) and decreases the effect of density-dependent processes with competition and predation (Lowe-McConnell 1987a; Araujolima 1994). This expansion of the floodplain also increases the amount of organic matter available in the system for the larvae (Godinho et al. 2010), by submersion and decomposition of marginal vegetation (Junk et al. 1983).

The ichthyoplankton distribution observed in the present work is influenced by the physiographic features of the São Marcos Bay, together with the river discharge of Rio Mearim as others study cases described in the literature (PARRISH et al. 1981; CHIAPPA-CARRARA et al., 2003). The large tidal regime appears to contribute to the recruitment and the reproductive success of fish (ARTHUR; BALL; BAUGHMAN, 1996; BENNET; MOYLE, 1996; MORIYAMA et al., 1998) in the center of the CESM. The south-east channel of the CESM is therefore a nursery area for many species of fish, requiring priority actions for environmental protection.

REFERENCES

1. Allen JRL (1992) Large-scale textural patterns and sedimentary processes on tidal salt marshes in the Severn Estuary, southwest Britain. Sediment Geol 81:299–318. doi: 10.1016/0037-0738(92)90077-5
2. Araujolima CARM (1994) Egg Size and Larval Development in Central Amazonian Fish. J Fish Biol 44:371–389. doi: 10.1111/j.1095-8649.1994.tb01219.x
3. Aurenhammer F (1991) Voronoi Diagrams — A Survey of a Fundamental Data Structure. ACM Comput Surv 23:345–405. doi: 10.1145/116873.116880
4. Barkley R a. (1964) The Theoretical Effectiveness of Towed-Net Samplers as Related to Sampler Size and to Swimming Speed of Organisms. ICES J Mar Sci 29:146–157. doi: 10.1093/icesjms/29.2.146
5. Carvalho-Neta RNF, Torres AR, Abreu-Silva AL (2012) Biomarkers in catfish Sciades herzbergii (teleostei: ariidae) from polluted and non-polluted areas (São Marcos' Bay, Northeastern Brazil). Appl Biochem Biotechnol 166:1314–1327. doi: 10.1007/s12010-011-9519-1
6. Carvalho Neta R, Castro A (2008) Diversity of the estuarine fish assemblages on Crabs Island, Maranhao State, Brazil. AN - prod.academic_MSTAR_1323813019; 17832325. Arq ciencias do mar 41:48–57.
7. Carvalho Neta RNF, Abreu-Silva AL (2013) Glutathione S-Transferase as biomarker in Sciades herzbergii (Siluriformes: Ariidae) for environmental monitoring: the case study of São Marcos Bay, Maranhão, Brazil. Lat Am J Aquat … 41:217–225. doi: 10.3856/vol41-issue2-fulltext-2
8. Chia F-S, Buckland-Nicks J, Young CM (1984) Locomotion of marine invertebrate larvae: a review. Can J Zool 62:1205–1222. doi: 10.1139/z84-176
9. Cowen RK, Lwiza KM, Sponaugle S, et al (2000) Connectivity of marine populations: open or closed? Science 287:857–859. doi: 10.1126/science.287.5454.857

10. Fortune S (1992) Voronoi diagrams and Delaunay triangulations. Comput Euclidean Geom 1:2. doi: 10.1016/0098-3004(93)90062-A
11. Godinho AL, Lamas IR, Godinho HP (2010) Reproductive ecology of Brazilian freshwater fishes. Environ Biol Fishes 87:143–162. doi: 10.1007/s10641-009-9574-4
12. González-Gorbeña E, Rosman PCC, Qassim RY (2015) Assessment of the tidal current energy resource in São Marcos Bay, Brazil. J Ocean Eng Mar Energy 1:421–433. doi: 10.1007/s40722-015-0031-5
13. Green AL, Maypa AP, Almany GR, et al (2014) Larval dispersal and movement patterns of coral reef fishes, and implications for marine reserve network design. Biol Rev n/a-n/a. doi: 10.1111/brv.12155
14. Helfman GS, Collette BB, Facey DE, Bowen BW (2009) The diversity of fishes: biology, evolution, and ecology.
15. INMET (2015) Instituto Nacional de Meteorologia, Banco de Dados Meteorológicos para Ensino e Pesquisa (BDMEP), Precipitações históricas (1961 – 1990) para Ilha de São Luis. http://www.inmet.gov.br/portal/index.php?r=tempo/graficos.
16. Lowe-McConnell RH (1987a) Ecological Studies in Tropical Fish Communities.
17. Lowe-McConnell RH (1987b) Ecological studies in tropical fish communities.
18. MMA (1999) No Title. In: Ministério do Meio Ambient. Programa Nac. da Biodiversidade Biológica. http://mapas.mma.gov.br/mostratema.php?temas=zcestuarios.

Estimating the Position of Sites for Ligands in Serum Albumins from Spectrofluorimetric Data

Juliana Almeida, Felipe da Costa Thadeu, Dilson Silva, Celia Martins Cortez[a]

Postgraduation in Computational Sciences, Rio de Janeiro State University, Brazil.
Rua São Francisco Xavier, 524 – 20550-900, RJ, Brazil,
[a)] ccortezs@ime.uerj.br

Abstract.
This work presents a mathematical-computational model designed to assess the position of binding sites for ligands in human and bovine serum albumins. The model associates geometric resources to the phenomenon of fluorescence quenching in albumin. The results showed that the mean distance between the binding site for risperidone and tryptophan residue 212 of bovine serum albumin would be 2.59 (± 0.92) nm, and the mean distance between this binding site and the tryptophan residue 134 would be 2.25 (± 0.80) nm. Thus, the binding site would be slightly closer to tryptophan residue 134 than the residue 212.

Keywords: Mathematical and Computational Modeling, Endocrine Cell, Hormone storage control, adrenal epinephrine.

PACS: xx

INTRODUCTION

In previous work [1], we presented a mathematical-computational model to estimate the relative position of binding sites for ligands in human serum albumin (HSA) and bovine (BSA), based on the theory of fluorescence quenching, considering the molecular and spectrofluorimetric differences and similarities between these albumins. The fluorescence emission by HSA excited at 290 nm is due to its single one tryptophan (Trp) residue at position 214 (Trp-214) along the chain, and BSA contains two Trp residues at positions 212 (Trp-212) and 134 (Trp-134) [2]. The folding of the amino acid chain creates domains and subdomains, where binding sites for several ligands may be present [3]. The knowledge of the location of binding sites in albumin is very important to the pharmacokinetic study of therapeutic agents [4-6].

Expanding a previous model [1], here we present a mathematical-computational model designed to assess the position of primary binding sites for ligands in human albumin and bovine albumins. The model associates geometric resources to the phenomenon of fluorescence quenching in albumin.

DESCRIPTION OF THE MODEL

Note in Figure 1 a schematic diagram of fluorescent light fluxes emitted by BSA, in presence of a quencher molecule (q), passing through the slit of a spectrofluorimeter (space between the two brown straight lines parallel to the Y axis). In the diagram the two Trp residues, T_1 and T_2, representing Trp-212 and Trp-134 residues, respectively, are spaced apart by a distance D.

As modeled by Cortez *et al*. [1], here we also consider that the total fluorescence intensity emitted by protein solution results from the sum of the fluorescence emitted by each Trp residue, $F_{Alb} = \sum_{i=1}^{n} F_{T_i}$. Thus, for BSA and HSA we can write that

$$F_{BSA} = F_{T_1} + F_{T_2} \tag{1}$$

and

$$F_{HSA} = F_{T_1} \tag{2}$$

where F_{BSA} and F_{HSA} are total fluorescence emitted by BSA and HSA respectively, and F_{T_i} is the fluorescence emitted by each tryptophan residue.

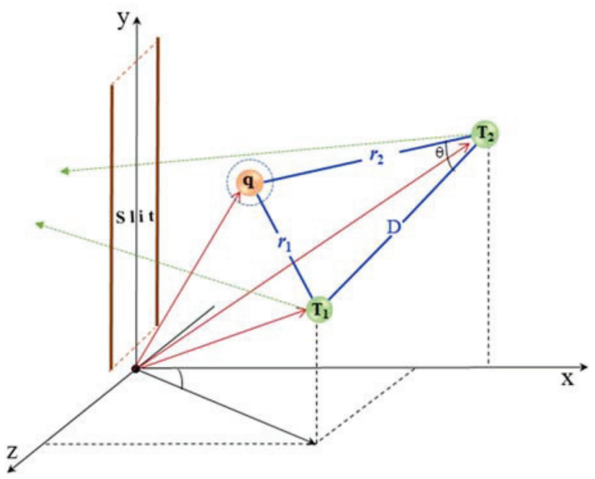

FIGURE 1. Schematic diagram of fluorescent light fluxes emitted by the two tryptophan residues (T_1 = Trp-212 and T_2 = Trp-134) of BSA, in presence of a quencher molecule (q), passing through the slit of a spectrofluorimeter (space between the two brown straight lines parallel to the Y axis): r_1 and r_2 are the distances from q to T_1 and T_2, respectively.

For a given quencher concentration (Q), the fluorescence of each Trp residue is quenched of $x_i F_{\mathrm{T}_i}$, thus the total quenched fluorescence of albumin is [1]:

$$F_{\mathrm{Alb}}|Q = F_{\mathrm{Alb}} - \sum_{i=1}^{n} x_i F_{\mathrm{T}_i}, \tag{3}$$

where the factor x_i is the fluorescence ratio quenched from Trp i. Dividing Eq. (3) by $\boldsymbol{F_{Alb}} = \sum_{i=1}^{n} \boldsymbol{F_{T_i}}$, we obtain that

$$\frac{F_{Alb}|Q}{F_{Alb}} = 1 - \frac{1}{F_{Alb}}\sum_{i=1}^{n} x_i F_{\mathrm{T}_i}, \tag{4}$$

The factor x_i is related to the distance (r_i) between T_i residue and the binding site for quencher.

Using Förster resonance energy transfer equation, $k_T = (1/\tau_0)(R_0/r)^6$ [7], for representing the factor x_i, we get that [1]

$$\frac{r_1}{r_2} = \sqrt[6]{\left(\frac{F_{B_0} - F_B}{F_{H_0} - F_H}\right) - 1}, \tag{5}$$

Aiming to improve accuracy of binding site localization in albumin, we applied geometric concepts to the previous model [1], since connecting the binding site to the Trp residues forms a triangle, as shown in Figure 2. In this, one can see the representation of possible positions of quencher binding sites in relation to residues T_1 and T_2, where $\boldsymbol{r_1}$ is the distance from the site q to the residue T_1, and $\boldsymbol{r_2}$ is the distance to residue T_2. To calculate these distances, we can use the equation:

$$r_1^2 = r_2^2 + \mathrm{D}^2 - 2r_2.D.\cos(\theta). \tag{6}$$

where θ is the angle between r_2 and D (Figure 2).

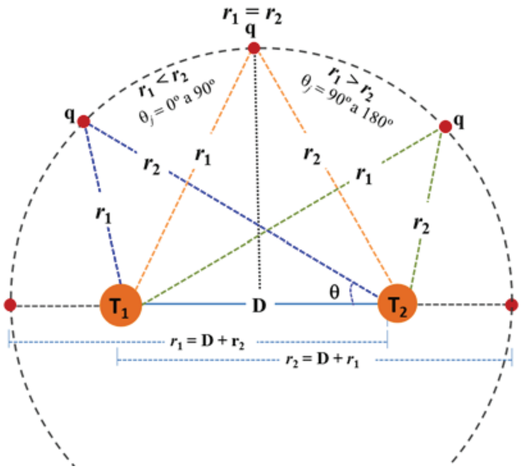

FIGURE 2. Representation of possible positions of quencher binding sites in relation to Trp residues, T_1 and T_2. Line segments r_1, r_2 and D form a triangle. D is the distance between T_1 and T_2; r_1 and r_2 are the distances from the binding site to T_1 and T_2 residues, respectively; and θ is the angle between r_2 and D.

Using Eq. (5) in Eq. (6), finally we obtain the following expressions:

$$\left(\left(\sqrt[6]{\left(\frac{F_{B_0} - F_B}{F_{H_0} - F_H}\right) - 1}\right)^2 - 1\right).r_2^2 = \mathrm{D}^2 - 2r_2.D.\cos(\theta) \quad (7)$$

or

$$\left(\left(\frac{r_1}{r_2}\right)^2 - 1\right).r_2^2 = \mathrm{D}^2 - 2r_2.D.\cos(\theta). \quad (8)$$

Knowing values of r_1 / r_2 and D, we can give values for r_2 and θ to solve the Eq. (8) numerically, and to find the distances r_1 and r_2. For this, the following boundary conditions must be considered:

(1) for $\theta = 0$ and $r_1 + r_2 = D$: the binding site is on the axis D, between T_1 and T_2.

(2) for $r_1 = r_2$ and $\theta \neq 0$: r_1 and r_2 form a isosceles triangle with D.

(3) for $r_1 < r_2$: the binding site is located at some point on left side of circle shown in Figure 2, and when $r_1 < r_2$, it is on right side.

RESULTS AND DISCUSSION

Using in Eq. 8, the value of the distance between the two Trp residues (D = 3.5 nm) found in the literature [8] and the ratio r_1 / r_2 estimated for risperidone (r_1/r_2 =1.15±0.04) by Fragoso *et al*. [9], it was possible to estimate r_1 and r_2, for the risperidone-BSA interaction. Figures 3 show the variation of distance r_1 and r_2 *versus* θ for this interaction at 25 ºC. Plots in Figure 3(*a*) display discontinuity for 60º ≤θ≤ 120º. The values of r_1 and r_2 increase with *θ*, from $\theta = 0^o$and to $\theta = 60^o$, where tend to infinity. For 120º ≤θ≤ 180º, r_1 and r_2 values are negative. For $\theta < 60^o$, the site is located in the left region of the circle shown in Figure 2, and for 120º ≤θ≤ 180º, the site is located in the left region.

For risperidone, the mean value estimated for r_1 was 2.59 (±0.92) nm, and for r_2 was 2.25(±0.80) nm. These means are next to the distance between two Trp residue (3.5 nm), and the difference $r_1 - r_2$ was 0.86 (±0.13) nm, suggesting that the triangle formed by the binding site and Trp residues would be a nearly isosceles triangle, being the binding site slightly closer to Trp-134 than Trp-212.

The shape of BSA is usually ellipsoidal with dimensions of 4 nm x 4 nm x 14 nm [10]. We could not find any information about the length of BSA domains in literature. Thus, considering that each domain would occupy 1/3rd of the molecule (smaller diameter ≈1.3 nm and the larger diameter ≈4.6 nm), the mean values estimated for r_1 and r_2 were larger than the smaller diameter of BSA domains, but they were smaller than the larger diameter.

Syrejshchikova et al. [11] suggested that risperidone binds to the HSA drug-binding site I. This site is a big hydrophobic cavity within the core of BSA and HSA subdomain IIA, where several drugs may bind at the same time [12]. Our results do not contradict the suggestion of those authors, because the binding site can be within the domain IIA, where is Trp-212, but slightly closer to Trp-134, since the shapes of domains also may be ellipsoidal.

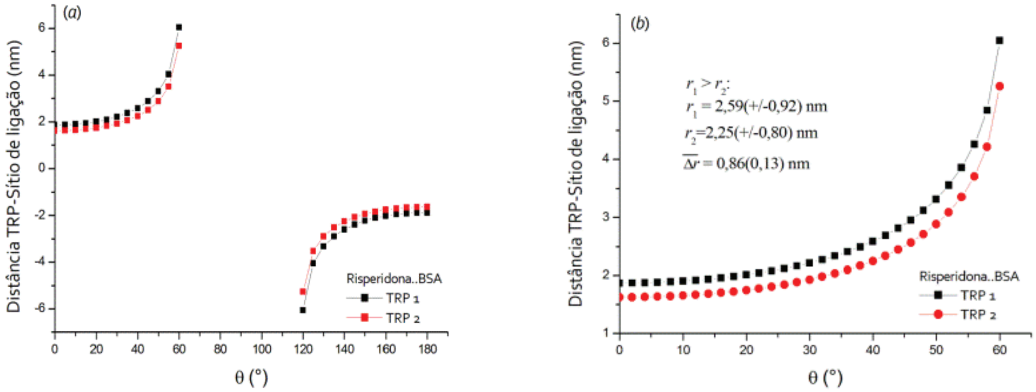

FIGURE 3. Distances r_1 e r_2 in function of the angle θ for interaction of risperidone with BSA, at 25 ºC, r_1/r_2 = 1.15(±0.04): (*a*) θ varying from 0 a 180º and (*b*) region for $r_2 > 0$ and $r_1 > 0$.

CONCLUSION

According to our model, the mean distance between the binding site for risperidone and Trp-212 ($\overline{r_1}$) in BSA would be 2.59 (± 0.92) nm, and the mean distance between this binding site and Trp-134 ($\overline{r_1}$) would be 2.25 (± 0.80) nm. The binding site for risperidone would be slightly closer to Trp-134 than Trp-212. Although the mean values estimated for r_1 and r_2 are larger than the smaller diameter considered for BSA domains (≈1.3 nm), they are smaller than the larger diameter (≈4.6 nm).

ACKNOWLEDGMENTS

Research Support Foundation *of the State of Rio de Janeiro* (FAPERJ) and *National Council for Scientific and Technological Development* (CNPQ) supported this work.

REFERENCES

1. C.M. Cortez, A. Pires Neto, A.A.E.A. Motta. *AIP Conf. Proc.* (New York) 1790, 100004.
2. J.R. Lakowicz. *Principles of Fluorescence Spectroscopy*, 3rd ed.; Springer Science: Philadelphia, PA, 2006.
3. U. Kragh-Hansen. *Dan. Med.Bull*. 37, 57-84 (1990).
4. C.M. Cortez, D. Silva, C.M.C., S.Missailidis. *Spectrochim. Acta. Part A* 95, 270-275 (2012).
5. C.M. Cortez, V.M. S. Fragoso, D. Silva. *AIP Conf. Proc*. (New York) 1618, 602 (2014); doi: 10.1063/1.4897810.
6. D. Silva, C.M. Cortez, S.R.W. Louro, J. Cunha Bastos*. Toxic. Letters* 147, 53-61 (2004).
7. P.L.Hernandez-Martinez, A.O. Govorov, H.V. *Demir J. Phys Chem C* 117 (2013) 10203-10212.
8. Peters Jr. T. All about albumin, biochemistry, genetics, and medical applications. Academic Press, New York, 1996.
9. V.M.S. Fragoso, D. Silva, F.A.O. Cruz, C.M. Cortez. *Environ Toxicol Pharmac* 33, 262-266 (2012).
10. Q. Tang, C.H. Xu, S.Q. Shi, L.M. Zhou. *Synthetic Metals* 147, 247-252 (2004).
11. T. Syrejshchikova, N. Smolina, V. Kondratyuk, G. Dobretsov, M. Uzbekov. *Curr Drug Discov Technol* 15, 263-269 (2018).
12. F Yang, Y Zhang, H Liang. *Int J Mol Sci* **1**5, 3580-3595 (2014).

Model for the Storage Control in an Endocrine gland based on Lyapunov Function

Vanessa Henriques Borges, Maria Clicia Stelling de Castro, Carlos Antonio de Moura, Celia Martins Cortez[a]

Postgraduation in Computational Sciences, Rio de Janeiro State University, Brazil.
Rua São Francisco Xavier, 524 – 20550-900, RJ, Brazil,
[a]ccortezs@ime.uerj.br

Abstract. The work presents a mathematical modeling of the hormonal storage control in an endocrine cell, with computational simulation in C language using the Lotka-Volterra equations and the Lyapunov optimization. To test the proposed model, we take as an example the regulation of catecholamine synthesis–storage-release in the adrenal medulla.

Keywords: Mathematical and Computational Modeling, Endocrine Cell, Hormone storage control, adrenal epinephrine.

INTRODUCTION

The nervous and endocrine systems are responsible for the regulation and coordination of almost all functions of the body. Endocrine System is the set of glands that secrete hormones, which reach their target of action through the bloodstream. Like any secretory cell, the endocrine cells have several cytoplasmic granules or vesicles having the product to be secreted [1].

For the functional equilibrium of these endocrine glands is essential an optimal balance between the synthesized and stored hormone amounts. Anomalies in storage-secretion balance contribute to the development and progress of diseases. Thus, to find mechanisms behind many diseases, it's essential to understand how hormones are synthesized and processed and how intracellular mechanisms interact to regulate their synthesis and storage [1,2,3].

In 2017, Cortez et al. [3] presented a simple mathematical model to simulate the control dynamics of synthesis, storage and secretion in an endocrine gland, based on the classical theory enzymatic kinetics to Lotka-Volterra equations. The results found were in the order of magnitude of that found in experimental studies.

Continuing the work of Cortez et al. [3], we are associating Lotka-Volterra equations to Lypuanov equations and Bellman optimization model to find an optimal control function to model the regulation of processes of storage-degradation control in an endocrine gland, using as an example the hormonal dynamic in adrenal medulla.

ADOPTED MODEL FOR STORAGE CONTROL IN ENDOCRINE GLAND

In our modeling, such as the Cortez et al. [3], we considered the synthesis of the hormone H uninterrupted, from the substrate S available in the blood, and the H synthesis velocity was depending of the cytoplasmic concentration of S, and of the activity of group of synthesizer enzymes. In this way, the hormone was accumulated in the cell and, if not released, its excess would go to degradation. At this stage, the hormone molecule is dissociated and the resulting parts of this dissociation can be reused in a new synthesis. Here we are interested in the control of intracellular processes related to the synthesis-stock-degradation of H.

Figure 1 shows the scheme of adopted model to represent hypothetic endocrine cell and its dynamic control for the synthesis and storage of hormone H. After the synthesis, H passes for storage via S. From storage, the hormone can follow one of two routes, via R (release) or via D (degradation). The degradation is ativated when the storage capacity exceeds the maximum limit, and the hormone molecule is broken to control the hormone quantity in the cell. Thus recovered S can return to phase synthesis or blood.

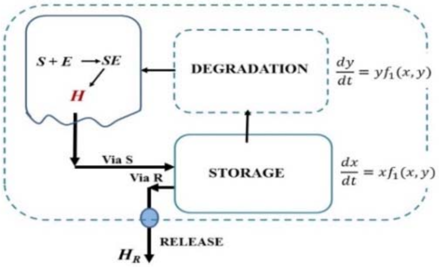

FIGURE 1. Model adopted for the dynamic control of the synthesis, storage and release of hormone. *S*=substrate, *E*= enzyme, *SE* = substrate-enzyme complex, v_T= uptake rate from blood, H = hormone, v_H=synthesis rate. Via S = storage pathway, Via D = degradation pathway and Via R = release pathway from the storage, H_R=released hormone.

To represent the dynamics of storage-degradation we have a system of two differential equations, Lotka-Volterra equations. One of them is related to the process of storage and involves the function $f_1(x,y)$, and the other refers to the degradation, which involves $f_2(x,y)$, where *x* is referent to the storage process and *y*, to the degradation process [4]. Thus [3],

$$\frac{dx}{dt} = x(a - ry - px), \tag{1}$$

$$\frac{dy}{dt} = y(-b + sx + C), \tag{2}$$

where a, b, r e s are positive constants, the term *ax* defines the rate of the stored hormone, *by* refers to degradation rate, *rxy* and *sxy* refer to the interdependence between storage e degradation. The term *C* is introduced to ensure the maintenance of optimal control, and characterizes the number of antagonistic conditions present in the cell at time *t*, being that

$$C = \xi y + V, \tag{3}$$

where ξy represents any compensatory process that at any stage of the system leads the system to the optimal equilibrium point, and *V* is the stability term.

Boundary conditions should be considered, because there are velocity limits for the synthesis/storage/ secretion that determine the normal functioning of gland. For the function *V* that stabilizes the system to be a Lyapunov function must be positive and guarantee an asymptotic stability, that is, $dV/dt < 0$.

At equilíbrium, Eq. 3 is positive, $C > 0$, and when $t \to \infty$, $V \to 0$ e $C = \xi y$. We considered the existence of optimal equilibrium point (x*□□y*) for storage-degradation dynamics, such as $df(x^*, y^*)/dt = 0$. Thus, from Eq. (2*a*) we have: $-px^* - rx^* = 0$, and $y^* = (a - px^*)/r > 0$. In this way $a - px^* > 0$. Using Eq. (2*b*), $-b + sx^* + \xi y_o = 0$, we obtain $\xi = b - sx^*/y$, being □ > 0 and $x^* < b/s$. For optimal deterministic control over a period of time (*0, T*), the control function can be determined from

$$V(y(0),0) = \min_V \left\{ \int_0^T C(y(t), V(t))\, dt + D(y(T)) \right\}, \tag{4}$$

where *D(y(T))* is the function that defines the system performance. For linear stochastic dynamics and performance described by a quadratic function, the optimal control problem can be reduced to the Hamilton-Jacobi-Bellman partial differential equation [4], $\min_V \left\{ \frac{dV(y(t),t)}{dt} + \omega \right\} = 0$, where

$$\omega = m_1(x - x^*) + m_2(y - y^*) + V^2 \tag{5}$$

and function *V*, by definition, is:

$$V(y(t),t) = \min_V \left\{ \int_0^T [m_1(x - x^*)^2 + m_2(y - y^*)^2 + V^2] dt \right\} \tag{6}$$

where m_1 and m_2 are positive constants. The solution of Eq. (6) should be investigated among the Lyapunov functions, according to the Lotka-Volterra type models [5].

For the nonlinear stochastic dynamics, to determine the solution *V* (*x, t*) in Eq. (5), we used the Lyapunov function in the following way [4]

$$V(x,y) = v_1 \left(x - x^* - x^* ln\left(\frac{x}{x^*}\right) \right) + v_2 \left(y - x^* - y^* ln\left(\frac{y}{y^*}\right) \right), \tag{7}$$

where v_1 e v_2 are positive constants to be determined, whose values can be determined by the Hamilton-Jacobi-Bellman equation [6]. The derivative of Eq. (7), considering Eqs. (1) and (2), gives:

$$\frac{dV(x,y)}{dt} = v_1(x - x^*)(a - px - ry) + v_2(y - y^*)(-b + sx + \xi y + V). \tag{8}$$

Replacing the results for *w*, from Eq. 5 and *dV(x,y)/dt*, Eq. 7, in Eq. 5, we have:

$$\min_V\{v_1(x - x^*)(a - px - ry) + v_2(y - y^*)(-b + sx + \xi y + V) + m_1(x - x^*)^2 + m_2(y - y^*)^2 + V^2\} = 0 \tag{9}$$

The function *V(t)* is not limited and can be found by ∂/∂V, from Eq. (9), being $V^* = \frac{-v_2}{2}(y - y^*)$, where V^* is the optimal value for control function; the value $V^* y$ represents the ideal enzymatic activity of system in each instant *t*. Replacing $V = V^*$ in Eq. (9), we obtain, and assuming that $v_1 = m_1/p$ and $v_1 = -sv_2/r$; and for $v_2 > 0$, $v_2 = 2\left(\delta + \sqrt{\delta^2 + m_2}\right)$, finally, we have that:

$$\frac{dV}{dt} = -m_1(x - x^*)^2 - \left(\sqrt{\delta^2 + m_2}\right)(y - y^*)^2 < 0 \tag{10}$$

TESTING THE MODEL

To test the proposed model, we used as an example the production of catecholamines, epinephrine (EPI) and norepinephrine (NEPI). This is an endocrine gland consisting of a cortex (superficial layer) and a medulla (inner layer). In adrenal medulla, cromaffin cells store and secrete catecholamines [1], and each cell has approximately 30,000 secretory granules with about 0.3 µm diameter containing about 0.5 □M of catecholamines [7]. The EPI and NEPI concentrations in the normal human adrenal are 412 to 633 □g and 37 to 123 □g, respectively [8]. From all the NEPI formed, 15% remain in the granules and 85% pass into the cytoplasm [9]. In this, NEPI is methylated forming EPI, which is captured and stored in the granules of chromaffin cells [10,11]. EPI is normally produced very quickly, so that the depletion of its EPI supply occurs only in unusual circumstances [12, 13].

Figures 2 *(a)* and 2 *(b)* show the plot of the storage and degradation velocities as a function of time, according to our model, for the parametric values included in the legend of these images.

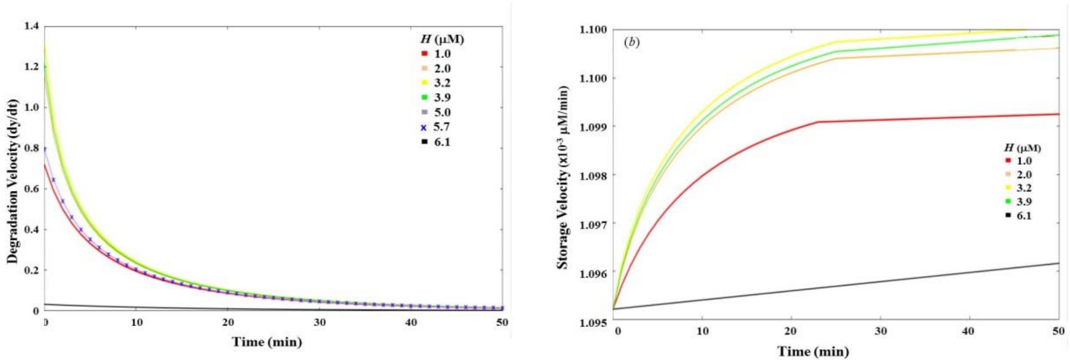

FIGURE 2. – Storage (a) and Degradation (b) velocity as a function of time, for a = 0.86; r = 0.001; b = 0.56; s = 0,05; p = 0.14; E = 0.09; m_1 = 0,03; e H = 1.0, 2.0, 3.2, 3,9, 5.0, 5.7, 6.1 □M.

In Figure *2(a),* we observed that at this rate it decreases with time, for all tested hormone concentrations (from H = 1.0 to 6.1 □M), and tends to zero for $t > 50$ min. Figure *2 (b)* shows that, unlike storage, the rate of degradation increases with time, from H = 1.0 to 3.9 □M, and reaches a plateau to $t > 10$ min. This plateau corresponds to the maximum degradation phase. But, while still growing, the chart for H = 6.1 □M is linear, showing that in this case the equilibrium would occur for a very long-time interval.

It's important to mention that a random variation of the input parameters (*a*, *b, r, s, p, m1, h* and *e*) didn't produce valid results. It wasn't possible to find in the literature the variation of the enzymatic action over time. In this way, we looked for, through simulations, what function could represent the rate of growth of the enzymatic

action that led us to a more realistic result. Thus, we adopted a linear function with a low angular index. In contrast, the behavior of the storage rate plot as a function of time didn't increase and stabilize after a certain time. We looked for other functions that could represent enzymatic variation, such as exponential, quadratic or logarithmic. But these weren't adequate. At the end, we adopted the function $E = EH - H / 100000$ (11), or $y = xy - x / 100000$, with which we could observe the behavior of the storage speed as a function of time.

Figures *3(a)* and *3(b)* present the graphs of the storage and degradation variations in time for the parametric values shown in the caption of the figures, considering the equation of the variation of E (Eq.11).

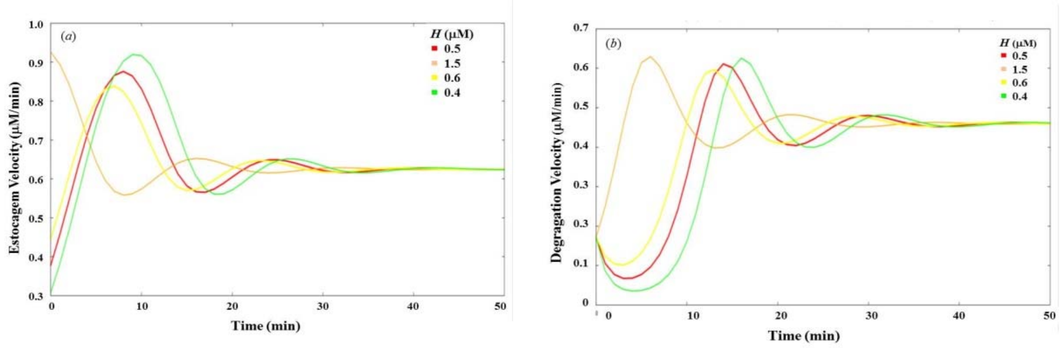

FIGURE 3. – Storage (a) and Degradation (b) velocity as a function of time, for $a = 0.86; r = 1.1; b = 4.56; s = 0.05; p = 0.14; E = 0.03; m_1 = 0.09;$ *e* $H = 0.5, 1.5, 0.6, 0.4$ □M.

Cortez et al. (2017) observed, using a simple mathematical model based on the classical Lotka-Volterra equations, that the degradation process started about 20 min after storage reaches its maximal capacity, and the degradation activity increased until $y = 0.103$ mg at $t = 35$ min, and then stabilized at $y = 0.0873$ mg. The storage and degradation velocities came into equilibrium for $v_S = v_D \approx$□1.53 □g/min (about 0.008 □moles/min). This value is in the order of magnitude of that found in experimental studies [13].

The results obtained are favorable to the proposal that the present model associating the Lyapuanov equations to those of Lokta-Voltera can be used to represent the control dynamics of the synthesis-storage and degradation of the catecholamines in the medulla of the adrenal gland, since the parametric values pointed to the system equilibrium condition of equations of the mathematical model are in the magnitude order of values found in the literature. Furthermore, the simulations used realistic values for a (0.86) and p (0.14), which were also obtained in the literature, resulting from experimental measurements.

ACKNOWLEDGMENTS

Research Support Foundation of the State of Rio de Janeiro (FAPERJ) and National Council for Scientific and Technological Development (CNPQ) supported this work.

REFERENCES

1. J.E. Hall. *Guyton and Hall Textbook of Medical Physiology.* Saundres- Elsevier, BIOS Sci Publishers (2010).
2. K. Tsaneva-Atanasova, H.M. Osinga, J. Tabak, M.G. Pedersen. *Acta Biotheor* **58**, 315-327. (2010).
3. C.M. Cortez, A. Pires Neto, A.A.E.A. Motta. AIP Conf. Proceedings (New York) **1790**, 100004 (2016).
4. C.C. Feltrin, Rafikov, M. Trends App Comp Math **3**, 83–92 (2002).
5. C. Zhu, G.Yin. J. Math Anal Applic 357:154-17- (2009)
6. R. Bellman. *Dynamic Programming*. [S.l.]: Courier Corporation (2013).
7. J.D. Deupree, J.A. Weaver, D.A. Downs, *Biochim Biophys Acta* **714**(3):471-8 (1982)
8. Mc.C. Goodall, B.W. Haynes, *J Clin Invest* **39**, 1927–1932 (1960).
9. J.H. Phillips, *Biochem J* **144**, 311–318 (1974).
10. J. Axelrod, J Biol Chem **237**, 1657-1660 (1962).
11 E.N. Marieb, K.Hoehn. *Human Anatomy & Physiology*. 9th Ed. (2010).
12. D.S. Goldstein, C. Holmes S.M. Frank, M. Naqibuddin et al., *Am J Cardiol* **91**, 53-58 (2003).
13. R. Comline, M. Silver. British Medical Bulletin, Oxford University Press **22**,16–20 (1966).

The International Symposium of Computational and Mathematical Modeling of Biology and Medicine Targets in the ICCMSE

Dilson Silva[a] and Sotiris Missailidis[b]

Technology Institute of Immunobiologics – Biomanguinhos/ Fiocruz / Brazil
Post-Graduation Program in Medical Sciences of Rio de Janeiro State University/ Brazil
Post-Graduation Program in Computational Sciences of Rio de Janeiro State University / Brazil

[a]dilson.silva@bio.fiocruzj.br; [b]sotiris.missailidis@bio.fiocruz.br

Abstract. Along these last six years, we have been organizing the above titled symposium, focused in general, on biological targets, and more specifically on computational methods and tools applied to health and environmental themes. We have brought then a meaningful number of good talks and presentations broadcasting research results as well as a sort of correlated models. The use of computational methods and mathematical tools in biological and medicine targets has been successfully supporting scientists to understand physical and biological phenomena. As we recently discussed in our previous symposium, current technological advances allow the simulation of larger systems, with greater accuracy. Our expectation is that scientists take advantage of the increasing computational power now available to model and simulate more complex structures. In this sense each edition of the symposium registers the path we have been grooving along the time since we joined the ICCMSE to overtake this challenge.

Keywords: High Performance Computing, Computation Models, Bioinformatics
PACS: 87.15.A-

The Conference, Sessions & Symposia

The ICCMSE is the annual event promoted by the European Society of Computational Methods in Sciences and Engineering (ESCMSE), with support of the American Institute of Physics (AIP) in whose Conference Proceedings all extended abstracts are whole published. ICCMSE is now in its 15th edition, and stands as a well stabilished event since 2003 when it was held in Kastoria/Greece. The Conference consider itself as an open space for scientists and engineers to expose works and ideas in their proper scopes, once ever linked to the use of computational methods which could improve results and so enhance activities.
In this context we have submitted a first symposium in 2014 for the 10th edition of the conference and have kept ourselves joined to ICCMSE until now. Thus it is the 6th time we attended to the event with our symposium, which with some minor changes in the thematic profile, has been stated with the title “VI International Symposium of Computational and Mathematical Modeling of Biology and Medicine Targets”.

Historic Panorama of the Symposium since 2014

We list below all oral presentations ordered by year which give us a complete view of our participation in the conference. We can observe that the title of the first sessions has varied although in a general view they have kept the main idea which support their scope. And so we invite you to know what was our contribution to the ICCMSE, congratulating with its nice and competente staff as well as with all participants who gently attended the symposium.

2014 - X ICCMSE – Athens, 04-07 April
Session 157 - "Drug Binding to Transport Proteins – Exploring Modeling and Computational Methods to get Better Results in Human and Ecosystem Health".
Organizers: Dr. Dilson Silva and Dr. Sotiris Missailidis

1) Audalio Torres - An Integrated model Supporting Histological And Biometric Responses As Predictive Biomarkers Of Fish Health Status.
2) Dilson Silva - Analyzing Models for Interactions of Aptamers to Proteins.
3) Raimunda Fortes - Fish Biomarkers For Environmental Monitoring: An Integrated Model Supporting Enzyme Activity.
4) Celia Cortez - Estimating the Relative Position of Risperidone Primary Binding Site in Sera Albumins. Modeling from Spectrofluorimetric Data.
5) Carla Coura - Using the Fluorescence Quenching Model to Compare the Plasmatic Transport of Two Antipsychotic Drugs by Serum Albumin.
6) Debora Sousa - Micronucleus Frequency and Hematologic Index in *Colossoma macropomum* (Pisces, Ariidae) for Environmental Impact Assessment at a Protected Area in Brazil.
7) Marilena Carqueja - Applying a Mathematical Model to Estimate the Fractional Accessibility to the Fluorescence Quenching of Serum Albumin by Risperidone.

2015 - XI ICCMSE – Athens, 20-23 March
Session 33 – "Ligand Binding to Proteins – Exploring Modeling and Computational Tools to Get Better Results in Human and Ecosystems Health".
Organizers: Dr. Dilson Silva, Dr. Raimunda N. F. Carvalho Neta and Dr. Sotiris Missailidis

1) Dilson Silva - Drug bind to Proteins - why modeling?
2) Viviane M. S. Fragoso – Interaction of sulpiride and serum albumin: Modeling from spectrofluorimetric data.
3) Janaina Dantas - Morphological biomarkers in *Prochilodus lineatus* (Pisces, Prochilodontidae) for Environmental Impact Assessment in the Region of the Baixada Maranhense, Brazil.
4) Sotiris Missailidis - Morphological biomarkers in *Prochilodus lineatus* (Pisces, Prochilodontidae) for Environmental Impact Assessment in the Region of the Baixada Maranhense, Brazil.
5) Eleuza Tenório - Antimicrobial activity of honey of stingless bees, tiúba (*Melipona fasciculata*) and jandaira (*Melipona subnitida*) compared to the strains of *Staphylococcus aureus*, *Escherichia coli* and *Pseudomonas aeruginosa.*
6) Ticianne Andrade - Oxidative Stress Enzyme and Histopathological Lesions in *Colossoma macropomum* (Pisces, Ariidae) for Environmental Impact Assessment.
7) Carla Coura - A Mathematical Model for Nonlinear Fluorescence Quenching

Session 34 – "International Symposium on Computational Modeling in Neurobiology"
Organizers: Dr. Celia M Cortez and Dr. Thiago Matos Pinto

1) Thiago M. Pinto - Unravelling how CaMKII controls the direction of plasticity at parallel fibre-Purkinje cell synapses.
2) Dilson Silva - Magnetic and electric fields across sodium and potassium channels. Effects of surface charges.
3) Celia M. Cortez - A Simple Model for Electrophoretic Transport of Charged Particles in Membrane Pore.
4) Maria Clicia S. de Castro - A Model for Reverberating Circuits with Controlled Feedback.
5) Celia M. Cortez - Applying backpropagation neural network in the control of medullary reflex pattern.
6) Dilson Silva - Measuring the electric Heart activity through 16 Bit Audio Card Monitored by the Goldwave™ Software

2016 - XII ICCMSE – Athens, 17-20 March
Session 23 – “International Symposium of Computational and Mathematical Modeling of Biologic and Medicine Targets”
Organizers: Dr. Dilson Silva and Dr. Celia M Cortez

1) Dilson Silva - Computational Challenges in Modeling and Simulating Living Matter.
2) Maria Clicia S. de Castro - Modeling Gene Regulatory Networks: A Network Simplification Algorithm.
3) Celia M Cortez - Dynamics for the Storage Control of an Endocrine Gland: A Model for Adrenal Epinephrine.
4) Ethel C. N. Valdez - Modeling the Accessibility of the Interaction of Clonazepan to Albumins.
5) Bruno Viveiros - Greenhouse Effect Simulation – An Educational Application.
6) Raimunda Fortes - In situ Assessment of Two Catfish Species (Pisces, Ariidae) to Evaluate Pollution in a Harbor.
7) Felipe Thadeu - Mathematical-Computational Modeling for Calculations Involved in the Stern-Volmer Theory.
8) Carla Coura - Serum Albumin and the Haloperidol Pharmacokinectics. Study Using a Computational Model.
9) Maria Clicia S. Castro - A Guide to Parallel Execution of Sequence Alignment.
10) Maria Clicia S. de Castro - The Influence of the Pentose’s Pathway of the *Clostridium acetobutylicum* on the Production of Butanol: Insights from Mathematical Modeling.
11) Victor Gomes - Modeling the Interaction of the Carbamate Fungicide Maneb, with Bovine Albumin.
12) Marilia Soares - A Model for the Neural Control of Pineal Periodicity.
13) Maria Clicia S. de Castro - Simulation Step Size Analysis of a Whole-Cell Computational Model of Bacteria.
14) Dilson Silva - A Computational Solution to Analyze Hydrophobic Characteristics in Protein Chains.

2017 - XIII ICCMSE – Thessaloniki, 21-25 April
Session 32 – “IV International Symposium of Computational and Mathematical Modeling of Biologic and Medicine Targets”
Organizers: Dr. Dilson Silva and Dr. Celia M Cortez

1) Dilson Silva - Process Modeling of a HLA Research Lab.
2) Rafaela Brum - A Whole-Cell Simulator in GNU Octave.
3) Celia Cortez - Verifying the Competition between Haloperidol and Biperiden in Albumin through a Model based on Spectrofluorimetry.
4) Debora Batista - Micronuclei and Erythrocytic Abnormalities Frequencies of Frechwater Fishes: Establishing a Baseline for Health Status.
5) Audalio Torres - Fourier Shape Descriptors in Fish Preliminary Results with Prochilodus.
6) Carolina Grassini - A Model to Estimating the Relative Position of Site for Ligands in Serum Albumins.
7) Eleuza Tenório - Antimicrobial Activity of Honey of Africanized Bee (*Apis mellifera*) and Stingless Bee, Tiuba (*Melipona fasciculata*) Against Strains of *Echerichia coli*, *Pseudomona aeruginosa* and staphylococcus *aureus.*
8) Celia Cortez - A Model based on Spectrofluorimetry to Study the Interaction between Glyphosate and Serum albumin of *Salminus brasiliensis.*

2018 - XIV ICCMSE – Thessaloniki, 14-18 March
Session 20 – "V International Symposium of Computational and Mathematical Modeling of Biologic and Medicine Targets"
Organizers: Dr. Dilson Silva and Dr. Celia M Cortez

1) Raimunda Fortes - A Model to Environmental Risk Assessment Based on Biochemical and Morphological Biomarkers in catfish.
2) Ligia Tchaicka - Micronucleus Test in *Centropomus undecimalis* (BLOCH, 1972) for the Assessment of the Water Quality of two Brazilian Estuaries.
3) Raimunda fortes - Models of Sexual Maturation as a Tool for the Conservation of Commercial Fish in a RAMSAR Site of Brazil.
4) Lais N. Alves - Selection and Evaluation of the Binding of Aptamers Against NS5 Zika Virus Using Fluorescence Spectroscopy.
5) Francisco Albuquerque - Modelling the Energy Balance and Turbulent Flows for Urban Surface Temperature Estimation Using the Improved Force Restore Technique.
6) Liliane Morais – DNA Aptamer as Molecular Tool for ZIKV NS1 Protein Detection.
7) LigiaTchaicka – Molecular Differentiation of Colletotrichum spp. Associated with Tropical Fruit Anthracnose.
8) Audalio Torres - The Eventual Presence of Freshwater of Amazonas River Over the Continental Shelf of the State of Maranhão – Brazil.

2019 - XVI ICCMSE – Rhodes, 1-5 May
Session 22 – "VI International Symposium of Computational and Mathematical Modeling of Biologic and Medicine Targets"
Organizers: Dr. Dilson Silva and Dr. Sotiris Missailidis

1) Alana L. Sousa - Scientific and Technological Research on the use of Molecular Markers in Turtles.
2) Alessandra Abalo - Fluorescence Spectroscopy Study of Single-Stranded Nucleic Acid Aptamer Species Against NS5 Zika Virus.
3) Audalio Torres - Fish Larval Distribution in a Macro-tidal Regime: an *in situ* Study in São Marcos Bay (Brazilian Equatorial Margin).
4) Celia M. Cortez - Estimating the Position of Sites for Ligands in Serum Albumins from Spectrofluorimetric Data.
5) Clicia S. Castro - Model for the Storage Control in an Endocrine Gland based on Lyapunov Function.
6) Dilson Silva - The International Symposium of Computational and Mathematical Modeling of Biology and Medicine Targets in the ICCMSE.
7) Ethel C. N. Valdez - Evaluation of HSA Activity on Selected Hantavírus Aptamers.
8) Ethel C. N. Valdez - Preliminary Evaluation of Selected Aptamers Against Hantaviruse.
9) Ligia A. Pereira - Population Analysis of Kinosternon scorpioides Using SSR Markers.
10) Raimunda Fortes - A Model to Environmental Risk Assessment Based on Biomarkers in crab *Ucides cordatus* (Crustacea, Decapoda) .
11) Sotiris Missailidis - Aptamers against the Zika virus NS1 protein, for a serological diagnostic assay development.

ACKNOWLEDGMENTS

The authors would like to thank FAPERJ, CNPq and CAPES for the financial support to this work.

Evaluation of HSA Activity on Selected Hantavírus Aptamers

Ethel C N Valdez[1], Ana PC Argondizzo [2], S Missailidis[3,a], Georgia D da C Machado [4], Ana PV dos S Esteves[4], C de S Motta Luis[4], C de S. Luis [4]

[1] *Centro Universitário Serra dos Órgão, Curso de Graduação em Farmácia Teresópolis/Campus Quinta do Paraiso(Estrada da Pratao s/n.25976-340) Brazil*

[2] *Laboratório de Tecnologia Recombinante, Pavilhão Rockfeller, Bio-Manguinhos/Fiocruz, Av. Brasil, 4365-Manguinhos, Rio de Janeiro, RJ, CEP 21040-900, Brazil*

[3] *Vice Diretoria de Desenvolvimento Tecnológico, Edifício Rocha Lima, Bio-Manguinhos/Fiocruz, Av. Brasil, 4365-Manguinhos, Rio de Janeiro, RJ, CEP 21040-900, Brazil*

[4] *Centro Universitário Serra dos Órgão, Curso de Graduação em Medicina, Campus Antonio Paulo Capanema de Souza (Avenida Alberto Torres, 111 - Alto - 25964-004), Brazil*

[a)] Corresponding author. E-mail: sotiris.missailidis@bio.fiocruz.br

Abstract. Hantaviruses are enzootic viruses that maintain persistent infections in their rodent hosts without apparent disease symptoms. The spillover of these viruses to humans can lead to serious illnesses as, hantavirus pulmonary syndrome and hemorrhagic fever with renal syndrome. In recent years, there has been an improved understanding of the epidemiology, pathogenesis, and natural history of these viruses following by the necessity to investigate a diagnostic mechanism.

.**Keywords:** Hantavirus, human albumin, fluorescence quenching, computational model.

INTRODUCTION

Hantavirus is a zoonotic, viral respiratory disease. The causative agent belongs to the genus Hantavirus, family Bunyaviridae. Is acquired primarily through inhalation of aerosols or contact with the excreta, droppings or saliva of infected rodents (Apodemus agrarius). Is referred as hemorrhagic fever with renal syndrome (HFRS) or as hantavirus pulmonary syndrome (HPS) or hantavirus cardiopulmonary syndrome (HCPS). These viruses can cause serious diseases in humans and have reached mortality rates of 12% (HFRS) and 60% (HPS) in some outbreak [1]. The application of rational treatment is necessary to obtain a positive prognosis as well as controlling the spread ability of the virus. Diagnosis preceded a rational action; thus, a diagnostic assays method is required. This work proposed to prove the efficiency of aptamer in a fluorometric identification method in recognizing the hantavirus protein, ANDES in the presence or human serum albumin (HSA) a significance Stern-Volmer constant performance to assit a qualitative etiological identification agent at HAS presence. Preliminary data showed that aptamers C2526 is less reactive in the presence of HAS, being a promise reactive recognizing agent.

METHODOLOGY

Aptamers Selection

Aptamers are oligonucleic acid or peptide molecules that bind a specific target and can be used for both biotechnological and clinical purposes, since they present molecular recognition properties like that commonly found in antibodies. Two aptamers previously selected against hantavirus, ANDES, have been produce applying a

random RNA library to select sequences the nitrogenous bases that recognize the specific virus, through the Systematic Evolution of Binding by Exponential Enrichment (SELEX) method. The aptamers selection against Hantavirus, was performance using a protocol, described by Simmons et al [2].

Fluorescence Quenching Experiments

The fluorescence quenching determination used 1µmL of 2 µM Hantavirus solution (phosphate buffer, pH 7.4) to which was added in increasing volume of 1 µL aptamer DNA free water solution (aptamers tested: C07; C0203; e C2526) following the final concentration in the curvette: 1µM; 2µM; 3µM; 4µM; 5µM; 6µM; 7µM; 9µM; 11µM; 15µM e 19µM. Fluorescence quenching plots of titrations of HSA, and aptamers for each point in the plot is the average of three values .Experiments were performed at 25 ºC. Fluorescence spectra were recorded in the range 300-400 nm, and with a 290 nm excitation wavelength, both emission and excitation slits width were 5 nm. Fluorescence measurements were performed on a Cary Eclipse from Agilent Co. fluorimeter and optical spectroscopy were performed in a UV-visible Shimatzu-160A. Experiments data were analyzed using Microcal Oring 6 and and the equilibrium association constant (Ksv determined using the equation described by [3]. Reproducibility and quenching average tendency and inter filter effect were verified.

The quenching constant (KD) due to the binding have been computed for each aptamer with hantavirus protein using modified Stern-Volmer equation [1].

$$\frac{Fo}{Fo-F\alpha} = \frac{1}{F\alpha} + \frac{1}{F\alpha KD[Q]} \tag{1}$$

where F0 e F are fluorescence intensities emitted by HSA in absence and presence of aptamers, respectively, and fa is the fraction of the initial fluorescence that is accessible to the quencher. The model proposed by Carqueja and Cortez [4] was used to verify the fluorescence intensity variation emitted by the hantavirus protein, during the interaction with the aptamers.

RESULTS

The quenching plots for HSA, show a downward curvature, as observed in figure 1,botowm, for the used range of aptamer concentration [Q]. Fluorescence quenching plots of titrations of HSA protein with the aptamers shown in Fig.1, which standard deviation is less than 8% around the maximum emission (λmax).

The quenching constant (KD) due to the binding have been computed for each aptamer with HAS using modified Stern-Volmer equation [5].

Comparing the stern-volmer graphs for the 3 aptamers, the quenching fluorescence is less intense in C2526 as showed in the bottom figure 1, reveled low affinity for the HAS, since the estimated Stern-Volmer constant (1,9(±05) x 10^4 / M) is the lower, as show in table 1

TABLE 1. Aptamers parameters

Aptamers	K_{sv}	r
C2526	1,9 (+/-0,5) 10^4/M	0,99992
C07	5,1(+/-0,1) 10^4/M	0,99959
C0203	5,9(+/-0,2) 10^4/M	0,9959

Figure 1, top, shows a linearity decrease result of the fluorescence emitted by biding of the HSA with the aptamers at low concentrations. Curvature graph shape are consequence of the presence of one fluorophores biding in a HSA chain [6]. Due to this preliminary result we can predict that HSA have low affinity to C2526 aptamers and it may not compete with hantavirus protein ANDES for the aptamers biding.

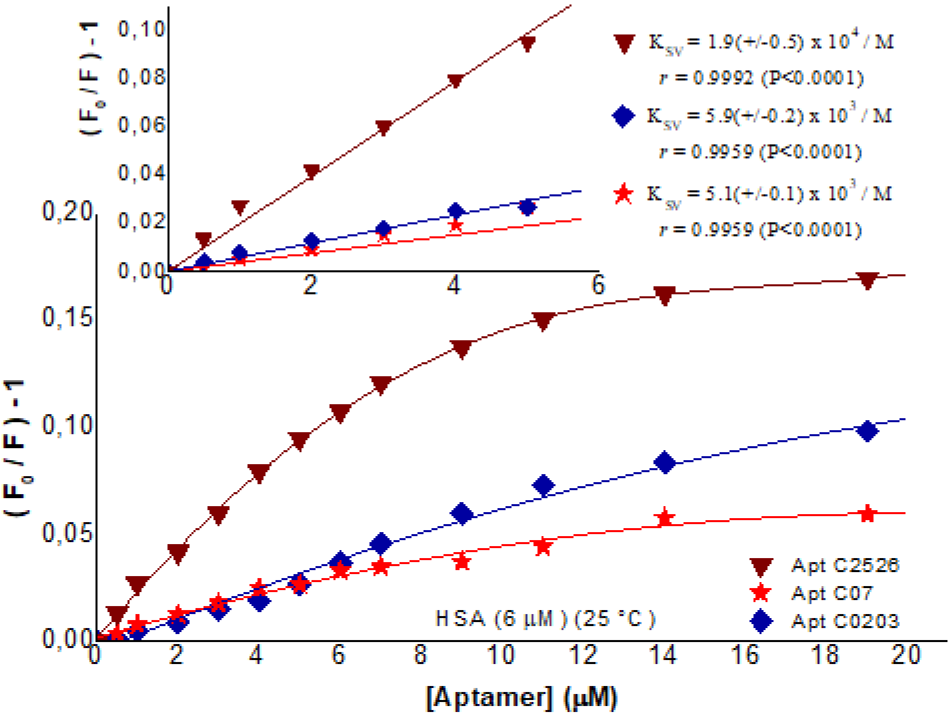

FIGURE 1. The figure shows the Stern-Volmer graphs for the interaction of the 3 aptamers under study, C2526, C07 and C0203, with HAS at 25^{0}C. The detail shows the region of the graphs for the lowest binder concentrations, which were used to estimate the constant revisions of Stern-Volmer, since this region depicts the binding of the aptamers to their primary sites of the protein

As a future perspective we plan, among other goals, to determine the type of quenching, which could verify the existence of the binding complex formation between the aptamer studied in this experiment to HAS.

REFERENCES

1. Jonsson,, Collen B., Figueredo, Luiz T. M., Vapalahti, Olli. A Global Perspective on Hantavirus Ecology, Epidemiology, and Disease. Clin Microbiol Rev. 2010 Apr; **23**(2): 412–441.doi: 10.1128/CMR.00062-09
2. .Simmons, S, McKenzie E, Harris, L.K., Aplin, J.D., Brenchley PEC, Velasco-Garcia M.N., Missailidis, S. Development of Novel Single-Stranded Nucleic Acid Aptamers against the Pro-Angiogenic and Metastatic Enzyme Heparanase (HPSE1). Plos One., v. 7, p. e37938, 2012. https://doi.org/10.1371/journal.pone.0037938, Google ScholarCrossref
3. C. Cortez, D. Silva, C.M.C. Silva, S. Missailidis, Spectroch Acta. Part A 95, 270-275 (2012).
4. M. Carqueja, C.M. Cortez, AIP Conf Proc 1618, 609 (2014); doi 10.1063/1.4897813
5. J.R. Lakowicz, Principles of fluorescence spectroscopy, 3nd Edition, Springer, New York. (2006).
6. Valdez, ECN, Paulino, ET, Coura, CPde Morais, Cortez CM., e Fragoso VMda Silva. Modeling the accessibility of the interaction of clonazepan to albumins
7. http://dx.doi.org/10.1063/1.4968697.: http://aip.scitation.org/toc/apc/1790/1

Preliminary Evaluation of Selected Aptamers against Hantaviruse

E. C.N. Valdez [1]., C.M. Cortez [1], R.P.O. dos Santos Oliveira [2], S. Vidal [3], D. Silva [4,a]., E. R S de Lemos [4]., S. S. Missailidis [5]

[1]*Programa de Pós-Graduação em Ciências Médicas, UERJ, R. São Francisco Xavier, 524, Maracanã, Rio de Janeiro,- RJ, CEP 20550-900, Brazil*
[2]*IOC/Fiocruz, Av. Brasil, 4365-Manguinhos, Rio de Janeiro, RJ, CEP 21040-900, Brazil.*
[3] *Centro Universitário Serra dos Órgão, Curso de Graduação em Efermagem, Campus Antonio Paulo Capanema de Souza (Avenida Alberto Torres, 111 - Alto - 25964-004) Brazil*
[4]*Latam/ Biomanguinhos//Fiocruz, Av. Brasil, 4365-Manguinhos, Rio de Janeiro, RJ, CEP 21040-900, Brazil.*
[5] *VDTEC/BioManguinhos/Fiocruz, Av. Brasil, 4365-Manguinhos, Rio de Janeiro, RJ, CEP 21040-900, Brazil*

[a)] Corresponding author. E-mail: dilson.,silva@bio.fiocruz.br

Abstract. Hantavirus is a zoonotic, viral respiratory disease and is recent associated with human diseases that need a qualitative diagnosis method to promote a rational treatment as well as controlling the spread ability of the virus. Thus a early rational treatment is necessary in the outcome of the disease that on a identification etiological agent is essential. This paper shows results obtained from hantavirus aptamers interaction with the hantavirus protein, ANDES solution, throw fluorometric methods, that will assist in the determination of a secure path to aim an identification mechanism to identify the virus. The investigation revels that aptamer C2526 shows a high affinity binding with hantavirus protein, ANDES, being a promise reactive for recognizing assays.

.**Keywords:** Hantavirus, aptamers, fluorescence quenching, computational model.

INTRODUCTION

Hantavirus is a zoonotic, viral respiratory disease. The causative agent belongs to the genus Hantavirus, family Bunyaviridae. Infections are acquired primarily through inhalation of aerosols or contact with the excreta, droppings or saliva of infected rodents. Usually human hantavirus infection occurs in rural areas (forests, fields, farms, etc.), where rodents hosting the virus might be found. Infected individuals may experience headache, dizziness, chills, fever and myalgia. They may also experience gastrointestinal (GI) symptoms including nausea, vomiting, abdominal pains, and diarrhea, followed by sudden onset of respiratory distress and hypotension [1]. The disease treatment and virus dissemination require a diagnostic method. This work proposed a fluorometric identification method using hantavirus aptamers showing a significance Stern-Volmer constant performance to assit a qualitative etiological identification agent. Aptamer C2526 maintained a good performance in the recognition of hantavirus protein, ANDES.

METHODOLOGY

Aptamers Selection

Aptamers are oligonucleic acid or peptide molecules that bind a specific target and can be used for both biotechnological and clinical purposes, since they present molecular recognition properties like that commonly found in antibodies. Two aptamers previously selected against hantavirus, ANDES, have been produce applying a random RNA library to select sequences the nitrogenous bases that recognize the specific virus, through the

Systematic Evolution of Binding by Exponential Enrichment (SELEX) method. The aptamers selection against Hantavirus, was performance using a protocol, described by Simmons et al [2].

Fluorescence Quenching Experiments

The fluorescence quenching determination used 1µmL of 2 µM Hantavirus solution (phosphate buffer, pH 7.4) to which was added in increasing volume of 1 µL aptamer DNA free water solution (aptamers tested: C07; C0203; e C2526) following the final concentration in the curvette: 1µM; 2µM; 3µM; 4µM; 5µM; 6µM; 7µM; 9µM; 11µM; 15µM e 19µM. Fluorescence quenching plots of titrations of hantavirus protein, ANDES, and aptamers for each point in the plot is the average of three values .Experiments were performed at 25 ºC. Fluorescence spectra were recorded in the range 300-400 nm, and with a 290 nm excitation wavelength, both emission and excitation slits width were 5 nm. Fluorescence measurements were performed on a Cary Eclipse from Agilent Co. fluorimeter and optical spectroscopy were performed in a UV-visible Shimatzu-160A. Experiments data were analyzed using Microcal Oring 6 and and the equilibrium association constant (Ksv determined using the equation described by [3]. Reproducibility and quenching average tendency and inter filter effect were verified.

The quenching constant (KD) due to the binding have been computed for each aptamer with hantavirus protein using modified Stern-Volmer equation [1].

$$\frac{Fo}{Fo-F\alpha} = \frac{1}{F\alpha} + \frac{1}{F\alpha KD[Q]} \quad (1)$$

where F0 e F are fluorescence intensities emitted by hantavirus protein, ANDES in absence and presence of aptamers, respectively, and fa is the fraction of the initial fluorescence that is accessible to the quencher. The model proposed by Carqueja and Cortez [4] was used to verify the fluorescence intensity variation emitted by the hantavirus protein, during the interaction with the aptamers.

RESULTS

The quenching plots for hantavirus protein, ANDES, show a downward curvature, as observed in figure 1,botowm, for the used range of aptamer concentration [Q]. Fluorescence quenching plots of titrations of Hantavirus protein with the aptamers shown in Fig.1, which standard deviation is less than 8% around the maximum emission (λmax).

The quenching constant (KD) due to the binding have been computed for each aptamer with hantavirus protein, ANDES using modified Stern-Volmer equation [5].

Comparing the stern-volmer graphs for the 3 aptamers, the quenching fluorescence is more intense in C2526 as showed in the figure 1, reveled the highest affinity for the hantavirus protein, ANDES, since the estimated Stern-Volmer constant ($8.2\pm0.1 \times 10^4$ / M) is the highest of the three, as shown in table 1

TABLE 1. Aptamers parameters

Aptamers	K_{sv}	R
C2526	8,2(+/-0,1) 10^4/M	0,99992
C07	7,3(+/-0,2) 10^4/M	0,99949
C0203	5,7(+/-0,3) 10^4/M	0,9872

Figure 1, top, shows a linearity decrease result of the fluorescence emitted by biding of the Hantavirus protein, ANDES with the aptamers at low concentrations. Curvature graph shape are consequence of the presence of more them one fluorophores biding in a hantavirus protein, ANDES, chain [6]

correlated to the increasing amount of CNPZ.

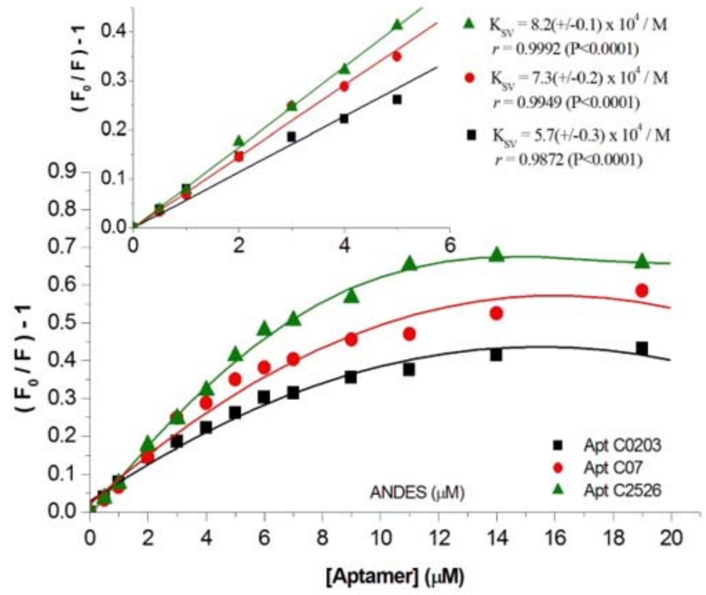

FIGURE 1. The figure shows the Stern-Volmer graphs for the interaction of the 3 aptamers under study, C2526, C07 and C0203, with the hantavirus protein ANDES at 25^{0}C. The detail shows the region of the graphs for the lowest binder concentrations, which were used to estimate the constant revisions of Stern-Volmer, since this region depicts the binding of the aptamers to their primary sites of the protein

As a future perspective we plan, among other goals, to determine the type of quenching, which could verify the existence of the binding complex formation between the aptamer studied in this experiment to hantavirus protein, ANDES.

REFERENCES

1. WHO | Hantavirus disease – Republic of Panama. https://www.who.int/csr/don/04-January-2019-hantavirus..
2. .Simmons, S, McKenzie E, Harris, L.K., Aplin, J.D., Brenchley PEC, Velasco-Garcia M.N., Missailidis, S. Development of Novel Single-Stranded Nucleic Acid Aptamers against the Pro-Angiogenic and Metastatic Enzyme Heparanase (HPSE1). Plos One., v. 7, p. e37938, 2012. https://doi.org/10.1371/journal.pone.0037938, Google ScholarCrossref
3. C. Cortez, D. Silva, C.M.C. Silva, S. Missailidis, Spectroch Acta. Part A 95, 270-275 (2012).
4. M. Carqueja, C.M. Cortez, AIP Conf Proc 1618, 609 (2014); doi 10.1063/1.4897813
5. J.R. Lakowicz, Principles of fluorescence spectroscopy, 3nd Edition, Springer, New York. (2006).
6. Valdez, ECN, Paulino, ET, Coura, CPde Morais, Cortez CM., e Fragoso VMda Silva. Modeling the accessibility of the interaction of clonazepan to albumins
7. http://dx.doi.org/10.1063/1.4968697.: http://aip.scitation.org/toc/apc/1790/1

Population Analysis of Kinosternon Scorpioides using SSR markers.

Lígia Almeida Pereira[a,*], Edyane Moraes dos Santos[b], Ligia Tchaicka[a] and Alana Lislea de Sousa[c].

[a]*Department of Chemistry and Biology, Maranhão State University, Brazil.*
[b] *Warwick Kerr Molecular Biology and Genetics Laboratory, Maranhão State University, Brazil.*
[c]*Departament of Veterinary Clinics, Maranhão State University, Brazil.*
[*]ligialmeida.uema@gmail.com

Abstract. Three natural populations of *Kinosternon scorpioides* located in the region of Baixada Maranhense were studied in order to quantify and compare levels of diversity and genetic structure using SSR markers. Ten microsatellite loci were validated for analysis in 56 individuals. The observed heterozygosities (Ho) were 0.838; 0.691 and 0.741 and the expected (He) 0.824; 0.819 and 0.815 for the populations of São Bento, Pinheiro and Anajatuba, respectively. AMOVA test showed that 98.97% of the total genetic variation is within populations while 1.03% is among populations. The estimated gene flow of 6,882 corroborates the small population differentiation (FST = 0.044). The populations of São Bento and Pinheiro are closer together genetically, according to the presented grouping analysis. These genetic data are important for the elaboration of strategic actions of management and conservation of the chelonians and especially *Kinosternon scorpioides*.

Keywords: genetic diversity; populational structure; *Kinosternon scorpioides,* SSR.

PACS: 00 - General; 06. Metrology, measurements, and laboratory procedures

INTRODUCTION

Kinosternon scorpioides is a small turtle distributed from western Panama to the north of South America and from the Amazon basin to the north of Argentina [1]. In Maranhão, it is found mainly in Baixada Maranhense, where it has been dislocated for at least four decades, especially in the reproductive period, when females migrate to terrestrial habitat and are captured by burning.

Molecular markers have shown to be efficient in the study of turtles, allowing the understanding of biological issues that are important for their conservation[2]. In this context, studies on the genetic diversity of *Kinosternon scorpioides* are necessary for the population evaluation of the species. Thus, the objective of this research was to evaluate the diversity of populations of this turtle, using SSR (Simple Sequence Repeat) markers to generate data that can be used in programs of sustainable management and conservation of the natural stocks of these animals in nature, directing strategies of actions in the balanced use of living species by man.

MATERIALS AND METHODS

The study was carried out in three municipalities of the Baixada Maranhense region (Maranhão, Brazil): Anajatuba, São Bento and Pinheiro. A total of 56 samples of *K. scorpioides* were obtained by SISBIO authorization No. 47635-4 / 2016 IBAMA / MA and a license from the Animal Ethics and Experimentation Committee of Maranhão State University - UEMA (nº 08/2015 of 11/24/15). Approximately 1.0 ml of blood was collected from each animal from the cervical sinus in a sterile syringe. Two drops of each sample were deposited on FTAcard ® type paper, previously identified and later packed in plastic bags. The remainder of the blood was immediately packed into EDTA-containing tubes and maintained at -20 ° C until DNA extraction. After blood collection, the animals were returned to their local environment. DNA extractions were performed using commercial Wizard® Genomic DNA Purification Kit Technical Manual. PCR products were initially analyzed by electrophoresis in 1%

agarose, stained with GelRedTM Nucleic Acid, with 1X TBE and later submitted to genotyping at the Laboratory of Genetics and Molecular Biology - UEMA, in an automatic sequencer, ABI 3500 eight capillaries (Applied Biosystems). GeneMarker version 2.6.3 (Soft Genetics, LLC) and genetic diversity, GenAIEx program [3], were used to identify genotypes. The verification of null alleles was performed through the Micro Checker program [4] and inbreeding coefficient through the FSTAT. In order to analyze population differentiation and structuring, GenAIEx program was used and the genetic differences within and among populations were verified through the software ARLEQUIN [5] by AMOVA test. The number of groups (k) was inferred by means of Structure [6] and verification of results by Structure Harvester [7].

RESULTS AND DISCUSSION

Analysis of the ten markers revealed the presence of polymorphism in 100% of them. In the ten loci analyzed, the number of alleles per locus ranged from 8 to 16. The lowest observed heterozygosity was obtained for the Kinsco locus 3155 (0.314) and the highest for the Kinsco locus 2505 (0.941). Table 1 shows the validated locus, number of alleles, observed and expected heterozygosity of the analyzed samples.

TABLE 1. - Validated loci, number of alleles, observed and expected heterozygosity in the analyzed samples of *Kinosternon scorpioides*, Maranhão, Brazil.

Locus	A	Ho	He
197	9	0,735	0,851
765	13	0,824	0,855
808	10	0,681	0,868
988	8	0,833	0,837
2000	10	0,810	0,829
2474	16	0,833	0,842
2505	14	0,941	0,877
2609	14	0,865	0,864
3155	16	0,314	0,865
3686	14	0,741	0,871

In a study with *Podocnemis unifilis*, heterozygosity values ranging from 0.3645 to 0.875 were found in eighteen microsatellite loci developed for the species, with the number of alleles ranging from 3 to 11 [8]. Comparatively, populations of *P. unifilis* numerically showed similar genetic diversity to the population of *K. scorpioides*.

Regarding the genetic structure, FST index expresses the proportion of genetic variability among populations, with values of FST equal to or less than 0.05, indicating a small population structure. In *K. scorpioides*, FST value obtained from the comparison between the population samples (0.044) indicates a low genetic differentiation that correlates with the existence of gene flow among the populations (Table 2). This flow is evidenced by the number of migrants (Nm), which average in the ten loci analyzed was 6,882, indicating sharing of some alleles in the three populations sampled.

TABLE 2. - Statistics F calculated for each individual locus and for all loci together

Locus	F_{IS}	F_{IT}	F_{ST}	Nm
Kinsco 197	0,088	0,136	0,052	4,530
Kinsco 765	0,019	0,059	0,041	5,893
Kinsco 808	0,186	0,224	0,046	5,195
Kinsco 988	-0,036	-0,008	0,027	9,050
Kinsco 2000	-0,012	0,047	0,058	4,044
Kinsco 2474	-0,022	0,038	0,059	3,958
Kinsco 2505	-0,088	-0,071	0,015	16,254
Kinsco 2609	-0,024	0,008	0,032	7,579
Kinsco 3155	0,539	0,578	0,086	2,650
Kinsco 3686	0,124	0,146	0,025	9,670
Média	**0,077**	**0,116**	**0,044**	**6,882**

Coefficient of inbreeding (FIS), Global Fixation Index (FIT), Fixed Index (FST), Estimated Gene Flow (Nm) as Nm = 0.25 (1 - FST) / FST.

The estimation of the number of biological groups of *K. scorpioides* present in the studied region through the Structure program indicated K = 2, suggesting the grouping of individuals into two groups [9], as observed in Figure 1, diverging from the number of populations sampled.

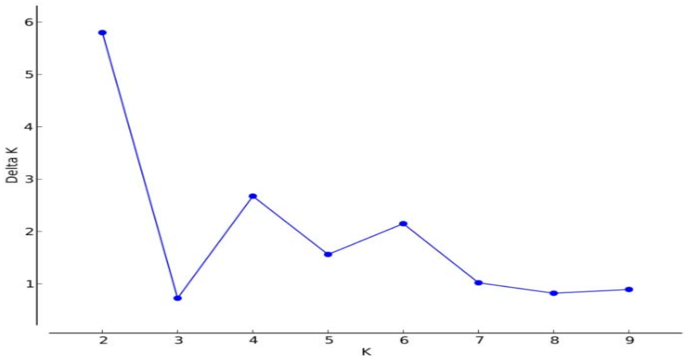

FIGURE 1 - Graphical representation of ΔK obtained from ten independent simulations for each number of possible groupings (K).

Genetic diversity within and between populations is the result of complex processes involving mutation, migration, genetic drift and selection, and this diversity is critical to ensure the viability and continuous evolution of populations [10]. In the detection of population structuring carried out by the Structure program, there was no sharp subdivision of the species within the sampled area, revealing the possibility of a slight structuring between the populations, by the suggestion of two biological groups: I- São Bento and Pinheiro and II - Anajatuba, with a small genetic discontinuity between them. Gene flow and population genetic structure are commonly shaped by environmental heterogeneity [11]. The presence of a discrete population structure suggests that these populations have a recent evolutionary history.

ACKNOWLEDGMENTS

We would like to acknowledge the Molecular Pathology Laboratory (PATOMOL); Molecular Biodiversity Laboratory (LABIMOL); Dr. Warwick Kerr Laboratory (LABWICK) and Genetics and Molecular Biology Laboratory (GENBIMOL), Maranhão State University for equipment, and Technological Development - FAPEMA, for financial support.

REFERENCES

1. TTWG - Turtle Taxonomy Working Group. Chel. Res. Found., p. 000-97(2010).
2. T. N. Engstrom, T. Edwards, M. F. Osentoski, E. M. Myers**.** Eds. Chelonian Research Monographs, **4**:124-141 (2007).
3. R. Peakall, P. E. Smouse. Mol Ecol Notes. **6**: 288–295 (2006).
4. C. Van Oosterhout, W. F. Hutchinson, D. P. M. Wills, P. F. Shipley. Mol Ecol Notes **4**:535-538. (2004).
5. S. Schneider, D. Roessli, L. Excoffier. Genetics and Biometry Laboratory, University of Geneva, Switzerland (2000).
6. J. Pritchard, M. Stephens, P. Donnelly. Gen, **155**: 945–959. (2000).
7. D. A. Earl. V. Holdt, M. Bridgget. Cons. Gen. Res, **4**(2):359-361 (2012).
8. C. Fantin, C. F. Carvalho, T. Hrbek, J. R. J. W Sites, L. A. S. Monjeló, S. Astolfi-Filho, I. P. Farias. Mol. Ecol. Notes. **7,** 1235-1238 (2007).
9. G. Evanno, S. Regnaut, J. Goudet. Mol. Ecol, **14**: 2611–2620 (2005).
10. K. Berthier, M. Galan, J. C. Foltete, N. Charbonnel, J.F. Mol. Ecol, **14**: 2861–2871 (2005).
11. S. Manel, M. Schwartz, G. Luikart, P. Tren. Ecol. Evol, **18**: 189–197.(2003).

A Model to Environmental Risk Assessment Based on Biomarkers in crab *Ucides cordatus* (Crustacea, Decapoda)

Raimunda Nonata Fortes Carvalho Neta[a,*], Suelen Rosana Sampaio de Oliveira[b], Ticianne de Sousa de Oliveira Mota Andrade[c], Wanda dos Santos Batista[c] and Audalio Rebelo Torres Junior[d]

[a]*Department of Chemistry and Biology, State University of Maranhão, Brazil;*
[b]*Master Program in Oceanography, Federal University of Maranhão, Brazil*
[c]*Master Program in Aquatic Resources and Fisheries, State University of Maranhão, Brazil*
[d]*Marine Science Institute, Federal University of Maranhão, Brazil*
[*]raifortes@gmail.com.br

Abstract. In this research, we present a mathematical model to environmental risk assessment based on biomarkers (glutathione-S-Tranferase activity and branchial lesions) in in crab *Ucides cordatus* (Crustacea, Decapoda) from São Luís Island (port area) and Facão Island (reference area) in Brazil. Adult males were captured bimonthly for a period of one year. Glutathione S-transferase (GST) was measured spectrophotometrically, and branchial lesions were examined by light microscope. GST activity values were correlated with those of the branchial lesion scale (independent variable) by fitting third order polynomials using the least squares method (0.05 significance level). Higher GST activity (1.03±0.07 µmol min mg^{-1} $protein^{-1}$) was observed in crabs at the potentially contaminated site ($p < 0.05$). However, null values (0.00 µmol min mg^{-1} $protein^{-1}$) were also recorded (only) for the crabs in the port area. The greatest number of branchial lesions (serious alterations) was recorded only for the port region. The activity of the enzyme increases until the serious lesions appear; after this limit, GST activity decreases dramatically to very low (or even null) levels, thus resulting in irreversible lesions (lamella collapse). The mathematical model based on the two parameters evaluated in *U. cordatus* show that the port area experience greater impact, while the reference area presented moderate environmental quality.

Keywords: glutathione S-transferase, stress, branchial lesions, harbor.
PACS: 00 - General; 06. Metrology, measurements, and laboratory procedures

INTRODUCTION

Benthic species that live in direct contact with the sediment such as the crab *Ucides cordatus* (Linnaeus, 1763) are particularly exposed to chemical stress in port areas [1,2]. The crustacean *U. cordatus* is an endemic species of the Atlantic coast of the American continent, found in mangroves (Brazil), being one of the main sources of income for local human communities [3]. This crab is an bioindicator of mangrove pollution and may undergo several types of changes under the influence of xenobiotics [4,5]. Such changes (biochemical, morphological, physiological and behavioral) are recognized as biomarkers, and their use shows good results for environmental risk assessment [6].

Mathematical models for the prediction of impacts in port regions can be elaborated to gather a set of data related to different types of biomarkers in an aquatic species [2,7]. In this context, the implementation of these predictive models should consider the standardization of methods based on individual species and ecosystems, given the large geographic and biological diversity of Brazil [8]. The main goal of this study was to test a mathematical model to environmental risk assessment based on biomarkers (glutathione-S-Tranferase activity and branchial lesions) in *Ucides cordatus* in order to verify how the species is responding to an environmental contamination in Brazil.

MATERIALS AND METHODS

The São Marcos Bay is an important fishing spot and has the most important public maritime port on the north coast of Brazil. This port region was considered here as potentially impacted area (A1), because is the second most important port in Brazil (in iron ore handling), it also experiences large vessel transit in which several types of

chemicals (iron, manganese, fertilizers, bauxite, and alumina) and petrol are imported and exported [2]. In contrast, the island chosen as reference area (A2), known as Facão Island, is located in São José Bay and does not have any port developments in its vicinity (Fig. 1). These estuary, which has a large area of mangrove, is used for ecotourism and fishing, including *U. cordatus* (uçá crab) fishing.

The male crabs (only adults) were captured bimonthly for a period of one year (August 2015 to June 2016). Only males (carapace width or CW > 60 mm) were analyzed, avoiding any effect of phase ecdise changes and sex hormones [9]. In the field the crabs were dissected with sterile scissors and samples of hepatopancreas and gills were removed with the aid of sterilized tweezers. The hepatopancreas samples were placed in Eppendorf tubes, frozen and kept in liquid nitrogen until the time of the enzymatic analyzes. The gills removed from each specimen were fixed in Davidson's solution for 24 hours. They were then washed and maintained in 70% alcohol until the usual histological processing. The Glutathione S-transferase activity in hepatopancreas of each crab was determined by the increase in absorbance to 340 nm, using reduced glutathione (GSH) and 1-chloro-2,4-dinitrobenzene (CDNB) as substrates [10]. Branchial lesions of each crab were classified according to Bernet et al. [11].

The values for the GST activity were correlated with those from the scale of branchial lesions (independent variable) by means of the fitting of polynomials of the third order, using the least squares method, accepting 0.05 of significance level.

.

RESULTS AND DISCUSSION

Increased GST activity was observed in the hepatopancreas of *U. cordatus* from the potentially contaminated site (port area) than in those in the reference area ($p < 0.05$). However, null values (0.00 µmol mg-1 protein-1) were also recorded only for crabs in the port area (Fig. 1).

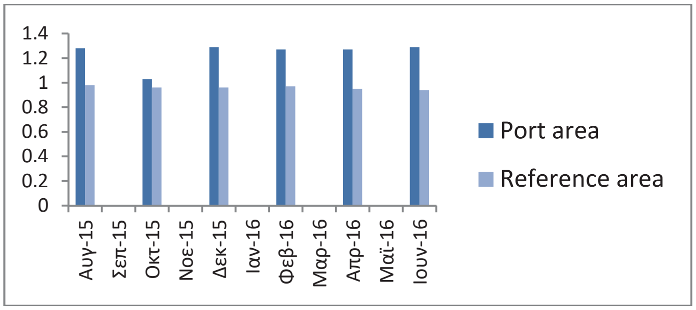

FIGURE 1. GST activity for the port area and for the reference area, Maranhão, Brazil.

In crabs of the port area were observed eight kinds of deformations in the gills, such as marginal channel deformation (MCD), necrosis (Ne), hemocytic infiltration (HI), swelling of the lamellae (SL) and collapse of the lamellae (CL) (Table 1). On the other hand, only three types of branchial lesions were identified in a small percentage (<1%) of the crabs caught in the reference area.

TABLE 1. Percentage of branchial lesions in crabs for the port area and for the reference area, Maranhão, Brazil.

	Port Area					Reference Area				
	MCD	SL	CL	Ne	HI	MCD	SL	CL	Ne	HI
Aug/2015	20%	12%	10%	9%	13%	0%	0%	0%	0%	0.3%
Oct/2015	20%	14%	15%	8%	15%	0.5%	0%	0%	0%	0.1%
Dec/2015	14%	18%	12%	18%	17%	0.2%	0%	0%	0%	0.4%
Feb/2016	16%	12%	13%	22%	17%	0.1%	0%	0%	0%	0%
Apr/2016	15%	22%	25%	23%	18%	0.1%	0%	0%	0%	0%
Jun/2016	15%	22%	25%	20%	20%	0%	0%	0%	0%	0%

* MCD = channel deformation, SL = swelling of the lamellae, CL = collapse of the lamellae, Ne = necrosis, HI = hemocytic infiltration.

The mathematical model (Fig. 2) used to correlate GST activity with branchial lesions in *U. cordatus* crabs from the analyzed port area showed that enzyme activity increases gradually with the appearance of mild and moderate lesions and decreases drastically to very low (or even null levels) with irreversible lesions (lamella collapse). These results can be explained by the biotransformation action performed by GST, since this enzyme acts in the metabolic transformations of pollutants, thus facilitating its excretion and elimination of the organism [2].

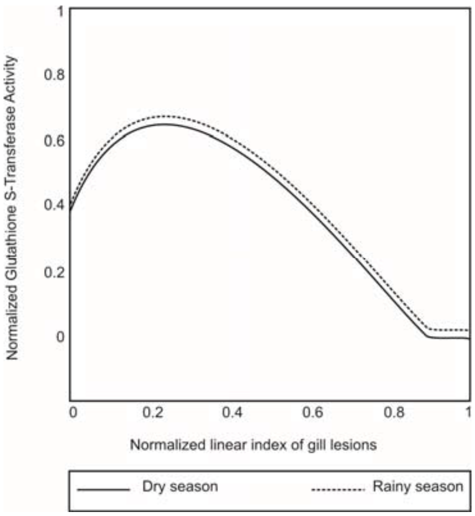

FIGURE 2. GST activity for the port area and for the reference area, Maranhão, Brazil

Chronic exposure to sublethal concentrations of toxic products in the aquatic environment can cause a number of effects, such as increased GST activity (above background level) at first and thereafter until the exhaustion of the biochemical- enzymatic, allowing the appearance of lesions in different tissues and organs, such as gills; these changes do not cause the immediate death of organisms, but represent important disturbances that prevent the organism from performing its functions in the ecosystem [12, 13, 14].

ACKNOWLEDGMENTS

We would like to acknowledge the "Laboratory of Biomarkers in Aquatic Organisms" (LABOAq/UEMA) for the supply of the fish and equipments, and Technological Development – FAPEMA, for financial support.

REFERENCES

1. R. R. Harris and M. C. F. Santos. *Mar Biol* **137**, 691-703 (2000).
2. R. N. F. Carvalho Neta and A. R. Torres Junior. *Appl Biochem Biotechnol* **166**, 1314–1327 (2012).
3. R. H. S. F. Vieira, E. A. de Lima, D. B. R. Sousa. *Rev Inst Med Trop Sao Paulo* **46**, 179–182 (2004).
4. M. A. A. Pinheiro, P. P. G. Silva, L. F. A. Duarte, A. A. Almeida, F. P. Zanotto. *Ecotoxicol Environ Saf* **81,** 114–121 (2012).
5. L. F. de Almeida Duarte, C. A. Souza, C. R. Nobre, C. D. S. Pereira, M. A. A. Pinheiro. *Ecotoxicol Environ Saf* **133,** 176–187 (2016).
6. R. Van der Oost, J. Beyer and N. P. E. Vermeulen, *Environ Toxicol Phar* **13**, 57-149 (2003).
7. R. N. Fortes Carvalho Neta, A. R. Torres Junior. AIP Conference Proceedings (American Institute of Physics, Melville, NY, 2017), pp.130008.
8. F. V. Valdez Domingos, M. Azevedo, M. D. Silva, M. A. F. Randi, C. A. Freire, H. S. de Assis, C. O. Ribeiro. *Environ Res* **105,** 350-363 (2007).
9. M. A. A. Pinheiro, L. F. A. Duarte, T. R. Toledo, M. L. Adam, R. A. Torres. *Environ Monit Assess* **185,** 8273-8285 (2013)
10. J. H. Ken, W. H. Habig, W. B. Jakoby. *J Biol Chem* **251**, 6183–6188 (1976).
11. D. Bernet, H. Schimidt, W. Meier and T. Whali *J Fish Dis* **22**, 25-34 (1999).
12. R. N. F Carvalho Neta, D. B. P. Sousa, Z. S. Almeida, D. M. S. Santos, L. Tchaicka, *Aquat Byosis* **10**, 1-12 (2014).
13. R. N. Fortes Carvalho Neta, G. L. Barbosa, H. S. Torres, D. B. Pinheiro Sousa, J. S. Castro, D. M. S. Santos, L. Tchaicka, Z. S. Almeida, E. G. Teixeira, A. R. Torres Junior. *Arch Environ Contam Toxicol* **72**, 132-138 (2017).
14. D. P. Magalhães, A. S. Ferrão Filho. *Oecol Bras* **12**, 355-381 (2008).

Aptamers against the Zika Virus NS1 Protein, for a Serological Diagnostic Assay Development

L.M. Morais [1], A.P.C. Argondizzo [2], D. Silva [3], S. Missailidis [4, a)]

[1]*Laboratório de Tecnologia Virológica, Edifício Rocha Lima, Bio-Manguinhos/Fiocruz, Av. Brasil, 4365-Manguinhos, Rio de Janeiro, RJ, CEP 21040-900, Brazil*
[2] *Laboratório de Tecnologia Recombinante, Pavilhão Rockfeller, Bio-Manguinhos/Fiocruz, Av. Brasil, 4365-Manguinhos, Rio de Janeiro, RJ, CEP 21040-900, Brazil*
[3] *Laboratório de Tecnologia em Anticorpos Monoclonais, Pavilhão Rockfeller, Bio-Manguinhos/Fiocruz, Av. Brasil, 4365-Manguinhos, Rio de Janeiro, RJ, CEP 21040-900, Brazil.*
[4] *Vice Diretoria de Desenvolvimento Tecnológico, Edifício Rocha Lima, Bio-Manguinhos/Fiocruz, Av. Brasil, 4365-Manguinhos, Rio de Janeiro, RJ, CEP 21040-900, Brazil*

[a)] Corresponding author. E-mail: sotiris.missailidis@bio.fiocruz.br

Abstract. Zika virus (ZIKV) belongs to the *Flaviviridae* family and its recent outbreak and association with human diseases (e.g. neurological disorders and microcephaly in babies) have raised global health concerns. Its differentiation from Dengue in accurate diagnostic assays are of great importance. The viral NS1 protein is a secreted protein and can be an ideal target for diagnostic assay development. We have thus selected NS1 as target for aptamer selection and study. Single-stranded DNA oligonucleotides aptamers have been previously selected for this target, and here we present the study of such aptamers by fluorescent spectroscopy, CD and ELISA in order to characterize their interaction and select the best candidate for further future assay development.

INTRODUCTION

Viral infections are difficult to distinguish, especially at the onset. If acute infection appears, the patient presents the set of nonspecific signs and symptoms. It has been more than twenty years since aptamers were first developed. Yet, up to date, studies on their exploitation in viral diseases are not developed enough, mostly focused on the well-known viruses, such as HIV-1, HCV, HBV, HPV, SARS and influenza. Studies on other viruses have not been carried out systematically, with only occasional experiments conducted against some arboviruses [1, 2].

Zika virus was first identified in a blood sample taken from a rhesus monkey captured in the Zika forest of Uganda in 1947. The first human infection was reported in 1952 in Nigeria (Macnamara, 1954), and the virus was isolated from Aedes mosquitoes [3, 4]. The first isolation of ZIKV in Asia was from Aedes aegypti mosquitoes in Malaysia in 1969 [4, 5]. Zika virus poses great dangers to women at pregnancy as the virus can be passed from pregnant women to their fetus, resulting in microcephaly. It has been also reported that Zika virus infection could be associated with Guillain-Barré syndrome (GBS) and meningoencephalitis in adult [6]. ZIKV circulation has been documented in two ecologically and evolutionarily distinct transmission cycles: an enzootic, sylvatic cycle, where the virus circulates between arboreal Aedes spp. mosquitoes and non-human primates; and a human or urban cycle, between humans and peridomestic/domestic Aedes spp. mosquitoes [7]. Symptoms appear within 3–11 days of the mosquito bite. These usually start with mild headache followed by maculo-papular rash (neck, face, trunk, and upper arms, and spread to palms and soles), fever, malaise, conjunctivitis, and joint pains along with some other manifestations that include diarrhoea, constipation, abdominal pain, anorexia, dizziness, and conjunctivitis. [8].

For the development of a zika diagnostic, an aptamer-based ELISA assay for highly specific and sensitive detection of Zika NS1 protein has been proposed [6]. The NS1 is a glycosylated protein and this is significant for

effective emission, virulence, and replication of the virus. The protein may be in the form of a monomer, a dimer (a membrane-bound protein, mNS1) or a hexamer (a secreted protein, sNS1). Homo dimer of NS1 plays a key role in the viral replication, while membrane-bound NS1 is secreted and is responsible for provoking immune responses [8]. SELEX was carried out to identify Zika NS1-binding ssDNA aptamers using a ssDNA aptamer library and magnetic beads protein coated for every cycle. After 7 rounds of selection with increasingly reduced amounts of the target Zika NS1 protein, the enriched aptamer pool binds to Zika NS1 protein more significantly than the initial random ssDNA library, suggesting that Zika NS1-binding aptamers have been successfully enriched. Two selected aptamers, with the best binding affinity and the best specificity, were chosen for structure optimization, analysis and determination of their minimum binding domain. Whilst one of the aptamers showed affinity for both Zika and Dengue NS1, the other did not, but neither bind to unrelated proteins such as interferon-γ and bovine serum albumin. The authors showed that Zika NS1 can be reliably detected using a two aptamer or an antibody/ aptamer pair in a sandwich ELISA [6]. In a similar approach, we have identified aptamers against the NS1 ZikV protein, in its glycosylated and non-glycosylated form, as well as linear peptide epitopes in order to develop a sensitive diagnostic assay for acute Zika virus infections.

OBJECTIVE

To study aptamers against the NS1 for their affinity and capture capacity using fluorescent spectroscopy, circular dichroism and ELISA assays, so as to identify lead molecules for use in serologic platform development.

METHODOLOGY

Fluorescence Quenching

This method is described by Silva et al. [25, 26] and involves the quenching of tryptophan residues contained in the enzyme, as a means to show interactions with the aptamers. Fluorescence was measured in the range between 300 and 450 nm, using a 1 ml cuvette (Hellma, Ref CXA-145-298S 104F QG). Instrument settings on the Horiba, Jobin Yvon Fluoromax-P Fluorimeter, including bandwidth, excitation wavelength and integration time, were established to maximise hK6 emission, and minimise aptamer emission. This is because any fluorescent measurement is the combined sum of all dissolved fluorophores, and thus the compounding effects of any aptamer fluorescence would add to the detected signal. Fluorimeter parameters were determined as follows: 280 nm excitation, bandwidth settings of 5 nm excitation and 1 nm detection of emission, iterations of 2 nm and integration time of 0.05 seconds, 5 scans were averaged for each titration point. Each titration series was performed three times, allowing warming up time of 5 minutes before any recordings were taken, measurements performed at 37°C, 0.5 μM of NS1 were used and titrations of aptamer between 0.01 to 0.1 μM from stock of 8 μM were performed.

Ruthenium displacement assay

Ruthenium binding to the aptamer (in binding solution): A stock solution of ruthenium was titrated into 50nM aptamer. Upon each aliquot, the emission spectrum (excitation wavelength: 434nm) of the solution was recorded (until no spectral changes could be observed upon further additions). To quantify the binding, fluorescence changes at 610nm were plotted as a function of Ru(phen)2.dppz.BF4 concentration. Data best fit to a sigmoidal function from which a value for Kd was determined. Peptide binding to the aptamer and displacement of the ruthenium dye: The individual aptamers (50nM) were mixed with near saturating concentrations of the dye and incubated until no fluorescent changes could be observed (~30min). Subsequently, a stock solution of the 20mer peptide was titrated into the aptamer-dye solution and the emission spectrum recorded. The relative fluorescence decrease at 610nm was plotted as a function of peptide concentration and data could equally well fit to a sigmoidal or quadratic function.

CD spectroscopy

The CD spectrum of 10mM S11 aptamer in binding solution was recorded. A stock solution of ruthenium was subsequently added to the aptamer in the following ratios: 1:2, 1:4 and 1:5. The spectrum for the 1:4 and 1:5 ratios overlapped, hence it was assumed that no more changes would be observed upon further additions of the dye. The final dye concentration of ruthenium in the aptamer solution was 52mM. Following on, the 20mer peptide was added to the ruthenium-aptamer complex with the final peptide concentration of 2.18mM. The experiment was repeated in

KPBB with 10mM S11, followed by the addition of ruthenium at a final concentration of 52 mM. The 20mer peptide, at a final concentration of 2mM, was subsequently added to the dye-aptamer complex.

ELISA

ELISA assays were performed in order to define the ability of selected aptamers to detect the presence of NS1 in test samples. ELISA plates were covered with poly-lysine that added a positive charge and thus created a surface capable of deposition of the aptamers. Poly-lysine was deposited overnight (50µM), followed by washing of the plate 5 times with washing buffer. Subsequently, aptamer was deposited overnight on the plate covered with poly-lysine, and a sandwich ELISA was performed. Increasing amounts of ZikV NS1 were added and incubated for 1h at 37ºC, washed and the selected NS1 monoclonal antibody (1:1000) was added. After another incubation at 37ºC and washing of the plate, the reaction was revealed using an anti-mouse/HRP (1:30.000), TMB and NaCl 1N and results were read at 450nm, using a SpectraMax 190 (Molecular Devices).

RESULTS

Interaction of aptamers with the NS1 protein was confirmed with fluorescence spectroscopy, demonstrating a high affinity of the aptamer for the protein.

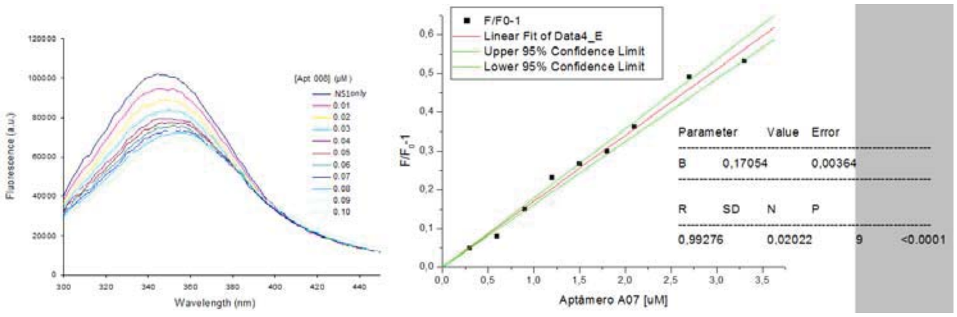

FIGURE 1. NS1 titration with increasing concentration of aptamers

Aptamers have been shown to bind to the NS1 protein, using fluorescence spectroscopy, with an affinity measured by the Stern-Volmer equation on the range of 10^5 M.

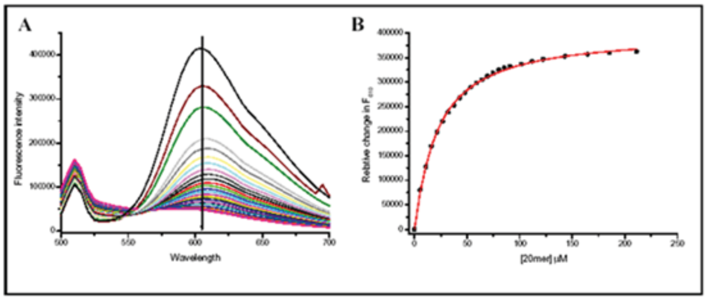

FIGURE 2. Fluorescence changes observed upon titration of a 20mer target peptide into the aptamer-dye complex. (A) emission spectra, (B) fluorescence changes plot as a function of the peptide concentration

An alternative to measure the binding interaction between the aptamers and peptides that have no inherent fluorescence, without directly labeling the aptamer, can be using a DNA intercalator, such as Ru(phen)2.dppz.BF_4 (figure 2). CD was used to assess the effect of the buffer on the assay. CD spectra for the aptamer-dye complex and the aptamer-dye complex plus peptide, in the binding salt solution and KPBB are shown below.

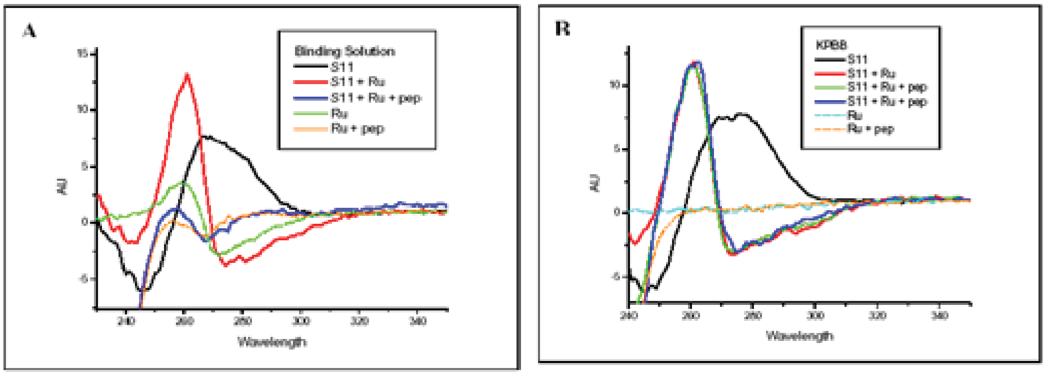

FIGURE 3. CD spectra of the aptamer, aptamer-dye complex and the aptamer-dye complex plus the 20mer test peptide, in binding solution (A) and in KPBB (B) demonstrated that aptamers can change their conformation and binding activity depending on the buffer composition

Aptamers were tested in a sandwich ELISA assay with the plate covered with Poly-Lysine, the aptamer as a capture agent and the selected anti-NS1 MAb as a revealing agent. The rNS1z_19 aptamer showed the highest optical density (O.D. = 1.22) and appeared as the best candidate for future assay development.

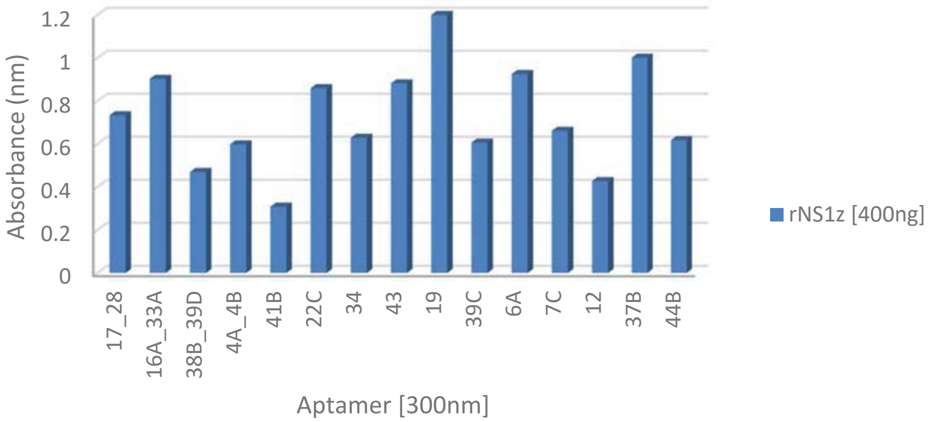

FIGURE 4. Sandwich ELISA assay showing the binding of aptamers to the NS1 non-glycocylated protein.

REFERENCES

1. Wandtke, T., Woźniak, J., Kopiński, P. Aptamers in Diagnostics and Treatment of Viral Infections. Viruses. 7, 751-780 (2015).
2. González V M, Martín M E, Fernández G, García-Sacristán A. Use of Aptamers as Diagnostics Tools and Antiviral Agents for Human Viruses. Pharmaceuticals. 9, 1-34 (2016).
3. Dick G W, Kitchen, S F, Haddow, A J. Zika virus. I. Isolations and serological specificity. Trans. R. Soc. Trop. Med. Hyg. 46, 509–520 (1952).
4. Lin H, Yip B, Huang L,Wu S. Zika virus structural biology and progress in vaccine development. Biotechnology Advances. 36, 47–53 (2018).
5. Marchette, N J, Garcia, R, Rudnick, A. Isolation of Zika virus from Aedes aegypti mosquitoes in Malaysia. Am. J. Trop. Med. Hyg. 18, 411–415 (1969).
6. Lee K H, Zeng H. Aptamer-Based ELISA Assay for Highly Specific and Sensitive Detection of Zika NS1 Protein. Anal. Chem. 89, 12743−12748 (2017).
7. Vasilakis N, Weaver S C. Flavivirus transmission focusing on Zika. Current Opinion in Virology. 22, 30–35 (2017).
8. Javed F, Manzoor K N, Ali M, Haq I U, Khan A A, Zaib A, Manzoor S. Zika virus: what we need to know?. J Basic Microbiol. 58, 3–16 (2017).

Preface of the "The Second Symposium on Information, Intelligent, Education and Engineering Application (IIEEA 2019)"

Chialiang Lin[1,a)] Chenglian Liu[2,b)] and Chiehwen Hsu[3,c)]

[1]School of Art, Ningbo Polytechnic, Ningbo 315800, China.
[2]Department of Computer Science and Technology, Neusoft Institute of Guangdong, Foshan 528225, China.
[3]Economics and Management College, Zhaoqing University, Zhaoqing 526000, China.

[a)]tronic1983@gmail.com
[b)]897599247@qq.com
[c)]2857509314@qq.com

The second symposium on Information, Intelligent, Education and Engineering Application (IIEEA 2019) is a part of the 15th International Conference of Computational Methods IN SCIENCES AND ENGINEERING (ICCMSE 2019, http://www.iccmse.org/). The IIEEA 2019 supports an academic platform for researchers who contribute on information technology, intelligent, education and engineering application. The IIEEA focuses on new methods, technologies and applications of computer science, educational technology and mathematics. The aim is to amalgamate some recent theoretical and empirical contributions that reflect current changes in technology and develop associations and interactions between ranges of disciplines. We hope that the discussions about exchange of ideas that took place contribute to advancements technology in the near future. We would like to express our greatest gratitude to the authors and reviewers of all papers, as well as to all attendees, for their participation.

Chialiang LIN

He spent that past 3 years of his life receiving his Bachelor of Arts Degree in Chang Jung Christian University (Taiwan). After that, He studied his Master of Arts course from 2007 to 2009 at National Dong Hua University (Taiwan). Now, he has been working as an associate professor at Quanzhou Institute of Technology, China. His interesting researches are Computer Programming, Image Processing and Virtual Reality Technology Development.

Chenglian LIU

Chenglian Liu received his B.S degree in information management from National Union University in 1992 and the MSc degree in National Defence from National Defence University in 2004. He studied his doctorate course at Royal Holloway, University of London from 2006 to 2009 under the supervised by Chris Mitchell. His research interests are in Key Agreement and Password Authentication, Number Theory and Cryptology so on.

Chiehwen HSU

He received his B.S degree in department of mathematics Tamkang University in 1992 and the Master degree in National Cheng Kung University in 1994(Taiwan). He completed his Ph.D of financial management from 2006 to 2010 at National Kaohsiung University of Science and Technology (Taiwan).Now, he has been working as an associate professor at Economics and Management college of Zhaoqing University in China. His research interests are in Information Analysis, Investment Strategy and Finance Engineering and so on.

Applying Distance Maintaining Calculation Method on Multi-rotor UAV Swarm

Jwu-jenq Chen[1, a)] Yung-gi Wu[2, b)] and Chia-liang Lin[3, c)]

[1] *Department of Computer Science and Information Engineering, Chang Jung Christian University, Tainan 71101, Taiwan.*
[2] *Department of Computer Science and Information Engineering, Chang Jung Christian University, Tainan 71101, Taiwan.*
[3] *School of Art, Ningbo Polytechnic, Ningbo 315800, China.*

[a)] jchen@mail.cjcu.edu.tw
[b)] wyg@mail.cjcu.edu.tw
[c)]Corresponding author: tronic1983@gmail.com

Abstract. Over the past few years, multi-rotor drones have been widely used for the both military and civilian purposes. In this paper, we are taking steps for finding a method to calculate and keep the distance in order to make the ranges of photos of every UAVs connected according to the lens and flight height. Finally, we succeeded to develop the distance maintaining calculation method via implementing angel of view formula.

INTRODUCTION

During the past years, some of studies [1–4] revealed that multi-rotor unmanned aerial vehicles (multi-rotor UAVs) that equipped single aerial filming system widely utilised for numerous purposes, containing executing disaster rescue missions and monitoring wild fires. Also, numerous researchers [6–12] found that developing a swarm control system for unmanned aerial vehicles was feasible and plausible. Moreover, some of findings [13, 14] revealed that the angle of view can be completely defined by the effective focal length and the dimension of film or image sensor as shown in Figure 1. Thus, we have been inspired by these researches and findings to develop a new distance maintaining calculation method on multi-rotor UAV swarm by using the angel of view formula.

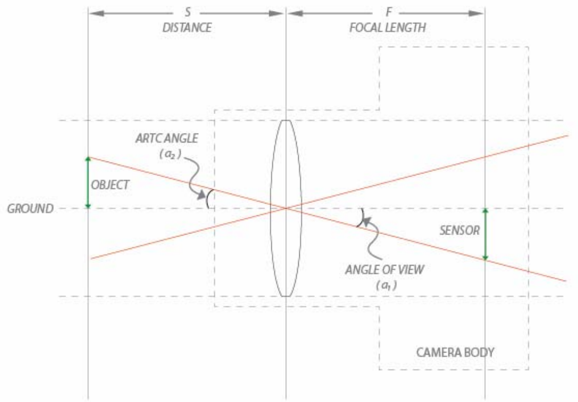

FIGURE 1. The diagram of commercial camera imaging

THE ANGEL OF VIEW CALCULATION FOR UAV

Additionally, we found that the aerial camera works like a commercial camera that rotates 90 degrees counterclockwise as shown in figure 2.

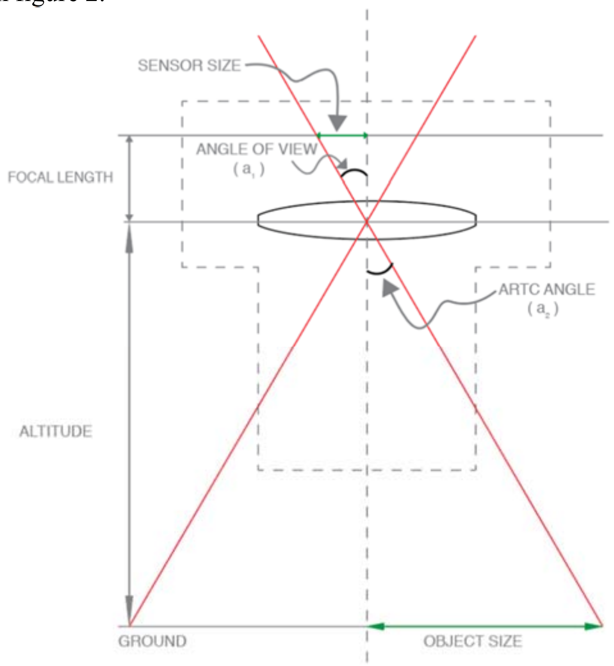

FIGURE 2. The diagram of drone's camera filming

Therefore, the drone camera's angle of view can be calculated from the chosen dimension and effective focal length using basic trigonometry as follows:

$$ANGLE\ OF\ VIEW\ (\propto_1) = \tan^{-1}\frac{SENSOR\ SIZE/2}{FOCAL\ LENGTH} \tag{1}$$

Then, calculating the artc angle ($\propto_2$) using the following equation.

$$ARTC\ ANGLE\ (\propto_2) = \tan^{-1}\frac{OBJECT\ SIZE}{ALTITUDE} \tag{2}$$

Since $\propto_2 = \propto_1$, we find:

$$\tan^{-1}\frac{SENSOR\ SIZE/2}{FOCAL\ LENGTH} = \tan^{-1}\frac{OBJECT\ SIZE}{ALTITUDE} \tag{3}$$

To eliminate $\tan^{-1}$ and rewrite the equation as follows:

$$\frac{SENSOR\ SIZE/2}{FOCAL\ LENGTH} = \frac{OBJECT\ SIZE}{ALTITUDE} \tag{4}$$

Finally, we get the formula of object size calculation presented below.

$$OBJECT\ SIZE = \left(\frac{SENSOR\ SIZE/2}{FOCAL\ LENGTH}\right) \times ALTITUDE \tag{5}$$

DISTANCE MAINTAINING CALCULATION FORMULA

After that, we exhibit our design concept of distance maintaining calculation formula as shown in figure 3.

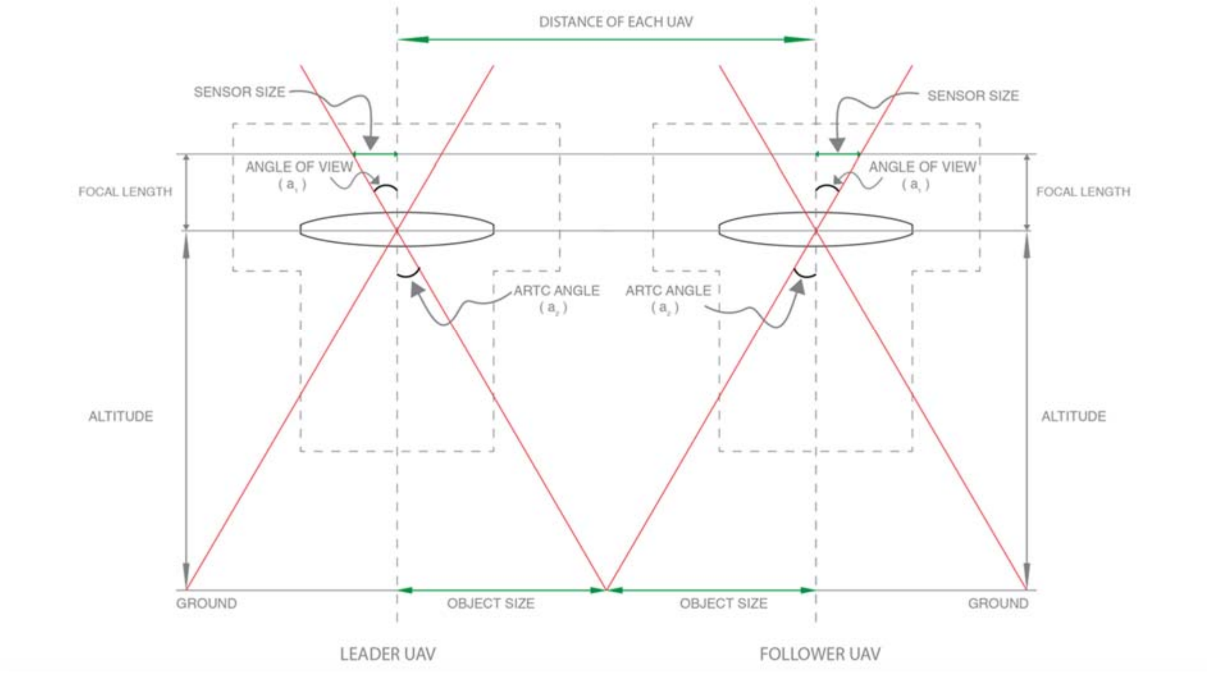

FIGURE 3. The concept of distance maintaining calculation formula.

According to the design concept, the distance of each UAV can be defined by distant object sizes as follows:

$$DISTANCE\ of\ EACH\ UAV = OBJECT\ SIZE + OBJECT\ SIZE + \cdots \tag{6}$$

Thus, we present the distance maintaining calculation formula as follows:

$$DISTANCE\ of\ EACH\ UAV = \left(\frac{SENSOR\ SIZE/2}{FOCAL\ LENGTH}\right) \times ALTITUDE + \left(\frac{SENSOR\ SIZE/2}{FOCAL\ LENGTH}\right) \times ALTITUDE + \cdots \tag{7}$$

CONCLUSION

This research has successfully developed a novel calculation formula of distance maintaining for multi-rotor UAVs through implementing the angel of view formula. This new method is able to significantly increase the effectiveness for the drone filming missions. Finally, this study provides its contribution and idea for discovering more possibilities of future researches.

ACKNOWLEDGEMENTS

The authors would like to appreciate the partial support from the Minister of Science & Technology, Taiwan under the project no. 106-2813-C-309-002-E

REFERENCES

1. C. C. Pai, Y. C. Liu, Y. S. Hsiao, H. P. Lien and P. H. Lin, Analysis of Accuracy for UAV-derived Topography from a GoPro Camera, Journal of Chinese Soil and Water Conservation. **46**, 142–149 (2015)

2. J. Y. Rau, C. Y. Chen, J. P. Jhan, K. Liu and W. Lee, Accuracy Analyses of UAV Photogrammetry and Direct Georeferencing, Taiwan Journal of Geoinformatics, **2**, 1–22 (2013)
3. W. Chang, Y. S. Hsiao, and J. C. Chang, Feasibility Analyses of River Sediment Estimation and Mountain Mapping by UAV Techniques, Journal of Chinese Soil and Water Conservation. **48**, 1–13 (2017)
4. S. H. Chio, Accuracy Elevation of Orthoimages for Aviation Occurrence Site from Rotary UAS Images, Journal of Aviation Safety and Management. **2**, 400–417 (2015)
5. D. James, 14 DRONES WITH THE BEST FLIGHT TIMES [PROFESSIONAL & HOBBY GRADE], (2017), available at http://www.dronesglobe.com/guide/long-flight-time/
6. J. Richardson, The Coming Drone Swarm, (2017), available at https://www.defenceprocurementinternational.com/features/air/drone-swarms
7. A. G. Madey, Unmanned Aerial Vehicle Swarms: The Design and Evaluation of Command and Control Strategies using Agent-Based Modeling, International Journal of Agent Technologies and Systems. **5**, 1–13 (2013)
8. S. N. Romaniuk and T. Burgers, China's Swarms of Smart Drones Have Enormous Military Potential , (2018), available at https://thediplomat.com/2018/02/chinas-swarms-of-smart-drones-have-enormous-military-potential/
9. P. Vincent and I. Rubin, "A framework and analysis for cooperative search using UAV swarms," in *ACM Symposium on Applied Computing-2004*, The 2004 ACM Symposium on Applied Computing, edited by H. M. Haddad *et al*. (ACM, New York, NY, 2004), pp. 79–86.
10. R. J. Bamberger, D. P. Watson, D. H. Scheidt and K. L. Moore, Flight Demonstrations of Unmanned Aerial Vehicle Swarming Concepts. Johns Hopkins Apl Technical Digest, **27**, 41–55 (2006)
11. P. Dasgupta, A Multiagent Swarming System for Distributed Automatic Target Recognition Using Unmanned Aerial Vehicles, IEEE Transactions on Systems, Man, and Cybernetics - Part A: Systems and Humans. **38**, 549–563 (2008)
12. A. Bandala, E. P. Dadios, R. R. P. Vicerra and L. A. G. Lim, Swarming Algorithm for Unmanned Aerial Vehicle (UAV) Quadrotors: Swarm Behavior for Aggregation, Foraging, Formation, and Tracking, Journal of Advanced Computational Intelligence and Intelligent Informatics. **18**, 745–751 (2014)
13. E. McCollough, *Photographic Topography* (Industrial Publishing Company, San Francisco, 1893). pp. 399–406
14. K. Y. Yeung, The Calculation and Application for the Angle of View (Chinese), (2006), available at: http://www.kyyeung.com/Photo/060525/060525.htm

Integrating Team-Assisted Individualisation Method into the Teaching of Art History Course

Chia-Liang Lin[1, a)] Yu-Cheng Shen[2, b)] Cheng-Wu Hu[1, c)] Dou-Ze Wu[1, d)] Si-Yong Feng[1, e)] and Wen-Jing Gao[1, f)]

[1]*School of Art, Ningbo Polytechnic,*
Ningbo, 315800, China.
[2]*Huaiyin Normal University,*
Huaiyin, 223300, China.

a) tronic1983@gmail.com
b) Corresponding author: roscoeshen@gmail.com
c) 179234763@qq.com
d) wuduoze2018@163.com
e) 331008900@qq.com
f) gwj3666409@126.com

Abstract. The history has usually been deemed a useless subject for many years. Meanwhile, most students have lost the passion of learning history-related subjects. Thus, this study is taking steps for introducing the method of Team-Assisted Individualisation (TAI) to attempt improving the teaching environment of art history course. Finally, this study has discovered problems in the art history teaching process due to we closely follow the current educational difficulties. Therefore, it can provide its contributions for the relevant researches in the future.

INTRODUCTION

For a long time, the history has been regarded as a useless subject in these education fields that related social science. Wu [1] revealed that most teachers have not paid too much attentions to the teaching method of history-related subjects, including the historical knowledge establishment and communication. Meanwhile, Wu [1] deemed most students have eliminated their passion for learning history-related subjects through the learning process of memorising significant historical events' names, years and dates. Henceforth, this subject has been marginalised into useless learning, becoming a pile of memories and unable to cultivate students' basic skills. Therefore, this study adopts the "Team-Assisted Individualisation (TAI)" proposed by Slavin [2] in 1985, to enhance students' interest in learning about art history through the design of events, containing group exercises, study evaluation and mutual praise. Finally, students will become the protagonists of the art history course to improve the learning outcomes, including historical understanding enhancement, historical thinking cultivation and historical consciousness establishment, by changing the education and learning methods of art history.

RESEARCH QUESTIONS

This study will address and answer the following questions related to integrate "Team-Assisted Individualisation (TAI)" method into the teaching of art history course at the Ningbo Polytechnic.

1. The satisfaction of integrating "Team-Assisted Individualisation" method into the art history teaching and learning.
2. The skill enhancement of historical thinking using the methods of learning by doing and narrative knowledge.

METHODOLOGY

Firstly, we introduce "Team-Assisted Individualisation (TAI)", one of cooperative learning theories, largely due to Fu [3] considered that it is the easiest implementation way of cooperative learning. This method focusses on these skills of group-based interaction and collaboration by grouping students heterogeneously with different abilities in order to achieve the interactive effects of cooperative learning. Weng [4] believed that cooperative learning is to use the division of members, exchange of opinions, sharing feedback and mutual learning among the members. The main purpose is to create a proactive learning environment, so that each team member can energetically participate in classroom teaching activity. Also, each team member will be trained to have the ability to listen and tolerate, and to accept the opinions of others, work together and respect the learning objectives of the team for promoting learning in the field of affection. Furthermore, some of findings [5-9] revealed that flipped classroom not only promote the change of students' learning style, lifestyle and survival mode, but also promote the renewal of teachers' teaching concepts, professional growth and teaching quality improvement. Therefore, this study is to analyse and review the situation of current art history course, and attempt to implement different teaching methods for improving the shortcomings of the art history classroom.

In the meantime, this method guides students to carry out historical thinking training to develop narrative types of students' historical thinking via focusing on the comparison of different evaluations for historical figures and events. Finally, we focus on the background, history and causality of historical events to shape students generating their own evaluations of historical events through empathising life style, background and culture.

RESEARCH FINDINGS

This study used the "Team-Assisted Individualisation (TAI) collaborative learning approach to conduct classroom activities. We grouped students according to the heterogeneity of different grades, traits and abilities. Therefore, each group formed a heterogeneous group of about 3 to 5 students to collaboratively learn and compete with each other as shown in figure 1. Finally, the results of the student learning competition are praised as their learning achievements.

(a) (b)

FIGURE 1. (a) showed the students were grouped heterogeneously. (b) revealed that students were collaboratively learning and competing with each other.

Also, we combined cooperative learning theory to construct knowledge of art history and explore the relationship between historical consciousness, historical thinking and historical teaching methods. Furthermore, this study used a combination of "Team-Assisted Individualisation (TAI)" teaching method applying to the establishment of art history knowledge to avoid the return of the scene of art history course to the old-school teaching way.

Thus, in terms of curriculum design, the teacher led the students to know the story of the artist and carried out "Vincent in Ningbo" painting creation activities. We designed these painting activities to replace the examination with the activity participation, enthusiasm, vitality and activity results to assess and understand the students' learning situation.

Finally, we obtained the feedback from those students who were taking art history course using online questionnaire. Thus, the details pertinent to results of students' feedbacks for integrating cooperative learning method into art history course were shown as Table 1 below.

Table 1. **The Satisfaction of Students for Team-Assisted Individualisation (TAI) teaching method**

Items	Percentage
The Moral Virtues of Teachers	81.81
The Content of Course	78.82
The Method of Teaching	81.15
The Effectiveness of Teaching	76.87
Total Average	80.03

According to the statistic, the total average percentage of evaluation results was 80.03%. Meanwhile, the highest percentage of evaluation item was the moral virtues of teachers, 81.81%. It was followed by the method of teaching, 81.15%. Therefore, it means that over 80% of students were satisfied with the moral virtues of teachers and the method of teaching method. However, the rest of two items, including the content of course and the effectiveness of teaching, were 78.82% and 76.87%.

CONCLUSION

The main research feature of this project is to try a new teaching method and break through the traditional performance model to bring new experiences to students. In addition, this study has the innovation of practical significance, largely because we follow the current educational difficulties to explore the problems in the art history teaching process. Finally, this study can provide contributions and ideas for the relevant researches from the two aspects, containing the method of teaching and the creation of the scene atmosphere.

REFERENCES

1. L. C. Wu, *Teaching Theory and Practice of History* (Chinese) (Wu-Nan Book Inc, Taipei, 2004), pp. 1–30.
2. R. E. Slavin, in *Learning to Cooperate, Cooperating to Learn*, edited by R. Schmuck (Springer, Boston, MA, 1985), pp 177–209.
3. M. L. Fu, "The Research of Cooperative Learning of Mathematics at Elementary School," Master thesis, National Changhua University of Education, 2001.
4. C. Weng, Using Lego Robotics in Program Learning, International Journal on Digital Learning Technology. **6**, 1–12 (2014)
5. H. Foot and C. Howe. The psychoeducational basis of peer-assisted learning. In K.J. Topping and S.W. Ehly, editors, Peer-Assisted Learning (Lawrence Erlbaum Associates, Mahwah, NJ, 1998), pp 27–43
6. M. B. Gilboy, S. Heinerichs and G. Pazzaglia, Enhancing Student Engagement Using the Flipped Classroom, Journal of Nutrition Education and Behavior. **47 (1)**, 109–114 (2015)
7. C. F. Herreid and N. A. Schiller, Case Studies and the Flipped Classroom, Journal of College Science Teaching. **42**, 62–66 (2013)
8. N. B. Milman, The Flipped Classroom Strategy: What Is it and How Can it Best be Used, Distance Learning. **11**, 9–11 (2012)
9. H. N. Mok, Teaching tip: The flipped classroom, Journal of Information Systems Education. 25, 7–11 (2014)

A Study of Android Calculator Based on Legendre's Conjecture

Yongzhang Luo[1, b)] Junjie Huang[2, c)], Chenglian Liu[2, a)], Huiwen Chen[2,d)] and Biying Zhao[3, e)]

[1] *School of Business Management, Neusoft Institute of Guangdong, Nanhai Software and Technology Park, Foshan 528225, Guangdong, China*

[2] *School of Computing, Neusoft Institute of Guangdong, Nanhai Software and Technology Park, Foshan 528225, Guangdong, China.*

[3] *School of Applied Economics, Guangdong Baiyun University, No. 1 Xueyuan Road, Baiyun District, Guangzhou 510450, Guangdong, China*

[a)]Corresponding author: 897599247@qq.com
[b)] 931785605@qq.com
[c)] 969318963@qq.com
[d)] halo@4fk.me
[e)] beyinzhao@outlook.com

Abstract. Legendre's s conjecture is an unproven idea in number theory. Legendre's conjecture states that there is a prime number between n^2 and $(n+1)^2$ for every positive integer *n*. In this article, we will demonstrate a common modern application that uses a new method to analyze the conjecture. Legendre's conjecture was found by the French mathematician Adrien-Marie Legendre put forward the prime conjecture.

INTRODUCTION

Determining the number of primes in an interval is a very important issue for mathematicians. This is because their use in applications is very strong. For example, applications that accurately require prime numbers include cloud computing, big data and internet security. With advances in computer technology, such as increases in memory and speed, the computer has become an important tool to expand artificial intelligence. With expanded memory and speed, the computer has become a great tool for work that requires many prime numbers. Legendre's conjecture [1] that trouble mathematicians for years still unproved. Its content is, in the set of natural numbers N, there is at least one prime number between n^2 and $(n+1)^2$. In 1855, a mathematician named Depov proposed the same idea, and is called Depov's conjecture [2; pp. 149-150]. Foreign sources indicate that this conjecture is Legendre's conjecture. China data and books are expressed as Depov's conjecture, to avoid confusion, the authors unified use the Legendre conjecture in this article. At the 1912 International Congress of Mathematicians (ICM), Edmund Landau summed up the four basic problems of prime Numbers at that time, the Legendre's conjecture it was one of them. Since then, many mathematicians have done research on Legendre. In 1995, Ye Zailiang [3] proposed two method to prove the conjecture. Danilo Bazzanela [4] has done some Legendre's Conjecture research prove. Fayez Fok Al Adeh [5] explain the conjecture using the method of complexity. Germán Paz [6] briefly explored the method of proving Legendre's conjecture in 2013, and Mehdi Hassani [7] partially proves Legendre's conjecture with the following formula:

$$\left\lfloor \frac{1}{2}\left(\frac{(\mathrm{n}+1)^2}{\log(\mathrm{n}+1)} - \frac{n^2}{\log n}\right) - \frac{\log^2 n}{\log\log n}\right\rfloor \le \pi((n+1)^2) - \pi(n^2) \qquad (1)$$

The author thinks this formula is too complicated and the proof is rather complicated, and author will describe the Legendre's conjecture in a more intuitive way.

RELATED WORK

In this article, we will discuss relevant features of Legendre's conjecture, and we will design and implement a computing application based on Android development environment. The results of Legendre's conjecture are analyzed in detail. The author will discuss some extensions of Legendre's conjecture in a simple and intuitive way, hoping that the results can provide reference value.

Legendre's Conjecture

Legendre's conjecture states that there is at least a prime number between n^2 and $(n+1)^2$ for every positive integer n. For example: if n is 5, n^2 is 25, and $(n+1)^2$ is 36. In the interval of (25, 36) there are two prime numbers: 29 and 31.

The Number of Primes in Legendre's Conjecture

Given a positive integer n=200, there are 33 prime numbers in the interval of (40000，40401), We call "33"，when n = 200, in the n^2 to $(n+1)^2$ interval there were number of prime numbers, and use L(X) expressed. shown in In table 1, Given a natural number, we can slow calculation in the n^2 to $(n+1)^2$ interval has how many prime Numbers and column into the form below, and more intuitive. Until now, however, it has not been possible to know directly how many prime numbers are in the interval.

TABLE 1. When n=100，n^2=10000，$(n+1)^2$=10201，prime number listed

10007	10009	10037	10039
10061	10067	10069	10079
10091	10093	10099	10103
10111	10133	10139	10141
10151	10159	10163	10169
10177	10181	10193	

OUR METHODOLOGY

We calculated the natural Numbers from n = 1 to n = 50000, in the n^2 to $(n+1)^2$ all primes in the interval. Based on this, we estimate a budget line, and from another angle to observe Legendre conjecture, we use a visual representation of table 2 and figure1.

Notation:

n: the natural number,

L(X): number of prime numbers in Legendre's conjecture,

L'(X): estimated number of prime numbers in Legendre's conjecture .

TABLE 2. Estimated number of prime numbers in Legendre's conjecture

n	n^2	$(n+1)^2$	L(X)	L'(X)
1	1	4	2	7
2	4	9	2	8
3	9	16	2	8
……	……	……	……	……
2500	6250000	6255001	328	338
2501	6255001	6260004	322	338
2502	6260004	6265009	333	338
……	……	……	……	……
50000	2500000000	2500100001	4605	4658

Based on the experimental data, the approximate formulas of the asymptotic curve obtained in this study are as follows.

$$L'(X) = \lceil -0.00000046 * n^2 + 0.1105 * n + n^{0.5198} + 5.6923 \rceil \quad (2)$$

In table 2, we can intuitive see when n is equal to what value corresponding to the n^2 and $(n+1)^2$ value, and in the n^2 to $(n+1)^2$ all primes in the interval expressed in L(X). And we can calculated by formula (2) n at this time the asymptote of L'(X).

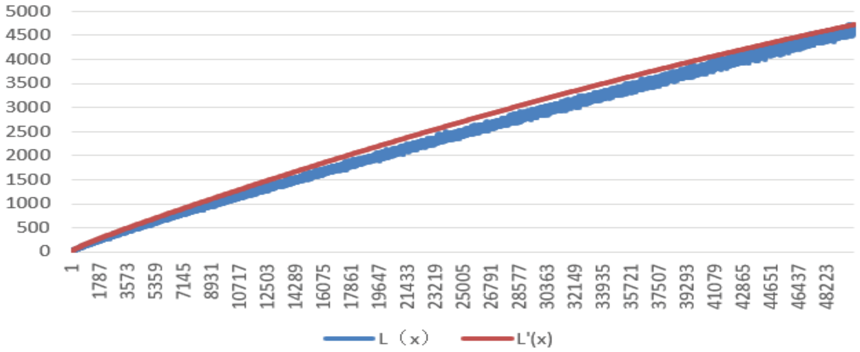

FIGURE 1. Asymptote curves of the number of prime numbers in Legendre's conjecture

In figure 1, the x-axis represents the value of n, the y-axis represents the number of prime Numbers, and the blue part is what n is corresponding to the value in the n^2 to $(n+1)^2$ all primes in the interval, the red part is the value of the experimental result, namely the experimental result of formula (2). The relationship between L'(X) and L(X) can be intuitively observed through this figure.

The Experimental Result

In the figure 2, we designed and developed an app based on the android development environment. This app is used formula (2) to calculate and estimated in the n^2 to $(n+1)^2$ all primes in the interval.

In the figure 2 it has two parts: the first, of all inputs a natural number n in the left half, and then outputs the result according to formula (2) and actual accurate results. Then in the right half is the range of a natural number n, which can be directly listed according to formula (2) the estimated number of prime numbers in Legendre's conjecture. The result of pre-valuation is L'(X) and Actual accurate results L(X).

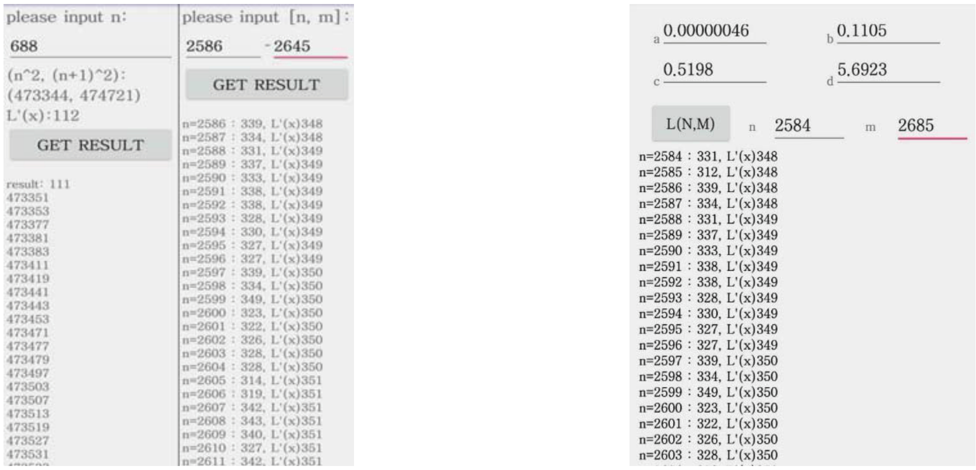

(a) (b)

FIGURE 2. (a) is the first APP demo, for example, enter an n=688 on the left side, the desired range is (473344,474721), which We can get the (n^2, $(n+1)^2$) value. Then calculate L'(X) according to formula (2) to get a value of 112, and we see figure 2 the "result" also know that in the n^2 to $(n+1)^2$ interval have a 111 prime numbers, and list each of them. Enter an interval range on the right part to get L(X)and L'(X) and compare. (b) revealed the dynamic adjustment of approximate formula APP

In figure 2 is the second app developed based on the android environment. It can dynamically adjust the asymptote formula to obtain a more optimized approximate formula. The previous formula (2) in this article is the static expression.

In the APP of figure 3, you can enter four parameters of the asymptote formula (2), where "a" is the coefficient of $-n^2$, "b" is the coefficient of n, "c" is the exponent of $n^{0.5198}$, and "d" is the constant term, and N and M represent the range of values of n. For example, the adjusted asymptote formula and the actual value can be obtained by inputting a=0.00000046, b=0.1105, c=0.5198, d=56923, N=2584, M=2685. Through this repeated operation, the parameters of the asymptote formula can be dynamically adjusted to obtain a more optimized asymptote. Through the mutual use and adjustment of the APP, we can get the number of primes in the correlation interval faster and more accurately, thus indirectly proving the validity of Legendre's conjecture.

CONCLUSION

The author designed and developed the APP based on the android development environment, which is used to calculate the number of prime numbers in Legendre's conjecture. In this paper, the author proposed a formula for estimating the number of primes in Legendre's conjecture by means of asymptotes. According to this estimation formula, the distribution of primes in different regions can be seen more intuitively and clearly. The author intends to continue to study the APP in order to make more accurate estimates of the asymptotes of the number of primes in different range of Legendre conjecture.

REFERENCES

1. Wikipedia. Legendre's conjecture. https://en.wikipedia.org/wiki/Legendre%27s_conjecture#cite_ref-4
2. Lou Shituo, Wu Donghua. Riemann Hypothesis. Liaoning education press, 1987:149-150.
3. Ye Zailiang. Two ways to solve Depov's conjecture. Journal of Shangluo normal college (natural science edition), vol.6, no.4, 1995.
4. Danilo Bazzanella. Primes between consecutive squares. Arch. Math. 75 (2000).
5. Fayez Fok Al Adeh. There is always a prime between n^2 and $(n+1)^2$. http://www.gsjournal.net/Science-Journals/Research%20Papers-Mathematical%20Physics/Download/1797
6. Germán Paz. On Legendre's, Brocard's, Andrica's, and Oppermann's Conjectures. https://arxiv.org/pdf/1310.1323.pdf
7. Mehdi Hassani .Counting primes in the interval (n^2, $(n+1)^2$). https://arxiv.org/pdf/math/0607096v1.pdf
8. Madieyna Diouf. A conditional proof of Legendre's Conjecture and Andrica's conjecture. https://arxiv.org/pdf/1810.02191.pdf

Security Analysis of Enhanced Schmidt-Samoa Scheme

Huiwen Chen[1,b)], Chenglian Liu[1,a)], Jungjie Huang[1,c)] and Sonia C-I Chen[2,d)]

[1]*School of Computing, Neusoft Institute of Guangdong, Foshan 528225, China*
[2]*School of Economics and Finance, Huaquiao University, Xiamen 361021, China*

[a)]Corresponding author: chenglian.liu@gmail.com
[b)]halo@4fk.me
[c)]legnirdrepus@qq.com
[d)]drsoniachen@mail.com

Abstract. Thangavel and Varalakshmi proposed "Enhanced Schmidt-Samoa cryptosystem for data confidentiality in cloud computing" in 2016, they modified the Schmidt-Samoa (SS) scheme, namely Enhanced Schmidt-Samoa (ESS) scheme into cloud computing environment. According to this algorithm, the authors develop two tiny programs those are Android app and HTML version used to mobile phone in any where. In the same time; the authors also analyze the security flaw of ESS algorithm in this article.
Keywords: RSA algorithm; Schmidt-Samoa scheme; Euler totient function; Flaw

Instruction

Thangavel and Varalakshmi modified the Schmidt-Samoa algorithm which it used four primes into their scheme. As we all know, the Schmidt-Samoa algorithm is very slow in encryption phase. Thangavel and Varalakshmi may want to improve the disadvantage of SS on this reason. In order to improve efficiency and security, the ESS scheme introduces the concept of four prime numbers, which is different from the original SS scheme. Although the ESS version of Thangavel and Varalakshmi used the RSA dual modulus framework, it is essentially a "Like RSA type". In this article the author analyses and points out the shortcomings of ESS scheme proposed by Thangavel and Varalakshmi, and points out unknown doubts.

Review of Enhanced Schmidt-Samoa Scheme

The RSA algorithm [1] is well known public key cryptosystem. It is widely used many application such as traitor tracing scheme, multi-secrect sharing scheme, and anonymous multi-receive encryption scheme so on. We briefly introduce the principle of RSA in this section.

The RSA scheme

Step 1. Randomly select two prime numbers p and q before to find n such as Equation (1)

$$n = p \cdot q \tag{1}$$

Step 2. To compute $\phi(n)$ where it satisfy the Equation (2)

$$\phi(n) = (p-1)(q-1) \tag{2}$$

Step 3. Choose an integer e where it $1 < e < \phi(n)$ and satisfies two Equation (3) and (4).

$$\gcd(e, \phi(n)) = 1, \tag{3}$$
$$e \cdot d \equiv 1 \pmod{\phi(n)} \tag{4}$$

published the public key e and keep the secret key d.

Step 4. Encryption phase, use the public key e to encrypt the digitize message M before the ciphertext C such as Equation (5).

$$C \equiv M^e \pmod{n} \tag{5}$$

Step 5. Decryption phase, use the private key to recover the ciphertext by Equation (5).

$$M \equiv C^e \pmod{n} \tag{6}$$

From Equation (1) to (6), those are RSA algorithm.

The ESS Scheme

The ESS is the abbreviation of Enhanced Schmidt-Samoa algorithm, meaning Schmidt-Samoa advanced version. The algorithm describes the following steps:

- Random select four prime numbers p, q, r and s to find

$$X = p \cdot q, \tag{7}$$
$$Y = r \cdot s. \tag{8}$$

- And then compute

$$L = (p - 1, q - 1) \tag{9}$$
$$M = (r - 1, s - 1) \tag{10}$$

- If holds

$$\gcd(X, L) = 1, \tag{11}$$

then find

$$X' \equiv X^{-1} \pmod{L} \tag{12}$$

- Else if compare

$$\gcd(Y, M) = 1 \tag{13}$$

then

$$Y' \equiv Y^{-1} \pmod{M} \tag{14}$$

- Calculate

$$Z = X' \cdot Y'. \tag{15}$$

- To generate the public key N and private key d, we should compare

$$\gcd(Z, L) \stackrel{?}{=} 1. \tag{16}$$

If it holds, then compute

$$N \equiv Z \pmod{L} \tag{17}$$
$$d \equiv N^{-1} \pmod{L} \tag{18}$$

We obtain the public key parameters {N,X}, else if skip to Step 9.

- Encrypt the message m such as

$$C \equiv m^N \pmod{X} \tag{19}$$

- Decrypt the cipher C as follow

$$m \equiv C^d \pmod X \quad (20)$$

- Re-compute the public key and private key where

$$\gcd(Z, M) \stackrel{?}{=} 1 \quad (21)$$

If holds, to find

$$N \equiv Z \pmod M \quad (22)$$
$$d \equiv N^{-1} \pmod M. \quad (23)$$

The parameter {N,Y} are public key pairs.

- Encrypt the message m such as

$$C \equiv m^N \pmod Y \quad (24)$$

- Decrypt the cipher C as follow

$$m \equiv C^d \pmod Y \quad (25)$$

Original Example

Randomly chooses four primes where $p = 7$, $q = 11$,$r = 13$, and $s = 17$, to find

$$X = 11 * 7 = 77. \quad (26)$$
$$Y = 13 * 17 = 221. \quad (27)$$
$$\phi(X) = 10 * 6 = 60. \quad (28)$$
$$\phi(Y) = 12 * 16 = 192. \quad (29)$$

And

$$L = (10, 6) = 30). \quad (30)$$
$$M = (12, 16) = 48. \quad (31)$$

Compare the Equation (32)

$$\gcd(X, L) \stackrel{?}{=} 1 \quad (32)$$

then to find X',

$$X' \equiv 77^{-1} \pmod{30} = 23. \quad (33)$$
$$Y' \equiv 221^{-1} \pmod{48} = 5. \quad (34)$$

Calculate Z, where

$$Z = 23 * 5 = 115. \quad (35)$$

Since

$$\gcd(Z, L) = (115, 30) = 5 \neq 1 \quad (36)$$

compare Equation (37) if it holds

$$\gcd(Z, M) = (115, 48) \stackrel{?}{=} 1 \quad (37)$$

If holds, then compute

$$N \equiv 115 \pmod{48} = 19. \quad (38)$$
$$d \equiv 19^{-1} \pmod{48} = 43. \quad (39)$$

Assume

$$e_n = 5, d_n = 194. \quad (40)$$
$$e_m = 3, d_m = 169. \quad (41)$$

Set digitize message m where

$$m = 25. \tag{42}$$

Encryption Phase:

$$C \equiv 32^{19} \pmod{221} = 111. \tag{43}$$

Decryption Phase:

$$m \equiv 111^{43} \pmod{221} = 25. \tag{44}$$

Security Analysis

Selecting Parameter Problem

In original RSA algorithm version, the Euler's totient function [5] use by

$$\phi(n) = (p-1)(q-1), \tag{45}$$

then to generate the public and private key, where

$$c \cdot d \equiv 1 \pmod{\phi(n)} \tag{46}$$

However, the Carmichael's totient function [2] increase secure degree and reduce the security risk, because the Carmichael totient function is less than the Euler's totient function [3]. Thus, the revised RSA version has changed to

$$\lambda(n) = (p-1, q-1) \tag{47}$$

In short, that is

$$\begin{cases} m^{\phi(Y)} \equiv m^{\lambda(Y)} \equiv 1 \bmod Y \\ 32^{192} \equiv 32^{48} \equiv 1 \bmod 221 \end{cases} \tag{48}$$

According to this experiment, does it exist an integer Ω less then the Carmichael's function? By citation [2], we traverse 1 to M, from 1 to 48, we found a positive integer 24 where it satisfies

$$m^{\Omega} \equiv 1 \bmod Y, \ while\ \Omega \leq \lambda(Y) \tag{49}$$

since

$$32^{24} \equiv 1 \pmod{221}. \tag{50}$$

From above, we know that the ESS algorithm has security risks.

Algorithm Defect Problem

As know the public parameters $\{N, Y\}$, does it exist an integer B to satisfy

$$\begin{cases} B - Y = N \\ B = \phi(Y) + M, \end{cases} \tag{51}$$

promptly

$$\begin{cases} 240 - 221 = 19 \\ 240 = 192 + 48 \end{cases} \tag{52}$$

From the example, if there satisfy an integer B, it can be decomposed in polynomial time. Figure 1 shows that there are 15 different combinations of permutations by the number 240, one of which ($4 * 48 = 192$) is the correct solution, namely $\phi(Y)$.

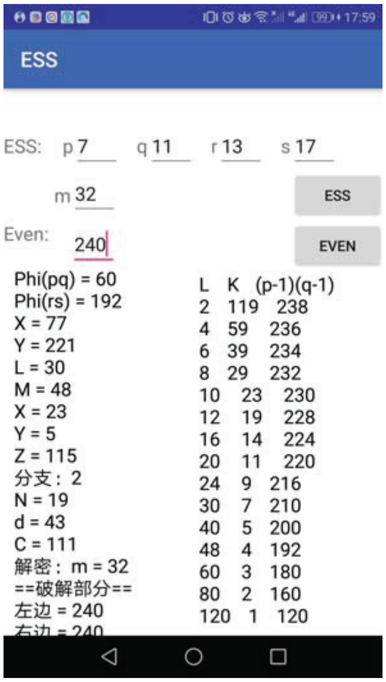

FIGURE 1. The ESS Android App.

CONCLUSION

This paper analyses the ESS algorithm from two perspectives, and deeply analyses the potential security risks or vulnerabilities of the improved ESS scheme. However, RSA involves extensive and profound knowledge of number theory, and the author's research is limited. The future goal is still devoted to the advanced research of ESS algorithm in this scheme.

ACKNOWLEDGMENTS

The authors would like to thank the anonymous reviewers for their useful comments. This work is partially supported from university project under the number NUIT2018-001. This work also partially supported by Guandong province special funds to foster the student's science and technology innovation under the number PDJH2019B0569 (Climbing program funds).

REFERENCES

[1] R. L. Rivest, A. Shamir, and L. Adleman, Communications of the ACM **21**, 120–126 (1978).
[2] Wikipedia website, Carmichael totient function, Feb 2019.
[3] Wikipedia website, Euler totient function, Feb 2019.
[4] M. Thangavel, P. Varlalshmi, M. Murrali, and K. Nithya, International Journal of Information and Computer Security **7**, 177–195 (2015).
[5] M. Thangavel and P. Varalakshmi, International Journal of Information systems and change Management **8**, 160–188 (2016).
[6] K. Schmidt-Samoa, Journal of Electronic Notes in Theoretical Computer Science **157**, 79–94May (2006).

CAE Analysis on the Mechanical Properties of a 3D-Printed Lattice Structure from Ti-6Al-4V for Biomedical Applications

Yu-Lian Lin[1], Chun-Ying Lee[1, a)] and Jhewn-Kuang Chen[2]

[1]*Graduate Institute of Manufacturing Technology, Taipei, Taiwan*
[2]*Department of Materials and Mineral Resources Engineering*
National Taipei University of Technology, Taipei 10608, Taiwan

[a)]Corresponding author: leech@ntut.edu.tw

Abstract. This study investigates the structural compression properties of the additive manufactured (AM) Ti-6Al-4V lattice structure using LS-Dyna simulation analysis software and calculates its mechanical properties under different porosities and different pattern designs. Ti-6Al-4V alloys formed by using additive manufacturing produced elliptic holes with long and short axes due to the difference in the direction of construction. These holes could be eliminated and the materials could be compacted by hot isostatic pressing (HIP) treatment. Compactness of the frame element achieved 99.9% and drastically reduced the anisotropic behavior caused by the fabrication process. For the experimental testing, the samples with different porosities and the A-type and AZ-type designs were employed in compression experiment. In the meantime, the Young's modulus, the yield strength, plateau stress and other mechanical behavior were investigated by CAE simulation. The plateau stress, which is an important property for some biomedical applications, was calculated with satisfactory accuracy compared with experimental measurements. The simulated results of the designed lattice structures with different porosity contents were able to adopt the Gibson-Ashby model to determine their failure mechanisms. Finally, the CAE simulation for the design of an auxetic material was demonstrated.

INTRODUCTION

Recently, additive manufacturing has been widely used in the industry for its unique adaptability for different applications. Without the expansive molding, parts with complicate shape and dimensions can be built in the cost-effective and time-efficient fashions. More importantly, tailor-made parts without excessive material waste are less energy-consuming and more eco-friendly. Nevertheless, the customized design for individual application requires more computer-aided engineering (CAE) design and analysis to reduce the trial-and-error process and to minimize the development cost.

With the limited available materials which can be used in additive manufacturing, the incorporation of structural design to tailor the required mechanical properties of the fabricated part poses a feasible solution. 3D-printed part with internal lattice structure has been a common practice to reduce the manufacturing cost and tune the mechanical property. With the same material, different lattice designs can influence the mechanical property such as strength and failure mechanism. Gibson and Ashby [1] proposed a theoretical model to correlate the relationship between the mechanical property and volume fraction of porous structure. Their theoretical model had successfully demonstrated its capability in predicting the elastic modulus and yield strength of porous aluminum alloy with different void volume fractions [2]. Kadhodapour and coworkers [3] studied the failure mechanisms of lattice structures consisted of cubic and diamond lattice unit cells. Both the finite element analysis and experimental measurement were used in their study. A lattice exponent n was distilled to determine the failure mode of the lattice structures. When the exponent is close to 1, tension/compression is the dominant failure mechanism. Bending becomes the main failure mechanism as the exponent n approaches 2.

With the availability of additive manufacturing, more degrees of freedom in design provide the emergence of different and unusual material structures. The physical properties of these metamaterials [4] can be impossible to be obtained from their natural counterparts, such as negative reflectivity, negative mass and negative Poisson's ratio. Their potential applications both in academia and industry are to be explored. Therefore, an auxetic material which has negative Poisson's ratio is designed and studied by both theoretical analysis and experimental measurement.

DETAILS IN CAE SIMULATIONS

Material and Lattice Structure Design

Table 1 lists the unit cells of the lattice structure and their dimensions used in this study. The lattice specimen for mechanical testing was 13 mm in diameter and 25 mm in height. In order to transmit the loading uniformly onto its two ends, a solid end tab was built directly at each end of the specimen. The specimen was fabricated by using Ti-6Al-4V powders through selective laser melting (SLM) process. A post-treatment with hot isostatic pressing (1000°C, 150 MPa, 1 hr) was conducted shortly after printing to homogenize the specimen. A solid specimen was also prepared with the similar procedure and used in the uniaxial compression test to obtain the material mechanical behavior. The stress-strain curves for the material loaded in y and z directions, respectively, are presented in Fig. 1. It is seen that after H.I.P. treatment the material remained ductile and nearly isotropic. This stress-strain curve was employed in the finite element analysis of this study. As presented in Table 1, two types of unit cell structure were considered in this study: A and AZ. The only difference in A-Z type lattice design from that of A type was the addition of extra column in z-direction through its center. Therefore, with similar dimensions, the AZ type lattice structure had less porosity than its A type counterpart. For each type, there were three designs with different porosities which was controlled by the diameter of its constituent members.

TABLE 1. Unit cells of the lattice structure and their dimensions 5

Specimen for mechanical testing	**A type unit cell**	**AZ type unit cell**
		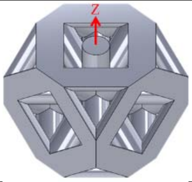

A type			
Specimen code	A46	A59	A69
Porosity	46%	59%	69%
Diameter of frame member (μm)	300	250	200
AZ type			
Specimen code	AZ33	AZ50	AZ84
Porosity	33%	50%	84%
Diameter of frame member (μm)	300	250	150

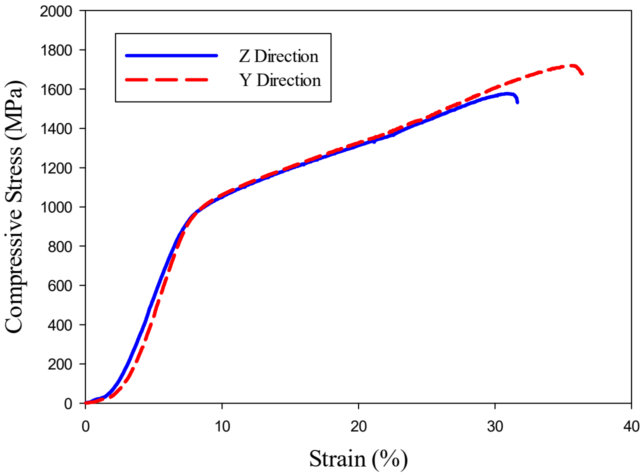

FIGURE 1. The measured stress-strain curves of an SLM printed solid Ti-6Al-4V specimen after hot isostatic pressing 5.

Compression Analysis

According to the dimensions listed in Table 1 for each specimen, a computer model with 3×3×3 lattice structure sandwiched between two solid end tabs was built. Figure 2 presents the simulation models for compression analysis. The cylindrical model was to simulate the specimen configuration used in experimental measurement. However, in terms of completeness and simplicity in simulation modeling, tetragonal model was easier to build. Comparison on the simulation results will be discussed later on. In the simulation analysis, the bottom face of the lower end tab was fixed while the upper end tab was assigned with a 0.125 mm/min compression speed which coincided with the magnitude adopted in experimental measurement. In the solution with LS-Dyna®, the contact among element surface was set at single surface to avoid the inter-penetration between elements.

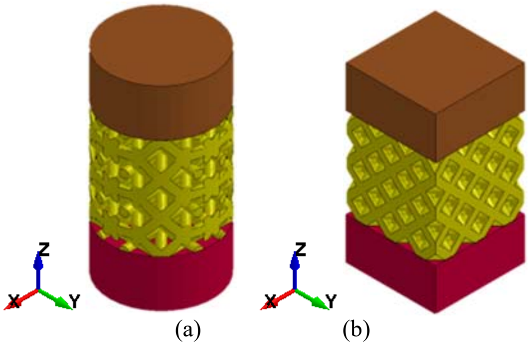

FIGURE 2. Simulation models for compression analysis: (a) Cylindrical Model, (b)Tetragonal Model

Shear Analysis

Under uniaxial compression test, the maximum shear occurs at 45° plane with respect to the loading direction. Therefore, in order to align the unit cell with the maximum shear direction, the simulation model of the lattice structure was rebuilt as shown in Fig. 3. It should be noted that for the same inclusion of 3×3×3 unit cells in this shear model, the dimensions became slightly larger than its compression counterpart. All the other simulation settings were the same as those used in compression analysis.

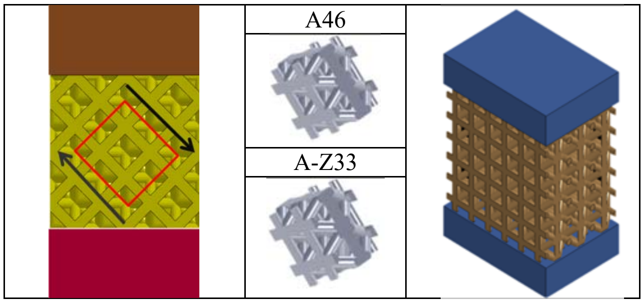

FIGURE 3. The simulation model for shear analysis of the lattice structure.

RESULTS AND DISCUSSION

Simplification of Simulation Model

As shown in Fig. 2, cylindrical and tetragonal specimens were used in the simulation analysis. Considering the possibility of using this lattice structure design in hip joint implant [5], the experimental specimen was built in cylindrical form. As mentioned previously, tetragonal model was easier to build and had merits in simulation such as higher meshing quality. Figure 4 presents the simulation results of cylindrical and tetragonal models under compression test. It can be seen that the difference between these two models was within 4%. The accuracy of simulation using tetragonal model was quite acceptable. Therefore, for simplicity the simulation analyses afterwards were all based on the tetragonal model.

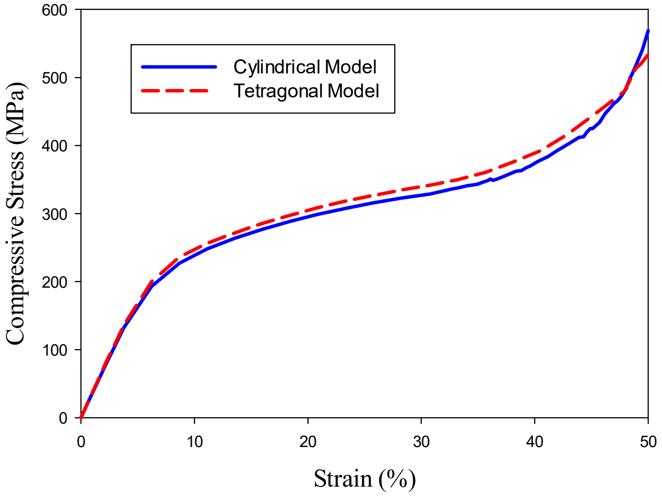

FIGURE 4. The simulation results of cylindrical and tetragonal models under compression test.

Failure Mode of Different Lattice Designs

The simulated stress-strain curve from the model was employed to extract the Young's modulus and yield strength. With these data and their corresponding porosity ratios for each type of lattice structure, the lattice exponent n could be fitted from the Gibson-Ashby model. The results are presented in Table 2. The exponents for the A and AZ type of lattice structures were 1.93 and 1.32, respectively. A-type lattice structure with n close to 2 denoted a shear dominant failure mode while AZ-type lattice structure with n near 1 revealed a compression dominant failure mode. The pictures of the failed specimens presented in Table 2 confirmed the failure mode predicted by Gibson-Ashby model. To further check on the individual simulation result of different lattice structures, Figures 5 and 6 show the pre-yield stress-strain curves of A46 and AZ33 specimens under both shear and compression loading, respectively. The dot lines in these figures are auxiliary lines with 0.2% offset to locate the

corresponding yield points. The lower yield strength in shear for A46 and lower yield strength in compression for AZ33 all complied with the aforementioned failure mechanisms.

TABLE 2. The fitted lattice exponent of Gibson-Ashby model for two different types of lattice structure

A Design	AZ Design
n=1.89	n=1.32

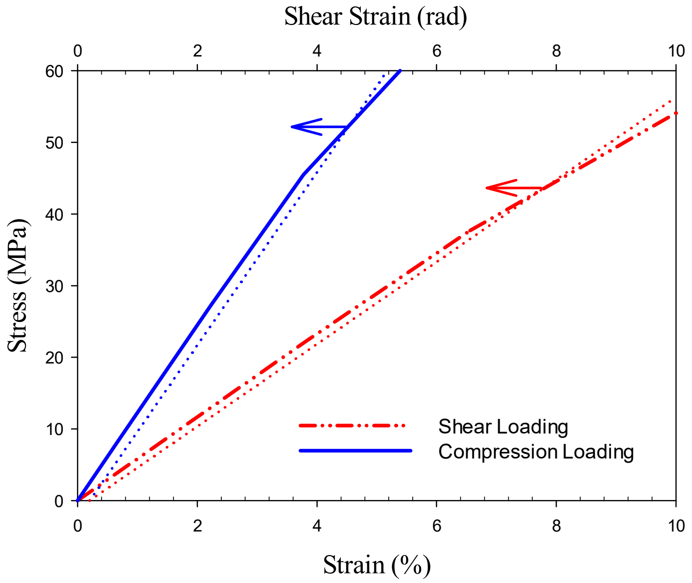

FIGURE 5. The pre-yield stress-strain curves of A46 specimen under shear and compression loading, respectively.

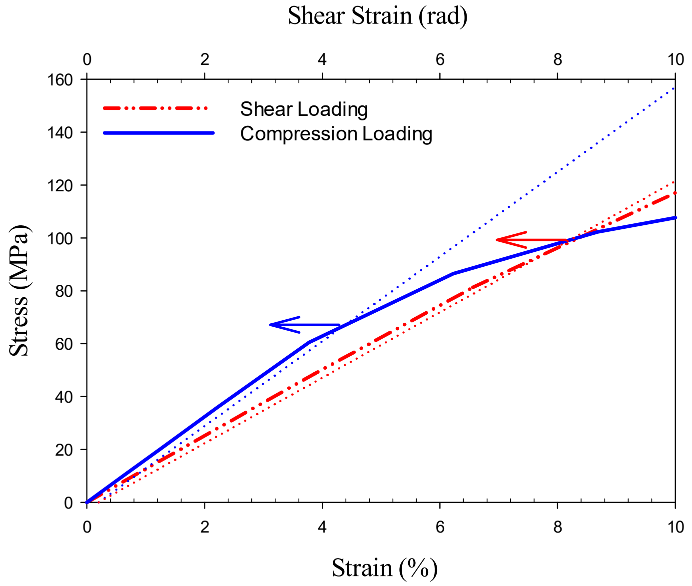

FIGURE 6. The pre-yield stress-strain curves of AZ33 specimen under shear and compression loading, respectively.

Design of Auxetic Structure

In the application of CAE analysis in the design of auxetic material, a 2-D lattice structure as shown in Fig. 7 was used as an example. Similar settings in simulation were adopted from the previous work in lattice structure except the material was replaced by thermoplastic polyurethane (TPU). TPU had lower elastic modulus and higher ductility to facilitate the deformation measurement under loading. Under uniaxial compression loading, both the axial and lateral deformations were measured to calculate the corresponding Poisson's ratio. The measured and simulated results at different compression deformations are presented in Fig. 8. It is obviously seen that a hysteresis occurred during the loading-unloading cycle. Nevertheless, the simulated result fitted very well with the measurements. The variation of the Poisson's ratio with the magnitude of the compression denoted the nonlinearity of this auxetic structure which could be derived from the material nonlinearity of TPU and the geometrical nonlinearity from large deformation.

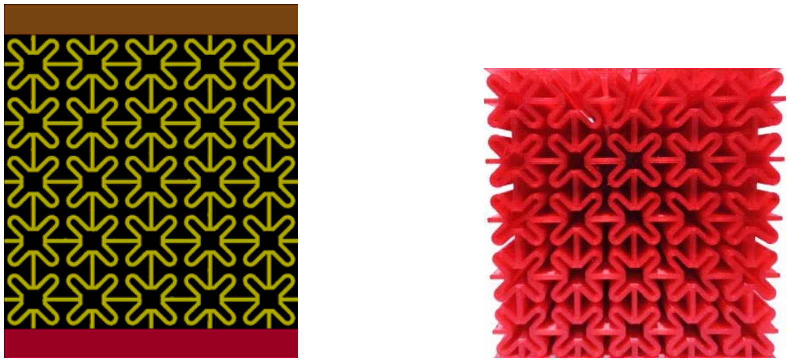

(a) (b)

FIGURE 7. A 2-D auxetic structure used in this study, (a) simulation model, (b) 3-D printed specimen.

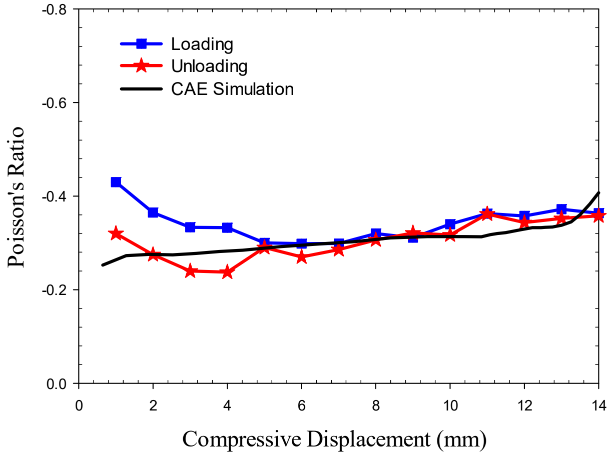

FIGURE 8. The variation of Poisson's ratio with respect to the magnitude of compression of the auxetic structure proposed in this study.

CONCLUSION

A nonlinear finite element analysis on the design of lattice structures fabricated by additive manufacturing was conducted in this study. The important findings can be summarized as:

- A 3×3×3 unit cell tetragonal model used in the simulation was good enough to obtain accurate result comparing with circular model and other more unit cell model.
- The simulated results of the designed lattice structures with different porosity contents were able to adopt the Gibson-Ashby model to determine their failure mechanisms. The prediction in shear or compression failure

mode of different lattice structure designs was consistent with the experimental observation.

- The finite element analysis on a proposed auxetic material consisting of lattice structure was shown to have negative Poisson's ratio which possessed slight nonlinearity over large compression deformation and was validated by experiment.

ACKNOWLEDGMENTS

The experimental data for the Ti-6Al-4V alloy provided by Mr. Tien-Lin Cheng is greatly appreciated.

REFERENCES

1. L.J. Gibson, M.F. Ashby, *Cellular Solids: Structure and Properties*, 2nd ed., (Cambridge University Press, Cambridge, MA. 1999)
2. L. E. Murr, S. M. Gaytan, F. Medina, H. Lopez, E. Martinez, B.I. Machado, D.H. Hernandez, L. Martinez, M.I. Lopez, R.B. Wicker and J. Bracke, "Next-generation Biomedical Implants Using Additive Manufacturing of Complex, Cellular and Functional Mesh Arrays," Philosophical Transactions: Mathematical, Physical and Engineering Sciences, Vol. 368, No. 1917, Advanced Processing of Biomaterials, 2010, pp. 1999-2032.
3. J. Kadkhodapour, H. Montazerian, A.Ch. Darabi, A.P. Anaraki, S.M. Ahmadi, A.A. Zadpoor, S. Schmauder, "Failure Mechanisms of Additively Manufactured Porous Biomaterials: Effects of Porosity and Type of Unit Cell," Journal of the Mechanical Behavior of Biomedical Materials **50**, 180-191 (2015).
4. R. S. Kshetrimayum, "A Brief Introduction to Metamaterials," IEEE Potentials **23**, 44-46 (2005).
5. T.-L. Cheng, "Compressive Properties of Porous Ti-6Al-4V Manufactured by Selective Laser Melting," Master Thesis, Department of Materials and Mineral Resources Engineering, National Taipei University of Technology, Taipei, Taiwan, 2016.

A Study on Accelerating Convolutional Neural Networks

Hsien-I Lin[a)] and Chung-Sheng Cheng[b)]

Graduate Institute of Automation Technology, National Taipei University of Technology, Taipei ,Taiwan

[a)]Corresponding author: sofin@ntut.edu.tw
[b)]laserlighteye@gmail.com

Abstract. Recent deep-learning methods have been paid more attention than shallow-learning ones because they have deep and complex structures to approximate functions. The salient feature of deep neural networks is to use many layers where many of them are used to extract data features and few are for classification or regression. The most severe problem of a deep neural network is using too many parameters that cause too much memory usage and computing resources for both training and inference. Thus, deep learning approaches are not suitable for real-time industrial applications that have limited computing resources such as memory and CPU. For example, a famous convolutional neural network (CNN), AlexNet, uses up to 60 million parameters to train ImageNet dataset and many imaging projects apply AlexNet to their own applications as transfer learning. Thus, this work proposes a feasible solution to trim the CNN, speed it up, and keep the accuracy rate similar. Two main types of CNNs and AlexNet, were validated, respectively, in THUR15K, Caltech-101, Caltech-256, and GHIM10k datasets. The results show that the parameter amount greatly decreased (76%) but the recognition rate dropped slightly (1.34%).

Introduction and Motivation

Machine learning is a multidisciplinary subject that involves probability theory, statistics, and other theories to improve the traditional way of logical reasoning and allow computers to learn the rules themselves through massive amounts of information. For example, machine learning has been applied to object identification and inspection in many industrial applications. In machine learning algorithms, features are manually designed to capture the characteristics of images. It is necessary to analyze and understand the characteristics of images in order to obtain useful features and when the images in the real environment are different from the trained images, the accuracy of these images inferred by the trained models usually decreases. Thus, the more different types of datasets need to be collected to design features, and it is necessary to test whether the features are valid. If the image features are complex or subtle, it may take more time to do the front-end processing of the data, and the ability to generalize the model underlying finite samples is limited.

Until Hinton *et al*. [1] proposed the concept of deep learning, deep learning can approximate complex functions through massive training data and linear and nonlinear transformations in multiple hidden layers of neural networks. Deep learning is able to automatically capture features that are sufficient to represent the entire data characteristics without complex pre-processing of the data. Taking image recognition as an example, the original image is directly fed into the deep neural network for training, and through the hierarchical calculation of the neural network, the network automatically learns the high-level characteristics of the image and is used for prediction. The results of deep learning methods are obviously better than traditional machine learning ones, and the same deep model can be easily adapted to other problems. It has excellent generalization for similar domain problems because deep learning adopts a complex model and learns data features from a great number of training samples. However, the disadvantage of deep learning is that the large amount parameters cause heavy computing power than the traditional machine learning. Therefore, how to effectively condense the network to speed it up is an important issue. If the network can be faster and keep the same prediction capability, it is feasible for industrial real-time applications. This paper focuses on how to reduce the overall parameter size of the deep convolutional network and accelerate the network model. Meanwhile, it can still keep the accuracy similar to the original network model.

Review of Related Studies

Deep learning is very popular in recent years. One of the prevalent deep-learning methods is convolutional neural network (CNN). It has been applied to many aspects, such as speech recognition [2], pedestrian detection [3], scene segmentation [4], etc. LeNet [5], the earliest convolutional neural network, was proposed to identify handwritten numbers. LeNet used multi-layer convolutions to extract image features distributed throughout the images, used pooling layers to take into account the relevance of adjacent pixels in space, and reduced the dimension of the feature map to reduce the computational complexity and retained the most significant features. Even though LeNet had good recognition results, it was limited by hardware performance at the time and did not receive much attention.

With the hardware improvement, AlexNet [6] was proposed to use the techniques of modified linear unit [7], dropout [8], batch size, and paralleled GPUs to accelerate the convergence speed and reduce the overfitting problem in the ILSVRC (ImageNet Large Scale Visual Recognition Competition) competition. There were 1.2 million images in 1,000 different types of objects. The accuracy of the model far exceeded that of all the participating teams at that time, winning the championship. Thus, the research boom of deep learning started out. Later, many network models such as GoogLeNet [9] and VGG-Net [10] appeared, and the spread of deep learning applications was rapid. For example, [11] used local features such as ear, mouth, and nose as training data to train deep the network for face recognition.

In addition to hardware enhancements, many works have also proposed a series of methods for accelerating CNN models [12, 13, 14, 15, 16]. For example, [13] proposed a multi-layer-perceptron (MLP) with more complex operations at each convolutional layer. In addition to the basic convolution, their work used a 1x1 convolution kernel to perform two more convolutions and global mean pooling to replace the full connection layer because global pooling greatly reduced the network parameters, speed up the network, and avoid overfitting. [14] proposed a mini network model structure to use the least amount of parameters without losing accuracy. Their approach was to replace the 3x3 convolution kernel with a 1x1 convolution kernel so that the parameters were reduced by 9 times. The pooling layer was placed at the last of the network because the higher resolution feature maps could be kept in the network to provide the higher the accuracy. [15] carried out to delete some weight parameters to sparse the network. They believed that the weight approaching zero had less contribution to the network. In the process of trimming the weight value, the weights approaching zero were directly set to zero. At the same time, the weights were grouped and the weights of the same group were shared by one weight to reduce the number of weights to be stored. [16] considered the similarity between the weights among the hidden layers. If the two weights were similar or equal, one of them was eliminated. [17] accelerated the network by not making the network model shallower but narrowing the network model. They removed the filters that were less important to the network by calculating the sum of the absolute values of the filter weights in each layer, and eliminating the filter with the smaller absolute value. Each time after deletion, a re-training process was performed to ensure the performance of the network.

Acceleration on CNN

Table 1 shows the network scale in terms of layer, parameter amount, and accuracy of several popular CNNs using ImageNet dataset in recent years. It is obvious that the convolutional neural network continues to improve recognition accuracy, while its network scale continues to grow. Such a large model cannot be implemented on real-time platforms in industrial applications. Pruning the network is an essential topic to be investigated. In the deep neural network, its complex architecture is used to improve the training error; meanwhile it increases the redundant parameters as well. AlexNet uses Dropout to reduce the amount of parameters during training to speed up the training time and alleviating overfitting. Figure 1 shows the distribution of parameter quantity of AlexNet.

From Fig. 1, it can be found that the total parameter amount of the eight-layer network model is about 58M and more than half of the parameters are concentrated in FC1, that is, where the feature maps are connected to the fully connected layer. In AlexNet, the convolutional layers and the pooling layers mostly appear in the first few layers. Their main purpose is to capture various local features and sub-sample the image. The fully-connected layer often appears in the last few layers. The local features are weighted and combined by weights. The fully connected layer is equivalent to a feature transformation space. The fully connected layer converts the feature map of the previous layer from a multi-dimensional feature to a one-dimensional array and maps to the label for classification. In the convolutional neural network, the parameters in the fully connected layer is determined by the size of the feature map. The size of the feature map can be calculated as follow. If the feature map size is large, the amount of weight generated will be very large, and it is easy to cause over-fitting problems.

TABLE 1. Layer and parameter scale of popular network architectures.

Model	Layers	Parameters (M)	Top-5 error
AlexNet	8	60	16.4%
VGG16	16	138	7.3%
GoogleNet	22	6.8	6.7%
ResNet	152	60	3.57%

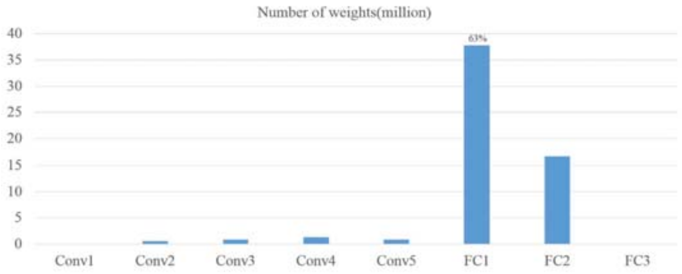

FIGURE 1. Distribution of parameter quantity of AlexNet.

$$\text{Feature}_{size} = ((N - F + 2 * padding)/stride + 1). \quad (1)$$

Thus, the proposed method is to reduce the dimension of the feature map by adding the pooling operation, reducing the input number to the fully connected layer. The method is to reduce the feature map into a one-dimensional array by using the maximum and average pooling operations. To implement it, firstly, the feature maps to be the input to the full-connection layer are divided into four areas: upper left, lower left, upper right, and lower right. The most significant features of the four regions of the feature map are retained by the maximum pooling operation, and then the average pooling operation is used to combine with the features of each region. The feature map is then converted into a 1x1 size, and fed to the fully connected layer for training.

To be clear, it is assumed that the last feature map to the fully connected layer is the size of NxN. In order to divide the feature map into a feature map of 2x2 size, it is required to design the corresponding KxK size mask and stride to do the maximum pooling operation. The KxK mask captures the most prominent features of the four regions, so the KxK mask changes according to the original image size, which is a quarter of the original image. If the stride is set to 1, the salient feature is just in the middle region and after the maximum pooling operation is performed, it is easy to repeatedly obtain the intermediate features. If a larger stride is set, the problem of not being able to design a mask is caused for a smaller feature map. In order not to repeat the same feature, the size of the stride will vary according to the size of the feature map, and is set to a size of N/2.

In order to convert a 2x2 feature map into a one-dimensional array, it is necessary to design an M-size mask to do the average pooling operation and combine the features in the four regions to form a 1x1 size feature map, where the stride is set to 1 and does not do any filling operation. The formula for calculating the size of the feature map can be rewritten from Eq.(1) to Equation (2) and we can find M=2. Thus, after the feature map is processed by the maximum pooling by the mask of size 2x2, the feature map becomes the 1x1. Figure 2 shows the concept, and the weighted sum is made at the connection of the fully connected layers. That is to use the pooling operation as dimension reduction while retaining the most significant features in the final feature map.

$$\text{Feature}_{1x1} = ((2 - M) + 1). \quad (2)$$

Figure 3 shows that AlexNet originally needs to connect a 6x6 size feature map to the fully connected layer, which produces 6x6x256x4,096=37,748,736 (about 37M) parameters. Figure 4 shows our proposed method that passes the 6x6 size feature map to the 4x4 size mask, performs the maximum pooling operation to become a 2x2 size feature

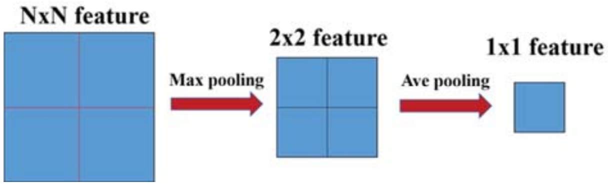

FIGURE 2. Concept of the proposed method on the feature map.

map, and then use a 2x2 mask to perform an average pooling operation to become a 1x1x256 one-dimensional array. The operation preserves the most significant features of each region of the feature map, and then uses the average pooling operation to combine the features of each region. That is, it is hoped that this 1x1 feature map can replace the original 6x6 feature map. Thus, the parameter amount between the feature map and the fully connected layer is reduced from the original parameter amount of about 37M to 1x1x256x4,096=1,048,576 (about 1M) parameter amount, which is 2.7% of the original parameter.

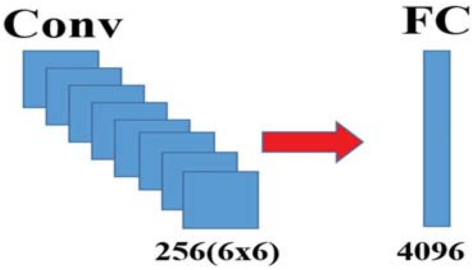

FIGURE 3. AlexNet: 6x6 size feature map to the fully connected layer.

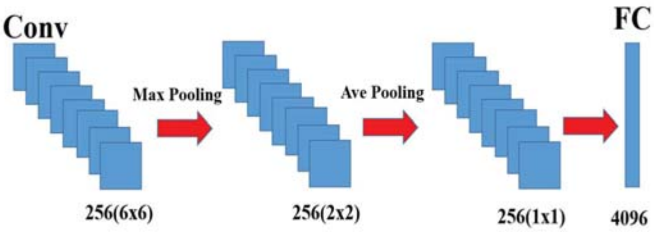

FIGURE 4. Modified AlexNet: 6x6 size feature map to the fully connected layer.

Results

To validate the proposed method, it is mainly focused to reduce the parameter amount of a convolutional neural network without significantly decreasing the recognition accuracy. Three experiments were performed. (1) Using the LeNet and experimenting with its original database. (2) Using the modified AlexNet network to test other datasets based on the proposed method.

Experiment 1 used LeNet and the original dataset MINST. MINST was a dataset containing 0 9 handwritten numbers. It had 60,000 training images and 10,000 test images. The purpose of this experiment was to test the modified network architecture on the original dataset. Figure 5 compares the recognition rate between the modified and original networks. and Figure 4.6 shows the comparison of the overall parameter amounts. The experimental results show that

although the modified LeNet had the recognition rate reduced by 0.43%, it reduced the overall parameter size by about 77%.

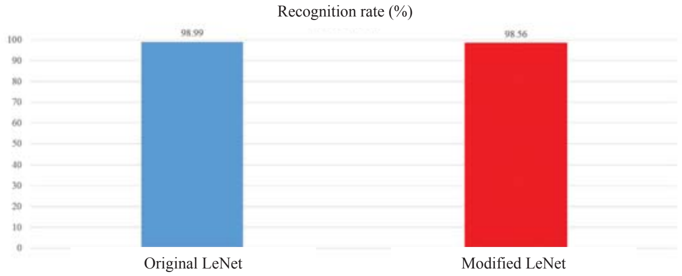

FIGURE 5. Comparison on the recognition rate between original and modified LetNets.

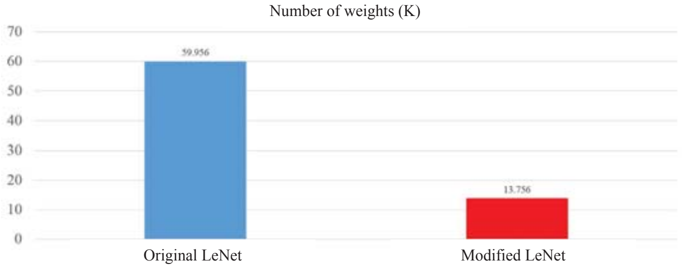

FIGURE 6. Comparison on the parameter amount between original and modified LetNets.

In the second experiment, AlexNet was used as for training, and four datasets were used for training and prediction, namely THUR15K [18], Caltech-101 [19], Caltech-256 [20], and GHIM10k [21]. 10% of the data in each dataset was used as verification data, 5% was used as test data, and the training results after adding our method were compared. Taking THUR15K as an example, the database was divided into five categories, and the amount of data for each category is shown in Table 2. In a total of 15,531 images, 13,201 were used as training materials, 1,553 were used as validation data and 777 were used as test data. The data distributions are shown in Figs. 7, 8, and 9.

TABLE 2. Categories of THUR15K.

Category	Images
Butterfly	3,457
Coffee Mug	3,281
Dog Jump	2,892
Giraffe	2,932
Plane	2,969

Figures 10 and 11 show the training results after using original and modified AlexNets on THUR15K, Caltech-101, Caltech-256, and GHIM10k datasets. The overall parameter amount was about 63% less by our method. Figure 4.14 shows the result using the computer with the i7 CPU, 8GB of memory, and no GPU. The average execution time of the image by the proposed method was greatly reduced. For the recognition rate, the modified AlexNet outperformed to the original AlexNet in all the datasets except Caltech-101.

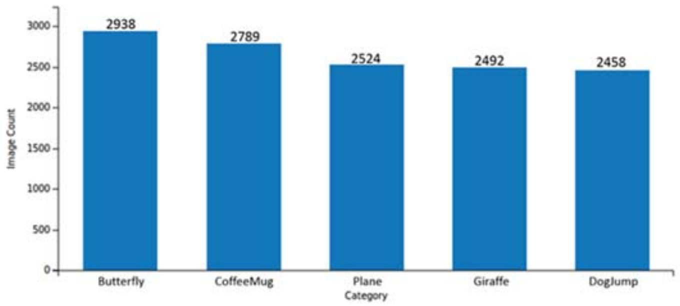

FIGURE 7. Distribution of training set of THUR15K.

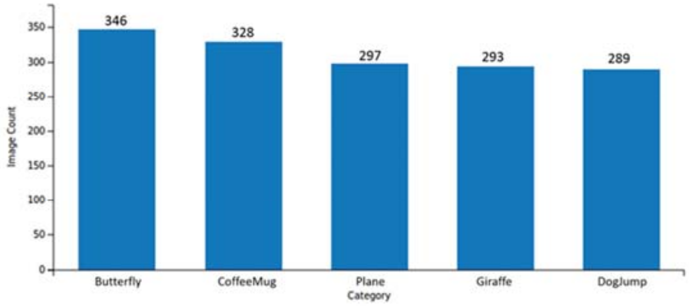

FIGURE 8. Distribution of validation set of THUR15K.

Conclusions

This paper proposes a method that can significantly reduce the parameters of deep learning convolutional neural networks. This study found that in deep convolutional neural networks, the parameters are mostly concentrated in the connection of the fully connected layer, and the size of the feature map with the fully connected layer is the bottleneck determining the number of parameters. The proposed method makes the size of the last feature map reduced by the pooling operation and retains the most significant features of each region of the feature map. This study did the feasibility of two experimental tests. Experiment 1 used LeNet and its original dataset MINST to validate the proposed method. The experimental results show that using the method of this study, the recognition rate was reduced by 0.43%, but it reduced the overall parameter by about 77%. Experiment 2 used AlexNet on different datasets such as THUR15K, Caltech-101, Caltech-256, and GHIM10k. The experimental results show that the recognition rate of the model using the Caltech-101 database was reduced, the recognition rate of other models was improved, and the overall parameter amount was reduced by about 63%.

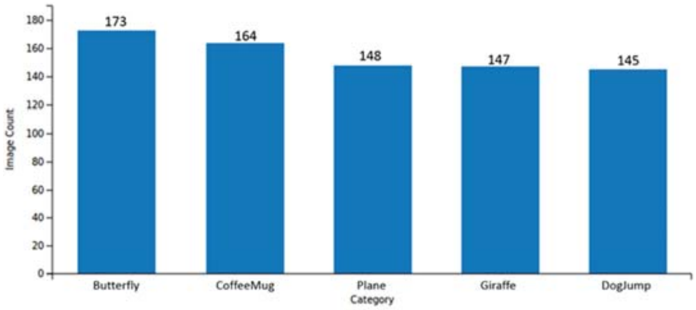

FIGURE 9. Distribution of test set of THUR15K.

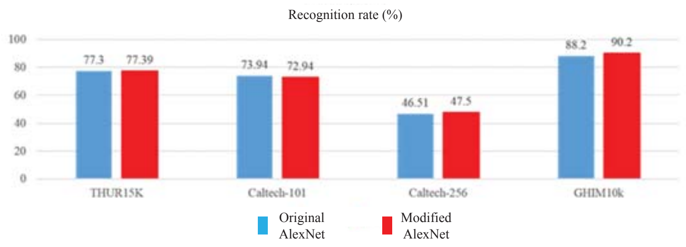

FIGURE 10. Comparison on the recognition rate between original and modified AlexNets.

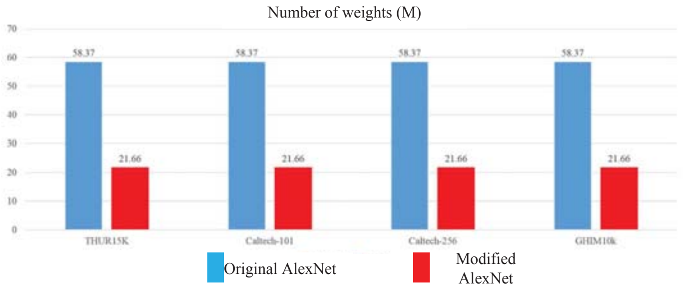

FIGURE 11. Comparison on the weight amount between original and modified AlexNets.

REFERENCES

[1] S. O. G. E. Hinton and Y.-W. Teh, Neural computation **18**, 1527–1554 (2006).

[2] J. Huang and B. Kingsbury, "Audio-visual deep learning for noise robust speech recognition," in *Acoustics, Speech and Signal Processing (ICASSP)* (IEEE, 2013), pp. 7596–7599.

[3] W. Ouyang and X. Wang, "Joint deep learning for pedestrian detection," in *Proceedings of the IEEE International Conference on Computer Vision* (IEEE, 2013), pp. 2056–2063.

[4] C. Farabet, C. Couprie, L. Najman, and Y. LeCun, IEEE transactions on pattern analysis and machine intelligence **35**, 1915–1929 (2013).

[5] Y. LeCun, L. Bottou, Y. Bengio, and P. Haffner, "Gradient-based learning applied to document recognition," in *Proceedings of the IEEE* (IEEE, 1998) p. 2278–2324.

[6] A. Krizhevsky, I. Sutskever, and G. E. Hinton, Advances in neural information processing systems 1097–1105 (2012).

[7] X. Glorot, A. Bordes, and Y. Bengio, "Deep sparse rectifier neural networks," in *Proceedings of the Fourteenth International Conference on Artificial Intelligence and Statistics* (2011) p. 315–323.

[8] G. E. Hinton, N. Srivastava, A. Krizhevsky, I. Sutskever, and R. R. Salakhutdinov, arXiv preprint arXiv:1207.0580 (2012).

[9] C. Szegedy, W. Liu, Y. Jia, P. Sermanet, S. Reed, D. Anguelov, D. Erhan, V. Vanhoucke, and A. Rabinovich, "Going deeper with convolutions," in *Proceedings of the IEEE conference on computer vision and pattern recognition* (IEEE, 2015), pp. 1–9.

[10] K. Simonyan and A. Zisserman, arXiv preprint arXiv:1409.1556 (2014).

[11] S. Srisuk and S. Ongkittikul, "Robust face recognition based on weighted deepface," in *International Electrical Engineering Congress (iEECON)* (IEEE, 2017), pp. 1–4.

[12] Y. Cheng, D. Wang, P. Zhou, and T. Zhang, arXiv preprint arXiv:1710.09282 (2017).

[13] M. Lin, Q. Chen, and S. Yan, arXiv preprint arXiv:1312.4400 (2013).

[14] F. N. Iandola, S. Han, M. W. Moskewicz, K. Ashraf, W. J. Dally, and K. Keutzer, arXiv preprint arXiv:1602.07360 (2016).

[15] S. Han, H. Mao, and W. J. Dally, arXiv preprint arXiv:1510.00149 (2015).

[16] S. Srinivas and R. V. Babu, arXiv preprint arXiv:1507.06149 (2015).

[17] H. Li, A. Kadav, I. Durdanovic, H. Samet, and H. P. Graf, arXiv preprint arXiv:1608.08710 (2016).

[18] M.-M. Cheng, N. J. Mitra, X. Huang, and S.-M. Hu, The Visual Computer **30**, 443–453 (2014).
[19] F.-F. Li, R. Fergus, and P. Perona, Computer vision and Image understanding **106**, 59–70 (2007).
[20] G. Griffin, A. Holub, and P. Perona, (2007).
[21] G.-H. Liu, J.-Y. Yang, and Z. Li, pattern recognition **48**, 2554–2566 (2015).
[22] H. Schulz and S. Behnke, "Learning object-class segmentation with convolutional neural networks." in *ESANN* (2012).
[23] A. Krizhevsky, I. Sutskever, and G. E. Hinton, "Imagenet classification with deep convolutional neural networks," in *Advances in neural information processing systems* (2012), pp. 1097–1105.
[24] S. Ioffe and C. Szegedy, arXiv preprint arXiv:1502.03167 (2015).

Preface of the Symposium " Traffic Infrastructure and Modelling" (TIAM-19)

Tiziana Campisi[1,a] , Dario Ticali[1,b], Aleksandra Deluka-Tibljaš[2,c] and Sanja Šurdonja[2,d]

[1]*University of Enna Kore - Enna, Italy*
[2]*University of Rijeka –Rijeka,Croatia*
[a]tiziana.campisi@unikore.it
[b]dario.ticali@unikore.it
[c]aleksandra.deluka@gradri.uniri.hr
[d]sanja.surdonja@gradri.uniri.hr

The session "TRAFFIC INFRASTRUCTURE AND MODELLING"(TIAM-19) was born recently and it focuses on new results related to engineering research, on rigorous mathematical and stochastic systems applied to transport systems and infrastructures using innovative models, methods and approaches. Recently, both advanced ITS applications and new approaches based on powerful stochastic analyses and computational methods have proved particularly effective in the treatment of transport engineering and road design to mention some possible scenarios of interest. Technological approaches to the development of the most relevant research in the sectors of road network and infrastructures design, numerical modelling, infrastructure production / management, engineering technological applications and materials.
The aim of the Session is to collect the most relevant researches dealing with innovative approaches in order to resolve typical engineering problems in the field of infrastructure and transport system.
The conference has also emphasized the integration between miscellaneous themes and ICT opportunities, which offer design, solutions and innovative models for the challenging problems of several fields, where the technologies are very useful to resolve different problems for motorised [1] and un-motorised road users[2]
This approach linked to the global vision of the user's needs and the improvement of infrastructures and services is becoming increasingly important and includes different aspects, from the modernization of public transport [3], to the improvement of transport infrastructures to solutions technological to map the quality and access in the public or confined space[4], especially in complex quality issues of life and satisfaction with the neighbourhood and the community [5][6] and possibilities for participation in the urban environment that affect the quality of life [7]
The contributions are focused on the need for close collaboration between scientists operating in different branches.

The paper entitled **" Use of AHP Method In The Traffic Planning - Example Of Selecting An Optimal Intersection Type** " deals with the topic of multi-criteria analysis and the possibility of its application in the process of planning, design, maintenance or reconstruction of transport infrastructure [8].
The AHP method, one of the most commonly used multi-criteria method [9], was used as a tool for selecting the optimal between 3 alternative solutions for intersection reconstruction, based on 5 criteria and 12 sub-criteria. In addition, paper showed a significant role of AHP method in sensitivity analysis which shows how the change in criteria importance affects the outcome, that is, the ranking of individual alternative.

The paper entitled **"The Influence Of Porous Asphalt Mix Design On Reveling Resistance"** deals with the possibilities for improvement of porous asphalt durability by using different type of aggregate, bitumen and additives. Porous asphalt despite many environmental benefits, can suffer from problems which can affect its performanse and service life [10]. Rapid agening of binder results in loss of adhesion and particle loss [11] which can be improved with usage of different type of aggregate, binder and aditives. Results of laboratory testing shows that asphalt mixtures with less discontinued grading envelopes have better particle loss resistance. In addition, paper show a significant dependance of type of bitumen and particle loss resistance

The paper entitled " **The Management Of Pedestrian Emergency Through Dynamic Assignment: Some Consideration About The "Refugee Hellenism" Square Of Kalamaria (Greece)**", is linked to pedestrian safety that is constantly pursued by urban areas that want to develop in accordance with sustainability and transport.

Terrorist phenomena or catastrophes lead to a preventive assessment of a possible approach in order to mitigate its effects [12]-

Daily situations such as maintenance infrastructures need analysis on variations in service levels in order to minimize disruption. This work focuses on one of the largest pedestrian areas in the city of Kalamaria (Greece) and through the definition of different scenarios, highlights how a square adjacent to the pedestrian artery may be useful for waiting or escape areas in case of evacuation. The work is a first step of evaluation which consists in the definition of incremental scenarios justified by the increase of the pedestrian flow during some periods of the year and is closely connected to the construction of a nearby metro station that will easily facilitate to increase the demand for pedestrian transport and therefore for transit and access in that area

The paper entitled "**The Evolution Of The Maas As A Mobility Solution Based On The Individual Needs Of Users "** shows an overview of the development of Maas-type mobility services by highlighting the fundamental parameters to be observed and affecting users in order to be able to create a service that satisfies the user's needs in an exhaustive manner[13] Even technological development allows a greater diffusion of the Maas. This research also highlights that there are still small cities where the development of the demand-based mobility system could reduce the criticalities encountered by users in moving or making multimodal choices.

The paper entitled "**The Surrogate Safety Measures Evaluation Of A Staggered Crossing On The Delta Area Of Rijeka**" focuses on pedestrian safety assessment in a traffic light intersection considering the state of affairs and two hypotheses of change to the geometry of the crossing itself. Pedestrian safety is of fundamental importance to maintain high Levels of Service (LOS) and several studies in the literature [14] highlight the possibility of using dedicated tools for evaluating surrogate security parameters that can provide a global overview of the infrastructure and users. A comparison of the current geometry has been approached by comparing the real case with two design hypotheses which, using current trafficked and pedestrian figures, respectively foresee the road intersection at grade with a long pedestrian ,implementing a pedestrian island and a staggered one that allow users to cross without being hit by vehicles.

The paper entitled "**The Evolution Of The Advance Space Line (ASL) Systems To Increase The Safety Of Cyclists In Traffic Light Junctions"** examines the diffusion of certain techniques for regulating traffic and relocation of areas reserved for cyclists in order to reduce their exposure to vehicle emissions and make turning and crossing maneuvers easier, reducing potential conflicts between weak users and vehicles.

The development of technologies applied to smart cities will reduce some critical issues affecting cyclists [15]

Through the SWOT assessment, the critical issues and the benefits of the construction of these portions of road infrastructure were highlighted, with reference to some European case studies.[16]

The paper entitled "**The Role Of Urban And Social Factors In The Accessibility Of Urban Areas For People With Motor And Visual Disabilities**" focuses on the concept of accessibility of urban spaces .This research starts from the definition and administration of a questionnaire to a sample of the population affected by disability. The results are fundamental for the calibration of some accessibility indicators and therefore allow to provide a more realistic value. The survey shows that the negative experience for people with disabilities in traffic spaces is extremely frequent. Furthermore, through the cataloging of problems relating to each type of urban space, it has been noticed how they largely affect the movement in public space and therefore can be used as a real guide for interventions in public spaces.

The paper entitled "**Value Of Travel Time: An Economic Assessment For Transport Appraisal Decision-Makers**" focuses on the economic *value of travel time* (VTT) as one of the most important factors for the displacement between two junctions of a transport network. This paper discusses on the guidelines and software tools adopted for the economic evaluation of transport interventions in UK and Italy, highlighting particularly, the values and methods for estimating the *value of time (VOT)* in both countries. We propose a strong integration of the two models taking into account the numerous parameters examined in UK and at the same time the method's easy applicability for countries with different development conditions and needs.

The paper entitled **"Evaluation Of Infrastrctures: Application Of TOD To Catania Underground Metro Station** " focuses on Catania metropolitan area which is characterized by a highly urbanized settlement with high percentage of urban sprawl. Lately these conditions are changing as a consequence of the development of the

underground metro network that connects the main city's service centers like the hospitals, the university (and soon also the Airport) to the city center. To achieve sustainable transportation and resolve the aforementioned problems, we have applied TOD criteria to some of the main city's transport junctions (selected using the Multi Criteria Decision Aid methodology) in order to fulfills the principle of sustainable transportation.

The paper entitled "**Validation Of Infrastructures Through BIM** " investigates on the one of the most interesting Building Information Modelling (BIM) [17]applications that can be developed in urban and infrastructural design (*Infra-BIM)*, where the processes and the controls implemented by BIM can be managed effectively and at a higher efficiency level. The paper focuses on the phase of *BIM Validation* viewed as a support for a proper work-flow: it not only allows to analyse the whole set of information associated with a parametric object but also how the entire model matches the specific design requirements [18]BIM Validation process in design is not defined yet, but it is important to aim at a correct procedure so as to guarantee quality of design and future management of the project.

References

1. Tollazzi, T., Renčelj, M., Rodošek, V., & Zalar, B. (2010). Traffic safety of older drivers in various types of road intersections. Promet-Traffic & Transportation, 22(3), 193-201.
2. Deluka-Tibljaš, A., Lucic, S., & Benigar, M. (2003). Soluzione non motorizzata accettabile per il traffico urbano. Contemporary Traffic , 23 (5), 333-337.
3. Thynell, M., Mohan, D., & Tiwari, G. (2010). Sustainable transport and the modernisation of urban transport in Delhi and Stockholm. Cities, 27(6), 421-429.
4. Campisi, T., Canale, A., Tesoriere, G., Lovric, I., & Čutura, B. (2019). The Importance of Assessing the Level of Service in Confined Infrastructures: Some Considerations of the Old Ottoman Pedestrian Bridge of Mostar. Applied Sciences, 9(8), 1630.
5. Mrak, I., Nuždić, S., Franković, M., & Matan, C. (2018, November). Preliminary research: Inclusiveness of cultural heritage-a model of evaluation. In Cultural Heritage for All Unlocking Europe's potential through Design for All.
6. Campisi T.,Canale A. &Tesoriere G., "The development of walkability in the historic centre of Enna: the case of the Sant Tommaso neighbourhood" (European Transport \ Trasporti Europei n. 73, ISSN 1825-3997, 2019
7. Keles R. , "The Quality of Life and the Environment" (Procedia - Social and Behavioral Sciences, ISSN: 1877-0428, Vol: 35, 2012, Page: 23-32)
8. Karleuša, B., Dragičević, N., & Deluka-Tibljaš, A. (2013). Review of multicriteria-analysis methods application in decision making about transport infrastructure. doi: https://doi.org/10.14256/JCE.850.2013
9. Barić, D., Pilko, H., & Strujić, J. (2016). An analytic hierarchy process model to evaluate road section design. Transport, 31(3), 312-321.
10. L.D. Poulikakos, S. Takahashi and M.N. Partl, "A comparison of Swiss and Japanese Porous Asphalt Through various Mechanical Test" in Proceedings of 4th Swiss Transportation Research Conference STRC 2004, p. 12
11. M.R. Hainin, L.A.Cooley Jr and B.D. Prowell, "An investigation factors influencing permeability of Superpave mixes" (International Journal of Pavements, Vol 2, University of Mississippi, 2003)
12. Cova, T. J., & Johnson, J. P. (2002). Microsimulation of neighborhood evacuations in the urban–wildland interface. Environment and Planning A, 34(12), 2211-2229.
13. Sochor, J., Karlsson, I. M., & Strömberg, H. (2016). Trying out mobility as a service: Experiences from a field trial and implications for understanding demand. Transportation Research Record, 2542(1), 57-64.
14. Gettman, D., & Head, L. (2003). Surrogate safety measures from traffic simulation models. Transportation Research Record, 1840(1), 104-115.
15. Stamatiadis, N., Pappalardo, G., & Cafiso, S. (2017, June). Use of technology to improve bicycle mobility in smart cities. In 2017 5th IEEE International Conference on Models and Technologies for Intelligent Transportation Systems (MT-ITS) (pp. 86-91). IEEE.]
16. Campisi, T., Canale, A., & Tesoriere, G. (2017, November). Study of emergency setting for urban facility using microsimulation tool. In AIP Conference Proceedings (Vol. 1906, No. 1, p. 190004). AIP Publishing
17. Acampa, G., Forte F.& De Paola P.. "BIM Models and Evaluations." Values and Functions for Future Cities. Springer, Cham, 2020. 351-363.]
18. Acampa, G.,Crespo Cabillo I.,& Marino G.. "Representación del dibujo frente a simulación de los sistemas BIM. Oportunidad o amenaza para la arquitectura. 2019"].

Tiziana Campisi

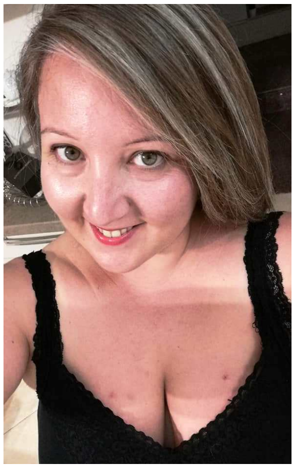

Kore University of Enna, Italy – tiziana.campisi@unikore.it

Tiziana Campisi,PhD is Assistant Professor at the Faculty of Engineering and Architecture, Kore University of Enna, Italy. She received her Bachelor's Degree in Civil and Environmental Engineering from the University of Catania, Italy; and her degree (cum Laude) in Safety and Civil Protection Engineering and doctorate at the Kore University of Enna, Italy. She has obtained the master (II level) in "Road Quality Management" and also a master in "Virtual Reality Design" (I level) She has published more than 20 articles in journals and conferences. She serves as a member of different Editorial Board (such as Proceedings — Journal MDPI; Electronic Journal of the Faculty of Civil Engineering Osijek e-gfos;etc..) and she is a reviewer for several international journal and conferences. Her research interests include transport supply/demand, road safety, road vulnerable users, road traffic microsimulation.

Aleksandra Deluka-Tibljaš

University of Rijeka ,Croatia -aleksandra.deluka@gradri.uniri.hr

Aleksandra Deluka Tibljaš, PhD is Full Professor at the University of Rijeka, Faculty of Civil Engineering, Croatia. She is head of Department for transportation engineering at the Faculty of Civil Engineering. Her main research interests are in the field of transportation engineering and urban traffic infrastructure and she teaches different courses regarding road and intersection design, urban transport and traffic safety at all levels of studies. She is also involved in laboratory and field research of macrotexture of asphalt pavements.

During her research activities she published 25 papers in different journals and more than 30 conference papers. She is member of editorial board of two journals indexed in Web of Science (Engineering Review, Građevinar) and she took part in many editorial boards of international conferences in Croatia and abroad.

Presently she leads research group at the University project “Traffic infrastructure in the function of sustainable urban mobility”

Sanja Surdonja

University of Rijeka ,Croatia -sanja.surdonja@gradri.uniri.hr

Sanja Šurdonja, PhD, is an Assistant Professor at Faculty of Civil Engineering at the University of Rijeka. She received her PhD in 2017 at the Faculty of Civil Engineering, University of Zagreb. Her main research interests are in the field of transportation engineering and urban traffic infrastructure. Currently she participates in teaching courses about road and intersection design, urban transport and traffic safety and railways at all levels of studies. She is also involved in different researches done in Transportation laboratory at Faculty. She published 29 papers in different journals and conferences. She is also a reviewer for several journals.

Dario Ticali

Kore University of Enna, Italy - dario.ticali@unikore.it

Dario Ticali , PhD is Associate Professor at the Faculty of Engineering and Architecture, Kore University of Enna, Italy.

He obtained his degree in Civil Transportation Engineering (5 years degree course cycle) in 2001 at the University of Palermo with a final thesis dealt on “Airport Acoustic Pollution”. A Master in Project Management and Public Policies, 2001 – 2002, University of Palermo (Italy). Since 2002 has taught several lessons in Master and Courses post lauream (Airport Infrastructure, Road Infrastructure Design, Transport Engineering, Road Materials). He obtained Ph.Doctorate on the subject of Road, Railway and Airport Infrastructure, at the Doctorate School of Palermo.

He was a consultant for the Architecture Faculty at University of Palermo for project on “Public Transport Analysis at Sicilian Region – a new planning and regulation” and for the “REMOMED project (rèseau europèen intermodal pour un dèvelopment intègrè des espaces de la mèditerranèe occidentale – Interreg III b mediterranèe occidentale) for the Architecture Faculty at University of Palermo. During his research activities he published more than 20 papers in different journals and more than 30 conference papers.

His research interests include transport supply/demand, road safety, road design, transport environmental assessment.

Use of AHP Method in the Traffic Planning - Example of Selecting an Optimal Intersection Type

Sanja Šurdonja[a)] Ivan Kišić[b)] Aleksandra Deluka-Tibljaš[c)] Barbara Karleuša[d)]

University of Rijeka, Faculty of Civil Engineering, Radmile Matejčić 3, Rijeka, Croatia .

[a)] Corresponding author: sanja.surdonja@uniri.hr

[b)] ivan.kisic@student.uniri.hr

[c)] aleksandra.deluka@uniri.hr

[d)] barbara.karleusa@uniri.hr

Abstract. Reconstruction of the intersection on the traffic network is necessary to maintain the required level of traffic safety for all road users, intersection capacity, and the functioning of the intersection in the changed conditions which occur due to, for example, increasing or redistributing traffic or connecting new roads on the network. Before reconstruction, it is necessary to analyze the existing situation, identify deficiencies or potential problems and propose several alternative solutions. Different alternative solutions are usually compared by using predefined criteria and sub-criteria. In some cases, due to a greater number of criteria and sub-criteria, the process of selecting the optimal solution (alternative) can be very complex. In the selection process of the optimal alternative, the application of the multi-criteria analysis method has a significant role. This paper presents the application of AHP (Analytic Hierarchy Process) method in the case of reconstruction of sub-urban intersection, the connection to the motorway. The AHP method is one of the most commonly used multi-criteria method in choosing solutions in the planning, design, maintenance and reconstruction of transport infrastructure. The AHP method, in this case, was used as a tool for selecting the optimal between 3 alternative solutions based on 5 criteria and 12 sub-criteria. In addition, to choosing the optimal solution, the AHP method plays a significant role in sensitivity analysis which shows how the change in criteria importance affects the outcome, that is, the ranking of individual alternative.

INTRODUCTION

The complexity of traffic planning and design imposes the need of finding new methods and tools for decision making process to make the process as objective as possible. Traditionally used cost-benefit method, based on estimation of costs and potential benefits (all expressed in money values) is no longer enough and in last decades methods that enable combination of different types of criteria – multicriteria analyses methods (MCA) – are used for selection of optimal solution for different types of traffic and transport problems.

Multicriteria analyses methods allow for taking into account subjective decisions maker's and interveners' preferences and transforming them into objective quantitative measures (Zak and Kruszynski, 2015).

The application of MCA methodology includes the following algorithm (Hajkowicz, 2007.)

1. elaboration of more alternative solutions,
2. definition of criteria,
3. evaluation of solutions with regard to criteria,
4. definition of the weight (importance) of each criterion,
5. ranking or sorting of solutions,
6. performation of the sensitivity analysis,
7. final decision.

Overview of the use of MCA in decision making about transport infrastructure (Deluka-Tibljaš et al., 2013.) showed that the MCA has been dominantly used in the phase of transport infrastructure planning and significantly less

in the process of design, or maintenance and reconstruction, of transport infrastructure. The usual criteria applied on a strategic selection of a traffic facility are: traffic criteria, economic criteria, environmental criteria and social criteria. The newest research considers also, as separate criteria those connected with traffic safety (Barić et al., 2016; Fancello et al., 2019) as enhancement of traffic safety is one of the most emphasized problems regarding traffic infrastructure.

Analyses also showed that mostly the used MCA method in making decision about transport infrastructure in urban areas is Analytic Hierarchy Process (AHP) (Deluka-Tibljaš et al., 2013; Barić et al., 2016). The application of AHP is specially stressed if it is applied on different levels of strategic or tactical traffic planning where there are no precisely quantified data (which is, as a rule, the case in operational planning) (Deluka-Tibljaš et al., 2011) Unlike the usual multi-criteria assessment of every alternative regarding each criterion separately, the possibility of pair-wise comparison of alternatives in relation to a specific criterion, which is enabled by the AHP method, significantly simplifies the procedure.

In this paper the application of MCA methodology, precisely AHP method, for the selection of optimal sub-urban intersection type is presented. There are available examples of researches and case studies for the application of MCA in different kind of problems regarding road intersections: selection of optimal type (Stanić et al., 2011) or optimisation of geometric elements (Pilko et al., 2017; Mehmood et al., 2006).

The AHP method, in this case, was used as a tool for selecting the optimal solution among 3 alternative solutions (signalised intersection and two alternatives of roundabout solutions). Five main criteria were defined: safety, traffic-technology, economic, environmental and spatial – urbanistic criteria. Main criteria were than divided in 12 sub-criteria which were used to make pair-wise comparison among three proposed solutions.

Alternatives were than compared according to two scenarios: Scenario A in which the safety criteria was most important and Scenario B in which safety and economic criteria were equally important in relation to other criteria. Ranking of the alternatives resulted different.

AHP METHOD

Numerous methods of multi-criteria analysis, are being applied in certain aspects of traffic planning. Analytic Hierarchy process (AHP) is a priority method applicable to problems that can be represented by a hierarchical structure (Saaty,1994; Saaty 1996) where the hierarchy consists of the goal at the highest level, one level lower are criteria and even lower sub-criteria, while the lowest level is represented by alternatives.

TABLE 1. AHP pair-wise comparison scale (Saaty, 1996)

Intensity of weight, importance, preference	Definition
1	Equal importance (no preference)
3	Moderate importance (moderate preference)
5	Strong importance (strong preference)
7	Very strong importance (very strong preference)
9	Extreme importance (extreme preference)
2, 4, 6, 8	Intermediate values

AHP method is based on estimating relative priorities (weights / importance) of criteria and alternatives on which pair-wise comparison criteria matrix and pair-wise comparison alternatives matrices (one matrix for each criterion) are generated. The matrices are normalized in order to calculate the priority weightings for criteria and for alternatives on the basis of each criterion. Combining the criteria priorities and the priorities of each alternative relative to each criterion enables the development of an overall priority ranking of the alternatives. Pairwise comparison of criteria and of alternatives is done using the scale presented in Table 1.

CASE STUDY – INTERSECTION ROGOVIĆI

Intersection Rogovići was used as a case-study to examine the possibility of applying AHP method in intersection design. This intersection is a part of a diamond-type interchange situated at the crossroads of the A8 highway and D48 State Road and County Road 5190 in the Region of Istria, Croatia. For the purpose of this paper only at grade intersection (approaches 1, 2, 2a, 3, 4 and 4a) was analysed (Fig. 1).

FIGURE 1. The existing situation of interchange Rogovići

Capacity analysis of the existing intersection showed a very good level of service as well as a capacity reserve for all approaches. Analysis of transit speed data (V85) was also done for all approaches. On the minor directions (ramps 2, 2a, 4 and 4a, which represent the entrances and exits of the highway A8), V_{85} speed is not problematic due to the necessary stop at the toll stations. Unlike the minor directions, the speed data analyses on the main directions (approaches 1 and 3) showed significant exceeding (65% - 91%) the speed limit of 50 km/h. The analysis of visibility on minor directions showed also unsatisfactory results.

Due to all of the above, 3 alternatives for intersection reconstruction have been proposed (Fig.2):

- Alternative 1 (A1): installation of traffic lights at the existing intersection
- Alternative 2 (A2): two roundabouts
- Alternative 3 (A3): one big roundabout.

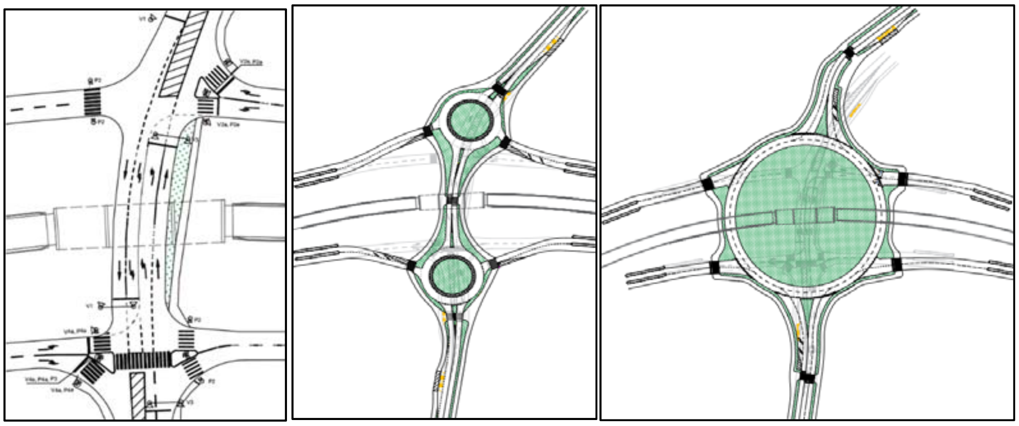

(a) (b) (c)

FIGURE 2. Possible alternatives: a) installation of traffic lights; b) two-roundabouts; c) one big roundabout

The first alternative was chosen assuming the most economic and fastest reconstruction while alternatives 2 and 3 were selected because various studies have shown that roundabouts are a good measure of traffic calming at highway entry/exit locations. Although many new alternative types of roundabouts are introduced in recent years (Tollazzi et al., 2016.) as a better solution then two-lane roundabout, in this paper conventional two-lane roundabout was considered as the alternative 3 since estimation of future traffic load and also a small number of accidents at this location do not require/justify application of alternative types of roundabouts whose construction costs are often higher than conventional roundabouts (Tollazzi et al., 2015).

CRITERIA AND SENSITIVITY ANALYSIS

The criteria applied on selection of optimal alternative for intersection reconstruction are:

- safety (S);
- traffic-technology (TT),
- economic (E),
- environmental (EN)
- spatial – urbanistic (SU) criteria.

Within the safety criterion the following sub-criteria were considered: conflict points (S1), potential traffic accidents (S2), the safety of non-motorized participants (S3) and visibility (S4). The traffic-technology criterion implied checking the capacity of each alternative. The economic criterion determined the profitability of a specific alternative, and within this criterion the costs of reconstruction (E1), land purchase (L2), maintenance (L3) and the complexity of reconstruction (L4) were considered. Environmental criterion has been taken into account in this analysis through the sub-criteria emission (EN1) and noise (EN2). The spatial-urbanistic criterion was considered through 2 sub-criteria, environmental disturbance (SU1) and space occupation (SU2). All sub-criteria within a given criterion were assumed with a specific importance.

Based on all above defined criteria a pair-wise comparison of 3 alternatives was conducted. The values in Table 2 are preferences of alternatives written in lines in relation to the alternatives written in columns with respect to a specific criterion. The preference value written without brackets defines the alternative in that line to be better than the alternative in that column with respect to the criterion. If the alternative preference is written in brackets, then the alternative in that line is worse than the alternative in the column.

TABLE 2. AHP Pair-wise comparison of alternatives in relation to each criterion

SAFETY (S)				**TRAFFIC-TECHNOLOGY (TT)**				**ECONOMIC (E)**				**ENVIRONMENTAL (EN)**				**SPATIAL – URBANISTIC (SU)**			
S1	A1	A2	A3	**TT**	A1	A2	A3	**E1**	A1	A2	A3	**EN1**	A1	A2	A3	**SU1**	A1	A2	A3
A1		1	6	A1		(5)	(3)	A1		4	9	A1		(4)	(8)	A1		4	9
A2			6	A2			2	A2			3	A2			(2)	A2			3
A3		Inc.	0,00	A3		Inc.	0,00	A3		In.	0,01	A3		Inc.	0,00	A3		Inc	0,01
S2	A1	A2	A3					**E2**	A1	A2	A3	**EN2**	A1	A2	A3	**SU2**	A1	A2	A3
A1		(5)	2					A1		4	9	A1		(4)	(7)	A1		(4)	(2)
A2			5					A2			3	A2			(2)	A2			2
A3		Inc.	0,05					A3		Inc.	0,00	A3		Inc.	0,00	A3		Inc.	0,00
S3	A1	A2	A3					**E3**	A1	A2	A3								
A1		5	7					A1		(7)	(4)								
A2			1					A2			2								
A3		Inc.	0,01					A3		Inc.	0,00								
S4	A1	A2	A3					**E4**	A1	A2	A3								
A1		(3)	(3)					A1		5	9								
A2			1					A2			2								
A3		Inc.	0,00					A3		Inc.	0,00								

The consistency of alternative pair-wise comparison matrices must be examined according to each criterion by applying the inconsistency index. The same also goes for defining the sub-criteria pair-wise comparison matrices in relation to criteria and criteria pair-wise comparison matrix in relation to the goal.

When selecting the optimal alternative for intersection reconstruction, it is necessary to determine the importance of the criteria (and sub-criteria). From an engineering point of view, the most important criterion of the above is safety. On the other hand, without neglecting the importance of safety criteria, economic criteria most often play a major role in choosing the optimal alternative.

To implement a sensitivity analysis, two scenarios are provided: Scenario A, in which the safety criteria is the most important, and Scenario B in which safety and economic criteria are equally important in relation to other criteria (Table 3). However, it must be noted that importance of sub-criteria were not changed in these two scenarios.

TABLE 3. Criteria importance according to different scenario

SCENARIO A						**SCENARIO B**					
	S	**TT**	**E**	**EN**	**SU**		**S**	**TT**	**E**	**EN**	**SU**
S		3	4	5	7	**S**		3	1	5	7
TT			3	4	6	**TT**			(3)	4	6
E				3	4	**E**				5	7
EN					2	**EN**					2
SU				Inc.	0,05	**SU**				Inc.	0,03

RESULTS OF AHP MEHOD APPLICATION

Alternatives analysis according to the scenario A and B were conducted by AHP method application (Fig. 3). As it can be seen from the Figure 3a, in the case when safety criteria was chosen as the most important, alternative 2 (two roundabouts) stand out as the optimal alternative for intersection reconstruction. In the case of Scenario B (Fig. 3b), when safety and economic criteria are identified, alternative 1 (installation of traffic lights at the existing intersection) stands out as the optimal alternative.

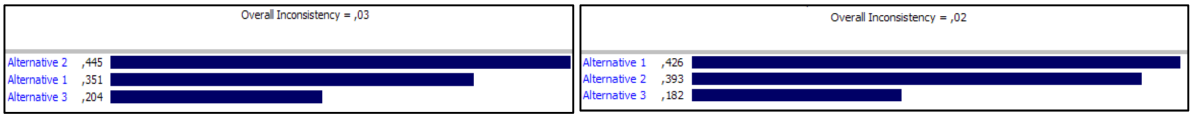

(a) (b)

FIGURE 3. Result of AHP method application for the scenario A (a) and scenario b (b)

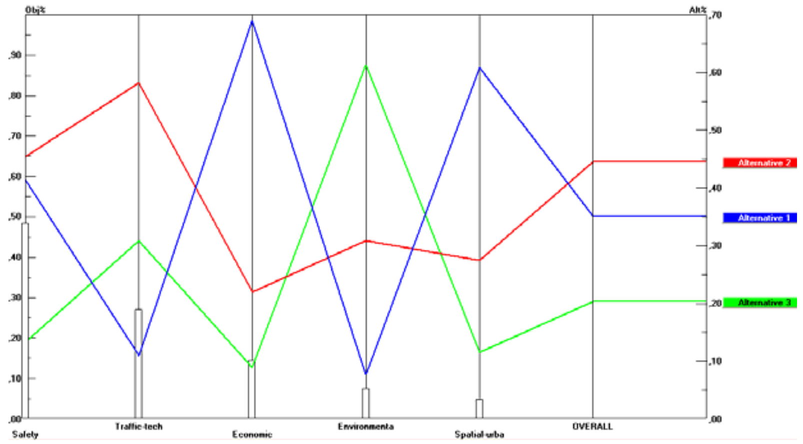

FIGURE 4. Performance sensitivity graph for scenario A

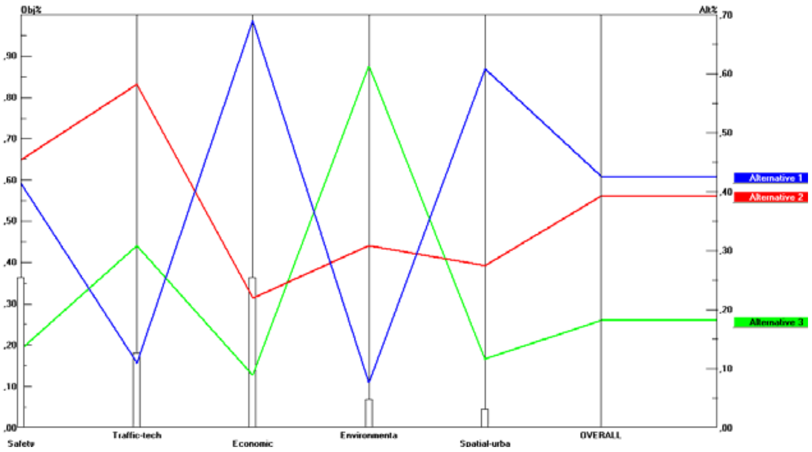

FIGURE 5. Performance sensitivity graph for scenario B

Based on the conducted sensitivity analysis according to the scenario A (Fig. 4) the optimal alternative for intersection reconstruction is the alternative 2 and according to scenario B (Fig. 5) alternative 1. Alternative 3 in both scenarios resulted as the worst alternative. Difference between alternative 1 and 2 is more emphasised if Scenario A is applied than in the case of Scenario B, main advantage of alternative 1 is low cost of implementation.

CONCLUSION

In this paper the application of Analytic Hierarchy Process (AHP) in the selection of optimal solution of the sub-urban intersection is presented. The AHP method, in this case, was used as a tool for selecting the optimal between 3 alternative intersection solutions based on 5 criteria and 12 sub-criteria. Overview of recent researches showed that multi-criteria analyses methods are used for estimation of traffic safety level so the priority in this research was given to the (traffic) safety criteria. Two scenarios were defined, one that gives exclusive priority to traffic safety criteria and one that gives equal importance to traffic safety and economic criteria. The ranking of alternatives resulted different so it can be concluded that methodology is sensitive to different use of criteria and their importance. It can be confirmed that AHP method is applicable for selection of the optimal intersection type and can serve as a tool for decision making when traffic safety improvements are considered as priority.

ACKNOWLEDGEMENTS

This paper is the result of the research done under the project "Research Infrastructure for Campus-based Laboratories at the University of Rijeka" (RC .2.2.06-0001) co-financed via the European Fund for Regional Development (EFRD) Ministry of Science, Education, and Sports of the Republic of Croatia. Publication of this paper is supported by the University of Rijeka under the project „Traffic Infrastructure in the Function of Sustainable Urban Mobility" (uniri-tehnic-18-143) and project „Implementation of Innovative Methodologies, Approaches and Tools for Sustainable River Basin Management" (uniri-tehnic-18-129).

REFERENCES

1. Żak, J., & Kruszyński, M. (2015). Application of AHP and ELECTRE III/IV methods to multiple level, multiple criteria evaluation of urban transportation projects. Transportation Research Procedia, 10, 820-830.
2. Hajkowicz, S. (2007). A comparison of multiple criteria analysis and unaided approaches to environmental decision making, Environmental Science & Policy, Elsevier, Vol. 10., No. 2., pp. 177-184., 2007.
3. Deluka-Tibljaš, A.; Karleuša, B., Dragičević, N. (2013). Review of multicriteria-analysis methods application in decision making about transport infrastructure, GRAĐEVINAR, 65 (2013) 7, pp. 619-631, doi: https://doi.org/10.14256/JCE.850.2013
4. Barić, D., Pilko, H., & Strujić, J. (2016). An analytic hierarchy process model to evaluate road section design. Transport, 31(3), 312-321.
5. Fancello, G., Carta, M., & Fadda, P. (2019). Road intersections ranking for road safety improvement: comparative analysis of multi-criteria decision making methods. Transport Policy, 80, 188-196.
6. Deluka-Tibljaš, A., Karleuša, B., & Benac, Č. (2011). AHP methodology application in garage-parking facility location selection. Promet-Traffic&Transportation, 23(4), 303-313.
7. Stanić, B., Tubić, V., & Čelar, N. (2011). Design and evaluation of a grade-separated intersection: a case study of the proposed Belgrade 'Hipodrom'. Transportation planning and technology, 34(6), 625-636.
8. Pilko, H., Mandžuka, S., & Barić, D. (2017). Urban single-lane roundabouts: A new analytical approach using multi-criteria and simultaneous multi-objective optimization of geometry design, efficiency and safety. Transportation Research Part C: Emerging Technologies, 80, 257-271.
9. Mehmood, A.; Easa, M. Said (2006). Optimizing geometric design of roundabouts: multi-objective analysis, Canadian Journal of Civil Engineering, Vol 33, 29-40
10. Saaty, T. L.(1994). Fundamentals of Decision Making and Priority Theory, RWS Publications, Pittsburg, USA
11. Saaty, T. L.(1996). The Analytic Hierarchy Process, second edition, RWS Publications, Pittsburg, USA
12. Tollazzi, T., Mauro, R., Guerrieri, M., & Rençelj, M. (2016). Comparative Analysis of Four New Alternative Types of Roundabouts:" Turbo"," Flower"," Target" and" Four-Flyover" Roundabout. Periodica Polytechnica Civil Engineering, 60(1), 51-60.
13. Tollazzi, T., Tesoriere, G., Guerrieri, M., & Campisi, T. (2015). Environmental, functional and economic criteria for comparing "target roundabouts" with one-or two-level roundabout intersections. Transportation research part D: transport and environment, 34, 330-344.

The Influence of Porous Asphalt Mix Design on Raveling Resistance

Marijana Cuculić[1,a], Aleksandra Deluka Tibljaš[1,b], Fabian Vasić[1,c], Ivana Pranjić[1,d]

[1]*University of Rijeka, Faculty of Civil Engineering, Croatia*

a) marijana.cuculic@gradri.uniri.hr
b) aleksandra.deluka@gradri.uniri.hr
c) fabian.vasic@student.uniri.hr
d) ivana.pranjic@gradri.uniri.hr

Abstract. Porous asphalt is type of open graded bituminous mixture for wearing courses. The reasons for its recent frequent usage as well as increase of research interest are the environmental benefits for example storm water management. However, there are some kinds of defects which can provoke deterioration of this type of pavement surface before expected project life.

The dominant defect type of porous asphalt pavements is raveling. Raveling is process of dislodgement of aggregate particles caused by loss of bond between aggregate particles and asphalt binder. In order to assess the raveling resistance in porous asphalt pavements, the Cantabro abrasion test was performed on the series of specimens.

Subject of this paper is divided in two phases: the first phase is to determine dependence of particle size distribution, bitumen content and percent of air voids on raveling resistance and the second phase deals with optimization of mix design from first phase in order to propose measures for asphalt properties improvement.

The analysis shows that usage of polymer modified bitumen has the greatest influence on raveling resistance of porous asphalt.

INTRODUCTION

Porous asphalt is bituminous material with bitumen as a binder prepared so as to have a very high content of interconnected voids which allow passage of water and air in order to provide the compacted mixture with drain and noise reducing characteristic [1]. Porous asphalt is used worldwide and offers a number of solutions to pavement problems. It is appreciated for its benefits in noise reduction and improved safety under wet conditions.

Permeability of porous asphalt mixtures mostly depend on the air voids. High air void content provided in the mixture will improve the permeability but reduces its modulus and durability [2]. Too much air voids also can cause the mixture having excessive aging and stripping problems. On the other hand, inadequacy of air void within the mixture will lead to the loss in permeability and clogging problem. Normally, porous asphalt is designed to achieve the desired air voids content between 16 and 26% [3]. To use low fines and optimum bitumen content in the mixture is critical in order to provide adequate interconnected voids [2].

Despite the environmental benefits, porous asphalt can suffer from problems, which can affect both its performance and service life. The open structure of porous asphalt adversely affects its durability due to high surface area exposure to air and water. This causes rapid ageing of the binder resulting in loss of adhesion and particle loss which culminates into raveling [4]. Standard laboratory tests for porous asphalts include Testing of hydraulic properties such as void content and permeability and mechanical properties such as Cantabro test.

According to HRN EN 12697-17 and other analyzed national standards the Cantabro test is a special test for porous asphalt to evaluate its resistance to particle loss by abrasion and impact forces. Furthermore, it is used as an important parameter to evaluate bonding properties between aggregate and bitumen [1].Comparison of the requirements for particle loss among analyzed standards is shown in Table 1.

TABLE 1. Requirements [5]

State	Air void	Particle loss
USA	18%-22% (>18%)	<20% at 25°C
Denmark	>26%	-
Australia	20%-25% (>20%)	20%-25%
Spain	>20%	25% at 25°C
Italy	18%-23%	25% at 25°C

This study was undertaken to investigate the effect of different gradation envelopes of porous asphalt made according to Croatian standard on the performance of porous asphalt mixture. In the first phase of laboratory testing was established that mixtures done according to Croatian standards for medium traffic loading did not give expected results. To improve mixture characteristics modified binders and additives are often used [6,7]

LABORATORY (EXPERIMENTAL) TESTING

Laboratory testing was divided into 2 phases. The aim of the first phase was to determine dependence of particle size distribution, bitumen content and percent of air voids on raveling resistance. The aim of the second phase was the optimization of mix design used in first phase testing in order to propose measures for asphalt properties improvement.

First Phase Laboratory Testing

In first phase, asphalt samples of different particle size distribution and binder content were made according to requirements for porous asphalt mixtures defined in HRN EN 13108-7 and Croatian technical requirements for asphalt pavements. For chosen asphalt mixture PA 11 BIT 50/70 three cases of particle size distribution were defined (Figure 1):

Case 1 – grading envelope near minimum values for selected grading envelope

Case 2 – grading envelope in the middle of minimum and maximum values for selected grading envelope

Case 3 – grading envelope near maximum values for selected grading envelope

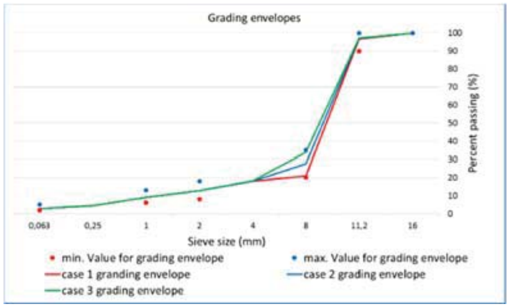

FIGURE 1. Grading envelopes – Case 1, Case 2 and Case 3

For each case variations of the content of asphalt binder was used as follows: 3.2%, 4.2% and 5.2%.

For durability purpose, porous asphalt wearing course should have good particle loss (raveling) resistance itself. In order to assess the particle loss resistance Cantabro test according to EN 12697-17 was done. Cantabro test enables to evaluate the resistance of the mixture to its disintegration by impact and abrasion caused by traffic. The test consists of introducing into the Los Angeles abrasion machine cylindrical Marshall specimens. Each specimen

was initially weight and placed into a machine. After 300 revolutions of the drum, specimens ware weighted again in order to determine percentage of mass loss during the test. According to EN 13108-7 particle loss values are in range 10% - 50%. Upper limits for particle loss resistance are different for different countries and regulated with national standards. Result of extended study carried out in Switzerland shows strong dependence of temperature on particle loss values. Given recommendation was to set up upper limits of particle loss values in dependence of environmental conditions of in situ asphalt pavement. States with high percentage of porous pavements monitor pavement performance during exploitation and give recommendation for correcting performance values [8]. According to Croatian technical requirements for asphalt pavement allowable limit for particle loss is set to 30%. Material components and Limit values of physical and mechanical properties of porous asphalt mixture are shown in Table 2 [4].

TABLE 2. Limit values [4]

Asphalt mixture materials	**Porous asphalt mixture PA 11**
Conventional bitumen 50/70	+
Polymer modified bitumen	Not allowed
Recycled aggregate	Not allowed
Physical and mechanical properties	**Porous asphalt mixture PA 11**
Void content V, %	$V_{min} = 16$, $V_{max} = 26$
Particle loss PL, % (m/m)	PL_{30}

TABLE 3. Asphalt mixture characterization

Asphalt mixture materials	**CASE 1**	**CASE 2**	**CASE 3**
Sample number	1 / 2 / 3	4 / 5 / 6	7 / 8 / 9
Bitumen content	3,2 / 4,2 / 5,2	3,2 / 4,2 / 5,2	3,2 / 4,2 / 5,2
Density of a bituminous mixture	2,57 / 2,53 / 2,49	2,57 / 2,53 / 2,49	2,57 / 2,53 / 2,49
Bulk density - procedure D	2,01 / 2,05 / 2,1	2,05 / 2,07 / 2,07	2,04 / 2,07 / 2,06
Air voids content	21,8 / 18,80 / **15,78**	20,34 / 18,06 / 16,81	20,69 / 18,19 / 17,36
Void in the mineral aggregate	28,08 / 27,23 / 26,45	26,74 / 26,57 / 27,34	27,06 / 26,69 / 27,82
Void filled with binder	22,37 / 30,97 / 40,32	23,94 / 32,03 / 38,53	23,56 / 31,85 / 37,62
Particle loss - Cantabro test	**46,1%** / **36,5%** / 26,5%	**52,8%** / **32,6%** / 28,1%	**42,7%** / 28,4% / 26,9%

Table 3 shows asphalt mixture characterization. Samples 1 and 2 from Case 1, samples 4 and 5 from Case 2 and sample 7 from Case 3 donot meet requirements according to particle loss resistance. Sample 3 from Case 1 doesn`t meet requirements according to air void content (all bold in the Table 2).

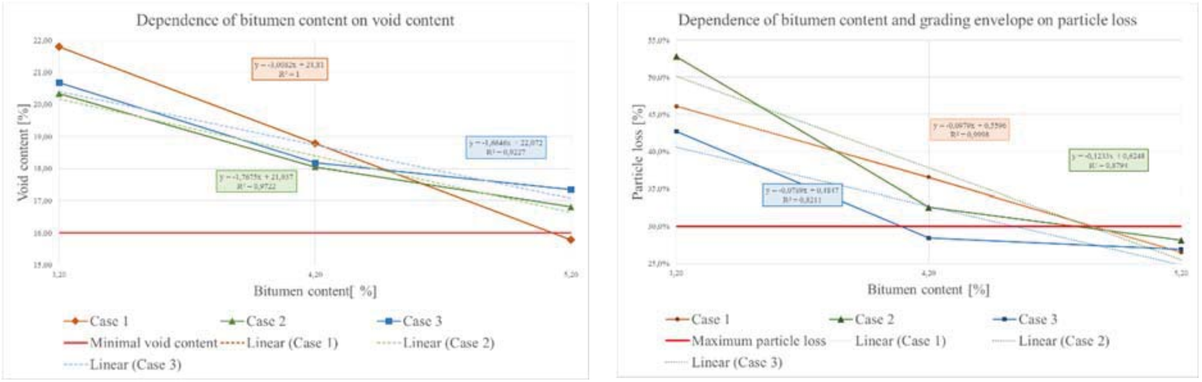

(a) (b)

FIGURE 2. (a) Dependence of bitumen content on void content (b) Dependence of bitumen content and grading envelope on particle loss

Figure 2 (a) shows dependence of bitumen content on void content. It can been seen that only sample 3 from Case 1 does not meet minimal void content requirements according to Croatian technical requirements for asphalt pavements so that kind of asphalt mixture can`t be used for surface courses of asphalt pavements. Generally, it can be concluded that with increasing of binder content percentage of void content is decreasing. Also is interesting that results from Case 2 and Case 3 have lower values of void content for the values of binder content in range 3,2 – 4,2% than in Case 1 and higher values of void content for the values of binder content in range 4,2 -5,2 %. Result of that phenomena can be in higher proportion of coarse aggregate (4-8 mm) which results with less discontinued grading envelope. Higher proportion of coarse aggregate means increasing of specific aggregate area which results in higher percentage of binder content used for enclosing aggregate particles.

Figure 2 (b) shows dependence of bitumen content and grading envelope on particle loss. Generally it can be concluded that particle loss is decreasing with increasing binder content. Figure 2 (b) shows linear correlation between binder content and particle loss for Case 1 while nonlinear correlation for Case 2 and Case 3. For Case 2 and Case 3 is visible that increasing binder content in range 4,2% - 5,2% has less impact on particle loss that increasing binder content in range 3,2 - 4,2%.

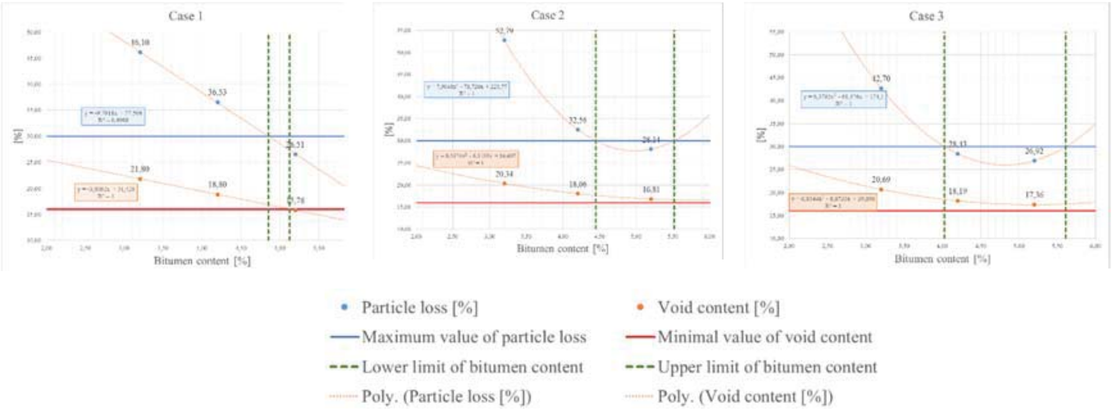

(a) (b) (c)

FIGURE 3. (a) Void content and particle loss – Case 1, (b) Void content and particle loss – Case 2, (c) Void content and particle loss – Case 3

Figure 3 shows influence of void content and particle loss on defined optimal bitumen content. Optimal mix design according to criteria of maximal particle loss (30%) and minimal void content (16%) was done. For Case 1 optimal bitumen content is in range 4,9% - 5,1%, for Case 2 is in range 4,4% - 5,5% and for Case 3 is in range 4,0% - 5,6%.

Analysis shows that with decreasing of discontinuities of grading envelopes range of optimal bitumen content is increasing. According to Croatian technical requirements for asphalt pavements only sample 3 (Case 1), sample 6 (Case 2) and samples 8 and 9 (Case 3) meet requirements for maximal particle loss. Sample 3 (Case 1) doesn`t meet requirements for minimal void content. From foregoing results, samples 6, 8 and 9 are chosen for determination of optimal mix design for further analysis.

Second Phase Laboratory Testing

According to Croatian technical requirements for asphalt pavements only sample 3 (Case 1), sample 6 (Case 2) and samples 8 and 9 (Case 3) meet requirements for maximal particle loss. Sample 3 (Case 1) doesn`t meet requirements for minimal void content. From foregoing results, samples 6, 8 and 9 are chosen for determination of optimal mix design for further analysis (Table 4).

TABLE 4. Asphalt mixture characterization – samples 6, 8 and 9

Sample number	Bitumen content	Void content	Particle loss
6 – Case 2	5,2 %	16,81 %	28,1 %
8 – Case 3	4,2 %	18,19 %	28,4 %
9 – Case 3	5,2 %	17,36 %	26,9 %

Sample 8 has maximal void content which indicate good permeability properties, but also has maximal percentage of particle loss which indicate lower durability properties. Sample 8 is the only sample with 4,2 % bitumen content. According the Figure 2 (b) it is establish that increasing bitumen content in range 4,2 – 5,2 % have no significant impact on particle loss. In comparison with samples 6 and 9, increase of bitumen content to 5,2 % (increasing of 24 %) will decrease particle loss for 6 %. As indicated in results, sample 8 was chosen as optimal mix design for further analysis. Further analysis include modification of mix design: type of mineral aggregate, type of bitumen and additives. Results of laboratory testing are shown in Table 5.

TABLE 5. Modified asphalt mixture characterization

Sample number	1 – Phase 2	2 – Phase 2	3 – Phase 2	4 – phase 2
Type of bitumen	PmB 45/80-65	BIT 50/70	PmB 45/80-65	PmB 45/80-65
Type of mineral aggregate	Carbonate	From ingenious rocks	Carbonate	From ingenious rocks
Type of filler	Carbonate	Carbonate	Calcite hydraulic lime	Calcite hydraulic lime
Additives	-	-	Cellulose fiber 0,3 % weight mass	Cellulose fiber 0,3 % weight mass
Bitumen content	4,2	4,2	4,2	4,2
Density of a bituminous mixture	2,53	2,554	2,513	2,527
Bulk density – procedure D	2,078	1,962	2,045	1,912
Air voids content	17,8	23,2	18,6	24,3
Void in the mineral aggregate	26,40	31,25	27,03	32,21
Void filled with binder	32,39	25,78	31,12	24,42
Particle loss – Cantabro test	6,94	29,16	10,00	13,89

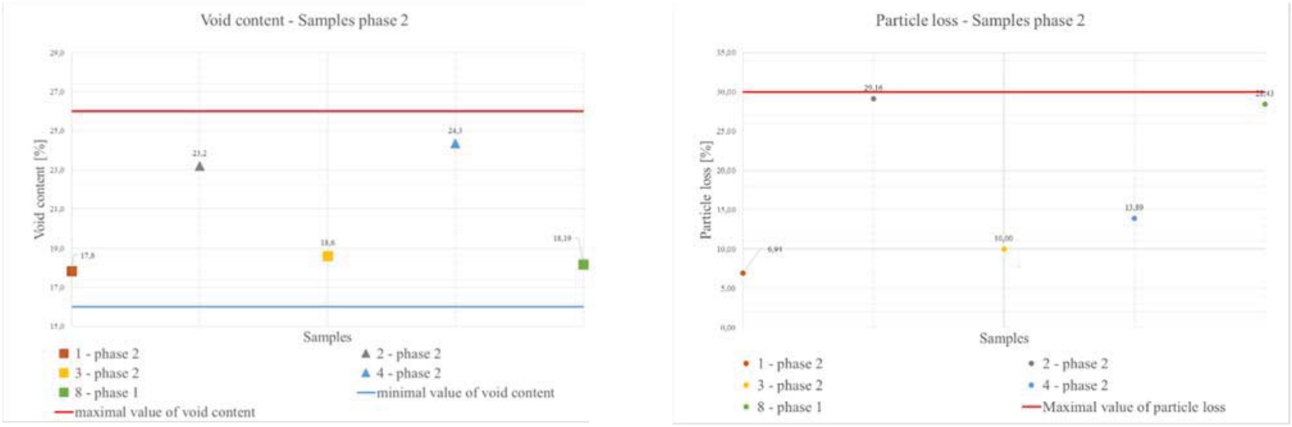

(a) (b)

FIGURE 4. (a) Void content – Samples phase 2, (b) Particle loss – Samples phase 2

Figure 4 (a) shows differences in void content between samples with carbonate aggregate (samples 1 and 3) and samples with aggregate from ingenious rock (samples 2 and 4). This can be result of carbonate aggregate crushing due to less abrasion resistance. Also it can be concluded that cellulose fibers and calcite hydraulic lime contribute to higher values of void content (sample 1 vs sample 3 and sample 2 vs sample 4).

Use of polymer modified bitumen results in better values of particle loss (Figure 4 (b)). Comparing sample 1 from phase 2 and sample 8 from phase 1 (difference in type of bitumen) it can be seen that sample 1 has 0,4% less value of void content and 21,5% less value of particle loss. Comparing sample 2 from phase 2 and sample 8 from phase 1 (difference in type of aggregate) it can be seen that sample 8 has 0,8% less value of particle loss. Usage of additives in combination with polymer modified bitumen (samples 3 and 4) show no improvements in particle loss resistance. In this results it can been seen a slight increase in values of void content (less than 1%) which can be result of usage of additives and usage of filler with less density values.

CONCLUSION

Dependence of grading envelopes, type of binder and binder content on air voids content and particle loss resistance for porous asphalt are shown. In phase 1, three types of porous asphalt mixture composed of carbonate mineral aggregate with conventional bitumen (3 types of grading envelopes and 3 values of bitumen content) were analyzed. From results it can be concluded that better particle loss resistance have samples with less discontinued grading envelopes and higher values of bitumen content. Lower values of void content results in better particle loss resistance.

For phase 2, sample 8 from phase 1 was chosen. The aim of phase 2 was to establish dependence of type of binder, type of mineral aggregate, type of filler and usage of additives on values of void content and particle loss resistance. . From results it can be concluded that greatest influence on particle loss resistance have usage of polymer modified bitumen. Results show that type of aggregate has no significant influence on particle loss resistance. Usage of additives and modification of type of filler in combination with polymer modified bitumen has no improvements in particle loss resistance.

Further analysis should include analysis of influence additives and different type of filler on porous asphalt mixtures composed of mineral aggregate with conventional bitumen.

ACKNOWLEDGMENTS

This paper is the result of the work under the project “Research Infrastructure for Campus-based Laboratories at the University of Rijeka” (RC.2.2.06-0001) co-financed via the European Fund for Regional Development (ERDF) Ministry of Science, Education and Sports of the Republic of Croatia. It was supported by the University of Rijeka under the project “Traffic Infrastructure in the Function of Sustainable Urban Mobility” (uniri-tehnic-18-143).

REFERENCES

1. HRN EN 13108-7, *Bituminous mixtures – Material specification – Part 7: Porous asphalt*
2. M.R. Hainin, L.A.Cooley Jr and B.D. Prowell, “An investigation factors influencing permeability of Superpave mixes” (International Journal of Pavements, Vol 2, University of Mississippi, 2003)
3. Croatian technical requirements for asphalt pavements, Croatian roads, 2017.
4. L.D. Poulikakos, S. Takahashi and M.N. Partl, “A comparison of Swiss and Japanese Porous Asphalt Through various Mechanical Test*”* in *Proceedings of 4th Swiss Transportation Research Conference STRC 2004,* p. 12
5. M.O. Hamzah, M.R.M Hasan, G. Van Bochove, “Rational control parameters for determination of design binder content of porous asphalt*”* in *Proceedings of 5th Euroasphalt & Eurobitume congress 2012.*
6. V.S Arrieta, J.E. Cordoba Maquilon “Resistance to degradation or cohesion loss in Cantabro test on specimens of porous asphalt friction courses” in *Proceedings of XVIII Panamerican Conference of Traffic and Transportation Engineering and Logistics PANAM 2014,* p290-299
7. M. Xiang, L. Qiang, Y.C. Cui, A.Q. NI, “Performance of porous asphalt mixture with various additives” (International Journal of Pavement Engineering, 2016, pp. 355-361)

   L.D. Poulikakos, M. Pittet, L. Arnaud, A. Junod, R.Gubler, E. Simond, M.Partl, A.G.Dumont, *Mechanical properties of porous asphalt, recommendations for standardization,* Swiss Federal Laboratory, Empa, Epfl, Lavoc, 2006

The Management Of Pedestrian Emergency Through Dynamic Assignment: Some Consideration About The "Refugee Hellenism" Square Of Kalamaria (Greece)

Giovanni Tesoriere[1,a)], Antonino Canale[1,b)], Alessandro Severino[2,c)], Iva Mrak[3,d)], Tiziana Campisi[1,e)]

[1]*University of Enna "Kore" - Faculty of Engineering and Architecture – Cittadella Universitaria 94100 Enna (EN) – ITALY*
[2]*University of Catania - Department of Civil Engineering and Architecture, Università degli Studi di Catania, Via Santa Sofia 64, 95125 Catania (CT),-ITALY*
[3]*University of Rijeka - Faculty of Civil Engineering, Građevinski fakultet. Radmile Matejčić 3 51000 Rijeka-CROATIA*

[a)]giovanni.tesoriere@unikore.it
[b)]antonino.canale@unikore.it
[c)]severinoalessandro@yahoo.it:
[d)]iva.mrak@gradri.uniri.hr
[e)]Corresponding author: tiziana.campisi@unikore.it

Abstract. Generally the safety of public areas plays a fundamental role in the liveability of a city. Different evacuation simulations are carried out over the years in order to mitigate the problems connected to a chaotic movement of pedestrians. The panicgenerated by a possible risky event, often involves variations in the trajectories assumed in the same spaces in safe conditions. This is due to the variations in speed, pedestrian density in the sub-areas and if not properly evaluated, the evacuation process could generate crowds and therefore congestion, reducing the distance from the area object of an event.
The present study focuses on the evaluation of different scenarios applied to the named square of Kalamaria (Greece) which is located near the two biggest pedestrian areas of the city. The study approach, based on pedestrian micro-simulation, is focused on the dynamic assignment,implemented in order to shape the path pedestrian choice behaviour by omitting the creation of static routes and using the OD matrix as flow input instead. Different steps are established in order to enquire input data, to calibrate the tool and obtain the results. These are based on the definition of areas and sub-areas in accordance with the pedestrian social force model.Through dynamic pedestrian assignment, different parameters were compared including speeds, density pedestrian and the LOS (Level Of Service), crossing the main square which may lead to benefits or criticalities as the risk level increases.

Keywords: Dynamic Assignment, pedestrian, emergency, micro-simulation, Viswalk

INTRODUCTION

The emergency can be defined as any critical condition that manifests itself as a result of an unwanted event, be it natural or of another nature (for example an earthquake, a fire, a violent act) that determines a potentially dangerous situation for the safety of people and public and private assets and which requires exceptional and urgent interventions to be managed and resolved.

It can therefore be confirmed that "emergencies" can also derive from human behavior such as errors, negligence, neglect, or as a consequence of natural events such as earthquakes, etc.

The management of an emergency consists of implementing a series of actions aimed at limiting damage to people or things and restoring normal conditions as quickly as possible.

So managing the emergency means, first of all, managing the moment between the emergence of the emergency itself and the arrival of structured relief, in order to safeguard the safety of the people and the goods present in the area affected by the event, limiting at minimum the negative consequences determined by the event.

The emergency management also consists in undertaking a series of preventive actions aimed at mitigating the factors that could potentially generate the emergency.

The main purpose of the emergency plan is to:

- Identify the scenarios in which emergencies can be generated during the course of the demonstration and how to intervene;
- Plan a series of preventive interventions aimed at cancelling or mitigating the unwanted effects;
- Organize a structure that can collect information and provide a rapid response in the event of an emergency.

Different types of studies can preventively evaluate the benefits or negativities of an area, think for example of the simpler approach through SWOT analysis [1][2] or in more complex terms through multi-criteria type evaluations [3,4,5]or BIM model in agreement with [6]

Safety in public spaces, especially during mass events where thousands of people gather in a small space in accordance with[7]

This area, is a sector of great interest especially since several terrorist attacks have occurred and since moreover there is a more careful assessment of seismic risk. [8,9,10,11,12].

Overcrowding, if not properly evaluated, can lead to the definition of crowds and congestions with even morenegative effects, increasing the number of deaths and injuries.

Therefore, in recent years we have noticed a thriving research activity on pedestrians and evacuation dynamics. This research aims not only to improve the qualitative and quantitative assessment of the general phenomena observed in large human crowds, but has led to a development in the field of pedestrian flow research not only in terms of public spaces but also in indoor spaces such as train stations and airports [13,14,15]

After validating and calibrating appropriate tools, such as microsimulation software, these models can be used for large planning events with consequent optimization of evacuation routes.

The present study starts from the awareness of a seismic risk in the high Kalamaria area. This involves an assessment of mitigation and risk reduction strategies, especially for the population. Therefore, one of the features of the Greek city characterised by the presence of pedestrian areaand by a great number of commercial and religious activities and of the Municipality, strategic site in the case of earthquake. Several scenarios have been hypothesized that allow the population to consider the square “ΠροσφυγικούΛληνισμού-Refugee Hellenism “of Kalamariaas a filter to access secondary roads in order to evacuate the Komninon road. The case study was selected both for the importance of the location of offices and commercial offices but also to understand how the square can act as a filter and then allow the evacuation from a main pedestrian street to other mixed secondary ones where they could find space emergency and hospital vehicles.

A significant contribution to the resolution of the problems of calculating the movement of people is offered by modern calculation systems, which allow the modeling of the exodus also taking into account the continuous interaction between the purely physical expression of motion and behavioral factors.

However, it should be pointed out that there is no right or wrong model, just as the achievable results cannot begeneralised, since each instrument is subject to experience of the person who applies it and the priorities that it identifies.

The scenarios represented are, in fact, the materialization of the contents that have been entered andthe correct model to use is above all that able to guide the user in the "construction" of his own representation model referred to the case study.

The models analysed are listed in Table 1 collected in three categories with the aim of expressing the relative levels of sophistication and potential:

- movement-based models,in which it is not possible to describe the behavior of people who are generically represented with a geometrical figure (ellipse);

- partially behavioural models, in which the behavior of the occupant can be implicitly modeled;
- behavioural models, in which the decision-making capacity of the individual occupant and the consequent behavior can be fully considered

There are various software dedicated to the simulation of pedestrian emergencies and evacuations as shown in the table below where they have been divided by type of model and purpose.

TABLE 1. Comparison of different tool linked to evacuation phenomenon

	Software					
Model type	Common building type		Residential buildings	Buildings <20m (h)	Areas closed to public transport	Single escape route
Models based on movement	Evacnet4 Takahashi's Fluid M. Pathfinder	Magnetic Model Steps	N.D.	Timtex	N.D.	Eescape Wayout Egresspro Entropy
Partially behavioral models	Exit89 Simulex Gridflow				Pedroute/Paxport Viswalk	Allsafe Viswalk
Behavioral models	Crisp Aseri Buildingexodus Egress 2000 Vegas E-Scape	Bgraf Evacsim Legion Myriad	Exitt	Bfires-2		

METHODOLOGY

It is assumed that the area of the square will be used as an evacuation filter in the event of various types of events, allowing people in the pedestrian area and offices in front of the square to leave this area without stopping in the square itself.

This work aims to explore the condition of the service level of the exit in case of escape from the square towards the neighboring arterial roads.

Through pedestrian micro-simulation, various scenarios have been hypothesized, of which the first concerning pedestrian flow data recorded in peak time, while the other scenarios are hypothesized considering a doubling, triplication and quadrupling of the observed data in order to understand which flow can generate congestion and therefore problems of leaving the square.

Literature has led to an empirical, internationally accepted formula e proposed in the most important manuals of engineering[16]due to phenomena of fire evacuation, for example, which relates to speed and density of crowding, for values of the latter ranging from 0.55 to 3.8 people / m2, otherwise the following conditions apply:

- for density along routes less than 0.55 people / m2 there is not is no interference between people and therefore the speed of displacement is the individual one;
- for values over 3.8 people / m2 in the motion interface

$$v = k - akD \tag{1}$$

where is it:

v = speed [m / s]

D = density [people / m2]
k = expressed constant
a = constant equal to 0.266 m2 / person
For densities less than 0.55 people / m2 the report is simplified as follows v = 0.85 k

The micro-simulation of vehicular and pedestrian traffic, as anticipated, provides a dynamic and timely viewof the phenomenon. For this purpose, the characteristics of the motion must be taken into considerationof individual pedestrians interacting with each other. Through the micro-simulation it is therefore possible to represent several families of displacements, each characterized by different behavioural parameters and by different types of pedestrians on which the movement speed depend.

The micro-simulator analyses and processes instant by instant the movement of every single pedestrian on the network, based on laws related to pedestrian movement and behaviour in accordance with the social force model of Helbing [17] and considering specific parameters and calibration model process like described by [18].

In order to be able to analyse and compare the simulated scenarios, it was necessary to identify a series of indicators capable of providing judgment parameters.

In this perspective, three fundamental parameters have been identified like road Level of Service (LOS);average journey times and average length of any queues and slowdowns.

The microsimulation model calculates the current LOS (determined on the basis of the provided and analyzed traffic surveys) and forecasts (defined on the basis of the results deriving from the use of the latter, applied to the different scenarios envisaged), on the basis of the classical methodology contained in the HCM manual. [19]

The micro-simulation of the traffic allows to evaluate congestion phenomena considering only one transport mode or more (i.e. pedestrian, vehicles, cliclyst).

Output is linked to different evaluation such as the travel times and queues length linked to the dynamic approach of the real traffic on the transport network.

This tool is useful for assessing scenarios that can be implemented to improve security and reduce problems related to traffic saturation. Several urban applications are present in the literature and focus not only on software calibration but also on the comparison of scenarios through Service levels as defined by the HCM. In agreement with [20] it is possible to study confined environments by evaluating non-flat geometries and in agreement with it is possible to evaluate areas where conflict points increase as in pedestrian crossings. Some studies in the literature use different mathematical methodologies and software for estimating evacuation phenomena [21].

The level of service (LOS) can be related to the possible traffic congestion but it can also be a useful parameter for assessing the accessibility of some public spaces if accompanied by an assessment of traffic components with disabilities and an assessment of the obstacles present along the route.

The analyzed area is marked red in figure1 and it has been divided into 30 subareas in order to obtained more performed results.

FIGURE 1. Evaluated area and relative sub areas

The figure 2 below shows the outgoing flow directions from the areas (in blue) respectively originating from the pedestrian area and from the municipal offices located on the pizza. The red arrows instead show the hypothesized escape routes.

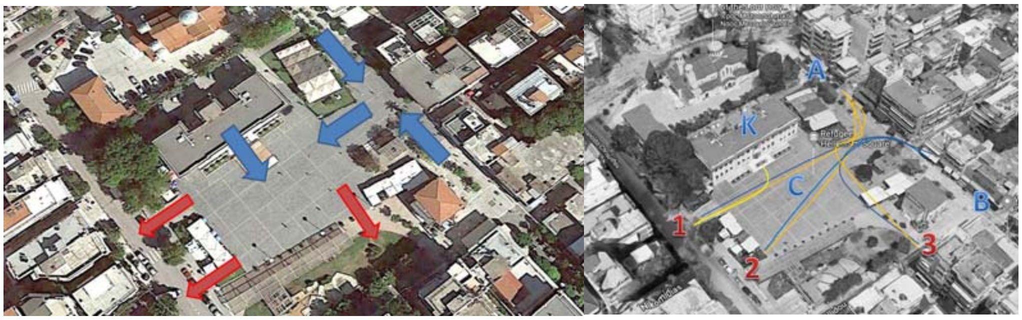

FIGURE 2. Entrance (blue) and exit (red) of monitored square in Kalamaria (Greece)

The evaluated scenarios consider an estimated flow (1st scenario) equal to 678 ped / h which was brought up to 4068 in the sixth scenario with gradual doubling increases, triplication etc.

Theacquisition of the data relating to the scenario was carried out in May 2019, finding a balanced pedestrian composition between men and women and at the same time between young people, adults and the elderly. A 2% of people with wheelchairs / people with impaired mobility characterize this composition.

RESULTS

The use of the micro-simulation tool starting from the choice of the input data to the calibration with reference to the mathematical models to which it is based, allowed to compare different scenarios, evaluating up to what point the examined area presents a good level of service and therefore a good degree of security in the evacuation of people who pass through the examined area daily.

Generally the microscopic simulation of pedestrians and crowds is particularly suitable for urban planning, for pedestrian use, for planning evacuation measures and for many other applications that guarantee an easy pedestrian circulation. The safety of groups of people is an element of great importance, especially in public places.

Therefore, the definition of innumerable structural and organizational measures to reduce and control the unexpected behavior of people in emergency situations is fundamental.

The software used in this work analyzes the potential risks and plans the entry and exit of flows in buildings, stadiums and other structures to ensure the security of flows of people. It also allows the modeling of escape routes and evacuation scenarios for skyscrapers and tunnels; simulates the emergency exits of a station or a road tunnel.

In order to be able to compare the different scenarios it was considered appropriate to consider the variation of the LOS connected to the pedestrian density and the travel times, considering a standard evacuation speed commensurate with the different types of pedestrian analyzed. The study in this first analysis aims at the study of evacuation with varying flows, leaving the geometries and compositions of pedestrian flow unchanged in accordance with the data recorded in the area through the use of video cameras located on the sides of the square and of the Komninon road.

The following are the LOS values relating to the different areas as the pedestrian flows increase. It is possible to notice that the areas adjacent to the H and I nodes are those that present a greater variation of the LOS going from a level A to a level D in concomitance of the section restrictions.

Likewise also in the square exits there is a variation from A to D of the LOS with similar values in the first two scenarios and then a variable reduction in the service level proportional to the increase in flows.

TABLE 2. Level of Service LOS in accordance with HCM manual and comparison of different scenarios in terms of LOS

Level of Service LOS	A	B	C	D	E	F
Pedestrian density Ped/m^2	0,080	0,080-0,270	0,270-0,450	0,450-0,690	0,690-1,660	>1,660

LOS distribution

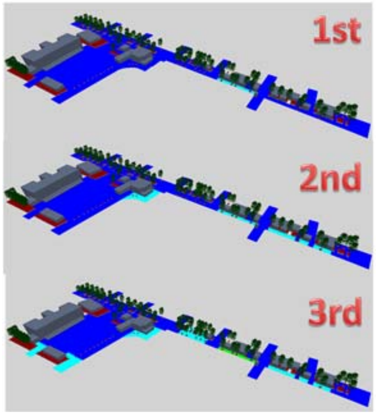

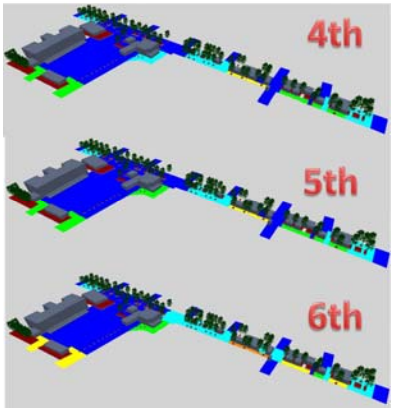

Through the comparison shown in the previous figure it is possible to observe a reduction in the LOS value in the last part to the right of the area resulting in a more restricted geometry that forces users to stand in a row and with reduced movement speeds.

The following are the travel themes between the main nodes A, B and C, which respectively represent the beginning and the end of the pedestrian street and C the square from which to reach the escape routes.The number 1-2-3 on Figure 3 (right) is linked to the actual exit and K is the Office of Municipality on the square.

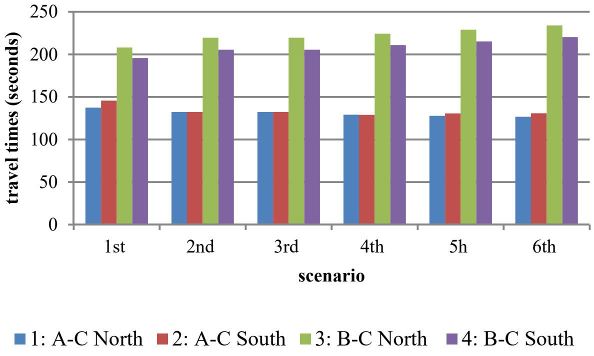

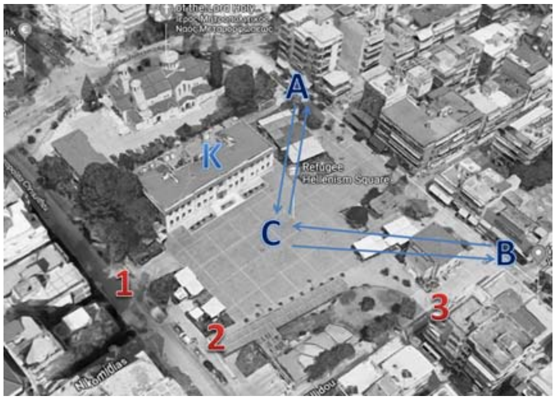

FIGURE 3. Travel time estimation considering the main nodes of the monitored area

The travel time longer in direction B than in A is not so much due to the central position of point C that is the square but the more it is connected to the presence of restrictions due to flowerbeds and tables of the rooms that limit the movement of pedestrians.

In the most congested areas due to the geometric shrinkage the travel times with respect to node C from which the exits depart as shown below are also evaluated and from which we can infer variable times between 110 and 210 seconds with average evacuation speed of pedestrians of 3,5 - 4m / s.

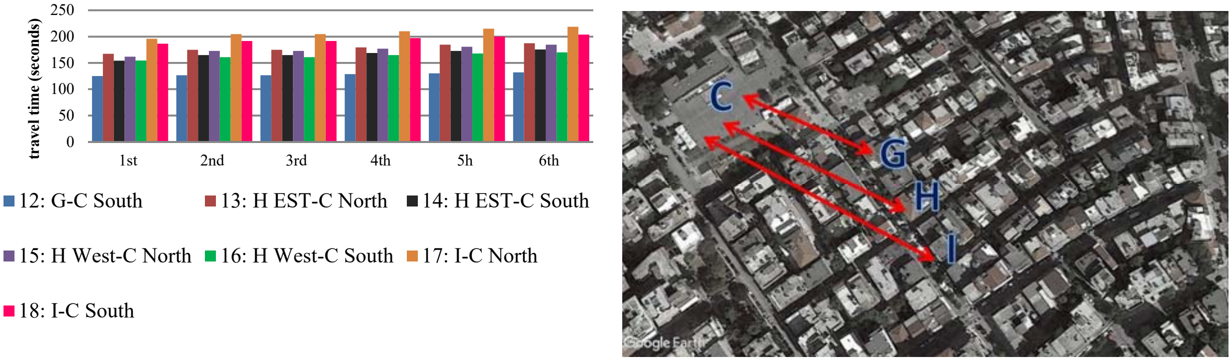

FIGURE 4. Travel time comparison on secondary nodes

These assessments do not contemplate the presence of further obstacles or barriers that could limit or reduce the speed of evacuation and therefore this work is fundamental for further evaluation of scenarios and emergency conditions. The evaluations shown in the graphs consider an ordinary condition of the area without obstacles or maintenance areas that could reduce the space that can be walked and therefore increase travel times.

CONCLUSION

Through micro simulation it has been possible to compare different scenarios relating to the main square of Kalamaria in a preventive manner considering only a gradual increase of the crowd that has to pass through the square to reach outside the examined area.

The scenarios have been scheduled considering an observed pedestrian flow of about 670 ped / h in the area examined and estimating 5 hypothetical cases by exponentially multiplying the observed data. meter that will bring many more users to travel the analysed area.

The comparison in terms of travel time and pedestrian density and relative LOS was carried out keeping constant the composition of the pedestrian flow in terms of gender, age and people moving alone or in groups or with wheelchairs.

This work is fundamental for other evaluations related for example to the change in the composition of pedestrian flows or to the presence of obstacles and maintenance areas in the area that can make the evacuation manoeuvre more critical.

REFERENCES

1. T. Campisi, A. Canale, and G. Tesoriere, (2018, November). “SWOT analysis for the implementation of spaces and pedestrian paths at the street markets of Palermo” (AIP Conference Proceedings, Vol. 2040, No. 1, p. 140003)
2. I, Mrak, “Evaluation Methods in the Protection of Built Heritage / Metodeprocjene u funkciji očuvanja graditeljsko gnaslijeđa” (Journal Civil Engineer, 66, 2014, 2, 127-138)
3. B. Karleuša, M. Benigar and A. Deluka-Tibljaš, “Use of AHP Multicriteria Optimisation Method for the Optimisation of Garage Facility DOK 3 in Rijeka” (11th International Symposium on Electronics in Traffic ISEP 2003, Proceedings / Anžek, Mario ur.. Ljubljana: Electrotechnical Society of Slovenia, 2003. U6)
4. I. Mrak, “An Evaluation Model For Cultural Heritage In Spatial Planning” (Inderscience International Journal of Global Environmental Issues IJGEnvI special issue “Cities as Sustainable Wealth Creators”, 2014, 13 2/3/4; 206-234)
5. I. Mrak, ”Locally Based Development—Tools for Identifying Opportunities and Evaluating Port Area Strategies of Rijeka” (MDPI-Sustainability 2013, 5, 9, 4024-4056)
6. G. Acampa, N. Bona, M. Grasso and D. Ticali, “BIM: Building information modeling for infrastructures” (AIP Conference Proceedings, Vol. 2040, No. 1, 2018, p. 140008)

7. T. Campisi, A. Canale, G. Tesoriere, I. Lovric and B. Čutura, "The Importance of Assessing the Level of Service in Confined Infrastructures: Some Considerations of the Old Ottoman Pedestrian Bridge of Mostar" (Applied Sciences, 9(8), 2019, 1630)
8. X. Romão, E. Paupério, N. Pereira, "Avaliação expedita do riscosísmico de bensculturais imóveis" (Conservar Património 25, 2017, 23-36)
9. A. H. Barbat, M. L. Carreño, L. G. Pujades, N. Lantada, O. D. Cardona and M. C. Marulanda, "Seismic vulnerability and risk evaluation methods for urban areas. A review with application to a pilot area" (Structure and Infrastructure Engineering, 6:1-2, 2010, 17-38)
10. E. Taniguchi, R.G. Thompson and T. Yamada, "Incorporating risks in City Logistics" (Citation Data Procedia - Social and Behavioral Sciences, ISSN: 1877-0428, Vol: 2, Issue: 3, 2010, Page: 5899-5910)
11. O. Renn and A. Klinke, "A Framework of Adaptive Risk Governance for Urban Planning" (Sustainability 2013, 5, 2036-2059)
12. G. Vogelbacher, I. Häring, K. Fischer et al., "Empirical Susceptibility, Vulnerability and Risk Analysis for Resilience Enhancement of Urban Areas to Terrorist Events" (Eur J Secur Res, 2016)
13. T. Campisi, A. Canale and G. Tesoriere, "Study of emergency setting for urban facility using microsimulation tool" (AIP Conference Proceedings, Vol. 1906, No. 1, 2017, p. 190004)
14. G. Tesoriere, T. Campisi, A. Canale, A. Severino and F. Arena, "Modelling and simulation of passenger flow distribution at terminal of Catania airport" (AIP Conference Proceedings, Vol. 2040, No. 1, 2018, p. 140006)
15. A. Deluka-Tibljaš, S. Šurdonja and M. Benigar, "Location Selection Criteria for the Sea Passenger Terminal in Relation to the Urban Structure of the Town" (Promet - Traffic & Transportation. 18, 2006, 3, 159-164)
16. A. S. Zanut, and T. Villani "Tempi di evacuazione e modelli automatici di simulazione del movimento delle persone", 2007
17. Helbing, D., & Molnar, P. (1995). Social force model for pedestrian dynamics. Physical review E, 51(5), 4282
18. T. Kretz, J. Lohmiller and P. Sukennik, "Some Indications on how to Calibrate the Social Force Model of Pedestrian Dynamics" (Transportation Research Record, 2672, 20, 2018, 228-238)
19. Manual-HCM, H. C. 2010. Transportation research board. National Research.
20. T. Campisi, G. Tesoriere and A. Canale, "The pedestrian micro-simulation applied to the river Neretva: The case study of the Mostar "old bridge" (AIP Conference Proceedings, Vol. 2040, No. 1, 2018, p. 140004)
21. L. Zheng, X. Peng, L. Wang and D. Sun, "Simulation of pedestrian evacuation considering emergency spread and pedestrian panic" (Physica A, 2019)

The Maas Development as a Mobility Solution Based On the Individual Needs of Transport Users

Antonino Canale[1,a)], Giovanni Tesoriere[1,b)] and Tiziana Campisi[1,c)]

[1]*University of Enna "Kore" - Faculty of Engineering and Architecture – Cittadella Universitaria 94100 Enna (EN) - ITALY*

[a)]antonino.canale@unikore.it
[b)]giovanni.tesoriere@unikore.it
[c)]Corresponding author: tiziana.campisi@unikore.it

Abstract. The MAAS (Mobility As A Service) is nothing more than a new business model for the provision of transport services. Like all "as a service", it provides a monthly flat-rate subscription that guarantees the personalized use of a bundle of public and private transport: trains, buses, taxis, car and bike sharing, which can be used unlimitedly with a single subscription, all in one. To enjoy the service in complete tranquility, it is possible to rely on an ad hoc app that includes all levels of mobility. By entering departure and destination you can choose the ideal transport mix that meets own needs. With a single operation it is therefore possible to use services that are different from one another but perfectly integrated. Gradually the perception of an economic benefit associated with owning a car will go into crisis and it will be much more convenient to rely on on-demand and / or self-driven services considering that with their progressive diffusion, they will become increasingly cheaper. Finally, let's not forget the green factor: more integration, more sharing, less cars, less CO2. The present work shows the evolution in Europe of this concept considering some cases present in the literature and highlights the needs of users at the service of the specific area of implementation

INTRODUCTION

The need of the citizen to move is closely connected to the cause but also to the need to do it with safety and comfort. Various studies in the literature show how infrastructures can increase the users safety [1,2]but also how it is possible to determine levels of walkability that allow primarily to man to move easily with the cheapest way on foot [3,4].

An integrated approach that evaluates the needs of citizens right from the planning stage is fundamental in order to build an optimal MAAS architecture.

Actually, the demand for transport is growing and more and more users are involved in multi-modal movements to reach their destinations. Being time wasters, a variable must be zeroed, each user searches for the most advantageous transport solution both from a temporal point of view that economic.

On the other hand, the offer of public and private transport has spread and is varied.

The technologies and applications now widespread through smartphones and tablets can facilitate modal choice, encouraging the user to use public or shared transport, reducing atmospheric emissions and traffic congestion.

Customers, transport authorities, companies and governments understand the enormous opportunities for mobility within a wider and more integrated system.

It is possible to distinguish different approaches to be pursued for the evolution of the MAAS. In particular the users aimed at improving user needs with innovative, personalized and intelligent mobility services. These seamless transport services work efficiently and provide easy access to mobility, a strong user orientation. In terms of public

sector approach, the information and communication technologies (ICT) improve the effectiveness of the global transport system.

The advantages include the ability to allocate resources efficiently (based on the user's real needs), create new activities and jobs, improve the management of road accidents and have a more reliable transport system through an analysis advanced data.

Finally in terms of business approach, the MAAS is a profitable market for new transport services.

The transport sector and new technologies are products and services that are fundamentally transforming expectations and opportunities of expectations for people and at the same time the market of intelligent mobility is rapidly becoming evolving.

MAAS DEFINITION

Mobility as a service was mainly developed in urban areas with strong public transport networks, which are fundamental for the definition of MaaS offers.

However, the organization of public transport in rural areas with declining population remains a challengeGenerally this approach is founded on:

• Collaboration and combination of various public subsidized transport services (social assistance, national health insurance services, school transport and public transport);
• Develop the attractiveness of public transport using on-demand (and automated) transport services;
• Development of transport service centers using a one-stop-shop principle, which allows the purchase of multiple services through a single user interface with interoperable ticketing;
• Complete traditional transport services with cars and ridesharing.

New opportunities for the transport and traditional infrastructure sectors are part of these innovative service and cooperation concepts Success in some new services markets, including apps for both private vehicle and car sharing, clearly has the potential to interfere with existing urban mobility services and can also encourage a shift to use of car, putting far more sustainable ways aside.

The predominance of individual modes of transport and the low visibility given to public transport in the context of developments and ongoing discussions on mobility as a service are certainly a cause for concern. Secondly, mobility as a service involves higher costs for the user or supplier and unequal services.

The digitization of transport services can create further detachment for less technologically sustainable people, which leads to a widening of the so-called digital divide.

The transport system focuses on an integrated vision, ie the focus shifted from the simple provision of transport services to the question of what the demand for services is, where it is and how to satisfy them more effectively.It takes into account the integration and convergence of services since different types of transport are now an integral part of transport networks.

Walking or cycling are essential parts of the entire system.

The flow chart below explains better this concept.

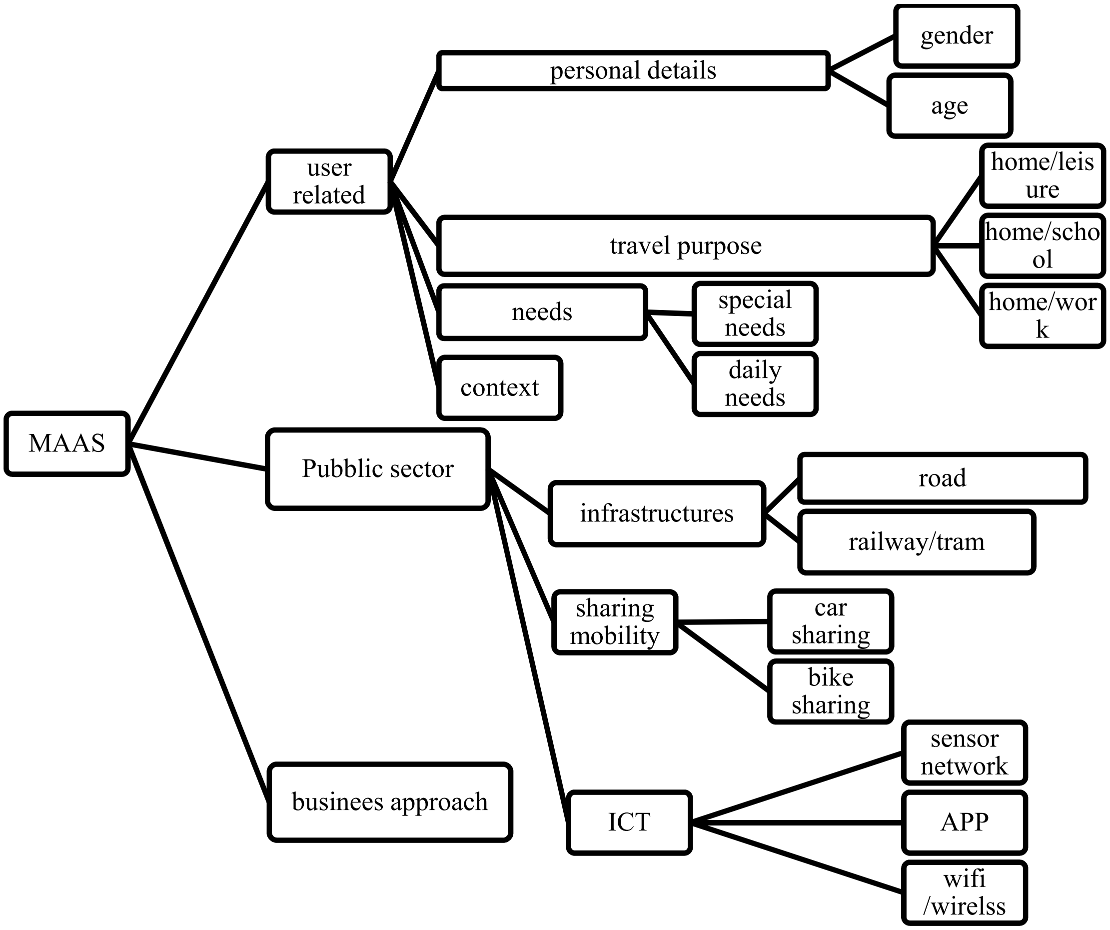

FIGURE 1. MAAS's architecture

Mainly based on software, MaaS is the precursor of "Mobility on Demand" which is specifically designed for hardware and transport services.

The integrated mobility services on demand can contribute to the modal shift towards public transport and also addressing the spatial inefficiencies of private motorized transport.

Focused on the urban user, mobility systems provide users with access to both inter- mediate multimodal mobility on demand with an improvement in overall transport efficiency.

It is possible to select an Intelligent integration of rate structures, data and user interfaces and rolling stock arrangement which requires new business models and scheduling, booking, ticketing etc.

The user experience is also one of the most important parameters during the calibration step with its ability to share information and new business models linked to new technologies and people request.

Furthermore, the development of the vision of transport as accessible and unrestricted: in fact having access to mobility rather than having the means of mobility is transforming the landscape.

Furthermore, the collaborative economy and technological developments will allow users to be more selective together, pursuing this trend.

The use of a combination of technologies in the entire approach makes it possible to put the user and his needs in the foreground with respect to his move: it is the key factor behind these changes.

In order to better understand what is meant by MAAS it is considered appropriate not only to give a definition of the concept of Mobility as a service but also to define the roles of various stakeholders in integrated development mobility services. It is important also to identify of the prerequisites for the development of integrated mobility services both in cities and in rural areas and evaluate user experiences from emerging mobility services in accordance with the flow chart below :

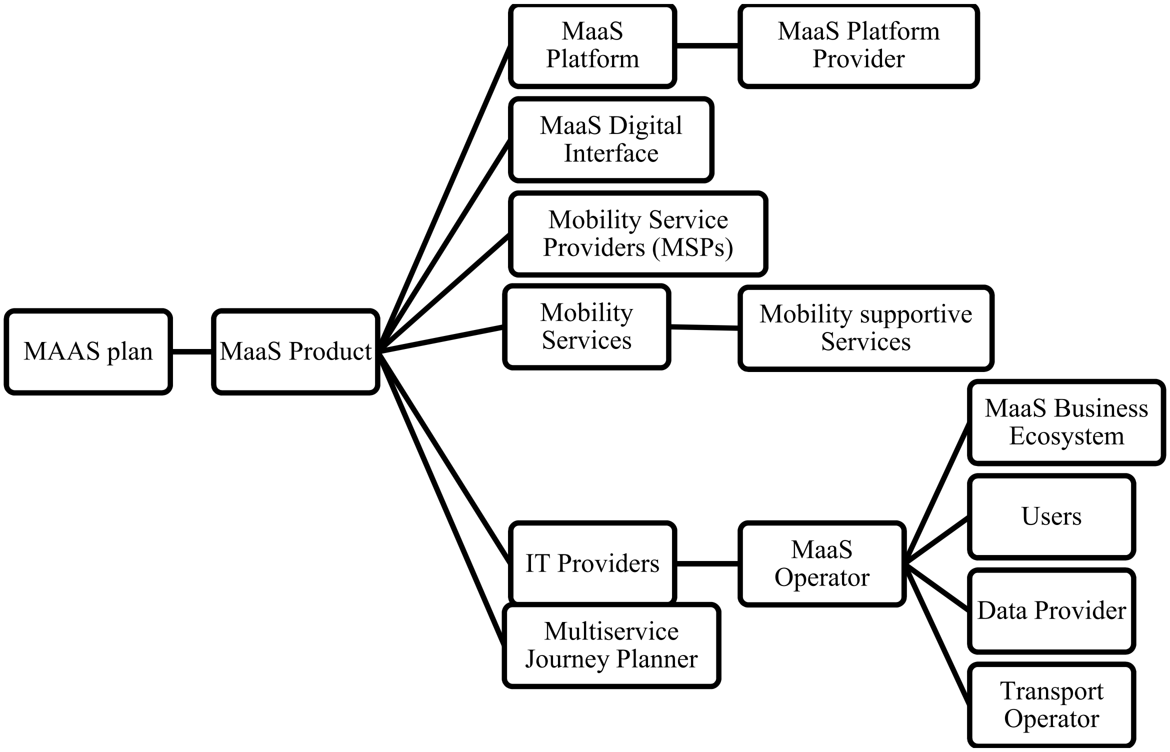

FIGURE 2. MaaS plan

The cooperation of many different actors, public transport companies, operators of shared mobility, telecommunications companies, payment processors, local authorities and urban planning bodies is fundamental for the implementation of shared mobility.

However, unlike the big cities and cities, it is important to remember that still many cities, especially the smaller ones with a small percentage of inhabitants, often of advanced age, are not characterized by continuous transport services[5].

Therefore the spread of sustainable mobility must take place by shaping the service with respect to the places of applicationThese critical issues will lead to an evaluation of the on demand system in order to ensure travel.

The MaaS digital platforms allow the planning of end-to-end trips (literally "from one point to another") by aggregating all the public and private means of transport available in the city and allowing the payment of the service through a monthly subscription or based on use.

By creating and using a single application it is possible to identify, book and pay separately for each means of transport, from public transportation to taxis and travel sharing, from bike sharing to car or scooter sharing. The users' preferences are therefore addressed considering all the parameters made available in real time by the platform, such as for example from weather conditions to traffic conditions up to the cost / duration of the trip. From this point of view, the mobility service is innovative and involves a reduction in the gap between public and private transport operators at city, interurban and national level. This is done through the integration of the currently fragmented tools and services that a traveler must travel considering the daily stages of travel planning with reservation, access to real-time information, payment and ticketing.The use of interviews allows a better understanding of the transport demand thanks to the focus groups in agreement with [6]

In agreement with [7] transport industry demand experts should include in their research not only how a MaaS system as a whole influences travel behavior and car ownership, but also how each component affects the demand for this service. Specifically, in-depth information on the architecture and intuitive design of the MaaS apps is highlighted in turn could increase the intention to use this service. Also, willingness to pay for the MaaS e subscription the willingness to pay for the purchase of a package (such as pay-as-you-go or a monthly / annual package) should be defined.A travel survey tool was created by [8] with smartphone-based guided recall and was extended using information on the actual travel behavior of the respondent. The attributes considered for each transport mode are the plan price and the transferability, which is the option of

taking unused trips with them the following month. In addition to these, innovative features were included and a number of London residents were surveyed. in agreement with [9] even if individuals do not prefer certain modes of transport, including shared mobility, the MaaS product, in fact, can provide sufficient added value to the respondents who would consider buying it.

EUROPEAN EXPERIENCES AND CITIES DEVELOPMENT

The first application took place in Finland, more precisely in Helsinki, where since 2016 where an application called WHIM was created, to plan and book public and private means of transport such as trains, taxis, buses, even cars and shared bicycles.

The objective of this integrated approach is to reduce traffic congestion and noise and air pollution levels. in big cities, the density is progressively increasing.

In cities that adopt a MaaS solution, in fact, a solid physical infrastructure is needed to make the service even more accessible:

The table below summarizes the literature on the subject over the last twenty years, highlighting the countries of implementation

TABLE 1. Literature review considering Maas development in accordance with [10-14]

Authors	Period	Focus	Location
Baliga et al.	2011	Virtual Private Mobile Network Towards MaaS	General
Sochor et al.	2015	Implementation of MaaS Mobility considering Challenges in Integrating User, Commercial, and Societal Perspectives	Gothenburg, Sweden
Karlsson et al.	2016	description of the experiences from a field trial of an innovative travel brokerage	Gothenburg, Sweden
Kamargianni et al.	2016	A critical review of new mobility services for urban transport	General
Melis et al.	2016	Crowd Sensing for smart mobility through a service-oriented architecture	Italy
Kamargianni et al.	2017	The business ecosystem of MaaS	General
Hensher et al.	2017	Potential definition of the future contexts in which bus services might be offered	General
Li et al.	2017	Challenges of implementation and policy required	Europe
Mathyas et al.	2018	The potential of mobility as a service bundles as a mobility management tool	Great London (UK)

However, many countries do not have Maas mobility or applications that can be technologically defined in this sector.Current and above all future transport and mobility services cannot be considered as independent solutions; on the contrary, urbanization in Europe will have to be taken into consideration as a significant fact and therefore, urban strategies aimed at increasing the efficiency of urban resources and decarbonisation.

Furthermore, mobility services and systems will have to interface with multi-sectoral and urban strategies to optimize the use of energy, space, economic and material resources.

The development of cities therefore focuses not on autonomous systems but on integrated systems on a regional, European and global scale with sustainable and efficient connections between urban and extra-urban transport networks under development, including other rail and air transport systems.

Considering the development of Smart Cities, intelligent mobility and transport systems are integrated with a broader integration of urban systems in the fields of energy, public services and intelligent infrastructures [16,17]

In particular, intelligent mobility services must take into account the contribution to wider performance in a smart city, both for renewable energies and electrification strategies, as well as urban management and planning infrastructures.

TRANSPORT USERS NEEDS

Some significant changes in the users of transport systems can be observed in their behavior and lifestyle, influencing the decarbonisation of new service models in the transport sector. In fact, gradually the population is opting for a reduction in the rates of motorization and use of the private vehicle towards the multimodal public or towards shared mobility.

Furthermore, transport users are largely developing the propensity to digitize and use smartphones, mobile web applications and social media.

These behavioral changes are supporting new models, services and markets for shared mobility and transport, which allow greater development of sustainable mobility considering not only the race but also the parking phases [5] or different types of vehicles.

The sustainable integration of users, vehicles and infrastructure creates great potential for multi sectoral and profound optimization impact on decarbonisation. The open flow of data across user infrastructure and domains is an important enabling factor for intelligent mobility service and system innovation; however planning, governance and maintenance of public digital the infrastructure will require public resources and dedicated regulatory frameworks.

European cities are pursuing a range of smart city projects, local emissions regulations (including CO2, NOX and noise) and spatial governance strategies aimed at increasing the complexresource and space efficiency of urban systems and improvement of the general quality of life of citizens. Consider, for example, the relocation of low-emission or congestion charging areas, or to transit and public development spatial reconfigurations that recover road surfaces for other urban and environmental functions.

Cities are also trying to reuse space in the city center dedicated to individual motorized transport for different economic uses. Urban planning and spatial planning will continue to turn into smart cities and mobility systems to evolve. By reducing congestion, pollution and energy use, intelligent mobility solutions can simultaneously reduce the cost of travel but also lead to faster exurbanization

Smart urban design and spatial governance are increasingly enabling the design of alternative vehicles
and a transition to individual micro-motorization not based on cars with small and light dimensions and low speed

The adoption of MaaS will therefore have to consider a combination of multiple aspects. In fact, it will have to focus on a service with sufficient added value, which provides an economically viable alternative without having to compromise (too much) on their needs for autonomy, flexibility and reliability is essential. Access to the service by all sections of the population is fundamental.

Furthermore, mobility packages could be used to influence travel behavior patterns, altering the way people perceive travel alternatives rather than physically altering alternatives. This could stimulate the use of more sustainable methods, in particular shared mobility modes.

Skills, values, age and place of residence and other socio-economic, socio-demographic and cultural characteristics can play a role in the adoption of MaaS and potential subsequent changes in travel behavior. In agreement with [19] the role of young people results in this development, since it is the part of the population that most closely approaches the development of these trends in society.

First, today's youth show different attitudes and behavior towards car ownership and driving. Despite the growing global trend of both overall travel and car ownership of young people tend to drive less and this will probably do increase their demand for alternative mobility solutions like MaaS. Secondly, young people are the first to adopt new technologies [20] and are the first generation that has not lived a life without a mobile phone. Their lifestyle, in which the mobile is often constantly present, has both reduced the demand for some type of travel, due to a change in the way they socialize, but has also increased the demand for a transport system in which in addition to travel displacement is essential where it is possible work, write messages or talk on the phone The travel behavior of young people today will persist when they pass to adulthood and then the development of MaaS according to the needs and visions of young people could have the potential to increase use at long-term and adoption of such mobility services. Furthermore, current research on mobility and travel behavior has been conducted on adult populations while the travel behavior of young people is limited.

CONCLUSIONS

The current scenario of mobility is characterized by numerous technological, organizational and cultural innovations that are found in the definition of "Mobility-as-a-Service" (MaaS), or rather the idea that transport will be increasingly organized around the "service" of mobility rather than the "medium" to be used.Conceptually simple and technically feasible with the development of adequate digital platforms for the optimization of travel solutions, this transition has however complex, objectively “revolutionary” organizational, technological and cultural implications. In fact, some traditional pillars of the current balance between transport demand and supply will lose relevance: the individual ownership of the vehicle, the clear differentiation of the segments of the offer (the bus service, the taxi service, the rental service...), the option “single-mode ". From literature it is clear that they will dominate the "watchwords" of integration, sharing, flexibility, optimization, inter / multi-mode. All lines of progression that will be sustained by an intensive use of digital devices (platforms, apps, aggregators, etc.), by a radical change in the offer players and the products / services put on the market, by a technological leap in vehicle handling (electric traction, autonomous driving...). In terms of generating new economic, social and environmental costs, the process is not without risks for the community as a whole and for the individual citizen-user. For example, the aforementioned "travel solution optimization" could push citizens to choose the car (their own or shared), even for only one leg of the journey, because it is more functional in terms of time and / or costs to reach the desired destination But perhaps the most dangerous risk is a potential social cost. It is the risk connected on the one hand to the node of the digital divide and on the other, on the territorial level, to what we can call the "mobility divide". In Italy a majority share of the population does not use info-mobility devices for travel by public transport, a fact inevitably correlated above all with the age of the citizens and, to a lesser extent, with the size of the municipalities of residence (those who live in large cities use more info-mobility services). This segment of the population would be cut off from access to the hyper-digitized infrastructure that powers the new system.

As for the mobility divide, the dominant concentration of innovative services in a few large urban centers is likely to widen the gap - already very marked today - between North and South and, even more, between small and large centers, in availability and use of sustainable mobility solutions.

REFERENCES

1. C. Gruden, T. Campisi, A. Canale, G. Tesoriere and M. Sraml, “A cross-study on video data gathering and microsimulation techniques to estimate pedestrian safety level in a confined space” (IOP Conference Series: Materials Science and Engineering, Vol. 603, No. 4, 2019, p. 042008)
2. I. I. Otković, H. Krstić and M. Zagvozda, “The Comparison between the Risk Perception of Drivers and Statistic Indicators of Traffic Safety in the Analysis of Effects of Reconstruction of Selected Urban Intersections” (26th ICTCT Workshop on: Sustainable and safe road design from a human behaviour point of view-Challenges for interdisciplinary work in road safety, 2013)
3. T. Campisi, A. Canale and G. Tesoriere, “SWOT analysis for the implementation of spaces and pedestrian paths at the street markets of Palermo” (AIP Conference Proceedings, Vol. 2040, No. 1, 2018, p. 140003)
4. T. Campisi, A. Canale, G. Tesoriere, I. Lovric and B. Čutura, “The Importance of Assessing the Level of Service in Confined Infrastructures: Some Considerations of the Old Ottoman Pedestrian Bridge of Mostar” (Applied Sciences, 9, 8,2019, 1630)
5. S. Farrell, D. McNamara and B. Caulfield, “Estimating the potential success of sustainable transport measures for a small town” (Transportation Research Record, 2163, 1, 2010, 97-102)
6. M. Kamargianni and M. Matyas, “The business ecosystem of mobility-as-a-service” (Transportation research board, Vol. 96, 2017)
7. M. Kamargianni, W. Li, M. Matyas, A. Schäfer, “A critical review of new mobility services for urban transport” (Transportation Research Procedia, 14, 2016, 3294-3303)
8. M. B. Matyas and M. Kamargianni, “Stated preference design for exploring demand for “mobility as a service” plans” (2017)
9. M. Matyas and M.Kamargianni, “The potential of mobility as a service bundles as a mobility management tool” (Transportation, 2018, 1-18)
10. A. Baliga, X. Chen, B. Coskun, G. de los Reyes, S. Lee, S. Mathur and J. E. Van der Merwe, “VPMN: virtual private mobile network towards mobility-as-a-service” (Proceedings of the second international workshop on Mobile cloud computing and services, 2011, pp. 7-12)

11. J. L. Sochor, H. Strömberg and M.Karlsson, “Challenges in integrating user, commercial, and societal perspectives in an innovative mobility service” Proceedings of the 94th Annual Meeting of the Transportation Research Board, Washington, DC, 2015)
12. I. M. Karlsson, J. Sochor and H. Strömberg, “Developing the ‘Service’in Mobility as a Service: experiences from a field trial of an innovative travel brokerage” (Transportation Research Procedia, 14, 2016, 3265-3273)
13. A. Melis, S. Mirri, C. Prandi, M. Prandini, P. Salomoni and F. Callegati, “Crowdsensing for smart mobility through a service-oriented architecture” (2016 IEEE International Smart Cities Conference, 2016)
14. D. A. Hensher, “Future bus transport contracts under a mobility as a service (MaaS) regime in the digital age: Are they likely to change?” (Transportation Research Part A: Policy and Practice, 98, 2017, 86-96)
15. Y. Li and T. Voege, “Mobility as a service (MaaS): challenges of Implementation and Policy Required” (Journal of transportation technologies, 7, 02, 2017, 95-106)
16. H. Schaffers, N. Komninos, M. Pallot, B. Trousse, M. Nilsson and A. Oliveira, (2011, May). “Smart cities and the future internet: Towards cooperation frameworks for open innovation” (The future internet assembly, 2011, pp. 431-446, Springer, Berlin, Heidelberg)
17. V. Torrisi, M. Ignaccolo and G. Inturri, “Innovative Transport Systems to Promote Sustainable Mobility: Developing the Model Architecture of a Traffic Control and Supervisor System” (International Conference on Computational Science and Its Applications, 2018, pp. 622-638, Springer, Cham)
18. M. Pitsiava–Latinopoulou, S. Basbas, K. Papoutsis and E. Sdoukopoulos, “Parking policies for supporting sustainable mobility” (Procedia-Social and Behavioral Sciences, 48, 2012, 897-906)
19. M. Johansson, “Mobility as a service: exploring young people’s mobility demands and travel behavior” (2017)
20. E. Blumenberg, et al., “What´s Youth Got To Do With It? Exploring the Travel Behavior of Teens and Young Adults” (UC Berkley: University of California Transportation Center, Los Angeles, 2012)

The Surrogate Safety Measures Evaluation of a Staggered Crossing on the Delta Area of Rijeka

Tiziana Campisi[1,a)], Iva Mrak[2,b)], Antonino Canale[1,c)], Giovanni Tesoriere[1,d)]

[1]*University of Enna "Kore" - Faculty of Engineering and Architecture – Cittadella Universitaria 94100 Enna (EN) - ITALY*
[2]*University of Rijeka - Faculty of Civil Engineering, Građevinski fakultet. Radmile Matejčić 3 51000 Rijeka-CROATIA*

[a)]Corresponding author: tiziana.campisi@unikore.it
[b)]iva.mrak@gradri.uniri.hr
[c)]antonino.canale@unikore.it
[d)]giovanni.tesoriere@unikore.it

Abstract. The causes of accidents in the crossings are many and cannot be alone traced back to the "irresponsible" action of the pedestrian, but should instead be sought above all in the failure to plan urban pedestrian itineraries, in the disorderly organization of the urban functions, in poor vehicle traffic planning and in the poor quality of road infrastructure design.The presence of pedestrian areas allows greater safety during the crossing, especially for users with reduced mobility or for the elderly as they provide a protected area where they can stop especially if the crossing is wide and the pedestrian traffic light cycle has a phase of reduced green.Generally the area bounded by the perimeter of the island is forbidden to the circulation of all vehicles, but can be used by pedestrians as a refuge for crossing the roadway, when the island is affected by a pedestrian crossing.The present work shows a comparison of traffic and safety scenarios hypothesizing the addition of a pedestrian island in an urban area of the city of Rijeka characterized by a very wide pedestrian crossing and by large pedestrian and vehicular flows. The traffic level of service level (LOS) and the surrogate safety parameters with and without the pedestrian area were evaluated through microsimulation of traffic.

INTRODUCTION

Pedestrian safety is one of the most debated research topics and deserves an in-depth assessment especially if they regard people with disabilities. The increase in vehicular traffic leads to an increase in the probability of conflicts during the crossing phases. Different road geometries in urban areas are used to reduce the points of conflict as they allow a sorting of the flow and a reduction in speeds, for example in unconventional roundabouts[1][2].

If it is not possible to change the geometry for economic or spatial reasons, it is possible to intervene by inserting pedestrian islands in the crossings characterized by high vehicular and pedestrian flow with reduced pedestrian green times. This strategy allows pedestrians to cross in two stages, protecting themselves from inside the protective area.The pedestrian island is the part of the road, suitably delimited and protected, destined to shelter and stop pedestrians during the carriageway crossing. Its function is to divide and separate the sections of road to cross, with the goal of increasing the safety and protection of pedestrians who are about to cross it [3][4]

The island reduces the time spent by pedestrians on the roadway where the conflicts between pedestrian and vehicle occur, and causes conflict with one single current of traffic at a time. It can also be of help in determining the optimal duration of the traffic light phases[3];for example: in case of traffic lights cycles of excessive duration (> 120 sec), the insertion of a life preserver island, with the reduction of pedestrian green times, can allow a reduction in the duration of the cycle, even if the pedestrian is forced to cross in two stages. It also represents a channeling of traffic currents, resulting in a reduction in the speed of vehicles in transit, with further benefits for security.In the literature there are several works on the evaluation of road safety and on the level of service linked to the road

geometry [5],crossings [6][7]]or of confined spaces always linked to pedestrians[8][9]or spaces characterized by large pedestrian flows in transit such as airport terminals[10] Different sensor-based technologies are applied in signalized crossings and not to increase the safety of weak real-time users[11][12].

DESCRIPTION OF CURRENT ASL IN EUROPE

It should also be pointed out that in many European countries the construction of a pedestrian crossing is based on a fluxogram that takes into account both pedestrian and vehicular flows, when the width of the crossing exceeds the two lanes, a pedestrian island is implemented. The Federal Highway Administration (FHWA), in its official document Sidewalks devotes an entire chapter to the correct layout of the various elements that make up a pedestrian crossing, giving information on: vertical and horizontal signs, island life buoy, sidewalk, ramp, crossing time and tactile route. A purely geometric analysis of the stretch of road involvedis required to implement a pedestrian crossing. In particular the study of the number of lanes to cross is required because it influences the length of the crossing for pedestrians and the choice to build, or not, a pedestrian island in the middle. The life preserver island is advisable in the case of crossing more than 3 lanes , however, it is mandatory in the case of more than 4 lanes to cross. It is also mandatory in the longitudinal slope of the pedestrian crossing (which corresponds to transversal slope to the direction of travel of the vehicles - it is advisable that this value not exceed 5%; higher values represent an obstacle to the accessibility of weak users) or cross slope of the pedestrian crossing (which corresponds to the slope longitudinal to the direction of travel of the vehicles - it is advisable that this value not be lower than 2%, to guarantee the outflow of rainwater over the section used for the crossing itself).

Particular attention must be paid to the analysis of the visibility distance (Dv): i.e. the length of the part of the road that the driver of the vehicle can see in front of him when driving along a road, rather than the distance required to stop the vehicle.

The construction of a life preserver island is advisable in the case of pedestrian crossing with more than three lanes and, in any case, it is mandatory in the case of a crossing of more than five lanes.

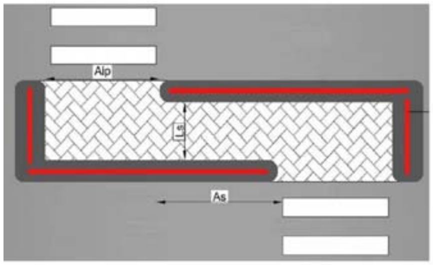

Legend
Aip= crossing width
Ls= island depth
As= net offset of pedestrian crossing
Red line =protection railing

FIGURE 1. Geometrical details of staggered crossing

The sizing of the pedestrian area must be proportional to the extent of the flows of pedestrians who engage it; precise indications are required for their design especially from the point of view of horizontal and vertical signs like described on figure below :

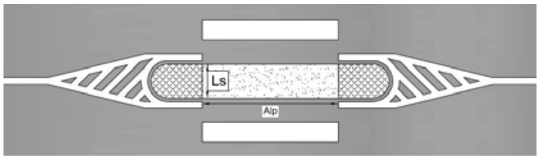

Legend
Aip= crossing width
Ls= island depth

FIGURE 2. Classic pedestrian islands at grade

In the different European and non-European countries, which are specifically regulated on pedestrian crossings and on pedestrian areas that dictate specific measures as shown in the summary Table 1

TABLE 1. Comparison of geometrical details related to pedestrian island in accordance with different rules

State	Standard	Pedestrian Islands	Passage width (Aip)
Italy	sized according to pedestrian flow and footprint of wheelchair	1.20 m (MIN) 2.50 m (MIN) for staggered crossing	at least as much as the width of thepedestrian crossing
Swiss	variablewith the flow of pedestrians and depending on the presence of the traffic light	from 1.50 to 5.00 m 2.00 m recommended	
UK	sized so that the adjacent lanes		not wider than 3.50 m
Croatia	For 3 or more lanes Coordinated by regulation on accessibility	1,8m (MIN) central part at least 1,5mat level with the road or with ramps	3 m
UnitedStates		1,50 m (raccommended) 1,22 m (MIN)	0,91 m (MIN)
Australia	at least as wide of the strips	2,40 m (MIN)	
India	at least as wide of the strips	from 1.20 to 2.20 m 1.50 m (MIN) Pedestrian island (if plants are present)	
New Zeland		1.80 m (MIN) Pedestrian area 2.00 m (recommended)	1,50 m (MIN)

In particular, the approach of a pedestrian area and its better visibility is enhanced by:

- continuous white stripes, of sufficient length and appropriate zebra pattern, in the part of road paving that precedes the head of the island;
- appropriate elements protruding from the road surface in the zebra zone;
- vertical stripes, yellow reflective and black, at the edges of the pedestrian islands;
- yellowown light or reflected light devices at the headers of the pedestrian area.

The pedestrian area is recommended in the satin type, at road level. Pedestrian areas are better raised only in case of depths greater than 3.50 m, which allows for a space necessary for the correct realization of the two access ramps for strollers and wheelchair users.Of particular interest is the so-called "staggered crossing" solution, which includes one longitudinal offset, in the direction of travel of the vehicles, of the two sections that the pedestrian must cross and the construction of a suitable central island, adequately protected, where the pedestrian is safe during the period between the first and the second section crossing.The realization of this type of pedestrian island, allowing a large waiting area, it is recommended when pedestrian flows are high. Moreover, in case of high vehicular and pedestrian flows, it is preferable for the protection of pedestrians, against vehicles in transit, to use separation railings at least 1.00 m high, as an alternative to curbs.

METHODS AND RESULTS

The present study analyzes the traffic light intersection located in Rijeka, Croatia, near the Delta area in the city center, characterized by a high pedestrian component that from 2020 will become even greater due to the location of many events for Rijeka European Capital of Culture. The study shows how the inclusion of two different pedestrian islands can increase pedestrian safety, comparing actual and supposed scenarios in terms of Level of Service of the road. The analyzed intersection is located in the area of the Delta in Rijeka between the main direction of the vehicular flow of the Ivana Zajca /Brajdica road and the secondary direction of the Ribarska / Wenzelova street and is characterized in the main direction by the presence of the pedestrian crossing analyzed along 28,15 m.

The area near the intersection is characterized by the presence of the open-air market and the municipal theater. These are main attractors for pedestrian flows together with the Exportdrvo area and the neighboring parking lot.This area is undergoing big changes (especially Exportdrvo area) related to Capital of culture activities and will

be subjected to an increase in pedestrian flows from 2020 as several events belonging to the "Rijeka Capital of Culture" will be located in the Exportdrvo building and in the Delta area.The traffic light cycle is of 100 seconds with 25 seconds of pedestrian green, 65 of pedestrian red and 10 of yellow.The pedestrian flows recorded in the rush hour amount to around 420ped / h, while the vehicular flow related to 1300-1500veh / h on weekdays and holidays with a composition related to 70% of light vehicle, 10% of heavy vehicle, 10% of bus and 10% of other types.The pedestrian composition analyzed during the month of June-July 2019 is made up of 50% of men and 50% of women (with up to 65% of men during Sunday mornings) with a large percentage of elderly people. An image of the analyzed intersection is shown below.

FIGURE 3. Monitored zebra crossing without pedestrian islands

The comparison of the current and hypothetical scenario was made possible through the use of the VISSIM / Viswalk software based respectively on the car following model of Wiedemann [13] and the social force model of Helbing [14]. The micro-simulation was based on a first phase of implementation of the scenario, a second phase of the calibration of the system and a third phase of acquisition of the outputs and comparison of the same.The images below show the names of the areas examined with the various directions.The micro-simulation can facilitate the choices of the best design solution in a preventive manner and become a useful tool for administrations together with the implementation of the BIM which is a method for optimizing the planning, construction and management of constructions through the help of a software in agreement with [15] Both micro simulation and BIM can be related to each other through output files.The intersection is linked to the 4 directions described on figure 2 below

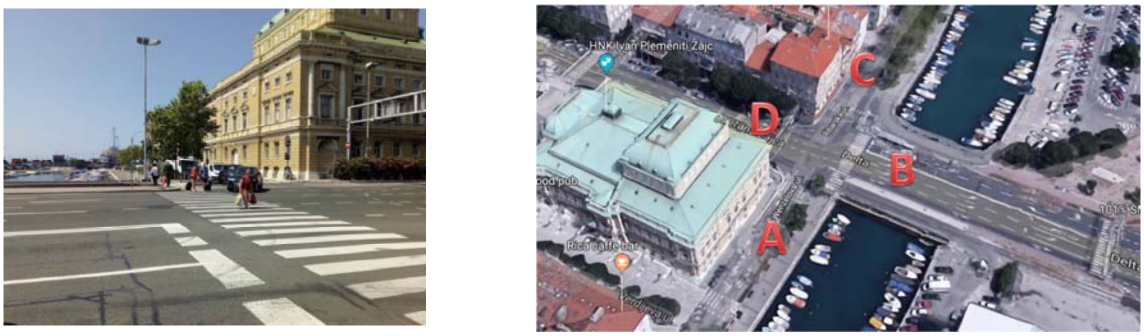

FIGURE 4. Monitored intersection and definition of each arms

Through the files with the trj extension it was possible to evaluate the quantity and type of conflicts for the two scenarios, finally reaching the evaluation of the Time to Collision (TTC) and the Post encroachment Time (PET)in accordance with [15]. The comparison of the three different scenarios, considering both a weekday and a holiday has been summarized in the table below in which it is possible to view the geometries considered along the 4 arm of the monitored crossing, maintaining constant the vehicular and pedestrian flow values recorded through the monitoring in June 2019.

TABLE 2. Definition of observed and supposed scenarios

Scenarios	Description	Weekday/Holiday	Scenario geometrical details
1stW	Monitored condition on actual site	Weekday	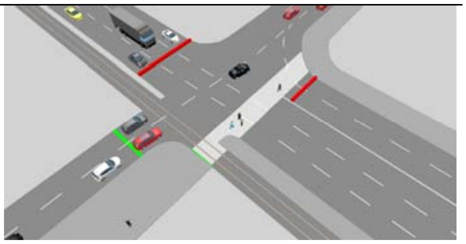
1stH	Monitored condition on actual site	Holiday	
2nd W	Scenario hypothesis with classic pedestrian islands at grade	Weekday	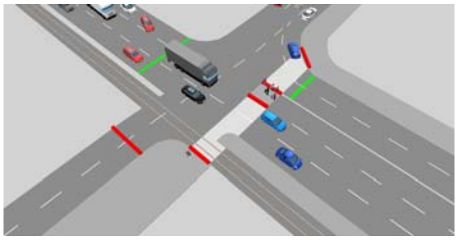
2nd H	Scenario hypothesis with classic pedestrian islands at grade	Holiday	
3rdW	Scenario hypothesis with staggered crossing	Weekday	
3rdH	Scenario hypothesis with staggered crossing	Holiday	

The results shown in Figure 3show the average and maximum variation of the length of the queuestaken along three of the intersection arms.The arm A has the maximum average length values of the queues comprised between 13 and 35 vehicles in the queue while in terms of maximum value the arm D assumes the highest values

The outgoing vehicle traffic from arm C does not affect the overall service level of the infrastructure examined before and after the insertion of two new types of crossing. On the contrary the remaining three arms are characterized by an average length of the queues of about 40 m along the arm A while the maximum length of things is on the arm D. These results are connected to the monitored vehicular flows which are huge in entry and exit from arm D.

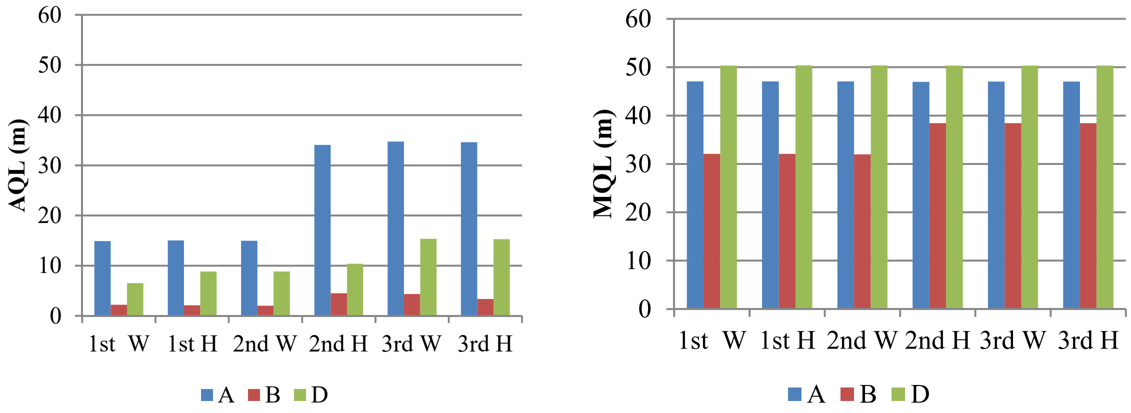

FIGURE 5. Comparison of AQL(left) and MQL (right) considering different scenarios

The evaluation of the LOS was made considering the values ranging from A to F (and therefore from infrastructure with excellent traffic circulation to congestion infrastructure and reduced safety and driving comfort) according to the HCM2000 [16]From the comparison of the LOS it is shown that the presence of the two islands leads the LOS from values of B to values of Eespecially on arm A with the insertion of the islands and the evaluation during the holidays.In arms B and D,like defined on the previous figure, the presence or absence of the pedestrian area does not entail a substantial change in the level of service like described on Figure 6 below.

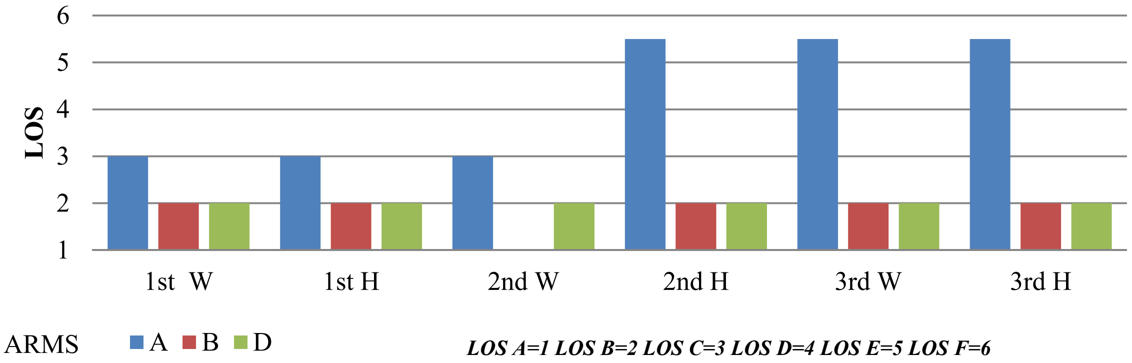

FIGURE 6. Comparison of LOS considering different scenarios

In addition the scenarios were compared through the estimation of the PET and TTC parameters, obtaining for the first values equal to 1,5s andfor the second equal to 2,3-2,5.

In general, only encounters with a minimum TTC less than 1.5s are considered critical and trained observers appear to operate rather consistently in applying this threshold value. In addition, the possible types of collision were analyzed, arriving at what is shown in the graphs in figure 7.

The scenario that has the greatest number of collisions in total is the second in festive conditions, especially in terms of both rear end and lane change.

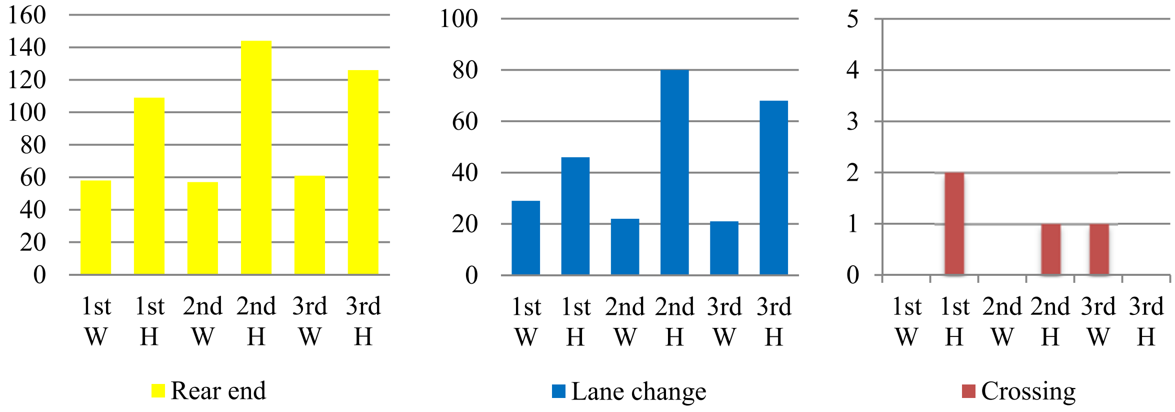

FIGURE 7. Comparison of different collision type linked to each scenarios

Furthermore the distribution of the aforementioned possible collisions in the various scenarios as described below.

Scenarios	*Collision type*	*Total accident distributions for each scenario*
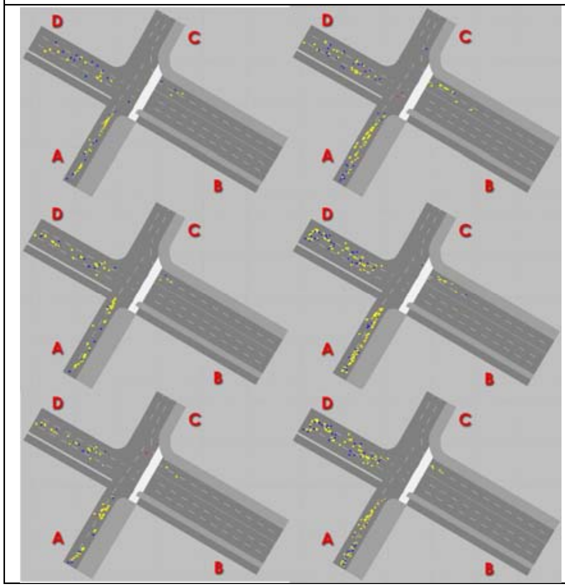	*Yellow* Rear end	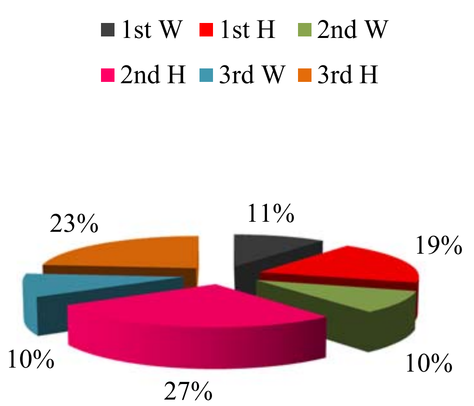
	Blue Lane change	
	Red Crossing	

FIGURE 8. Distribution of the possible collisions in the various scenarios

CONCLUSIONS

During the monitoring phase, up to 7,7% (and on average 5,6%) of all pedestrians were elderly persons with visible difficulties of movement. Also persons with mobility issues (wheelchair users, crutch users…) comprised on average 1,2% of pedestrians which is quite below the general share of these groups in general population (where the persons with disabilities represent 8,1% of the population of the County, and where 22,3% of the population +65 present some kind of disability)[17]

This dataindicate that these groups were underrepresented in thepedestrians on the crossing which can probably be related to both the issues at this particularcrossing (dynamic cycles with often not adequateduration of green pedestrian lights) and general issues with using public space.

The proposed modifications improve highly the LOS for the pedestrians while simultaneously allow for high quantity of traffic.

The inclusion of a protected crossing can mainly affect the safety of pedestrians, especially in a long crossing.

The presence of a greater number of pedestrian flows, and in particular of the elderly can be evaluated as the next step of analysis, leading to more exhaustive results in the conditions of slow and reduced mobility.

The improvement of the traffic light cycle with a cracking of the pedestrian green will have to be correlated to the choice of one of the two solutions, both at low cost, and also connected to a more in-depth study of the vehicular flows in order to be able to guarantee high levels of service of vehicular traffic and pedestrian.

REFERENCES

1. G. Tesoriere, T. Campisi, A. Canale and T. Zgrablić, “The Surrogate Safety Appraisal of the Unconventional Elliptical and Turbo Roundabouts” (Journal of Advanced Transportation, 2018)
2. I. I. Otković, T. Tollazzi and M. Šraml, “Calibration of microsimulation traffic model using neural network approach” (Expert systems with applications, 40,15, 2013, 5965-5974)
3. S. Šurdonja, M. Cuculić, I. Pranjić, A. Deluka-Tibljaš and M. Renčelj, “Analysis of the possibility of improving safety in pedestrian crossings areas outside the crossroads-example of the city of Rijeka” (6. hrvatski kongres o cestama, 2015)

4. E. Paschalidis, I. Politis, S. Basbas and P. Lambrianidou, “Pedestrian compliance and cross walking speed adaptation due to countdown timer installations: A self report study” (Transportation research part F: traffic psychology and behaviour, 42, 2016, 456-467)
5. S. Šurdonja, A. Deluka-Tibljaš and S. Babić, “Impact of design elements on roundabout level of service” (Zbornik radova Građevinskoga fakulteta Sveučilišta u Rijeci, 14, 2011, 295-314)
6. J. Yang, W. Deng, J. Wang, Q. Li and Z. Wang, “Modeling pedestrians’ road crossing behavior in traffic system micro-simulation in China” (Transportation Research Part A: Policy and Practice, 40(3), 2006, 280-290)
7. Y. Li and G. Fernie, “Pedestrian behavior and safety on a two-stage crossing with a center refuge island and the effect of winter weather on pedestrian compliance rate” (Accident Analysis & Prevention, 42, 4, 2010, 1156-1163)
8. T. Campisi, A. Canale, G. Tesoriere, I. Lovric and B. Čutura, “The Importance of Assessing the Level of Service in Confined Infrastructures: Some Considerations of the Old Ottoman Pedestrian Bridge of Mostar” (Applied Sciences", 9, 8, 2019, 1630)
9. L. Jian, Y. Lizhong and Z. Daoliang, “Simulation of bi-direction pedestrian movement in corridor” (Physica A: Statistical Mechanics and its Applications, 354, 2005, 619-628)
10. G. Tesoriere, T. Campisi, A. Canale, A. Severino and F. Arena, “Modelling and simulation of passenger flow distribution at terminal of Catania airport” (AIP Conference Proceedings, Vol. 2040, No. 1, 2018, p. 140006)
11. G. Pau, T. Campisi, A. Canale, A. Severino, M. Collotta and G. Tesoriere, “Smart Pedestrian Crossing Management at Traffic Light Junctions through a Fuzzy-Based Approach” (Future Internet, 10, 2, 2018, 15)
12. T. Giuffrè and G.Tesoriere, “Implications of Adaptive Traffic Light Operations on Pedestrian Safety” (IOSR J. Mech. Civ. Eng, 13, 2017, 58-63)
13. R. Wiedemann, “Simulation des Strassenverkehrsflusses. Wiedemann” (1974)
14. D. Helbing and P. Molnar, “Social force model for pedestrian dynamics” (Physical review E, 51, 5, 1995, 4282)
15. G. Acampa, N. Bona, M. Grasso and D. Ticali (2018, November). “BIM: Building information modeling for infrastructures” (AIP Conference Proceedings, Vol. 2040, No. 1, 2018, p. 140008)
16. T. Campisi, G. Tesoriere and A. Canale, “The variability of Level Of Service and Surrogate Safety Assessment of urban turbo-roundabout with BRT system” (JMEST Journal of Multidisciplinary Engineering Science and Technology, 2018)
17. H. C. Manual, Highway capacity manual. (Washington, DC, 2, 2000)
18. Hrvatski zavod za javno zdravstvo, Izvješće o osobama s invaliditetom u Republici Hrvatskoj, Zagreb, 2013

The Developing Benefits of the Advance Space Line (ASL) Systems for Planning Safer Traffic Light Intersections

MarkoRenčelj[1,a)], Tiziana Campisi[2,b)], Antonino Canale[2,c)], Giovanni Tesoriere[2,d)]

[1]University of Maribor - Faculty of Engineering and Architecture - Smetanova 17, 2000 Maribor-SLOVENIA
[2]University of Enna "Kore" - Faculty of Engineering and Architecture – Cittadella Universitaria 94100 Enna (EN) - ITALY

[a)]marko.rencelj@uni-mb.si
[b)]Corresponding author: tiziana.campisi@unikore.it
[c)]antonino.canale@unikore.it
[d)]giovanni.tesoriere@unikore.it

Abstract. The safety of the road vulnerable users is the subject of recent research, considering not only different strategies applied to priorities but also to road geometries, with particular reference to crossings and waiting areas adjacent to traffic light lanterns.This document presents an exploratory study of bicycle boxes considering some European and American case studies. The bicycle boxes, also known as advanced stopping lines or advanced stopping boxes, have been installed to increase the visibility of the cyclists and reduce the conflicts between motor vehicles and cyclists, in particular in the potential situations of "right hooking". A bicycle box is a space of the traffic light intersection located between the walkway, and the stop line of the vehicle used to supply the cyclists a dedicated space to wait for the signal during the red light intersections. In this area the positioning of the cyclists in view of the vehicle stop improves visibility and reduces conflicts between all users. They also provide cyclists with an initial advantage cross the intersection, which helps make cyclists turn difficult and improves safety and comfort due to the difference in acceleration rates between bicycles and motor vehicles. It allows a cyclist to be in front of motor vehicles, which is not the case it only improves the visibility and awareness of motorists, but allows cyclists to "reclaim the lane" if desired. Both the reversal of motor vehicles and bicycles in pedestrian crossing decreased significantly at the points where the bicycles were located compared to the control intersections. Bike boxes have had mixed effects on the invasion of motorists on the bike path. The number of conflicts observed at the pit stations has decreased, while the total number of cyclists and motor vehicles has increased, promoting a safer crossing. Starting from the comparison of case studies examined in the literature of the last 20years, an attempt was made to define the benefits and criticalities produced by this implementation, reporting all of them to a SWOT analysis useful in the preliminary design phase but also a simple control tool.

INTRODUCTION

Vulnerable road users such as pedestrians and cyclists risk their safety in road infrastructures. Many studies, however, have led to the definition of design choices that have brought to the fore the presence of these traffic components, limiting potential conflicts with the vehicle component[1,2].

Among the solutions adopted in recent years there are the preferential lanes for cyclists [3]or the transformation of traffic light intersections and not into single-lane roundabouts of the traditional type [4]or in turbo roundabout[5,6]

A bicycle box or ASL is a designated area at a signalized intersection between an advance stop line and the intersection stop line, intended to provide bicycles a space in which to wait in front of stopped motor vehicles during the red signal phase so that they are more visible to motorists at the start of the green signal phase.Slow mobility is

the subject of new transport policies not only in terms of road safety but also in terms of environmental sustainability with the reduction of atmospheric emissions to zero.In some countries and particularly in some cities, cycling is a frequently used means of transport.

To mitigate accidents, bicycle facilities are included, such as cycle paths (separated by curbs) and cycle paths (separated by road) with painted lines). However, studies have shown that cycle paths do not improve cyclists' safety Among the accident scenarios that concern cyclists, a higher percentage is highlighted of cornering accidents compared to intersections without cycle lanes Incidents are more numerous in the intersections reported Bicycle lanes are less safe for cyclists on stretches of road than both bike lanes and no bicycle facilities, but the bike paths seem to have no influence on the number of injured cyclists at intersections compared to no cycle structure

In accordance with [7] asmall increase still exist in terms of the number of injured cyclists and cyclists mopeds at intersections and on road sections after the construction of cycle paths.

The differences in the effects on the safety of bicycle lanes and cycle paths suggest that, although the bicycle facilities are shown more accidents involving cyclists at intersections, some layouts may be safer than others. Previous studies have mainly has compared various geometric layouts of the cycle structures at the intersections indicated assuming the best layout it is safer for cyclists regardless of the volume of traffic and therefore has compared layouts with different traffic volumes by controlling these differences So far, only a few studies have evaluated the risk of cyclists for different bicycle systems that use variable traffic volumes.In general, the best layout of bicycle structures depends on the volume of traffic at the intersection, although the literature is not present in ranges that include the most correct value to associate with good design Good cycling patterns separate cycling, temporally and / or spatially, in the main junctions, or involve a reduction in the levels of car traffic to the point where the ASLs are redundant. In some countries such as the Netherlands the ASLs are disappearing because the maximum threshold of car traffic for their use is roughly equivalent to the point at which road signs can and must be removed. Even if the advanced stop lines work, they do it only part-time. When road signs are green, they offer absolutely no advantage: they are just a large area painted on the ground.

When road signs are red, anyone who does not wish to be in a potentially dangerous situation must go through a complex evaluation process, judging the risk of attempting to reach the ASL.

The problem is that human beings are fallible and will make wrong decisions or errors on trying to reach the ASL or on safe waiting. Impatience cannot be designed by the man who promotes progress.

ASLs represent a very poor way of trying to address that human fallibility, especially because they can encourage bad decision-making and do nothing to prevent dangerous outcomes [8,9,10]

In agreement with [11]the safety of cyclists for commonly used was compared layout of bicycle structures at marked intersections to assess which layout is better at various traffic volumes and to be developed methods to facilitate this comparison. Moving transport has often been considered as a mode of transport - rather than taking a whole of transport approach, ie integrated transport.It is more critical that proper integration is to support and resource constraints. In accordance with [12] five critical success factors are identify for integration:

- Institutions - to ensure the right transport choices are made for commuters;
- Infrastructure - to ensure that commuters can enjoy the most convenient travel experience possible;
- Network - to ensure commuter can make a joined up journey from origin to destination;
- Making informed decisions before and during their journey;
- Fares to ensure commuters are not penalized for making the most efficient use of an integrated transport system.
- Passenger transport functions need to be vested in a single agency which is responsible for policy, planning, pricing, and operations across modes.

AMERICAN AND EUROPEAN CASE STUDY

Modes must physically connect as seamlessly as possible, especially way finding and integration of transport and commercial precincts. Connecting services is also critical - bus services meet train services etc. The move to turn up and go high volume routes is also important to reduce the reliance on timetables. Providing intermodal journey information is becoming easier with smartphone apps, especially when real time service information is embedded.Active transport modes, such as walking and cycling are very effective alternatives for shorter journeys and need to be part of the strategy. To be a truly integrated transport system requires a regular review of the existing and proposed transport infrastructure and services - not just the incremental additions.

An ASL is a space dedicated to bicycles and located between the pedestrian crossing and the stopping line of the vehicle used to provide cyclists with a dedicated space to wait during the red light at intersections with traffic lights.

FIGURE 1. Some examples of ASL in Europe

In general, this area allows cyclists to wait in front of the vehicular traffic that awaits the traffic light green, improves visibility and reduces conflicts between all users.

Cyclists are also facilitated in traversing the species in performing difficult turning movements and improves safety and comfort due to the difference in acceleration rates between bicycles and vehicles. Bicycle boxes also offer more space for more cyclists waiting at a red light instead of being tied to a bike path. In Boston, the first bicycle boxes were installed on Commonwealth Avenue in Back Bay.

Bicycle boxes should be taken into account for any project to improve bicycle speciesin places with high volumes of turning movements by cyclists

Depending on the context of the bike path, left or right side, cyclists can move to the sides of the road to align themselves with the vehicles making the same movement through the intersection.In places where motor vehicles can go straight or turn right through a bicycle lane on the right side, the bicycle box allows cyclists to move in front of the traffic queue and make their movement first, minimizing conflicts between the right-hand driver and the cyclist.

In the city of Boston the bicycle boxes are usually painted green and their design should be integrated with adequate signage according to the latest version of the MUTCD. Where there are only right hand lanes for motor vehicles, bicycle lanes must be designed to the left of the turning lane.

In France (where the 'SAS vélo' are part of the highway code since 1998), the use of the ASL and the cycle paths unfortunately sees the presence in them of motorcycles and scooters, so that recently the mayor of Paris has proposed the introduction of video recording as only possible tool to contain it.

Some studies conclude that a separate cycle path that crosses the intersection in a more lateral position with respect to its main axis is the best solution In Holland the geometry in rotatory motion is preferred to that of intersection with traffic lights as the geometry reduces the number of conflicts according to [] ASL can reduce waiting times for the turn and increase travel speed. But in the case of 'slow' cyclists, often with children, it is preferable not to go along with the vehicles but, if available, to use the all red traffic light phase for cars and all green for bikes and pedestrians to turn right rather than reach the ASL, stand on his right and then stay in the middle of the road waiting for the space to turn. The ASL certainly have a certain potential and here in Great Britain they often justify their use based on a 2007 study for the London transport agency (TfL). Similar results were proposed by previous studies, in 2002 in New Zealand, and in 2005, again in England.More elements to judge ASL come from a 2011 report, in which, through an analysis of the specialist literature on the different types of intersections with traffic lights, the authors conclude, based on a series of criteria (conflicts with pedestrians, safety and convenience for cars and bicycles, journey times, costs, need or not for important regulatory changes), that the ASL are the best possible solution.

LITTERATURE REVIEW

A review of literature that focuses on the safety impacts of the advanced stop line or bike boxes on traffic conflicts was also performed in the Table 1.

TABLE 1. The methods and findings from six previous studies that have examined the effects of bike boxes in accordance with [13-20]

Period	Authors	Details	Case Study location	N° site (Intersection/ BikeBox/ Control Site/Layout)	ASL	Video recorded data	Signal details
1994	Herrstedt et al.	Study about the reduction of the number of crashes between right-turning motorists and cyclists going straight through the intersection.			yes		
1998	Garder et al.	before-and-after study of four cycle track intersection crossings	Gothenburg, Sweden				Red
2000	Hunter	study on the connection of cycle lanes on the right and left side and on the correct extension in the lanes of the ASL	Eugene (OR)		yes		Not Coloured
2000	Hunter et al.	The study applied on 3 intersections covered bicycle box layout expecially considering the cyclist right manouver.	Eugene (Oregon)	7 I		yes	Blue
2002	Newman	examined the effect of bike boxes and advanced cycle-lane installations on vehicles and cyclists	Christchurch, NZ	7 I		yes	Not Coloured
2003	Wall et al.	study capacity implications of four bike box installations and included a useful overview of previous research into ASL in the Netherlands and UK	UK and Netherlands	4 BB	yes		Coloured
2005	Atkins	study on the geometry related to the implementation of ASL considering different case studies and maneuver lanes	South London(UK)	10 CS		yes	Green
2017	Madsen, &Lahrmann	Comparison of the safety of cyclists in five bicycle facility layouts in signalized intersections at various traffic volumes	Danemark	5L		yes	

ASLs and the technique looking to introduce a single colored cycle lane through a junction feature on the top considering value for money. The technique looking to straighten staggered toucans features in both the best schemes for cyclists as well as the best overall. The reason that it does not feature on the best when considering value for money is that to straighten a staggered crossing requires expensive civil engineering works as well as significant traffic management costs. In comparison, many of the schemes listed in the assessment section do not require a large outlay of cost as they require reconfiguration of existing equipment or additional road markings. This scheme is still considered a well-rounded solution.To emphasis, the point of selective implementation both the dwell on green and straightening of staggered crossings also feature on the worst performer's lists when considering capacity and delay of vehicles The use of uncontrolled crossings, also, to allow cyclists to bypass signals when at a cross roads has appeared on the worst performers list for safety, worst overall, worst for cyclists and worst value for money.

TABLE 2. Benefits and criticalities related to ASL

Parameters	**Benefits**	**limitation**
Visibility	+	Only if the cyclist manages to reach the ASL in relative speed and safety does the benefit
Simplest Right Manouver	+	The advantages for the right turn decrease when pedestrians (who must take precedence) are crossing the side street
Simplest Left manouver	+/-	when the ASL is not very deep (generally less than 4m between the two stop lines perpendicular to the road axis), they seem to match the blind zone ('blind spot') of the trucks
Travel time reduction	+	
Crossover efficiency	+	
Decrease of emission exposure	+	
Reduction of waiting time	+	
Reduction of n° conflict	+	
Reductions in the number of avoidance manouvres by both bicyclists and motorists.	+	
Reductions in the number of bicycles and motor vehicles encroaching	+	
proper usage of the bicycle box by cyclist	+	

The dangerousness of the streets of our cities, the traffic, the speed and sometimes the carelessness of motorists are in fact the main deterrents to the daily use of the bicycle, especially for cyclists who are not yet very experienced.The fact that the seriousness of road accidents involving car-bikes is directly proportional to the speed with which the motor vehicle impacts a cyclist is not very comforting since it means that the cyclist is responsible for own safety only up to a certain point.

Although every passive safety tool and accessory (helmet, lights, jacket, etc...) is advisable and can do its part under certain circumstances, there is no protection that keeps you in front of a collision with a car that travels to speeds above 30 km / h (this is why the EU, the World Health Organization and others recommend the introduction of the 30 km / h limit in the city).

Where the percentage of accidents to the detriment of cyclists in relation to the number of completed journeys is very low (see Netherlands and Denmark), the merit is in fact of the administrations that have been able to create an urban context suitable for cycling and pedestrians, slowing down the speed of cars in the urban center and separating the car-bike flow with appropriate cycle lanes on medium-fast roads.

In order to consider the implementation of ASLs in urban areas, it was assumed to evaluate the design and implementation process considering the SWOT approach in accordance with [21][22].

SWOT ANALYSIS

The aim of the SWOT analysis is to identify strengths and weaknesses (Strengths and Weaknesses) as wellas opportunities and external dangers (Opportunity and Threat). The identification comes carried out through interviews with stake holders (government representatives, associations, companies engaged in the transport sector) and is of a qualitative nature.

A plan should be implemented considering the following critical success factors, defined on Table below and ri-adapted to case study.

TABLE 3. SWOT parameters related to ASL

Strengths	Weaknesses
• Reduction of environmental and acoustic pollution • Reduction of vehicular congestion • Economic advantages • Policies supporting the bicycle industry • Increased safety • Increased number of cyclists • Economical transport system	• Design and maintenance quality • Shortage of financial resources • Lack of specialist skill
Opportunities	**Threats**
• Being able to visit a place in a fun way and avoid walking • Change that helps the operation of the sector • Develop the market • Strategic alliances	• Lack of cycle paths • Lack of parking • Lack of incentives to use the bike • Decrease in demand • limited transport offer

CONCLUSION

ASL design is optimal especially where space is limited for other types of interventions, certainly it costs relatively little, perhaps it is better than nothing especially if it follows the geometric requirements of installation and is also placed in the presence of a video surveillance system It should not be a substitute for an integrated cycling network that includes crossroads (which is safer and therefore more inclusive, and can bring more benefits). Finally, the cyclist's decision to reach an ALS and wait for the green in it, or remain in line can depend on:

- the number and type of vehicles in front (and those that could already occupy it), and the time before the green is triggered
- the direction after the traffic lights
- the direction of other vehicles
- the presence or absence of a cycle lane
- the presence or not of a dedicated traffic light
- the type of road and intersection, the number of lanes,the geometrical parameters…

ASLs were the best overall technique in that they provide good benefits for cyclists whilst having little to no effect on motorised traffic.

ASLs have a proven safety benefit for cyclists and subsequently offer value for money.

Therefore, it is recommended that ASLs continue to be supported and promoted as a notable technique for aiding cyclists through signalised intersections.

REFERENCES

1. F. Wegman, F. Zhang and A. Dijkstra, "How to make more cycling good for road safety?" (Accident Analysis & Prevention, 44(1), 2012, 19-29)
2. P. Schepers, D. Twisk, E. Fishman, A. Fyhri and A. Jensen, "The Dutch road to a high level of cycling safety" (Safety science, 92, 2017, 264-273)

3. J. P. Schepers, P. A. Kroeze, W. Sweers and J. C. Wüst, “Road factors and bicycle–motor vehicle crashes at unsignalized priority intersections” (Accident Analysis & Prevention, 43, 3, 2011, 853-861)
4. L. Sakshaug, A. Laureshyn, A. Svensson and C. Hydén, “Cyclists in roundabouts—Different design solutions” (Accident Analysis & Prevention, 42, 4, 2010, 1338-1351)
5. T. Tollazzi, M. Rencelj and S. Turnšek, “Slovenian experiences with turbo-roundabouts” (Proceedings of the 3rd International book on Roundabouts, TRB, USA, 2011)
6. L. G. H. Fortuijn, “Pedestrian and Bicycle-Friendly Roundabouts; Dilemma of Comfort and Safety” (Annual Meeting of the Institute of Transportation Engineers ITE, Seattle, Washington, USA, 2003)
7. C. C. Reynolds, M. A. Harris, K. Teschke, P. A. Cripton and M. Winters, “The impact of transportation infrastructure on bicycling injuries and crashes: a review of the literature” (Environmental health, 8, 1, 2009, 47)
8. L. Basford, S. Reid, T. Lester, J. Thomson and A. Tolmie, “Drivers' perceptions of cyclists” (Department for Transport, 42, 2002)
9. H. Nicholls, G. Rose, M. Johnson and R. Carlisle, “Cyclists and Left Turning Drivers: A Study of Infrastructure and Behaviour at Intersections” (Australasian Transport Research Forum ATRF, 39th, 2017, Auckland, New Zealand)
10. N. Stamatiadis, S. Cafiso and G.Pappalardo, “A Comparison of Bicyclist Attitudes in Two Urban Areas in USA and Italy” (The 4th Conference on Sustainable Urban Mobility, 2018, pp. 272-279, Springer, Cham)
11. J. Pucherandand, R. Buehler, “Cycling for everyone: lessons from Europe” (Transportation research record, 2074, 1, 2008, 58-65
12. Booz & Co, “Integrating Australia’s Transport Systems: a strategy for an efficient transport future” (Infrastructure Partnerships Australia, 2012)
13. L. Herrstedt, M. A. Nielsen, K. M. L. Krogsgaard, E. Jorgensen and N. O. Jorgensen, “Safety Of Cyclists In Urban Areas. Danish Experience” (No. 10, 1994)
14. P. Gårder, L. Leden and U. Pulkkinen, “Measuring the safety effect of raised bicycle crossings using a new research methodology” (Transportation Research Record, 1636, 1, 1998, 64-70)
15. W. W. Hunter, “Evaluation of Innovative Bike-Box Application in Eugene, Oregon” (Transportation Research Record 1705, 2000, 99-106)
16. W. W. Hunter, W. E. Pein and J. C. Stutts, “Bicycle-Motor Vehicle Crash Types: The Early 1990s” (Transportation Research Record 1502, 1995, 65-74)
17. A. Newman, “Marking of Advanced Cycle Lanes and Advanced Stop Boxes at Signalized Intersections, the Report” (Christchurch, NZ: Christchurch City Council, City Streets Unit, 2002)
18. A. Newman, C. P. Officer, C. S. Unit and C. C. Council, “The marking of advanced cycle lanes and advanced stop boxes at signalised intersections” (City Streets Unit, Christchurch City Council, Christchurch, New Zealand, 2002)
19. G. T. Wall, D. G. Davies and M. Crabtree, “Capacity implications of Advanced Stop Lines for cyclists” (Transport Research Laboratory, 2003)
20. T. K. O. Madsen and H. Lahrmann, “Comparison of five bicycle facility designs in signalized intersections using traffic conflict studies” (Transportation research part F: traffic psychology and behaviour, 46, 2017, 438-450)
21. T. Campisi, A. Canale and G. Tesoriere, “SWOT analysis for the implementation of spaces and pedestrian paths at the street markets of Palermo” (AIP Conference Proceedings, Vol. 2040, No. 1, 2018, p. 140003). AIP Publishing)
22. A. Bugheanu, “SWOT analysis of public transport system in Bucharest” (Management Research and Practice, 7, 1, 2015, 14-31)

The Role of Urban and Social Factors in the Accessibility of Urban Areas for People with Motor and Visual Disabilities

Iva Mrak[1,a)],Tiziana Campisi [2,b)], Giovanni Tesoriere [2,c)], Antonino Canale [2,d)], Margareta Cindrić[1)]

[1] *University of Rijeka - Faculty of Civil Engineering, Građevinski fakultet. Radmile Matejčić 3 51000 Rijeka-CROATIA*
[2]*University of Enna "Kore" - Faculty of Engineering and Architecture – Cittadella Universitaria 94100 Enna (EN) – ITALY*

[a)] Corresponding author: iva.mrak@gradri.uniri.hr
[b)] Corresponding author: tiziana.campisi@unikore.it
[c)] giovanni.tesoriere@unikore.it
[d)] antonino.canale@unikore.it

Abstract. The accessibility of urban areas and pedestrian networks is closely linked to the ease with which people can move in their environment. This depend on environmental factors, and can be divided into physical or social factors. An optimal integrated analysis of accessibility requires the analysis of both types of factors, social and physical. The research is based on preliminary research in which the persons with disabilities are asked to comment on problems and elements of accessibility in public space. Based on the answers, the survey was formed about the problems and solutions for accessibility in opens spaces of pedestrian traffic. The survey was oriented to persons with mobility and visual disability and aims to highlight the criticalities and benefits produced by three different urban spaces, such as parking lots, streets and squares and also to grade the perceived importance of various problems and solutions by persons with disabilities (motor and visual)..

INTRODUCTION

The accessibility of urban areas and pedestrian networks is closely linked to the ease with which people can move in their environment. This depends on environmental factors, and can be divided into physical or social factors. An optimal integrated analysis of accessibility requires the analysis of both types of factors, social and physical.

This approach is becoming more and more important and include different aspects, from modernization of public transport [1,2,3], improvement of infrastructure of public transport [4], IT solutions to map the barriers and their solutions [5] quality and access in public space [6], analysis of barriers in urban space [7], impact of different spatial barriers on users [8], determination of the best route [9] complex issues of quality of life and satisfaction with neighborhood and community [10,11], and possibility of participation in urban environment that impacts the quality of life [12].

These surveys are useful also for the definition and calibration of walkability indicators in urban areas in accordance with [13]and also allow attention to be paid to the assessment of infrastructural problems related to the people with special needs in order to be able to consider micro-simulation approaches in a more exhaustive manner[14,15],to evaluate carefully benefits and criticalities trough theSWOT analysis [16] and also inferential and statistical approaches.

These research mostly focus on the possibilities of new technology for mapping, and analysis of perception of participation and quality of life. The topics on possible barriers and solutions is still not widely researched, possibly because of the great reliance on adequacy of codes and case by case interventions when notified of problems, and less on understanding types of barriers and adequacy of solutions.

The goals of this research were to identify the most common and biggest barriers encountered by the users with mobility problems and/or visual impairment in open spaces of pedestrian traffic (pedestrian paths, public squares, roads, parking and garage spaces and public transport stops), their overlapping or lack of it for different groups, perceived best usefulness of proposed solutions for different groups, and their overall perceived importance.

METHODOLOGY AND MATERIALS

Based on the answers of previous research conducted at University of Rijeka (presented in bachelor theses [17]), some possible aspects of physical and social factors contributing to accessibility and inclusiveness of open spaces for mobility were identified. Based on those aspects, the survey "Critical points and accessibility of open spaces" was formed about the problems and solutions for accessibility in open spaces of pedestrian traffic[18].

The survey "Critical points and accessibility of open spaces" was conducted with help of several associations of persons with mobility and visual impairment (that wished to stay anonymous) from Croatia and Italy. The survey was done through google forms and word document formats (because of technological requirements of some associations). The abstract of the survey is given in Table 1.

The survey was conducted with 56 persons, of which 62,5% men and 37,5% women. The age distribution was 18-25 years 12,50%, 26-45years 53,57% and +45 years 33,93%. 82,14% of the surveyed were persons with mobility problems (group A) and 17,86% with visual impairment (group B). The Table 2 gives the distribution (%) of persons by category of disability.

TABLE 1. Abstract of the survey "Critical points and accessibility of open spaces"

1) Did you have negative experience about space – PEDESTRIAN COMUNICATIONS?
   □ YES □ NO
2) What was the negative experience about – case of SIDEWALK
   a. Width too small
   b. Slope to high
   c. Sidewalk without elements of boundary definition
   d. Cars or other objects (including infrastructure) occupy the sidewalk
   e. Lack of handrail
   f. Elements of drainage (especially on pedestrian crossing)
3) What was the negative experience about – case of RAMPS
   a. Lack of ramps to get up/off the sidewalk
   b. Not adequate ramps (slope to high, width too small…)
   c. Ramps occupied by objects (including infrastructure)
   d. Lack or partial presence of handrail
4) What was the negative experience about – case of TRAFFIC LIGHTS
   a. Duration of traffic light too brief
   b. Traffic lights without tactile plan of the road
   c. Lack of horizontal signalling
   d. Other
5) Indicate the usefulness of possible solutions (from 1 – less useful to 5 – very useful)

Ramp built according to legislation	□1 □2 □3 □4 □5
Path of adequate width	□1 □2 □3 □4 □5
Adequate surface of the path	□1 □2 □3 □4 □5
Limits of the path well defined	□1 □2 □3 □4 □5
Adequate duration of traffic light	□1 □2 □3 □4 □5
Sidewalk and ramp clear of objects on the path	□1 □2 □3 □4 □5
Adequate position of ramps and other infrastructural elements	□1 □2 □3 □4 □5
More dedication to solutions defined by regulation and adequate management	□1 □2 □3 □4 □5
Realisation of handrails on the main critical positions	□1 □2 □3 □4 □5
Other (describe)_________________________	□1 □2 □3 □4 □5

TABLE 2. Distribution (%) of persons by category of disability

Persons surveyed by type of disability	%
Wheelchair user – classic	25,00
Person using 2 crutches	14,29
Persons with visual impairment	14,29
Non specified/other disabilities that impact mobility	10,71
Person with psychological difficulties that impact mobility	8,93
Wheelchair user – motorized	8,93
Walker user	5,36
Cane user	5,36
Persons with low vision	3,57
Persons using one crutch	1,79
Persons with chronic illness that impact mobility	1,79

DISCUSSION OF RESULTS

Most persons had negative experience with pedestrian paths (98,21%), and least persons had negative experience with parking and garage spaces (high 83,64%). The negative experience as measured by survey is given in Table 3.

TABLE 3. Negative experience for groups A and B

Negative experience regarding space	% total	% of persons with mobility difficulties (group A)	% persons with visual difficulties (group B)
Pedestrian communications	98,21	97,83	100,00
Roads	89,29	89,1%	90,0%
Public transport	87,50	84,7	100
Public squares	85,71	84,8%	90,0%
Parking and garage spaces	83,64	83,6%,	80,0%

The barriers of overall highest importance were considered “Cars or other objects (including infrastructure) occupy the sidewalk” (>70% of answers), “Duration of traffic light too brief” and “Traffic lights without tactile plan of the road”. Also in other answers the problem of paths occupied by objects is noticeable, therefore it is clear that besides basic technical interventions, the management of the paths (maintenance of ordinance, education…) is crucial factor. The crossing is obviously a problem for both groups, both for duration and intelligibility of the crossing.

As seen in Table 4 the major barriers for the 2 groups often do not correspond, making understanding of situation on site and also the possible solutions more complex.

Regarding Pedestrian communications, we can see that almost all persons (both groups A and B, 97,83% and 100,00% respectively) had negative experience. In case of sidewalks (as elements of pedestrian communications), most persons had chosen as the most problematic “Cars or other objects (including infrastructure) occupy the sidewalk” (74,55%). This was chosen as the most problematic by both group A and group B (73,91% and 70,00% - although 30% of group B could not choose between multiple factors). For the ramps as an element of the pedestrian communications, as most problematic was chosen “Not adequate ramps (slope to high, width too small…)” (with 33,96%) and “Ramps occupied by objects (including infrastructure)” (close 30,19%), with group A choosing “Not adequate ramps (slope to high, width too small…)” (36,96%), and group B choosing ““Ramps occupied by objects (including infrastructure)” (60,00%) which could be explained with the need of persons with visual impairment to count on the knowledge of certain space (every change is very problematic even for the person who uses the space regularly).Regarding the traffic lights, as the most problematic, was chosen “Duration of traffic light too brief” (58,49%), with group A chose this option as the most problematic (67,39%), while the group B has chosen the option “Traffic lights without tactile plan of the road” (70,00%) - which is actually still not common feature even in western countries.As for the possible solutions, as the most helpful was selected “Sidewalk and ramp clear of objects on the path” (4,7/5), and the least “Ramp built according to legislation” (4,3/5). It can be seen that therefore, all solutions proposed were considered very important, even the least graded. The average grade for proposed solutions was 4,5/5). There is some difference for group preference, with group A selecting “Sidewalk and ramp clear of objects on the path” (4,8/5), and group B selecting “Limits of the path well defined” (4,4/5). Besides proposed

negative experiences, the groups also reported problems with damages, parked cars, traffic lights that are not coordinated, and suggested information about the elements of vertical mobility, bigger parking spaces and consultation with persons with disabilities as very important for improving the existent spaces.

TABLE 4. Major obstacles when using paths

Space	Major negative experience – group A	%	Major negative experience group B	%	Correspondence
Pedestrian communications					
Sidewalks	Cars or other objects (including infrastructure) occupy the sidewalk	73,9	Cars or other objects (including infrastructure) occupy the sidewalk	70,0	+
Ramps	Not adequate ramps (slope to high, width too small…)	36,9	Ramps occupied by objects (including infrastructure)	60,0	-
Traffic lights	Duration of traffic light too brief	67,4	Traffic lights without tactile plan of the road	70,0	-
Public squares	Space occupied by cars or other objects	50,0	Space occupied by cars or other objects	40,0	+
Roads					
Sidewalks	Lack of sidewalk	65,2	Paths occupied by vehicles or other objects (including infrastructure)	60,0	-
Ramps	Ramps for pedestrian crossing inadequate (slope to high, ramp too narrow, inadequate materials…)	36,9	Ramps occupied by vehicles or other objects (including infrastructure)	50,0	-
Crosswalk	Ramp on just one side of the road	34,8	Crosswalks position in areas with low visibility	50,0	-
Parking and garage spaces	"The width of the dedicated parking spaces too narrow"	30	"Positioning of the parking spaces too distant from entrance	30	+
Public transport stops	Lack of ramps on the vehicles	34,8	More factors	40,0	-

Regarding Public squares, we can see that most persons (85,71%, with both groups A and B, 84,8% and 90,0% respectively) had negative experience. Both groups selected "Space occupied by cars or other objects" as the biggest factor (50% and 40% respectively). They also reported non adequate renewal and multiple negativities as very important. As for the possible solutions, as the most helpful was selected "Transferring the objects (cars, urban equipment, infrastructural elements)" (4,7/5), and the least "IT apps" (4,1/5). All solutions were graded above "very important" with the average of 4,4.

Regarding the roads, most persons (89,3%, with both groups A and B, 89,1% and 90,0% respectively) had negative experience. As regarding the sidewalks, the biggest negativity was considered "Lack of sidewalk" (65,45%, also 65,2 % from group A), but also "Paths occupied by vehicles or other objects (including infrastructure)" (from group B). In case of the ramps, the most negative was "Ramps for pedestrian crossing inadequate (slope to high, ramp too narrow, inadequate materials…)" (35,85% for total and 36,96% for group A) and "Ramps occupied by vehicles or other objects (including infrastructure)" (50,0% for group B). In case of the crosswalk, the biggest negativity was "Crosswalks position in areas with low visibility" (33,33% for total), but differed for groups ("Ramp on just one side of the road", 34,78% for group A, and "Crosswalks position in areas with low visibility", 50,0% for group B). Many participants suggested multiple answers.As the most helpful solution was selected "Renewal of surfaces and other elements of the road" (4,6/5), "Path of adequate width" and "Adequate duration of traffic lights" (4,6/5 for group A) and "Path of adequate width" (4,9/5 for group B).

Regarding the parking and garage spaces, most persons (83,6%, with both groups A and B, 82,6% and 80,0% respectively) had negative experience. The most negative element was selected "The width of the dedicated parking spaces too narrow" (37,7% of total, and 30% of group A), and "Positioning of the parking spaces too distant from entrance" (30% of group B). Some participants had chosen multiple aspects, and some added additional possible problems such as abuse of licenses for parking at spaces for person of disabilities, lack of culture of other drives.As for the possible solutions, as the most helpful was selected "Add more dedicated parking spaces" (4,5/5), and the

least “Positioning of parking spaces near entrance” (4,1/5). All solution were graded above “very important” with the average of 4,4. Group A had graded as the best “Add more dedicated parking spaces” and “Parking spaces well defined by Traffic plan and with accessible cost” (4,6/5) and group B “Spaces for pedestrian passage dedicated and signalized” (4,9/5).

Regarding the public transport stops, most persons (87,5%, with both groups A and B, 84,7% and 100,0% respectively) had negative experience. As the most negative element was selected “Lack of ramps on the vehicles” (35,85% for total and 34,78% for group A) and more factors (40% for group B). As for the possible solutions, as the most helpful was selected “Hight of sidewalk and entrance of the public transport vehicle coordinated” (4,6/5) for group A and “Ramps on vehicles” (4,4/5) for group B.

Participants in the survey also accentuated the need of better education of general public and drives of public transport, creation of sidewalks and ramps (many places are still not designed according to regulation), and generally to consider the needs of persons with disabilities as important and a priority.

All highest graded solutions are also graded as very important but differ considerably for 2 groups (Table 5). Besides the highest rated solution, also the average grade of the solutions is between 4,2 and 4,5 or very important (Table 6).

TABLE 5. Highest graded solutions for groups A and B

Space	Major solution – group A	Rating	Major solution – group B	Rating	Correspondence	Above rating of very important (4/5)
Pedestrian communications	Sidewalk and ramp clear of objects on the path	4,8/5	Limits of the path well defined	4,4/5	-	+
Public squares	Transferring the objects (cars, urban equipment, infrastructural elements)”	4,8/5	Transferring the objects (cars, urban equipment, infrastructural elements)”	4,5/5	+	+
Roads	Path of adequate width, Adequate duration of traffic lights	4,6/5	Path of adequate width	4,9/5	+	+
Parking and garage spaces	Add more dedicated parking spaces, Parking spaces well defined by Traffic plan and with accessible cost	4,6/5	Spaces for pedestrian passage dedicated and signalized	4,9/5	-	+
Public transport stops	Hight of sidewalk and entrance of the public transport vehicle coordinated	4,6/5	Ramps on vehicles	4,4/5	-	+

TABLE 6. Average grading of proposed solutions for groups A and B

Space	Min result	Max result	Average
Pedestrian communications	4,3	4,7	4,5
Public squares	4,1	4,7	4,4
Roads	3,9	4,6	4,2
Parking and garage spaces	4,1	4,5	4,4
Public transport stops	4,4	4,6	4,5

CONCLUSIONS

Negative experience for persons with disabilities in spaces of traffic is extremely frequent. The grading of the problems and the comments of the participants indicate that the problems were quite well defined in the survey and largely impact the movement in public space for both groups and therefore can be used as real guidance for interventions in public spaces.

The comments about ramps indicate that often these major elements are still not realized according to regulations.Besides technical solution defined by regulations, both groups rated highly the importance of maintenance of order and management (for example cars parked on the paths are the problem), education of professionals and public, management of crossing – green traffic light of adequate duration, tactile plans and green lights not at the same moments as the green for cars. This is particularly interesting, as the common solution for green pedestrian light is to be on at the same moment as the green for the cars turning right. This indicate that the solutions for better mobility would include not just building code standards, but overall management of movement in space. The same can be concluded for the problem of lack of sidewalks, indicating that the building codes are probably still less considered in opens spaces.

It is also interesting to note that the parking spaces dedicated to person with disabilities are considered to narrow, indicating that the building standards should maybe be reconsidered as those spaces are already designed in accordance with the regulation. The positioning of the spaces is also considered inadequate, which indicates that the regulation should maybe be clearer on this point.

Average grading of the proposed solutions is above 4/5 which indicate that the proposed solutions are largely deemed important and therefore relevant for improving the movement for persons with disabilities. Maintaining the paths in functioning order is priority for both groups (again indicating the importance of both technical and management interventions).

Also the 2 groups often have different priorities – spatial definition and orientation. It is interesting that, especially for group A, it is important to have parking spaces, which is in line with the importance of contemporary traffic options for ease of transport of more sensitive groups.

ACKNOWLEDGMENTS

Authors thank the members of the associationswho participated in this and preliminary research.A special thanks goes to Dr. Andrea Fornaia

REFERENCES

1. A. P. Zając, "City Accessible for Everyone – Improving Accessibility of Public Transport Using the Universal Design Concept" (Transportation Research Procedia, ISSN: 2352-1465, Vol: 14, 2016, Page: 1270-1276)
2. N. N. Sze and K. M. Christensen, "Access to urban transportation system for individuals with disabilities" (ATSS Research, ISSN: 0386-1112, Vol: 41, Issue: 2, 2017, Page: 66-73)
3. R. Velho, "Transport accessibility for wheelchair users: A qualitative analysis of inclusion and health" (International Journal of Transportation Science and Technology, ISSN: 2046-0430, Vol: 8, Issue: 2, 2019, Page: 103-115)
4. S. H. K. Soltani, M. Sham, M. Awang and R. Yaman, "Accessibility for Disabled in Public Transportation Terminal" (Procedia - Social and Behavioral Sciences, ISSN: 1877-0428, Vol: 35, 2012, Page: 89-96)
5. R. A. Mollá-Sirvent, H. Mora,V. Gilart-Iglesias, R. Pérez-delHoyo and M. D. Andújar-Montoya, "Accessibility Index for Smart Cities" (Proceedings, 2018, 2, 1219)
6. N. Tyler, "Safety accessibility and sustainability: The importance of micro-scale outcomes to an equitable design of transport systems" (IATSS Research, ISSN: 0386-1112, Vol: 41, Issue: 2, 2017, Page: 57-65)
7. R. Pérez-DelHoyo et al., "Improving urban accessibility: a methodology for urban dynamics analysis in smart, sustainable and inclusive cities" (Int. J. Sus. Dev. Plann. Vol. 12, No. 3, 2017, 357–367)
8. P. Clarke, J. A. Ailshire, M. Bader, J. D. Morenoff and J. S. House, "Mobility Disability and the Urban Built Environment, American Journal of Epidemiology" (Johns Hopkins Bloomberg School of Public Health, Vol. 168, No. 5, 2008)
9. Y. Inadaa, S. Izumia, M. Kogab and S. Matsubarac, "Optimal Route Finding for Wheelchair Users" (12th International Conference on Design and Decision Support Systems in Architecture and Urban Planning, DDSS 2014 Development of Planning Support System for Welfare Urban Design, Procedia Environmental Sciences 22, 2014, 61 – 69 1878-0296)
10. R. W. Marans, "Quality of Urban Life Studies: An Overview and Implications for Environment-Behaviour Research" (Procedia - Social and Behavioral Sciences, ISSN: 1877-0428, Vol: 35, 2012, Page: 9-22)

11. I. Mrak, S. Nuždić, M. Franković and C. Matan, “Preliminary research: Inclusiveness of cultural heritage - a model of evaluation Poster Cultural Heritage for All Unlocking Europe’s potential through Design for All” (Pescara, Italy, 2018, unpublished)
12. R. Keles, “The Quality of Life and the Environment” (Procedia - Social and Behavioral Sciences, ISSN: 1877-0428, Vol: 35, 2012, Page: 23-32)
13. T. Campisi, A. Canale and G. Tesoriere, “The development of walkability in the historic centre of Enna: the case of the Sant Tommaso neighbourhood” (European Transport \ Trasporti Europei n. 73, ISSN 1825-3997, 2019)
14. T. Campisi, A. Canale, G. Tesoriere, I. Lovric and B. Čutura (2019). “The Importance of Assessing the Level of Service in Confined Infrastructures: Some Considerations of the Old Ottoman Pedestrian Bridge of Mostar” (Applied Sciences, 9, 8, 2019, 1630)
15. T. Campisi, G. Tesoriere and A. Canale, “The pedestrian micro-simulation applied to the river Neretva: The case study of the Mostar “old bridge” (AIP Conference Proceedings, Vol. 2040, No. 1, 2018, p. 140004)
16. T. Campisi, A. Canale and G. Tesoriere, “SWOT analysis for the implementation of spaces and pedestrian paths at the street markets of Palermo” (AIP Conference Proceedings, Vol. 2040, No. 1, 2018, p. 140003)
17. M. Cindrić, “Universal architectural design for social spaces” (University of Rijeka, Faculty of Civil Engineering, bachelor theses, 2018)
18. A. Deluka-Tibljaš, S.Lučić, and M. Benigar, “Nonmotorised Traffic - Acceptable Solution for Urban Traffic” (Suvremenipromet, 23, 2003, 5; 333-337)

Value of Travel Time: An Economic Assessment for Transport Appraisal Decision-Makers

G. Acampa[1, a)] D. Ticali [1, b)] C.M. Parisi [2, c)]

[1] *Associate Professor – Faculty of Engineering and Architecture, Kore University of Enna, Italy*
[2] *PhD Candidate – Faculty of Engineering and Architecture, Kore University of Enna, Italy*

[a)] *giovanna.acampa@unikore.it*
[b)] *dario.ticali@unikore.it*
[c)] *claudia.parisi@unikore.it*

[a)] Corresponding author: giovanna.acampa@unikore.it

Abstract. The continuous growth of vehicles on the road and the consequent traffic congestion, especially in suburban areas, is a source for major concern. It impacts negatively on the operating costs of infrastructures and on the social and economic life in the surrounding area. From an economic perspective, travel time for the displacement between two junctions of a network is one of the most significant factors to be taken into consideration. On this basis, the designer decides on the level of service and the type of infrastructure to be built and the traveller assesses the alternatives to the existing modes of transport and his willingness to face the associated cost. In Europe, United Kingdom (UK) was the first country to value travel time in the early 1960s. Moreover, until 2011, it contributed to the estimation of the monetary value of time for 60% of international studies within the EU. The UK Department for Transport (DfT) adopts the *Transport Analysis Guidance (WebTAG)* as useful transport planning and design tool. This paper discusses on the guidelines and software tools adopted for the economic evaluation of transport interventions in UK and Italy, highlighting particularly, the values and methods for estimating the *value of time (VOT)* in both countries. We propose a strong integration of the two models taking into account the numerous parameters examined in UK and at the same time the method's easy applicability for countries with different development conditions and needs.

ECONOMIC ASSESSMENT IN TRANSPORT SYSTEM

Introduction

The transportation system plays a central role in the development of any modern economy and territory [1].

The continuous growth in traffic congestion is generated by the increase in transport demand to reach an increasingly concentrated small portion of the territory. Thus, the transport means for passengers and freight should become more efficient, taking into account the economic limits in public and private funding, which are linked to the users' economic interest [2] [3].

There is no unique methodology to evaluate transport policies [4]. In the international literature, there is a wide range of approaches to assess impact of transport: Cost-Benefit Analysis (CBA) [5][6], Cost-Effectiveness Techniques [7], Life-Cycle Analysis [8], Multicriteria Analysis (MCA), [9] etc.

Cost-benefit analysis is one of the most widely adopted methods in design, management and evaluation of the transport investment decisions [10]. It is based on welfare economy theory [11] whose objective is to optimize financial resources while maximizing social benefits.

Within the cost-benefit analysis applied to the economic assessment of a transport infrastructure, the *value of time* (VOT) plays a central role and accounts for one of the highest costs.

This paper analyses the current state of the research and the methods used to assess the value of travel time. We especially focused on the United Kingdom which, from 1963 to 2011, contributed to the estimate the monetary value of time in 60% of international studies within the EU [12].

VALUE OF TIME (VOT)

Definitions and State of Art

Travel time is one of the largest categories of transport costs, and time savings are often the greatest expected benefit from transport improvement projects [13]. Therefore, from an economic point of view, the VOT become one of the main factors in estimating the benefits for travellers. It is used in transport models to monetize travel time related to the socio-economic background of travellers [14].

The value of travel time (VTT) is defined as the amount that a traveller would be willing to pay in order to save time (acquiring an additional unit of time [15] [16]), or the amount that a traveller would accept as compensation for lost time [17].

The value of travel time savings varies according to both socio-economic variables (income, family situation, type of work, etc.) and specific features of the travel (length of journey, time, purpose of travel and comfort) [18].

The concept of value of travel time (VOT) was first introduced in the 1960's after the development of the time allocation model [19]. Since 1963, several studies were carried out on different European environments such as high speed trains, new toll roads, light rapid transit networks, congestion pricing, quality improvements on local bus services and inter-urban train services, and infrastructure improvements for cyclists and pedestrians [12].

Since 1994, the European Commission has been providing guidance on cost-benefit analysis in the transport sector, and some countries (Netherlands, Norway, Sweden, Finland, United Kingdom) have attached official values to travel time so that transport projects, programmes and policies can be assessed objectively and uniquely [20]. Nevertheless, there are still significant differences in the estimation methods and in the values obtained themselves.

Valuation Methods for Travel Time Saving

Economic theory suggests different methods to evaluate VTTS according to the purpose of the journey, differentiating among working travel, non-working travel and commercial goods traffic [21]. For each, there are different methodologies to assess time savings:

- Wage rate or cost savings approach
- Hensher approach
- Willingness to pay (WTP)

Cost saving approach is often used in relation to working travel and commercial goods traffic. It is based on classical theory of marginal productivity. *Any savings in production costs will be met through an increase in production up until the point that the marginal cost of production once again equals marginal revenue. Reductions in labour costs (due to shorter journeys) will therefore result in more units of labour being hired to increase production. This will occur up to the point that the value of an extra unit of labour is equal to the cost of that labour. Thus the cost savings approach suggests that the value of in-work time savings is the wage rate plus the overhead costs associated with the employment of an extra unit of labour* [22]. This approach is open to criticism because it overlooks the social impacts on users, but rather focusing on the assumption that all travel time savings can be transferred to the production process [23].

Hensher method [24] is an alternative to the cost saving approach. It assumes that there are two elements in a work trip: a business one, i.e. that not all travel time is unproductive, and a private one, by which not all time savings are transferred to extra work but are used for non-work purposes. This method certainly provides a sophisticated assessment of travel time, as it considers that part of the travel time is productive and that time savings have meaningful impacts on workers private life. However, its implementation is complex and for this reason cost saving approach is preferable [25] [26].

According to the Willingness to pay method, the value of non-directly productive travel time is based on the methods of stated (SP) and revealed (RP) preferences. These methods represent the main monetary valuation techniques for estimating costs and benefits. Both methods use data collection to determinate VTTS in both passenger and freight transport. RP studies take into account the actual behaviour of persons or firms, while SP studies try to investigate the preferences of economic actors among alternatives which are only hypothetical [27].

Revealed preference method is the most direct way to estimate willingness to pay and are based on actual passenger behaviour (e.g. surveys on users of toll roads and alternative routes).

However, it is difficult to collect data on revealed preferences having sufficient quality and quantity to estimate robust VTTS. For this reason, the best alternative is the stated preference method.

TRAVEL TIME VALUATION IN UK AND ITALY

WebTAG Guidelines

Since 1998, the UK Department for Transport (DfT) adopts the *Transport Analysis Guidance (WebTAG)* as useful transport planning and design tool [28]. It consists of guidelines and a toolkit for transport modelling and appraisal methods applicable to actions on highways and public transport.

Figure 1 shows the standard procedures and economic parameters adopted by the United Kingdom Department for Transport in the transport sector.

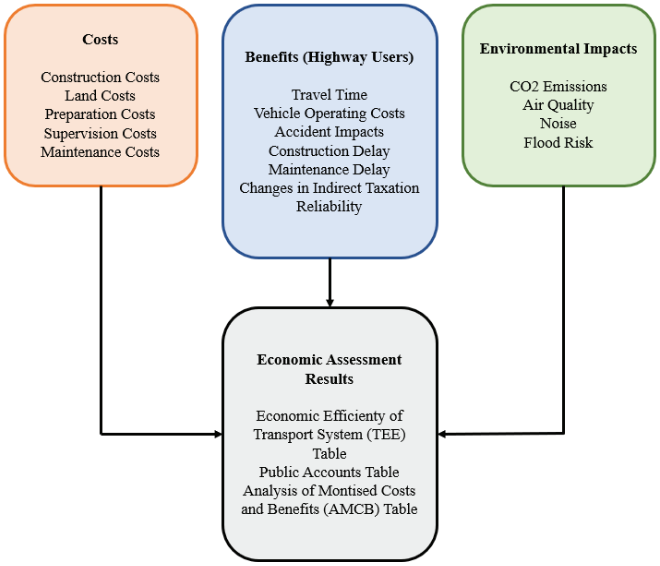

FIGURE 1. Economic Assessment Components

The UK Department for Transport provided an excel file, called TAG Data Book [29] which is divided into several units for modelling and evaluating transport (Fig.2).

TAG Unit	Section Title	Unit Title	Worksheet	Table Title
			Cover	Department for Transport contact information
			User Parameters	User - defined price year and initial forecast year
			Audit	Version log
			TAG1	TAG1 table look-up
			Annual Parameters	Forecast annual economic and demographic parameters
A 1.1	Cost Benefit Analysis		**A 1.1.1**	Discount rates
A 1.3	User &	Values of time	**A 1.3.1**	Values of time per person (working and non-working)
	Provider		**A 1.3.2**	Forecast values of time per person (working and non-working)
	Impacts		**A 1.3.3**	Car and vehicle occupancies (2000); Annual percentage change in car passenger occupancy up to 2036
			A 1.3.4	Proportion of travel and trips in work and non-work time
			A 1.3.5	Market price values of time per vehicle based on distance travelled
			A 1.3.6	Forecast market price values of time per vehicle based on distance travelled
		Operating costs	**A 1.3.7**	Fuel and electricity prices and components
			A 1.3.8	Fuel / energy consumption parameter values
			A 1.3.9	Forecast proportion of car, LGV and other vehicle kilometres using petrol / diesel / electricity
			A 1.3.10	Forecast assumed vehicle fuel efficiency improvements to 2035
			A 1.3.11	Forecast fuel / energy consumption parameters
			A 1.3.12	Forecast vehicle fuel / energy cost formulae parameters (work)
			A 1.3.13	Forecast vehicle fuel / energy cost formulae parameters (non-work)
			A 1.3.14	Non-fuel resource vehicle operating costs
			A 1.3.15	Forecast non-fuel resource car operating costs to 2035
		Social Impact of buses	**A 1.3.16**	Proportion of bus trips by car ownership, trip purpose and concessionary travel pass status.
			A 1.3.17	Proportion of bus trips by that would "not go" if bus not available.
			A 1.3.18	Value of the social impact per return bus trip
A 3.1	Environmental	Noise Impacts	**A 3.1**	Monetary valuation of changes in noise
A 3.2	Impacts	Air Quality Impacts	**A 3.2**	Damage cost and marginal abatement cost values by pollutant
A 3.3		Greenhouse Gases	**A 3.3**	Carbon dioxide emissions per litre of fuel burnt / kWh used
A 3.4			**A 3.4**	Forecast non-traded, £ per tonne of CO_2e
A 4.1	Social &	Social Impact	**A 4.1.1**	Average value of prevention per casualty by severity and element of cost
	Distributional	Appraisal	**A 4.1.2**	Average value of prevention per road casualty by class of road user
	Impacts		**A 4.1.3**	Average value of prevention of road accidents by severity and element of cost
			A 4.1.4	Average value of prevention per road accident by severity & class of road: all hours
			A 4.1.5	Rail injury classification, weights and values
			A 4.1.6	Value of journey quality benefit of cycle facilities, relative to no facilities
			A 4.1.7	Values of aspects of pedestrian environment, used in valuation of London Strategic Walk Network
			A 4.1.8	Option and non-use values
A5.3	Uni-Modal	Rail Appraisal	**A 5.3.1**	Operating cost and revenue forecasting series
			A 5.3.2	Journey purpose / ticket type splits by flow category
A 5.4	Appraisal	Marginal External	**A 5.4.1**	Proportion of total traffic by region, congestion band, area type & road type
		Congestion Costs	**A 5.4.2**	Marginal external costs by road type and congestion band
			A 5.4.3	Car traffic shares by time of day
			A 5.4.4	Marginal external costs by region and time of day
			A 5.4.5	Car diversion factors by PDFH flow category
			A5.4.6	Bus diversion factors by recipient/source mode
			A5.4.7	Cycling diversion factors by recipient/source mode
M 2.1	Variable Demand Modelling		**M 2.1**	Values of time by income band for non-work purposes (£/hr)
M 2.2			**M 2.2**	Values of time by income band for work purposes (£/hr)
M 3.2	Assignment Modelling		**M 3.2.1**	Segmented values of bus quality interventions (generalised minutes)
M 4.2	Model Forecasting & Uncertainty		**M 4.2.1**	Forecast fuel price and income adjustment factors
			M 4.2.2	Car cost series for rail demand forecasting
			M 4.2.3	Car and bus journey time series for rail demand forecasting
			M 4.2.4	Rail forecasting parameters
COBALT	Accidents & Casualties		**COBALT 1**	Costs per accident / casualty
			COBALT 2	Annual rates of growth of accident values
			COBALT 3	Link & Combined Link / Junction: accident rates & change factors
			COBALT 4	Severity rates (Link / Combined)
			COBALT 5	Link & Combined Link / Junction: casualty rates & change factors
			COBALT 6	Junction only: accident parameters
			COBALT 7	Junction only: accident change factors
			COBALT 8	Severity rates (Junction only)
			COBALT 9	Junction only: casualty rates & change factors

FIGURE 2. Contents of TAG Data Book (updated on 2019 may)

The TAG Data Book contains all the necessary parameters for an economic assessment including a description of the of scheme costs, user benefits for travel time, journey time reliability, vehicle operating costs, accidents and wider economic impacts.

The spreadsheet A.1.3.1 "Values of time per person (working and non-working)" contains values of travel time savings for working and non-working time that should be used when evaluating from an economic point of view most of the transport projects.

The Department for Transport uses the Willingness to pay method and in particular the Stated Preferences technique. A key distinction in the valuation of travel time savings is by purpose of journey, and specifically between values for trips made on working time (or employers' business), and non-working time values including commuting and transport all leisure purposes.

Error! Not a valid bookmark self-reference. and TABLE 2 give the average values of working time per person by mode and, for car and rail trips, by distance. These values apply only to journeys made in working time and thus excludes commuting journeys.

TABLE 1. Values of Working (Employers' Business) Time by Mode

Mode	Factor Cost	Perceived Cost	Market Price
(£ per hour, 2010 prices, 2010 values)			
Car driver	14,86	14,86	17,69
Car passenger	14,86	14,86	17,69
LGV (driver or passenger)	10,24	10,24	12,18
OGV (driver or passenger)	12,06	12,06	14,35
PSV driver	12,32	12,32	14,66
PSV passenger	8,42	8,42	10,02
Taxi driver	10,89	10,89	12,96
Taxi / Minicab passenger	14,86	14,86	17,69
Rail passenger	24,52	24,52	29,18
Underground passenger	8,42	8,42	10,02
Walker	8,42	8,42	10,02
Cyclist	8,42	8,42	10,02
Motorcyclist	14,86	14,86	17,69
Average of all working persons	16,19	16,19	19,27

TABLE 2. Values of Working (Employers' Business) Time by mode per person (distance banded)

Values of Working (Employers' Business) Time by mode per person (distance banded)

Mode	Resource Cost	Perceived Cost	Market Price
Car (driver or passenger) 0-50km	8,42	8,42	10,02
Car (driver or passenger) 50-100km	13,62	13,62	16,21
Car (driver or passenger) 100-200km	18,49	18,49	22,00
Car (driver or passenger) 200km+	23,77	23,77	28,28
Rail passenger 0-50km	8,42	8,42	10,02
Rail passenger 50-100km	13,62	13,62	16,21
Rail passenger 100-200km	23,72	23,72	28,23
Rail passenger 200km+	34,22	34,22	40,72

Values of working vary according traveller income, trip time, trip cost and trip distance.

According to the advices in the Wardman's research (2013) on "Valuation of Travel Time Savings for Business Travellers" [30], values of working time varies according only to distance and mode. This variation is represented by a continuous function, where the value of time is assumed to vary with trip distance according to a logistic functional form. The parameters of this function, including the minimum and maximum thresholds, can be found in the spreadsheet "A1.3.1" of the TAG Data Book. The continuous function is shown below:

$$VTTS = \frac{U}{1 + e^{\frac{x_{min} - D}{k}}} \tag{1}$$

where:

VTTS = Value of travel time savings (£/hr, in 2010 prices and values)

D = Distance (measured in km)

U = Upper limit of the function (the 'asymptote') (measured in £/hr, 2010 prices and values)

x_{mid} = Distance at the inflexion point of the curve (where $VTTS = U/2$) (measured in km)

K = A scale parameter which is inversely proportional to the steepness of the curve

The spreadsheet A1.3.1 also give the values of time savings for “commuting” (travelling to and from the normal working place) and “other” (all other non-work trips, e.g. for leisure) journey purposes (TABLE 3).

TABLE 3. Values of Non-Working Time by Trip Purpose

Values of Non-Working Time by Trip Purpose (£ per hour, 2010 prices, 2010 values)			
Trip Purpose	**Factor Cost**	**Perceived Cost**	**Market Price**
Commuting	8,36	9,95	9,95
Other	3,82	4,54	4,54

The values within the TAG Data Book are based on research conducted by the Institute for Transport Studies (ITS) and Accent for the Department for Transport, reported in 2015, and published as ‘Provision of market research for value of travel time savings and Reliability: Phase 2 Report’ [31]. The values have been converted to 2010 values and prices in line with the growth in income (with a GDP/capita elasticity of 1) and changes in prices (using the GDP deflator) between 2010 and 2014 [32].

In order to carry out a correct cost-benefit analysis, the UK Department for Transport provides TUBA (Transport User Benefit Appraisal) software conforms to the WebTAG guidelines. This software implements a "willingness to pay" approach to economic evaluation for multimodal schemes with fixed or variable demand.

Italian Guidelines on Guide to Economic Valuation of Investment Project

For the economic evaluation of transport infrastructures, the reference text in Italy is "Guidelines for the evaluation of investments in public works under the responsibility of the Ministry of Infrastructure and Transport pursuant to Legislative Decree 228/2011" edited by the Directorate General for Spatial Development, Planning and International Projects and the Board of Evaluation and Verification of Public Investments [33].

In principle, it is based on the European guidelines (“Guide to Cost-Benefit Analysis of Investment Projects”) [22]. According to these guidelines, the main benefits are measured on the basis of the "consumer surplus" defined as the excess of users’ willingness-to-pay over the prevailing generalised cost of transport for a specific trip. The generalised cost of transport takes into account the variation in operating costs (i.e. tariff, toll, fuel, etc.) and value of travel times (and/or a travel time equivalents, such as the inconvenience of long intervals). Any reduction in the general cost of transport to move goods and people brings to an increase in the consumer surplus.

With regard to the value of travel time, the guidelines provide for a minimum level of segmentation that takes into account:

- systematic travel for work purposes (*commuting*);
- occasional business trips (*business*);
- occasional travel for other reasons (leisure and free time).

Travel time values vary not only according to purpose but also according to distance classes: short distance (Urban and metropolitan displacements) and long distance (Moving over medium and long distances) (Tab.4)

TABLE 4. VTTS due to travel and distance class (passengers)

	Value of Time (€ 2016/pass.-h)		
	Business	**Commuting**	**Other**
Urban and metropolitan displacements	12-20	5-10	5-15
Moving over medium and long distances	20-35	10-15	10-25

Existing guidelines do not suggest the use of simulation software for cost-benefit analysis of actions in the transport sector. Yet, a commercial software could be developed from existing software such as the TUBA used in the UK.

DISCUSSION AND CONCLUSION

In the present paper, we collected and analysed information and details on the assessment methods related to the cost-benefit analysis of existing transport systems, their implementation and new infrastructure integrations.

The comparison between the ITA/EU and UK methodologies highlights some critical issues in the approach to the analysis, which depend on the level of detail the parameters taken into account.

The UK model, WebTAG and TUBA, analyse transport costs according to an economic and social approach, linked to marginal productivity and at the same time to user comfort.

The approach is complete and immediately applicable for the analyst who can use tables and models already equipped with defined analytical logic. The input data depends on the type of transport and the user involved; the output is unique and objective and can thus be easily compared to alternative solutions. On the other hand, the UK model is limited by the rigidity of the variables that are not immediately applicable to the new modes of transport. Moreover, changes in user interests are not taken into account. In fact, over the years, users have changed their behavioural attitudes as a result of the use of new technologies and the widespread use of internet.

The comparison between the two systems provides the following considerations:

- the EU model has a direct approach that depends on a few parameters and is therefore flexible and dynamic with regard to the different modes of transport and to compare them;
- the EU model has the limit of examining a small number of parameters and therefore is subject to numerical inaccuracies and may issue assessments that are not always consistent with the actual needs of the territory and the demand for transport. The range assigned by the model for each type of movement (business, commuting, other) should be identified according to a logical function or proportional to factors that strictly identify the reference territory (e.g. GDP, socio-economic conditions, population density, etc.).
- the UK model is much more dated than the EU one and was built following with a much more detailed analysis. It takes into account many factors and is unambiguous and objective, thus facilitating the role of the analyst.
- the UK model is closely linked to the country's standards and is not easily and immediately applicable to other areas. In fact, it is necessary from time to time to review the parameters and indices according to the country of application and the evolution in the behavior.

For the above reasons, we believe that the EU and UK models should be strongly integrated to take into account the numerous parameters highlighted in UK, but at the same time developing an approach easier to apply even to different areas, taking into account the different development conditions and needs of other countries.

In addition, the EU should have a unique model that makes assessments as unambiguous and objective as possible in order to be able to assess the entities and forms of funding to be allocated to individual infrastructures.

REFERENCES

1. I. Athira, C. Muneera, K. Krishnamurthy and M. Anjaneyulu, *Estimation of Value of Travel Time for Work Trips* (Transportation Research Procedia 2016), pp. 116-123. doi:10.1016/j.trpro.2016.11.067
2. European Commission, *Transport in the European Union. Current Trends and Issues*, Available online: https://ec.europa.eu/transport/sites/transport/files/2019-transport-in-the-eu-current-trends-and-issues.pdf, (Accessed on 27 August 2019).
3. T. Vörös, M. Juhász and K. Koppány, *The measurement of indirect effects in project appraisal* (Transportation Research Procedia, 13, 2016), pp.114 – 123. https://doi.org/10.1016/j.trpro.2016.05.012
4. P. B. Cadena, J. M. Vassallo and K. Cheung, *Sustainability Assessment of Transport Infrastructure Projects: A Review of Existing Tools and Methods* (Transport Reviews 35(5), 2015), pp.1-28. doi: 10.1080/01441647.2015.1041435
5. OECD, *Cost-Benefit Analysis and the Environment: Recent Developments* (OECD, Paris, 2005)
6. R. Brent, *Applied Cost-Benefit Analysis* (Edward Elgar Publishing, United Kingdom, 2008)
7. World Bank, *Where to Use Cost Effectiveness Techniques Rather than Cost-Benefit Analysis* (Transport Economics, Policy and Poverty Thematic Group, Washington, 2005)
8. G. Flintsch, *Life-cycle assessment as a tool for sustainable transportation Infrastructure management* (John Wiley & Sons Inc, Hoboken, NJ, USA, 2008)
9. R. Vreeker and P. Nijkamp, *Multicriteria evaluation of transport policies* (Elsevier, Netherlands, 2005)

10. P. Nijkamp, B. Ubbels and E. Verhoef, *Transport Investment Appraisal and the Environment* (SSRN Electronic Journal, 2002). doi: 10.2139/ssrn.339080
11. N. Kaldor, *Welfare propositions of economics and interpersonal comparisons of utility* (Economic journal 49(195), 1939), pp. 549-552
12. M. Wardman, V. Phani, K. Chintakayala and Gerard de Jong, *Values of travel time in Europe: review and meta-analysis* (Transportation Research Part A: Policy and Practice 94), pp. 93-111
13. *Victoria Transport Policy Institute, Transportation Cost and Benefit Analysis II – Travel Time Costs,* Available online: https://www.vtpi.org/, (Accessed on 29 August 2019)
14. L. Ambarwati, A. K. Indriastuti and P. Kusumawardhani, *Estimating the Value of Time and Its Application* (Open Science Journal 2(1), 2017), pp.1-9. doi: https://doi.org/10.23954/osj.v2i2.639
15. M. Huq, Explaining Variations in the Value of Time Saving, *In The All China Economics (ACE) International The Second Conference* (City University of Hong Kong, 2007)
16. K. A. Small, *Valuation of Travel Time* (Economics of Transportation (1)1, 2012), pp.1-39. doi:10.1016/j.ecotra.2012.09.002
17. A. Younis, "Review of value of travel time savings and its variation with income and distance", Thesis for MSc Transport Planning, University of Leeds, 2013
18. M. Borjesson and J. Eliasson, *Experiences from the Swedish Value of Time Study* (Transportation Research Part A Policy and Practice 59, 2012) doi: 10.1016/j.tra.2013.10.022
19. G. Becker, *A theory of the allocation of time* (Economy journal 75(299), 1965), pp.493-517
20. P. Mackie, P. Worsley, and J. Eliasson, *Transport Appraisal Revisited* (Research in Transportation Economics 47, 2014), pp. 3-18. https://doi.org/10.1016/j.retrec.2014.09.013
21. E. Ustaoglu and B. Williams, "Cost-Benefit Evaluation Tools on the Impacts of Transport Infrastructure Projects on Urban Form and Development", in *Smart Urban Development*, edited by Sara Shirowzhan (IntechOpen, University of New South Wales, 2019) doi: 10.5772/intechopen.86447
22. European Commission*, Guide to Cost-Benefit Analysis of Investment Projects, Economic Appraisal Tool for Cohesion Policy 2014–2020*, Available online: https://ec.europa.eu/regional_policy/sources/docgener/studies/pdf/cba_guide.pdf, (Accessed on 2 September 2019)
23. HEATCO, *Funded by 6th Framework Programme IER, Germany* 2004-2006 (HEATCO: Stuttgart, Germany, 2007)
24. D. Hensher, *The Value of Business Travel Time* (Pergaman, Oxford, 1977)
25. Department for International Development, *The Value of Time in Least Developed Countries* Available online: https://assets.publishing.service.gov.uk/media/57a08d4340f0b64974001762/R7785.pdf, (Accessed on 4 September 2019)
26. P. Mackie, M. Wardman, A. Fowkes, G. Whelan, J. Nellthorp and J. Bates, *Values of Travel Time Savings in the UK* (Institute of Transport Studies, University of Leeds, 2003)
27. L. Zamparini and A. Reggiani, "The Value of Travel Time in Passenger and Freight Transport: An Overview", in *Policy Analysis of Transport Networks* (Ashgate,England, 2016), pp.145-161
28. P. C. Bueno, J. M. Vassallo and K. Cheung, *Sustainability Assessment of Transport Infrastructure Projects: A Review of Existing Tools and Methods* (Transport Reviews 35(5), 2015), pp.622-649. https://doi.org/10.1080/01441647.2015.1041435
29. Department for Transport, *TAG Data Book*, Available online: https://www.gov.uk/government/publications/tag-data-book (Accessed on 9 September 2019)
30. M. Wardman, R. Batley, J. Laird, P. Mackie, T. Fowkes, G. Lyons, J. Bates and J. Eliasson, *Valuation of Travel Time Savings for Business Travellers* (Institute for Transport Studies, University of Leeds, 2013)
31. Department for Transport*, Provision of market research for value of travel time savings and reliability*, Available online: *https://assets.publishing.service.gov.uk/government/uploads/system/uploads/attachment data /file/470229/vtts-phase-2-report-non-technical-summary-issue-august-2015.pdf., (Accessed on 9 September 2019)*
32. Department for Transport, *TAG UNIT A1.3 User and Provider Impacts*, Available online: *https://www.gov.uk/guidance/transport-analysis- guidance-webtag* (Accessed on 9 September 2019)
33. Ministry of Infrastructure and Transport, *Linee guida per la valutazione degli investimenti in opere pubbliche*, Available online: http://www.mit.gov.it/sites/default/files/media/notizia/2017-07/Linee%20Guida%20Val%20OO%20PP_01%2006%202017.pdf, (Accessed on 10 September 2019)

Evaluation of Infrastructure: Application of TOD to Catania Underground Metro Station

Giovanna Acampa[1, a)] Francesco Contino[2,] Mariolina Grasso[1, b)] Dario Ticali[1, c)]

[1] *Faculty of Engineering and Architecture, Kore University of Enna, Italy*
[2]*Governmental Management Ferrovia Circumetnea Ministry of Transport, Italy*

[a)] giovanna.acampa@unikore.it
[b)] mariolina.grasso@unikore.it
[c)] dario.ticali@unikore.it

Abstract. In recent years, the concept of transit-oriented development (TOD) is increasingly applied to urban development based on the principles of smart growth and sustainable development. The growing complexity of urban systems and metropolitan areas requires an integrated strategic vision. This means addressing the issues of mobility and accessibility and their impact on the urban environment. Catania metropolitan area is characterized by a highly urbanized settlement with high percentage of urban sprawl. The General Master Plan of the city, shaped in 1964 and finally endorsed in 1969, severely reduced the opportunity for new developments by allocating areas for new urban facilities. The process of urban sprawl is mainly characterized by residential settlements. This aspect together with an inadequate road network and an insufficient public transport service brought to the growth of private cars on the roads, generating serious traffic congestion and making Catania based on a car-oriented model. Lately these conditions are changing as a consequence of the development of the underground metro network that connects the main city's service centers like the hospitals, the university (and soon also the Airport) to the city center. To achieve sustainable transportation and resolve the aforementioned problems, we have applied TOD criteria to some of the main city's transport junctions (selected using the Multi Criteria Decision Aid methodology) in order to fulfills the principle of sustainable transportation.

URBAN PLANNING AND EVALUATION METHODS: AN INTEGRATED APPROACH

Evaluation methods for urban planning

Evaluation can be defined as a set of activities aiming at organizing the information necessary to make a choice, enabling each actor involved in the decision-making process to take a balanced decision [1]. In this perspective, a Multi-Criteria Decision Aid (MCDA) approach provides a useful tool to understand not only the structure of the issue addressed in the decision-making process but also its multiple and different dimensions.

Thus, it is possible to face problems that do not have unique solutions. Many of these problems are characterized by variety and uncertainty [2], triggering a collaboration process both among technicians and those who are directly or indirectly involved in the choices [3].

Urban and regional planners depend heavily upon the interaction between objectives and evaluation methods in their analysis, planning, and implementation processes. There is obviously a need for tools by which planners and other professionals may take stock of their work. [4]

Urban planning analysis requires that several factors such as natural system constraints, compatibility with existing land-uses, existing land-use policies, should be taken into consideration [5].

Therefore, quantitative approaches such as MCDA techniques in land suitability procedures can be used in an appropriate manner.

An important question concerns the choice of the appropriate evaluation method for the specific decision context in which it has to be applied. To ease this selection, a list of quality criteria was developed by De Montis et al. (2004). It can be used to reveal strengths and weaknesses of MCDA methods with respect to three main aspects:

1) operational components of MCDA methods;
2) applicability of MCDA methods in the user context;
3) applicability of MCDA methods considering the problem structure.

Taking into account the aim of this study (selection of underground station junctions in Catania where the application of Transit Oriented Development[1] criteria can lead to significant benefits) the most suitable analysis turned out to be the Analytic Hierarchy Process (AHP)[2].

AHP is a mathematical technique used for multi-criteria decision-making, it considers the assessment of consistency among decision maker(s). It is used for making selection, evaluation, cost and benefit analysis, resource allocations, planning and development, priority and ranking, and forecasting. [6]

A decision-making process involves three main stages: structuring the problem, constructing the decision model, and analyzing the problem. Structuring includes the definition of the problems with their required elements and the visualization [7]. The elements are designed in the hierarchic structure descending from the goal to a set of criteria, sub-criteria and a set of alternatives[3] [8]. The steps of the classical AHP method can be explained as follows:

• Defining the decision problem and determining the evaluation criteria;
• Structuring the hierarchy starting from the goal (top of the hierarchy) through the mid-levels (criteria, sub-criteria) to the set of alternatives;
• Constructing the pairwise comparison matrices for comparison the criteria with respect to the parent criteria;
• Doing the calculations for each level with respect to the upper levels and calculating the overall and global priorities until the final priorities of the alternatives obtained.

SUSTAINABLE TRASNPORTATION AND "USERFRIENDLY" URBAN MODEL

Transit Oriented Development for urban systems

The concept of TOD stems from urban planning theories that emerged in response to urban sprawl, including smart growth, new urbanism and sustainable development.

The principles of smart growth include high-density development, mixed land use, constructing accessible pedestrian spaces and diversifying the selection of transportation vehicles [9].

Calthorpe in 1993 introduced the concept of TOD, defining it as "moderate and high-density housing, along with complementary public uses, jobs, retail and services, concentrated in mixed-use developments at strategic points along the regional transit systems."

In particular, Calthorpe addressed the importance of creating pedestrian-friendly spaces. As example, concentrating various facilities for day to day activities in a TOD region can improve pedestrian accessibility.

La Greca, Barbarossa, Ignaccolo, Inturri, and Martinico (2011) verified that concentrating urban development near transportation facilities improves pedestrian accessibility to such stations within walking distance, thereby further promoting the financial sustainability of public transportation systems [10].

TOD designs can be examined according to the scale definition proposed by Calthorpe (1993), in which typical of a TOD project is a mixed-use community where the area scale of the community is within approximately 2000 pedestrian steps[4] to a central commercial station.

---

[1] The concept of TOD is derived from urban planning theories that emerged in response to urban sprawl including smart growth, new urbanism, and sustainable development. Calthorpe (1993) defined it as "moderate and high-density housing, along with complementary public uses, jobs, retail and services, concentrated in mixed-use developments at strategic points along the regional transit systems."

[2] AHP, introduced by Saaty (1988), is a multi-criteria decision making technique for modeling unstructured problems. It provides a comprehensive framework to overcome the basic problem of decision making which is to choose the best in a set of competing alternatives under conflicting criteria.

[3] Hierarchic structure shows the effects of changes in priorities of upper level on priorities of lower levels. To structure a decision problem as a hierarchy, the upper-level elements have to be independent from the lower-level elements and it does not involve interaction.

[4] walking time: approximately 10 min, walking distance: approximately 500 - 600 m.

When Calthorpe (1993) proposed the concept of TOD, it was divided into two types: urban TOD and neighborhood TOD according to the types of public transportation systems. The types of public transportation systems for urban TOD are light and heavy rail systems as well as express buses (similar to bus rapid transit systems).

Urban TOD areas feature high-density businesses and work opportunities as well as moderate high density of residential areas. The primary types of public transportation systems in neighborhood TOD areas are local transportation systems and bus extensions. The travel time to a primary transportation system should not exceed 10 minutes. Neighborhood TOD areas have a moderate residential density and the primary commercial behavior is retail businesses. The principal goal of developing this type of region is to create a positive living environment with abundant public open spaces and recreational zones.

Regarding the land-use distribution ratios, urban (neighborhood) TOD areas feature a public space usage ratio of 5%e15%, a central commercial/office zone ratio of 30%e70%, and a residential ratio of 20%e60% [11].

However, not all stations are suitable for TOD of the surrounding area, due to the more or less suitable natural environment close to them and to the limited government budgets to implement such approach. Therefore, stations closest to the target of sustainable transportation must be selected for TOD planning following a thorough evaluation[5] [12].

CASE STUDY: APPLICATION OF TOD CRITERIA TO CATANIA UNDERGROUND METRO STATION NODES

Catania urban system

Catania metropolitan area is characterized by highly urbanized settlement with a high percentage of urban sprawl. The General Master Plan of the city, shaped in 1964 and finally endorsed in 1969, severely reduced the opportunity for new developments by allocating areas for new urban facilities. In fact, despite many attempts, the Catania Metropolitan Area still does not have either a Master Plan or a Strategic Plan [13].

The process of urban sprawl is mainly marked by residential settlements. Almost 70% of the total built up area (within 19 municipalities), are principally made of detached or semidetached housing, built between 1964 and 1985. This aspect together with an inadequate road network and an insufficient public transport service encouraged the spread of private cars, generating serious traffic congestion.

Thus, the city has adopted a car-oriented model in which the lack of quality and environmental standards helps to create a metropolitan environment among the least sustainable in Europe.

To build new sustainable urban scenarios for the metropolitan city of Catania, rail transport plays a central role.

The metro of Catania (in service form July 11, 1999) is managed by the local authority “Ferrovia Circumetnea - FCE”. It is originated from the project of replacing the urban path of the Circumetnea railway. In fact, the first section was developed on the old route from the Port to the “Borgo” station.

The works began on December 13, 1986 and on June 27, 1999 after almost 13 years, the first lot “Borgo-Porto” with 6 stations (“Borgo”, “Giuffrida”, “Italia”, “Galatea”, “Stazione Centrale FS e Porto”) for a total of 3 km, was opened.

In the last few years, in order to deal with the increased (and time-shifted) mobility needs, the management of FCE and the Ministry of Transport kicked off an upgrading project of the railway infrastructure.

To date, the situation of the metro line is the following: 8.8 km in operation with 8 stations (Giovanni XXXIII-Galatea-Italia-Giuffrida-Borgo-Milo-San Nullo-Nesima) and 2.2 km under construction (lots Nesima -Misterbianco and Stesicoro-Palestro).

In addition to the existing line and to the sections under construction, further sections are planned to reach the airport “Fontanarossa -Vincenzo Bellini” and the south-western Etna countries (lots Palestro-Aeroporto and Monte Po-Misterbianco).

By the end of 2024 the entire line (from Misterbianco to the Airport), for a total of 19.4 km, is forecasted to be completed. This project (when completed) will allow to connect the center of Catania with the main urban and suburban centers [14].

---

[5] As aforementioned we have used the analytic hierarchy process to select the best options among all the underground station nodes of Catania.

An interesting data concerns the increasing number of passengers after completing the first phases of the upgrading works. An average of 5 million passengers was recorded in 2018, compared to 600.000 of the year before the woks ended[6].

Selection process of the underground metro station junctions

The selection process of the underground metro stations consists of two phases. In fact the AHP multi criteria decision aid allows to hierarchize up to a maximum of 7 alternatives. Considering this limit, applying the ELECTRE method[7], we excluded 4 of the 8 stations and selected the other 4: “Milo”, “San Nullo”, “Stesicoro” and “Giovanni XXXIII”.

Regarding those stations, we implements AHP according to the following path.

First of all we established the criteria to be used:

1) proximity to points of interest (hospitals, University, sport center etc);
2) usability (pedestrian accessibility, parking, etc.)
3) areas to be regenerated (empty urban spaces)

These criteria have been selected taking into account TOD principles, allowing the selection of the most suitable stations (among those currently in operation).

To make a decision in an organized way we have decomposed the decision into the following levels (Table 1):

TABLE 1

Level 1	**objective**	Stations choice			
Level 2	**criteria**	Proximity to points of interest	Usability	Regeneration	
Level 3	**alternatives**	Giovanni XXXIII	San Nullo	Milo	Stesicoro

Level 2 - weighting the criteria: we have constructed a set of 3x3[8] pairwise comparison matrices. It has allowed to compare the criteria among each other and establish which the more relevant.

To make these comparisons, we have chosen a number from the following scale (Figure 1) that indicates how many times one element is more important or dominant over another element.

---

[6] Source: Ferrovia Circumetnea FCE - http://www.circumetnea.it

[7] The acronym ELECTRE stands ELimination Et Choix Traduisant la REalit´e (ELimination and Choice Expressing the REality), consists in setting the concordance threshold (Tc) and the discordance threshold (Td). Once these thresholds are defined, it is possible to proceed with the elimination of dominated alternatives. An alternative dominates or out-performs another only if its value is higher than the concordance threshold (Tc) and, at the same time, the discordance value is lower than discordance threshold (Td).
In case in which we have not an alternative dominating the others, the thresholds are relaxed through a decrease of the concordance threshold value and an increase in the discordance threshold value

[8] The structure of the matrix depends on the numbers of criteria

Intensity of Importance	*Definition*	*Explanation*
1	Equal Importance	Two activities contribute equally to the objective
2	Weak or slight	
3	Moderate importance	Experience and judgement slightly favour one activity over another
4	Moderate plus	
5	Strong importance	Experience and judgement strongly favour one activity over another
6	Strong plus	
7	Very strong or demonstrated importance	An activity is favoured very strongly over another; its dominance demonstrated in practice
8	Very, very strong	
9	Extreme importance	The evidence favouring one activity over another is of the highest possible order of affirmation
Reciprocals of above	If activity *i* has one of the above non-zero numbers assigned to it when compared with activity *j*, then *j* has the reciprocal value when compared with *i*	A reasonable assumption
1.1–1.9	If the activities are very close	May be difficult to assign the best value but when compared with other contrasting activities the size of the small numbers would not be too noticeable, yet they can still indicate the relative importance of the activities.

FIGURE 1 - The fundamental scale of absolute numbers

Matrix A - Criteria weight

	Proximity to points of interest	**Usability**	**Regeneration**
Proximity to points of interest	1	5	4
Usability	0,2	1	1
Regeneration	0,25	1	1
Sum of columns	1,45	7	6

Matrix A - normalize

	Proximity to points of interest	**Usability**	**Regeneration**
Proximity to points of interest	0,69	0,71	0,67
Usability	0,14	0,14	0,17
Regeneration	0,17	0,14	0,17
Cheking	1,00	1,00	1,00

Priority Vector

P.P.o.I.	0,69
Usability	0,15
Regeneration	0,16

After having assigned a weight to the criteria, Matrix A has been normalized in order to obtain the priority vector. The priority vector is the synthesis of the weights of each criterion. The one achieving the highest score has the major impact on alternatives. Considering this case study, the proximity of the stations to points of interest had the highest impact on the alternative choice.

Once determined the priority vector, it was important to understand whether the matrix of comparisons among pairs was consistent or not. In order to do that, we calculated the Consistency Ratio CR[9]= CI/RI (Consistency Index/Random Index). Considering this case study, CR was equal to 0,01 and Matrix A was verified to be consistent.

Level 3[10] - the third and last step has been about comparing all the alternatives to each other (and to each criteria) in order to obtain the priority vectors[11].

Matrix B1

Proximity to points of interest	Giovanni XXXIII	Milo	San Nullo	Stesicoro
Giovanni XXXIII	1,00	0,14	0,25	0,50
Milo	7,00	1,00	0,50	2,00
San Nullo	4,00	1,00	1,00	0,50
Stesicoro	1,00	0,50	2,00	1,00
Sum of columns	13,00	2,64	3,75	4,00

Matrix B1 normalized

Proximity to points of interest	Giovanni XXXIII	Milo	San Nullo	Stesicoro
Giovanni XXXIII	0,08	0,05	0,07	0,13
Milo	0,54	0,38	0,13	0,50
San nullo	0,31	0,38	0,27	0,13
Stesicoro	0,08	0,19	0,53	0,25
Cheking	1,00	1,00	1,00	1,00

	Priority vector
Giovanni XXXIII	0,08
Milo	0,39
San nullo	0,27
Stesicoro	0,26

As mentioned before we repeated this procedure for all the 4 alternatives until we obtained the final priority matrix and the percentage of preference[12]:

Priority matrix

	Proximity to points of interest	Usability	Regeneration
Giovanni XXXIII	0,08	0,20	0,10
Milo	0,39	0,24	0,30
San nullo	0,27	0,09	0,50
Stesicoro	0,26	0,47	0,10

	% of preference
Giovanni XXXIII	10%
Milo	35%
San nullo	28%
Stesicoro	27%

As result of this process, we obtained the following hierarchization: 1) Milo 2) San Nullo 3) Stesicoro 4) Giovanni XXXIII.

In order to apply TOD principles we have finally select the first two station of the ranking (Milo and San Nullo).

---

[9] The condition for the matrix to be consistent is that CR<0,1 (10%).

[10] as demonstration of the work carried out we have reported one of the three matrices of comparison between criterion and alternative

[11] The priority vector is given by the average of each row of the matrix. The higher score implies the prevalence of one criterion (or alternative) over another

[12] The percentage of preferences is given by the matrix product between each row of the priority matrix and the column of the criteria priority vector.

Strategies and actions

Within a circumference having as center the underground stations of “San Nullo” and “Milo” and as radius 500 meters, TOD “ingredients” such as functional mix, high density, public spaces has been implemented. (Figure 2)

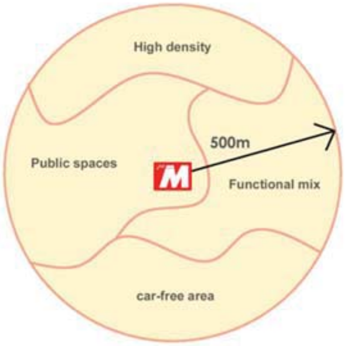

FIGURE 2 – Transit Oriented Development main principles

According to the principles of TOD, the actions foreseen for the junctions were the following:

1) Improvement of cycle/pedestrian accessibility
2) Regeneration of San Nullo urban empty
3) Regeneration of FCE railway sediments

As regards to point (1), i.e. the improvement of cycle/pedestrian accessibility, we identified new routes creating a network around the stations. The "network" is divided into:

- new cycle/pedestrian routes (as foreseen in PRG 2012[13] proposal);
- cycle/pedestrian routes on existing roads;
- cycle/pedestrian route on FCE sediments.

The second action concerned the regeneration of San Nullo urban empty. The project has the aim to transform the empty area into an urban park marked by:

1) urban polarities with functional mix[14]
2) cycle/pedestrian route crossing the area and connecting it to the entire network of cycle/pedestrian paths planned[15]. (Figure 3)

The third and final action concerned the regeneration of the disused FCE railway by putting in place an exclusively cycle/pedestrian route. This last proposal could allow the connection not only of the selected stations (Milo and San Nullo) but also of Nesima, Fontana and Cibali[16] covering a fairly large part of the territory. (Figure 4)

FIGURE 3 – Project of San Nullo empty area

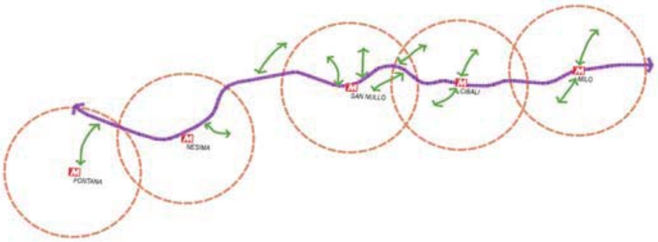

FIGURE 4 – Cycle/pedestrian route network

[13] Proposal of the general masterplan (PRG 2012) not yet approved
[14] Construction of new buildings with different functions within them: parkings, commercial areas, offices and residences
[15] In this way, non-motorized access to the node will be guaranteed.
[16] The stations of Cibali and Fontana will be opening soon.

CONCLUSION

Taking into account the main goal of this study, we employed the AHP method to ensure that the criteria and the alternatives selection approach will be as objective as possible. The criteria were established taking into account TOD principles. This in order to select the most suitable underground station junctions in Catania where the application of Transit Oriented Development criteria could lead to significant benefits. The selection process involved 8 stations. Since the AHP allows to select up to 7 alternatives we discarded some using the ELECTRE method.

At the end of the process of hierarchization the stations of San Nullo and Milo were selected. The main actions foreseen can be summarized as follows:

1) Improvement of cycle/pedestrian accessibility
2) urban regeneration San Nullo
3) regeneration of FCE railway sediments

The study carried out around the area of the stations under examination shed light on several issues. The problem that has become particularly evident is the lack of a forecast for slow mobility. This condition involved a large part of the territory. Catania is based on a car-oriented model in which the lack of quality and environmental standards helps to create a metropolitan environment among the least sustainable in Europe.

In view of the construction of new sustainable urban scenarios for the metropolitan city of Catania, the extension of rail transport in conjunction with the application of TOD principles could play a central role within the overall project.

REFERENCES

1. Nijkamp P., Rietveld P. & Voogd H. *Multicriteria Evaluation in Physical Planning* , Elsevier 1990, Amsterdam, The Netherlands.
2. Fusco Girard L., Cerreta M. & De Toro P. *Integrated assessment for sustainable choices* (Scienze Regionali, 2014) vol 13, pp 111-142.
3. Mendas A. & Delali A. *Integration of multi-criteria decision analysis in GIS to develop land suitability for agriculture: application to Durum wheat cultivation in the Region of Mleta in Algeria* Computers and Electronics in Agriculture, 2012) vol. 83 pp. 117-126.
4. Deluka-Tibljaš, Aleksandra; Karleuša, Barbara; Šurdonja, Sanja; Dragičević, Nevena. *Use of AHP Multi-Criteria Method for Transportation Infrastructure Planning* (International Scientific Conference People, Buildings And Environment, 2014) pp. 123-124
5. Mosadeghi, R., Warnken, J., Tomlinson, R., & Mirfenderesk, H. *Comparison of Fuzzy-AHP and AHP in a spatial multi-criteria decision making model for urban land-use planning* (Computers, Environment and Urban Systems, 2015) vol. 49, pp. 54–65.
6. Vaidya, O. S., & Kumar, S. *Analytic hierarchy process: An overview of applications* (European Journal of Operational Research, 2006) vol. 169(1), pp. 1–29.
7. Saaty, T. L., & Shih, H.-S. *Structures in decision making: On the subjective geometry of hierarchies and networks* (European Journal of Operational Research 2009) vol. 1699, pp. 867–872.
8. Saaty, T. L. *Rank from comparisons and from ratings in the analytic hierarchy/network processes* (European Journal of Operational Research, 2006) vol. 168, pp. 557–570.
9. Grant, G., & Tsenkova, S. *New urbanism and smart growth movements* International encyclopedia on housing & home Oxford: Elsevier, 2012.
10. L. Barbarossa, M. Ignaccolo, P. La Greca, F. Martinico, *The density dilemma. A proposal for introducing smart growth principles in a sprawling settlement within Catania Metropolitan Area* (Cities, 2011) vol 28 pp 2-3.
11. Wey, W.-M., et al., *Alternative transit-oriented development evaluation in sustainable built environment planning* (Habitat International, 2016) http://dx.doi.org/10.1016/j.habitatint.2016.03.003
12. Deluka-Tibljaš, Aleksandra; Lučić, Sanja; Benigar, Milivoj *Nonmotorised Traffic - Acceptable Solution for Urban Traffic* (Suvremeni promet, 2003) vol. 5 pp. 333-337
13. G. Acampa, N. Bona, M. Grasso, D. Ticali, *BIM: Building Information Modeling for Infrastructures* (AIP Conference Proceedings, 2018) vol. 2040, Issue 1; https://doi.org/10.1063/1.5079197
14. G. Tesoriere, T. Campisi, A. Canale, F. Arena *Modelling and simulation of passenger flow distribution at terminal of Catania airport* (AIP Conference Proceedings, 2018) https://doi.org/10.1063/1.5079195

Validation of Infrastructures through BIM

Giovanna Acampa[1, a)] Giorgia Marino[2, b)] Dario Ticali[1, c)]

[1] *Associate Professor – Faculty of Engineering and Architecture, Kore University of Enna, Italy*
[2] *PhD Candidate – Faculty of Engineering and Architecture, Kore University of Enna, Italy*

[a)] giovanna.acampa@unikore.it
[b)] giorgia.marino@unikorestudent.it
[c)] dario.ticali@unikore.it

Abstract. Building Information Modelling is the latest phase of a revolutionary process that over the last thirty years has profoundly transformed the world of design in the construction sector in all its different disciplines: architecture and engineering design, mechanical/electrical/plumbing engineering, operation and maintenance, cost and safety, etc. From 2D and 3D assisted design to parametric design, the innovation has led to a profound change of perspective as far as the way of conceiving the work in all its phases is concerned, from concept to execution and consequently to management. BIM methodological approach, based on sharing and interoperability, opens up a potential range of future applications, although nowadays it is mainly used in the MEP (mechanical, electrical and plumbing engineering) sector. One of the most interesting applications can be developed in urban and infrastructural design (*Infra-BIM)*, where the processes and the controls implemented by BIM can be managed effectively and at a higher efficiency level. The term *Infra-BIM* is used in reference to the adoption of the BIM methodology in the infrastructure sector. An area that by itself calls for a strong disciplinary interconnection with Geographic Information Systems (GIS) and involves many aspects, from the analysis of the area analysed to the relations and interferences with other infrastructures. A multidisciplinary approach that, consequently, requires the correct implementation of the BIM methodology reached by checking the coherence and quality of the information input in the models. The paper focuses on the phase of *BIM Validation* viewed as a support for a proper work-flow: it not only allows to analyse the whole set of information associated with a parametric object but also how the entire model matches the specific design requirements. BIM Validation process in design is not defined yet, but it is important to aim at a correct procedure so as to guarantee quality of design and future management of the project.

.

INTRODUCTION

Simulation for the rational control and management of information

The new technologies huge potentials are fully expressed in foreshadowing the future reality through models, visual simulations able to tell the space and time, fully uncovering technical details and not only through simplified graphics. [1] [2]

The radical change in design concept has taken place at the most significant space level, the "simulated space", which is the most familiar intangible medium for designers, where they create, understand, manipulate and explore models in real time through a digital methodology. It is no longer a tool that only helps in preparing a project, but which is able to transfer the entire methodological process (analysis-project-verification-management) in digital form, working on a design model that can be viewed with continuous accessibility in space and time. The design object is then interpreted as a single integrated project archive, where the architectural and engineering sections are defined both in terms of technical choices and in terms of economic impact of their implementation and management. [3]

Initially, the BIM was introduced to support the design of the systems, then extended to the entire building and finally also to the linear infrastructure.

The application of BIM design to linear infrastructures is not yet widespread, but in strong growth as requested by the contracting authorities and by large construction companies having international experience.[4] [5] [6].

In this context, BIM Model Checking plays an important role, thanks to which it is possible to verify and validate projects not only at the design stage, but at all stages of the process [7].

The main objective of this paper is to provide an approach to the process of verification and validation of a BIM design, applied to civil infrastructure and in particular to a road. This tool is now missing from the contracting stations that on the one hand promote design using BIM methodology but on the other hand are not equipped with the necessary tools to verificy and operate the BIM product.

The next step will be to develop of automatic validation systems, their functionalities and the advantages that stem from their use. In particular, we will see how the Solibri validation software works and how it can generate project quality control through customisable sets of rules, especially during the management and monitoring phases of an infrastructure project.

I-BIM AND THE IMPORTANCE OF VALIDATION ABOUT QUALITY CHECKING

State of the Art

The acronym I-BIM (Infrastructure - Building Information Modelling) is used in the AEC (Architecture-Engineering-Construction) sector and refers to use of BIM models in infrastructure design, construction and management. [8]

I-BIM and BIM, which are substantially the same, have, however, a different approach to modelling. In civil infrastructures such as roads or bridges, all specific items are positioned horizontally with respect to the reference line, thus defining the transverse sections which are then extended horizontally along the designated alignments. Building models are instead created vertically one plane after the other. For this reason, building projects are also called "vertical projects", while civil infrastructure projects are usually called "horizontal projects". [9]

An infrastructure project prepared according to high quality standards, will have to jointly approach , because they always interact, both the intrinsic elements , which have to do with infrastructure itself, and the extrinsic elements, which are related to its place in the overall urban and territorial environment. [10]

While the intrinsic elements are related just to the technical characteristics of building (materials, performance, etc..), the extrinsic ones are strongly interconnected to the Geographic Information Systems (GIS) and involve various issues in the analysis of the area on interest: from climatic conditions to geological and geotechnical up to interference with existing infrastructure. The GIS tool, moreover, is potentially capable to check the position of the planned work in the space and to provide stratified data on the territory which helps the designer to put his work in context. [11] [12] The BIM platform allows in particular to generate three-dimensional models of the infrastructure, defining superstructures, substructures, sub-services and any work in completion and support, while highlighting the relationship with the surrounding environment. In fact, detailed and updated images of the existing situation and the boundary conditions (e.g. orthophotos taken with a drone, clouds of laser scanning points...) can be added to the model, together with any other available graphic information that could influence the project implementation. [13]

To guarantee the quality of the BIM model, it is essential to validate it:

"Validation is a check/evidence that demonstrates the acceptability or congruity of an operation with respect to a set of criteria or constraints. The negative result of the verification or test entails the rebuttal of the said operation ". Validation generally refers to the project as a design process carried out according to quality, conformity, fulfilment of requirements standards. [14]

Having high quality model can save money and time and helps keeping order while sharing information, thus increasing the level of security. In fact, Quality Checking validates the technical integrity and information contained in it. [7]

BIM AND PROCUREMENT

BEP and EIR as tools for achieving quality in tenders: Italferr's experience in railway sector

'Quality' may be defined as the fulfilment of requirements and expectations [15], according to a concept that goes beyond any possible certification. A digital model that can be considered as qualitative, needs to be analysed to understand whether or not it adheres to such a definition.

In order to do so, models are evaluated through procedures and validation tools that over the years are gradually getting more reliable thanks to the new technologies. In this general framework, BIM methodology fits perfectly into all types of design processes, from architectural to infrastructural. [16]

For the first time, the new European Directive 2014/24 [17] introduced the possibility of using a BIM approach: "*For public works contracts and design contests, Member States may require the use of specific electronic tools, such as electronic modelling tools for construction*". Italy adopted this Directive with the Ministerial Decree n.560/2016 [18], which dictates that electronic modelling tools have to be progressively used in public procurement procedures.

The decree, in particular, forces on Contracting Authorities to define a comprehensive program relating to the introduction of BIM: staff training, acquisition of appropriate tools, concrete implementation of digitized processes and interoperability, which requires the use of open formats and that data used in the process have to be connected according to the methods indicated in the information requirements. The use of information systems can only be requested, however, by Contracting Authorities with trained personnel, especially in tenders for infrastructures.[19]

In tenders, documents such as the BEP (Building Execution Plan) or the CI (Informative Specifications) - more commonly known as the Employer Information Requirements (EIR) – present the requirements that the contractor should meet and that will then be compared with what it offers. The Invitation to Tender (Capitolato Informativo) includes the requirements for the information management system, to which the contactors will have to respond through an offer of Information Management (oGI) which is followed, for successful bidder, by the BEP.

The Building Execution Plan (BEP), which describes in details also the methods of control and exchange of information, the information tools that will effectively be implemented if accurately drafted, ensures that quality level of the project increases significantly. It essentially presents the plan drawn up by designer and the contractor to show the methods and tools aimed at achieving the objectives and requirements established by the client in the EIR. [20]

In the infrastructure sector, the two Italian companies Italferr, a railway engineering company, and ANAS, a company that manages the national primary road network, have been using BIM since 2013, and in particular have been enhancing the so-called Change Management for tenders by identifying the following objectives: [21]

- Setting the requirements to be included in the Informative Specifications;
- Drafting a BIM Execution Plan (BEP) and a company BIM Guide, project templates, certified libraries and specifications for tenders;
- Drawing up the library of rules to railway sector aimed at Model Checking. [22] [23]

The modelling of the Apice-Hirpinia segment, prepared in 2018, is one of the first examples in which the design in BIM was used for the entire railway line and not only for parts of the works carried out there. This necessarily called for a particular co-ordination among various software, that manage the different modelling activities on linear and spot works, so that they merge correctly in a general integrated model. Linear structures included designing the following: tunnels, trenches, embankments, yards, viaducts and station/stops.

The figures here below show how the various elements involved contribute to the creation of the integrated model: from purely infrastructural models such as tunnels and viaducts, to architectural models of specific works such as stations. By displaying the integrated model, the interference between the various models becomes evident.

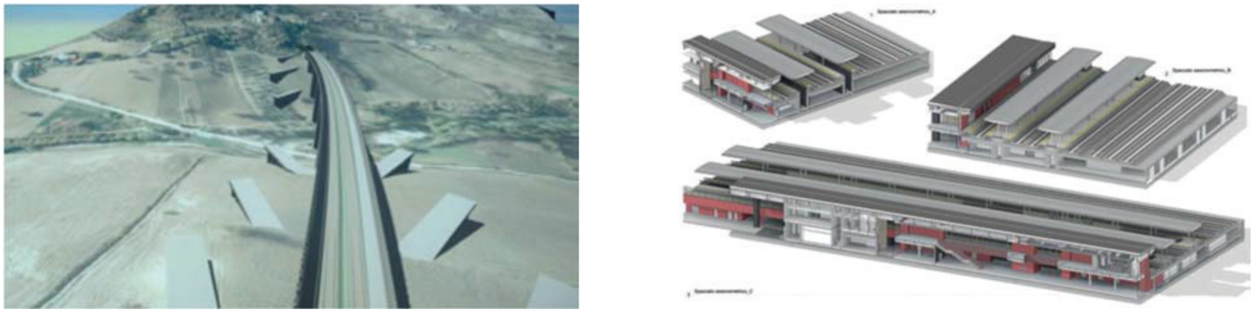

(a) (b)

FIGURE 1. On the right, the viaduct of Apice-Hirpinia section and on the left, axonometric cross-sections of the BIM Hirpinia Station models.

MODEL CHECKING E IL PROGETTO INNOvance

Le tre fasi del Model Checking e i primi approcci verso una libreria BIM

During the Model Checking phase, thanks to neutral IFC interchange format, geometric and non-geometric parameters implemented in information models are analysed and validated; the Building Information Model undergoes different validation processes. These include the set of control rules, called rule-sets, which are applied to the model in three phases of consequential verification: the BIM Validation, to control the attributes and procedures of the modelling procedure, Clash Detection, to verifiy interferences, and Code Checking, to verify the compliance with the reference standards (Figure 2). [7]

FIGURE 2. The three phases of Model Checking

The first phase of BIM Validation is essential for subsequent controls to be correct, as the application of rules to verify the mandatory requirements, asks for enriching the model with a set of data and information to be used as input.

Critical issues that can be detected in this phase concern the alphanumeric contents of the parametric model, such as the attributes, or its geometric structure.

Reference is therefore made to the so-called LOD (Level of Development), where each level corresponds to precise attributes to be defined for each object. Depending on its design phase and its stage of development, the model will be more or less enriched with information content and, in the same way, the controls will be more or less precise.

In the infrastructural works, appropriate libraries are not easy to get access to and the geometry of the objects is difficult to parametrize. In Italy, in 2011 the Ministry for Economic Development financed the INNOVance research project, promoted by ANCE (Associazione Nazionale Costruttori Edili), with the aim of creating a new platform for the construction sector, based on a wide BIM library:

"The INNOvance project aims to create the first national database containing all technical, scientific and economic information useful to construction industry.".

Some of the objectives are:

- The creation of a standardized digital data sheet for each product, whose information content is made available to users in paper, electronic and/or multimedia formats, in order to ensure businesses a valid technical support; [24]
- The set of data contained in each sheet will be associated to the representation of new objects as required BIM 'Building Information Model allowing a rapid and comprehensive consultation of information about the object itself.

The technical sheet contains information useful to all actors in the supply chain, from customers, builders, designers, and concerning: coding, name, description, use, manufacturer data, performance, sustainability, safety, geometry and shape, visual and/or construction, size, physical-chemical properties, composition tolerances, approvals, transport, packaging, product declarations and attachments.

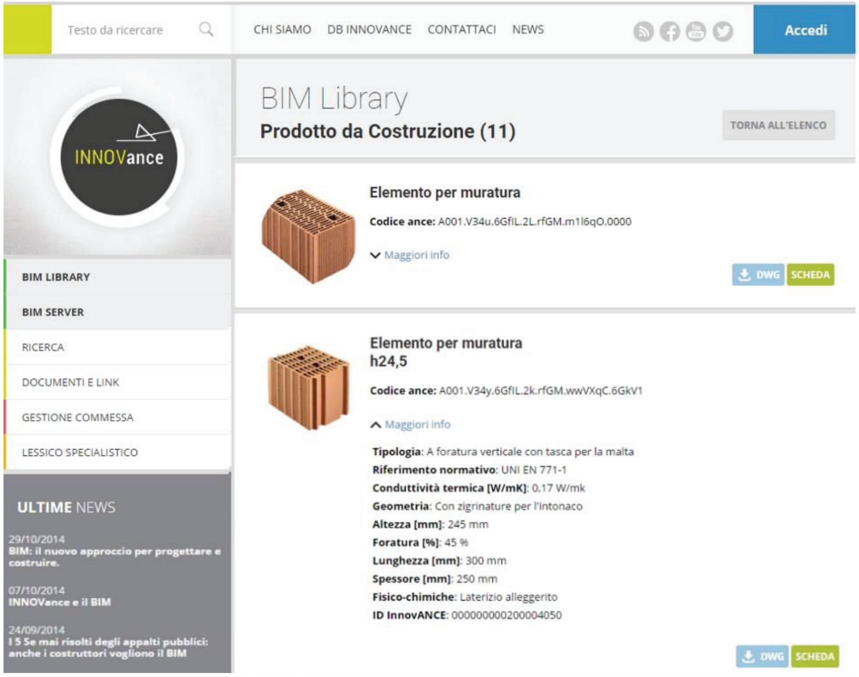

FIGURE 3. BIM Library INNOVance Website

The second phase of the Model Checking is the Clash Detection or interference control that is developed step by step; first of all, the designer must detect any interference for the part of its competence in the same platform of BIM Authoring and then for the next phase of multidisciplinary coordination there are several validation software such as BIM Viewer, Solibri Model Viewer and Autodesk Navisworks.

After correctly setting the desired rule-set, it should first be applied to the individual disciplinary models, and then detect any coordination problems in the Merged Model. Moreover, the clash and the criticalities that can be detected are not only due to physical interference, but through a Rule-based Model Checking tool it is also possible to verify

the proximity between objects and determine the minimum tolerance, for example, for the installation or maintenance of the different components present in the building. [7]

Finally, the third and final phase of Code Checking is able to validate the project by comparing the parameters contained in the model with the standards and regulations of reference. Building processes are regulated by numerous local, national and international laws [9] and the information contained in these documents can be translated into parametric rules. It is used to verify compliance with accessibility requirements, minimum room heights and areas, air-lighting ratios, and more sophisticated controls, such as sustainability analysis, acoustic, energy and structural requirements. Thanks to the creation of rule sets, the validation process is increasingly objective.

VALIDATION IN SOLIBRI MODEL CHECKER

The creation of customizable rule-set and their application for infrastructure work

For validation purposes, a parametric model has to be integrated with information attributes necessary to the control phase. To apply an automated validation process, BIM models ought not only contain purely geometric data generated automatically by platforms but ought also to be integrated with all information needed to verify the project compliance with regulations and in reference to performance standards.

Specifically, Solibri Model Checker (SMC) is a software whose main aim is to support the activity of project verification which allows the automatic control of compliance with current regulations by highlighting any critical issue, for instance the overlap of structures and facilities to be installed. The action of verification and preliminary control allows avoiding design changes that could lead to increases in cost during the execution phase.

The validation process consists of the following phases:

1) Uploading files in IFC format regarding the entire project in all its sections (structural, plant engineering, architectural);
2) Decide the rule-set corresponding to the chosen type of control (Figure 4);

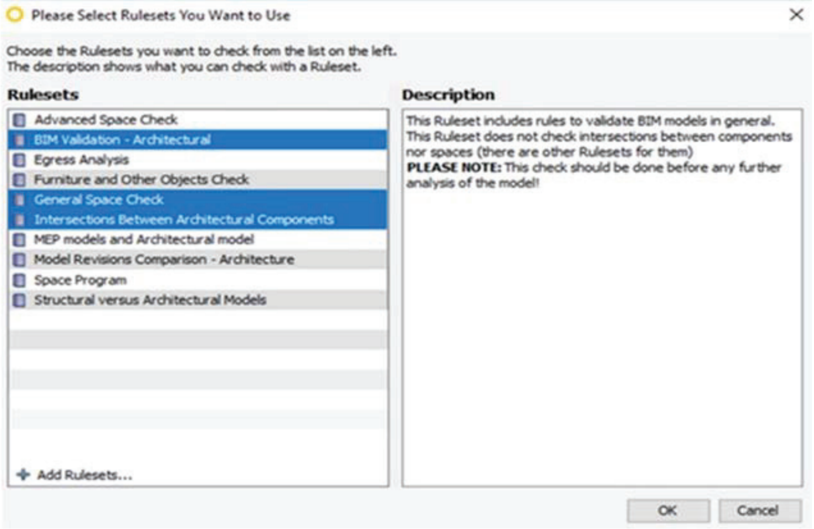

FIGURE 4. Rule selection for checking in SMC

3) Classify the model elements to be checked (classifications can follow different settings: Omniclass, Masterclass, Uniclass);
4) Verify project completeness according to the specific LOI (Level of Information) or LOG (Level of Geometry) of elements.

The conflicts and inconsistencies found are automatically listed in a table and identified with triangles having different colours according to on the different level of severity (critical, moderate or less critical). The colour coding helps the user in identifying priorities (Figure 5).

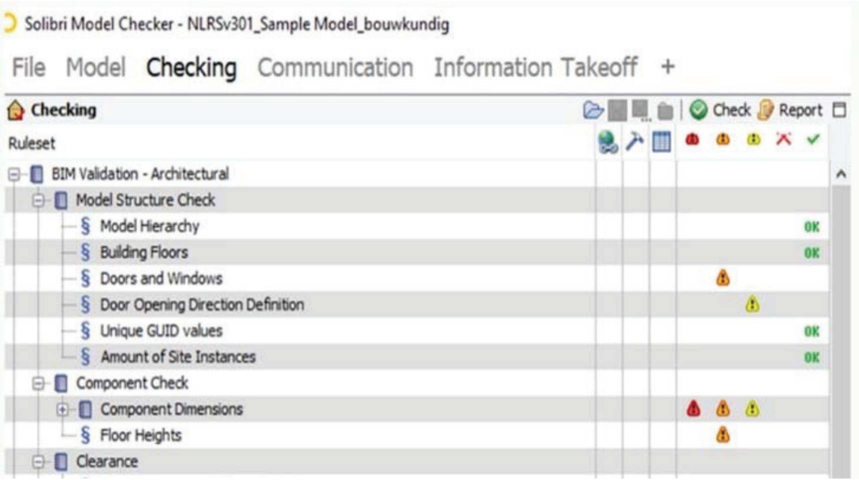

FIGURE 5. Severity of issues as shown in SMC

As far as I-BIM is concerned, at design stage, a working control system should allow to verify the infrastructure correct execution and its compliance with reference standards. It should also make possible managing all information regarding works maintenance status.

In the specific case of road infrastructure, the most critical element to verify is the degradation in the superstructure which impacts on the road functionality and service level.

Secondly, the design and control activities must address the issue of road signs and street furniture.

To design and planning maintenance operations, managing institutions should define performance standards in relation to the road's functional classification (motorways, urban, suburban) and the service level to be achieved. Subsequently, the focus should shift on setting the indices related to the performance standards that should be monitored. In the case of road functionality, such indices should measure also the pavement status and its deterioration. The trend of those parameters can be estimated in a predictive manner according to the type and amount of expected or monitored traffic.

In order to define the maintenance interventions that have to be carried out on the superstructure, it is necessary to know degradation curves trend of the related main parameters (adhesion, regularity, bearing capacity) which are defined as follows:

- Adherence guarantees suitable contact between tyre and pavement, enabling wheel rolling rather than slipping. The parameter is measured by direct and indirect tests.
- Regularity indicates the maintenance of superstructure design dimension, i.e. the continuity of the profile in all directions. The value of the I.R.I. (International Roughness Index) is assessed by correlating it with measurements obtained by profilometers or by high performance tests.
- Bearing capacity is defined as the ability to withstand to the stresses caused by vehicle transit. The measurement is obtained by localised load tests or by high performance measurements (HWD, FWD).

Through BIM validation tools, parameters can be constantly measured through appropriate monitoring activities, and then processed by a dedicated software. The number and type of data to be acquired for road evaluation depend on the road classification and to the area (urban or suburban) which it belongs to. For instance, we attach here below the table defined by the Lombardy Region in Italy in which it lists the parameters to be measured in relation to each road type (table 1).

TABLE 1

Sigla	Caratteristiche superficiali e strutturali da rilevare	Indicatore di stato consigliato	Modalità di misura	Unità di misura	Metodologia di misura/valutazione
RL	Longitudinal regularity	IRI	Not punctual	m/km	Profilometers
		Irregularity depth	Punctual	Mm	3 m bar
RT	Transversal regularity	Footprint depth	Not punctual	Mm	3 m bar
			Punctual	Mm	3 m bar
A	Aderenza	CAT	Non puntuale	--	SCRIM or equivalent device
M	Macrotessing	ETD	Not punctual	Mm	Texture meter or equivalent device
P	Lift	Deflection	Not punctual	Mm/100	FWD
			Punctual	Mm/100	Benkelman beam
DS	Surface instability	The organization identifies the types of disruptions to be detected in relation to type of flooring	Punctual	Dipendente dal tipo di dissesto	Catalogue of breakdowns

Model Checking management activity can be carried out by monitoring these indices and it provides the following elements:

- Most appropriate type of intervention (surface treatments, reinforcements through addition of new layers, reconstruction of only linked layers through milling and replacement, deep renovations, etc.);
- Thickness of the intervention in relation to the actual constraints (lateral curbs, manhole covers, thickness of layers to be milled, etc.);
- Intervention durability, i.e. degradation trend of the indices; the degradation depends on the traffic and on certain environmental features;
- Possible use of specific materials or technologies suitable for achieving particular performances (e.g.: binders with polymers, etc.);
- Cost in relation to available resources.

The validation of the maintenance criteria with the relative status indexes (such as the representation of general state of a trunk or road network, the definition of performance standards, the representation of degradation evolution (degradation curves) or even the definition of benefit intervention), will provide the Maintenance Plan, with all the technical and economic information required during the reference period and with basic contents. Its implementation will ensure to the superstructure a longer useful life.

CONCLUSIONS

This paper has highlighted the usefulness of applying BIM also in extended linear works such as transport infrastructure and roads. A correct application of BIM turns infrastructure design and management processes more efficient. The validation process through Model Checking will be able to ensure continuous monitoring of the infrastructure through the inclusion of some indices that will determine its deterioration state.

If we also consider that road infrastructures are becoming richer and richer in technological content with the installation of systems for driving aid (intelligent infrastructures) and users aid in general (road and pedestrian), it is

natural to think that the BIM will become increasingly useful for an overall assessment at design stage, and for the subsequent work management and maintenance planning stages.

REFERENCES

1. G. Acampa, F. Forte. and P. De Paola «*B.I.M. models and evaluations*» In: Mondini G., Oppio A., Stanghellini S., Bottero M., Abastante F. (eds) Values and Functions for Future Cities. Green Energy and Technology. Springer, Cham DOI https://doi.org/10, 2019.
2. C. Eastman, R. Sacks and K. Liston, *BIM handbook: a guide to building information modelling for owners, managers, designers, engineers, and contractors*, Wiley, 2011.
3. G. Acampa, I. Crespo and G. Marino, «*Representación Del Dibujo Frente A Simulación De Los Sistemas Bim. Oportunidad O Amenaza Para La Arquitectura*,» ACE Arquitectura, Ciudad y Entorno– Universitat Politecnica Catalunya*,* n.40 DOI: http://dx.doi.org/, 2019.
4. G. Dell'Acqua, «*BIM per Infrastrutture Lineari, Infrastructure-BIM, "Heavy-BIM", "Horizontal-BIM".*» Ingenio*,* 2016.
5. E. Hjalmarsson and M. Hoier, «*Use of BIM in infrastructural projects A cross country comparative analysis between the use of BIM in Australia and SwedenMaster of Science*», Thesis in the Master's Programme Design and Construction, Chalmers University of Technology, Göteborg, Sweden , 2014.
6. W. Liu, H.Guo, H. Li and Y. Li, «*Using BIM to improve the design and construction of bridge projects: a case study of a long-span steel-box arch bridge project*» vol. Int. J. Adv. Robot. Syst. 11 (125), pp. 1-11, 2014.
7. A. Ciribini, M. Bolpagni e S. Ventura, «*La validazione del contenuto informativo è la chiave del successo di un processo BIM-based*,» Ingenio. DOI: 10.14609/Ti_2_15_1i.
8. G. Acampa, N. Bona, M. Grasso and D. Ticali, « *BIM: Building information modeling for infrastructures*» AIP Conference Proceedings - 2040, n. 140008- doi.org/10.1063/1.5079197, 2018.
9. Q. LU, «*Evaluation of the BIM Adoption for Civil Infrastructure and Development of a 5D BIM Financial Decision Making Framework*» A Thesis Submitted to The Hong Kong University of Science and Technology in Partial Fulfillment of the Requirements for the Degree of Master of Philosophy in Department of Civil and Environmental Engineering, Hong Kong, 2015.
10. E. Fattinnanzi, Acampa G., Forte F. and F. Rocca , «*La Valutazione complessiva della qualità nel progetto di architettura*» *Valori e valutazioni ,* n. 21, 2018.
11. A. Galiano, C. Brebbia, L. Mahdjoubi and R. Laing, *Building Information Systems in the Construction Industry*, WIT Press, 2018.
12. H. Kim, Z. Chen, C.S. Cho, H. Moon, K. Ju, and W. Choi, «*Integration of BIM and GIS: Highway cut and fill earthwork balancing»* vol. In Computing in Civil Engineering, p. 468–474, 2015.
13. S. Boddy and L. Koskela, «*Challenges and Opportunities in Implementing Lean and BIM on a Infrastructure Project*» In: Formoso, C.T. and Tzortzopoulos, 21th Annual Conference of the International Group for Lean Construction*.* Fortaleza, Brazil, 2013.
14. D. Patassini, «*Cultura della valutazione, Rassegna di approcci, metodi e tecniche*» 2019. [Online]. Available: http://www.iuav.it/Ateneo1/docenti/docenti201/Patassini-/materiali-/index.htm.
15. F. Fontana, «*I linguaggi del BIM: la digitalizzazione dei processi tra prassi e teoria, il caso studio del Lefay Resort & SPA Dolomiti*,» Tesi di laurea Politecnico di Torino, 2017/2018.
16. M. Bolpagni, «*The implementation of BIM within the public procurement. A model-based approach for the construction industry*,» VTT Technology, 2013.
17. European Parliament, 2014. *Directive 2014/24/EU of the European Parliament and of the Council of the 26 February 2014 on public procurement and repealin*g Directive 2004/18/EC.
18. D.Lgs 50 del 2016 (Codice dei Contratti Pubblici).
19. A. Pavan, C. Mirarchi and M. Giani, «*BIM: metodi e strumenti*» Tecniche Nuove, Milano, 2017.

20. M. Bolpagni and Ciribini A., «*An Innovative Approach to e-public Tendering Based on Model Checking, Procedia Economics and Finance*,,» 8thNordic Conference on Construction Economics and Organization, vol. 21, pp. 32-39, 2013.
21. A. Daniela, «*Evoluzione del Processo (digitale)»* Ingenio*,* 2018.
22. Italferr Gruppo Ferrovie dello Statoitaliane, *Innovare per progettare il futuro, primo libro bianco sul Building Information Modeling*, 2018.
23. O. Anna, «*Industria 4.0 BIM e InfraBIM tra didattica e ricerca al Politecnico di Torino*,» Ingenio, 2018.
24. A.Pavan, F. Re Cecconi, S. Maltese, E. Oliveri and G. Aracri, «*La scheda prodotti interattiva di INNOVance*».
25. N. Hjelseth and E. Nisbet, «*Overview of concept for model checking*» in CIB W78, 27th International Conference, Cairo, Egitto, 2010.
26. J. Wangara, *Quality Management in BIM, Use of Solibri Model Checker and CoBIM Guidelines for BIM,* Thesis of Helsinki Metropolia University of Applied Sciences, 2018.
27. Solibri, «*Getting Started with Solibri Model Checker V9*», PDF 2017.
28. C. Eastman., J. Lee, Y. Jeong and L. Lee, «*Automatic rule-based checking of building designs»* Automation in Construction, vol. vol. 18, n. issue 8, pp. 1011-1033, 2009.
29. Harpaceas, «*Il BIM nella fase di verifica: l'utilizzo di Solibri Model Checker in un progetto di Italferr*» Ingenio 2018.
30. A. Viola, «*Sviluppo di un modello BIM per la manutenzione delle infrastrutture stradali*» Tesi di laurea magistrale in Ingegneria Civile, Politecnico di Torino, 2018.
31. T Campisi, A Canale, G Tesoriere, I Lovric, B Čutura, *The Importance of Assessing the Level of Service in Confined Infrastructures: Some Considerations of the Old Ottoman Pedestrian Bridge of Mostar* Appl. Sci. 2019 9, https://doi.org/10.3390/app9081630
32. Načinović Margan, Andrea; Arbanas, Željko; Deluka-Tibljaš, Aleksandra; Cuculić, Marijana. *Deformational properties of unbound granular pavement materials,* Road and Rail Infrastructure III Lakušić, Stjepan (ur.).Zagreb: Faculty of Civil Engineering University of Zagreb, 2014. 649-656

Numerical Evaluation of an Internally Cracked Autofrettaged Spherical Pressure Vessel

M. Perl[1, a)] and M. Steiner[2]

[1]*Department of Mechanical Engineering - Pearlstone Center for Aeronautical Engineering Studies*
Ben-Gurion University of the Negev
Beer-Sheva 84105, Israel
[2]*Faculty of Aerospace Engineering*
Technion Israel Institute of Technology, Haifa 3200003, Israel.
[a)]merpr01@bgu.ac.il

Abstract. Internally cracked, fully or partially autofrettaged, spherical pressure vessels are analyzed by numerically calculating 3-D Stress Intensity Factor (SIF) distributions along the fronts of radial lunular or crescentic cracks emanating from the vessel's bore. The finite element (FE) method is used employing singular elements along the crack front. A novel realistic autofrettage residual stress field incorporating the Bauschinger effect is embodied in the FE model using an equivalent temperature field. The SIFs are extracted by using both the J-integral and the displacement extrapolation methods, and are calculated for three vessel geometries, a wide range of crack depth to wall thickness ratios, various ellipticities, and three levels of autofrettage. A detailed study of the influence of the above parameters on the prevailing SIF is conducted. The results attest to the favorable effect of autofrettage in reducing the SIF, delaying crack initiation, slowing down crack growth rate, and thus, substantially prolonging the fatigue life of the vessel. They also emphasize the importance of properly accounting for the Bauschinger effect including re-yielding, and highlight the significance of the 3-D analysis.

INTRODUCTION

More than one hundred years ago, the process of autofrettage was suggested by Col. L. Jacob of the French Artillery [1] for the purpose of increasing the allowable pressure in gun barrels in order to extend their firing range. Further on, it was found that the autofrettage process has an additional substantial benefit in decreasing the vessel's susceptibility to cracking, i.e., delaying crack initiation and slowing down crack growth rate, thus considerably increasing the total fatigue life of the barrel. This process has been further developed and has been widely used for cylindrical pressure vessels in a variety of industries.

Spherical pressure vessels, though less common than cylindrical ones, are widely used in industry mainly due to their optimal specific strength (strength/weight) and their ease of packing. Moreover, whenever ***extremely high pressure*** take place as in high explosion containment tanks, spherical pressure vessels are actually the only feasible solution. Some of these spherical pressure vessels are manufactured from a series of double curved petals welded along their meridional lines. These vessels are susceptible to cracking along the welds due to one or more of the following factors: cyclic pressurization-depressurization, the existence of a heat-affected zone near the welds, tensile residual stresses within this region, and the presence of corrosive agents. Consequently, radial cracks develop from the inner surface of the vessel on the welded planes.

Nowadays, autofrettage is rarely applied to spherical pressure vessels and the possible beneficial effect on such vessels has only recently been investigated for the first time [2]. It is the objective of the present analysis to examine and consequently determine the beneficial influence of autofrettage in reducing the SIF for an inner radial lunular or crescentic crack in spherical pressure vessels. The 3-D analysis is performed by the FE method and a novel realistic residual stress field incorporating the Bauschinger effect. The autofrettage residual stress field is embodied in the FE model, using an equivalent temperature field.

The distributions along the crack front of K_{IA}, the negative[1] stress intensity factor due to autofrettage, for various lunular[2] and crescentic[3] shapes (see Fig. 1) are evaluated for three vessel geometries (R_0/R_i=1.1, 1.2, and 1.7), a wide range of crack depth to

---

1 It is only in the context of superposition of loads that a SIF can be considered negative.
2 A lunular crack is defined as a planar, part-through crack, whose shape is enclosed by two circular arcs of different radii, one concave and one convex, which intersect at two points, having an ellipticity of a/c=1 (Fig.1b).
3 A Crescentic crack is defined as a planar, part-through crack whose shape is enclosed by two intersecting arches, the concave one which is elliptical, and the convex one which is circular, having an ellipticity of $a/c \neq 1$(Fig. 1c-d).

wall thickness ratios (a/t=0.01-0.8), various crack ellipticities(a/c=0.2-1.5), and three levels of autofrettage (ε=50%, 75%, and 100%). The SIFs are numerically evaluated using J-integral and the displacement extrapolation method.

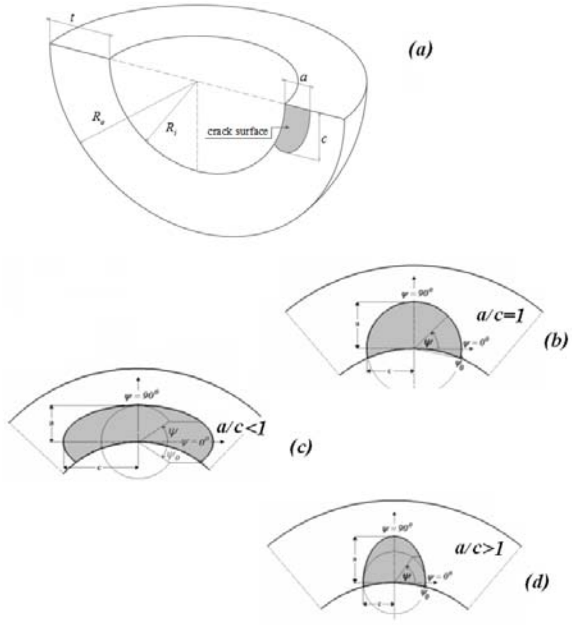

FIGURE 1. (a) quarter of the spherical vessel containing one crack; (b) the parametric angle ψ defining the points on the crack fronts of a lunular crack, (c) a slender crescentic crack, and (d) a transverse crescentic crack.

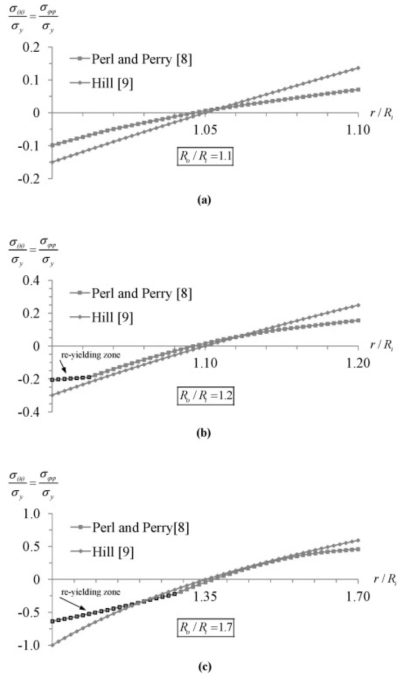

FIGURE 2. The distribution of the hoop/meridional residual stress component through the wall of a fully autofrettaged spherical pressure vessel of radii-ratio of (a) R_o/R_i=1.1, (b) R_o/R_i=1.2, (c) R_o/R_i=1.7

THE AUTOFRETTAGE MODEL AND ITS SIMULATION

Although the process of autofrettage has been used for more than a century, the calculation of the residual stress field resulting from this process has been problematic. This is due to the fact that a realistic quantitative evaluation of the autofrettage residual stress field is highly dependent on the particular assumptions made regarding the material's elasto-plastic behavior, as well as on any other simplifications made to yield a more tractable problem. As the calculated residual stress field induced by the autofrettage process serves as an essential input to the stress analysis of the intact as well as the cracked vessel, its realistic evaluation has a paramount impact on the end results.

The first attempt to evaluate the residual stress field due to autofrettage in a spherical pressure vessel was made by Hill [3] in 1950. In order to obtain an elegant analytical solution, Hill assumed an incompressible elasto-perfectly-plastic material. As a result of these assumptions, this approach overestimates the magnitude of the residual stress components. In recent years, several attempts were made by Adibi-Asl and Livieri [4], Parker and Huang [5] and others to improve the modeling of autofrettage in spherical pressure vessels by choosing more realistic material behaviors. The most recent solution was suggested by, Perl and Perry [6] who evaluated the residual stress field in an autofrettaged spherical pressure vessel fully incorporating the Bauschinger effect, by adapting their previously proposed experimental-numerical model for solving autofrettage in a cylindrical pressure vessel. This model is presently one of the two most realistic models[4] that are completely based on the experimentally measured stress-strain curve under repeated reversed loading, which enables an accurate determination of the material behavior including the Bauschinger effect both in tension and in compression.

This new model was recently evaluated for a typical pressure vessel made of AISI 4340 steel. Fig. 2 represents the residual hoop (meridional) stress component distribution through the wall thickness of a fully autofrettaged (ε =100%) spherical vessel of radii ratios of R_o/R_i=1.1, 1.2 and 1.7. For comparison purposes, Hill's solution for the same vessel is also presented. In terms of the

[4] The other model is that by Parker and Huang [5].

beneficial effect of autofrettage, one should examine the stress distribution near the inner surface of the vessel. It is evidently clear that in this critical region the two solutions differ considerably.

The greatest difference between the two models occurs in the most sensitive zone, i.e., the inner portion of the sphere's wall. The realistic residual hoop stress at the bore is much smaller, in absolute value, than the one estimated by Hill's solution in vessels of R_o/R_i=1.1, 1.2, and 1.7 by about 34%, 31%, and 36% respectively.

The autofrettage residual stress field prevailing in a spherical pressure vessel is evaluated discretely applying the Perl and Perry model, and is embodied in the FE analysis using an equivalent temperature field emulating it very accurately. The discrete values of the equivalent temperature field are calculated using the general algorithm developed by Perl [7].

THREE DIMENSIONAL FINITE ELEMENT ANALYSIS

The three dimensional analysis of the cracked sphere is based on Linear Elastic Fracture Mechanics (LEFM). The pressure vessel is modeled as an elastic sphere of inner radius R_i, outer radius R_O, and wall thickness t. The spherical vessel contains an inner radial, lunular or crescentic crack of a $2c$ length and a depth (see Fig. 1). The crack is symmetric with respect to the equatorial plane as described in Fig. 1a.

Due to the various symmetries of the geometrical configuration, only a quarter of the spherical vessel must be analyzed (see Fig.1a). The autofrettage residual stress field is embodied in the FE model by an equivalent temperature field. The model is solved using the commercial ANSYS 14.0 FE code [8]. To accommodate the singular stress field in the vicinity of the crack front, this area is covered with a layer of 20-node isoparametric brick elements collapsed to wedges, forming singular elements at the crack front [9]. On top of this layer, at least four additional layers, consisting of 20-node isoparametric brick elements, are meshed. The rest of the model is meshed with 10-node tetrahedron elements. Near the crack front the elements are chosen to be small, and their size is gradually increased when moving away from it. SIFs are extracted using two methods built into ANSYS: J-integral [10], and the crack-face displacement extrapolation. SIFs are calculated at discrete points equally spaced along the crack front. For very slender cracks a/c=0.2, SIFs were calculated at 140 points along half of the crack front. For cracks of a/c=0.4, 75 points were used, and for cracks of $a/c \geq 0.6$, SIFs were calculated at 55 points along half of the crack front.

Validation of the Model

Presently, to the best of the authors' knowledge there are no available solutions for K_{IA}, the stress intensity factor due to autofrettage. Therefore, the model is validated by two different procedures: Convergence tests of the SIF as a function of the number of degrees of freedom (DOF) in the model, and comparison between two independent methods for evaluating the SIF: J-integral and the displacement extrapolation procedure.

Fig. 3 represents a typical convergence test. In this case, the convergence criterion was chosen to be the value of the SIF at the crack's deepest point $\psi = 90°$. The results clearly indicate that as the number of DOF increases, the SIF converges to a practically constant value. In order to further validate the model, a second approach is used: K_{IA} is evaluated by the J-integral along four paths at different distances from the crack tip, and the results are compared to K_{IA} independently obtained by the crack-face displacement extrapolation procedure for all the points along the crack front. Fig. 4 represents the SIFs calculated by the two methods for a typical case. The results obtained by the two methods are practically identical except for a small discrepancy of less that 3% that occurs near the inner wall of the sphere as can be expected. The results also indicate that the SIF obtained by the J-integral converges as the integration path becomes closer to the crack tip [11]. The maximal difference between the SIFs obtained using different integration paths is less than 1% for shallow cracks and up to 3% for deeper ones. For very deep cracks a comparison only between J-integral along the smallest path and the SIF determined by displacement extrapolation was made, yielding differences of less than 3%.

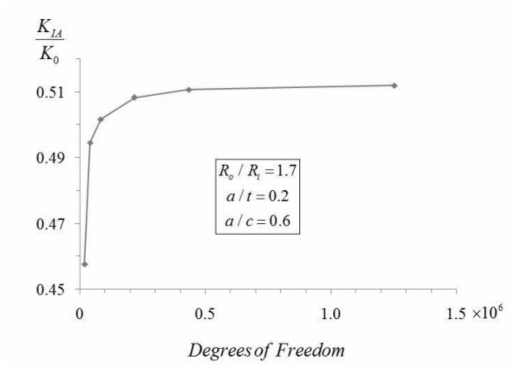

FIGURE 3. K_{IA}/K_0 at ψ=0° as a function of the number degrees of freedom for a crack of a/t=0.2, a/c=0.6 in a spherical vessel of R_0/R_i=1.7.

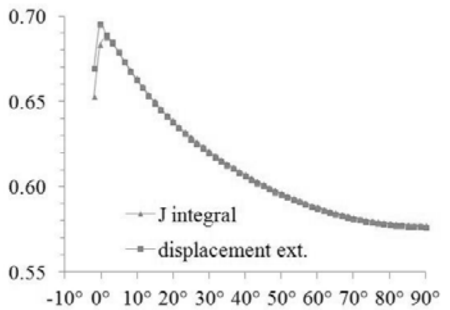

FIGURE 4. K_{IA}/K_0 vs. ψ calculated by J-integral and of the Displacement Extrapolation Method for R_0/R_i=1.7, a/t=0.1, a/c=1

RESULTS

Typical results representing the influence of crack's relative depth and the vessel's relative thickness on K_{IA}/K_0 distribution along a slender crescentic crack of ellipticity $a/c=0.6$ are presented in figures 5 and 6 for a thin, R_0/R_i=1.1, and a very thick fully autofrettaged vessel, R_0/R_i=1.7. In these two cases as the crack's relative depth, a/t, increases, K_{IA}/K_0 value at $\psi=90°$ decreases while remaining almost unchanged at the inner portion of the vessel's wall ($\psi\approx 0°$). As the relative thickness of the vessel increases, the magnitude of the residual field increases as well. As a result, the absolute value of K_{IA} increases and thus the values of K_{IA}/K_0, and K_{IAmax}/K_0, increase as well.

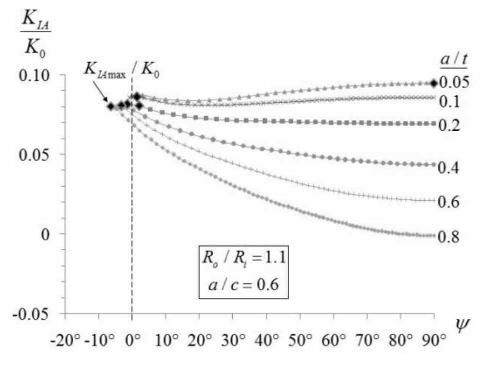

FIGURE 5. Variation of K_{IA}/K_0 as a function of ψ along the front of a slender crescentic crack a/c=0.6 for various relative crack depths in a fully autofrettaged vessel ε=100% of relative thickness of R_0/R_i=1.1.

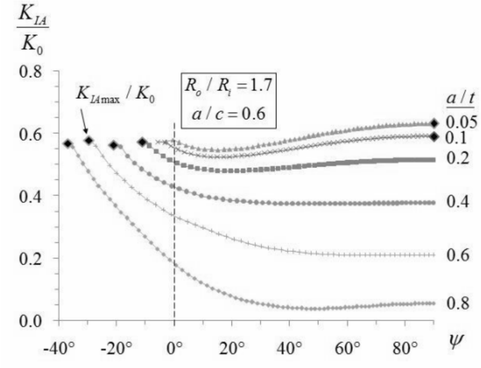

FIGURE 6. Variation of K_{IA}/K_0 as a function of ψ along the front of a slender crescentic crack a/c=0.6 for various relative crack depths in a fully autofrettaged vessel ε=100% of relative thickness of R_0/R_i=1.7.

CONCLUSIONS

1. The thicker the vessel, the higher the magnitude of the residual stress field and the higher $|K_{IA}|$ is.
2. The location of the maximum SIF K_{IAmax} depends on crack depth and ellipticity. For shallow and very slender cracks ($a/t\leq$ 0.1and $a/c\leq$ 0.6), K_{IAmax} occurs at ψ=90°. In the case of shallow cracks of larger ellipticity ($a/t\leq$ 0.1and a/c>0.6), K_{IAmax} shifts to the vicinity of $\psi\approx$0°.As cracks become deeper, K_{IA}/K_0 near ψ=90° becomes smaller and cracks of small ellipticity may reach K_{IAmax} at either ψ=90° or $\psi\approx$0°.
3. Once K_{IA} is determined, it is possible to assess the favorable effect of autofrettage on the fatigue life of spherical pressure vessels. K_{IA} can considerably reduce the prevailing effective stress intensity factor, $K_{IN}=K_{IP}-|K_{IA}|$, delaying crack initiation, slowing down crack growth rate, and thus increasing the total fatigue life of the spherical pressure vessel substantially.
4. The magnitude of the negative residual hoop stress is a decreasing function of r and therefore, as the crack penetrates deeper into the vessel's wall, it encounters smaller and smaller compressive stresses which become tensile beyond a certain depth. This mainly affects the deepest part of the crack front, and has almost no effect on the crack front near the inner surface of the vessel. As a result, K_{IA}/K_0 values decrease as the crack's relative depth a/t increases.

REFERENCES

1. L. Jacob, *La Résistance et L'équilibre Élastique des Tubes Frettés* (Mémoire de L'artillerie Navale, 1, 1907) pp. 43-155.
2. Perl, M., et al. "3-D Stress Intensity Factors due to Autofrettage for an Inner Radial Lunular or Crescentic Crack in a Spherical Pressure Vessel," Engineering Fracture Mechanics, 131, 2014, pp. 282-295.
3. R. Hill, 1950, *The Mathematical Theory of Plasticity* (Oxford University Press, New York 1950).
4. R. Adibi-Asl and P. Livieri, Journal of Pressure Vessel Technology **129**, 3, pp. 411-419 (2007).
5. A. P. Parker and X. Huang, Journal of Pressure Vessel Technology, **129**, pp. 83-88 (2007).
6. M. Perl and J. Perry, Journal of Pressure Vessel Technology **132**, 011204 (2010
7. M. Perl, Journal of Pressure Vessel Technology **130**, 03, 031201(2008).
8. ANSYS 14.0, Verification Manual, Swanson Analysis Systems Inc. (2011).
9. R. S. Barsom, International Journal of Numerical Methods in Engineering, **10**, 1, pp. 25- 37 (1976).
10. J. R. Rice, Journal of Applied Mathematics*,* 35, pp. 379-386 (1968).
11. N. Omer and Z. Yosibash, International Journal of Fracture, 136, pp. 1-36 (2005).

Fast Inverse Laplace Transform for the Unsteady Thermal Response of Geothermal Heat Exchangers

Miguel Hermanns[1]

[1] *Departamento de Mecánica de Fluidos y Propulsión Aeroespacial, Escuela Técnica Superior de Ingeniería Aeronáutica y del Espacio, Universidad Politécnica de Madrid, Plaza Cardenal Cisneros 3, E-28040 Madrid, Spain*

miguel.hermanns@upm.es

Abstract. The successful harnessing of geothermal energy for the efficient heating and cooling of buildings relies upon the correct sizing of geothermal heat exchangers. This is done during the building's design phase using extensive numerical simulations to forecast the unsteady thermal response of the geothermal heat exchanger and its surrounding ground for the next 25, 50, or even 100 years of operation. In the present work, an efficient numerical Laplace inversion formula is proposed, which applied to the obtained solution in the complex Laplace plane, allows the fast and accurate prediction of the sought unsteady thermal response.

INTRODUCTION

For the heating and cooling of buildings, the harnessing of geothermal energy represents one of the most energy efficient solutions available nowadays. An HVAC (heating, ventilation, and air conditioning) system based on that renewable energy source consists in a water-to-water heat pump connected to a geothermal heat exchanger composed of multiple vertical geothermal boreholes. Each of these boreholes is typically equipped with a U-shaped pipe through which a heat carrying liquid flows and exchanges heat with the surrounding ground. Such an HVAC system can only be considered truly renewable, however, if the geothermal heat exchanger is correctly designed and sized. Otherwise, an excessive drift in the operating temperatures of the heat carrying liquid builds up over time, negatively affecting the energy efficiency of the heat pump, and consequently of the whole HVAC system.

Advanced theoretical/numerical models are regularly used to study the unsteady thermal response of geothermal heat exchangers. One such model is the *Superposition Borehole Model* (SBM) that exploits the large disparity in time and length scales present in the equations to strongly simplify the three-dimensional unsteady heat conduction problem in the ground [1, 2]. By numerically solving multiple axisymmetric unsteady heat conduction problems, with each one centered around each borehole, and then superimposing them, the SBM obtains the sought unsteady thermal response. In the original formulation of the model, those axisymmetric problems are discretized using finite differences for the spatial derivatives and an explicit Euler scheme for the time derivative.

In recent years, the SBM has been reformulated in terms of point sources of heat, allowing the problem and its solution to be expressed in terms of integral operators instead of differential equations [3, 4, 5, 6]. Additionally, the Laplace transform is used to convert the time-marching problem into an algebraic problem, whose solution is much simpler to obtain [3, 6]. Once the results in the complex Laplace plane are known, the sought time evolution of the geothermal heat exchanger is recovered through the inverse Laplace transform. The benefit of all this is a significantly reduced computational cost, with only 790 seconds of wall-clock time required on an Intel Core i5-2500K processor to obtain the unsteady thermal response of a typical geothermal heat exchanger composed of 100 boreholes [3].

Further reductions in computational time can be achieved by improving the employed numerical Laplace inversion formula. In [3], a method based on the Fast Fourier Transform is used, which needs to be invoked for each time instant to compute. In the present work, a different numerical Laplace inversion formula is developed that allows the unsteady thermal response of a typical geothermal heat exchanger composed of 100 boreholes to be obtained in just 206 seconds using a single core of an Intel Core i7-7700K processor. Even after factoring out the performance difference between the two microprocessors, the proposed numerical Laplace inversion formula still leads to a three-fold speedup, with its computational cost not depending on the total number of time instants to compute.

THE SUPERPOSITION BOREHOLE MODEL IN THE COMPLEX LAPLACE PLANE

A geothermal heat exchanger is composed of N_b vertical geothermal boreholes. Each borehole j is characterized by its nondimensional depth h_j, its nondimensional buried depth d_j, its slenderness Λ_j, its network of nondimensional thermal resistances (A_j, B_j, and S_j), and its nondimensional operating conditions Ω_j [4, 5, 7]. The thermal state of each borehole j is given by the nondimensional temperature difference Δ_j between the two legs of the U-shaped pipe, the nondimensional weighted mean fluid temperature Θ_j, and the nondimensional heat injection rate per unit borehole length $\bar{q}_j$, all of which are functions of the nondimensional vertical coordinate ξ and the nondimensional time τ [6].

To obtain the functions $\Delta_j(\xi, \tau)$, $\Theta_j(\xi, \tau)$, and $\bar{q}_j(\xi, \tau)$, the unsteady heat conduction in the ground and the grout and the unsteady convective heat transport along the U-shaped pipes need to be modeled and solved. Using the simplifying assumptions and hypotheses of the Superposition Borehole Model, and the Laplace transform to address the resulting time-marching problem, the following set of equations is obtained for each borehole j [4, 5, 6, 7]:

$$\frac{d\tilde{\Delta}_j}{d\xi} = -\tilde{q}_j, \qquad \frac{d\tilde{\Theta}_j}{d\xi} = \frac{\Omega_j S_j}{h_j}\tilde{q}_j - \frac{\Omega_j^2}{h_j^2 A_j}\tilde{\Delta}_j, \qquad \tilde{\Theta}_j - \tilde{\Theta}_{bj} = \tilde{q}_j B_j, \tag{1}$$

where the superscript ~ denotes the Laplace transform of the corresponding variable. The nondimensional mean azimuthal borehole wall temperature $\tilde{\Theta}_{bj}(\xi)$ of borehole j, that accounts for the thermal response of the ground and for the thermal influences exerted by the neighboring boreholes, is given by

$$\tilde{\Theta}_{bj} = \tilde{\Theta}_\infty + \sum_{n=1}^{N_b} \frac{1}{4\pi} \int_{d_n}^{h_n} \tilde{q}_n(\xi_0) \left[\frac{\mathrm{e}^{-\sqrt{s}\sqrt{\eta_{jn}^2 + (\xi-\xi_0)^2}}}{\sqrt{\eta_{jn}^2 + (\xi-\xi_0)^2}} - \frac{\mathrm{e}^{-\sqrt{s}\sqrt{\eta_{jn}^2 + (\xi+\xi_0)^2}}}{\sqrt{\eta_{jn}^2 + (\xi+\xi_0)^2}} \right] \mathrm{d}\xi_0, \tag{2}$$

where $\tilde{\Theta}_\infty(\xi)$ is the nondimensional unperturbed ground temperature. The nondimensional planar distance between boreholes j and n is η_{jn}, with $\eta_{jj} = h_j/\Lambda_j$, and s is the complex number in the Laplace plane.

Each of the N_b boreholes is subject to the following boundary conditions at its top, $\xi = d_j$, and its bottom $\xi = h_j$,

$$\xi = d_j: \quad \tilde{\Delta}_j = \tilde{f}_j, \qquad \xi = h_j: \quad \tilde{\Delta}_j = 0, \tag{3}$$

with $\tilde{f}_j$ being the nondimensional heat injection rate of borehole j. The values of $\tilde{f}_j$ result from imposing a set of global constraints, being the first one the energy conservation at geothermal heat exchanger level [5]:

$$\tilde{f} = \sum_{j=1}^{N_b} \tilde{f}_j, \tag{4}$$

where $\tilde{f}$ is the nondimensional heat injection rate imposed by the HVAC system onto the geothermal heat exchanger. Further constraints emerge from the condition that the heat carrying liquid fed to the boreholes comes from a horizontal network of distribution pipes. In case all boreholes are connected in parallel to that network, all the borehole inlet temperatures must be equal to the a priori unknown nondimensional inlet temperature $\Theta_{\mathrm{in}}(\tau)$. This leads to the following set of N_b constraints to be satisfied by the solution in the complex Laplace plane [5]:

$$\tilde{\Theta}_j(d_j) + \frac{\Omega_j}{2h_j}\left(S_j + 1\right)\tilde{\Delta}_j(d_j) = \tilde{\Theta}_{\mathrm{in}}, \qquad j = 1, \ldots, N_b. \tag{5}$$

The solution to the integro-differential system of equations formed by (1), (2), (3), (4), and (5) has to be obtained numerically for each value of the complex number s. To correctly capture the strong variations close to the borehole endings of the nondimensional heat injection rates per unit borehole lengths $\tilde{q}_j$, a grid point distribution based on the extrema of the Chebyshev polynomials of the first kind is used, where $N+1$ is the total number of grid points:

$$\xi_{ij} = d_j + (h_j - d_j)\frac{1 - \cos\left(\pi \frac{i}{N}\right)}{2}, \qquad i = 0, \ldots, N. \tag{6}$$

By approximating the derivatives using first order finite differences and the integrals using the trapezoidal rule, a large system of linear algebraic equations is constructed. Its solution is obtained using an iterative GMRES solver, whose convergence is strongly accelerated using a physics-based preconditioner analogous to the one employed by the author in [8], thereby completing the formulation and solution of the SBM in the complex Laplace plane. The sought time evolution of the geothermal heat exchanger is then obtained by applying the inverse Laplace transform.

INVERSE LAPLACE TRANSFORM

Given the function $F(s)$, that represents any of the results of interest that arise from the solution procedure described in the previous section, its temporal counterpart $f(\tau)$ is obtained using the inverse Laplace transform. In the present work, this inverse transformation is expressed through the Bromwich integral defined as

$$f(\tau) = \frac{1}{2\pi i} \lim_{T\to\infty} \int_{\sigma-iT}^{\sigma+iT} F(s)\, \mathrm{e}^{s\tau}\, \mathrm{d}s, \tag{7}$$

where $i = \sqrt{-1}$ and σ places the integration contour to the right of all singularities of $F(s)$. In order to exploit this expression, the integral along the line $\mathrm{Re}(s) = \sigma$ needs to be discretized using any of the well known quadrature rules. The convergence of the so obtained numerical Laplace inversion formula can be vastly improved by deforming the integration path. The aim is to exploit the exponential factor of the integrand by choosing a new path along which it decays rapidly, so that a reduced number of discretization points is required by the quadrature rule. This idea is valid as long as the new integration path is also located to the right of all singularities of $F(s)$.

Several different integration paths $z(\theta)$ have been proposed in the literature, with θ being the argument of the complex number s [9, 10, 11]. All of them share the property that $\mathrm{Re}(z(\pm\pi)) = -\infty$, which ensures the rapid decay of the aforementioned exponential factor. Application of $z(\theta)$ to (7) leads to an integral between $-\pi$ and π, which can then be discretized, as shown in Figure 1, using the midpoint rule and the $2N$ uniformly-spaced discretization points $\theta_k = \pi(2k-1)/(2N)$, with k ranging from $1-N$ till N. Since the function $F(s)$ satisfies that $F(s^*) = F(s)^*$, where the superscript $*$ represents the conjugate of a complex number, the final expression for the numerical Laplace inversion formula is

$$f(\tau) = \frac{1}{2\pi i} \int_{-\pi}^{\pi} F(z(\theta))\, \mathrm{e}^{z(\theta)\tau} z'(\theta)\, \mathrm{d}\theta$$

$$= \frac{1}{N} \sum_{k=1}^{N} \mathrm{Im}\Big[F(z(\theta_k))\, \mathrm{e}^{z(\theta_k)\tau} z'(\theta_k)\Big]. \tag{8}$$

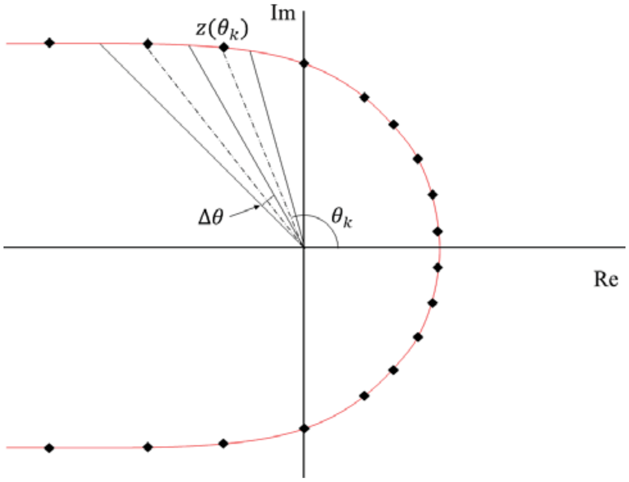

FIGURE 1. Sketch of the deformed integration path $z(\theta)$ with the employed uniformly-spaced discretization points θ_k.

The number of evaluations N required for a certain error level ε depends on the chosen integration path. In the present work, the path proposed by Dingfelder and Weideman is used [11], for which $\varepsilon \approx \mathrm{e}^{-2.719N}$. Hence, for single precision accuracy ($\varepsilon = 10^{-8}$), just $N = 7$ evaluations would be required. Nevertheless, since the chosen integration path depends on the considered time instant τ,

$$z(\theta) = \frac{2N}{\tau}\left(-0.6122 + 0.5017\frac{\theta}{\tan(0.6407\theta)} + 0.2645 i\theta\right), \tag{9}$$

and if N_τ time instants are to be computed, a total of $N_\tau N$ evaluations of the costly function $F(s)$ result, which can still be too computationally expensive.

In the present work a novel strategy is proposed to overcome the just highlighted problem. The idea is to use the same integration path for multiple time instants that are not too far apart, so that the same N evaluations of the costly function $F(s)$ can be reused. This strategy works, despite the dependence of $z(\theta)$ on the considered time instant, thanks to the weak degradation the convergence rate of the employed integration path experiences for time instants that are not too far apart from the one used for the definition of $z(\theta)$.

The proposed strategy is implemented as follows. Consider the N_τ time instants of interest to be contained in the time interval $[\tau_{\min}, \tau_{\max}]$. This time interval is then divided into octaves, with each octave n covering a time subinterval $[\tau_{\max}/2^n, \tau_{\max}/2^{n-1}]$. Thus, a total number of $N_o = \lceil \ln(\tau_{\max}/\tau_{\min}) / \ln(2) \rceil$ octaves results, where the operator $\lceil x \rceil$ represents the least integer greater or equal than x. For each octave n, one single integration path $z_n(\theta)$ is used, whose parameters are computed for the reference time $\tau_{\max}/2^{n-1}$ contained in the octave.

RESULTS AND CONCLUSIONS

For the proposed numerical Laplace inversion formula, the total number of evaluations of the costly function $F(s)$ is $N_o N$, which coincides with $N_\tau N$ when only a single time instant of interest is contained in each octave. Figure 2 shows the relative errors committed by the numerical Laplace inversion formula (with $\varepsilon = 10^{-4}$) in the computation of the nondimensional inlet temperature $\Theta_{\text{in}}(\tau)$ of the geothermal heat exchanger composed of 100 boreholes described in [3]. Using the same spatial resolution as in [3], the shown results required a wall-clock time of just 206 seconds using a single core of an Intel Core i7-7700K processor.

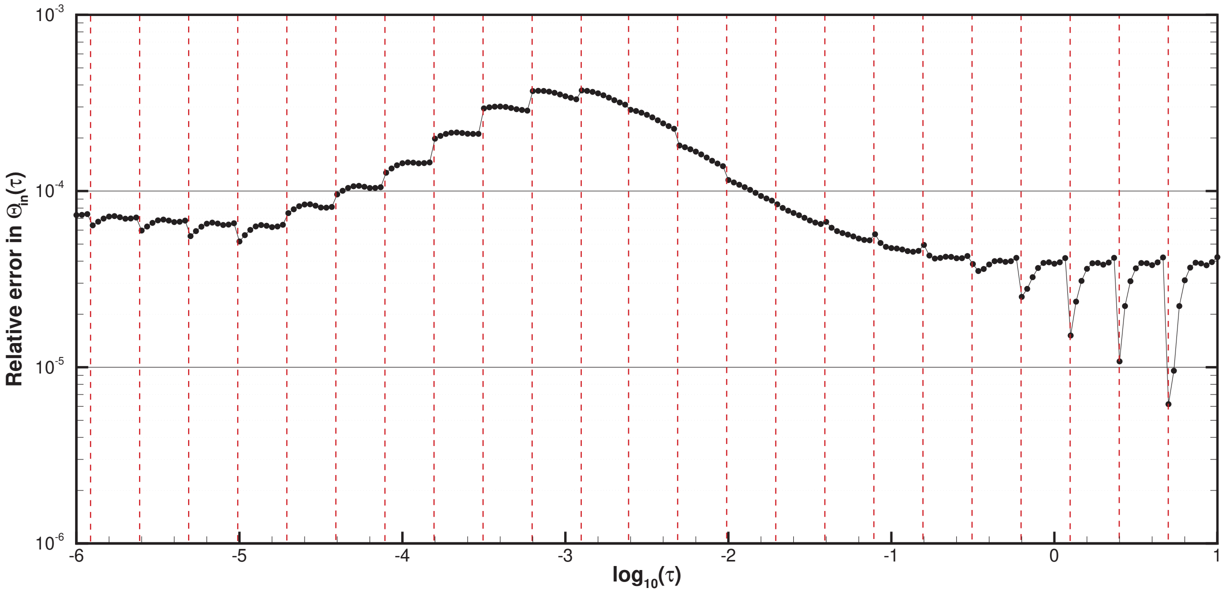

FIGURE 2. Relative error in the nondimensional inlet temperature Θ_{in} of a typical geothermal heat exchanger composed of 100 boreholes as a function of the nondimensional time τ. The error level imposed onto the numerical Laplace inversion formula is $\varepsilon = 10^{-4}$, and the vertical dashed lines mark the limits of the octaves used to divide the time interval $[\tau_{\min}, \tau_{\max}] = [10^{-6}, 10^{+1}]$.

ACKNOWLEDGMENTS

Work was funded by Spanish *Ministerio de Economía y Competitividad* through project ENE2015-68703-C2-2-R.

REFERENCES

[1] P. Eskilson, *Superposition Borehole Model, Manual for Computer Code*, Department of Mathematical Physics, University of Lund, Lund, Sweden (1986).

[2] P. Eskilson, "Thermal analysis of heat extraction boreholes," Ph.D. thesis, Department of Mathematical Physics, Lund Institute of Technology, Lund, Sweden 1987.

[3] M. Cimmino, International Journal of Heat and Mass Transfer **91**, 1119–1127 (2015).

[4] M. Hermanns and S. Ibáñez, SIAM Journal on Applied Mathematics **79**, 230–256 (2019).

[5] M. Hermanns and S. Ibáñez, Submitted to SIAM Journal on Applied Mathematics (2018).

[6] M. Hermanns, In preparation for SIAM Journal on Applied Mathematics (2019).

[7] S. Ibáñez and M. Hermanns, SIAM Journal on Applied Mathematics **78**, 1658–1681 (2018).

[8] M. Hermanns, AIP Conference Proceedings **2040**, 150002–1–150002–4 (2018).

[9] A. Talbot, IMA Journal of Applied Mathematics **23**, 97–120 (1979).

[10] J. A. C. Weideman, SIAM Journal on Numerical Analysis **44**, 2342–2362 (2006).

[11] B. Dingfelder and J. A. C. Weideman, Numerical Algorithms **68**, 167–183 (2015).

Prediction of Non-Metallic Inclusions in Steel Wires for Tire Reinforcement by means of Machine Learning Algorithms

Miguel Cuartas[1, b)], Estela Ruiz[2, c)], Diego Ferreño[3, a)], Jesús Setién[3, d)], Valentín Arroyo[1, e)] and Federico Gutiérrez-Solana[3, f)]

[1] *GTI (Group of Information Technologies), University of Cantabria. E.T.S. de Ingenieros de Caminos, Canales y Puertos, Av. Los Castros 44, 39005 Santander, Spain.*
[2] *Global Steel Wire, GSW. Nueva Montaña s/n, 39011, Santander, Spain*
[3] *LADICIM (Laboratory of Science and Engineering of Materials Division), University of Cantabria. E.T.S. de Ingenieros de Caminos, Canales y Puertos, Av. Los Castros 44, 39005 Santander, Spain.*

[a)]ferrenod@unican.es
[b)]miguel.cuartas@unican.es
[c)]estela.ruiz@globalsteelwire.com
[d)]jesus.setien@unican.es
[e)]valentin.arroyo@unican.es
[f)]federico.gutierrez-solana@unican.es

Abstract. This study was aimed at developing a reliable Machine Learning algorithm to classify castings of steel for tire reinforcement depending on the number and properties of inclusions, experimentally determined. 855 castings were available for training, validation and testing. 140 parameters are monitored during fabrication, which are the features of the analysis; the output is 1 or 0 depending on whether the casting is rejected or not. The following algorithms have been employed: Logistic Regression, K-Nearest Neighbors, Support Vector Classifier, Random Forests, AdaBoost, Gradient Boosting and Artificial Neural Networks. The reduced value of the rejection rate implies that classification must be carried out on an imbalanced dataset. Resampling methods and specific scores for imbalanced datasets (Recall, Precision and AUC rather than Accuracy) were used. Random Forest was the most successful method providing an area under the curve in the test set of 0.85. No significant improvements were detected after resampling. It has been proved that this tool allows the samples with a higher probability of being rejected to be selected, improving the effectiveness of the quality control. In addition, the optimized Random Forest has enabled to identify the most important features, which have been satisfactorily interpreted on a metallurgical basis.

INTRODUCTION

Monitoring the final properties of steel manufactured products is an indispensable procedure to guarantee their final quality. After the fabrication of steel, composition, mechanical behavior or microstructure are determined to verify the quality requirements of the product. Steelmaking is a complex process, involving chemical reactions extremely sensitive to the environmental conditions (temperature, composition, mass and heat transfer processes, etc.). For this reason, the relationship between the input parameters of the process and the outcome is highly complex and non-linear. Modelling these phenomena is very difficult with traditional methods since it involves synergies between input variables that are unknown in most cases. The most outstanding virtue of traditional methods is the development of experimental and/or numerical procedures that allow the very specific processes behind the formation of non-metallic inclusions (NMIs) to be understood. However, for these very same reasons, they are of limited use when it

comes to making reliable predictions between the steel fabrication parameters and the presence of NMIs in the final product. To the best of these authors' knowledge, no previous study has addressed the prediction of NMIs in a steel manufactured by continuous casting employing Machine Learning (ML) algorithms. The processing parameters (inputs or features) were collected over the years in the context of the quality control program of the company Global Steel Wire (GSW, Spain). The amount and characteristics of the NMIs present in the steel (outputs) were obtained throughout this time by the laboratory LADICIM of the University of Cantabria.

MATERIALS AND METHODS

Steel for Tire Reinforcement

Continuous casting is the procedure employed to obtain the steel. After the fusion of the raw material, the billet is obtained through a molding process and then, hot rolling is applied to produce a wire rod with a diameter of 5.5 mm which is then drawn down to 0.2 mm or less. These fine filaments are twisted into strands being subjected in this process to significant stresses that can eventually cause their fracture; for this reason, the strict quality of the filament is demanded along its entire length. Steel cleaning directly affects the quality of steel cord for tire reinforcement; consequently, the presence of NMIs must be minimized in order to reduce unexpected breakages [1]. The introduction of new approaches based on ML algorithms can be of great help to optimize steel quality and cleanliness controls. The GSW protocol is based on the characterization of samples taken from randomly selected castings by means of scanning electron microscopy (SEM) and microanalysis (EDX) techniques. For each casting, six samples are obtained and examined in the SEM. An area of 6.86 mm^2 (1.14 mm^2 per sample) is randomly chosen and all the inclusions larger than 1 μm in size are quantitatively analyzed. The report includes the total number of inclusions, the distribution of sizes and the composition of each inclusion which is represented within the ternary diagram Al_2O_3 / SiO_2 / CaO + MgO + MnO. The ternary diagram is divided into three regions, A, B and C. According to the quality protocol, there is a maximum limit to the percentage of particles allowable in regions B and C. Otherwise, the casting should be rejected ('non-accepted').

Features, Algorithms, Imbalanced Datasets

During the manufacture of the steel for tire reinforcement, 140 parameters are monitored, which can be classified according to the phases of the fabrication process: Electric arc furnace (EAF), ladle furnace (LF) and continuous casting (CC). These numeric parameters are the features of the classification algorithm. The targets are represented by the results of the ternary diagrams experimentally obtained after fabricating the steel. The most relevant result is the acceptance or rejection of the casting. The data used in this study included 855 observations (castings), 793 of which were classified as 'accepted' (class 0) and the rest as 'non-accepted' (class 1). The rejection rate of the process is therefore 7.25%. The ML models have been developed and evaluated in Python using the libraries numpy, pandas, scikit-learn, matplotlib and seaborn. The following classification algorithms have been used in this research: Logistic Regression, K-Nearest Neighbors (KNN), Support Vector Machines (SVM), Algorithmic Ensemble Techniques and Artificial Neural Networks (ANN).

The rejection rate in this dataset is 7.25%. This corresponds to an imbalanced class distribution, common in anomaly detection. In this situation, standard classifier algorithms tend to predict the majority class data ignoring the minority class. There are different methods for dealing with imbalanced sets, which may be categorized as follows [2]: a) Resampling techniques, b) alternative scores and c) ensemble methods. The ML analysis in this research has been organized in two phases. First, the previously mentioned algorithms were trained and tested without resampling. Then, they were applied to the resampled dataset (random oversampling).

RESULTS AND DISCUSSION

Evaluation of Machine Learning algorithms.

20% of the observations were randomly extracted to form a test dataset used to provide an unbiased evaluation of the models. Models were trained and the hyper-parameters were refined using the remaining 80%. 5-fold cross-validation was used for training and validation. Parameter selection and model evaluation was conducted with

GridSearchCV. Features were scaled through the StandardScaler. Next, the main characteristics of the algorithms employed after tuning are described:

- Logistic regression, LR: For the best hyper-parameters of the model, the 'saga' solver was selected with an L1 penalty. A strong regularization was achieved with C=0.1; tol=1e-5 was selected as the optimum tolerance value for stopping criteria. Finally, a maximum number of 10000 interactions guaranteed convergence.
- K-Nearest Neighbors, KNN: The optimum number of neighbors found was 7, and the best distance metric was manhattan (minkowski with p=1). The algorithm used to compute the nearest neighbors was BallTree with a leaf size of 10. Finally, the weight of the points was considered by the inverse of the distance.
- SVM: the linear kernel was used as a baseline model. Then, the Radial Basis Function (RBF) kernel was fine-tuned determining C and gamma through grid search, to obtain C=20 and gamma=0.01.
- Random Forest, RF: The optimum number of decision trees in the forest was 750; 'entropy' was the function to measure the quality of a split.
- AdaBoost, AB: The optimum number of estimators (decision trees with max deep of 1) was 15 with a learning rate of 0.5. The algorithm used was SAMME.R.
- Gradient Boosting, GB: The optimum number of boosting stages was 1200 with a learning rate of 0.01 that shrinks the contribution of each tree and a fraction of samples to be used for fitting each individual base learner (subsample) of 0.5. The maximum depth of the individual estimators was 3.
- Artificial Neural Networks, ANN: the optimum MLP consisted in two hidden layers with 10 nodes each. The activation function was ReLu. The Learning rate was established as 'invscaling' An L2 penalty of alpha=0.1 was applied as a regularization term to prevent overfitting.

Table 1 shows the Accuracy ('Acc.') and AUC on the original dataset and after oversampling. The most significant outcomes are summarized below:

- As expected, Accuracy is a substantially insensitive metric for imbalanced datasets.
- The performance of the algorithms is not improved after using oversampling.
- The best results (in the non-resampled dataset) are obtained through the RF algorithm. The AUC for the train+validation set amounts to 0.83 ± 0.13 while for the test set it is 0.85. AUC=0.85 is equivalent to a probability of 85% that a randomly picked point of the positive class (rejected casting) will have a higher score according to the classifier than a randomly picked point from the negative class (non-rejected casting).

Figure 1 shows a comparison between the ROC (Receivertile Operating Characteristic) curves provided by RF in the original dataset and after applying resampling. As can be seen, this technique does not represent any perceptible improvement in this case. To carry out an independent evaluation of the selected classifier, 149 additional castings have been considered. Three of these new instances were rejected based on the SEM analysis. The features of these 149 instances have been introduced in the optimized RF algorithm and the results have been sorted in descending order of the probability of belonging to class 1. According to the result obtained through the optimized RF, these three castings have been classified in positions 3, 10 and 43, with failure probabilities of 26%, 21% and 11%, respectively.

Feature Importance

Scikit-learn enables to compute the importance of a node in a decision tree. The following four features were obtained: number of uses of the ladle, amount of Al_2O_3 and SiO_2 in the slag and amount of carbon in the final steel.

TABLE 1. Accuracy and AUC scores for the train+validation and test sets. Original and resampled datasets.

	Original dataset				**Resampled data**			
	Train + validation		**Test**		**Train + validation**		**Test**	
Model	**Acc.**	**AUC**	**Acc.**	**AUC**	**Acc.**	**AUC**	**Acc.**	**AUC**
LR	0.93 ± 0.01	0.78 ± 0.09	0.90	0.78	0.90 ± 0.03	0.95 ± 0.02	0.78	0.76
KNN	0.93 ± 0.01	0.70 ± 0.10	0.91	0.73	0.90 ± 0.02	0.98 ± 0.01	0.81	0.74
SVC (RBF)	0.94 ± 0.01	0.81 ± 0.10	0.92	0.78	1.00 ± 0.00	1.00 ± 1.00	0.91	0.78
SVC (linear)	0.87 ± 0.03	0.69 ± 0.14	0.83	0.73	0.95 ± 0.02	0.93 ± 0.01	0.82	0.73
RF	0.93 ± 0.01	0.83 ± 0.13	0.91	0.85	1.00 ± 0.00	1.00 ± 0.00	0.92	0.83
AB	0.93 ± 0.03	0.84 ± 0.18	0.89	0.82	0.89 ± 0.03	0.96 ± 0.02	0.82	0.77
GB	0.93 ± 0.03	0.80 ± 0.20	0.91	0.79	0.98 ± 0.01	1.00 ± 0.00	0.91	0.79
ANN	0.91 ± 0.02	0.73 ± 0.08	0.91	0.79	0.97 ± 0.01	0.99 ± 0.02	0.88	0.79

Business Impact

This research enables to optimize the process of sample selection for the experimental control of NMIs. Consider, for example, a sample consisting of 1000 castings; using the optimized RF algorithm with a threshold = 0.10, 204 of the 1000 castings would have been classified as class 1, correctly identifying 55 out of the 73 castings to be rejected. In case of randomly selecting 204 castings, on average, only 0.073 * 204 = 15 of the 73 castings would have been rejected. Based on this argument, a new metric to be referred to as Improvement Ratio (IR) is defined; in the previous example, IR = 55/15 = 3.7. A word of caution is necessary at this stage: as indicated previously, there is no silver bullet to define the threshold because decision-making depends on economic aspects too.

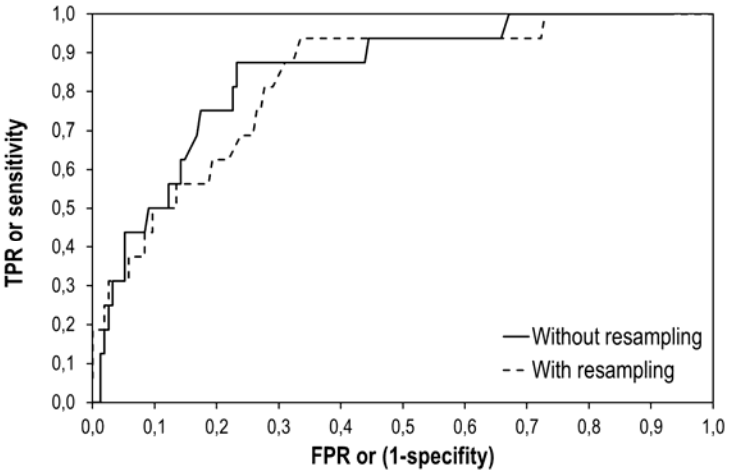

FIGURE 1. ROC curves obtained with RF with and without resampling.

CONCLUSIONS

Different approaches were employed to deal with the imbalanced class distribution motivated by the small rejection rate, such as resampling (random oversampling), alternative scores (Precision, Recall and AUC rather than Accuracy) and ensemble methods (Random Forest, AdaBoost and Gradient Boosting). The best results were obtained with Random Forest on the non-resampled dataset (AUC for training+validation equals 0.83 ± 0.13 while for testing it is 0.85). There have been no improvements after using random oversampling but a slight tendency to overfitting, which has been previously reported by other authors [3].

ACKNOWLEDGMENTS

This Project was carried out with the financial grant of the program I+C=+C, 2017, FOMENTO de la TRANSFERENCIA TECNOLÓGICA. The financial contribution from SODERCAN and the European Union through the program FEDER Cantabria is gratefully acknowledged. The authors would also like to express their gratitude to the technical staff of GLOBAL STEEL WIRE and, specially, to Mr. Rafael Piedra, Mr. Santiago Pascual and Mr. Jean-Francois Fourquet, without whom it would not have been possible to conduct this research.

REFERENCES

[1] Millman S. Clean steel basic features and operation practices. In: Wúnnenberg K, Millman S, editors. IISI Study Clean Steel, Brussels, Belgium: IISI Committeee on Technology; 2004, p. 39–60.
[2] Guido S, Müller A. Introduction to Machine Learning with Python. A Guide for Data Scientists. O'Reilly Media; 2016.
[3] Mukherjee U. How to handle Imbalanced Classification Problems in machine learning? Anal Vidhya 2017. https://www.analyticsvidhya.com/blog/2017/03/imbalanced-classification-problem/.

The Numerical Studies Of the Multi-Stage Damage Behavior of an Explosively-Driven HR2 Cylinder

Jiang Yuxi[1,a)], Jiang Songqing [1,b)], Liu Wentao [1,c)], Xiong Jun [1,d)]

[1]*Institute of Applied Physics and Computational Mathematics, No.2 Fenghao Donglu, Haidian District, Beijing, China*

[a)] Corresponding author: Jiang_yuxi@iapcm.ac.cn

[b)] Jiang_Songqing@iapcm.ac.cn

[c)] Liu_Wentao@iapcm.ac.cn

[d)] Xiong_Jun@iapcm.ac.cn

Abstract. The damage in the metallic thick-walled cylinder expanded by explosive load is highly complicated and is particularly important to the design of munitions and armaments. A serial of experiments with different strain rate in steel have been done to explore the fracture behavior in the metallic cylinder [1] ~ [8]. Figure 1 shows the sketch of the experimental specimen and the field [8]. The experimental results in the Fig. 2 revealed that the shear fracture was dominant while the cylinder deformed at a high strain rate [1], [3]. As the Fig.3, the recovered fragments showed the damage in the cylinder contained many fracture mechanisms such as spallation, tensional fraction and adiabatic shear band [3].

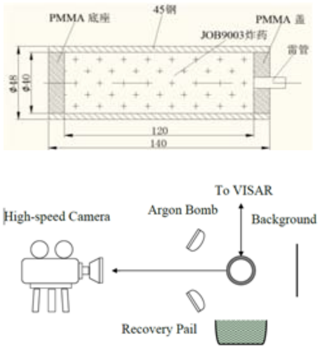

FIGURE 1. The sketch of the specimen and experimental field[8]

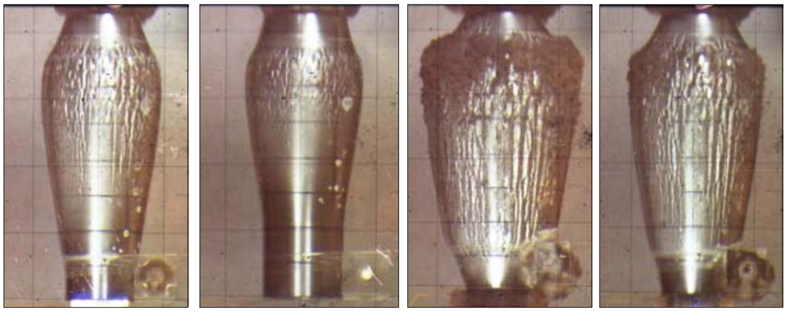

FIGURE 2. The typical photos of the expanding cylinder shell taken by the high-speed camera[1],[3]

(a) (b) (c)

FIGURE 3 The recovered fragments: a) Spallation and shear fracture; b) Tensional and shear fracture; c) Typical shear fracture

In this paper, the multi-stage damage behaviors of the HR2 thick-walled cylinder expanded by explosive load were numerically studied by using CHAP3D code, a program developed by our research group. The maximum tensional stress model was used to describe the spallation and tensional fracture. The Johnson-Cook model was adopted to characterize the adiabatic shear band, whereas it was induced by the competition between the stain harden and the thermal softening. The Gruneisen EOS for the HR2 was used. Table 1 and Table 2 show the parameters about relative materials.

TABLE 1. The parameters of Johnson-Cook constitutive model and the Shear modulus for the cylinder

Shear modulus	*A*	*B*	*n*	*C*	*m*
0.77	0.00464	0.0202	0.85	0.045	1.39

TABLE 2. The parameters of the Gruneisen EOS for HR2 cylinder

density	C	S_1	S_2	S_3	γ_0	α
7.82	0.4693	1.339	0.0	0.0	1.678	0.0

As an instability process, the initiation of the damage in the HR2 cylinder shell was strongly dependent on the non-uniformities of the material. A distribution of the local yield stress satisfied the Gaussian distribution was introduced to describe the non-uniformity of the material, and several factitious disturbances of the local yield stress were used to describe the disfigurement of the specimen from the work-hardening, as shown in Fig.4.

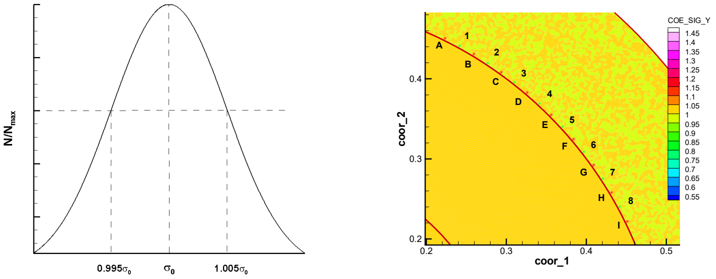

FIGURE. 4 The distribution of the local yield stress satisfied the Gaussian distribution and several factitious disturbances

Due to the complexity of the damage in the expanded cylinder, 2D simulation was firstly carried out to study the propagation and the "self-organized" of the adiabatic shear bands, as shown in the Fig. 5. The 2D numerical simulation results show that the initial disturbing in the material can cause the ASBs. The shear bands tended to initiate from the inner surface, and organized themselves and along a counter clockwise direction (Fig. 6). This phenomenon was called the single direction spiral[8].

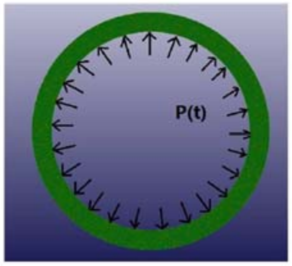

FIGURE 5 The geometry of 2D model

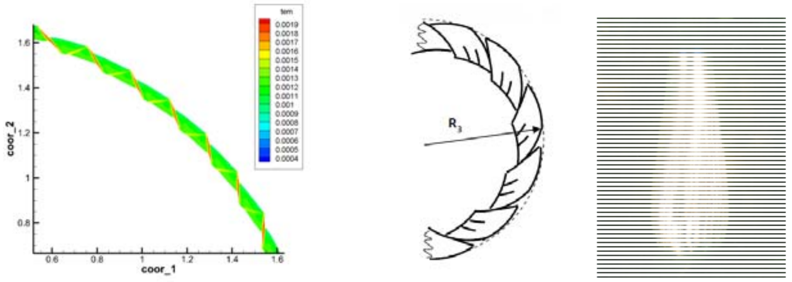

FIGURE 6 The phenomena of the ASB single direction spiral patter

Then the 3D simulation is taken to investigate the multi-stage damage behaviors of the expanded HR2 thick-walled cylinder. The initiation and propagation of the shear bands, and the spallation and tensional fracture were successfully simulated.

The numerical results showed that the radial spallation occurred in the early stage (t = 3.5 μs) of the damage, shown in the Fig.7. In the same time, the concentration of the effective plastic strain, caused by shear, appeared from the inner surface, while the shear bands have not been formed yet.

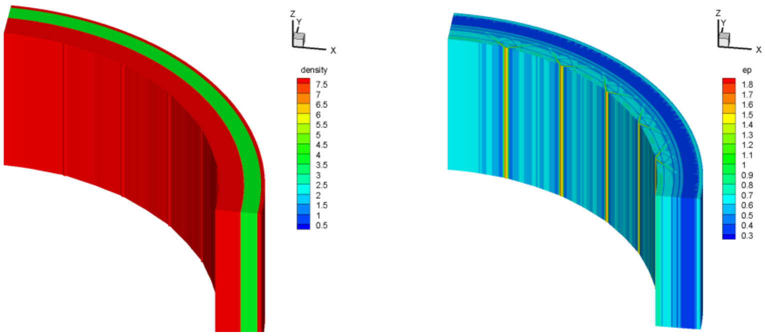

FIGURE 7 The distributions of the density and effective plastic strain in the early-stage (t = 3.5 μs) of the damage

Then, Fig.8 shows the shear bands tended to initiate from the inner surface in the middle stage (t = 4.0 μs). After that, the shear bands propagated, organized themselves. However the radial spallation would interrupt the extension of the shear bands and only some of them could extend to outer surface to become macro fracture.

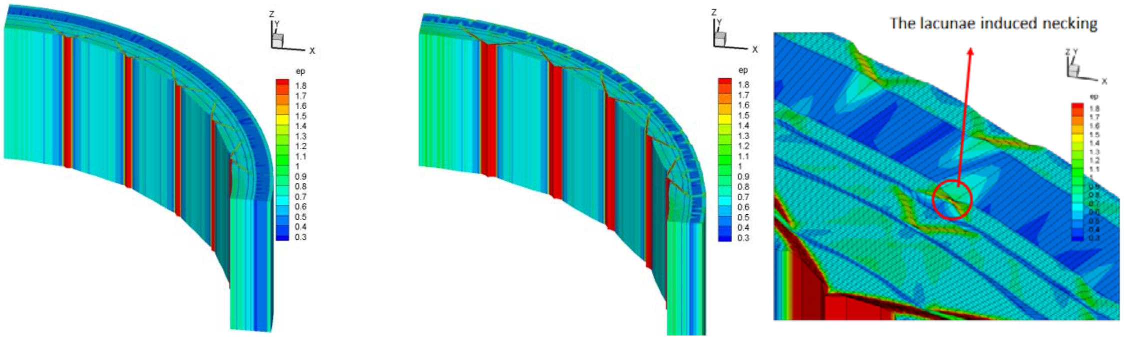

t = 4.0 μs t = 4.5 μs

FIGURE 8 The distributions of the effective plastic strain in the middle-stage (t = 4.0 μs) and the last-stage (t = 4.5 μs)

Also, Fig.8 shows, in the later stage ($t = 4.5\ \mu s$), the necking appeared in the spallation fragment, and gradually became the tensional fracture, caused by the typical hoop strain, the shear bands and the lacunae in the material. The computational results showed that the damage observed on outer surfaces was the competition result of the several fracture patterns. In these fracture modes, the shear bands were dominating. The numerical results agreed with the experimental observations.

REFERENCE

1. Tiegang Tang, Qingzhong Li, Xueling Sun, et al. Strain-rate effects of expanding fracture of 45 steel cylinder shells driven by detonation. Explosion Shock Waves, 2006, 26(2):129–33. (in Chinese)
2. Goto DM, Becker R, Orzechowski TJ, et al. Investigation of the fracture and fragmentation of explosively driven rings and cylinders. International Journal of Impact Engineering, 2008, 35(12):1547–56.
3. Haibo Hu, Tiegang Tang, Shan Jin, et al. Some experimental aspects of fracture on cylindrical metal shells under intensive explosive loading. Khariton Topical Scientific Readings, Extreme states of substance Detonation Shock Waves, Sarov, Russia, March 18-22, 2013.
4. Minzu Liang, Xiangyu Li, Jianguang Qin, et al. Improved expanding ring technique for determining dynamic material properties. Review of Scientific Instruments, 2013, 84(6):065114.
5. Xiangyu Li, Minzu Liang, Mafa Wang, et al. Experimental and numerical investigations on the dynamic fracture of a cylindrical shell with grooves subjected to internal explosive loading. Propellants, Explosives, Pyrotechnics, 2015, 39(5):723–32.
6. Guowu Ren, Zhaoliang Guo, Cheng Fan, et al. Dynamic shear fracture of an explosively-driven metal cylindrical shell. International Journal of Impact Engineering, 2016, 95: 35-39.
7. Mingtao Liu, Zhaoling Guo, Cheng Fan, et al. Modeling spontaneous shear bands evolution in thick-walled cylinders subjected to external High-strain-rate loading. International Journal of Solids and Structures, 2016, 98: 336-354.
8. Mingtao Liu, Guowu Ren, Cheng Fan, et al. Experimental and numerical studies on the expanding fracture behavior of an explosively driven 1045 steel cylinder. International Journal of Impact Engineering, 2017, 109: 240-252

An Unstructured Spectral Element Method for Hydrodynamic Instability and Bifurcation Analysis

Dong-Jun Ma[1,a)], Da-Wei Chen[1], De-Jun Sun[2] and Pei Wang[1]

[1]*Institute of Applied Physics and Computational Mathematics, Beijing 100094, China*
[2]*Department of Modern Mechanics, University of Science and Technology of China, Hefei 230027, Anhui, China*

[a)]Corresponding author: ma_dongjun@iapcm.ac.cn

Abstract. A high order unstructured spectral element method with a domain decomposition Stokes solver is presented for the hydrodynamic instability and bifurcation analysis. A Jacobian-Free Inexact-Newton-Krylov algorithm with a Stokes time-stepping preconditioning technique is introduced for the steady-state solution of incompressible flow. A matrix-free arc-length approach with Householder transformation is used for the numerical continuation near a turning point. An Arnoldi method is utilized to calculate the leading eigenvalues and their corresponding eigenvectors for the big system of linearized incompressible Navier-Stokes equations, which are responsible for initiating the hydrodynamic instability. The new method can do the steady and unsteady simulations in the similar way without time-splitting divergence error, it do not form the Jacobian matrix, which can reduce the memory allocation, decrease the computation cost, and speed up the convergence rate. The symmetric-breaking Hopf and Pitchfork bifurcations are considered in the flow passed a circular cylinder between two parallel plates. An antisymmetric sinusoidal velocity driven cavity problem is considered and the stable and unstable patterns are analyzed by checking the leading eigenvalues of their steady states. Besides the stable patterns of steady symmetric and steady asymmetric solutions£a new pair of unsteady asymmetric solutions are found depending on the different initial conditions.

INTRODUCTION

Flow instability has always been one of the focuses of hydrodynamics and nonlinear dynamics. The local instability for simple parallel flow can be analyzed by solving the Orr-Sommerfeld equation, whereas the global linear and weak nonlinear instability analysis deserves more wider attention for non-parallel flows [1]. The instability and transition mechanism of the complex flows can be studied by the general eigenvalue problem from the linearized equation with small perturbation on the basic state, while the basic state of non-parallel flow can be obtained by the direct numerical solution of Navier-Stokes equations. The nonlinear bifurcation path and flow patterns can be followed by the numerical continuation and cross-validated by the direct numerical simulation of full NSE to reveal the evolution process. The spectral element method is a high-order weighted residual method for solving partial differential equations by combining the flexibility of finite element and the accuracy of spectral method, which is very suitable for the analysis of the global hydrodynamic instability and bifurcation path of the flow in complex regions, such as non-parallel flows.

In this paper, the high-order spectral element method is used to analyze the global instability and bifurcation path. Tuckermann et al. [2] developed a methodology for bifurcation analysis based on unsteady Stokes preconditioning, which has been widely used with spectral element method [3] and finite difference method [4, 5, 6]. However its divergence error due to time splitting [7] may affect the stability analysis results. In this paper, the unstructured spectral element method with domain decomposition Stokes solver [8] without splitting divergence error is used as the basis for global instability analysis. The steady state is achieved by a Jacobian-free Newton-Krylov method with a time-stepping preconditioning, which is consistent with the unsteady solver. An arc-length continuation method is used for the bifurcation path following with special treatment for the turning point. Furthermore, the dominant eigenvalues is calculated by Arnoldi method for the stability analysis of steady state. Some examples will be demonstrated to verify the feasibility and accuracy of the proposed method for the bifurcation analysis of non-parallel flows.

GOVERNING EQUATIONS AND NUMERICAL METHODS

Considering the two dimensional unsteady incompressible flow where both the density and viscosity of the fluid are constant, the governing equations are the classical Navier-Stokes equations:

$$\nabla \cdot \boldsymbol{u} = 0 \tag{1a}$$

$$\partial_t \boldsymbol{u} = -\nabla p - \boldsymbol{u} \cdot \nabla \boldsymbol{u} + \mathrm{Re}^{-1} \nabla^2 \boldsymbol{u} \tag{1b}$$

An unstructured spectral/hp element method with a domain decomposition Stokes solver [8] is utilized to solve the governing Eq. (1). The computation domain is decomposed into non-overlapping unstructured spectral elements. Within each element Gauss-Lobatto-Jacobi and Gauss-Radau-Jacobi quadrature points are used in two directions respectively. Dubiners modified triangular bases are introduced to the approximating expansion. The second-order stiff stable scheme is adopted for the unsteady time integration. The linear terms are treated implicitly and the nonlinear terms explicitly. Then the discretized equation can be re-formed with an unsteady Stokes operator on the left-hand side and explicit forcing terms on the right-hand side. With the domain decomposition approach, the interior and marginal degrees of freedom are decoupled and the divergence-free condition is satisfied strictly. The resulting small linear system in each element can be solved by direct method.

The Navier-Stokes equations (1) can be re-formed as

$$\begin{aligned} \partial_t \boldsymbol{u} &= -\nabla p - \boldsymbol{u} \cdot \nabla \boldsymbol{u} + \mathrm{Re}^{-1} \nabla^2 \boldsymbol{u} = -(I - \nabla \nabla^{-2} \nabla \cdot)(\boldsymbol{u} \cdot \nabla \boldsymbol{u}) + \mathrm{Re}^{-1} \nabla^2 \boldsymbol{u} \\ &= \mathbf{N}(\boldsymbol{u}) + \mathbf{L}\boldsymbol{u} \end{aligned} \tag{2}$$

where $\mathbf{N}$ and $\mathbf{L}$ represent the nonlinear and linear operators, respectively. For semi-implicit scheme we have

$$\frac{\boldsymbol{u}^{n+1} - \boldsymbol{u}^n}{\Delta t} = \mathbf{N}(\boldsymbol{u}^n) + \mathbf{L}\boldsymbol{u}^{n+1} = (\mathbf{I} - \Delta t \mathbf{L})^{-1} (\mathbf{N} + \mathbf{L}) \boldsymbol{u}^n \tag{3}$$

The steady-state solution for Navier-Stokes equations $(\boldsymbol{u}, \mathrm{Re})$ read

$$f(\boldsymbol{u}, \mathrm{Re}) = \mathbf{N}\boldsymbol{u} + \mathbf{L}\boldsymbol{u} = 0 \tag{4}$$

Applying Newton's method to Eq. (4), the linear equation for the correction $\delta \boldsymbol{u}$ is $(\mathbf{N_u} + \mathbf{L})\, \delta \boldsymbol{u} = -(\mathbf{N} + \mathbf{L})\, \boldsymbol{u}$ where $\mathbf{N_u}$ is the Jocabian matrix associated with the nonlinear term $\mathbf{N}$ evaluated at state $\boldsymbol{u}$. A Jacobian-free Newton-Krylov method is used to obtain stable or unstable steady solutions. Using the unsteady Stokes operator $\mathbf{P} = (\mathbf{I} - \Delta t \mathbf{L})^{-1} \Delta t$ as a preconditioner, the linear system for Newton iteration can be reformulated as

$$(\mathbf{I} - \Delta t \mathbf{L})^{-1} \Delta t (\mathbf{N_u} + \mathbf{L})\, \delta \boldsymbol{u} = -(\mathbf{I} - \Delta t \mathbf{L})^{-1} \Delta t (\mathbf{N} + \mathbf{L})\, \boldsymbol{u} \tag{5}$$

Inexact Newton method is used for accelerating convergence, where the right- and left-hand side of Eq. (5) are calculated by a time-stepping based on Eq. (3).

In order to follow the bifurcation path of the dynamic system, an arc-length numerical continuation method is used to avoid the difficulty due to the turning point. Eq. (5) is re-formed to an extended system based on the vector $(\boldsymbol{u}, \mathrm{Re})$:

$$\mathbf{P} D_{\mathbf{u}} f(\boldsymbol{u}^k, \mathrm{Re}^k) \cdot \Delta \boldsymbol{u}^k + \mathbf{P} D_{\mathrm{Re}} f(\boldsymbol{u}^k, \mathrm{Re}^k) \Delta \mathrm{Re}^k = -\mathbf{P} f(\boldsymbol{u}^k, \mathrm{Re}^k) \tag{6}$$

The system is solved by a Jacobian-free Newton-Krylov method with a Householder transformation.

An iterative Arnoldi method [2] is utilized to calculate the leading eigenvalues and their corresponding eigenvectors for the big system of linearized incompressible Navier-Stokes equations. The detailed implementation can refer to the published papers [5, 6].

NUMERICAL RESULTS

The laminar flow past a stationary cylinder between two parallel plates [9] is analyzed to verify the accuracy of the proposed method. Cliffe et al. show that the flow will lose stability to a periodic flow at a supercritical Hopf bifurcation point as the flow rate is increased, and there is another Hopf bifurcation to restabilize the flow above a critical Reynolds number. Furthermore, steady asymmetric flows exist at the same blockage ratio B (the ratio of

cylindrical diameter to plate width). We performed the bifurcation analysis at the special blockage ratio $B = 0.7$, where steady symmetric solutions, steady asymmetric solutions and periodic solutions are obtained, and the critical Reynolds and Strouhal numbers are given in Table 1. The computational region is divided into 130 iso-parametric quadrilateral elements, each of which has an interpolation order of $p = 11$. Table 1 shows the comparisons between higher order spectral element method and finite element method [9]. The critical parameters agree well with the first two Hopf bifurcations. We also give the pitchfork bifurcation point clearly. Figure 1 shows the streamlines of different symmetric and asymmetric steady solutions near the critical bifurcation points.

TABLE 1. Critical Reynolds and Strouhal numbers for blocked cylinder flow ($B = 0.7$).

	Bifurcation type	Re_{cr}	St	Re_{cr} (Cliffe *et al.)*	St (Cliffe *et al.)*
1	Hopf	91.99	0.5694	91.9944	0.5694
2	Hopf	174.70	0.5806	174.7156	0.5806
3	Pitchfork	180.02	0		

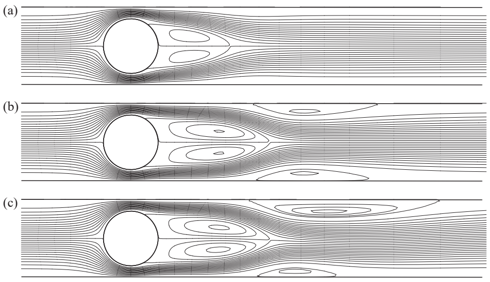

FIGURE 1. Streamline for blockage ration B=0.7; (a) Re = 90; (b) Re = 175; (c) Re = 185.

The driven cavity problem [10] with a sinusoidal velocity on the top cover of a square cavity has rich flow patterns and complex bifurcation processes. It is very good benchmark case for the bifurcation analysis and path following. Considering the computational region of unit square cavity $[0, 1] \times [0, 1]$, the top cover ($y = 1$ boundary) has an antisymmetric sinusoidal velocity boundary condition $u(x) = U_0 \sin(2\pi x)$, the other three sides are fixed-wall boundary conditions, and the whole system has the symmetry relative to the vertical centerline.

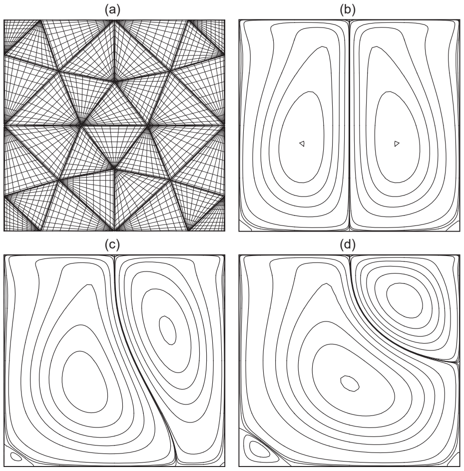

FIGURE 2. Streamlines for sinusoidal velocity driven cavity Re = 800: (a) Computational mesh; (b) Stable symmetric solution; (c) Stable asymmetric solution; (d) Unstable asymmetric solution.

This paper calculates various cases when Re = 800, which are shown in Fig. 2. The stable solutions, (including a symmetric and a pair of asymmetric solutions) are in good agreement with the previous results [10]. In addition, a new pair of unstable asymmetric solution are obtained by numerical continuation method as shown in Fig. 2(d).

The main eigenvalues and eigenvectors of the steady solutions are also solved, where the dominant eigenvalues of (b) $\lambda_m = -0.1274 \pm 0.1602\,i$, (c) $\lambda_m = -0.1984$, (d) $\lambda_m = 0.1149$. It can be judged from the positive and negative real parts of dominant eigenvalues that the steady solutions (b) and (c) are stable while the steady state (d) are unstable. Figure 3 shows the detailed bifurcation diagram where a turning point is captured with the arc-length method.

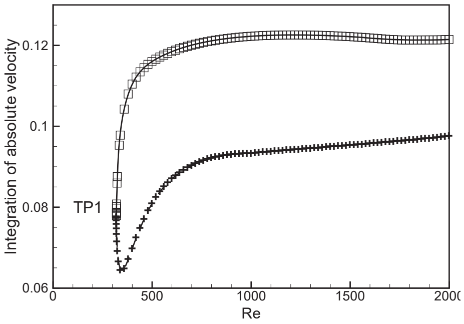

FIGURE 3. Bifurcation diagram for sinusoidal velocity driven cavity.

CONCLUSIONS

A high order unstructured spectral element method with a domain decomposition Stokes solver is presented for the hydrodynamic instability and bifurcation analysis. A Jacobian-Free Inexact-Newton-Krylov algorithm with a Stokes time-stepping preconditioning technique is used for the steady-state solution of incompressible flow. A matrix-free arc-length approach with Householder transformation is used for the numerical continuation near a turning point. The new method can do the steady and unsteady simulations in the similar way without time-splitting divergence error.Two verification benchmark cases are considered. The symmetric-breaking Hopf and Pitchfork bifurcations are calculated for the flow passed a cylinder between two parallel plates and agree well with the reference. An antisymmetric sinusoidal velocity driven cavity problem is also considered. Besides the stable patterns of symmetric and asymmetric solutions, a new pair of unstable asymmetric solutions are found. This subcritical flow with multi-state and turning point can be served as an effective benchmark for the global instability and bifurcation analysis of non-parallel flows.

ACKNOWLEDGMENTS

This work is supported by the Natural Science Foundation of China under Grant Nos. 11772065, 11702028, the Joint Fund of the National Natural Science Foundation of China and the China Academy of Engineering Physics (Grant No. U1530261), and the Science Challenge Project, China (Grant No. TZ2016001).

REFERENCES

[1] B. R. Noack and H. Echelmann, J. Fluid Mech. **270**, 297–330 (1994).
[2] L. S. Tuckerman and D. Barkley, in *Numerical Methods for Bifurcation Problems and Large-Scale Dynamical Systems*, Vol. 119, edited by E. Doedel and L. S. Tuckerman (Springer, New York, 2000), pp. 453–466.
[3] A. Bergeon, D. Henry, H. BenHadid, and L. S. Tuckerman, J. Fluid Mech. **375**, 143–177 (1998).
[4] D. J. Ma, D. Henry, and H. BenHadid, Phys. Fluids **17**, p. 124101 (2005).
[5] D. J. Ma, D. J. Sun, and X. Y. Yin, Phys. Rev. E **74**, p. 037302 (2006).
[6] B. F. Wang, D. J. Ma, C. Chen, and D. J. Sun, J. Fluid Mech. **711**, 27–39 (2012).
[7] G. E. Karniadakis, M. Israeli, and S. A. Orszag, Journal of Computational Physics **97**, 414–443 (1991).
[8] S. J. Sherwin and M. Ainsworth, Applied Numerical Mathematics **33**, 357–363 (2000).
[9] K. A. Cliffe and S. J. Tavener, J. Fluid Mech. **501**, 125–133 (2004).
[10] J. E. Farias and J. P. McHugh, Phys. Fluids **14**, 3179–3188 (2002).

A Natural Formulation Versus an Extended Formulation for the K Clusters with Fixed Cardinality Problem

Graça Marques Gonçalves[1,b)] and Lídia Lampreia Lourenço[1,a)]

[1] *Centro de Matemática e Aplicações (CMA), FCT, UNL, Departamento de Matemática, FCT, UNL, Portugal*

[a)] Corresponding author: lll@fct.unl.pt
[b)] gmsg@fct.unl.pt

Abstract. A natural formulation for the K clusters with fixed cardinality problem is presented. This formulation is compared with an extended formulation and it is strengthened by valid inequalities. The quality of this natural and the strengthened model are tested on randomly generated instances, by using standard software, with good results.

Keywords: K clusters problem, fixed cardinality, natural formulation, valid inequalities.

Introduction

The K clusters with fixed cardinality problem (KCCP) consists in computing K disjoint clusters with fixed size from a set of N items. The objective of this problem is to maximize the total similarity among the items placed in the same cluster. KCCP is a clustering type problem. Although with different objectives or constraints, related clustering type problems are described in [2]. A survey of mathematical programming models for clustering problems can also be found in [6].

The KCCP is a NP-hard combinatorial optimization problem with many applications which include software design for web search, customer segmentation, marketing area, document categorization, and scientific data analysis. For instance, when making a product search in the web, groups of other similar products are proposed in advertising windows to the user, based on previous searches. These products are grouped by similarity into groups with different sizes. Another application comes up in large supermarkets to select different products to be placed together, in view of a specific marketing strategy ([3]). In this case, each cluster has a fixed number of products, and the similarity between each pair of products is based on the frequency that they are simultaneously bought. Another important application of this problem arises in the financial area, to group N customers in K portfolios with fixed customers each one, maximizing the similarity between customers based on their profiles.

The natural mixed-integer formulation of the KCCP involves a number of variables of the same order of the data dimension. This is an advantage over the extended formulations which involve additional variables, resulting in prohibitive large mixed-integer programming problems. Another advantage of the natural formulation is the possibility to add a small subset of valid inequalities, obtaining a better approximation of the convex hull of the problem's feasible region. The inclusion of valid inequalities in the natural formulation results in a problem with lower dimension than the extended formulations with valid inequalities.

Natural Formulation

Consider the following notation for the mixed-integer linear formulation for KCCP:

N	-	number of items ($N \in \mathbb{N}$)
K	-	number of clusters ($K \in \mathbb{N}, K < N$)
i, j	-	items indexes ($i, j \in \{1, \ldots, N\}$)
k	-	cluster index ($k \in \{1, \ldots, K\}$)
M_k	-	number of items per cluster k ($M_k \in \mathbb{N}, \sum_k M_k < N$)
s_{ij}	-	similarity between items i and j, element of a symmetric matrix with diagonal elements equal to zero ($0 \leq s_{ij} < 1$)

Consider now the following binary decision variables:

x_{ik}- binary variable which indicates whether item i is in cluster k (=1) or not (=0), ($i = 1, \ldots, N$; $k = 1, \ldots, K$)

y_{ij} - binary variable which indicates whether items i and j are in the same cluster k (=1) or not (=0) ($i = 1,\ldots,N-1$; $j = i+1,\ldots,N$).

According to the parameters and the variables defined above, the KCCP can be formulated as a natural mixed integer linear programming problem (MILP) as follows:

$$
(F_1)\quad
\begin{array}{lll}
max \quad \sum_{i=1}^{N-1}\sum_{j=i+1}^{N} s_{ij}y_{ij} & & (1)\\
s.t. \quad y_{ij} \geq x_{ik} + x_{jk} - 1 & 1 \leq i < j \leq N; k = 1,\ldots,K & (2)\\
\sum_{i=1}^{j-1} y_{ij} + \sum_{i=j+1}^{N} y_{ji} = \sum_{k=1}^{K}(M_k - 1)x_{jk} & j = 1,\ldots,N & (3)\\
\sum_{k=1}^{K} x_{ik} \leq 1 & i = 1,\ldots,N & (4)\\
\sum_{i=1}^{N} x_{ik} = M_k & k = 1,\ldots,K & (5)\\
x_{ik} \in \{0,1\} & i = 1,\ldots,N; k = 1,\ldots,K & (6)\\
0 \leq y_{ij} \leq 1 & 1 \leq i < j \leq N & (7)
\end{array}
$$

The objective function (1) gives the total similarity, i.e., the sum of the similarity values between pairs of items placed in the same cluster. Constraints (2) relate the variables y_{ij} and x_{ik}. Constraints (3) force, for each j, $(M_k - 1)$ variables y_{ij} to be equal to 1, when j is in cluster K. The set of constraints (4) assures that each item belongs to one cluster at most. Cardinality constraints (5) do not allow violation of the number of items in each cluster. Constraints (6)-(7) are the variables' domain.

Note that, although the variables y_{ij} are continuous, between 0 and 1, they only take the values 0 or 1 in the optimal solution, due to the maximization objective and the constraints (2)-(3).

In order to strengthen the model F_1, the following triangular inequalities are included in the model, resulting in the problem F_1^{cut}:

$$y_{ij} \geq y_{ti} + y_{tj} - 1 \quad t < i < j\,; \quad y_{ij} \geq y_{it} + y_{tj} - 1 \quad i < t < j\,; \quad y_{ij} \geq y_{it} + y_{jt} - 1 \quad i < j < t.$$

Grötschel and Wakabayashi [5] use the triangular inequalities to formulate the partition problem of a network with N nodes into cliques. These inequalities result from the transitiveness of the items' relations. These same inequalities are presented in the paper of Park, Lee and Park [7] as facets for the convex hull of the set of feasible solutions for the edge-weighted maximal clique problem.

An Extended Model for the KCCP

An extended formulation (F_2) with disaggregated variables for the KCCP, due to Gonçalves and Lourenço [4], is considered. The decision variables are binary variables that assign the items to the clusters:

y_{ijk} - binary variable which indicates whether items i and j are in the same cluster k (=1) or not (=0) ($i = 1,\ldots,N-1$; $j = i+1,\ldots,N; k = 1\ldots,K$).

The notation and the other variables are the same as the ones in F_1 formulation. The KCCP can be formulated as an extended MILP problem as follows:

$$
(F_2)\quad
\begin{array}{lll}
max \quad \sum_{k=1}^{K}\sum_{i=1}^{N-1}\sum_{j=i+1}^{N} s_{ij}y_{ijk} & & (8)\\
s.t. \quad y_{ijk} \leq x_{ik} & 1 \leq i < j \leq N; k = 1,\ldots,K & (9)\\
y_{ijk} \leq x_{jk} & 1 \leq i < j \leq N; k = 1,\ldots,K & (10)\\
\sum_{k=1}^{K} x_{ik} \leq 1 & i = 1,\ldots,N & (4)\\
\sum_{i=1}^{N} x_{ik} = M_k & k = 1,\ldots,K & (5)\\
x_{ik} \in \{0,1\} & i = 1,\ldots,N; k = 1,\ldots,K & (6)\\
0 \leq y_{ijk} \leq 1 & 1 \leq i < j \leq N; k = 1,\ldots,K & (11)
\end{array}
$$

The objective function (8) gives the total similarity, i.e., the sum of the similarity values between pairs of items placed in the same cluster. Constraints (9) and (10) allow the value 1 for y_{ijk} if x_{ik} and x_{jk} are equal to 1 simultaneously. Constraints (11) are the variables' domain.

Note that, similar to formulation F_1, the y_{ijk} variables are continuous, but in the optimal solution they are 0 or 1.

Computational Experience - Test Instances

This section reports the computational experience performed with the natural and the extended MILP models and the corresponding continuous linear relaxations, for the KCCP. As no benchmark instances exist for the KCCP, a set of instances was generated, based on the instances for the k-cluster Problem, reported in the CEDRIC's Library of instances (http://cedric.cnam.fr/ lamberta/Library/k-cluster.html) (Billionnet [1]).

In the generation scheme we consider $N = 40$. Each one of the CEDRIC's instances is defined by a graph with density (d) and with a number M_1 of items in the cluster, which can be equal to 10 ($\frac{1}{4}N$), 20 ($\frac{1}{2}N$) or 30 ($\frac{3}{4}N$). Three different graph densities with values 0.25, 0.50 and 0.75 were considered. For each M_1 fixed and each density d fixed, there are 5 different graphs, with all edge weights equal to 1. The total number of different graphs is 15, and the set of 15 graphs considered for different M_1 values is always the same. Note that, for each graph, 3 different instances exist, each one with a different number M_1 of items in the cluster. The final number of instances is 45.

The KCCP test instances were then obtained by considering $N = 40$ and they were based on the 15 graphs mentioned above. For each edge graph $[i, j]$, a positive weight s_{ij} was randomly generated strictly between 0 and 1, defining the similarity between items i and j. The remaining data of these instances were defined as follows.

Instances with $K = 1, 2$ and $\sum_{k=1}^{K} M_k = 10, 20, 30$ were generated. For $K = 1$ we generated 45 instances, 15 for each M_1 value. For $K = 2$, 90 instances were generated, 15 for each value of $\sum_{k=1}^{K} M_k$ and for each choice of M_k. Two different options for the M_k values were considered, one with balanced and another one with unbalanced values of M_k. As there are 6 different options for M_k, then there exists $6 \times 15 = 90$ instances.

Note that, for $K = 2$, for d fixed and $\sum_k M_k$ also fixed, there are 2 different instances related to the same graph. Then, for those d and $\sum_k M_k$ fixed, there are 10 instances because 5 different graphs exist for each density.

Computational Results

All models were solved by using the standard mathematical software CPLEX. The algorithm provided by the IBM ILOG CPLEX 12.6, ran on a i7 computer with 3.60 GHz processor and 8 GB RAM. In all tests the following CPLEX parameters were considered: time limit=7200 seconds, clocktype=1, mip tol absmipgap=0.0, mip tol mipgap=0.0, mip tol integrality=0.0, feasopt tolerance=0, threads=8, while the other CPLEX parameters were used with their default values. The computational tests were made for the instances described in the previous section.

In Tables 1 and 2 presented below, the first two columns are the graph density and the values of $\sum_k M_k$, respectively. The Gap and the CPU time of the linear relaxation (CPU time LR) are the average values for the 5 instances in Table 1 and average values for the 10 instances in Table 2. The Gap at the root node of the search tree is equal to $\frac{v(\bar{P})-v(P)}{v(P)} * 100\%$, where $v(P)$ is the optimum value of the problem and $v(\bar{P})$ is the linear relaxation optimum value of the same problem. When there is no optimal solution available, the best integer solution is considered for the gap computation. Columns 3, 5 and 7 (headed by 'Average gap') give the average gap in percentage. This value measures the gap between the optimal or the best lower bound known for the instance and the upper bound from the linear relaxation. In columns 4, 6 and 8 (headed by 'Average CPU time LR'), we find the average CPU time (in seconds) required to solve the linear relaxation of each formulation F_2 , F_1 and F_1^{cut}, respectively.

TABLE 1. Results for models F_2, F_1 and F_1^{cut} for K=1.

d	$\sum_k M_k$	F_2 Average gap (%)	Average CPU time LR (s)	F_1 Average gap (%)	Average CPU time LR (s)	F_1^{cut} Average gap (%)	Average CPU time LR (s)
25	10	**56.0**	0.1	177.3	0.0	133.6	1.7
	20	**21.0**	0.2	298.8	0.0	61.9	1.4
	30	**5.3**	0.3	34.8	0.0	10.6	2.2
50	10	107.4	0.2	**84.8**	0.0	**72.4**	1.9
	20	**39.7**	0.1	148.3	0.0	47.7	1.5
	30	**12.2**	0.3	15.9	0.0	**6.4**	2.2
75	10	148.8	0.1	**52.0**	0.0	**44.5**	1.7
	20	**54.0**	0.1	90.7	0.0	**35.3**	1.6
	30	18.3	0.3	**9.8**	0.0	**4.2**	1.8

From table 1, we note that the optimal solution for all models was obtained within the limit of 7200 sec. The average gap for the set of instances corresponding to $d = 25$ and $\sum_k M_k = 10$, is 56.0 for F_2 and 177.3 for F_1, i.e., in this case F_2 is better than F_1. However, in the same table, for $d = 50$ and $\sum_k M_k = 10$ the opposite result is observed. For $d = 50$ and $d = 75$, the model F_1^{cut} gives always the better linear relaxation value, with exception of the density

$d = 50$ and $\sum_k M_k = 20$. Therefore, for instances with higher density, the F_1^{cut} model performs better than other models.

TABLE 2. Results for models F_2, F_1 and F_1^{cut} for K=2.

d	$\sum_k M_k$	F_2 Average Gap (%)	F_2 Average CPU time LR (s)	F_1 Average Gap (%)	F_1 Average CPU time LR (s)	F_1^{cut} Average Gap (%)	F_1^{cut} Average CPU time LR (s)
25	10	104.8	0.0	**100.6**	0.6	**86.2**	2.5
	20	**54.7**	0.0	218.8	0.0	79.6	1.6
	30	**36.3**	0.0	218.4	0.0	**34.1**	1.5
50	10	209.6	0.0	**48.4**	0.0	**44.3**	2.2
	20	**99.8**	0.2	108.5	0.0	**61.2**	1.9
	30	**61.0**	0.0	106.3	0.0	**33.0**	1.8
75	10	**303.9**	0.0	1220.1	0.0	1192.3	1.8
	20	127.5*	0.0	**69.5**	0.0	**41.3**	1.9
	30	77.0*	0.0	**63.5**	0.0	**21.7**	1.8

From Table 2, we observe that the models did not gave the optimal value for the instances tested, with medium and large densities ($d = 50$ and $d = 75$), in the time limit of 7200 seconds. The CPLEX gave the message out of memory for 3 instances marked with (*). The best average gap for the set of instances, is obtained a few times for F_2, others for F_1. However, for all instances, except two sets, F_1^{cut} model gave the best average gap value.

Observe that, the upper bounds given by the linear relaxation of the formulation F_1 were significantly improved with the inclusion of the valid inequalities in the model.

Conclusions

This paper presents a natural formulation for the K clusters with fixed cardinality problem, and compares this formulation with an extended formulation. Some valid inequalities were imposed to strengthen the linear relaxation bound obtained from the natural formulation.

Computational experiments show that the upper bounds provided by the strengthened model F_1^{cut} are better than the bounds resulting from the original linear relaxation. Note also, that the strength model never gave the message "out of memory" as opposed to the extended model F_2. Moreover, the CPLEX solved all the small instances of the problem, for all models.

Research should be continued to developed heuristics in order to obtain lower bounds for the instances of medium and large size. The study of other formulations and valid inequalities should also be made to reinforce linear relaxations to get better upper bounds for the optimal value.

Acknowledgments

This work was partially supported by the Fundação para a Ciência e a Tecnologia (Portuguese Foundation for Science and Technology) through the project UID/MAT/00297/2019 (Centro de Matemática e Aplicações).

REFERENCES

[1] Billionnet A. (2005). "Different formulations for solving the heaviest k-subgraph problem". *Information Systems and Operational Research* 43 (3): 171-186.

[2] Bruglieri, M., Ehrgott, M., Hamacher, H. and Maffioli, F. (2006). "An annotated bibliography of combinatorial optimization problems with fixed cardinality constraints". *Discrete Applied Mathematics*, 154, pp. 1344-1357.

[3] Cavique L. (2004). "Graph-based structures for the market baskets analysis". *Investigação Operacional* 24: 233-246.

[4] Gonçalves, G. M. and Lourenço, L. L. (2009). A strengthened mixed-integer linear formulation for the K clusters problem with fixed cardinality. *Recent Advances in Applied Mathematics, Proceedings of the 14th WSEAS International Conference on Applied Mathematics (Math'09)*, Canary Islands, Spain, pp. 229-232.

[5] Grötschel, M. and Wakabayashi, Y. (1989). "A cutting plane algorithm for a clustering problem". *Mathematical Programming*, 45, pp. 59-96.

[6] Hansen, P. and Jaumard, B. (1997). "Cluster analysis and mathematical programming". *Mathematical Programming*, 79, pp. 191-215.

[7] Park, K., Lee and Park, S. (1996). "An extended formulation approach to the edge-weighted maximal clique problem". *European Journal of Operational Research*, 95, pp. 671-682.

User Story Technique in Scientific Software Product Project: Measuring Rock Block Displacement.

Dagan Bakun-Mazor [1, a)], Moshe Davidian[2, b)] and Shlomo Mark [2, c)]

[1] *Department of Civil Engineering Shamoon College of Engineering, Beer Sheva 84100, Israel*
[2]*Department of Software Engineering Shamoon College of Engineering, Ashdod 77245, Israel*

[a)] daganba@sce.ac.il
[b)] moshikodavi@gmail.com
[c)]Corresponding author: marks@sce.ac.il

Abstract. User Story technique is a tool for writing requirements in a way of short and simple descriptions of the system's features from the perspective of the user. This paper discusses and represent the adjust User Story technique for a conceptual verifier produced as part of scientific software development process. We will demonstrate this by using a user story technique in order to write requirements for a scientific software used to. In this paper we describe and demonstrate the use of the adjusted user story technique for software scientific product as expressed in the development of a measuring rock block displacement.

INTRODUCTION

A *Scientific Software product* is one that serves the scientist in order to help analyze, visualize, or simulate processes or data [1]. A scientific software product is aimed towards scientific computations where the scientific development life cycle encompasses the design, analysis, and development of algorithms and software for solving problems in science and engineering [2] [3]. A *conceptual verifier* software product belongs to this family of software tools and characterized by that the software tool serves to assist in the corroboration of research claims. Some of the most challenging projects that software engineering developments deal with are focused on the conceptual verification needs of the software product. There are many reasons for this, and one of the most important is the understanding that most of scientific studies require a software in order to translate, analyze, accessible and understand the results, and many cases all the progress of the research depends on the pace of completion of the software product. Therefore, in most cases we can find that a code development begins with in-house development when computational scientists develop codes, and when the complexity, dependencies and limitations of the computing, together with the need for high performance computing applications [4], requires the researcher to demand professional intervention that specializes in proven principles, approaches, and tools— the software engineer. A professional software development process requires different professional steps - requirements, specifications, design, implementation, and integration - with close cooperation with researcher's scientists. Under the process of the development of scientific software product, we can find two main different stakeholders; the "scientists" and the professional software engineers [5]. The scientist is the one who asked for the *conceptual verifier* software product in order to explore some issues in his science, while computational software engineers are software engineers who provide useful and proven principles, approaches, and tools for developing scientific software products [6] [7]. The development process is usually characterized and accompanied by many disputes between these two main stakeholders arising from different points of view, and a different understanding of the need for an orderly and controlled development process. Much of the literature [5] [8] [4] [9] [10] [11] deals with the understanding of factors that affect scientific software development, where most emphasize the wide gap between general software development and scientific software product development [1] [5] [12] [13]. Software systems are complex and, in order to meet always pressing needs and deadlines, are often built in a rush, with a lack of comprehensive documentation, but with the understanding that it is impossible to escape the need to continue developing and improving the software. Demeyer et al. [14] say that “there is good evidence to support the notion that a culture of continuous re-engineering is necessary to obtain healthy, maintainable software systems”. hence, in order to enable maintainability, refactoring and re-engineering, the software engineers required to spend a substantial amount of time to write a structural, understandable and clear behavior requirements as well as source code [15], which because of the unique nature of *conceptual verifier* software product, is not always possible. Software maintenance is a very important part of the software life-cycle, especially in scientific software products and even more so in the case of *conceptual verifier* software product. When there is a short deadline

or limited resources, developers have a tendency to prefer writing quick code over replacing it with a simpler design, if it means spending more time on the simpler design. Once we have a working software, we want to improve our understandability and simplify the maintenance process. In order to achieve this goal, we have to improve the software. The improving process needed to be done in small steps so it would not affect code execution. Fowler [16] called this refactoring, which he defines as “a change made to the internal structure of software to make it easier to understand and cheaper to modify without changing its observable behavior.” In order to achieve success at all stages of the development process and to reach a quality software product that will best serve the scientist, it is important to ensure that the development process is based on the right things from the beginning i.e. the development of reliable and quality software is based on writing a proper, clear understandable and comprehensive requirement. When it comes to scientific software product is even more important, because the scientist and the software developer usually come from different knowledge worlds. It is important to create a common language that will enable them to define the software requirements effectively, which will cover all the scientist's needs in the most efficient, simple and best manner. In order to bridge these gaps and enable optimal writing of requirements in this paper we describe and demonstrate the use of the adjusted user story technique as part of the efforts to ensure quality in the development of scientific software product.

CASE STUDY: ROCK SLOPE STABILITY ANALYSES

A geology engineering research group specializing in soil and rock mechanics turned to our research team with the request that we develop a tool that could help them to improve the analytical capacity in order to support their model in the field of Rock Slope Stability. The client – in this case, the head of the research team contacted us after he recognized that the software they wrote in the research group was very cumbersome, and almost unmaintainable. In order for them to achieve significant results, they require more professional intervention, which will enable them to expand the software capabilities so as to enable continuous and long-term automation, as well as improved measurement, identification and accuracy.

Rock Slope Stability Analyses

When geologists analyze problems of stability of rock slopes or the rate of natural weathering along rock slopes, it is a common practice to refer the rock mass as an assemblage of block material separated by discontinuities, mostly by joints, bedding planes, dykes and fault planes. The stability of rock slopes is controlled by the mechanical properties of the entire rock blocks, but mostly by the shear strength along the interfaces between the rock blocks, while failure typically occurs by deformation along those pre-existing discontinuities. Various environmentally controlled mechanisms are considered in an attempt to explain slope failures in rock masses along discontinuities. High-magnitude earthquakes, pore pressure buildup in rock joints, and freezing and thawing of water in joints, have been suggested as trigger factors for landslides and rock avalanches. In the last two decades, more attention has been given to the effect of temperature changes on rock block deformations along rock slopes. Considering daily and seasonal temperature influences, many researchers have detected extremely slow, creep-like, slope displacements due to cyclic temperature changes in long-term monitoring surveys. In order to explain how cyclic thermal oscillations, induce intermittent expansion and contraction of a tension crack, thereby causing seasonal translation of rock blocks, a thermally-induced wedging-ratcheting mechanism has been suggested [17]. A conceptual system of thermally-induced block sliding is schematically illustrated in Fig. 1 as it appears on natural rock slopes (a) and as a discrete conceptual model (b). The system consists of a discrete removable block that is separated from the rock mass by a tension crack and rests on an inclined bedding plane. The tension crack is filled with rock fragments or a single wedge block. According to the suggested mechanism, plastic displacement occurs during heating and cooling cycles, while the rock fragments or the wedge play the role of ratcheting mechanism.

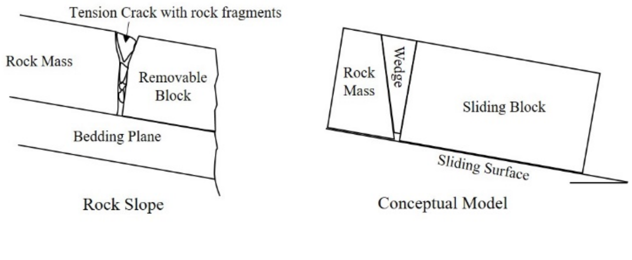

FIGURE 1. Structural components of the thermally - induced wedging-ratcheting mechanism

Measuring Thermally Induced Rock Block Displacement

In order to validate the thermally-induced wedging-ratcheting mechanism, a large-scale physical model is tested in a thermally controlled environment. The physical model consists of an assemblage of concrete blocks. A lower block serves as a sliding surface, and above it positioned three blocks: a sliding block, a fixed block representing the rock mass, and a wedge in the space between that represents the tension crack in the field. The block system on the tilted table is placed inside the Climate Controlled Room.

In order to obtain reliable measurement of the displacement, three different measurement methods are used: 1) image processing of visual range camera, 2) Vibrating Wire displacement transducers, and 3) Potentiometer displacement transducers. A high-resolution (6576X4384 pixels) visual range camera tracks the focus area (15.95 cm in height and 10.63 cm in width) between the wedge, the fixed block, and the sliding block (see Fig. 2A and 2B). Within the focus area six screws are drilled and attached to the blocks in order to serve as marker points for image processing (Fig. 2C).

FIGURE 2. Layout of the measurement system

Requirements of the Research Group

The Preliminary Initiation Document received by the research team stated that they are asking us to develop software tools whose function is to connect to a camera and to identify known shape objects in each image. Objects can be stickers in different shapes or alternatively screws attached to elements within the system. The software is required to identify the element in each image, to calculate and mark the center of each element, and to associate the shapes with other images in order to identify and track the movement from image to image. The software is required to give the camera a command to take pictures at intervals defined by the user. The output required from the software is the central location of the various elements as a function of the time. Another feature that the software requires is the ability to calculate in real time the relative distance between two centers of elements. In the thought of the researcher who commissioned the software, the software should allow the user to identify the elements in advance, to define pairs of elements and calculate the distance between the centers of elements in real time. In such a situation, the user can monitor the relative displacement of each element in the system, or track deformations that develop within different elements.

THE USER STORY TECHNIQUE

The "User Story" [18] is a technique to write requirements, the source of User Stories (US) is in the development methodology Extreme programing (XP) [19]. Kent Beck, the creator of XP, noted that the method came to meet the specific needs of software development facing changing and obscure requirements. The User Stories has to be:1. A short piece of text describing and representing the user story.2. Conversations between stakeholders to exchange perspectives on the user story. 3. Acceptance criteria. Currently, there is no unification in the use of US templates, but in this article we will suggests an adjust template which is appropriate for the special characteristics of scientific software product in general and in *conceptual verifier* software product particular

The suggested engineering approach of the development of scientific software product following a request for new requirements includes the following stages:

1. **The layout stage** – The developer must inspect the codes or the software that was written by the scientist in order to lay out the functionality, structure, behavior, and computational resources of the software – by re-writing fitted User Stories that will use as a basis for particularly appropriate understanding of the code and the needs.
2. **The positioning stage** – the end-user writes the new requirements by using the adjusted User Story technique. At this stage the developer is required to identify and define all requirement interfaces in order to position the new demand.

3. **The refactoring stage** – The development approach is to keep the process as simple as possible, so that immediately after verifying compliance with the requirements we refactor the code to engineered software product. This stage is in order to improves the understandability of the software in order to improve the ability to easily maintain the software in the future.

The implementation of these stages in the development of scientific software product depends on the development of a customized technique, to write requirements based on the User Story technique.

The steps used in user stories technique:

1. User stories has to be short, simple descriptions of a feature from the end-user perspective - in our case, usually the scientist himself.
2. The process start when the user (the scientist) is the one who writes the User Story.
3. The User Story is transferred to one member of the development team, how is responsible to edits it in his words - for this purpose it is required for customer availability.
4. The developer adds estimates of the difficulty level and the effort required to perform. Ideally, a User Story should be able to implement within two to three days. If the estimate is longer, developers should split the user's story into a series of smaller series [20].
5. The edited User Stories, will be forwarded to the evaluation of the all development team at a coordination meeting that also includes the presence of the scientist how invite the development of the software.
6. At the coordination meeting, as a basis for the software system to be developed, user stories should be: Independent, Negotiable, Valuable to users and customers, Estimable, Small, and Testable - this is known as the INVEST model [21].
7. The edited User Stories will be transferred to a client whose job it is to prioritize them.
8. The development team responsible to broken up the prioritize User Stories into development tasks.
9. Responsibility for each task is assigned to a team member.
10. The order of implementation will decided by the team based on multiple factors [22].

A generic modified framework for a User Story for an SSP project will comprise five parts:

1. Roles: - For who belongs the need described next.
2. Status: Does the requirement/functionality have any written code? or this is a new requirement.
3. Description of the functionality the system must perform (mandatory).
4. Justify why the demand why this functionality is needed (mandatory). (for better understanding the origin and related requirements.
5. Difficulty and effort estimation (work-point) (developer).

The format we propose is: "[As a < User >,] [like in < Name of the right function >,] I want <goal>, [so that <why>]."

The User Stories for Rock Slope Stability Analyses software product

Story # 1 describe requirement that existed in the first software and describe the reason for the requirement. In contrast, in story # 2, we can see requirement that existed in the first program and are not describe the reason for the requirement. In Story 3 we can see a new requirement, which did not exist in the previous system, and is without a description of why it is required. While in Story 4 we can see a new requirement with a description of why the scientist needs it.

1. Like in "Identifying_Object" function, I want to recognize objects in the system, so that it can calculate their center.
2. Like in "Time_to_Pic" function, I want to automatically command the camera to take pictures at user-defined intervals.
3. I want to mark and pre-number the shapes in the picture.
4. I want to calculate in real time the relative distance between two centers of shapes, so that it can track the relative displacements of each element in the system.

CONCLUSION

Writing requirements for Scientific Software Product using the user story technique contributed greatly to all stakeholders of the software. On the one hand, in the development process, it makes it very clear to understand what

are the user requirements, software functionality and constraints the software needed to meet. On the other hand, the structure of the user stories in writing requirements allows to limit misunderstanding of the constraints. Moreover, the technique for writing the requirements as a short stories allows modular division into sub-requirements. The effort and difficult estimation helps to control and evaluate the overall development process and enabled better management and timeliness. In conclusion, we believe that using the "User Story" technique improves the quality of writing requirements that lead to improve of the development process, which eventually lead to improvement in the software quality and better science.

References

[1] J.E. Hannay, C. MacLeod, J. Singer , "How do scientists develop and use scientific software?," in *SECSE '09 Proceedings of the 2009 ICSE Workshop on Software Engineering for Computational Science and Engineering*, 2009.

[2] Mark, S & Ronen, Y , " The Milne and Numorov methods as independent approaches for solving the Schroedinger equation: test case for the deuteron model for odd - odd N = Z nuclei," *Physica Scripta,* vol. 82, no. 4, pp. 1-8, 2010.

[3] Dubi C,Yaar I, and Mark S,., " Two independent approaches used for estimating 2d contamination distribution on the ground level- based on air monitoring information," *mathematics in engineering, science and aerospace ,* vol. 3, no. 2, pp. 151-158, 2012.

[4] J. C. Carver, R. P. Kendall, S. E. Squires, and D. E. Post. , "Software development environments for scientific and engineering software: A series of case studies." in *International Conference on Software Engineering*, 2007.

[5] S. Mark and Y. Lurie, "Customized project charter for computational scientific software products," *Journal of Computational Methods in Sciences and Engineering,* vol. 18, no. 1, pp. 165-176, 2018.

[6] L. Aronshtam, H. Cohen, D. Sohacheski and S. Mark, "Grading scale model for knowledge based repositories," *J. of Computational Methods in Sciences and Engineering,* vol. 18, no. 4, pp. 931-938, 2018.

[7] H. Cohen, D. Khankin, S. Mark and S. Mordechai, "Resource Management and Optimization Efficiency Issues in a Simulation Software Package," in *SIMUL 2015 : The Seventh International Conference on Advances in System Simulation*, 2015.

[8] V. R. Basili, D. Cruzes, J. C. Carver, L. M. Hochstein, J. K. Hollingsworth, and M. V. Zelkowitz., "Understanding the high-performance computing community: A software engineer's perspective," *IEEE Software,* vol. 25, no. 4, pp. 29-36, 2008.

[9] R. Sanders and D. Kelly., "Dealing with risk in scientific software development," *IEEE Software,* vol. 25, no. 4, pp. 21-28, 2008.

[10] J. Segal, "When software engineers met research scientists," *Empirical Software Engineering, vol. 10, no. 4, pp. 517-536, 2005. ,* vol. 10, no. 4, pp. 517-536, 2005.

[11] J. Segal and C. Morris, "Developing scientific software," *IEEE Software,* vol. 25, no. 4, pp. 18-20, 2008.

[12] J. Segal, "Some problems of professional end user developers," in *IEEE Visual Languages and Human-Centric Computing*, 2007.

[13] Nguyen-Hoan, Luke, Shayne Flint, and Ramesh Sankaranarayana, " A survey of scientific software development," in *Proceedings of the 2010 ACM-IEEE International Symposium on Empirical Software Engineering and Measurement. ACM*, 2010.

[14] S. Demeyer, S. Ducasse, and O. Nierstrasz, Object-Oriented Reengineering Patterns, Morgan Kaufmann and DPunkt, 2002.

[15] Hui Zhou, Wencai Du, Shaochun Xu, Qinling Xin, "Computer Network Reverse Engineering," *Computer and Information Science 2011, Studies in Computational Intelligence Volume 364, 2011, pp 227-239.*

[16] Fowler, Martin, Refactoring: improving the design of code y, New York: Addison-Wesle, 1999.

[17] D. Bakun-Mazor, Y. H. Hatzor, S. D. Glaser and C. J. Santamarina, "Thermally vs. seismically induced block displacements in Masada rock slopes," *International Journal of Rock Mechanics and Mining Sciences,* vol. 61, pp. 196-211, 2013.

[18] K. Beck, "Embracing change with extreme programming," *Computer,* vol. 10, pp. 70-77, 1999.

[19] K. Beck and E. Gamma, Extreme programming explained: embrace change, addison-wesley professiona, 2000.

[20] X. Jie, D. Ho and . L. F. Capretz, "An empirical study on the procedure to drive software quality estimation models." *International Journal of Computer Science & Information Technology,,* vol. 2 (4), p. 1–16, 2010.

[21] ISO/IEC/IEEE, "24765:2010 Systems and software engineering – Vocabulary".

[22] N. F. Schneidewind, "Body of knowledge for Software quality measurement.," *IEEE Computer,* vol. 35 (2), p. 77–83, 2002.

Computational Formula for the Impact of Stochastic Dependence on the Insurance Premium

Ji Hwan Cha[1, a)], Hyunju Lee[1, b)] and Maxim Finkelstein[2,c)]

[1]*Department of Statistics, Ewha Womans University, Seoul 120-750, Rep. of Korea*
[2]*Department of Mathematical Statistics, University of the Free State 339 Bloemfontein 9300, South Africa.*

[a)]Corresponding author: jhcha@ewha.ac.kr
[b)]hyunjlee@ewhain.net
[c)]FinkelM@ufs.ac.za

Abstract. Standard actuarial theory of multiple life insurance traditionally postulates independence for the remaining lifetimes mainly due to computational convenience rather than realism. In this paper, we propose a general common shock model for modelling dependent coupled lives and apply it to a life insurance model. Under the model, we derive the computational formula for the impact of stochastic dependence on the pricings of insurance policies involving multiple lives which are subject to common shocks.

INTRODUCTION

Traditionally, in evaluating the amount of premium relating to an insurance contract involving multiple life insurance, the independence for the lifetimes has been assumed mainly due to simplicity. However, in practice, the involved lifetimes are frequently stochastically dependent rather than being completely independent. A good example for dependence among insured persons is certainly a contract issued to a married couple. For example, it is observed that there is a very high positive correlation in the times of deaths between coupled lives (see Carriere 2000). Indeed, the husband and wife are more or less exposed to the same types of risks or hazards since they share a common living environment and a common way of life. In this paper, we develop a general dynamic common shock model for modelling dependent coupled lives. In the common shock model studied by Denuit et al. (2006), it is assumed that a shock just kills both individuals simultaneously. However, in practice, several different situations can dynamically occur due to a critical event or a shock. For example, some types of events are not too critical so that such events may cause just injuries of the individuals, not actually causing their deaths. Also, one of the individuals or both of them can survive the critical event or shock, but they may suffer from it and their remaining lifetimes can be affected by the event. Motivated by it, in the model studied in this paper, we assume that (i) each shock (critical accident) can kill both individuals simultaneously; or (ii) it can kill only one of the individuals; or (iii) it does not kill any individuals. Furthermore, even if an individual survives shocks, it is assumed that the effects of shocks are accumulated in the hazard rate of the individual according to a standard shot-noise process. Applying the developed shock model to the life insurance, we investigate the influence of dependence on the pricings of insurance policies involving multiple lives which are subject to the general shock model.

The paper is organized as follows. In Section 2, we briefly introduce the stochastic model and suggest the joint distribution of the lifetimes of the individuals. In Section 3, we derive the computational formula for the impact of stochastic dependence on the pricings of insurance policies. In Section 4, some concluding remarks are given.

The Stochastic Model and Bivariate Survival Function

Denote by L_1 and L_2 the 'baseline' coupled lives which represent the individual lifetimes of the couple when the shock process is not present, i.e., the lifetimes in the absence of shocks. We denote by $r_1(t)$ and $r_2(t)$ the force of mortalities (hazard rate) of L_1 and L_2, respectively. The individuals are subject to a common external shock process and let the external shock process $\{N(t), t \geq 0\}$ be the nonhomogeneous Poisson process (NHPP) with rate (i.e., intensity function) $\lambda(t)$. On each event of shock, with probability $p_0(t)$ both individuals survive the shock (shock of type 0); with probability $p_i(t)$ only the i th individual is killed (shock of type i), $i = 1,2$, respectively; with probability $p_3(t)$ both individuals are killed simultaneously (shock of type 3), where t is the shock occurrence time and $p_0(t) + p_1(t) + p_2(t) + p_3(t) = 1$. In practice, even though the individuals survive the shocks, they may injure and suffer from it, and their remaining lifetimes can be seriously affected by the event. This effect is modelled by a standard shot noise process (Lemoine and Wenocur (1985, 1986)) as follows. When the i th individual has survived until time t, the level of accumulated damage of this individual at time t, caused by the total $N(t)$ survived shocks, is modelled as

$$W_i(t) = \sum_{j=1}^{N(t)} D_j h_i(t - T_j), \; i = 1,2, \tag{1}$$

where T_j is the j th arrival time of the shock process, $D_j, j = 1,2,...$ (i.i.d.) are the corresponding magnitudes of shocks having common probability density function (pdf) $f_D(u)$ and $h_i(t)$ is a nonnegative and deterministic function with $h_i(t) = 0$ for $t < 0$, $i = 1,2$. The shock process $\{N(t), t \geq 0\}$ and the sequence $\{D_1, D_2, ...\}$ are supposed to be independent, which is the typical assumption in the studies of a standard shot noise process (see also Lemoine and Wenocur (1985, 1986)). The usual assumption for considering asymptotic properties of $W_i(t)$ is that $h_i(t)$ is monotonically decreasing, vanishing as $t \to \infty$, and its integral in $[0, \infty)$ is finite. However, here, we formally do not need this rather restrictive assumption and it can be relaxed considering practical aspects. For example, (i) if the effect of a shock (i.e., caused damage) is not decreasing and it remains at the same level, then a constant function of $h_i(t) = c_i$, $t \geq 0$, can be applied; (ii) if the effect of a damage becomes severer as t increases, then an increasing function of $h_i(t)$ can be employed; (iii) if the effect of a damage decreases (e.g., by suitable medical treatments), then $h_i(t)$ can be assumed to be decreasing. Thus, the shot- noise process model in (1) allows much flexibility in modelling the shock effect.

The accumulated damage may eventually result in the deaths of individuals, which can be probabilistically described by assuming that the corresponding conditional hazard rate (excluding the baseline hazard $r_i(t)$), on condition that $\{N(t), T_1, T_2, ..., T_{N(t)}\}$ and $\{D_1, D_2, ..., D_{N(t)}\}$ are given and the life is still alive, is proportional to $W_i(t)$. This is a reasonable assumption that describes the proportional dependence of the probability of death in the infinitesimal interval of time on the level of damage. Thus, on condition that $\{N(t), T_1, T_2, ..., T_{N(t)}\}$, $\{D_1, D_2, ..., D_{N(t)}\}$ are given and shocks of types i and 3 have not occurred yet, the conditional hazard rate of the i th individual λ_{it} is formally described by

$$\lambda_{it} \equiv r_i(t) + k_i \sum_{j=1}^{N(t)} D_j h_i(t - T_j), \; i = 1,2, \tag{2}$$

where $k_i > 0$, $i = 1,2$, are the constants of proportionality. Under the stochastic model given in (2), the joint survival function of the coupled lives is given in the following result. In the following, for convenience, we define

$\Lambda(t) \equiv \int_0^t \lambda(s)ds$ and $H_i(t) \equiv \int_0^t h_i(s)ds$, $i = 1,2$. Then, under the model suggested in (2), it can be shown that the joint survival function of (X_1, X_2) is given as follows (see Lee and Cha (2018)):

$$P(X_1 > x_1, X_2 > x_2) = \exp\left\{-\int_0^{x_1} r_1(s)ds\right\}\exp\left\{-\int_0^{x_2} r_2(s)ds\right\}$$

$$\times \exp\left\{-\int_0^{x_2}\left(1-\int_0^{\infty} p_0(s)\exp\{-k_1uH_1(x_1-s)-k_2uH_2(x_2-s)\}f_D(u)du\right)\lambda(s)ds\right\}$$

$$\times \exp\left\{-\int_{x_2}^{x_1}\left(1-\int_0^{\infty}(p_0(s)+p_2(s))\exp\{-k_1uH_1(x_1-s)\}f_D(u)du\right)\lambda(s)ds\right\},\ \textit{if } x_1 \geq x_2,$$

$$P(X_1 > x_1, X_2 > x_2) = \exp\left\{-\int_0^{x_1} r_1(s)ds\right\}\exp\left\{-\int_0^{x_2} r_2(s)ds\right\}$$

$$\times \exp\left\{-\int_0^{x_1}\left(1-\int_0^{\infty} p_0(s)\exp\{-k_1uH_1(x_1-s)-k_2uH_2(x_2-s)\}f_D(u)du\right)\lambda(s)ds\right\}$$

$$\times \exp\left\{-\int_{x_1}^{x_2}\left(1-\int_0^{\infty}(p_0(s)+p_1(s))\exp\{-k_2uH_2(x_2-s)\}f_D(u)du\right)\lambda(s)ds\right\},\ \textit{if } x_1 < x_2 . \quad (3)$$

The Impact of Stochastic Dependence

An annuity is a series of payments made either continuously or at certain intervals (as months or years) during some period which is random. A typical example is the life annuity which involves a benefit payable until the first death. An important type of life annuity is the joint-life annuity. In the case of a married couple, the continuous n-year joint-life annuity pays \$ 1 per year as long as both spouses survive (with a maximum of n years). The corresponding net single premium is given by

$$\bar{a}_{xy;\overline{n}|} = \int_0^n \exp\{-\int_0^t \delta_u du\} P(X_1 > t, X_2 > t)dt ,$$

where δ_u is the instantaneous interest rate at time u .

Note that

$$\bar{a}_{xy;\overline{n}|} = \int_0^n \exp(-\int_0^t \delta_u du)\Pr(X_1 > t, X_2 > t)dt$$

$$= \int_0^n \exp(-\int_0^t \delta_u du)\cdot \exp\left\{-\int_0^t r_1(s)ds\right\}\exp\left\{-\int_0^t r_2(s)ds\right\}$$

$$\times \exp\left\{-\int_0^t\left(1-\int_0^{\infty} p_0(s)\exp\{-k_1uH_1(t-s)-k_2uH_2(t-s)\}f_D(u)du\right)\lambda(s)ds\right\}dt$$

$$= \int_0^n \exp(-\int_0^t (\delta_u - \phi(u))du)\cdot \exp\left\{-\int_0^t r_1(s)ds\right\}\exp\left\{-\int_0^t r_2(s)ds\right\}$$

$$\times \exp\left\{-\int_0^t\left(1-\int_0^\infty (p_0(s)+p_2(s))\exp\{-k_1uH_1(t-s)\}f_D(u)du\right)\lambda(s)ds\right.$$

$$\left.-\int_0^t\left(1-\int_0^\infty (p_0(s)+p_1(s))\exp\{-k_2uH_2(t-s)\}f_D(u)du\right)\lambda(s)ds\right\}dt$$

$$=\int_0^n \exp(-\int_0^t \delta_u^* du)\Pr(X_1^\perp > t, X_2^\perp > t)dt,$$

where $(X_1^\perp, X_2^\perp)$ is the independent version of (X_1, X_2) and $\delta_u^* \equiv \delta_u - \phi(u)$ and $\phi(u)$ is defined by

$$\phi(t) \equiv (1-((p_0(t)+p_2(t)))\lambda(t) + (1-((p_0(t)+p_1(t)))\lambda(t)$$

$$+\int_0^t\left(\int_0^\infty (p_0(s)+p_2(s))\{k_1uh_1(t-s)\}\exp\{-k_1uH_1(t-s)\}f_D(u)du\right)\lambda(s)ds$$

$$+\int_0^t\left(\int_0^\infty (p_0(s)+p_1(s))\{k_2uh_2(t-s)\}\exp\{-k_2uH_2(t-s)\}f_D(u)du\right)\lambda(s)ds - (1-p_0(t))\lambda(t)$$

$$-\int_0^t\left(\int_0^\infty p_0(s)\{k_1uh_1(t-s)+k_2uh_2(t-s)\}\exp\{-k_1uH_1(t-s)-k_2uH_2(t-s)\}f_D(u)du\right)\lambda(s)ds$$

(see also Lee and Cha (2018)). Thus, δ_u^* corresponds to the shifted instantaneous interest rate. Therefore, the effect of the dependency of the bivariate distribution in (3) is the decrease in the interest rate by $\phi(u)$, compared with the case when the remaining lifetimes are independent.

Concluding Remarks

The findings obtained in this study suggest some general insights into the relationship between the modeling parameters in the dependent lifetime model and the pricings of insurance policies. In this paper, the main source of dependence is the environment shared by the individuals in a couple. In the future study, other sources of dependence could be additionally incorporated into the proposed bivariate model.

REFERENCES

1. J. F. Carriere, Bivariate survival models for coupled lives, *Scandinavian Actuarial Journal* **2000**, 17-32 (2000).
2. M. Denuit, E. Frostig, and B. Levikson, Shifts in interest rate and common shock model for coupled lives, *Belgian Actuarial Bulletin* **6**, 1-4 (2006).
3. H. Lee and J. H. Cha, A dynamic bivariate common shock model with cumulative effect and its actuarial application, *Scandinavian Actuarial Journal* **2018**, 890-906 (2018).
4. A. J. Lemoine and M. L. Wenocur, On failure modeling, *Naval Research Logistics* **32**, 497-508 (1985).
5. A. J. Lemoine and M. L. Wenocur, A note on shot-noise and reliability modeling, *Operations Research* **34**, 320-323 (1986).

Computation of the Ideal Step-Size - A Constant and Adaptive Approach

Simon Genser[1,a)], Franz Holzinger[1] and Georg Stettinger[1]

[1] *VIRTUAL VEHICLE Research Center, Inffeldgasse 21a, 8010 Graz, Austria*

[a)]Corresponding author: simon.genser@v2c2.at

Abstract. The correct or ideal step-size of a signal is a crucial information for many different applications in simulation, control engineering or signal processing to name a few. Introduced will be a constant approach, where an ideal constant step-size of a signal will be computed, and an adaptive approach where a signal will be ideal sampled with a time varying step-size. Both approaches are validated at a simple sinus signal and at an industrial example, utilizing a speed signal which is part of a co-simulated hybrid vehicle. How to choose the tolerance parameters and the accuracy of the ideal sampled signal and the amount of saved memory will be discussed.

INTRODUCTION

The selection of the correct step-size for signals is an important question in many fields like control systems, simulation, or signal processing. In many different applications the problem of oversampling, i.e. too small step-size respectively sampling rate, is present, which is leading to an unnecessary memory consumption. An oversampled signal results in bad excitation, for details see [1], therefore the utilization of system identification tools, like least square methods [1], subspace methods [2], state space identification [3] or similar, is problematic and will lead to a poor quality of the identified model. For co-simulation [4] or parallel computation oversampled signals are leading to an overhead in communication, which can decrease the speed of the overall simulation or computation. For those reasons the computation of an ideal step-size is beneficial for a lot of different fields and applications.
For the computation of the ideal step-size two different approaches will be introduced in chapter 2. First a constant approach, where the determined ideal step-size is constant for the whole signal and second a so-called adaptive approach, where a time varying step-size is computed. Both approaches are not designed to be executed at runtime (post-process), the whole signal has to be computed and stored before and then the ideal step-sizes can be determined. Nevertheless this information is crucial for a signal analysis. Both methods are validated at an industrial example, utilizing the speed signal of a hybrid electric vehicle.

COMPUTATION OF THE IDEAL STEP-SIZE

There are two different approaches for the computation of the ideal step-size, the constant version where the ideal constant step-size $\Delta\tilde{T}$ is determined and the adaptive approach where the output is the time-varying ideal step-size. To keep the derivations as simple as possible the following notation is utilized and the following assumptions are made:

- T_k denotes the k-th sampling point
- $\Delta T_{12} := T_2 - T_1$ denotes the step-size between T_1 and T_2
- $y(.)$ describes the original sampled, scalar signal
- $\tilde{y}(.)$ describes the ideal sampled, scalar signal
- $y_k := y(T_k)$ stands for the value of y at the sampling point T_k

Note: Due to the fact that one can identify a n-dimensional vector-valued signal as n scalar signals, this method can easily be generalized for multidimensional vector-valued signals.

Constant Approach

The computation of the ideal constant step-size $\Delta\tilde{T}$ is carried out with the utilization of

$$Int_y := \int_{T_{start}}^{T_{end}} \underbrace{y(t) - min\,(y(t))}_{>0}\, dt, \tag{1}$$

and it is realized via the following pseudo code:

set $l = 2$
$\tilde{y}$ consists every l-th data point from y
compute $Int_y, Int_{\tilde{y}}$
compute $\epsilon_{const} := \frac{|Int_y - Int_{\tilde{y}}|}{Int_y + \epsilon}$
while $\epsilon_{const} < tol_{const}$ **do**
    $l = l + 1$
    $\tilde{y}$ consists every l-th data point from y
    compute $Int_{\tilde{y}}$
    compute $\epsilon_{const} = \frac{|Int_y - Int_{\tilde{y}}|}{Int_y + \epsilon}$
end while
$\Delta\tilde{T} = (l - 1) \cdot \Delta T$

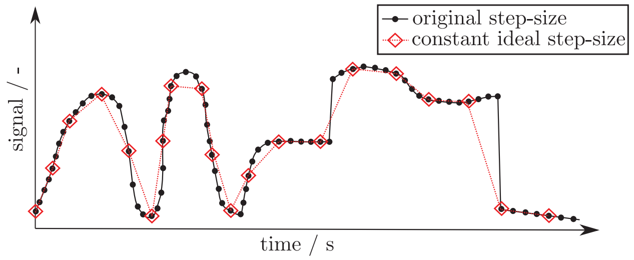

FIGURE 1: schematic visualization of the constant approach

The original signal y has to be sampled with a constant step-size ΔT. The number of samples in $\tilde{y}$ is as long reduced as the difference from Int_y and $Int_{\tilde{y}}$ is sufficiently small, which is ensured via the condition $\epsilon_{const} < tol_{const}$.

Note: The computation of the integral in (1) should be carried out with a trapezoidal method, so that the linear interpolated signal $\tilde{y}$ is integrated exactly.

Adaptive Approach

Compared to the constant approach, the adaptive approach is also capable of signals with time-varying step-sizes, there are no additional assumptions. The method is based on the following two definitions:

$$A(T_1, T_2, T_3) \;:=\; \frac{(y_1 + y_2 - 2 \cdot min\{y_1, y_2, y_3\})}{2} \cdot \Delta T_{12} + \ldots$$
$$\frac{(y_2 + y_3 - 2 \cdot min\{y_1, y_2, y_3\})}{2} \cdot \Delta T_{23}$$
$$A(T_1, T_3) \;:=\; \frac{(y_1 + y_3 - 2 \cdot min\{y_1, y_3\})}{2} \cdot \Delta T_{13}$$

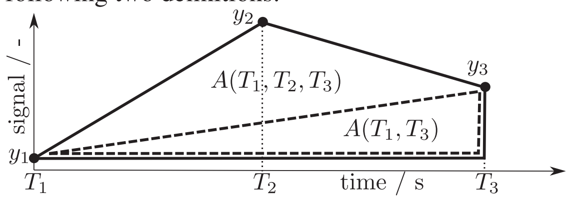

FIGURE 2: visualization of the nearby definitions

The ideal adaptive step-size is is computed with the following method, displayed in pseudo code as:

for $k = 1, ..., N$ **do**
    $A_1 = A(T_k, T_{k+1}, T_{k+2})$
    $A_2 = A(T_k, T_{k+2})$
    $\epsilon_{rel} := \left|\frac{A_1 - A_2}{A_2 + \epsilon}\right|$
    $\epsilon_{abs} := |A_1 - A_2|$
    cnt=1
    while $\epsilon_{rel} < tol_{rel}$ and $\epsilon_{abs} < tol_{abs}$ **do**
        cnt=cnt+1
        $A_1 = A(T_k, T_{k+cnt}, T_{k+cnt+1})$
        $A_2 = A(T_k, T_{k+cnt+1})$
        $\epsilon_{rel} = \epsilon_{rel} + \left|\frac{A_1 - A_2}{A_2 + \epsilon}\right|$
        $\epsilon_{abs} = \epsilon_{abs} + |A_1 - A_2|$
    end while
    $\tilde{y}(T_k) = y(T_k)$
    $\tilde{y}(T_{k+cnt}) = y(T_{k+cnt})$
    k=k+cnt+1
end for

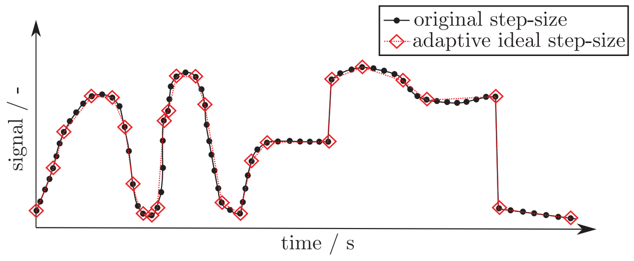

FIGURE 3: schematic visualization of the adaptive approach

The method iterates through every of the N data points in the original signal y and decides if a data point contains important information compared to a linear interpolated signal without this data point, if not, this data point is ignored in the ideal sampled signal $\tilde{y}$. Via entering the while loop the data points at $T_{k+1}, \ldots, T_{k+cnt-1}$ are ignored. Therefore the signal y is filtered and just the important data points are kept, leading to $\tilde{y}$ with an ideal adaptive step-size, respectively sampling time.
Note: For the case of constant signals where $A_1, A_2 = 0$ respectively $Int_y, Int_{\tilde{y}} = 0$ the parameter ϵ is necessary, so that the criteria $\left|\frac{A_1-A_2}{A_2+\epsilon}\right| < \epsilon_{rel}$ for the adaptive approach and $\frac{|Int_y-Int_{\tilde{y}}|}{Int_y+\epsilon} < tol_{const}$ for the constant approach are true. And for the case, that $A_1 \ll A_2$ respectively $Int_y \ll Int_{\tilde{y}}$ or vice-versa, $\epsilon \approx 10^{-14}$ does not influence the criteria above.

Choosing the Tolerance Parameters for the Adaptive Approach

The ϵ_{rel} describes the local behaviour of the signal, i.e. the change of the derivative of the signal. This means, if there are sudden changes in the signal, the data points representing those, will be included in the ideal-sampled signal $\tilde{y}$. Therefore the choice of tol_{rel} should be chosen small, if one is interested in taken fast, but maybe small, changes in the signal into account, as discontinuities for example. Choosing tol_{abs} can be accomplished with the approach

$$tol_{abs} := c_{abs} \cdot [max(y) - min(y)], \tag{2}$$

where $c_{abs} > 0$ should be chosen appropriate. For $tol_{rel} \to 0$ or $c_{abs} \to 0$ holds $\tilde{y} \to y$.
Note: It is not possible to differentiate between the case that the original step-size is ideal, or if the step-size is chosen too large, leading to aliasing effects. This means that with the two mentioned approaches the step-size can only be enlarged or kept as it is.
Note: The constant and adaptive approach are both insensitive to scaling or offsets of the signal, this is beneficial for choosing the tolerance parameters.

EVALUATION AT SINUS SIGNAL & SPEED SIGNAL FROM HYBRID VEHICLE

For the computation of the ideal constant and adaptive step-size for an industrial signal, the choice of the tolerance parameters is crucial. The tuning of the parameters is accomplished by a sinus function, which is depicted in the upper part of Figure 4. There it is clearly visible that the ideal adaptive step-size is smaller when the change of the derivative is fast and the step-size is larger when the change of the derivative is slow.
The parameters $tol_{const} = 1.2$, $tol_{rel} = 0.5$ and $c_{abs} = 0.0012$, which were tuned at the sinus function, are utilized for analyzing the speed signal of a co-simulated hybrid vehicle, for details see [5]. It is obvious, that the tuned parameters from the sinus function work well for the industrial example too. Comparing the ideal constant and the ideal adaptive step-size, it is obvious that with the adaptive approach the approximation of the original signal is more accurate than with the constant approach, see therefore Table 1. Especially for the case of sudden changes in the signal, as they appear between 0.5 and 2 seconds. Taken the memory saving and the accuracy from Table 1 for both signals into account, the ideal adaptive step-size is preferable, because the representation of the signal is much more accurate and the memory saving is still high. A tradeoff between accuracy and memory saving is always mandatory.

	sinus signal	speed signal
saved memory - constant approach	98.31 %	96.97 %
saved memory - adaptive approach	96.02 %	89.67 %
ϵ_{err} - constant approach	0.019	23.53
ϵ_{err}- adaptive approach	0.005	2.42

TABLE 1: Comparison of the memory saving and approximation error $\epsilon_{err} = \text{mean}(|y - \tilde{y}|)$ of the constant and adaptive approach.

SUMMARY, CONCLUSION & FUTURE WORK

Both introduced methods for determining the ideal step-size, the constant and adaptive approach, are capable of signals which do not have zero mean and they are both invariant to scaling or shifting of the signal. Both investigated examples showed, that an accurate approximation of the signal is possible and the potential memory saving is high with 90 %

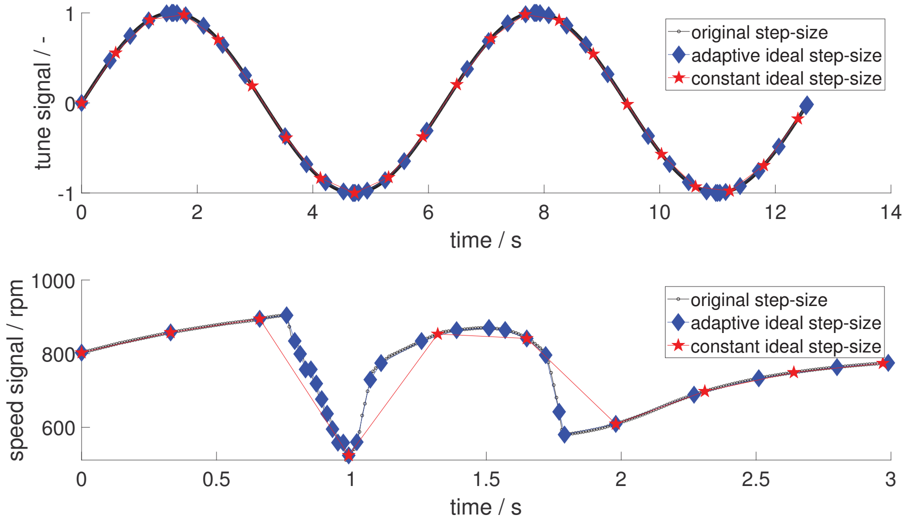

FIGURE 4: Computation of the ideal step-size, with the constant and adaptive approach. The upper part depicts a sinus and the lower part a speed signal from a hybrid vehicle, Details in [5]. The original step-size is $\Delta T = 10\ ms$ for both signals.

- 98 %. This is of special interest in co-simulation because, there the signals have to be communicated between subsystems and therefore the reduction of the required memory of a signal is significant, for a better performance of the co-simulation.
In every application where a time-/ or state-discretization is utilized, the question of the appropriate discretization-size alias the ideal step-size arises. Therefore the possible applications of the herein proposed methods is very broad, the focused ones for the future are: approximation of the dynamics and the relative degree of a model; finding the best trigger sequence of a co-simulation; preparing an online step-size controller for the communication step-size for co-simulation; the determination of the ideal quantization height for Quantized State System Simulations [6].

ACKNOWLEDGMENTS

The publication was written at VIRTUAL VEHICLE Research Center in Graz, Austria. The authors would like to acknowledge the financial support of the COMET K2 Competence Centers for Excellent Technologies Programme of the Federal Ministry for Transport, Innovation and Technology (bmvit), the Federal Ministry for Digital, Business and Enterprise (bmdw), the Austrian Research Promotion Agency (FFG), the Province of Styria and the Styrian Business Promotion Agency (SFG).

REFERENCES

[1] L. Ljung, *System Identification: Theory for the User*, 2nd ed. (PTR Prentice Hall Information and System Sciences Series, Prentice Hall, New Jersey,, 1999).

[2] P. V. Overschee and B. D. Moor, *Subspace Identification for Linear Systems*, 1st ed. (Kluwer Academic Publishers, London, 1996).

[3] M. Giesbrecht, G. Barreto, and C. P. Bottura, eds., *State Space Identification Algorithm based on Multivariable Impulse Response* (2018).

[4] R. Kübler and W. Schiehlen, eds., *Two Methods of Simulator Coupling* (Mathematical and Computer Modelling of Dynamical Systems, 2010).

[5] G. Stettinger, M. Horn, M. Benedikt, and J. Zehetner, eds., *A Model-Based Approach for Prediction-Based Interconnection of Dynamic Systems* (53rd IEEE Conference on Decision and Control, 2014).

[6] F. Cellier, E. Kofman, G. Migoni, and M. Bortolotto, eds., *Quantized State System Simulation* (2008).

The Influence of Consolidation Coefficients on Wave Attenuation and Dispersion Based on General Linear Solid Framework

Shuna Chen[1, a)], Xiaotao Wen[1, b)] and Zhege Liu[1, c)]

[1]*Institute of Geophysics, Chengdu University of Techology, Chengdu 610000, China*

[a)]chen_shuna@163.com
[b)] Corresponding author: wenxiaotao@cdut.cn
[c)]liuzhege@163.com

Abstract. This paper investigates the impact of consolidation coefficients on wave attenuation and dispersion based on the general linear solid framework. Through the numerical experiments with the published mechanical properties of the brine-saturated sandstone, the dispersion and attenuation of fast P-wave and slow P-wave are discussed under four different consolidation conditions.

INTRODUCTION

Since the poroelasticity theory was fundamentally established by Boit (1956a, b) and Gassmann (1951), the attenuation and dispersion of compressional seismic waves including the fast P-wave and slow P- wave in fluid-saturated porous media have received widely public attention.

The general linear solid (GLS) framework was proposed by Morozov and Deng (2016a, 2016b). It only needs to input the physical properties of rocks, which are independently measurable in physical experiments. Deng and Morozov (2016) used GLS framework to illustrate the dispersion and attenuation of the fast P-wave in fluid-saturated media. But there is no discussion about the impact of consolidation state on the wave attenuation and dispersion, neither about the propagation characteristic of the slow P-wave based on GLS framework. In this context, we will discuss these questions through numerical experiments based on GLS framework at seismic frequencies.

GLS FRAMEWORK

According to the GLS framework presented by Morozov and Deng (2016a, 2016b), for the incident harmonic plane P-wave in which all spatial displacements are oriented in the direction of axis x, the matrix form equation of

motion they derived in their paper is (Deng and Morozov, 2016),

$$\boldsymbol{\rho}\ddot{\mathbf{u}} = -\mathbf{d}\dot{\mathbf{u}} + \mathbf{M}^{*}\mathbf{u}'' \tag{1}$$

Where the complex-valued compressional wave modulus is$\mathbf{M}^{*} \equiv \mathbf{K}^{*} + \frac{4}{3}\boldsymbol{\mu}^{*} \equiv \mathbf{M} - i\omega\boldsymbol{\eta}_{M}$, and corresponsively the bulk modulus is $\mathbf{K}^{*} = \mathbf{K} - i\omega\boldsymbol{\eta}_{K}$, shear modulus is $\boldsymbol{\mu}^{*} \equiv \boldsymbol{\mu} - i\omega\boldsymbol{\eta}_{\mu}$. What's more, there is $\mathbf{M} \equiv \mathbf{K} + \frac{4}{3}\boldsymbol{\mu}$, and $\boldsymbol{\eta}_{M} \equiv \boldsymbol{\eta}_{K} + \boldsymbol{\eta}_{\mu}$.

$$\mathbf{M}\mathbf{u}'' + \boldsymbol{\eta}_{M}\dot{\mathbf{u}}'' = (\mathbf{K}^{*} + \frac{4}{3}\boldsymbol{\mu}^{*})\mathbf{u}''. \tag{2}$$

An important variable introduced in GLS is the complex-valued density $\boldsymbol{\rho}^{*} \equiv \boldsymbol{\rho} + \frac{i}{\omega}\mathbf{d}$, its real part is mass density, and its image part is the density caused by the relative movement between multi-phase materials. Thus, based on mathematical derivation, the relationship between $\boldsymbol{\rho}^{*}$ and $\mathbf{M}^{*}$ from equation 2 can be expressed by equation 3:

$$\boldsymbol{\rho}^{*}\boldsymbol{v}^{(n)} = \gamma^{n}\mathbf{M}^{*}\boldsymbol{v}^{(n)}. \tag{3}$$

Where $\gamma \equiv (k+i\alpha)^2/\omega^2$, the complex-valued wave modes $\mathbf{v}^{(n)}$ and the corresponding eigenvalues $\gamma^{(n)}$ can be obtained from the equation 3. From the corresponding values of γ, the phase velocity of the wave is acquired for each wave mode:

$$\text{Vphase} \equiv \frac{\omega}{k} = \frac{1}{Re\sqrt{\gamma}} \ . \tag{4}$$

And the energy dissipation factor is $Q^{-1} \equiv 2\alpha/k = 2\mathrm{Im}(\sqrt{\gamma})/\mathrm{Re}(\sqrt{\gamma})$.

Assume that the fluid-saturated porous rock with different level of consolidation, the dry rock moduli of single porosity are obtained from following effective medium formula (Zhao et al.,2015):

$$K_d^i = (1-\phi)K_s/(1+c_i\phi), \tag{5}$$
$$\mu_d^i = (1-\phi)\mu_s/(1+c_i\phi)$$

Where c is the consolidation coefficient and ϕ is porosity. K_d and μ_d is the bulk modulus and shear modulus of the rock respectively. Refer to Zhao's paper (2015), for the brine-saturated sandstone we research in this context, we empirically take c=4, 6, 8 and 10 respectively when i=1,2,3,4.

For the two-phase porous medium (solid porous rock frame plus saturating pore fluid) we research here, the form of the bold parameters in above equations is 2 × 2 matrices, including density, elastic-moduli, and Darcy friction. They are shown as follows (Deng and Morozov, 2016):

$$\boldsymbol{\rho} = \begin{bmatrix} \rho & -\rho_f \\ -\rho_f & \frac{\tau}{\Phi}\rho_f \end{bmatrix} \qquad \mathbf{d} = \begin{bmatrix} 0 & 0 \\ 0 & \eta/\kappa \end{bmatrix}, \tag{6}$$
$$\mathbf{K} = \begin{bmatrix} K_U & -\alpha M \\ -\alpha M & M \end{bmatrix} \qquad \boldsymbol{\mu} = \begin{bmatrix} \mu_d & 0 \\ 0 & 0 \end{bmatrix}.$$

Where Ku is the bulk modulus of saturated porous rock, and α is Biot-Willis coefficient.

Besides, the inverse of K is the elastic compliance:

$$\mathbf{J} \equiv \mathbf{K}^{-1} = J_D \begin{bmatrix} 1 & \alpha \\ \alpha & K_U/M \end{bmatrix}. \tag{7}$$

Where $J_D \equiv K_d^{-1}$ and $K_U \equiv K_d + \alpha^2 M$.

NUMERICAL EXPERIMENT

In the numerical expriments, we use the published mechanical properties of the brine-saturated sandstone (Carcione and Gurevich, 2011) to study the wave attenuation and dispersion in seismic frequencies. Deng and Morozov (2016) had used this data to analyze the solid viscosity of fluid-saturated porous rock with squirt flows at seismic frequencies less than approximately 1 kHz. Based on their work, we add the consolidation coefficients into their Lagrangian model including solid viscosity due to squirt flows. This model schematically designs a rock containing two different types of pores: relatively compliant and planar “soft” pores or cracks and “stiff” pores. Noted that when they fomulated this squirt-flow model, they considered a fluid-saturated rock with only stiff pores. What’s more, at lower frequencies, the effects of fluid flows within compliant pores are considered as bulk and shear solid viscosities of the effective porous frame (Deng and Morozov, 2016). Similarly with Deng and Morozov’s work (2016), we also take the fluid-saturated rock as a two-phase medium. In table 1, comparing with the values of porosity and soft porosity, it shows that the porosity is 1000 times of the soft porosity in the porous rock, therefore it is reasonable that in the equation 5, we only consider the porosity and neglect the soft porosity. The soft porosity works in the calculation of the effective bulk and shear viscosities in the equation 7 in Deng and Morozov’s paper (2016).

TABLE 1. Mechanical properties of brine-saturated sandstone used in the examples (Carcione and Gurevich,2011)

	Solid	
K_s	50 GPa	Bulk modulus of solid grains
K_h	20 GPa	bulk modulus
μ_d	12 GPa	Drained shear modulus
ρ_s	2650 kg/m^3	Density of solid grains
φ	0.2	Porosity
φ_c	0.0002	Soft Porosity
k	200 mD	Permeability
f	0.93	Volume fraction
σ	0.0004	Grain-contact aspect ratio
τ	2.3	Tortuosity
	Brine	
K_{fl}	2.25 GPa	Bulk modulus
ρ_{fl}	1040 kg/m^3	Density
η	1 cP	Viscosity

Based on GLS framework and the data shown in table 1, we obtain the result shown in figure 1. Now let’s analyze the influence of consolidation on the wave dispersion and attenuation of fast P-wave and slow P-wave at seismic frequencies less than approximately 1 KHz.

Firstly, we found that the phase velosities of fast P-wave have no obvious dispersion characteristic at seismic frequencies below 1KHz, but the phase velosities of slow P-wave have. It is consistent with the Biot theory. Secondly, the phase velocities of fast P-wave show significant difference with different consolidation coefficients. The fast P-wave velocity becomes higher when the rock is in a better consolidation, the smaller consolidation

coefficient means the better consolidation. However, the consolidation coefficients only have a very little of influence on the phase velocities of slow P-wave at seismic frequencies.Thirdly, the phase velocity of slow P-wave does have dispersion characteristic, but its value is so low and its attenution is so high that the slow P-wave is hard to be recorded by instruments at seismic frequencies. At the same time, the consolidation coefficients easily affect the fast P-wave attenuation, but hardly affect the slow P-wave attenuation. This is because the fast P-wave propagates in the solid rock frame and the slow P-wave propagates in the fluid in pores, and the consolidation coefficients significantly affect the effective dry rock moduli according to equation 5.

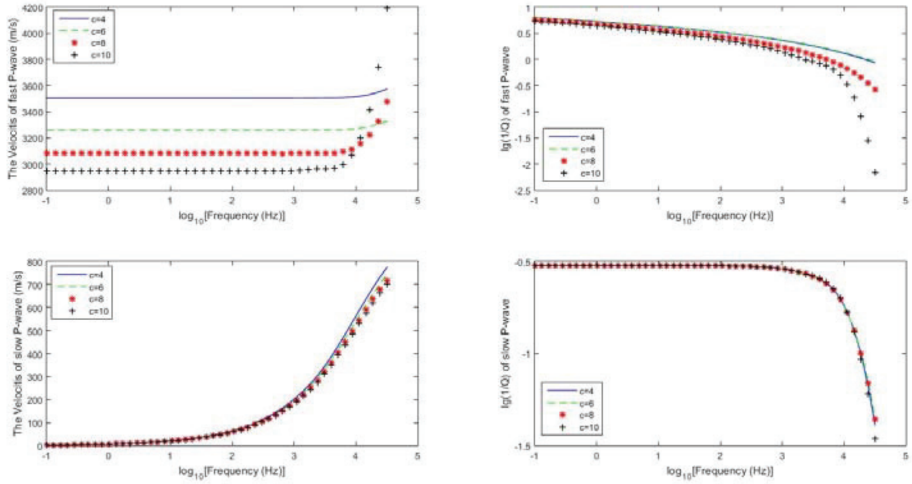

FIGURE 1. Velocities and lg(Q^{-1}) of the fast P-wave and slow P-wave in brine-saturated sandstone with different consolidation coefficients.

CONCLUSION

The influence of consolidation coefficients on the dispersion and attenuation of fast P-wave and slow P-wave based on GLS framework is discussed in this paper. Based on the numerical experiments, during the seismic frequencies less than 1 KHz, the phase velocities of fast P-wave have no obvious dispersion and their values are significantly influenced by the consolidation level. However, the phase velocities of slow P-wave have dispersion characteristic and their values are hardly affected by consolidation coefficients. To get more accurate and quantitative analysis, it is worth to do more work to obtain more accurate consolidation coefficients suitable for the fluid-saturated rocks.

ACKNOWLEDGMENTS

The authors sincerely acknowledge the support from the National Natural Science Foundation of China (grants 41774142).

REFERENCES

1. J. Carcione, and B. Gurevich, Geophysics **76** (6), 55–64 (2011).
2. L. Zhao, De-hua Han, Q. Yao, R. Zhou and F. Yan, Geophysics **80** (3), 221-235 (2015).
3. I. B. Morozov and W. Deng, Geophysics **81** (1), 1-13 (2016a).
4. I. B. Morozov and W. Deng, Geophysics **81** (4), 405-417 (2016b).
5 I. B. Morozov and W. Deng, Geophysics **83** (2), 67-79 (2018a).
6. W. Deng and Igor B. Morozov, Geophysics **81** (4), 395-404 (2016).

Solving Travelling Salesman Problem with Sparse Graphs

Seeja K.R.[1]

[1] *Indira Gandhi Delhi Technical University for Women, Delhi- 110006, India*

Corresponding author: seeja@igdtuw.ac.in
URL: http://www.igdtuw.ac.in

Abstract. The travelling salesman problem is one of the most explored combinatorial optimization problem by mathematicians as well as computer scientists. The state-of-the-art algorithms for solving TSP assume that the underlying graph of the TSP is a complete graph. There has not been many works that take a sparse graph as an input to an algorithm for finding the TSP tour, even though the graph corresponding to many practical applications that are formulated as an instance of TSP are sparse. In this research an efficient hybrid heuristic is proposed to get a near optimal TSP solution from sparse graph instances. The proposed heuristic is a combination of many heuristics like rotational transformation, unreachable vertex heuristic and 2-opt exchanges. The experimental evaluation on benchmark datasets show that the proposed approach efficient in terms of optimality as well as running time than the state of the art heuristics.

INTRODUCTION

Travelling Salesman Problem (TSP) is a well known NP-hard problem and its objective is to find the shortest route that a salesman has to travel by visiting each city exactly once and returning back to the original city. It can also be defined as identifying a minimum cost Hamiltonian Cycle in a weighted graph. A cycle which contains all vertices of an undirected graph exactly once is called Hamiltonian Cycle. Most of the real world applications, like routing of vehicles, door-to-door salesmen, genome sequencing etc., formulated as an instance of TSP are sparse. A graph with relatively few edges is called a sparse graph. Most of the existing algorithms for TSP works on complete graphs and hence the sparse graphs are converted into complete graphs by adding high cost edges. The literature hardly contains any algorithm for TSP, which takes a sparse graph as input. Emami Taba's master thesis[1] is the only exception. In his thesis, he has suggested some algorithms to convert a complete graph into a non-complete graph by removing some irrelevant edges. Then he had suggested a combination of greedy and modified 2-opt algorithm to find TSP tour from the non-complete graph. However, the literature contains many algorithms for finding Hamiltonian Cycles from sparse graphs providing exact solutions or approximate solutions. The exact solution methods like cutting plane method[2], branch-and-cut[7,8] and branch-and-bound. These algorithms become highly inefficient as we increase the number of cities in the tour. Approximate algorithms give near optimal solutions using heuristics[10] like Nearest Neighbour, Greedy, Clarke-Wright savings heuristic [3], The Lin-Kernighan heuristic[4,5] etc. Many researchers [6] explored the application of metaheuristics to the TSP problem.

The proposed method is a combination of three different heuristics like Rotational Transformation[9], 2-opt Transformation[11] and unreachable vertex heuristic[12].

PROPOSED METHODOLOGY

The proposed algorithm takes a weighted graph as input and returns a near optimal TSP tour. The proposed algorithm works in four phase – initial path creation, conversion to Hamiltonian path, conversion to Hamiltonian Cycle and tour improvement.

The algorithm uses the following subroutines: Visited(x) – returns true if the vertex x is already present in the partial tour found so far, RotationTransformation(P,x) - returns the new end vertex of P after performing rotation transformation on the end vertex x of path P, ReversePath(P,x,y) - reverses the part of the path P from vertices x to y, TwoOpt(P,n) – performs 2-opt transformations on the cycle P with n vertices by replacing high cost vertices in the cycle with low cost vertices, FindAdj(x) - returns the set of vertices adjacent to x, FindMinAdj(x,A) - returns the vertex z of the edge (x,z), which is the minimum weighted edge connecting x and the vertices in set A, Reachable(x) - returns true if the unvisited neighbors of x has more than one unvisited neighbor.

```
HybridTSP(b,V,n)
    i=1; // Create a low cost initial path
    P[i]=V[i];
    Y=P[i];
    Visited(y)=true;
    ExtendPath(P,y,i,n);
    While (i is less than n) //Extend Initial Path
        Y= RotationTransformation(P,i);
        ExtendPath(P,y,i,n);
        if(i!=n)then ReversePath(P,1,i);
    While(b(P(1),P(n))==0) //Convert path into cycle
        y=RotationTransformation(P,n,b)
        if (b(p(1),y)==0)then ReversePath(P,1,n)
    TwoOpt(P,n) //Tour Improvement
End

ExtendPath(P,y,i,n)
    While( i is less than n)
        A=FindAdj(y);
        If (i is less than n-2)
            While(A is not empty set)
                x=FindMinAdj(y,A);
                if(!reachable(x))then A=A- (x);
                else break;
        If(A is not empty)
            i=i+1;
            P[i]=x;
            Visited(x)=true;
        Else break;
        y= P[i];
End
```

RESULT AND DISCUSSION

The proposed algorithm is implemented in MATLAB 13RA in a system with 4GB RAM and Intel Core i7 processor. The performance of the proposed approach is compared with that of other heuristics. There is no standard dataset containing sparse instances of TSP. Hence the HCP and Symmetric TSP instances of TSPLIB [14] are modified to create sparse instances of TSP.

Experiment 1: Modified HCP instances

In experiment 1, HCP instances of TSPLIB are converted into sparse instances of TSP by assigning random weights to the edges. The HybridTSP() could find the Least Cost Hamiltonian Cycle or TSP tour in reasonable time as shown in Table 1.

Experiment 2: Modified Symmetric TSP instances

In experiment 2, the complete graph instances of Symmetric TSP instances are converted into sparse instances by removing some high cost edges from the graph. Each vertex in the graph needs to have a minimum degree d to have

TABLE 1. HCP Instances

Sl.No.	Library	No.of Cities	Running Time(Sec.)
1	alb1000	1000	1.3438
2	Alb2000	2000	5.1094
3	Alb3000a	3000	11.0313
4	Alb3000b	3000	10.7656
5	Alb3000c	3000	10.9375
6	Alb3000d	3000	10.9844
7	Alb3000e	3000	11.3438
8	Alb4000	4000	19.8438
9	Alb5000	5000	29.6250

a Hamiltonian Cycle. According to Dirac's theorem[13], if each vertex in an n-vertex graph have at least n/2 degree then the graph must have a Hamiltonian cycle. Hence the top n/2 high cost vertices are removed from the Symmetric TSP instances to create sparse TSP instances. The performance comparison of the HybridTSP() with other state of the art heuristics for some selected instances are shown in Table 2. The implementation of the heuristics available in Concorde[15] is used for performance evaluation.

CONCLUSION

This research proposes a novel hybrid heuristic for finding TSP tour directly from weighted sparse graphs. The experimental evaluation of proposed algorithm is performed on TSPLIB instances of HCP and Symmetric TSP (upto 6000 vertices) and finds that the proposed algorithm is efficient in finding near optimal TSP tours in less time. The algorithm has a polynomial time complexity of O(n^3) even though the solution is not guaranteed theoretically in all cases.

ACKNOWLEDGMENTS

The research presented in this manuscript is supported University Grants Commission Major Project Grant F.No.42-136/2013(SR).

TABLE 2. Symmetric TSP Instances

Library	Optimal	Hybrid TSP	Nearest Neighbour	Greedy	Lin Kernighn	Boruvka	Quick Boruvka	Running Time(Sec.)
rl1323	270199	295090	327639	307420	273063	315903	327840	18.3125
berlin52	7542	8918	9790	9951	7542	10117	9529	0.0469
a280	2579	2879	3367	3161	2611	3126	3029	0.2500
bier127	118282	122578	150939	138036	119051	139202	131357	0.0938
d493	35002	36620	43745	40524	35037	40621	39861	0.8594
d198	15780	17596	18549	19480	15874	18508	18221	0.1563
d657	48912	52683	63479	58053	49018	57365	57539	1.9844
d1291	50801	53855	62613	62850	53084	61865	60914	14.8438
d1655	62128	67329	77917	74806	64573	72035	75446	32.5938
1d2103	80450	83603	90904	94001	82535	91507	85896	59.9844
eil51	426	461	503	521	426	545	480	0.0625
eil76	538	568	613	631	538	612	609	0.0469
eil101	629	671	847	787	629	744	739	0.0938
fl417	11861	12957	15770	13341	11870	15498	16223	0.5469
fl1400	20127	21759	27331	25955	20141	24585	26356	13.4063
fl1577	22249	45769	28067	25583	22239	25606	27778	29.1875
fl3795	28772	30697	38106	34711	29457	33885	36396	435.1406
fnl4461	182566	195740	225417	211944	183222	207297	210194	899.2813
gil262	2378	2548	3073	2748	2382	2849	2881	0.2656
kroB150	26130	27939	36417	31427	26130	30254	30036	0.1563
kroA200	29368	31685	38037	34554	29368	34811	35504	0.1563
kroB200	29435	31894	36915	35975	29440	33758	34924	0.1406
lin105	14379	15781	18248	16766	14492	16479	17582	0.0625
lin318	42029	45883	53655	49744	42121	48811	54090	0.3281
nrw1379	56638	61135	69347	65355	56784	65481	66204	21.2344
p654	34643	36160	43730	39938	34675	41065	42619	2.8281
pcb442	50778	55035	64959	62220	51495	61269	60623	0.5469
pcb1173	56892	62470	73481	66819	56988	67213	66155	9.3125
pcb3038	137694	177635	175586	160275	138349	160390	162454	195.8281
pr76	108159	112429	150840	140349	108159	140574	127137	0.0938
rd400	15281	16657	19279	17359	15285	18716	18004	0.6563
rl1304	252948	282961	316455	302069	258870	294566	301220	14.3438
rl1889	316536	345573	387460	390328	332665	372541	384674	56.8906
rl5915	565530	615951	709022	634723	581960	654985	648841	1.7398e+003

REFERENCES

[1] M. S. E. Taba, "Solving traveling salesman problem with a non-complete graph," Master thesis, University of Waterloo 2009.

[2] M. Hahsler and K. Hornik, Journal of Statistical Software **23**, 1–21 (2007).

[3] G. Clarke and J. W. Wright, Operations research **12**, 568–581 (1964).

[4] S. Lin and B. Kernighan, Operations research **21**, 498–516 (1973).

[5] K. Helsgaun, Operations research **126**, 106–130 (2000).

[6] M. Gendreau, G. Laporte, and D. Vigo, Computers and Operations Research **26**, 699–714 (1999).

[7] J.-J. S.-G. Hipólito Hernández-Pérez, Discrete Applied Mathematics **145**, 126–139 (2004).

[8] B. Roberto, E. Hadjiconstantinou, and A. Mingozzi, Networks **42**, 26–41 (2003).

[9] L. Posa, Discrete Mathematics **14**, p. 359–364 (1976).

[10] G. Mosheiov, European Journal of Operational Research **79**, 299–310 (1994).

[11] G. Croes, Operations research **6**, 791–812 (1958).

[12] K. R. Seeja, Journal of Optimization **2018**, p. 10 (2018).

[13] G. A. Dirac, Proc. Lond. Math. Soc **2**, p. 69–81 (1952).

[14] G. Reinelt, ORSA Journal on Computing **3**, 376–384 (1991).

[15] D. Applegate, R. E. Bixby, V. Chvátal, and W. J. Cook, Concorde ŤSP solver, `http://www.math.uwaterloo.ca/tsp/concorde/` (), [downloaded on September 2015].

Deterministic and Stochastic Models Of Labor Forces Dynamics in the Industry with Pure Competition

Irina Zaitseva[1, a)], Oleg Malafeyev[2, b)], Natalya Poddubnaya[1, c)], Dmitry Shlaev[1, d)] and Svetlana Bogdanova[1, e)]

[1]Stavropol State Agrarian University, 12, Zootechnicheskiy alley, Stavropol, Russia, 355017
[2]Saint Petersburg State University, 7/9 Universitetskaya nab., St. Petersburg, Russia, 199034

[a)] Corresponding author: irina.zaitseva.stv@yandex.ru
[b)]malafeyevoa@mail.ru
[c)]cherkasovanatas@mail.ru
[d)]shl-dmitrij@yandex.ru
[e)]svetvika@mail.ru

Abstract. This article discusses two classes of models that describe the development dynamics of the industry labor force with pure competition. In the first case, it is assumed that the factors influencing the production process are strictly deterministic. The second class of models is based on the assumption of stochastic dynamics of external (exogenous) parameters. In the first case, a deterministic model of the development dynamics of the industry labor forces is formulated. In the second case, its generalization to the stochastic case is considered.

INTRODUCTION

Effective production planning by both an individual manufacturer and the industry as a whole must take into account a variety of factors affecting both the production process and the market condition. The behavior of some of these factors can be described with deterministic ratios with a sufficient degree of accuracy. The dynamics of others turns out to be difficult and in this case it seems natural to assume that it can be described as a random process with certain properties. The production process itself can be understood in a generalized sense, as the production of any goods, the issuance of securities, etc. In this connection, mathematical models of the industry development dynamics are of interest, taking into account the presence of external parameters with both deterministic and stochastic dynamics and allowing them to be used for forecasting in various situations.

MODELS OF THE DEVELOPMENT DYNAMICS OF THE INDUSTRY LABOR FORCES

Deterministic Model of Labor Forces Development in the Industry

The proposed model summarizes the standard dynamic model of the industry with pure competition in the case when the components of the industry firms interact with each other on the basis of the Cournot's competitive model. Suppose there are n firms, $i \in I = \{1, \ldots, n\}$.. The process of producing a product is described by means of the relations:

$$M_i = m_i Q_i\,,\ L_i = a_i + b_i Q_i + c_i Q_i^2\,,$$

where $Q_i -$ release per unit time, $L_i -$ the amount of labor used by labor forces, $M_i -$ amount of material used, $m_i, a_i, b_i, c_i > 0 -$ constants.

At the current time, each company seeks to maximize profits H_i from the sale of a product at a price p determined from the ratio

$$p = \alpha - \beta\left(\sum_{k=1}^{n} Q_k\right)$$

where $\alpha, \beta > 0 -$ constants.

At the wage rate of labor forces w and the price of the material p_m

$$H_i(Q) = pQ_i - wL_i - p_m M_i = Q_i[\alpha - p_m|m_i - b_i w - \beta \sum_{k\in I, k\neq i} Q_k] - Q_i^2[c_i w + \beta] - a_i w.$$

We believe that the volumes of product release by firms are set at the Cournot's equilibrium point determined from the ratio

$$\frac{\partial H_i}{\partial Q_i} = [\alpha - p_m m_i - b_i w - \beta \sum_{k\neq i} Q_k] - 2Q_i[c_i w + \beta] = 0\,.$$

From here we get that

$$\overline{Q_i}(Q\|Q_i) = \frac{\left[\alpha - p_m m_i - b_i w - \beta \sum_{k\neq i} Q_k\right]}{2[c_i w + \beta]}\,.$$

Here $Q\|Q_i = (Q_1 \ldots Q_{i-1}, Q_{i+1} \ldots Q_n)$.

Let, for definiteness, $n = 2$:

$$H_1(Q_1, Q_2) = Q_1[\alpha - p_m m_1 - b_1 w - \beta Q_2] - Q_1^2(c_q w + \beta) - a_1 w,$$

$$H_2(Q_1, Q_2) = Q_2[\alpha - p_m m_2 - b_2 w - \beta Q_1] - Q_2^2(c_2 w + \beta) - a_2 w,$$

$$\overline{Q_1} = \frac{[\alpha - p_m m_1 - b_1 w - \beta Q_2]}{2(c_1 w + \beta)} = f_1(Q_2)\,,$$

$$\overline{Q_2} = \frac{[\alpha - p_m m_2 - b_2 w - \beta Q_1]}{2(c_2 w + \beta)} = f_2(Q_1)\,.$$

Looking for a fixed point display

$$(Q_1, Q_2) \to (f_1(Q_2), f_2(Q_1))\,.$$

We have ratios

$$Q_1 = \frac{\alpha - p_m m_1 - b_1 w - \beta[\alpha - p_m m_2 - b_2 w - \beta Q_1]/2(c_2 w + \beta)}{2(c_1 w + \beta)},$$

$$Q_2 = \frac{(\alpha - p_m m_2 - b_2 w - \beta[\alpha - p_m m_1 - b_1 w - \beta Q_2]/2(c_1 w + \beta)}{2(c_2 w + \beta)}.$$

Let, for simplicity, $m_1 = m_2 = m,\ c_1 = c_2 = c,\ b_1 = b_2 = b.$ Then

$$Q_1 = \frac{(\alpha - p_m m - bw)}{2(cw + \beta)} - \beta(\alpha - p_m m - bw - \beta Q_1) = \beta^2 Q_1 + (\alpha - p_m m - bw)\left[\frac{1}{2(cw + \beta)} - \beta\right].$$

From here we get

$$Q_1 = Q_2 = (\alpha - p_m m - bw)\left[\frac{1}{2(cw + \beta)} - \beta\right]/(1 - \beta^2). \qquad (1)$$

Thus, they described the formation process of the product manufacturing rate by firms in accordance with the Cournot's game model, depending on the prices of materials, labor wage rates, the number of materials. The total demand is assumed linear by the buyer's income and product price, so

$$X = \frac{kY - lp}{p_0} + \mu. \qquad (2)$$

Here $X = \sum_{i=1}^{n} X_i$, $X_i -$ product sales by firm i, $Y -$ buyer's income, $p_0 -$ price index for other products, $k, l, \mu > 0 -$ constants.

We can assume that prices are rising at a rate proportional to the difference between sales and production. This is done, for example, by an intermediary who buys the product from the manufacturer at the Cournot's equilibrium price and sells it with some additive. Formally, this is described by the price adaptation equation:

$$\dot{p} = \gamma\left(X - \sum_{k=1}^{n} Q_k\right).$$

For $n = 2$ the equation has the form:

$$\dot{p} = \gamma(X - Q_1 - Q_2) = -\gamma\frac{lp}{p_0} + \gamma\left[\frac{kY}{p_0} + \mu - \frac{2}{1-\beta^2}(\alpha - p_m m - bw)(\frac{1}{2(cw + \beta)} - \beta)\right] \qquad (3)$$

Relations (1) - (3), describing the behavior in time of this model, allow by the change of variables w, p_m, p_0, Y to predict variables changes Q, X, p. In the equilibrium state when $X = Q_1 + Q_2, \dot{p} = 0,$ we obtain that

$$p^* = \frac{p_0\left[\frac{kY}{p_0} + \mu - \frac{2}{1-\beta^2}\left(\alpha - p_m m - bw\right)\left(\frac{1}{2(cw + \beta)} - \beta\right)\right]}{l}.$$

We now find a common solution, considering that w, p_m, p_0, Y are constants

$$p(t) = p^* + (p(0) - p^*)e^{\frac{-\gamma l}{p_0}t}, \ X(t) = X^* + (X(0) - X^*)e^{\frac{-\gamma l}{p_0}t}.$$

This model can be studied further numerically with different variables $L_i, M_i, a_i, b_i, c_i, m_i, w, p_m, p_0, Y$. Suppose, for example, that for a certain period of time $w = w_0 + w_1 t,\ Y = Y_0 + Y_1 t,\ p_m = p_{m0} + p_{m1} t.$

In this case

$$p(t) = \big(AEg - Atg - A - AE^2 Ei\,(1, g(E+t)\big)e^{g(E+t)}g^2 - Bg + BEEi(1, g(E+t))e^{g(E+t)}g^2 -$$
$$- Ei(1, g(E+t))Ce^{g(E+t)}g^2 + e^{gt}(-AEg + Bg + A + AE^2 Ei(1, Eg)e^{Eg}g^2 + Ei(1, Eg)Ce^{Eg}g^2 -$$
$$- BEEi(1, Eg)e^{Eg}g^2 + p(0)g^2))/g^2,$$

where $Ei(*,*) -$ exponential integral,

$$g = -\frac{\gamma l}{p_0},\ A = \frac{\gamma\left(2p_0 m p_{m1}\beta - kY_1 + 2p_0 b w_1 \beta + kY_1\beta^2\right)}{p_0\left(\beta^2 - 1\right)},$$

$$B = \gamma(-kY_1 c w_0 - kY_1\beta + kY_1\beta^2 c w_0 + kY_0\beta^2 c w_1 + +kY_1\beta^3 - kY_0 c w_1 - \mu p_0 c w_1 + 2p_0 m p_{m1}\beta c w_0 +$$
$$+ \mu p_0\beta^2 c w_1 + 2p_0 m p_{m1}\beta^2 - 2p_0\alpha\beta c w_1 + 4p_0 b w_0 \beta c w_1 + 2p_0 m p_{m0}\beta c w_1 - p_0 b w_1 - p_0 m p_{m1} +$$
$$+ 2p_0 b w_1 \beta^2)/(p_0(\beta^2 - 1)c w_1),$$

$$C = \gamma(p_0\alpha - kY_0\beta + kY_0\beta^3 - \mu p_0\beta - 2p_0\alpha\beta^2 - p_0 m p_{m0} - p_0 b w_0 - kY_0 c w_0 - 2p_0\alpha\beta c w_0 + kY_0\beta^2 c w_0 +$$
$$+ 2p_0 m p_{m0}\beta c w_0 + \mu p_0\beta^2 c w_0 + 2p_0 m p_{m0}\beta^2 - \mu p_0 c w_0 + 2p_0 b w_0^2\beta c + 2p_0 b w_0\beta^2)/(p_0(\beta^2 - 1)c w_1),$$

$$E = \frac{c w_0 + \beta}{c w_1}.$$

We note that the dynamics models of various parameters of the labor market can be formulated in the same way. Of course, the meaning of the parameters will be different, but the main controls will remain the same.

Stochastic Model of the Industry Development

We introduce the stochastic dynamics for the external parameters of the model. Suppose that these parameters p_m, p_0, Y can be represented as a three-component stochastic process. For definiteness, consider the case $n = 2$.

Suppose first that one external parameter is stochastic, and all others are fixed. Let such a parameter be the cost of labor forces Y. Then the process of price regulation can be described by a stochastic differential equation of the 1st order:

$$dp(t) = \left[\delta - \sigma p(t)\right]dt + \psi d\xi(t),$$

где $\delta \equiv \gamma\left[\mu - \frac{2}{1-\beta^2}(\alpha - p_m m - bw)\left(\frac{1}{2(cw+\beta)} - \beta\right)\right]$, $\sigma \equiv \frac{\lambda l}{p_0}$, $\xi \equiv \frac{\gamma k}{p_0}$, $Ydt \equiv d\xi$,

Here $\xi(t)-$ stochastic process.

This linear stochastic equation and its general solution is:

$$p(t) = p^* + [p(0) - p^*]e^{-\sigma t} + \frac{kY(t)}{l}(e^{-\sigma t} - 1) + \frac{\gamma k}{p_0} e^{-\sigma t}\int_0^t e^{\sigma s} d\xi(s)$$

The situation in which the random price of the material p_m, can be described similarly.

We now consider a stochastic differential equation for the variable p_0.

It looks like: $dp(t) = \delta dt + [\varepsilon - \sigma p(t)]d\xi(t)$,

where $\delta \equiv \gamma\left[\mu - \frac{2}{1-\beta^2}(\alpha - p_m m - bw)\left(\frac{1}{2(cw+\beta)} - \beta\right)\right]$, $\sigma \equiv \gamma l$, $\varepsilon \equiv \gamma kY$, $d\xi(t) \equiv \frac{dt}{p_0(t)}$.

Its solution is as follows:

$$p(t) = e^{-\sigma t - \gamma l\xi(t) + \gamma l\xi(0)}\left[p(0) + (\delta + \sigma\varepsilon)e^{-\gamma l\xi(0)}\left(\int_0^t e^{\sigma s + \gamma l\xi(s)} ds + \varepsilon\int_0^t e^{\sigma s + \gamma l\xi(s)} d\xi(s)\right)\right].$$

Now assume the random behavior of all three variables of the model. The simplest replacement implies:

$$d\xi_1 = \frac{dt}{p_0},\ d\xi_2 = \frac{Y}{p_0}dt,\ d\xi_3 = p_m dt,$$

and we get the following price control:

$$dp(t) = \gamma\left[\mu - \frac{2}{1-\beta^2}\left(\frac{1}{2(cw+\beta)} - \beta\right)(\alpha - bw)\right]dt + \gamma A\mathrm{E}(t),$$

where $A = \left(-lp, k, \frac{2m}{1-\beta^2}\left(\frac{1}{2(cw+\beta)} - \beta\right)\right)$ and $\vec{\mathrm{E}}(t) = (\xi_1(t), \xi_2(t), \xi_3(t))-$ stochastic process for external variables.

CONCLUSION

Thus, the considered two classes of models allow us to describe the development dynamics of labor forces in various industries with pure competition. If the factors influencing the production process are strictly deterministic, then we get a deterministic model of the development dynamics of the industry labor forces. The assumption of the stochastic dynamics of the external (exogenous) models parameters is based on the generalization of the deterministic model to the stochastic case. The presented models of the labor forces development in various industries with pure competition, will allow to research and manage the selected parameters.

ACKNOWLEDGMENTS

The work is partially supported by the RFBR grant # 18-01-00796.

REFERENCES

1. A. Kirjanen, O. Malafeyev, N. Redinskikh, "Developing industries in cooperative interaction: Equilibrium and stability in processes with lag", Statistics, Optimization and Information Computing, 2017.
2. E. Kriulina, N. Tarasenko, N. Miroshnitchenko, I. Zaitseva, and I. Dedyukhina, "Environmental Management in Agriculture: Problems and Solutions", Research Journal of Pharmaceutical, Biological and Chemical Sciences, no. 7(3), pp. 1908-1912, 2016.
3. E. Neverova and O. Malafeyev, "A model of interaction between anticorruption authority and corruption groups", AIP Conference Proceedings, (American Institute of Physics, 2015).
4. E.G. Neverova, O.A. Malafeyev, G.V. Alferov and T.E. Smirnova, "Model of interaction between anticorruption authorities and corruption groups" in International Conference on "Stability and Control Processes" in Memory of V.I. Zubov, (SCP, Proceedings, SPb, 2015), pp. 488-490.
5. G. Drozdov, O. Malafeyev and S. Nemnyugin, "Multicomponent dynamics of competitive single-sector economy development", International Conference on "Stability and Control Processes" in Memory of V.I. Zubov (SCP 2015 – Proceedings, 2015).
6. I. Kolesin, O. Malafeyev, M. Andreeva and G. Ivanukovich "Corruption: Taking into account the psychological mimicry of officials", AIP Conference Proceedings (American Institute of Physics, 2017).
7. I. Zaitseva and M. Popova, "Technique to study the employment potential of the region: economic-mathematical aspect", (World Applied Sciences Journal, 2013), no. 22 (1), pp. 22-25.
8. I. Zaitseva, E. Kriulina, A. Ermakova, E. Shevchenko and Y. Vorokhobina, "Application of Factor Analysis to Study the Labour Capacity of Stavropol Krai", (Research Journal of Pharmaceutical, Biological and Chemical Sciences, 2016), no. 7(4), pp. 2183-2186.
9. I. Zaitseva, M. Popova, A. Ermakova, S. Bogdanova and D. Rezenkov, "Determination Prospects Of Development Labor Potential In Agriculture Stavropol Territory Based On Assessment His Condition", (Research Journal of Pharmaceutical, Biological and Chemical Sciences, no. 7(3), 2016), pp. 2592-2595.
10. I. Zaitseva, O. Malafeyev, S. Strekopytov, A. Ermakova and D. Shlaev, "Game-theoretical model of labour force training", Journal of Theoretical and Applied Information Technology, 2018.
11. I. Zaitseva, O. Malafeyev, S. Strekopytov, G. Bondarenko and D. Lovyannikov, "Mathematic model of regional economy development by the final result of labor resources", AIP Conference Proceedings, 2018.
12. I.V. Zaitseva, A.N. Ermakova, D.V. Shlaev, E.A. Shevchenko, and S.I. Lugovskoy. "Workforce planning redistribution of the region's results", (Research Journal of Pharmaceutical, Biological and Chemical Sciences. 2017), 8(1), pp. 1862-1866.
13. K. Kostyukov, I. Zaitseva, G. Bondarenko, T. Svechinskaya and S. Nechayeva, "Workforce Planning as An Element of Control System", (Research Journal of Pharmaceutical, Biological and Chemical Sciences, no. 7(6), 2016), pp. 2315–2319.
14. M.A. Vlasov, V.V. Glebov, O.A. Malafeyev and D.N. Novichkov, "Experimental study of an electron beam in drift space", (Soviet journal of communications technology & electronics, 1986), 31(3), pp. 145-149.
15. O. A. Malafeyev, and N. D. Redinskikh Compromise solution in the problem of change state control for the material body exposed to the external medium AIP Conference Proceedings 1959, 080017 (2018); https://doi.org/10.1063/1.5034734
16. O. A. Malafeyev, N. D. Redinskikh, S. A. Nemnyugin, I. D. Kolesin, and I. V. Zaitseva The optimization problem of preventive equipment repair planning AIP Conference Proceedings 1978, 100013 (2018); https://doi.org/10.1063/1.5043757
17. O. Malafeev and S. Nemnyugin, "Generalized dynamic model of a system moving in an external field with stochastic components", (Theoretical and Mathematical Physics, no. 107(3), 1996), 770 p.
18. O. Malafeev, "On the existence of nash equilibria in a noncoope rative n-person game with measures as coefficients", (Communications in Applied Mathematics and Computational Science, no. 5(4), 1995), pp. 689-701.
19. O. Malafeyev, A. Awasthi, I. Zaitseva, D. Rezenkov and S. Bogdanova, "A dynamic model of functioning of a bank", AIP Conference Proceedings, (American Institute of Physics, 2018).
20. O. Malafeyev, D. Rylow, I. Zaitseva, M. Popova and L. Novozhilova, "Game-theoretic model of dispersed material drying process", AIP Conference Proceedings, (American Institute of Physics, 2017).

21. O. Malafeyev, D. Saifullina, G. Ivaniukovich, V. Marakhov and I. Zaytseva, “The model of multi-agent interaction in a transportation problem with a corruption component”, AIP Conference Proceedings, (American Institute of Physics, 2017).
22. O. Malafeyev, K. Farvazov, O. Zenovich, I. Zaitseva, K. Kostyukov and T. Svechinskaya, “Geopolitical model of investment power station construction project implementation”, AIP Conference Proceedings, (American Institute of Physics, 2018).
23. O. Malafeyev, S. Nemnyugin, D. Rylow, E. Kolpak and A. Awasthi, “Corruption dynamics model”, AIP Conference Proceedings, (American Institute of Physics, 2017).
24. O. Malafeyev, A. Awasthi, K. Kambekar, A. Kupinskaya, “Random walks and Market Efficiency in Chinese and Indian equity markets”, K.S., 2019, Statistics, Optimization and Information Computing, 7(1), pp. 1-25.
25. V.N. Kolokoltsov, O.A. Malafeyev, “Corruption and botnet defense: a mean field game approach”, International Journal of Game Theory, 2018, pp. 1-23.
26. I. Zaitseva, O. Malafeyev, I. Kolesin, A. Ermakova, D. Shlaev, “Modeling of the labour force redistribution in investment projects with account of their delay”, 2018 IEEE International Conference on Power, Control, Signals and Instrumentation Engineering, ICPCSI 2017, pp. 68-70.
27. Y.A. Pichugin, O.A. Malafeyev, D. Rylow, I. Zaitseva, “A statistical method for corrupt agents detection”, 2018, AIP Conference Proceedings, https://doi.org/10.1063/1.5043758.
28. O. Malafeyev, D. Rylow, I. Zaitseva, A. Ermakova, D. Shlaev, “Multistage voting model with alternative elimination”, 2018, AIP Conference Proceedings, http://doi.org/ 10.1063/1.5043756.
29. O. Malafeyev, N. Redinskikh, “Quality estimation of the geopolitical actor development strategy”, Source of the Document 2017 Constructive Nonsmooth Analysis and Related Topics (Dedicated to the Memory of V.F. Demyanov), CNSA 2017 – Proceedings, http://dx.doi.org/10.1109/CNSA.2017.7973986.
30. V.N. Kolokoltsov, O.A. Malafeyev, “Mean-Field-Game Model of Corruption”, Dynamic Games and Applications, 2017, 7 (1), pp. 34-47.
31. O.A. Malafeyev, N.D. Redinskikh, “Stochastic analysis of the dynamics of corrupt hybrid networks”, Proceedings of 2016 International Conference "Stability and Oscillations of Nonlinear Control Systems" (Pyatnitskiy's Conference), STAB 2016, http://dx.doi.org/10.1109/STAB.2016.7541208.
32. Y.A. Pichugin, O.A. Malafeyev, “Statistical estimation of corruption indicators in the firm”, Applied Mathematical Sciences, 2016, 10 (41-44), pp. 2065-2073.
33. O.A. Malafeyev, S.A. Nemnyugin, “Model of the optimal parameters choice for the charged particles beam”, 2016, 25th Russian Particle Accelerator Conference, RuPAC 2016, pp. 437-439.
34. Y. Pichugin, G. Alferov, O. Malafeyev, “Parameters estimation in mechanism design”, Contemporary Engineering Sciences, 2016, 9 (1-4), pp. 175-185.
35. G.V. Alferov, O.A. Malafeyev, A.S. Maltseva, “Game-theoretic model of inspection by anti-corruption group”, AIP Conference Proceedings, 1648, 450009 (2015), http://dx.doi.org/10.1063/1.4912668.
36. G.V. Alferov, O.A. Malafeyev, A.S. Maltseva, “Programming the robot in tasks of inspection and interception”, International Conference on Mechanics - Seventh Polyakhov's Reading,Conference Proceedings,(2015),1-3,http://dx.doi.org/10.1109/Polyakhov.2015.7106713.
37. O.A. Malafeyev, S.A. Nemnyugin, G.A. Ivaniukovich, “Stochastic models of social-economic dynamics”, 2015 International Conference on "Stability and Control Processes" in Memory of V.I. Zubov, SCP 2015 – Proceedings, pp. 483-485.
38. X. Grigorieva, O. Malafeev, “A competitive many-period postman problem with varying parameters”, Applied Mathematical Sciences,8(145-148), 2014, pp. 7249-7258.

Model of Information Multi-Stage Process in Structured System

Oleg Malafeyev[1, a)], Nadezhda Redinskikh[1,b)], Irina Zaitseva[2,3,c)], Tatiana Smirnova[1,d)] and Dmitry Kolesov[1,e)]

[1]*Saint-Petersburg State University, 7/9 Universitetskaya nab., St. Petersburg, 199034 Russia*
[2]*Stavropol State Agrarian University, Zootechnical lane, 12, Stavropol, 355017, Russia*
[3]*Stavropol branch of the Moscow Pedagogical State University, Dovatortsev str. 66 g, Stavropol, 355042, Russia*

[a)]malafeyevoa@mail.ru
[b)]redinskich@yandex.ru
Corresponding author: [c)]irina.zaitseva.stv@yandex.ru
[d)]t.smirnova@spbu.ru
[e)]d.kolesov@spbu.ru

Abstract. The information process consisting of the stages of collection, processing, storage and protection of information is considered in this paper. The process is formalized in the form of a structurally logical scheme consisting of stages of the information process. It is assumed that the process of collecting, processing and storing information is carried out by special equipment. The analysis of the process under investigation is presented. A numerical example is given.

INTRODUCTION

The implementation of information technologies and new technological solutions in various areas of production contributed to the change in the production process and the quality of products. New information technologies have also contributed to the emergence of a large amount of information obtained in the production process. Such information may include data received from controllers installed on the main units and parts of machines, from sensors installed on individual parts of mechanisms. During the operation of the equipment, information is collected, processed and stored. Processing and interpretation of data prevent an unplanned cessation of operation of production, to eliminate possible damage to equipment. The collection, processing and storage of large amounts of data is an information process. The unexpected termination of one of the stages of such information process can lead to additional costs for the repair of equipment for storage and processing of the received information. Therefore, the main task is to ensure the smooth operation of the information process.

Such information process can be represented in the form of the structural and logical scheme consisting of the stages of information process responsible for search, storage, processing and protection of information. The process of collecting, processing and storing information in the information process is carried out by special equipment.

The information process consisting of four stages is considered in this paper. There is a problem of ensuring uninterrupted synchronous operation of all stages of the information process. This papers makes use the ideas from the approaches of [1-8].

FORMALIZATION OF THE PROBLEM OF INFORMATION MULTI-STAGE PROCESS IN A STRUCTURED SYSTEM

The system of information processing, transmission and protection is considered. Such system can be presented in the form of a structural and logical scheme consisting of $A = \{a_1, ..., a_n\}$ performers responsible for information retrieval, $B = \{b_1, ..., b_m\}$ performers responsible for storage, received information, $C = \{c_1, ..., c_l\}$ performers of information processing, and $D = \{d_1, ..., d_k\}$ technical tools necessary for information protection.

At the first stage of the complex-structural information process, the performers $A = \{a_1, ..., a_n\}$ responsible for the search for information, carries out its search, according to its task. Finding the necessary information can be carried in many ways: observation, implementation of queries to information systems and databases etc. Collected information transferred to the performers $B = \{b_1, ..., b_m\}$ responsible for the storage and collection of obtained information. It is assumed that the collected information is stored on electronic devices. The received information is transmitted through communication channels to the information processing performers $C = \{c_1, ..., c_l\}$. The information processing executors receives the input information and processes it. Information is processed according to the specified algorithm of information processing. Information processing devices can communicate with each other, transmitting the processed information through message channels $Y = \{y_1, ..., y_s\}$. The processed information is transferred to the stage of information protection, which according the set $D = \{d_1, ..., d_k\}$. At the stage of information security, each of the performers is responsible for the storage of key data sets, installation of software necessary for the protection of information, etc.

The problem of ensuring the smooth functioning of the all stages of the information process is occurred. It is assumed that there are no restrictions on the capacity of communication channels when transferring information from the stage of collection and storage to the stage of information processing.

NUMERICAL EXAMPLE

The system of information processing, transmission and protection is considered. Such system can be represented in the form of a structural and logical scheme consisting of 3 performers responsible for information retrieval, 4 performers responsible for storage, received information, 4 performers of information processing, and 5 technical tools necessary for information protection (Fig.1).

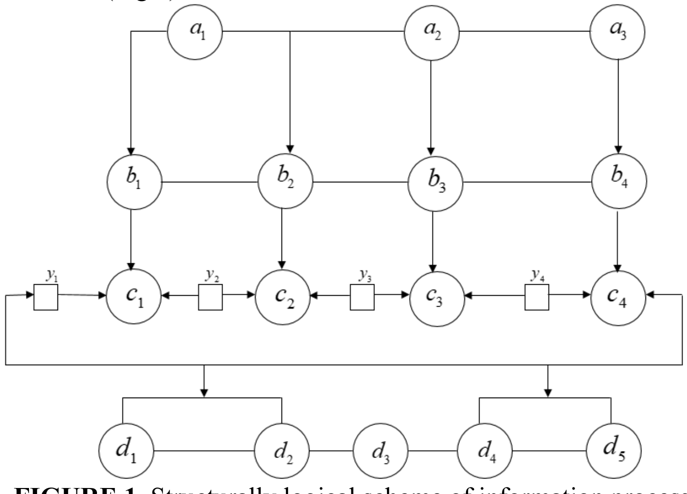

FIGURE 1. Structurally logical scheme of information process

The performers $A = \{a_1, a_2, a_3\}$ responsible for the search for information find the necessary information. Collected information transferred to the performers $B = \{b_1, b_2, b_3, b_4\}$ responsible for the storage and collection of

obtained information. The received information is transmitted through communication channels to the information processing performers $C = \{c_1, c_2, c_3, c_4\}$. The information is processed according to the specified algorithm of information processing. Through the message channels $Y = \{y_1, y_2, y_3, y_4\}$ information processing performers are communicated with each other. The processed information is transferred to the stage of information protection, which according the set $D = \{d_1, d_2, d_3, d_4, d_5\}$.

It is known that for the simultaneous stable functioning of all four stages, it is necessary to operate at least one of the three performers responsible for the information search. It is assumed that there are no restrictions on the bandwidth of communication channels when transferring information from the stage of collection and storage to the stage of information processing.

Also it is known, that probability of stable functioning of performers responsible for information search equals to $p(a_1) = 0.7$, $p(a_2) = 0.6$, $p(a_3) = 0.95$. The probability of stable functioning of performers responsible for storage and collection information equals to $p(b_1) = 0.8$, $p(b_2) = 0.85$, $p(b_3) = 0.9$, $p(b_4) = 0.78$. The probability of stable functioning of information processing performers and message channels is identical and equals to 0.93. The probability of stable functioning the performers responsible of information protection equals to $p(d_1) = 0.9$, $p(d_2) = 0.8$, $p(d_3) = 0.6$, $p(d_4) = 0.72$. So let us compute the probability of stable functioning of all information process $(0.7 \cdot 0.6 \cdot 0.95) \cdot (0.8 \cdot 0.85 \cdot 0.9 \cdot 0.78) \cdot 0.93^8 \cdot (0.9 \cdot 0.8 \cdot 0.6 \cdot 0.72) = 0.0314$.

CONCLUSION

So in this paper we consider information process as structurally complex scheme. Such scheme allows to consider more detail complex information process, consisting of several stages. Also it is possible to compute the probability of stable functioning of information process.

ACKNOWLEDGMENTS

The work is partly supported by grant RFBR № 18-01-00796

REFERENCES

1. A. Kirjanen, O. Malafeyev, N. Redinskikh, “Developing industries in cooperative interaction: Equilibrium and stability in processes with lag”, Statistics, Optimization and Information Computing, 2017.
2. E. Kriulina, N. Tarasenko, N. Miroshnitchenko, I. Zaitseva, and I. Dedyukhina, “Environmental Management in Agriculture: Problems and Solutions”, Research Journal of Pharmaceutical, Biological and Chemical Sciences, no. 7(3), pp. 1908-1912, 2016.
3. E. Neverova and O. Malafeyev, “A model of interaction between anticorruption authority and corruption groups”, AIP Conference Proceedings, (American Institute of Physics, 2015).
4. E.G. Neverova, O.A. Malafeyev, G.V. Alferov and T.E. Smirnova, “Model of interaction between anticorruption authorities and corruption groups” in International Conference on "Stability and Control Processes" in Memory of V.I. Zubov, (SCP, Proceedings, SPb, 2015), pp. 488-490.
5. G. Drozdov, O. Malafeyev and S. Nemnyugin, “Multicomponent dynamics of competitive single-sector economy development”, International Conference on "Stability and Control Processes" in Memory of V.I. Zubov (SCP 2015 – Proceedings, 2015).
6. I. Kolesin, O. Malafeyev, M. Andreeva and G. Ivanukovich “Corruption: Taking into account the psychological mimicry of officials”, AIP Conference Proceedings (American Institute of Physics, 2017).
7. I. Zaitseva and M. Popova, “Technique to study the employment potential of the region: economic-mathematical aspect”, (World Applied Sciences Journal, 2013), no. 22 (1), pp. 22-25.
8. I. Zaitseva, E. Kriulina, A. Ermakova, E. Shevchenko and Y. Vorokhobina, “Application of Factor Analysis to Study the Labour Capacity of Stavropol Krai”, (Research Journal of Pharmaceutical, Biological and Chemical Sciences, 2016), no. 7(4), pp. 2183-2186.

9. I. Zaitseva, M. Popova, A. Ermakova, S. Bogdanova and D. Rezenkov, “Determination Prospects Of Development Labor Potential In Agriculture Stavropol Territory Based On Assessment His Condition”, (Research Journal of Pharmaceutical, Biological and Chemical Sciences, no. 7(3), 2016), pp. 2592-2595.
10. I. Zaitseva, O. Malafeyev, S. Strekopytov, A. Ermakova and D. Shlaev, “Game-theoretical model of labour force training”, Journal of Theoretical and Applied Information Technology, 2018.
11. I. Zaitseva, O. Malafeyev, S. Strekopytov, G. Bondarenko and D. Lovyannikov, “Mathematic model of regional economy development by the final result of labor resources”, AIP Conference Proceedings, 2018.
12. I.V. Zaitseva, A.N. Ermakova, D.V. Shlaev, E.A. Shevchenko, and S.I. Lugovskoy. “Workforce planning redistribution of the region's results”, (Research Journal of Pharmaceutical, Biological and Chemical Sciences. 2017), 8(1), pp. 1862-1866.
13. K. Kostyukov, I. Zaitseva, G. Bondarenko, T. Svechinskaya and S. Nechayeva, “Workforce Planning as An Element of Control System”, (Research Journal of Pharmaceutical, Biological and Chemical Sciences, no. 7(6), 2016), pp. 2315–2319.
14. M.A. Vlasov, V.V. Glebov, O.A. Malafeyev and D.N. Novichkov, “Experimental study of an electron beam in drift space”, (Soviet journal of communications technology & electronics, 1986), 31(3), pp. 145-149.
15. O. A. Malafeyev, and N. D. Redinskikh Compromise solution in the problem of change state control for the material body exposed to the external medium AIP Conference Proceedings 1959, 080017 (2018); https://doi.org/10.1063/1.5034734
16. O. A. Malafeyev, N. D. Redinskikh, S. A. Nemnyugin, I. D. Kolesin, and I. V. Zaitseva The optimization problem of preventive equipment repair planning AIP Conference Proceedings 1978, 100013 (2018); https://doi.org/10.1063/1.5043757
17. O. Malafeev and S. Nemnyugin, “Generalized dynamic model of a system moving in an external field with stochastic components”, (Theoretical and Mathematical Physics, no. 107(3), 1996), 770 p.
18. O. Malafeev, “On the existence of nash equilibria in a noncoope rative n-person game with measures as coefficients”, (Communications in Applied Mathematics and Computational Science, no. 5(4), 1995), pp. 689-701.
19. O. Malafeyev, A. Awasthi, I. Zaitseva, D. Rezenkov and S. Bogdanova, “A dynamic model of functioning of a bank”, AIP Conference Proceedings, (American Institute of Physics, 2018).
20. O. Malafeyev, D. Rylow, I. Zaitseva, M. Popova and L. Novozhilova, “Game-theoretic model of dispersed material drying process”, AIP Conference Proceedings, (American Institute of Physics, 2017).
21. O. Malafeyev, D. Saifullina, G. Ivaniukovich, V. Marakhov and I. Zaytseva, “The model of multi-agent interaction in a transportation problem with a corruption component”, AIP Conference Proceedings, (American Institute of Physics, 2017).
22. O. Malafeyev, K. Farvazov, O. Zenovich, I. Zaitseva, K. Kostyukov and T. Svechinskaya, “Geopolitical model of investment power station construction project implementation”, AIP Conference Proceedings, (American Institute of Physics, 2018).
23. O. Malafeyev, S. Nemnyugin, D. Rylow, E. Kolpak and A. Awasthi, “Corruption dynamics model”, AIP Conference Proceedings, (American Institute of Physics, 2017).
24. O. Malafeyev, A. Awasthi, K. Kambekar, A. Kupinskaya, “Random walks and Market Efficiency in Chinese and Indian equity markets”, K.S., 2019, Statistics, Optimization and Information Computing, 7(1), pp. 1-25.
25. V.N. Kolokoltsov, O.A. Malafeyev, “Corruption and botnet defense: a mean field game approach”, International Journal of Game Theory, 2018, pp. 1-23.
26. I. Zaitseva, O. Malafeyev, I. Kolesin, A. Ermakova, D. Shlaev, “Modeling of the labour force redistribution in investment projects with account of their delay”, 2018 IEEE International Conference on Power, Control, Signals and Instrumentation Engineering, ICPCSI 2017, pp. 68-70.
27. Y.A. Pichugin, O.A. Malafeyev, D. Rylow, I. Zaitseva, “A statistical method for corrupt agents detection”, 2018, AIP Conference Proceedings, https://doi.org/10.1063/1.5043758.
28. O. Malafeyev, D. Rylow, I. Zaitseva, A. Ermakova, D. Shlaev, “Multistage voting model with alternative elimination”, 2018, AIP Conference Proceedings, http://doi.org/ 10.1063/1.5043756.
29. O. Malafeyev, N. Redinskikh, “Quality estimation of the geopolitical actor development strategy”, Source of the Document 2017 Constructive Nonsmooth Analysis and Related Topics (Dedicated to the Memory of V.F. Demyanov), CNSA 2017 – Proceedings, http://dx.doi.org/10.1109/CNSA.2017.7973986.
30. V.N. Kolokoltsov, O.A. Malafeyev, “Mean-Field-Game Model of Corruption”, Dynamic Games and Applications, 2017, 7 (1), pp. 34-47.

Psychological Model of the Project Investor and Manager Behavior in Risk

Oleg Malafeyev[1,a)], Irina Zaitseva[2,3,b)], Sergey Sychev[4,c)], Tatiana Smirnova[1,d)], Anastasia Malova[1,e)] and Aleksandra Tsybaeva[1,f)]

[1] Saint Petersburg State University, 7/9 Universitetskaya nab., St. Petersburg, Russia, 199034
[2]Stavropol State Agrarian University, 12, Zootechnicheskiy alley, Stavropol, Russia, 355017
[3]Stavropol branch of the Moscow Pedagogical State University, 66G, Dovatortsev Street, Stavropol, Russia, 355042
[4)]Saint Petersburg State University of Architecture and Civil Engineering, 4 Vtoraya Krasnoarmeiskaya, St. Petersburg, Russia, 190005

[a)]malafeyevoa@mail.ru
Corresponding author: [b)]irina.zaitseva.stv@yandex.ru
[c)]sasychev@ya.ru
[d)]t.smirnova@spbu.ru
[e)]anastasya.malova97@yandex.ru
[f)]aleksandra_tsybaeva@mail.ru

Abstract. All people have to make risky decisions in everyday life. And we do not know how true they are. But is it possible to mathematically assess the correctness of our choice? This article discusses the model of decision making under risk on the example of project management. This is a game with two players, one of which is Investor, and the other is the Project Manager. Each player makes a risky decision for himself, based on his past experience. With the help of a mathematical model, the players form a level of confidence, depending on who the player accepts the strategy or does not accept. The project manager assesses the costs and compares them with the level of confidence. An investor evaluates past results. Also visit the case where the strategy of the player accepts the part.

INTRODUCTION

A person is subject to different emotions while making a decision, which depends on many factors. One of them is the memory of past events. Bad experience can cause uncertainty in the correctness of the decision that would entail the rejection of this strategy. Also, there may be a reverse situation: success in the past encourages a person to make a decision.

There is evidence that a person is inclined to memorize more negative events of his life, rather than positive ones. For example, the pain of losing a small amount of money will be remembered longer than the joy of winning this amount in the lottery. That is why this article aims to show how life experience influences decision making.

One of the most illustrative examples of this problem is investing in projects. In this situation, a decision is made whether to invest money in a project or not, since there is a large share of the risk of losing the invested amount without having received any profit in the future. Further in the article we will consider the choice of an investor in the conditions of risk and draw up a game-theoretic model.

FORMULATION OF THE PROBLEM

Let us analyze how the Investor forms the choice of his strategy. Let A denote the Investor's strategy, which implies a contribution to the project. Adopting strategy A, there is both a risk and an opportunity to make a profit. As

a rule, the greater the risk of investing, the greater the expected return. The question arises, what (logical, psychological) mechanism can lead an agent to the most effective outcome of this problem? This question remains one of the central in modern game theory. We assume that the main problem of acceptance is confidence, or rather its absence. Certainly, confidence can be influenced by past experience of the Investor: which of his investments justified themselves and which of them did not. In this model, we believe that it is the past experience that affects confidence, and thus the likelihood of the investor getting the maximum profit.

Formalization Of The Game-Theoretic Model Of Strategy Choice Under Risk Conditions

Investor strategy selection. Formation of the level of investor confidence

The beginning of the procedure for concluding a potential transaction will correspond to the strategy chosen by the Investor A, which will mean in the future that the Investor has decided to invest in the project. Let us analyze how the Investor forms the choice of his strategy. Let $p^0 \in [0,1]$ be the Investor's confidence level in the successful outcome of the choice of strategy A in a risky transaction. Let $\psi^0 \in [0,1]$ be the actual probability of a successful outcome when choosing strategy A. We assume that when an Investor analyzes a decision, his level of confidence is based on memories of the outcomes of his past projects. An investor, in whose memory there are more successful investments, will have a higher level of confidence in the successful outcome of this situation. At the same time, the Investor, in whose memory there are more unsuccessful investments, will have a lower level of confidence in the successful outcome. Let s^0be the number of successful outcomes of strategy A in the memory of the Investor. And f^0 is the number of negative outcomes of strategy A.

We assume that the Investor confidence level is $p^0 = \beta(s^0,f^0)$, where β satisfies the following properties:

1) For any s^0,f^0 $0 < \beta(s^0,f^0) < 1$;

2) $\beta_s' > 0$, $\beta_f' < 0$ (with an increase in the number of successes, confidence increases, and with an increase in the number of failures, confidence decreases);

3) For any $a > 0, \lim_{f\to\infty} \beta(af^0, f^0) = \frac{a}{a+1}$.

The third property is fundamental, since it can be concluded from the fact that when the number of outcomes tends to infinity when choosing strategy A, the level of confidence tends to the empirical frequency of success.

Thus, the Investor forms in the memory the number of successful and unsuccessful outcomes. But we cannot say that he does it objectively, since it was previously stated that failures are perceived more deeply and are remembered more strongly. Investor's perception is distorted, which will necessarily affect our model. Consequently, we must formalize the description of the model and consider various options for the perception of the Investor.

Model Formalization

Variants of the distorted perception of the Investor

Let $y^0 \in Y^0$be the impulse received by the Investor, after each end of the project in which he invested. The investor remembers this impulse and records it in his past experience, which he will consider when choosing the strategy A. Also, let's say about the set of all possible outcomes of the transaction X^0.

We introduce the investor perception matrix. For each $y^0 \in Y^0$and $x^0 \in X^0$we denote $u^0_{x^0,y^0}$ - the probability that the momentum was y^0, when the true outcome is x^0.Since there are only two outcomes of the transaction, $X^0 = \{S^0, F^0\}$. And also only two types of impulse $Y^0 = \{n, m\}$, where n is the normal (correct) perception of the Investor, m is the false one. Let γ^0be the probability that the Investor assigns a negative outcome to a negative state of affairs. Then we can create an investor perception matrix:

$$u^0 = \begin{pmatrix} & n & m \\ S^0 & 1 & 0 \\ F^0 & 1-\gamma^0 & \gamma^0 \end{pmatrix}$$

This matrix is important in order to assess the past experience of the Investor.

Let the Investor can accurately count the number of successful investments made (sometimes the memory may not allow him to do this), for which $x^0 = s^0$. Next, we formalize the concept of “experience” as a pair $w^0 = (x^0, y^0)$,

as for each outcome x^0 there is a momentum y^0(the investor responds to each outcome in a certain way, so a positive outcome is not always written by an investor in a positive experience). Due to the fact that a person does not always assess the situation objectively, at this moment there is a distortion of the actual data, and, therefore, we must introduce a random variable such as $c^0(w^0, s^0)=\{1,0\}$. 1 if experience $w^0 \in s^0$and 0 otherwise. Thus, c^0=1 if the experience that the Investor received (in his opinion) is related to a positive outcome.

Let the Investor recollection process be the vector $g^0 = \{g^0{}_{\omega^0, s^0}\}_{\omega^0, s^0}$, where $g^0{}_{\omega^0, s^0} = P\{c^0(w^0, s^0) = 1\}$(the probability that the random variable $c^0 = 1$, as the experience obtained by the Investor is related to a positive outcome). Let also the random variable $\delta^0(s^0) = \sum_{w^0 \in W} c^0(w^0, s^0)$, where W is the set of all Investor's experiments.

Since the number of positive and negative outcomes deposited in memory for a given set of past experiments is a random variable, then $s^0 = \delta^0(S^0)$, $f^0 = \delta^0(F^0)$.

We can conclude that when the Investor forms the confidence level p^0, only those outcomes that he attributed to the normal (correct) one, ie those for which $y^0 = n$.

From where, the process of remembering an investor g^0 has the form: $g^0{}_{\omega^0, s^0} = 1$if $x^0 = s^0$ and$y^0 = n$; $g^0{}_{\omega^0, s^0} = 0$ otherwise.

Consider the frequency of positive implementations of strategy A, due to normal circumstances, according to Investor. This will be a function of the true frequency of outcomes when choosing strategy A.

Let $\alpha^0 = (\alpha^0_{x^0})_{x^0 \in X^0}$ be the true frequency of Investor outcomes.

The expected number of events when counting positive outcomes s^0 is

$$E_{(u^0, g^0, \alpha^0)}\delta^0(s^0) = \sum_{x^0 \in X^0, y^0 \in Y^0} g^0{}_{(x^0, y^0), s^0}\, u^0_{x^0, y^0}\, \alpha^0_{x^0}$$

Thus, the Investor's confidence level in investing p^0, based on past experience, is expressed by the following relationship:

$$\frac{E_{(w^0, g^0, \alpha^0)}\delta^0(s^0)}{E_{(w^0, g^0, \alpha^0)}\delta^0(s^0) + E_{(w^0, g^0, \alpha^0)}\delta^0(f^0)} \qquad (1)$$

Note:

Formula (1) is an approximate calculation of Investor's confidence, since at any time t the number of successes in a transaction s^0 is a random variable. With an increase in past experience, its values will be close to the values of the relation (1).

The investor's correct adoption of the strategy A:

In order for the investor to invest his money in the project, it is necessary that

$$p^0 \geq \mu, \quad where\ \mu \in (0.5; 1]$$

Now we will consider such a scenario that the Investor can invest in the project not all the funds, but part of them. So, for example,

$$\mu^1 \in (0.5; 0.65]$$

$$\mu^2 \in (0.65; 0.8]$$

$$\mu^3 \in (0.8; 1]$$

Then if $\mu^1 \leq p^0 < \mu^2$, then the Investor invests 1/3 of the sum at his disposal, if $\mu^2 \leq p^0 < \mu^3$, then 2/3, and if $p^0 \geq \mu^3$, then the whole amount is full.

CONCLUSION

This work is an attempt to bring agents to the effective outcome of their interaction. Throughout the work, we were of the opinion (in common with psychology) that agents form their level of confidence based on simple heuristics and the choice of attribution style.

Undoubtedly, there are a large number of heuristics, psychological patterns and personal associations that agents use when forming their choice. But our main goal is not to compile an exhaustive catalog with which agents can form their determination, but to present a new way of optimization for the risk interaction between the two agents.

The results obtained in this article show that personal perception of the situation, a tendency toward optimistic or pessimistic distortions of perception can affect the formation of a person's confidence about his ability to succeed in a risky transaction. As well as the same mechanisms affect the opponent and how they are combined with each other.

From the obtained results a number of conclusions follow.

For example:

* if agents could find any control over their level of confidence, then this could lead them to improve the results of the risky deals they concluded.

* if agents could find any control over the level of confidence of the opponent, then this could lead them to improve the results of risky deals they make.

* Risky deals are "safer" to conclude with agents whose past experience is most positive.

Thus, careful attention to oneself and one's own reactions to the perception of situations, to the personality of the opponent and his past experience, is a very important step in the intention to conclude a risky deal.

ACKNOWLEDGMENTS

The work is partially supported by the RFBR grant # 18-01-00796.

REFERENCES

1. A. Kirjanen, O. Malafeyev, N. Redinskikh, "Developing industries in cooperative interaction: Equilibrium and stability in processes with lag", Statistics, Optimization and Information Computing, 2017.
2. E. Kriulina, N. Tarasenko, N. Miroshnitchenko, I. Zaitseva, and I. Dedyukhina, "Environmental Management in Agriculture: Problems and Solutions", Research Journal of Pharmaceutical, Biological and Chemical Sciences, no. 7(3), pp. 1908-1912, 2016.
3. E. Neverova and O. Malafeyev, "A model of interaction between anticorruption authority and corruption groups", AIP Conference Proceedings, (American Institute of Physics, 2015).
4. E.G. Neverova, O.A. Malafeyev, G.V. Alferov and T.E. Smirnova, "Model of interaction between anticorruption authorities and corruption groups" in International Conference on "Stability and Control Processes" in Memory of V.I. Zubov, (SCP, Proceedings, SPb, 2015), pp. 488-490.
5. G. Drozdov, O. Malafeyev and S. Nemnyugin, "Multicomponent dynamics of competitive single-sector economy development", International Conference on "Stability and Control Processes" in Memory of V.I. Zubov (SCP 2015 – Proceedings, 2015).
6. I. Kolesin, O. Malafeyev, M. Andreeva and G. Ivanukovich "Corruption: Taking into account the psychological mimicry of officials", AIP Conference Proceedings (American Institute of Physics, 2017).
7. I. Zaitseva and M. Popova, "Technique to study the employment potential of the region: economic-mathematical aspect", (World Applied Sciences Journal, 2013), no. 22 (1), pp. 22-25.
8. I. Zaitseva, E. Kriulina, A. Ermakova, E. Shevchenko and Y. Vorokhobina, "Application of Factor Analysis to Study the Labour Capacity of Stavropol Krai", (Research Journal of Pharmaceutical, Biological and Chemical Sciences, 2016), no. 7(4), pp. 2183-2186.
9. I. Zaitseva, M. Popova, A. Ermakova, S. Bogdanova and D. Rezenkov, "Determination Prospects Of Development Labor Potential In Agriculture Stavropol Territory Based On Assessment His Condition", (Research Journal of Pharmaceutical, Biological and Chemical Sciences, no. 7(3), 2016), pp. 2592-2595.
10. I. Zaitseva, O. Malafeyev, S. Strekopytov, A. Ermakova and D. Shlaev, "Game-theoretical model of labour force training", Journal of Theoretical and Applied Information Technology, 2018.
11. I. Zaitseva, O. Malafeyev, S. Strekopytov, G. Bondarenko and D. Lovyannikov, "Mathematic model of regional economy development by the final result of labor resources", AIP Conference Proceedings, 2018.
12. I.V. Zaitseva, A.N. Ermakova, D.V. Shlaev, E.A. Shevchenko, and S.I. Lugovskoy. "Workforce planning redistribution of the region's results", (Research Journal of Pharmaceutical, Biological and Chemical Sciences. 2017), 8(1), pp. 1862-1866.
13. K. Kostyukov, I. Zaitseva, G. Bondarenko, T. Svechinskaya and S. Nechayeva, "Workforce Planning as An Element of Control System", (Research Journal of Pharmaceutical, Biological and Chemical Sciences, no. 7(6), 2016), pp. 2315–2319.
14. M.A. Vlasov, V.V. Glebov, O.A. Malafeyev and D.N. Novichkov, "Experimental study of an electron beam in drift space", (Soviet journal of communications technology & electronics, 1986), 31(3), pp. 145-149.

15. O. A. Malafeyev, and N. D. Redinskikh Compromise solution in the problem of change state control for the material body exposed to the external medium AIP Conference Proceedings 1959, 080017 (2018); https://doi.org/10.1063/1.5034734
16. O. A. Malafeyev, N. D. Redinskikh, S. A. Nemnyugin, I. D. Kolesin, and I. V. Zaitseva The optimization problem of preventive equipment repair planning AIP Conference Proceedings 1978, 100013 (2018); https://doi.org/10.1063/1.5043757
17. O. Malafeev and S. Nemnyugin, "Generalized dynamic model of a system moving in an external field with stochastic components", (Theoretical and Mathematical Physics, no. 107(3), 1996), 770 p.
18. O. Malafeev, "On the existence of nash equilibria in a noncoope rative n-person game with measures as coefficients", (Communications in Applied Mathematics and Computational Science, no. 5(4), 1995), pp. 689-701.
19. O. Malafeyev, A. Awasthi, I. Zaitseva, D. Rezenkov and S. Bogdanova, "A dynamic model of functioning of a bank", AIP Conference Proceedings, (American Institute of Physics, 2018).
20. O. Malafeyev, D. Rylow, I. Zaitseva, M. Popova and L. Novozhilova, "Game-theoretic model of dispersed material drying process", AIP Conference Proceedings, (American Institute of Physics, 2017).
21. O. Malafeyev, D. Saifullina, G. Ivaniukovich, V. Marakhov and I. Zaytseva, "The model of multi-agent interaction in a transportation problem with a corruption component", AIP Conference Proceedings, (American Institute of Physics, 2017).
22. O. Malafeyev, K. Farvazov, O. Zenovich, I. Zaitseva, K. Kostyukov and T. Svechinskaya, "Geopolitical model of investment power station construction project implementation", AIP Conference Proceedings, (American Institute of Physics, 2018).
23. O. Malafeyev, S. Nemnyugin, D. Rylow, E. Kolpak and A. Awasthi, "Corruption dynamics model", AIP Conference Proceedings, (American Institute of Physics, 2017).
24. O. Malafeyev, A. Awasthi, K. Kambekar, A. Kupinskaya, "Random walks and Market Efficiency in Chinese and Indian equity markets", K.S., 2019, Statistics, Optimization and Information Computing, 7(1), pp. 1-25.
25. V.N. Kolokoltsov, O.A. Malafeyev, "Corruption and botnet defense: a mean field game approach", International Journal of Game Theory, 2018, pp. 1-23.
26. I. Zaitseva, O. Malafeyev, I. Kolesin, A. Ermakova, D. Shlaev, "Modeling of the labour force redistribution in investment projects with account of their delay", 2018 IEEE International Conference on Power, Control, Signals and Instrumentation Engineering, ICPCSI 2017, pp. 68-70.
27. Y.A. Pichugin, O.A. Malafeyev, D. Rylow, I. Zaitseva, "A statistical method for corrupt agents detection", 2018, AIP Conference Proceedings, https://doi.org/10.1063/1.5043758.
28. O. Malafeyev, D. Rylow, I. Zaitseva, A. Ermakova, D. Shlaev, "Multistage voting model with alternative elimination", 2018, AIP Conference Proceedings, http://doi.org/ 10.1063/1.5043756.
29. O. Malafeyev, N. Redinskikh, "Quality estimation of the geopolitical actor development strategy", Source of the Document 2017 Constructive Nonsmooth Analysis and Related Topics (Dedicated to the Memory of V.F. Demyanov), CNSA 2017 – Proceedings, http://dx.doi.org/10.1109/CNSA.2017.7973986.
30. V.N. Kolokoltsov, O.A. Malafeyev, "Mean-Field-Game Model of Corruption", Dynamic Games and Applications, 2017, 7 (1), pp. 34-47.
31. O.A. Malafeyev, N.D. Redinskikh, "Stochastic analysis of the dynamics of corrupt hybrid networks", Proceedings of 2016 International Conference "Stability and Oscillations of Nonlinear Control Systems" (Pyatnitskiy's Conference), STAB 2016, http://dx.doi.org/10.1109/STAB.2016.7541208.
32. Y.A. Pichugin, O.A. Malafeyev, "Statistical estimation of corruption indicators in the firm", Applied Mathematical Sciences, 2016, 10 (41-44), pp. 2065-2073.
33. O.A. Malafeyev, S.A. Nemnyugin, "Model of the optimal parameters choice for the charged particles beam", 2016, 25th Russian Particle Accelerator Conference, RuPAC 2016, pp. 437-439.
34. Y. Pichugin, G. Alferov, O. Malafeyev, "Parameters estimation in mechanism design", Contemporary Engineering Sciences, 2016, 9 (1-4), pp. 175-185.
35. G.V. Alferov, O.A. Malafeyev, A.S. Maltseva, "Game-theoretic model of inspection by anti-corruption group", AIP Conference Proceedings, 1648, 450009 (2015), http://dx.doi.org/10.1063/1.4912668.

Study of the Equilibrium of Labor Resources in Differential Games of Supporting the Projects' Joint Investment Processes

Oleg Malafeyev[1, a)], Irina Zaitseva[2,3, b)], Denis Lovyannikov[4, c)], Konstantin Kostyukov[3, d)] and Tatiana Svechinskaya[3, e)]

[1]Saint Petersburg State University, 7/9 Universitetskaya nab., St. Petersburg, Russia, 199034
[2]Stavropol State Agrarian University, 12, Zootechnicheskiy alley, Stavropol, Russia, 355017
[3]Stavropol branch of the Moscow Pedagogical State University, 66G, Dovatortsev Street, Stavropol, Russia, 355042
[4]North-Caucasus Federal University, 2, Kulakova Street, Stavropol, Russia, 355035

[a)]malafeyevoa@mail.ru
[b)]Corresponding author: irina.zaitseva.stv@yandex.ru
[c)]denlov1@mail.ru
[d)]kostukovki@mpgu26.ru
[e)] svechinskayata@mpgu26.ru

Abstract. The article presents a mathematical model for the study of the equilibrium of labor resources. The problem of finding a sufficient equilibrium condition in differential games with many participants is solved. The article deals with a differential game of X persons with terminal gain, and sufficient conditions are derived in the class of positional strategies. The task is to find a sufficient equilibrium condition. The results obtained are adjacent to the results of [1,2,5], in which sufficient optimality conditions for optimal control problems and antagonistic differential games are stated.

INTRODUCTION

For the task of studying the equilibrium of labor resources, a high level of complexity of the solution should be noted. To find the equilibrium, a game-theoretic method is used, in which the game under consideration at a fixed position (t, x) is a game in normal form with forbidden situations. Determining the parameters of the equilibrium state of labor resources as a complex economic system will provide the required or maximum possible degree of their stability.

To simulate the stability of labor resources, it is necessary to determine some sufficient equilibrium conditions for admissible situations, provided that they satisfy the system of dynamic programming equations on a given set.

This requires the development of a qualitatively new methodological approach to solving the problem of studying the equilibrium of labor resources.

ISSUE DEFINITION

Let $I = \{1,2,...,n\}$ - be the set of labor resources, which we will consider as players, $U_i \subset R^{m_i}$ - a closed set, t, x, u_i - variables, from spaces R^1, R^m, R^{m_i}, $u = (u_1,...,u_n) \in U = \prod_1^n U_i$, $f(t,x,u)$ - continuous vector function $(f : R^1 \cdot R^m \cdot U \to R^m)$, continuously differentiated with respect to x.

Define $(\bar{t},\bar{x})$ the initial position of the game. Let a smooth manifold $M=\{(t,x)/\varphi_i(t,x)=0, i=1,...,\ell\}\subset R^{m+1}$ be a terminal manifold of a game, where φ_i - be a terminal manifold of a game, and $H_i(t_i,x(t_1))$ - a smooth terminal function of winning a player $i\in I$.

Define $u(t,x)=(u_1 t_1 x),...,u_n(t,x)$ - the situation in positional strategies, definitions on the set $Q\subset R^{m+1}$, if $u(t_1 x)\in U$ and for any point $(\bar{t},\bar{x})\in Q$ there is a unique solution to the equation

$$x=f(t,x,u(t,x)) \quad (1)$$

on the segment $[\bar{t},t_1(\bar{t},\bar{x})]$ with initial conditions $x(\bar{t};\bar{t},\bar{x})=\bar{x}$ and $u(t,x(t;\bar{t},\bar{x}))\in U$ for $t\in[\bar{t},t_1(\bar{t},\bar{x})]$ and $(t_1(\bar{t},\bar{x}),x(t_1(\bar{t},\bar{x});\bar{t},\bar{x})\in M$. Here denote by $x(t;\bar{t},\bar{x})$ a trajectory with initial conditions $\bar{t},\bar{x}$.

Thus, the game in question at a fixed position (t,x) is a game in normal form with forbidden situations. Consider the positional situation $u(t,x)$ of the game trajectory $x(t;\bar{t},\bar{x})$ and the corresponding control $u(t)=u(t,x(t;\bar{t},\bar{x}))$. Suppose the situation $u(t,x)$ is equilibrium for a point $(\bar{t},\bar{x})$.

In the following presentation, we will be analyzing the smoothness of the players' $H=(H_1,...,H_n)$ win function in equilibrium situations In order for the corresponding reasoning to be correct, we need to make some assumptions about the game. We will consider the set U_i of controlling parameters of the player as a smooth closed manifold.

It's important to remember that in this case the space γU_n of games with smooth payoff functions defined on $U=\prod_1^n U_i$, is divided into connected open components γe, $e=1...,\bar{e}$ ..., regularities, and a singular part $\gamma_U\setminus\bigcup_{e=1}^{\bar{e}}\gamma_e$. Each game $\Gamma_н\in\gamma_e$ game has a finite number of equilibrium situations that smoothly depend on $\Gamma_н$ within this component.

Fix one smooth branch γ_e of the equilibrium situation over each component $Vae\Gamma_н$ and denote by the vector of values of the players' winnings function in the corresponding situation. They will also smoothly depend on $\Gamma_н$ within each component.

In our further considerations, only finite-dimensional families of games of the space γ, will appear, and the parameters of the game are the positions of the differential game.

SUFFICIENT CONDITION OF EQUILIBRIUM

Consider cellular decompositions of the game space Q and assume that for each cell the set of games parametrized by its points is such that there exists a smooth mapping branch for it, which compares the equilibrium situation to the games. Smoothness is understood in the sense that this branch can be smoothly continued to an open neighborhood Q in with a given cell.

A valid situation is a function $u(t,x)=(u_1(\cdot),...,u_n(\cdot))$, defined on Q, for which there is a cellular partition $Q_0\subset Q_1\subset Q_2\subset...\subset Q_m\subset Q$, that satisfies the conditions given below Q. Cells from a set $Q\setminus Q_m$ is an open subset R^{m+1}, and for every non-empty set C from $Q_j\setminus Q_{j-1}$ there is a smooth mapping defining it from a neighborhood of a set $Q\setminus\overline{Q}$ $\varphi_c:\overline{Q}\to R^{m+1-i}$, moreover, this cell is a subset of the set in the induced topology.

1. For every cell C there is a smooth mapping $u_c(t,x)$, defined in a neighborhood C, such that $u_c(t,x)=u)t,x)$ with $(t,x)\in C$. The cell family is assumed to be locally finite, i.e. every compact of interests Q have only a finite number of cells. The variety M is contained in Q_m and is the union of a finite number of cells.

The set of K of all cells is divided into three classes. $K = K_I U K_{II} U K_{III}$. Every cell from $Q \setminus Q_m$ belongs to K_I. If $C \in K_I$, then there exists a cell Π_c, for which the function φ_{Π_c} has one component φ^j more, than φ_c. From any point $(\bar{t}, \bar{x}) \in c$ a single trajectory of equation (1), emanates C в which falls in from in a finite time and intersects Π_c at a nonzero angle, so that if $(t,x) \in \Pi_c$, then $\frac{\partial \varphi^j(t,x)}{\partial t} + \sum_{k=1}^{m} \frac{\partial \varphi^j(t,x)}{\partial x_k} f_k(t,x,u_c(t,x)) \neq 0$ or, in short, denoting the derivative by subscript,

$$\varphi_t^j(t,x) + \varphi_x^j(t,x) f(t,x,u_c(t,x)) \neq 0. \tag{2}$$

If $C \in K_{II}$, then there exists a cell $\delta_c \in K_I$, for which the function φ_{δ_c} function has one component less than φ_{δ_c}. From each point (t,x), there is a single trajectory of equation (1), that enters the cell δ_c and has one common point with the cell (t,x).

The function $u(t,x)$ is continuously differentiated on $C \cup \delta_c$.

Cells from M form a set K_{II}. Every trajectory reaches a manifold M, in a finite time by intersecting a finite number of cells in the following sequence: from C to Π_c, if $\Pi_c \in K_I$, of from to C в δ_{Π_c}, if $\Pi_c \in K_{II}$, without leaving Q.

Let $C_1,...,C_\infty$ – be the cells from K_I, which the trajectory passes successively $x(t;\bar{t},\bar{x})$. Let us denote $\tau_j(\bar{t},\bar{x})$ by the moment of reaching the trajectories $x(\cdot)$ of the cell Π_{cj} and put for brevity:

$$x_j(\bar{t},\overline{x}) = x(\tau_j(\bar{t},\overline{x});\bar{t},\overline{x}). \tag{3}$$

Then $(\tau_j(\bar{t},\bar{x});\bar{t},\bar{x}), x_j(\bar{t},\bar{x})) \in \Pi_{cj}$ and $(t, x(t;\bar{t},\bar{x})) \in C_{j+1}$ with $\tau_j(\bar{t},\bar{x}) \le t \le \tau_{j+1}(\bar{t},\bar{x})$, if $\Pi_{cj} \in K_I$, or with $\tau_j(\bar{t},\bar{x}) < t < \tau_{j+1}(\bar{t},\bar{x})$, if $\Pi_{cj} \in K_{II}$.

PROPOSITION 1. Let $C \in K_I, (\bar{t},\bar{x}) \in C$ and $x = x(t;\bar{t},\bar{x}))$ – be the trajectory of the equation $\dot{x} = f(t,x,u(t,x))$.

Then:

1) the position $(\tau_j(\bar{t},\bar{x}), x_j(\bar{t},\bar{x})$ of the exit point $(t; x(t;\bar{t},\bar{x}))$ from the cell C_j is continuously differentiable on the set C by $(\bar{t},\bar{x})$;

2) $x(t;\bar{t},\bar{x})$ continuously differentiable on the set $\{(t;\bar{t},\bar{x}) \mid (\bar{t},\bar{x}) \in C, \tau_{j=1}(\bar{t},\bar{x}) < t < \tau_j(\bar{t},\bar{x})\}$, $j = \overline{1,Q}$.

Matrix $x_{\bar{x}}(t;\bar{t},\bar{x})$ satisfies the equation

$$\dot{x}_{\bar{x}}(t;\bar{t},\bar{x}) = \left[f_x(t, x(t;\bar{t},\bar{x}), u(t, x(t, x(t;\bar{t},\bar{x})) + f_u(t, x(t;\bar{t},\bar{x}), u(t, x(t;\bar{t},\bar{x}))) \cdot u_{cjx}(t; x(t;\bar{t},\bar{x}))\right] x_{\bar{x}}(t;\bar{t},\bar{x}) \tag{4}$$

at $\tau_{j-1}(\bar{t},\bar{x}) < t < \tau_j(\bar{t},\bar{x})$;

3) for moments of time τ_{j-1}, τ_j the function $x_{\bar{x}}(t;\bar{t},\bar{x})$ has limits on the right and left:

$$x_{\bar{x}}(\tau_{j-1}) = -f(\tau_{j-1}, x_{j-1}, u_{cj}(\tau_{j-1}, x_{j-1}))\tau_{(j-1)\bar{x}} + x_{(j-1)}\bar{x}; \tag{5}$$

$$x_{\bar{x}}(\tau_{\bar{j}}) = -f(\tau_{\bar{j}}, x_j, u_{cj}(\tau_j, x_j))\tau_{j\bar{x}} + x_{j\bar{x}}. \tag{6}$$

Conditions similar to (5)-(6), are fulfilled when replacing with $x_{\bar{t}}$ and $\tau_{j\bar{x}}, x_{j\bar{x}}$ to $\tau_{j\bar{t}}, x_{j\bar{t}}$. The proof is presented in [1].

THEOREM 1. The value of the gain function in any equilibrium situation $u*$ cannot increase along any trajectory $\chi(u*//u_i)$.

PROOF. Suppose the contrary, that is, along a certain trajectory $\chi(u*i/u_i)V_i(\cdot)$ strictly increases. We use the strategy $u_i(\cdot)$. Following the trajectory $x(u*i/u_i)$, we get a great value of the player's gain. We get a contradiction.

THEOREM 2. The value $v_i(x,t)$ along the equilibrium trajectory is constant.

PROOF. Let be $\chi(u^*)$ on $[t_0,t_1]$ – the equilibrium trajectory for the initial state x_0, corresponding to the equilibrium situation $u*$. By Theorem 1, since a restriction $u*$ on $[t\ ,t_1]$ for any $t_0 \le t \le t_1$ is admissible for the initial state $x*(t)$, $V_i(t,x*(t)) \ge H_i(t_1,x*(t_1))$. But due to the equilibrium $u*$ for t_0,x_0 $v_i(t_0;x_0) = H_i(t_1,x*(t_1))$ and since $V_i(t,x*(t))$ it is non-increasing, then $V_i(t,x*(t)) = H_i(t_1,x*(t_1))$ $t_0 \le t \le t_1$.

THEOREM 3. Let $i \in I, W_i(t,x)$ be a real-valued function defined on R^{m+1}, such that $W_i(t,\bar{x}) = H_i(t,\bar{x})$ with $(t,x) \in M$. Let (t_0,x_0) the initial position of the game and for all trajectories $x = \chi(u*i/u_i)$, corresponding to admissible situations $(u*i/u_i)W_i(\cdot)$;; not rising on $[t_0,t_1]$ along $x(\cdot)$. If $u*$ – is a situation, for which $\chi(u^*)$ the function $W_i(t,x*(t))$ is constant, then $u*$ – equilibrium and $W_i(t_0,x_0) = V_i(t_0,x_0)$.

PROOF. Indeed, for any valid player controls $u_i(\cdot)$ and $x = \chi(u*i/u_i)$ we have: $W_i(t_0,x_0) \ge H_i(t_1,x(t_1))$.

For control $u*$ we have: $W_i(t_0,x_0) = H_i(t_1,x*(t_1))$ for any $i \in I$, т. е. $u*$ that is equilibrium.

Let the game end in a situation $u*i/u_i$. Assume that the function "values" $v_i(t,x)$ is differentiable at a point (t,x). Then fair.

THEOREM 4. Let $u_i^*(i' \ne i, i' \in I)$ – fixed, equilibrium, V_i – differentiable in a neighborhood of a point (t,x), then for every $u_i \in \upsilon_i$ V_i satisfies the partial differential inequality:

$$\frac{\partial V_i}{\partial t} + \nabla V_{iT}^{1}(t,x,u*i/u_i) \le 0. \tag{7}$$

If $u*_i$ $(i' \ne i)$ – equilibrium strategies, then

$$\max_{u_i \in \upsilon}\left(\frac{\partial V_i}{\partial t} + \nabla V_i f_i(t,x,u*//u_i) = 0.\right. \tag{8}$$

The maximum in (8) is reached at the right-hand limit $u_i^*(x*(t))^+$ at the moment t.

PROOF. Consider the right derivative of the function v_i along the trajectory $x*$. By proven, v_i non-increasing, therefore, $D^+V_i(t,x(t)) \le 0$.

Writing it in detail according to the rule of differentiation of a complex function, we get:

$$\frac{\partial V_i}{\partial t} + (\nabla V_i f(t,x,(u//u_i)) \le 0$$

with all such u_i, that $\chi(u^*//u_i) \neq \varnothing$ with beginnings in (t,x). If u^* is equilibrium, then $V_i(t,x^*(t)) = H_i(t_1,x^*(t_1))$ at $t \in [t_0,t_1]$. Consequently, $\frac{\partial V_i}{\partial t} + (\nabla V_i f(t,x,(u//u_i^+(t))) = 0$.

Here u_i^{*+} – is the limit $H_i^*(\cdot)$ on the right at t at the point t. From here we obtain the statement of the theorem. Next we will consider the question of the differentiability of the function of value $V = (V_1,...,V_n)$. Here the following note is significant.

COMMENT. If $u^*(t,x)$ – is an equilibrium situation, $t_1(t,x), x_1(t_1(t,x),t,x)$ – is the final position in this situation with a starting point (t,x), then the value $V(t,x)$ is differentiable at each point at which $t_1(t,x), x_1(t_1(t,x);t,x)$ is a differentiable function with respect to (t,x).

THEOREM 5. Let $V_i(t,k)$, $i \in I$ – be a smooth solution of the system of dynamic programming equations

$$o = \max_{u_i \in \upsilon} \left(\frac{\partial V_i(t,x)}{\partial t} + \nabla V_i(t,x) f(t,x,u^*(\cdot)//u_i(t,x)) \right),$$

$i \in I$, satisfying the condition $V_i(t,x) = H_i(t,x)$ at $(t,x) \in M$. Let (t_0,x_0) – be a point from the set $Q, u(t,x)$ – an admissible situation, $\chi(u) = x$ – the corresponding solution of the system $x = f(t,x,u(\cdot))$.

Then $V_i(t,x(t)), i \in I$ – is a non-decreasing function of t. If u^* – is an admissible situation, and $x^* = \chi(u^*(\cdot))$ – is an appropriate trajectory, such that

$$\frac{\partial V_i(x)}{\partial t} + \nabla V_i(t,x(t)) \cdot f(t,x^*,u^*(t,x^*)) = 0,$$

then u^* – is an equilibrium situation, and aV_i, $j \in I$ – is a function of value.

EVIDENCE. From the equations of dynamic programming we get:

$$\frac{d}{dt} V_j(t,x(t)) = \frac{\partial V_i}{\partial t} + \nabla V_i(t,x(t)) \cdot f(t,x(t),u(t)) \leq 0.$$

Consequently, $V_j(t,x(t))$ – is a non-decreasing function. And from the condition (*) we get that $\frac{d}{dt} V_j(t,x^*(t)) = 0$ as $V_j(t,x^*(t))$. Consequently, u^* – equilibrium by Theorem 3.

NOTE 2. If there is an admissible situation $u(t,x)$, then the function $\overline{H_i}(t,x,u) = H_i(t_f,x(t_f,t,x))$ is continuously differentiated with respect to (t,x) on the set $Q \setminus Q_m$. This follows directly from the definition $\overline{H_i}$ and theorem 1.

We now find some sufficient equilibrium conditions for admissible situations, provided that they satisfy the system of dynamic programming equations on the set $Q \setminus Q_m$.

THEOREM 6. Let $Q \subset R^{m+1}$ be a set, containing interior points, $V_j(t,x), i \in I$ – continuous functions, defined on Q и and satisfying the condition $V_i(t,x) = H_i(t,x), (t,x) \in M \cap Q, K \subset Q$ – be such that $Q \setminus K$ the open R^{m+1} intersection K with any compact set of Q lies in the union of a finite number of sets given by the equations $\varphi(t,x) = 0$, where φ – where is a smooth map defined on neighborhood $\widetilde{Q}$ set $\widetilde{Q}$, such, then $\nabla \varphi(t,x) \neq 0$ when $(t,x) \in K$.

Let further on the set Q / K of functions $V_j(\cdot)$ are continuously differentiable and satisfy the system of equations:

$$\max_{u_j \in U_i} \left\{ \frac{\partial V_i(t,x)}{\partial t} + \nabla V_i(t,x) f(t,x,u) \right\} = 0 \cdot$$

Let $(t_0, x_0) \in Q$ and all the trajectories, corresponding to the admissible equations lie in Q with $t \in \lfloor t_0, t_f \rfloor$. Let u^* be a situation, for which $V_i(t_0, x_0) = H_i(t_f, x^*(t_f^*))$, then u^* – an equilibrium situation.

PROOF. Let $u(t) = (u_1(t), \ldots, u_n(t))$ be the control along some trajectory emanating from a point (t_0, x_0), corresponding to the situation $u(t,x)$. It is known from [1] that in a neighborhood of a point x_0 there exist such points y', that a solution to the equation $\dot{x} = f(t,x,u)$ exists on an interval $\lfloor t_0, t_f \rfloor$ and its intersection with K contains no more than a finite number of points. Consider the sequence y_k of points such that $y_k \to y_0$.

Let for such a point $y_k, \tau_1, \ldots, \tau_{\bar{e}}$ – be the set of moments at which the trajectory $x(t, t_0, y_k)$ intersects K and $\tau_{K+1} = t_f, \tau_0 = t_0$. Then from the condition of continuity of the derivatives $\frac{\partial V_i}{\partial t}, \frac{\partial V_i}{\partial xp}$, at the points $(t, x(t, t_0, y_k))$, where $\tau_{e-1} < t < \tau_e$, and the continuity of the functions $V_i(t,x)$ we obtain:

$$0 \ge \int_{\tau_{e-1}}^{\tau_e} \left[\frac{\partial V_i}{\partial t}(t,x(t,t_0,y_k)) + \nabla V_i(t,x(t,t_0,y_k) \cdot f(t,x(t,t_0,y_k),u(t,x(t,t_0,y_k)) \right] dt = V_i(\tau_i,x(\tau_i,t_0,y_k)) - V_j(E_0,y_k)$$

The inequalities are summed to e from 1 to $\bar{e}+1$, we get:

$$0 \ge V_i(t_f, x(t_f, t_0, y_k)) - V_i(t_0, y_k) .$$

Letting y_k to y_0 k and using the continuity of the function $V_i(t,x)$ k and using the continuity of the function $x(t, t_0, y_k)$ to $x(t, t_0, y_k)$ we get:

$$\lim_{k\to\infty} V_i(t_f, x(t_f; t_0, y_k)) = V_i(t_f, x(t_f; t_0, x_0) = H_i(t_0, x(t_f; t_0, y_k)) = \overline{H_i}(t_0, x_0, u) \le \lim_{k\to\infty} V_i(t_0, y_k) = V_i(t_0, x_0) .$$

Consequently, the value of the gain function $H_i(t_0, x_0, u^* // u_i)$ in any strategy u_i, such that $(u^* // u_i)$ – is an admissible situation, is less or equal $V_i(t_0, x_0)$. Hence, by definition u^* is equilibrium.

THEOREM 7. Let $u^*(t,x)$ be an admissible situation, and a function $\overline{H_i}(t,x,u^*)$ – be continuous on Q. Then, to be $u^*(\cdot)$ balanced, it is necessary and sufficient that the following conditions be fulfilled:

1) $H_i(t,x,u^*), i \in \tau$ there is a continuously differentiable solution of the system of dynamic programming equations for Q/Q_m;

2) For anyone $(t,x) \in Q/Q_m$ .is executing $\frac{\max}{u_i \in U_i} \nabla \overline{H_i}(t,x,u^*) f(t,x,u^* // u_i) = \nabla \overline{H_i}(t,x,u^*)$.

PROOF. The necessity follows from Theorem 4 and Remark 2. The sufficiency is proved in the previous theorem.

CONCLUSION

Thus, the paper presents a solution to an important socio-economic problem related to finding a sufficient equilibrium condition in differential games with many participants. A methodical approach has been developed and a mathematical apparatus has been proposed for the study of the equilibrium of labor resources. A differential game of X persons with terminal gain, for which sufficient conditions in the class of positional strategies are derived, is considered. The results obtained will allow us to investigate the stability of labor resources using sufficient optimality conditions for optimal control problems and antagonistic differential games.

ACKNOWLEDGMENTS

The work is partially supported by the RFBR grant # 18-01-00796.

REFERENCES

1. W. Fleming and R. Richel, *Optimal control of deterministic and stochastic systems (*M.: World, 1978), 316 p.
2. N. N. Krasovskii and A. I. Subbotin. *Positional differential games* (M.: FIZMATLIT, 1974), 456 p.
3. V. I. Zubov, *Methods of A. M. Lyapunov and their application* (L.: Publishing house LSU, 1957), 242 p.
4. L. A. Petrosyan, *Differential games of pursuit* (L.: Publishing house of LSU, 1977), 224 p.
5. L.D. Berkovitz, *A variational approach to differential games*. In: Dresher, M., Shapley, L.S., Tucker, A.W. (eds.) (Advances in Game Theory, Princeton University Press, Princeton, 1964), pp. 127–174.
6. A. Kirjanen, O. Malafeyev, N. Redinskikh, "Developing industries in cooperative interaction: Equilibrium and stability in processes with lag", Statistics, Optimization and Information Computing, 2017.
7. E. Kriulina, N. Tarasenko, N. Miroshnitchenko, I. Zaitseva, and I. Dedyukhina, "Environmental Management in Agriculture: Problems and Solutions", Research Journal of Pharmaceutical, Biological and Chemical Sciences, no. 7(3), pp. 1908-1912, 2016.
8. E. Neverova and O. Malafeyev, "A model of interaction between anticorruption authority and corruption groups", AIP Conference Proceedings, (American Institute of Physics, 2015).
9. E.G. Neverova, O.A. Malafeyev, G.V. Alferov and T.E. Smirnova, "Model of interaction between anticorruption authorities and corruption groups" in International Conference on "Stability and Control Processes" in Memory of V.I. Zubov, (SCP, Proceedings, SPb, 2015), pp. 488-490.
10. G. Drozdov, O. Malafeyev and S. Nemnyugin, "Multicomponent dynamics of competitive single-sector economy development", International Conference on "Stability and Control Processes" in Memory of V.I. Zubov (SCP 2015 – Proceedings, 2015).
11. I. Kolesin, O. Malafeyev, M. Andreeva and G. Ivanukovich "Corruption: Taking into account the psychological mimicry of officials", AIP Conference Proceedings (American Institute of Physics, 2017).
12. I. Zaitseva and M. Popova, "Technique to study the employment potential of the region: economic-mathematical aspect", (World Applied Sciences Journal, 2013), no. 22 (1), pp. 22-25.
13. I. Zaitseva, E. Kriulina, A. Ermakova, E. Shevchenko and Y. Vorokhobina, "Application of Factor Analysis to Study the Labour Capacity of Stavropol Krai", (Research Journal of Pharmaceutical, Biological and Chemical Sciences, 2016), no. 7(4), pp. 2183-2186.
14. I. Zaitseva, M. Popova, A. Ermakova, S. Bogdanova and D. Rezenkov, "Determination Prospects Of Development Labor Potential In Agriculture Stavropol Territory Based On Assessment His Condition", (Research Journal of Pharmaceutical, Biological and Chemical Sciences, no. 7(3), 2016), pp. 2592-2595.
15. I. Zaitseva, O. Malafeyev, S. Strekopytov, A. Ermakova and D. Shlaev, "Game-theoretical model of labour force training", Journal of Theoretical and Applied Information Technology, 2018.
16. I. Zaitseva, O. Malafeyev, S. Strekopytov, G. Bondarenko and D. Lovyannikov, "Mathematic model of regional economy development by the final result of labor resources", AIP Conference Proceedings, 2018.
17. I.V. Zaitseva, A.N. Ermakova, D.V. Shlaev, E.A. Shevchenko, and S.I. Lugovskoy. "Workforce planning redistribution of the region's results", (Research Journal of Pharmaceutical, Biological and Chemical Sciences. 2017), 8(1), pp. 1862-1866.
18. K. Kostyukov, I. Zaitseva, G. Bondarenko, T. Svechinskaya and S. Nechayeva, "Workforce Planning as An Element of Control System", (Research Journal of Pharmaceutical, Biological and Chemical Sciences, no. 7(6), 2016), pp. 2315–2319.
19. M.A. Vlasov, V.V. Glebov, O.A. Malafeyev and D.N. Novichkov, "Experimental study of an electron beam in drift space", (Soviet journal of communications technology & electronics, 1986), 31(3), pp. 145-149.
20. O. A. Malafeyev, and N. D. Redinskikh Compromise solution in the problem of change state control for the material body exposed to the external medium AIP Conference Proceedings 1959, 080017 (2018); https://doi.org/10.1063/1.5034734

Stability of a Flow due to Nonhomogeneous Heat Sources in a Magnetic Field

Andrei Kolyshkin[1,a)] and Valentina Koliskina[1,b)]

[1]*Department of Engineering Mathematics, Riga Technical University, Daugavgrivas street 2, Riga, Latvia, LV 1007*

[a)]Corresponding author: andrtejs.koliskins@rtu.lv
[b)]valentina.koliskina@rtu.lv

Abstract. Linear stability of a convective flow generated by nonhomogeneous internal heat sources between two parallel vertical planes is investigated in the paper. A uniform magnetic field is applied in the direction perpendicular to the planes. Analytical solution for the base flow velocity and temperature distribution is obtained. Linear stability of the base flow is analyzed numerically. Numerical results show stabilizing effect of the magnetic field and destabilizing effect of inhomogeneity of internal heat sources.

INTRODUCTION

The development of methods for biomass utilization and energy production is related to extensive mathematical and experimental modeling with the objective to identify factors that enhance mixing and promote more efficient energy conversion [1]. It is shown in [1] that internal heat sources and external magnetic field play an important role in the developoment of flow instability. Linear stability of flows with internal heat generation is investigated in many papers (see, for example, [2],[3],[4]). In the present paper linear stability of a convective flow caused by nonhomogeneous internal heat sources in an external magentic field perpendicular to the direction of the flow is investigated. It is found that inhomogeneity of internal heat sources destabilizes the flow while the increase in the strength of the magnetic field stabilizes the flow.

MATHEMATICAL MODEL

Consider a convective flow of a viscous incompressible fluid between two parallel vertical planes $\tilde{x} = \pm h$. The constant temperatures of both planes, $\tilde{T}_1$ and $\tilde{T}_2$, are assumed to be equal ($\tilde{T}_1 = \tilde{T}_2$). The flow is caused by inhomogeneous heat sources of density $\tilde{Q} = A + B\tilde{x}$. A uniform magnetic field of strength B_0 is applied in the direction perpendicular to the planes. The following dimensionless quantities are chosen as measures of length, time, velocity, temperature, magnetic field and pressure, respectively: h, h^2/ν, $g\beta Q_0 h^4/(2\nu)$, $Q_0 h^2/2$, B_0, $\rho g\beta Q_0 h^3/2$. The density of internal heat sources in dimensionless form is $Q = Q_0(1+ax)$, where a is constant. The problem is described by four dimensionless parameters $G = g\beta Q_0 h^5/(2\nu^2)$ (the Grashof number), $Ha = B_0 h\sqrt{(\sigma/(\rho\nu))}$ (the Hartmann number), $Pr = \nu/\xi$ (the Prandtl number) and $Pr_m = 1/(\nu\sigma)$ (the magnetic Prandtl number). Here ρ is the density of the fluid, β is the coefficient of thermal expansion, σ is the conductivity, ν is the kinematic viscosity and ξ is the thermal conductivity.

There exists a steady solution of the magnetohydrodynamic equations of thermal convection in the Boussinesq approximation:

$$\mathbf{v} = (0, 0, v_0(x)), \quad \mathbf{B} = (1, 0, b_0(x)), \quad T = T_0(x), \quad p = p_0(z). \tag{1}$$

The functions $v_0(x)$, $T_0(x)$, $b_0(x)$ and $p_0(z)$ satisfy the following system of ordinary differential equations:

$$-\frac{dp_0}{dz} + v_0'' + \frac{Ha^2}{GPr_m} b_0' + T_0 = 0, \tag{2}$$

$$GPr_m v_0' + b_0'' = 0, \tag{3}$$

$$T_0'' + 2(1 + ax) = 0, \tag{4}$$

where dp_0/dz is constant. The boundary conditions are

$$v_0(\pm 1) = 0, \quad T_0(\pm 1) = 0, \quad b_0(\pm 1) = 0. \tag{5}$$

The fluid layer is assumed to be closed so that the total fluid flux through the cross-section of the channel is zero:

$$\int_{-1}^{1} v_0(x)\, dx = 0. \tag{6}$$

It follows from (2)–(6) that the velocity and temperature distribution of the steady flow are given by

$$\begin{aligned} v_0(x) &= \frac{2(\cosh Hax - \cosh Ha)}{3Ha(Ha\cosh Ha - \sinh Ha)} + \frac{2a}{Ha^4 \sinh Ha}\sinh Hax \\ &\quad + \frac{(1-x^2)}{Ha^2} + \left(\frac{a}{3Ha^2} - \frac{2a}{Ha^4}\right) - \frac{a}{3Ha^2}x^3, \qquad (7) \\ T_0(x) &= 1 - x^2 + \frac{ax}{3}(1-x^2). \qquad (8) \end{aligned}$$

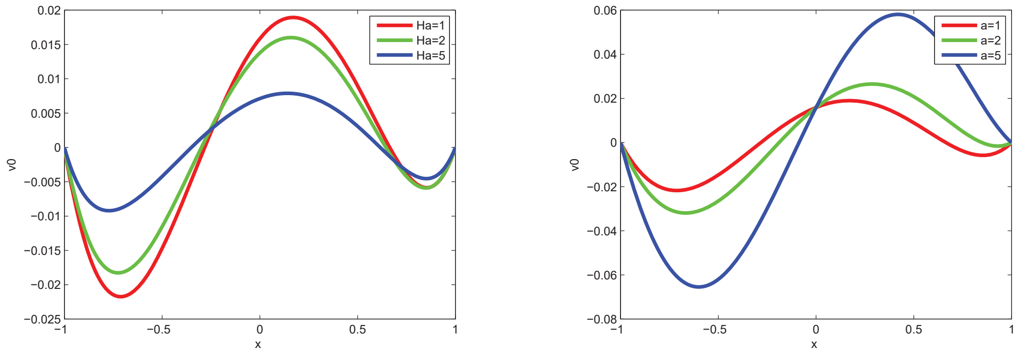

FIGURE 1. Base flow velocity distribution

Base flow velocity distribution is shown in Fig. 1. The velocity profiles for different values of the Hartmann number and $a = 1$ are shown in the left part of the graph. The right part of the graph plots the velocity ptofiles for $Ha = 1$ and different values of a. Fig. 2 shows the base flow temperature distribution for different values of a.

Consider a perturbed motion of the form

$$\mathbf{v} = \mathbf{v}' + v_0\mathbf{k}, \quad T = T' + T_0, \quad p = p' + p_0, \quad \mathbf{b} = \mathbf{b}' + b_0\mathbf{k}, \tag{9}$$

where $\mathbf{v}'$, T', $\mathbf{b}'$ and p' are small unsteady perturbations. Substituting (9) into the system of the magnetohydrodynamic equations under the Boussinesq approximation, linearizing the system in the neighborhood of the base flow (7), (8), dropping the primes, introducing the stream function by the relations $v_x = -\psi_z$, $v_z = \psi_x$ and assuming perturbations of the form

$$\psi(x,z,t) = \varphi(x)\exp(ikz - \lambda t), \tag{10}$$

$$T(x,z,t) = \theta(x)\exp(ikz - \lambda t), \tag{11}$$

where k is the wave number and λ is a complex eigenvalue, we obtain the system of two ordinary differential equations for the functions $\varphi(x)$ and $\theta(x)$ subject to noslip boundary conditions for the function $\varphi(x)$ and zero boundary conditions for the function $\theta(x)$. The boundary value problem is discretized using collocation method. The corresponding generalized eigenvalue problem (after discretization) is solved numerically for different values of the parameters of the problem.

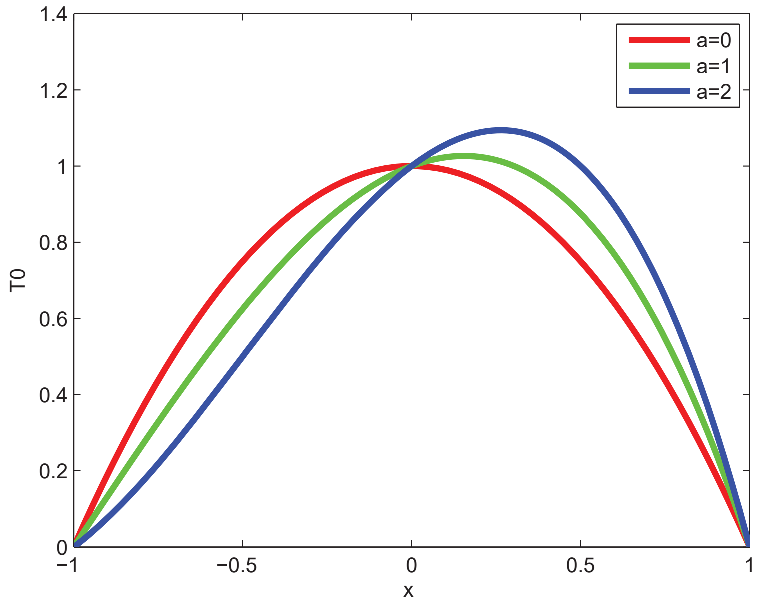

FIGURE 2. Base flow temperature distribution.

NUMERICAL RESULTS

Marginal stability curves are shown in Fig. 3 for two different sets of the parameters of the problem. The graph on the left in Fig. 3 shows three marginal stability curves for the case $Ha = 0$ and three values of a, namely, $a = 0, 1, 2$ (from top to bottom). Thus, the increase in the parameter a destabilizes the flow. The graph on the right in Fig. 3

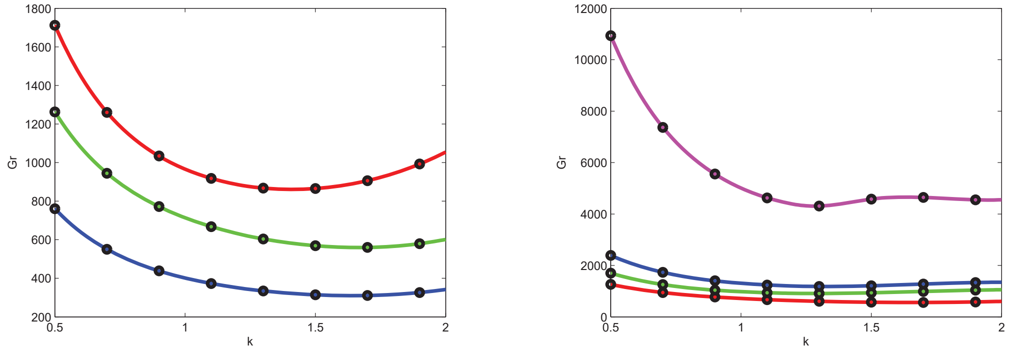

FIGURE 3. Marginal stability curves.

shows marginal stability curves for the case $a = 1$ and four values of Ha, namely, $Ha = 0, 1, 2, 5$ (from bottom to top). Hence, the increase in the strength of the magnetic field stabilizes the flow.

Fig. 4 plots the critical values of the Grashof number versus a and Ha.

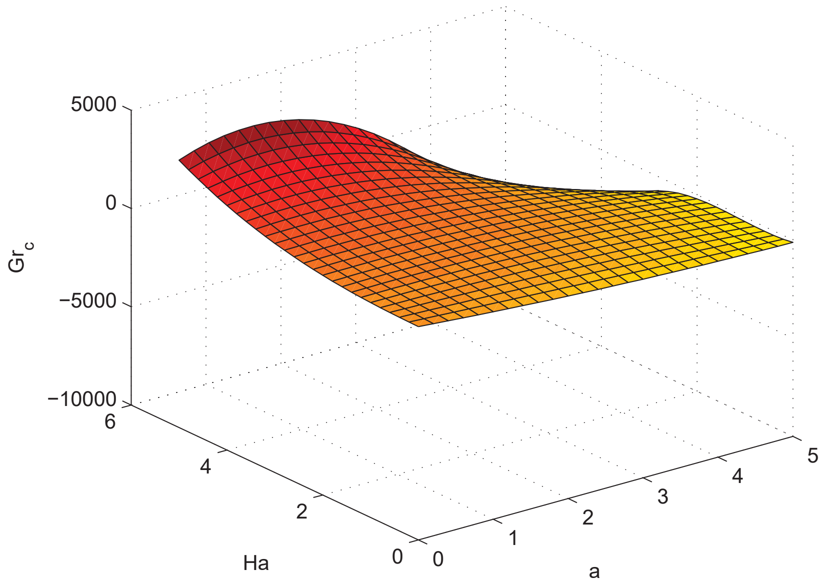

FIGURE 4. Marginal stability surface.

The stabilizing effect of the magnetic field and destabilizing effect of the nonhomogeneity of the heat sources is clearly seen from the graph.

CONCLUSIONS

Linear stability of a convective flow generated by nonhomogeneous heat sources in a magnetic field is investigated in the paper. It is found that the flow is governed by the concurrence between stabilizing effect of the magentic field and destabilizing effect of inhomogeneity of the internal heat sources. Nonuniform internal heating is recommended to enhance mixing processes during biomass thermal conversion.

REFERENCES

[1] I. Barmina, I. Kolmickovs, R. Valdmanis, M. Zake, and H. Kalis, Chem. Eng. Trans. **50**, 121–126 (2016).
[2] A. Kolyshkin and V. Koliskina, JP J. Heat Mass Transfer **15**, 515–530 (2018).
[3] B. F. Wang, D. J. Ma, C. Chen, and D. J. Sun, J. Fluid Mech. **711**, 27–39 (2012).
[4] B. F. Wang, L. Zhou, Z. H. Wan, D. J. Ma, and D. J. Sun, Phys. Review E **94**, p. 013108 (2016).

Identification of Informative Time Frames for System Identification Purposes - A Time-Varying Order of Excitation Assessment Approach

Simon Genser[1,a)], Georg Stettinger[1] and Franz Holzinger[1]

[1] *VIRTUAL VEHICLE Research Center, Inffeldgasse 21a, 8010 Graz, Austria*

[a)] Corresponding author: simon.genser@v2c2.at

Abstract. The most informative time-frame for performing system identification is crucial for a satisfying performance of every system identification based method or algorithm, which is often applied in control systems, simulations or signal processing for example. A detailed signal analysis leading to a time-varying order of excitation is utilized for the determination of the most informative time frame for identifying the required surrogate model. A short-time fourier transformation based approach for computing this time-varying order of excitation is introduced. The method is robust against noise or small disturbances. It is evaluated at an artificially generated signal and at a speed signal of co-simulated hybrid electric vehicle.

INTRODUCTION

Model-based algorithms and methods are widespread in many different fields, for example control systems, signal processing or simulation to name a few. Especially in the field of co-simulation, see [1], the utilization of model-based coupling methods, see [2, 3, 4, 5], leads to improved aspects according stability, accuracy and performance. The question of access to the necessary model information is always crucial and in most cases not easy to answer. The model itself provides this information just in rare cases, therefore typically system identification methods are utilized to identify the required surrogate model. Classical system identification approaches strongly rely on so called persistently exciting signals, these are signals which are rich of specific model information, see [6] for more details.
Least Square methods, see [6], Subspace methods, see [7], or state space identification, see [8], require the in- and output signals of the real model to create the surrogate model. All these algorithms assume that the input signal contains enough information, more precisely the excitation of the input signal has to be sufficient. To measure this the computation of the so-called order of the excitation is required. The higher the order of excitation is, the more detailed the underlying model can be and the more accurate the model parameters can be identified.
The herein proposed method computes the order of the excitation as a time-varying function, this makes it possible to determine the most informative time frame where the required surrogate model should be identified. Therefore the computation of the time-varying order of excitation is a perfectly suited method for a post-process signal analysis. Based on the determined known informative time-frame for the system identification, the simulation can be rerun and the identified surrogate model can be improved by identifying it exclusively at the appropriate time frames.
The paper is organized as follows: Section 2 describes the introduced method for the computation of the time-varying order of excitation, which is based on a short-time fourier transformation, see [9]. The validation of the introduced method is carried out at an artificially generated signal and at a speed signal from a co-simulated hybrid electric vehicle, to demonstrate the practical value of the proposed method.

COMPUTATION OF THE TIME-VARYING ORDER OF EXCITATION

This section describes the method for the computation of the time-varying order of excitation. The order of excitation can be determined with the help of the fourier transformation, because a signal with an order of excitation n has n

spectral lines in the frequency domain, see therefore [6]. This directly leads to the conclusion that a signal consisting of n different sinusoids has an order of excitation of $2n$. In the following pseudo-code u denotes the scalar input signal of a model, all details to the pseudo-code are explained next to it:

```
1: compute the ideal sampled signal ũ from u
2: choose the parameters ws and n
3: for i = 1, . . . , #windows do
4:     ũ(window_i) = ũ(window_i) − mean(ũ(window_i))
5:     compute P(i) := intensity distribution with FT of ũ(window_i)
6: end for
7: th := mean(P)
8: for i = 1, . . . , #windows do
9:     ooe(i) := 2· number of local maxima in P(i) > th
10: end for
```

In line 1 the problem of oversampling is avoided by determining the ideal sampled signal $\tilde{u}$. This is performed by an approach of computing the ideal constant step-size, see therefore [10]. In line 2 the two parameters, the window size ws and the number of frequency partitions n, of the fourier transformation FT are chosen. Due to the window size and the entire number of samples of $\tilde{u}$ the number of windows $\#windows$ is determined.

The signal $\tilde{u}$ is made zero-mean for every window independently in line 4, which makes it invariant against offsets. The intensity distribution $P(i)$ of the frequencies of $window_i$ is computed based on the fourier transformation FT in line 5. The threshold th computed in line 7 is needed to cancel out noise and disturbances in the intensity distribution. This is carried out in line 9, where the order of excitation ooe is computed for every window individually, leading to a time-varying order of excitation. The multiplicative factor 2 in line 9 arises from the fact that the herein-used fourier transformation computes the single-sided spectrum only.

Note: The determination of pauses (e.g. engine idle phase), time frames where the order of excitation is zero, is also possible with this approach.

VALIDATION

The validation of the introduced method is carried out at an artificially generated signal because therefore the analytic time-varying order of excitation is known and can be utilized as a reference solution. For representing the practical value and applicability at an industrial example, a speed signal from a co-simulated hybrid electric vehicle, for details see[3], has been chosen.

Artificially Generated Signal

The artificially generated signal, see Fig. 1, is made up of a sinusoids function between 0 and 2 seconds, following a constant phase between second 2 and 4. From second 4 until 7 the signal is composed of the superposition of three sinusoid with different frequencies following a constant phase with noise from second 7 until 9. From second 9 until 10 the signal is composed of jumps with different height. The identified time-varying order of excitation coincides with the reference solution, because for every sinusoid in a signal the order of excitation increases for 2. Therefore a constant function is of order 0 and jumps has theoretically an order of ∞, which is here depicted with a high order of excitation, as can been seen in the lower part of Fig. 1 from second 9 until 10. Due to the filtering based on the threshold th, see line 7 in the pseudo-code, the noisy phase between second 7 and 9 is assigned with an order of excitation of 0, which is perfectly correct. This means that, the introduced method for computing the time-varying order of excitation perfectly works for dynamical signals including pauses and noisy parts.

Hybrid Electric Vehicle - Speed Signal

For demonstration of the practical applicability of the introduced method a speed signal of a co-simulated hybrid vehicle has been chosen, see middle part of Fig. 2. There, the most informative time frames for system identification are highlighted with a green dashed rectangular and also the identified pauses are denoted with a red dotted rectangular. These rectangulars are constructed based on the order of excitation, depicted in the lower part of Fig. 2. Every time frame where the order of excitation is beneath the red dotted line is a pause and where it is above the green dashed line, it is a informative time frame for system identification. The parameter of the window size ws should be chosen in such a way that, the dynamics of the system can be displayed in a window but choosing it too large, would blur the results. Therefore the rule of thumb is to choose the window size as big as necessary and as small as possible.

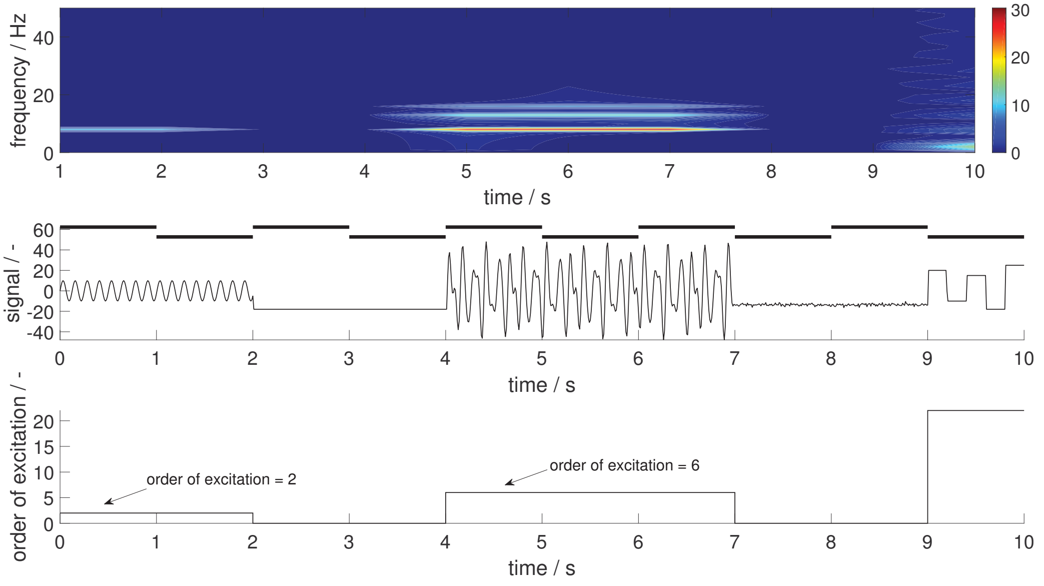

FIGURE 1. Artificially generated signal: the upper part depicts the intensity distribution based on the short-time fourier transformation; the middle part shows the signal and the black bars denote the non-overlapping windows; the lower part denotes the time-varying order of excitation, used parameters: $ws = 1\ s$, $n = 100$, $Ts = 0.01\ s$.

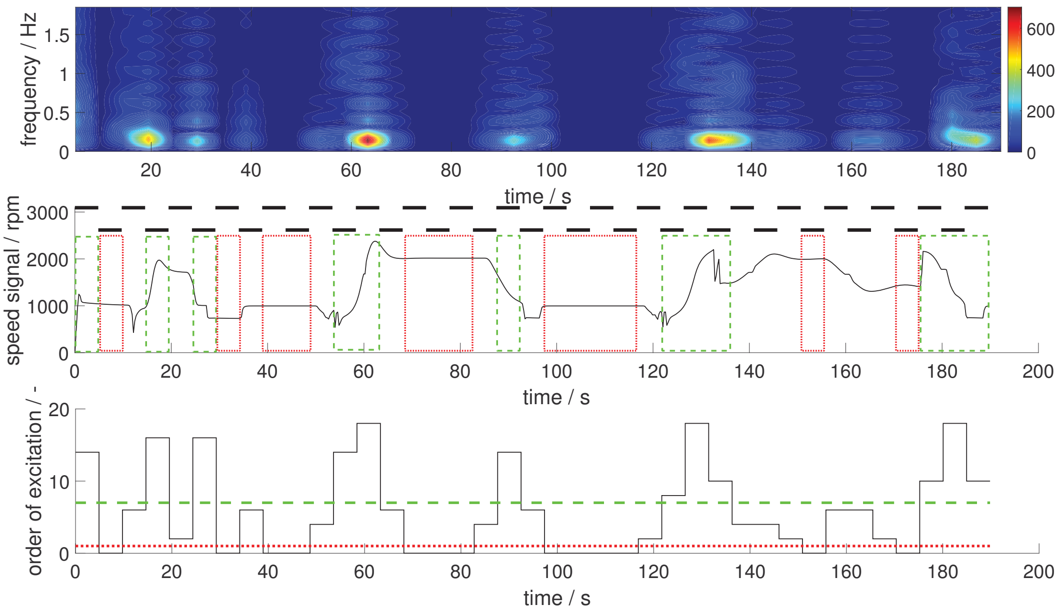

FIGURE 2. Speed-signal of a co-simulated hybrid electric vehicle: the upper part depicts the intensity distribution based on the short-time fourier transformation; the middle part shows the signal and the black bars denote the non-overlapping windows, the green dashed rectangulars denotes the parts with a high order of excitation and the red dotted rectangulars the identified pauses; the lower part denotes the time-varying order of excitation, where the time frames with a high order of excitation (above green dashed line) and the pauses (beneath red dotted line) are highlighted, used parameters: $ws = 5\ s$, $n = 100$, $Ts = 0.01\ s$.

SUMMARY, CONCLUSION & FUTURE WORK

The introduced method computes a time-varying order of excitation based on a short-time fourier transformation of the input signal. This is a crucial information for determining the optimal time frames for performing system identification tasks, due to the fact that the order of excitation is too low the identified model is of poor quality or unusable if the model order is greater than the order of excitation. Additional, pauses in the signal can be identified. Due to a filtering, based on the intensity of the frequencies, noise or disturbances in the signal are ignored and does not distort the computed order of excitation. The method is also robust against offsets in the signal, because the signal is made zero-mean for every window independently.

The validation of the method at an artificially generated signal shows that it coincides exact with the known reference solution. The performance of the method is also satisfying for the case of a speed signal from a co-simulated hybrid electric vehicle. This shows that the introduced method produces useful and satisfying results also for industrial cases.

A detailed analysis of the influence of the window size to the results will be carried out in the future. Improving the quality of the identified surrogate model for model-based co-simulation coupling algorithms, especially for [2] and [3], will also be a focus in the future.

ACKNOWLEDGMENTS

The publication was written at VIRTUAL VEHICLE Research Center in Graz, Austria. The authors would like to acknowledge the financial support of the COMET K2 Competence Centers for Excellent Technologies Programme of the Federal Ministry for Transport, Innovation and Technology (bmvit), the Federal Ministry for Digital, Business and Enterprise (bmdw), the Austrian Research Promotion Agency (FFG), the Province of Styria and the Styrian Business Promotion Agency (SFG).

REFERENCES

[1] R. Kübler and W. Schiehlen, eds., *Two Methods of Simulator Coupling* (Mathematical and Computer Modelling of Dynamical Systems, 2010).

[2] S. Genser and M. Benedikt, eds., *A Pre-Step Stabilization Method for Non-Iterative Co-Simulation and Effects of Interface-Jacobians Identification*, Simulation and Modeling Methodologies, Technologies and Applications - Advances in Intelligent Systems and Computing (Springer Verlag, 2019 - submitted).

[3] G. Stettinger, M. Horn, M. Benedikt, and J. Zehetner, eds., *A Model-Based Approach for Prediction-Based Interconnection of Dynamic Systems* (53rd IEEE Conference on Decision and Control, 2014).

[4] T. Haid, G. Stettinger, D. Watzenig, and M. Benedikt, "A model-based corrector approach for explicit co-simulation using subspace identification," (The 5thJoint International Conference on Multibody System Dynamics, 2018).

[5] M. Arnold, "Numerical stabilization of co-simulation techniques, the ODE case," (Martin Luther University Halle-Wittenberg NWF II-Institute of Mathematics, 2011).

[6] L. Ljung, *System Identification: Theory for the User*, 2nd ed. (PTR Prentice Hall Information and System Sciences Series, Prentice Hall, New Jersey,, 1999).

[7] P. V. Overschee and B. D. Moor, *Subspace Identification for Linear Systems*, 1st ed. (Kluwer Academic Publishers, London, 1996).

[8] M. Giesbrecht, G. Barreto, and C. P. Bottura, eds., *State Space Identification Algorithm based on Multivariable Impulse Response* (2018).

[9] J. Allen, ed., *Short term spectral analysis, synthesis, and modification by discrete Fourier transform* (IEEE Transactions on Acoustics, Speech, and Signal Processing, 1977).

[10] S. Genser, F. Holzinger, and G. Stettinger, "Computation of the ideal step-size - a constant and adaptive approach," (ICCMSE 2019 - 15th International Conference of Computational Methods in Sciences and Engineering, 2019 - submitted).

Micromagnetic Simulation of Fast GHz Gyromotion of Magnetic Vortex Core in Permalloy Disk with Antidot

Je-Ho Shim[1,2,3], Yikyung Yu[4,5], Daniel M. Tartakovsky[4,7], Hong-Guang Piao[5,6], Sang-Hyuk Lee[1,5], Dong Eon Kim[2,3], Seong-Cho Yu[1], and Dong-Hyun Kim[1,5 a)]

[1] *Department of Physics, Chungbuk National University, Cheongju 28644, South Korea*

[2] *Center for Attosecond Science and Technology and Department of Physics, POSTECH, Pohang 37673, South Korea*

[3] *Max Planck Center for Attosecond Science, Pohang, 37673, South Korea*

[4] *Department of Mechanical and Aerospace Engineering, University of California, San Diego, La Jolla, CA 92093 USA*

[5] *Research Institute for Nanoscale Science and Technology, Chungbuk National University, Cheongju 28644, Chungbuk, South Korea*

[6] *College of Science, China Three Gorges University, Yichang 443002 P. R. China*

[7] *Department of Energy Resources Engineering, Stanford University, Stanford, CA 94305, USA*

[a)] Corresponding author: donghyun@cbnu.ac.kr

Abstract. We report our micromagnetic simulation investigation of the magnetic vortex core motion in a disk with an antidot. With variation of antidot geometry, faster core gyration is expected, where gyrotropic motion near antidots becomes quite sensitively depending on the antidot geometry, with frequency up to several GHz. Our finding opens a possibility to boost up the core motion of a ferromagnetic nanostructure with introducing geometrical modulation.

The control of magnetic vortex dynamics becomes essential in realization of future spintronic devices based on vortex core (VC). In particular, a gyromotion of magnetic VC has attracted much attention for application as a frequency generator [1,2]. However, the gyro-frequency is observed to be usually around few hundreds MHz in case of typical ferromagnetic nano- or micro-disk, which is considered to be relatively slow for some applications requiring a faster operation. Various work has been devoted to understanding of the VC motion in a disk. Generally, it is known that the VC can be described by a collective coordinate motion in terms of gyrotropic and damping terms. VC is observed to exhibit a gyrotropic motion around the center of a disk under external magnetic fields or spin currents and find an equilibrium point, usually at the center of the disk, with losing kinetic energy due to the damping term. Numerous studies have been devoted to modify the gyrotropic motion frequency since it is directly linked to the generated frequency by the VC-based oscillator.

In this work, we have carried out micromangnetic simulations of the gyromotion of the magnetic VC in a permalloy disk with a square antidot at the center, by means of object oriented micromagnetic framework (OOMMF) [3], where we have systemically varied the size of the antidot. The cell size was $2.5\times2.5\times2.5\ nm^3$, and the damping constant was set to be 0.01. Locating the antidot at the center, it is expected that the VC motion should experience severe modification. Schematic diagram of the ferromagnetic disk under consideration in the present study is illustrated in Fig. 1(a). The diameter of the disk is 500 nm, and the thickness is 15 nm. The length of the antidot (d)

of 5,10, and 15nm and the height (h) of 5,10, and 15 nm are considered. Initially, the VC is off from the center of the disk under a constant magnetic field. After turning off the applied field, VC is back to center with gyrotropic motion of ~300 GHz frequency. The VC trajectory in this case for the region far from the antidot is plotted on the left of Fig. 1(b), while the VC trajectory near the antidot is plotted on the right of Fig. 1(b).

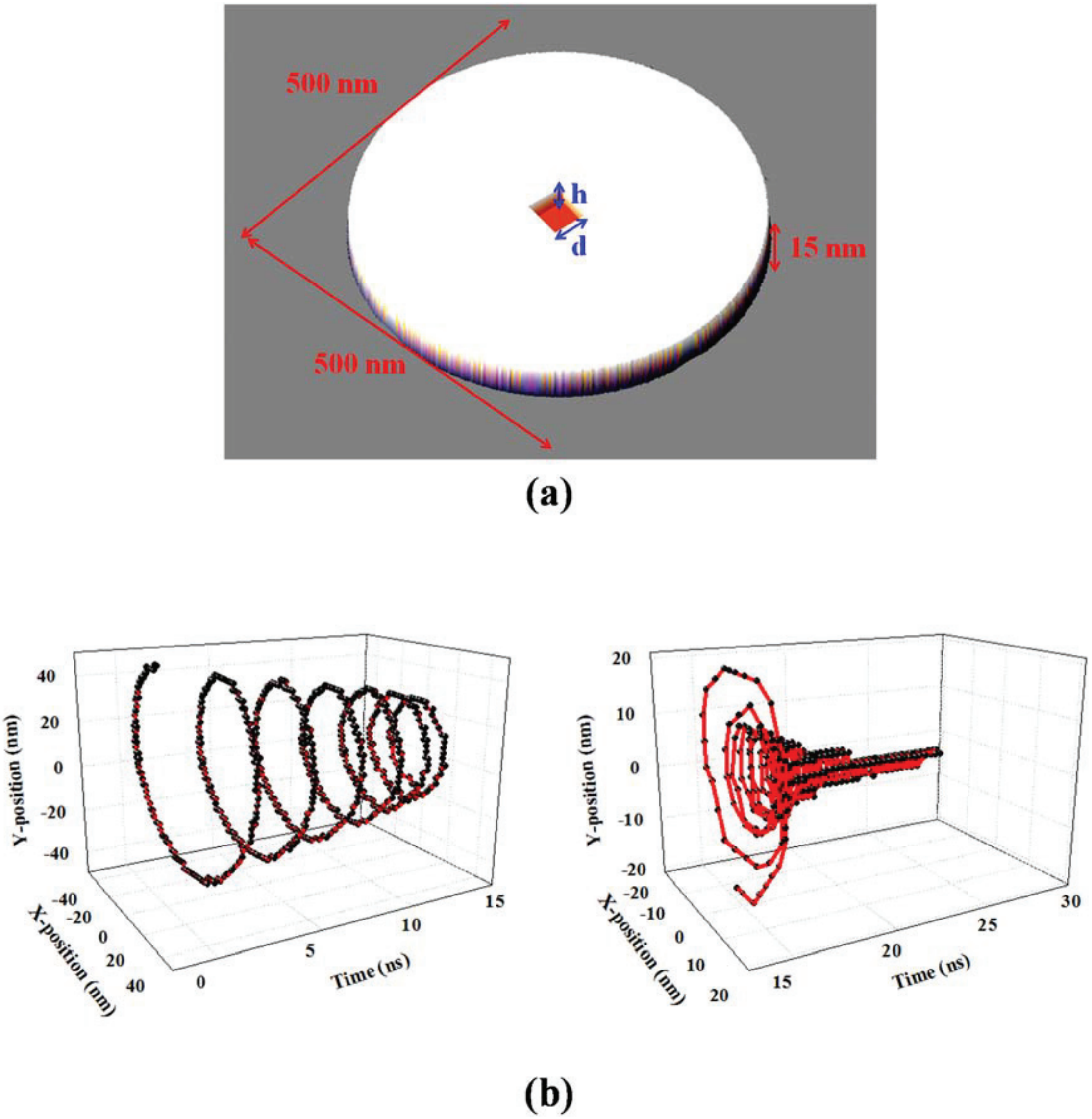

FIGURE 1. (a) The geometry of the permalloy disk with the antidot. (b) The trajectory of the VC in the permalloy disk with the antidot. (Left) Initial VC trajectory away from the antidot and (right) near the antidot.

It is interesting to note that, when VC is close to the antidot, gyrotropic motion becomes substantially faster, reaching, surprisingly to the range of GHz with period of well below sub-ns. To investigate further, we have analyzed magnetization profiles with respect to time, as seen in Fig. 2.

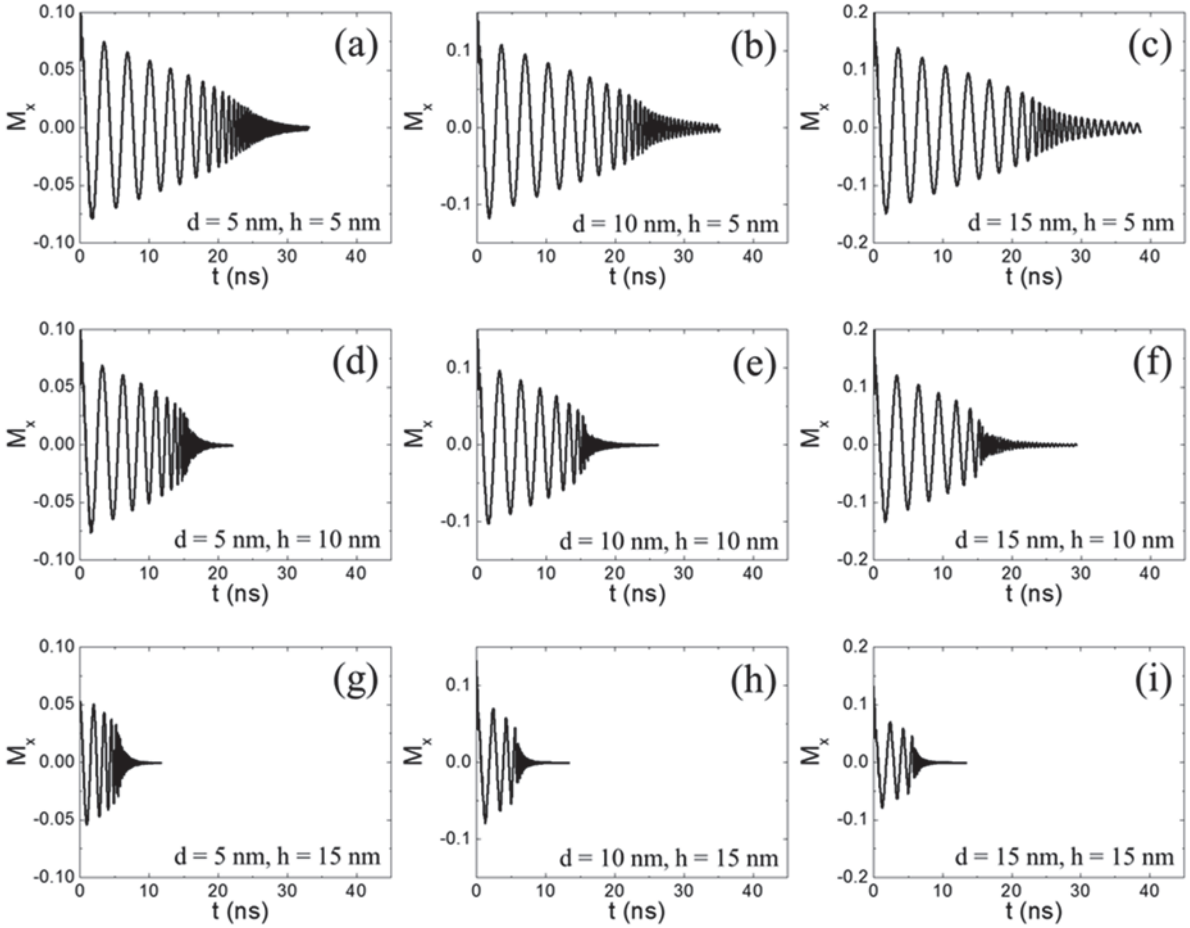

FIGURE 2. Magnetization profiles along the x-axis (a certain direction in the disk plane) are plotted for various combinations of d and h. (a) (5,5), (b) (10,5), (c) (15,5), (d) (5,10), (e) (10,10), (f) 15,10), (g) (5,15), (h) (10,15), (i) (15,15).

As seen in the figure, a drastic change of motion is observed when the VC approaches to the antidot region. The frequency increases extremely while the amplitude decreases significantly, but with a still detectable oscillation. Considering the main drawback of the VC is the slow frequency limited to the sub-GHz, our finding might be meaningful for future application based on the VC. In case of full antidot (hole), the VC trajectories are shown in Fig. 2(g)-(i), where similar behaviors are found, but core motion lifetime becomes substantially shorter due to the earlier annihilation of the VC in the hole.

To investigate further, we have carried out Fast Fourier Transformation (FFT) analysis, as depicted in Fig. 3. In all cases, the main gyrotropic frequency peak is observed under 1 GHz. Very interestingly, the second peak, corresponding to the boosted VC motion near the antidot, is clearly observed for all cases. The most interesting case is for d = 5 and h = 10 (Fig. 3(d)), where the boosted VC gyrotropic motion frequency reaches up to 6 GHz. In case of full antidot, the frequency even reaches up to 7 GHz, while the lifetime of the VC motion is less than 10 ns, as in the case of Fig. 2(g)-(i).

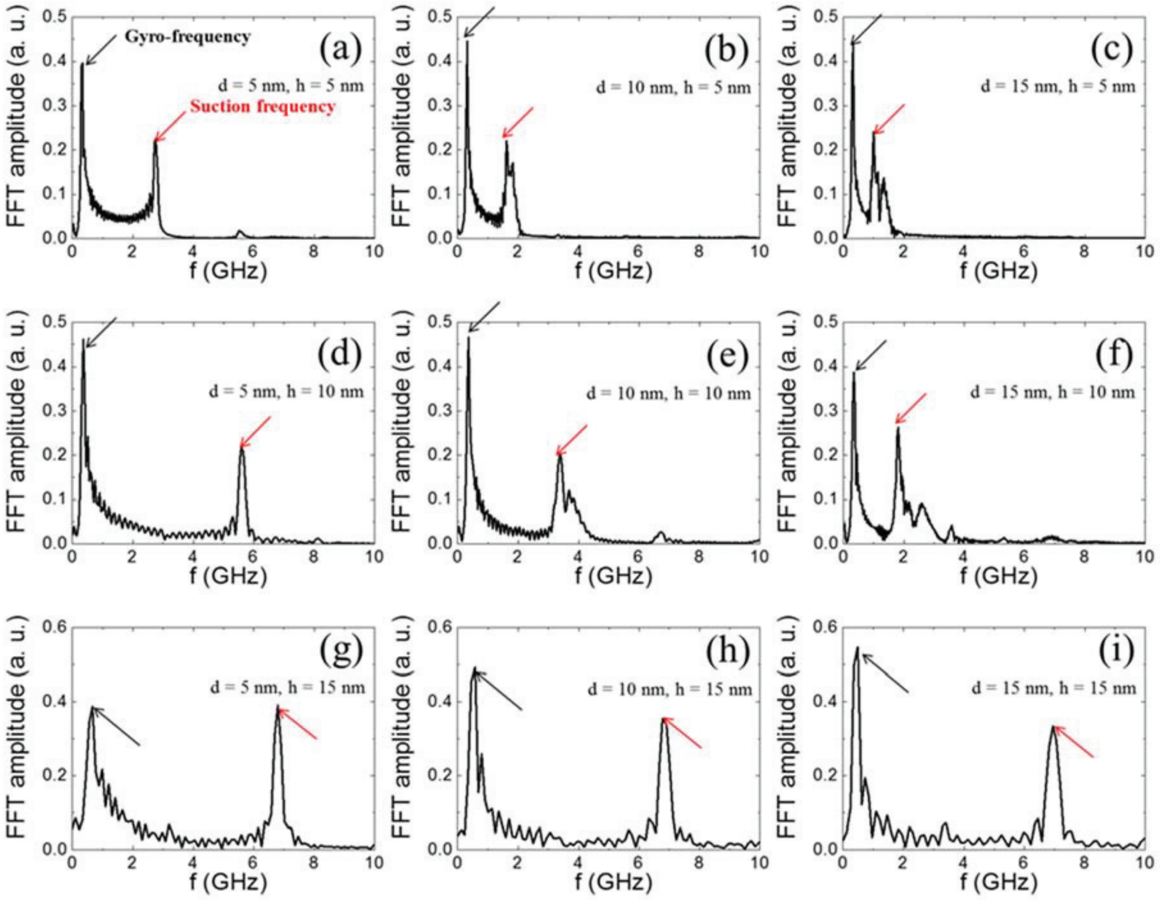

FIGURE 3. FFT results for various combination of d and h, corresponding to the Fig. 2. (a) (5,5), (b) (10,5), (c) (15,5), (d) (5,10), (e) (10,10), (f) (15,10), (g) (5,15), (h) (10,15), (i) (15,15).

In summary, we report our micromagnetic investigation on the possibility of controlling gyrotropic motion of VC, boosting the frequency up to several GHz ranges simply by introducing the antidot structure. In practice, this antidot can be easily introduced using various lithographic technique such as focused ion beam so that the possibility of boosting VC motion up to GHz range might be doable for real applications.

ACKNOWLEDGMENTS

This research has been supported in part by Global Research Laboratory Program [Grant No 2009-00439] and by Max Planck POSTECH/KOREA Research Initiative Program [Grant No 2016K1A4A4A01922028] through the National Research Foundation of Korea (NRF) funded by Ministry of Science, ICT & Future Planning. This research was supported by Basic Science Research Program through the National Research Foundation of Korea (NRF) funded by the Ministry of Education [Grant No 2017R1A6A3A04011173]. This study was supported by Korea Research Foundation (NRF) grant No. 2018R1A2B3009569 and a KBSI Grant D39614.

REFERENCES

1. B. Pigeau, et al. *Appl. Phys. Lett.* **96**, 132506 (2010).

2. A. Dussaux, et al. *Appl. Phys. Lett*. **98**, 132506 (2011).

3. M. J. Donahue and D. G. Porter. OOMMF User's Guide, http://math.nist.gov/oommf (2002).

Identification and Classification of Signal Types and Critical Loops to Support Configuration of Co-Simulation

Franz Rudolf Holzinger[1,a)], Simon Genser[1] and Georg Stettinger[1]

[1] *VIRTUAL VEHICLE Research Center, Inffeldgasse 21a, 8010 Graz, Austria*

[a)]Corresponding author: franzrudolf.holzinger@v2c2.at

Abstract. An approach to identify critical loops within connected systems especially in co-simulation frameworks is presented. Therefore a classification of the coupling signals is done to distinguish between different types of signals: continuous, discontinuous, discrete and flat. Based on this classification structural loops between the connected subsystems are identified and rated to get critical loops in sense of coupling effort. This information supports application engineers to identify critical signals from a coupling point of view and to set proper coupling methods to handle these coupling signals efficiently.

INTRODUCTION

The growing complexity of simulation models makes it almost impossible to solve complete systems within a simulation environment. Different systems and domains have developed their own specific simulation environments and solvers to provide proper tools for specific tasks. Co-simulation is a technology which has been developed to integrate the different subsystems to a closed simulation.
However, co-simulation has some drawbacks. For instance, a causality problem exists when subsystems possess bidirectional dependencies. Extrapolation filters are used in order to avoid causality problems, but these induce coupling errors to the co-simulation [1]. A number of coupling methods to compensate these coupling errors exist: for example signal based coupling approaches, which (nearly) compensate the energy of the extrapolation error [2] and model based techniques, that use an estimated model for the extrapolation and compensate the overall coupling error [3, 4, 5].
Nevertheless, the compensation methods have to be configured in a proper way. The increasing number of subsystems in co-simulation models and so the increasing number of coupling signals makes it more and more difficult for application engineers to focus on the relevant coupling signals during the configuration. The classification of signals and identification of critical loops is an important information for each co-simulation application engineer and can also be used as a possible method to handle an automated configuration for co-simulation [6].

IDENTIFICATION OF SIGNAL TYPES

Different signal types enable the application of special coupling approaches or disqualify them. For instance, discrete and discontinuous signals can only be reasonably coupled by ZOH (zero-order-hold) extrapolation technique, where the last known value is used for the next coupling step. In the following an identification method is shown, which categorizes piecewise a signal in one of four following types: *continuous, discontinuous, discrete* and *flat*.
Therefore four samples $x_i, x_{i-1}, x_{i-2}, x_{i-3}$ are used to determine gradients between the samples $\Delta x_i = x_i - x_{i-1}$, $\Delta x_{i-1} = x_{i-1} - x_{i-2}$ and $\Delta x_{i-2} = x_{i-2} - x_{i-3}$. The change of the differences sign is a measure of the signal type. Table 1 shows the classification of the different signal types with an illustration.

To describe the whole signal a calculation window with 4 samples is moved over the signal. One of the four signal types is assigned to each window. In order to obtain a quantitative value for the entire signal, each signal type is weighted by a value $w_i \in [0, 1]$. For instance, a continuous identification is assigned by $w_i = 0$ and a discrete one is

TABLE 1. Classification of signal types

Classification	Plot	Description	Weight w_i
continuous	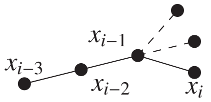	*sign* $\{\Delta x_i, \Delta x_{i-1}, \Delta x_{i-2}\}$ changes max. once: e.g. $\pm\{1,1,0\}$, $\{-1,1,1\}$ etc.	0
flat	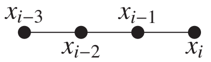	*sign* $\{\Delta x_i, \Delta x_{i-1}, \Delta x_{i-2}\}$ is zero: $\{0,0,0\}$	*unused*
discontinuous	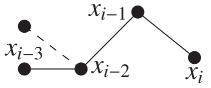	*sign* $\{\Delta x_i, \Delta x_{i-1}, \Delta x_{i-2}\}$ changes more than once: e.g. $\{1,-1,1\}$, $\{1,0,-1\}$, $\{0,1,-1\}$, etc.	0.9
discrete	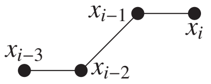	*sign* $\{\Delta x_i, \Delta x_{i-1}, \Delta x_{i-2}\}$ is zero and change once in between: $\{0,\pm 1,0\}$	1

weighted by $w_i = 1$. At the end the mean value s of all weights w_i along several windows are determined, except the flat (unused) windows. The flat identification is ambiguous and can be interpreted as continuous as well as discrete signal and so, it does not include additional information and is not considered in the calculation of the signal type s. Figure 1 shows an example of the identification of the signal types. On the top left figure a mixed benchmark signal is shown. The signal includes discrete, continuous, discontinuous and flat parts. The bottom left plot shows the classification by the presented approach. All discontinuities and the discrete jumps are identified correctly, as well as the flat region at the beginning of the signal.

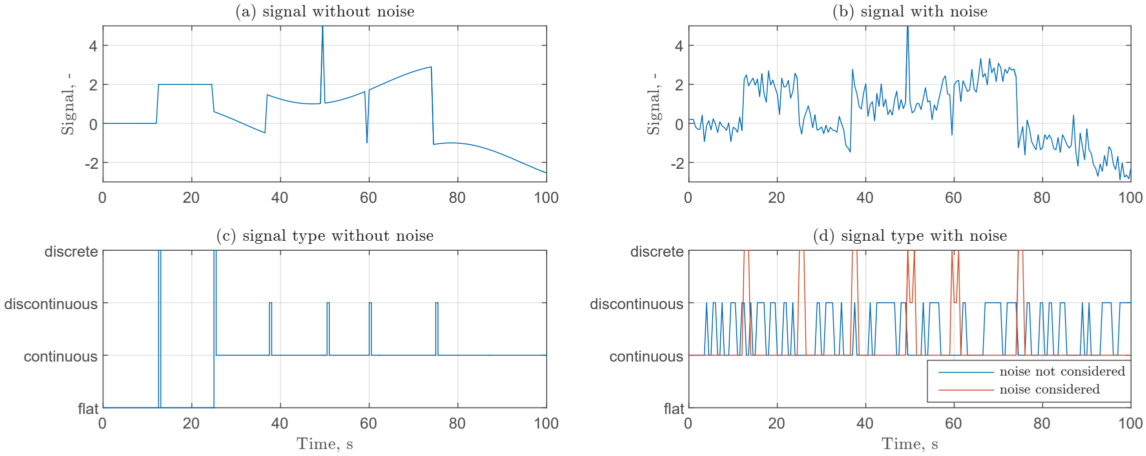

FIGURE 1. Identification of signal types: (a) signal without noise; (b) signal with additional noise; (c) identified signal types of signal without noise; (d) identified signal types of signal with additional noise.

The signal on the top right side is corrupted by noise. If the approach is directly applied to the signal, many discontinuities are identified, as shown in the first signal below right. In order to interpret the signal types of noisy signals noise, the variance of the signal is additionally determined for the identification. In the determined windows, all samples within an ϵ range are interpreted as continuous. The ϵ range depends on the variance σ^2 of the noise and can be defined as $\epsilon = 2 \cdot \sigma$. This approach enables a classification for noisy signals. The identification of flat signals is not possible any more, due to the fact, that the four considered samples with noise do not allow a differentiation between flat and continuous. Details to determine the variance can be found in [7]. This method requires measurements to determine the variance. Therefore, the signal type identification for noisy signals is done after the simulation.

CLASSIFICATION OF SIGNALS AND LOOPS

The identification and quantification of the signals can be used to categorize signals and loops in the co-simulation framework. Figure 2 shows the classification signals and loops. Therefore the identified signal types from the previous chapter are used. The presented categories allow an extraction of critical and relevant signals in the context of co-simulation to define suitable extrapolation filters and coupling algorithms. In the following the categories of the signals and loops are described in detail.

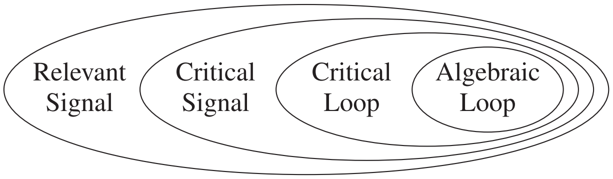

FIGURE 2. Classification of signals and loops

RELEVANT SIGNAL

The term *relevant signal* covers all continuous and physically motivated coupling signals. These signals enable special coupling methods and extrapolation filters. Nearly all of these methods use the dynamics of the signals to extrapolate the next value, by a signal- or model-based estimator. Discrete signals, like status signals cannot be handled by these methods. From the coupling point of view, discrete and discontinuous signals are difficult to treat and to extrapolate in co-simulation. A signal with a calculated signal type s_i is called relevant, if $s_i < \hat{s},\ s_i \in [0, 1]$, where $s_i = 0$ represents a continuous signal and $s_i = 1$ a discrete signal. The level $\hat{s}$ represents a threshold for classifying relevant signals. Discrete and discontinuous signals beyond this level can only be coupled using ZOH extrapolation technique. For signals below the threshold $\hat{s}$, higher order extrapolation techniques as well as advanced coupling approaches can be used.

CRITICAL SIGNAL

Critical signals with a weight c_i are a subset of relevant signals of signal type s_i and contain all coupling variables that are difficult to extrapolate without additional coupling methods, such as special extrapolation filters or correctors. The weight c_i is a measure that results from the dynamics of the signal as well as the subsystems and describes the property of the signal. Details to determine signal weights can be found in [6].
A signal with a weight c_i is called critical if $c_i \geq \hat{c},\ c_i \in [0, 1]$, where $c_i = 0$ qualifier a non-critical and $c_i = 1$ a critical signal.
A critical signal can be treated in several ways. If the co-simulation supports subsystems to be executed sequentially, i.e. that one subsystem calculates after the other, an execution sequence can be selected in which critical signals are not extrapolated. An other possibility is to use advanced coupling methods to handle the critical signals.

CRITICAL LOOP

A critical loop is the result of several critical signals forming a closed loop. For this purpose, all possible loops between the subsystems of the co-simulation are identified. Details to determine loops in a connected system can be found in [8].
A loop is called critical if the sum of the weights c_i within the loop C_j exceeds a limit $\hat{m}$:

$$\frac{1}{N_C} \sum_i c_i > \hat{m} \quad with \quad c_i \geq \hat{c},\ c_i \in C_j.$$

In the case of a critical loop, it is helpful to reduce the coupling step size and/or to use advanced model-based coupling approaches [3, 4, 5].

ALGEBRAIC LOOP

An algebraic loop is given, if several subsystems with direct feed-throughs form a closed loop. A direct feed-through of a subsystem means, that a change at the input is immediately presented at the output. Algebraic loops are hard to handle with co-simulation, so it is very important to identify them. If the knowledge of direct feed-through of a subsystem is known (e.g. FMU [9]), it is straight forward to identify an algebraic loop. Otherwise the property of direct feed-throughs has to be estimated, e.g. by correlation coefficient. An algebraic loop can be understood as a special case of a critical loop.

CO-SIMULATION APPLICATION

Related to co-simulation, an understanding of the signal properties and loops is necessary to define a proper co-simulation configuration, in terms of trigger sequence, extrapolation filter and coupling time steps. The proposed identification and classification approach delivers important information for this purpose. The identified signal types allow at least the exclusion of some extrapolation filters and restricts the usage of appropriate filters. The application engineer's work is made much easier if he can neglect many coupling signals in advance and only has to concentrate on a few important signals instead of dozens. In addition, signal classification in combination with identified loops allows the definition of execution order with respect to all critical signals in the loop.

CONCLUSION AND FURTHER WORK

The presented classification approach allows a simple and fast recognition of signal types. This in turn serves as a basis for the identification of critical signals and loops. The knowledge of these variables makes it possible to identify signals, which require advanced filter techniques. This can be understood as a support for application engineers in co-simulation. In a further step, this information can also be used for an automatic co-simulation configuration approach.

ACKNOWLEDGMENTS

The publication was written at VIRTUAL VEHICLE Research Center in Graz, Austria. The authors would like to acknowledge the financial support of the COMET K2 Competence Centers for Excellent Technologies Programme of the Federal Ministry for Transport, Innovation and Technology (bmvit), the Federal Ministry for Digital, Business and Enterprise (bmdw), the Austrian Research Promotion Agency (FFG), the Province of Styria and the Styrian Business Promotion Agency (SFG).

REFERENCES

[1] C. Gomes, C. Thule, D. Broman, P. G. Larsen, and H. Vangheluwe, "Co-simulation: A survey," (ACM, New York, NY, USA, 2018), pp. 49:1–49:33.

[2] M. Benedikt, D. Watzenig, and A. Hofer, "Modelling and analysis of the non-iterative coupling process for co-simulation," (2013), pp. 451–470.

[3] G. Stettinger, M. Horn, M. Benedikt, and J. Zehetner, eds., *A Model-Based Approach for Prediction-Based Interconnection of Dynamic Systems* (53rd IEEE Conference on Decision and Control, 2014).

[4] S. Genser and M. Benedikt, eds., *A Pre-Step Stabilization Method for Non-Iterative Co-Simulation and Effects of Interface-Jacobians Identification*, Simulation and Modeling Methodologies, Technologies and Applications - Advances in Intelligent Systems and Computing (Springer Verlag, 2019 - submitted).

[5] T. Haid, G. Stettinger, D. Watzenig, and M. Benedikt, "A model-based corrector approach for explicit co-simulation using subspace identification," (The 5thJoint International Conference on Multibody System Dynamics, 2018).

[6] M. Benedikt and F. R. Holzinger, "Automated configuration for non-iterative co-simulation," in *2016 17th International Conference on Thermal, Mechanical and Multi-Physics Simulation and Experiments in Microelectronics and Microsystems (EuroSimE)* (2016), pp. 1–7.

[7] D. Garcia, "Robust smoothing of gridded data in one and higher dimensions with missing values," (2010), pp. 1167–1178.

[8] D. C. Kozen, "Depth-first and breadth-first search," in *The Design and Analysis of Algorithms* (Springer New York, New York, NY, 1992), pp. 19–24.

[9] T. Blochwitz, M. Otter, J. Åkesson, M. Arnold, C. Clauss, H. Elmqvist, M. Friedrich, A. Junghanns, J. Mauss, D. Neumerkel, H. Olsson, and A. Viel, "Functional mockup interface 2.0: The standard for tool independent exchange of simulation models," in *Proceedings of the 9th International Modelica Conference* (The Modelica Association, 2012), pp. 173–184.

Numerical Simulation of Fatigue Crack Growth in Steel-Aluminium Transition Joint

Mateusz Kowalski[1, a)] and Dariusz Rozumek[1, b)]

[1] Department of Mechanics and Machine Design, Opole University of Technology, Mikolajczyka 5, 45-271 Opole, Poland

[b)] *Corresponding author: d.rozumek@po.opole.pl*
[a)] *m.kowalski@po.opole.pl*

Abstract. The paper presents the results of fatigue crack growth simulation of the transition joint for S235JR steel and A5083 aluminum with the Grade 1 titanium interlayer coat and A1050 aluminum. Calculations were performed using ANSYS software. The publication presents the crack growth phenomena observed during fatigue testing. Additionally, calculations of residual stresses distributions induced by the process of joining materials during welding were carried out. Results of crack length calculations were comparable with experimantal data.

INTRODUCTION

The use of welding connectors in various branches increased in recent years, especially in the shipbuilding industry [1]. In the ship constructions, deck components (aluminium alloy) are joined with the steel hull in an example with the screw connections. Traditional screw connections can be replaced with the multilayer transition joints. Joints between materials with different mechanical properties in example steel and aluminum requires the use of appropriate treatments [2–4]. To optimize the process of joining materials one should take into account, among others, the influence of temperature, deformation, resulting in microcracks or residual stresses induced by the welding process. At the design stage, part of the fatigue analysis is performed in the range of fracture mechanics. Crack growth simulations are performed for important construction nodes [5]. Prediction of the fatigue properties and fracture propagation influence operational safety of the designed structures.

The aim of the paper is to present the results of numerical calculations of the welding transition joint using the ANSYS software. The stress distribution results in the connector model were presented without damage and during the crack growth.

MATERIALS PROPERTIES AND CALCULATION MODEL

The analysis was performed for the structural transition joint consisting of fallowing layers: aluminum A5083 (5 mm), aluminum A1050 (1.5 mm), titanium Grade 1 (1 mm), steel S235JR+N (5 mm). Chemical compositions (in mass-%) of the A5083 aluminum are as follows 0.22Si, 0.36Fe, 0.05Cu, 0.60Mn, 4.80Mg, 0.05Zn, 0.03Ti; of the A1050 are: 0.09Si, 0.31Fe, 0.01Mn, 0.01Mg, 0.03Ti; of the Grade 1 are: 0.20Fe, 0.18O, 0.03N, 0.1C, 0.01H and S235JR steel are: 0.14C, 0.67Mn, 0.17Si, 0.019P, 0.011S, 0.020Cr, 0.015Cu, 0.009Ni, 0.009Mo, 0.036Al. Basic mechanical properties of the materials were presented in Table 1. Shape and dimensions of the transition joint specimen were presented in Figure 1. For crack propagation analysis linear model behavior was used.

Analysis of the crack propagation was performed in the ANSYS software using the SMART crack growth tool. For this purpose, two analyses were made: one for the whole specimen, the other for a simplified model of the weldment on the aluminum side.

TABLE 1. Mechanical properties of materials before cladding in the room temperature.

Materials	σ_{02}, MPa	σ_u , MPa	E, MPa	G, MPa	ν	E_t MPa
S235JR+N	235	370	220000	84000	0,3	592
Grade 1	200	324	100000	38000	0.37	420
A1050	114	120	69000	25900	0.33	232
A5083	168	308	71000	26800	0.33	1994

Where: σ_{02} – yield strength at 0.2 plastic strain, σ_u – ultimate strength, E – Young's modulus, G – Shear modulus , ν – Poisson's ratio, E_t – tangent modulus

Comparison between obtained results indicated negligible differences between stress fields (error below 5%). Simulation of the fatigue crack development was carried out using simplified model type.

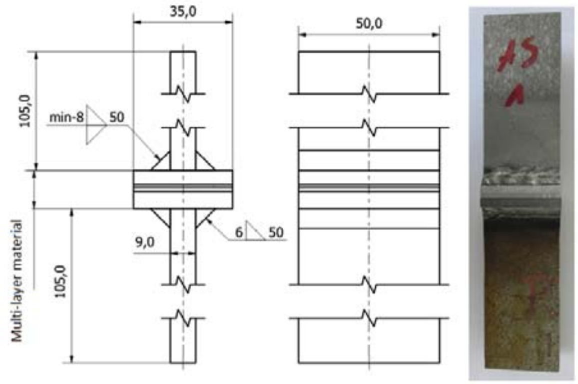

FIGURE 1. Steel-aluminum transition joint and shape and dimensions of the simulated joint.

THE RESULTS OF NUMERICAL CALCULATIONS

Calculations of the residual stress distribution were performed with coupled thermo – mechanical FEM analysis. Heat loading was realized with Goldak volumetric heat source distribution. Temperature dependent mechanical and thermal properties were used in presented model. Length of simulated specimen was equal to 70 mm but distance on which weld was placed was 50 mm with 10mm margins on sides. More detailed description of the calculation process can be found in [6]. Examples of residual stress fields according to Huber-Mises were presented in Figure 2. Figure 2b presents graphs of residual stress present in the structure after welding. Normal stress in the web members obtain maximal values near weld face. The maximum stress value in A5083 was about 164 MPa. In steel plate

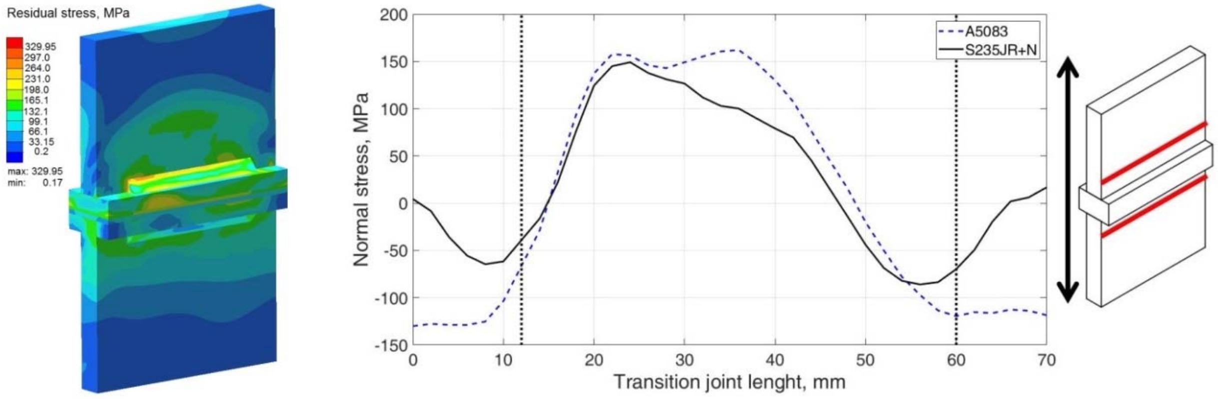

(a) (b)

FIGURE 2. Residual stress distribution (a), normal stress in web members at a distance of 2 mm from weld faces, and stress direction (b) [6].

normal stress reached 150 MPa. The stresses in the range of 100 to 144 MPa have been found in the joints of the multilayer material. Stress level exceed yield strength of Grade 1 titanium and A1050 aluminum. Asymmetry of the stress pattern results from the welding sequence. Pause time between aluminum and steel welding influence transition joint cooling process. The finite element mesh (FEM) and the introduced crack shape for the fatigue crack propagation process were shown in Figure 3. The shape of the crack results from the observation of cracks during experimental tests and confirms the information obtained from the literature [5]. A semi-elliptical fatigue crack propagating from the center of the joint was assumed. Total number of finite elements in the model was 700280, number of nodes 500297. Calculation model consisted of tetrahedral nonlinear elements. In the analysis, a linear material model was used, taking into account material constants taken from the literature [7, 8]. The hardness distribution is given in the paper [9].

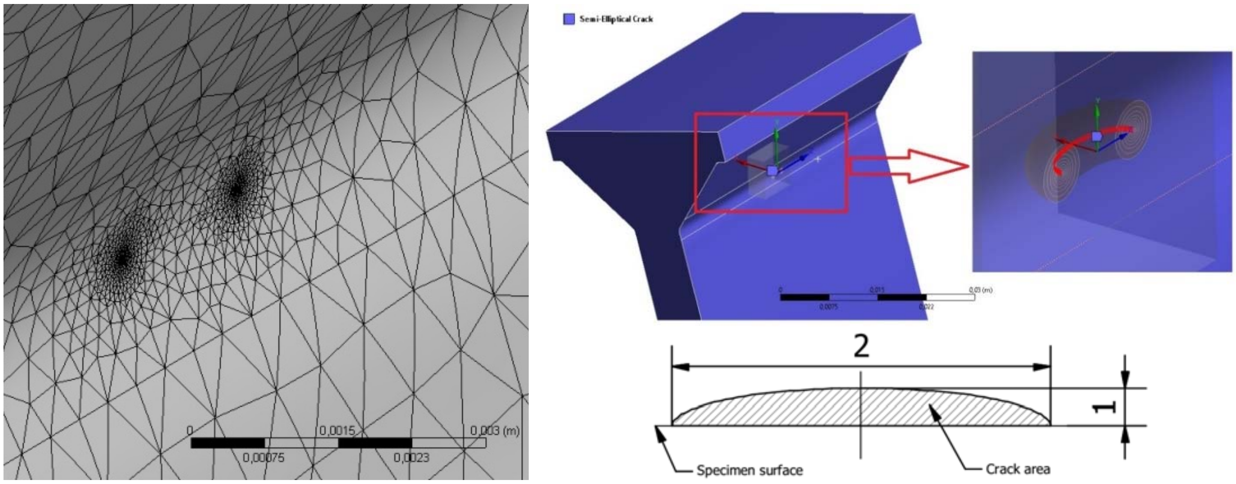

(a) (b)

FIGURE 3. Modeling semi-elliptical cracking with (a) finite element mesh, (b) crack orientation and dimensions.

Figure 4 shows exemplary results of numerical computations designed by using the Ansys software for tension in the form of maps of normal and equivalent Huber-Mises stresses.

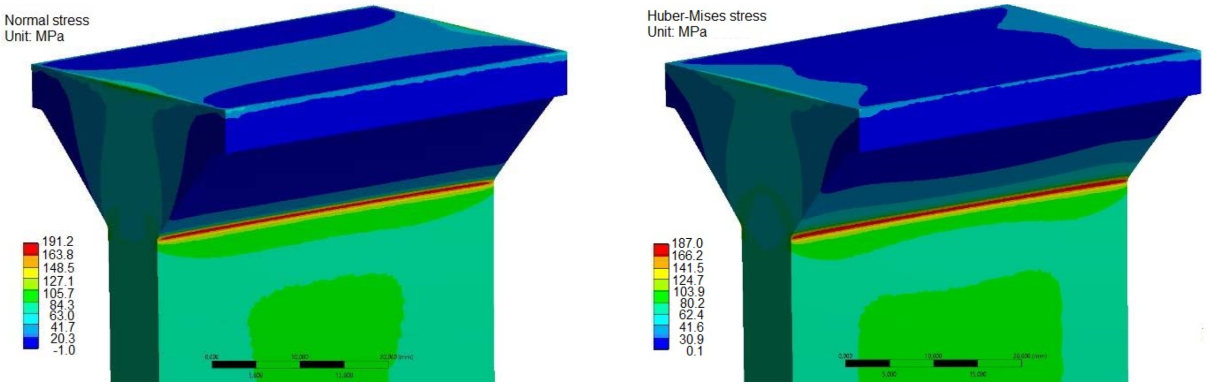

(a) (b)

FIGURE 4. The obtained values of calculated stresses (a) normal, (b) equivalent Huber-Mises.

The analysis shows that the presence of other material layers does not significantly affect the stress distribution in the welded joint. The obtained values of normal and equivalent stresses differ from each other in a negligible degree. Registration of the crack length was performed during fatigue test of transition joint specimen. Tests were performed according to ASTM standards. Crack length measurements were performed with portable microscope. Development of fatigue cracks was observed on the lateral surface of the specimens. Result of the analysis is the relationship between the crack length and the number of cycles (see Figure 5). Figure 5 shows a comparison between experimental and numerical simulation results. It can be seen that the results are convergent up to a crack length of

0.6 mm. Fig. 5a indicates the application range (rectangle) of the linear elastic fracture mechanics (LEFM). Figure 5b also shows how the stress intensity factor (SIF) changes as a function of the crack length. It can be observed that the largest SIF values were in the range of 0.8 to 1.4 mm. In experimental studies, the crack was initiated centrally in the specimen (same as it was simulated in the FEM) or in the area of the notch. Surface crack (semi-elliptical) developed similarly to Fig. 3b. If the crack initiated in the region of the notch, it increased into the material.

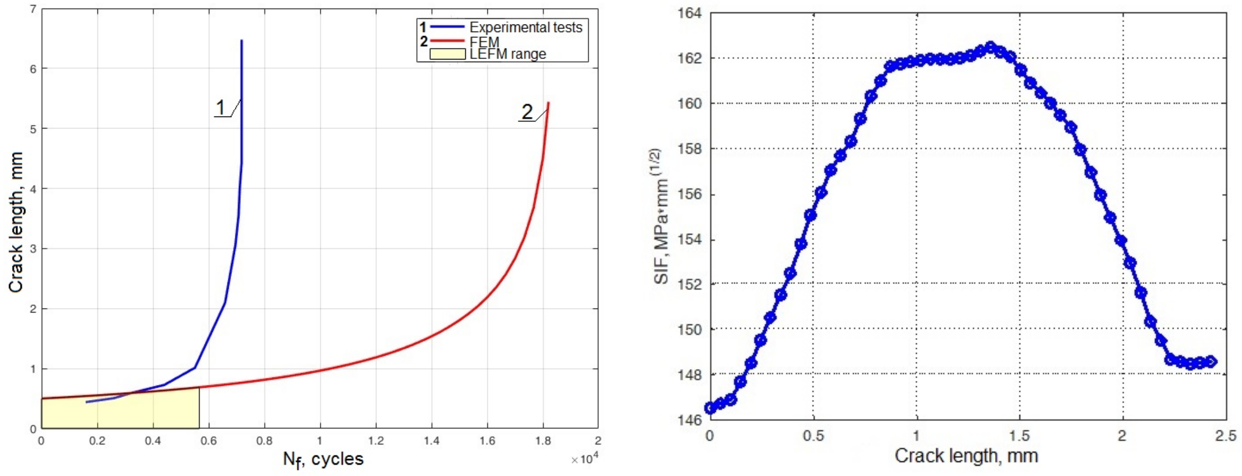

(a) (b)

FIGURE 5. Test and simulation results for (a) development of cracks, (b) stress intensity factor.

CONCLUSIONS

On the basis of the calculations made, the following conclusions and observations were formulated:

1. Residual stress after welding, calculated using FEM, was 164 MPa in alloy A5083.
2. The initiation and growth of the crack occurred only in aluminum.
3. The program used allows calculating the development of fatigue cracks in the welding process.
4. The results of calculations of crack growth obtained numerically were comparable with the test results to the length of 0.6 mm.

REFERENCES

1. W. Liu, J. Ma, M. Mazar Atabaki, and R. Kovacevic, Joining of advanced high-strength steel to AA 6061 alloy by using Fe/Al structural transition joint, Materials & Design **68**, 146–157 (2015).
2. T. Kr and L. Gt, Explosion-bonded transition joints for structural applications, Construction and Building Materials **3**,64–72 (1989).
3. M. Rathod and M. Kutsuna, Joining of Aluminum Alloy 5052 and Low-Carbon Steel by Laser Roll Welding, Welding Journal **83**, 16–26 (2004).
4. Y.-N. Du, M.-L. Zhu, and F.-Z. Xuan, Transitional behavior of fatigue crack growth in welded joint of 25Cr2Ni2MoV steel, Engineering Fracture Mechanics **144**, 1–15 (2015).
5. S. Mikheevskiy, G. Glinka, and T. Cordes, Total Life Approach for Fatigue Life Estimation of Welded Structures, Procedia Engineering **101**, 177–184 (2015).
6. M. Kowalski and M. Bohm, "Numerical Simulation of Residual Stress Induced by Welding of Steel-Aluminum Transition Joint, " in *Proceedings of the 14th Int. Scientific Conf.: Computer Aided Eng*, pp. 346–352. (2019).
7. S. KumarSingh, R. Mohan Tiwari, A. kumar, S. Kumar, Qasim Murtaza, S. Kumar, "Mechanical Properties and Microstructure of Al-5083 by TIG, " *Materials Today: Proceedings* 5, no. 1, Part 1, pp. 819–822 (2018).
8. K. Gotoh, K. Murakami, and Y. Noda, Fatigue crack growth behaviour of A5083 series aluminium alloys and their welded joints, J Mar Sci Technol **16**(3), p. 343 (2011).
9. M. Kowalski, A. Kurek, D. Rozumek, A. Kurek, Fatigue testing of a steel-aluminum welding connector with a titanium interlayer, Welding Technology Review **90**, 69-72 (2018) (in Polish).

Unsupervised Anomaly Detection in Time Series exploiting Local and Global Information

Emanuele La Malfa[1,a)] and Gabriele La Malfa[2,b)]

[1]*Computer Science Engineer, France*
[2]*Student EMLYON Business School, 23 Avenue Guy de Collongue, 69130 Ecully, France*

[a)]Corresponding author: emanuele.la.malfa@outlook.it
[b)]Corresponding author: gabriele.lamalfa@edu.emlyon.com

Abstract. We introduce a novel machine learning ensemble architecture for anomaly detection, that exploits global and local information from a 1d time series. A double step validation is performed to decide if a time period is anomalous: from one side a Long Short-Term Memory is trained to be reliable at forecasting, hence a parametric test on the forecasting's error is used spot the anomalies. Concurrently, a Variational Autoencoder is trained to compress both global and local information from the series to a low-dimensional normal distribution, raising an anomaly if a time step's likelihood is below a threshold. While anomaly detection with deep learning techniques often comes with the assumption that forecasting error is gaussian, we prove that this is in general a wrong assumption: we show that error function is better approximated by a distribution chosen dynamically. We validate our work on some public physical datasets, outperforming the current deep learning methods in terms of precision and recall.

INTRODUCTION

Forecasting and anomaly detection represent two critical research topics in the analysis of continuous phenomena over time. These studies are applied to different disciplines: physics, healthcare, robotics, artificial intelligence, finance, product analysis etc. Each discipline employs its own corpus of knowledge [1, 2], build on the top of many factors: from the nature of input variables and their relashionships, to the presence of trends, seasonality in the time series etc. [3, 4]. Often physical processes exhibit patterns that can be modeled with simple functions that repeat themselves around their fundamental period, while for many others, like financial and economical series, random walks models [5] are employed and their predictability is still an open issue [6]. A fundamental factor, in terms of predictability of the process, is how information propagates through time. If from one side in Markovian processes the information useful to forecast the next time period depends only on the previous state of the system, on the other in chaotic system a small perturbation of the initial state may influence the behavior or the phenomenon in a remote future.

Sequential models applied to time series have been widely used in recent years in many disciplines [7, 8, 9]. Particular attention has been devoted to explore learning methods [10, 11], enabled by the capacity of those models to process unidimensional and multidimensional datasets, extract features autonomousely [12] and model complex systems' dynamics. [13]. Malhotra et al. [16] use Long Short-Term Memory Networks (LSTM) [17] on physical time series: once forecasting is reliable, anomaly detection is based on modeling the prediction errors. On the other hands, Tsang et al. [18] provide a learning method applied to financial time series: after preprocessing data with a Symlet Wavelet Thresholding, a Stacked Autoencoder (SAE) is used for a pre-train session and finally an LSTM is used to forecast and identify anomalies. When it comes to financial time series forecasting, is often necessary a multivariate dataset which provides the missing information about the stochastic process that is not present in the monovariate market index. Laptev et al. [14] feed the features extracted from an autoencoder to a LSTM model, hence the model is used for anomaly detection. Being able to extract only the relevant features for the process may also benefit extreme event forecasting [15].

In this work, we combine two different approaches to do anomaly detection. From one side we processes the data through a LSTM network, improving precision and recall of the current state of the art method [19]. The same input data is processed by a Variational Autoencoder (VAE) [20]. If from one side LSTMs effectively detect anomalies once

temporal dependencies among distant timesteps are learnt, from the other the VAE model learns to compress each input sequence to a low-dimensional gaussian distribution, labeling as anomalous low probability timesteps.
The paper is organized as follows: in Section II the model is described in details. In Section III the experiments' results are presented. The last Section is dedicated to the conclusion and future directions of this work.

METHOD

We approach anomaly detection with an ensemble of two methods: a Long Short-Term Memory and a Variational Autoencoder. Each method identifies its own set of anomalies independently, while the final prediction is made by the union of the two sets. As the LSTM network spots anomalies based on the temporal dependencies learnt between distant timesteps, hence from a global perspective, a Variational Autoencoder learns to map each input to a point belonging to a low-dimensional gaussian distribution, hence emphasizing the local characteristics of each sequence. Figure 1. shows the complete process. For each method, details are presented in the following subsections.

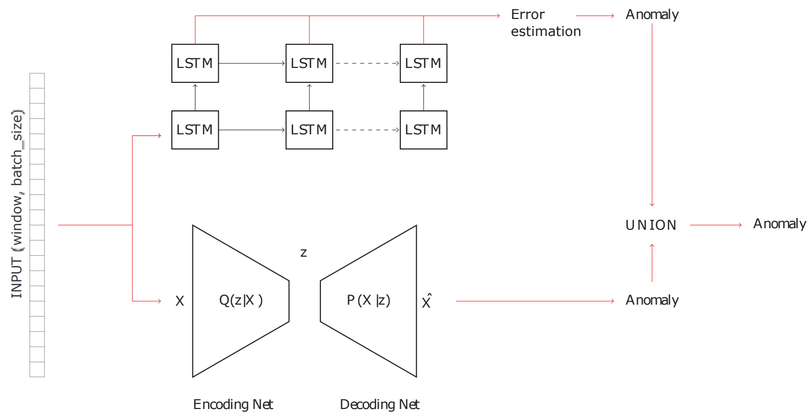

FIGURE 1: The LSTM-VAE model proposed in this work.

LSTM Network

LSTM is a model that extends Recurrent Neural Networks introducing Cells with specific gates for update, forget and output, in order to mitigate the vanishing gradient problem (Figure 3.). The gate Γ_u is used to update the previous state of the process C_{t-1} (previous cell), the forget gate Γ_f is dedicated to the reset operations for the actual cell C_t, while the output gate Γ_o works for the actual activation function a_t. In Eq. 1 it is reported the general formula for the update of a generic gate Γ, being$W$ and b the parameters for the respective gate. Consequently the process at time t is represented by the state of the process C_t (Eq. 2), with $\hat{C}_t$ as the updating of C_{t-1} (Eq. 3), and by the activation function a_t (Eq. 4).

$$\Gamma = \sigma \cdot (W \cdot [a_{t-1}, X_t] + b) \tag{1}$$

$$C_t = \Gamma_u \cdot \hat{C}_t + \Gamma_f \cdot C_{t-1} \tag{2}$$

$$\hat{C}_t = tanh \cdot (W_c \cdot [a_{t-1}, X_t] + b_c) \tag{3}$$

$$a_t = \Gamma_o \cdot C_t \tag{4}$$

In this work we propose a model where each LSTM Cell takes as input one chunk of the time series $x_i(t : t + len)$, whose length is defined by the *sequence length* parameter (len in the formula): the *stride* parameter, s in the formula, controls how many time steps sequence $x_i(t : t+len)$ overlaps with the subsequent one, $x_{i+1}(t+s : t+s+len)$. Another important parameter is the number of LSTM Cells, named *batch size*: this parameter is crucial to define the length of the LSTM network, hence the temporal dependencies between each sequence. The model aims at minimizing the forecasting error on each $x_i(t : t + len)$'s next input step, defined as $\sum_i(y_i(t) - \hat{y_i(t)})$: in the previous formula, $y_i(t)$ is the expected output of the i-th LSTM Cell when $x_i(t : t + len)$ is presented as input, while $\hat{y_i(t)}$ is the value predicted by the i-th LSTM cell.

The first training phase is performed on data D_{train} that does not contain anomalies: once the prediction is reliable (we use sMAPE as performance metric [21, 22] but many others can be employed [23]), we evaluate the error on an unseen dataset $D_{validation}$, that comes from the same distribution of D_{train} while being temporally subsequent. If one models the error on validation as a random variable from a specific probability distribution, it is possible to estimate the parameters that best fit the error's distribution with Maximum a Posteriori principle. While some relevant works [16, 19] assume as fixed the aforementioned family distribution (i.e. gaussian), we empirically found out that this is wrong in general: the best fitting distribution may change according to a specific instance of the model. Our approach mitigate this wrong hypothesis by choosing the best fitting distribution among a pool of *tractable* (with respect to MAP parameters estimation) distributions, and the one that better approximates the error on $D_{validation}$ is employed for the specific MAP parameters' estimation. Finally, on another unseen, identically distributed and subsequent part of the dataset D_{test}, we estimate for each input sequence the forecasting output: since we modeled the error distribution in the previous phase, we can calculate the probability of each forecasting error and if the value is below a threshold that maximizes a specific metric (like F1 score), mark the timestep as anomalous.

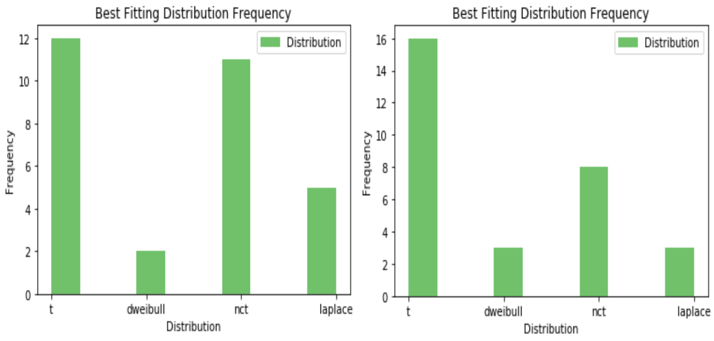

FIGURE 2: Best Fitting Distributions: Power Consumption (left) and Space Shuttle (right) Datasets.

Variational Autoencoder

A Variational Autoencoder is used to make inference and learning using a probabilistic based method characterized by latent variables with posterior intractable distributions [20]. By defining latent variables z that describe our data it is possible to obtain a non-blind generative model (i.e. it is possible to make sampling). Formally, one can model the probability of the input data as $P(X) = \int P(X|z)P(z)dz$, where $P(z)$ is the probability distribution function of the latent variable z and $P(X|z)$ the conditional distribution of data. In order to obtain $P(z)$, one can use the conditional probability $P(z|X)$: unfortunately approximating this ditribution is often hard. Hence variational inference approximates $P(z|X)$ with another tractable distribution $Q(z|X)$. This approximation problem can be optimized by a neural network where the first half layers, the *encoder*, maps X to the low-dimensional gaussian distribution $P(z)$ employing $Q(z|X)$, while the second part of the network rebuilds (hence the name *decoder*) the input by approximating $P(X|z)$ from its low-dimensional representation: the VAE's parameters are learnt through backpropagation, by minimizing the Kullback-Leibler (KL) divergence between ecnoder and decoder distributions.The objective function takes the following form: $logP(x) - D_{KL}[Q(z|X)||P(z|X)] = E[logP(X|z)] - D_{KL}[Q(z|X)||P(z)]$. In Figure 3. (right) VAE architecture is depicted. In our work we train the VAE on data D_{train} that does not contain anomalies and test it on unseen data D_{test} that instead may contain anomalies: in this way, when the compressed representation of an input sequence from D_{test} is very different from the pool of patterns seen so far in the time series, it will be assigned a low probability and marked as anomalous.

Anomaly Detection

We test our model on two publicly available physical datasets[1]: both of them do not contain anomalies in train and validation parts, while in the test part one or more anomalies need to be detected. The datasets come in the form of univariate quasi predictable time-series, still they set different challenges: data from Space Shuttle Marotta Valve

[1] http://www.cs.ucr.edu/ eamonn/discords

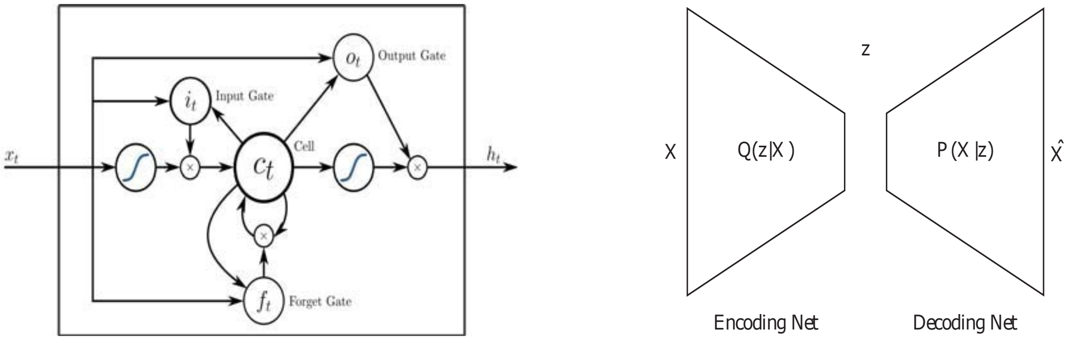

FIGURE 3: LSTM Cell (left), VAE encoder-decoder architecture (right).

contain a localized anomaly which can be easily spotted when a sequence is long enough to capture the unseen descending and climbing pattern, while in the Power Consumption dataset the anomaly can be spotted if and only if the algorithm *understands* that data is periodic and in the test phase two out of five consumption's peaks are not present at the end of the sequence. Data are preprocessed with normalization methods and subsampled (up to a factor of 3) when possible, to speedup computation.
The results obtained with LSTM algorithm are reported in Table [1], while on Table [2] we present the results obtained with VAE. Finally in Table [3] we report the score of the LSTM-VAE model, comparing precision and recall to the currently recognized state of the art method on the same challenge [19].

TABLE 1: In the right Table the results for the LSTM, in the right Table the results for the VAE network.

Model - Dataset	Precision	Recall	sMAPE
LSTM - Power Demand	1.	0.112	11.87
LSTM - Space Shuttle	1.	0.1	12.90

Model - Dataset	Precision	Recall
VAE - Power Demand	1.	0.25
VAE - Space Shuttle	1.	0.25

TABLE 2: LSTM-VAE Network, compared to previous SotA method [19]

Datasets	Precision	Recall	Precision-Recall (previous SotA)
Power Demand	1.	0.25	(0.92 - 0.04)
Space Shuttle	1.	0.3	(0.83 - 0.08)

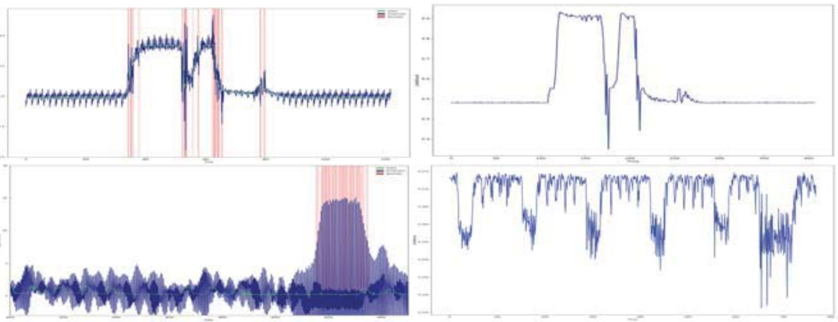

FIGURE 4: Top-left and top-right images represent anomaly detection results on test set for LSTM model and VAE on Space Shuttle dataset, while bottom-left and bottom-right refer to Power Consumption dataset.

CONCLUSION

We have presented an ensemble method for anomaly detection that exploits two different neural networks architectures, outperforming the current state of the art methods on two physics datasets. We reserve to extend the analysis on other datasets: in future works the aim is to apply those methods also to multidimensional financial time series, to capture the highly complex relations between features and hidden variables.

REFERENCES

[1] V. Chandola, A. Banerjee, V. Kumar, *Anomaly detection: A survey*, ACM Computing Surveys (CSUR), Vol. 41, Issue 3, 2009.

[2] V. J. Hodge, J. Austin, *A Survey of Outlier Detection Methodologies*, Artificial Intelligence Review, Vol. 22, Issue 2, pp. 85126, 2004.

[3] R. H. Shumway, D. S. Stoffer, *Time Series Analysis and Its Applications with R Examples*, Springer International Publishing, 2017.

[4] R. S. Tsay, *Analysis of Financial Time Series*, John Wiley & Sons, 3rd Edition, Hoboken, 2010.

[5] E. F. Fama, *Random Walks in Stock Market Prices*, Financial Analysts Journal, Vol. 21, no. 5, pp. 55-59, 1965.

[6] A. W. Lo, A. C. MacKinlay, *A Non-Random Walk Down Wall Street*, Princeton University Press, 2002.

[7] L. Deng, *Three classes of deep learning architectures and their applications: a tutorial survey*, APSIPA Transactions on Signal and Information Processing, 2012.

[8] Y. LeCun, Y. Bengio, G. Hinton, *Deep learning*, Nature, Vol. 521, no. 7553, 2015.

[9] A. Graves, *Supervised Sequence Labelling with Recurrent Neural Networks*, Springer-Verlag Berlin Heidelberg, Vol. 385, 2012.

[10] K. Yamanishi, J. Takeuchi, *A unifying framework for detecting outliers and change points from time series*, IEEE Transactions on Knowledge and Data Engineering, Vol. 18, Issue 4, pp. 482-492, 2006.

[11] Z. Che, S. Purushotham, K. Cho, D. Sontag, Y. Liu , *Recurrent Neural Networks for Multivariate Time Series with Missing Values*, Scientific Reports 8, Article Number 6085, 2018.

[12] M. Assaad, R. Bon, H. Cardot, *A New Boosting Algorithm for Improved Time-Series Forecasting with Recurrent Neural Networks*, Information Fusion 9, pp. 41-55, 2008.

[13] O. Ogunmolu, X. Gu, S. Jiang, N. Gans, *Nonlinear systems identification using deep dynamic neural networks*, arXiv: 1610.01439, 2016.

[14] N. Laptev, J. Yosinski, L. E. Li, S. Smyl, *Time-series Extreme Event Forecasting with Neural Networks at Uber*, Uber AI, ICML, 2017.

[15] L. de Haan, A. Ferreira, *Extreme Value Theory: An Introduction*, Springer Series in Operations Research and Financial Engineering, 2006.

[16] P. Malhotra, L. Vig, G. Shroff, A. Puneet, *Long short term memory networks for anomaly detection in time series*, ESANN 23rd European Symposium on Artificial Neural Networks, Computational Intelligence and Machine Learning, 2015.

[17] S. Hochreiter, J. Schmidhuber, *Long short-term memory*, Neural Computation, Vol. 9, Issue 8, pp. 1735-1780, 1997.

[18] G. Tsang, J. Deng, X. Xie, *Recurrent Neural Networks for Financial Time-Series Modelling*, 24th International Conference on Pattern Recognition, ICPR, 2018.

[19] P. Malhotra, A. Ramakrishnan, G. Anand, L. Vig, G. Shroff, A. Puneet, *LSTM-based Encoder-Decoder for Multi-sensor Anomaly Detection*, ArXiv: 1607.00148, 2016.

[20] D. P. Kingma, M. Welling, *Auto-Encoding Variational Bayes*, arXiv: 1312.6114, 2014.

[21] J. Armstrong, F. Collopy, *Error Measures for Generalizing about Forecasting Methods: Empirical Comparisons*, International Journal of Forecasting, Vol. 8, Issue 1, pp. 69-80, 1992.

[22] S. Makridakis, *Accuracy Measures: Theoretical and Practical Concerns*, International Journal of Forecasting, Vol. 9, Issue 4, pp. 527-529, 1993.

[23] R. J. Hyndman, A. B. Koehler, *Another Look at Measures of Forecast Accuracy*, International Journal of Forecasting, Vol. 22, Isuue 4, pp. 679-688, 2006.

Composite Structures Optimization Using Hybrid Genetic algorithm for space applications

Leila Gharsalli[1, a)] and Yannick Guerin[1, b)]

[1] *DLA/SDT/STM, 52 Rue Jacques Hillairet, 75012 Paris*
[a)] Leila.gharsalli@cnes.fr, [b)]Yannick.guerin@cnes.fr

Abstract. The aim of this study is to develop a hybrid genetic algorithm (H-GA) that combines a genetic algorithm (GA) and a descent local search technique to pursue the optimization of a sandwich composite inter-stage skirt located in the upper bound of the launcher. Total number of plies forming the sandwich composite skin and fiber orientations (predefined ply angles) are considered as design variables. The H-GA is chosen as an optimization tool thanks to its ability to deal with discrete optimization problems, of which the design of composites stacking is an example. First, the proposed approach is presented and explained. Then, its performances are compared and discussed against those offered by the classical GA.

INTRODUCTION

The development and application of hybrid optimization methods is attracting more and more the academic interest. Indeed, these methods have the advantage to combine different concepts or components of various algorithms and try to merge their strengths and eliminate their weaknesses to solve real-world problems in several applications' fields [1, 2, 3, 4], etc., such as the design of composites structures notably used in the aeronautical and space industries due to the economic benefit of composites materials [5].

Indeed, composites materials are made by the combination of two or more materials that have very different properties in order to generate a new one with improved strength and lightness. Hence, the latter may become a feasible alternative as a replacement for conventional homogeneous materials [6]. However, although such aggregation is more efficient, the raw materials are often expensive. Therefore, the composite structures should be optimized to make the best use of materials and minimize their total mass. For this purpose, many methods have been proposed to optimize the composite laminate performance using various design variables such as plies orientations, plies thicknesses, lamina thickness, stacking sequence, or even geometric parameters [7, 8, 9, 10] etc.,.

In this work, an integration between a based-population metaheuristic: a Genetic Algorithm (GA) and an iterated local search technique is used to pursue the optimization of laminated sandwich composite applied to the mechanical sizing of a launcher's structure. Aiming to reduce the structure's weight under various mechanical and design constraints, the total number of plies forming the sandwich composite skin and their several orientations are considered as design variables. The GA is used as a global zero-order optimization technique whereas the local search approach is chosen to attempt to explore more in details the identified promising areas. Hybridization is done by coupling sequentially an iterative local search technique with the GA where it complements genetic operators to reach the optimum. A special attention is given to the genetic representation of the laminated sandwich composite given its indispensability for the proper functioning of the algorithm.

This article is organized around four sections. In the first section we present the classical GA's principles. The second section is about the proposed approach. The application and the obtained results are discussed in the third section. Finally, the last section is devoted to conclusions and prospects.

PRINCIPLES OF GA

General mechanics of GA

GA try to simulate the process of natural evolution following the Darwinian model and use therefore a vocabulary similar to that of natural genetics with more or less some complexity [11]. The core of this vocabulary is the individual that belongs to a set of individuals called population. This individual is composed of a chromosome which is itself composed of genes that contain the hereditary characteristics of the individual. The main genetic operators are firstly selection, that include generally, two different operators; the parental selection devoted for reproduction and replacement selection devoted to keeping the population size constant by individuals who will survive in the next generation. A selection preferably retains the best individuals but must also give a chance to the less good to avoid the problems of premature convergence. Secondly, the crossover operation makes it possible to explore the research space by diversifying the population. It usually manipulates the chromosomes of two parents to generate two children. There are different types of crossover such as at one-point or at two-points. Finally, the mutation operation causes a small perturbation on an individual's chromosome and tries to bring into the population new characteristics or gene values which are nonexistent in the population pool.

It is nonetheless crucial to mention that GAs need a genetic representation of the desired problem by coding its parameters. Hence, the algorithm can evaluate the 'fitness' of every individual and computes the problem's objectives and constraints based only on coding without any further knowledge of real parameters. Note that the 'fitness' function evaluates how close a given solution is to the optimum one. References [12] and [13] provide further discussion on the theoretical properties of GAs and on standard genetic operators.

Encoding Scheme

From now on, we focus only on the specific framework of laminated sandwich composites optimization. Note that a sandwich composite is obtained from two skins bonded to a core made of a very light material. The sandwich is preferred to the monolithic one because it allows to discard the skins that improves the buckling behavior while limiting the longitudinal stiffness [6]. The encoding of composites is done based on the concepts of genetics in the following way; the initial population is composed of a set of random individuals (sets of skin plies characterized by orientation angles) where each individual is equivalent to a laminate. Therefore, the population refers to a set of laminates. An individual can be then represented by one chromosome. Each chromosome contains a chain of genes of the same type representing the coded variables of the problem. For example, the chromosome devoted to orientation angles (0°, 90°, until last angle, see **TABLE 1**). Note that the number of chromosomes as well as the number of genes of each chromosome necessary for the individual representation depend specifically on the studied problem.

PROPOSED HYBRID APPROACH

Local Search Technique

Combining a local search strategy with a GA can be done in various ways ([14,15]). In this work, the proposed hybrid GA (H-GA) approach consists in strong cooperation between GA and a local descent search technique for the entire course of the algorithm. The local search algorithm is integrated at the beginning of the GA in order to intensify research only around promising solutions (**FIGURE 1**) because applying the local search to every individual will waste the resources. Hence, for every new generation, a set of best solutions reached by the GA is selected as an initialization for the local search approach. Then, a set of neighbors is built for every individual where each neighbor is evaluated. If one neighbor shows an improved fitness, then it is introduced in the population to replace that individual. This process is repeated for a certain amount of iterations set by the user.

TABLE 1. Orientations' chromosome representation

Encoded	0	1	2	3	4
Decoded	0°	±45°	±90°	Empty	±30°

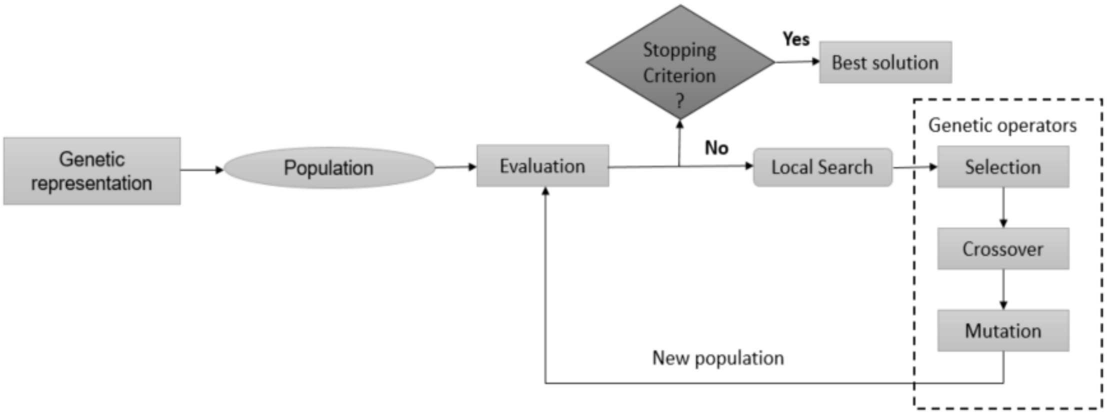

FIGURE 1. The proposed hybrid genetic algorithm (H-GA) flowchart

Neighborhood Structure

The classical GA uses the mutation operator to diversify some selected individuals of the population. However, this operator mutates a random gene by any value belonging to the domain according to the same probability. Therefore, the larger the domain is, the lower the probability that a gene will be mutated by its neighbor is. For this reason, a well-defined neighborhood is used during the local search procedure as seen in [16]. To determine a given individual's two neighbors, a randomly selected gene is flipped to either the previous or the next value in the chromosome's domain. For example, if the domain contains 5 possible values $\{0,1,2,3,4\}$, then if the value of the fifth gene is 3, the value of this gene will be replaced by 4 in the first neighbor and by 2 in the second (**TABLE** ***2***). However, if the randomly selected gene is the domain's upper bound (herein 4), then the two neighbors are built by flipping firstly the gene to the previous value in the domain (3) then to the lower bound (0) and conversely if the randomly selected gene is the domain's lower bound.

TABLE 2. Example of Neighbors' building

Chromosome	2	0	1	4	**3**	4	2	1
Neighbor 1	2	0	1	4	**4**	4	2	1
Neighbor 2	2	0	1	4	**2**	4	2	1

APPLICATION AND RESULTS

To compare the efficiency of the H-GA against the classical GA, this test case is considered: a sandwich composite inter-stage skirt optimization. This structure is located on the upper part of the launcher and is subject to pressure oscillations from engines upstream. In order to limit the vibratory levels at the launcher's top, the skirt has a filtering role. In order to better filtering these oscillations, the structure must be mechanical sizing according to a compromise between stiffness and flexibility related to the need to avoid buckling. Hence, the optimization's aim is to minimize the total mass while respecting a longitudinal stiffness constraint and buckling strength. Note that these constraints are managed during the H-GA selection process whereas the composite design constraints (mirror symmetry, balancing, grouping etc.,[17]) are overcome by using a repair technique during the orientations' chromosome decoding step.

For the sake of simplicity, sandwich skin plies and core thicknesses are considered as fixed ($0.1\ mm$ per ply and $22\ mm$ respectively) and individuals are represented each by only one orientation chromosome (design variable encoded as seen in **TABLE** ***1***) that have initially 8 genes which can take 5 different values in $\{0,1,2,3,4\}$. Fitness of every individual is calculated by interrogating the finite element analysis (FEA) program called NASTRAN [18] which interacts with H-GA when evaluating, in order to associate with each stacking the structure's mass, the

longitudinal stiffness and the corresponding buckling eigenvalue. Nevertheless, for the purpose of accelerating the optimization process, a database containing individuals already assessed and their respective fitness is created during the optimization process. In this way, before each evaluation, H-GA runs through the database and look for fitness from the stacks previously evaluated. The population size is equal to 30 individuals in all the analysis. GA and H-GA are computed using the same parameters (**TABLE *3***).

After 500 generations, the best reached stacking is composed of 6 plies per skin against 8 initially and respects all the design constraints of composite structures besides both stiffness and buckling constraints. Note that the margins obtained from constraints highlights the primary objective of the GA which is to minimize the total mass. Indeed, the total mass is decreased by 8.4 % compared to the one given by NASTRAN. Besides, a more efficient result is offered by H-GA in terms of needed number of iterations to reach the optimum and the associated elapsed time, buckling and stiffness (**TABLE *4***). In the other hand, the graph **FIGURE *2***- (a) perfectly illustrates the usefulness of the based-neighborhood local search. Indeed, since the 30th generation, H-GA starts to converge by spreading better individuals in the population and offering simultaneously a wide choice of new different individuals to explore thanks to the research intensification around the best solution than that given by the GA. **FIGURE *2***- (b) supports this result by showing the frequency of appearance of the dominant solution reached by both H-GA and GA. In fact, while the best solution given by the latter is appearing constantly more than 20 times per generation since the 200th iteration, that one given by H-GA oscillates allowing the algorithm to explore more possible solutions.

TABLE 3. H-GA parameters

Parameters	Values
Probability of mutating	0.2
Mutant genes per individual	1
Probability of crossing	1
Individuals reported in the next generation	1
Neighbors per individual	2
Iterations for local search	5

TABLE 4. Results

	Convergence (Iterations/ Time CPU)	Stacking (°)	Stiffness < 2.10^{8} (N/m)	Buckling > 2,03	Mass (Kg)
Nastran	1	45/0/30/0/30/0/-45/90	5.2e-09	2,73	357
GA	58/7h	0/30/-30/30/-30/90	6.9e-09	2,15	327
H-GA	28/5h	45/90/-45/30/-30/ 0	5.8e-09	2.22	327

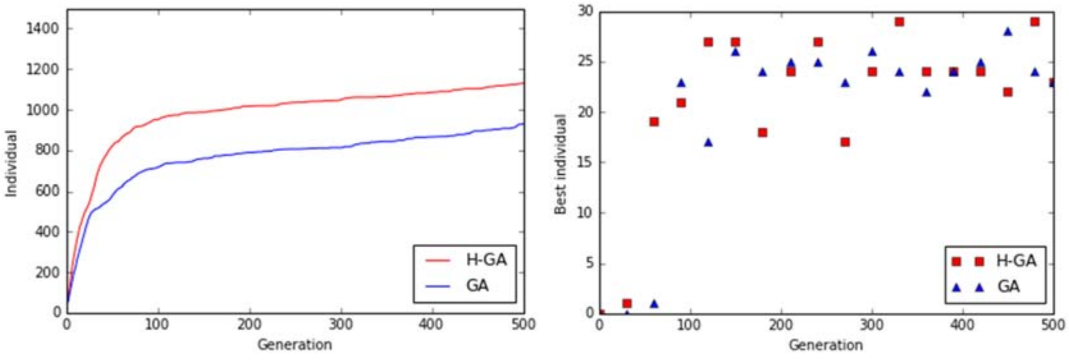

(a) (b)

FIGURE 2. (a) Evolution of new individuals during the optimization process, (b) frequency of appearance of the best individual

CONCLUSIONS AND PROSPECTS

In this paper, a promising hybrid genetic algorithm is introduced to deal with sandwich composite optimization. In the proposed hybrid approach, the population was treated in a sequential manner by both the genetic operators and the local search technique. A spatial test case was performed to identify the performances of the hybrid technique against the classical GA. The obtained results reveal a better convergence of the hybrid algorithm. However, work in progress concerns firstly including the sandwich core thickness among the design variables and secondly the finding of a better different way to hybridize the GA in order to improve much more its convergence performances notably on other test cases.

REFERENCES

1. P. Moscato, C. Cotta and A. Mendes, Memetic algorithms. New optimization techniques in engineering, Springer, 2004, p. 53–85.
2. C. Vanaret, "Hybridization of evolutionary algorithms and interval-based methods for optimizing difficult problem," 2015.
3. H. Hachimi, "Hybridization of metaheuristic algorithms in global optimization and their applications," 2013.
4. N. El Hami, "Contribution to hybrid heuristic optimization methods: Distribution and application on information systems interoperability," 2012.
5. J. I. Pelaez, J. A. Gomez-Ruiz, J. Veintimilla, G. Vaccaro and P. Witt, "Memetic Computing Applied to the Design of Composite Materials and Structures," Mathematical Problems in Engineering, vol. 2017, p. 16.
6. T. Reinhart, "Overview of Composite Materials," in Peters S.T. (eds) Handbook of Composites, Boston, MA, Springer, 1998.
7. A. Rama Mohan Rao and N. Arvind, "Optimal stacking sequence design of laminate composite structures using tabu embedded simulated annealing," Structural Engineering and Mechanics, vol. 25, no. 2, p. 239–268, 2007.
8. A. Carpentier, "Optimisation multi-niveaux de panneaux Composites," 2008.
9. A. Lasseigne, "Optimization of variable-thickness composite structures. Application to a CROR blade," 2016.
10. F.-X. Irisarri, A. Lasseigne, H. Leroy François and R. Le Riche, "Optimisation des empilements dans les structures composites stratifiées avec arrêts de plis," in 18èmes Journées Nationales sur les Composites, Nantes, 2013.
11. J. H. Holland, Adaptation in Natural and Artificial Systems: An Introductory Analysis with Applications to Biology, Control and Artificial Intelligence, Ann Arbor, MI: University of Michigan Press, 1975.
12. D. Whitley, "A Genetic Algorithm Tutorial," Statistics and Computing, vol. 4, pp. 65-85, 1994.
13. D. E. Goldberg, Genetic Algorithms in Search, Optimization and Machine Learning, I. Addison-Wesley Longman Publishing Co., Ed., 1989.
14. C. Blum, M. Aguilera, A. Roli and M. Sampels, "Hybrid Metaheuristics – An Emerging Approach to Optimization," Studies in Computational Intelligence, vol. 114, 2008.
15. Y. G. Xu, G. Li and. Z. Wu, "A novel hybrid genetic algorithm using local optimizer based on heuristic pattern move," Applied Artificial Intelligence, vol. 15, no. 7, pp. 601-631, 2001.
16. F. Girard, "Optimisation de Stratifiés en Utilisant un Algorithme Génétique," Québec, Canada, 2006.
17. D. Gay and S.V. Hoa and S.W. Tsai, " Composite Materials: Design and Applications," CRC Press, 2002.
18. M. Software, MSC Nastran 2012 Quick Reference Guide, M. Software, Ed., 2011.

Symbolic-Numeric Research of Leaky Modes in Planar Dielectric Electromagnetic Waveguide As Inhomogeneous Waves

D.V. Divakov[1,a)], A.A.Egorov[2,b)], K.P. Lovetskiy[1,c)] and L.A. Sevastianov[1,d)]

[1] *Department of Applied Probability and Informatics, Peoples' Friendship University of Russia (RUDN University), 6 Miklukho-Maklaya St, Moscow, Russia, 117198.*
[2] *Prokhorov General Physics Institute, Russian Academy of Sciences, 38, Vavilov Street, Moscow, 119991, Russia;*

[a)] divakov-dv@rudn.ru
[b)] yegorov@kapella.gpi.ru
[c)] lovetskiy-kp@rudn.ru
[d)] sevastianov-la@rudn.ru

Abstract. In the case of guided and radiation modes of open waveguides, the Sturm-Liouville problem is formulated for self-adjoint second-order operators on the axis and the corresponding eigenvalues are real quantities for dielectric media. The search for eigenvalues and eigenfunctions corresponding to the leaky modes involves a number of difficulties: the boundary conditions for the leaky modes are not self-adjoint, so that the eigenvalues can turn out to be complex quantities. The problem of finding eigenvalues and eigenfunctions is associated with finding the complex roots of the nonlinear dispersion equation.

The presence of complex eigenvalues corresponding to the leaky modes leads to an infinite increase of eigenfunctions corresponding to the leaky modes. In the present work, the leaky modes are considered as solutions of the problem for the wave equation and are analyzed as a wave process. Complex eigenvalues define the leaky modes as inhomogeneous waves. The proposed approach allows to obtain a mathematically sound representation of the leaky modes, within which one can see the region of existence of each particular leaky mode. The calculations of model structure, demonstrating the application of the described approach, are presented in the paper.

INTRODUCTION

In the books by Marcuse[1, 2], Adams[3], Snyder and Love[4], Tamir[5], and other authors the terms "leaky rays" and "leaky modes" appear when discussing the propagation of polarized light in fiber optical waveguides with the refractive index of the core smaller than that of the cladding, and in planar waveguides with plates of material optically denser than the waveguide layer itself. In this case, Marcuse writes that the outflow of light from such a waveguide is akin to tunneling through a potential barrier in quantum mechanics. The "leaky light", in contrast to the "emitted light", propagates for quite a long time along the axis of the optical fiber. Similarly, in a planar waveguide, the resulting electromagnetic radiation propagates for some time at some distance along the waveguide, in contrast to the emitted light. The description of leaky modes in planar waveguides, given in the book by Nefedov[6], in our opinion seems to be the most complete one among the books of that time both from the physical and mathematical points of view.

In our opinion, a more rigorous justification of the model of leaky waves of open waveguide systems can be obtained by starting calculations not from the Helmholtz equation, as is traditionally done, but from the wave equation preceding the Helmholtz equation, and most importantly, more adequately reflecting the wave nature of leaky modes.

Statement of the problem of modeling leaky modes of symmetric waveguides

Consider a symmetric three-layer planar waveguide consisting of a dielectric film having the height h with real refractive index n_f, surrounded by a cladding layer with real refractive index $n_c < n_f$. The generally accepted model of the

electromagnetic field in a planar (infinitely extended along the Oy-axis) are fields that are independent of the variable y. In this case, Maxwell's equations are considerably simplified, since $\partial E_\alpha/\partial y = \partial H_\alpha/\partial y \equiv 0$ for any $\alpha = x, y, z$, and they are divided into two independent subsystems — the subsystem for the so-called TE-modes and for the TM-modes. The subsystem for the TE-modes can be represented as a single wave equation for E_y

$$\left(\frac{\partial^2}{\partial x^2} + \frac{\partial^2}{\partial z^2} - \frac{n^2(x)}{c^2}\frac{\partial^2}{\partial t^2}\right)E_y = 0, \tag{1}$$

where c is the electrodynamic constant, $n(x)$ is the variable refractive index of the considered three-layer waveguide, defined below. The subsystem for the TE-mode also includes two equations for the connection of components H_x, H_z with the master component E_y.

As a model of leaky modes propagation, we will consider Eq. (1), i.e., in other words, we will consider the propagation of leaky modes in terms of a wave process. As asymptotic boundary conditions, we will consider the conditions of "outgoing waves" corresponding to the Gamow-Siegert model [8, 9, 10].

In the case under consideration, the function describing the refractive index depends only on x, which makes it possible to separate the variables in Eq. (1). As a result, we obtain solutions corresponding to leaky modes propagating in the positive direction of the z-axis:

$$\left.E^+_{yj}\right|_{x>h} = A^+_{cj}\cdot\exp\left\{ik_0\sqrt{n_c^2-\beta_j{}^2}x + ik_0\beta_j z - i\omega t\right\}, \tag{2}$$

$$\left.E^+_{yj}\right|_{\substack{x<h\\x>0}} = A^+_{fj}\cdot\exp\left\{ik_0\sqrt{n_f^2-\beta_j{}^2}x + ik_0\beta_j z - i\omega t\right\} + B^+_{fj}\cdot\exp\left\{-ik_0\sqrt{n_f^2-\beta_j{}^2}x + ik_0\beta_j z - i\omega t\right\}, \tag{3}$$

$$\left.E^+_{yj}\right|_{x<0} = B^+_{cj}\cdot\exp\left\{-ik_0\sqrt{n_c^2-\beta_j^2}x + ik_0\beta_j z - i\omega t\right\}, \tag{4}$$

where ω is the frequency, and β_j are the eigenvalues of the non-self-adjoint Sturm-Liouville problem with boundary conditions that extract the leaky modes[3, 7, 11, 12]:

$$\begin{cases} X'' + k_0^2 n^2(x)X = k_0^2\beta^2 X, \\ X'(0) + ik_0\sqrt{n_c^2-\beta^2}X(0) = X'(h) - ik_0\sqrt{n_c^2-\beta^2}X(h) = 0, \end{cases} \tag{5}$$

Analysis of leaky modes in terms of inhomogeneous waves

Consider the complex values $p_{cj} = \sqrt{n_c^2-\beta_j^2} = p'_{cj} + ip''_{cj}$, $p_{fj} = \sqrt{n_f^2-\beta_j^2} = p'_{fj} + ip''_{fj}$, and $\beta_j = \beta'_j + i\beta''_j$ in the solutions (2)–(4), explicitly distinguishing their real and imaginary parts, which will allow us to reformulate Eq. (2) (and the same for Eqs. (3,4)) in terms of inhomogeneous waves, whose amplitude is also a function of x and z:

$$\left.E^+_{yj}\right|_{x>h} = A^+_{cj}\cdot\exp\left\{-k_0 p''_{cj}x - k_0\beta''_j z\right\}\cdot\exp\left\{ik_0 p'_{cj}x + ik_0\beta'_j z - i\omega t\right\}, \tag{6}$$

Consider Eq. (6) in the form of an inhomogeneous wave: $\left.E^+_{yj}\right|_{x>h} = A_{cj}(x,z)\cdot\exp\left\{ik_0 p'_{cj}x + ik_0\beta'_j z - i\omega t\right\}$, where $A_{cj}(x,z)$ is the amplitude of the inhomogeneous wave defined as

$$A_{cj}(x,z) = A^+_{cj}\cdot\exp\left\{-k_0 p''_{cj}x - k_0\beta''_j z\right\}. \tag{7}$$

Consider in more detail the inhomogeneous wave with variable amplitude $A_{cj}(x,z)$. If such waveguide parameters exist for which the inhomogeneous wave of some j-th mode propagates in the direction $\vec{s}_j = \left(k_0 p'_{cj},\ \ k_0\beta'_j\right)^T$, along which $A_{cj}(x,z) \to 0$, then such wave will decay (of course, if such direction exists). If a direction $\vec{s}_j = \left(k_0 p'_{cj},\ \ k_0\beta'_j\right)^T$ exists, along which $A_{cj}(x,z) = Const$, then the wave will become homogeneous and, correspondingly, if a direction $\vec{s}_j = \left(k_0 p'_{cj},\ \ k_0\beta'_j\right)^T$ exists, along which $A_{cj}(x,z) \to \infty$, then the wave will have infinitely growing amplitude along such a direction.

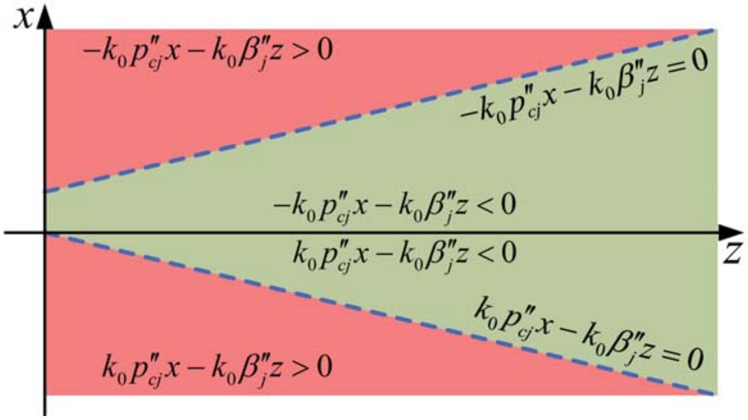

FIGURE 1: Amplitude growth/attenuation regions and a constant amplitude line of an inhomogeneous wave on a plane

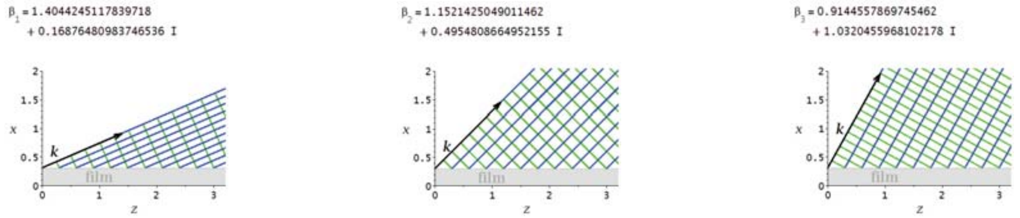

FIGURE 2: Lines of constant amplitude (blue), constant phase (green) and wave vectors (black) of the first three outgoing modes in a cladding layer of a symmetric waveguide with n_c=1.47, n_f=1.565, $\lambda = 0.55\mu m$ and $h = 1.1\lambda$

Consider first the case $A_{cj}(x, z) = Const$. The representation (7) allows choosing a direction in the plane xOz, along which $A_{cj}(x, z) = Const$. This direction is described by the equation $-k_0 p''_{cj} x - k_0 \beta''_j z = 0$. The symmetric direction $k_0 p''_{cj} x - k_0 \beta''_j z = 0$ will be responsible for the constant amplitude of the inhomogeneous wave. The domain above the line $-k_0 p''_{cj} x - k_0 \beta''_j z = 0$ corresponds to the domain of the amplitude growth, as well as the domain below the line $k_0 p''_{cj} x - k_0 \beta''_j z = 0$ (see Fig. 1).

The region of existence of leaky modes corresponding to non-uniform waves with non-increasing amplitude is shown green in Fig. 1. Namely, if the wave vector of the non-uniform wave is located in the green color region, then this leaky mode has a non-increasing amplitude and can propagate in the positive direction of the z-axis.

Numerical analysis of leaky modes of symmetric three-layer waveguides

Let us proceed to numerical analysis of the obtained representation of the leaky modes. Since the structure of the waveguide under consideration is symmetric, it is sufficient to consider only Eq. (6). Below we give the calculated values of the complex phase deceleration coefficient calculated for a waveguide with n_c=1.47, n_f=1.565, $\lambda = 0.55\mu m$ and $h = 1.1\lambda$. Let us analyze, by the example of the waveguide in question, the lines of constant phase and constant amplitude for the first three leaky modes (Fig. 2).

It is commonly assumed that for the leaky modes the amplitude increases with the distance x from the waveguide along the vertical axis (at a fixed longitudinal distance $z$and in the absence of losses in the waveguide). However, as it propagates along the axis z, this mode decays due to permanent energy losses from the waveguide layer to the environment. Functionally, the fields of leaky modes (vertical profile) are identical to the fields of ordinary guided modes; however, since unlike normal guided (homogeneous) modes, the leaky modes are inhomogeneous waves, they have planes of equal phases and planes of equal amplitudes that are not perpendicular to each other. This is exactly what our results confirm (Fig. 2). In this regard, the representation of leaky waves of planar waveguides using the solutions of the wave equation seems to be preferable for us, compared to the traditionally used representation using

the solutions of the Helmholtz equation.

At the same time, some features were revealed that we plan to analyze in our further publications. It is important to emphasize that the region of existence of leaky modes corresponding to inhomogeneous waves with non-increasing amplitude is detected (green area in Fig. 1). Moreover, if the wave vector of an inhomogeneous wave is located in the region of green, then such a leaky mode has a non-increasing amplitude and can propagate for a sufficiently long distance in the waveguide without absorption.

Conclusion

This paper discusses the guided modes that exist when the waveguide thickness is below the critical one. Such modes are referred to as leaky modes. These waves occur when the thickness of the waveguide layer is less than the critical value, below which waveguide properties cannot take place in the usual sense. It is important to emphasize that the number of leaky modes with a gradual leakage is limited, unlike the continuum of radiative modes. The resulting gradual leakage waves form a discrete spectrum and are plane inhomogeneous waves. On the contrary, the radiative modes form a continuum (their spectrum is continuous) and are plane homogeneous waves. As a result, the replacement of one kind of these waves with another kind requires serious analysis in each specific case. From this point of view, the methods developed by us are undoubtedly useful for theoretical and numerical studies of dielectric and, in particular, optical waveguides supporting leaky modes.

ACKNOWLEDGMENTS

The publication has been prepared with the support of the RUDN University Program 5-100 and funded by RFBR (projects No. 18-07-00567 and No. 18-51-18005).

REFERENCES

[1] D. Marcuse, [*Light Transmission Optics*], Van Nostrand Reinhold, New York, (1972).
[2] D. Marcuse, [*Theory of Dielectric Optical Waveguides*], Academic, New York, (1973).
[3] M.J. Adams, [*An Introduction to Optical Waveguides*], Wiley, Chichester, (1981).
[4] A.W. Snyder and J. D. Love, [*Optical Waveguide Theory*], Chapman and Hall, London, (1983).
[5] T. Tamir, [*Integrated Optics*], Berlin, Germany: Springer-Verlag, (1982).
[6] E.I. Nefedov, [*Diffraction of Electromagnetic Waves by Dielectric Structures*] [in Russian], Nauka, Moscow, (1979).
[7] E.I. Golant and K.M. Golant, ”New Method for Calculating the Spectra and Radiation Losses of Leaky Waves in Multilayer Optical Waveguides,” *Technical Physics,* **51**(8), 1060–1068, (2006).
[8] G. Gamow, ”Zur quantentheorie de atomkernes,” *Z. Phys.,* **51**, 204–212, (1928).
[9] A. Bohm, M. Gadella and B. Mainland, ”Gamow vectors and decaying states,” *Am. J. Phys.,* **57**, 1103–1108, (1989).
[10] A. F. J. Siegert, ”On the derivation of the dispersion formula for nuclear reactions,” *Phys. Rev.,* **56**, 750–752, (1939).
[11] D. Divakov, A. Tiutiunnik and A. Sevastianov, ”Symbolic-Numeric Computation of the Eigenvalues and Eigenfunctions of the Leaky Modes in a Regular Homogeneous Open Waveguide,” *MATEC Web of Conferences,* **186**, 01009, (2018).
[12] D. Stowell, J. Tausch, ”Guided and leaky modes of planar waveguides: Computation via high order finite elements and iterative methods,” *PIERS Online,* **6**(7), 669–673, (2010).

Symbolic-Numeric Implementation of The Four Potential Method for Calculating Normal Modes of Square Electromagnetic Waveguide with Rectangular Insert

A.A. Tiutiunnik[1,a)] and M.D. Malykh[1,b)]

[1]*Department of Applied Probability and Informatics,*
Peoples' Friendship University of Russia (RUDN University),
6 Miklukho-Maklaya St, Moscow, Russia, 117198.

a) tyutyunnik-aa@rudn.ru
b) malykh-md@rudn.ru

Abstract. In this paper, the Maple computer algebra system is used to construct a symbolic-numeric implementation of the method for calculating normal modes of square closed waveguides in a vector formulation. The method earlier proposed by Malykh et al. [M.D. Malykh, L.A. Sevastianov, A.A. Tiutiunnik, N.E. Nikolaev. On the representation of electromagnetic fields in closed waveguides using four scalar potentials // Journal of Electromagnetic Waves and Applications, 32 (7), 886-898 (2018)] will be referred to as the method of four potentials. The Maple system is used at all stages of treating the system of differential equations for four potentials: the generation of the Galerkin basis, the substitution of approximate solution into the system under study, the formulation of a computational problem, and its approximate solution.

The paper presents the results of the verification method.

INTRODUCTION

Computer algebra systems have recently been actively used to construct symbolic-numeric methods for approximate solution of computational problems of mathematical physics (see. e.g., [1, 2, 3, 4, 5]).

Particularly efficient is the use of a computer algebra system in the application of methods based on Galerkin and Kantorovich decompositions. Approximate solutions within the framework of these methods are represented as partial sums of a series over some complete system of basis functions. When computerising the methods of Galerkin and Kantorovich [6, 7], it becomes necessary to apply projection relations, including integrals (often from rapidly oscillating functions) (see [3]). If the basic functions of the Galerkin and Kantorovich methods are known in symbolic form (for example, polynomials, trigonometric functions, etc.), then it is convenient to set up an approximate problem in a computer algebra system.

In this paper, we have developed a symbolic-numeric implementation of the four potential method [1] for computing the normal modes of a rectangular closed waveguides in vector formulation using the Maple computer algebra system.

Preliminary information: four potential method

In the framework of the four potential method [1, 2], a waveguide of constant cross section S with ideally conducting walls is considered. The axis Oz with unit vector $\vec{e}_z$ is directed along the axis of the waveguide; the normal to the side wall will be denoted by $\vec{n}$, and the tangent vector perpendicular to both $\vec{e}_z$ and $\vec{n}$ by $\vec{\tau}$ (Fig. 1).

In a closed waveguide, the components of the electromagnetic field E_z, H_z are expressed in terms of $\vec{E}_\perp = \left(E_x,\ E_y\right)^T$ and $\vec{H}_\perp = \left(H_x,\ H_y\right)^T$ [8, 9, 10], therefore, within the framework of the method, the electromagnetic field can be represented as $\vec{E}_\perp = \nabla u_e + \nabla' v_e$, $\vec{H}_\perp = \nabla v_h + \nabla' u_h$, where $u_{e,h}$ and $v_{e,h}$ are scalar functions that satisfy

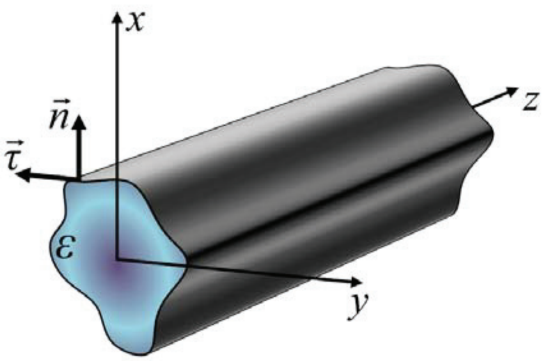

FIGURE 1. Waveguide of constant section S

the Dirichlet and Neumann conditions at the waveguide boundary. The Maxwell equations in this representation are reduced to a system of differential equations for four potentials [1]:

$$\begin{cases} \nabla' \left(\partial_z v_h - \frac{1}{ik\mu} \Delta v_e \right) + ik\varepsilon \nabla' v_e - \nabla \partial_z u_h + ik\varepsilon \nabla u_e = 0, \\ \nabla' \left(\partial_z u_e + \frac{1}{ik\epsilon} \Delta u_h \right) - ik\mu \nabla' u_h - \nabla \partial_z v_e - ik\mu \nabla v_h = 0, \end{cases} \tag{1}$$

where $\nabla = (\partial/\partial x, \partial/\partial y)^T$, $\nabla' = (-\partial/\partial y, \partial/\partial x)^T$. The boundary conditions for the potentials are as follows [1]:

$$u_e|_{\partial S} = u_h|_{\partial S} = 0, \ \ \nabla v_e \cdot \vec{n}\big|_{\partial S} = \nabla v_h \cdot \vec{n}\big|_{\partial S} = 0. \tag{2}$$

The Dirichlet and Neumann boundary conditions (2) that are classical for mathematical physics [11, 12] often allow constructing an approximate solution applying the Galerkin method with, e.g., the eigenfunctions of the Laplace operator with appropriate boundary conditions as the basis. In the case of a complex cross section geometry, it is more convenient to construct an approximate solution by means of the finite element method [3, 13, 14]. However, in the case of simple geometry that allows separation of variables, e.g., a rectangular cross section, an approximate solution can be constructed using the Galerkin method.

To test the performance of the method, we will first consider waveguides of square cross section with an arbitrary rectangular insert. In this case, we will construct an approximate solution using the incomplete Galerkin method [15, 16] and then investigate the numerically obtained solutions.

Setting a computational problem

We first consider a waveguide homogeneous along the axis z with square cross section $S = \{x \in [0; 1], y \in [0; 1]\}$.

Let the permittivity and permeability ε, μ do not change along the axis z on a certain segment $a < z < b$. We decompose the approximate solution in a finite number of linearly independent functions satisfying the boundary conditions (2). A suitable basis in this case is the basis $\left\{\vec{\varphi}_j\right\}_{j=1}^{4N^2-2}$ composed of eigenfunctions of the Laplace operator with Dirichlet conditions and Neumann conditions, namely [11]:

$$\left\{\vec{\varphi}_j\right\}_{j=1}^{N^2-1} = (\psi_{nm}(x,y), 0, 0, 0)^T, \ \left\{\vec{\varphi}_j\right\}_{j=N^2-1}^{2N^2-2} = (0, \psi_{nm}(x,y), 0, 0)^T, \quad m, n = 0, \ldots, N-1, m+n > 0, \tag{3}$$

$$\left\{\vec{\varphi}_j\right\}_{j=2N^2-2}^{3N^2-2} = (0, 0, \phi_{nm}(x,y), 0)^T, \ \left\{\vec{\varphi}_j\right\}_{j=3N^2-2}^{4N^2-2} = (0, 0, 0, \phi_{nm}(x,y))^T, \quad m, n = 1, \ldots, N, \tag{4}$$

where $\psi_{nm}(x,y) = \cos(\pi n x)\cos(\pi m y)$, $\phi_{nm}(x,y) = \sin(\pi n x)\sin(\pi m y)$ are eigenfunctions of the Neumann and Dirichlet problems for the two-dimensional Laplace operator in the square S. An approximate solution of the system will be constructed by analogy with the incomplete Galerkin method [15, 16] in the form of expansion

$$(v_h, v_e, u_e, u_h)^T = \sum_{j=1}^{4N^2-2} w_j(z)\,\vec{\varphi}_j(x,y). \tag{5}$$

After substituting the approximate solution into the equations of the system and applying the projection scheme of the Galerkin method, we arrive at a system of ordinary differential equations for the vector of the desired coefficient functions $\vec{w} = (w_1, w_2, \ldots, w_{4N^2-2})^T$:

$$B\vec{w}' + ik_0 A\vec{w} + (ik_0)^{-1} C\vec{w} = \vec{0}, \tag{6}$$

where A, B and C are square matrices, whose elements are double integrals over the waveguide section S:

$$a_{ij} = \iint_S \varepsilon\left(\nabla'\varphi_{j2} + \nabla\varphi_{j3}\right)\cdot(\nabla'\varphi_{i1} - \nabla\varphi_{i4})\,dxdy + \iint_S \mu\left(\nabla'\varphi_{j4} + \nabla\varphi_{j1}\right)\cdot(\nabla'\varphi_{i2} - \nabla\varphi_{i3})\,dxdy, \tag{7}$$

$$b_{ij} = \iint_S \left(\nabla'\varphi_{j1}\cdot\nabla'\varphi_{i1} + \nabla'\varphi_{j3}\cdot\nabla'\varphi_{i3} + \nabla\varphi_{j2}\cdot\nabla\varphi_{i2} + \nabla\varphi_{j4}\cdot\nabla\varphi_{i4}\right)dxdy, \tag{8}$$

$$c_{ij} = \iint_S \left(\Delta\varphi_{j2}\Delta\varphi_{i1}/\mu - \Delta\varphi_{j4}\Delta\varphi_{i3}/\varepsilon\right)dxdy, \tag{9}$$

where φ_{jn}, $n = 1, \ldots, 4$ denote the n-th component of the j-th vector function $\vec{\varphi}_j$ The homogeneous system of ordinary differential equations (6) has solutions that depend on z as $e^{ik_0\beta z}$; such solutions are called normal waveguide modes. Substituting the form $\vec{w}(z) = \vec{\psi} e^{ik_0\beta z}$ of the solution into Eq. (6) and cancelling the nonzero factors, we arrive at the eigenvalue problem

$$K\vec{\psi} = \beta\vec{\psi}, \tag{10}$$

where the matrix K is expressed through the matrices A, B and C as $K = B^{-1}\left(A - k_0^{-2}C\right)$. The eigenvalue problem (10) must then be solved numerically.

Numerical calculations are also implemented using Maple built-in numerical methods (using `LAPACK` library [18] with QR factorization [19]). Eigenvalues and eigenvectors are calculated using the function `Eigenvectors` from the `LinearAlgebra` library [17]. The described algorithm is implemented in Maple and is available at https://bitbucket.org/AnastasiiaTyu/waveguide/downloads/

Verification method (comparison with a hollow waveguide)

Consider a hollow square waveguide with a unit width and height, i.e., a waveguide without an insert ($p_x = p_y = 0$) with the permittivity $\varepsilon_1 = 1$ and permeability $\mu_1 = 1$. Let us calculate the eigenvalues β_j using the four potential method, which determines the phase constants of the corresponding normal modes of the considered hollow waveguide using the four potential method and compare the eigenvalues obtained as a result of a numerical calculation with the analytically known eigenvalues, expressed as $\beta_{1,2} = \pm\sqrt{1 - \pi^2/k_0^2}$, $\beta_{3,4} = \pm\sqrt{1 - 2\pi^2/k_0^2}$. The eigenvalues obtained in the framework of the proposed method will be denoted $\beta_j^{M(N)}$, where the parameter $M(N) = 4N^2 - 2$ is the number of eigenfunctions to be held in the expansion of the approximate solution. Next, we present the absolute and relative errors for the calculated eigenvalues with $N = 3, 4, 5, 6, 7$, which correspond to the dimensions $M =$ 34, 62, 98, 142, 194 of the matrices:

$$\left|\beta_j^{M(N)} - \beta_j\right| < 2.82\cdot 10^{-11}, \quad \left|\beta_j^{M(N)} - \beta_j\right| / \left|\beta_j\right| < 3.62\cdot 10^{-11}, \quad j = 1, 2, 3, 4. \tag{11}$$

The error values obtained in (11) demonstrate the high accuracy of approximate calculations of the eigenvalues β_j that determine the phase constants of the corresponding normal modes in a hollow waveguide.

Conclusion

The proposed approach, based on the introduction of potentials, allows adequate description of the normal modes in closed waveguides having square cross section. The symbolic-numeric implementation of the method allows reduction of the number of calculations needed to find double integrals from rapidly oscillating functions, due to the use of symbolic calculations. The validity of the four potential method within the frameworks of this study was verified by qualitative and numerical analysis of the resulting eigenvalues and eigenfunctions: in the example of a model structure (a hollow waveguide), for which the exact eigenvalues are known in analytical form, the proposed method yields an error of the order of 10^{-11}.

ACKNOWLEDGMENTS

The publication has been prepared with the support of the “RUDN University Program 5-100” and funded by RFBR according to the research projects No. 18-07-00567, 18-51-18005.

REFERENCES

[1] Malykh, M.D., Sevastianov, L.A., Tiutiunnik, A.A., Nikolaev, N.E.: On the representation of electromagnetic fields in closed waveguides using four scalar potentials. Journal of Electromagnetic Waves and Applications **32**(7) 886–898, (2018).

[2] Divakov, D.V., Lovetskiy, K.P., Malykh, M.D., Tiutiunnik, A.A.: The application of Helmholtz decomposition method to investigation of multicore fibers and their application in next-generation communications systems. Communications in Computer and Information Science **919**, 469–480 (2018).

[3] Gusev, A. A. et.al.: Symbolic-Numerical Algorithms for Solving the Parametric Self-adjoint 2D Elliptic Boundary-Value Problem Using High-Accuracy Finite Element Method. In: Gerdt V., Koepf W., Seiler W., Vorozhtsov E. (eds) Computer Algebra in Scientific Computing. CASC 2017. Lecture Notes in Computer Science **10490**, 151–166 (2017).

[4] Shapeev, V.P., Vorozhtsov, E.V.: Symbolic-Numerical Optimization and Realization of the Method of Collocations and Least Residuals for Solving the NavierStokes Equations. In: Gerdt V., Koepf W., Seiler W., Vorozhtsov E. (eds) Computer Algebra in Scientific Computing. CASC 2016. Lecture Notes in Computer Science **9890**, 473–488 (2016).

[5] Bertolazzi, E., Biral, F., Da Lio M.: Symbolic-numeric efficient solution of optimal control problems for multibody systems. Journal of Computational and Applied Mathematics **185**(2), 404–421 (2006).

[6] Kantorovich, L.V., Krylov, V.I.: Approximate Methods of Higher Analysis. Wiley, New York (1964).

[7] Fletcher, C. A. J.: Computational Galerkin Methods. Springer-Verlag, Berlin Heidelberg (1984).

[8] Adams, M. J.: An Introduction to Optical Waveguides. Wiley, New York (1981).

[9] Marcuse, D.: Light Transmission Optics. Van Nostrand, New York (1974).

[10] Tamir, T.: Guided-Wave Optoelectronics. Springer-Verlag, Berlin (1990).

[11] Ladyzhenskaya, O. A.: The Boundary Value Problems of Mathematical Physics. Berlin-Heidelberg-New York, Springer Verlag (1985).

[12] Hellwig, G.: Differential Operators of Mathematical Physics. MA: Addison-Wesley, (1967).

[13] Bathe, K.J.: Finite Element Procedures in Engineering Analysis. Prentice Hall, Englewood Cliffs (1982).

[14] Bogolyubov, A.N., Mukhartova, Yu.V., Gao, J., Bogolyubov, N.A.: Mathematical modeling of plane chiral waveguide using mixed finite elements. Progress in Electromagnetics Research Symposium 1216–1219 (2012).

[15] Sveshnikov, A.G.: The basis for a method of calculating irregular waveguides. Computational Mathematics and Mathematical Physics **3**(1), 170–179 (1963).

[16] Sveshnikov, A.G.: A substantiation of a method for computing the propagation of electromagnetic oscillations in irregular waveguides. Computational Mathematics and Mathematical Physics **3**(2), 314–326 (1963).

[17] Mathematics-based software and services for education, engineering, and research: https://www.maplesoft.com/

[18] LAPACK Users’ Guide Release: http://www.netlib.org/lapack/lug/node93.html.

[19] Kressner, D.: Numerical Methods for General and Structured Eigenvalue Problems. Berlin Heidelberg, Springer (2006).

Method of Adiabatic Waveguide Modes Formulation for Open Layered Dielectric Planar Waveguides in Symbolic Form

A.L. Sevastianov[1,a)], D.V. Divakov[1,b)] and L.A. Sevastianov[1,c)]

[1]*Department of Applied Probability and Informatics,*
Peoples' Friendship University of Russia (RUDN University), 6 Miklukho-Maklaya St, Moscow, Russia, 117198.

[a)]sevastianov-al@rudn.ru
[b)]divakov-dv@rudn.ru
[c)]sevastianov-la@rudn.ru

Abstract. Computational problems of electrodynamics require an approximate solution of the system of Maxwells vector equations for regions with different geometries. The main methods for solving problems with the Maxwell equations are either finite difference methods, or methods based on the Galerkin and Kantorovich expansions, or the finite element method. Each of the classes of methods is characterised by a wide range of permissible objects, but in each of the methods, the solution contains a large number of quantities known only in numerical form.

We have chosen a different approach, in which to describe the waveguide propagation of electromagnetic radiation we propose using the model of adiabatic waveguide modes. This model, firstly, allows for the vector character of electromagnetic radiation and, secondly, involves the amplitude vector function and the scalar function describing the phase as the main desired quantities. This model allows reducing Maxwell's equations to a system of ordinary differential equations, which allows analysis of its solutions at the symbolic level.

Introduction

Over the past 50-70 years, a tremendous development of numerical methods and computational capacities has occurred, which today allow solving tasks of huge computation volume. Computational problems of electrodynamics require an approximate solution of the system of Maxwells vector equations for regions that differ in both linear dimensions and geometry. The approach to solving vector problems with the Maxwell equations, based on modern numerical methods, requires either the introduction of grids to construct difference schemes in the space or space-time domains, or the series expansion of solutions in some complete systems of functions. The series are further truncated to partial sums and Galerkin and Kantorovich methods [2, 3] are used for the final formulation of the computational problem. However, there are also methods that occupy an intermediate place between grid and projection methods, namely, the finite element method [4, 6, 7]. As an alternative to the numerical methods described in the introduction, it is proposed to introduce a physically more understandable type of solution, liked by physicists because of the possibility of constructing several approximations that specify the solution, namely, an asymptotic expansion. A limitation of the validity of such a decomposition is the presence of a small parameter, the smallness of which will determine the class of waveguide structures suitable for consideration in the framework of the method and the range of electromagnetic radiation.

Setting of the problem

Solving the problem of waveguide propagation of electromagnetic radiation for Maxwell's equations without additional assumptions is an extremely difficult task. In our case, we limit the scope of the study to smoothly irregular integrated optical structures that satisfy the following constraints: $\left|\frac{\partial h}{\partial y}, \frac{\partial h}{\partial z}\right| \ll \frac{hk_0}{2\pi}, \quad \left|\frac{\Delta\varphi}{\nabla\varphi}\right| \ll \frac{k_0}{2\pi}$.

From the description of the class of integrated optical structures under consideration, it follows that in the absence of external currents and charges, the induced currents and charges are zero. In this case, the material coupling equations are assumed to be linear. Thus, the electromagnetic field in a space filled with dielectrics in the Gaussian system of units is described by the equations [8, 9, 10]:

$$rot\vec{H} = \frac{\varepsilon}{c}\frac{\partial \vec{E}}{\partial t}, \quad rot\vec{E} = -\frac{\mu}{c}\frac{\partial \vec{H}}{\partial t}. \tag{1}$$

Here $\vec{E} = \left(E_x, E_y, E_z\right)^T$ and $\vec{H} = \left(H_x, H_y, H_z\right)^T$ are vectors of electric and magnetic fields, and c is the speed of light in vacuum. At the interface between dielectric media, the following conditionss are satisfied [8, 9, 10]:

$$\left[\vec{n} \times \vec{H}^1\right]\Big|_{x=h(y,z)} = \left[\vec{n} \times \vec{H}^2\right]\Big|_{x=h(y,z)}, \quad \left[\vec{n} \times \vec{E}^1\right]\Big|_{x=h(y,z)} = \left[\vec{n} \times \vec{E}^2\right]\Big|_{x=h(y,z)}, \tag{2}$$

here $\vec{n}$ is the normal vector to the interface between the first and the second dielectric medium, $\vec{E}^1$, $\vec{E}^2$, $\vec{H}^1$, $\vec{H}^2$ are the vectors of the electric and magnetic field strength in the first and the second medium, respectively. Since an open integrated optical dielectric structure is considered, it is necessary to specify asymptotic boundary conditions at infinity for guided waveguide modes [8, 9, 10]: $\left\|\vec{E}\right\| \xrightarrow[x\to\pm\infty]{} 0$, $\left\|\vec{H}\right\| \xrightarrow[x\to\pm\infty]{} 0$.

In weakly inhomogeneous three-dimensional media, the propagation of electromagnetic radiation is described using locally plane waves or adiabatic approximations of the Maxwell equations obtained by the asymptotic method [1]. The propagation of electromagnetic radiation in the integrated optical structures can be described using the model of adiabatic waveguide modes (AWM). To construct the AWM model [5], we use the asymptotic method [1], in which the desired solutions of Maxwell's equations (1) are presented in the form:

$$\vec{E}(x,y,z,t) = \sum_{s=0}^{\infty} \frac{\vec{E}_s(x;y,z)}{(-i\omega)^{\gamma+s}} \exp\{i\omega t - ik_0\varphi(y,z)\}, \quad \vec{H}(x,y,z,t) = \sum_{s=0}^{\infty} \frac{\vec{H}_s(x;y,z)}{(-i\omega)^{\gamma+s}} \exp\{i\omega t - ik_0\varphi(y,z)\}, \tag{3}$$

In this representation, the following notation and variables are used: ω is the angular frequency of the propagating monochromatic electromagnetic radiation, s is the asymptotic expansion index, $\vec{E}_s$, $\vec{H}_s$ are the corresponding electric and magnetic strength vectors for the asymptotic expansion term of the order s, k_0 is the wave number, $\varphi(y,z)$ is the phase distribution. In this case, the angular frequency of propagating electromagnetic radiation should be large enough, so that the value $\frac{1}{\omega}$ is a small parameter of the asymptotic expansion (3) in the optical range of electromagnetic radiation. Let us substitute the expressions (3) into the system of Eqs. (1) and equate the coefficients for the same powers of $\frac{1}{\omega}$. As a result, in the zero approximation of the method, we arrive at the system of homogeneous equations:

$$\vec{u}' = A\vec{u}, \tag{4}$$

where the vector of the desired quantities $\vec{u} = \vec{u}(x;y,z)$ and the matrix of coefficients $A = A(y,z)$ are defined as follows:

$$u = \begin{pmatrix} H^z(x;y,z) \\ E^z(x;y,z) \\ H^y(x;y,z) \\ E^y(x;y,z) \end{pmatrix}, \quad A = \begin{bmatrix} 0 & \frac{ik_0}{\mu}\varphi_y\varphi_z & 0 & -\frac{ik_0}{\mu}{\varphi_z}^2 + ik_0\varepsilon \\ -\frac{ik_0}{\varepsilon}\varphi_y\varphi_z & 0 & \frac{ik_0}{\varepsilon}{\varphi_z}^2 - ik_0\mu & 0 \\ 0 & \frac{ik_0}{\mu}{\varphi_y}^2 - ik_0\varepsilon & 0 & -\frac{ik_0}{\mu} \\ -\frac{ik_0}{\varepsilon}{\varphi_y}^2 + ik_0\mu & 0 & \frac{ik_0}{\varepsilon}\varphi_y\varphi_z & 0 \end{bmatrix}, \tag{5}$$

where $\varphi_y = \frac{\partial\varphi}{\partial y}, \varphi_z = \frac{\partial\varphi}{\partial z}$.

It is important to note that the matrix of the system under consideration is sparse; in fact, half of the elements of the matrix are zero. In order to build a fundamental system of solutions (FSS) [13, 14] for Eq. (4) in symbolic form, it is necessary to derive symbolic expressions for the eigenvalues and eigenvectors of the matrix A. Moreover, for efficient qualitative analysis of the solutions of the system, symbolic expressions of eigenvalues and eigenvectors must be compact and applicable for such an analysis.

Using the Maple computer algebra system [15], we calculate eigenvalues γ_j and eigenvectors $\vec{\xi}_j$, $j = \overline{1,4}$ of the matrix A in a symbolic form. Let us denote by $\vec{\gamma}$ and X the vector composed of eigenvalues and the matrix of eigenvectors [11, 12]. For the eigenvalues, there are two eigenvalues $\gamma_\pm = \pm k_0\sqrt{-\varepsilon\mu + \left(\frac{\partial\varphi}{\partial y}\right)^2 + \left(\frac{\partial\varphi}{\partial z}\right)^2}$, each having a

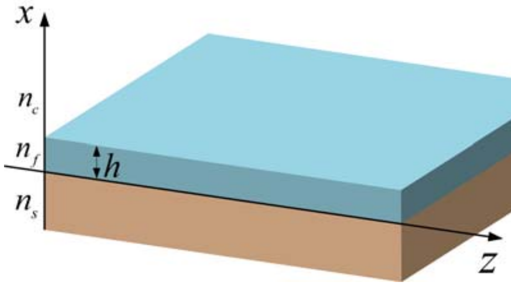

FIGURE 1. Open regular planar three-layer waveguide

multiplicity of 2, which may complicate the form of the FSS of the system under study. Using the computer algebra system, we obtain the matrix of eigenvectors:

$$X = \begin{bmatrix} \frac{-\varepsilon\mu+\varphi_y^2}{\varphi_y\varphi_z} & -\frac{i\mu\sqrt{-\varepsilon\mu+\varphi_y^2+\varphi_z^2}}{\varphi_y\varphi_z} & \frac{-\varepsilon\mu+\varphi_y^2}{\varphi_y\varphi_z} & \frac{i\mu\sqrt{-\varepsilon\mu+\varphi_y^2+\varphi_z^2}}{\varphi_y\varphi_z} \\ -\frac{i\varepsilon\sqrt{-\varepsilon\mu+\varphi_y^2+\varphi_z^2}}{\varphi_y\varphi_z} & \frac{-\varepsilon\mu+\varphi_z^2}{\varphi_y\varphi_z} & \frac{i\varepsilon\sqrt{-\varepsilon\mu+\varphi_y^2+\varphi_z^2}}{\varphi_y\varphi_z} & \frac{-\varepsilon\mu+\varphi_z^2}{\varphi_y\varphi_z} \\ 0 & 1 & 0 & 1 \\ 1 & 0 & 1 & 0 \end{bmatrix}$$

From the form of the matrix X, it can be noted that despite the presence of multiple eigenvalues, the eigenvectors are linearly independent. Using the obtained symbolic expressions for eigenvalues and eigenvectors, we construct the FSS for the SODE (4): $\vec{U}(x; y, z) = C_1\vec{\xi}_1 e^{\gamma_+ x} + C_2\vec{\xi}_2 e^{\gamma_- x} + C_3\vec{\xi}_3 e^{\gamma_+ x} + C_4\vec{\xi}_4 e^{\gamma_- x}$.

Taking into account the fact that the FSS is known in symbolic form and is amenable to qualitative analysis, we will use it to state the problems of finding the modes of multilayer dielectric waveguides.

Numerical calculation of guided modes of a planar open three-layer waveguide

As an example, consider an open three-layer regular planar dielectric waveguide, schematically presented in Fig. 1. Note that such planar structures are well described in the framework of the scalar model, therefore, for verification, we compare the phase constants obtained in the model of adiabatic waveguide modes with appropriate coefficients obtained in the scalar model [16, 17]. Now let us proceed to numerical calculations. For this purpose we specify the required values as follows: $\lambda = 0.55$; $k_0 = 2\pi/\lambda$; $n_c = 1.0$; $n_f = 1.565$; $n_s = 1.47$; $h = 2\lambda$.

To verify the described method, we compare the calculated phase constants with those obtained within the scalar model [16, 17]. The phase constants in the framework of the described method are denoted by β^{vector}, and the phase constants obtained in the scalar model are denoted by β^{scalar}. In the framework of the algorithm described above, we will find the phase constants (the zeros of the determinant function) with the accuracy $\varepsilon = 4.44 \times 10^{-18}$; with the same accuracy, we calculate the phase constants using the scalar model. Let us compare the calculated phase constants and determine the absolute $\delta_{abs} = \left|\beta^{scalar} - \beta^{vector}\right|$ and relative $\delta_{rel} = \left|\beta^{scalar} - \beta^{vector}\right| / \left|\beta^{scalar}\right|$ errors. The verification results are presented in the table below.

β^{scalar}	β^{vector}	δ_{abs}	δ_{rel}
1.5514927380692901290	1.5514927380692901222	6.8×10^{-18}	4.38×10^{-18}
1.5501811158901042864	1.5501811158901042882	1.8×10^{-18}	2.38×10^{-18}
1.5117506145374407068	1.5117506145374407104	3.6×10^{-18}	1.16×10^{-18}
1.5072749512764207624	1.5072749512764207660	3.6×10^{-18}	2.39×10^{-18}

Given the magnitude of the error $\varepsilon = 4.44 \times 10^{-18}$, we can conclude that the absolute error δ_{abs} has the order of the error of calculations, and the relative error does not exceed the error of the calculations. From the numerical results, it follows that the phase constants, calculated in the framework of the method under study and in the framework of the scalar model, coincide within the accuracy of the calculations performed.

Conclusion

In the paper, the vector problem of finding the guided modes of an open dielectric waveguide with an arbitrary number of dielectric layers having smooth boundaries is posed in symbolic form.

Thanks to the model of adiabatic waveguide modes, it is possible to obtain rather simple symbolic expressions when formulating the problem of finding guided modes, which radically distinguishes the model used from other approaches to the modelling of smoothly irregular integrated optical structures. A symbolic-numerical method for the approximate solution of the problem is developed. The method is implemented in the Maple computer algebra system. Verification was performed by comparing the phase constants calculated in the framework of the method under study with those obtained using the scalar model. The results coincide with an accuracy close to the accuracy of calculations, which demonstrates the consistency of the developed method. All results were obtained in the Maple computer algebra system using the LinearAlgebra and ArrayTools packages.

ACKNOWLEDGMENTS

The publication has been prepared with the support of the "RUDN University Program 5-100" and funded by RFBR according to the research projects No. 18-07-00567 and 19-01-00645.

REFERENCES

[1] Babich, V. M., and Buldyrev, V. S. : Asymptotic Methods in Short-Wave Diffraction Problems. Nauka, Moscow (1972) [English translation: Springer Series on Wave Phenomena 4. Springer, Berlin Heidelberg New York 1991]

[2] Kantorovich, L.V., Krylov, V.I.: Approximate Methods of Higher Analysis. Wiley, New York (1964).

[3] Fletcher, C. A. J.: Computational Galerkin Methods. Springer-Verlag, Berlin Heidelberg (1984).

[4] Gusev, A. A. et.al.: Symbolic-Numerical Algorithms for Solving the Parametric Self-adjoint 2D Elliptic Boundary-Value Problem Using High-Accuracy Finite Element Method. In: Gerdt V., Koepf W., Seiler W., Vorozhtsov E. (eds) Computer Algebra in Scientific Computing. CASC 2017. Lecture Notes in Computer Science **10490**, 151–166 (2017).

[5] Sevastyanov, L.A., Sevastyanov, A.L., Tyutyunnik, A.A.: Analytical Calculations in Maple to Implement the Method of Adiabatic Modes for Modelling Smoothly Irregular Integrated Optical Waveguide Structures. In: Gerdt V.P., Koepf W., Seiler W.M., Vorozhtsov E.V. (eds) Computer Algebra in Scientific Computing. CASC 2014. Lecture Notes in Computer Science **8660**, 419–431 (2014).

[6] Bogolyubov, A.N., Mukhartova, Yu.V., Gao, J., Bogolyubov, N.A.: Mathematical modeling of plane chiral waveguide using mixed finite elements. Progress in Electromagnetics Research Symposium 1216–1219 (2012).

[7] Bogolyubov, A.N., Mukhartova, Y.V., Gao, T.: Calculation of a parallel-plate waveguide with a chiral insert by the mixed finite element method. Mathematical Models and Computer Simulations **5**(5), 416–428 (2013).

[8] Adams, M. J.: An Introduction to Optical Waveguides. Wiley, New York (1981).

[9] Marcuse, D.: Light Transmission Optics. Van Nostrand, New York (1974).

[10] Tamir, T.: Guided-Wave Optoelectronics. Springer-Verlag, Berlin (1990).

[11] Coddington, Earl A.; Levinson, Norman.: Theory of Ordinary Differential Equations. New York: McGraw-Hill (1955)

[12] Hartman, Philip.: Ordinary differential equations, Classics in Applied Mathematics, 38, Philadelphia: Society for Industrial and Applied Mathematics,(2002) [1964]

[13] W. Johnson.: A Treatise on Ordinary and Partial Differential Equations, John Wiley and Sons, in University of Michigan Historical Math Collection (1913)

[14] A. D. Polyanin, V. F. Zaitsev, and A. Moussiaux.: Handbook of First Order Partial Differential Equations, Taylor & Francis, London (2002)

[15] Mathematics-based software and services for education, engineering, and research url:https://www.maplesoft.com/

[16] K.P. Lovetskiy, M.N. Gevorkyan, D.S. Kulyabov, A.L. Sevastyanov, L.A. Sevastyanov, Waveguide modes of a planar optical waveguide, Mathematical Modelling and Geometry, **3**(01), 43-63 (2015).

[17] E.A. Ayryan, A.A. Egorov, E.N. Michuk, A.L. Sevastyanov, L.A. Sevastianov, A.B. Stavtsev Representations of Guided Modes of Integrated-Optical Multilayer Thin-Film Waveguides E11-2011-31, LIT preprints (2011)

Willingness to Pay as an Index of Direct Taxation for Restoration of Seaside Environment

Odysseas Kopsidas

Department of Industrial Management & Technology, School of Maritime and Industrial Studies, University of Piraeus, 80, M. Karaoli & A. Dimitriou St., GR-18534, Piraeus, Grecce

Email: odykopsi@yahoo.gr

Abstract. Thermaic, Pagasetic and Saronic gulfs which surround the regional units of Thessaloniki, Magnesia and Attica respectively, do suffer from heavy pollution. In order to examine to what extend citizens of Thessaloniki, Volos and Piraeus were willing to pay (WTP) for restoration operations in their cities, questionnaires were given out. 240 individuals were interviewed, 80 people from each city were chosen to serve as a random sample and provide. The answers to various questions statistics show that volunteers in Volos are willing to pay more for the environmental recovery of the gulf, while respondents in Thessaloniki are willing to pay the least amount for the environmental restoration. Considering the results of this empirical analysis, it is safe to conclude that the respondents of the regional area of Thessaloniki would pay more money for the restoration of the gulf. At the same time they believe the protection of the sea is a significant issue. Respondents in close proximity to the sea declare that they would pay higher to restore it. It is also important to note that there are different parameters that affect the willingness of respondents to pay in each case. The above study, which has been conducted in three different areas of Greece aims to be part of a larger environmental protection plan and will hopefully be supported by every citizen, the Public Administration and Local Authorities.

Key –words: willingness to pay, WTP, direct taxation, seaside, environment, restoration

INTRODUCTION

Thermaic, Pagasetic and Saronic gulfs which surround the regional units of Thessaloniki, Magnesia and Attica respectively, do suffer from heavy pollution. Marine pollution occurs to great extend from residential and industrial waste, thus nowadays, environmental restoration initiatives are most compelling.

The contamination of water happens due to excessive use of fertilizers and pesticides, from various human activities taking place on land [1-2]. The soil absorbs all those harmful substances, which get incorporated into the water later on, through soil disassembly [3-4]. As urban and industrial waste water constitute major pollutants of the marine ecosystem, the results below indicate the willingness of citizens to contribute with money to the restoration of the marine environment [5-6].

IMPLEMENTATION

In order to examine to what extend citizens of Thessaloniki, Volos and Piraeus were willing to pay (WTP) for restoration operations in their cities, questionnaires were given out. 80 people from each city were chosen to serve as a random sample and provide answers to various questions as it can be seen below. The main question was about the amount of money the interviewees would donate each month to projects related to environmental regeneration, which along with a list of variables shed light to the survey [7-9]. The list of variables follows right below:

TABLE 1. List of Variables

X_1:	**Frequency of visits to the seaside**
X_2:	Information about the environmental situation of the gulf
X_3:	Current environmental situation of the gulf
X_4:	The main environmental problem of the gulf
X_5:	The reason of the main environmental problem of the gulf
X_6:	Protection of gulf by the Authorities
X_7:	Member of environmental group
X_8:	Financial participation of the Municipality for each 100 euro
X_9:	Financial participation of the interviewees for each 100 euro
X_{10}:	What would you wish to be done
X_{11}:	Willingness to pay for restoration (WTP)
X_{12}:	Willingness to pay if you leave near the sea (WTP_1)
X_{13}:	What would you like to be restored firstly
X_{14}:	Willingness to accept the seaside pollution (WTA)
X_{15}:	Industries
X_{16}:	Gender
X_{17}:	Age
X_{18}:	Live / living
X_{19}:	Individual whose residency is near the seaside
X_{20}:	Labor near the seaside
X_{21}:	Distance from seaside
X_{22}:	Job
X_{23}:	Sea job
X_{24}:	Family
X_{25}:	Children
X_{26}:	Level of education
X_{27}:	Personal Income
X_{28}:	Family Income

At this stage, the results of the descriptive statistical analysis regarding the decision of citizens to pay or not for environmental restoration projects (WTP) are listed below for each city.

TABLE 2. Descriptive Statistics for the variable WTP

	Mean	Standard Deviation	Range	Min	Max
Thessaloniki	2.89	0.852	4	1	4
Volos	24.18	12.231	38	0	40
Piraeus	9.25	14.566	38	0	40

As it can be seen on the table above, statistics show that volunteers in Volos are willing to pay more for the environmental recovery of the gulf, while respondents in Thessaloniki are willing to pay the least amount for the environmental restoration.

In the next part of the analysis, a linear regression model is applied considering X_{11} (WTP) as the dependent variable, while the others are independent. This method calculates the Variance Inflation Factor (VIF) with the SPSS - Statistics program. Based on the analysis, it can be seen that the variables X_{17}, X_{22} have a VIF value higher than 2. For this calculation, the X_{17} variable was excluded from the model.

The next step of this analysis is ANOVA for each sample. The results are presented in the following table.

TABLE 3. Linear Regression Analysis for each sea

Sea	Linear Regression Model
Thessaloniki	$X_{11} = 0.295 * X_4 + 0.449 * X_6 - 0.178 * X_{10} - 0.593 * X_{12}$
Volos	$X_{11} = 1.174 - 0.379 * X_9 + 0.84 * X_{12} - 0.157 * X_{14} - 0.183 * X_{19} + 0.213 * X_{28}$
Piraeus	$X_{11} = 0.843 + 0.272 * X_7 - 0.421 * X_9 + 0.584 * X_{12} - 0.272 * X_{19}$

Note 1: The coefficients that are not statistically significant and excluded from the models.
Note 2: The factors were considered at a 5% materiality level.

TABLE 4. ANOVA

Sea	Model	Sum of Squares	Df	Mean Square	F statistic	Sig
Thessaloniki	Regression	26.413	17	1.845	18.951	0.256*
	Residual	6.375	52	0.093		
	Total	52.125	93			
Volos	Regression	49.318	18	1.873	9.623	0.123*
	Residual	21.179	58	0.426		
	Total	42.782	96			
Piraeus	Regression	29.711	26	1.986	4.768	0.228*
	Residual	18.876	32	0.498		
	Total	47.984	52			

At this final stage, Logit Regression Analysis for each model (one for each gulf) has been applied. The results are presented in the following Table.

TABLE 5. Logit analysis for the effect of information

Sea	Model	−2Log Likelihood	Chi-square	Df	Sig
Thessaloniki	Intercept Only	175.14			
	Final	0.136	175.039	17	0.134*
Volos	Intercept Only	189.361			
	Final	76.188	128.174	28	0.345*
Piraeus	Intercept Only	153.183			
	Final	78.876	76.329	17	0.164*

The table below shows the results of each Logit model where coefficients show statistical significance at a 5% level, ie coefficients that are numerically less than 0.05.

TABLE 6. Model Logit Results

Sea	Variables for WTP
Thessaloniki	$X_{12}(+), X_{13}(+), X_{14}(-), X_{19}(+)$
Volos	$X_1(-), X_4(+), X_6(+), X_{10}(-), X_{12}(+), X_{15}(+)$
Piraeus	$X_{10}(-), X_{12}(+), X_{24}(-)$

The above Table shows that in the case of the Thermaic Gulf the proximity to the beach (X_{12}) is significant. The closer the distance of the respondent to the beach, the more money is available to pay. The same decision shares the ones whose property is located near the coastline(X_{19}).

CONCLUSION

Considering the results of this empirical analysis, it is safe to conclude that the respondents of the regional area of Thessaloniki would pay more money for the restoration of the gulf. At the same time they believe the protection of the sea is a significant issue. Furthermore, equally willing to pay are the respondents who live near the coastal area. Regarding the region of Volos, it has been found that the willingness of respondents to contribute with money increases according to the frequency of their visits to the coastal zone. The interviewees consider the environmental problem of the gulf to be in crucial condition, however the Local Government has been found unable to cope with it efficiently.

Additionally to the above, regarding the area of Piraeus, the willingness of respondents to pay for the restoration of the gulf is high because they estimate that the environmental status of the sea is in a very bad condition. Equally fond to contribute appear those interviewees whose residency is near the sea and those who according to their marital status, are married.

Moreover, one cannot ignore the fact that the three major gulfs in Greece continue to deteriorate environmentally. Respondents in close proximity to the sea declare that they would pay higher to restore it. It is also important to note that there are different parameters that affect the willingness of respondents to pay in each case. This is to be expected considering the different living conditions in each city which drive the population into different decisions based on their needs.

Finally, it is the parameter of the social dimension that appears in Piraeus and more specifically the participants who are married appeared as more eager to donate higher amounts, probably based on future concerns about their offspring and their wellbeing.

The above study, which has been conducted in three different areas of Greece aims to be part of a larger environmental protection plan and will hopefully be supported by every citizen, the Public Administration and Local Authorities.

REFERENCES

1. D. Xu, Chang, W., Hou, L., Zhao, T., Y. Measure of watershed ecological compensation standard based on WTP and WTA: A case study in Liaohe River Basin, *Resources Science* (2012).

2. L., Xu, B.Yu, Y. Li. Ecological compensation based on willingness to accept for conservation of drinking water sources, *Frontiers of Environmental Science & Engineering, Springer* (2015).

3. L. Huang, C. Zhao, Non market valuation of forest resources in Guiyang City of Guizhou Province based on comparative analysis of WTP and WTA. *Chinese Journal of Ecology* (2011).

4. K.M.A. Chan, T. Satterfield, J. Goldstein, Rethinking ecosystem services to better address and navigate cultural values. *Ecological Economics, Elsevier* (2012).

5. F. Carlsson, O. Johansson, Stenman, Annu. Behavioral economics and environmental policy. *Rev. Resour. Econ.* (2015).

6. D. C. Kingsley, T. C. Brown. Value learning and the willingness to accept–willingness to pay disparity. *Economics Letters, Elsevier* (2013).

7. T. Tunçel, J. K. Hammitt. A new meta-analysis on the WTP / WTA disparity. *Journal of Environmental Economics, Elsevier* (2014).

8. J. Talberth, M. Weisdorf . Genuine progress indicator 2.0: pilot accounts for the US, Maryland, and City of Baltimore 2012–2014. *Ecological Economics, Elsevier* (2017).

9. Y. Kim, C., L. Kling, , J. Zhao. Understanding behavioral explanations of the WTP-WTA divergence through a neoclassical lens: implications for environmental policy. *Annu. Rev. Resour. Econ.* (2015).

Determination of the Optical Properties of a-$Si_x ge_{1-X}$ Facilitated by Micro-Combinatory

György Sáfrán[1, a)], Benjámin Kalas[1)] and Miklós Serényi[1)]

[1]Centre for Energy Research, Hungarian Academy of Sciences, Konkoly Thege Miklós str. 29-33. 1121 Budapest, Hungary

[a)]Corresponding author: safran.gyorgy@energia.mta.hu

Abstract. The traditional "multiple-sample concept" combinatorial techniques produce numerous different samples, very effectively, however, handling and measuring dozens of samples is definitely not effective. We worked out the method "one-sample concept" micro-combinatory that provides extreme throughput in both preparation and measurement of composition dependent properties of binary films. Due to its technological importance gradient amorphous SiGe was studied to reveal the correlations between composition, structure, and optical properties. SiGe micro-combinatorial samples were deposited by DC magnetron sputtering and scanned by a Woollam M-2000DI rotating compensator spectroscopic ellipsometer. The dispersion of the layer was modeled using the Tauc-Lorentz (TL) approach. This approach allows that the total number of fitted parameters are kept at a reasonable value (thicknesses of the roughness layer and the film, and the TL parameters). The spectra measured at each position (each composition) have been fitted. To shorten the time of calculations of the fitting procedure we used the calculated parameters of the previous point as starting data to find the best match between the measured and calculated ellipsometry spectra.

Introduction

Spectroscopic ellipsometry (SE) is a premier tool for the optical characterization of layer structures consisting thin films. This method is based on the measurement of both the amplitude- and phase change of the light beam which was reflected on the surface of the sample to be investigated. From the measurement the ellipsometric angles, Ψ and Δ are obtained, defined by

$$\rho = \tan \Psi \exp(i\Delta)\,, \tag{1}$$

where ρ is the complex reflectance ratio and the angles Ψ **,** Δ are related to the amplitude ratio and the phase difference between p- and s-polarized light, respectively**.** SE is an indirect method, meaning that an optical model is necessary in order to obtain the true values of physically meaningful parameters (e.g. layer thickness, layer roughness or optical properties). To calculate these values usually random global fit is carried out and the root mean square error **(**RMSE**)** is computed numerically. The RMSE is defined as

$$RMSE = \sqrt{\frac{1}{3n-m}\sum_{j=1}^{n}\left[\left(\frac{N_j^m - N_j^c}{\sigma_{N_j}^m}\right)^2 + \left(\frac{C_j^m - C_j^c}{\sigma_{C_j}^m}\right)^2 + \left(\frac{S_j^m - S_j^c}{\sigma_{S_j}^m}\right)^2\right]}\,, \tag{2}$$

where n is the number of wavelengths, m is the number of the fit parameters of the model. $N=\cos(2\Psi)$, $C=\sin(2\Psi)\cos(\Delta)$ and $S=\sin(2\Psi)\sin(\Delta)$. The subscripts '*m*' and '*c*' indicate the measured and the calculated values, while σ is the standard deviation of the measured values.

Experimental

Due to technological importance, the correlations between composition, structure, and optical properties of amorphous SiGe were studied. Research of thin SiGe layers is motivated by the potential of widespread applications, e.g. solar cells, thin film transistors, Schottky diodes, thermal sensors, bolometers. Due to enhanced non-linear properties of Ge to Si, layers of high Ge content are of interest in the development of optoelectronics devices for the in mid-infrared range.

Combinatorial methods are widespread in chemistry and biology and have increasing importance in materials science. The traditional "multiple-sample concept" combinatorial techniques produce numerous different samples, in one experiment, very effectively, however, handling and measuring dozens of samples is definitely not efficient. Contrarily, we have been worked out the "one-sample concept" micro-combinatory [1] that provides an extreme high throughput in both preparation and measurement of composition dependent properties of binary films by transmission electron microscopy (TEM) and further analytical techniques. The micro-combinatorial sample is prepared in three sections that contain all compositions of a binary layer system. The first section exhibits pure component A, the second one is a concentration spread A-B section with a constant concentration gradient and the third one is of pure component B. As a result a single micro-combinatorial sample includes the entire binary system of components A_xB_{1-x} (where $0 \leq x \leq 1$) and, moreover, it is prepared to suit the wished measuring technique. The sample is deposited by dual DC magnetron sputtering through a narrow slot that travels above the substrate meanwhile the powers of the magnetrons are regulated, as preprogrammed. This creates the concentration spread within the deposited film. The experimental setup of the deposition is shown in Fig 1.

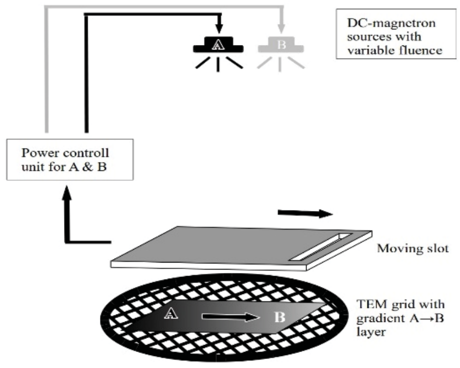

FIGURE 1. Setup of the synthesis of a micro-combinatorial TEM sample. "A" and "B" materials are deposited from regulated power DC magnetron sources onto a TEM grid, through a moving slot. The output powers of the sources A and B are adjusted in sync with the slot movement. The sample consists of 3 sections: pure A, gradient A ⇨ B and pure B arranged in a line.

The patented method [2] enables the collection of a whole data library of concentration dependent properties of a binary system within a single specimen and within the space of one measuring session. A combinatorial sample for TEM appears, on microgrid, as a 1x1.5 mm^2 size layer, while for RBS, XRD and ellipsometry it is deposited on a 12x25mm^2 size Si-wafer as depicted in Fig 2. Micro-combinatorial SiGe samples were deposited by DC magnetron sputtering. TEM, RBS and energy dispersive X-ray spectroscopy

(EDS) showed an amorphous structure of SiGe and a linear concentration change in the whole composition range.

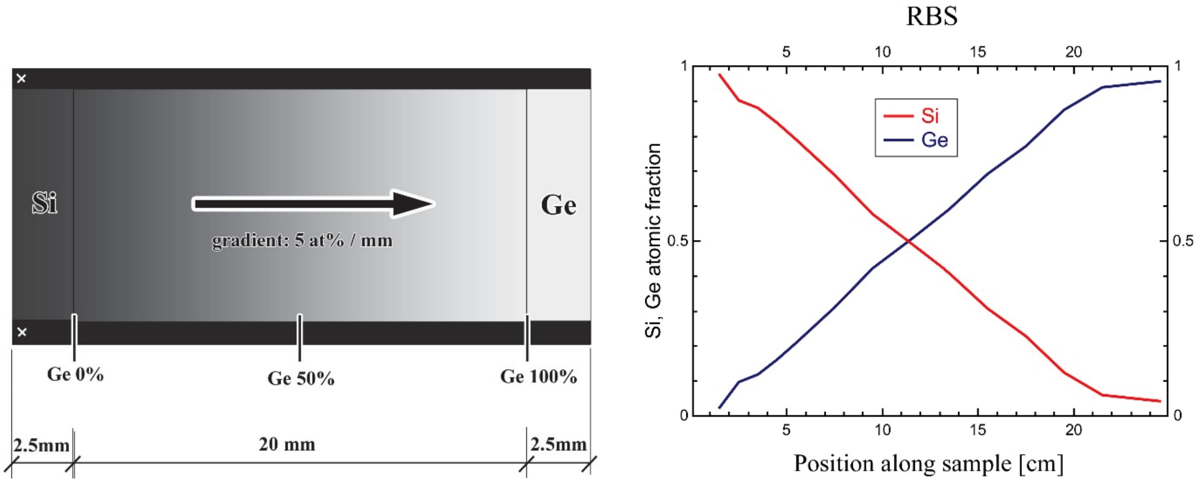

FIGURE 2. (a) Scheme of a micro-combinatorial SiGe sample deposited typically on Si wafer dedicated to X-ray diffraction (XRD), ellipsometry and nanoindentation measurements. The 10 x 25mm^2 overall size layer includes a 2.5 mm, 20 mm and 2.5 mm long sections of pure Si, gradient SiGe and pure Ge film, respectively. (b) Variation of Atomic fractions of Si and Ge along a sample shown in "a" measured by Rutherford Backscattering Spectrometry (RBS).

Discussion and results

For a mapping of the optical properties of the sample, it was scanned by a Woollam M-2000DI rotating compensator spectroscopic ellipsometer with a focused spot. A linescan has been implemented along the center line of the wafer parallel to the concentration gradient. The measurement took only a few seconds for scanning the mid infrared to ultraviolet wavelength range at each position. That provided high-resolution and high-accuracy data library with an acceptable acquisition time of the entire map. In order to determine the optical parameters of the deposited a-$Si_{1-x}Ge_x$ films, a model was constructed to calculate the ellipsometric angles and to fit the parameters in order to obtain a good match to the measured and fitted spectra.

The dispersion of the layer was modeled using the Tauc-Lorentz (TL) approach [3]. In this parameterization the imaginary part of the dielectric function is described as a combination of a Lorentz oscillator with the three usual parameters (the broadening, the amplitude and the peak energy of the oscillators) and an additional Tauc gap parameter. This approach allows that the total number of fitted parameters are kept at a reasonable value (thickness, roughness of the layer and the TL parameters). The spectra have been recorded at three angles of incidence providing six measured values at each wavelength, and a total of about 2000 measured values for each scanned position (Fig. 3.). In order to reduce the number of fitting iterations we used the calculated parameters of the previous point as starting data to find the best match between the actually measured and calculated ellipsometry spectra. Based on this algorithm the fit was calculated within relatively short time resulting in a smooth map of the optical spectra and collection of an entire data library for a-$Si_{1-x}Ge_x$ films as a function of composition.

The refractive index and extinction coefficient maps were obtained and plotted, as color coded, in the whole concentration range (Fig. 4). The possible value range of each parameter was carefully chosen. The effect of using the data calculated from the previous measurement point as a starting value was also considered. This analysis revealed that around 40% performance increase is achievable in computing time compared to the computation with random starting place.

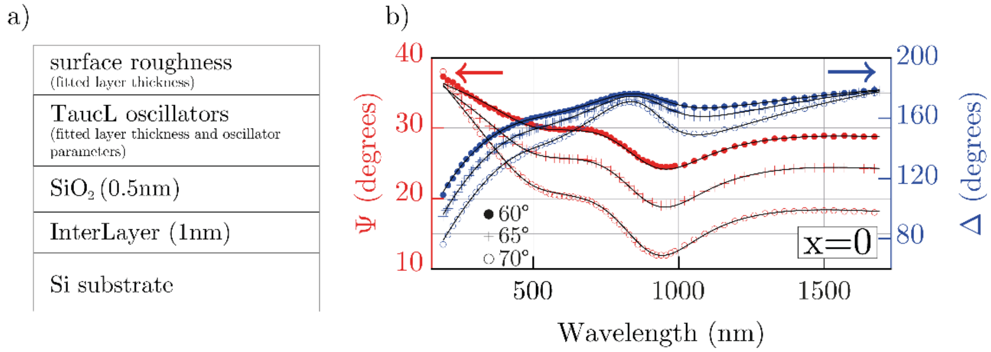

FIGURE 3. a) The optical model used for describing the SiGe samples and b) the evaluated spectra with fitted curves for x=0 (bare a-Ge side). The symbols show measured values and the solid lines are provided by the fitting process.

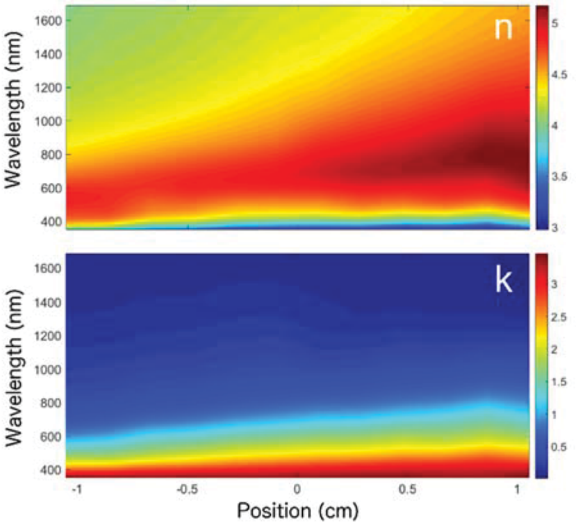

FIGURE 4. Color coded maps of the refractive index (n) and extinction coefficient (k) for a-Si_xGe_{1-x} in the whole concentration range of x .

REFERENCES

1. G. Sáfrán: Ultramicroscopy **187**, 50–55 (2018)
2. G. Sáfrán: Hung. Patent No. P 15 00500 (2015)
3. Jellison, G. E. & Modine, F. A. Parameterization of the optical functions of amorphous materials in the interband region. Appl. Phys. Lett. **69**, 371–373 (1996).

Microservices-Based Application for Fast Modeling of Microstrip Antenna Array Characteristics

Viacheslav Kizimenko [a)] and Roman Bogdanov [b)]

Belarusian State University of Informatics and Radioelectronics
P. Brovki str., 6 - 201b, R&D Department, Center 1.6
Minsk, Belarus

[a)] kizimenko_v@mail.ru
[b)] bogdanov@bsuir.by

Abstract. Microservices-based application for fast calculation of the characteristics and parameters of microstrip antennas and arrays using a resonator model and a modified Method of Integral Equations in a thin-wire approximation was developed. The comparison of achieved results with results calculated using wide known software of full 3D-electrodynamic modeling shows, that the developed thin-wire mathematical model basically corresponds to the real radiator with a solid plate and allows to simulate characteristics of both single microstrip radiators and arrays with rather high accuracy. Significant acceleration of the numerical modeling process is achieved through the use of CUDA technology and Intel Optane SSD.

INTRODUCTION

At the moment, a large number of published articles are devoted to modeling antennas with the use of Graphics Processing Units (GPU) and parallel computing architecture CUDA. At the same time, the main difficulty is the limited amount of video memory of graphics accelerator and its higher cost compared to conventional memory. The calculation is possible only for relatively small tasks and antenna arrays with a small number of radiating elements. For instance, the main difficulty in the case of the traditional finite element method (FEM) is an intensive data exchange between blocks of code. It can be seen that due to the growth of data exchange, the increase in the number of video cards does not give a corresponding increase in computing performance: the low speed of copying data into video memory is a limiting factor. For example, Nvidia GeForce RTX 2070 graphics card has the data bandwidth inside the card around 448 GB/s, but maximal total bandwidth for PCIe 3.0x16 bus is 32 GB/s. To solve the problem of modeling the characteristics and parameters of multi-element microstrip antenna arrays, a special method that allows reducing the calculation time and the dimension of the matrices, which reduces the time required to transfer data to the video memory was developed.

METHOD FOR CALCULATING THE CHARACTERISTICS OF MULTI-ELEMENT MICROSTRIP ANTENNA ARRAY AND ARCHITECTURE OF THE APPLICATION

To determine the initial dimensions of a single microstrip radiator, it is proposed to use a resonator model that allows to accurately determine the resonant frequency of the radiator. An analysis of various types of resonator models, showed, that the most accurate results are given by the F. Abboud, J.P. Damiano, A. Papiernik model [1] (the error in determining the resonance frequency is less than 1.8%).

After determining the initial dimensions of the microstrip radiator using the resonator model, a thin wire model is created on the basis of a modified Method of Integral Equations – MIE [2], which takes into account the effective dielectric permeability of the substrate. In Fig. 1 an example of a fine-wire approximation of a single rectangular microstrip element fed by a coaxial waveguide is shown. Parameters of the radiator: plate dimensions a x b = 17x11 mm, dielectric constant of the substrate ε = 2.33; thickness h = 3.175 mm.

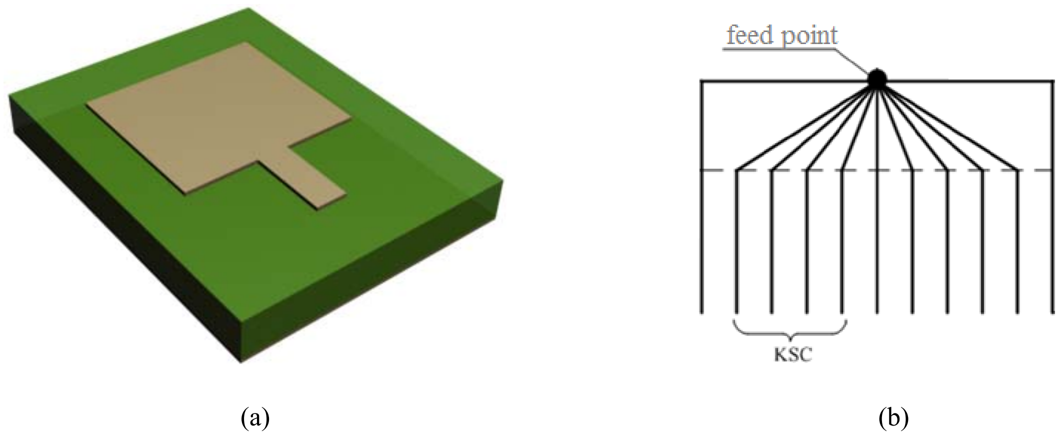

FIGURE 1. Approximation of the microstrip radiator (a) by a system of thin wires (b)

In Fig. 2 the results of calculating the dependences of the input resistance on frequency using the modified Method of Integral Equations in comparison with the experimental data are shown.

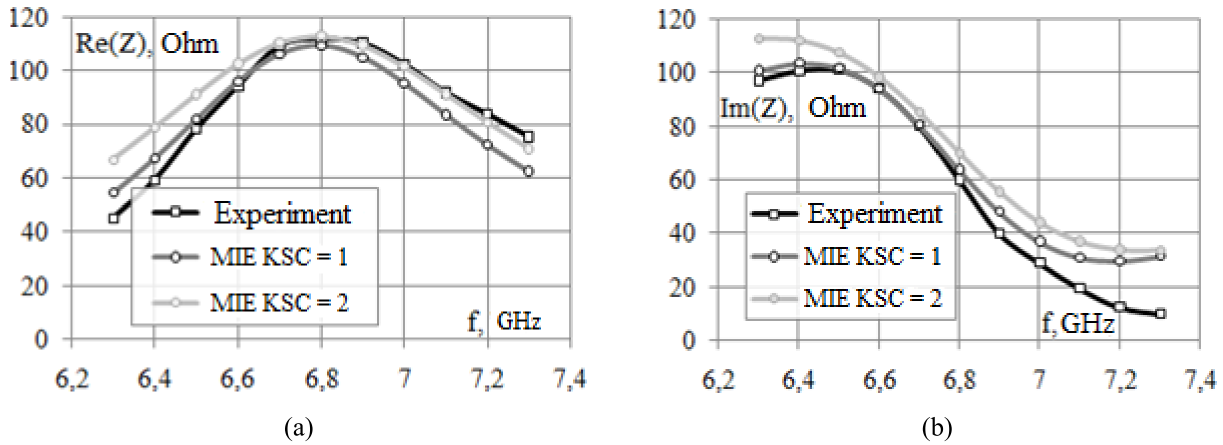

FIGURE 2. Frequency dependences of the active (a) and reactive (b) part of the input impedance of a microstrip antenna

Based on the calculated model of a single microstrip radiator, an antenna array model is created from such radiators with a predetermined arrangement and spacing between the elements.

Fig. 3 shows the result of calculating the direction of the square antenna array (7x7 elements) with a step between elements along both axes $\Delta = 0.5\lambda$.

The presented results show that the developed thin-wire mathematical model basically corresponds to the real radiator with a solid plate and allows to simulate characteristics of both single microstrip radiators and arrays from them with rather high accuracy.

During the process of solving this problem at the final stage, the current distribution was determined by solving the System of linear equations with the order of the matrix of mutual resistances 8428 (the total number of basis currents on the antenna array). To reduce simulation time, the source code was adapted to run on NVIDIA graphics accelerators using CUDA technology.

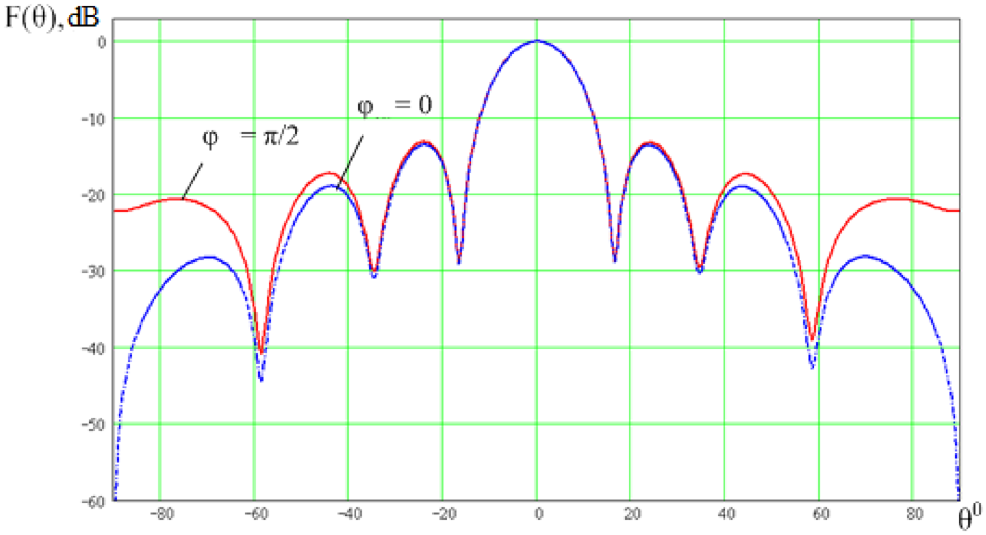

FIGURE 3. Farfield of the microstrip antenna array (7x7 elements) at two planes

Fig. 4 presents the printscreen of the window for monitoring the workload of the graphics accelerator, as well as a graph showing how many times the process of solving the System of linear equations on the GPU is faster in comparison with the usual CPU.

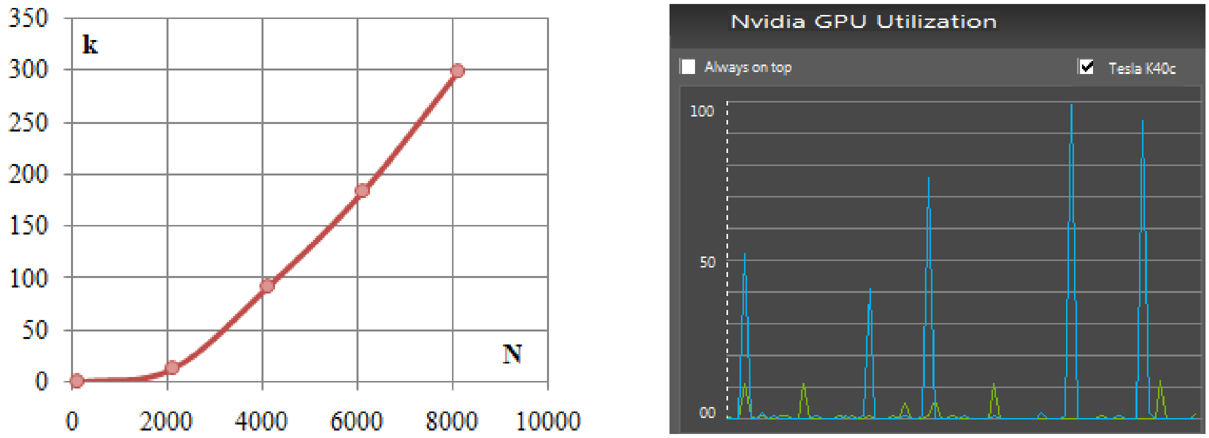

(a) (b)

FIGURE 4. Graph of the acceleration of the System of linear equations solution process on the GPU and graph of GPU workload

The process of modeling was held on a computer with the Core i7-5820K (3.3 GHz), 16 GB of RAM, and the NVIDIA Tesla K40C graphics accelerator. As can be seen from the graph in Fig. 4, with the increase of the number of matrix elements up to 8100, the acceleration of the calculation process compared to the CPU is 297 times. During the process of modeling we should save matrixes of large sizes on a hard drive. To achieve additional speedup, we have tried new storage solution - Intel Optane DC P4800X [3]. The total time, which was necessary for recording and reading blocks of various sizes, was measured. The comparison of results showed that with the size of the stored block up to 110 MB, Intel Optane is almost 2 times faster than the conventional SSD, achieving acceleration of 3.25 times at some points (2MB).

Taking into account the situation, that during the process of the optimisation of antenna array, the huge amount of variants should be modeled, the microservices-based software was developed. For managing the resources of computing cluster, the Kubernetes framework was used. Kubernetes is a portable, extensible open-source platform

for managing containerized workloads and services, which contains a load-balancer, distributing the workload between the nodes. The architecture of the developed software is presented in Fig. 5.

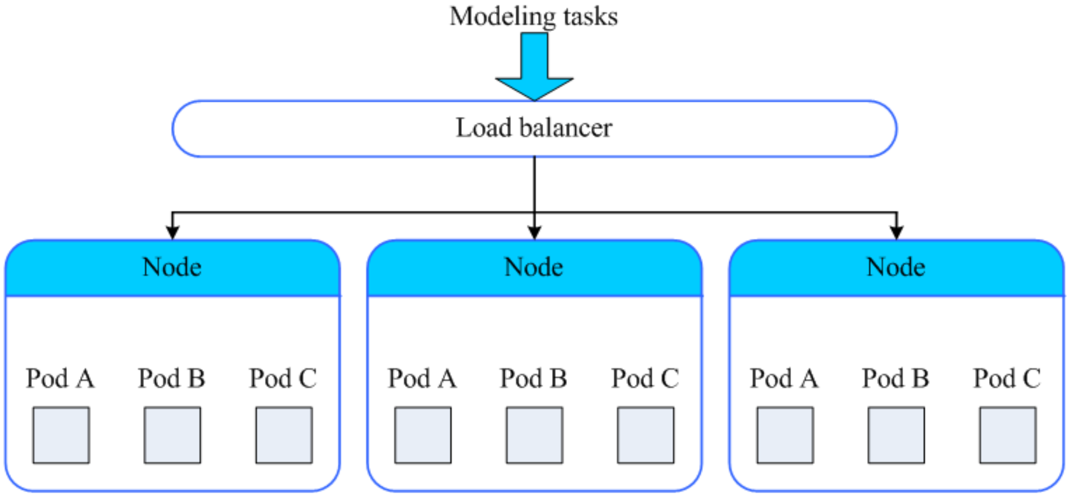

FIGURE 5. Architecture of the developed application

As it can be seen from Fig.5, the modeling tasks with different parameters (quantity of microstrip radiators, their geometrical size, value of dielectric permeability and thickness of the substrate, frequency, type of amplitude and phase distribution) come to the load balancer and then distributed among the computing nodes. The whole process of the modelling is divided into separate microservices: computation the matrix of mutual impedance, calculation the currents distribution and farfield of whole system. A key feature of the developed modeling methodology is the possibility of multiple reuse of the previously calculated matrix of mutual resistances. This reduces the simulation time by 30%.

CONCLUSIONS

A microservices-based application for fast calculating the characteristics and parameters of microstrip antennas and arrays modified Method of Integral Equations in a thin-wire approximation is developed. Significant acceleration of the calculation process is achieved through the use of CUDA technology and Intel Optane SSD and reuse of the previously calculated matrix of mutual resistances.

ACKNOWLEDGMENTS

Authors are grateful to the Associate Professor Alexander Ulanouski for help in developing a mathematical model and to Professor Oleg Yurtsev for many years of support and advisory.

REFERENCES

1. F. Abboud, J.P. Damiano, A. Papiernik, "Simple model for the input impedance of coax-fed rectangular microstrip patch antenna for CAD," in *IEE Proceedings of Microwaves, Antennas and Propagation*, Vol. 135, Iss. 5 (IET, 1988), pp. 323-326.
2. V.V. Kizimenko and A.V. Ulanouski, "Fine-wire approximation of a microstrip radiator taking into account the effective permittivity of the substrate," in *Electronica-INFO*, №6 (Minsk, Belarus, 2015), pp. 45-50.
3. V. Kizimenko, "First experience with Intel Optane P4800X" (2017), available at https://www.linkedin.com/pulse/first-experience-intel-optane-p4800x-viachaslau-kizimenko

Increased Motor Activity And Proper Nutrition for Prevention of Complications in the Elderly with Diabetes

Ruska Paskaleva[a], Galina Mratzkova, Magdalena Platikanova

Faculty of Medicine at the Trakia University - Stara Zagora, Bulgaria
[a)]e-mail: ruska64@abv.bg

Abstract.
One of the most significant diseases worldwide, with a rapid rate of development leading to severe economic losses is diabetes mellitus type 2 (non-insulin dependent diabetes). Chronic metabolic disease of carbohydrate metabolism is characterized by high blood glucose levels and relative insulin deficiency . Approximately 6% of the adult population, estimated globally from 2010 to date, shows that type 2 diabetes (285 million people) accounts for about 90% of diabetes. He exercise of regular physical activity maintains muscles in good condition, prevents the onset of inactive hypotrophies or contractions, and activates various types of modulating downward control (pain suppression) to maintain the emotional tone of the patient. The purpose of the present study is the active participation of the students of specialty "Medical rehabilitation and ergotherapy" in the implementation of rehabilitation activities at the Diabetes Center - Stara Zagora, in elderly people with type 2 diabetes.
Material and methods. *The subject* of the study is 120 diabetic patients at the Diabetes Center - Stara Zagora with different types of diabetes. Five rehabilitation groups were developed, depending on the motor skills. The exercises are for one year with consecutive group work twice a week by the students during the clinical practice.. This result is indicative of the stimulating effect of kinesitherapy and ergotherapy on the motor activity of patients. They all have increased motor skills in everyday activities
Key words: *motor activity, elderly people, diabetes, prevention of complications.*

Introduction

The prevalence of both sexes is almost uniform, but regional differences are observed. Its frequency is higher in the Eastern Mediterranean and the American region (11% for both sexes) compared to the European Region and the Western Pacific (8-9% for both sexes) [33]. Every year 3.5 million people die from the disease or its deviations [34]. The disease affects 8.3% of the population in Bulgaria, the death rate for 2008. is 23.3 per 100 000 [35].That is why the World Health Organization recognizes diabetes as a global epidemic [36].
Obesity along with the lack of physical activity, sleep that affects the metabolism of the body, bad eating habits, unhealthy eating, stress and urbanization are among the causes of the spread of type 2 diabetes [37,38]. For the development of the disease, the genetic predisposition is also of particular importance [39]. While some factors such as gender, age, genetic factors can not be controlled by the person, lifestyle factors can. This also determines the events associated with the prevention and prevention of type 2 diabetes. Life-related measures can reduce the risk of preventing the disease by more than 50 percent [40]. Proper nutrition and physical exercise occupy an important place in the prevention of the disease [41]. Seven percent of cases of type 2 diabetes are due to lack or insufficient physical activity [42]. Greater physical exercise combined with appropriate diet leads to better disease control results [43]
A basic element of diabetic treatment is dietary nutrition. Modern aspects of nutrition policy for type 2 diabetes at European and national level overlap the criteria and recommendations for healthy eating [44]. The diet should be individualized and tailored to the patient's eating habits and preferences. Energy is body-weight-dependent: normoenergy - in normal-body patients, hypoenergicity in obesity, hyper-energy in underweight patients.
The quality of life and its elements have many definitions and interpretations. They are subjective and objective indicators of the physical, psychological, and social characteristics of the patient. The quality of life is a broad understanding of the balance between good and bad in the individual's body, soul, and environment as well as his pessimistic or optimistic view of life [23,24,27].
I. Topuzov (2006) defines the quality of life as a synthesis of the standard of life, personal interests and their realization in the style of life. At the present stage, the importance of quality of life stands out due to the following

features: Increasing the number of chronic illnesses and prolonging their lives;Incomplete healing, only improving vital functions; Improving the role of the personality and hence the complexity of the psychological problems; Changing health goals and striving for health welfare, regardless of disease or disability;Taking into account the medical effects on treatment and quality of life, not just prolonging the life of the patient [16].

Quality of life is a measurable concept that includes as a constituent element the standard of life, the individual's personal interests and their realization in the style of life.

The standard of life is determined by the quantitative biological, social and economic dimensions of life. It is a measurable assessment of health, material, intellectual and formal interests.

Indicators of a person's standard of living are:Health status; Financial liability; Occupational employment; The structure of material and cultural consumption; Distribution of work and leisure time; Public insurances and healthcare; Democratic guarantees for the person. Personal interests reflect the qualitative and psychosocial dimensions of life. They assess the degree of satisfaction that the individual feels with his / her intellectual, cultural, aesthetic and moral values [28,29].

The lifestyle is the individual complex of the standard of living and personal interests. It is influenced by the country's traditions, the religion that confesses the person, the political system, the ideological and geographic conditions. As a collective expression, the style of life (of the person) is influenced by the individual's bio-psychological features [24].

According to modern authors in the field of ergotherapy, the quality of life is a more important factor, as a reflection of disability on the person than the disability itself [3].

The risks of deterioration in the quality of people with disabilities are: The severity of the disability; Level of functional working capacity; Level of pathological changes and symptoms; Subjective feeling of tolerable effort; Overall health self-confidence; Professional, social and financial problems preceding the disability. To assess the quality of life, we use: medical methods for assessing and determining the patient's rehabilitation potential (Clinical Quality of Life Scale in Grades 1 to 3); psychological assessment; sexological assessment; sociological assessment; a practical assessment and a comprehensive assessment of the quality of life, as a summary of the remaining estimates [17,30].

Improving the quality of life of elderly people with diabetes is achieved through the comprehensive approach of modern rehabilitation, including physical exercise, occupational activities in the form of ergotherapy and art-therapy activities.

Exercises and sports are used in the prevention and treatment of elderly people with diabetes. Their versatile healing and prophylactic effects counteract premature aging by keeping the aging organism at the highest possible structural and functional level. Group activity is recommended, but in the absence of such an opportunity, adults may also be self-employed by giving them the necessary instructions for self-control and proper exercise. [2,6,7]

Ergotherapy is an active process in which the patient is engaged in a purposeful activity, emotionally satisfying. [8,9]. It is used in the rehabilitation and re-socialization of elderly people with diabetes through various work activities and training in everyday life activities . It distracts the attention of old people by diverting them from different problems, has emotional effect in various activities and contributes to building new skills. [10,31,32] The classes are conducted individually or in groups; in different settings - in rehabilitation centers, in elderly homes and other specialized centers [21,26]. Patients belong to different age groups, when observing the specifics of each. Every age has its own model of everyday activities typical for that period of life. In middle-aged people are applied different types of work activities, and in the elderly - training in daily life activities and entertaining ergotherapy (horticulture, floristry, modeling, etc.). [4,5,20]

Art therapy serves to mobilize the creative potential. It is based on internal mechanisms for mobilization, activation, self-regulation and self-preservation of the individual. Increasingly, it enters the life of contemporary people as a scientific area of knowledge and as an increasingly practical practice with great impact effectiveness and with many different techniques of art-therapeutical work. It is based on the fact that the creative process associated with making art is curative and brings a positive change of life, stimulates the psychics, activates the creative potential, and develops new skills [15].

It is best to take care of adults with diabetes by specialists - rehabilitators, kinesitherapists and ergo-therapists - to follow the most appropriate approach to the realization of this high-level humanitarian work, such as preserving the health, employability and vitality of the a large proportion of the population [25,22].

The purpose of the present study is the active participation of the students of specialty "Medical rehabilitation and ergotherapy" in the implementation of rehabilitation activities at the Diabetes Center - Stara Zagora, in elderly people with type 2 diabetes.

Material and methods

The subject of the study is 120 diabetic patients in the Diabetes Social and Public Center - Stara Zagora. Rehabilitation events are applied depending on the motor skills. The activities are twice a week with a duration of 50 minutes, with the participation of the students of the specialty "Medical Rehabilitation and Ergotherapy" at the Faculty of Medicine at the Trakia University during the clinical practice and pre-graduate practice.

Methodology of the study. Anthropometric measurements, a specialized test for daily life activities(DLA) and a Quality of Life Test were performed. The latter consists of four parts (1. Physical health and daily life activities; 2. Psychological test and appearance; 3. Social and personal relationships; 4. Environment and financial resources). It gives a very accurate idea of the quality of life of diabetic patients. Tests were performed in 120 diabetic patients before and after rehabilitation formed in five rehabilitation groups, depending on their motor skills. A rehabilitation program of all groups is also implemented within one calendar year with voluntary and active participation of the students. The program includes*: kinesitherapy (physical exercise with a large therapeutic ball and dosed walking), proper nutrition, ergotherapeutic activities (DLA and functional ergotherapy) and art therapy (making souvenirs, cards, etc.).*

The following methodological guidelines have been followed in the implementation of the rehabilitation program for working with the elderly with diabetes: Simple physical exercise was used at the beginning of the activities of adults and elderly people; the method of display is used in the study and execution of physical exercises, gradually including the verbal method. The load is gradual, precisely metered, and this is determined by the reduced adaptive and recovery capabilities of the patient's body.

Statistical methods for processing the results were used. The results of the performed tests were marked in a specially developed card for diagnosis and rehabilitation of the patient and the data from the study was processed with the statistical computer program STATGRAPHICS, WINDOWS, EXCEL using the Wilcoxon rank test - statistical method for analysis and distribution of nonparametric data.

Results and discussion

The activities of everyday life are of the utmost importance for a person's autonomy. These are related to getting up in the morning, dressing up, taking breakfast, dressing and undressing. It refers to moving the body into space, changing its position, occupying different positions, moving with aids or without help. It is important for the everyday use of tools, appliances - they support the execution of DLA [14, 18, 19].

The results achieved in improving daily life activities (Figure 1) and gait stability confirm the thesis that exercise of regular physical activity in diabetic patients maintains well muscles, prevents the onset of complications by the nervous system and the locomotor apparatus.

Fig. 1represents the results of the DLA for residential and professional activities for upper limbs before and after rehabilitation, including computer manipulation, telephone use and other fine motor activities that did not pose serious difficulties for patients. Hy-square link test - the differences in the pre- and post-treatment assessments are highly statistically significant ($P < 0.001$).

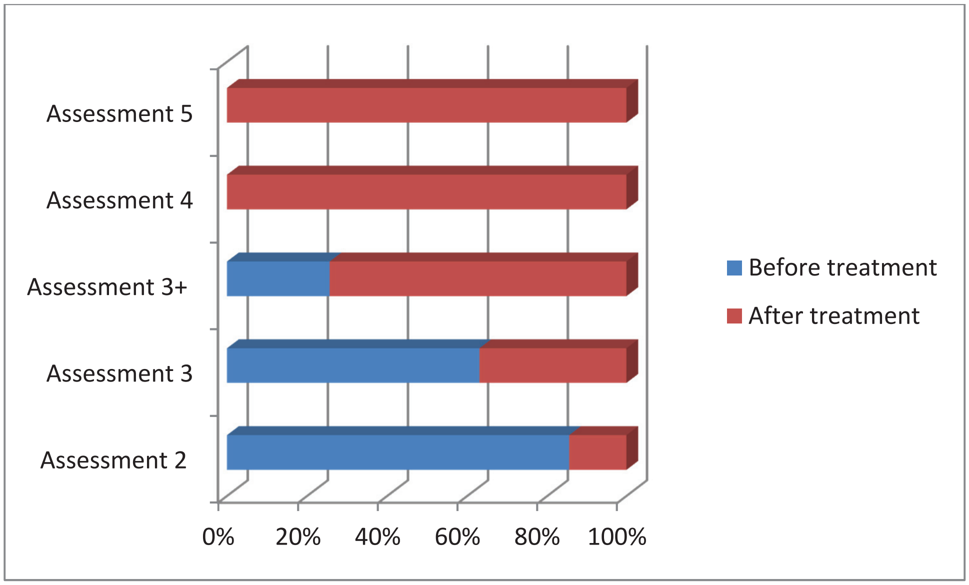

FIGURE 1. Results of the DLA test for residential and professional activities, associated with a travel before and after rehabilitation

This result is indicative of the stimulating effect of kinesitherapy, ergotherapy and art therapy on the motor activity of patients. All of them have increased motor skills in everyday activities, become more confident in these activities and have developed creative potential and art-therapy skills. All crafted articles were arranged in an exhibition.

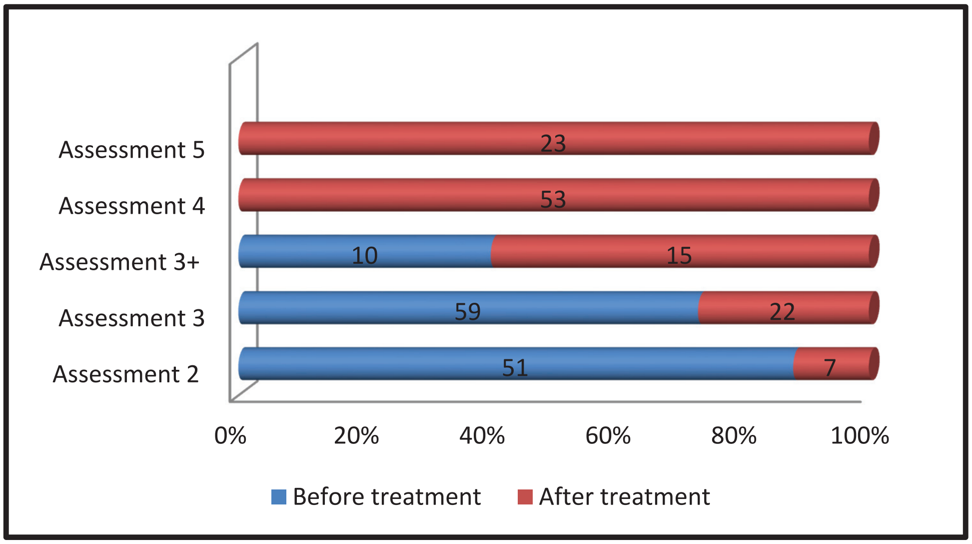

FIGURE 2. Results of the DLA test for residential and professional activities for lower limbs and gait stabilization before and after rehabilitation

The results of the DLA test for domestic and professional activities for lower limbs and gait stabilization before and after rehabilitation (Figure 2) are indicative of the good functioning of the complex procedures on the balance and maintaining the equilibrium of sitting and standing, walking - incline, forward and back, climb and descend on stairs.

Hy-square link test - the differences in the pre- and post-treatment assessments are highly statistically significant ($P < 0.001$).

This is evidence of the incomparable influence of motor activity on the quality of life of diabetic patients in interaction with proper diet and social interactions at the Diabetes Association of Stara Zagora.

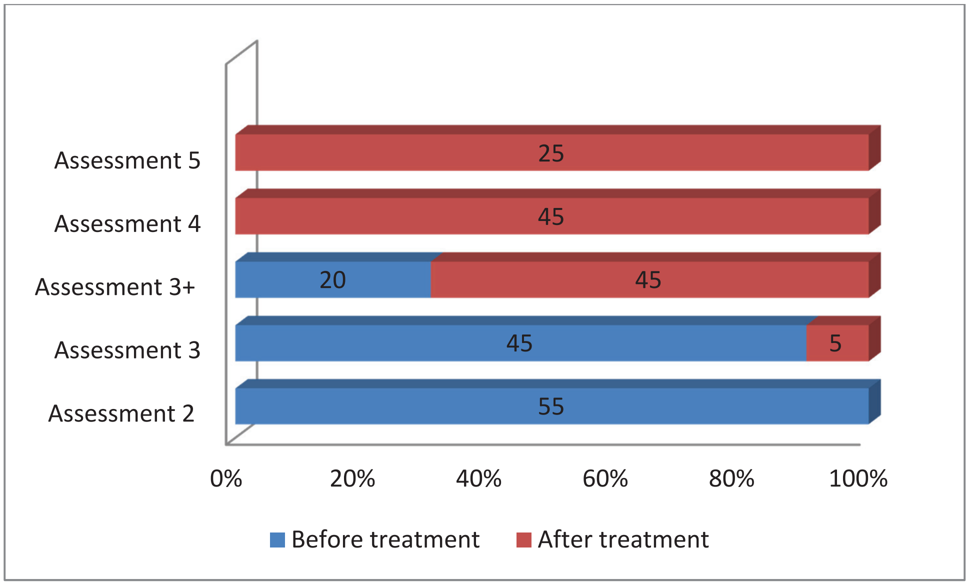

FIGURE 3. Results of the DLA test for residential and professional travel related activities before and after rehabilitation

In Fig. 3there are presented the results of the DLA for domestic and professional activities related to travel before and after the rehabilitation, including: crossing the streets, using personal and public transport (descent and boarding), driving and other motor activities. The joint events organized by the Diabetes Association of Stara Zagora and students of the Medical Rehabilitation and Ergotherapy course at the Faculty of Medicine at the Trakia University stimulate and motivate elderly people with diabetes to a more active way of life and more social contacts. Culinary exhibitions and art-therapy workshops are organized for the great Christian holidays with many guests and pleasant emotions. There are organized outdoor tours along the routes to Metodi Kusev Park (Ayazmoto).

All these joint actions improve the quality of life of the elderly with diabetes and are voluntarily carried out by the students [11,12,13].

The results of the Quality of Life Test: The correlation between the influence of physical and mental health of patients is direct, significant in strength and statistically significant ($R = 0.61$, $p < 0.05$). This is proof of the significant impact of rehabilitation and art therapy on the quality of life of older people with diabetes.

Inferences and conclusions

The implementation of complex rehabilitation in patients with diabetes type 2 requires prolonged activities in specialized rehabilitation centers to stimulate motor activity and social integration; to achieve good results in the rehabilitation of diabetic patients and to improve self-care, it is essential to start early, to include work and training in self-sustaining activities from everyday life, Ergotherapy and art therapy stimulate patient autonomy, mental health and social activity; a continuous improvement and diversification of the activities are needed to improve the quality of life of diabetic patients.

REFERENCES

1. Andonova, A., Future Medical Specialists on the Specifics of Working with Older People, Sofia 2012, XXX Scientific and Technological Session "Contact 2012" - "The Interdisciplinary Idea in Action" 26.10.2012, ed. TEMTO pp. 193-195
2. Bankov, Occupational Therapy Manual. Sofia, Medicine and Physical Education, 1979.
3. Vacheva D. Occupational therapy activities in the rehabilitation of patients with postdisciplinary hemiparesis in UMHAT - Pleven. - Collection of materials at the first national conference on medical rehabilitation and ergotherapy, Pleven, 37, 2007.
4. Vacheva D. Types of gripping and their testing for various injuries and diseases of the hand , Neurorehabilitation, Vol. 3, 1-2, 26-31, 2009.
5. Vacheva D. Recognizing the recovery of daily life activities (toilet and personal hygiene) in patients with cerebrovascular disease. Neurorehabilitation, Volume 5, 2, 68-69, 2011.

6. Dimitrova E. Muscular relaxation and stretching in manual therapy. NSA PRESS; Sofia; p.223, 2008.
7. Karansev G., Milcheva D. Methods for Diagnostics and Research in the Physical Education. Sofia, VIF, 1984.
8. Koleva, I., Ergotherapy - Philosophy and Principles. - Prevention and Rehabilitation, p.3, 1-2, 53-58, 2009.
9. Koleva, I. Functional evaluation in medical rehabilitation and ergotherapy. A textbook for students of Medical rehabilitation and ergotherapy at the Medical University - Pleven. - Sofia: RIC "SIMEL", p.154 , 2008.
10. Koleva, I. Significance of Ergotrapy in Neurorehabilitation Clinical Practice. - Clinical Rehabilitation and Balneology,p. 3, 1-6, 4-9, 2008.
11. Kyuchukova S. The Challenges of Modern Ethics towards Volunteer Students in the Field of Health Care, Academic Journal of Management and Education, vol. VI (4) 2010, ISSN 13126121, Bourgas, pp.268-271, 2010.
12. Kyuchukova, S., Voluntary Work in the European Union, Sister's magazine, issue 2-3 /, ISSN 1310-7496, Sofia University, pp. 32-34, 2010.
13. Kyuchukova, S. Voluntary student work in the sphere of public health and health care. Dissertation for awarding educational and scientific degree "Doctor", p.223, 2013.
14. Mollova K., M. Albert, S. Filkova, R. Djurkova - Physical Activity in Elderly People with Osteoporosis - Proceedings of Scientific Conference with International Participation "Aging, Health, Geriatric Care", pp.189-194, 2017.
15. Paskaleva R., Innovative elements in kinesitherapy training, art therapy and ergotherapy for students rehabilitators, Monograph, Publishing House EKS-PRESS - Gabrovo, p. 120, 2012.
16. Topuzov I. Ergotherapy. First part. Sofia, RIC "Simel", 2006.
17. Topuzov I. Ergotherapy. Third part. Sofia, RIC "Simel", 2009.
18. Yancheva S., Milanov I., Georgiev D., Shotekov P. , Motor activity,Neurology - General Neurolog, Prof. Yancheva, Stara Zagora, Knowledge, 1998.
19. Andonova, A., Sereva, D., Physical Rehabilitation and Recreation in Surgery, The VIII International Scientific and Practical Internet Conference: Medical, Social, Psychological and Pedagogical Aspects of Health, 13-17 February, pp. 26-31 , 2017.
20. Koleva I, Ioshinov R. Automated system for Nosometric Studies, Diagnostics and Prescription of Rehabilitation Complex for Patients Suffering from Multiple Sclerosis. – In: Abstracts of the II Mediterranean Congress of Physical Medicine and Rehabilitation, May 1998, Valencia, Spain, 448.
21. Koleva I, Goranova Z, Ivanova S, Yoshinov R. Electrodiagnostical and Electrographical Evaluation of the Efficacy of Reflexotherapy in Neuropathic Diabetic Foot. - – In: Chinese therapeutic methods, v.2. (Proceedings of VI European Congress of Chinese Medicine “From the past to the future”, September - October 2006, Sofia). Sofia, 32-42, 2008.
22. Okafor, P.I., Sumaila, F.G., Mohammed, J., Badaru, U.M. Assessment of Functional and Musculoskeletal Problems, and Barriers to Obtaining Physiotherapy Services Among the Elderly in a Rural Community in Kano State, Nigeria. A JPARS Vol. 7, Nos. 1 & 2, pp. 1 -6, 2015.
23. Paskaleva R. Effect of innovations in kinesitherapy and ergotherapy training on the students’ motivation for practical work. British Medical Bulletin, Issue 1 (2), (December), Volume 120. „Oxfort University Press“, Pages 321-333, 2016.
24. Paskaleva R. Application of occupational therapy and kinesitherapy to improve the driving activity and activities of daily life (ADL) in children with cerebral damage. Medicine & Science in Sports & Exerciseq Issue 12 (2), (December), Volume 49. Lippincott Williams & Wilkins Ltd. Pages 2875-2884, 2017.
25. Paskaleva R. Increasing the motivation of students for practical work through motor activity and prevention of complications in elderly people with diabetes. KNOWLEDGE - International Journal, Vol 23.1, pp. 519-525, 2018.
26. Peurala, Sinikka H. Rehabilitation of Gait in Chronic Stroke Patients. Series of Reports, No 74, Department of Neurology, University of Kuopio, 108 p., 2005.
27. Platikanova M. Working conditions, labour organisation and musculoskeletal and optical system- related complaints when working with video displays. International scientific on-line journalu"Science & Technologies"; V (1):184-189, 2015.
28. Platikanova M., V. Slavova, V. Ivanov, S. Alekova. Role of neuro-psychlogical tension and fatigue in the daily activites of general practition from the Stara Zagora region. Trakia Journal of Sciences; 13 (2):180-183, 2015.
29. Sato Y. Diabetes and life-styles: role of physical exercise for primary prevention. The British Journal Of Nutrition [Br J Nutr] Dec; Vol. 84 Suppl 2, pp. S187-90, 2000.
30. Sinaki M. Basic clinical rehabilitation medicine. Toronto – Philadelphia, W. B. Saunders Co, 1987.

31. Titianova E., T. Chamova, S. Karakaneva, R. Dimova. Myosonographic Assessment of Triceps Surae Muscle in Chronic Post-Stroke Hemiparesis. Neurosonology And Cerebral Hemodynamics, vol. 2, 75-80, 2012.
32. Trombly CA. Occupational Therapy for Physical Dysfunction. – Boston – Baltimor – Philadelphia – Hong-Kong – London – New York – Sydney – Tokyo: Williams & Wilkins, 1996.
33. WHO. Global status report on noncommunicable diseases, 2014.
34. WHO. Aug 2011. Diabetes Fact sheet N°312. http://www.who.int/en/news-room/fact-sheets/detail/diabetes
35. Ripsin CM, Kang H, Urban RJ. Management of blood glucose in type 2 diabetes mellitus. Am Fam Physician 79 (1). January 2009, 29–36.
36. Pasquier F. Diabetes and cognitive impairment: how to evaluate the cognitive status? Diabetes & metabolism 36 Suppl 3. 2010 Oct. DOI:10.1016/S1262-3636(10)70475-4,100–105.
37. Touma C. Et all. Does lack of sleep cause diabetes?. Cleveland Clinic journal of medicine 78 (8). 2011 Aug. DOI:10.3949/ccjm.78a.10165, 549–558.
38. Raina Elley C, Kenealy T. Lifestyle interventions reduced the long-term risk of diabetes in adults with impaired glucose tolerance. Evid Based Med 13 (6). 2008, 173. DOI:10.1136/ebm.13.6.173.
39. Orozco LJ, Buchleitner AM, Gimenez-Perez G, Roqué I Figuls M, Richter B, Mauricio D. Exercise or exercise and diet for preventing type 2 diabetes mellitus.Cochrane
40. Lee I-Min et all. Effect of physical inactivity on major non-communicable diseases worldwide: an analysis of burden of disease and life expectancy. The Lancet. Volume 380, Issue 9838, 2012, 219-229. DOI:10.1016/S0140-6736(12)61031-9.
41. WHO, European Food and Nutrition Action Plan 2015-2020, www.euro. who.int/ data/assets/pdf_file/0008/253727/64wdl4e_FoodNutAP_140426.pdf
42. Vijan, S. Type 2 diabetes. Annals of internal medicine 152 (5). 2010-03-02. DOI:10.1059/0003-4819-152-5-201003020-01003. c. ITC31–15, quiz ITC316.
43. Thomas D, Elliott EJ. Low glycaemic index, or low glycaemic load, diets for diabetes mellitus.Cochrane Database Syst Rev (1). 2009. DOI:10.1002/14651858.CD006296.pub2. c. CD006296.
44. Risérus U, Willett WC, Hu FB. Dietary fats and prevention of type 2 diabetes. Progress in Lipid Research 48 (1). January 2009.

Analysis Of Research Results Of Physical Development In Children Aged 5-6 Years In Stara Zagora Municipality - Bulgaria

Ruska Paskaleva[a], Violeta Ivanova, Vanya Pavlova, Uliana Marinova, Katya Peeva

Faculty of Medicine at the Trakia University - Stara Zagora, Bulgaria
[a]e-mail: ruska64@abv.bg

Abstract. The high incidence of disturbed posture among preschool children is not only a public concern but also a public health problem for wider preventive measures to improve the motor activity of children. It is necessary to draw up large-scale national programs for early diagnosis and prevention of vertebral distortions at pre-school and school age. The purpose of the present study is to analyze the results of a research of the physical development study in pre-school children aged 5-6 to prevent vertebral distortions and overweight in kindergartens on the territory of the town of Stara Zagora and to prepare a rehabilitation program for prevention of vertebral distortions. The children in 25 kindergartens in Stara Zagora were studied for the period October - December 2017. Out of all 2,029 children, 1483 (73.1%) were examined, of whom 970 children (65.41%) have a disorder, 181 (12.2%) are overweight, the other 333 children (22.39%) have no problems. The largest share of the studied children (75-80%) is in six kindergartens (№7, №25, №3, №23, №10, №8) and the lowest is less than 50% in SG №11 . This is proof of the good scale of the study. Physical development study was performed with a specially designed Early Diagram Attachment Card, adapted to the age of the children, corresponding to their physical development, with the tests of OTT and Schober being modified for 5-6 years old children compared to the height. Overweight children were also surveyed by innovative methodology, compliant with the physical development and compared with the height and weight, individual peculiarities and eating habits. In the study of physical development, the total percentage of children with impaired standing was 65.41% with 95% CI (62.91%, 67.83%), confidence interval. Kindergartens with numbers 6, 24, 29 and 34 have statistically significantly higher values of the percentage of children with disordered posture compared to the total for all kindergartens ($P < 0.05$).
Key words: ***physical development, vertebral distortion, overweight, pre-school age, children.***

Introduction

Early diagnostics, systemic monitoring, treatment, and the actual motor regimen contribute to the favorable outcome of disturbed preschool posture in children [21, 12]. Of particular importance are the good organization of healing and healing measures including a timely diagnosis to prevent gross spinal and thoracic deformities with subsequent complications leading to severe disability [22, 5, 11].

Spinal deformities are among the most prevalent diseases in childhood and adolescence. [1] Contemporary lifestyle and reduced motor activity are factors that provoke the appearance of irregular pos ture and various deformities of the spine and thorax in preschool children [2]. The physical development of children and adolescents correlates with their motor and diet regime, with their constitution, with the hardening, early detection, prophylaxis and treatment of the acute and chronic diseases accompanying the growth [3, 4].

Several authors point to six major factors determining the anomalies of growth and deformities of the spinal cord and thorax. These are: the genetic factors affecting the growth and development of the locomotory system; hormonal and metabolic dysfunctions affecting calcium-phosphate metabolism; biomechanical factors due to decreased motor activity; environmental factors and lifestyle related to children's eating habits; abnormal skeletal growth and congenital abnormalities associated with the nervous system. Modern NMR studies of children with vertebral distortions confirm this thesis [25, 26, 27]. The most common spinal distortions in children and adolescents are habitual scoliosis. They are progressing and have an unprecedented evolution [24]. Scoliosis formation is a complicated pathological process. The first manifestation is lateral deviation of the spine (SG). In a functional curve, it is only justified in changing the shape of the intervertebral discs within the limits of the

physiological capabilities of the spine [16]. This scoliosis is reversible in most cases and it is considered as the result of static-dynamic disorders. Signs of scoliosis begin in early childhood, may develop during growth and become permanent if not treated. These occur in children aged 5 to 6 years but the spinal curve is labile, decreasing in the pelvic position and corrected for mobilization of the musculature [13, 14]. A thorough postural evaluation is required to check if the problems are related to lower limbs, pelvis, shoulder belt, torso, upper limbs, or functional reasons only [15, 17]. The basic principles defining the correct approach to correcting the disturbed posture and overcoming the spinal deformities are limited to: maintaining the motor activity of all the structures of the spine - intervertebral discs, joints, ligament apparatus and muscles; overcoming muscle imbalance because hypertonic muscles hamper flexibility and hypotonicity of spine stability; overcoming ligament abnormalities associated with bone growth and stimulation of postural control, nervous system and equilibrium reactions [7, 8, 10].

The purpose of the present study is to analyze the results of a research of the physical development study in pre-school children aged 5-6 to prevent vertebral distortions and overweight in kindergartens on the territory of the town of Stara Zagora and to prepare a rehabilitation program for prevention of vertebral distortions.

Material and methods.

The children in 25 kindergartens in Stara Zagora were studied for the period October - December 2017. Out of all 2,029 children, 1483 (73.1%) were examined, of whom 970 children (65.41%) have a disorder, 181 (12.2%) are overweight, the other 333 children (22.39%) have no problems. The largest share of the studied children (75-80%) is in six kindergartens (№7, №25, №3, №23, №10, №8) and the lowest is less than 50% in SG №11 . This is proof of the good scale of the study. A Student test was conducted to compare the relative shares of the surveyed indicators in each kindergarten with the corresponding general indicator for the city. A level of significance P <0.05 was used in all tests.

Study methodology: Physical development study was performed with a specially designed Early Diagram Attachment Card, adapted to the age of the children, corresponding to their physical development, with the tests of OTT and Schober being modified for 5-6 years old children compared to the height. Overweight children were also surveyed by innovative methodology, compliant with the physical development and compared with the height and weight, individual peculiarities and eating habits. There was a conducted a survey of the parents of all children with impaired posture and overweight for motor activity and eating habits. Statistical methods for processing the results were applied.

Results and discussion.

The children in 25 kindergartens in the OT for a period of three months - 2017 were studied. Of all 2,029 children, 1483 (73.1%) were examined, of which 970 children (65.41%) had a disorderly posture, 181 (12.2%) overweight, the remaining 22.39% had no problems ... Student test was conducted to compare relative stakes of the surveyed indicators in each kindergarten with the corresponding general indicator for the city. A level of significance P <0.05 was used in all tests.

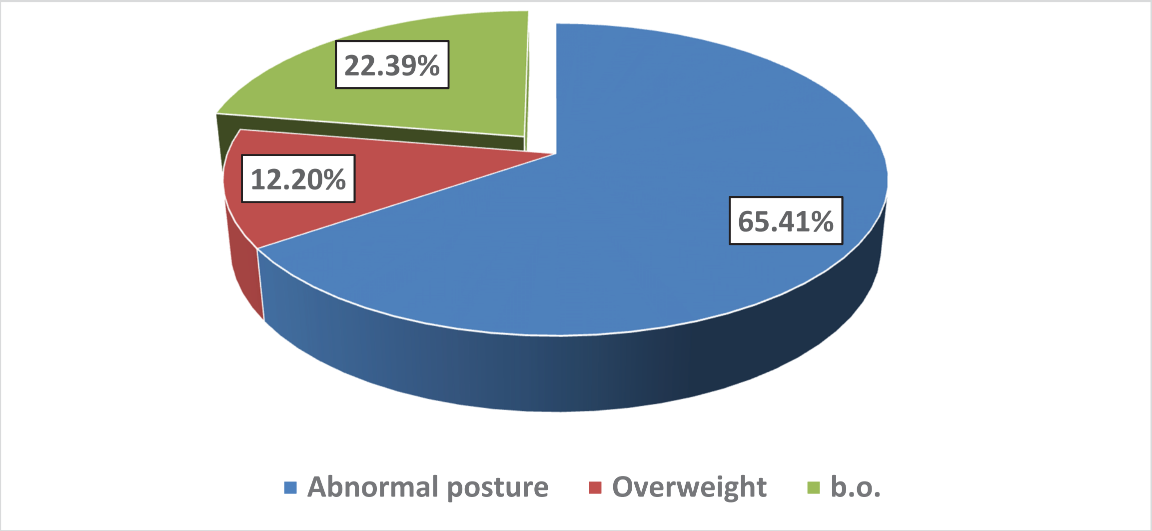

FIGURE. 1. Distribution of examined children

In the study of physical development (*Fig. 1., Tab. 1*), the total percentage of children with impaired standing was 65.41% with 95% CI (62.91%, 67.83%), confidence interval. Kindergartens with numbers 6, 24, 29 and 34 have statistically significantly higher values of the percentage of children with disordered posture compared to the total for all kindergartens (P <0.05). Kindergartens with numbers 5, 35 and 66 have statistically significant lower values of the percentage of children with disordered posture compared to the total for all kindergartens (P <0.05). They are a positive example of a very good practice to prevent the disturbed posture.
The total percentage of children aged 6 years with discontinuity was 34.05% with 95% CI (31.64%, 36.46%). Kindergartens with numbers 6, 7, 20 and 24 have statistically significantly higher percentages of 6-year-olds with disturbed posture compared to the total for all kindergartens (P <0.05). Kindergartens with numbers 5, 11, and 66 have statistically significantly lower percentages of children aged 6 years with a disturbed posture compared to the total for all kindergartens (P <0.05).
In children aged 5 years the total percentile rate of all surveyed was 31.29% with 95% CI (27.73%, 34.85%). Kindergartens with numbers 11 and 25 have statistically significantly higher percentages of 5-year-olds with a disturbed posture compared to the total for all kindergartens (P <0.05). Kindergartens with numbers 20 and 35 have statistically significant lower percentages of 5-year-old children with a disturbed posture compared to the total for all kindergartens (P <0.05).
The overall percentage of overweight children is 12.2% with 95% CI (9.68%, 14.73%).

Kindergartens with numbers 5 and 16 do not have overweight children, and kindergartens with numbers 3 and 23 have statistically significantly lower percentages of overweight children compared to the total for all kindergartens (P <0.05) and they can be taken as an example of good practice against overweight. The other kindergartens do not have statistically significant differences compared to the total for all kindergartens (P> 0.05).

TABLE 1. Distribution of examined children

Kindergarten number	Number of examined	Percent of children with abnormal posture	95% CI		SEM
			Lower bound	Upper bound	
66	37	33.33%	18.14%	48.52%	7.75%
35	63	37.50%	25.55%	49.45%	6.10%
5	35	45.71%	29.21%	62.21%	8.42%
68	21	48.65%	27.27%	70.03%	10.91%
33	30	50.00%	32.11%	67.89%	9.13%
4	85	55.29%	44.72%	65.86%	5.39%
10	62	58.06%	45.78%	70.34%	6.27%
8	111	59.46%	50.33%	68.59%	4.66%
2	53	60.38%	47.21%	73.55%	6.72%
58	45	61.90%	47.71%	76.09%	7.24%
20	41	65.31%	50.74%	79.88%	7.43%
Total for Stara Zagora	**1483**	**65.41%**	**62.99%**	**67.83%**	**1.24%**
17	98	67.78%	58.53%	77.03%	4.72%
7	154	68.18%	60.82%	75.54%	3.75%
13	40	70.00%	55.80%	84.20%	7.25%
3	74	71.62%	61.35%	81.89%	5.24%
23	43	73.17%	59.93%	86.41%	6.76%
1	44	75.00%	62.21%	87.79%	6.53%
25	89	75.00%	66.00%	84.00%	4.59%
31	18	75.38%	55.48%	95.28%	10.15%
16	90	76.19%	67.39%	84.99%	4.49%
11	18	77.78%	58.57%	96.99%	9.80%
24	84	79.07%	70.37%	87.77%	4.44%
29	65	79.78%	70.02%	89.54%	4.98%
34	56	86.67%	77.77%	95.57%	4.54%
6	27	88.89%	77.04%	100.74%	6.05%

Conclusion

The high incidence of disturbed posture among preschool children is not only a public concern but also a public health problem for wider preventive measures to improve the motor activity of children. It is necessary to draw up large-scale national programs for early diagnosis and prevention of vertebral distortions at pre-school and school age.

REFERENCES

1. Karaneshev, G., Sokolov B., Venova L. Theory and methods of healing gymnastics. Under the edition of G.Karaneshev. - Sofia: Medicine and Physical Education, 1987, p. 308.
2. Karaneshev, G., Sokolov B., Venova L. Guide to Practical Exercises in Medical Gymnastics. - Sofia: Medicine and Physical Education, 1991, p.182
3. Koleva I., Short Course on Kinesitherapy (for rehabilitators). 2nd Complete and Revised Edition. Textbook for rehabilitators from the first year of Medical College at Medical University - Sofia. - Sofia: RIM "SIMEL", 2009, p.168
4. Koleva I., Fundamentals of rehabilitation (with algorithms for socially significant diseases and damage to the nervous system and the locomotor system), Textbook. - Sofia, 2010, p. 264
5. Kraidjikova L., Manual Methods for mobilization in musculoskeletal dysfunctions in the spine, Monograph, Sofia, 2011, p.177
6. Mollova K., A. Uzunova, I. Popov, Hr. Milcheva. Analysis of screening results for postural distortion and flatness in children in first to fourth grade. Academic Magazine "Management and Education" Volume XIII (5), Bourgas 2017 pp.106-110
7. Paskaleva R., Innovative Elements in the Kinesitherapy Training, Art Therapy and Ergotherapy for Students Rehabilitators, Monograph, Publishing House EKS-PRESS - Gabrovo 2012, p. 120
8. Ilieva I, R. Paskaleva. Physical activity motivating effect of kinesitherapy in school settings. In "Student Team Practice for the Prevention of Metabolic Syndrome", Academic Publishing House - TU Stara Zagora, 2010; pp.108-111, pp.231-240.
9. Paskaleva R. Kinesitherapy in common diseases in childhood and relaxation techniques. Textbook. Publishing house: EKS-PRESS Gabrovo 2015; p.227.
10. Platikanova M. Illness in children and students from Stara Zagora region. Varna Medical Forum, 2015; 4 (3): pp.252-256.
11. Platikanova M., V. Karabayeva. Some indicators for physical development of children and students from Stara Zagora region. Varna Medical Forum, 2015; 4 (3): pp.257-261.
12. Platikanova M., V. Karabayeva, S. Naneva. The state of the sports facilities in the schools in Stara Zagora - a prerequisite for good health. Varna Medical Forum, 2015; 4 (3): pp.262-266.
13. Filkova S. Prophylaxis of spinal distortion in pre-school children. Author of the dissertation thesis for awarding educational and scientific PhD degree, Varna, 2017, p.78.
14. Filkova, S. Methodic for the prevention of vertebral distortions in preschool children. In: Collection of papers from the International Scientific Conference "European Standards in Sport Education", held in Veliko Tarnovo University "St. St. Cyril and Methodius ". Vratsa, 2013, pp. 419-425.
15. Beckner D., Ca. Beresoski2, M. Camargo, K. Fernandes, C. Siqueira, D. Fujisawa. Early signs of scoliosis in preschool childre. Fisioter Pesq. 2015;22(1):pp.69-75
16. Bogdanović Z., F. Mavrić, A. Mavrić. Effects of a Programmed Corrective Training on Postural Disorders in Lumbar and Thoracic Region. International Journal of Sports and Physical Education (IJSPE) Volume 3, Issue 1, 2017, pp. 7-13
17. Vacheva D. Rehabilitation and Occupational Therapy in Some Common Motor Deficits. – Saarbrucken: LAMBERT, 2013.
18. Kenyon L., M. Blackinton .Applying Motor-Control Theory to Physical Therapy Practice: A Case Report. Journal ListPhysiother Canv.63(3); Summer 2011
19. Konieczny M. R., H. Senyurt , R. Krauspe. Epidemiology of adolescent idiopathic scoliosis. J Child Orthop (2013) 7:3–9

20. Melo K., S. Bandeira de Barros, T. Santos, A. De Marco, V. Hirota, C. Amorim de Sa. The Relationship between Family Lifestyle and Physical Activity of Children from 4 to 6 Years. International Journal of Sports and Physical Education (IJSPE) Volume 3, Issue 4, 2017, pp. 12-16.
21. Mollova K., A.Uzunova, Flat feet – a neglegted problem with significant consequences, Twelfth International Scientific Conference KNOWLEDGE WITHOUT BORDERS 31.03-02.04.2017, Vrnjacka Banja, Serbia - International Journal Scientific Papers, KNOWLEDGE Skopje, Vol 16.4, 2017, pp.1564-1568
22. Paskaleva R. Diagnosis and rehabilitation of spinal deformities - new approach in practical training. Medicine & Science in Sports & Exerciseq Issue 12 (2), (December), Volume 49. Lippincott Williams & Wilkins Ltd., 2017. pp. 2855-2861.
23. Pfeiffer M, Kotz R, Ledl T, Hauser G, Sluga M.(2006), Prevalence of Flat Foot in PreschoolAged Children, Pediatrics Vol. 118 No.
24. Chiwaridzo Matthew, Nirmala Naidoo2Functional consequences and health-care seeking behaviour for recurrent non-specific low back pain in Zimbabwean adolescents: a cross-sectional study. Springer-Verlag Berlin Heidelberg. Eur Spine J (2016) 25:pp.643–650
25. Zadeh JR, Gleiber MA (2015) Adolescent Idiopathic Scoliosis: An in Depth Analysis and Historical Review. MOJ Orthop Rheumatol 3(4): 00105.
26. Winnie C. W. Chu, Darshana D. Rasalkar, Jack C. Y. Cheng Asynchronous neuro-osseous growth in adolescent idiopathic scoliosis—MRI-based research. Pediatr Radiol (2011) 41:1100–1111
27. Woggon A. D. Martinez Chiropractic treatment of idiopathic scoliosis with the CLEAR Institute method: a description of the protocol. Scoliosis. 2013; 8(Suppl 2): p.6.

Investigation of the Interface of Metamaterial and Topological Insulator

Tatjana Gric[1, 2, a)]

[1] *Department of Electronic Systems, Vilnius Gediminas Technical University, Vilnius, Lithuania*
[2] *Semiconductor Physics Institute, Center for Physical Sciences and Technology, Vilnius, Lithuania*
[a)]Corresponding author: tatjana.gric@vgtu.lt

Abstract. We investigate the propagation of surface plasmon polaritons (SPPs) at the boundary of metamaterial and topolological insulators. Instance of Bi_2Se_3 and metamaterial boundaries is investigated. The topological insulators under consideration are three dimensional topological insulators of the second generation. Dispersion relations, absorption characteristics and propagation lengths of SPPs are calculated. The key parameters making a dramatic impact on propagation lengths are acknowledged and mechanisms for engineering dispersion properties are suggested.

INTRODUCTION

Surface plasmons (SPs) are characterized as the localized excitations existing at the interface between two substances [1, 2]. Naturally their appearance is only possible in case of one substance having a real but at the same time negative permittivity ε and another material possessing real and positive permittivity. With losses taken into account phenomenologically, the complex-valued frequency dependent low-momentum dielectric response function in a substance with negative ε being an idealized metal is of the form

$$\frac{\varepsilon(\omega)}{\varepsilon_0} = 1 - \frac{\omega_p^2}{\omega(\omega + i\gamma)}, \tag{1}$$

where $\omega_p^2 = \frac{n_e e^2}{m\varepsilon_0}$ is the plasma frequency, n_e is the number density of electrons and m is their effective mass. The γ damping term is a small positive quantity setting the DC conductivity of the metal.

Herein, we consider the features of the SPs in case of their localization on a topologically non-trivial interface. The case of the material described by a permittivity of the form (1) leads to a fascinating realization of a topological interface. The former might take place in case of a substance demonstrating the topological bandstructure of a topological insulator has, attained a finite bulk carrier density via doping. Actually, mostly all practically realized 3d TI materials, for instance $BI_{1-x}Sb_x$ alloys, Bi_2Se_3 and Bi_2Te_3 have a non-vanishing bulk carrier density.

The paper is structured as following. In section 2, the theory of SPs in topological insulators will be reviewed. The corresponding formulas for the case of a topologically non-trivial boundary will be presented. Section 3 is dedicated to the investigation of the tunable features of the SPs. The main objective of the paper is to prove the principal possibility and find various scenarios of dynamical tuning of the characteristics of interest, which is expected to be achievable by engineering the chemical potential of graphene μ.

SURFACE PLASMONS IN TOPOLOGICAL INSULATORS

The model system under study being the boundary between a topological insulator and a MM is presented. For this case ε is positive inside the TI while ε in the MM can be negative, leading to the propagation of SP.

The interface of MM under study is depicted in Fig. 1. The MM is made of pairs of alternate dielectric layer (with thickness d_d) and graphene layer (with thickness d_g). The studied structure contains a

Graphene/Dielectric MM aiming to investigate the dispersive features of SPPs, assuming that ε_g is calculated using the parameters presented in [3].

Aiming to take on board an effective medium approach it is assumed that the wavelength of radiation is larger than thickness of any layer.

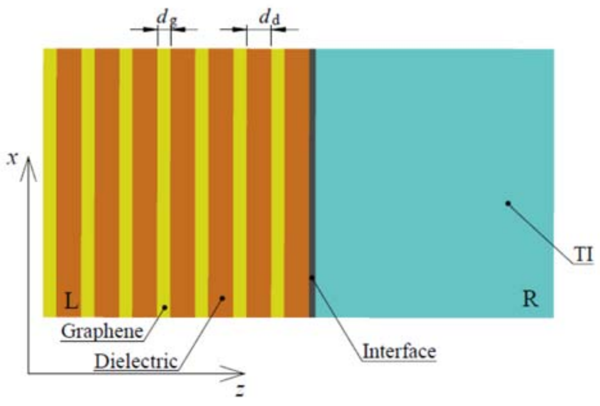

FIGURE 1. 1D MM made of graphene and dielectric layers. The MM/TI (MM/Bi_2Se_3 interface) is considered.

Now, let us consider the dispersion features of SPPs. In contrast to the approach in [4-6], we now make the step forward by taking the damping term in the graphene into account while studying and modelling the dispersion features. By applying effective medium approximation theory, this system can be treated as an anisotropic uniaxial medium, whose effective relative permittivity can be expressed in a tensor form:

$$\varepsilon = \varepsilon_0 \begin{pmatrix} \varepsilon_{\parallel} & 0 & 0 \\ 0 & \varepsilon_{\parallel} & 0 \\ 0 & 0 & \varepsilon_{\perp} \end{pmatrix} \tag{2}$$

The transverse and longitudinal relative permittivities are given by [7, 8]:

$$\varepsilon_{\parallel} = f_g \varepsilon_g + f_d \varepsilon_d \tag{3}$$

$$\varepsilon_{\perp} = \varepsilon_g \varepsilon_d / \left(f_g \varepsilon_d + f_d \varepsilon_g \right) \tag{4}$$

where $f_g = d_g / L$ and $f_d = d_d / L$, $L = d_d + d_g$ are the graphene and dielectric filling ratios, correspondingly. It is assumed, that $\varepsilon_d = 18.8$. The effective permittivity ε_g of graphene can be calculated as follows $\varepsilon_g = 1 + i\sigma / \varepsilon_0 \omega d_g$, where d_g is the thickness of graphene sheet, ε_0 is the permittivity in the vacuum. It is worthwhile noting that that MMs with a very large permittivity or a near-zero permittivity possess fascinating features [8]. One may use MMs with a near-zero permittivity as optical insulators [8]. Doing so, the zero point and divergence point of the principal values are of the high importance for the scientific community aiming to study the dispersion features of SPPs [9, 10]. The dispersion relationship between frequency ω and the propagation constant β is derived by using the transverse resonance method [11] with suitable periodic boundary conditions. After some mathematical manipulations, it is given by formula:

$$\beta = k \sqrt{\frac{\left(\varepsilon_{\parallel}^{R} - \varepsilon_{\parallel}^{L} \right) \varepsilon_{\perp}^{R} \varepsilon_{\perp}^{L}}{\varepsilon_{\perp}^{R} \varepsilon_{\parallel}^{R} - \varepsilon_{\perp}^{L} \varepsilon_{\parallel}^{L}}}, \tag{5}$$

where k is the is the free-space wave number and β is the wavevector parallel to the interface. Here, index R corresponds to the right-hand side material and the index L to the left-hand side material correspondingly (see Fig. 1).

The bulk optical properties of Bi_2Se_3 in the far and mid-IR are obtained from reflectance measurements [12, 13]. It has been concluded that the overall features of reflectance spectra in the range from 50 cm^{-1} to 1000 cm^{-1} in case of all three materials [12] can be described by isotropic Drude-Lorentz model with 3 or 4 oscillators. The Drude-Lorentz oscillator model is used to calculate the dielectric constant in the far-IR range and is given as follows:

$$\varepsilon\left(\omega, cm^{-1}\right)=\varepsilon_{\infty}-\frac{\omega_D^2}{\omega^2+i\omega\gamma_D}+\sum_{j=1}^{j=3,4}\frac{\omega_{pj}^2}{\omega_{0j}^2-\omega^2-i\omega\gamma_j} \tag{6}$$

Table 1 presents parameters for Bi_2Se_3 at room temperature [12]. Similar numbers in case of thin films of Bi_2Se_3 used in [14] are also shown.

TABLE 1. Drude-Lorentz model parameters for Bi_2Se_3 ($\varepsilon_{\infty}=1$) at room temperatures in far and mid-IR [12] and for the unpatterned Bi_2Se_3 at 300 K [14].

Oscillator	**ω_0, cm^{-1}**	**ω_0, cm^{-1}**	**γ, cm^{-1}**
Bi_2Se_3 ($\varepsilon_{\infty}=1$) at room temperatures			
Drude	0	908.66	7.43
Lorentz, α	63.03	657.9	17.5
Lorentz, β	126.94	100	10
Lorentz, Ω_{gap}	2029.5	11249	3920.5
Bi_2Se_3 at 300 K			
Drude	0	933.3	23.3
Lorentz, α	63.3	566.7	10.0
Lorentz, β	133.3	66.7	3.33
Lorentz, Ωgap	free	free	free

Based on [12], the Drude-Lorentz model for Bi_2Te_3 at room temperature requires the Drude term with $\omega_p=5651.5cm^{-1}$, $\gamma=111.86cm^{-1}$ and a single Lorentz oscillator with $\omega_0=8386.6cm^{-1}$, $\omega_0=66024cm^{-1}$, $\gamma=102660cm^{-1}$ ($\varepsilon_{\infty}=1$). Only the Drude term with $\omega_p=6906.7cm^{-1}$, $\gamma=183.69cm^{-1}$ ($\varepsilon_{\infty}=51$) is needed for the case of Sb_2Te_3. These numbers, compared to the data for Bi_2Se_3, show that at room temperature both Bi_2Te_3 and Sb_2Te_3 show highly metallic behavior in their optical response. The former is in line with the bulk band gap of Bi_2Se_3 being larger than the one of Bi_2Te_3 and Sb_2Te_3 [15]. Room temperature optical responses of Bi_2Te_3 and Sb_2Te_3 consequently are dominated by free electrons in the bulk.

Now we discuss dispersion relations, absorption characteristics and propagation lengths for SPPs at the MM/Bi_2Se_3 interface, following the approach of [16]. A MM boundary supports modes of different types [16].

In Figs. 2-4 we show dispersion curves dealing with different combinations of MM parameters (thickness of the dielectric, Fermi level, number of graphene sheets). It is worthwhile noting, that there are observable variations in the dispersion curves varying the mentioned parameters. The electrically tunable Fermi energy provides us a method to manipulate the characteristics as shown in Fig. 2. It should be mentioned that decreases in the Fermi energy μ will move the dispersion curves to lower frequencies; in contrast, increases in the Fermi energy μ move them to higher frequencies. As seen from Fig. 2, the smallest asymptotic frequency is achieved by employing the smallest Fermi energy. The former tunability property suggests that the surface wave can be engineered by the Fermi energy of the graphene sheets.

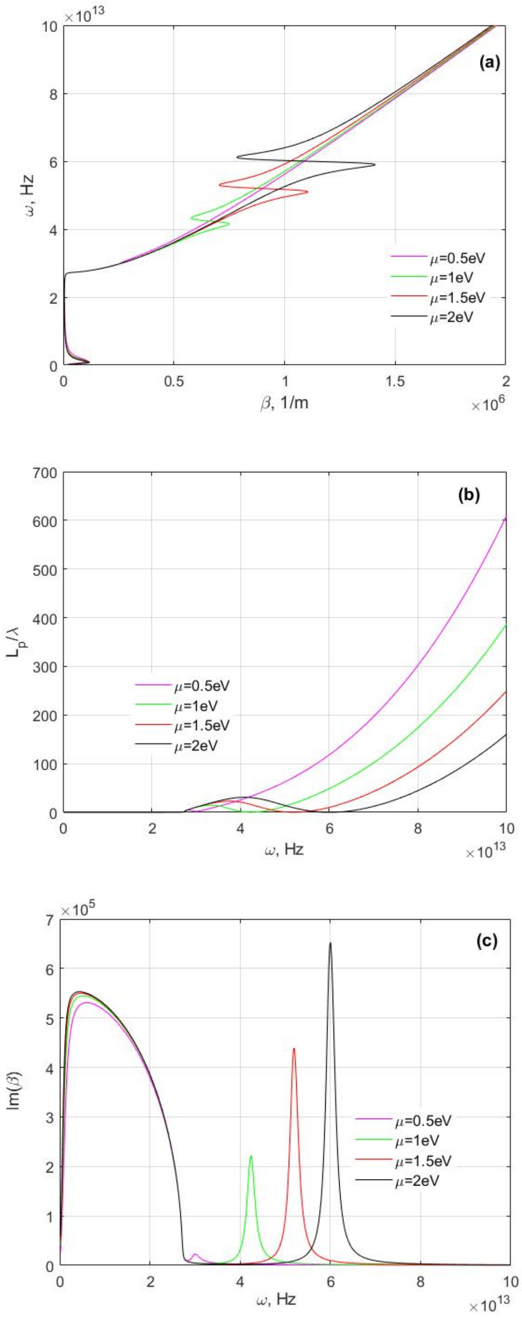

FIGURE 2. Dispersion relations of SPPs at the MM/Bi_2Se_3 boundary for different Fermi energy levels (a). Propagation lengths for corresponding parameters (b). Absorption characteristics (c).

We proceed further by performing modelling of the dispersion curves and normalized propagation lengths for changing values of the dielectric width and number of graphene layers.

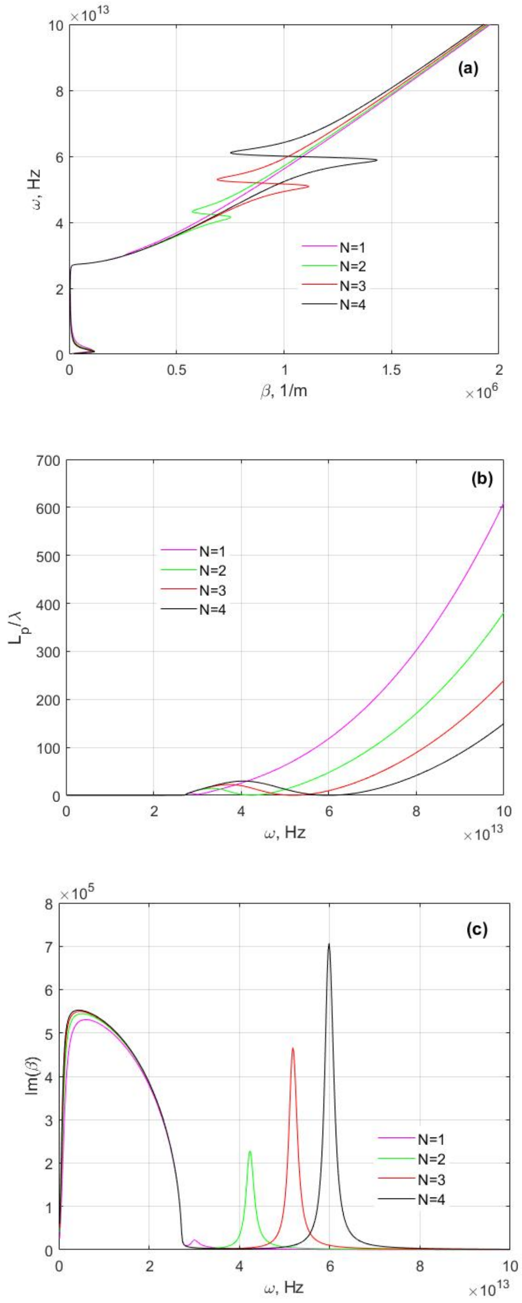

FIGURE 3. Dispersion relations of SPPs at the MM/Bi_2Se_3 boundary for different numbers of graphene layers (a). Propagation lengths for corresponding parameters (b). Absorption characteristics (c).

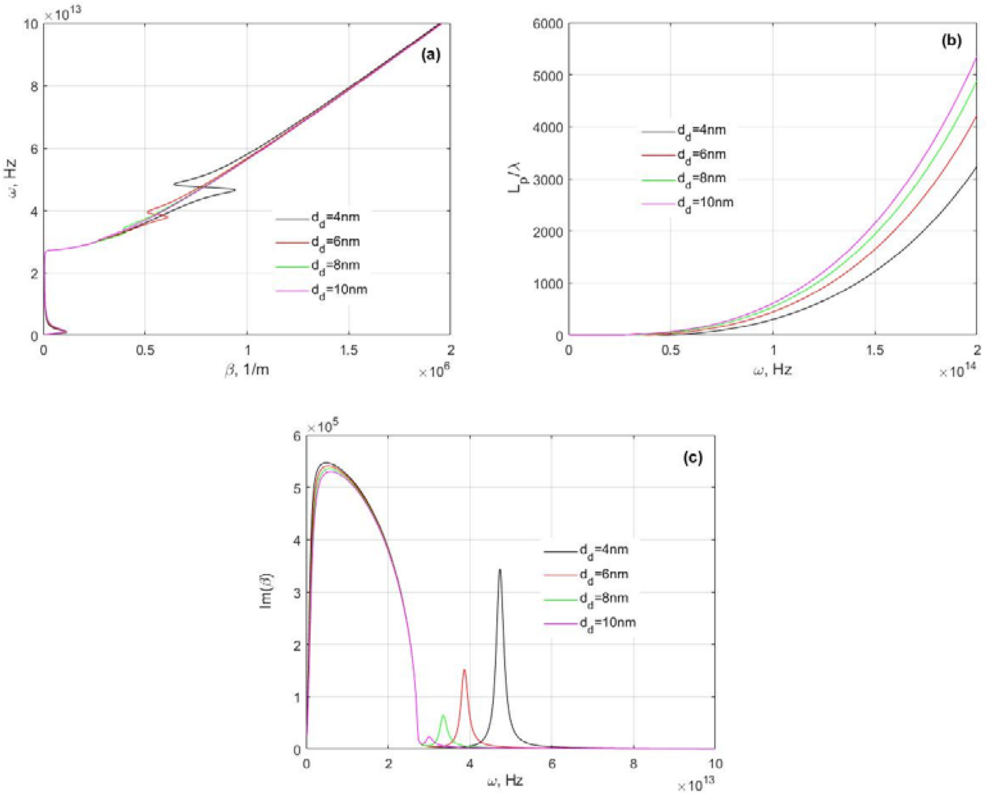

FIGURE 4. Dispersion relations of SPPs at the MM/Bi_2Se_3 boundary for different thicknesses of dielectric layers (a). Propagation lengths for corresponding parameters (b). Absorption characteristics (c).

It is worthwhile noting, that the most noteworthy property is the significant enhancement of the propagation length as either the dielectric thickness is increased or the Fermi level and number of graphene layers are decreased.

It should be mentioned, that negative values of the absorption in Figs. 2-4 (c) which result from non-physical solutions of the dispersion equation and have been omitted. Moreover, the sketched graphs imply the presence of the surface waves propagating for a long distance. This is caused by the fact that the real part of β is very low within this spectral region.

CONCLUSIONS

1. Dispersion relations and propagation lengths of SPPs at the Bi_2Se_3/MM boundary were calculated applying realistic material parameters. Bi_2Se_3 is treated as the substance of preference if larger propagation lengths are preferred.
2. The Fermi level, number of graphene sheets and thickness of dielectric layer are found to be the key parameters making a dramatic impact on the propagation length. Lowering E_F by gating is a reasonable technique to engineer the propagation lengths of SPPs. Graphene is an ideal material for electrochemical sensing and biosensing since it has large surface-to-volume ratio, excellent electrical conductivity, high carrier mobility, and many other unique properties.
3. The theory developed by stacking MMs and insulators is discussed in terms of applications to engineer dispersion relation of SPPs. In this relation, an interesting question if the SPP frequency can be shifted by stacking up into the spectral range of e. g. quantum cascade lasers. This case may provide a fertile ground for engineering SPPs in terahertz range.

REFERENCES

1. R. H. Ritchie, Phys. Rev. **106**, 874 (1957).
2. E. A. Stern and R. A. Ferrell, Phys. Rev. **120**, 130 (1960)
3. R. Mondal et al., Phy. Rev. B **97**, 144306 (2018).
4. M. G. Cattom and D. R. Tilley, Introduction to Surface and Superlattice Excitations (IOP Publishing, Bristol, 2005), Chaps. 8–9. 276 277.
5. R. Li, C. Cheng, F.-F. Ren, J. Chen, Y.-X. Fan, J. Ding, and H.-T. Wang, Appl. Phys. Lett. **92**, 141115 (2008).
6. J. A. Sorni, M. Naserpour, C. J. Zapata-Rodriguez, and J. J. Miret, Opt. Commun. **355**, 251 (2015).
7. O. Takayama, D. Artigas, and L. Torner, Opt. Lett. **37**, 4311 (2012).
8. A. Orlov, P. M. Voroshilov, P. A. Belov, and Y. S. Kivshar, Phys. Rev. B **84**, 045424 (2011).
9. Y.-L. Zhang, Q. Zhang, and X.-Z. Wang, J. Opt. Soc. Am. B **33**, 543 (2016)
10. T. Gric, O. Hess, Journal of Applied Physics **122**, 193105 (2017).
11. I. Iorsh, A. Orlov, P. Belov, and Y. Kivshar, Appl. Phys. Lett. **99**(15), 151914 (2011).
12. M. S. Wolf, Infrared and Optical Studies of Topological Insulators Bi2Se3, Bi2Te3 and Sb2Te3, (Thesis, The University of Akron, 2011).
13. W. Richter, H. Kohler, and C. R. Becker, Phys. Stat. Sol. (b) **84**, 619–628 (1977).
14. P. Di Pietro, M. Ortolani, O. Limaj, A. Di Gaspare, V. Giliberti, F. Giorgianni, M. Brahlek, N. Bansal, N. Koirala, S. Oh, P. Calvani, and S. Lupi, Nat. Nanotechnol. **8**, 556–560 (2013).
15. H. Zhang, C. X. Liu, X. L. Qi, X. Dai, Z. Fang, and S. C. Zhang, Nat. Phys. **5**, 438–442 (2009).
16. T. Gric, O. Hess, Opt. Express **25**, 11466-11476 (2017).

Contribution to Individualized Environmental Education

Aspasia Karagiannopoulou, Fragiskos Batzias[a], Odysseas Kopsidas

Dep. Industrial Management and Technology, Univ. Piraeus
80 Karaoli & Dimitriou, GR 18534 Piraeus, Greece
[a]email: fbatzi@unipi.gr

Abstract. In this work, we modify the Holland' s methodology for the categorization of human personalities by including queries (in the corresponding questionnaire that serves as an evaluation tool) investigating its responders attitude as regards his/her willingness to be professionally engaged with the natural or/and anthropogenic environment. The population used as representative sample consisted of 250 students following courses at high school and university level. The quantitative methods used were descriptive statistics, parametric and non-parametric statistics hypothesis (on causal relations) testing, categorical semantics, ontological mapping fuzzy sets and interval algebra. The results obtained showed relative significant internal consistency at macro-level for almost half of the interviewees, but the dependence of answers to environmental queries on the rest responds to the rest queries was insignificant, indicating lack of specific knowledge and clarification of the corresponding concepts at micro-level.

Keywords: Environmental Education, Holland's Theory, Questionnaire Design, Hypothesis Testing, Vocational Typology.

INTRODUCTION

The central hypothesis in Holland's theory is that the vocational interest is a key aspect of the individual. People can be described by their degree of resemblance to six theoretical personality types: Realistic (conforming, hard-headed, practical, inflexible, un-insightful), Investigative (independent, intellectual, precise, rational, reserved), Artistic (emotional, imaginative, introspective, nonconforming, sensitive), Social (cooperative, friendly, helpful, responsible, warm), Enterprising (agreeable, ambitious, energetic, extroverted, sociable), and Conventional (conforming, conscientious, efficient, obedient, practical) [1]. Each type is characterized by distinctive preferences, outlooks, competencies, and self perceptions. In practical applications, information about a person's preferences, goals, and self estimates is used to assess the degree to which an individual resembles each of the six personality types; these types are not always clear and pure, and a variety of mixed personalities are not uncommon. At what level of the same kind of work will influence a person is determined by one's intelligence, self-knowledge and professional information/background [2].

Environmental attitudes are conceptualized in terms of behavioral theory as being composed of beliefs towards an object [3]. The environment as an object is difficult to define; it may be an attitude object which has been forced on the respondent by journalists and researchers, but it may not make sense to respondents who see the environment much more in terms of its component parts that they personally experience. The factors that may influence one's environmental attitudes are: knowledge, background, experience, perception, values and context. Environmental concern appears to be a specific belief which is largely embedded in cognitive structures and should be considered an opinion rather than an attitude. While changes in this opinion have been documented, it is not clear that environmental attitudes or values have shifted, although attitudes have most probably became more differentiated over the last decade.

The investigation of the attitudes of young people is very important to environmental education, whose role is to shape positive behaviors towards the environment. Linking environmental and vocational type helps grouping of personalities. The psychometric tools available in the literature are in the form of census questionnaires used to

assess job characteristics [1]. In this work, we modify the Holland' s methodology for the categorization of human personalities by including queries (in the corresponding questionnaire that serves as an evaluation tool) investigating its responders attitude as regards his/her willingness to be professionally engaged with the natural or/and anthropogenic environment.

METHODOLOGY

We used Holland's methodology to develop a questionnaire with 42 Likert-type questions, grouped in seven to six clusters according to Holland's vocational types [3]. Each group includes questions of vocational interest and one or two of environmental interest. We worked mainly with students samples, aged between 15 and 24, of both sexes, interviewed in person. The sample includes students of technical vocational schools and high schools, as well as, by undergraduate and post-graduate university students. Respondents filled the questionnaire by themselves at class, at the presence of their teacher/lecturer for any clarification needed. Scoring followed the five-point scale, from 1= strongly disagree to 5 = agree completely. At the end of each questionnaire the student had to describe himself by ranking the six personality types with descending order of preference. That gave two sets of scores (i.e., the summation of the scores that each respondent gave to the questions) on occupational preferences, one from the responses to the questions and another from his ranking preferences (initial and final, respectively). The questionnaires data were registered in excel and processed with SPSS-Statistics, using R^2, weighted rank (r_T), Pearson's, Kendall's and Spearman's coefficient correlations [4,5].

RESULTS

The survey was conducted within 20/5-20/6 2011,using the high school and technical vocational schools of Zografos (east suburb of Athens) and undergraduate and post-graduate students of the University of Piraeus. Some problems have been registered during the completion of questionnaires, mainly due to miscomprehension of the questions (especially at the lower levels of education), lack of time, and the influence of the classmates. The study extends to the diversification of respondents according to age, sex and educational level. The students sample consisted of the 47% women and 53% men. The distribution according to the students' origin is 40% from technical vocational schools , 42% from high schools, 7% in undergraduate university courses and 11% in post-graduate courses. The age distribution is given in Fig. 1. As regards the personality types, 12.3% of respondents belong to type A, 17.5% are registered as type B, 15.8% fit in type C, 25.7% belong to type D, 10.5% are type E, and 18.1% are assigned under type F.

The correlation of personality type with the degree of environmental awareness has been used herein as a tool to determine the approach (extend, intensity and depth) that environmental education should follow on each of the six Holland's types. The most friendly type to environment is type D (Social), followed closely by type C (Artistic), type E (Enterprising), type F (Conventional), type B (Investigative), whereas type A (Realistic) appears the least predisposed. The correlation between personality types and awareness of respondents on environmental issues (Fig. 2) showed that social type is the most sensitive to environmental issues. We have associated the type of personality of each respondent, as it is deduced from his/her answers, with his/her personal beliefs, as they are derived from his/her ranking of types: the internal consistency of the first type selected is 43%, whereas the internal consistency between the first and second choice is 81%. We have also associated each type's environmental question with the other questions in the group. The results gave R^2 values between 0.71-0.95, indicating medium to high correlation between the average values of scores of all other questions and the score of question that measures the environmental sensitivity.

The top-down correlation analysis, considering the ranking score of the respondents and the classification chosen by the respondent, gave the following weighted rank correlations, r_T: (i) for the technical vocational school students, the range is between -0.053 and +0.707, with an average value of 0.355 and a standard deviation of 0.78; (ii) for the undergraduate students, the range is between +0.159 and +0.771, with an average value of 0.482 and a standard deviation of 0.218. Evidently, there is significant agreement between the two rankings for the six personality types, at least for the higher values of correlation. We formed the hypothesis for the Pearson's, the Kendall's and the Spearman's correlation coefficients. H_0 : if $r=0$, then there is no correlation. H_1 : if $r>0$ or $r<0$, then there is correlation. The confidence level is $a=5\%$. Thus, if p-value (two-tailed) < 0.05 , then H_0 is rejected and H_1 is accepted. If $r > 0$, there is a positive correlation whereas if $r < 0$, there is a negative correlation; in these cases, H_0 is

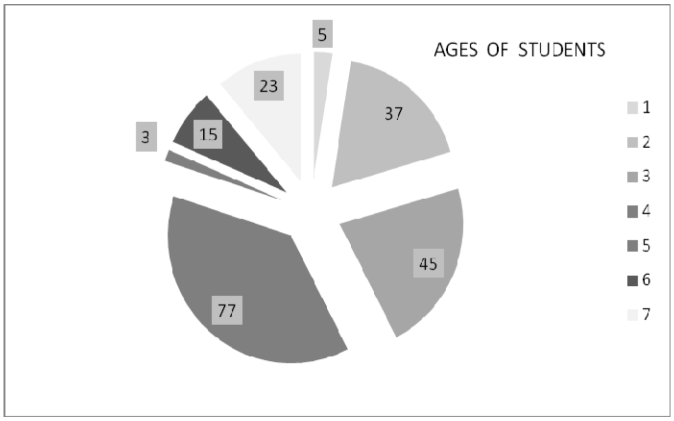

FIGURE 1. Students' ages chart, where: 1=14; 2=15; 3=16; 4=17; 5=18; 6=22; 7=24 years old.

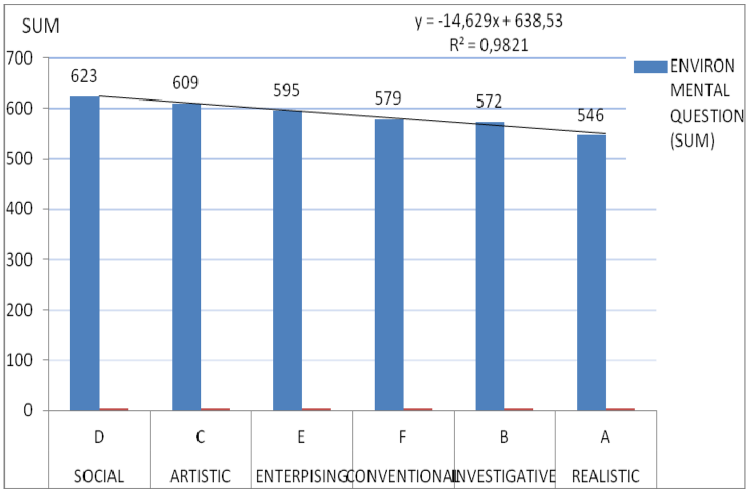

FIGURE 2. Environmental Question (SUM) of each type.

TABLE 1. Coefficients of Correlation

HOLLAND'S TYPE	$r_{Pearson}$	$r_{Kendall}$	$r_{Spearman}$	REMARKS
A	0,382	0,292	0,382	p(two-tailed)<0,05
B	0,315	0,252	0,329	p(two-tailed)<0,05
C	0,411	0,324	0,429	p(two-tailed)<0,05
D	0,180	0,158	0,208	p(two-tailed)<0,05
E	0,219	0,154	0,204	p(two-tailed)<0,05
F	0,348	0,274	0,350	p(two-tailed)<0,05

accepted and H_1 is rejected. The results are presented in Table 1. As there is no linear relationship between variable "Initial Score" and "Final Score", our assumptions are based on Kendall and Spearman correlation coefficient.

DISCUSSION AND CONCLUDING REMARKS

In Greek primary and secondary education, environmental education is included in the curriculum, yet it still depends on the educators' will to be applied. Administration bottlenecks, in addition to the uncertainty teachers are feeling concerning their knowledge background on environmental issues, the lack of existence of a suitable

educational or training material and the restriction of the school timetable, usually hamper the environmental education course.

The theory of Holland's vocational personalities has been confirmed and validated by many researchers [6-10]. Using the modified questionnaire of personality types of Holland, without direct reference to them, our research has helped to elicit indirectly the views of students about the environment, so as to provide educators valuable information that they may use to formulate a proper educational material. Certain conclusions have been drawn at comparing personality types to environmental awareness, assigning a degree of environmental predisposition to each type.

Social is the first type of personality that is sensitive to environmental issues. The causal relationship that form the social type fully justifies this predisposition, as the main characteristics of the type are consistent with environmental sensitization: the social type is friendly and responsible, he enjoys team work, he prefers educational activities, he cares for the public benefit and he tries to maximize social welfare. After all, the environment is a public good and its protection relies on willingness of the citizens.

The second type of personality that is sensitive to environmental issues is the artistic one. This type develops positive feelings about the environment, is creative and unconventional. For this type, clean environment is a source of inspiration and creativity.

In conclusion, the modification of Holland's methodology for determining the degree of environmental awareness of young people has been proven suitable to evaluate attitudes and beliefs of students as regards their willingness to be actively engaged with the environment. The results obtained showed relative significant internal consistency at macro-level for almost half of the interviewees, but the dependence of answers to environmental queries on the rest responds to the rest queries was insignificant, indicating lack of specific knowledge and clarification of the corresponding concepts at micro-level.

ACKNOWLEDGMENTS

Financial support provided by the Post-Graduate Degree Programme (MSc) on 'Systems of Energy Management and Environmental Protection', through the Research Centre of the University of Piraeus, is kindly acknowledged.

REFERENCES

1. J. L. Holland, *Making Vocational Choices*, USA, Psychological Assessment Resources,1997.
2. G.D. Gottfedson, J.L. Holland, *Dictionary of Holland Occupational Codes*, USA, Psychological Assessment Resources, 1982.
3. A. Kyridis, E. Mavrikaki, H. Tsakiridou, Int*. J.Sustain. Higher Edu.* **6**, 54-64 (2005).
4. J.H Zar, *Biostatistical Analysis*, USA, Prentice Hall International,1996, pp.371-406
5. B. Bolton, *J. Voc. Behav.* **27**, 210-217 (1985).
6. N.E. Amundson, J. Harris-Bowlsbey, S.G. Niles*, Essential elements of career counseling: processes and techniques,* USA, Pearson Merrill Prentice Hall, Colombus Ohio, 2nd Edition 2008.
7. T.A. Heberlein*. Environmental Attitudes ,* Madison, Wisconsin, Abhandlungen, ZfU 2/81,241—270.
8. T.A. Timmerman, *J. Bus. Psychol.*, **12**, Fall 1997.
9. Greek Ministry of National Education and Religious Affairs and Pedagogical Institute, 2002
10. R.E. Dunlap, K.D. Van Liere, A.G. Mertig, R. Emmet Jones, Measuring Endorsement of the New Ecological Paradigm: A Revised NEP Scale.

Knowledge Acquisition for Reconstruction and Identification of Dimensionless Groups by Means of Case Based Reasoning

Fragiskos Batzias[a] and Odysseas Kopsidas

Laboratory of Simulation of Industrial Processes
Department of Industrial Management and Technology
University of Piraeus
Karaoli & Dimitriou 80, 18534 Piraeus, Greece
[a]fbatzi@unipi.gr

Abstract. When searching with Data Mining Techniques to identify or find out dimensionless groups (DGs) in technical literature, it is possible to meet errors/faults/omissions concerning both, the form and the content of such groups. In the present study, a methodological framework has been developed in terms of a logical flow chart, including 11 activity stages and 7 decision nodes, to acquire/process/store/retrieve knowledge for reconstruction and identification of these groups. Case Based Reasoning (CBR), especially modified to meet the needs of this work, has been used for tracing causality paths by similarity and making correction suggestions. Two case examples are presented to prove the functionality of the proposed methodology.

Keywords: dimensional analysis, knowledge acquisition, dimensionless groups, case based reasoning, data mining, Blake number, modified Reynolds number, adsorption, sedimentation, flocculation, filtration, scale up.

INTRODUCTION

Dimensional analysis was initially developed early in the last century [1-6] by scientists and engineers for expressing the behavior of a physical system in term of the minimum number of independent variables and in a form that is unaffected by changes in the magnitude of the units of measurement. The first attempt to a similar approach in Economics was made by Allais [7], who presented a systematic treatment of the theory of dimensions and its foundations. Later, some authors contributed to the diffusion of this scientific topic (e.g., see [8]) or used relevant techniques either for simply stressing the distinction between stock and flow variables [9,10] or for techno-economic analysis [11,12] or for model checking [13]. The physical and/or economic magnitudes are usually arranged in dimensionless groups (DGs), the number of which is $m=n-r$, where n is the number of dimensional variables/ parameters/constants (VPCs) and r is the number of primary quantities used, like mass M, length L, time T, and temperature G. This rule is a general relation based on Linear Algebra and Group Theory and is mostly quoted as Buckingham's pi theorem.

DGs may have physical meaning and in such a case we can search for similar groups through Case Based Reasoning (CBR) in order to properly describe quantitatively and solve similar problems, possibly occurring due to errors either in dimensions or in form or in content. CBR has been formalized for purposes of computer-aided processing as a four-step algorithmic procedure, which might be named 4R from the initial letter of the four verbs used as computer program commands in the corresponding steps: (I) Retrieve the cases considered to be relevant to solving a given target problem. (II) Re-use the solution (if it was successful) from the previous case to the target problem by making the necessary modifications to adapt the solution as needed to fit the new situation. (III) Revise by testing the solution of the new problem directly in the real world or indirectly under suitable conditions or reliable simulation. (IV) Retain by storing the solution as a new case in the computer memory, provided that the adaptation was a successful one.

Computer-aided solving by CBR the problems quoted above is a difficult task, especially when this approach uses unpublished evidence as its main Knowledge Base (KB); since the available information from the past may be

not relevant/reliable to the required level for backing a successful 'implementation-by-analogy', there is no guarantee that the necessary generalization (that ensures applicability) is correct. Nevertheless, inductive reasoning in case of scarce data/information for statistical relevance/reliability is usually based on incomplete evidence in practice. Moreover, there is always the possibility of developing CBR within a statistical framework and formalizing case-based inference as a specific type of probabilistic/possibilistic inference; therefore, it becomes feasible to make case-based estimates with a preset level of confidence.

METHODOLOGY

The methodological framework we have developed, in terms of a logical flow chart with 11 activity stages and 7 decision nodes (interconnected as shown in Fig. 1), to acquire/process/store/retrieve knowledge for reconstruction and identification of dimensionless groups by means of CBR, is presented below:

1. Analysis of the DG in error or the dimensionally inconsistent VPC.
2. Checking of the definitions of the VPCs registered under widely known names in relevant KBs and, subsequently, in the corresponding original sources of technical literature.
3. Translation of these verbal or symbolic definitions into dimensional definitions in accordance with the dimensional system adopted from the start as most appropriate.
4. Replacement of the VPCs suspected to be in error with the new/checked ones and testing of the DG under consideration for dimensional homogeneity.
5. Checking for operability within a proper/successful paradigm extracted from a KB by means of data mining and knowledge acquisition techniques to be used in accordance with CBR.
6. Combinations of DGs to find out those which are more close to the DG under consideration.
7. Checking these combinations for operability *ab initio* (i.e., without having necessarily a past successful paradigm).
8. Discrimination of relevant DGs and ranking of them in descending order of similarity degree as regards the DG to be corrected.
9. DA by replacing *a priori* the DG under correction with the most similar (but unexamined so far) DG within the set of DGs resulted as the solution of the dimensional matrix corresponding to the system of equations obtained according to Rayleigh's Method of Indices.
10. Multicriteria ranking of combinations performed in stage 6, according to the order of decreasing degree of closeness to the DG under consideration.
11. Checking of the first combination (among the ones not examined so far) for operability.

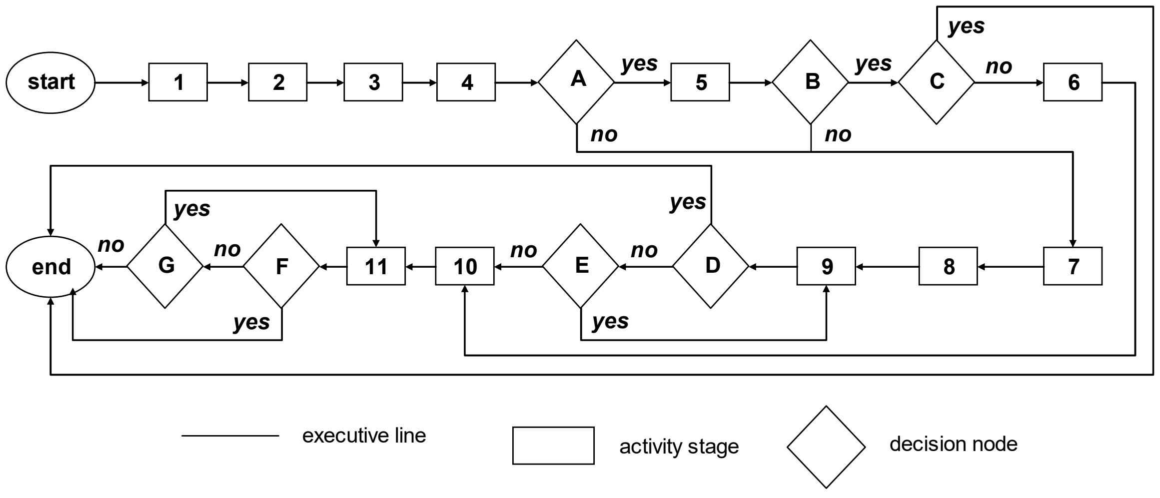

FIGURE 1. The logical flow chart developed for acquiring/processing/storing/retrieving knowledge for identification and correction of either dimensionally inconsistent VPCs or/and DGs in error.

A. Has dimensional homogeneity been restored?

B. Is operability satisfactory?
C. Is the new DG identified as the correction of the old one?
D. Is this replacement successful?
E. Is there another ranked DG with lower similarity degree?
F. Is its operability satisfactory?
G. Is there another ranked combination not examined?

IMPLEMENTATION BY CASE EXAMPLES

We have implemented successfully the methodology described above in a plethora of cases. Subsequently, we present two of them. The first refers to modified Reynolds or Blake Number, defined in Perry's Chemical Engineering Handbook [14] as $B = V\rho / [\mu(1-\varepsilon)S]$, where V: characteristic or average fluid velocity (m/s); ρ: fluid density (kg/m^3); μ: fluid viscosity (Pa s); ε: void fraction (m^3); S: particle area/volume (1/m); all magnitudes measured in SI units. By replacing the units with the corresponding dimensions, we obtain $B \in [LT^{-1}]$ $[ML^{-3}]$ $[ML^{-1}T^{-1}]^{-1}$ $[L^3]^{-1}[L^2L^{-3}]^{-1}$ or $B \in [L^{-3}] \neq [1]$. Evidently, this is in error, since the result should be $B \in [1]$, i.e., dimensionless. Searching in external KBs by means of data mining and knowledge acquisition techniques incorporated within an Intelligent Agent (IA), according to [15], we find the most recent reference source [16] with all common DGs, where $B = V\rho / [\mu(1-\varepsilon)d]$, with $\varepsilon \in [1]$, while d is the characteristic particle diameter $d \in [L]$ as recognized by the computer aided DA procedure adopted herein and thoroughly described in [17]. Working out as above, we obtain $B \in [LT^{-1}][ML^{-3}][ML^{-1}T^{-1}]^{-1}[L]^{-1}[L^2L^{-3}]^{-1}$ or $B \in [L^{-1}] \neq [1]$. By continuing the automatic searching, as shown in the flow chart of Fig. 1, the computerized procedure identified finally the correct dimensions to be $\varepsilon \in [1]$ and $S \equiv d \in [L^{-1}]$, giving $B \in [1]$.

The second case example used for implementation is the Freundlich isotherm, which we have used recently [18] to study by experimental simulation the dye adsorption in batch and fixed-bed systems:

$Q = KC^{1/n}$

where q = the amount of mass adsorbed per unit mass of the adsorbent [1]; C = the equilibrium concentration of the adsorbate, $[ML^{-3}]$; K = parameter related to adsorption capacity; n = parameter related to adsorption intensity, [1]. Most authors do not specify the dimensions of K, while several of the rest of them assign either $[L^3M^{-1}]$ or [1] (e.g., see [19] or [20,21], respectively). Evidently, these dimensional assignments are in error, as the dimensional homogeneity of this isotherm requires $K \in [M^{-1/n} L^{3/n}]$, although this assignment is meaningless, when its physical content is considered thoroughly. By referring mass M to dye in solution, dye adsorbent, adsorbent itself, we can split this primary dimension to M_s, M_d, M_t, respectively. Consequently, we can write the isotherm model in dimensional form as follows: $q = K_s K_d K_t C^{1/n}$, where $q \in [M_d M_t^{-1}]$, $C \in [M_s L^{-3}]$, $K_s \in [M_s^{-1} L^3]^{1/n}$, $K_d \in [M_d]$, $K_t \in [M_t^{-1}]$,which is meaningful as representing the real situation (facilitating also the scale up/down of the corresponding simulation procedures).

DISCUSSION AND CONCLUDING REMARKS

Even in physical sciences and engineering/technology, this identification attempt becomes cumbersome and the computer program may fail to suggest a realistic solution without substantial human intervention. The probability to fail increases when the DG under investigation is incorporated into relations that change the original VPCs with others for sake of better fitting to system's specifications. For example, when the system is 'fluid flow through porous media', B can be combined with the 'resistance coefficient' DG expressed by the ratio $\Psi = A^2\varepsilon^3 P / [Q^2\rho(1-\varepsilon)lS]$ to give a relation of the general form $\Psi = K/B^n$ in the procedure known as the Blake-Carman correlation, where A is the cross-sectional area of packing perpendicular to flow direction, P is the pressure difference, Q is the volumetric flow rate ($Q=VA$), l is the length of packing in the flow direction, K and n are parameters. In the low B-range (approximately, $B<1$), $n=1$, and by re-arranging the VPCs, we obtain the Kozeny-Carman equation $Q = A\varepsilon^3 P / [K\mu(1-\varepsilon)^2 S^2 l]$, which is dimensionally homogenous, since $Q \in [L^3T^{-1}]$ and $A\varepsilon^3 P / [K\mu(1-\varepsilon)^2 S^2 l] \in [L^2][1][ML^{-1}T^{-2}][1][ML^{-1}T^{-1}][L^{-1}]^{-2}[L]^{-1} = [L^3T^{-1}]$.

In such a case, we cannot investigate any dimensional inhomogeneity in *B* since this DG does not appear *per se* in the final model while the investigation of any error propagation should be based on CBR where the similar cases to be retrieved should belong to a broader family of Kozeny-Carman equations. If, according to [16], *S* is replaced by *d* in *B*, then the Kozeny-Carman equation becomes $Q = A\varepsilon^3 P / \left[K\mu(1-\varepsilon)^2 Sdl\right]$. Consequently, the dimensional vector of the right-hand side of this equation becomes [LT^{-1}] which is inconsistent with the left hand-side dimensional vector [L^3T^{-1}] denoting the correct dimensions of volumetric flow rate *Q*. The IA cannot identify the source of error unless provided with further information corresponding to ancestor relations. On the other hand, the inference engine searching within the KB may identify *Q* with the 'superficial velocity' u_0 (i.e., the average linear velocity the fluid would have in the column if no packing were present) quoted as the dependent variable of Blake-Kozeny equation in the classic work [22].

As a matter of fact, searching for the possible routes of error propagation and the corresponding implications is a 'direct problem' while searching for the possible source of error through an identification procedure is the 'inverse problem'. In the case examined herein, searching for implications of error in Blake Number *B* is the direct problem while searching for the possible source of error in Kozeny-Carman equation is the inverse problem. It is also worthwhile noting that the same family of equations is frequently met under all pairwise combinations (i.e., Kozeny-Carman, Blake-Carman, Blake-Kozeny) leading to additional difficulties faced by the IA searching in external KBs using the keywords interface suggested in [15].

In conclusion, we have indicated the functionality of the methodological framework presented herein by analyzing two simple cases, one for DG and another for VPC. If the DGs or VPCs in eror have been incorporated/combined into/with other expressions, traceability decreases and human intervention, at least for changing the searching pattern through CBR, increases the effectiveness of computer aided performance while facilitates the KB's enrichment/restructuring.

REFERENCES

1. L. Rayleigh, *Proc Roy. Soc. London* **66**, 68 (1899-1900).
2. L. Rayleigh, *Nature* **95**, 66 (1915).
3. E. Buckingham, *Phys. Rev.,* **4**, 345-376 (1914).
4. H.E. Langahaar, *Dimensional Analysis*, London, 1951.
5. H.E. Huntley, *Dimensional Analysis,* London, MacDonald, 1952
6. J. Palacios, (translated by P. Lee with L.Roth), *Dimensional Analysis*, London, Mac Millan, 1964 (originally published in Spanish, 1956).
7. M. Allais, *Traite d' economie pure*, Vol. I, *Les Donnees generals de l' economie pure* , Paris and vol. IV, *Annexes* (2nd Ed. of a textbook published in 1943 under the title *A la recherché d' une discipline economique*).
8. F.J. de Jong, *Dimensional Analysis for Economists*, Amsterdam, North Holland Publ. Co, 1967.
9. K.E. Boulding, *Economic Analysis*, 4th Ed., Vol. II, New York, 1966.
10. G. Auckley, *Macroeconomic Theory*, New York, 1961 .
11. T. Nussbaumer and P. Neuenschwander. *Biomass Bioenerg.* **18**, 181-188 (2000).
12. Le Corre, O., GuillaumB. and Mohand, T., *Appl. Thermal Eng.* **84**, 177-185 (2002).
13. F.A. Batzias, D.K. Sidiras, *J. Hazard. Mater.* **114**, 167-174 (2004).
14. R.H. Perry, D.W. Green, *Perry's Chemical Engineers' handbook,* 7th Ed., McGraw-Hill 1997, pp. 648-650.
15. F.A. Batzias, E.C. Marcoulaki, *Comp. Aided Chem. Eng.* **10**, 829-834 (2002).
16. http://www.uni-magdeburg.de/ivt/mvt/englisch/framemvt.html and R.H. Perry, D.W. Green, J.O. Maloney, Perry's Chemical Engineers' Handbook (CD version), pp. 6-49, McGraw-Hill, New York, 1999.
17. F.A. Batzias, A.S. Kakos, N.P. Nikolaou, *J. Computat. Meth. Sci. Eng.* **5**, 47-60 (2005).
18. F.A. Batzias, D.K. Sidiras, *J Hazard. Mater.*, **114**, 167-174 (2004).
19. G.M. Walker, L.R. Weatherley, *J. Chem. Eng.* **83**, 201-206 (2001).
20. C. Costa, M.C. Marquez, *Wat. Res.* **32**, 107-114 (1998).
21. C. Ng, J.N. Losso, W.E. Marshall, R.M. Rao, *Bioresour. Technol.* **84**, 177–185 (2002).
22. R.B. Bird, W.E. Stewart, E.N. Lightfoot, *Transport Phenomena*. Wiley International, New York, 1960, pp. 196-200.

Scale Up Of Adsorption Column Packed With Conditioned Waste Lignocellulosics

O.N. Kopsidas, I.G. Konstantinou, D.K. Sidiras[a] and F.A. Batzias

Laboratory of Simulation of Industrial Processes, Department of Industrial Management and Technology, University of Piraeus, 80 Karaoli and Dimitriou, GR 18534 Piraeus, Greece.

[a)]sidiras@unipi.gr

Abstract. The present work deals with the scale up of adsorption column for the removal of basic dyes from wastewaters, using methylene blue as a representative adsorbate and barley straw as a representative waste biomass adsorbent. The pilot scale column used herein was 137 cm in height with 19 cm inner diameter. The flow rate was determined so that the linear velocity for the pilot scale column is approximately the same with the linear velocity for the two laboratory scale columns (15 and 25 cm in height, respectively, with 2.5 cm inner diameter). In the case of the pilot scale column the time required for breakthrough (predetermined at C=2 mg/L) was 140 min and the corresponding required influent volume was 220 L (C_i=14 mg/L), where the C, Ci are concentrations for adsorbate output and input, respectively. The results indicate that barley straw exhibits satisfactory adsorption properties. Considering the abundance and the low cost of this lignocellulosic material, barley straw could serve as a cost-effective adsorbent for basic dyes.

Keywords: adsorption; barley straw; packed bed column; methylene blue; scale up.

INTRODUCTION

The environmental impact of dye effluents in the wastewater streams of many industrial sectors, such as dyes, textiles, paper, tanneries and chemicals, has drawn a lot of attention for the last decades, emphasizing on the necessity of their removal at acceptable cost. The utilization of inexpensive and locally available materials as potential substitutes of commercial activated carbon for the removal of dyes in industrial wastewater is commonly discussed in literature [1-9]. A variety of low cost materials have been proposed [1-9], including cotton waste, rice husk, betonite clay, neem leaf powder, powdered activated sludge, perlite, bamboo dust, coconut shell, groundnut shell, rice husk and straw, sawdust, duck weed, sewage sludge, gram husk, bagasse fly ash, and blast furnace slag. The suitability of these materials as dye adsorbents is often established using (i) the kinetics of methylene blue adsorption during batch and continuous (column) processes [10, 11] and (ii) the BET surface area [12]. Notwithstanding, most of these studies report on bench scale experiments, whereas literature on scale-up of column adsorption processes is scarce. A column adsorption process represents a complex system with many inherent difficulties in scaling up, especially in predicting performance and in evaluating scale-up factors [13]. From an economic point of view, the column adsorption process should be designed to give a maximum recovery of the desired product from a fluid phase, with an optimum schedule to handle a certain amount of material. To achieve this goal, extensive laboratory and pilot plant experiments are normally required to find the optimum conditions.

In the present study, the scale up of adsorption column, and the removal of methylene blue by barley straw were studied. The pilot scale column used herein was 137 cm in length and 19 cm in diameter. The flow rate was determined such as the linear velocity for the pilot scale column to be approximately the same with the linear velocity for the two laboratory scale columns (15 and 25 cm in length, respectively, and 2.5 cm in diameter). The results indicate that barley straw shows high adsorption properties.

METHODS

Material Development: Barley straw used was obtained from Thessaly (Central Greece), as a suitable source for full-scale/industrial applications. Barley straw contains 27% w/w hemicelluloses, 33% w/w cellulose, lignin 28% w/w and 12% w/w ash. The moisture of the material measured was 8.5% w/w. After grinding in a hummer mill and screening, the fraction with particle sizes between 1 and 2 cm was isolated as ‘coarse grinded barley straw’. The material was saturated for 24 hours prior to adsorption experiments.

Experimental Setup: Fixed-bed up-flow adsorption studies were conducted in a 137 cm x 19 cm Plexiglas column, in a 15 cm x 3 cm stainless steel column and in a 25 cm x 3 cm stainless steel column filled with 2730 g, 14 g and 22 g of coarse grinded barley straw, respectively. The experimental set-up consisted of one column, fed by a peristaltic pump at a constant flow rate, Q=22.5 mL/min and 16.8 mL/min for the 15 cm and 25 cm laboratory scale columns, respectively, and Q=1.36 L/min for the pilot scale column. The methylene blue influent concentration was 14 $mg.L^{-1}$. Interconnective tubing and fitting were made of polytetrafluoroethylene (PTFE). Effluent samples were analyzed to yield output concentration breakthrough curves. In the case of the laboratory scale stainless steel columns, the cross-section was E=4.91 cm^2 and the adsorbent (coarse grinded barley straw) was 0.19 g/mL. In the case of the pilot plant Plexiglas column, the cross-section was E=283.39 cm^2 and the adsorbent was 0.07 g/mL, i.e. the column was filled with 2730 g of coarse grinded barley straw.

Analytical Techniques: Following the technique proposed by Saeman et al. [14], the lignocellulosic materials were hydrolyzed to glucose and reducing sugars in nearly quantitative yields; the filtrates were analyzed for glucose and xylose. Based on these results the cellulose and hemicelluloses contents of the adsorbents were estimated. Finally, the acid-insoluble lignin (Klason lignin) was determined according to the Tappi T222 om-88 method. The samples were dried under vacuum at 150ºC overnight. The concentration of methylene blue in the solution was obtained by measuring O.D. at 663 nm, using a HACH DR4000U UV–visible spectrophotometer.

RESULTS AND DISCUSSION

Oulman [15] proposed the use of a bed depth service model for simulating GAC (granular activated carbon) adsorption beds. The model, first developed by Bohart and Adams [16], was based on surface reaction theory and is equivalent to the logistic curve [17-20]. The Bohart-Adams equation is as follows:

$$ln\left(\frac{C_i}{C}-1\right)=\frac{K\cdot N\cdot x}{u}-K\cdot C_i\cdot t \quad \text{or} \quad ln\left[\frac{C_i}{C}-1\right]=ln\,A-r\cdot t \tag{1}$$

in which C=effluent concentration ($mg.L^{-1}$); C_i=influent concentration ($mg.L^{-1}$); K=an adsorption rate coefficient ($L.mg^{-1}.min^{-1}$); N=an adsorption capacity coefficient ($mg.L^{-1}$); x=bed depth (cm); u=linear velocity ($cm.min^{-1}$); and t=time (min). $lnA=K.N.x/u$ and $r=K.C_i$.

The values of A and r can be thus estimated from the column effluent data assuming C_i=column influent and C=the column effluent at time t. We can calculate K, N from the equations $K=r/C_i$ and $N=u\cdot lnA/(x\cdot K)= C_i\cdot u\cdot lnA/(x\cdot r)$. As shown in Fig. 1, the theoretical model expressed by Eq. (1) simulates the experimental data satisfactorily. In addition, the adsorption rate coefficient (K) and the adsorption capacity coefficient (N), shown for pilot scale column in Table 1, were estimated from the A and r parameter -values obtained using the same equation.

The simulation of the 15 cm laboratory scale column gave adsorption capacity coefficient N=786 mg/L, adsorption rate coefficient K=0.00079 Lmg^{-1} min^{-1} and correlation coefficient R=-0.9413. The simulation of the 25 cm laboratory scale column gave N=2395 mg/L, K=0.00045 $Lmg^{-1}min^{-1}$, R=-0.96984. The results of the simulation of the pilot plant column for methylene blue adsorption on Barley Straw according to the Bohart-Adams bed depth service model are presented in Table 1.

Equation (1) can be rewritten as:

$$C=\frac{C_i}{1+Ae^{-rt}} \tag{2}$$

This is the well known logistic model, which can be used as an independent phenomenological kinetic expression, since all break through curves exhibit a sigmoid profile. The disadvantage of applying this expression is its symmetry round the inflection point at $t=(ln\,A)/r$, $C=C_i/2$, as it can be easily proved by replacing t in the corresponding differential (rate) function with two t-values, symmetrical round $t=(ln\,A)/r$. When the goodness of fitting of the logistic function is not satisfactory because of its symmetry, we can apply one of the following empirical asymmetrical sigmoid models [21]:

$$y=\frac{K}{1+me^{-bt^a}}\ \text{(I)},\quad y=\frac{K}{\left(1+me^{-bt}\right)^a}\ \text{(II)},\quad y=\frac{K}{\left(1+me^{-bat}\right)^{1/a}}\ \text{(III)},\quad y=\frac{K}{\left(1+me^{-bat}\right)^a}\ \text{(IV)} \tag{3}$$

where $y=C$, $K=C_i$, $m=A$, $b=r$ and a=exponent. For a=1 we obtain eq. (2).

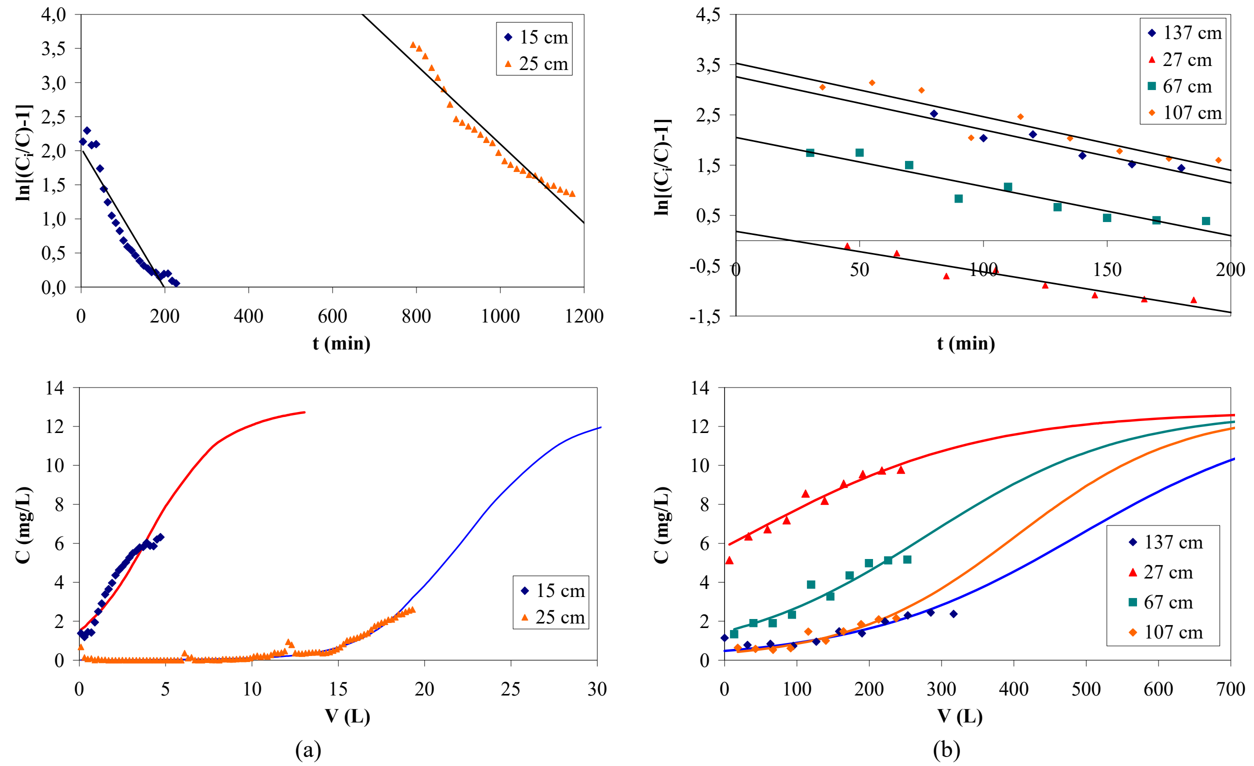

FIGURE 1. Breakthrough curves in the linearized/logarithmic form and in the original/non-linear form (a) for the laboratory scale columns with bed height x=15 cm and 25 cm, and (b) for the pilot plant column with bed height x=137 cm (sampling at 27, 67, 107, and 137 cm). Fixed bed: barley straw; Methylene Blue solution flow rate 22.5 mL/min, 16.8 mL/min and 1.36 L/min for the three columns, respectively; inflow concentration C_i=14 mg/L.

FIGURE 2. (a) Laboratory scale column of 15 cm height with 25 L tank, (b) laboratory scale pump, and (c) pilot scale column of 137 cm height with 1000 L tank.

TABLE 1. Estimated parameter values for methylene blue adsorption on barley straw according to the Bohart-Adams bed depth service model for the case of the pilot scale column.

Fixed bed height x (cm)	Adsorption capacity coefficient N (mg/L)	Adsorption rate coefficient K (Lmg^{-1} min^{-1})	Flow rate Q (L/min)	Correlation Coefficient R	Standard error of estimate SEE
27	50	0.00063	1.32	-0.9599	0.4138
67	188	0.00076	1.33	-0.9502	0.4559
107	170	0.00083	1.22	-0.9333	0.2449
137	161	0.00083	1.58	-0.9568	0.3584

CONCLUDING REMARKS

The adsorption column scale-up studied herein, for the removal of basic dyes from wastewaters, using methylene blue as a representative adsorbate and barley straw as a representative waste biomass adsorbent, was successful, as regards consistency and reliability (judged by low absolute and relative standard deviation) of results. Moreover, the goodness of fitting of the Bohart-Adams (B-A) model to experimental data was satisfactory, as judged by the corresponding low values of the standard error of estimate (SEE), while the correlation coefficient, estimated on the basis of the corresponding linearized regression equation, was quite acceptable (i.e., negative and close -1). By transforming the original B-A model to the well known logistic expression, we suggested a family of empirical alternative models to cope with adsorption kinetic data that do not follow the symmetric pattern, which is the main characteristic of the logistic function. The creation of this family was achieved by introducing a fourth parameter in different modes, which represents a measure of deviation from symmetry. When the experimental data come close to a symmetrical path, this parameter approaches unit and the empirical model tends to coincide with the logistic function, i.e., the B-A model. This feature enhances the applicability of the B-A model under its modified version, since the lack of symmetrical data does not prevent the use of the most appropriate model of the family while giving the opportunity of coming back from empirical to scientific when the obstacles giving rise to asymmetry have been removed by reconditioning the process.

ACKNOWLEDGMENTS

The financial support provided by the Research Center of the University of Piraeus is kindly acknowledged.

REFERENCES

1. G. McKay, G. Ramprasad and P.P. Mowli, *Water Air Soil Pollut.* **29**, 273-283 (1986).
2. K. R. Ramkrishna and T. Viaraghavan, *Water Sci. Technol.* **36**, 189-196 (1997).
3. K. G. Bhattacharya and A. Sharma, *Dyes Pigm.* **65**, 51-59 (2005).
4. M. Dogan, M. Alkan, A. Turkyilmaz and Y. Ozdemir, *J. Hazard. Mater.* **109**, 141-148 (2004).
5. P. Waranusantigul, P. Pokethitiyook, M. Kruatrachue and E. S. Upatham, *Environ. Pollut.* **125**, 385-392 (2003).
6. M. Otero, F. Rozada, L. F. Calvo, A. I. Garcia and A. Moran, *Biochem. Eng. J.* **15**, 59-68 (2003).
7. R. Jain, and S. Sikarwar, *Int. J. Environ. Pollut.* **27**, 158-178 (2006).
8. A. Mittal, L. Kurup (Krishnan) and V. K. Gupta, *J. Hazard. Mater.* **117**, 171-178 (2005).
9. V. K. Gupta, D. Mohan, S. Sharma and M. Sharma, *Separat. Sci. Technol.* **35**, 2097-2113 (2000).
10. F. A. Batzias, D.K. Sidiras, *J. Hazard. Mater*. **149**, 8-17 (2007).
11. F. A. Batzias, D.K. Sidiras, *Biores. Technol*. **98**,1208-1217 (2007).
12. F. Batzias, D. Sidiras, E. Schroeder, C. Weber, Chem. Eng. J., **148** , 459-472 (2009).
13. F. Augier, C. Laroche, E. Brehon, Sep. Purific. Technol., **63**, 466-474 (2008).
14. J. F. Saeman, J. F. Bubl and E. E. Harris, *Ind. Eng. Chem. Anal. Ed.* **17**, 35-37 (1945).
15. C. S. Oulman, *J. Am. Wat. Works Assoc.* **72**, 50-53 (1980).
16. G. S. Bohart and E. Q. Adams, *J. Chem. Soc.* **42**, 523–544 (1920).
17. S. J. Allen, Q. Gan, R. Matthews and P. A. Johnson, *Bioresource Technol.* **88**, 143-152 (2003).
18. G. M. Walker and L. R. Weatherley, *Chem. Eng. J.* **84**, 125-131 (2001).
19. U. Kumar and M. Bandyopadhyay, *J. Hazard. Mater.* B**129**(1-3), 253-259 (2006).
20. A. Cambiella, E. Ortea, G. Ríos, J. M. Benito, C. Pazos and J. Coca, *J. Hazard. Mater.* B**131**(1-3), 195-199 (2006).
21. F. Batzias, «Forecasting and decision making», pp. 231-362, Chapter in the book «Decision Making» by F. Batzias and Z. Res,, Hellenic Open University Ed., Patra 2005.

Applying a Modified Contingent Valuation Method (CVM) For the Preservation/Restoration of the Lake Kastoria in Northern Greece

Elsa Zoupanidou, Fragiskos Batzias[a], Odysseas Kopsidas

Laboratory of Simulation of Industrial Processes,
Dep. Industrial Management and Technology, Univ. Piraeus
80 Karaoli & Dimitriou, GR 18534 Piraeus, Greece
[a]email: fbatzi@unipi.gr

Abstract. The preservation/restoration of natural environment is frequently entailing excessive cost (paid by people through taxation) while it is a source of additional income for both, the State and the people, due to tourism. Since the evaluation of this good cannot be in market terms, we apply herein a modified version of the Contingent Valuation Method (CVM), which is used in Experimental Economics in order to investigate the significance that people put on this good and how much they might be willing to pay (WTP) for supporting activities concerning the preservation/restoration of Lake Kastoria. The WTP dependence on (i) external diseconomies, (ii) the expectations for property values' rise as a result of the restoration, (iii) the proximity of interviewees' residence to the lake, (iv) the opinion of the interviewee on the time and money spent to visit the lake, (v) the time and money the interviewees spent to visit the lake, as well as other dependencies (all taken as independent variables) are estimated by means of Logit, Probit, Logistic and Linear Regression Models.

Keywords: Contingent Valuation Method (CVM), Environmental impact, Willingness To Pay (WTP), Logit Model, Parametric Approach, Non-Parametric Approach, Probit Model.

INTRODUCTION

Lake Kastoria covers an area of 28 Km^2 at an altitude of 630 m in the Kastoria Prefecture, northwestern Greece (Fig. 1), extending to the Municipalities of Kastoria, Makedni and Vitsi. The lake, subject to the provisions of the Bern Convention (1979), the Bonn Convention (1979), and Council Directives 79/409 and 92/43, is part of the Natura 2000 network. Lake Kastoria is a very fragile shallow aquatic ecosystem, long stressed by the various rural (logging, agricultural wastes, stockbreeding, etc.), craft (tanneries, fur/leather production), and urban (e.g., sewer discharges, rubble depositions and extensive littering) activities of the area. The nearby wastewater treatment plant of Dispilio, which operates since 1991, managed to reduce to some extent wastewater inflows, yet the lake faces increasing water pollution problems, ecological degradation of the coastal line and loss in its aesthetic value [1].

The aim of this study is to provide policy-makers with much needed information on the economic value of the benefits generated by the sustainable management of the Lake Kastoria. The preservation/restoration of natural environment is frequently entailing excessive cost (paid by people through taxation) while it is a source of additional income for both, the State and the people, due to tourism. Since the evaluation of this good cannot be in market terms, we apply herein a modified version of the Contingent Valuation Method (CVM), which is used in Experimental Economics in order to investigate the significance that people put on this good and how much they might be willing to pay (WTP) for supporting activities concerning the preservation/restoration of Lake Kastoria.

The WTP dependence on (i) external diseconomies, (ii) the expectations for property values' rise as a result of the restoration, (iii) the proximity of interviewees' residence to the lake, (iv) the opinion of the interviewee on the time

FIGURE 1. Photo (left) and satellite image (right) of Lake Kastoria. Nine rivulets flow into the lake; its depth varies from nine to ten meters which defines the lake as a shallow one.

and money spent to visit the lake, (v) the time and money the interviewees spent to visit the lake, as well as other dependencies (all taken as independent variables) are estimated by means of Logit, Probit, Logistic and Linear Regression Models.

METHODOLOGY

Members of the public were randomly intercepted in city and town centres, cafes and markets, and were interviewed face-to-face. The sample size was 80 questionnaires. For the processing of answers in stages 10, 12, 17 (pilot, main, follow-up study, respectively) we use the following measures/indices [2-4]: R^2, Efron's R^2, MacFadden's log likelihood of the intercept model, Cox & Snell's R^2, adjusted Cox & Snell's R^2. The non-linear regression models we used are the Probit and the Logit ones. Probit is a popular specification for an ordinal or a binary response model that employs a link function. In this model, the response variable y is binary and may represent a certain condition. A generalized form of this model is the following:

$$\Pr(y = 1/x) = \Phi(x'\beta) \tag{1}$$

where Pr denotes probability and Φ is the cumulative distribution function of the standard normal distribution. The parameters β are typically estimated by maximum likelihood. There exists an auxiliary random variable:

$y^* = x'\beta + \varepsilon$, where error $\varepsilon \in N(0,1)$

Then y can be considered as an indicator for whether this latent variable is positive:

$$y = 1_{\{y^*>0\}} = \begin{cases} 1 & \text{if} \quad y^*>0, \quad i.e., -\varepsilon < x'\beta \\ 0 & \text{otherwise} \end{cases} \tag{2}$$

The Logit model gives the logistic function:

$$f(z) = \frac{e^z}{e^z + 1} = \frac{1}{1 + e^{-z}} \tag{3}$$

where the variable z is usually defined as: $z = \beta_0 + \beta_1 x_1 + ... + \beta_k x_k$ where β_0 is the intercept and $\beta_1,...,\beta_k$ are the regression coefficients of $x_1,...,x_k$, respectively. Actually, R^2, the coefficient of determination, is the relative power of the Probit and the Logit models.

RESULTS AND DISCUSSION

The survey sample consisted of 51.25% women and 48.56% men, the majority between 26 and 35 years old, since young people were more willing to participate in the survey; 27.5% of the respondents hold a university degree, whereas 37.50% had high school education. The majority of the interviewees belonged to the intermediate

income class and enjoy full-time employment. About 50% of the respondents live or work in close proximity of the lake; however, average WTP does not differ significantly with proximity or distance. Given that extensive media coverage during the recent years, most people were well aware about the problems of the lake. When respondents were asked to assign a level of importance to the protection of the lake on a 3-point scale (very, enough and slightly), 93.75% placed it at the highest scale, 11.25% at the medium scale, and only 5% at the lowest.

The present survey examined, among other factors, the attitude of citizens towards the general environmental problems of the area and the benefits that would derive from restoring the lake's ecosystem. The majority of the interviewees allocate the responsibility of environmental degradation to the failure or limited capacity of the State and local authorities, whereas they support all of the restoration activities we proposed, with 69.03% giving high priority to biological agriculture for decreasing the input of chemical contaminants. The participants were also asked to determine the amount of money, among six fixed alternatives and a seventh open option, that each was willing to pay for 12 months to help maintain or even improve the state of the lake, taking into consideration that the subsidy which was given by the government and the local authorities should remain the same. The proportion of all respondents who expressed a willingness to pay any amount was 90% (Fig. 2); the mean WTP was 13.16€, while the amount of 5€ was the most frequent.

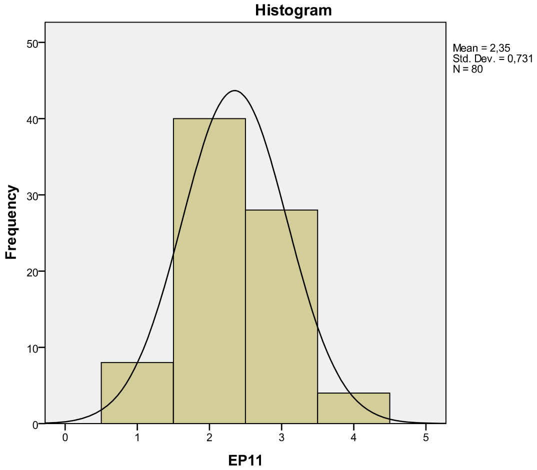

Statistics

(N)	80
Mean	2,35
Std. Error of Mean	0,082
Median	2
Mode	2
Std. Deviation	0,731
Variance	0,534
Skewness	0,142
Std. Error of Skewness	0,269
Range	3
Min	1
Max	4

FIGURE 2. Distribution of WTP and sample summary statistics.

Regression analysis was also used to investigate the relationship between WTP and socio-economic factors; the Durbin–Watson statistic of ca. 2 is indicative of small residual autocorrelation (Table 1), whereas the ANOVA is shown in Table 2. The analysis results found which independent variables are statistically significant at the 5% significance level: X_9: the importance of lake Kastoria; X_{12}: willingness to pay IFF the respondent was living close to lake; X_{14}: accept a compensation to forgo an improvement in lake; X_{19}: own property close to lake; X_{28}: household income in relation to that of residents of Kastoria. The reduced form of the resulting Linear regression function becomes: $WTP=1.164-0.27X_9+0.82X_{12}-0.14X_{14}-0.01X_{19}+0.11X_{28}$.

TABLE 1. Regression Analysis Model Summary

R	*R Square*	*Adjusted R Square*	*Std. Error of the Estimate*	*Durbin-Watson*
0.929	0.863	0.819	0.311	1.885

TABLE 2. The ANOVA results, with predictors: X_1, …, X_{16} and WTP-value as the dependent variable.

Model	*Sum of Squares*	*df*	*Mean Square*	*F*	*Sig.*
Regression	36.408	19	1.916	19.851	0.00
Residual	5.792	60	0.097		
Total	42.200	79			

The results of the Logit and Probit regression analysis are shown in Table 3. The independent variables, statistically significant at the 5% significance level, for Probit regression are X_{12} and X_{14}, whereas Logit regression adds also the variable X_{19}.

TABLE 3. Probit and Logit Regression Analysis

Probit			
	Chi-square test	df	Significance
Pearson	35.065	218	1.000
Deviance	42.050	218	1.000
	Chi-square test		
Cox & Snell	0.888		
Nagelkerke	1.000		
McFadden	1.000		
Logit			
	Chi-square test	df	Significance
Pearson	28.297	218	1.000
Deviance	27.774	218	1.000
	Chi-square test		
Cox & Snell	0.888		
Nagelkerke	1.000		
McFadden	1.000		

DISCUSSION AND CONCLUDING REMARKS

Economic valuation is a two-part process in which the first part (demonstration) displays and measures the economic value of environmental assets, while the second part (appropriation) finds ways to capture the value of such. The present survey has managed to demonstrate the economic value of preserving Lake Kastoria; the appropriation of this value requires policies, rules, and regulations on the part of concerned agencies and institutions.

The willingness to pay, a so-called 'restoration fee', which is actually a 'user's fee' [5], indicates the possibility of fund raising from the community, especially when lake restoration is linked to tourist economy. On the other hand, non-use values for the lake, which this study shows to be substantial, can be captured through appropriate policy instruments. Designing appropriate policy instruments is one big task in itself and there are possible options to be considered like voluntary contribution or council taxation. Since education is a determinant that increases WTP in the medium/long-run, future surveys should target schools, colleges, and universities in the area, so as to increase potential 'capturable' non-use values and acquire relevant information useful for sensitizing young people.

In conclusion, our analysis demonstrates that social science research can provide useful information for complex environmental policy problems such as the restoration of a lake system. Policy analysis for such cases is especially difficult because these systems provide multiple, interdependent services that vary by type of lake, location, ecohydrological management, and other factors. The work presented herein has been proven a useful comprehensive tool for determining the realistic cognitive burden for stakeholders and third parties.

ACKNOWLEDGMENTS

Financial support provided by the Post-Graduate Degree Programme (MSc) on 'Systems of Energy Management and Environmental Protection', through the Research Centre of the University of Piraeus, is kindly acknowledged.

REFERENCES

1. N. Mantzafleri, A. Psilovikos, A. Blanta, *Water Resour Manage* **23**, 3221–3254 (2009).
2. T.F. Liao, *Interpreting Probability Models: Logit, Probit, and other Generalized Linear Models*. SAGE Publications Inc., 1994.
3. S. Menard, *Applied Logistic Regression Analysis*, 2nd ed., SAGE Publications Inc., 2001.
4. D.W. Hosmer, S. Lemeshow, *Applied Logistic Regression*, 2nd ed., John Wiley & Sons, 2000.
5. R. Mitchell, R. Carson. *Using surveys to value public goods: the contingent valuation method*. Resources for the Future. Washington DC, 1989.

A New Family of Hybrid Six–Step Embedded Explicit Algorithms with Eliminated Phase–Lag and its Derivatives

Ibraheem Alolyan[1] and T.E. Simos[1,2,3,4,a]

[1]*Department of Mathematics, College of Sciences, King Saud University, P. O. Box 2455, Riyadh 11451, Saudi Arabia*

[2]*Data Recovery Key Laboratory of Sichuan Province, Neijiang Normal University, Dongtong Road 705, Neijiang 641100, China*

[3]*Group Leader, Group of Modern Computational Methods, Ural Federal University, 620002,19 Mira Street,Ekaterinburg, Russian Federation,*

[4]*Section of Mathematics, Department of Civil Engineering, Democritus University of Thrace, Xanthi, Greece (Visiting Professor)*

[a]e-mail: tsimos.conf@gmail.com

Abstract. In this paper we propose a hybrid six–step method with algebraic order the highest possible. The area of application of this newly obtained algorithms is the numerical solution of second order initial and/or boundary-value problems with solutions which present periodical and/or oscillating behavior.

In order the above newly introduced family to be obtained we establish the following requirements:

- phase–lag $= 0$
- phase–lag$^{(n)} = 0$,

where where phase–lag$^{(n)}$ is the n-th derivative of the phase–lag. The above requirements lead to systems of of equations for each scheme of the new proposed family. The solution of the above mentioned system of equations leads to the designation of the free parameters of the each scheme of the family of algorithms.

In order to examine the above newly developed family of methods, we establish the following theoretical analysis which consists of the following stages:

1. Designation of the local truncation error (LTE) of each scheme of the newly proposed family.
2. Investigation of the asymptotic form of the LTE which is produced using as model problem the radial time independent Schrödinger equation.
3. Assessment of the asymptotic forms of LTEs for all the schemes of the newly obtained family. The above-mentioned assessment leads to conclusions on the accuracy of the algorithms of the newly obtained family.
4. Investigation of the stability and the interval of the periodicity of all the schemes of the newly obtained family.
5. Investigation of the computational efficiency of all the schemes of the newly obtained family, by applying them to the numerical solution of several second order problems like the radial Schrödinger equation, astronomical problems, etc.

Keywords: Numerical solution, Schrödinger equation, embedded multistep methods, interval of periodicity, P-stability, phase–lag, phase-fitted, derivatives of the phase–lag
PACS: 02.60, 02.70.Bf, 95.10.Ce, 95.10.Eg, 95.75.Pq

INTRODUCTION

The computational solution of the initial and/or boundary value problems of the form:

$$\kappa''(x) = f(x, \kappa(x)). \tag{1}$$

is the subject of the research of this paper (see for bibliography [1] - [15]):

We pay special attention to problems of the form (1) with periodical and/or oscillating behavior of their solution. Many areas in sciences and engineering have problems which can be expressed with equations or system of equations

of the form (1) (examples: Schrödinger's equation, Duffing's equation, van der Pol equation, Astronomical and Astrophysical problems etc).

In the Flowchart of Figure 1 the development of the newly family of algorithms is presented (for developing flowcharts in LaTeX one can see [16]).

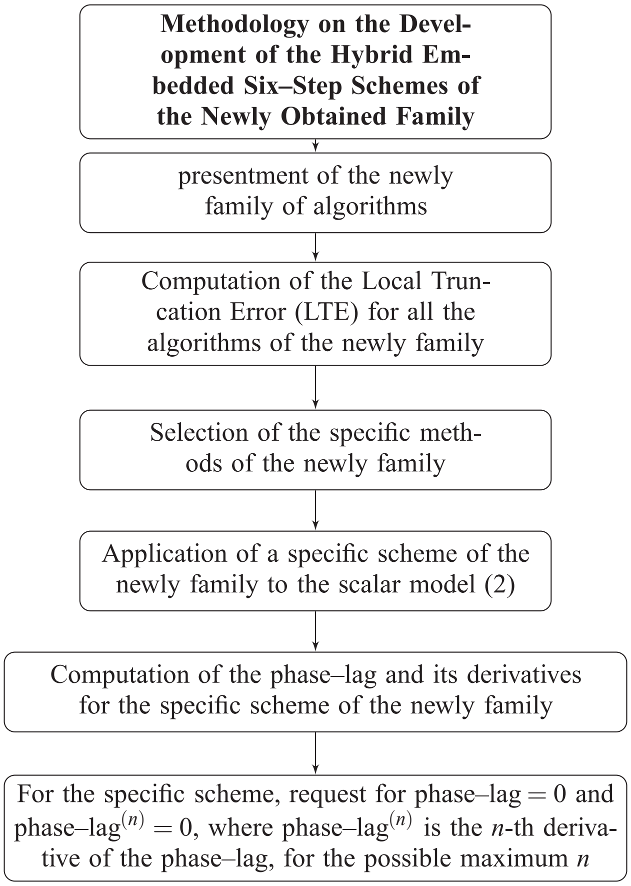

FIGURE 1. Flowchart for the Development of the Hybrid Embedded Six–Step Schemes of the Newly Obtained Family

The following categories of problems can be solved using the newly introduced family:

- problems with solution which presents oscillating and / or periodical behavior,
- problems with solution involving the functions cos and sin,
- problems with solution involving combinations of the functions cos and sin.

The newly obtained algorithms have the following properties:

- Algebraic order of highest possible value.
- $phase--lag = 0$.
- phase–lag$^{(j)} = 0$, where phase–lag$^{(n)}$ is the j-th derivative of the phase–lag, with $j = 1, 2, \dots, n$.
- Maximum possible stability area and the largest possible interval of periodicity.

Remark 1
- *In order to calculate the phase–lag, we use the direct formula for symmetric $2k$-step methods, $k \in \mathbb{N}$, obtained in [10], [11] and [12] by Simos and his co-authors.*
- *In order to calculate the derivatives of the phase–lag, we use the above mentioned direct formula.*

The effectiveness of the new family of methods is assessed as follows:

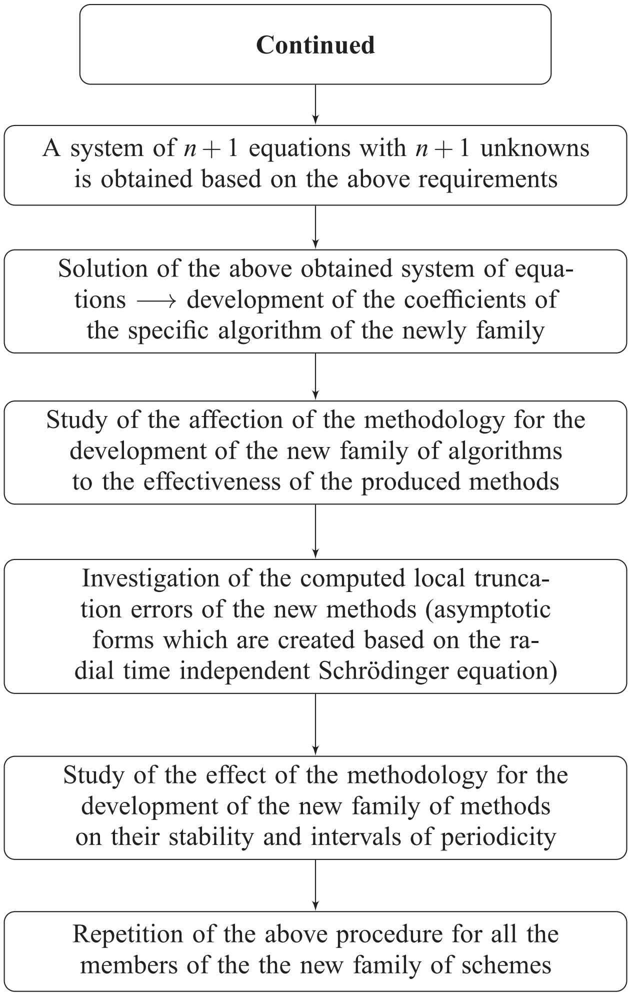

FIGURE 1. Continued

Theoretical Evaluation

- Investigation of the asymptotic forms of the local truncation errors ($ASFOLTEs$) for all the members of the family.
- Comparison of the $ASFOLTEs$ with those of of other similar algorithms (comparative error analysis).
- Investigation of the stability and interval of periodicity analysis of all the members of the newly proposed family methods.

Computational Evaluation

- Assession of the numerical tests obtained by the application of all the members of the new introduced family of algorithms to several second order problems (see for more details [13]).

SYMMETRIC MULTISTEP METHODS

Let us consider the scalar equation:

$$\kappa'' = -\phi^2 \kappa. \tag{2}$$

We define as $2m$-step methods as:

$$\Phi(m) : \sum_{i=-m}^{m} \alpha_i \kappa_{n+i} = h^2 \sum_{i=-m}^{m} \beta_i f(x_{n+i}, \kappa_{n+i}) \tag{3}$$

where

- $\{x_i\}_{i=-m}^{m} \in [a,b]$ where $[a,b]$ is the integration domain,
- $h = |x_{i+1} - x_i|, \quad i = 0(1)m-1$, is the step length of the integration.

Definition 1

$$\Phi(m) \rightarrow \begin{cases} \beta_m \neq 0 & \textit{implicit}; \\ \beta_m = 0 & \textit{explicit}. \end{cases} \tag{4}$$

Definition 2

$$\Phi(m) \ \textit{with} \ \alpha_{i-m} = \alpha_{m-i}, \beta_{i-m} = \beta_{m-i}, i = 0(1)m \rightarrow \textit{symmetric} \tag{5}$$

$$(3) \stackrel{(2)}{\longrightarrow} DiffEqt\,(m) \text{ and } ChrEqt\,(m) \tag{6}$$

where

$$DiffEqt\,(m) = \Lambda_m(v)\,\kappa_{n+m} + \cdots + \Lambda_1(v)\,\kappa_{n+1} + \Lambda_0(v)\,\kappa_n + \Lambda_1(v)\,\kappa_{n-1} + \cdots + \Lambda_m(v)\,\kappa_{n-m} = 0 \tag{7}$$

and

$$ChrEqt\,(m) = \Lambda_m(v)\,\lambda^m + \cdots + \Lambda_1(v)\,\lambda + \Lambda_0(v) + \Lambda_1(v)\,\lambda^{-1} + \cdots + \Lambda_m(v)\,\lambda^{-m} = 0. \tag{8}$$

where $v = \phi\, h$, h is the step length and $\Lambda_j(v)\; j = 0(1)m$ are the stability polynomials of v.

Remark 2 *Condition of the algebraic order s + Conditions of consistency* $\stackrel{\textit{for the methods (3)}}{\longrightarrow}$ *[14].*

Definition 3 [15] $(0, v_0^2)$ *for the symmetric* $2m$*-step method with (8)* $\stackrel{\textit{if for all } v \in (0, v_0^2)}{\longrightarrow}$ *the roots* $s_i, i = 1(1)2m$ *of Eq. (8) satisfy:*

$$s_1 = e^{i\theta(v)},\, s_2 = e^{-i\theta(v)},\ \textit{and}\ |s_i| \leq 1,\, i = 3(1)2m \tag{9}$$

where $\theta(v)$ *is a real function of v and* $(0, v_0^2) =$ *a non empty interval of periodicity.*

Theorem 1 [10] *The symmetric method (3) with (8) has a phase–lag order* ρ *and a phase–lag constant* ϑ *given by:*

$$-\vartheta v^{\rho+2} + O(v^{\rho+4}) = \frac{2\sum_{j=1}^{m} \Lambda_j(v)\cos(jv) + \Lambda_0(v)}{2\sum_{j=1}^{m} j^2 \Lambda_j(v)} \tag{10}$$

For a symmetric six–step method, the phase–lag order ρ and the phase–lag and phase–lag constant ζ are given by:

$$-\vartheta v^{\rho+2} + O(v^{\rho+4}) = \frac{2\Lambda_3(v)\cos(3v) + 2\Lambda_2(v)\cos(2v) + 2\Lambda_1(v)\cos(v) + \Lambda_0(v)}{18\Lambda_3(v) + 8\Lambda_2(v) + 2\Lambda_1(v)} \tag{11}$$

THE NEW FAMILY OF SIX–STAGES EMBEDDED METHODS

The form of the new proposed family of six–stages symmetric six–step embedded methods is given by:

$$
\begin{aligned}
B &= -\kappa_{n-2} - c_1\,(\kappa_{n+1}+\kappa_{n-1}) - c_0\,\kappa_n \\
\tilde{\kappa}_{n+2} &= B + h^2\left[\delta_1\left(\kappa''_{n+1}+\kappa''_{n-1}\right)+\delta_0\,\kappa''_n\right] \\
\check{\kappa}_{n+2} &= B + h^2\left[\varepsilon_2\left(\tilde{\kappa}''_{n+2}+\kappa''_{n-2}\right)+\varepsilon_1\left(\kappa''_{n+1}+\kappa''_{n-1}\right)+\varepsilon_0\,\kappa''_n\right] \\
A &= -a_2\left(\kappa_{n+2}+\kappa_{n-2}\right)-a_1\left(\kappa_{n+1}+\kappa_{n-1}\right)-a_0\,\kappa_n-\kappa_{n-3} \\
\hat{\kappa}_{n+3} &= A + h^2\left[\gamma_2\left(\check{\kappa}''_{n+2}+\kappa''_{n-2}\right)+\gamma_1\left(\kappa''_{n+1}+\kappa''_{n-1}\right)+\gamma_0\,\kappa''_n\right] \\
\overline{\kappa}_{n+3} &= A + h^2\left[\beta_3\left(\hat{\kappa}''_{n+3}+\kappa''_{n-3}\right)+\beta_2\left(\kappa''_{n+2}+\kappa''_{n-2}\right)+\beta_1\left(\kappa''_{n+1}+\kappa''_{n-1}\right)+\beta_0\,\kappa''_n\right] \\
\check{\kappa}_{n+3} &= A + h^2\left[\beta_3\left(\overline{\kappa}''_{n+3}+\kappa''_{n-3}\right)+\beta_2\left(\kappa''_{n+2}+\kappa''_{n-2}\right)+\beta_1\left(\kappa''_{n+1}+\kappa''_{n-1}\right)+\beta_0\,\kappa''_n\right] \\
\tilde{\kappa}_{n+3} &= A + h^2\left[\beta_3\left(\check{\kappa}''_{n+3}+\kappa''_{n-3}\right)+\beta_2\left(\kappa''_{n+2}+\kappa''_{n-2}\right)+\beta_1\left(\kappa''_{n+1}+\kappa''_{n-1}\right)+\beta_0\,\kappa''_n\right] \\
\tilde{\kappa}_n &= \kappa_n + h^2\left[\zeta_3\left(\tilde{\kappa}''_{n+3}+\kappa''_{n-3}\right)+\zeta_2\left(\kappa''_{n+2}+\kappa''_{n-2}\right)+\zeta_1\left(\kappa''_{n+1}+\kappa''_{n-1}\right)+\zeta_0\,\kappa''_n\right] \\
\kappa_{n+3} &= A + h^2\Bigg[b_3\left(\tilde{\kappa}''_{n+3}+\kappa''_{n-3}\right)+b_2\left(\kappa''_{n+2}+\kappa''_{n-2}\right) \\
&\qquad +b_1\left(\kappa''_{n+1}+\kappa''_{n-1}\right)+b_0\,\tilde{\kappa}''_n\Bigg], \qquad (12)
\end{aligned}
$$

where

- $h \longrightarrow$ step length for the integration ,
- $n \longrightarrow$ number of steps,
- $\kappa_n \longrightarrow$ approximated value of the function κ at the x_n,
- $x_n = x_0 + n\,h$ and
- $x_0 \longrightarrow$ initial value point.

If we apply the newly introduced algorithm (12) to the scalar equation (2), we obtain the difference equation (7) with $m = 3$ and:

$$\Lambda_3(v)\,(\kappa_{n+3}+\kappa_{n-3})+\Lambda_2(v)\,(\kappa_{n+2}+\kappa_{n-2})+\Lambda_1(v)\,(\kappa_{n+1}+\kappa_{n-1})+\Lambda_0(v)\,\kappa_n=0 \qquad (13)$$

where

$$
\begin{aligned}
\Lambda_3(v) &= 1,\ \Lambda_2(v) = -v^{10}a_2b_0\beta_3{}^3\zeta_3+v^{10}b_0\beta_2\beta_3{}^2\zeta_3 \\
&+ v^8a_2b_0\beta_3{}^2\zeta_3+v^8a_2b_3\beta_3{}^3-v^8b_0\beta_2\beta_3\zeta_3 \\
&- v^8b_3\beta_2\beta_3{}^2-v^6a_2b_0\beta_3\zeta_3-v^6a_2b_3\beta_3{}^2 \\
&+ v^6b_0\beta_2\zeta_3+v^6b_3\beta_2\beta_3+v^4a_2b_0\zeta_3 \\
&+ v^4a_2b_3\beta_3-v^4b_0\zeta_2-v^4b_3\beta_2-v^2a_2b_3 \\
&+ v^2b_2+a_2 \\
\Lambda_1(v) &= -v^4b_0\zeta_1+v^{14}b_3\beta_3{}^3\delta_1\varepsilon_2\gamma_2 \\
&+ v^{12}b_3\beta_3{}^3c_1\varepsilon_2\gamma_2
\end{aligned}
$$

$$
\begin{aligned}
& + \quad v^2 b_1 - v^{12} b_3 \beta_3{}^3 \varepsilon_1 \gamma_2 - v^{10} b_3 \beta_3{}^3 c_1 \gamma_2 \\
& - \quad v^{12} b_0 \beta_3{}^3 \gamma_1 \zeta_3 - v^{10} a_1 b_0 \beta_3{}^3 \zeta_3 \\
& + \quad v^{10} b_0 \beta_1 \beta_3{}^2 \zeta_3 + v^8 a_1 b_0 \beta_3{}^2 \zeta_3 \\
& - \quad v^8 b_0 \beta_1 \beta_3 \zeta_3 - v^6 a_1 b_0 \beta_3 \zeta_3 + a_1 + v^{10} b_3 \beta_3{}^3 \gamma_1 \\
& + \quad v^8 a_1 b_3 \beta_3{}^3 - v^8 b_3 \beta_1 \beta_3{}^2 - v^6 a_1 b_3 \beta_3{}^2 \\
& + \quad v^6 b_3 \beta_1 \beta_3 + v^4 a_1 b_3 \beta_3 - v^2 a_1 b_3 - v^4 b_3 \beta_1 \\
& - \quad v^{16} b_0 \beta_3{}^3 \delta_1 \varepsilon_2 \gamma_2 \zeta_3 - v^{14} b_0 \beta_3{}^3 c_1 \varepsilon_2 \gamma_2 \zeta_3 \\
& + \quad v^4 a_1 b_0 \zeta_3 + v^6 b_0 \beta_1 \zeta_3 + v^{14} b_0 \beta_3{}^3 \varepsilon_1 \gamma_2 \zeta_3 \\
& + \quad v^{12} b_0 \beta_3{}^3 c_1 \gamma_2 \zeta_3 \\
\Lambda_0(v) & = \quad -v^{12} b_3 \beta_3{}^3 \varepsilon_0 \gamma_2 \\
& - \quad v^{10} b_3 \beta_3{}^3 c_0 \gamma_2 + a_0 + v^6 b_0 \beta_0 \zeta_3 \\
& + \quad v^4 a_0 b_0 \zeta_3 + v^{10} b_3 \beta_3{}^3 \gamma_0 + v^8 a_0 b_3 \beta_3{}^3 \\
& - \quad v^8 b_3 \beta_0 \beta_3{}^2 - v^6 a_0 b_3 \beta_3{}^2 + v^6 b_3 \beta_0 \beta_3 \\
& + \quad v^4 a_0 b_3 \beta_3 + b_0 v^2 - v^4 b_3 \beta_0 - v^2 a_0 b_3 + v^{14} b_3 \beta_3{}^3 \delta_0 \varepsilon_2 \gamma_2 \\
& + \quad v^{12} b_3 \beta_3{}^3 c_0 \varepsilon_2 \gamma_2 - v^{16} b_0 \beta_3{}^3 \delta_0 \varepsilon_2 \gamma_2 \zeta_3 \\
& - \quad v^{14} b_0 \beta_3{}^3 c_0 \varepsilon_2 \gamma_2 \zeta_3 + v^{14} b_0 \beta_3{}^3 \varepsilon_0 \gamma_2 \zeta_3 \\
& + \quad v^{12} b_0 \beta_3{}^3 c_0 \gamma_2 \zeta_3 + v^8 a_0 b_0 \beta_3{}^2 \zeta_3 \\
& - \quad v^8 b_0 \beta_0 \beta_3 \zeta_3 - v^6 a_0 b_0 \beta_3 \zeta_3 - v^{10} a_0 b_0 \beta_3{}^3 \zeta_3 \\
& + \quad v^{10} b_0 \beta_0 \beta_3{}^2 \zeta_3 - v^{12} b_0 \beta_3{}^3 \gamma_0 \zeta_3 - v^4 b_0 \zeta_0
\end{aligned} \tag{14}
$$

Requesting:

- the vanishing of the phase–lag,
- the vanishing of the phase–lag's derivatives of the maximum possible order,

using also the formulae (13) and (14)), we obtain a system of equations. The solution of the obtained system leads to the computation of the unknown coefficients for the specific scheme of the newly introduced family of embedded methods.

Remark 3 *The vanishing of the phase–lag's derivatives of the maximum possible order is dependent from*

- *the unknown coefficients of the specific scheme of the family,*
- *the satisfaction of the requested maximum possible algebraic order and*
- *the satisfaction of the consistency's conditions.*

The above methodology leads to the construction of several embedded algorithms of the newly produced family of methods of the form (12).

The production of the specific embedded scheme is followed by:

1. the computation of the local truncation error (LTE),
2. the computation of the stability and the interval of periodicity of the method and
3. the assessment of the efficiency of the produced schemes by applying them to several well known second order problems.

REFERENCES

1. L. Abia, J.M. Sanz-Serna, Partitioned Runge-Kutta methods for separable Hamiltonian problems, *Math. Comput.* **60** 617-634(1993).
2. Forest E. Ruth R., Fourth order symplectic integration, *Physica D* **43** 105-117(1990).

3. J.M. Franco, Exponentially fitted symplectic integrators of RKN type for solving oscillatory problems, *Computer Physics Communications* 177(2007) 479-492.
4. Ruth R.D., A canonical integration technique, *IEEE Trans. Nuclear Sci.* **NS 30** 2669-2671(1983).
5. J. M. Sanz Serna and L. Abia, Order conditions for canonical Runge Kutta schemes, *SIAM J. Numer. Anal.* **28** 1081-1096(1991).
6. Sanz-Serna, J.M., Calvo, M.P., *Numerical Hamiltonian Problem*, Chapman and Hall, London, 1994.
7. A. Tocino and J. Vigo-Aguiar, Symplectic Conditions for Exponential Fitting Runge-Kutta-Nyström methods, *Mathematical and Computer Modelling* 42 (2005) 873-876.
8. Hans Van de Vyver, A symplectic exponentially fitted modified Runge-Kutta-Nyström method for the numerical integration of orbital problems, *New Astronomy*, 10 (2005) 261-269.
9. Yoshida H., Construction of higher order symplectic integrators, *Physics Letters A* 150(1990),262-268
10. T.E. Simos and P.S. Williams, A finite difference method for the numerical solution of the Schrödinger equation, *Journal of Computational and Applied Mathematics* **79**, 189-205(1997).
11. T.E. Simos and P.S. Williams, On finite difference methods for the solution of the Schrödinger equation, *Computers & Chemistry* **23** 513-554(1999).
12. A.D. Raptis and T.E. Simos: A four-step phase-fitted method for the numerical integration of second order initial-value problem, BIT, 31, 160-168(1991)
13. Ibraheem Alolyan and T.E. Simos, A Runge-Kutta type four-step method with vanished phase–lag and its first and second derivatives for each level for the numerical integration of the Schrödinger equation, *Journal of Mathematical Chemistry*, **52(3)** 917-947(2014)
14. J.D. Lambert, Numerical Methods for Ordinary Differential Systems, *The Initial Value Problem*, Pages 104-107, John Wiley and Sons, 1991.
15. L.D. Lambert and I.A. Watson, Symmetric multistep methods for periodic initial value problems, *J. Inst. Math. Appl.* **18**, 189202, (1976).
16. Stefan Kottwitz, LaTeX Cookbook, Pages 231-236, Packt Publishing Ltd., Birmingham B3 2PB, UK (2015)